

# APPLIED GROUNDWATER MODELING

## Simulation of Flow and Advective Transport

**Second Edition**

**MARY P. ANDERSON**

Department of Geoscience, University of Wisconsin-Madison,  
Madison, Wisconsin

**WILLIAM W. WOESSNER**

Department of Geosciences, University of Montana, Missoula,  
Montana

**RANDALL J. HUNT**

U.S. Geological Survey, Wisconsin Water Science Center, Cross Plains,  
Wisconsin



Amsterdam • Boston • Heidelberg • London  
New York • Oxford • Paris • San Diego  
San Francisco • Singapore • Sydney • Tokyo  
Academic Press is an imprint of Elsevier



Academic Press is an imprint of Elsevier  
125 London Wall, London EC2Y 5AS, UK  
525 B Street, Suite 1800, San Diego, CA 92101-4495, USA  
225 Wyman Street, Waltham, MA 02451, USA  
The Boulevard, Langford Lane, Kidlington, Oxford OX5 1GB, UK

Copyright © 2015, 2002 Elsevier Inc. All rights reserved.

No part of this publication may be reproduced or transmitted in any form or by any means, electronic or mechanical, including photocopying, recording, or any information storage and retrieval system, without permission in writing from the publisher. Details on how to seek permission, further information about the Publisher's permissions policies and our arrangements with organizations such as the Copyright Clearance Center and the Copyright Licensing Agency, can be found at our website: <http://elsevier.com/permissions>.

This book and the individual contributions contained in it are protected under copyright by the Publisher (other than as may be noted herein).

### Notices

Knowledge and best practice in this field are constantly changing. As new research and experience broaden our understanding, changes in research methods, professional practices, or medical treatment may become necessary.

Practitioners and researchers must always rely on their own experience and knowledge in evaluating and using any information, methods, compounds, or experiments described herein. In using such information or methods they should be mindful of their own safety and the safety of others, including parties for whom they have a professional responsibility.

To the fullest extent of the law, neither the Publisher nor the authors, contributors, or editors, assume any liability for any injury and/or damage to persons or property as a matter of products liability, negligence or otherwise, or from any use or operation of any methods, products, instructions, or ideas contained in the material herein.

ISBN: 978-0-12-058103-0

### British Library Cataloguing in Publication Data

A catalogue record for this book is available from the British Library

### Library of Congress Cataloging-in-Publication Data

A catalog record for this book is available from the Library of Congress

For information on all Academic Press publications  
visit our website at <http://store.elsevier.com/>



Working together  
to grow libraries in  
developing countries

[www.elsevier.com](http://www.elsevier.com) • [www.bookaid.org](http://www.bookaid.org)

### Acknowledgment

The front cover image is provided courtesy of Schlumberger Water Services. The image represents a uniform grid for a multi-layer finite-difference MODFLOW model and was produced using the software Visual MODFLOW Flex. Colors at the top of the image represent changes in land surface elevation; colors in the bottom layers represent geologic variability. The back cover graphic is a word cloud created using all text contained in Chapters 1–12. Word-cloud graphics included with the introductory sections of the book consist of text contained in each section. All word clouds were generated using Wordle, created by Jonathon Feinberg ([www.wordle.net](http://www.wordle.net)).

*...to Charles, Jean, and Lori*

## LIST OF FIGURES

<b>Figure 1.1</b>	Workflow for groundwater modeling. As presented, the workflow assumes the objective of the model is a forecast but the workflow can be adapted for other modeling purposes, as described in the text. Although not shown in the figure, field data are critical for the workflow, especially conceptual model design and the calibration process.	10
<b>Figure 1.2</b>	The scientific method ( <i>modified from: <a href="http://www.sciencebuddies.org/science-fair-projects/project_scientific_method.shtml">http://www.sciencebuddies.org/science-fair-projects/project_scientific_method.shtml</a></i> ).	16
<b>Figure B1.1.1</b>	Springflow calculated using an ANN model and multiple linear regression compared with results from process-based models for continuous porous media (Theis or Hantush–Jacob solutions) and conduit flow (Darcy–Weisbach equation). Measured springflow is also shown ( <i>Sepúlveda, 2009</i> ).	7
<b>Figure 2.1</b>	Generic conceptual model of a large riverine valley with terraces ( <i>Winter et al., 1998</i> ).	29
<b>Figure 2.2</b>	Data and analyses leading to (a) hydrogeologic site conceptual model; (b) hydrologic system conceptual model ( <i>modified from Kolm, 1996</i> ).	32
<b>Figure 2.3</b>	Hydrogeologic boundaries of a conceptual model of the groundwater system in Long Island, NY, USA, and mathematical representation in the numerical model ( <i>Buxton and Smolensky, 1999</i> ).	36
<b>Figure 2.4</b>	Faults form boundaries for a model of the San Bernardino, CA, USA, groundwater system ( <i>Danskin et al., 2006</i> ).	37
<b>Figure 2.5</b>	Potentiometric surface maps showing head in the lower surficial aquifer (see Fig. 2.9(b)), Dover Air Force Base, Delaware, USA, under average recharge conditions, October 1959: (a) regional; (b) site ( <i>Hinaman and Tenbus, 2000</i> ).	38
<b>Figure 2.6</b>	Generic conceptual models of aquitards showing: (a) timescales for flow through aquitards ( <i>Winter et al., 1998</i> ); (b) discontinuous beds ( <i>Alley et al., 1999</i> ).	40
<b>Figure 2.7</b>	Hydrostratigraphic units at the Savannah River Site, South Carolina, USA. Geophysical logs and layers in the numerical	

	model are also shown. Note that nomenclature in Georgia is different from South Carolina ( <i>Clarke and West, 1998</i> ).	43
<b>Figure 2.8</b>	Geologic facies model of a fluvial depositional setting ( <i>Fielding et al., 2009</i> ).	44
<b>Figure 2.9</b>	Conceptual models in cross section. (a) Hydrofacies with information on depositional setting and estimates of hydraulic conductivity, Cape Cod, MA, USA ( <i>Reilly and Harbaugh, 2004; modified from Masterson et al., 1997</i> ). (b) Hydrostratigraphic units for the upper groundwater flow system at the Dover Air Force Base, Delaware, USA, with estimates of hydraulic conductivity. Note that the confining bed (upper Calvert Formation) is discontinuous ( <i>Hinaman and Tenbus, 2000</i> ).	45
<b>Figure 2.10</b>	Isopach map of the confining bed (upper Calvert Formation, Fig. 2.9(b)) in the area surrounding the Dover Air Force Base, Delaware, USA ( <i>Hinaman and Tenbus, 2000</i> ).	47
<b>Figure 2.11</b>	Fence diagram showing hydrogeologic units for a model of Yucca Mountain, NV, USA ( <i>Faunt et al., 2010</i> ).	48
<b>Figure 2.12</b>	Groundwater flow in the vicinity of the Savannah River Site, Georgia, and South Carolina, USA ( <i>Clarke and West, 1998</i> ).	49
<b>Figure 2.13</b>	Graphics created with the GIS software Rockworks™ v. 2006 for a 25.7 by 19 mile site in southeastern Wisconsin, USA: (a) well logs displayed as cylinders in three-dimensional space; (b) solid models show 690 ft of section at the surface and at a depth of 400 feet. The legend gives values of hydraulic conductivity in ft/day ( <i>modified from Dunkle, 2008</i> ).	50
<b>Figure 2.14</b>	Conceptual models of settings characterized by fractures and solution conduits. (a) Carbonate rock in karst terrain showing fractures, conduits, and sinkholes ( <i>modified from Runkel et al. 2003</i> ); (b) Fractures and faults in igneous and metamorphic terrain ( <i>Whitehead, 1994</i> ); (c) Lava flows and dikes in Hawaii, USA. Low-permeability dikes act as barriers to groundwater flow ( <i>modified from Oki et al., 1999</i> ).	52
<b>Figure 2.15</b>	Block diagram showing groundwater flow directions and water budget components in an arid setting (Southern Arizona, USA) ( <i>Healy et al., 2007</i> ).	53
<b>Figure 2.16</b>	Block diagram showing Long Island, New York, USA, and the hydrologic budget (left-hand side table) and groundwater budget (right-hand side table) under predevelopment conditions. Both water budgets assume equilibrium conditions with no change in storage ( <i>Alley et al., 1999</i> ).	57

<b>Figure P2.1</b>	Geologic map of the Red River Valley.	<b>62</b>
<b>Figure B2.1.1</b>	Modified screen capture of a GIS-based graphical user interface showing the estimated recharge and discharge map of a groundwater basin in a humid setting in Central Wisconsin, USA. Blue and green colors denote recharge areas; red and yellow denote discharge areas. Surface water features are shown as colored lines and polygons ( <i>Lin et al., 2009</i> ).	<b>34</b>
<b>Figure 3.1</b>	Representative elementary volume ( $\Delta x \Delta y \Delta z$ ) showing the components of flow along the $y$ -coordinate axis.	<b>71</b>
<b>Figure 3.2</b>	Principle of superposition showing (a) the field setting; (b) superposition of drawdowns from two wells to represent the effect of an impermeable boundary (or the effect of two wells pumping at the same rate) ( <i>Ferris et al., 1962</i> ).	<b>81</b>
<b>Figure 3.3</b>	Map view of an area modeled using analytic elements showing elements for hydraulic conductivity domains ( $K$ ); no-flow barriers ( $B$ ) including faults at $B1$ and $B2$ ; far-field features ( $F$ ) including rivers; near-field discharge ( $H$ ), including springs at $H1$ and $H2$ ; and recharge ( $R$ ) ( <i>Johnson and Mifflin, 2006</i> ).	<b>82</b>
<b>Figure 3.4</b>	Finite-difference (FD) grid and notation. (a) Two-dimensional (2D) horizontal FD grid with uniform nodal spacing; $i$ = columns and $j$ = rows. Sometimes a different indexing convention is used. For example, in MODFLOW $i$ = rows and $j$ = columns. The cells are block-centered; the heavy dark line represents the problem domain. Inactive cells (those outside the boundary of the problem domain) are shaded. (b) 2D horizontal FD grid with notation for the group of five nodes comprising the FD computational module (star) centered around node $(i,j)$ . (c) Three-dimensional notation where $\Delta z$ represents the vertical distance between nodes and $k$ is the vertical index. The group of blocks at the right is shown in 2D space (the two blocks perpendicular to the page along the $y$ -axis are not shown). The group of seven nodes including node $(i,j,k)$ comprise the FD computational module in three dimensions.	<b>85</b>
<b>Figure 3.5</b>	Two-dimensional horizontal finite-element mesh with triangular elements and notation. (a) A representative triangular element with nodes $i$ , $j$ , and $m$ , labeled in counterclockwise order, with spatial coordinates $(x,y)$ ; (b) Triangular elements, with element numbers inside circles, are defined by numbered nodes. The elements are fitted to the boundary of the problem domain ( <i>modified from Wang and Anderson, 1982</i> ).	<b>86</b>

- Figure 3.6** FD notation for irregularly spaced nodes in the  $x$ -direction in a block-centered grid. The grid and notation are shown in one dimension only. 87
- Figure 3.7** Representation of head in the finite-element (FE) and finite-difference (FD) methods. (a) In the FE method, head ( $h^c$ ) is a continuous function within each element. In the FE mesh shown in the figure, the elements are triangular with heads at nodes designated  $h_i$ ,  $h_j$ , and  $h_m$ . (b) In the FD method, head ( $h_{i,j}$ ) is defined only at the node. 89
- Figure 3.8** (a) Plan view of a patch of elements around node L in a finite-element mesh. (In Fig. 3.5, for example, the elements 1, 3, 5, 7, 4, and 2 form a patch around node 4.) (b) Three-dimensional view of the nodal basis function  $N_L(x,y)$  (modified from Wang and Anderson, 1982 and Cheng, 1978). 90
- Figure 3.9** Schematic diagram showing the relation of the element coefficient matrices and their assembly into the global coefficient matrix for the finite-element mesh shown in the inset (Wang and Anderson, 1982). 92
- Figure 3.10** Plan view of finite-difference cells (n and m) in an unstructured grid as used in the control volume finite-difference method. Nodes are located in the center of the cell. (a) Connection lengths are measured from the center of the cell. The horizontal connection between cells is  $L_{nm} + L_{mn}$  and the flow area (shown in gray) for the connection is  $a_{nm}$  ( $=a_{mn}$ ). The connection lengths bisect the shared face at right angles. (b) The line connecting the centers of cells n and m (shown as filled black circles) does not bisect the shared face at a right angle, requiring a more complicated definition of  $L_{nm}$  and  $L_{mn}$ . The process is as follows: locate the midpoint of the shared face ( $P_{nm}$ ); extend a perpendicular line outward from this point in both directions. Then,  $L_{nm}$  and  $L_{mn}$  are defined as the distances between the midpoint of the shared face and points on the perpendicular line (shown as open circles) closest to the cell centers (Panday et al., 2013). 93
- Figure 3.11** Example output from MODFLOW showing nonconvergence of the solution after 100 iterations. The head closure criterion was specified to be  $0.1E-4$  ft ( $0.1 \times 10^{-4}$ ). The output gives the maximum residual error in head in each of the 100 iterations, listed in order from left to right. Read the output by row from left to right (e.g., the 99th iteration is

the second to last entry in the last row). The location of the maximum residual for each iteration is given in parentheses as the layer, row, and column numbers. Results suggest the residual error cannot be reduced below  $0.31\text{E-}4$  ft, which is the lowest error computed (for iteration number 99).

Nevertheless, the error in the water budget for this run was only 0.22%. Based on the good water budget and the oscillation of the solution around an error of  $0.4\text{E-}4$ , the solution could be accepted or the convergence criterion could be increased to  $0.1\text{E-}3\text{ft}$ .

**97****Figure 3.12**

Water budget for a transient problem calculated by MODFLOW showing the cumulative water budget in volumes of water (left-hand side of figure) and the water budget in volumetric rates (right-hand side of figure) for time step 5 in stress period 12. (See Section 7.6 for an explanation of stress periods.) The problem has two specified head boundaries (itemized as “constant head” in the budget) that represent surface water bodies; areal recharge from precipitation (itemized as “recharge”); and a pumping well (itemized as “wells”). Note that water is both entering and leaving the system through the specified head boundaries. Water enters the system as recharge and is removed through the pumping well. There is a change in storage listed under inflow, which means that there is a net removal of water from storage (i.e., water leaves storage and enters the system). The error in the cumulative water budget for this time step is  $250\text{ ft}^3$ , which is less than 0.01% of the total inflow or outflow and thus the error (percent discrepancy) is listed as zero.

**100****Figure P3.1**

(a) Map view of an 800 m by 500 m portion of a confined aquifer showing the locations of wells A and B. (b) Cross section of the aquifer. The datum for head is the base of the confined aquifer.

**109****Figure P3.2**

Map view of the steady-state cone of depression (blue lines) for a pumping well (red dot) penetrating a confined aquifer. Drawdown decreases as distance from the well increases. The blue square is the location of the  $400 \times 400$  m grid in Fig. P3.3.

**110****Figure P3.3**

Head distribution in a  $400 \times 400$  m area shown in Fig. P3.2. Heads at the boundaries are given in meters; heads at the four interior nodes are unknown (after Wang and Anderson, 1982).

**110**



- Figure B3.1.1** Global and local coordinate systems in two dimensions. Two-dimensions are shown for convenience but the concepts are easily extended to three dimensions. (a) The  $x$ - $z$  global coordinate system is aligned with the principal directions of  $\underline{\mathbf{K}}$  ( $K_{xx} = K_x$  and  $K_{zz} = K_z$ ). The governing equation for two-dimensional (2D) transient flow has only two hydraulic conductivity terms. (b) Complicated hydrogeology requires four components of  $\underline{\mathbf{K}}$ . Local coordinates ( $x'$ - $z'$ ) are defined to align with the principal components of the local hydraulic conductivity tensor  $K'_{xx}, K'_{zz}$ . The governing equation for 2D transient flow in the global coordinate system requires four components of  $\underline{\mathbf{K}}$  defined in the global coordinate system:  $K_{xx}, K_{zz}$ , and  $K_{xz} = K_{zx}$ . 74
- Figure B3.2.1** Conceptual model for one-dimensional flow problem. 79
- Figure 4.1** Schematic representation of two-dimensional (2D) areal models. (a) Confined aquifer bounded by an upper and lower confining bed. The upper confining bed may be overlain by an unconfined aquifer (see Fig. 4.2), which provides a source of water to the confined aquifer via leakage through the confining bed. Heads represent the potentiometric surface defined by the elevation of water levels in wells penetrating the confined aquifer (see Fig. 4.2). (b) Head in an unconfined aquifer is equal to the elevation of the water table,  $h$ , above the base of the aquifer (see Figs. 4.2 and 4.3). The thickness of the model layer is equal to  $h$  and varies spatially. (c) A 2D areal model may simulate both confined and unconfined conditions within the same model layer. 119
- Figure 4.2** Schematic diagram showing an unconfined aquifer and a confined aquifer within a regional groundwater flow system (Waller, 2013). 120
- Figure 4.3** Horizontal flow (blue arrows) in an unconfined aquifer under the Dupuit-Forchheimer (D-F) approximation. The D-F approximation is inaccurate near the discharge face and close to the water table. Equipotential lines (red lines) in the true flow field deflect at the water table and near the discharge face where there are vertical gradients and a seepage face; the D-F approximation assumes vertical equipotential lines (shown in blue). In the true flow field, the water table intersects the discharge face above the free surface of the surface water body (red line) creating a seepage face. Under the D-F approximation,

- the water table is continuous and meets the free surface of the surface water body without a seepage face. 121
- Figure 4.4** Equipotential lines (faint gray lines) and flowpaths (heavy blue lines) with schematic flow arrows in a profile model. A two order of magnitude contrast in hydraulic conductivity effectively creates a no-flow boundary at the base of the upper layer. Figure was created using TopoDrive (Hsieh, 2001). 127
- Figure 4.5** Axisymmetric profiles. (a) An FE mesh for an axisymmetric profile model of transient groundwater flow into a cavity (i.e., a well with a central perforated interval, shown at left) (modified from Keller et al., 1989). (b) An axisymmetric profile to simulate flow to a partially penetrating pumping well at the point of the pie-shaped section of aquifer shown in the FD grid at the right. The thickness of the profile and the transmissivity assigned to a cell increase with distance from the well. Adjustments to storativity are also needed to reflect the change in profile thickness. Pumping rate is adjusted according to the angle (here equal to 20°) of the aquifer wedge. The grid for a three-dimensional model, which assumes radial flow and uses symmetry to model only one quarter of the aquifer is shown on the left-hand side of the figure (modified from Land, 1977). 132
- Figure 4.6** Schematic diagram showing the hydrogeology and model layers for a seven layer quasi-3D model of the Savannah River Site, SC, USA. Confining beds are not represented in the FD grid but are indirectly included in the model by representing the vertical resistance of the confining beds by leakance and flow through the layers by leakage terms (Clark and West, 1998). 133
- Figure 4.7** Physical boundaries. (a) Two-dimensional areal FD grid showing perimeter boundaries defined by physical boundaries. Relatively impermeable bedrock outcrops are no-flow boundaries; specified head boundaries represent wetlands, Lake Wausau, and the Eau Claire River, WI, USA (modified from Kendy and Bradbury, 1988). (b) Relatively impermeable bedrock across a fault creates a physical boundary for the alluvial aquifer. The intermittent stream is separated from the water table by a thick unsaturated zone but contributes water to the aquifer via percolating conditions (Fig. 4.16(d)) (Niswonger and Prudic, 2005). 135
- Figure 4.8** Flow across fault zones shown in schematic cross sections of an unconfined aquifer. Simulations of the profile were done in TopoDrive (Hsieh, 2001). Equipotential lines (faint gray lines)

- and flowpaths (heavy blue lines) are shown. There is a two order of magnitude contrast between the hydraulic conductivity ( $K$ ) of the aquifer and the fault zone. Both aquifer and fault are isotropic. (a) Fault as a conduit. The fault zone is shaded in blue;  $K$  of the fault is larger than  $K$  of the aquifer. Groundwater flows up the fault and discharges in the valley bottom. (b) Fault as a barrier (dam). The fault zone is shaded in pink;  $K$  of the fault is smaller than  $K$  of the aquifer. There is an abrupt drop in the water table across the fault and water is dammed against the fault. **138**
- Figure 4.9** Fully and partially penetrating surface water bodies. (a) Schematic cross section through an unconfined aquifer showing groundwater divides beneath a topographic high and beneath a stream. The stream partially penetrates the aquifer physically but is hydraulically fully penetrating. The lake (at right) is both physically and hydraulically fully penetrating (*Granneman et al., 2000*). (b) Cross section through an unconfined aquifer showing streamlines in the vicinity of a shallow ditch. Streamlines flow beneath the ditch indicating underflow. The ditch is both physically and hydraulically partially penetrating (*modified from Zheng et al., 1988*). **139**
- Figure 4.10** Freshwater—seawater interface in a coastal aquifer showing the transition from freshwater to seawater in the zone of dispersion. The interface acts as a barrier to groundwater flow; freshwater flows upward along the interface and discharges to the ocean (*Barlow, 2003*). **140**
- Figure 4.11** Boundary representation in FD grids and FE meshes of a two-dimensional areal model. (a) For purposes of illustration, relatively impermeable rock at the mountain front forms a physical no-flow boundary. Streamlines, defined from a water-table map, form hydraulic no-flow boundaries. The fully penetrating river is a physical specified head boundary. (b) Block-centered FD grid showing that no-flow boundaries are located at the edges of FD cells and specified heads are located on the nodes. The grid is larger than the problem domain. (c) Point-centered FD grid showing that both no flow and specified head boundaries are placed directly on the nodes. The grid coincides with the problem domain. (d) Triangular FE mesh. Node numbers are shown; element numbers are circled. Both no flow and specified head boundaries are located directly on the nodes. (e) Quadrilateral FE mesh. Node numbers are shown; element

- numbers are circled. Both no flow and specified head boundaries are located directly on the nodes. 146
- Figure 4.12** Hydraulic boundaries. Schematic water-table contour maps for a regional problem domain (on the left) bounded by physical features and a local problem domain (on the right) with three hydraulic boundaries taken from the solution of the regional problem; the circled dot represents a pumping well (*modified from Townley and Wilson, 1980*). 147
- Figure 4.13** Implementation of specified flow conditions. (a) In an FD grid, a volume of water is placed into an FD cell/block (or extracted from the cell/block) using wells (Q) or areal recharge (R). Lateral flows (i.e., underflow) can be introduced using a code's well or recharge option or using a head-dependent boundary. For underflow input via a well,  $Q = U\Delta x\Delta z$  where U is the lateral flux (L/T). When underflow (U) is input as recharge,  $R = U\Delta z/\Delta y$ . (b) In an FE mesh, diffuse flow ( $Q_s$ ) along the boundary is discretized along the sides of triangular elements and then assigned to nodes (*modified from Townley and Wilson, 1980*). 149
- Figure 4.14** Default no-flow boundaries in a two-dimensional block-centered FD grid are implemented by setting transmissivity (T) equal to zero in inactive cells/ghost cells (shaded) outside the problem domain. The ghost cells with  $T = 0$  that are used to implement no flow conditions along the groundwater divides and the ghost cells to the right of the underflow boundary are not shown. Constant head and specified flow (injection wells) conditions are imposed in boundary cells to cancel the effect of the default no-flow boundaries (*adapted from McDonald and Harbaugh, 1988*). 150
- Figure 4.15** FD grid showing implementation of head-dependent boundary (HDB) conditions for boundary flows (designated as general head boundary cells), drains, and evapotranspiration. Stream cells and lake cells use more sophisticated representation of HDB conditions as discussed in Sections 6.5 and 6.6, respectively (*Gannett et al., 2012*). 151
- Figure 4.16** Implementation of HDB conditions for representing surface water bodies using a stream in an FD cell for illustration. (a) Representation of the stream in an FD cell. The stream is conceptualized to be embedded in the cell and to exchange water with the aquifer but the stream does not occupy space within the grid. (Representation in an element of an FE mesh is similar.)

- As shown, the stage of the stream is lower than the head in the cell and the width of the stream is less than the width of the cell. (b) When the stream is gaining, the head in the aquifer,  $h_{i,j,k}$ , is higher than the head in the stream,  $h_s$ . The elevation of the bottom of the streambed sediments is SBOT; the thickness of the sediments is  $b'$ .  $Q_{GW}$  is the volumetric rate ( $L^3/T$ ) of groundwater discharge to the stream. (c) For a losing stream  $h_{i,j,k} < h_s$  and  $Q_{GW}$  is the volumetric rate ( $L^3/T$ ) of induced recharge from the stream to the aquifer. (d) Under percolating conditions, the stream is separated from the aquifer and  $Q_{GW}$  is constant. (e) Discretization of a stream into 12 reaches. The width,  $W$ , of the stream is much less than the grid spacing ( $\Delta x$ ); the length of the stream reach,  $L_R$ , is not equal to the length of the cell ( $\Delta y$ ). Each reach can have different values for  $h_s$ , SBOT,  $K'_z/b'$ , as well as  $L_R$  and  $W$  (*modified from McDonald and Harbaugh, 1988*). 154
- Figure 4.17** Examples of drains with associated cross-sectional area used to compute conductance (*composite of images modified from Yager, 1987; Fipps et al., 1986 and McDonald and Harbaugh, 1988*). 156
- Figure 4.18** Representation of ET as a head-dependent boundary (Eqn (4.6)) showing extinction depth ( $d$ ), land surface elevation ( $h_s$ ),  $h_s - d$ , and calculated head ( $h$ ). 157
- Figure 4.19** Head-dependent boundary used to represent flow between the modeled area and a distant physical boundary, shown here as a large lake. The boundary flow ( $Q$ ) is controlled by the head at the distant boundary, shown here as the head in a large lake,  $h_B$ .  $C$  is conductance (Eqn (4.4b)). 158
- Figure 4.20** Grid refinement for setting boundary conditions showing shared nodes in the horizontal FD grids of intermediate- and local-scale models. Hydraulic boundaries for the local-scale model are extracted from the solution of an intermediate-scale model. The grid for a regional-scale model that provides boundary information for the intermediate-scale model is not shown (*Hoard, 2010*). 160
- Figure 4.21** Hydraulic boundary conditions for a 3D FD model (basin model) are extracted from the solution of a 2D regional analytic element (AE) model. Lake and stream analytic elements are outlined in blue and pink. Heads (dashed lines) calculated by the AE model were used to compute fluxes along the perimeter boundaries (outlined in red) of the FD model. Fluxes extracted from the AE model were uniformly distributed vertically along the perimeter of the five layer FD model (*modified from Hunt et al., 1998*). 161

- Figure 4.22** Representation of hydraulic conditions at the water table and seepage face. (a) The water table is a streamline when there is no recharge (left hand side figure) but is not a streamline when recharge is present (right hand side figure). In both cases, the pressure head at the water table is zero. (b) A seepage face (DC) along a streambank (left hand side figure). Schematic flowlines and arrows are shown. The location of the water table (DE) and the point of intersection of the water table with the streambank (D) are unknown. Right hand side figure shows detailed schematic depiction of flow near the seepage face. The pressure head at the seepage face is zero so that head at the seepage face is equal to elevation head (*modified from Fitts, 2013*). (c) The water table computed as the surface of zero pressure in a variably saturated model. The aquifer is shown in cross section with vertical exaggeration = 10. Equipotential lines are computed in the unsaturated–saturated continuum and are closely spaced near the discharge face at the ocean (shaded in green). The ocean level and seepage face are also shown (*modified from Ataie-Ashtiani, 2001*). **163**
- Figure 4.23** Water table in a three-dimensional FD grid showing that head calculated at the water-table node (h) is higher than the bottom elevation of the top layer of the model but is not necessarily equal to the elevation of the node. (A similar situation occurs in a fixed node FE mesh.) **164**
- Figure 4.24** Movable nodes and deformable elements (shaded) in FE meshes. (a) Movable nodes are placed along the water-table boundary (*modified from Mitten et al., 1988*). (b) Movable nodes are placed along the water-table boundary and along the exit face and in the interior of a permeable earthen dam. The model solves for the location of the water table and associated seepage face; nodes 25 and 30 are on the seepage face (*modified from Neuman, 1976*). **166**
- Figure P4.1** (a) The five-point star computational module for an interior node (filled circle) in a two-dimensional FD grid. The numbers refer to the weighting of heads in the FD equation (Eqn (B4.3.2) in Box 4.3). (b) The computational module for a boundary node (shaded) in a block-centered FD grid; the no-flow boundary is to the left of the node. The head at the ghost node at  $i-1,j$  (not shown) equals the head at  $i,j$ . (c) The computational module for a boundary node (shaded) in a point-centered FD grid; the no-flow boundary is directly on

	the node. The head at the ghost node at $i-1,j$ (not shown) equals the head at $i+1,j$ . (d) Point-centered FD grid for the profile model in Box 4.3.	171
<b>Figure P4.2</b>	Cross section of an aquifer with overlying dam and reservoir. The inset shows the dam in map view; the line shows the approximate location of the cross section.	172
<b>Figure P4.3</b>	Map and cross section of the aquifer adjoining the Green Swamp. Location of a proposed fully penetrating pumping well 1500 m from the river is also shown.	174
<b>Figure B4.1.1</b>	Cross sections through a regional groundwater flow system showing flowpaths. (a) Vertical flow is slightly exaggerated (vertical exaggeration = 2.5). (b) Without vertical exaggeration flowpaths are dominantly horizontal. System parameters are typical of an aquifer in a humid climate (recharge = 25.4 mm/yr; $K_h = K_v = 0.3$ m/d). The ratio of system length to thickness is approximately 25 ( <i>modified from Haitjema and Mitchell-Bruker, 2005</i> ).	122
<b>Figure B4.1.2</b>	Kirkham's (1967) "slotted" porous medium. The slots at A through I provide no vertical resistance to flow. Vertical flow occurs along a stepped flowpath LMNPQRc (red line), which is smoothed to the path MkjRd (blue line) when the slots are closely spaced ( <i>modified from Kirkham, 1967</i> ).	123
<b>Figure B4.1.3</b>	Water-table contours and capture zones for seven partially penetrating, high-capacity pumping wells in a heterogeneous system computed by (a) a 2D areal model using D-F conditions; (b) a 3D eight-layer model. The pumping wells create 3D flow that affects the shapes of the capture zones ( <i>Reilly and Harbaugh, 2004</i> ).	124
<b>Figure B4.2.1</b>	Profile model aligned parallel to groundwater flow shown by purple arrows. Water-table contours (numbered in meters) are also shown. Slice orientation, simulated in a three-dimensional model, is the preferred orientation for profile modeling.	125
<b>Figure B4.2.2</b>	In layer orientation (bottom three figures) the profile is simulated as an areal two-dimensional model. The thickness of the layer equals the width of the profile. Slice orientation (top figure) is shown for comparison.	126
<b>Figure B4.3.1</b>	Conceptual model showing boundaries and schematic flowline in a cross section of a regional groundwater system ( <i>after Tóth, 1962</i> ).	128

- Figure B4.3.2** Mathematical model showing the governing equation and boundary conditions for the conceptual model in Fig. B4.3.1 (after Tóth, 1962). 129
- Figure B4.3.3** Numerical model for the problem in Fig. B4.3.2. (a) Block-centered grid showing boundary location and placement of the 11 columns and six rows of nodes within the problem domain. (b) FD equations for each cell in an Excel<sup>®</sup> spreadsheet model of the problem. Specified head boundary values (in meters) are entered in the first row to represent the water table. Ghost nodes in columns A and M and row seven are outside the problem domain and are used to implement no-flow boundary conditions at the outside edge of the FD cells along the boundaries. (c) Solution showing heads in meters. For the purpose of calculating flux across the water table, hydraulic conductivity is equal to 10 m/day (cell B10). Flow (Q) at the water table is calculated in m<sup>3</sup>/day for the 1 m width of the cross section. Total recharge (RTotal) and total discharge (DTotal) across the water table and the error (i.e., the difference between RTotal and DTtotal) in the water budget, are also computed. 130
- Figure B4.4.1** The freshwater—seawater interface: (a) under hydrostatic conditions as assumed by the Ghyben—Herzberg relation (Eqn (B4.4.1b)) (Barlow, 2003); (b) in a multiaquifer system simulated using a quasi-three-dimensional model (Section 4.1). The offset in the interface between aquifers (along EF in the figure) is small when vertical resistance between layers is small (i.e., leakance is large). The offset is relatively large when there is a confining bed between aquifer layers (Fitts et al., 2015). 141
- Figure B4.4.2** Cross section of a sharp interface model as simulated with MODFLOWs SWI2 Package. (a) Conceptual model showing native (seawater) head and equivalent freshwater head at the interface. The freshwater—seawater interface (dotted line) separates freshwater (zone 1) from subsurface seawater (zone 2). (b) One-layer model of a coastal aquifer. The thickness of the layer varies in space; vertical variations in density within the layer represent freshwater and subsurface seawater. The code solves for the transient movement of the interface (Bakker et al., 2013). 143
- Figure B4.6.1** Schematic diagram of a regional flow system when the water table is controlled by topography, based on Tóth's (1963) profile model. A sinusoidal specified head condition, intended to mimic



- topography, was imposed at the water table. The model simulates nested local, intermediate, and regional flow cells (*Winter et al., 1998*). 168
- Figure B4.6.2** Water table controlled by recharge in a 2D profile model. The water table was specified using heads determined from a Hele-Shaw analog model (Section 1.2) in which uniform recharge was infiltrated at a sinusoidal land surface. The water table does not follow the sinusoidal function of the land surface and nested flow cells are not present (*modified from Shahbazi et al., 1968*). 168
- Figure B4.6.3** Conceptual model of one-dimensional flow under the D-F approximation in an unconfined aquifer under uniform recharge,  $R$ . The maximum terrain rise,  $d$ , is the largest vertical distance between the datum (defined by the heads at the boundaries) and the land surface. The vertical scale is greatly exaggerated for purposes of illustration. 169
- Figure 5.1** Connections among nodes. (a) In a 3D structured grid or mesh, a node has, at most, six connections to neighboring nodes; in 2D there are a maximum of four connections (<http://doi.ieeecomputersociety.org/cms/Computer.org/dl/mags/cs/2012/03/figures/mcs20120300483.gif>). (b) A horizontal 2D unstructured FD grid where the central node is connected to six other nodes; in 3D this grid would have eight connections (*modified from Tyson and Weber, 1964. This material may be downloaded for personal use only. Any other use requires prior permission of the American Society of Civil Engineers*). 183
- Figure 5.2** Orientation of an FD grid. (a) The FD grid for a model of the Edwards aquifer, Texas, USA, is oriented to align with northeast–southwest trending faults shown in (b). Note that the grid is larger than the problem domain defined by boundary conditions. Areas outside the boundaries contain inactive nodes (*Lindgren et al., 2004*). 185
- Figure 5.3** Coordinate axes in an FE mesh are oriented to coincide with the principal components of the  $K$  tensor as shown by the stratification at the left. The detailed mesh near the sheet pile is not shown (*modified from Townley and Wilson, 1980*). 186
- Figure 5.4** Structured and unstructured grid designs (*Panday et al., 2013*). 187
- Figure 5.5** Irregular grids shown using MODFLOW convention where  $i = \text{rows}$  and  $j = \text{columns}$ . Spacing between columns (spacing along rows) is  $\Delta r_j$  and spacing between rows (spacing along columns) is  $\Delta c_i$ : (a) block-centered grid; (b) point-centered grid (*modified from McDonald and Harbaugh, 1988*). 188

- Figure 5.6** Irregular FD grid designed to provide fine nodal spacing in the vicinity of a superfund site, New Jersey, USA (*Lewis-Brown et al., 2005*). 189
- Figure 5.7** Nested cells in an unstructured FD grid; each cell is numbered (*Panday et al., 2013*). 192
- Figure 5.8** Quadtree grid for a CVFD model of the Biscayne aquifer, Florida, USA, based on an 800-m structured grid. Cells are refined down four levels to a cell size of 50 m within 1000 m of a municipal well and along canals and the coastline. The quadtree grid was smoothed so that every cell is connected to no more than two cells in any direction (*Panday et al., 2013*). 193
- Figure 5.9** Two types of cell connections in an unstructured FD grid. (a) A line connecting the centers of adjacent cells passes through the shared face at a right angle; (b) a connecting line does not intersect the shared face at a right angle thereby violating the CVFD requirement (*Panday et al., 2013*). 194
- Figure 5.10** Placement of ghost nodes in an unstructured FD grid to correct for violation of the CVFD requirement (*Panday et al., 2013*). 194
- Figure 5.11** Two-dimensional finite elements; linear, quadratic, and cubic refer to the type of basis function used (Section 3.5): (a) triangular elements; (b) quadrilateral elements (serendipity family); (c) quadrilateral elements (Lagrange family) (*adapted from Huyakorn and Pinder, 1983*). 196
- Figure 5.12** Three-dimensional finite elements: (a) tetrahedrons; (b) hexahedrons; (c) prisms (*adapted from Huyakorn and Pinder, 1983*). 197
- Figure 5.13** Discretization in an FE model of the Nile Delta, Egypt. (a) Map showing head contours and boundary conditions (circled numbers) where 3 indicates a head-dependent boundary (Section 3.3). (b) Triangular elements are shaped to fit the irregular boundary. (c) Nodal numbers in a truncated version of the mesh. Nodes are numbered sequentially along the shortest dimension of the mesh (*modified from Townley and Wilson, 1980*). 198
- Figure 5.14** Mesh refinement. (a) FE mesh for a peninsula jutting into Green Bay, Wisconsin, USA, constructed with a mix of triangular and quadrilateral elements. Fine nodal spacing is used to represent the shoreline area where groundwater discharges to Green Bay (*Bradbury, 1982*). (b) FE mesh showing local mesh refinement near a barrier wall designed to protect a nuclear reactor from a high water table when the Po River floods, NW Italy. The river forms the southern boundary; the river bank is represented by

	fine nodal spacing. The northern and southern boundaries are specified head and the eastern and western boundaries are no-flow boundaries ( <i>modified from Gambolati et al., 1984</i> ).	199
<b>Figure 5.15</b>	Faults in an FE mesh. (a) Non-connected nodes represent an impermeable fault. (b) Thin elements (shaded) represent a fault. Hydraulic conductivity, or transmissivity, values assigned to the elements determine whether the fault is permeable or impermeable ( <i>modified from Townley and Wilson, 1980</i> ).	204
<b>Figure 5.16</b>	Tubular discrete feature elements (DFEs) to represent a multi-layer pumping well and a horizontal pumping well in an FE mesh ( <i>Diersch, 2014</i> ).	204
<b>Figure 5.17</b>	Conduits in an FD grid simulated using the Conduit Flow Process ( <i>Reimann and Hill, 2009</i> ).	206
<b>Figure 5.18</b>	Characteristic leakage length, $\lambda$ , for (a) a surface water body represented as a head-dependent boundary condition ( <i>adapted from Haitjema, 2006</i> ); (b) a pumping well in a leaky confined aquifer.	207
<b>Figure 5.19</b>	Representation of layers as hydrogeologic units, Long Island, NY, USA. (a) Hydrogeologic cross section showing the hydrogeologic units; (b) representation of the dipping units as deformed model layers (see Fig. 5.20) ( <i>Reilly and Harbaugh, 2004; modified from Buxton et al., 1999</i> ).	209
<b>Figure 5.20</b>	Hydrogeologic units as deformed layers in an FD grid. Each cell in the layer has different top and bottom elevations so that $\Delta z$ effectively varies with space, causing an irregularly shaped (deformed) layer as in Fig. 5.19 ( <i>modified from McDonald and Harbaugh, 1988</i> ).	216
<b>Figure 5.21</b>	Pinchouts. (a) Confining bed and pinchout aquifer shown at left are represented by the second model layer shown at the right. Hydraulic properties assigned to nodes within the layer reflect the change from aquifer to confining bed ( <i>modified from Leahy, 1982</i> ). (b) Pinchouts in cross section in an unstructured FD grid ( <i>Panday et al., 2013</i> ).	218
<b>Figure 5.22</b>	Representation of faults in an unstructured FD grid. (a) Offset of units along a fault shown in cross section; (b) representation in an unstructured FD grid ( <i>Panday et al., 2013</i> ).	219
<b>Figure 5.23</b>	Misalignment of the hydraulic conductivity tensor with the model's coordinate axes. (a) FD grid in profile showing dipping beds of fractured rock (shown by shading) superimposed over horizontal model layers. The horizontal change in geology caused by the dip of the units is captured by spatial variation in $K$ within the layer. $K_{\min}$ is vertical hydraulic conductivity and	

- $K_{\max}$  is horizontal hydraulic conductivity (Yager *et al.*, 2009). (b) FE mesh showing dipping and folded beds (hydrogeologic units B and C) beneath a dam in a 2D profile model. Under field conditions, the principal components of the  $K$  tensor ( $K_x$ ,  $K_y$ ) for hydrogeologic units B and C align with the dipping and folded bedding planes. In the model, units B and C are assumed to be isotropic so that  $K_{xx}$  and  $K_{yy}$  are equal and are aligned with the global coordinate system. For hydrogeologic unit A, the principal components of the hydraulic conductivity tensor are aligned with the global coordinate axes where  $K_{xx}$  is parallel to horizontal bedding in the sand and gravel and  $K_{yy} = K_{xx}/4$ . The fine resolution in the mesh beneath the dam is not shown (*modified from Townley and Wilson, 1980*). (c) FD grid in profile showing dipping hydrogeologic units represented by spatial variation in hydraulic conductivity within model layers (*modified from Groschen, 1985*). 220
- Figure 5.24** Example representation of dipping hydrogeologic units as horizontal layers in an FD grid. The full grid is three dimensional with 71 layers. (a) Hydrogeologic cross section showing the dipping beds and fault zone. The dip angle in this setting ranges from  $15^\circ$  to  $70^\circ$  with the largest dips occurring near the fault zone. (b) Horizontal model layers that represent the geology in (a) showing areas of active (yellow and green), pseudo-active (purple), and inactive (tan) cells (*modified from Lewis-Brown and Rice, 2002*). 221
- Figure 5.25** Range in hydraulic conductivity of geologic materials (Healy *et al.*, 2007; *modified from Heath, 1983*). 224
- Figure 5.26** Schematic representation of discontinuous and interfingering laminae in a cell block in a layer of an FD grid (*modified from McDonald and Harbaugh, 1988*). 224
- Figure 5.27** Assignment of storage parameters in a five-layer model with three hydrogeologic units: an upper sand aquifer under unconfined conditions, a shale confining unit, and a confined sandstone aquifer. Under the conditions shown the water table (dashed line) is only in layer 1 and layers below layer 1 are fully saturated. Storage in layer 1 is represented by specific yield ( $S_y$ ); layers 2, 3, 4, and 5 are under confined conditions with confined storativity equal to specific storage ( $S_s$ ) times the thickness of the layer. In practice, all layers should be designated as convertible layers (Section 5.3) and then both specific yield and specific storage (or confined storativity) would be input for all layers.

	The code would automatically use specific yield only for unconfined layers (i.e. layers where a water table is present).	237
<b>Figure 5.28</b>	Parameter assignment of hydraulic conductivity in an FD grid: (a) zonation; (b) inverse distance interpolation; (c) linear interpolation ( <i>Reilly and Harbaugh, 2004</i> ).	239
<b>Figure 5.29</b>	Examples of parameter zonation: (a) hydraulic conductivity zones ( <i>Gannett et al., 2012</i> ); (b) recharge zones ( <i>Gannett et al., 2012</i> ); (c) storage parameters ( <i>Johnson and Njuguna, 2002</i> ).	240
<b>Figure 5.30</b>	Variograms defined by the separation distance of measurement points, $h$ , and the variance of the separation distance or variogram function, $\gamma$ . Variograms and kriging were first used in mining applications where the sill, $\sigma$ , represents the horizontal and vertical dimensions of an ore body. In hydrogeologic applications, the sill represents the dimensions of heterogeneities ( <i>modified from Journel and Huijbregts, 1978</i> ).	241
<b>Figure 5.31</b>	Box and whisker plot showing ranges in hydraulic conductivity in hydrogeologic units for a model of Bear Creek Valley, TN, USA ( <i>modified from Connell and Bailey, 1989</i> ).	242
<b>Figure P5.1</b>	Areal view of a rectangular island. The lines that divide the island into four quadrants are groundwater divides that form in this homogeneous and isotropic aquifer in response to the imposed flow regime ( <i>Wang and Anderson, 1982</i> ).	244
<b>Figure P5.2</b>	The model domain for Problem P5.3 in map view and as a 3D block. The width of the problem domain is 11,700 m. Heads along the side boundaries are 120 and 90 m. $K_1$ is the hydraulic conductivity in layer 1 where the horizontal hydraulic and vertical conductivities ( $K_x$ and $K_z$ ) are $K_{1h}$ and $K_{1v}$ , respectively. $K_2$ and $K_3$ are the hydraulic conductivities for layers 2 and 3, respectively. The blue square is the pond. The dashed line represents the water table. The average saturated thickness of layer 1 is 25 m. The land surface elevation is 130 m above datum.	246
<b>Figure P5.3</b>	Problem domain of an arid valley for Problem P5.4, showing geologic boundaries of two alluvial fans and locations of field measured hydraulic conductivities (red dots) reported in Table P5.1. The area shown in blue is the inferred location of a gravel-rich buried channel that is tapped by wells B and F.	248
<b>Figure B5.1.1</b>	(a) Regular FD grid; (b) irregular FD grid. Both are shown in one dimension. Nodes are filled circles; locations halfway between nodes are designated by red X's. The location $i + 1/2$ is halfway between	

- nodes  $i$  and  $i + 1$ ;  $i - 1/2$  is halfway between nodes  $i - 1$  and  $i$ ;  $\Delta x_{i+1/2}$  is the distance between nodes  $i$  and  $i + 1$ ;  $\Delta x_{i-1/2}$  is the distance between nodes  $i - 1$  and  $i$ ;  $\Delta x_i$  is the width of the cell around node  $i$ . In the regular grid,  $\Delta x_{i-1/2} = \Delta x_{i+1/2} = \Delta x$ . For illustration purposes, the irregular grid was expanded using a factor of four rather than the recommended factor of 1.5 (Section 5.1). **190**
- Figure B5.2.1** Flow nets showing flow beneath a dam. Equipotential lines are heavy dotted lines and flow lines are shown by solid light blue lines. Flow is from left to right. (a) In the transformed (isotropic) section ( $X$ - $Z$  coordinates) equipotential lines and flow lines meet at right angles. (b) In the true (anisotropic) system ( $x$ - $z$  coordinates), equipotential lines and flow lines are not at right angles (*Fitts, 2013*). **201**
- Figure B5.3.1** Layered sequence of seven isotropic units that form a model layer of thickness  $B_{i,j}$  at node  $(i,j)$  in the horizontal nodal network. The layered heterogeneity in the sequence of isotropic layers can be represented by a homogeneous and anisotropic block, which may be an FD cell or a finite element. Equations (B5.3.2) and (B5.3.3) can be used to calculate the equivalent horizontal and vertical hydraulic conductivity, respectively, for the block. **212**
- Figure B5.3.2** Effects of layered heterogeneity. Representation of layered heterogeneity at three different scales is shown at the left. At scale 0 the layers are isotropic; values of  $K$  (cm/s) are given in parentheses. The equivalent horizontal hydraulic conductivity,  $K_h$ , and vertical anisotropy ratio,  $K_h/K_v$ , at scales 1 and 2 were calculated using Eqns (B5.3.2) and (B5.3.3). Equipotential lines (contour interval = 0.0034 cm) under 2D flow are shown in the figures at the right; in each representation the sides and left-hand side of the top boundary are under no flow conditions while the right-hand side of the top boundary is specified at  $h = 0.1$  cm and the bottom boundary is specified at  $h = 0$ . All three models were discretized into nine layers with each layer 20 cm thick. The same relative effects would be observed if the layers were scaled to represent flow at a larger scale, e.g., if each layer were 20 m thick (*modified from Anderson, 1987*). **213**
- Figure B5.4.1** Schematic profile of the subsurface (left-hand side) and plot of total head (potential) in the subsurface continuum (right-hand side) showing the zero flux plane in the unsaturated (vadose) zone. The soil root zone is the upper part of the unsaturated

zone between the land (soil) surface and the zero flux plane. Here, evaporation includes both evaporation and transpiration (i.e., evapotranspiration). Runoff shown here represents infiltration excess overland flow rather than rejected recharge. Recharge crosses the water table at the top of the saturated zone. The gradient in total head ( $dH/dz$ ) changes direction at the zero flux plane (whereas pressure head = 0 at the water table) (modified from Khalil et al., 2003).

233

**Figure B5.4.2**

Comparison of recharge estimated from a soil water balance with recharge calculated by a one-dimensional (column) unsaturated flow approximation for each node by using the MODFLOW-UZF Package (Niswonger et al., 2006) for a humid temperate climate in northern Wisconsin, USA. The tops of the soil columns were placed at the zero flux plane (Figure B5.3.1). Recharge rates from the soil water balance were calculated by using a soil water balance approach. (a) Results when the unsaturated zone was less than 1 m thick. Recharge at the water table simulated by using the UZF Package (blue bars) was less than recharge estimated from a soil water balance (blue + pink) that did not account for rejected recharge and associated saturation excess overland flow. (b) Results when the unsaturated zone was greater than 15 m thick show differences in the timing and magnitude of recharge events. Infiltration derived from the soil water balance is shown by the pink line; water passing the simulated water table by using the UZF Package is shown by the blue line. Note that recharge (blue line) during October 1990 does not return to the baseline observed in the summer owing to the mixing of the fall 1990 infiltration front with the previous spring's infiltration (modified from Hunt et al., 2008).

234

**Figure 6.1**

Representation of a well in a layered FE model. The well is open to the aquifer through the screened sections and is simulated using 1D tubular discrete feature element (DFE) (Diersch, 2014).

259

**Figure 6.2**

Effect of nodal spacing on simulated heads near pumping wells in a 2D areal FD model. In figures (a) and (b) two wells, separated by a distance of 200 ft, are each pumping at a rate of 100,000 ft<sup>3</sup>/day. (a) Nodal spacing is 300 ft; the well node represents both pumping wells. (b) Nodal spacing is 100 ft; each well pumps from a separate well node. (c) The model design is the same as in (a) and (b) except that there is only one well pumping at a rate of 200,000 ft<sup>3</sup>/day. The figure shows the drawdown

- along the row that contains the well node (*Reilly and Harbaugh, 2004*). 261
- Figure 6.3** Representation of a pumping or injection well in an FD grid. (a) Conceptual representation of the well as a point source or sink; (b) representation of discharge from a pumping well ( $Q$ ) in an FD model as areally distributed discharge where  $W^*$  ( $T^{-1}$ ) is a general sink/source term (see Eqn 3.12). 263
- Figure 6.4** Multinode wells. (a) The well fully penetrates the top four layers and is partially penetrating in layer 5. (b) Formation of a seepage face along the well bore causes additional head loss in the well; note that discharge from the well follows MODFLOW convention where a negative value of  $Q$  represents pumping (*Konikow et al., 2009*). 263
- Figure 6.5** Distributed recharge. (a) Recharge from infiltration is applied as a flux ( $L/T$ ) to the top (unconfined) layer of a three-dimensional FD cell.  $W^*$  is the sink/source term in the general governing equation (Eqn (3.12)). (b) Recharge to the shaded area in the FE mesh is applied as a volumetric recharge rate ( $L^3/T$ ) to node 2. The specified flow rate assigned to node 2 is a weighted average based on the rates in the shaded area. (c) Discharge assigned (as negative recharge) to a side face of an FD block to represent underflow,  $U$ , (Fig. 2.15). If input as a rate ( $L/T$ ) via the code's recharge array, side fluxes must be adjusted as shown when assembling input data. In an FE code, underflow is assigned to a node as a specified flow boundary condition using a volumetric rate ( $L^3/T$ ). 271
- Figure 6.6** Conceptual models of stream and groundwater exchange showing the water table position relative to the stream stage: (a) gaining stream; (b) losing stream; (c) flow through stream; (d) parallel flow stream (*after Woessner, 2000*). 274
- Figure 6.7** Complex stream channel geometry approximated using eight points along the channel (*Prudic et al., 2004*). 277
- Figure 6.8** Representation of streams and lakes in an FD grid. (a) The River Package in MODFLOW was used to represent far-field streams and far-field lakes as fixed level lakes; the SFR and Lake Packages were used to simulate near-field streams and lakes, respectively (*Feinstein et al., 2010*). (b) The River Package in MODFLOW was used to represent fixed level lakes. Areas of outflow from the lakes to the groundwater system in response to



- pumping are indicated by red triangles; blue triangles indicate areas of groundwater inflow (*modified from Hunt et al., 2001*). **278**
- Figure 6.9** Lakes classified by groundwater flow regime. (a) A discharge lake receives inflow from groundwater. (b) A recharge lake recharges the groundwater system. (c) A flow-through lake receives groundwater inflow through some of the lakebed and recharges the groundwater system through the remainder of the lakebed (*Winter et al., 1998*). (d) A lake with a complex flow regime has shallow discharge conditions (circled arrows), intermediate flow-through conditions, and deep recharge (*modified from Anderson and Cheng, 1993*). **280**
- Figure 6.10** Representation of a lake in MODFLOW with the LAK3 Package. (a) Lake nodes occupy space in the FD grid. Water budget components are also shown. (b) General equations for calculating conductance,  $C_{lkbd}$  and  $C_{aq}$  are used in Eqn (6.16) to compute average conductance values; (c) both horizontal and vertical flow between the lake and groundwater are simulated (*Parts (a), (b) and (c) are from Markstrom et al., 2008; modified from Merritt and Konikow, 2000*). **281**
- Figure 6.11** Representation of wetlands in MODFLOW with the Wetlands Package. (a) Schematic representation of field conditions. (b) Two-layer model consisting of an upper wetland layer coupled to a subsurface layer. The upper layer simulates the wetland including overland surface water flow and flow through the wetland sediments (*modified from Restrepo et al., 1998*). **284**
- Figure P6.1** Areal 2D model domain showing the locations of a pumping well (blue dot) and a monitoring well (red dot) that fully penetrate a 10-m-thick confined aquifer. **293**
- Figure P6.2** Areal 2D model domain of an unconfined aquifer showing a reservoir (in blue) created by mining a sand and gravel quarry. A subdivision is shown in the lower left-hand corner of the figure. **294**
- Figure P6.3** (a) Areal 2D model domain of an unconfined aquifer between two lakes crossed by a 200-m-wide river with a constant stage of 130 m. Drains are installed in a 200 m wide area (shaded in tan) to lower the water table to 125 m. (b) A north–south cross section through the drain area. **295**
- Figure B6.1.1** Well node in an FD grid. (a) The well node is shown at the center of an FD cell; the effective well radius,  $r_e$ , is the radius at which the head is equal to the average head in the cell,  $h_n (=h_{i,j})$ . (b) FD

- cells in the vicinity of the well node  $(i,j)$ . The pumping rate is  $Q$ . The cell containing the pumping node receives one-fourth of the pumping discharge from each of the four neighboring cells. **267**
- Figure B6.1.2** Well node in an FE mesh consisting of equilateral triangular elements. The well node is surrounded by six neighboring nodes; each is located at a distance equal to  $a$  (Eqn B6.1.7) from the well node. The radius of the well is  $r_w$  and the effective well radius is  $r_e$  (*modified from Diersch et al., 2011*). **268**
- Figure B6.2.1** Trout Lake surface watershed (outlined with dotted line) and groundwatershed (outlined with dashed line) in glaciated terrain in a temperate climate (northern Wisconsin, USA). Water table contours (m) are also shown. A regional analytic element model was used to define hydraulic perimeter boundary conditions for the rectangular problem domain of the FD model shown in the figure; also see Fig. 4.21. Groundwater divides (shown by the dashed line) were delineated based on heads calculated by the FD model (*modified from Pint et al., 2003*). **285**
- Figure B6.2.2** Components of the hydrologic cycle for a hydrologic response model (*modified from Freeze and Harlan, 1969*). **286**
- Figure B6.2.3** Components of a GSFLOW model of the snowmelt-dominated montane watershed near Truckee, CA, USA. (a) Hydrologic Response Units (HRUs; Box 6.3) used in the rainfall-runoff model to represent surface and soil zone processes. (b) FD grid and values of hydraulic conductivity used in MODFLOW (*Markstrom et al., 2008*). **287**
- Figure B6.3.1** Field data from a watershed in a humid temperate climate (central Wisconsin, USA) showing the importance of the variable source area in generating peak streamflows. When the water table is below land surface (bottom graph) precipitation infiltrates and becomes groundwater recharge and streamflows (middle graph) are dominated by groundwater-derived base-flow. When the water table rises to the land surface (green arrow) in response to high precipitation (upper graph), precipitation runs off rather than infiltrates. The resulting peak streamflow (middle graph) is over 9 times higher than average streamflow (*modified from Hunt et al., 2000*). **289**
- Figure B6.3.2** Importance of saturation excess overland flow on nonpeak streamflows in a humid temperate climate (northern Wisconsin, USA). Streamflow is simulated at the outlet of a large lake, which receives inflow from five tributary streams. Two

- simulations used the same spatially and temporally distributed precipitation rate; results from the simulation that omitted saturation excess overland flow (pink line) are biased low when compared to measured flows at the lake outlet (shown by black dots). When saturation excess overland flow is routed to the five tributary streams there is a better match between simulated streamflow (green line) and measured flows (*modified from Hunt et al., 2008*). 291
- Figure 7.1** Box and whisker plot showing the mean, median, and range in head in observation wells in hydrogeologic units for a temperate climate in Oregon, USA (*Snyder, 2008*). 305
- Figure 7.2** Hydrograph for a monitoring well in New Zealand. The period 1990–2000 was used to derive an average head target (shown by dashed line) for a steady-state model (*Scott and Thorley, 2009*). 306
- Figure 7.3** Hydrograph for a monitoring well in the Trinity aquifer, Texas, USA (July 2009–July 2012), showing pseudo-steady-state conditions at the end of summer 2011 when pumping rates are low and before fall rains occur (*modified from Central Texas Groundwater Conservation District, The Hydro Blog, August 2012, <http://www.centraltexasgcd.org/the-hydro-blog/>*). 307
- Figure 7.4** Water table profiles showing the effect of storage on the approach to steady state for a one-dimensional model of an unconfined aquifer using different values of storativity,  $S$ , (=specific yield). The aquifer receives recharge at a constant rate, and groundwater discharges to a stream located at distance equal to zero. The transient response is initiated by an increase in recharge rate; the head at  $t = 0$  represents initial conditions;  $t$  is time in months. At steady state, the solution is independent of storativity (*Zucker et al., 1973*). 309
- Figure 7.5** Examples of output from a transient model of the Lake Michigan Basin, USA. (a) Calculated groundwater levels at pumping centers shown from predevelopment conditions to recent time. (b) Simulated water budgets at selected times. (c) Simulated flows in selected cross sections for 2005 (*Feinstein et al., 2010*). 311
- Figure 7.6** Schematic depiction of three types of initial conditions, shown for one-dimensional horizontal flow in an unconfined aquifer between two streams. The spatial variation of head,  $h(x)$ , is shown on the right; corresponding hydrographs at the location

- $x_1$  are shown at left. (a) Static steady state; head is constant in space and time; (b) Dynamic steady state; head varies in space but is constant in time; (c) Dynamic cyclic equilibrium conditions; head varies in both space and time. The water table configuration on the right is for one point in time. 313
- Figure 7.7** Schematic hydrograph showing transient model spin up to generate initial conditions. Arbitrary initial conditions at the beginning of the spin up might be based on historical information about predevelopment water levels (blue dot). Simulated results are shown by the red line. Results for the spin-up period are not used but heads at the end of the spin up are matched to field observations (dashed blue line). The calculated heads at the end of the spin-up period (shown by the brown dot) effectively provide initial conditions for the rest of the transient simulation. 313
- Figure 7.8** Stress periods for: (a) groundwater withdrawals from pumping; the simulation used 78 stress periods of variable length between 1891 and 2009 (*Kasmarek, 2012*); (b) recharge; recharge rates were estimated from residuals in a soil-water balance model (Box 5.4). Rates for stress periods 3–12 are shown (*Feinstein et al., 2000; Reeves, 2010*). 317
- Figure 7.9** Effect of the size of the time step ( $\Delta t$ ) on the numerical solution (dots) for the decay of a groundwater mound compared to an analytical solution (solid line). Small time steps in (a) and (b) give results that match the analytical solution very well. The larger time step in (c) also provides an acceptable match to the analytical solution. The time step in (d) produced results that do not match the solution within the first 30 days (*modified from Townley and Wilson, 1980*). 319
- Figure 7.10** Effect of the number of time steps on numerical solutions of drawdown in response to pumping. (a) Numerical solutions using four different time steps (DELTA) are compared to the Theis analytical solution. Drawdown is shown at an observation point 1000 ft from the pumping well (*modified from Prickett and Lonngquist, 1971: Comparison of theoretical and digital computer solutions near a pumped well with DELTA as a variable, by Thomas A. Prickett and Carl G. Lonngquist, Bulletin 55, Illinois State Water Survey, Champaign, IL*). (b) Numerical solutions for drawdown in a pumping well using from 1 to 20 time steps. Except for the 1 time step simulation each time step was 1.5 times longer than the last. The solutions for 10 and 20 time steps are indistinguishable

	at the scale of the plot. The solution for 6 time steps is in good agreement with the 10 and 20 time step solutions ( <i>Reilly and Harbaugh, 2004</i> ).	321
<b>Figure 7.11</b>	Simulated and observed water levels for two monitoring wells in California, USA, with different periods of record ( <i>Gannett et al., 2012</i> ).	322
<b>Figure 8.1</b>	Workflow of the particle tracking process.	334
<b>Figure 8.2</b>	Velocities and flowpaths. (a) Simulated horizontal groundwater velocity vectors around a water table mound ( <i>Walter and Masterson, 2003</i> ); (b) Flowpaths produced by a particle tracking code originate at a boundary and discharge to a large group of springs at the Snake River, South Central Idaho, USA ( <i>Skinner and Rupert, 2012</i> ).	337
<b>Figure 8.3</b>	Comparison of flowpaths associated with a weak sink (pumping well) in a 5-layer model; the well is in layer 3. Flow is from top to bottom of the figures with forward tracking of particles. In the boxed inset at the bottom of the figure: (i) the coarse grid is 500 ft by 500 ft in the horizontal dimension and has 10-ft spacing in the vertical dimension; (ii) the fine grid has 10-ft spacing in the cell containing the well. (a) Flowpaths in the finely discretized grid ((ii) in the inset); (b) Flowpaths in the coarse grid ((i) in the inset) showing that all flow bypasses the well (i.e., no particles are captured by the well); (c) Flowpaths in the coarse grid but with a velocity refinement procedure ( <i>Zheng, 1994</i> ).	339
<b>Figure 8.4</b>	Capture zone for a well pumping a heterogenous aquifer. (a) Zoned hydraulic conductivity (K) distribution where circled numbers are values of K in ft/day; (b) Potentiometric surface; (c) 20-year capture zone ( <i>modified from Shafer, 1987</i> ).	340
<b>Figure 8.5</b>	Velocity interpolation for a transient simulation uses the ending head distribution of a time step to calculate a velocity field for particle tracking to represent conditions during that time step. In other words, the head distribution at $t_{n+1}$ represents heads (and associated velocities) between $t_n$ and $t_{n+1}$ .	341
<b>Figure 8.6</b>	Capture zone for a transient simulation in a homogenous confined aquifer where the pumping rate is constant but recharge varies with space and time; there are four stress periods of four time steps each. (a) The correct capture zone (yellow shading) for the pumping well (black dot) defined by flowpaths generated by back tracking particles released at the pumping well at all time steps. Flowpaths (green lines) are shown only for	

- the last time step of each stress period. Contour lines of head are shown for stress period 4 (blue lines) and stress period 2 (red lines). (b) Incorrect capture zone (blue shading) defined by reverse tracking of particles released only at the beginning of the PT simulation (i.e., at the last time step of the last stress period of the groundwater flow model) (Rayne et al., 2013). 342
- Figure 8.7** A portion of a finite-difference grid showing the locations of nodes and internodal positions (shown by  $x$ 's), where velocity components  $v_x$  and  $v_y$  are calculated. The quadrants (circled and numbered) associated with node  $(i,j)$  are used in bilinear interpolation of velocities. 343
- Figure 8.8** Definition diagram for inverse distance interpolation: (a) Points used in the calculation of  $v_x$ ; (b) Points used in the calculation of  $v_y$  (modified from Franz and Guiguer, 1990). 345
- Figure 8.9** Improvement of interpolation of velocity by subdividing triangular finite elements into four subtriangles in which separate velocity vectors are computed (modified from Cordes and Kinzelbach, 1992). 346
- Figure 8.10** Semianalytical particle tracking within a finite-difference cell showing the computation of travel time and flowpath from the particle location  $(x_p, y_p)$  to an exit point  $(x_e, y_e)$  (modified from Pollock, 2012). In this figure, MODFLOW numbering convention is used where  $i = \text{row}$  and  $j = \text{column}$  (Fig. 5.5). 347
- Figure 8.11** Schematic diagram for the fourth-order Runge-Kutta method showing trial locations of the particle  $p_1$  after moving one full ( $p_4$ ) and two half steps ( $p_2, p_3$ ). The final particle location is  $(x_{n+1}, y_{n+1})$  (modified from Zheng and Bennett, 2002). 349
- Figure 8.12** Methods to control the tracking step in particle tracking where  $\Delta s$  is the error. For additional discussion of these methods see Section 8.6. (a) Use of two half-tracking steps ( $\Delta t/2$ ) in PATH3D (modified from Zheng, 1989); (b) reverse tracking used in FLOWPATH (modified from Franz and Guiguer, 1990). 350
- Figure 8.13** Schematic diagram of flows in model cells associated with (a) a weak sink and (b) a strong sink. Flow rate is proportional to the length of the arrow (modified from Spitz et al., 2001). 350
- Figure 8.14** Contributing areas. (a) Forward particle tracking to delineate the contributing area to Allequash Lake (salmon pink) and Allequash Creek (green) in a humid temperate climate in Northern Wisconsin, USA. Contours indicate time of travel in years. Particles were placed at the water table in every active cell

in the model and tracked forward in time. All weak sinks were converted to strong sinks (*Pint et al., 2003*). (b) Contributing areas as shown in (a) but allowing all particles to pass through weak sinks (*Masbruch, 2005*). 352

**Figure 8.15** Reverse particle tracking showing capture zone projections for a well field of five wells. The configuration of the capture zones is irregular owing to the highly heterogenous aquifer and the three-dimensional flow field. (a), (b), and (c) show horizontal plane projections at 10, 40, and 280 years, respectively; the blue squares show the position of particles that have reached the surface; for example, 93.1% of particles have reached the surface after 280 years. Open circles show the end position of particles that have not reached the surface; for example, 6.9% of particles have not reached the surface after 280 years. (d) a vertical plane projection at 280 years (*modified from Frind and Molson, 2004; Frind et al., 2002*). 353

**Figure 8.16** Reverse particle tracking to identify sources of water to a deep sewer tunnel system. (a) Map view showing extent of a MODFLOW model set in a regional analytic element (GFLOW) model. The tunnel is shown as line segments representing the Inline Storage System (ISS) (see the legend). (b) West—east cross section. The tunnel (Inline Storage System (ISS)) is shown in purple. Travel times are indicated by the arrowheads; each arrowhead represents 75 years of travel time (*Dunning et al., 2004*). 354

**Figure 8.17** Advective particle tracking from contaminated areas (labeled as grassy area source and north edge of apron area source) at a former airfield, showing flowpaths and travel times (*Haugh et al., 2004*). 356

**Figure 8.18** Flowpaths in three-dimensions. Particles released at the surface move down through the bedrock and back up to Quaternary deposits at the surface. Travel times are indicated by colors. Main flowpaths are shown by dashed black lines with arrowheads. Streams and lakes at the surface are outlined in red (*Bosson et al., 2013*). 357

**Figure 8.19** Advective age of particles along different flowpaths. Flowpaths of vastly different ages discharge in close proximity suggesting that mixing of waters of different ages occurs in the discharge location. (For example, flowpath I discharges near flowpath II.) Groundwater sampled in discharge areas will have a mean or apparent age that is different from the advective age of an individual flowpath (*Pint et al., 2003*). 358

- Figure 8.20** Different capture zones (red lines) are computed by reverse particle tracking when particles are released from slightly different locations around the well node. Equipotential lines are shown in blue. Particles were released 0.01, 0.1, 1, and 4 ft off-center of the well. Particles released 4 ft and 1 ft off-center underestimate the width and downgradient extent of the capture zone. Particles released 0.1 and 0.01 ft off-center produce virtually the same capture zone width, but the 0.01 ft release points show slightly greater downgradient capture (*Courtesy of Kurt Zeiler, Brown and Caldwell*). 359
- Figure 8.21** Schematic diagram showing the retarding effect of linear adsorption and definition of the retardation factor. In particle tracking, solutes are transported by plug flow (*modified from Zheng and Bennett, 2002*). 363
- Figure P8.1** Model domain of a portion of saturated rock located at depth below an area undergoing oil and gas development. The domain is composed of three layers that have similar properties on the left side of fault 2. The geologic material to the right of fault 2 is the same in each layer and represents a different rock type that has been faulted into this location. Faults each represent a zone 400-m wide and extend completely through each layer. Specified head boundaries are located on the left- and right-hand sides and extend to each layer in the domain. The remaining boundaries are no flow. Locations of injection wells I1 and I2 and pumping well P1 are also shown. 368
- Figure P8.2** Model domain of a 10-m thick single layer confined aquifer. Location of the pumping well is shown. The letter A (red dot) represents a monitoring well location. 369
- Figure B8.2.1** Schematic flow net with equipotential lines of constant head (dashed lines) and streamlines (blue lines with arrowheads) representing constant values of the streamfunction,  $\psi$ . If the contour interval of  $\psi$  is constant, the flow rate,  $\Delta Q$  ( $L^3/T$ ), through a streamtube is constant and can be calculated (see Section 3.4, Eqn (3.21)) (*Fitts, 2013*). 335
- Figure B8.2.2** Flow net generated using a numerical solution. (a) The system is anisotropic and heterogenous in piecewise constant zones with values of horizontal hydraulic conductivity ( $K_x$ ,  $K_y$ ) shown. Boundary conditions are no flow except at either end of the aquifer (middle layer) where values of head,  $h$ , are shown. (b) Flow net for the system shown in (a). Streamlines are the



- horizontal lines in the center of the figure; the other lines are equipotential lines (*modified from Bramlett and Borden, 1990*). **336**
- Figure B8.3.1** Capture zones. (a) Capture zone (labeled as zone of contribution) shown in 3D with bounding flowpaths (*Paschke et al., 2007*). (b) Time of travel (TOT) capture zones and bounding streamline shown in map view for a two-dimensional, steady-state, uniform flow field with ambient flow of  $Q_0$  ( $L^2/T$ ; discharge rate per unit thickness) and pumping rate of  $Q$  ( $L^3/T$ ); recharge rate is zero.  $\tilde{T}$  is a dimensionless time parameter ( $=2\pi t Q_0^2 / nbQ$  where  $t$  is the time particles along a TOT line take to reach the well;  $n$  is the effective porosity; and  $b$  is the average saturated thickness of the aquifer prior to pumping) (*modified from Ceric and Haitjema, 2004*). **360**
- Figure B8.3.2** Stream capture zones resulting from pumping at a constant rate for 50 years from the lower basin-fill in a semiarid basin, Arizona, USA. The color at any location represents the fraction of the withdrawal rate by a well at that location that is contributed by streamflow depletion (*Barlow and Leake, 2012*). **361**
- Figure B8.3.3** Contributing and release zones around a circular lake delineated by bounding flowpaths. The release zone delineates flow leaving the lake through the groundwater system (*modified from Townley and Trefry, 2000*). **362**
- Figure 9.1** General workflow for manual trial and error, the first phase of history matching a model intended for forecasting (ME, mean error; MAE, mean absolute error; RMSE, root mean squared error). **377**
- Figure 9.2** History matching to the depth of the interface between a plume of lake water and terrestrially recharged groundwater at three locations. The interface was located in the field by using measurements of stable isotopes of water (observed) and in the model by advective particle tracking (simulated) (*modified from Hunt et al., 2013*). **381**
- Figure 9.3** Map view of observed (green) and simulated (red) water table (shown by contours) in an arid inland river basin in China. Topographic elevations are shown by color shading (*Yao et al., 2014*). **386**
- Figure 9.4** Four ways to visualize the comparison of history matching observed (blue) to simulated (reddish-brown) targets in a transient model. (a) Hydrograph of observed and simulated streamflow with Nash–Sutcliffe coefficient (Eqn (9.4))

- reported; Fig. 7.11 shows an example of this type of plot using observed and simulated heads. (b) Monthly plot of mean observed and simulated streamflow over the same months in different years using data shown in panel (a). (c) Comparison of mean observed and simulated heads. (d) Comparison of the observed and measured range of values for mean head values shown in panel c (*modified from Hunt et al., 2013*). **387**
- Figure 9.5** Scatter plot (a) and categorized scatter plot (b) of simulated to observed fit of water levels. The categories in (b) can convey the modeler's assessment of target quality, here ranging between observations roughly estimated (small, gray dots) and more accurate observations (larger, colored symbols). The 1:1 perfect fit line is also shown for reference to visualize bias (*modified from Juckem et al., 2014*). **388**
- Figure 9.6** Two examples of representing residual errors. (a) Similar size symbols with different colors can be effective when many data are shown, as is the case for head data from the large-scale groundwater model shown in the figure. With such a representation the spatial bias of simulated heads is effectively conveyed. (b) Different sizes and colors can be used when data are few, such as with flux targets in the same model domain as shown in (a). Color relates to degree of fit and symbol size relates to magnitude of the measured flux target—information important when judging the fit of a regional model. Small data sets of lesser quality from synoptic measurements and seasonal stream gages are highlighted to distinguish them from higher quality long-term streamflow measurements (*modified from Juckem, 2009*). **389**
- Figure 9.7** History match of flux targets: (a) flux targets with residual error related to uncertainty in measured values (*D'Agnese et al., 2002*); (b) Spatial flux difference targets of baseflow in five streams for three different models showing uncertainty in measured values (*modified from Hunt et al., 1998*). **390**
- Figure 9.8** A schematic workflow diagram of the mechanics of each forward run automated by a universal nonlinear regression parameter estimation code. The shaded background in the figure indicates that the steps are performed internally by the code without user intervention. Two types of ASCII (American Standard Code for Information Interchange) files are required before the parameter estimation code can be run: (1) a template file that specifies where to place new values of calibration

parameters in the model input file; and (2) an instruction file that extracts relevant model outputs for comparison to observed calibration targets. Both required files are typically created by a graphical user interface (GUI). 398

**Figure 9.9** A schematic diagram of a general workflow for parameter estimation, the second phase of history matching for a model designed for forecasting. Shaded box contains steps automated by the parameter estimation code; steps in the unshaded areas require modeler action. An objective function is appropriate when all targets are included but targets important to the modeling objective are more prominently weighted (GUI, graphical user interface). 399

**Figure 9.10** (a) Idealized objective function surface for a two-parameter problem (*modified from Himmelblau, D.M., 1972, Applied Nonlinear Programming, McGraw-Hill, New York, reproduced with permission of McGraw-Hill Education*). (b) improvement in the solution via parameter upgrade in successive parameter estimation iterations (shown by the dashed line) leading to the objective function minimum (*from Doherty, 2010a*). 402

**Figure 9.11** Objective function surfaces from a two-parameter model of a field site where contour lines with warmer colors represent lower objective function value: (a) example of a solution that did not converge; that is, the objective function surface has no unique minimum (shaded pink trough). Nonconvergence was caused by using only head data as calibration targets; (b) the objective function surface for a solution that converged. The solution included both heads and groundwater temperature as observation targets. Dashed lines represent the approach to the surface minimum and reddish circles represent parameter upgrades (*modified from Bravo et al., 2002*). 404

**Figure 9.12** Cross section of an objective function surface showing local and global minima (*modified from Zheng and Bennett, 2002*). 404

**Figure 9.13** Plot of change in model outputs (y-axes) to small increments of change in one model parameter (x-axes) for two different observations. Each dot represents one model run; the straight line is the best fit through the dots. Because the true parameter sensitivity derivative is approximated using a 1% parameter perturbation sequential 1% perturbations should provide a coherent change (e.g., a monotonically changing line, shown in (b)). Poor derivatives calculated by

- perturbation (a) can confound derivative-based parameter estimation methods; tighter solver closure as shown in (b) provides more coherent derivatives. An influence statistic (Cook's D, Box 9.6) for the two observations is also listed, where higher values represent more influence on the regression (*modified from Feinstein et al., 2008*). 405
- Figure 9.14** An example of a Jacobian matrix with 6 columns of parameters and 14 rows of observations. Each entry in the matrix is a parameter sensitivity (sensitivity coefficient) calculated from Eqn (9.7). The numbers in the left-hand column are the labels for head targets where best, fair, and poor indicate the quality of the target. 407
- Figure 9.15** Pilot Points. (a) Network of pilot points in a watershed-scale groundwater flow model (left); linkages between pilot points (right) used to calculate Tikhonov regularization constraints for preferred homogeneity (*modified from Muffels, 2008*). (b) Network of pilot points used to represent two hydraulic conductivity zones where Tikhonov regularization is applied to pilot points within the same zone (*modified from Davis and Putnam, 2013*). 415
- Figure 9.16** Visualization of parameter estimation using alternative Tikhonov regularization, where the same parameter estimation problem is solved using two different values of the target objective function (PHIMLIM variable in PEST). (a) When the target objective function is set unrealistically low ( $\text{PHIMLIM} = 1$ ), user soft knowledge is disregarded and optimality of the inverse solution is defined solely by the model's fit to calibration targets (i.e., minimization of the measurement objective function,  $\Phi$ ). The resulting field has extreme contrasts and parameter "bulls eyes" that reflect the code's unchecked pursuit of the best fit. (b) When the target objective function is set to a value around 10% higher than the best  $\Phi$  obtained ( $\text{PHIMLIM} = 1\text{e}6$ ), the resulting fit is slightly worse (as shown by a slightly larger spread around the 1:1 line in the scatter plot of heads), but heterogeneity in the optimal parameter field is reduced. Whether the heterogeneity expressed is reasonable is the decision of the modeler; thus both models might be considered part of the Pareto front shown in Fig. 9.17 (*modified from USGS unpublished data*). 419
- Figure 9.17** A Pareto front diagram. Multiple calibrations by Tikhonov regularized inversion of the same model are shown by dots,

which coalesce into a thick black line along a “front”; the only difference among calibrations is the strength of the soft knowledge constraint expressed during parameter estimation. The Pareto front illustrates the inherent trade-off between a perfect model fit (zero on x-axis) and perfect adherence to the modeler’s soft knowledge (zero on y-axis). The “best” model is the modeler’s subjective pick of one calibration from the many calibration results along the Pareto front (*modified from Moore et al., 2010*).

420

**Figure 9.18**

A schematic depiction of the relation of two parameters ( $p_1$  and  $p_2$ ) to the solution space and null space defined by a set of calibration targets. Because neither parameter lies on the plane of the solution space, the parameters are not perfectly constrained by the observations. Parameter  $p_1$  is partially informed by the observations; thus it has a projection into the solution space and can be estimated during parameter estimation. Parameter  $p_2$ , however, cannot be projected onto the solution space and cannot be estimated given the calibration targets (*modified from Doherty et al., 2010b*).

423

**Figure 9.19**

A schematic diagram of a general workflow for parameter estimation using a hybrid SVD-Assist (SVDA)/Tikhonov regularization approach. Shaded box contains the steps performed internally by the parameter estimation code without user intervention; unshaded steps require modeler action. The trade-off between soft knowledge and the model’s fit to hard knowledge is adjusted by changing the target objective function for Tikhonov regularization (the PHIMLIM parameter in PEST); (GUI, graphical user interface; SVD, singular value decomposition).

426

**Figure P9.1**

Map view and cross section of an unconfined sand and gravel aquifer. The areal dimensions of the problem domain are 1500 m by 1500 m and the nodal spacing is uniformly 100 m. Impermeable bedrock along the northern boundary of the problem domain and north of the river does not contribute water to the river. Numbers refer to river stage in meters above sea level. Letters refer to pumping and observation wells (Table P9.1). The cross section is oriented N–S along column 9. Elevations are given in meters above sea level.

433

**Figure B9.2.1**

Pie charts of an initial objective function that is: (a) unbalanced because the number of head targets is much larger than other

- targets and (b) more balanced because no one target type dominates or is dominated by other groups. The more balanced objective function was obtained by simply normalizing the observation weights by the number of targets in each group. **409**
- Figure B9.4.1** Singular value decomposition of a photographic image. When the matrix is perfectly known (defined by 240 pixels/singular values in the image), it reflects the highest resolution and thus the highest number of singular values can be shown visually. For reference, the image with 20 singular values represents less than 10% of the information contained in the original image in the upper left, yet it contains enough information that the subject matter can be easily identified. A similar concept applies to groundwater problems—if too few singular values are selected, a needlessly coarse and blurry representation of the groundwater system results. When the information content of the calibration data set is increased, a larger number of data-supported singular values can be included, resulting in a sharper “picture” of the groundwater system. In practice, most field observations only support a relatively blurry depiction of subsurface properties (*from Doherty and Hunt, 2010; image and SVD processing by Michael N. Fiennen, USGS*). **422**
- Figure 10.1** A simple example of hindcasting groundwater—surface water interaction in a humid temperate climate (Wisconsin, USA). A model calibrated to current pumping conditions (a) is re-run to simulate groundwater—surface water interaction before pumping (b). Red symbols identify areas of induced flow from surface water in response to pumping, a dam, and high hydraulic conductivity fluvial sediments in the river valleys. Blue symbols represent areas of groundwater discharge to surface water. Comparison of (a) and (b) shows the expansion of losing stream conditions caused by pumping. The effect of the dam is evident during both time periods (horizontal red band near top of figures) (*modified from Hunt et al., 2003*). **444**
- Figure 10.2** Minimum Message Length (MML) curves as described by Wallace and Boulton (1968) and Moore and Doherty (2005). (a) A typical MML conceptualization showing sources of uncertainty in the base model as measurement error (blue-green line) and structural error (gray line) and their relation to model complexity and forecast uncertainty. Increasing complexity results in increasing the measurement error components of

uncertainty because the noise within the measurements is amplified (right-hand portion of the figure). Very simple models (left-hand portion of the figure), on the other hand, are also characterized by relatively high forecast uncertainty because the model's ability to forecast is adversely affected by parameter simplification error. The minimum forecast uncertainty is found when the total uncertainty in the base model (thick black line; the sum of measurement uncertainty and structural uncertainty) is minimized (*modified from Hunt, 2012.*) (b) MML curve (thick black line) for a groundwater model of an arid setting (Yucca Mountain, Nevada, USA). Model complexity is represented by the number of singular values (parameters or parameter combinations) included in the error analysis (x-axis). The error variance in the forecast (thick black line) caused by error in the base model is the sum of structural error (thin solid line) and measurement error (dashed line). Forecast error is high when the model is oversimplified (0–10 singular values), and again when the model is overly complex (>18 singular values). The smallest total error occurs when 11–16 singular values are used (*James et al., 2009.*)

448

**Figure 10.3**

A schematic picture of Bayesian updating using a one-parameter distribution, where the possible range of the parameter spans from  $-10$  to  $20$ . The probability density function representing the prior distribution  $P(A)$  of the calibration parameter is diffuse (gray dashed line), meaning the variance is relatively high and, correspondingly, uncertainty in the parameter is high. The likelihood function  $L(B|A)$  (solid gray line), on the other hand, has lower variance, suggesting a history-matching process brings a higher level of certainty to the estimation of the parameter than given by the prior distribution only. The resulting posterior distribution  $P(A|B)$  (solid black line) is a convolution of the prior and likelihood functions. The peak is higher indicating more certainty resulted after history matching, is shifted significantly from the prior toward the likelihood, and is narrower, representing less uncertainty (*modified from Fioren et al., 2009, 2013.*)

451

**Figure 10.4**

An example of a Bayesian posterior uncertainty evaluation of log hydraulic conductivity (shown by colors) after a number of aquifer (pumping) tests were performed using hydraulic tomography. Areas stressed by multiple aquifer tests are characterized by lower uncertainty (lower standard deviation of

- log(K), blue areas). Areas distant from the pumping locations have higher uncertainty (*Cardiff et al., 2013*). 452
- Figure 10.5** An example of a forecast of future reductions in streamflow resulting from continuing an existing pumping regime. The forecast has relatively less uncertainty because it is reported as a mean annual value rather than the range of all simulated values. In addition, the forecast can be expected to contain less uncertainty because it is presented as a difference rather than absolute model output, and concerns a quantity (pumping stress) included in the calibration history matching (*modified from Ely et al., 2011*). 457
- Figure 10.6** Schematic diagram of a potential workflow for performing basic uncertainty analysis. 458
- Figure 10.7** A forecast of baseflow summarizing 15 scenario forward runs (maximum, minimum, and average conditions in each of three emission scenarios). Forecast uncertainty is shown by the envelope around the means of the three scenarios (colored lines). The forecasts derived from the mean of each emission scenario were based on the mean results from 5 different General Circulation Models. Note how the uncertainty envelope increases with time (*Hunt et al., 2013*). 459
- Figure 10.8** A visual representation of final calibrated model parameters and their associated 95% confidence interval calculated by linear uncertainty methods. HK = hydraulic conductivity (ft/d), RCH = recharge (ft/d), and RIV = conductance (ft<sup>2</sup>/d) (*modified from Ely and Kahle, 2004*). 461
- Figure 10.9** Precalibration and postcalibration parameter contribution to total error variance (sum of all bars in a row) for a forecast of lake level under drought conditions (using MODFLOWs Lake Package, Section 6.6). The error variance (calculated from Eqn (10.2)) represents uncertainty around the model forecast. The bars show the contribution of each parameter to the total forecast error (precalibration = 0.96 m<sup>2</sup>; postcalibration 0.60 m<sup>2</sup>). Forecast uncertainty is lower after calibration, as shown by the reduction in height in the bars for a number of calibration parameters used in the forecast simulation. Note that postcalibration reduction in forecast uncertainty was most notable for the lakebed leakance (lk leakance) parameter. Thus, less gain is expected from future data-collection activities targeting only this parameter because the value of the parameter



is already well constrained by existing history matching data, i.e., the parameter has good identifiability (*modified from Hunt and Doherty, 2006*). Parameter types are: man = Manning’s n, por = effective porosity, lk leakance = lakebed leakance, rstage = far-field river stage boundary, inc = stream elevation increment boundary condition, rchg = recharge, k1 through k4 = horizontal hydraulic conductivity of layers 1 through 4, kz1 through kz4 = vertical hydraulic conductivity of layers 1 through 4. 466

**Figure 10.10** Linear uncertainty analysis for a groundwater flow model of an arid hydrologic setting (Yucca Mountain, Nevada, USA). Parameter identifiability is used to judge parameters that are not constrained by the observation targets. A value of 1.0 indicates a completely identifiable parameter, i.e., one that is well constrained by the calibration targets and can be estimated by history matching. An identifiability of 0.0 represents complete unidentifiability—that is, the observations have no information to constrain the parameter and it cannot be estimated by history matching. Identifiability between the two extremes is more qualitative, whereby small bars are less identifiable and larger bars are relatively more identifiable. The color coding represents the strength of identifiability. Warmer colors represent parameters more supported by observation targets; cooler colors are parameters less supported by observation targets (*James et al., 2009*). 467

**Figure 10.11** Schematic illustration of nonlinear calibration-constrained forecast maximization—minimization for a two-parameter problem (*Doherty et al., 2010*). 470

**Figure 10.12** A comparison of measured streamflow to maximum and minimum forecasts calculated by using a constrained maximization and minimization approach shown in Fig. 10.10 (*modified from Bahreman and De Smedt, 2010*). 470

**Figure 10.13** Schematic representations of three different types of Probability Density Functions (PDFs—top row) and Cumulative Density Functions (CDFs—bottom row) used for parameters sampled in Monte Carlo analysis (*after NIST, 2012*). 474

**Figure 10.14** Schematic workflow for performing Monte Carlo uncertainty analysis. 474

**Figure 10.15** Simulated probability due to uncertainty in advective transport parameters affecting a plume emanating from treatment lagoons.

- Blue color represents high probability flowpaths; orange colors represent low probability flowpaths (*Juckem et al., 2014*). **476**
- Figure 10.16** Markov Chain Monte Carlo results showing the best estimate (solid line) and upper and lower 95% confidence intervals (dashed lines) for hypothetical injection and advective transport of bromide (*modified from Fiennen et al., 2006*). **477**
- Figure 10.17** Distribution of objective functions computed from 100 realizations with stochastic parameters: (a) before null-space projection and recalibration; (b) after null-space projection. Realizations sampled from (b) are much more likely to meet conditioning criteria. As a result, null-space Monte Carlo reduces the computational burden needed for the Monte Carlo process to converge (*Doherty et al., 2010*). **477**
- Figure B10.2.1** Details of the synthetic aquifer: (a) model domain and grid with the 12 head observation locations (representing wells) shown as large circles and pilot point locations shown as small circles. (b) The “true” hydraulic conductivity field. (c) Head contours (solid lines) and particle track (dotted line) calculated for the true hydraulic conductivity field (*modified from Moore and Doherty, 2005; Moore et al., 2010*). **455**
- Figure B10.2.2** A Pareto front diagram showing a forecast of particle travel time in days (vertical axis) versus the calibration objective function (horizontal axis). Each dot represents a forecast made with a different calibrated model. Well-calibrated models have low objective functions and poorly calibrated models have relatively higher objective functions. The true travel time through the synthetic aquifer (Fig. B10.2.1) is 3256 days, which is only sampled when the objective function is at its upper limit of feasibility (*modified from Moore et al., 2010*). **456**
- Figure B10.4.1** Results of Monte Carlo simulations: (a) convergence of the Monte Carlo process is indicated by the relatively stable moving average MAE after 25 realizations; (b) large errors in head (large MAE) were addressed by conditioning the 200 runs by removing runs where the MAE was greater than 7.68 m (*Hunt and Steuer, 2000*). **472**
- Figure B10.4.2** Visualizing uncertainty as a probabilistic area of contribution for a spring complex. The graphic is based on 136 conditional simulations and shows low (blue) to high (red) probability for the extent of the area of contribution (*modified from Hunt et al., 2001*). **473**
- Figure 11.1** Generic outline of a modeling report. **499**

## LIST OF TABLES

<b>Table 2.1</b>	Types of data potentially used in construction of a hydrogeologic site conceptual model (Alley et al., 1999)	<b>31</b>
<b>Table 2.2</b>	Groundwater budget for the San Bernardino area, California, USA, 1945–1998, showing possible ways to account for the imbalance in the budget represented by the residual; values are in acre-ft per year (modified from Danskin et al., 2006)	<b>55</b>
<b>Table 2.3</b>	Example of estimated error (second set of numbers in each column) associated with measurements (first set of numbers in each column) of components in a groundwater budget. Groundwater inflow to three sites in a wetland in Wisconsin was estimated using four different techniques. $K_v$ is vertical hydraulic conductivity; $K_h$ is horizontal hydraulic conductivity (modified from Hunt et al., 1996)	<b>58</b>
<b>Table P2.1</b>	Lithostratigraphy and water yield of sediment in Orangeburg County, South Carolina, USA (Colquhoun et al., 1983; after Aadland et al., 1995; Gellici, 2007)	<b>61</b>
<b>Table 3.1</b>	Example of a simulation log (modified from Aquaterra Consulting Pty Ltd, 2000)	<b>103</b>
<b>Table 5.1</b>	Typical values of specific yield ( $S_y$ ) (Morris and Johnson, 1967)	<b>228</b>
<b>Table 5.2</b>	Typical values of specific storage ( $S_s$ ) (adapted from Domenico, 1972)	<b>229</b>
<b>Table 5.3</b>	Methods of estimating recharge and discharge. Most methods can be used for estimating both recharge and discharge although a given method may be better suited for one than the other (modified from NRC, 2004; Scanlon et al., 2002)	<b>231</b>
<b>Table P5.1</b>	Hydraulic conductivity values from aquifer (pumping) tests. Well locations are given by coordinate locations and are shown in Fig. P5.3	<b>249</b>
<b>Table 7.1</b>	Types of transient calibration data for confined aquifers in a regional model of the Lake Michigan Basin, USA (modified from Feinstein et al., 2010). Higher observation weights reflect increased importance of the observation in model calibration (Section 9.5)	<b>323</b>
<b>Table P7.1</b>	Estimated average monthly recharge rates for the Hubbertville aquifer	<b>325</b>
<b>Table B8.1.1</b>	Values of effective porosity from field tracer tests compiled by Gelhar et al. (1992)	<b>333</b>

<b>Table 9.1</b>	Estimated accuracy of head data by measurement method (modified from Nielson, 1991). Measurement method is but one source of error for head targets	<b>379</b>
<b>Table P9.1</b>	Head targets for the aquifer shown in Fig. P9.1	<b>434</b>
<b>Table 10.1</b>	Examples of intrinsic and epistemic uncertainties in hydrologic modeling (adapted from Beven and Young, 2013)	<b>450</b>
<b>Table 10.2</b>	An example of a simple <b>C(p)</b> matrix for a three-parameter model (K = hydraulic conductivity). (a) Input for the matrix; (b) the <b>C(p)</b> matrix constructed from information in (a)	<b>464</b>
<b>Table 10.3</b>	Uncertainty terms and related forecast probability (IPCC, 2014)	<b>480</b>
<b>Table P10.1</b>	Measured heads after 1 year of pumping	<b>484</b>
<b>Table 11.1</b>	Minimum information required for model replication and reproducibility	<b>509</b>

# PREFACE

*Art and science have their meeting point in method.*

*Edward George Bulwer-Lytton*

This second edition is motivated by the many significant developments in groundwater modeling since the first edition was published in 1992. The increased computational speed and capacity of present day multicore computers as well as the availability of sophisticated graphical user interfaces (GUIs) and geographical information systems have transformed groundwater modeling. But more importantly, new ways of calibrating models and analyzing uncertainty and new powerful codes that provide enhanced modeling tools are revolutionizing the science of groundwater modeling. In this second edition, we discuss many of the important advances in applied groundwater modeling introduced since 1992 and also update the treatment of fundamentals of groundwater flow modeling covered in the first edition. The chapters on model calibration and forecasting (Chapters 9 and 10 in the second edition) are entirely new and include discussion of new tools for parameter estimation and uncertainty analysis in forecast simulations. Similar to the first edition, our book is intended as an introduction to the applied science of modeling groundwater flow. We focus on groundwater modeling practice. For a more theoretical approach to groundwater modeling, the reader is referred to textbooks by [Diersch \(2014\)](#) and [Bear and Cheng \(2010\)](#).

Quantitative analysis of groundwater flow is essential to all hydrogeological problems, and groundwater models are the essential tools in such analyses. Groundwater flow models solve for what cannot be fully observed or measured—the distribution of head in space and time. Important associated information such as water budgets, flow rates, and flowpaths to and from surface water bodies and wells can be calculated from the head distribution. The focus of our book is mastering groundwater flow models, a critical first step for a groundwater modeler.

Although many groundwater problems can be solved by analyzing groundwater flow alone, some problems require analysis of the movement of solutes or contaminants in the subsurface. A transport model includes representation of advective transport, dispersion, and chemical reactions to solve for solute or contaminant concentrations. Transport modeling is beyond the scope of our textbook but is covered in detail by [Zheng and Bennett \(2002\)](#). However, the starting point for transport modeling is a good groundwater flow model because a transport code uses output from a groundwater flow model. Moreover, some transport problems can be addressed by considering only advective transport using a particle tracking code as a postprocessor to a groundwater flow model to calculate flowpaths and travel times. We discuss those types of problems in a chapter on

particle tracking (Chapter 8 in the second edition) that was revised and updated from the first edition.

Mastery of groundwater modeling requires both art and science. The science of groundwater modeling includes basic modeling theory and numerical solution methods. There are many textbooks that provide advanced, intermediate, and elementary treatments of the science and underlying mathematics of numerical modeling of groundwater flow. Since 1992, applied groundwater science has expanded to include theory and methods for parameter estimation (inverse solutions) and uncertainty analysis, and there are books devoted exclusively to those topics (e.g., [Doherty, 2015](#); [Aster et al., 2013](#); [Hill and Tiedeman, 2007](#)). Although our text provides some of the background information for applying groundwater models to field problems, we assume that the reader knows the basic principles of hydrogeology and modeling as covered in standard textbooks such as [Fitts \(2013\)](#), [Kresic \(2007\)](#), [Todd and Mays \(2005\)](#), [Schwartz and Zhang \(2003\)](#), and [Fetter \(2001\)](#). A rudimentary knowledge of the theory of groundwater modeling including the basics of finite-difference and finite-element methods as contained in [Wang and Anderson \(1982\)](#) is also helpful.

Our book is meant to be accessible to those who want to apply groundwater models as tools. To use an analogy presented to us years ago by Professor John Wilson (New Mexico Tech), using a model is like driving a car. A good driver knows the rules of the road and has the skill to control the car under a wide variety of conditions and avoid accidents, but does not necessarily understand the intricacies of what goes on under the hood of the car. The goal of this book is to help the reader learn how to be a good driver and operate a model under a wide variety of conditions and avoid “accidents.” To help in this, we have included a section at the end of each chapter in which we list common modeling errors—some we have encountered and many we have made ourselves. Eventually, after learning how to drive well, a modeler may want to explore the mechanics of a code (i.e., look under the hood of the car); familiarity with code mechanics helps the modeler understand the strengths and limitations of a specific code and will help the modeler modify the code if necessary.

The art of modeling is gained mainly through experience; by developing and applying groundwater models one develops “hydrosense” and modeling intuition ([Hunt and Zheng, 2012](#)). Our book provides guidance in the fundamental steps involved in the art of modeling: developing a conceptual model, translating the qualitative conceptual model to a quantitative (numerical) model, and assessing model input and output. Given that “art and science have their meeting point in method,” our objective is to describe methods of applying groundwater flow models, and thereby provide a compact comprehensive reference to assist those wishing to develop proficiency in the art of modeling.

The book comprises four sections. Section 1, Modeling Fundamentals (Chapters 1, 2, and 3), lays out the motivation for modeling, describes the process of formulating a conceptual model, and provides the theoretical and numerical base. Section 2, Designing the

Numerical Model (Chapters 4 through 7), describes how to translate the conceptual model of groundwater flow into a numerical model, including grid/mesh design, selecting boundary and initial conditions, and setting parameter values. Section 3, Particle Tracking, Calibration, Forecasting, and Uncertainty Analysis (Chapters 8 through 10) discusses particle tracking and model performance. Section 4, The Modeling Report and Advanced Topics (Chapters 11, 12) discusses the modeling report and archive, model review, and briefly covers topics beyond basic groundwater flow modeling.

In the first edition, we made extensive reference to specific flow and particle tracking codes to illustrate examples of modeling mechanics. However, the number and capabilities of groundwater codes have increased dramatically since 1992. In the second edition, we illustrate how fundamental modeling concepts are implemented in two representative groundwater flow codes: MODFLOW (for finite-difference methods) and FEFLOW (for finite-element methods). We use MODFLOW (<http://water.usgs.gov/ogw/modflow/MODFLOW.html>) because it is freeware, open-source, well-documented, versatile, used worldwide and in the US is the standard code in regulatory and legal arenas. The proprietary code FEFLOW is widely used, versatile, well-supported, and well-documented both online (<http://www.feflow.com/>) and in a textbook (Diersch, 2014). We selected the PEST software suite (<http://www.pesthomepage.org>) to illustrate how concepts of parameter estimation can be implemented. The PEST suite of codes (Doherty 2014, 2015; Welter et al., 2012; Fioren et al., 2013) is freeware and open-source, includes widely used approaches for parameter estimation with many advanced options. A version of PEST (PEST++ by Welter et al., 2012) is supported by the U.S. Geological Survey (<http://pubs.usgs.gov/tm/tm7c5/>). In practice, the modeler will typically use these codes within a GUI. The details of how the codes work within a GUI are not covered in our book. The reader should expect to spend practice time with a GUI to be accomplished in using these or any other codes.

The many new developments and advances in groundwater modeling since the first edition are supported by an enormity of literature. Therefore, we developed some general guidelines for presentation of material in the second edition.

- We focus on “the norm” rather than “the exception” in order to guide the reader to the most likely productive approach for most problems.
- We use language and mathematics accessible to the beginning and intermediate level groundwater modeler and try to avoid jargon. Necessarily, the advanced modeler may find our presentation at times overly simple or lacking in rigor.
- For the most part, we reference widely available software; the vast majority of applied groundwater modeling is done with off-the-shelf software.
- We recognize that software, jargon, and methods will change in the future. Therefore, our text focuses on the basic principles of groundwater modeling that will endure. However, we use code-specific language and variable names when we believe that such specificity is beneficial.

- We mainly cite work published in the twenty-first century, as well as classic (benchmark) papers. References cited should be regarded as portals into the large body of pertinent literature on a specific topic. That is, the provided reference is cited not only for itself but also for all the work cited therein. In this way, the reader is given the opportunity to consult a broad body of literature and explore a research thread. Reports published by the U.S. Geological Survey are available for free download at <http://www.usgs.gov> or at the provided Universal Resource Locators (URLs).

With the maturing of the science, groundwater modeling has become more interdisciplinary and relevant publications are distributed across a wide variety of journals. No textbook can fully cover all the relevant literature. Therefore, we apologize in advance to those who may feel we have overlooked their contributions.

The second edition has an associated Web site that will contain background material, example problems, and links to other modeling resources (<http://appliedgwmodeling.elsevier.com>). We hope this material, together with the textbook, will be useful on two levels: (1) for teaching undergraduate and graduate level courses in applied groundwater modeling; (2) as a reference for environmental consultants and those in industry and governmental agencies. In its broadest intent, our book is meant for those who want to learn how to build, use, and assess groundwater flow models. We hope that reading this book will facilitate a life-long journey in groundwater modeling.

*All things are ready, if our minds be so.*

*—Henry V, Act IV*

**Mary P. Anderson**, Madison, Wisconsin  
**William W. Woessner**, Missoula, Montana  
**Randall J. Hunt**, Cross Plains, Wisconsin

## REFERENCES

- Aster, R.C., Borchers, B., Thurber, C.H., 2013. Parameter Estimation and Inverse Problems, second ed. Elsevier, 360 p.
- Bear, J., Cheng, A.H.D., 2010. Modeling Groundwater Flow and Contaminant Transport. In: Theory and Applications of Transport in Porous Media, vol. 23. Springer, 834 p.
- Diersch, H.-J.G., 2014. FEFLOW: Finite Element Modeling of Flow, Mass and Heat Transport in Porous and Fractured Media. Springer-Verlag, Berlin, Heidelberg, 996 p.
- Doherty, J., 2014. PEST, Model-independent Parameter Estimation. User Manual (fifth ed., with slight additions). Watermark Numerical Computing, Brisbane, Australia.
- Doherty, J., 2015. Calibration and Uncertainty Analysis for Complex Environmental Models. Watermark Numerical Computing, Brisbane, Australia, ISBN: 978-0-9943786-0-6, 227 p.
- Fetter, C.W., 2001. Applied Hydrogeology, fourth ed. Pearson Education Limited, Prentice Hall, Upper Saddle River, N.J., 612 p.



- Fienen, M.N., D’Oria, M., Doherty, J.E., Hunt, R.J., 2013. Approaches in Highly Parameterized Inversion: BgaPEST, a Bayesian Geostatistical Approach Implementation with PEST. U.S. Geological Survey Techniques and Methods Report 7(C9), 86 p. <http://pubs.usgs.gov/tm/07/c09/>.
- Fitts, C.R., 2013. Groundwater Science, second ed. Academic Press, London, 672 p.
- Hill, M.C., Tiedeman, C.R., 2007. Effective Groundwater Model Calibration. John Wiley & Sons, Hoboken, N.J., 455 p.
- Hunt, R.J., Zheng, C., 2012. The current state of modeling. Groundwater 50 (3), 329–333.
- Kresic, N., 2007. Hydrogeology and Groundwater Modeling, second ed. CRC Press, Boca Raton, FL, 807 p.
- Schwartz, F.W., Zhang, H., 2003. Fundamentals of Ground Water. John Wiley & Sons, Hoboken, N.J., 583 p.
- Todd, D.K., Mays, L.W., 2005. Groundwater Hydrology, third ed. John Wiley & Sons, Inc., Hoboken, N.J., 636 p.
- Wang, H.F., Anderson, M.P., 1982. Introduction to Groundwater Modeling: Finite Difference and Finite Element Methods. Academic Press, San Diego, CA, 237 p.
- Welter, D.E., Doherty, J.E., Hunt, R.J., Muffels, C.T., Tonkin, M.J., Schreüder, W.A., 2012. Approaches in Highly Parameterized Inversion—PEST++, a Parameter ESTimation Code Optimized for Large Environmental Models. U.S. Geological Survey Techniques and Methods 7(C5), 47 p. <http://pubs.usgs.gov/tm/tm7c5/>.
- Zheng, C., Bennett, G.D., 2002. Applied Contaminant Transport Modeling, second ed. John Wiley & Sons, New York, 621 p.

## DISCLAIMER

The material in this book is intended to guide those familiar with the basics of hydrogeology and groundwater flow modeling in developing numerical groundwater flow models of field problems. Although the information in this book is presented in the belief that it will help the reader to minimize errors, no responsibility is assumed by the authors, the U.S. Government and other institutions with which the authors are affiliated, or the publishers for any errors, mistakes, or misrepresentations that may occur from the use of this book, and no compensation will be given for any damages or losses whatever their cause.

Any use of trade, firm, or product names is for descriptive purposes only and does not imply endorsement by the U.S. Government.

## ACKNOWLEDGMENTS

We are indebted to the many valuable comments by our reviewers who read the book in manuscript form. We especially thank Charles Andrews and Rodney Sheets who read the entire book and provided many helpful technical and editorial comments and Kevin Breen for his thorough and careful review of a near final version of the manuscript. Michael Cardiff, Michael Fienen, Andrew Leaf, and Jeremy White provided thoughtful and detailed comments on Chapters 9 and 10. Hans-Jörg Diersch, Henk Haitjema, and Kurt Zeiler gave us valuable comments on other chapters.

We also thank the many individuals who provided insights and help in conversations and via email over the years, including Daron Abby, Daniel Abrams, William Arnold, Jean Bahr, Mark Bakker, Paul Barlow, Brian Barnett, Okke Batelaan, Jordi Batlle-Aguilar, Steffen Birk, Kenneth Bradbury, John Bredehoeft, Philip Brunner, John Cherry, Steen Christensen, Brian Clark, K. William Clark, Thomas Clemo, Peter Cook, Le Dung Dang, Alyssa Dausman, Geoff Delin, Martin Dietzel, John Doherty, Matthew Ely, Daniel Feinstein, Charles Fitts, Devin Galloway, Joseph Guillaume, Keith Halford, Randall Hanson, Arlen Harbaugh, Glenn Harrington, David Hart, Mary Hill, Joseph Hughes, Steven Ingebritsen, Dylan Irvine, Anthony Jakeman, Scott James, Igor Jankovic, Paul Juckem, Elizabeth Keating, Victor Kelson, Stefan Kollet, Leonard Konikow, James Krohelski, Eve Kuniansky, Christian Langevin, Stanley Leake, Yu-Feng Lin, Fabien Magri, Marco Maneta, Steve Markstrom, Gregoire Mariethoz, Luis Marin, Ghislain de Marsily, Paul Martin, James McCallum, David McWhorter, Steffen Mehl, Allen Moench, Leanne Morgan, Eric Morway, Shlomo Neuman, Christopher Neuzil, Christopher Neville, Tracy Nishikawa, Richard Niswonger, Saskia Noorduijn, Gunnar Nützmann, Thomas Osborne, Sorab Panday, Berh Parker, Adam Perine, Eileen Poeter, Vincent Post, David Prudic, Larry Putnam, Todd Rayne, R. Steve Regan, James Rumbaugh, Willem Schreüder, Margaret Shanafield, Craig Simmons, Campbell Stringer, Otto Strack, Michael Sukop, Amelia Tallman, Michael Teubner, Lloyd Townley, Herbert Wang, Lieke Van Roosmalen, Chani Welch, David Welter, Adrian Werner, Stephen Westenbroek, Gerfried Winkler, Ray Wuolo, Yueqing Xie, Richard Yager, Chunmiao Zheng, Vitaly Zlotnik, and members of the 2011 and 2012 NCGRT Modeling and Research Groups at Flinders University, Australia. Marie Dvorzak provided library assistance at UW-Madison. Mary Devitt and her Crossroads Coffeehouse staff are kindly thanked for providing “office space” and “fuel” for a portion of the writing process.

Last but not least, we thank our families especially our spouses, and James and Johanna Hunt for their patience.

*I can no other answer make but thanks,  
And thanks, and ever thanks*

—*Twelfth Night, Act III, Scene III*



# CHAPTER 1

## Introduction

*Science, like art, is not a copy of nature but a re-creation of her.*

*Jacob Bronowski (1956, Science and Human Values Part 1)*

### Contents

1.1 Motivation for Modeling	3
1.2 What Is a Model?	5
1.2.1 Physical Models	5
1.2.2 Mathematical Models	5
1.3 Purpose of Modeling	9
1.3.1 Forecasting/Hindcasting Models	9
1.3.2 Interpretative Models	11
1.4 Limitations of Models	11
1.4.1 Nonuniqueness	12
1.4.2 Uncertainty	12
1.5 Modeling Ethics	13
1.5.1 Model Design	14
1.5.2 Bias	14
1.5.3 Presentation of Results	15
1.5.4 Cost	15
1.6 Modeling Workflow	16
1.6.1 Steps in the Workflow	17
1.6.2 Verification and Validation	19
1.7 Common Modeling Errors	20
1.8 Use of This Text	20
1.9 Problems	21
References	22

### Boxes

Box 1.1 Data-Driven (Black-Box) Models	6
--	---

## 1.1 MOTIVATION FOR MODELING

Groundwater hydrologists are often asked questions about groundwater flow systems and management of groundwater resources. The following is a representative sampling of these types of questions.

*How will pumping affect groundwater levels in the North China Plain in the next 100 years?  
How will proposed land use change affect groundwater discharge to wetlands and streams in  
Madison, Wisconsin, USA?*

*How will water management decisions related to water diversions affect groundwater levels in the  
Nubian Sandstone of Egypt and Libya in the next 50 years?*

*How will climate change affect groundwater levels and groundwater discharge to surface water  
bodies in temperate forests in northern Wisconsin, USA?*

*How long will it take for water levels in a lake created as a result of open pit mining in Guyana to  
reach equilibrium after dewatering operations cease?*

*What is the capture area of a well field that supplies municipal water to Graz, Austria?*

*Where and when should groundwater be sampled to identify potential leakage of a clay liner  
beneath a landfill in Mexico City?*

*How long will it take contaminants leaching into groundwater from an abandoned industrial site  
in Tokyo to reach the property boundary?*

Providing answers to these seemingly straightforward questions requires considerable specific hydrogeologic information and analyses, as well as general hydrogeologic knowledge, insight, and professional judgment. Even relatively simple groundwater problems require values of aquifer parameters and hydrologic stresses such as pumping and recharge rates.

A groundwater model provides a quantitative framework for synthesizing field information and for conceptualizing hydrogeologic processes. The organization imposed by a model helps alert the modeler to errors in assumptions and to processes not previously considered. In other words: "...applying a model is an exercise in thinking about the way a system works" (Anderson, 1983). For this reason, mathematical modeling should be performed at the beginning of every hydrogeological study that addresses nontrivial questions (e.g., see Bredehoeft and Hall, 1995).

Tóth (1963) gave compelling justification for modeling, which is still valid today: "Whereas it is practically impossible to observe separately all phenomena connected with a regime of groundwater flow, a correct theory discloses every feature and draws attention to the most important properties of the flow." Or put another way, given that the subsurface is hidden from view and analysis is hampered by lack of field observations, a model is the most defensible description of a groundwater system for informed and quantitative analyses as well as forecasts about the consequences of proposed actions.

Therefore, although not all hydrogeological problems require a model, almost every groundwater problem will benefit from some type of model, if only as a way to organize field data and test the conceptual model. A corollary to the question "why model?" is the question "what else if not a model?" In the 1st edition of this book we included discussion of the debate over the worth of models then current in the literature. Today, groundwater models are accepted as essential tools for addressing groundwater problems.

## 1.2 WHAT IS A MODEL?

A *model* is a simplified representation of the complex natural world. For example, a road map is a kind of model (Wang and Anderson, 1982); it depicts a complex network of roads in a simplified manner for purposes of navigation. Similarly, a conceptual model of a groundwater system simplifies and summarizes what is known about the hydrogeology in the form of written text, flow charts, cross sections, block diagrams, and tables. A conceptual model is an expression of the past and current state of the system based on field information from the site, and knowledge available from similar sites (Section 2.2). A more powerful groundwater model is one that quantitatively represents heads in space and time in a simplified representation of the complex hydrogeologic conditions in the subsurface. Broadly speaking, groundwater models can be divided into physical (laboratory) models and mathematical models.

### 1.2.1 Physical Models

Physical models include laboratory tanks and columns packed with porous material (usually sand) in which groundwater heads and flows are measured directly. For example, in pioneering work Darcy (1856) measured head in sand-packed columns of various diameters and lengths to show that flow in porous media is linearly related to the head gradient. Physical models are mostly used at the laboratory scale (e.g., Mamer and Lowry, 2013; Illman et al., 2012; Sawyer et al., 2012; Fujinawa et al., 2009). Analog models are laboratory models that rely on the flow of electric current (electric analog models; e.g., Skibitzke, 1961) or viscous fluids (Hele-Shaw or parallel plate models; e.g., Collins and Gelhar, 1971) to represent groundwater flow. Analog models of groundwater flow, especially electric analog models, were important in the 1960s before digital computers were widely available (e.g., see Bredehoeft, 2012).

### 1.2.2 Mathematical Models

We consider two types of mathematical models: data-driven models and process-based models. *Data-driven or “black-box” models* (Box 1.1) use empirical or statistical equations derived from the available data to calculate an unknown variable (e.g., head at the water table) from information about another variable that can be measured easily (e.g., precipitation). *Process-based models* (sometimes called physically based models although that usage is discouraged by Beven and Young, 2013) use processes and principles of physics to represent groundwater flow within the problem domain. Process-based models are either stochastic or deterministic. A model is *stochastic* if any of its parameters have a probabilistic distribution; otherwise, the model is *deterministic*. The focus of our book is process-based deterministic models, although we briefly discuss stochastic models in Boxes 10.1 and 10.4 and Section 12.5.

A process-based mathematical groundwater flow model consists of a *governing equation* that describes the physical processes within the problem domain; *boundary conditions* that specify heads or flows along the boundaries of the problem domain; and for time-dependent problems, *initial conditions* that specify heads within the problem domain at the beginning of the simulation. Mathematical models can be solved analytically or numerically. Mathematical models for groundwater flow are solved for the distribution of head in space and also in time for transient problems.

Analytical models require a high level of simplification of the natural world in order to define a problem that can be solved mathematically to obtain a closed-form solution. The resulting analytical solution is an equation that solves for a dependent variable (e.g., head) in space and for transient problems also in time. Simple analytical solutions can be solved using a hand calculator but more complex solutions are often solved using a spreadsheet or a computer program (e.g., Barlow and Moench, 1998), or special software (e.g., MATLAB, <http://www.mathworks.com/products/matlab/>). Assumptions built into analytical solutions limit their application to relatively simple systems and hence they are inappropriate for most practical groundwater problems. For example, few analytical solutions allow for three-dimensional flow or hydrogeological settings with heterogeneity or boundaries with realistic geometries. Numerical models are even replacing the Theis (1935) analytical solution for aquifer test analysis (e.g., Li and Neuman, 2007; Yeh et al., 2014). Nevertheless, analytical solutions are still useful for some problems

### Box 1.1 Data-Driven (Black-Box) Models

Data-driven models use equations that calculate system response (e.g., head) to input stresses (e.g., recharge from precipitation) without quantifying the processes and physical properties of the system. First, a site-specific equation is developed by fitting parameters either empirically or statistically to reproduce the historical record (time series) of fluctuations in water levels (or flows) in response to stresses. Then, the equation is used to calculate the response to future stresses. Data-driven models require a large number of observations of head that ideally encompass the range of all expected stresses to the system. They are used by themselves (e.g., Bakker et al., 2007) or with a process-based model (e.g., Gusyev et al., 2013; Demissie et al., 2009; Szidarovszky et al., 2007).

Early applications of data-driven models analyzed the response of karst aquifers (Dreiss, 1989) and applications to karst systems continue to be popular and successful (Fig. B1.1.1). Artificial neural network (ANN) models are data-driven models that have received much interest in the recent literature (e.g., Sepúlveda, 2009; Feng et al., 2008; Coppola et al., 2005). Data-driven models are also developed using Bayesian networks (e.g., Fioren et al., 2013).

Generally, process-based models are preferred over data-driven models because process-based models can make acceptable forecasts when large numbers of observations are not available and when future conditions lie outside the range of stresses in the historical record, such as response to climate change.



Box 1.1—cont'd

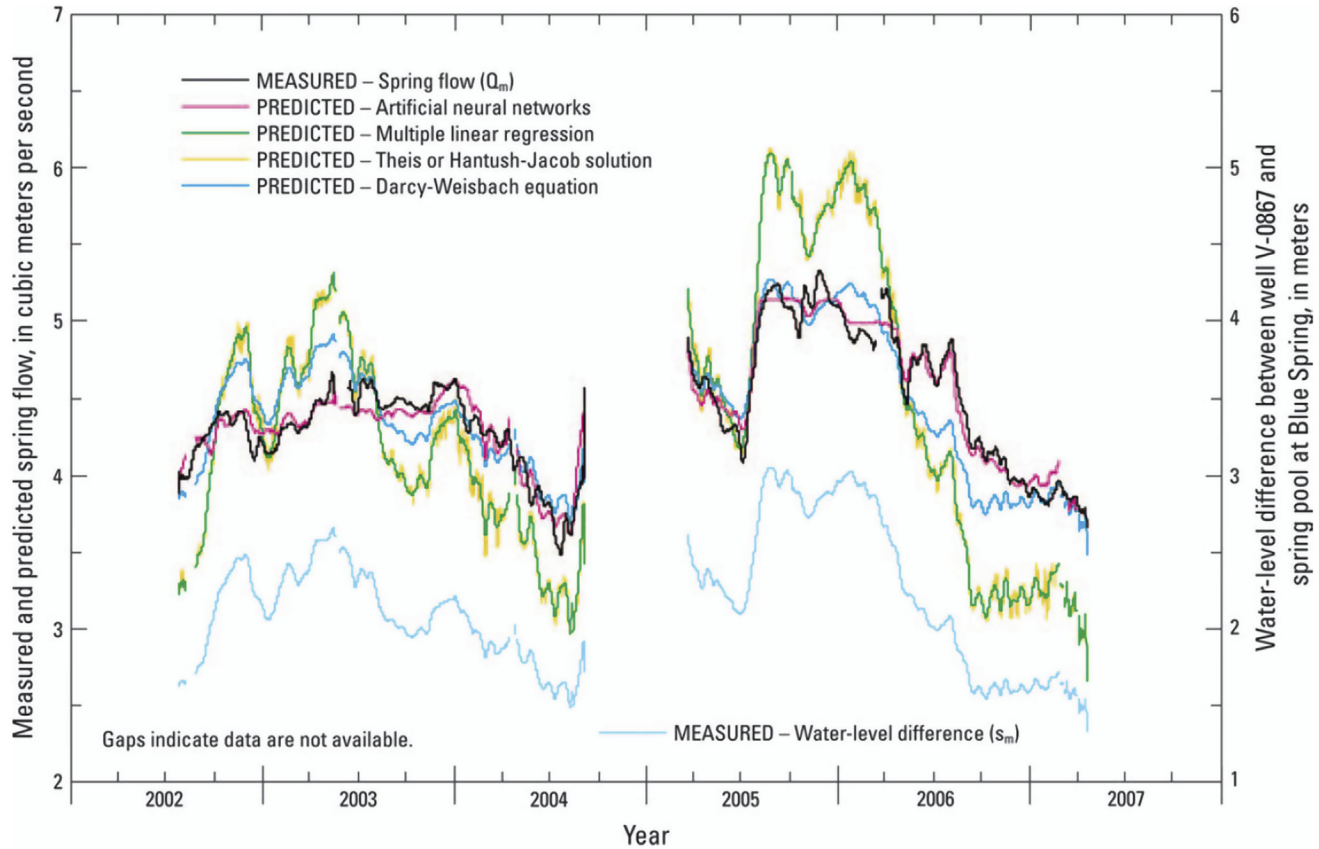


**Figure B1.1.1** Springflow calculated using an ANN model and multiple linear regression compared with results from process-based models for continuous porous media (Theis or Hantush–Jacob solutions) and conduit flow (Darcy–Weisbach equation). Measured springflow is also shown (Sepúlveda, 2009).

and also provide important insight into the behavior of groundwater systems (Box 3.2). Analytical models can be useful interpretive tools to guide construction of more complex numerical models (Haitjema, 2006). Analytical solutions are also used to verify that codes that solve numerical models are programmed correctly (Section 1.6).

The analytic element (AE) method (Haitjema, 1995; Strack, 1989) provides a way to extend analytical solutions to more complex problems. The AE method relies on a computer code to superpose certain types of analytical solutions, known as analytic elements, which are based on Green's functions and include solutions with point/line sources and sinks. AE models can incorporate complex boundary geometry and zones of heterogeneity, but currently have limited applicability for highly heterogeneous and transient problems (Hunt, 2006), although development of new AE solutions is an active area of research (e.g., Kulman and Neuman, 2009). Currently, AE models are most commonly applied to two-dimensional and steady-state groundwater flow problems (e.g., see Hunt, 2006; Haitjema, 1995). AE models are also useful for guiding assignment of regional boundary conditions for three-dimensional and transient modeling (Section 4.4).

Numerical models, typically based on either the finite-difference (FD) or the finite-element (FE) method, allow for both steady-state and transient groundwater flow in three dimensions in heterogeneous media with complex boundaries and a complex network of sources and sinks. Owing to their versatility, FD and FE models are most commonly used to solve groundwater problems and are the focus of our book.

Mathematical groundwater models are used to simulate both local and regional settings. Although some questions can, and should, be addressed with analytical models or simple numerical models, many problems require a more sophisticated representation of the groundwater system. Increased computing power and new codes and tools allow complex and large regional systems to be efficiently simulated. The sophistication, or complexity, of a numerical model is often measured by the number of processes included and the number of layers, cells/elements, and parameters it contains. Numerical methods assign parameter values to points (nodes) in the model domain and it is not uncommon for models to have millions of nodes. For example, Frind et al. (2002) described a three-dimensional, 30-layer FE model of the Waterloo Moraine aquifer system (Ontario, Canada) that used 1,335,790 nodes and 2,568,900 elements. A three-dimensional FD model of the Lake Michigan Basin (Feinstein et al., 2010) used over two million nodes. Kollet et al. (2010) discussed groundwater models that contained  $8 \times 10^9$  FD cells. Although values of hydrogeologic parameters must be assigned to every node, cell, or element, in practice it is usual to delineate areas (zones) in the problem domain in which a constant value is assigned to all the nodes (Section 5.5). Hence, zonation effectively reduces the number of parameters. Other methods of parameterization and the issue of complexity in groundwater models are discussed in Chapter 9.

We use the term *groundwater model* or model to mean the mathematical representation and associated input data for a specific problem. A *code* is a computer program that

processes the input data for a specific model and solves the process-based equations (Section 3.2) that describe groundwater processes. A code is written in one or more computer languages and consists of a set of equations that is solved by a computer. For example, PEST and the FD code MODFLOW are written in the computer language Fortran; PEST++ and the FE code FEFLOW are written in C/C++. A code that solves for groundwater flow calculates head in space and time, along with associated quantities such as flow. A *particle tracking code* takes output from a groundwater flow code and calculates groundwater flowpaths and associated travel times (Chapter 8). Codes are sometimes called groundwater models but we distinguish between a specific application of a code, which is a model, and the code itself, which is the tool for solving the model. A different groundwater model is designed for each application whereas the same code is used to solve many different problems.

### 1.3 PURPOSE OF MODELING

The starting point of every groundwater modeling application is to identify the purpose of the model (Fig. 1.1). The most common purpose is to forecast the effects of some future action or hydrologic condition, but models are also used to re-create past conditions (hindcasting) and also as interpretive tools. Reilly and Harbaugh (2004, p. 3) identify five broad categories of problems for groundwater modeling: basic understanding of groundwater systems; estimation of aquifer properties; understanding the present; understanding the past; and forecasting the future. We group the first three of these categories into interpretive models and the last two into forecasting/hindcasting models. We discuss forecasting/hindcasting models first.

#### 1.3.1 Forecasting/Hindcasting Models

The objective of the vast majority of groundwater models is to forecast or predict results of a proposed action/inaction. Forecasting simulations are designed to address questions like those listed at the beginning of this chapter. We prefer the term forecast over prediction to emphasize that a forecast always contains some uncertainty. For example, a weather forecast is typically stated in terms of a probability (of rain, for example). Forecasting models (Chapter 10) are typically first tested by comparing model results to field measurements in a history matching exercise that is part of model calibration (Chapter 9). In history matching, parameters are adjusted within acceptable limits until model outputs, primarily heads and flows, give a satisfactory match to field-measured (observed) values. The calibrated model is then used as the base model for forecasting simulations.

*Hindcasting (or back-casting) models* are used to re-create past conditions. Hindcasting models may involve both a groundwater flow model and a contaminant transport model to simulate the movement of a contaminant plume. Examples of hindcasting models include those used in the well-known Woburn, Massachusetts Trial (Bair, 2001) and

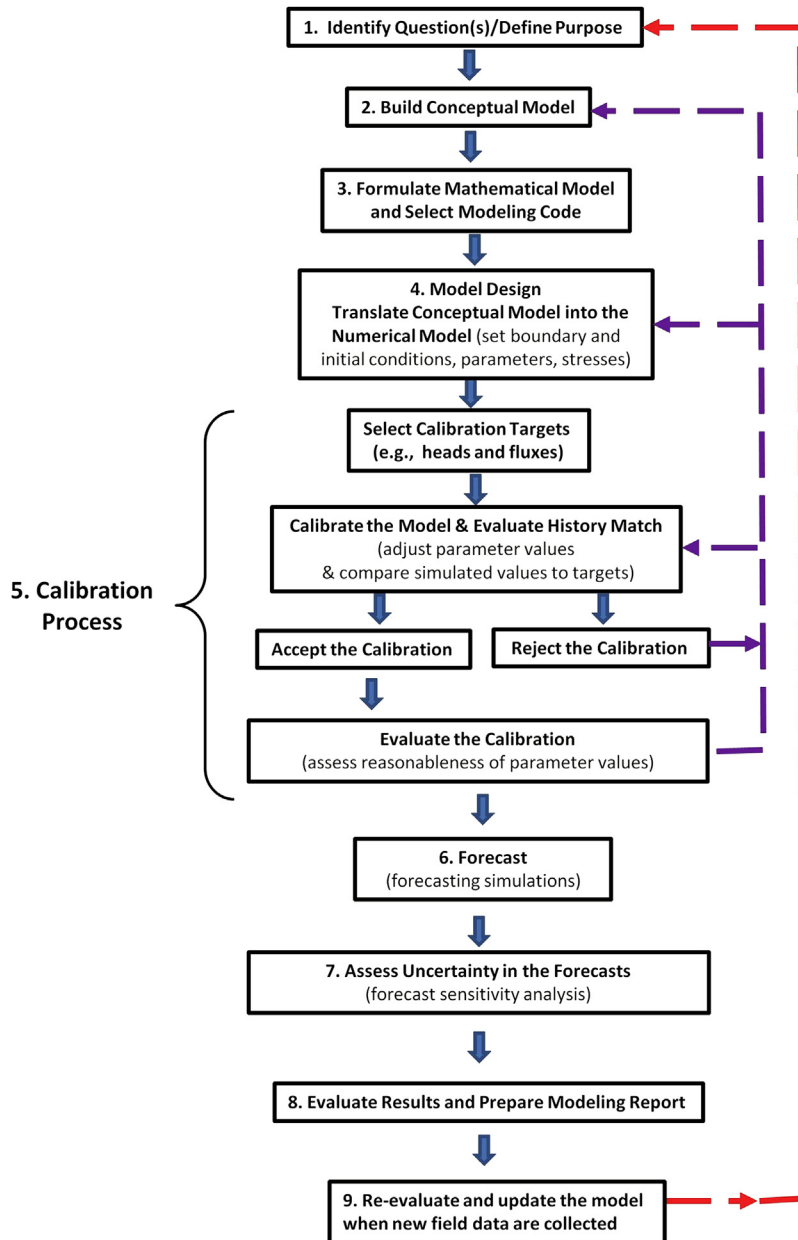


**Figure 1.1** Workflow for groundwater modeling. As presented, the workflow assumes the objective of the model is a forecast but the workflow can be adapted for other modeling purposes, as described in the text. Although not shown in the figure, field data are critical for the workflow, especially conceptual model design and the calibration process.

at a military base in North Carolina (Clement, 2011). Hindcasting applications are “uniquely challenging” (Clement, 2011) because it is not possible to collect additional observations to augment the existing historical dataset, which is often meager.

### 1.3.2 Interpretative Models

Interpretive models include those used as: (1) *engineering calculators* that quickly give an answer to a specific engineering question; (2) *screening models* that help the modeler develop an initial understanding of a groundwater system and/or test hypotheses about the system; (3) *generic models* that explore processes in generic hydrogeologic settings. Models used as engineering calculators and generic models usually are not calibrated. Screening models may or may not be calibrated.

An example application of an interpretive model as an engineering calculator is the use of analytical and numerical models to calculate aquifer parameters from drawdown data obtained in an aquifer (pumping) test. Analytical models and sometimes numerical models are used as engineering calculators to verify new codes (Section 1.6).

A screening model vets a conceptual model or tests hypotheses about the flow system. A screening model might help in designing a more complex numerical model. For example, Hunt et al. (1998) developed a two-dimensional AE model as a screening model to develop boundary conditions for a three-dimensional FD model. Interpretive models also are used to conceptualize system dynamics and provide general insights into controlling parameters or processes at a field site. For example, during a major oil spill from a damaged well in the Gulf of Mexico, Hsieh (2011) quickly developed an interpretive MODFLOW model (adapted to simulate flow in a petroleum reservoir) to determine if measured shut-in pressure in the damaged well was indicative of a potential future catastrophic rupture of the capped well. The results were used to make the decision not to uncap the well to reduce reservoir pressure, which proved to be the correct course of action.

Generic models are interpretive models applied to idealized groundwater systems. Generic models were used in the early days of numerical modeling of groundwater flow and continue to be useful. For example, Freeze and Witherspoon (1967) and Zlotnik et al. (2011) used two-dimensional generic models to study the effects of heterogeneity on regional groundwater flow in cross section. Woessner (2000) and Sawyer et al. (2012) used generic models to study exchange between groundwater and streams at the aquifer/stream interface (the hyporheic zone). Sheets et al. (2005) used generic models to assess the effect of pumping near regional groundwater divides.

## 1.4 LIMITATIONS OF MODELS

Groundwater models are simplifications of reality and thus are limited by underlying simplifying approximations as well as by nonuniqueness and uncertainty (Chapters 9

and 10). Groundwater models never uniquely represent the complexity of the natural world. Therefore, groundwater models that represent the natural world have some level of uncertainty that must be evaluated and reported. In that respect, forecasting simulations for groundwater are similar to weather forecasts. Weather forecasts combine extensive datasets, representations of atmospheric physics, meteorology, and real-time satellite images within a highly sophisticated model, but the daily forecast is always given with probabilities. Similarly, results from groundwater models should be qualified by specifying the nature and magnitude of uncertainty associated with a forecast (Section 10.6).

### 1.4.1 Nonuniqueness

Nonuniqueness in groundwater models means that many different combinations of model inputs produce results that match field-measured data. Consequently, there will always be more than one possible reasonable model. Although early groundwater modeling applications typically reported only one calibrated model and presented only one possible forecast, this is unacceptable practice today. Either multiple calibrated models are carried forward in the analysis or the modeler chooses a preferred calibrated model and constructs error bounds around forecasted outputs. In either case, it is acknowledged that a groundwater model cannot give a single true answer.

Although models are critical tools, professional judgment, guided by modeling intuition and hydrogeological principles, is always required during a modeling project. Recognition of model uncertainty and nonuniqueness motivates the following underlying philosophy of modeling: "...a model cannot promise the right answer. However, if properly constructed, a model can promise that the right answer lies within the uncertainty limits which are its responsibility to construct" (Doherty, 2011).

### 1.4.2 Uncertainty

Uncertainty in groundwater models (Sections 10.2, 10.3) arises from a number of factors related to representing groundwater processes. In selecting a particular code, the modeler indirectly makes assumptions about the set of hydrologic processes important to the modeling objective because the selection of a code in effect reduces all processes under consideration to only those included in the code. Furthermore, current and future hydrogeologic conditions represented in a model cannot be fully described or quantified. Hunt and Welter (2010) described one source of uncertainty as "unknown unknowns," which are "...things we do not know we don't know" (from Former US. Secretary of Defense Donald Rumsfeld, February 12, 2002 press briefing). In groundwater models, *unknown unknowns* include unexpected (and hence unmodeled) hydrogeologic features such as heterogeneities in subsurface properties, as well as unanticipated future stresses. Bredehoeft (2005) cautioned modelers to anticipate the model "surprise" that occurs when new data reveal system responses caused by unmodeled hydrologic processes. For example, in a forecasting model there is uncertainty over future hydrological

conditions (e.g., recharge rates) as well as future pumping rates and locations of new wells, which depend on uncertain societal and economic drivers.

Although some types of forecasts are more uncertain than others (Section 10.3), uncertainty can only be reduced, never eliminated. Therefore, groundwater modelers need to develop an awareness of the uncertainties that influence modeling results and a healthy skepticism of modeling output. Modeling intuition (Haitjema, 2006) and “hydrosense” (Hunt and Zheng, 2012) help a modeler evaluate modeling output and identify flawed results. Modeling processes and results need to undergo rigorous “sensitivity analyses” that are rooted in basic hydrogeologic principles.

## 1.5 MODELING ETHICS

Ethics refer to pursuing a course of action that leads to morally right outcomes. Ethics in groundwater modeling means that the groundwater modeler acts in a morally responsible manner when planning, designing, and executing models and presenting modeling results. Ethics also means that the modeler remains unbiased and objective and strives to model according to the best available science for the modeling purpose. The modeler must maintain scientific integrity even when the results are not what the client expects, and when models enter regulatory and legal arenas. Tensions can arise between the modeler and teams of interdisciplinary scientists, lawyers, regulators, and stakeholders including industrial clients and the public-at-large. The modeler must resist inappropriate pressure from those groups as well as the pressure of societal, environmental, and regulatory concerns and steadfastly perform ethical modeling.

Modeling may be driven by regulatory concerns or even mandated by regulations. For example, groundwater models are required by the European Water Framework Directive (Hulme et al., 2002) or regulations may be written in such a way that the best (perhaps even only) way to satisfy a regulatory obligation is by groundwater modeling. When models are discussed in the courtroom, the modeler must be especially vigilant to present objective, unbiased results based on sound science. The U.S. Federal Court trial regarding groundwater contamination in Woburn, Massachusetts, which was the subject of a popular book (Harr, 1995) and a movie (*A Civil Action*), was notable for the conflict and confusion that surrounded the interpretation of the hydrogeologic system (Bair, 2001; Bair and Metheny, 2011; also see *Science in the Courtroom: The Woburn Toxic Trial*: <http://serc.carleton.edu/woburn/index.html>). In that case, competing groundwater models (a one-dimensional steady-state model and a three-dimensional, transient model) and differences in opinion among three expert witnesses over the basic hydrogeology and appropriate parameter values led to difficulties in fact-finding needed to reach a verdict.

Ethical issues may arise over decisions about model design (especially as related to model complexity), model bias, presentation of results, and costs of modeling. Each of these is discussed below.

### 1.5.1 Model Design

In designing a model, the groundwater hydrologist, sometimes in concert with the client, regulators and stakeholders, proposes the analyses best suited to address the question(s) being posed. A numerical groundwater model may not be necessary if the questions can be answered more effectively using an analytical solution, an AE model, a data-driven model (Box 1.1), or analysis of field data without a model. For example, Kelson et al. (2002) showed that a simple AE model quickly provided the same insight into the effects of dewatering caused by a proposed mine as complex three-dimensional numerical models. However, for many complex problems a numerical model may be the best way to answer the questions. For the mine site considered by Kelson et al. (2002), questions about on-site disposal of mine tailings and the potential for contamination of groundwater and surface water were best addressed with a more comprehensive numerical model.

It may be clear before, during, or after a modeling effort that the available data are inadequate to constrain modeling results to a reasonable range suitable for decision-making. Clement (2011) discussed a highly complex state-of-the-art numerical hindcasting model where the historical data were judged insufficient to support the modeling effort. An independent panel of experts recommended that future hindcasting models for other parts of the site utilize simpler models including analytical models. The modelers disagreed with that assessment (Maslia et al., 2012), arguing that complex models are useful even when not fully supported by field data. The argument over simplicity *vs* complexity when designing groundwater models is a common topic in the literature (e.g., Simmons and Hunt, 2012; Hunt et al., 2007; Hill, 2006; Gómez-Hernández, 2006). Models should include processes and parameters essential to addressing the model's purpose, but exclude those that are not. Defining the optimal compromise between simplicity and complexity is part of the art of modeling and is one of the biggest challenges in modeling (Doherty, 2011). Simplifications come in many forms—for example, in the processes included or excluded from the model, and in the discretization of space and time, selection of boundary conditions, and parameter assignment. Each decision to simplify the complex natural world will influence the model's ability to simulate some facet of the actual hydrogeologic conditions.

### 1.5.2 Bias

Critics of modeling argue that models can be designed to produce whatever answer the modeler wants. Professionalism and ethics, however, require the modeler to design the model without introducing approximations that bias results. A simple example of deliberate bias is if a modeler consciously and inappropriately assigns a specified head boundary condition in order to minimize drawdown from pumping. (A specified head boundary allows an infinite amount of water to flow into the model and thereby mitigates the effect



of pumping by maintaining heads at unnaturally high levels (Section 4.3).) Concerns over bias motivate a requirement for peer review of modeling reports (Section 11.4). In-house review by senior hydrogeologists or engineers and by outside experts, regulators, opposing parties, and even the interested public is common. Quality assurance review can be helpful to the modeler in identifying inadvertent modeling errors, but when performed by an independent party, especially one engaged by an opposing party, such errors can support concerns of deliberate bias. The perception of bias is reinforced if either the modeler or reviewers neglect to reveal any potential conflicts of interest and areas of personal bias.

Critics often question whether a modeler paid by a client can remain independent and avoid bias. It is essential that modelers maintain their independence and preserve their professional credibility. The modeler has the obligation to give honest scientific and engineering assessments in return for compensation for work performed. The payment for work performed is not itself at issue but there may be the perception that the resulting model is biased to produce results favorable to the client. Such concerns over perceived bias can be addressed by careful and deliberate presentation of results, as discussed below.

### 1.5.3 Presentation of Results

With today's sophisticated codes and graphics packages it is relatively easy to produce visually impressive figures and tables. But ethics require that assumptions and approximations built into the model are clearly identified in the modeling report and in oral presentations. Inadequacies in field data should be discussed and uncertainties in modeling results should be quantified and discussed. Directly addressing potential concerns about the model's trustworthiness helps safeguard the modeler against claims of bias. Preparation of the modeling report is discussed in Chapter 11.

### 1.5.4 Cost

The cost of designing and executing a numerical model is sometimes cited as a limitation of modeling, but we consider it an ethical concern. After an investment in hardware and software, the costs of modeling are primarily for the modeler's and modeling team's time. Obviously, a complicated model requires more time and money to construct than a simple model. Missteps in conceptualization, construction, execution, and interpretation of models cost time and money but are often an unavoidable part of the modeling process. Of course, models need field data, but field data are needed for any type of hydrogeologic analysis. Availability of funds may limit the type of model that can be constructed and the scope of the modeling effort; the modeler is ethically bound to provide the best possible model given the time and resources available. When cost is the dominant driver for the model presented, the report should clearly state how constraints on funding affected the design of the model and the output.

## 1.6 MODELING WORKFLOW

Steps in groundwater modeling (Fig. 1.1) follow the scientific method (Fig. 1.2). In the scientific method, a question is asked, a hypothesis is constructed and tested, then accepted or rejected. If rejected, the testing process is repeated with a revised hypothesis. Similarly, the workflow for groundwater modeling starts with a question. Modeling should never be an end in itself; a model is always designed to answer a specific question or set of questions. The question underpins all facets of the resulting groundwater model. A workflow for applying groundwater models in forecasting is presented in Fig. 1.1. The steps in the workflow build confidence in the model. Although not shown in the figure, field data and soft knowledge (i.e., any information that is not evaluated directly by model output) inform almost every step of the modeling process, especially the design of the conceptual model, parameterization, selection of calibration targets, and ending the calibration process.

The modeling process may start over when new field data become available and when there are new questions to answer. The cyclic nature of the workflow allows for the

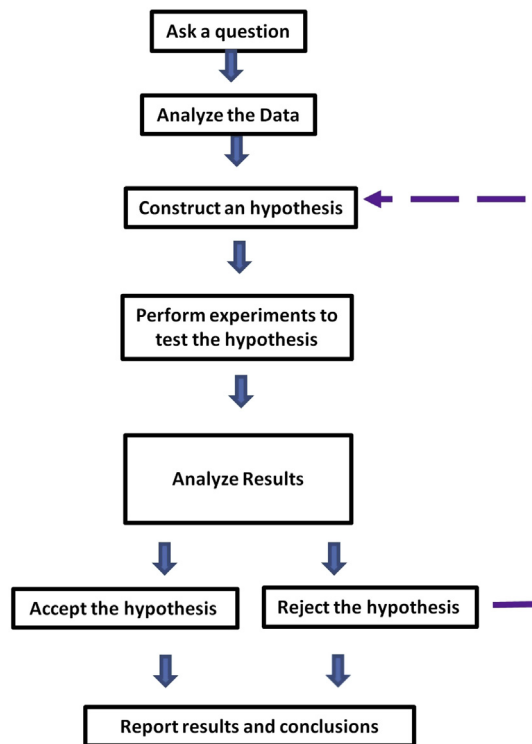


**Figure 1.2** The scientific method (modified from: [http://www.sciencebuddies.org/science-fair-projects/project\\_scientific\\_method.shtml](http://www.sciencebuddies.org/science-fair-projects/project_scientific_method.shtml)).

potential to improve and update the model when a calibrated groundwater model is used routinely as a decision-making tool in water resources management. Modelers in the UK are working toward establishing a set of calibrated models for aquifer systems throughout the UK for water resources management (Shepley et al., 2012). The Netherlands has a countrywide AE groundwater model (De Lange, 2006) and multimodel system for water resources management (De Lange et al., 2014); large regional models designed for water resources management are also being developed in the US (Reeves, 2010). More often, however, a model is developed to answer a specific question and after the decision is made, the model is rarely used again.

### 1.6.1 Steps in the Workflow

Our book is structured to discuss each of the steps in Fig. 1.1 as summarized below.

1. The purpose of the model (Chapter 2) is to answer a specific question or set of questions. The purpose is the primary factor in deciding appropriate simplifications and assumptions and thereby determines the characteristics of the mathematical model and drives code selection and model design.
2. The conceptual model (Chapter 2) consists of a description of the groundwater flow system including associated surface water bodies, as well as hydrostratigraphic units and system boundaries. Field data are assembled and the hydrogeologic system is described; water budget components are estimated. Multiple conceptual models may be constructed in order to account for uncertainty in describing the field setting. If the modeler did not collect the field data, a visit to the field site is recommended. A field visit will help put the hydrogeologic setting in perspective, give context to the assignment of parameter values and guide decisions during the modeling process.
3. The modeling purpose and the conceptual model drive the choice of a mathematical model and associated code(s) (Chapter 3). The mathematical model consists of a governing equation, boundary conditions, and, for transient problems, initial conditions. Numerical methods programmed into the code approximate the mathematical model.
4. Model design (Chapters 4–7) involves translating the conceptual model into a numerical groundwater flow model by designing the grid/mesh, setting boundaries, assigning values of aquifer parameters, and hydrologic stresses, and, for transient models, setting initial conditions and selecting time steps. The model is run using an initial set of parameter values (Section 5.5) based on the conceptual model. A particle tracking code (Chapter 8) is used to check flow directions and interactions with boundary conditions, and calculate flowpaths and travel times.
5. Arguably calibration (Chapter 9) is the most important step in the modeling process because it helps establish the legitimacy of the conceptual and numerical models. Moreover, the calibrated model is the base model for forecasting simulations. During

the calibration process, the modeler selects calibration targets and calibration parameters, and performs history matching. History matching consists of adjusting the initial parameter assignments in sequential model runs until field observations are sufficiently matched by the model and final parameter values are reasonable. A parameter estimation code helps find the values of calibration parameters that give the best possible match to the field observations (calibration targets). Modelers often do not allow sufficient time for calibration; a guideline is to start calibration no later than halfway (defined by the timeline and budget) through the project and preferably earlier.

6. Forecasting simulations (Chapter 10) use the calibrated model or a set of acceptably calibrated models to forecast the response of the system to future events; or the calibrated model is used to reconstruct past conditions in a hindcasting simulation. In both forecasts and hindcasts, the model is run using calibrated values for aquifer parameters and stresses except for stresses that change under future (or past) conditions. Estimates of anticipated future hydrologic conditions (e.g., recharge rates and pumping rates) are needed to perform the forecast; past hydrologic conditions are needed in hindcasts.
7. Uncertainty (Chapter 10) in a forecast (or hindcast) arises from uncertainty in the calibrated model, including its parameters, as well as uncertainty in the magnitude and timing of future (or past) hydrologic conditions. A forecasting uncertainty analysis includes assessment of measurement error, errors in the design of the model, and uncertainty in future (or past) hydrologic conditions important to the forecast (or hindcast). A particle tracking code may be used to forecast flowpaths and travel times (Chapter 8).
8. The results are presented in the modeling report and stored in the modeling archive (Chapter 11). The modeling report chronicles the modeling process, presents model results and states conclusions and limitations. It includes introductory material, information on the hydrogeologic setting, explanation of the data and assumptions used to formulate the conceptual model, and a reference to the numerical methods and code selected. The report also describes how the model domain is discretized and how parameters were assigned, documents model calibration and presents calibration results, forecasts and associated uncertainty. Modeling reports are accompanied by an archive that contains datasets, codes, input and output files and other materials needed to re-create and execute the model in the future.
9. When the opportunity arises it is useful to evaluate model performance by performing a postaudit. A *postaudit* (Section 10.7) compares the forecast with the response that actually occurred in the field as a result of the action that was simulated by the model. The postaudit is performed long enough after the forecast to allow adequate time for significant changes to occur in the field system. New field data collected during a postaudit may be used to improve the model. In *adaptive management* the model is routinely updated as new data become available and used to guide management decisions.

A forecasting simulation proceeds through steps 1 through 8. Engineering calculators and generic models require steps 1 through 4 and then skip to step 6. The steps in the workflow for a screening model depend on the purpose; the workflow always includes the first four steps and might proceed through step 5 or even steps 6, 7, and 8. If multiple possible conceptual models are considered (e.g., [Neuman and Wierenga, 2002](#)), the workflow is executed multiple times.

## 1.6.2 Verification and Validation

The terms model verification, code verification, and model validation are not in the workflow because verification and validation, as historically used, are no longer critical elements in groundwater modeling. However, because these terms are still in use, we discuss them below and also in Box 9.5.

*Model verification* refers to a demonstration that the calibrated model matches a set of field data independent of the data used to calibrate the model. However, given the large number of parameters involved in calibrating most field-based groundwater models, it is advisable to use all available data in the calibration exercise itself ([Doherty and Hunt, 2010](#), p. 15) rather than save some data for verification. Thus, groundwater model verification per se generally is not a useful exercise.

*Code verification* refers to a demonstration that a code can reproduce results from one or more analytical solutions or match a solution from a verified numerical code. Code verification is an important step in developing a code ([ASTM, 2008](#)) and information on code verification should be included in the user's manual. However, given that most applied modeling makes use of standard codes that have been verified by the code developer and well tested by the modeling community, additional code verification is not required for most modeling projects. Rather, it is reserved for cases when a new code is developed specifically for the modeling project or when an existing code is modified.

The term model validation has been much debated in the groundwater literature (e.g., [Konikow and Bredehoeft, 1992](#); associated comments and reply; [Bredehoeft and Konikow, 1993, 2012](#); [Anderson and Bates, 2001](#); [Hassan, 2004a,b](#); [Moriasi et al., 2012](#)). Validation has been equated with model calibration to suggest, incorrectly, that a calibrated model is a validated model. Furthermore, the term validation may incorrectly imply to nonmodelers that a model is capable of making absolutely accurate forecasts. This is fundamentally not supportable—truth cannot be demonstrated in any model of the natural world, or in any forecast using that model, because the truth is unknown ([Oreskes et al., 1994](#)). Therefore, models of the natural world cannot be validated in the same way as a computer code is verified or as a controlled laboratory experiment might be validated. Although such philosophical subtleties are not universally accepted, most groundwater modelers concur that a groundwater model cannot make absolutely

accurate forecasts and therefore cannot be validated. We recommend the term “validation” not be used in reference to a groundwater model.

The modeling workflow described above provides a generic structure for best modeling practice. Modeling guidelines also provide strategies for modeling but are formulated as required or recommended steps tailored to application in a regulatory procedure (e.g., Barnett et al., 2012; Neuman and Wierenga, 2002). Technical guidance manuals (e.g., Ohio EPA, 2007; Reilly and Harbaugh, 2004) describe general modeling procedures usually intended for a specific audience of modelers. The ASTM International (<http://www.astm.org/>) has published a variety of technical guidance documents on groundwater modeling (e.g., ASTM, 2006, 2008).

## 1.7 COMMON MODELING ERRORS

At the end of each chapter, we present modeling errors that we have found to be common mistakes and misconceptions in groundwater modeling. Because no such list can be inclusive, the reader will undoubtedly make modeling errors and encounter errors in the work of other modelers that are not included in our lists.

- The modeler does not allow enough time for calibration. Certainly formulation of the conceptual model and design of the numerical model are critical steps in groundwater modeling. However, modelers often spend so much time on those initial steps that they run out of time and budget for robust model calibration; we suggest that half of the project’s time and budget should be allocated for calibration.
- The modeler does not allow enough time for forecasting simulations. Modelers tend to think that the hard work of modeling is over when the model has been calibrated and assume that the forecasting simulations will be straightforward “production” runs. However, it is essential to perform an uncertainty analysis in conjunction with the forecast (Chapter 10) and uncertainty analysis may occupy more time than the modeler anticipates. Furthermore, sometimes surprises are encountered during the forecasting simulations that may require the modeler to revisit some of the earlier steps in the modeling workflow.
- The modeler does not allow enough time for report preparation. A readable and comprehensive modeling report is invaluable for reconstructing important modeling decisions and outcomes. A model is diminished without a good report to describe the model and its results.

## 1.8 USE OF THIS TEXT

Readers should be familiar with the basic principles of groundwater hydrology and basic concepts of groundwater modeling presented in standard hydrogeology textbooks such as Fitts (2013), Kresic (2007), Todd and Mays (2005), Schwartz and Zhang (2003), and

Fetter (2001). In Chapter 3, we review basic principles of FD and FE methods drawing on the elementary level text by Wang and Anderson (1982).

The problems following each chapter are intended to illustrate the main points of the chapter. Starting with Chapter 4, most of the problems require the use of an FD or FE code. Boxes amplify topics mentioned in the main text.

To supplement the material covered in the text, the reader is encouraged to consult the literature cited throughout the book as well as groundwater journals and modeling reports published by the US. Geological Survey and other governmental and regulatory groups. We have included links to many such resources on the companion Web site for this text (<http://appliedgwmodeling.elsevier.com>). The modeler can develop modeling intuition and hydrosense by studying the models described in journal papers and technical reports, starting with those cited in our book, and by the experience of developing and solving problems with models.

## 1.9 PROBLEMS

Problems for Chapter 1 are intended to introduce the modeling process and stimulate thinking about the level of modeling needed to address a stated modeling purpose.

- P1.1** List the type of groundwater model (i.e., forecasting or interpretive (engineering calculator, screening, or generic)) that would most likely be used to solve each of the following problems. List the assumptions you made to reach your decision.
- a. A regulatory agency wants to understand why the ages of water discharging from various springs that flow from an anisotropic and homogeneous sandstone aquifer are so variable. It is suggested that each spring is discharging water that is a mix of water coming from several different flowpaths, or that stratigraphic and structural controls affect groundwater residence times and thus determine the age of the spring discharge.
  - b. A lawyer wants a consultant to estimate seasonal fluctuations in the water table of an alluvial fan aquifer in Spain resulting from a change in the timing and distribution of groundwater recharge originating from flood irrigation practices. The change in recharge was brought about by recent litigation involving land ownership.
  - c. A consulting firm is tasked to determine the scales and magnitudes of aquifer heterogeneities that would cause a 25% reduction in the size of the capture zone of a well designed to pump contaminated water from what was thought to be a homogeneous unconfined outwash aquifer.
  - d. A stream ecologist wants to quantify the seasonal exchange of water between a stream and its contiguous floodplain aquifer.
  - e. An agency is planning a secure landfill for disposal of low-level nuclear waste in thick low permeability sedimentary deposits. The agency would like to assess

the effect of changes in recharge on rates and directions of groundwater flow at the proposed site.

- P1.2** Make a list of criteria you would use to determine if a model appropriately represented a particular hydrogeological system. Justify your selection and save the list for future reference.
- P1.3** Read a recent report prepared by a consultant or governmental agency that describes the application of a groundwater flow model in your geographical area. Identify the purpose of the model and the modeling question(s). How was the conceptual model presented (e.g., in text, cross sections, tables)? Describe the mathematical model and identify the code used to solve the model. Describe the calibration process. If the model was used for forecasting, discuss how the modeler(s) evaluated forecast uncertainty. Create a flow chart of the modeling process used and compare and contrast it to Fig. 1.1.

## REFERENCES

- Anderson, M.G., Bates, P.D. (Eds.), 2001. *Model Validation: Perspectives in Hydrological Science*. John Wiley & Sons, Ltd, London, 500 p.
- Anderson, M.P., 1983. Ground-water modeling—the emperor has no clothes. *Groundwater* 21 (6), 666–669. <http://dx.doi.org/10.1111/j.1745-6584.1983.tb01937.x>.
- ASTM International, 2006. Standard guide for subsurface flow and transport modeling, D5880–06. American Society of Testing and Materials, Book of Standards 04 (09), 6 p.
- ASTM International, 2008. Standard guide for developing and evaluating groundwater modeling codes, D6025–08. American Society of Testing and Materials, Book of Standards 04 (09), 17 p.
- Bair, E.S., 2001. Models in the courtroom. In: Anderson, M.G., Bates, P.D. (Eds.), *Model Validation: Perspectives in Hydrological Science*. John Wiley & Sons Ltd, London, pp. 55–77.
- Bair, E.S., Metheny, M.A., 2011. Lessons learned from the landmark “A Civil Action” trial. *Groundwater* 49 (5), 764–769. <http://dx.doi.org/10.1111/j.1745-6584.2008.00506.x>.
- Bakker, M., Maas, K., Schaars, F., von Asmuth, J., 2007. Analytic modeling of groundwater dynamics with an approximate impulse response function for areal recharge. *Advances in Water Resources* 30 (3), 493–504. <http://dx.doi.org/10.1016/j.advwatres.2006.04.008>.
- Barlow, P.M., Moench, A.F., 1998. *Analytical Solutions and Computer Programs for Hydraulic Interaction of Stream-aquifer Systems*. USGS Open-File Report: 98-415-A, 85 p. <http://pubs.usgs.gov/of/1998/of98-415A/>.
- Barnett, B., Townley, L.R., Post, V., Evans, R.F., Hunt, R.J., Peeters, L., Richardson, S., Werner, A.D., Knapton, A., Boronkay, A., 2012. *Australian Groundwater Modelling Guidelines*. Waterlines Report. National Water Commission, Canberra, 191 p. [http://nwc.gov.au/\\_\\_data/assets/pdf\\_file/0016/22840/Waterlines-82-Australian-groundwater-modelling-guidelines.pdf](http://nwc.gov.au/__data/assets/pdf_file/0016/22840/Waterlines-82-Australian-groundwater-modelling-guidelines.pdf).
- Beven, K., Young, P., 2013. A guide to good practice in modeling semantics for authors and referees. *Water Resources Research* 49, 5092–5098. <http://dx.doi.org/10.1002/wrcr.20393>.
- Bredehoeft, J., 2005. The conceptualization model problem—surprise. *Hydrogeology Journal* 13 (1), 37–46. <http://dx.doi.org/10.1007/s10040-004-0430-5>.
- Bredehoeft, J., 2012. Modeling groundwater flow—the beginnings. *Groundwater* 50 (3), 324–329. <http://dx.doi.org/10.1111/j.1745-6584.2012.00940.x>.
- Bredehoeft, J., Hall, P., 1995. Ground-water models. *Groundwater* 33 (4), 530–531. <http://dx.doi.org/>.
- Bredehoeft, J.D., Konikow, L.F., 1993. Ground-water models: Validate or invalidate. *Groundwater* 31 (2), 178–179 (Reprinted in *Groundwater* 50 (4), pp. 493–494). <http://dx.doi.org/10.1111/j.1745-6584.1993.tb01808.x>.



- Bredehoeft, J.D., Konikow, L.F., 2012. Reflections on our model validation editorial. *Groundwater* 50 (4), 495. <http://dx.doi.org/10.1111/j.1745-6584.2012.00951.x>.
- Clement, T.P., 2011. Complexities in hindcasting models—When should we say enough is enough? *Groundwater* 49 (5), 620–629. <http://dx.doi.org/10.1111/j.1745-6584.2010.00765.x>.
- Collins, M.A., Gelhar, L.W., 1971. Seawater intrusion in layered aquifers. *Water Resources Research* 7 (4), 971–979. <http://dx.doi.org/10.1029/WR007i004p00971>.
- Coppola, E., Rana, A., Poulton, M., Szidarovszky, F., Uhl, V., 2005. A neural network model for predicting aquifer water level elevations. *Groundwater* 43 (2), 231–241. <http://dx.doi.org/10.1111/j.1745-6584.2005.0003.x>.
- Darcy, H.P.G., 1856. Determination of the Laws of Water Flow through Sand, the Public Fountains of the City of Dijon, Appendix D – Filtration, Section 2 of Appendix D on Natural Filtration. Translated from the French by Patricia Bobeck. Kendall/Hunt Publishing Company, Iowa, 455–459.
- De Lange, W.J., 2006. Development of an analytic element ground water model of the Netherlands. *Groundwater* 44 (1), 111–115. <http://dx.doi.org/10.1111/j.1745-6584.2005.00142.x>.
- De Lange, W.J., Prinsen, G.F., Hoogewoud, J.C., Veldhuizen, A.A., Verkaik, J., Oude Essink, G.H.P., van Walsum, P.E.V., Delsman, J.R., Hunink, J.C., Massop, H.Th.L., Kroon, T., 2014. An operational, multi-scale, multi-model system for consensus-based, integrated water management and policy analysis: The Netherlands Hydrological Instrument. *Environmental Modelling & Software* 59, 98–108. <http://dx.doi.org/10.1016/j.envsoft.2014.05.009>.
- Demissie, Y., Valocchi, A.J., Minsker, B.S., Bailey, B., 2009. Integrating physically-based groundwater flow models with error-correcting data-driven models to improve predictions. *Journal of Hydrology* 364 (3–4), 257–271. <http://dx.doi.org/10.1016/j.jhydrol.2008.11.007>.
- Doherty, J., 2011. Modeling: Picture perfect or abstract art? *Groundwater* 49 (4), 455. <http://dx.doi.org/10.1111/j.1745-6584.2011.00812.x>.
- Doherty, J.E., Hunt, R.J., 2010. Approaches to Highly Parameterized Inversion: A Guide to Using PEST for Groundwater-Model Calibration. U.S. Geological Survey Scientific Investigations Report 2010–5169, 60 p. <http://pubs.usgs.gov/sir/2010/5169/>.
- Dreiss, S.J., 1989. Regional scale transport in a karst aquifer: 2. Linear systems and time moment analysis. *Water Resources Research* 25 (1), 126–134. <http://dx.doi.org/10.1029/WR025i001p00126>.
- Fienen, M.N., Masterson, J.P., Plant, N.G., Gutierrez, B.T., Thieler, E.R., 2013. Bridging groundwater models and decision support with a Bayesian network. *Water Resources Research* 49 (10), 6459–6473. <http://dx.doi.org/10.1002/wrcr.20496>.
- Feinstein, D.T., Hunt, R.J., Reeves, H.W., 2010. Regional Groundwater-Flow Model of the Lake Michigan Basin in Support of Great Lakes Basin Water Availability and Use Studies. U.S. Geological Survey Scientific Investigations Report 2010–5109, 379 p. <http://pubs.usgs.gov/sir/2010/5109/>.
- Feng, S., Kang, S., Huo, Z., Chen, S., Mao, X., 2008. Neural networks to simulate regional ground water levels affected by human activities. *Groundwater* 46 (1), 80–90. <http://dx.doi.org/10.1111/j.1745-6584.2007.00366.x>.
- Fetter, C.W., 2001. *Applied Hydrogeology*, fourth ed. Prentice Hall, 598 p.
- Fitts, C.R., 2013. *Groundwater Science*, second ed. Academic Press, London, 672 p.
- Freeze, R.A., Witherspoon, P.A., 1967. Theoretical analysis of regional ground-water flow: 2. Effect of water table configuration and subsurface permeability variations. *Water Resources Research* 3 (2), 623–634. <http://dx.doi.org/10.1029/WR003i002p00623>.
- Frind, E.O., Muhammad, D.S., Molson, J.W., 2002. Delineation of three-dimensional well capture zones for complex multi-aquifer systems. *Groundwater* 40 (6), 586–598. <http://dx.doi.org/10.1111/j.1745-6584.2002.tb02545.x>.
- Fujinawa, K., Iba, T., Fujihara, Y., Watanabe, T., 2009. Modeling interaction of fluid and salt in an aquifer/lagoon system. *Groundwater* 47 (1), 35–48. <http://dx.doi.org/10.1111/j.1745-6584.2008.00482.x>.
- Gómez-Hernández, J.J., 2006. Complexity. *Groundwater* 44 (6), 782–785. <http://dx.doi.org/10.1111/j.1745-6584.2006.00222.x>.
- Gusyev, M.A., Haitjema, H.M., Carlson, C.P., Gonzalez, M.A., 2013. Use of nested flow models and interpolation techniques for science-based management of the Sheyenne National Grassland, North Dakota, USA. *Groundwater* 51 (3), 414–420. <http://dx.doi.org/10.1111/j.1745-6584.2012.00989.x>.

- Haitjema, H.M., 1995. Analytic Element Modeling of Groundwater Flow. Academic Press, Inc., San Diego, CA, 394 p.
- Haitjema, H., 2006. The role of hand calculations in ground water flow modeling. *Groundwater* 44 (6), 786–791. <http://dx.doi.org/10.1111/j.1745-6584.2006.00189.x>.
- Harr, J., 1995. *A Civil Action*. Random House, New York, 512 p.
- Hassan, A.E., 2004a. Validation of numerical ground water models used to guide decision making. *Groundwater* 42 (2), 277–290. <http://dx.doi.org/10.1111/j.1745-6584.2004.tb02674.x>.
- Hassan, A.E., 2004b. A methodology for validating numerical ground water models. *Groundwater* 42 (3), 347–362. <http://dx.doi.org/10.1111/j.1745-6584.2004.tb02683.x>.
- Hill, M.C., 2006. The practical use of simplicity in developing ground water models. *Groundwater* 44 (6), 775–781. <http://dx.doi.org/10.1111/j.1745-6584.2006.00227.x>.
- Hsieh, P.A., 2011. Application of MODFLOW for oil reservoir simulation during the Deepwater Horizon crisis. *Groundwater* 49 (3), 319–323. <http://dx.doi.org/10.1111/j.1745-6584.2011.00813.xs>.
- Hulme, P., Fletcher, S., Brown, L., 2002. Incorporation of groundwater modeling in the sustainable management of groundwater resources. In: Hiscock, K.M., Rivett, M.O., Davison, R.M. (Eds.), *Sustainable Groundwater Development*. Special Publication 193, Geological Society of London, pp. 83–90.
- Hunt, R.J., 2006. Review paper: Ground water modeling applications using the analytic element method. *Groundwater* 44 (1), 5–15. <http://dx.doi.org/10.1111/j.1745-6584.2005.00143.x>.
- Hunt, R.J., Anderson, M.P., Kelson, V.A., 1998. Improving a complex finite difference groundwater-flow model through the use of an analytic element screening model. *Groundwater* 36 (6), 1011–1017. <http://dx.doi.org/10.1111/j.1745-6584.1998.tb02108.x>.
- Hunt, R.J., Doherty, J., Tonkin, M.J., 2007. Are models too simple? Arguments for increased parameterization. *Groundwater* 45 (3), 254–261. <http://dx.doi.org/10.1111/j.1745-6584.2007.00316.x>.
- Hunt, R.J., Welter, D.E., 2010. Taking account of “unknown unknowns”. *Groundwater* 48 (4), 477. <http://dx.doi.org/10.1111/j.1745-6584.2010.00681.x>.
- Hunt, R.J., Zheng, C., 2012. The current state of modeling. *Groundwater* 50 (3), 329–333. <http://dx.doi.org/10.1111/j.1745-6584.2012.00936.x>.
- Illman, W.A., Berg, S.J., Yeh, T.-C.J., 2012. Comparison of approaches for predicting solute transport: Sandbox experiments. *Groundwater* 50 (3), 421–431. <http://dx.doi.org/10.1111/j.1745-6584.2011.00859.x>.
- Kelson, V.A., Hunt, R.J., Haitjema, H.M., 2002. Improving a regional model using reduced complexity and parameter estimation. *Groundwater* 40 (2), 132–143. <http://dx.doi.org/10.1111/j.1745-6584.2002.tb02498.x>.
- Kollet, S.J., Maxwell, R.M., Woodward, C.S., Smith, S., Vanderborght, J., Vereecken, H., Simmer, C., 2010. Proof of concept of regional scale hydrologic simulations at hydrologic resolution utilizing massively parallel computer resources. *Water Resources Research* 46, W04201. <http://dx.doi.org/10.1029/2009WR008730>.
- Konikow, L.F., Bredehoeft, J.D., 1992. Ground-water models cannot be validated. *Advances in Water Resources* 15, 75–83. [http://dx.doi.org/10.1016/0309-1708\(92\)90033-X](http://dx.doi.org/10.1016/0309-1708(92)90033-X) (Also see comment by Marsily, G. de, Combes, P., Goblet, P., 1993. *Advances in Water Resources* 15, pp. 367–369. Reply by Bredehoeft, J.D., Konikow, L.F., pp. 371–172.).
- Kresic, N., 2007. *Hydrogeology and Groundwater Modeling*, second ed. CRC Press, Boca Raton, FL, 807 p.
- Kulman, K.L., Neuman, S.P., 2009. Laplace-transform analytic-element method for transient, porous-media flow. *Journal of Engineering Math* 64, 113–130. <http://dx.doi.org/10.1007/s10665-008-9251-1>.
- Li, Y., Neuman, S.P., 2007. Flow to a well in a five-layer system with application to the Oxnard Basin. *Groundwater* 45 (6), 672–682. <http://dx.doi.org/10.1111/j.1745-6584.2007.00357.x>.
- Mamer, E.A., Lowry, C.S., 2013. Locating and quantifying spatially distributed groundwater/surface water interactions using temperature signals with paired fiber-optic cables. *Water Resources Research* 49, 1–11. <http://dx.doi.org/10.1002/2013WR014235>.
- Maslia, M.L., Aral, M.M., Faye, R.E., Grayman, V.M., Suarez-Soto, R.J., Sautner, J.B., Anderson, B.A., Bove, J.F., Ruckart, P.Z., Moore, S.M., 2012. Comment on “complexities in hindcasting models—when should we say enough is enough”. *Groundwater* 50 (1), 1–16. <http://dx.doi.org/10.1111/j.1745-6584.2011.00884.x>.

- Moriasi, D.N., Wilson, B.N., Douglas-Mankin, K.R., Arnold, J.G., Gowda, P.H., 2012. Hydrologic and water quality models: Use, calibration and validation. *Transactions American Society of Agricultural and Biological Engineers* 55 (4), 1241–1247. <http://dx.doi.org/10.13031/2013.42265>.
- Neuman, S.P., Wierenga, P.J., 2002. A Comprehensive Strategy of Hydrogeologic Modeling and Uncertainty Analysis for Nuclear Facilities and Sites. NUREG/CF-6805, 236 p. <http://www.nrc.gov/reading-rm/doc-collections/nuregs/contract/cr6805/>.
- Ohio EPA (Environmental Protection Agency), 2007. Ground Water Flow and Fate and Transport Modeling, Technical Guidance Manual for Ground Water Investigations. Chapter 14, 32 p. <http://www.epa.state.oh.us/ddagw/>.
- Oreskes, N., Shrader-Frechette, K., Belitz, K., 1994. Verification, validation, and confirmation of numerical models in the Earth Sciences. *Science* 263 (5147), 641–646. <http://dx.doi.org/10.1126/science.263.5147.641>.
- Reeves, H.W., 2010. Water Availability and Use Pilot: A Multiscale Assessment in the U.S. Great Lakes Basin. U.S. Geological Survey Professional Paper 1778, 105 p. <http://pubs.usgs.gov/pp/1778/>.
- Reilly, T.E., Harbaugh, A.W., 2004. Guidelines for Evaluating Ground-Water Flow Models. U.S. Geological Survey Scientific Investigation Report 2004-5038, 30 p. <http://pubs.usgs.gov/sir/2004/5038/>.
- Sawyer, A.H., Cardenas, M.B., Buttle, J., 2012. Hyporheic temperature dynamics and heat exchange near channel-spanning logs. *Water Resources Research* 48. W01529. <http://dx.doi.org/10.1029/2011WR011200>.
- Schwartz, F.W., Zhang, H., 2003. *Fundamentals of Groundwater*. John Wiley & Sons, 583 p.
- Sepúlveda, N., 2009. Analysis of methods to estimate spring flows in a karst aquifer. *Groundwater* 47 (3), 337–349. <http://dx.doi.org/10.1111/j.1745-6584.2008.00498.x>.
- Sheets, R.A., Dumouchelle, D.H., Feinstein, D.T., 2005. Ground-Water Modeling of Pumping Effects Near Regional Ground-water Divides and River/Aquifer Systems – Results and Implications of Numerical Experiments. U.S. Geological Survey Scientific Investigations Report 2005-5141, 31 p. <http://pubs.usgs.gov/sir/2005/5141/>.
- Shepley, M.G., Whiteman, M.I., Hulme, P.J., Grout, M.W., 2012. Groundwater resources modelling: A case study from the UK, the Geological Society, London. Special Publication 364, 378 p.
- Simmons, C.T., Hunt, R.J., 2012. Updating the debate on model complexity. *GSA Today* 22 (8), 28–29. <http://dx.doi.org/10.1130/GSATG150GW.1>.
- Skibitzke, H.E., 1961. Electronic computers as an aid to the analysis of hydrologic problems. *International Association of Scientific Hydrology, Publ. 52* 347–358. *Comm. Subterranean Waters*, Gentbrugge, Belgium.
- Strack, O.D.L., 1989. *Groundwater Mechanics*. Prentice Hall, Englewood Cliffs, New Jersey, 732 p.
- Szidarovszky, F., Coppola, E.A., Long, J., Hall, A.D., Poulton, M.M., 2007. A hybrid artificial neural network-numerical model for ground water problems. *Groundwater* 45 (5), 590–600. <http://dx.doi.org/10.1111/j.1745-6584.2007.00330.x>.
- Theis, C.V., 1935. The relation between lowering of the piezometric surface and rate and duration of discharge of a well using ground-water storage. *Transactions of the American Geophysical Union* 16, 519–524.
- Todd, D.K., Mays, L.W., 2005. *Groundwater Hydrology*, third ed. John Wiley & Sons, Inc. 636 p.
- Tóth, J., 1963. A theoretical analysis of groundwater flow in small drainage basins. *Journal of Geophysical Research* 68, 4795–4812. <http://dx.doi.org/10.1029/JZ068i016p04795>.
- Wang, H.F., Anderson, M.P., 1982. *Introduction to Groundwater Modeling: Finite Difference and Finite Element Methods*. Academic Press, San Diego, CA, 237 p.
- Woessner, W.W., 2000. Stream and fluvial plain ground water interactions: Rescaling hydrogeologic thought. *Groundwater* 38 (3), 423–429. <http://dx.doi.org/10.1111/j.1745-6584.2000.tb00228.x>.
- Yeh, T.-C.J., Mao, D., Zha, Y., Hsu, K.-C., Lee, C.-H., Wen, J.C., Lu, W., Yang, J., 2014. Why hydraulic tomography works? *Groundwater* 52 (2), 168–172. <http://dx.doi.org/10.1111/gwat.12129>.
- Zlotnik, V.A., Cardenas, M.B., Toundykov, D., 2011. Effects of multiscale anisotropy on basin and hyporheic groundwater flow. *Groundwater* 49 (4), 576–583. <http://dx.doi.org/10.1111/j.1745-6584.2010.00775.x>.

## CHAPTER 2

# Modeling Purpose and Conceptual Model

*Everything should be made as simple as possible, but not simpler.*

*attributed to Albert Einstein*

### Contents

2.1 Modeling Purpose	28
2.2 Conceptual Model: Definition and General Features	29
2.3 Components of a Conceptual Model	35
2.3.1 Boundaries	35
2.3.2 Hydrostratigraphy and Hydrogeological Properties	37
2.3.3 Flow Direction and Sources and Sinks	51
2.3.4 Groundwater Budget Components	54
2.3.5 Ancillary Information	57
2.4 Uncertainty in the Conceptual Model	59
2.5 Common Modeling Errors	59
2.6 Problems	60
References	63

### Boxes

Box 2.1 Geographical Information Systems (GIS)	33
Box 2.2 Describing the Void Space	42

The first two steps in the modeling workflow (establishing the purpose and developing the conceptual model; Fig. 1.1) drive the rest of the modeling process. The modeling purpose distills the motivation and provides direction and context for the modeling exercise; the purpose dictates the selection of appropriate assumptions and simplifications and helps the modeler decide whether the calibrated model produced an acceptable match to field observations. The conceptual model summarizes what is known about the hydrogeological system and thereby provides a framework for designing the numerical model. Poor model calibration and/or failure to make accurate forecasts often can be attributed to an inappropriate, inaccurate, or insufficient conceptual model (Ye et al., 2010). Reviewers who perform quality assurance evaluations of models often spend a significant portion of time examining the strengths and weaknesses of the conceptual model.

## 2.1 MODELING PURPOSE

Constructing a numerical model is never an end in itself. The model is always designed to answer a specific question or set of questions. In practice, modeling is most commonly performed to forecast the effects of some future action or hydrologic condition, but models are also used to recreate past conditions and as interpretive tools (Section 1.3).

When defining the purpose, the modeler considers the question(s) that motivate the modeling exercise and specifies what will be learned from the model. A carefully constrained statement of the model's purpose is important because the purpose guides the design of the numerical model and is used to judge if the model appropriately met its objective. The purpose may be modified if the hydrogeological data are found to be inadequate to meet initial modeling objectives. Once the purpose is defined, the modeler should also confirm that a model is the best way to answer the question(s). The modeling purpose and the time and money available will determine whether the groundwater flow model is analytical or numerical; one-, two-, or three-dimensional; steady state or transient, and whether particle tracking or a solute transport model is needed in addition to a flow model.

Examples of effective statements of purpose for forecasting models are:

*This report provides estimates of water demand for Union County, Mississippi, to the year 2050 and describes the simulated ground-water drawdown in the Coffee Sand and Eutaw-McShan aquifers in northeastern Mississippi from 2000 to 2050, which are a result of the projected increases in pumpage.*

**Hutson et al., 2000**

*The purpose of this report is to document the results obtained using the regional ground-water flow model to estimate potential effects of implementing the proposed water-rights applications filed by LVVWD.*

**Schaefer and Harrill, 1995**

The following is an example of a statement of purpose for interpretive screening models that, if calibrated, might also be used for forecasting:

*The report describes how the models were used to support ARNG investigations, including determination of monitoring well locations, identification of potential source areas, and delineation of areas contributing recharge to municipal wells.*

**ARNG = U.S. Army National Guard; Walter and Masterson, 2003**

Examples of statements of purpose for interpretive generic models are:

*We developed a steady-state model of a simple hypothetical ground water/lake system to test the sensitivity of the calculated lake level to the value of hydraulic conductivity used to represent the lake ( $K_2$ ) relative to the hydraulic conductivity of the aquifer ( $K_1$ ).*

**Anderson et al., 2002**

*In this study, potential nets obtained from two-dimensional hypothetical models are examined qualitatively to show the effect of variations in the controlling parameters on the regional groundwater flow system.*

*Freeze and Witherspoon, 1967*

## 2.2 CONCEPTUAL MODEL: DEFINITION AND GENERAL FEATURES

To solve any site-specific groundwater problem, the hydrogeologist must assemble and analyze relevant field data and articulate important aspects of the groundwater system. The synthesis of what is known about the site is a conceptual model (Kresic and Mikszewski, 2013). Commonly, U.S. state and federal regulations related to groundwater development, contaminant source identification and remediation require the formulation of a site conceptual model (SCM), also known as a conceptual site model. For example, the U.S. Environmental Protection Agency (U.S. EPA, 2003, p. 13) states that an SCM for evaluating the feasibility of groundwater restoration at RCRA and Superfund sites: “synthesizes data acquired from historical research, site characterization, and remediation system operation. ...The conceptual model serves as a foundation for evaluating the restoration potential of the site.”

A conceptual model is usually built for a site-specific hydrogeological setting, but can also be constructed for a generic geologic setting (Fig. 2.1; Winter, 2001). Most groundwater problems will be addressed with a mathematical model developed from the conceptual model. In general, the closer the conceptual model approximates the field situation, the more likely the numerical model will give reasonable forecasts. The level of detail necessary is determined by the modeling purpose, the available field data, and the practical limits of building complexity into the numerical model. In practice, it is desirable to strive for parsimony in the design of the conceptual model, which implies that the conceptual model is simplified to include only those processes important for addressing the purpose

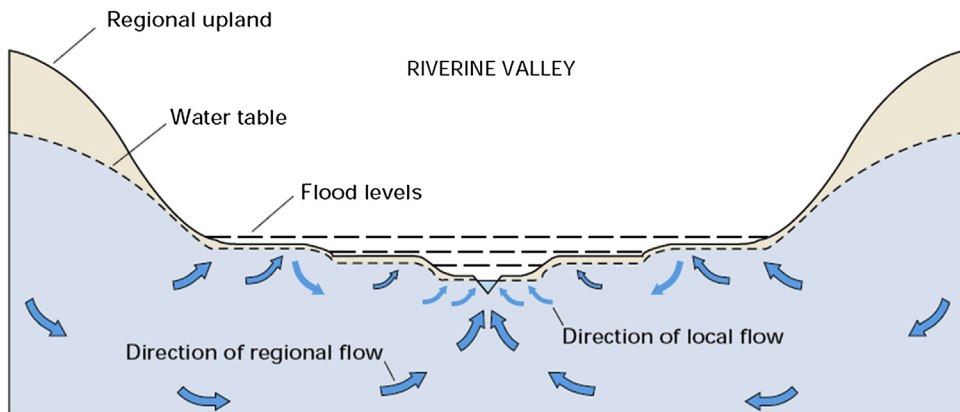


**Figure 2.1** Generic conceptual model of a large riverine valley with terraces (Winter et al., 1998).

yet still has sufficient complexity to represent relevant system behavior. If necessary, more complexity can be added later in the modeling process by revising the conceptual model.

Building on the general concepts presented above has produced many definitions of a conceptual model in the hydrogeological literature. According to [Zheng and Bennett \(2002\)](#), the development of a conceptual model is “synonymous with site characterization” so that the conceptual model is an integration of relevant local and regional hydrogeologic information using simplifying assumptions and qualitative interpretations of site-specific flow and transport processes. A sampling of other definitions is given below.

*A conceptual groundwater flow model is a simplification of a real-world groundwater problem such that (1) it captures the essential features of the real-world problem and (2) it can be described mathematically.*

**Haitjema, 1995**

*...conceptual model—an interpretation or working description of the characteristics and dynamics of the physical system.*

**ASTM, 2008**

*A conceptual hydrogeologic model is a mental construct or hypothesis accompanied by verbal, pictorial, diagrammatic and/or tabular interpretations and representations of site hydrogeologic conditions as well as corresponding flow/transport dynamics.*

**Neuman and Wierenga, 2002**

*A conceptual model is an evolving hypothesis identifying the important features, processes and events controlling fluid flow and contaminant transport of consequence at a specific field site in the context of a recognized problem.*

**NRC, 2001**

*A conceptual model consolidates the current understanding of the key processes of the groundwater system, including the influence of stresses, and assists in the understanding of possible future changes.*

**Barnett et al., 2012**

We define a *conceptual model* to be a qualitative representation of a groundwater system that conforms to hydrogeological principles and is based on geological, geophysical, hydrological, hydrogeochemical, and other ancillary information ([Table 2.1](#)). Design of a conceptual model should typically consider nine data sources: geomorphology, geology, geophysics, climate, vegetation, soils, hydrology, hydrochemistry/geochemistry, and anthropogenic aspects ([Kolm, 1996](#)). As such, a conceptual model includes characterization of both the hydrogeological framework ([Fig. 2.2\(a\)](#)) and the hydrologic system ([Fig. 2.2\(b\)](#)).

**Table 2.1** Types of data potentially used in construction of a hydrogeologic site conceptual model (Alley et al., 1999)

---

**Physical framework**

---

Topographic maps showing the stream drainage network, surface water bodies, landforms, cultural features, and locations of structures and activities related to water  
 Geologic maps of surficial deposits and bedrock  
 Hydrogeologic maps showing extent and boundaries of aquifers and confining units  
 Maps of tops and bottoms of aquifers and confining units  
 Saturated thickness maps of unconfined (water table) and confined aquifers  
 Average hydraulic conductivity maps for aquifers and confining units and transmissivity maps for aquifers  
 Maps showing variations in storage coefficient for aquifers  
 Estimates of age of groundwater at selected locations in aquifers

---

**Hydrologic budgets and stresses**

---

Precipitation data  
 Evaporation data  
 Streamflow data, including measurements of gain and loss of streamflow between gaging stations  
 Maps of the stream drainage network showing extent of normally perennial flow, normally dry channels, and normally seasonal flow  
 Estimates of total groundwater discharge to streams  
 Measurements of spring discharge  
 Measurements of surface water diversions and return flows  
 Quantities and locations of interbasin diversions  
 History and spatial distribution of pumping rates in aquifers  
 Amount of groundwater consumed for each type of use and spatial distribution of return flows  
 Well hydrographs and historical head (water-level) maps for aquifers  
 Location of recharge areas (areal recharge from precipitation, losing streams, irrigated areas, recharge basins, and recharge wells), and estimates of recharge

---

**Chemical framework**

---

Geochemical characteristics of earth materials and naturally occurring groundwater in aquifers and confining units  
 Spatial distribution of water quality in aquifers, both areally and with depth  
 Temporal changes in water quality, particularly for contaminated or potentially vulnerable unconfined aquifers  
 Sources and types of potential contaminants  
 Chemical characteristics of artificially introduced waters or waste liquids  
 Maps of land cover/land use at different scales, depending on study needs  
 Streamflow quality (water-quality sampling in space and time), particularly during periods of low flow

---



In developing a conceptual model, the modeler organizes, analyzes, and synthesizes relevant hydrogeological data, often with the help of a database tool such as a geographical information system (GIS) (Box 2.1). In addition to GIS-based data, data are taken from reports produced by consultants, state geological and water surveys, and federal agencies such as the U.S. Geological Survey, along with papers published in professional journals. Key components of a conceptual model include boundaries; hydrostratigraphy and estimates of hydrogeological parameters; general directions of groundwater flow and sources and sinks of water; and a field-based groundwater budget. Although the data for a conceptual model may be stored within a GIS, the conceptual model is typically presented in a series of diagrams, including cross sections, fence diagrams, and tables.

When developing a conceptual model it is helpful to consider the regional setting in order to understand how the regional hydrogeology influences groundwater flow in the study area. For models in the United States, information about regional hydrogeological

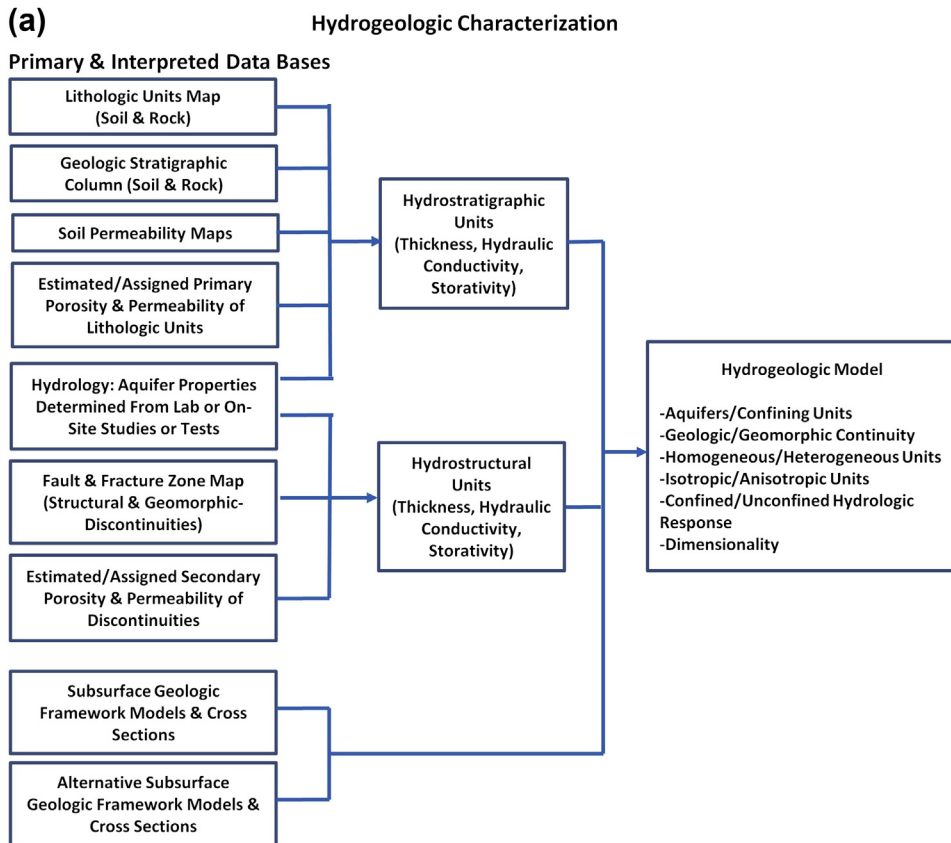


Figure 2.2 Data and analyses leading to (a) hydrogeologic site conceptual model.

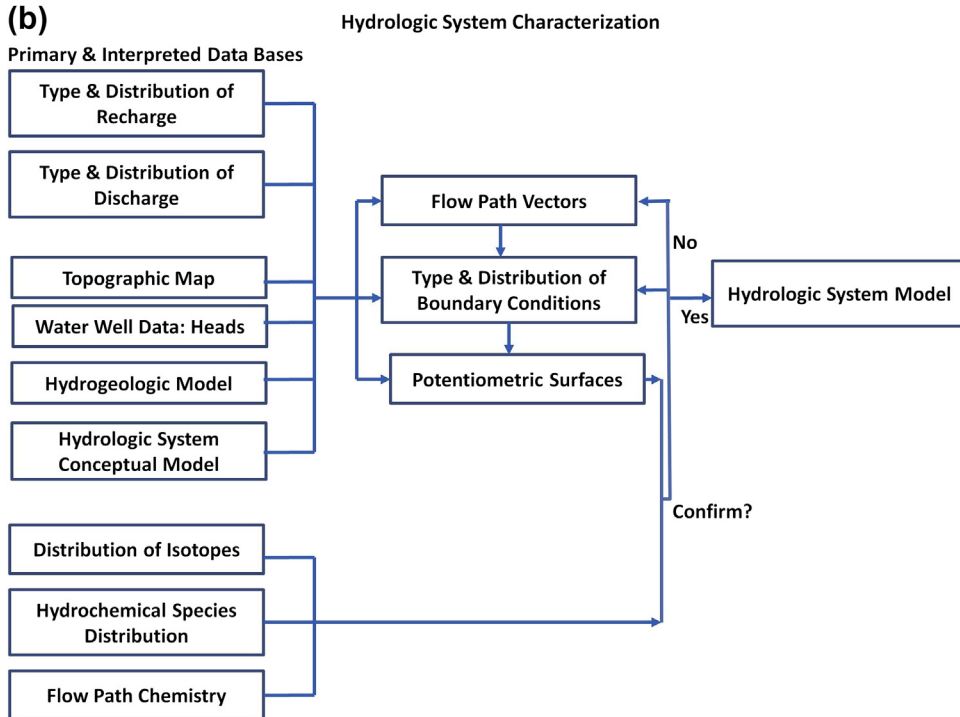


Figure 2.2 Cont'd. (b) hydrologic system conceptual model (modified from Kolm, 1996).

### Box 2.1 Geographical Information Systems (GIS)

A geographical information system (GIS) is a computer program or set of programs that stores, manipulates, analyzes, retrieves, and displays data referenced in space and time. As such, a GIS is a convenient tool for storing, organizing, and displaying data that form the conceptual model of a groundwater flow system. There are many GIS programs including QGIS, which is free and open source. Data from a GIS can be input to a graphical user interface (GUI; Section 3.6), and most GUIs have built-in GIS capabilities.

In addition to geographic position, data in a GIS have associated properties (called “meta-data”). Properties include type of measurement, such as water level elevation or hydraulic conductivity. The time period associated with the measurement is also typically specified. USGS (2007) present a general overview of GIS. Kresic and Mikszewski (2013) discuss GIS within the context of designing a hydrogeological site model and review the suite of programs in ArcGIS for Desktop (see their Chapter 3). Although some relatively simple groundwater analyses can be performed within a GIS (e.g., see Minor et al., 2007), a GIS by itself is not a groundwater model. Data are passed from the GIS for input to a groundwater model, or the GIS may be linked directly to a groundwater code (e.g., Martin et al., 2005; also see Tsou and Whittemore, 2001; Pint and Li, 2006; Steward and Bernard, 2006). Pinder (2002) provided detailed

(Continued)

### Box 2.1 Geographical Information Systems (GIS)—cont'd

instructions on modeling with the Argus ONE GIS linked to the Princeton Transport Code, MODFLOW, and MT3D.

There are also special function GIS tools that interface with groundwater codes (e.g., Lin et al., 2009; Meyer et al., 2012; Ajami et al., 2012). A screen capture from one such tool designed to calculate groundwater recharge and discharge is shown in Fig. B2.1.1.

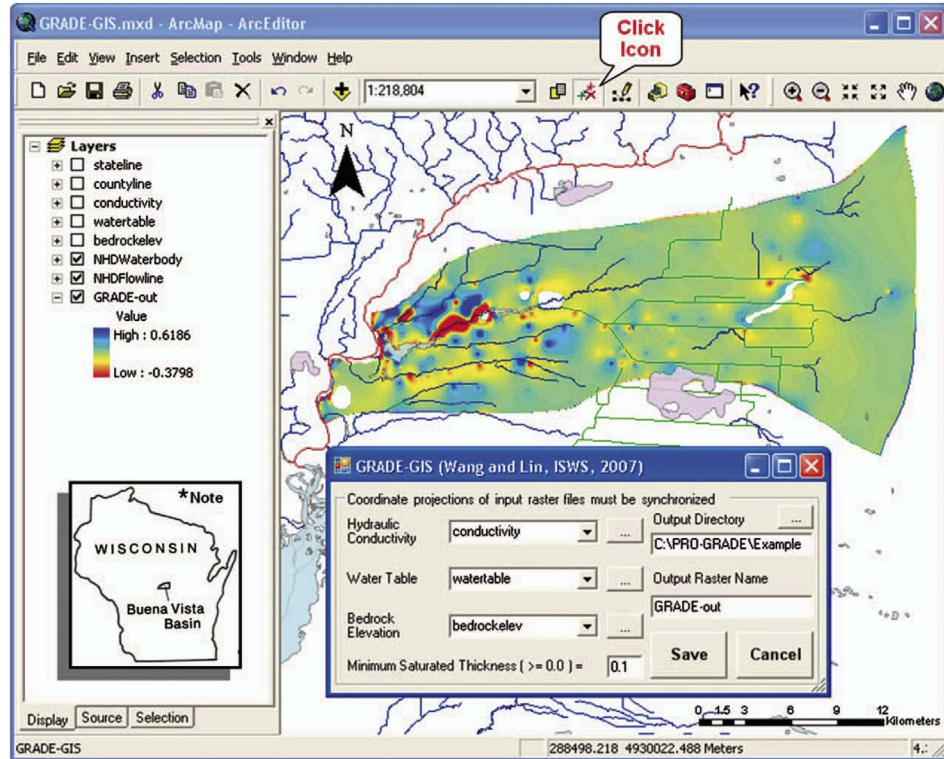


**Figure B2.1.1** Modified screen capture of a GIS-based graphical user interface showing the estimated recharge and discharge map of a groundwater basin in a humid setting in Central Wisconsin, USA. Blue and green colors denote recharge areas; red and yellow denote discharge areas. Surface water features are shown as colored lines and polygons (Lin et al., 2009).

conditions may be found in the *Ground Water Atlas of the United States* available online from the U.S. Geological Survey (<http://capp.water.usgs.gov/gwa/index.html>) and in Back et al. (1988). Johnston (1997) gives regional water budget information for some important aquifer systems in the United States. Regional hydrogeology for other countries is summarized in Zektser and Everett (2006), among others.

## 2.3 COMPONENTS OF A CONCEPTUAL MODEL

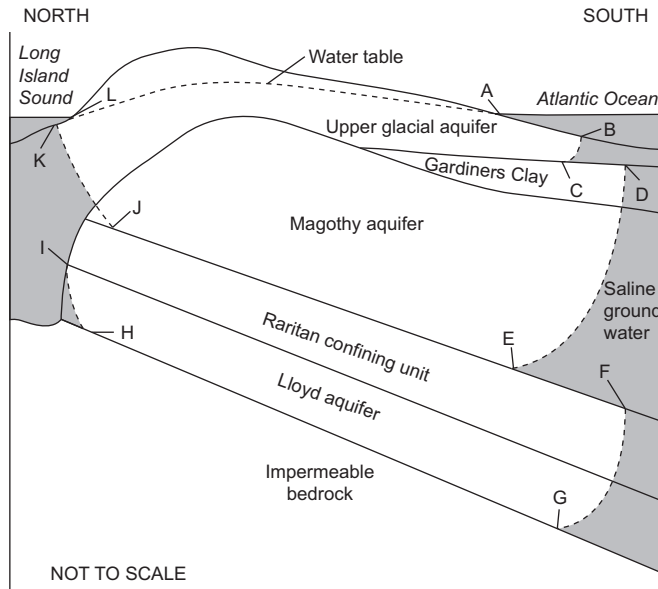
A conceptual model designed for most groundwater flow modeling, at a minimum, includes information on boundaries; hydrostratigraphy and hydrogeologic properties; flow directions and sources and sinks; and a field-based estimate of components of the groundwater budget. Additionally, any information that helps define and constrain the conceptualization, such as information on water chemistry, is used when available. Engineering calculators and generic models (Section 1.3) do not require a fully developed conceptual model.

### 2.3.1 Boundaries

The hydrological conditions along the boundaries of the conceptual model determine the mathematical boundary conditions (Section 3.3) of the numerical model. Boundary conditions are a key component of a mathematical model (Section 1.2) and strongly influence the flow directions calculated by a steady-state numerical model and most transient models.

Boundaries include hydraulic features such as groundwater divides and physical features such as bodies of surface water and relatively impermeable rock. The water table usually forms the upper boundary of a three-dimensional numerical model. Ideally, lateral and bottom boundaries should be aligned with physical or hydraulic features that do not move or change as hydrologic conditions change. These include relatively stable groundwater divides; the ocean and associated relatively stable saltwater/freshwater interface in a coastal aquifer (Fig. 2.3); large lakes and rivers that are connected to the groundwater system; relatively impermeable rock (e.g., unfractured granite, shale, clay) (Fig. 2.3); and relatively impermeable fault zones (Fig. 2.4). However, the modeler should be aware that in some settings groundwater divides may move in response to pumping (e.g., Sheets et al., 2005) or changes in recharge. Similarly, water levels in lakes and rivers, and even the ocean (Konikow, 2011), might change in response to pumping, climate change, and changes in land use. The modeler must assess whether the potential for changed conditions along a boundary will compromise modeling results. Transient changes in the location and hydraulic conditions along a boundary in principle can be incorporated into a numerical model; however, this assumes those fluctuations have been measured or can be estimated a priori, which is often difficult to do.

Boundaries are identified from potentiometric, topographic, and geologic maps of the region and site. If the location of a groundwater divide is determined from a topographic map, the modeler should recognize that groundwater divides do not always coincide with topographic divides (Winter et al., 2003; Pint et al., 2003). It may not be possible or convenient to surround the entire problem domain with hydraulic or physical features. If there are no hydraulic or physical features near the



BOUNDARY SEGMENT	HYDROGEOLOGIC FEATURE	MATHEMATICAL REPRESENTATION
LA	Water table and streams	Specified flow (free surface) Specified flow and head-dependent flow <sup>1</sup>
HG	Consolidated bedrock	No flow (streamline)
AB, KL	Shore discharge	Constant head
BC, DE, FG, HI, JK	Saltwater-freshwater interface	No flow (streamline)
CD, EF, IJ	Subsea discharge	Specified head

<sup>1</sup>Stream boundaries are specified differently in different simulations.

**Figure 2.3** Hydrogeologic boundaries of a conceptual model of the groundwater system in Long Island, NY, USA, and mathematical representation in the numerical model (Buxton and Smolensky, 1999).

area of interest that can serve as boundaries, the SCM is set within a larger (regional) conceptual model (Fig. 2.5). Then, the numerical model will have two levels of detail with more detailed representation in the primary model domain (*near-field*) and less detail in the larger regional groundwater system (*far-field*). Boundary conditions in the near-field numerical model are determined from conditions in the regional conceptual model, or may be calculated from the far-field solution of the regional numerical model (Section 4.4).

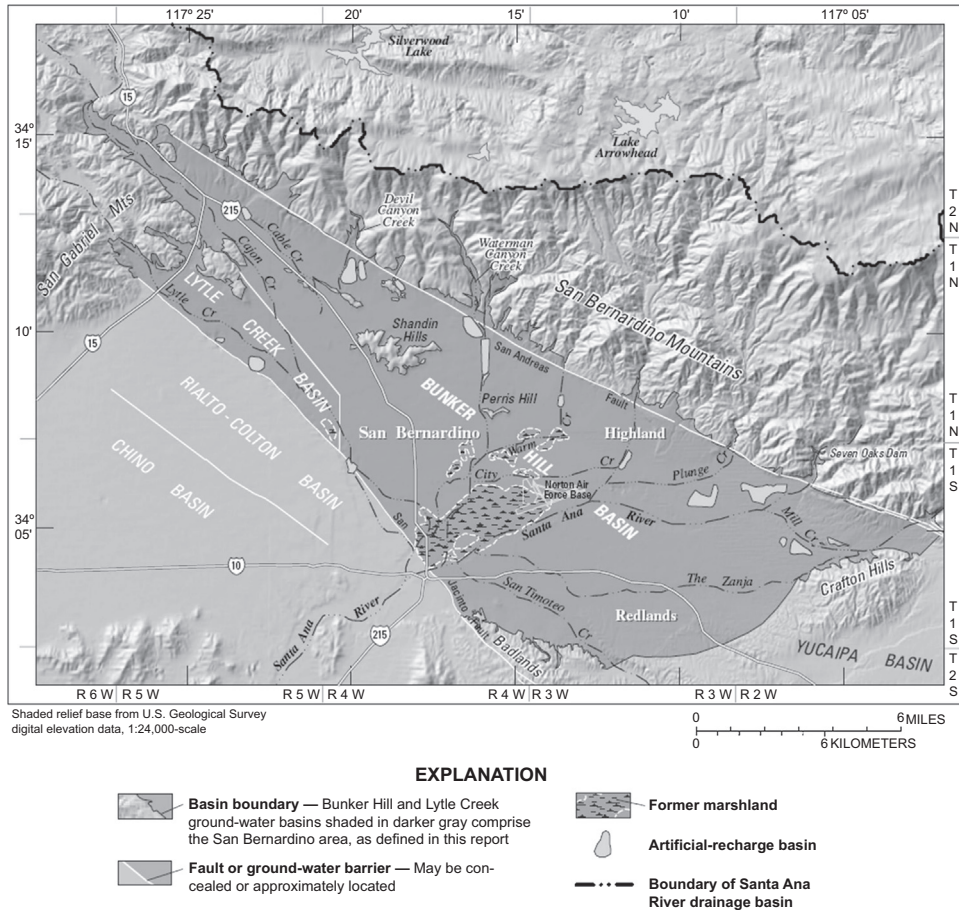


**Figure 2.4** Faults form boundaries for a model of the San Bernardino, CA, USA, groundwater system (Danskin et al., 2006).

### 2.3.2 Hydrostratigraphy and Hydrogeological Properties

Geological material in the interior of the conceptual model should be described as comprehensively as practical. Traditionally, a groundwater system is characterized as an aquifer or a sequence of aquifers and confining beds (Fig. 2.6(a)). An *aquifer* is a geological unit, or series of hydraulically connected geological units, that stores and transmits significant amounts of groundwater (definition modified from Kresic and Mikszewski, 2013, p. 49), where “significant” is understood to be subjective and related to the amount of water that can be pumped for a specific use (e.g., individual domestic, municipal, agricultural, or industrial).

A *confining bed* is a geologic unit, or series of connected geologic units, of relatively low permeability that may store but does not transmit significant amounts of water.

A confining bed (or confining unit) hydraulically confines the aquifer beneath it so that the head in the aquifer rises above the elevation of the base of the upper confining bed. Units of low permeability can also occur below aquifers so that a confined aquifer may be bound by confining beds above and below (Fig. 2.6(a)). The terms aquitard, aquiclude, and aquifuge have been used to describe the relative transmission properties of confining beds: an aquitard retards but does not prevent flow; an aquiclude “precludes” flow but may allow some water to pass through; an aquifuge is impermeable. Currently confining

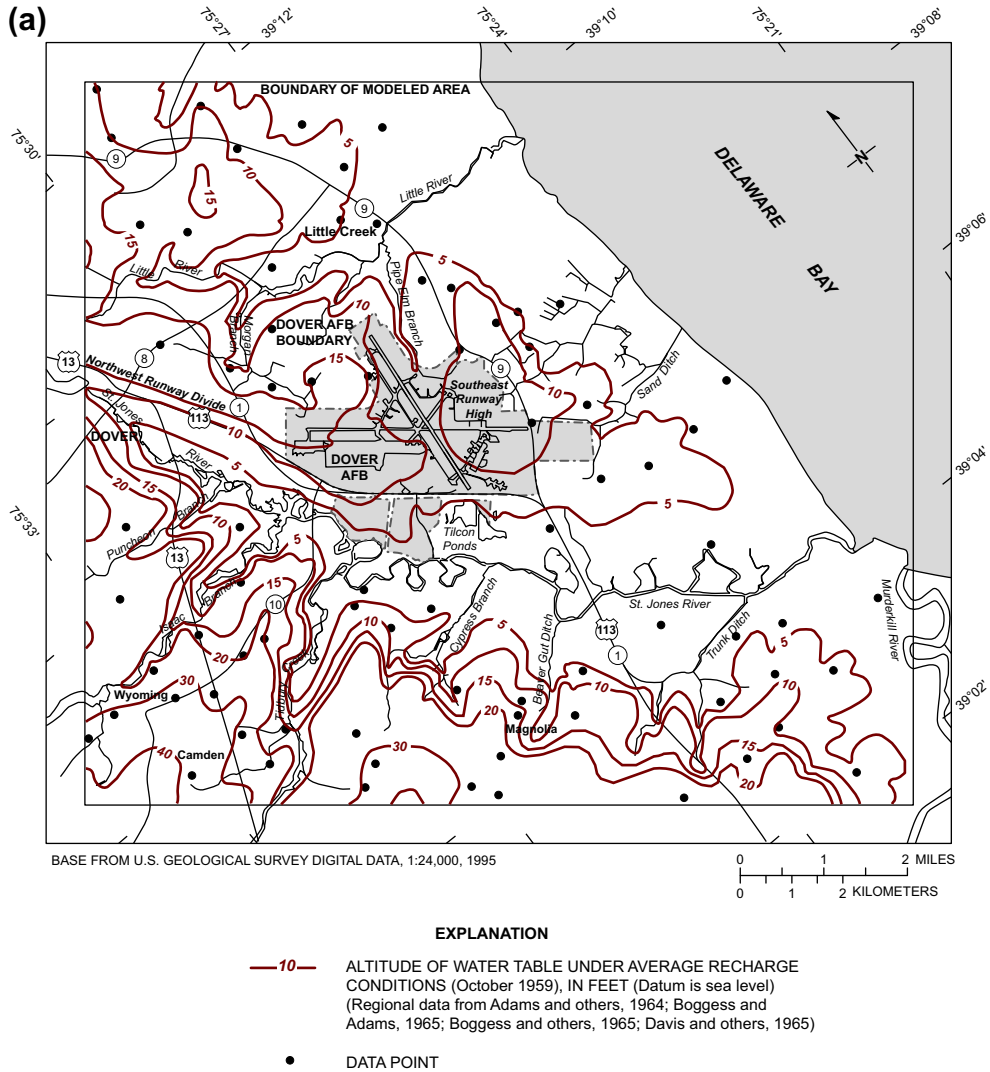


Figure 2.5 Potentiometric surface maps showing head in the lower surficial aquifer (see Fig. 2.9(b)), Dover Air Force Base, Delaware, USA, under average recharge conditions, October 1959: (a) regional.

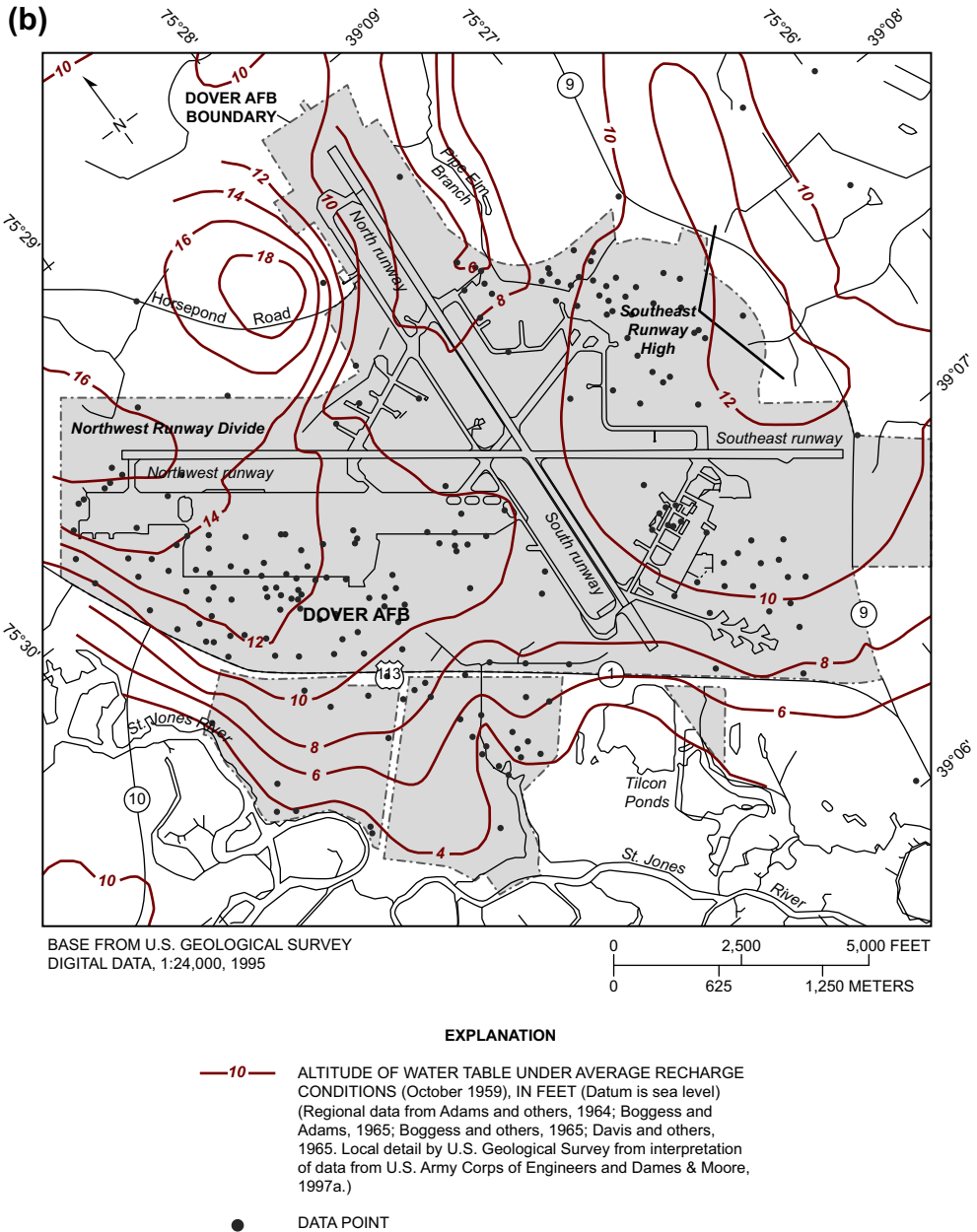
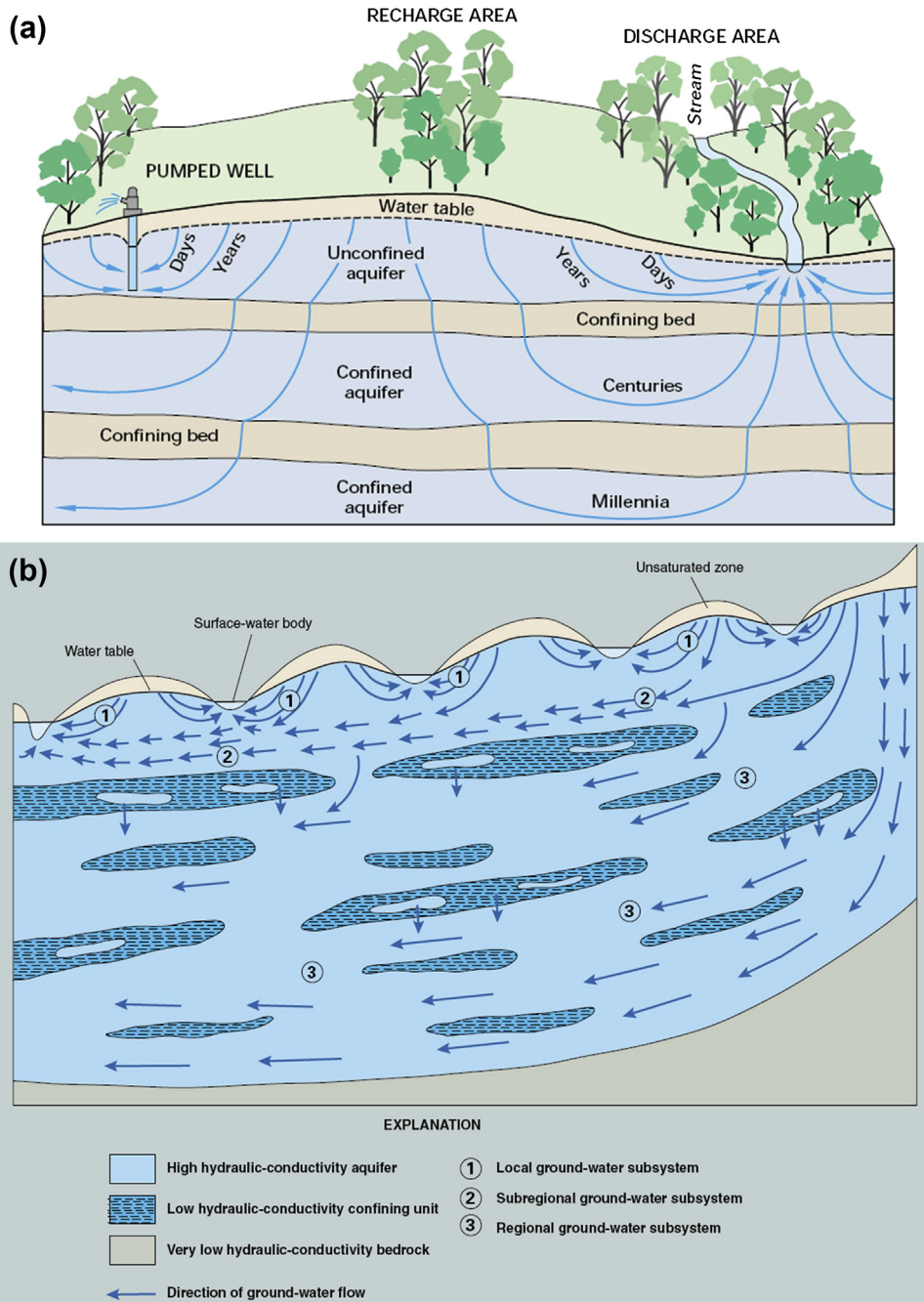


Figure 2.5 Cont'd (b) site (Hinaman and Tenbus, 2000).





**Figure 2.6** Generic conceptual models of aquitards showing: (a) timescales for flow through aquitards (Winter et al., 1998); (b) discontinuous beds (Alley et al., 1999).

bed and aquitard are the preferred generic terms for laterally continuous material of low permeability. Aquiclude and aquifuge are seldom used inasmuch as an aquiclude is an aquitard and aquifuge is not a useful term because few geologic units are completely impermeable (Fig. 2.6(a,b)) as was pointed out long ago by T.C. Chamberlin (1885). The terms aquitard and confining bed are often used interchangeably, but some authors (e.g., Cherry et al., 2006, p. 1) distinguish between the two, noting that not all aquitards hydraulically confine an aquifer. For example, the low hydraulic conductivity bedrock, in Fig. 2.6(b), is an aquitard but not a confining bed. Aquitards and confining beds may be discontinuous and/or leaky (owing to primary permeability and/or secondary fractures) (Fig. 2.6(b)). Discontinuities in a confining bed are sometimes called windows. Researchers in Minnesota (e.g., see Green et al., 2012) introduced the term “aquitardifer” to describe a confining bed that has low vertical hydraulic conductivity but horizontal hydraulic conductivity of the same magnitude as an aquifer.

Geologists divide rocks into three general categories based on genesis: sedimentary, igneous, and metamorphic. Igneous rocks are subdivided into intrusive rocks formed below the earth’s surface and extrusive rocks formed at the land surface. In the field, geologists group rocks into formations based on physical characteristics (lithology), including mineralogy and lateral extent. Hydrogeologists refine such groupings into hydrostratigraphic units based on the nature and connectivity of the openings (void space) in the rock (Box 2.2), which determine transmission and storage properties. The void space is characterized by porosity and permeability. Primary porosity refers to the void space present when the rock was formed; secondary porosity refers to the openings (e.g., fractures, solution channels) created after the rock was formed. Effective porosity, a measure of interconnected void space, is important in particle tracking (Box 8.1). Permeability quantifies the ability of the interconnected void space to transmit fluids. In groundwater hydrology, permeability is more explicitly expressed as hydraulic conductivity because the fluid of interest is usually water. Maxey (1964) introduced the hydrostratigraphic unit to encompass an identifiable aquifer and associated confining beds. He intended the hydrostratigraphic unit to be similar in concept to stratigraphic units defined by geologists, but his definition proved troublesome. For our purposes, a *hydrostratigraphic unit* consists of contiguous geological material having similar hydraulic properties (Seaber, 1988). Hydrostratigraphic units are also called hydrogeologic or geohydrologic units. Several geologic formations may be combined into a single hydrostratigraphic unit or a geologic formation may be subdivided into aquifers and confining beds; hydrostratigraphy of the same geologic units may vary regionally (Fig. 2.7).

Hydrostratigraphic units carry a regional connotation. At the site scale, it is common to refer to hydrofacies to connote a site-scale hydrostratigraphic unit; a *hydrofacies* encompasses interconnected porous material of relatively homogenous hydraulic properties (Poeter and Gaylord, 1990). Because a hydrofacies is defined based on hydraulic continuity it may not be the same as a geologically defined facies, which is a contiguous deposit that has similar

### Box 2.2 Describing the Void Space

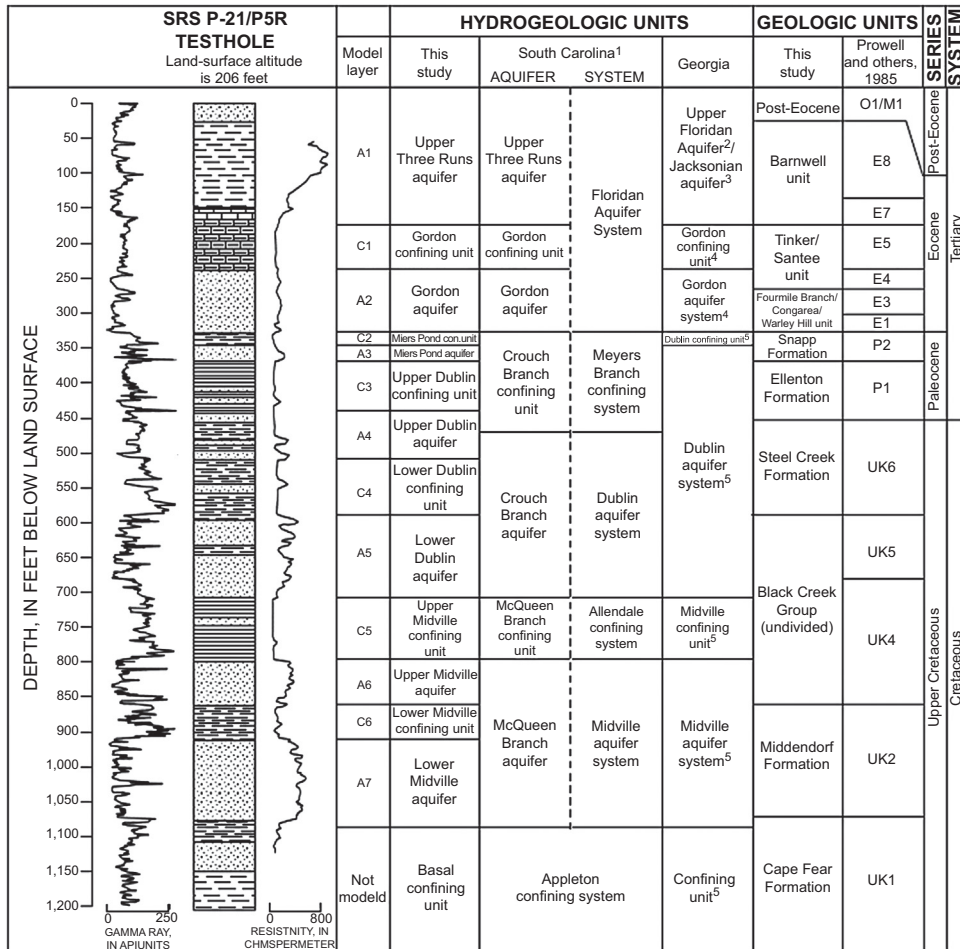
Geologists describe rocks in terms of grain size and mineralogy of the solid framework of porous material. Hydrogeologists instead focus on the void space within the solid framework. In this box, we provide some general information about the hydraulic characteristics of geological materials that typically comprise aquifers and confining beds and form hydrostratigraphic units and hydrofacies (Section 2.3). For a more extended discussion of these issues, the reader is referred to Sections 5.3, 5.4, 5.5 in Fitts (2013). Qualitative information on the nature and connectivity of the void space in hydrostratigraphic units and hydrofacies should be included in the conceptual model because this information is useful in evaluating initial parameter values for the conceptual model and in assessing the reasonableness of final calibrated parameter values.

Sand and sandstone typically have well-connected openings that result in high primary porosity and permeability. Eolian (wind-deposited) sand and sandstones are more homogeneous than other types of sands and sandstones. In some sandstones, primary porosity and permeability may be augmented by fractures. The hydraulic characteristics of carbonate sedimentary rock (e.g., limestone and dolomite) are highly variable (Fig. 2.14(a)); these rocks often contain fractures enhanced by solution. Some carbonate rocks have a dense network of well-connected fractures so that in large-scale models the unit effectively functions as a continuous porous medium, also known as an equivalent porous medium (EPM). This is important because when represented as an EPM the aquifer can be simulated using a standard groundwater flow code (e.g., Scanlon et al., 2002; Rayne et al., 2001). Terrain characterized by large open fractures and conduits, and solution features such as sinkholes on the landscape (Fig. 2.14(a)) is known as karst, which is usually underlain by carbonate rock. Conduit flow within a matrix of porous material can be simulated using special options included in most standard groundwater flow codes (Section 4.2) but if conduit flow is dominant, it may be necessary to use a special groundwater flow code that simulates flow within a network of fractures and conduits (Section 12.2).

Most metamorphic rocks and intrusive igneous rocks, which are collectively known as crystalline rock, have little or no primary porosity or permeability and are often simulated as physical boundaries to flow (Figs. 2.3, 2.6(b), 2.9(a)). However, depending on the geologic history of the area, crystalline rock may acquire appreciable secondary porosity and permeability in the form of fractures and weathered zones (Fig. 2.14(b)). Compressional and extensional tectonic stresses, pressure-release fracturing, and shrinkage during cooling contribute to secondary permeability. Weathering of crystalline rock forms a deposit known as saprolite that has high porosity of 40–50% and can yield water to wells (Fetter, 2001). In general, the fracture systems in crystalline rocks decrease in importance with depth. However, observations in mines and yields of boreholes finished in granite indicate fracture systems can be present at depths exceeding 1600 m (Fetter, 2001). Extrusive igneous rocks such as lava flows often have high secondary permeability in the form of fractures and void spaces created when the lava cooled at the surface. Consequently, volcanic rock may form productive aquifers (Fig. 2.14(c)). As in carbonate rocks, if fractures in metamorphic, igneous rocks, or sedimentary rocks and/or conduits in volcanic rock form the primary routes for transmission of water, it may be necessary to use a specialized groundwater flow code that solves for flow in sets of fractures or conduits (Section 1.2).

**Box 2.2 Describing the Void Space—cont'd**

Confining units (aquitards) are typically composed of shale or clay, which typically have low permeability. However, it is not uncommon for confining units to have fractures that may impart significant secondary porosity and permeability. For examples, aquitardifers (Green et al., 2012) are dominantly sedimentary rock with low vertical hydraulic conductivity and fractures parallel to bedding planes that impart high horizontal hydraulic conductivity.



<sup>1</sup> Aadland and others, 1992, 1995  
<sup>2</sup> Krause and Randolph, 1989;  
 Aadland and others, 1995  
<sup>3</sup> Vincent, 1982  
<sup>4</sup> Brooks and others, 1985  
<sup>5</sup> Clarke and others, 1985

**EXPLANATION**

- SAND
- MARL
- CLAYEY SAND
- MASSIVE CLAY
- LIMESTONE
- LAMINATED CLAY

MODEL LAYER—A, simulated aquifer;  
 C, simulated confining unit

**Figure 2.7** Hydrostratigraphic units at the Savannah River Site, South Carolina, USA. Geophysical logs and layers in the numerical model are also shown. Note that nomenclature in Georgia is different from South Carolina (Clarke and West, 1998).

physical properties and was deposited in the same geologic environment. Examples of depositional environments are: the ice margin of a glacier (ice-contact deposit), the ocean shoreline (beach sand), and along a mountain front (an alluvial fan deposit). Geologists use *facies models* to summarize generic information about depositional settings (Fig. 2.8). A geologic facies model might be helpful in interpreting site hydrostratigraphy (Anderson, 1989) and estimating the geometry and hydraulic characteristics of hydrofacies. However, deposits represented in a geologic facies model are for an idealized representation of a depositional environment and deposits at any specific field site will not be present exactly as represented in the model. Kresic and Mikszewski (2013), Fitts (2013), Fetter (2001), Back et al. (1988), and Davis and DeWeist (1966) present summary hydrogeological information for a

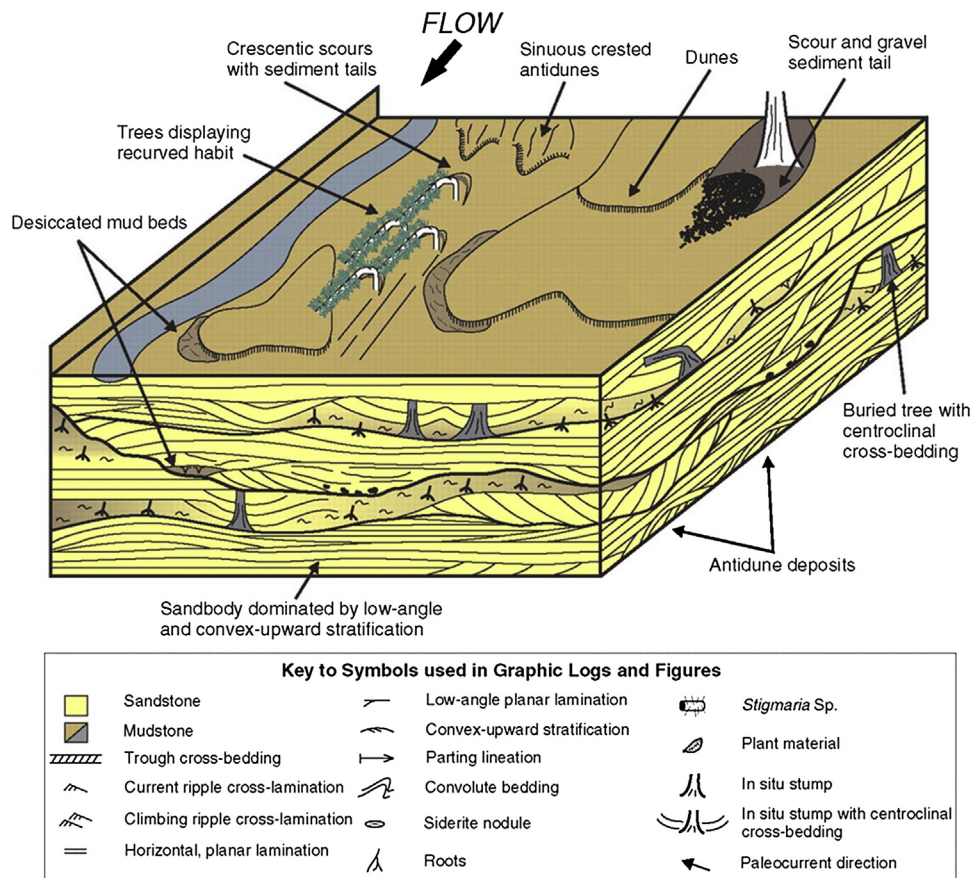
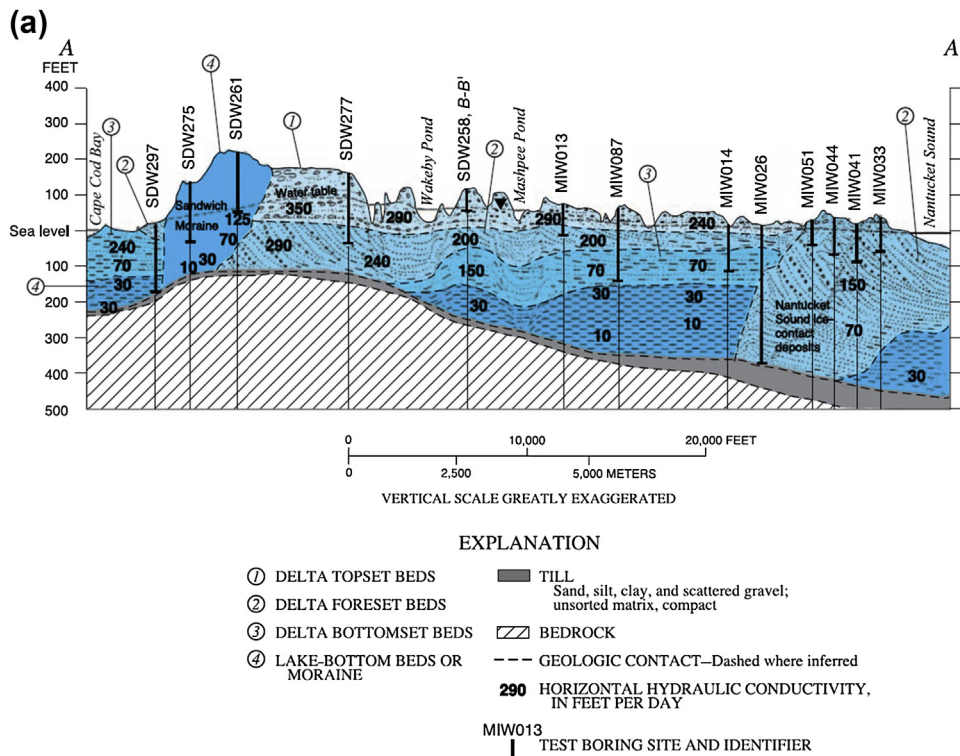


Figure 2.8 Geologic facies model of a fluvial depositional setting (Fielding et al., 2009).

variety of depositional settings including glaciated terrain, alluvial deposits, coastal settings, karst, and igneous and metamorphic terrains.

Information on depositional setting, geological history, and generalizations about hydraulic properties of hydrostratigraphic units and hydrofacies should be included in the conceptual model when possible (Fig. 2.9(a)). This information is useful in determining parameter values for the conceptual model, and later will be useful when evaluating the reasonableness of calibrated parameter values in the numerical model and in setting effective porosity values in a particle-tracking simulation (Box 8.1).

Kolm (1996) suggested defining hydrostructural units (Fig. 2.2(a)) as zones that are conduits or barriers to flow, such as fracture zones, conduits, and faults. These features might be assigned unique hydrogeological properties within a hydrostratigraphic unit or might constitute separate features. Such hydrostructural units are not commonly



**Figure 2.9** Conceptual models in cross section. (a) Hydrofacies with information on depositional setting and estimates of hydraulic conductivity, Cape Cod, MA, USA (Reilly and Harbaugh, 2004; modified from Masterson et al., 1997).

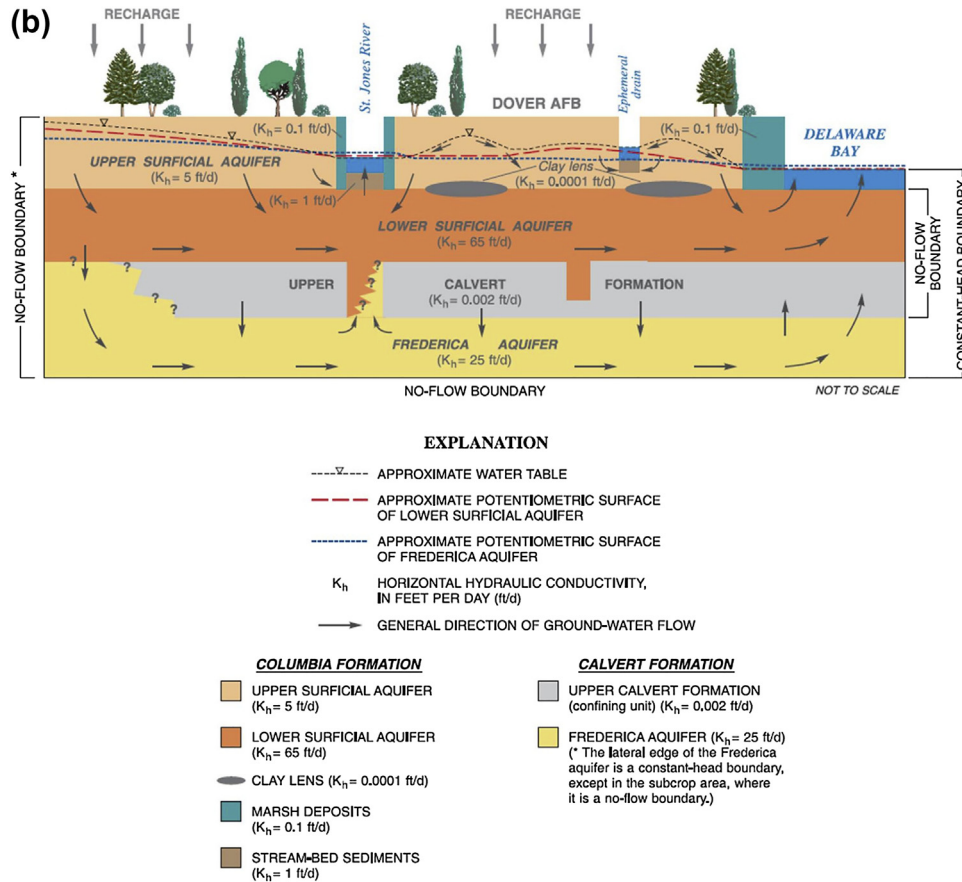


**Figure 2.9 Cont'd.** (b) Hydrostratigraphic units for the upper groundwater flow system at the Dover Air Force Base, Delaware, USA, with estimates of hydraulic conductivity. Note that the confining bed (upper Calvert Formation) is discontinuous (Hinaman and Tenbus, 2000).

used in current practice, but the concept is important and relevant to model design since it might be necessary to include these types of features in a SCM.

The modeler might find that hydrostratigraphic units are already defined for the region of interest in a form similar to Fig. 2.7. The thickness of hydrostratigraphic units can be determined from isopach maps, which show contours of equal thickness (Fig. 2.10), or from logs of boreholes and wells. At the site scale, hydrofacies are defined using on-site boreholes (Fig. 2.9(a)). Borehole geophysical logs help delineate hydrostratigraphic units (Fig. 2.7), and surface geophysical methods such as ground-penetrating radar provide “snapshots” of the hydrostratigraphy in some depositional environments (e.g., Lunt and Bridge, 2004; Lowry et al., 2009). Electrical and seismic methods are useful in coastal settings where saline water is present (e.g., Barlow, 2003).

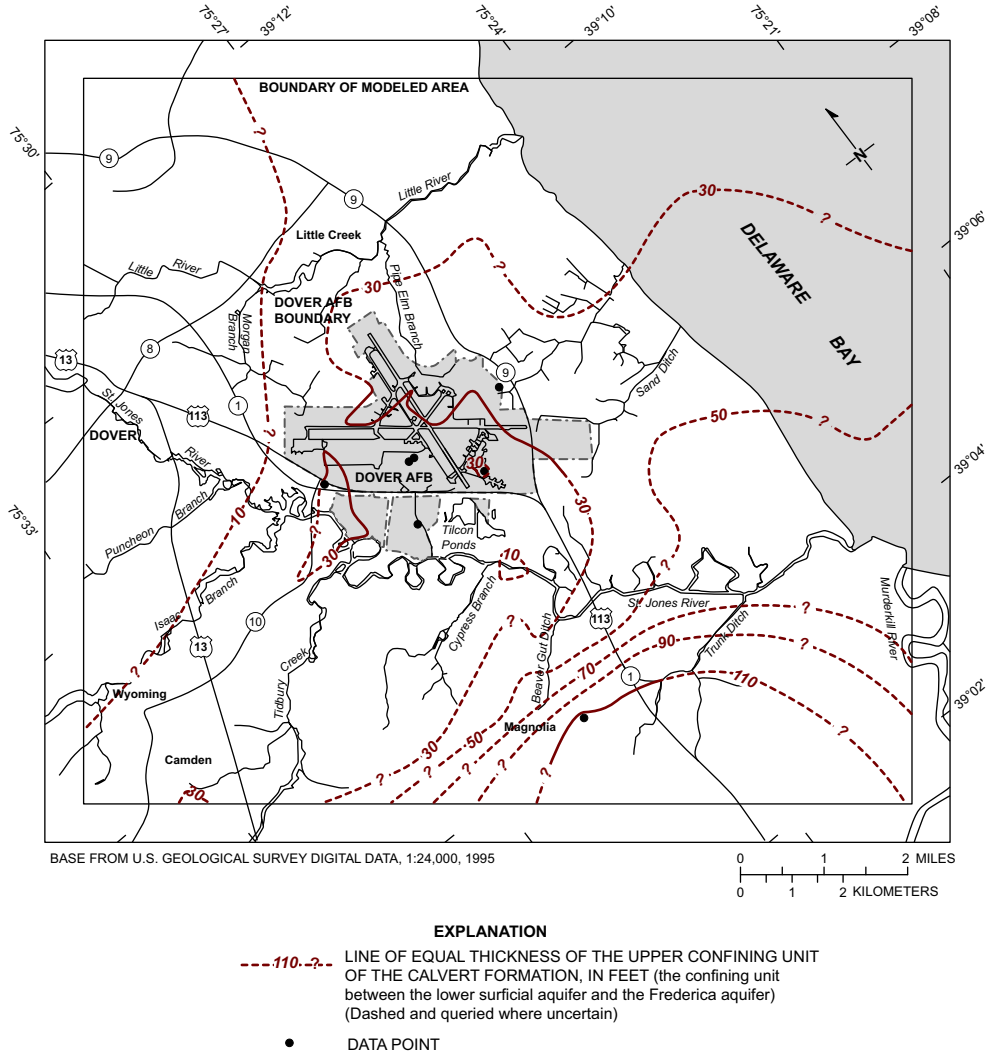
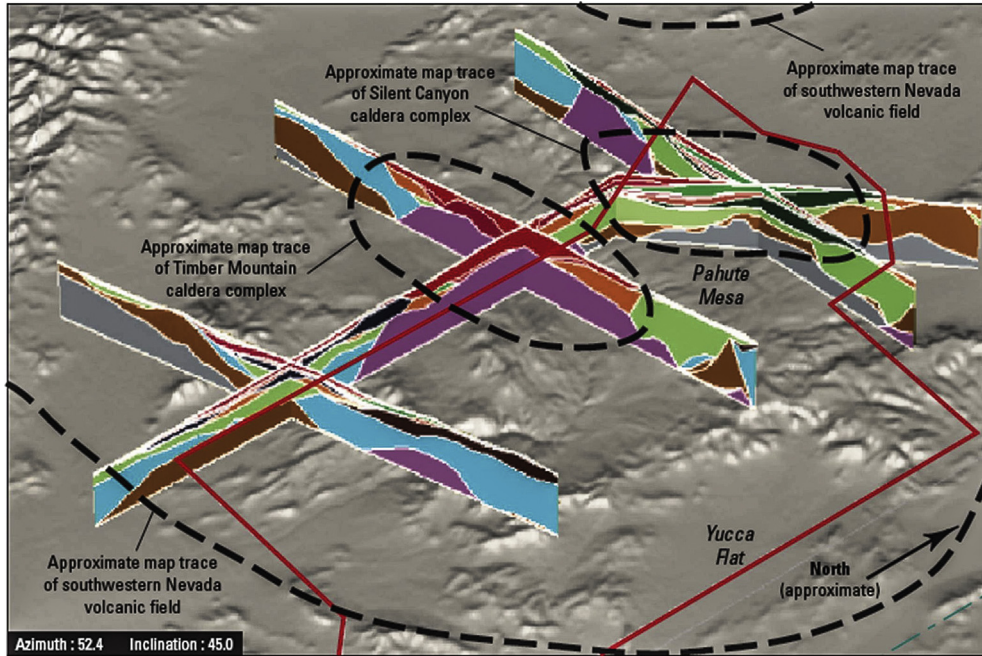


**Figure 2.10** Isopach map of the confining bed (upper Calvert Formation, Fig. 2.9(b)) in the area surrounding the Dover Air Force Base, Delaware, USA (Hinaman and Tenbus, 2000).

Hydrostratigraphic units and hydrofacies are displayed in stratigraphic columns (Fig. 2.7), cross sections (Fig. 2.9(a,b)), fence diagrams (Fig. 2.11), and block diagrams (Fig. 2.12). A GIS tool (Box 2.1) might be used to help organize and display information from boreholes (Fig. 2.13(a,b)).

Estimates of hydrogeological properties should be specified for each hydrostratigraphic unit or hydrofacies using field data when available (Fig. 2.9(a,b)). If relevant site-specific data are not available, values can be estimated from previous work





Azimuth : 52.4 Inclination : 45.0  
 Shaded-relief base from 1:250,000-scale Digital Elevation Model;  
 sun illumination from northwest at 30 degrees above horizon

**EXPLANATION**

**Hydrogeologic unit**

(Not all units appear on sections)

- Younger alluvial aquifer (YAA)
- Younger alluvial confining unit (YACU)
- Older alluvial aquifer (OAA)
- Older alluvial confining unit (OACU)
- Limestone aquifer (LA)
- Lava-flow unit (LFU)
- Younger volcanic-rock unit (YVU)
- Upper volcanic- and sedimentary-rock unit (upper VSU)
- Timber Mountain–Thirsty Canyon volcanic-rock aquifer (TMVA)
- Paintbrush volcanic-rock aquifer (PVA)
- Calico Hills volcanic-rock unit (CHVU)
- Wahmonie volcanic-rock unit (WVU)
- Crater Flat–Prow Pass aquifer (CFPPA)
- Crater Flat–Bullfrog confining unit (CFBCU)

- Crater Flat–Tram aquifer (CFTA)
- Belted Range unit (BRU)
- Older volcanic-rock unit (OVU)
- Lower volcanic- and sedimentary-rock unit (lower VSU)
- Sedimentary-rock confining unit (SCU)
- Lower carbonate-rock aquifer-thrust (LCA\_T1)
- Lower clastic-rock confining unit-thrust (LCCU\_T1)
- Upper carbonate-rock aquifer (UCA)
- Upper clastic-rock confining unit (UCCU)
- Lower carbonate-rock aquifer (LCA)
- Lower clastic-rock confining unit (LCCU)
- Crystalline-rock confining unit (XCU)
- Intrusive-rock confining unit (ICU)

Base of each cross section corresponds to the base of the regional hydrogeologic framework model (4,000 meters below sea level)

Azimuth—Specifies horizontal angle that north end of model has been rotated from north

Inclination—Specifies vertical angle that the model has been rotated from horizontal

— — County line

— — Nevada Test Site boundary

**Figure 2.11** Fence diagram showing hydrogeologic units for a model of Yucca Mountain, NV, USA (Faunt et al., 2010).

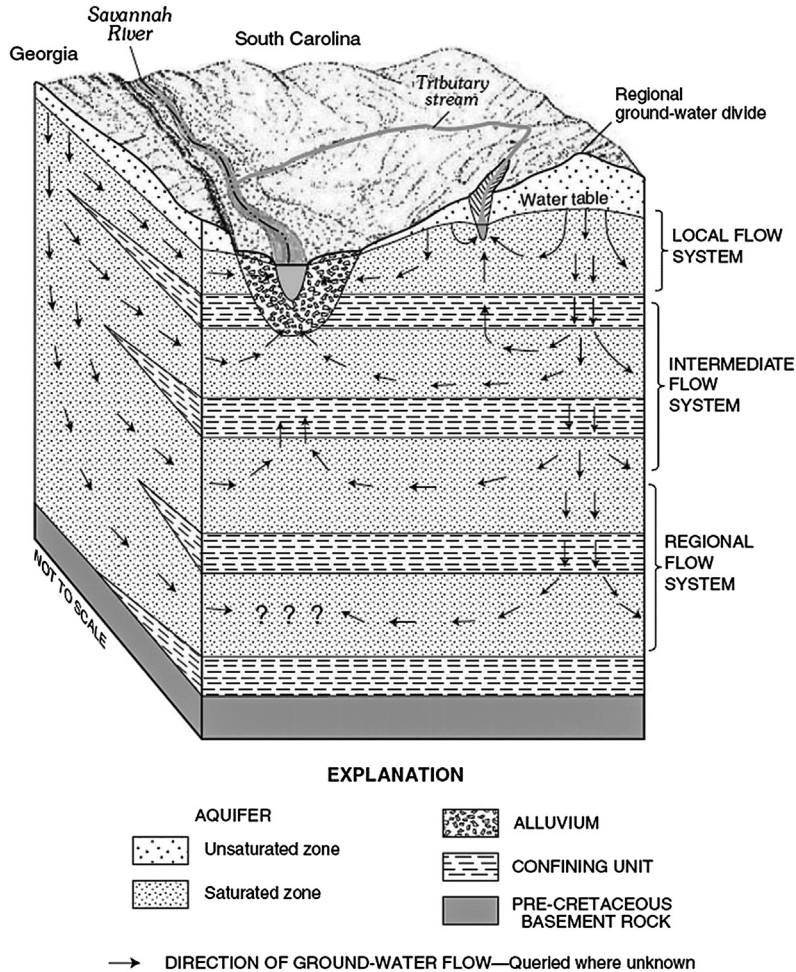


**Figure 2.12** Groundwater flow in the vicinity of the Savannah River Site, Georgia, and South Carolina, USA (Clarke and West, 1998).

from areas near the site and from the literature. To help in parameter assignment, information about depositional environment and geological history as well as generalizations on the amount and connectivity of void space in each hydrostratigraphic unit/hydrofacies are commonly included in the conceptual model (Box 2.2). The parameter values assigned to the conceptual model will be used as the initial parameter estimates at the start of model calibration (Fig. 9.1). All groundwater flow models require information on hydraulic conductivity. Time-dependent (transient) simulations (Chapter 7) also require values of storage parameters (Section 5.4) for each hydrostratigraphic unit/hydrofacies. Particle-tracking simulations require information on effective porosity (Box 8.1).

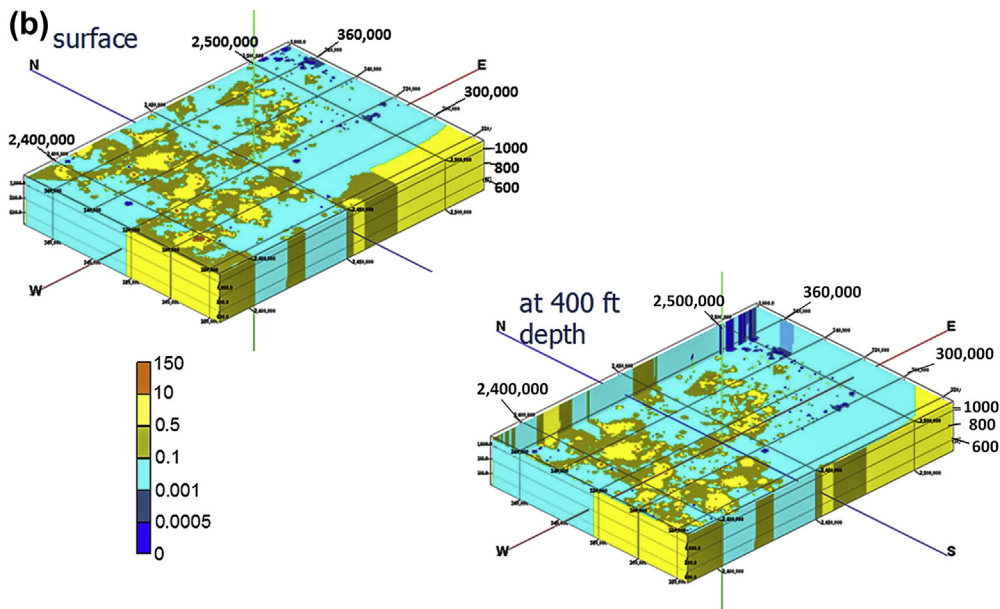
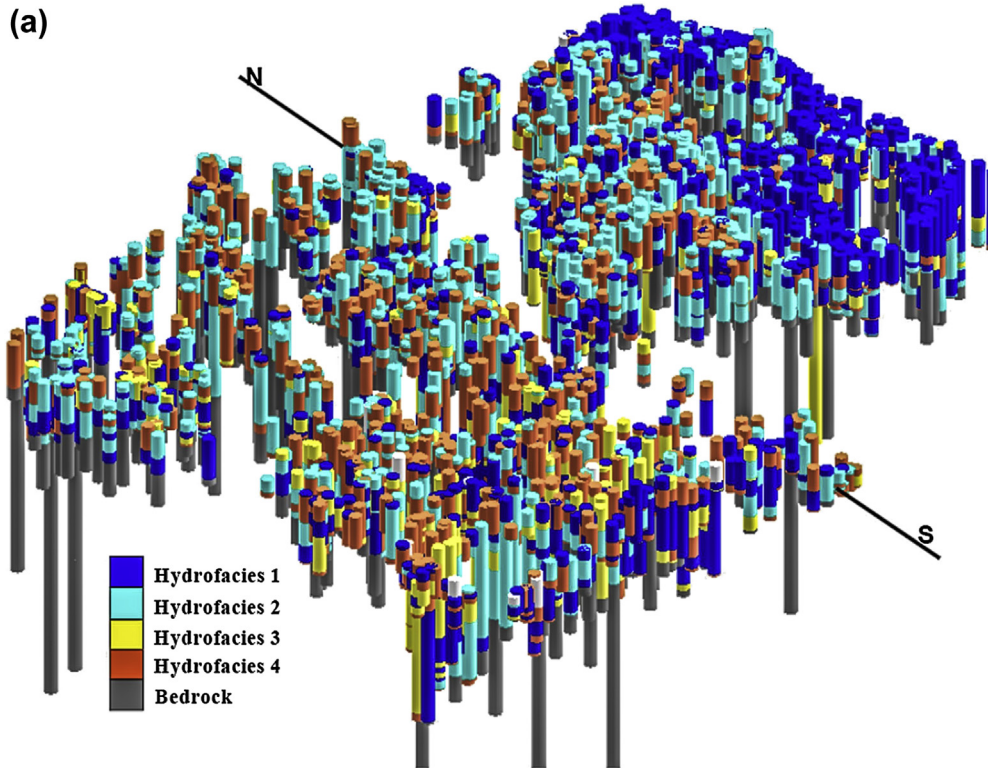


Figure 2.13 Graphics created with the GIS software Rockworks™ v. 2006 for a 25.7 by 19 mile site in southeastern Wisconsin, USA: (a) well logs displayed as cylinders in three-dimensional space; (b) solid models show 690 ft of section at the surface and at a depth of 400 feet. The legend gives values of hydraulic conductivity in ft/day (modified from Dunkle, 2008).

### 2.3.3 Flow Direction and Sources and Sinks

Groundwater flow within the problem domain of the conceptual model is depicted by schematic groundwater flow lines or arrows on potentiometric maps or hydrogeological cross sections (Figs. 2.1, 2.6, 2.9(b), 2.12, 2.14(b,c), 2.15). General flow directions are determined from contour maps of the water table and potentiometric surface (Fig. 2.5), if available, or from information on water levels, boundaries, and locations of recharge and discharge areas. If there is more than one aquifer present, flow directions are shown for each aquifer (Fig. 2.9(b)). Heads measured in nested wells, if available, provide information on the direction of vertical flow and help identify the depth of a flow system. Because flowpath visualizations are affected by anisotropy and vertical exaggeration (Box 5.2), it is good practice to include one cross section that has no vertical exaggeration (e.g., Fig. 4.1.1(b) in Box 4.1). A cross section with no vertical exaggeration is also useful to show the true relative scales of the groundwater system where the depth of the system is typically much less than its length (Box 4.1).

Hydrographs of water-level fluctuations in observation wells, especially long-term monitoring wells (Taylor and Alley, 2002; Feinstein et al., 2004), should be compiled, analyzed, and stored in the database of the conceptual model. This information will be useful in documenting whether a transient or steady-state model is needed to address the modeling objective (Section 7.2). Examples of hydrographs for wells finished in a wide range of aquifers in the United States can be viewed on the USGS Web site (<http://groundwaterwatch.usgs.gov/>).

Important sources and sinks of water inside the problem domain should be located and described. The addition of water commonly includes precipitation infiltrating the land surface that crosses the water table to become groundwater recharge (Fig. 2.9(b); Box 5.4). In some hydrogeological settings, the groundwater system can be recharged by mountain front or hillslope runoff (Fig. 2.15), seepage from sinkholes (Fig. 2.14(a)), and surface water bodies including lakes and rivers (Fig. 2.14(c)), as well as reservoirs, canals, and detention ponds (Fig. 2.15). Water can also be input by water reuse and disposal activities such as injection wells and artificial recharge infiltration galleries. Sinks of water include any feature that removes groundwater from the system, such as diffuse discharge to wetlands, surface water bodies and oceans (Figs. 2.1, 2.6(a,b), 2.9(b), 2.12), line discharge to drainage tiles and tunnels, and point discharge to pumping wells and springs (Fig. 2.14(c)). When the water table is close to the land surface, loss of water may also occur by evapotranspiration, which includes evaporation directly from the saturated zone and transpiration by plants whose roots penetrate the water table (Fig. 2.15). Sources and sinks of water from the outside edges of the problem domain (perimeter boundaries) should also be described. For example, some groundwater flow may enter or leave the problem domain via fractures in bedrock that forms the lower (and/or side) boundary of the model. Groundwater also may enter and leave the model along boundaries via underflow (Fig. 2.15).

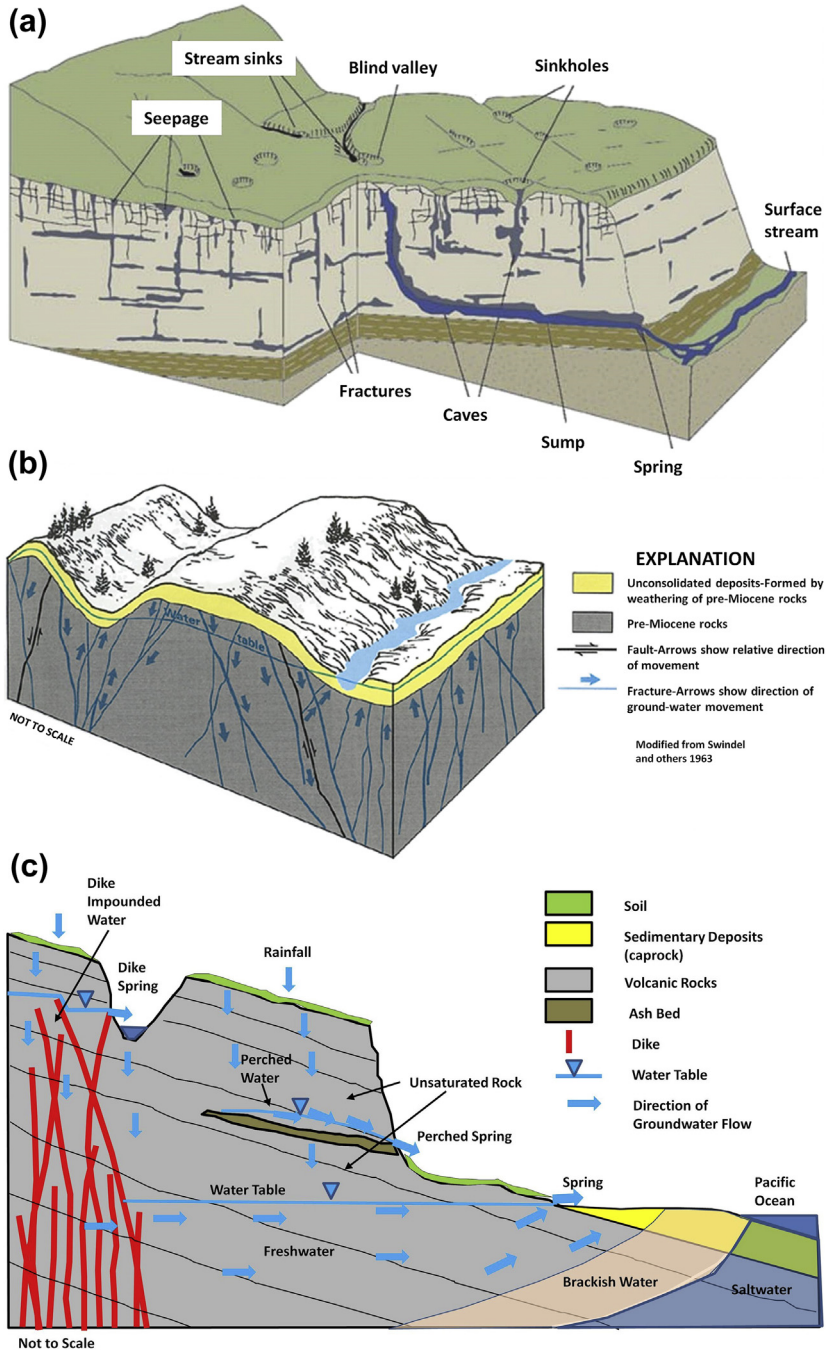


**Figure 2.14** Conceptual models of settings characterized by fractures and solution conduits. (a) Carbonate rock in karst terrain showing fractures, conduits, and sinkholes (*modified from Runkel et al. 2003*); (b) Fractures and faults in igneous and metamorphic terrain (*Whitehead, 1994*); (c) Lava flows and dikes in Hawaii, USA. Low-permeability dikes act as barriers to groundwater flow (*modified from Oki et al., 1999*).

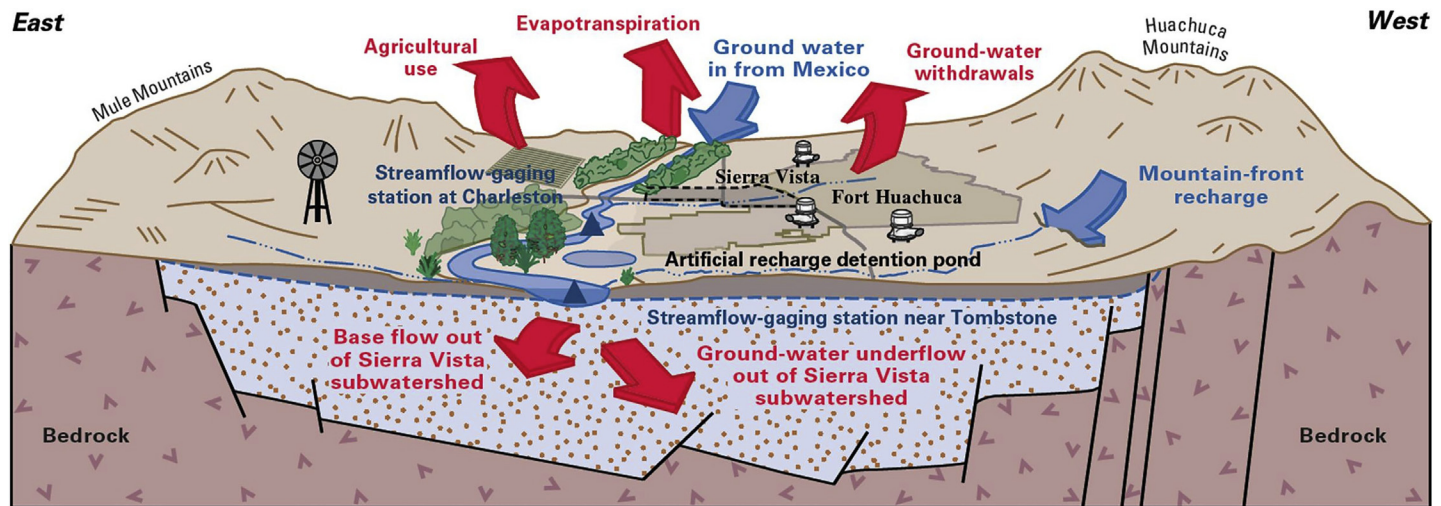


Figure 2.15 Block diagram showing groundwater flow directions and water budget components in an arid setting (Southern Arizona, USA) (Healy et al., 2007).

Representing the exchange of water between surface water features and groundwater is often a critical step when designing the numerical model. Fortunately, groundwater modeling codes typically include options for simulating groundwater–surface water interaction (Sections 4.3, 6.4, 6.5, 6.6, 6.7). In humid climates, surface water features are often well connected to near-surface groundwater systems and are important areas of discharge (Figs. 2.1, 2.6(a,b), 2.9(b), 2.12) (and/or recharge; Fig. 2.14(c)). However, surface water features, particularly in arid climates, can be hydraulically separated from the groundwater system by an unsaturated zone and have little or no direct influence on groundwater flow. In those situations the degree of interaction between surface water and the underlying groundwater is determined by the hydraulic properties of the unsaturated zone and surface water stage. Deep groundwater systems may have no direct connection with surface water features when aquitards divert flow into the horizontal direction (Fig. 2.6(b)). However, water from a deeper regional groundwater system may be recharged in a near-surface regional recharge area (Fig. 2.6(b)) and/or may discharge to overlying groundwater systems at a regional surface water discharge area (Fig. 2.6(a)). Thus, it may be necessary to include those deeper flow systems, or at least the contributions from those systems, in a model focused on near-surface groundwater flow.

When developing the conceptual model, information about rates for recharge, pumping, evapotranspiration, baseflow, springflow, as well as underflow and other boundary flows are compiled or estimated along with information on the temporal and spatial variability of recharge/discharge conditions. This information is also used for developing model input including calibration targets (Section 9.3).

### 2.3.4 Groundwater Budget Components

A tabulation of field-based estimates of groundwater budget components should be part of every conceptual model in order to provide an initial understanding of model inflows and outflows. During calibration of the numerical model, the field-based groundwater budget can be compared with the groundwater budget calculated by the numerical model. The groundwater budget is developed for the area or volume represented by the conceptual model and for a specified period of time, i.e., days, months, years, or even decades (Table 2.2), or for seasonal or annual average (equilibrium) conditions (Fig. 2.16).

The water budget equation in its simplest form is:

$$\text{Inflow} = \text{Outflow} +/\!-\ \Delta \text{ in Storage} \quad (2.1)$$

A comprehensive water budget for the entire hydrologic system (left-hand side table in Fig. 2.16) may be developed in addition to a groundwater budget (right-hand side table in Fig. 2.16). The *hydrologic budget* includes precipitation, evaporation, evapotranspiration, and surface water flows in addition to groundwater flows. For a groundwater budget, inflow includes recharge from precipitation or other sources of recharge (e.g., mountain front recharge), seepage from surface water bodies, flow into the groundwater system from bedrock or hydrogeologic units outside the model boundaries,

**Table 2.2** Groundwater budget for the San Bernardino area, California, USA, 1945–1998, showing possible ways to account for the imbalance in the budget represented by the residual; values are in acre-feet per year (modified from Danskin et al., 2006)

Component	Minimum	Average value	Maximum	Comment
<b>Recharge</b>				
Direct precipitation	0	1000	12,000	
Gaged runoff	27,000	116,000	423,000	
Ungaged runoff	4000	16,000	68,000	
Local runoff	2000	5000	12,000	
Imported water	0	3000	30,000	
Underflow	4000	5000	7000	
Return flow from pumpage	20,000	28,000	37,000	
Total	57,000	174,000	589,000	
<b>Discharge</b>				
Pumpage	123,000	175,000	215,000	
Underflow	4000	13,000	25,000	
Evapotranspiration	1000	7000	26,000	
Rising groundwater	0	5000	42,000	
Total	128,000	200,000	308,000	
Change in storage	−143,000	−4000	289,000	
Residual	na	−22,000	na	
<b>Sources of water to compensate for residual</b>				
Recharge from gaged runoff	0	4000	5500	Simulated values are 5500 acre-feet per year greater than original estimate, which required many assumptions.
Recharge from ungaged runoff	0	500	500	Original estimate is highly uncertain.
Recharge from local runoff	0	500	500	Round-off error of original estimate is 500 acre-feet per year.
Seepage from bedrock aquifer	0	6000	15,000	Some underflow from bedrock is likely, and has been estimated using a heat-transport model to be as much as 15,000 acre-feet per year.
Change in storage, unconfined part of the valley-fill aquifer	0	3000	7500	Groundwater flow model suggests a greater change in storage occurred.

*Continued*



**Table 2.2** Groundwater budget for the San Bernardino area, California, USA, 1945–1998, showing possible ways to account for the imbalance in the budget represented by the residual; values are in acre-ft per year (modified from Danskin et al., 2006)—cont'd

Component	Minimum	Average value	Maximum	Comment
Change in storage, confined part of the valley-fill aquifer	0	100	500	Original estimate for change in storage did not account for the confined aquifer.
Water released during land subsidence	0	500	1000	Some inelastic release of water from storage likely occurred, but the quantity is unknown.
Reduced evapotranspiration	0	1000	2000	Model may overestimate evapotranspiration.
Reduced underflow out of aquifer	0	6400	6400	Simulated value for underflow near Barrier J is 6400 acre-feet per yr less than original estimate.
Total	na	22,000	na	

(–, indicates a decrease in groundwater storage; na, not applicable; average values are well researched from measured and estimated data; values to compensate for calculated residual are speculative).

recharge from irrigation, injection of water through wells, and any other additions of water to the system. Outflow includes groundwater discharge to surface water bodies, evapotranspiration, pumping, springflow, discharge through seepage faces along hillslopes, and any other losses of water from the system. Change in storage occurs when inflow is not balanced by outflow, resulting in either a loss or gain in groundwater storage and accompanying change in groundwater head.

Constructing a groundwater budget for a conceptual model helps the modeler evaluate whether all the important components and processes of the groundwater system have been considered and how they interact. However, estimating components of a groundwater budget accurately is difficult and fraught with uncertainty, especially if literature values and professional judgment are the primary source of information. For that reason, conceptual models often rely on reasonable ranges in water budget components (Table 2.2) or may include an estimate of the error associated with each component of the budget (Table 2.3). Flux estimates used in developing a groundwater budget, such as those shown in Table 2.3, may also be used as flux targets during model calibration (Section 9.3). Standard hydrogeology texts, hydrogeology field manuals (e.g., Moore, 2012; Weight, 2008; Sanders, 1998), and the literature discuss techniques to quantify each component of the groundwater budget. If the groundwater budget does not balance, a residual is presented as part of the budget (Table 2.2) and sources of uncertainty in the water budget may be itemized as part of the residual (Table 2.2).

OVERALL PREDEVELOPMENT WATER-BUDGET ANALYSIS		GROUND-WATER PREDEVELOPMENT WATER-BUDGET ANALYSIS	
INFLOW TO LONG ISLAND HYDROLOGIC SYSTEM	CUBIC FEET PER SECOND	INFLOW TO LONG ISLAND GROUND-WATER SYSTEM	CUBIC FEET PER SECOND
1. Precipitation	2,475	7. Ground-water recharge	1,275
OUTFLOW FROM LONG ISLAND HYDROLOGIC SYSTEM		OUTFLOW FROM LONG ISLAND GROUND-WATER SYSTEM	
2. Evapotranspiration of precipitation	1,175	8. Ground-water discharge to streams	500
3. Ground-water discharge to sea	725	9. Ground-water discharge to sea	725
4. Streamflow discharge to sea	525	10. Evapotranspiration of ground water	25
5. Evapotranspiration of ground water	25	11. Spring flow	25
6. Spring flow	25	Total outflow	1,275
Total outflow	2,475		

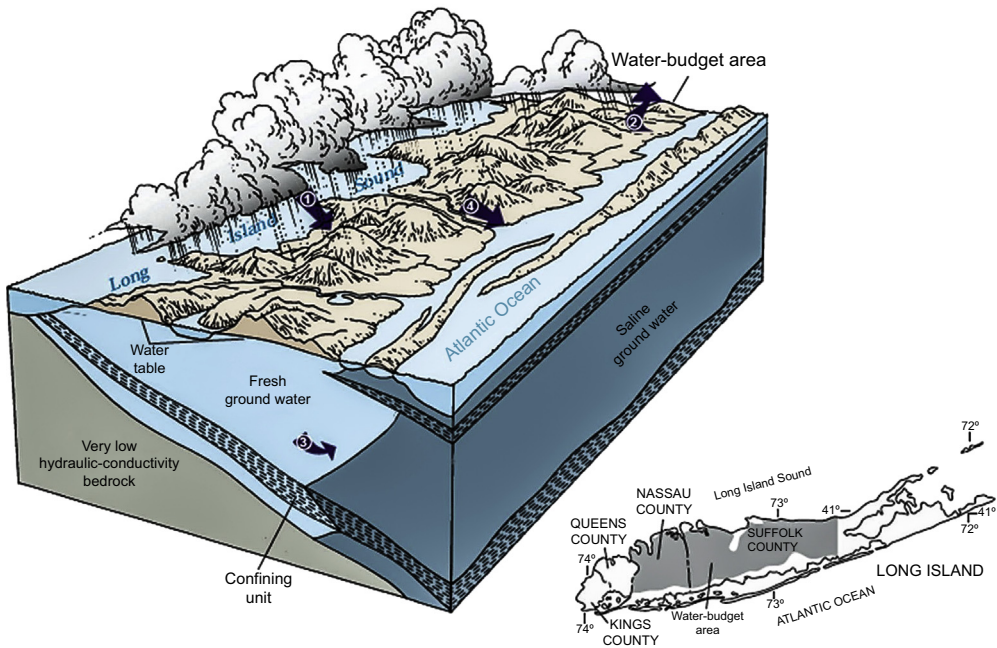


**Figure 2.16** Block diagram showing Long Island, New York, USA, and the hydrologic budget (left-hand side table) and groundwater budget (right-hand side table) under predevelopment conditions. Both water budgets assume equilibrium conditions with no change in storage (Alley et al., 1999).

### 2.3.5 Ancillary Information

Although the conceptual model is based primarily on geological and hydrological data, other types of data including water chemistry, geophysics, soils, vegetation, and ecological habitats may also be helpful in developing the conceptual model.

Chemical analyses of water samples typically include concentrations of major cations ( $\text{Ca}^{+2}$ ,  $\text{Mg}^{+2}$ ,  $\text{Na}^+$ , and  $\text{K}^+$ ) and anions ( $\text{SO}_4^{-2}$ ,  $\text{HCO}_3^-$ ,  $\text{Cl}^-$ ), specific conductance, total dissolved solids, dissolved oxygen, temperature, and pH. Depending on the purpose of the

**Table 2.3** Example of estimated error (second set of numbers in each column) associated with measurements (first set of numbers in each column) of components in a groundwater budget. Groundwater inflow to three sites in a wetland in Wisconsin was estimated using four different techniques.  $K_v$  is vertical hydraulic conductivity;  $K_h$  is horizontal hydraulic conductivity (modified from Hunt et al., 1996)

Site	Darcy's law Calculations ( $K_v = K_h$ ), cm/d		Isotope Mass Balance, cm/d		Temperature Profile Modeling, cm/d		Water Balance Modeling, cm/d	
	F2*	-0.02	±0.4	-0.6	±0.1	-1.0	±0.4	-1.1
W1†	-0.2	±4	-0.1	±0.1	-0.7	±0.5	-0.4	±0.4
W2†	-0.3	±6	-1.0	±0.2	-0.8	±0.3	+1.3‡	±2.8

Negative numbers denote groundwater inflow.

\*Constructed wetland.

†Natural wetland.

‡Site head data are sparse in this area; the head configuration and estimated flux are likely incorrect.

study, analyses may also include trace metals, stable and radiogenic isotopes, and organic compounds. Water chemistry data can help identify groundwater of similar geochemical composition and water entering the aquifer from a different flow system. Trends in water chemistry are sometimes helpful in identifying groundwater flow directions. Hydrochemical facies can be used to help identify the degree of separation between flow systems.

Both artificial and environmental tracers are useful in providing information about flowpaths. For example, artificial sweeteners are especially useful in tracing the source of groundwater flowpaths (Roy et al., 2014). Isotopic data give insight on sources, ages, and directions of groundwater flow and interaction with surface water (e.g., Kendall and McDonnell, 1998) and can be used as calibration targets (e.g., Hunt et al., 2006). Isotopic analyses using tritium, stable isotopes of oxygen and hydrogen, strontium, and synthetic organic compounds such as chlorofluorocarbons help identify sources and amounts of recharge and estimate groundwater flow rates (e.g., Cook et al., 2006; Solomon et al., 2006; Hunt et al., 2005) and groundwater age (e.g., McCallum et al., 2014). However, it should be recognized that groundwater samples extracted from wells and piezometers typically contain a mixture of water of different ages so that the determined age date is an apparent or effective age (Bethke and Johnson, 2002, 2008; Goode, 1996). Mixing of water of widely different ages occurs in heterogeneous aquifers (Weissmann et al., 2002), which can confound simple groundwater age estimates (McCallum et al., 2014). Mixing also can be important in groundwater systems characterized by complex converging flowpaths influenced by the presence of surface water bodies (Pint et al., 2003). Also see discussion on this topic in Section 8.5.

Data from surface and borehole geophysics help to estimate depth to water table and bedrock and delineate heterogeneities, geological structures, and bedding planes (e.g., Lowry et al., 2009; Lunt and Bridge, 2004). Geophysics can also locate a freshwater–saltwater interface (e.g., Barlow, 2003), which might be used as a boundary for a

conceptual model of groundwater flow (Figs. 2.3, 2.14(c)). Certain types of vegetation and ecological habitats are associated with groundwater discharge areas in streams and lakes (e.g., Van Grinsven et al., 2012; Pringle and Triska, 2000; Rosenberry et al., 2000; Lodge et al., 1989) and hydric soils are often indicative of a water table historically near the land surface.

## 2.4 UNCERTAINTY IN THE CONCEPTUAL MODEL

All conceptual models are qualitative and uncertain owing to our inability to represent the full complexity of even a simple hydrogeological system. Moreover, the field data on which the conceptual model is based are always incomplete and provide only an approximate description of true hydrogeological conditions.

Two approaches can be used to address uncertainty in the conceptual model:

1. The conceptual model is updated and revised as new information becomes available. The new information includes new field data as well as information gained during model calibration and uncertainty analysis (Fig. 1.1; also see Kresic and Mikszewski, 2013; Neuman and Wierenga, 2002). In this approach, the conceptual model is regarded as “an evolving hypothesis” (NRC, 2001).
2. Alternative versions of the conceptual model are developed. Wuolo (1993) likened this approach to T.C. Chamberlin’s (1897) well-known concept of multiple working hypotheses in which a geologist formulates several possible hypotheses that could account for the phenomenon being studied, but with better understanding of the system some of the hypotheses are eliminated and new ones may be proposed. In groundwater modeling, the alternative conceptual models are tested during calibration (Chapter 9) and forecast uncertainty analysis (Chapter 10). For example, Ye et al. (2010) tested five different conceptual models of the hydrostratigraphy and five different conceptual models of recharge rates and patterns, leading to a total of 25 different conceptual models for an arid setting in Nevada, USA.

In practice, the project budget and modeling purpose determine how much effort is devoted to identifying alternative conceptual models. A favored conceptual model might be updated and revised during the modeling process and retained as the final conceptual model if the numerical model on which it is based is satisfactorily calibrated and judged to perform well during forecast uncertainty analysis. If a numerical model fails either of these criteria, one or more alternative conceptual models can then be tested.

## 2.5 COMMON MODELING ERRORS

- The modeler constructs a model to learn something about the system without defining a specific purpose or framing specific questions. Although modeling without

a well-defined purpose might be helpful in the initial stages of an interpretive generic modeling exercise, even a generic model benefits from a well-defined purpose. The purpose helps the modeler select the processes, parameters, and level of detail to include in the conceptual and numerical models.

- The modeler becomes enamored with a conceptual model. Field data alone rarely support the selection of a single conceptual model, especially after project resources are depleted. Yet, a single conceptual model is often selected for convenience and the modeler might be reluctant to let go of the favored model, especially after significant investment of resources. However, during model calibration the presence of recalcitrant misfit and optimal calibrated parameter values that are at the extreme of a hydrogeologically reasonable range may require revising the conceptual model, or selecting an alternative conceptual model, and repeating the modeling process.
- The modeler builds a detailed “real-world” conceptual model that is inappropriately complex for constructing a numerical model given the modeling purpose, budget, and time available. In some scientific applications constructing the conceptual model is the sole objective; in those cases the conceptual model appropriately includes every possible process and parameter that might influence the outcome. However, in groundwater modeling, the purpose of constructing a conceptual model is to distill the real world to a representative set of processes and parameters that can be simulated in a groundwater flow code and is appropriate to the modeling purpose.

## 2.6 PROBLEMS

The problems for Chapter 2 focus on building the conceptual model including developing both a hydrologic budget and a groundwater budget.

**P2.1** Refer to the report you read for Problem P1.3.

- a. Based on the material presented in this chapter, is the modeling purpose clearly presented in the report and does the report title reflect the purpose?
- b. Critique the conceptual model of the hydrogeological system as presented in the report. Does it include all the components discussed in this chapter? Comment on the use of parsimony in the development of the conceptual model. Is an alternative conceptual model presented and if not, attempt to formulate one.

**P2.2** Consider the stratigraphic descriptions in [Table P2.1](#). Using the water-yielding characteristics given in the descriptions together with information in [Box 2.2](#) and your professional hydrogeological judgment, define hydrostratigraphic units for this setting. Prepare a hydrostratigraphic column (e.g., [Fig. 2.7](#)) showing the hydrostratigraphic units.

**P2.3** The geologic map in [Fig. P2.1](#) shows a river valley filled with 30 m of fluvial sand and gravel. The fluvial deposits are underlain by 200 m of clayey alluvial-fan deposits that are underlain by bedrock. The climate is humid and the river gains water from groundwater discharge as it flows southwest through the valley from

**Table P2.1** Lithostratigraphy and water yield of sediment in Orangeburg County, South Carolina, USA (Colquhoun et al., 1983; after Aadland et al., 1995; Gellici, 2007)

	Unconsolidated, clayey sand.
Cooper Group	Unconsolidated to indurated. Poorly sorted. Sandy clay, clayey sand, and limestone. 0-100 ft thick. Yields probably up to 100 gpm.
Orangeburg Group	Poorly consolidated. Fine sand in calcareous clay matrix. Glaucinitic and phosphatic at base. 0-150 ft thick.
	Unconsolidated. Moderately to poorly sorted. Sand and clayey sand. 50-100 ft thick. Yields probably up to 500 gpm.
	Poorly consolidated. Carbonaceous, laminated sand and clay. 25-100 ft thick.
Black Mingo Group	Poorly consolidated. Carbonaceous, laminated sand and clay. 25-100 ft thick.
Peedee Formation	Unconsolidated. Moderately to poorly sorted. Interbedded sand and clay. 150-250 ft thick. Yields up to 1,500 gpm.
Black Creek Formation	Poorly consolidated to well indurated. Laminated carbonaceous silt and clay. Sandy, silty marl. Calcite-cemented beds. 50-200 ft thick.
Middendorf Formation	Unconsolidated. Moderately to poorly sorted. Sand and clayey sand. 200-300 ft thick. Yields up to 2,000 gpm.
	Unconsolidated to indurated. Poorly to very poorly sorted. Gravel, sand, clayey sand, and clay. Weakly cemented with silica. 50-300 ft thick.
Crystalline rocks of the Piedmont	Sandstone and mudstone.

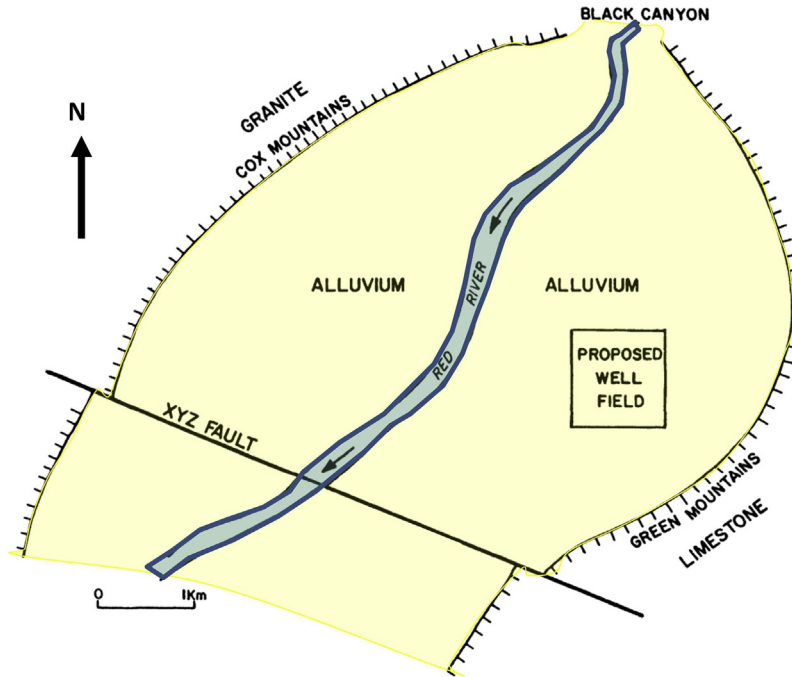


Figure P2.1 Geologic map of the Red River Valley.

Black Canyon. The water table is located about 3 m below land surface in most of the valley. A well field is proposed to tap the unconfined sand and gravel aquifer. The owners of the property where the well field is to be located would like to know if the flow (discharge) of the river will be affected if the discharge from the well field is  $500 \text{ m}^3/\text{min}$ . The estimated annual recharge is  $0.1 \text{ m}/\text{y}$ . Local consultants suggest the XYZ fault be used as a boundary.

- a. Develop a conceptual model of the system by specifying boundaries; hydrostratigraphy and hydrogeological parameters; flow directions and sinks and sources appropriate for addressing the owners' question. Justify your choices. Make a start on tabulating the groundwater budget and indicate the type of information needed to complete the budget.
- b. As you formulated your conceptual model, you probably noticed that with such limited hydrogeological information you needed to rely on your knowledge of the principles of hydrogeology to support a conceptual model. In this situation, another conceptual model might represent the system equally well, particularly with respect to placement of boundaries. Generate an alternative conceptual model with different boundaries. Justify your choices.
- c. List additional information that would be helpful in refining your boundary assignment.

- P2.4** In the conceptual model you developed for Problem P2.3 assume that: (1) precipitation exceeds evapotranspiration; (2) water is withdrawn from the river to flood irrigate a 4 km<sup>2</sup> area of the valley floor and some of that water infiltrates to the water table while some is used by crops, and some reenters the river as surface return flow; (3) water that is pumped from the aquifer by operating the well field is exported from the basin.
- a. Tabulate the components of an annual hydrologic budget for the conditions described above. Clearly define terms and state your assumptions.
  - b. Tabulate the components of an annual groundwater budget for the alluvial aquifer. Clearly define terms and state your assumptions.

## REFERENCES

- Aadland, R.K., Gellici, J.A., Thayer, P.A., 1995. Hydrogeologic Framework of West-Central South Carolina. South Carolina DNR Water Resources Division Report 5, 200 p.
- Ajami, H., Maddock, T., Meixner, T., Hogan, J.F., Guertin, D.P., 2012. RIPGIS-NET: A GIS tool for riparian groundwater evapotranspiration in MODFLOW. *Groundwater* 50 (1), 154–158. <http://dx.doi.org/10.1111/j.1745-6584.2011.00809.x>.
- Alley, W.M., Reilly, T.E., Franke, O.L., 1999. Sustainability of Ground-Water Resources. U.S. Geological Survey Circular 1186, 79 p. <http://pubs.usgs.gov/circ/circ1186/>.
- Anderson, M.P., 1989. Hydrogeologic facies models to delineate large scale spatial trends in glacial and glaciofluvial sediments. *Geological Society of America Bulletin* 101, 501–511. [http://dx.doi.org/10.1130/0016-7606\(1989\)101<0501:HFMTDL>2.3.CO;2](http://dx.doi.org/10.1130/0016-7606(1989)101<0501:HFMTDL>2.3.CO;2).
- Anderson, M.P., Hunt, R.J., Krohelski, J., Chung, K., 2002. Using high hydraulic conductivity nodes to simulate seepage lakes. *Groundwater* 40 (2), 117–122. <http://dx.doi.org/10.1111/j.1745-6584.2002.tb02496.x>.
- ASTM International, 2008. Standard guide for conceptualization and characterization of groundwater systems, D5979 – 96 (2008). American Society of Testing and Materials, Book of Standards 04 (09), 8 p.
- Back, W., Rosenshein, J.S., Seaber, P.R. (Eds.), 1988. Hydrogeology, DNAG (Decade of North American Geology) Series 2. Geological Society of America, Boulder, CO, 524 p.
- Barlow, P.M., 2003. Ground Water in Freshwater-Saltwater Environments of the Atlantic Coast. U.S. Geological Survey Circular 1262, 113 p. <http://pubs.usgs.gov/circ/2003/circ1262/>.
- Barnett, B., Townley, L.R., Post, V., Evans, R.F., Hunt, R.J., Peeters, L., Richardson, S., Werner, A.D., Knapton, A., Boronkay, A., 2012. Australian Groundwater Modelling Guidelines, Waterlines Report. National Water Commission, Canberra, 191 p. [http://nwc.gov.au/\\_data/assets/pdf\\_file/0016/22840/Waterlines-82-Australian-groundwater-modelling-guidelines.pdf](http://nwc.gov.au/_data/assets/pdf_file/0016/22840/Waterlines-82-Australian-groundwater-modelling-guidelines.pdf).
- Bethke, C., Johnson, T., 2002. Ground water age. *Groundwater* 40 (4), 337–339. <http://dx.doi.org/10.1111/j.1745-6584.2002.tb02510.x>.
- Bethke, C., Johnson, T., 2008. Groundwater age and groundwater age dating. *Annual Review of Earth and Planetary Science* 36, 121–152. <http://dx.doi.org/10.1146/annurev.earth.36.031207.124210>.
- Buxton, H.T., Smolensky, D.A., 1999. Simulation of the Effects of Development of the Ground-Water Flow System of Long Island, New York. U.S. Geological Survey Water-Resources Investigations Report 98-4069, 57 p. <http://pubs.usgs.gov/wri/wri984069/>.
- Chamberlin, T.C., 1885. Requisite and Qualifying Conditions of Artesian Wells. U.S. Geological Survey Annual Report 5, pp. 131–175.
- Chamberlin, T.C., 1897. The method of multiple working hypotheses. *Journal of Geology* 5, 837–848.
- Cherry, J.A., Parker, B.L., Bradbury, K.R., Eaton, T.T., Gotkowitz, M.B., Hart, D.J., Borchardt, M.A., 2006. Contaminant Transport through Aquitards: A State-of-the-Science Review. AWWA Research Foundation, IWA Publishing, Denver, CO, 126 p.



- Clarke, J.S., West, C.T., 1998. Simulation of Ground-Water Flow and Stream-Aquifer Relations in the Vicinity of the Savannah River Site, Georgia and South Carolina, Predevelopment through 1992. U.S. Geological Survey Water-Resources Investigations Report 98-4062, 135 p. <http://pubs.usgs.gov/wri/wri98-4062/>.
- Colquhoun, D.J., Woollen, I.D., Van Nieuwenhuise, D.S., Padgett, G.G., Oldham, R.W., Boylan, D.C., Bishop, J.W., Howell, P.D., 1983. Surface and Subsurface Stratigraphy, Structure and Aquifers of the South Carolina Coastal Plain. University of South Carolina, Department of Geology, 78 p.
- Cook, P., Plummer, L.N., Solomon, D., Busenberg, E., Han, L., 2006. Effects and processes that can modify apparent CFC age. In: Groning, M., Han, L.F., Aggarwal, P. (Eds.), Use of Chlorofluorocarbons in Hydrology. A Guidebook. International Atomic Energy Agency, Austria, pp. 31–58. [http://www.pub.iaea.org/MTCD/publications/pdf/Pub1238\\_web.pdf](http://www.pub.iaea.org/MTCD/publications/pdf/Pub1238_web.pdf).
- Danskin, W.R., McPherson, K.R., Woolfenden, L.R., 2006. Hydrology, Description of Computer Models, and Evaluation of Selected Water-Management Alternatives in the San Bernardino Area, California. U.S. Geological Survey Open-File Report 2005-1278, 178 p. <http://pubs.usgs.gov/of/2005/1278/>.
- Davis, S.N., De Wiest, R.J.M., 1966. Hydrogeology. John Wiley and Sons, New York, 463 p.
- Dunkle, K.M., 2008. Hydrostratigraphic and Groundwater Flow Model: Troy Valley Glacial Aquifer, Southeastern Wisconsin. M.S. thesis. Department of Geoscience, University of Wisconsin-Madison, 118 p.
- Faunt, C.C., Sweetkind, D.S., Belcher, W.R., 2010. Three-dimensional hydrogeologic framework model, Chapter E. In: Belcher, W.R., Sweetkind, D.S. (Eds.), Death Valley Regional Groundwater Flow System, Nevada and California—Hydrogeologic Framework and Transient Groundwater Flow Model. U.S. Geological Survey Professional Paper 1711, pp. 165–249. <http://pubs.usgs.gov/pp/1711/>.
- Feinstein, D.T., Hart, D.J., Krohelski, J.T., 2004. The Value of Long-term Monitoring in the Development of Ground-Water Flow Models. U.S. Geological Survey Fact Sheet 116-03, 4 p. <http://pubs.usgs.gov/fs/fs-116-03/>.
- Fetter, C.W., 2001. Applied Hydrogeology, fourth ed. Prentice Hall. 598 p.
- Fielding, C.R., Allen, J.P., Alexander, J., Gibling, M.R., 2009. Facies model for fluvial systems in the seasonal tropics and subtropics. *Geology* 37 (7), 623–626. <http://dx.doi.org/10.1130/G25727A.1>.
- Fitts, C.R., 2013. Groundwater Science, second ed. Academic Press, London. 672 p.
- Freeze, R.A., Witherspoon, P.A., 1967. Theoretical analysis of regional ground-water flow: 2. Effect of water table configuration and subsurface permeability variations. *Water Resources Research* 3 (2), 623–634. <http://dx.doi.org/10.1029/WR003i002p00623>.
- Gellici, J.A., 2007. Hydrostratigraphy of the ORG-393 Core Hole at Orangeburg. South Carolina, State of South Carolina DNR Water Resources Division Report 42, 31 p.
- Goode, D.J., 1996. Direct simulation of groundwater age. *Water Resources Research* 32 (2), 289–296. <http://dx.doi.org/10.1029/95WR03401>.
- Green, J.A., Runkel, A.C., Alexander Jr., E.C., 2012. Conduit flow characteristics of the St. Lawrence aquitardifer, conduits, karst, and contamination. In: Minnesota Ground Water Association Spring Conference April 19, 2012. [http://www.mgwa.org/meetings/2012\\_spring/2012\\_spring\\_abstracts.pdf](http://www.mgwa.org/meetings/2012_spring/2012_spring_abstracts.pdf).
- Haitjema, H.M., 1995. Analytic Element Modeling of Groundwater Flow. Academic Press, Inc., San Diego, CA. 394 p.
- Healy, R.W., Winter, T.C., LaBaugh, J.W., Franke, O.L., 2007. Water Budgets: Foundations for Effective Water-Resources and Environmental Management. U.S. Geological Survey Circular 1308, 90 p. <http://pubs.usgs.gov/circ/2007/1308/>.
- Hinaman, K.C., Tenbus, F.J., 2000. Hydrogeology and Simulation of Ground-Water Flow at Dover Air Force Base, Delaware. U.S. Geological Survey Water-Resources Investigations Report 99-4224, 72 p. <http://pubs.usgs.gov/wri/wri99-4224/>.
- Hunt, R.J., Coplen, T.B., Haas, N.L., Saad, D.A., Borchardt, M.A., 2005. Investigating surface water-well interaction using stable isotope ratios of water. *Journal of Hydrology* 302 (1–4), 154–172. <http://dx.doi.org/10.1016/j.jhydrol.2004.07.010>.
- Hunt, R.J., Feinstein, D.T., Pint, C.D., Anderson, M.P., 2006. The importance of diverse data types to calibrate a watershed model of the Trout Lake Basin, northern Wisconsin, USA. *Journal of Hydrology* 321 (1–4), 286–296. <http://dx.doi.org/10.1016/j.jhydrol.2005.08.005>.

- Hunt, R.J., Krabbenhoft, D.P., Anderson, M.P., 1996. Groundwater inflow measurements in wetland systems. *Water Resources Research* 32 (3), 495–507. <http://dx.doi.org/10.1029/95WR03724>.
- Hutson, S.S., Strom, E.W., Burt, D.E., Mallory, M.J., 2000. Simulation of Projected Water Demand and Ground-Water Levels in the Coffee Sand and Eutaw-McShan Aquifers in Union County, Mississippi, 2010 through 2050. U.S. Geological Survey Water Resources Investigation Report 00-4268, 36 p. <http://pubs.usgs.gov/wri/wri004268/>.
- Johnston, R.H., 1997. Hydrologic Budgets of Regional Aquifer Systems of the United States for Predevelopment and Development Conditions. U.S. Geological Survey Professional Paper 1425, 34 p. <http://pubs.er.usgs.gov/publication/pp1425>.
- Kendall, C., McDonnell, J.J. (Eds.), 1998. *Isotope Tracers in Catchment Hydrology*. Elsevier Science Publishers, 839 p.
- Kolm, K.E., 1996. Conceptualization and characterization of ground-water systems using Geographic Information Systems. *Engineering Geology* 42 (2–3), 111–118. [http://dx.doi.org/10.1016/0013-7952\(95\)00072-0](http://dx.doi.org/10.1016/0013-7952(95)00072-0).
- Konikow, L.F., 2011. Contribution of global groundwater depletion since 1900 to sea-level rise. *Geophysical Research Letters* 38 (17), L17401. <http://dx.doi.org/10.1029/2011GL048604>.
- Kresic, N., Mikszewski, A., 2013. *Hydrogeological Conceptual Site Models: Data Analysis and Visualization*. CRC Press, Boca Raton, 584 p.
- Lin, Y.-F., Wang, J., Valocchi, A.J., 2009. PRO-GRADE: GIS toolkits for ground water recharge and discharge estimation. *Groundwater* 47 (1), 122–128. <http://dx.doi.org/10.1111/j.1745-6584.2008.00503.x>.
- Lodge, D.M., Krabbenhoft, D.P., Striegl, R.G., 1989. A positive relationship between groundwater velocity and submersed macrophyte biomass in Sparkling Lake, Wisconsin. *Limnology and Oceanography* 34 (1), 235–239. <http://dx.doi.org/10.4319/lo.1989.34.1.0235>.
- Lowry, C.S., Fratta, D., Anderson, M.P., 2009. Ground penetrating radar and spring formation in a groundwater dominated peat wetland. *Journal of Hydrology* 373 (1–2), 68–79. <http://dx.doi.org/10.1016/j.jhydrol.2009.04.023>.
- Lunt, I.A., Bridge, J.S., 2004. Evolution and deposits of a gravelly braid bar, Sagavanirktok River, Alaska. *Sedimentology* 51 (3), 415–432. <http://dx.doi.org/10.1111/j.1365-3091.2004.00628.x>.
- Martin, P.H., LeBoeuf, E.J., Dobbins, J.P., Daniel, E.B., Abkowitz, M.D., 2005. Interfacing GIS with water resource models: A state-of-the-art review. *Journal of the American Water Resources Association* 41 (6), 1471–1487. <http://dx.doi.org/10.1111/j.1752-1688.2005.tb03813.x>.
- Masterson, J.P., Walter, D.A., Savoie, J., 1997. Use of Particle Tracking to Improve Numerical Model Calibration and to Analyze Ground-Water Flow and Contaminant Migration, Massachusetts, Military Reservation, Western Cape Cod, Massachusetts. U.S. Geological Survey Water-Supply Paper 2482, 50 p. <http://pubs.er.usgs.gov/publication/wsp2482>.
- Maxey, G.B., 1964. Hydrostratigraphic units. *Journal of Hydrology* 2 (2), 124–129. [http://dx.doi.org/10.1016/0022-1694\(64\)90023-X](http://dx.doi.org/10.1016/0022-1694(64)90023-X).
- McCallum, J.L., Cook, P.G., Simmons, C.T., 2014. Limitations of the use of environmental tracers to infer groundwater age. *Groundwater*. <http://dx.doi.org/10.1111/gwat.12237>.
- Meyer, S.C., Lin, Y.-F., Roadcap, G.S., 2012. A hybrid framework for improving recharge and discharge estimation for a three-dimensional groundwater flow model. *Groundwater* 50 (3), 457–463. <http://dx.doi.org/10.1111/j.1745-6584.2011.00844.x>.
- Minor, T.B., Russell, C.E., Mizell, S.A., 2007. Development of a GIS-based model for extrapolating meso-scale groundwater recharge estimates using integrated geospatial data sets. *Hydrogeology Journal* 15 (1), 183–195. <http://dx.doi.org/10.1007/s10040-006-0109-1>.
- Moore, J.E., 2012. *Field Hydrogeology: A Guide for Site Investigations and Report Preparation*. CRC Press, Boca Raton, FL, 190 p.
- National Research Council (NRC), 2001. *Conceptual Models of Flow and Transport in the Fractured Vadose System*. National Academy Press, Washington, DC, 374 p.
- Neuman, S.P., Wierenga, P.J., 2002. *A Comprehensive Strategy of Hydrogeologic Modeling and Uncertainty Analysis for Nuclear Facilities and Sites*, NUREG/CF-6805, 236 p. and Appendices. <http://www.nrc.gov/reading-rm/doc-collections/nuregs/contract/cr6805/>.

- Oki, D.S., Gingerich, S.B., Whitehead, R.L., 1999. Ground Water Atlas of the United States: Hawaii. U.S. Geological Survey Hydrologic Atlas, HA 730-N. [http://pubs.usgs.gov/ha/ha730/ch\\_n/index.html](http://pubs.usgs.gov/ha/ha730/ch_n/index.html).
- Pinder, G.F., 2002. Groundwater Modeling Using Geographical Information Systems. John Wiley & Sons, Inc., New York, 233 p.
- Pint, C.D., Hunt, R.J., Anderson, M.P., 2003. Flow path delineation and ground water age, Allequash Basin, Wisconsin. *Groundwater* 41 (7), 895–902. <http://dx.doi.org/10.1111/j.1745-6584.2003.tb02432.x>.
- Pint, T., Li, S.-G., 2006. ModTech: A GIS-enabled ground water modeling program. *Groundwater* 44 (4), 506–508.
- Poeter, E., Gaylord, D.R., 1990. Influence of Aquifer Heterogeneity on Contaminant Transport at the Hanford Site. *Groundwater* 28 (6), 900–909. <http://dx.doi.org/10.1111/j.1745-6584.1990.tb01726.x>.
- Pringle, C.M., Triska, F.J., 2000. Emergent biological patterns and surface-subsurface interactions at landscape scale. In: Jones, J.B., Mulholland, P.J. (Eds.), *Streams and Ground Waters*. Academic Press, San Diego, CA, pp. 167–193.
- Rayne, T.W., Bradbury, K.R., Muldoon, M.A., 2001. Delineation of capture zones for municipal wells in fractured dolomite, Sturgeon Bay, Wisconsin, USA. *Hydrogeology Journal* 9 (5), 432–450. <http://dx.doi.org/10.1007/s100400100154>.
- Reilly, T.E., Harbaugh, A.W., 2004. Guidelines for Evaluating Ground-Water Flow Models. U.S. Geological Survey Scientific Investigation Report 2004-5038, 30 p. <http://pubs.usgs.gov/sir/2004/5038/>.
- Rosenberry, D.O., Striegl, R.G., Hudson, D.C., 2000. Plants as indicators of focused ground water discharge to a northern Minnesota lake. *Groundwater* 38 (2), 296–303. <http://dx.doi.org/10.1111/j.1745-6584.2000.tb00340.x>.
- Roy, J.W., Van Stempvoort, D.R., Bickerton, G., 2014. Artificial sweeteners as potential tracers of municipal landfill leachate. *Environmental Pollution* 184, 89–93. <http://dx.doi.org/10.1016/j.envpol.2013.08.021>.
- Runkel, A.C., Tipping, R.G., Alexander Jr., E.C., Green, J.A., Mossler, J.H., Alexander, S.C., 2003. Hydrogeology of the Paleozoic Bedrock in Southeastern Minnesota. Minnesota Geological Survey Report of Investigations 61, 105 p., 2 pls.
- Sanders, L.L., 1998. *A Manual of Field Hydrogeology*. Prentice Hall, Upper Saddle River, NJ, 381 p.
- Scanlon, B.R., Mace, R.E., Barrett, M.E., Smith, B., 2002. Can we stimulate regional groundwater flow in a karst system using equivalent porous media models? Case study, Barton Springs Edwards aquifer, USA. *Journal of Hydrology* 276 (1–4), 137–158. [http://dx.doi.org/10.1016/S0022-1694\(03\)00064-7](http://dx.doi.org/10.1016/S0022-1694(03)00064-7).
- Schaefer, D.H., Harrill, J.R., 1995. Simulated Effects of Proposed Ground-Water Pumping in 17 Basins of East-Central and Southern Nevada. U.S. Geological Survey Water-Resources Investigations Report 95-4173, 71 p. <http://pubs.er.usgs.gov/publication/wri954173>.
- Seaber, P.R., 1988. Hydrostratigraphic units. In: Back, W., Rosenshein, J.S., Seaber, P.R. (Eds.), *Hydrogeology. The Geology of North America, DNAG (Decade of North American Geology) 0-2*, Geological Society of America, Golden, CO, pp. 9–14.
- Sheets, R.A., Dumouchelle, D.H., Feinstein, D.T., 2005. Ground-Water Modeling of Pumping Effects Near Regional Ground-Water Divides and River/Aquifer Systems — Results and Implications of Numerical Experiments. U.S. Geological Survey Scientific Investigations Report 2005-5141, 31 p. <http://pubs.usgs.gov/sir/2005/5141/>.
- Solomon, D., Plummer, L.N., Busenberg, E., Cook, P., 2006. Practical applications of CFCs in hydrological investigations. In: Groning, M., Han, L.F., Aggarwal, P. (Eds.), *Use of Chlorofluorocarbons in Hydrology. A Guidebook*. International Atomic Energy Agency, Vienna, Austria, pp. 89–103. [http://www-pub.iaea.org/MTCD/publications/pdf/Pub1238\\_web.pdf](http://www-pub.iaea.org/MTCD/publications/pdf/Pub1238_web.pdf).
- Steward, D.R., Bernard, E.A., 2006. The synergistic powers of AEM and GIS geodatabase models in water resources studies. *Groundwater* 44 (1), 56–61. <http://dx.doi.org/10.1111/j.1745-6584.2005.00172.x>.
- Taylor, C.J., Alley, W.M., 2002. Ground-Water-Level Monitoring and the Importance of Long-term Water-Level Data. U.S. Geological Circular 1217, 68 p. <http://pubs.usgs.gov/circ/circ1217/>.
- Tsou, M.S., Whittemore, D.O., 2001. User interface for ground water modeling: ArcView extension. *Journal of Hydrologic Engineering* 6 (3), 251–257. [http://dx.doi.org/10.1061/\(ASCE\)1084-0699\(2001\)6:3\(251\)](http://dx.doi.org/10.1061/(ASCE)1084-0699(2001)6:3(251)).

- USEPA (U.S. Environmental Protection Agency), 2003. Guidance for Evaluating the Technical Impracticability of Ground-Water Restoration, Interim Final, Directive 9234. 2–25, September. <http://www.epa.gov/superfund/health/conmedia/gwdocs/techimp.htm>.
- USGS (U.S. Geological Survey), 2007. Geographic Information Systems. [http://egsc.usgs.gov/isb/pubs/gis\\_poster/](http://egsc.usgs.gov/isb/pubs/gis_poster/).
- Van Grinsven, M., Mayer, A., Huckins, C., 2012. Estimation of streambed groundwater fluxes associated with coaster brook trout spawning habitat. *Groundwater* 50 (3), 432–441. <http://dx.doi.org/10.1111/j.1745-6584.2011.00856.x>.
- Walter, D.A., Masterson, J.P., 2003. Simulation of Advective Flow Under Steady-State and Transient Recharge Conditions, Camp Edwards, Massachusetts Military Reservation, Cape Cod, Massachusetts. U.S. Geological Survey Water-Resources Investigations Report 03-4053, 68 p. <http://pubs.usgs.gov/wri/wri034053/>.
- Weight, W., 2008. *Hydrogeology Field Manual*, second ed. The McGraw-Hill Companies, Inc., New York. 751 p.
- Weissmann, G.S., Zhang, Y., LaBolle, E.M., Fogg, G.E., 2002. Dispersion of groundwater age in an alluvial aquifer system. *Water Resources Research* 38 (10), 1198. <http://dx.doi.org/10.1029/2001WR000907>.
- Whitehead, R.L., 1994. Ground Water Atlas of the United States: Idaho, Oregon, Washington, U.S. Geological Survey Hydrologic Atlas, HA 730-H. [http://pubs.usgs.gov/ha/ha730/ch\\_h/index.html](http://pubs.usgs.gov/ha/ha730/ch_h/index.html).
- Winter, T.C., 2001. The concept of hydrologic landscapes. *Journal of the American Water Resources Association* 37 (2), 335–349. <http://dx.doi.org/10.1111/j.1752-1688.2001.tb00973.x>.
- Winter, T.C., Harvey, J.C., Franke, O.L., Alley, W.M., 1998. Ground Water and Surface Water, a Single Resource. U.S. Geological Survey Circular 1139, 79 p. <http://pubs.usgs.gov/circ/circ1139/>.
- Winter, T.C., Rosenberry, D.O., LaBaugh, J.W., 2003. Where does the ground water in small watersheds come from? *Groundwater* 41 (7), 989–1000. <http://dx.doi.org/10.1111/j.1745-6584.2003.tb02440.x>.
- Wuol, R.W., August 1993. Ground-water modeling and multiple working hypotheses. *The Professional Geologist*, 19–21.
- Ye, M., Pohlmann, K.F., Chapman, J.B., Pohll, G.M., Reeves, D.M., 2010. A model-averaging method for assessing groundwater conceptual model uncertainty. *Groundwater* 48 (5), 716–728. <http://dx.doi.org/10.1111/j.1745-6584.2009.00633.x>.
- Zektser, I.S., Everett, L.G. (Eds.), 2006. *Ground Water Resources of the World and Their Use*. NGWA Press, National Ground Water Association, Westerville, OH, 346 p.
- Zheng, C., Bennett, G.D., 2002. *Applied Contaminant Transport Modeling*, second ed. John Wiley & Sons, New York. 621 p.

## CHAPTER 3

# Basic Mathematics and the Computer Code

*The fascinating impressiveness of rigorous mathematical analysis, with its atmosphere of precision and elegance, should not blind us to the defects of the premises that condition the whole process. There is, perhaps, no beguilement more insidious and dangerous than an elaborate and elegant mathematical process built upon unfortified premises.*

*T.C. Chamberlin (1899)*

### Contents

3.1 Introduction	70
3.2 Governing Equation for Groundwater Flow	71
3.2.1 Assumptions	71
3.2.2 Derivation	71
3.3 Boundary Conditions	77
3.4 Analytical Models	78
3.4.1 Analytical Solutions	78
3.4.2 Analytic Element (AE) Models	80
3.5 Numerical Models	85
3.5.1 Finite Differences	86
3.5.2 Finite Elements	89
3.5.3 Control Volume Finite Differences	91
3.5.4 Solution Methods	95
3.6 Code Selection	96
3.6.1 Code Verification	99
3.6.2 Water Budget	99
3.6.3 Track Record	100
3.6.4 GUIs	101
3.7 Code Execution	102
3.7.1 Simulation Log	102
3.7.2 Execution Time	105
3.7.3 Closure Criteria and Solution Convergence	105
3.8 Common Modeling Errors	107
3.9 Problems	108
References	111

### Boxes

Box 3.1 The Hydraulic Conductivity Tensor	74
Box 3.2 Insights from Analytical Solutions	79

### 3.1 INTRODUCTION

The subsurface continuum is divided into the unsaturated zone above the water table, where pore space is filled with air and water, and the saturated zone below the water table, where pore space is completely filled with water. Our book focuses on flow in the saturated zone below the water table. Traditionally, water in the saturated zone is called groundwater and we follow that convention. Flow of water in the subsurface continuum is called variably saturated flow (Section 12.2); when we refer to simulating flow above the water table, we will use the term unsaturated flow.

All process-based models of groundwater flow are derived from two basic principles: conservation of mass, which states that water is not created or destroyed; and Darcy's law, which states that groundwater flows from high to low potential energy. A mathematical model for groundwater flow consists of a *governing equation* (derived from conservation of mass and Darcy's law) that represents processes within the problem domain; *boundary conditions* that represent processes along the boundaries; and, for time-dependent (transient) problems, *initial conditions* that specify values of the dependent variable (i.e., head) at the start of the simulation. In this chapter, we derive the governing equation for groundwater flow, introduce the mathematics of boundary conditions, and review commonly used methods for approximating the governing equation. A mathematical model can be solved analytically or numerically. Implementation of boundary conditions in a numerical model is discussed in Section 4.3 and initial conditions are covered in Section 7.4.

A model should simulate all processes important to addressing the modeling objective. Groundwater flow is usually the dominant process in all groundwater models. The focus of our book is modeling groundwater flow in a continuous porous medium without density effects. The basic governing equation for groundwater flow assumes that the density of groundwater is constant and approximately equal to  $1.0 \text{ gm/cm}^3$ , which is a reasonable assumption for water with concentrations of total dissolved solids (TDS) less than 10,000 mg/L and temperatures in the range of most shallow aquifers. For example, water at  $4^\circ\text{C}$  has a density of  $0.999973 \text{ gm/cm}^3$  but when heated to  $50^\circ\text{C}$  has a density of  $0.988047 \text{ gm/cm}^3$ . The most commonly encountered groundwater problem involving density effects is seawater intrusion in coastal aquifers (Box 4.4; Section 12.2); seawater has a density of  $1.025 \text{ gm/cm}^3$  and TDS of approximately 35,000 mg/L.

In Chapter 12, we briefly summarize approaches for simulating other processes the groundwater modeler will need to consider to solve advanced problems. In addition to variable density flow, those processes include flow through fractures and conduits; aquifer compaction; variably saturated flow; multiphase flow; and solute and heat transport. None of those processes is included in the general governing equation used in standard groundwater flow codes such as derived below. However, some codes have options for simulating flow through fractures and conduits, aquifer compaction, and variably saturated flow. Furthermore, groundwater flow codes can be coupled or linked to other codes that simulate multiphase flow, solute and heat transport, and rainfall and surface runoff processes. We describe options for simulating

additional processes throughout our book; however, in depth coverage of complex groundwater process simulation is beyond the scope of our text.

## 3.2 GOVERNING EQUATION FOR GROUNDWATER FLOW

### 3.2.1 Assumptions

Mathematical representation of hydrogeologic processes necessarily requires simplifying assumptions. Those assumptions are embodied in the governing equation. The governing equation derived below is the form most often used in groundwater flow modeling. It represents flow of a single phase fluid (water) at constant density in a continuous porous medium under Darcy's law.

In Section 3.1, we discussed the assumption of constant density. Single phase flow means that water is the only phase present in the system. In advanced problems, other phases could include gases, nonaqueous phase liquids, and oil (Section 12.2). In a continuous porous medium, water flows through connected pore space. An *equivalent porous medium (EPM)* is porous media that can reasonably be simulated as a continuous porous medium. For example, a carbonate aquifer with a well-connected network of fractures is usually simulated as an EPM. When fractures do not form a well-connected network, special options (Section 5.2) and codes (Section 12.2) may be used to simulate conduit flow through individual fractures or a network of fractures. When simulating solute transport, a dual domain approach can be used to simulate the transfer of solutes between fractures and the porous rock matrix (Section 12.3).

### 3.2.2 Derivation

The governing equation for flow through a porous medium is traditionally derived by referring to the flux of water through a cube of porous material that is large enough to be representative of the properties of the porous medium yet small enough so that the change of head within the volume is relatively small (Fig. 3.1). This cube of porous material is known as a *representative elementary volume or REV*, with volume equal to  $\Delta x \Delta y \Delta z$ .

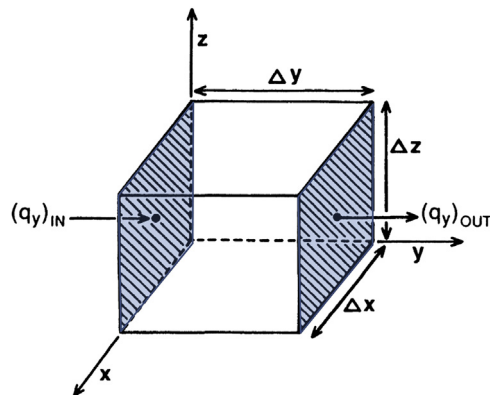


**Figure 3.1** Representative elementary volume ( $\Delta x \Delta y \Delta z$ ) showing the components of flow along the  $y$ -coordinate axis.

The flux through the REV,  $\mathbf{q}$ , is a vector whose magnitude is expressed by three components,  $q_x$ ,  $q_y$ , and  $q_z$ . Formally, we write:

$$\mathbf{q} = q_x \mathbf{i}_x + q_y \mathbf{i}_y + q_z \mathbf{i}_z \quad (3.1)$$

where  $\mathbf{i}_x$ ,  $\mathbf{i}_y$ , and  $\mathbf{i}_z$  are unit vectors along the  $x$ ,  $y$ , and  $z$  axes, respectively. Conservation of mass requires a water balance within the REV such that,

$$\text{outflow} - \text{inflow} = \Delta \text{ storage} \quad (3.2)$$

Consider flow along the  $y$ -axis of the REV in Fig. 3.1. Inflow occurs through the face  $\Delta x \Delta z$  and is equal to  $(q_y)_{\text{IN}}$ . Outflow is equal to  $(q_y)_{\text{OUT}}$ . The volumetric outflow rate minus the volumetric inflow rate along the  $y$ -axis is:

$$[(q_y)_{\text{OUT}} - (q_y)_{\text{IN}}] \Delta x \Delta z \quad (3.3)$$

which can be written as,

$$\frac{(q_y)_{\text{OUT}} - (q_y)_{\text{IN}}}{\Delta y} (\Delta x \Delta y \Delta z) \quad (3.4)$$

Dropping the IN and OUT subscripts and converting from difference notation to a derivative, the change in flow rate through the REV along the  $y$ -axis is:

$$\frac{\partial q_y}{\partial y} (\Delta x \Delta y \Delta z) \quad (3.5)$$

Similar expressions are written for the change in flow rate along the  $x$ - and  $z$ -axes. Using Eqn (3.2), the total change in flow rate is equal to the change in storage:

$$\left( \frac{\partial q_x}{\partial x} + \frac{\partial q_y}{\partial y} + \frac{\partial q_z}{\partial z} \right) \Delta x \Delta y \Delta z = \Delta \text{storage} \quad (3.6)$$

We must allow for the possibility of a sink (e.g., a pumping well) or source of water (e.g., an injection well or recharge) within the REV. The volumetric inflow rate from sources and sinks is represented by  $W^* \Delta x \Delta y \Delta z$ , where we use the convention that  $W^*$  is positive when it is a source of water. As a source of water,  $W^*$  is subtracted from the left-hand side of Eqn (3.6) (notice the minus sign in front of inflow in Eqn (3.2)), resulting in:

$$\left( \frac{\partial q_x}{\partial x} + \frac{\partial q_y}{\partial y} + \frac{\partial q_z}{\partial z} - W^* \right) \Delta x \Delta y \Delta z = \Delta \text{storage} \quad (3.7)$$

Now consider the right-hand side of Eqn (3.7). Change in storage is represented by specific storage ( $S_s$ ), which is the volume of water released from storage per unit change in head ( $h$ ) per unit volume of aquifer:

$$S_s = - \frac{\Delta V}{\Delta h \Delta x \Delta y \Delta z} \quad (3.8)$$



The convention in Eqn (3.8) is that  $\Delta V$  is intrinsically positive when  $\Delta h$  is negative, or in other words, water is released from storage when head decreases. The rate of change in storage in the REV is:

$$\frac{\Delta V}{\Delta t} = -S_s \frac{\Delta h}{\Delta t} \Delta x \Delta y \Delta z \quad (3.9)$$

Combining Eqns (3.7) and (3.9) and dividing through by  $\Delta x \Delta y \Delta z$  yields the final form of the water balance equation:

$$\frac{\partial q_x}{\partial x} + \frac{\partial q_y}{\partial y} + \frac{\partial q_z}{\partial z} - W^* = -S_s \frac{\partial h}{\partial t} \quad (3.10)$$

This equation is of little practical use, however, because we cannot easily measure  $\mathbf{q}$ . We want a governing equation written in terms of head because head is an observed quantity easily measured in wells. Darcy's law ( $\mathbf{q} = -\mathbf{K} \mathbf{grad} h$ ) relates specific discharge ( $\mathbf{q}$ ) to head ( $h$ ) where  $\mathbf{grad} h$  is the gradient of  $h$ . Both  $\mathbf{q}$  and  $\mathbf{grad} h$  are vectors and  $\mathbf{K}$  is the hydraulic conductivity tensor (Box 3.1). The components of the specific discharge vector,  $\mathbf{q}$ , are:

$$\begin{aligned} q_x &= -K_x \frac{\partial h}{\partial x} \\ q_y &= -K_y \frac{\partial h}{\partial y} \\ q_z &= -K_z \frac{\partial h}{\partial z} \end{aligned} \quad (3.11)$$

where  $K_x$ ,  $K_y$ , and  $K_z$  are the principal components of the hydraulic conductivity tensor  $\mathbf{K}$  and  $\partial h/\partial x$ ,  $\partial h/\partial y$ , and  $\partial h/\partial z$  are components of the vector  $\mathbf{grad} h$ , the gradient of head.

Equation (3.11) is substituted into Eqn (3.10) to give the general governing equation (differential equation) representing three-dimensional (3D) transient groundwater flow for heterogeneous and anisotropic conditions:

$$\frac{\partial}{\partial x} \left( K_x \frac{\partial h}{\partial x} \right) + \frac{\partial}{\partial y} \left( K_y \frac{\partial h}{\partial y} \right) + \frac{\partial}{\partial z} \left( K_z \frac{\partial h}{\partial z} \right) = S_s \frac{\partial h}{\partial t} - W^* \quad (3.12)$$

The variable of interest,  $h$ , is the dependent variable, while  $x$ ,  $y$ ,  $z$ , and  $t$  are the independent variables and  $K_x$ ,  $K_y$ ,  $K_z$ ,  $S_s$ , and  $W^*$  are parameters. The subscripts on  $K$  denote anisotropic conditions (Box 3.1), meaning that hydraulic conductivity can vary with direction,  $x$ ,  $y$ , and  $z$ . The placement of  $K$  within the differential signs allows for spatial variation (heterogeneity) in hydraulic conductivity.

### Box 3.1 The Hydraulic Conductivity Tensor

Hydraulic conductivity is a tensor, which means that its properties change with direction. Mathematically, a tensor operates on a vector and transforms it into another vector, potentially changing both its magnitude and direction. For example, in Darcy's law ( $\mathbf{q} = -\mathbf{K} \text{grad } h$ ) the hydraulic conductivity tensor  $\mathbf{K}$  relates the **grad**  $h$  vector to the specific discharge vector  $\mathbf{q}$ . The components of  $\mathbf{q}$  ( $q_x, q_y, q_z$ ) are aligned with the coordinate axes ( $x, y, z$ ). Then we align the principal components of the hydraulic conductivity tensor  $\mathbf{K}$  ( $K_x, K_y, K_z$ ) with the  $x$ -,  $y$ -, and  $z$ -axes (Fig. B3.1.1(a)).

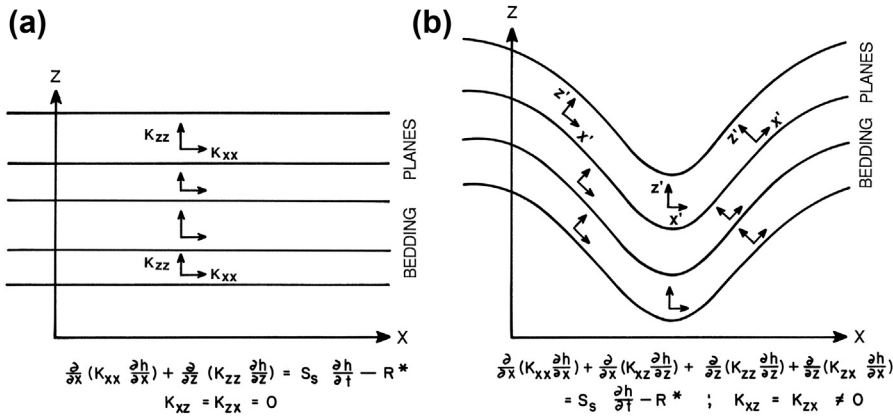


**Figure B3.1.1** Global and local coordinate systems in two dimensions. Two-dimensions are shown for convenience but the concepts are easily extended to three dimensions. (a) The  $x$ - $z$  global coordinate system is aligned with the principal directions of  $\mathbf{K}$  ( $K_{xx} = K_x$  and  $K_{zz} = K_z$ ). The governing equation for two-dimensional (2D) transient flow has only two hydraulic conductivity terms. (b) Complicated hydrogeology requires four components of  $\mathbf{K}$ . Local coordinates ( $x'$ - $z'$ ) are defined to align with the principal components of the local hydraulic conductivity tensor  $K'_{xx}, K'_{zz}$ . The governing equation for 2D transient flow in the global coordinate system requires four components of  $\mathbf{K}$  defined in the global coordinate system:  $K_{xx}, K_{zz}$ , and  $K_{xz} = K_{zx}$ .

When groundwater flow is represented by the usual form of Darcy's law (Eqn (3.11)), flow in any coordinate direction is related only to the gradient in that direction; for example,  $q_x$  is related to the head gradient in the  $x$ -direction. Of course, flow ( $\mathbf{q}$ ) can still be three-dimensional and is computed from Eqn (3.1). When the global and local coordinate systems are aligned (Fig. B3.1.1(a)), hydraulic conductivity,  $\mathbf{K}$ , is represented by a matrix, where  $K_{xx}, K_{yy}$ , and  $K_{zz}$  are the entries along the center diagonal and the off-diagonal components of  $\mathbf{K}$  are zero:

$$\mathbf{K} = \begin{bmatrix} K_{xx} & 0 & 0 \\ 0 & K_{yy} & 0 \\ 0 & 0 & K_{zz} \end{bmatrix} \quad (\text{B3.1.1})$$

Then Eqn (3.11) can be generated from the vector form of Darcy's law ( $\mathbf{q} = -\mathbf{K} \text{grad } h$ ) by matrix multiplication using Eqn (B3.1.1) for  $\mathbf{K}$ , where we drop the second subscript on the components of  $\mathbf{K}$  (i.e.,  $K_{xx} = K_x, K_{yy} = K_y$ , and  $K_{zz} = K_z$ ).

### Box 3.1 The Hydraulic Conductivity Tensor—cont'd

Sometimes (see Section 5.3), however, the hydrogeology is more complicated (Fig. B3.1.1(b)) and it is not possible to align  $\underline{\mathbf{K}}$  globally with the local coordinate axes. Then Eqn (3.11) does not adequately describe groundwater flow because  $q_x$ ,  $q_y$ , and  $q_z$  are each dependent on head gradients in all three coordinate directions. In that case, we need a way to relate the components of flow in each coordinate direction to gradients in all three directions. This is done by using the full form of the  $\underline{\mathbf{K}}$  tensor:

$$\underline{\mathbf{K}} = \begin{bmatrix} K_{xx} & K_{xy} & K_{xz} \\ K_{yx} & K_{yy} & K_{yz} \\ K_{zx} & K_{zy} & K_{zz} \end{bmatrix} \quad (\text{B3.1.2})$$

where  $K_{xx}$ ,  $K_{yy}$ ,  $K_{zz}$  are the principal components of  $\underline{\mathbf{K}}$  in the  $x$ ,  $y$ ,  $z$  directions, respectively, but they are not equal to the values  $K_x$ ,  $K_y$ ,  $K_z$  that we normally derive from field and/or laboratory measurements because those values assume that the principal components of  $\underline{\mathbf{K}}$  are aligned with the coordinate axes as in Fig. B3.1.1(a). When the principal components of  $\underline{\mathbf{K}}$  are not aligned with the coordinate axes, the components of  $\underline{\mathbf{K}}$  in the matrix shown in Eqn (B3.1.2) are best thought of as mathematical terms that relate a gradient of flow to a component of  $\mathbf{q}$  as expressed in the expanded form of Darcy's law:

$$\begin{aligned} q_x &= -K_{xx} \frac{\partial h}{\partial x} - K_{xy} \frac{\partial h}{\partial y} - K_{xz} \frac{\partial h}{\partial z} \\ q_y &= -K_{yx} \frac{\partial h}{\partial x} - K_{yy} \frac{\partial h}{\partial y} - K_{yz} \frac{\partial h}{\partial z} \\ q_z &= -K_{zx} \frac{\partial h}{\partial x} - K_{zy} \frac{\partial h}{\partial y} - K_{zz} \frac{\partial h}{\partial z} \end{aligned} \quad (\text{B3.1.3})$$

When Darcy's law is written as Eqn (B3.1.3), the governing equation for groundwater flow (Eqn (3.12)) is expanded as follows:

$$\begin{aligned} &\frac{\partial}{\partial x} \left( K_{xx} \frac{\partial h}{\partial x} + K_{xy} \frac{\partial h}{\partial y} + K_{xz} \frac{\partial h}{\partial z} \right) + \frac{\partial}{\partial y} \left( K_{yx} \frac{\partial h}{\partial x} + K_{yy} \frac{\partial h}{\partial y} + K_{yz} \frac{\partial h}{\partial z} \right) + \frac{\partial}{\partial z} \left( K_{zx} \frac{\partial h}{\partial x} + K_{zy} \frac{\partial h}{\partial y} + K_{zz} \frac{\partial h}{\partial z} \right) \\ &= S_s \frac{\partial h}{\partial t} - W^* \end{aligned} \quad (\text{B3.1.4})$$

When solving Eqn (B3.1.4), the  $x$ - $y$ - $z$  coordinate system refers to the global coordinate system for the entire problem domain and we must specify values of the principal and the off-diagonal components of  $\underline{\mathbf{K}}$  in the global coordinate system. Fortunately, the  $\underline{\mathbf{K}}$  matrix is symmetric across the center diagonal so that  $K_{yx} = K_{xy}$ ;  $K_{zx} = K_{xz}$ ;  $K_{zy} = K_{yz}$ . However, we still need to find values for those components and for the components along the center diagonal. The components of  $\underline{\mathbf{K}}$  in the global coordinate system could be measured in the field using an aquifer (pumping) test (e.g., Quinones-Aponte, 1989; Maslia and Randolph, 1987). More typically, we find those values by defining local coordinate systems for each cell or element in a model so that each local coordinate system is locally aligned with the principal components of  $\underline{\mathbf{K}}$  in that coordinate system (Fig. B3.1.1(b)). Then  $\underline{\mathbf{K}}$  in the local coordinate system has

(Continued)

### Box 3.1 The Hydraulic Conductivity Tensor—cont'd

only three nonzero components since the off-diagonal components are zero (Eqn (B3.1.1)); each cell or element is associated with its own local coordinate system and with cell- or element-specific values of  $K_x$ ,  $K_y$ , and  $K_z$ , which represent values of hydraulic conductivity measured in the normal way. The angle between the global and the local system relates the known (measured) values of  $K_x$ ,  $K_y$ , and  $K_z$  in the local system to the unknown components of  $\mathbf{K}$  in the global system. In other words, the components of  $\mathbf{K}$  in each cell or element transform with a coordinate rotation from local to global coordinates. Details for deriving equations to calculate the components of  $\mathbf{K}$  for each cell or element in the global system are given by Wang and Anderson (1982, Appendix A) for two dimensions and by Bear (1972) for three dimensions. Diersch (2014, p. 229, in Eqn (7.8)), gives the components of  $\mathbf{K}$  in two dimensions and instructions for calculating components in three dimensions.

Most groundwater flow codes are not designed to solve Eqn (B3.1.4), but some FE codes (e.g., FEFLOW, Diersch, 2014; SUTRA, Voss and Provost, 2002) have this capability. The finite-difference method considers cells within a globally defined grid so that the assignment of local coordinates is not straightforward. In the FE method, however, each element is always considered separately so that it is relatively easy to assign local coordinates to each element and incorporate the mathematics of coordinate rotation.

Fortunately, in most hydrogeological settings the principal components of  $\mathbf{K}$  can be aligned with the coordinate axis. Geologic beds generally dip at relatively low angles ( $<10^\circ$ ) and can be considered essentially horizontal so that  $K_x$ ,  $K_y$ ,  $K_z$  approximately align with the global  $x$ -,  $y$ -,  $z$ -coordinate axes. In that case,  $\mathbf{K}$  is still a tensor and is expressed mathematically as a matrix but the off-diagonal components of  $\mathbf{K}$  are zero (Eqn (B3.1.1)) and the usual form of Darcy's law (Eqn (3.11)) and the standard form of the governing equation (Eqn (3.12)) apply.

Equation (3.12) assumes that the principal components of the hydraulic conductivity tensor ( $K_x$ ,  $K_y$ ,  $K_z$ ) are aligned with the coordinate axes  $x$ ,  $y$ ,  $z$ . When this is not the case, it is necessary to use a version of the governing equation that includes all nine components of the hydraulic conductivity tensor, rather than just the three principal components in Eqn (3.12) (Box 3.1).

Equation (3.12) is used in most numerical groundwater flow codes. The equation simplifies when the problem is steady state ( $\partial h/\partial t = 0$ ) and/or when two-dimensional (2D). For 2D horizontal flow through a confined aquifer, vertically integrated parameters, i.e., transmissivity ( $T$ ) and storativity ( $S$ ), can be defined. Then the components of transmissivity in the  $x$ - and  $y$ -directions are  $T_x = K_x b$  and  $T_y = K_y b$ , respectively, where  $b$  is aquifer thickness;  $S = S_s b$ . The sink/source term,  $W^*$ , in Eqn (3.12) becomes a flux, expressed as volume of water per area of aquifer per time,  $R$  (L/T). Under these conditions Eqn (3.12) simplifies to:

$$\frac{\partial}{\partial x} \left( T_x \frac{\partial h}{\partial x} \right) + \frac{\partial}{\partial y} \left( T_y \frac{\partial h}{\partial y} \right) = S \frac{\partial h}{\partial t} - R \quad (3.13a)$$

For 2D horizontal flow in an unconfined, heterogeneous, anisotropic aquifer, the differential equation is:

$$\frac{\partial}{\partial x} \left( K_x h \frac{\partial h}{\partial x} \right) + \frac{\partial}{\partial y} \left( K_y h \frac{\partial h}{\partial y} \right) = S_y \frac{\partial h}{\partial t} - R \quad (3.13b)$$

where  $S_y$  is specific yield and  $R$  is recharge rate. Here, head ( $h$ ) is equal to the elevation of the water table measured from the base of the aquifer. 2D horizontal flow, expressed by Eqns 3.13(a) and (b), represents flow under the Dupuit–Forchheimer approximation (Section 4.1; Box 4.1). For steady-state flow with no recharge ( $R = 0$ ) in a homogenous and isotropic aquifer, Eqns 3.13(a) and (b) simplify to the well-known Laplace equation (Section 3.4).

### 3.3 BOUNDARY CONDITIONS

Mathematically, boundary conditions are classified into three types.

*Type 1. Specified head boundary (Dirichlet conditions)* where head along the boundary is set at a known value. Heads along a specified head boundary may vary with space. A constant head boundary is a special case Type 1 boundary where the heads along the boundary are set to the same value.

*Type 2. Specified flow boundary (Neumann conditions)* where the derivative of head at the boundary is specified. Flow is calculated from Darcy's law. For example, a flux boundary condition imposed at the  $\Delta x \Delta z$  face in Fig. 3.1 would be written:

$$\frac{\partial h}{\partial y} = -\frac{q_y}{K_y} \quad (3.14)$$

A no flow boundary is a special case Type 2 boundary where the flow across the boundary is zero.

*Type 3. Head-dependent boundary (Cauchy conditions)* where flow across the boundary is calculated from Darcy's law using a gradient calculated as the difference between a specified head outside the boundary and the head computed by the model at the node located on or near the boundary. This type of boundary condition is sometimes called a mixed boundary condition because it relates a boundary head ( $h_b$ ) to a boundary flow. For example, a head-dependent boundary condition imposed at the right-hand side  $\Delta x \Delta z$  face of the cell in Fig. 3.1 would be written in numerical form as:

$$q_y = -K_y \frac{h_b - h_{i,j,k}}{\Delta y/2} \quad (3.15)$$

where  $h_{i,j,k}$  is the head computed by the model in the center of the cell;  $h_b$  is the head specified at the boundary along the  $\Delta x \Delta z$  face, which is located a distance  $\Delta y/2$  from the center of the cell. This boundary condition induces flow through the boundary with the direction of flow dependent on the relative values of  $h_{i,j,k}$  and  $h_b$ .

The names Dirichlet, Neumann, and Cauchy refer to nineteenth-century mathematicians who studied problems involving the respective boundary condition that bears their name. These same three types of boundary conditions also pertain to other areas of science such as solute and heat transport, where the dependent variable is concentration and temperature, respectively.

Strictly speaking, boundary conditions, as used here, refer to hydraulic conditions along the perimeter of the problem domain. In Section 4.2, we introduce the concept of internal boundary conditions to represent sinks and sources within the interior of the problem domain. Dirichlet, Neumann, and Cauchy boundary conditions can be applied to both perimeter and interior boundaries. Moreover, all three types of boundary conditions can be time-dependent if boundary heads and/or flows are updated as the simulation progresses. Implementation of boundary conditions in a numerical model is discussed in Section 4.3.

### 3.4 ANALYTICAL MODELS

A mathematical model can be solved using analytical or numerical methods. Numerical models are the focus of our text, but in this section and in [Box 3.2](#) we briefly discuss analytical models.

#### 3.4.1 Analytical Solutions

Analytical solutions have the advantage over numerical solutions of being quicker to solve, numerically exact, and continuous in time and space. Analytical models use simpler forms of the governing equation than [Eqn \(3.12\)](#) and require simple system geometry and boundary conditions. The solution of relatively complex analytical models requires application of complicated mathematics and the solution is typically coded into a computer program for ease of application (e.g., [Barlow and Moench, 1998](#)).

Examples of analytical solutions can be found in most hydrogeology textbooks (e.g., [Fitts, 2013](#)) and in journal papers. [Bruggeman \(1999\)](#) provides a comprehensive volume of analytical solutions for groundwater problems. [Barlow and Moench \(1998\)](#) and [Reeves \(2008\)](#) present analytical solutions for aquifer-stream systems and computer programs for their solution. A simple analytical model is discussed in [Box 3.2](#).

Although an analytical model is a highly simplified approximation of a field setting, for some problems an analytical solution may be adequate to address the modeling purpose. For example, the standard approach for estimating hydraulic conductivity from aquifer (pumping) tests utilizes analytical solutions such as the Thiem or Theis equations for steady-state and transient conditions, respectively. Furthermore, analytical solutions are useful in verifying that a numerical solution has been coded properly ([Ségol, 1994](#)). They provide helpful guidelines for numerical modeling ([Haitjema, 2006](#); [Box 3.2](#)) and can test model conceptualization (e.g., [Kelson et al., 2002](#)).

### Box 3.2 Insights from Analytical Solutions

Simple analytical solutions are easily manipulated and solved by hand calculations or spreadsheets, and can give valuable insights into system behavior. For example, consider a model of one-dimensional, steady-state flow in a homogeneous, unconfined aquifer receiving recharge ( $R$ ) at a constant rate (Fig. B3.2.1). The aquifer is bounded on both ends by streams. The stage in the streams defines the datum for head. The saturated thickness of the aquifer below the datum,  $b$ , is much greater than the saturated thickness,  $h$ , above the datum, allowing us to linearize the unconfined flow equation by using transmissivity ( $T = Kb$ ) instead of hydraulic conductivity,  $K$ . In other words, we assume  $T = K(b + h) \cong Kb$ , so that  $T$  is a constant.

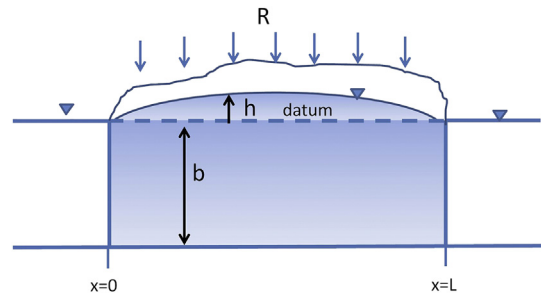


Figure B3.2.1 Conceptual model for one-dimensional flow problem.

The mathematical model is as follows:

**Governing equation:**

$$\frac{d^2h}{dx^2} = -\frac{R}{T} \quad (\text{B3.2.1a})$$

for  $0 < x < L$

**Boundary conditions:**

at  $x = 0$

$$h(0) = 0 \quad (\text{B3.2.1b})$$

at  $x = L$

$$h(L) = 0 \quad (\text{B3.2.1c})$$

The general solution of Eqn (B3.2.1a) is:

$$h(x) = -\frac{R}{T} \frac{x^2}{2} + a_1x + a_2 \quad (\text{B3.2.2})$$

where  $a_1$  and  $a_2$  are arbitrary constants that depend on the boundary conditions. Substituting the boundary conditions (Eqns (B3.2.1b) and (B3.2.1c)) into Eqn (B3.2.2) gives  $a_2 = 0$  and  $a_1 = RL/2T$ . Then the solution of the model is:

$$h(x) = \frac{R}{2T} (Lx - x^2) \quad (\text{B3.2.3})$$

We can learn quite a bit about how this system functions from Eqn (B3.2.3). First, we see that head is directly related to  $R$  (e.g., doubling  $R$ , doubles head everywhere in the interior of the

(Continued)

### Box 3.2 Insights from Analytical Solutions—cont'd

problem domain) and head is inversely related to  $T$ . Because  $L$  is determined by the dimension of the problem, any increase in  $R$  can be simply offset by corresponding increases in  $T$  to give the same calculated heads. Simulated head can be changed by adjusting  $R/T$ ; if we know the heads only from field measurements, we can estimate this ratio but not  $R$  or  $T$  individually.

If the model correctly simulates the head at the groundwater divide between the two streams (at  $x = L/2$ ), heads in the rest of the system will be at least approximately correct. From Eqn (B3.2.3), the head at the divide,  $h_D$ , is:

$$h_D = \frac{RL^2}{8T} \quad (\text{B3.2.4})$$

Equation (B3.2.4) shows that the head at the divide, like heads in the rest of the system, is directly related to  $R$  and  $1/T$ . However, the head at the divide is dependent on the length of the system squared ( $L^2$ ); in other words, the head at the divide increases by  $L^2$  as  $L$  increases. Hence, Eqn (B3.2.4) tells us that the head at the divide is most sensitive to the distance between the streams,  $L$ , and therefore  $L$  is the most important parameter in this system. Fortunately, the location of sinks is usually well known and distances can be accurately specified. Some additional insights from Eqn (B3.2.4) are explored in Box 4.6.

The analysis above was for a very simple system; however, the general observations about the relation between  $h$  and  $R$  and  $T$  (or  $K = T/b$ ), and between  $h_D$  and  $L$  also pertain to more complex problems (e.g., Box 4.6). Other useful parameters can be derived from analytical solutions including the characteristic leakage length,  $\lambda$ , and the aquifer response time,  $\tau$ . The characteristic leakage length,  $\lambda$ , is used for multiaquifer systems and groundwater–surface water interaction (Section 5.2). Aquifer response time,  $\tau$ , helps determine whether a system can be modeled under steady-state conditions or whether a transient simulation is necessary (Section 7.2).

## 3.4.2 Analytic Element (AE) Models

The AE method (AEM) uses superposition of multiple analytic solutions to solve relatively complex groundwater flow problems. The method was introduced by Professor Otto Strack and coworkers (Strack and Haitjema, 1981a,b; see Strack, 2003 for an overview of the history of the AEM). Fitts (2013) gives a good overview of the method; Haitjema (1995) presents a comprehensive introduction of the AEM for applied groundwater modeling, and Strack (1989) provides details on the wide range of AEs and related mathematics. A brief description of the AEM is given below.

The AEM relies on the *principle of superposition*, which allows linear solutions to be added (see Fitts, 2013; Reilly et al., 1987). For example, an analytical solution that solves for the cone of depression of a pumping well within a horizontal potentiometric surface may be added to a solution for regional flow so that the composite solution simulates pumping from a regionally sloping potentiometric surface. Superposition is also applied to problems involving overlapping cones of depression produced by two or more pumping wells (Fig. 3.2).



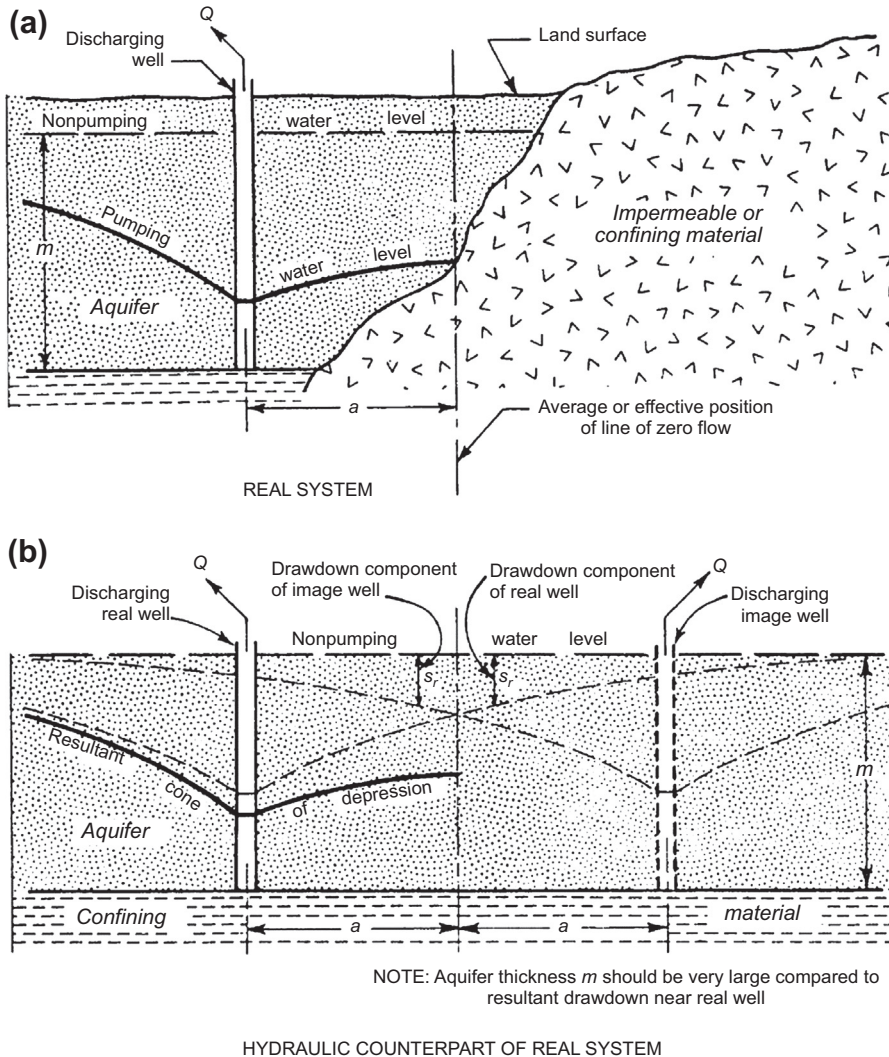


**Figure 3.2** Principle of superposition showing (a) the field setting; (b) superposition of drawdowns from two wells to represent the effect of an impermeable boundary (or the effect of two wells pumping at the same rate) (Ferris et al., 1962).

The AEM utilizes analytic solutions (i.e., analytical solutions for distinct flow features that influence groundwater flow) that are called *analytic elements*. An AE code superposes many AEs, sometimes thousands, to represent relevant hydrologic features and stresses. Each stress and hydrologic feature (recharge, pumping, surface water bodies) and each heterogeneity is represented by separate AEs (Fig. 3.3). AEs have been defined for a wide variety of features, including heterogeneities, thin barriers, line sources/sinks of

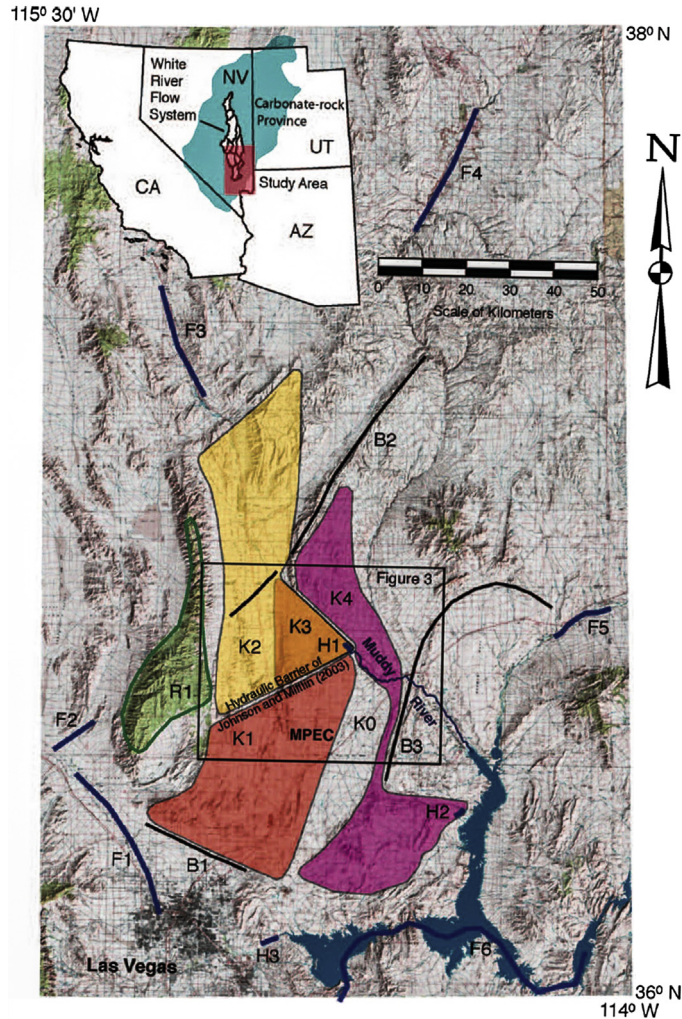


**Figure 3.3** Map view of an area modeled using analytic elements showing elements for hydraulic conductivity domains ( $K$ ); no-flow barriers ( $B$ ) including faults at  $B1$  and  $B2$ ; far-field features ( $F$ ) including rivers; near-field discharge ( $H$ ), including springs at  $H1$  and  $H2$ ; and recharge ( $R$ ) (Johnson and Mifflin, 2006).

specified head or specified discharge, leakage, areal and distributed recharge, fully and partially penetrating wells, and uniform flow. Fitts (2013) discusses some of the commonly used AEs. In designing an AE model, many AEs are used to define flow in the *near-field* region, while fewer are used in the *far-field* (Fig. 3.3). For most problems the AE solution is exact at all locations like an analytical solution, but some approximations are introduced by discretization of AEs within the problem domain to represent realistic geometries (Fig. 3.3).

The AEM assumes an infinite problem domain with boundary conditions set at infinity. To control flow to and from infinity, the area of primary interest (the near-field region) is delimited with internal boundary conditions in the far-field region (Fig. 3.3). An advantage of the AEM is that it is not necessary to set perimeter boundary conditions around the near-field region. Instead sources and sinks in the far-field control flow to and from the near-field region. Furthermore, an AE model can easily be extended by adding more AEs to the far-field, which theoretically extends to infinity, or modified by adding more elements in the near-field. Proper discretization of the internal boundaries, which often are surface water features, is important (e.g., Hunt et al., 1998).

In numerical models, head is typically the dependent variable (Eqns (3.12) and (3.13)) but in most AE codes the governing equation is written in terms of a discharge potential,  $\Phi$  (Haitjema, 1995; Strack, 1989). One advantage of this formulation is that the discharge potential gives linear partial differential equations that pertain to both confined and unconfined groundwater flow. Not only are linear equations necessary for superposition but in many groundwater modeling applications linearity is advantageous for numerical efficiency even in complex numerical models (e.g., see Sheets et al., 2015). Discharge potentials can be applied to many types of groundwater flow problems (see Strack, 1989; Box 4.4), but for simplicity we focus on the basic forms of the governing equation. The discharge potential,  $\Phi$  ( $L^3/T$ ), for a confined aquifer is:

$$\Phi = Th \quad (3.16)$$

where  $T$  is transmissivity and  $h$  is head; for an unconfined aquifer, the discharge potential is:

$$\Phi = \frac{Kh^2}{2} \quad (3.17)$$

The Laplace equation (for 2D, steady-state flow without recharge under homogeneous and isotropic conditions) can be written in terms of the discharge potential, as:

$$\frac{\partial^2 \Phi}{\partial x^2} + \frac{\partial^2 \Phi}{\partial y^2} = 0 \quad (3.18)$$

When  $R$  is not equal to zero the Poisson equation applies:

$$\frac{\partial^2 \Phi}{\partial x^2} + \frac{\partial^2 \Phi}{\partial y^2} = -R \quad (3.19)$$

When the Laplace equation (Eqn (3.18)) applies, the discharge potential has the advantageous feature that the derivative of  $\Phi$  defines the streamfunction,  $\psi$  ( $L^3/T$ ),

which can be used to calculate groundwater flowpaths without particle tracking. The streamfunction is defined from the discharge potential as follows:

$$\begin{aligned}\frac{\partial\psi}{\partial y} &= +\frac{\partial\Phi}{\partial x} = -Q'_x \\ \frac{\partial\psi}{\partial x} &= -\frac{\partial\Phi}{\partial y} = Q'_y\end{aligned}\tag{3.20}$$

where  $Q'_x$  and  $Q'_y$  are discharge per unit width ( $L^2/T$ ) in the  $x$ - and  $y$ -directions, respectively. The discharge,  $Q$ , between streamlines is the change in the streamfunction:

$$\Delta Q = \psi_1 - \psi_2\tag{3.21}$$

Plotting  $\Phi$  and  $\psi$  produces a flow net but flow nets can be constructed only for a limited set of conditions as described in Box 8.2. The AEM itself is not so restricted and in practice, AE codes use particle tracking methods (Chapter 8) to calculate flowpaths for realistic groundwater problems.

AE models are not limited to solutions of the Laplace and Poisson equations but can include both anisotropy and heterogeneity. Anisotropy is either assumed constant over the problem domain or allowed to vary by subdomains (Fitts, 2010). Heterogeneity can also be included in all AE models (as in Fig. 3.3). In applied modeling, typically the AEM is used to solve for 2D areal steady-state groundwater flow using the Dupuit-Forchheimer approximation (Section 4.1; Box 4.1). However, the method has been extended for special cases of 3D flow, as well as transient problems, and there also are some numerical experimental applications to dispersion of solutes in highly heterogeneous systems (e.g., Dagan et al., 2003; Jankovic et al., 2003). New AEs continue to be developed (e.g., Haitjema et al., 2006; Strack 2006) and researchers are expanding the method such that the types of problems the AEM handles continue to increase. The AEM has found a niche in applied groundwater modeling for easy to construct simulations of complex 2D horizontal flow problems (Hunt, 2006) at very large regional scales (e.g., Bakker et al., 1999; de Lange, 2006; Feinstein et al., 2006), regional scales (e.g., Kelson et al., 2002; Feinstein et al., 2003; Dripps et al., 2006), and even site scales (e.g., Zaadnoordijk, 2006). AE models are well suited as screening models because they can be constructed relatively quickly. Moreover, the AE solution in an aquifer of infinite areal extent can be used to simulate near-field boundaries for a numerical model (Section 4.4; Haitjema et al., 2010; Feinstein et al., 2003; Hunt et al., 1998).

A variety of AE codes are available such as SLAEM/MLAEM (<http://www.strackconsulting.com/aem-products/>), GFLOW (Haitjema, 1995; <http://www.haitjema.com/>), and AnAqSim (Fitts, 2010; <http://www.fittsgeosolutions.com/>). GFLOW is widely used for applied modeling (see review by Yager and Neville, 2002) to simulate single layer areal groundwater flow in two-dimensions. Specialized AE codes

simulate stratified and multilayer aquifers (e.g., AnAqSim, Fitts, 2010, see review by McLane, 2012; also TimML <http://code.google.com/p/timml/> and MLAEM <http://www.strackconsulting.com/aem-products/>), and include capabilities to simulate seawater intrusion (Box 4.4).

### 3.5 NUMERICAL MODELS

Numerical models use an approximate form of the governing equation to calculate head at selected locations. In contrast to analytical solutions and the AEM, a numerical solution is not continuous in space or time; head is calculated at discrete points (nodes) in space and for specified values of time. However, numerical models can solve the full transient, 3D, heterogeneous and anisotropic governing equation (Eqn (3.12)) under complex boundary and initial conditions.

The numerical methods most commonly used in groundwater modeling are the finite-difference (FD) method and the finite-element (FE) method. In the FD method, nodes are located in 3D space using indices  $(i,j,k)$  to assign relative locations within a rectangular grid (Fig. 3.4). In the FE method, the locations of nodes are designated using

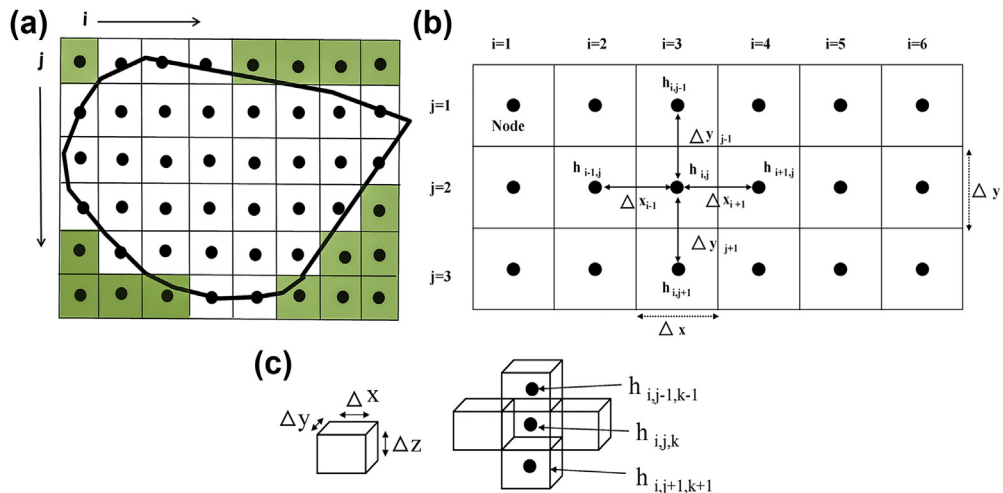


**Figure 3.4** Finite-difference (FD) grid and notation. (a) Two-dimensional (2D) horizontal FD grid with uniform nodal spacing;  $i =$  columns and  $j =$  rows. Sometimes a different indexing convention is used. For example, in MODFLOW  $i =$  rows and  $j =$  columns. The cells are block-centered; the heavy dark line represents the problem domain. Inactive cells (those outside the boundary of the problem domain) are shaded. (b) 2D horizontal FD grid with notation for five nodes comprising the FD computational module (star) centered around node  $(i,j)$ . (c) Three-dimensional notation where  $\Delta z$  represents the vertical distance between nodes and  $k$  is the vertical index. The group of blocks at the right is shown in 2D space (the two blocks perpendicular to the page along the  $y$ -axis are not shown). The group of seven nodes including node  $(i,j,k)$  comprise the FD computational module in three dimensions.

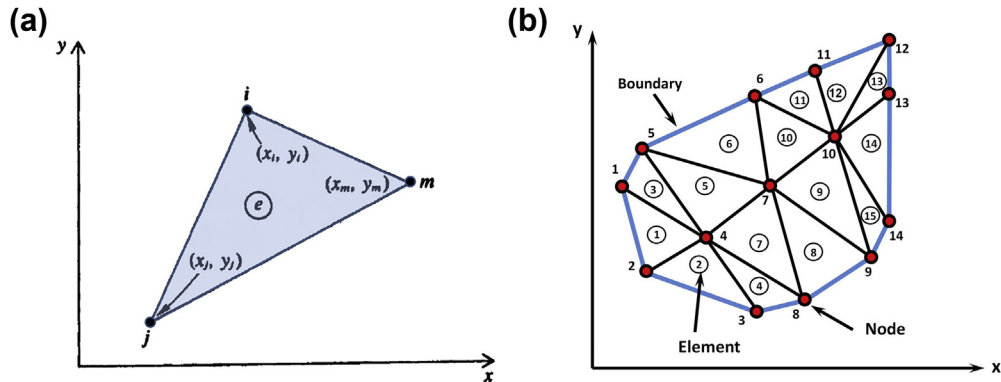


**Figure 3.5** Two-dimensional horizontal finite-element mesh with triangular elements and notation. (a) A representative triangular element with nodes  $i$ ,  $j$ , and  $m$ , labeled in counterclockwise order, with spatial coordinates  $(x,y)$ ; (b) Triangular elements, with element numbers inside circles, are defined by numbered nodes. The elements are fitted to the boundary of the problem domain (modified from Wang and Anderson, 1982).

spatial coordinates  $(x,y,z)$  in a mesh (Fig. 3.5). Numerous texts and reports cover the basic theory of these methods. For example, Remson et al. (1971) discuss finite differences and Diersch (2014), Huyakorn and Pinder (1983), Pinder and Gray (1977), and Istok (1989) discuss finite elements. Wang and Anderson (1982) provide an elementary introduction to both methods. Pinder and Gray (1976) and Wang and Anderson (1977, 1982), among others, have shown that the FD and FE formulations of the Laplace equation (Eqn (3.18)) yield the same set of algebraic equations. They also demonstrated that both methods yield the same results if nodal spacing is sufficiently small. Thus, while the methods differ in concept they yield similar results, even for more complex versions of the governing equation than the Laplace equation.

### 3.5.1 Finite Differences

In the FD method, nodes are designated by  $i, j, k$  indices, which here represent the column, row, and layer, respectively, of a node in 3D space (Fig. 3.4). The spacing of nodes along rows is designated by  $\Delta x$  and the spacing along columns by  $\Delta y$ , while the spacing between layers is  $\Delta z$ . The node is situated within an FD cell or block (Fig. 3.4(b) and (c)). Heads are defined only at nodes and the head at a node represents the average head in the FD cell/block. An approximate form of the governing equation is written by replacing the partial derivatives in Eqn (3.12) by differences. For example, for a representative node,  $i,j,k$ , in a grid with uniform nodal spacing in the  $x$ -direction ( $\Delta x = \text{a constant}$ ), the approximation to the first derivative of  $h$  with respect to  $x$  is:

$$\frac{\partial h}{\partial x} = \frac{h_{i+1,j,k} - h_{i-1,j,k}}{2\Delta x} \quad (3.22)$$

where  $2\Delta x$  is the distance between the nodes  $h_{i+1,j,k}$  and  $h_{i-1,j,k}$ . Under uniform nodal spacing in the  $x$ -direction, the second derivative is:

$$\frac{\partial^2 h}{\partial x^2} = \frac{1}{\Delta x} \left[ \frac{h_{i+1,j,k} - h_{i,j,k}}{\Delta x} - \frac{h_{i,j,k} - h_{i-1,j,k}}{\Delta x} \right] = \frac{h_{i-1,j,k} - 2h_{i,j,k} + h_{i+1,j,k}}{(\Delta x)^2} \quad (3.23)$$

Similar expressions are written for derivatives in the  $y$ - and  $z$ -directions. In FD notation, the time derivative is represented by:

$$\frac{\partial h}{\partial t} = \frac{h_{ij}^{n+1} - h_{ij}^n}{\Delta t} \quad (3.24)$$

where the superscripts  $n$  and  $n+1$  designate the current and subsequent time levels, respectively.

Allowing for irregularly spaced nodes (Fig. 3.6) the FD expression for Eqn (3.12) is written as follows:

$$\begin{aligned} & \frac{1}{(\Delta x)_{i,j,k}} \left[ K_{x(i+1/2,j,k)} \frac{h_{i+1,j,k}^{n+1} - h_{i,j,k}^{n+1}}{(\Delta x)_{i+1/2,j,k}} - K_{x(i-1/2,j,k)} \frac{h_{i,j,k}^{n+1} - h_{i-1,j,k}^{n+1}}{(\Delta x)_{i-1/2,j,k}} \right] \\ & + \frac{1}{(\Delta y)_{i,j,k}} \left[ K_{y(i,j+1/2,k)} \frac{h_{i,j+1,k}^{n+1} - h_{i,j,k}^{n+1}}{(\Delta y)_{i,j+1/2,k}} - K_{y(i,j-1/2,k)} \frac{h_{i,j,k}^{n+1} - h_{i,j-1,k}^{n+1}}{(\Delta y)_{i,j-1/2,k}} \right] \\ & + \frac{1}{(\Delta z)_{i,j,k}} \left[ K_{z(i,j,k+1/2)} \frac{h_{i,j,k+1}^{n+1} - h_{i,j,k}^{n+1}}{(\Delta z)_{i,j,k+1/2}} - K_{z(i,j,k-1/2)} \frac{h_{i,j,k}^{n+1} - h_{i,j,k-1}^{n+1}}{(\Delta z)_{i,j,k-1/2}} \right] \\ & = S_s \frac{h_{i,j,k}^{n+1} - h_{i,j,k}^n}{(\Delta t)} - W_{(i,j,k)}^* \end{aligned} \quad (3.25)$$

where  $(\Delta x)_{i+1/2,j,k}$  and  $(\Delta x)_{i-1/2,j,k}$  are indicated on Fig. 3.6; irregular nodal spacing in the  $y$ - and  $z$ -directions is defined similarly. The  $n+1$  superscripts on the left-hand side of the equation indicate that space derivatives are approximated at the  $n+1$  time level.

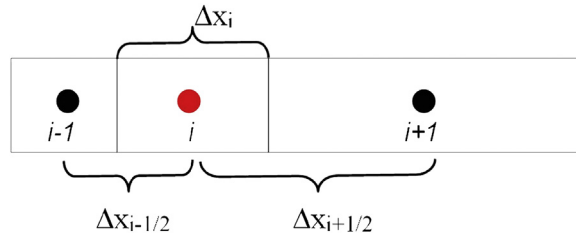


**Figure 3.6** FD notation for irregularly spaced nodes in the  $x$ -direction in a block-centered grid. The grid and notation are shown in one dimension only.

Equation (3.25) is simplified by introducing a parameter known as *conductance*. A general expression for conductance,  $C$ , between two cells in a rectangular FD grid is:

$$C = \frac{KA}{L} \quad (3.26)$$

where  $A$  is the area of the face between the two cells;  $L$  is the distance between the node centers in the two cells;  $K$  is the intercell hydraulic conductivity (i.e., the average hydraulic conductivity between the two nodes). Note that  $Q = C\Delta h$ . Equation (3.25) can be written in terms of conductance:

$$\begin{aligned} & CV_{i,j,k-1/2}h_{i,j,k-1} + CR_{i-1/2,j,k}h_{i-1,j,k} + CC_{i,j-1/2,k}h_{i,j-1,k} \\ & + (-CV_{i,j,k-1/2} - CR_{i-1/2,j,k} - CC_{i,j-1/2,k} - CV_{i,j,k+1/2} \\ & - CR_{i+1/2,j,k} - CC_{i,j+1/2,k} + HCOF_{i,j,k})h_{i,j,k} \\ & + CV_{i,j,k+1/2}h_{i,j,k+1} + CR_{i+1/2,j,k}h_{i+1,j,k} + CC_{i,j+1/2,k}h_{i,j+1,k} = RHS_{i,j,k} \end{aligned} \quad (3.27)$$

where  $CR$  and  $CC$  are horizontal conductances within rows and columns, respectively, and  $CV$  is the vertical conductance between layers. In Eqn (3.27), we use MODFLOW terms ( $CR$ ,  $CC$ ,  $CV$ ,  $HCOF$ ,  $RHS$ ) with the convention that  $i$  is the column index and  $j$  is the row index, which is consistent with Eqn (3.25) and Fig. 3.4. Readers should note, however, that in MODFLOW  $i = \text{rows}$  and  $j = \text{columns}$ . Consequently, the subscripts on  $CR$  and  $CC$  are different in the equivalent equation in MODFLOW (e.g., see Eqn (6-1) in Harbaugh, 2005).

In Eqn (3.25), the current (old) time level is  $n$  and we solve for head at  $n+1$ . In Eqn (3.27) we use a different convention for expressing time levels whereby, we solve for heads at time level  $t$ . Head,  $h$ , shown without a superscript is understood to be at time level  $t$ ; the previous (old) time level is  $t-1$ . Head at level  $t-1$  appears in the expression for  $RHS$ :

$$\begin{aligned} HCOF_{i,j,k} &= \frac{-SS_{i,j,k}V_{i,j,k}}{\Delta t} \\ RHS_{i,j,k} &= \frac{-SS_{i,j,k}V_{i,j,k}h_{i,j,k}^{t-1}}{\Delta t} \end{aligned} \quad (3.28)$$

where  $SS_{i,j,k}$  is the specific storage of the cell  $i,j,k$ ;  $V_{i,j,k}$  is the volume ( $\Delta x_{i,j,k}\Delta y_{i,j,k}\Delta z_{i,j,k}$ ) of cell  $i,j,k$ ;  $\Delta t$  is the time step;  $h_{i,j,k}^{t-1}$  is the head at node  $i,j,k$  at the previous time level ( $t-1$ ).

Equations (3.25 or 3.27) is written for every node in the interior of the grid. Boundary conditions are incorporated into the expressions for nodes that lie along the boundaries. The resulting set of algebraic equations is written as a global matrix equation:

$$[A]\{h\} = \{f\} \quad (3.29)$$



where  $[A]$  is the coefficient or conductance matrix that contains the conductances and HCOF;  $\{h\}$  is the array of unknown heads, and  $\{f\}$  contains R.H.S. Solution of the matrix equation is discussed below under solution methods.

### 3.5.2 Finite Elements

The mathematics of the FE method is less straightforward than the FD method. In the FE method, the problem domain is subdivided into elements (Fig. 3.5) that are defined by nodes. The dependent variable (e.g., head) is defined as a continuous solution within elements (Fig. 3.7(a)) in contrast to the FD method where head is defined only at the nodes and is considered piecewise constant between nodes (Fig. 3.7(b)). The FE solution is piecewise continuous, as individual elements are joined along edges. A large variety of element shapes and nodal locations are possible, although the most common elements are triangular (Fig. 3.5) and quadrilateral (Fig. 5.11). Elements are lines in one dimension, planes in two dimensions, and volumetric polygons in three dimensions (Fig. 5.12).

Locations of nodes in an FE mesh are designated using  $x$ ,  $y$ ,  $z$  coordinates (Fig. 3.5(a)). Both nodes and elements are numbered and the location of each element is defined in terms of the surrounding nodal numbers. For example, in Fig. 3.5(b), element number 5 is formed by nodes 5, 7, and 4. The FE method requires more bookkeeping of nodal locations than in FD because not only is the  $x$ ,  $y$ ,  $z$  location of each node required but the element number and the numbers of the nodes forming the element must be input to the code to generate the mesh. Mesh generation is both tedious and important because the sequence of nodal numbering can have an impact on computer memory during code execution (Wang and Anderson, 1982). Hence, FE codes usually include mesh generating software.

The FE equations are generated by introducing a trial solution of head within the element. For example, for the triangular element in Fig. 3.5(a), the trial solution is defined by interpolation functions, usually called *basis functions*, that relate head at the

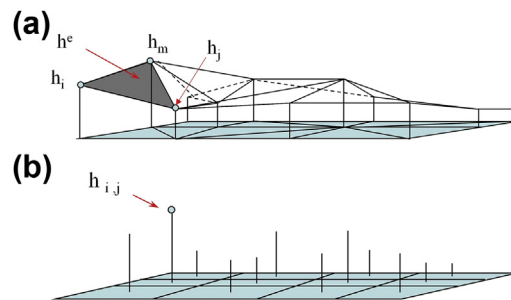


**Figure 3.7** Representation of head in the finite-element (FE) and finite-difference (FD) methods. (a) In the FE method, head ( $h^e$ ) is a continuous function within each element. In the FE mesh shown in the figure, the elements are triangular with heads at nodes designated  $h_i$ ,  $h_j$ , and  $h_m$ . (b) In the FD method, head ( $h_{i,j}$ ) is defined only at the node.

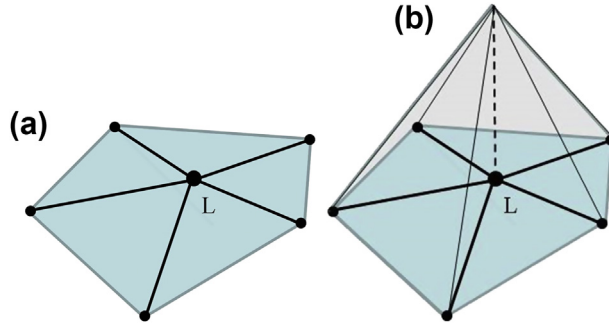


**Figure 3.8** (a) Plan view of a patch of elements around node L in a finite-element mesh. (In Fig. 3.5, for example, the elements 1, 3, 5, 7, 4, and 2 form a patch around node 4.) (b) Three-dimensional view of the nodal basis function  $N_L(x,y)$  (modified from Wang and Anderson, 1982 and Cheng, 1978).

nodes to head within the element (Fig. 3.8). Typically, a linear interpolation function is chosen, though more complex functions are possible.

Following Wang and Anderson (1982), in two dimensions, the general form of a linear interpolation function is:

$$h^e(x, y) = a_0 + a_1x + a_2y \tag{3.30}$$

where  $h^e(x,y)$  represents head within the element and  $a_0, a_1,$  and  $a_2$  are coefficients. Then, head within the element is computed using heads at the three nodes ( $i,j,m$ ; numbered counterclockwise) forming the triangular element,

$$\begin{aligned} h_i &= a_0 + a_1x_i + a_2y_i \\ h_j &= a_0 + a_1x_j + a_2y_j \\ h_m &= a_0 + a_1x_m + a_2y_m \end{aligned} \tag{3.31}$$

If Eqns (3.31) are solved for  $a_0, a_1, a_2$  and the expressions are substituted into Eqn (3.30), Eqn (3.30) can be rewritten as:

$$h^e(x, y) = N_i^e(x, y)h_i + N_j^e(x, y)h_j + N_m^e(x, y)h_m \tag{3.32}$$

where

$$\begin{aligned} N_i^e(x, y) &= 1/(2A^e) [(x_j\gamma_m - x_m\gamma_j) + (\gamma_j - \gamma_m)x + (x_m - x_j)\gamma] \\ N_j^e(x, y) &= 1/(2A^e) [(x_m\gamma_i - x_i\gamma_m) + (\gamma_m - \gamma_i)x + (x_i - x_m)\gamma] \\ N_m^e(x, y) &= 1/(2A^e) [(x_i\gamma_j - x_j\gamma_i) + (\gamma_i - \gamma_j)x + (x_j - x_i)\gamma] \end{aligned} \tag{3.33}$$

and

$$2A^e = (x_i\gamma_j - x_j\gamma_i) + (x_m\gamma_i - x_i\gamma_m) + (x_j\gamma_m - x_m\gamma_j) \tag{3.34}$$

$N_i^e(x, y)$ ,  $N_j^e(x, y)$  and  $N_m^e(x, y)$  are the basis functions. In this case, they are linear functions that define head within the triangular element of area  $A^e$  in terms of the heads at the three corner nodes (Fig. 3.5(a)). The general properties of the linear basis functions defined by Eqn (3.33) are:

1.  $N^e$  is 1 at node L, where L is either  $i$ ,  $j$ , or  $m$ , and 0 at the other two nodes.
2.  $N^e$  varies linearly with distance along any side.
3.  $N^e$  is  $1/3$  at the centroid of the triangle.
4.  $N^e$  is 0 along the side opposite node L.

These properties can be verified by substituting values into Eqn (3.33).

Because the trial solution of head defined by the basis functions is not the true solution, the governing equation is not represented exactly by using the trial solutions but includes a residual error term that is a measure of the degree to which the head does not satisfy the governing equation (see Chapter 6 in Wang and Anderson, 1982, for details). If the residuals over the problem domain are minimized so that the sum of residuals is forced to equal zero, the trial solution approaches the true solution. Commonly the FE method applies the method of weighted residuals to minimize the residuals and obtain approximate values of the dependent variable (e.g., head) at the nodes. To apply the method of weighted residuals, the Galerkin's method is typically used and the weighting functions are set equal to the basis functions (Eqn (3.33)).

Assembly of the matrix equation (Eqn (3.29)) for the problem domain is done by first considering the equation that pertains to the *patch of elements* around each node (Fig. 3.8). Then contributions from each element are assembled to form the global coefficient matrix (Fig. 3.9). Details for the 2D case are given by Wang and Anderson (1982; pp. 121–126). In transient problems, the nodal values of head are functions of time and the time derivative is approximated using finite differences. Hence “the finite element method of solving the transient flow equation is a hybrid of finite element and finite difference concepts” (Wang and Anderson, 1982, p. 152).

### 3.5.3 Control Volume Finite Differences

Standard FD methods require rectangular grids and rectangular cells within the grid. Although rectangular grids are simple to code and visualize, they often require inconvenient assumptions about system geometry. Furthermore, rectangular grids have two other drawbacks: they generate cells in areas of the model domain outside the main area of interest and they require that any increased resolution in discretization is extended areally to the edges of the model domain (Fig. 5.6) and vertically into all layers of a 3D model. For example, increased resolution (smaller node spacing and smaller FD cells) around surface water features for better representation of groundwater/surface water interaction in layer 1 of a model requires the same higher level of discretization in all lower layers even though the surface water features are present only in layer 1.

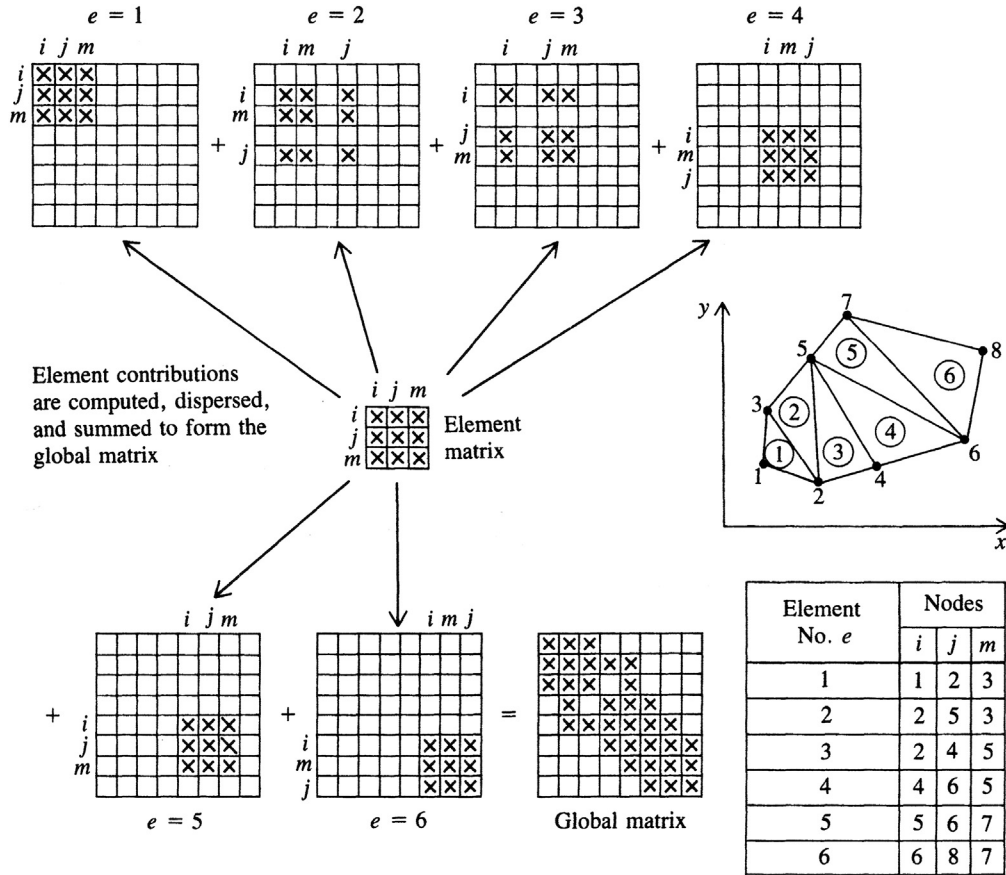


**Figure 3.9** Schematic diagram showing the relation of the element coefficient matrices and their assembly into the global coefficient matrix for the finite-element mesh shown in the inset (Wang and Anderson, 1982).

The control volume finite-difference (CVFD) method was used in one of the first applications of numerical models to a groundwater problem (Tyson and Weber, 1964) and was explored in detail by Narasimhan and Witherspoon (1976) in another early application. The method was called integrated finite differences in those early applications. The CVFD method gives FD methods much of the same flexibility in spatial discretization as the FE method. In a CVFD model, spatial discretization can include a combination of rectangular and square cells as well as hexagons, triangles, and irregular shapes (Figs. 5.4, 5.7, 5.8, 5.22). Moreover, spatial discretization can be different in each vertical layer. Recently, Panday et al. (2013) used CVFD to develop the code MODFLOW-USG, a version of the FD code MODFLOW with an unstructured grid (USG). As in an FE mesh, nodes in a USG are numbered sequentially, rather than using

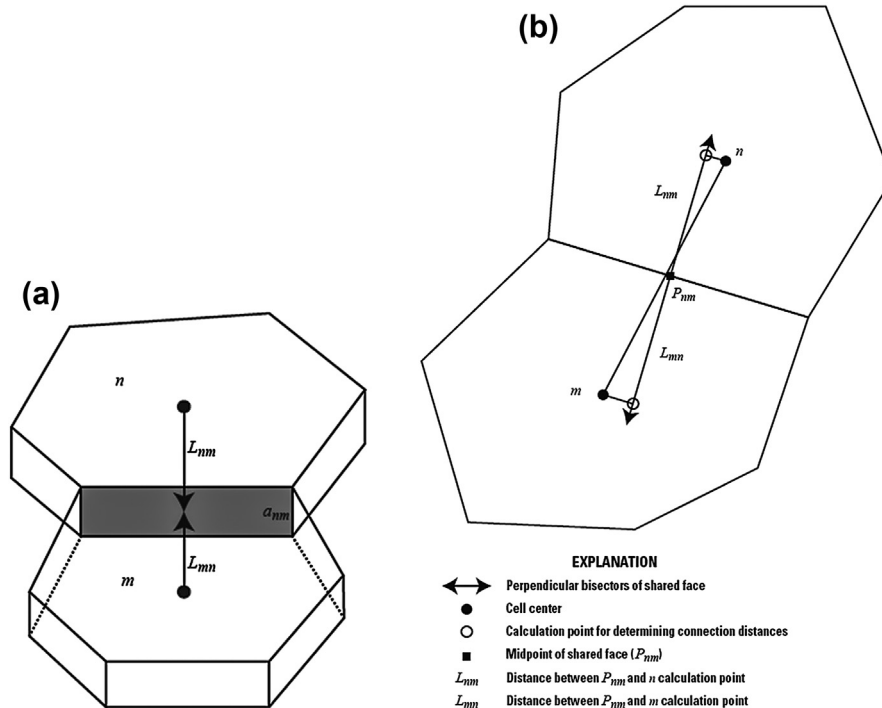


**Figure 3.10** Plan view of finite-difference cells ( $n$  and  $m$ ) in an unstructured grid as used in the control volume finite-difference method. Nodes are located in the center of the cell. (a) Connection lengths are measured from the center of the cell. The horizontal connection between cells is  $L_{nm} + L_{mn}$  and the flow area (shown in gray) for the connection is  $a_{nm}$  ( $=a_{mn}$ ). The connection lengths bisect the shared face at right angles. (b) The line connecting the centers of cells  $n$  and  $m$  (shown as filled black circles) does not bisect the shared face at a right angle, requiring a more complicated definition of  $L_{nm}$  and  $L_{mn}$ . The process is as follows: locate the midpoint of the shared face ( $P_{nm}$ ); extend a perpendicular line outward from this point in both directions. Then,  $L_{nm}$  and  $L_{mn}$  are defined as the distances between the midpoint of the shared face and points on the perpendicular line (shown as open circles) closest to the cell centers ([Panday et al., 2013](#)).

the  $i,j,k$  indexing convention of standard FD methods. Similar to FE, each cell is numbered ([Fig. 3.10\(a\)](#)). Adjacent nodes are said to be connected ([Fig. 3.10\(a\)](#) and [\(b\)](#)) and the user must input the area of the shared cell face for every cell connection. Given the complexity of assembling the data for a USG, a preprocessor code is recommended to assemble the grid ([Panday et al., 2013](#)). The equations used in the CVFD method are briefly discussed below but the details of the method are beyond the scope of our text. The interested reader should refer to [Narasimhan and Witherspoon \(1976\)](#) and [Dehotin et al. \(2011\)](#) for details of the theory, and to [Panday et al. \(2013\)](#), who show how to adapt the CVFD approach to the coding used in MODFLOW. We provide an overview of the CVFD method below, following [Panday et al. \(2013\)](#) and [Narasimhan and Witherspoon \(1976\)](#).

The CVFD method is a type of finite volume method (e.g., see [Bear and Cheng, 2010](#), pp. 537–541). Formally [Eqn \(3.12\)](#) is integrated over a small control volume  $V$ ;

$$\int_V (K\nabla h) dV = \frac{\partial}{\partial t} \int_V (S_s h) dV + \int_V W dV \quad (3.35)$$

The volume integral can be converted into a surface integral:

$$\int_s (K\nabla h) \cdot \mathbf{n} dS = S_s V \frac{\partial h}{\partial t} + WV \quad (3.36)$$

where  $\mathbf{n}$  is an outward pointing unit normal vector on the volume surface and  $S$  is the surface of the control volume. This representation of the governing equation is an expression of conservation of mass, or a water balance, where the inflows and outflows at the surface balance gain or loss from sources or sinks and change in storage within the volume.

In the CVFD method, the flow system is subdivided into small subdomains (the volumes,  $V$  in CVFD), sometimes called elements, and mass balance is calculated for each volume as represented in [Eqn \(3.36\)](#). The surface integral on the left-hand side of [Eqn \(3.36\)](#) represents the sum of fluxes over the surface,  $S$ , of the volume and measures the rate at which water is accumulating in the volume, subject to boundary and initial conditions. The right-hand side expresses the rate of accumulation of water as the average time rate of change in head in the volume ([Narasimhan and Witherspoon, 1976](#), p. 54).

In practice, FD expressions are written for the water balance for each volume and are then assembled into a global matrix equation ([Eqn \(3.29\)](#)). For example, [Panday et al. \(2013\)](#) give the general form of the CVFD water balance equation for cell  $n$  connected to each of its cell  $m$  neighbors ([Fig. 3.10\(a\)](#)):

$$\sum_{m \in \eta_n} C_{nm} (h_m - h_n) + \text{HCOF}_n (h_n) = \text{RHS}_n \quad (3.37)$$

where  $C_{nm}$  is the intercell conductance between cells  $n$  and  $m$ ;  $h_n$  and  $h_m$  are the hydraulic heads in cells  $n$  and  $m$ ;  $\text{HCOF}_n$  and  $\text{RHS}_n$  are equal to  $\text{HCOF}_{i,j,k}$  and  $\text{RHS}_{i,j,k}$  ([Eqn \(3.28\)](#)), respectively.

The first term in [Eqn \(3.37\)](#) represents the flow between cells  $n$  and  $m$  as calculated by Darcy's law. The summation of the first term in [Eqn \(3.37\)](#) is over all cells  $m$  associated with the volume (element)  $\eta_n$ , which is the set of cells connected to cell  $n$ . For the CVFD formulation, conductance ( $C_{nm}$ ) is generalized to represent intercell conductance between cell  $n$  and each of its neighbors  $m$ :

$$C_{nm} = \frac{a_{nm} K_{nm}}{L_{nm} + L_{mn}} \quad (3.38)$$

where  $a_{nm}$  is the saturated area perpendicular to flow between cells  $n$  and  $m$ ;  $K_{nm}$  is the intercell hydraulic conductivity;  $L_n$  and  $L_m$  are the perpendicular distances between the shared  $n$ – $m$  interface and a point between cells  $n$  and  $m$ , respectively (Fig. 3.10(b)).

The approximation of the general flow equation using standard FD (Eqn (3.27)), when rewritten in water balance form, is identical to Eqn (3.37) when the subscripts  $i,j,k$  in Eqn (3.27) are changed to the subscript  $n$  for the CVFD formulation and it is understood that cell  $n$  is connected to neighboring cells designated generally as cell  $m$  (Panday et al., 2013). Hence, the methods used to solve the standard FD equation can be applied to CVFD. The major and fundamental difference, however, is in the way the intercell conductances,  $C_{nm}$ , are computed. In standard FD, calculation of the intercell conductances is relatively straightforward (Eqn (3.26)) owing to the regular geometry and connections between cells in a rectangular grid. In CVFD, however,  $L_{nm}$  and  $L_{mn}$  (Eqn (3.38)) must be computed for each cell connection (Fig. 3.10(b)) and the area of the shared face, which is not necessarily rectangular, must also be specified (Fig. 3.10(a)).

### 3.5.4 Solution Methods

The set of algebraic equations resulting from applying a numerical approximation to the governing equation using the FD, FE, or CVFD method is solved for head using either direct methods or direct methods combined with iteration. Some general features of solution methods are discussed briefly in this section. Wang and Anderson (1982) discuss basic iterative and matrix solution techniques in more detail.

*Direct methods* solve the global matrix equation (Eqn (3.29)) using matrix solvers and give an exact numerical solution of the set of algebraic equations subject to numerical roundoff error. Roundoff errors are generated because the computer stores a finite number of digits to represent each numerical value. Although in principle direct method solutions are desirable, they often require large amounts of computer memory since all entries of the coefficient matrix must be stored in the computer and the number of entries is typically large. Moreover, owing to the large number of calculations required to solve a matrix equation directly, significant numerical roundoff error can occur. In practice, execution time of direct solvers is fastest with small, linear, groundwater problems, but can be unacceptably long if the modeling problem is highly nonlinear. Therefore, convergence problems (Konikow and Reilly, 1998) and computer memory have limited the application of direct solution methods. However, improved solution methods and improved computer power are motivating new developments in direct methods. The FE code FEFLOW (DHI-WASY, 2013; FEFLOW version 6.2) includes a direct solver that can accommodate up to 1 million nodes. There is also a direct solver for MODFLOW (DE4: Harbaugh, 1995, 2005). Nevertheless, direct solutions continue to be more appropriate for steady-state models, which solve for only one set of heads. Transient

models, especially models that use variable length time steps (Section 7.6; see Table 1 in Harbaugh, 1995), may be better served by a solver that combines direct methods with iteration.

An *iterative solution* is the simplest type of numerical solution and point iteration was used routinely to solve FD equations in the early years of groundwater flow modeling. Today, point iterative solutions for the groundwater flow equation are rarely used. Instead, direct (matrix) methods are combined with iteration. With point iteration, the FD equation is solved sequentially for head at each node in the problem domain and then the process is repeated until heads between iterations stop changing (i.e., the solution converges). For example, Eqn (B4.3.2) (Box 4.3) is an FD equation for point iteration to solve for heads in a 2D, homogenous aquifer under steady-state conditions. (Also see Problem P3.5.)

Methods that combine iteration with a direct solution first simplify the coefficient matrix in the global matrix equation (Eqn (3.29)) so that more efficient direct matrix solvers can be used. Because the resulting matrix equation has a coefficient matrix that is not exactly correct, the solution is not accurate and iteration is used to improve the solution. Wang and Anderson (1982, pp. 106–107) present examples of methods for combining direct and iterative solution methods for 2D groundwater flow problems. McDonald and Harbaugh (1988) discuss direct methods combined with iteration for solving the 3D flow equation (Eqn (3.27)). Codes generally include several different solvers from which the user may choose. The solution of large, complex groundwater models may require the modeler to experiment to find the solver that converges most efficiently.

Iterative solutions are inexact because the iteration process is stopped when the solution is (subjectively) judged to have converged. Moreover, iteration involves a large number of calculations making the solution prone to roundoff error and associated artifacts. Acceleration parameters and relaxation factors speed up convergence but the modeler has to select values for those parameters. A *residual error* in head (= the difference in heads at the start and end of an iteration) is calculated for each node. The modeler specifies a value for the *head closure criterion* (also called the head error criterion, error tolerance or convergence criterion) that sets the maximum allowed value of the residual error in head. Many solvers also use a similarly defined second closure criterion for the water balance. Both error criteria are discussed in Section 3.7. Typically a limit is also set on the number of iterations. Iteration stops when the closure criteria are met or the maximum number of iterations is reached (Fig. 3.11).

### 3.6 CODE SELECTION

The set of equations generated by applying a numerical method (FD, FE, or CVFD) is programmed into a computer code. The selection of a groundwater flow code for a particular modeling application depends on the problem to be solved, the options



```

100 ITERATIONS FOR TIME STEP 1 IN STRESS PERIOD 1
OMAXIMUM HEAD CHANGE FOR EACH ITERATION:
O HEAD CHANGE LAYER,ROW,COL HEAD CHANGE LAYER,ROW,COL HEAD CHANGE LAYER,ROW,COL HEAD CHANGE LAYER,ROW,COL HEAD CHANGE LAYER,ROW,COL
-----
-9.995 ( 1, 1, 5) -3.302 ( 1, 4, 5) -2.973 ( 1, 4, 5) -2.125 ( 1, 4, 5) -1.561 ( 1, 4, 5)
-0.6207 ( 1, 4, 5) -0.1787 ( 1, 4, 5) -0.1370 ( 1, 4, 5) -0.1538 ( 1, 9, 1) -0.1369 ( 1, 4, 5)
-0.7454E-01 ( 1, 4, 5) -0.2230E-01 ( 1, 4, 5) -0.1339E-01 ( 1, 4, 5) -0.1020E-01 ( 1, 4, 5) -0.9841E-02 ( 1, 4, 5)
-0.5095E-02 ( 1, 4, 5) -0.1651E-02 ( 1, 4, 5) -0.9778E-03 ( 1, 4, 5) -0.7224E-03 ( 1, 4, 5) -0.5151E-03 ( 1, 4, 5)
-0.2968E-03 ( 1, 4, 5) -0.8535E-04 ( 1, 4, 5) -0.5132E-04 ( 1, 4, 5) 0.4417E-04 ( 1, 1, 9) -0.5334E-04 ( 1, 1, 5)
0.4072E-04 ( 1, 1, 6) 0.4093E-04 ( 1, 1, 8) 0.4416E-04 ( 1, 1, 9) 0.4071E-04 ( 1, 1, 6) 0.4091E-04 ( 1, 1, 8)
0.4413E-04 ( 1, 1, 9) 0.4412E-04 ( 1, 1, 1) -0.5337E-04 ( 1, 1, 5) 0.4085E-04 ( 1, 1, 2) 0.4413E-04 ( 1, 1, 1)
0.4097E-04 ( 1, 1, 8) 0.4097E-04 ( 1, 1, 2) 0.4074E-04 ( 1, 1, 6) 0.4417E-04 ( 1, 1, 9) 0.4079E-04 ( 1, 1, 2)
-0.5333E-04 ( 1, 1, 5) 0.4416E-04 ( 1, 1, 9) 0.4417E-04 ( 1, 1, 1) 0.4073E-04 ( 1, 1, 6) 0.4090E-04 ( 1, 1, 8)
0.4415E-04 ( 1, 1, 9) 0.4071E-04 ( 1, 1, 6) 0.4092E-04 ( 1, 1, 8) -0.5335E-04 ( 1, 1, 5) 0.4389E-04 ( 1, 1, 1)
0.4092E-04 ( 1, 1, 8) 0.4090E-04 ( 1, 1, 2) 0.4412E-04 ( 1, 1, 9) 0.4399E-04 ( 1, 1, 1) 0.4095E-04 ( 1, 1, 2)
0.4074E-04 ( 1, 1, 6) -0.5336E-04 ( 1, 1, 5) 0.4089E-04 ( 1, 1, 2) 0.4068E-04 ( 1, 1, 6) 0.4417E-04 ( 1, 1, 9)
0.4417E-04 ( 1, 1, 1) 0.4073E-04 ( 1, 1, 6) 0.4095E-04 ( 1, 1, 8) 0.4417E-04 ( 1, 1, 9) -0.5333E-04 ( 1, 1, 5)
0.4093E-04 ( 1, 1, 8) 0.4414E-04 ( 1, 1, 9) 0.4408E-04 ( 1, 1, 1) 0.4096E-04 ( 1, 1, 8) 0.4094E-04 ( 1, 1, 2)
0.4413E-04 ( 1, 1, 9) 0.4411E-04 ( 1, 1, 1) -0.5334E-04 ( 1, 1, 5) 0.4066E-04 ( 1, 1, 6) 0.4418E-04 ( 1, 1, 9)
0.4097E-04 ( 1, 1, 2) 0.4074E-04 ( 1, 1, 6) 0.4417E-04 ( 1, 1, 9) 0.4418E-04 ( 1, 1, 1) 0.4068E-04 ( 1, 1, 6)
-0.5336E-04 ( 1, 1, 5) 0.4417E-04 ( 1, 1, 9) 0.4417E-04 ( 1, 1, 1) 0.4089E-04 ( 1, 1, 8) 0.4090E-04 ( 1, 1, 2)
0.4415E-04 ( 1, 1, 1) 0.4094E-04 ( 1, 1, 8) 0.4094E-04 ( 1, 1, 2) -0.5333E-04 ( 1, 1, 5) 0.4388E-04 ( 1, 1, 1)
0.4092E-04 ( 1, 1, 2) 0.4069E-04 ( 1, 1, 6) 0.4413E-04 ( 1, 1, 1) 0.4095E-04 ( 1, 1, 2) 0.4074E-04 ( 1, 1, 6)
0.4412E-04 ( 1, 1, 9) -0.5334E-04 ( 1, 1, 5) 0.4099E-04 ( 1, 1, 2) -0.3088E-04 ( 1, 1, 3) 0.4417E-04 ( 1, 1, 9)

```

**Figure 3.11** Example output from MODFLOW showing nonconvergence of the solution after 100 iterations. The head closure criterion was specified to be 0.1E-4 ft ( $0.1 \times 10^{-4}$ ). The output gives the maximum residual error in head in each of the 100 iterations, listed in order from left to right. Read the output by row from left to right (e.g., the 99th iteration is the second to last entry in the last row). The location of the maximum residual for each iteration is given in parentheses as the layer, row, and column numbers. Results suggest the residual error cannot be reduced below 0.31E-4 ft, which is the lowest error computed (for iteration number 99). Nevertheless, the error in the water budget for this run was only 0.22%. Based on the good water budget and the oscillation of the solution around an error of 0.4E-4, the solution could be accepted or the convergence criterion could be increased to 0.1E-3ft.

available in the code for representing special features such as surface water bodies (Section 6.1), and the preference of the user. The main difference intrinsically between a standard FD code and an FE or CVFD code is the nature of the spatial discretization. The FD method is easy to understand and spatial discretization is easy to set up compared to FE or CVFD. In FE and CVFD, the geometry of irregularly shaped boundaries, internal heterogeneities, sinks and sources, and features such as fault zones can be represented more realistically than with FD methods (Fig. 3.5). The FE method simulates variable anisotropy (Box 3.1; Section 5.3), seepage faces, and moving water tables more easily and better than FD and CVFD. However, FD models continue to be popular. Increased computer power allows standard FD codes to solve complex models effectively even though the requirement for a rectangular grid may entail a large number of nodes. Consequently, high-resolution FD models are sufficient for many problems.

The most widely used code for solving groundwater flow problems currently is the FD code MODFLOW by the U.S. Geological Survey (USGS) (<http://water.usgs.gov/ogw/modflow/>). MODFLOW allows for addition of modules and linking or coupling with other codes; it is freely available with detailed documentation. Although there is no single FE code that has attained the popularity of MODFLOW, the proprietary code FEFLOW (<http://www.feflow.com/>) is widely used (see review by Trefry and Muffels, 2007). Diersch (2014) has extensively documented the theoretical underpinnings of the FE method used in the FEFLOW code and user's manuals are freely available online. We use MODFLOW and FEFLOW throughout the text as representative codes to illustrate implementation of modeling concepts. The CVFD code MODFLOW-USG (Panday et al., 2013) is still relatively new to the modeling community, so current experience is limited.

General mathematical software packages such as MATLAB and COMSOL can be used to solve the general groundwater flow equation (Eqn (3.12)) as an alternative to off-the-shelf groundwater codes. MATLAB, and its public domain derivative OCTAVE, provide tools to solve analytical solutions (e.g., Zlotnik et al., 2011; Cortis and Berkowitz, 2005) as well as numerical recipes for solving a set of linear algebraic equations, such as generated from a numerical approximation of the groundwater flow equation (Eriksson and Ooppelstrup, 1994). COMSOL is an FE-based software package that solves a variety of partial differential equations including those for groundwater flow (e.g., Cardiff et al., 2009), solute transport, and heat transport (see review by Li et al., 2009). COMSOL also allows the modeler to build coupled models such as groundwater flow coupled to solute and/or heat transport; coupled groundwater and surface water flow (Cardenas, 2008; Ward et al., 2013); and groundwater flow coupled to other types of models such as a vegetation model (e.g., Loheide and Gorelick, 2007). However, to date such mathematical software packages have been applied to groundwater modeling primarily in academic and educational settings. In most applied groundwater modeling, codes specific to groundwater are used because they provide more options for simulating hydrologic features and are supported and tested on an on-going basis by the groundwater modeling community. Moreover, groundwater models applied to engineering

and management problems potentially will be questioned in the legal arena where using an industry standard code is expected.

Regardless of the code selected, the following questions should be asked: (1) Has the accuracy of the code been checked (verified) against analytical solutions and/or a verified numerical solution? (2) Does the code include a water budget computation? (3) Has the code been used in field studies and does it have a proven track record? (4) Does the code have a graphical user interface (GUI)? Each of these questions is discussed below.

### 3.6.1 Code Verification

Codes for groundwater flow are *verified* by comparing the numerical results with analytical solutions and sometimes with other numerical solutions. The purpose of code verification is to test that the numerical solution has been properly programmed (ASTM, 2008). The level of agreement of numerical results with an analytical solution depends on the choice of closure criteria, grid spacing, and time step. Example problems used in code verification are typically included in the user's manual.

### 3.6.2 Water Budget

Water budget calculations are standard features of most codes; the computed water budget helps the modeler assess the accuracy of the numerical solution and allows comparison with the field-based water budget, which is normally calculated as part of the conceptual model. The water budget computed by the code itemizes flows across boundaries, including the water table; to and from sources and sinks, including surface water bodies; and in transient simulations to and from storage (Fig. 3.12). Release of water from storage is counted as inflow and uptake is counted as outflow. Typically, cells or elements associated with specified head boundary nodes are not considered part of the problem domain for purposes of the water balance computation. For example, recharge applied to specified head nodes is considered captured by the specified head and is not included in the water balance computation. Likewise, flow between specified head nodes is not normally computed although flow between specified boundary heads and the active problem domain is included in the water budget (Fig. 3.12).

The governing equation for groundwater flow is derived using conservation of mass (i.e., water balance) and Darcy's law (Section 3.2). Hence, the numerical solution of the governing equation should conserve mass. Failure to conserve mass locally has been a criticism of the FE method (e.g., see Berger and Howington, 2002) but is unwarranted as is demonstrated by water budget calculations in modern FE codes. Water balance errors reported in early FE solutions arose from flawed methodology and are not inherent to the FE method; modern FE codes include procedures that compute a numerically accurate water budget. For example, the consistent boundary flux method is used in FEFLOW (Diersch, 2014, pp. 391–393).

The water budget should show that total inflow equals total outflow. Typically, the code computes the water budget error as the difference between inflow and outflow

VOLUMETRIC BUDGET FOR ENTIRE MODEL AT END OF TIME STEP		5	IN	STRESS PERIOD	12
CUMULATIVE VOLUMES	L**3	RATES FOR THIS TIME STEP			L**3/T
IN:		IN:			
---		---			
STORAGE =	0.11099E+08	STORAGE =	23927.		
CONSTANT HEAD =	330.70	CONSTANT HEAD =	24.778		
WELLS =	0.0000	WELLS =	0.0000		
RECHARGE =	0.17021E+08	RECHARGE =	21375.		
TOTAL IN =	0.28120E+08	TOTAL IN =	45327.		
OUT:		OUT:			
---		---			
STORAGE =	0.68859E+07	STORAGE =	0.0000		
CONSTANT HEAD =	0.13935E+08	CONSTANT HEAD =	25326.		
WELLS =	0.73000E+07	WELLS =	20000.		
RECHARGE =	0.0000	RECHARGE =	0.0000		
TOTAL OUT =	0.28121E+08	TOTAL OUT =	45326.		
IN - OUT =	-250.00	IN - OUT =	0.81250		
PERCENT DISCREPANCY =	0.00	PERCENT DISCREPANCY =	0.00		

**Figure 3.12** Water budget for a transient problem calculated by MODFLOW showing the cumulative water budget in volumes of water (left-hand side of figure) and the water budget in volumetric rates (right-hand side of figure) for time step 5 in stress period 12. (See Section 7.6 for an explanation of stress periods.) The problem has two specified head boundaries (itemized as “constant head” in the budget) that represent surface water bodies; areal recharge from precipitation (itemized as “recharge”); and a pumping well (itemized as “wells”). Note that water is both entering and leaving the system through the specified head boundaries. Water enters the system as recharge and is removed through the pumping well. There is a change in storage listed under inflow, which means that there is a net removal of water from storage (i.e., water leaves storage and enters the system). The error in the cumulative water budget for this time step is 250 ft<sup>3</sup>, which is less than 0.01% of the total inflow or outflow and thus the error (percent discrepancy) is listed as zero.

(Fig. 3.12). The water budget should be less than around 0.5% (ideally less than 0.1%; Konikow, 1978), but an error as high as 1% may be acceptable. A higher percent water budget error might mean that the solution has not converged because the closure criteria are set too high or the solution may not have converged within the maximum number of iterations allowed (Section 3.7). A large water budget error may reflect errors in input and/or model design or conceptualization, or may be an artifact of how the code simulates a head-dependent boundary (Box 4.5). The global water balance is typically itemized in model output; some solvers check the water balance locally during solution to meet a water balance closure criterion (Section 3.5). ZONEBUDGET (Harbaugh, 1990) for MODFLOW calculates the local water budget for user-specified zones in the problem domain, which can be helpful in analyzing local flows in the model.

### 3.6.3 Track Record

Ideally, a code applied to engineering or management problems should have a history of use and testing. For illustrative purposes in our text, we use MODFLOW and FEFLOW. The MODFLOW suite of codes is the most widely used set of groundwater codes in the world and the standard for litigation purposes in the United States. MODFLOW has been applied to numerous and diverse field problems and is the focus of a series of

international professional conferences (<http://igwmc.mines.edu/Conference.html>). Owing to MODFLOW's long history of use within the groundwater modeling community (McDonald and Harbaugh, 2003), errors are discovered and corrected, new modules (packages and processes) are developed and a variety of GUIs is available. FEFLOW (Diersch, 2014) is a proprietary FE code that has been continually improved and updated since it was first introduced in 1979. It was offered commercially in the 1990s (Trefry and Muffels, 2007) and is being applied increasingly to a variety of complex groundwater problems (DHI-WASY, 2013).

### 3.6.4 GUIs

A GUI serves as an intermediary between the modeler and the code. It facilitates model design and parameter input and helps avoid input errors that can result from entering data manually into a code. GUIs are also enormously helpful in the visualization, inspection, and analysis of output. Given the complexity of most numerical models, a GUI is an indispensable tool for groundwater modeling.

GUIs produce images of model domains including FD and CVFD grids and FE meshes and boundaries. Displays of calibration targets and parameters assist the user in visualizing the spatial distribution of data and editing values. The GUI formats and assembles data in the form required by the code, creates the input files, and can also execute the code. The GUI also processes output files from code execution and graphically displays results.

GUIs may be developed for a specific code, or may include multiple codes. For example, PetraSim is the GUI for the TOUGH2 family of codes (see review by Yamamoto, 2008). FEFLOW includes a GUI that produces input and output files and graphics (Diersch, 2014). ModTech integrates groundwater flow and transport codes within a GIS environment (see review by Pint and Li, 2006). MODFLOW does not include an embedded GUI but a number of GUIs have been developed for MODFLOW. The three most widely used commercially developed GUIs for MODFLOW are Groundwater Vistas (Rumbaugh and Rumbaugh, 2011) (see review by Langevin and Bean, 2005), Visual MODFLOW-flex (VM-Flex) (Schlumberger Water Services, 2012), and Groundwater Modeling Systems (Jones, 2014). The USGS developed the public domain GUI ModelMuse for MODFLOW (Winston, 2009) and ModelMate for parameter estimation using UCODE with MODFLOW (Banta, 2011). The Freeware PMWIN is also available for MODFLOW simulations (Cheng and Kinzelbach, 2013). Many of these GUIs also include parameter estimation, particle tracking, and solute transport codes that work with MODFLOW (e.g., PEST, PEST++; MODPATH, PATH3D; MT3DMS, SEAWAT). GUIs often handle several versions of MODFLOW codes (e.g., MODFLOW-SURFACT, MODHMS, MODFLOW-USG), as well as optimization methods. GUIs include various options for 3D visualization. In addition, there are software

packages dedicated to postprocessing and 3D visualization of output (e.g., see [Kresic and Mikszewski, 2013](#)). For example, Model Viewer is a 3D visualization and animation program developed by the USGS for groundwater models (see review by [Zheng, 2004](#)). GroundWater Desktop (<http://www.groundwaterdesktop.com/>) has extended visualization features.

Although a GUI releases the modeler from knowing all details of the file structure and input requirements for a particular code, troubleshooting code performance is greatly facilitated when the modeler has even a cursory knowledge of how the code operates. A quick read of the code's user's manual will give the modeler a first level of understanding of the inner workings of the code. An understanding of the code's input file structure is also helpful. Some GUIs provide access to the modeling code's input files, which are generated by the GUI from data input by the user, allowing the modeler to examine and modify input files outside of the GUI.

### 3.7 CODE EXECUTION

After the model is designed and data are entered into a GUI, the code is executed. Typically several preliminary runs are needed to correct errors in input data, adjust model design and parameter values for conceptual errors, and adjust solver settings and closure criteria. In the second phase of code execution, many runs will be required for model calibration. In the final phase, the model is run for forecasting and uncertainty analysis. It is recommended that the modeler keep a simulation log of runs performed during all three phases of code execution. In this section, we discuss the simulation log, execution time, and closure criteria and solution convergence.

#### 3.7.1 Simulation Log

Because the modeler will execute the code many times during model design, calibration, and forecasting and uncertainty analysis, it will be helpful to keep a *simulation log* ([Table 3.1](#)), which is a written record of actions and decisions associated with executing the code. The log includes the purpose of each run of the model and a short summary of the outcome, as well as a description of the changes, if any, that were made to the model as a result of the run. The simulation log serves to outline the process of model construction, calibration, and forecasting and list key decisions made during the modeling project. The log may also contain comments on how data sets were assembled and organized; how the grid/mesh was discretized, and how changes made to the conceptual (or numerical) model affected results. Keeping track of changes to parameter sets and hydrologic stresses during calibration and forecasting uncertainty analyses can be particularly helpful in relating the model's response to conditions different from those presented in the final modeling report. Typical records include: "modeler's name, the simulation data, the project name/number, the simulation number, the

<b>Table 3.1</b> Example of a simulation log (modified from <a href="#">Aquaterra Consulting Pty Ltd, 2000</a> )				
<b>Job 125</b>	<b>Steady-state and transient calibration</b>			
<b>Run</b>	<b>Issue</b>	<b>Model changes and/or previous model parameters</b>	<b>Comments/results</b>	<b>Filename and path</b>
A1	Start with previous model, and update to predict dewatering rates and impacts	Refine grid, adjust layer geometry and $K$ values, increase water balance and recalibrate in steady state, as described in hydrogeology report and below.	See below	125\Model\W1 M1.mdl (PMWin v4) (for Model No. 1)
A2	Grid refinement Around site, the existing model grid was about 1000 m square (some rows at site were less than this)—refers to separate notes on file.	The grid was refined to a minimum of 100 m cells at site, with a view that further refinement may prove necessary. The physical justification for the horizontal flow barrier (see opposite) is that measured water levels at the western end of valley show very steep hydraulic gradients across an inferred dyke (e.g., from BH3 to BH4).	Following grid refinement, some previously inactive layer 1 cells were activated, as finer grid resolution allowed more accurate representation of the boundary between the basement ridges and the layer 1 units (alluvium etc.). The $K_h$ and $K_v$ were also adjusted accordingly.	Data files for horizontal flow barrier packages comprise: LIHFBc.dat, LIHFBd.dat, L2HFBc.dat, L2HFBd.dat, (final letter indicating conductance (“c”) or direction (“d”))

*Continued*

Table 3.1 Example of a simulation log (modified from Aquaterra Consulting Pty Ltd, 2000)—cont'd				
Job 125	Steady-state and transient calibration			
Run	Issue	Model changes and/or previous model parameters	Comments/results	Filename and path
B1	General solution adjustments	<p>Feedback loop invoked to take heads from end of calibration simulations as initial heads for next set of calibration attempts continued throughout calibration.</p> <p>Rewetting was initially inactive, but many layer 1 cells dry, especially on margins. When rewetting was activated, very few of these cells rewet, because the base elevation for these cells is generally above the water table. Similarly, many layer 2 cells within western valley are also dry. Rewetting later turned off.</p> <p>PCG2 solver was Hclose = 0.01, Rclose = 100, Outer = 50, Inner = 30, Accl = 0.9</p>	<p>Layer 1 and 2 starting head files-&gt;</p> <p>Layer 1 and 2 boundary inflow data files—————→</p> <p>Rewetting parameters—every fifth iteration, Rewet = 0.9, Threshold = -2 m</p> <p>Monitoring bore data files→</p> <p>Hclose = 0.001 m, Rclose = 10 (L<sup>3</sup>/T), Accl = 0.99, Outer = 54, Inner = 20</p>	<p>LlstrtHD.dat, L2strtHD.dat Llwel.dat, L2wel.dat</p> <p>BorW1.bor = 52 bores (original data set)</p>
C1	Recharge	<p>In original model, recharge was <math>1.585 \times 10^{-5}</math> m/d over layer 1 cells only (to highest active cell). This value was initially doubled to <math>3 \times 10^{-5}</math> m/d as a global value. The physical justification for enhanced recharge to valley margins (see opposite) is that basement outcrop runoff is concentrated on the scree slopes adjacent to outcrop.</p>	<p>The rate was later decreased to zero across the broad valley areas, with enhanced recharge at <math>1 \times 10^{-4}</math> around the outcrop areas from site and eastward, and left at <math>3 \times 10^{-5}</math> in the narrow valleys west of site. Applied to layer 1 only. Overall, recharge volume is virtually doubled, compared to the previous model.</p>	<p>Llrch.dat = revised recharge rates</p>



code used (and versions), the purpose of the run, the input file names, comments on the input data, the output file names, and comments on the results” (ASTM, 2013). The simulation log can also facilitate report preparation and provide a record of model response to possible changes that may be requested by others after the modeling is completed.

### 3.7.2 Execution Time

The length of time necessary to run the code for a given set of input data is the *execution time*. The execution time primarily depends on: (1) the speed at which the computer loads input files and executes the code; (2) the efficiency of the solver and selection of settings of solver parameters; (3) the nonlinearity of the problem and number of nodes and layers, which affects the number of calculations the code will perform; (4) the number of iterations required for convergence of a solver that uses iteration; (5) how closely the steady-state starting heads provided by the modeler approximate the final head solution; (6) the number of stress periods and time steps (Section 7.6) in a transient simulation; and whether the simulation is for steady-state or transient conditions. Runtimes for transient models are usually longer than for steady-state models. In some cases, more rigorous closure criteria can reduce the total transient model run time because a better head solution in one time step can facilitate solution convergence in subsequent time steps.

In addition to computer speed, another consideration is having a computer with sufficient random access memory (RAM) to store the code and provide rapid access to input data and arrays created during execution of the code. Most computer workstations have sufficient RAM to run complex applied groundwater models. Direct solvers typically require more RAM than a solver that combines a matrix solution with iteration and thus direct solvers often cannot be used to solve large modeling problems (Section 3.5). Moreover, ancillary codes for calibration or uncertainty analysis (Chapters 9 and 10) entail additional computational burden and for models with many adjustable parameters and observations, the use of multiple processors associated with parallel processing may be required.

### 3.7.3 Closure Criteria and Solution Convergence

Solvers that include iteration require the modeler to specify closure criteria, typically for both head and water balance as well as a maximum number of iterations (Section 3.5). The values of closure criteria affect not only the execution time but the validity of the solution because they determine the maximum residual error allowed and, therefore, when the solution is judged to have converged. When the residual error equals or falls below the maximum value allowed, the solution is said to converge and iteration stops. The modeler also specifies a maximum number of iterations permitted; if the solution has not converged (met the closure criteria) within the permitted number of iterations,

execution stops prior to convergence. A code may compare the head closure criterion with the maximum computed residual or with the sum of residuals over the problem domain, or some other composite statistic. When the code uses the maximum computed residual, a general rule of thumb is to set the head closure criterion to be one to two orders of magnitude smaller than the level of accuracy desired in head. This means that the head closure criterion is typically set to values of the order  $1E-3$  to  $1E-5$ . For other types of residual comparisons, the modeler should consult the code's user's manual to set the value of the closure criterion.

The water balance closure criterion also depends on how the residual is calculated. Usually the water budget residual is reported as a percent error but other options are possible. Moreover, the code computes a global water balance for the entire problem domain but may also compute cell or element water budgets or zonal water budgets. The modeler should consult the code's user's manual to ensure that the correct order of magnitude is specified for the water budget closure criterion. The effects of both error criteria on the solution should be tested. Ideally, the selection of values for the closure criteria should balance desirable short runtimes with an acceptably low reported error in the computed water budget (Section 3.6; Fig. 3.12). For transient simulations, it is often important to review the computed water budget at the end of each time step to evaluate whether changes in the water budget through time are reasonable.

A solution may not converge simply because unreasonably small closure criteria were specified by the modeler. In that case, the solution does not converge because small numerical errors in the solution prevent the residual(s) from falling below the specified closure criteria. In that case, the head residual typically oscillates around some value higher than the head closure criterion (Fig. 3.11) even though the water budget error may be acceptable. Sometimes, convergence can be obtained by raising the head closure criterion. However, for some solvers loosening closure criteria may just result in oscillation around a higher residual error. Nonconvergence can also result from poor assignments of starting heads and parameters, improper boundary conditions, and/or errors in input values. Some codes (e.g., MODFLOW) monitor the approach to convergence and provide a listing of residual errors at nodes farthest from closure (Fig. 3.11). It may be possible to identify why a model is not converging by finding the areas in the model domain that have large residual error. Checking the input data read by the code for those areas may reveal errors in input data. Nonconvergence may also occur owing to a poor conceptual model. For example, a model designed to solve for steady-state heads in an aquifer receiving areally uniform recharge and surrounded by no-flow boundaries with no internal sinks is poorly conceived. The solution will not converge because there are no sinks to remove the water added; the model has no steady-state solution.

In some cases, the lack of convergence in and of itself may not indicate a poor solution. For example, large water budget errors can occur when using a head-dependent boundary condition even when the solution has converged. The water

budget errors are caused by artifacts in how the head-dependent condition is simulated but do not necessarily indicate that the solution is compromised. See Box 4.5 for more information. In a transient simulation, the solution may not converge in the first few time steps. This may not be a concern if heads in early time steps are not important and if the computed water budget error after the first several time steps is small. In this situation, the modeler can use an option included in some codes that allows the simulation to continue even if the solution has not converged. When a steady-state solver does not converge, a steady-state solution can be reached by running a transient model with many time steps and an arbitrary value for the storage parameter (e.g., [Feinstein et al., 2003](#), p. 198). Because the transient model is run until storage is exhausted, the storage parameter is arbitrary and simply serves to dampen the solution process and facilitate a stable approach to steady state.

### 3.8 COMMON MODELING ERRORS

- The modeler insists on using a particular code even when the problem would be better simulated by another code.
- The modeler trusts that input to a GUI is correctly translated to the code even when model output disagrees with expected system response and hydrogeological common sense.
- The modeler fails to check results from a complex numerical model against results from simpler models or analytical solutions. Simpler models may help identify conceptual errors that can be hidden in a complex numerical model.
- The modeler neglects to investigate alternative solvers available in the code and the range of solver settings. It is especially tempting to use the default solver and default values for solver settings provided in a GUI without testing their effect on the solution. However, adjusting solver settings or switching to another solver may decrease execution time and may be necessary to solve convergence problems.
- The modeler fails to check model output to determine if convergence problems are occurring within the problem domain. The reasons for nonconvergence can often be identified by examining the spatial distribution of head and flux residuals, residual statistics, and the computed water budget.
- The modeler assumes input to the code is correct because the model executed to completion. With the option to use free format input, many codes will complete execution even when input data are missing. A listing of the input data should always be evaluated for correctness and completeness.
- Nonconvergence occurs because the modeler has set too low a value on solution precision. The solution should be run using higher precision (e.g., double precision versions of the code).

### 3.9 PROBLEMS

Chapter 3 problems explore the equations presented in the chapter and selected analytical models.

- P3.1** This problem will give you practice in writing FD approximations.
- Write a FD approximation for Eqn (3.13a).
  - Write a FD approximation for Eqn (3.13b). What complication arises when writing an expression for this nonlinear equation compared to writing the approximation for Eqn (3.13a), which is linear? What causes the nonlinearity in Eqn (3.13b)? How could the equation be linearized?
- P3.2** Show how the standard FD approximation in Eqn (3.27) can be rewritten in water balance form as Eqn (3.37). That is, show the missing steps to transform Eqn (3.27) into Eqn (3.37).
- P3.3** Demonstrate that steady-state versions of Eqn (3.13a,b) are the same as Eqn (3.19).
- P3.4** Two wells fully penetrate a 20-m-thick confined aquifer that is isotropic and homogeneous (Fig. P3.1). Storativity is estimated to be  $2 \times 10^{-5}$ . The hydraulic conductivity is 100 m/d. The confining unit is composed of very low permeability material and is approximated as impermeable. Both wells have a radius of 0.5 m and are pumped continuously at a constant rate for 30 days; well A is pumped at 4000 L/min and well B is pumped at 12,000 L/min. Before pumping, the head is 100 m everywhere in the problem domain. The 800 m by 500 m problem domain in Fig. P3.1 is the near-field region of a problem domain that extends over many tens of square kilometers so that the aquifer effectively is of infinite extent and the composite cone of depression does not reach the boundaries after 30 days of pumping.
- Write the mathematical model (governing equation, boundary conditions, and initial conditions) for the problem.
  - Overlay a grid with uniform nodal spacing of 50 m on the 800 m by 500 m area of interest shown in Fig. P3.1. Be sure to locate each well exactly on a node. Use superposition with the Theis analytical solution to compute the drawdown (change in head from the initial head of 100 m) created by pumping both wells at the locations of the nodes. Contour the resulting drawdown to show the overlapping cones of depression. Does the Theis analytical solution solve the same form of the governing equation as given in your answer to part (a)? If not, write a mathematical model that uses the governing equation appropriate to the Theis analytical solution and explain why both mathematical models are valid for this problem.
  - List the components of a water budget for this problem. What is the source of water to the pumping wells? Using your results from part (b), calculate values for each component in the water budget. Does your water budget balance? What is the error in the water budget?

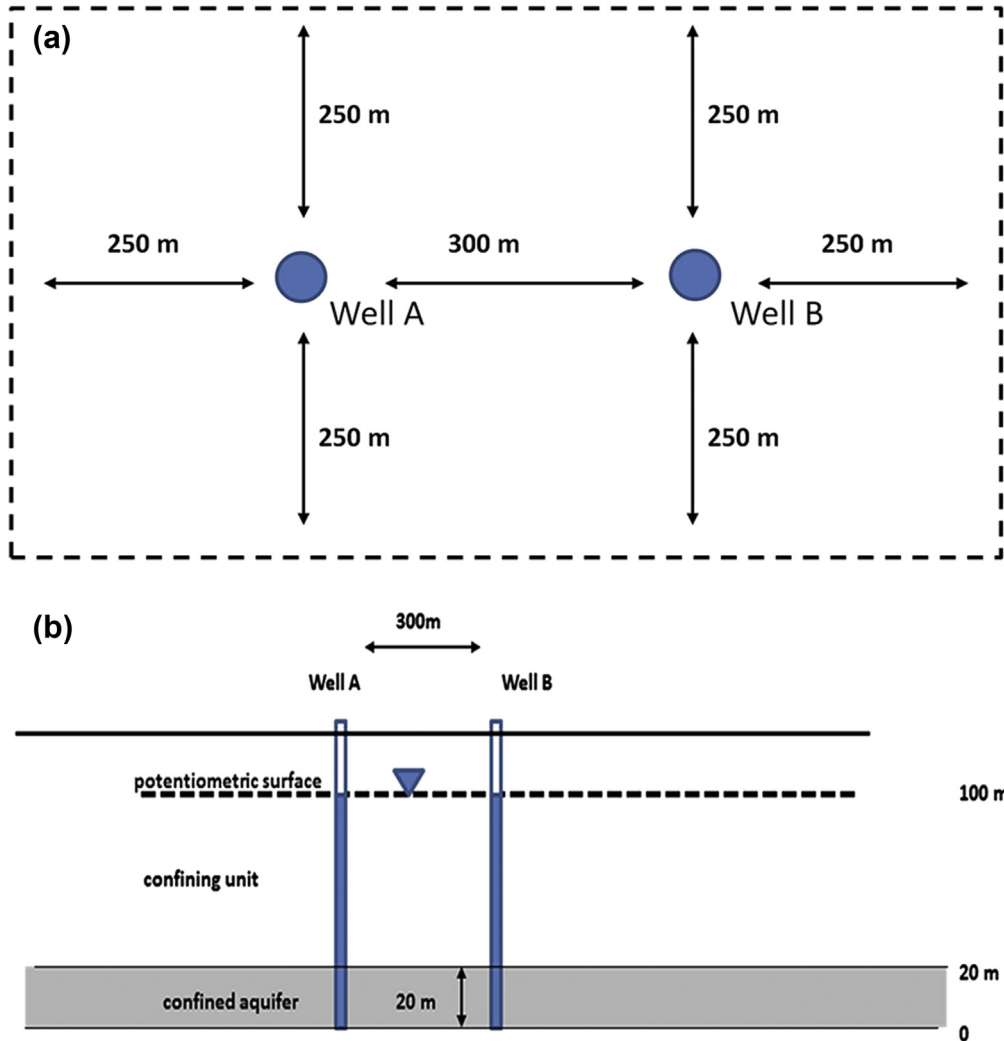


**Figure P3.1** (a) Map view of an 800 m by 500 m portion of a confined aquifer showing the locations of wells A and B. (b) Cross section of the aquifer. The datum for head is the base of the confined aquifer.

**P3.5** A single well is pumped to steady state in a confined isotropic homogeneous aquifer (Fig. P3.2). A square 400 m by 400 m grid is imposed as shown in Fig. P3.3 and heads are measured in wells along the boundaries of the grid.

- Write the mathematical model for the problem.
- Compute the heads at the four interior nodes by solving the four simultaneous equations.
- Standard spreadsheets (e.g., Excel) can solve FD approximations of a groundwater governing equation using point iteration (Box 4.3). Write the FD

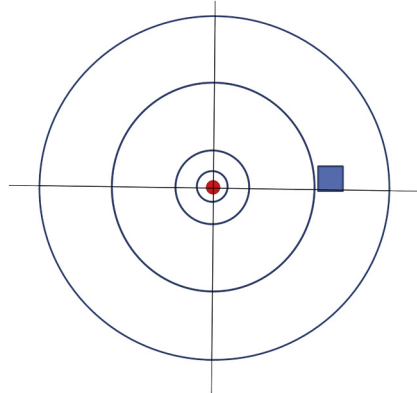


**Figure P3.2** Map view of the steady-state cone of depression (blue lines) for a pumping well (red dot) penetrating a confined aquifer. Drawdown decreases as distance from the well increases. The blue square is the location of the  $400 \times 400$  m grid in Fig. P3.3.

8.04 ●	8.18 ●	8.36 ●	8.53 ●
7.68 ●	$h_{2,2}$ ●	$h_{2,3}$ ●	8.41 ●
7.19 ●	$h_{3,2}$ ●	$h_{3,3}$ ●	8.33 ●
6.82 ●	7.56 ●	7.99 ●	8.29 ●

**Figure P3.3** Head distribution in a  $400 \times 400$  m area shown in Fig. P3.2. Heads at the boundaries are given in meters; heads at the four interior nodes are unknown (after Wang and Anderson, 1982).

expression for solving this problem using point iteration. Then develop a spreadsheet model and solve for the heads at the four interior nodes. (Note: when setting up the spreadsheet in Excel<sup>®</sup>, go to: tools > options > calculations and check manual; also check the iteration box. Press F9 to begin the calculation.) Use at least 1000 iterations and a head closure criterion of  $1E-4$  m to compare against the maximum value of absolute residual error.

- d. Compare results with the solutions in parts (b) and (c). Do all solutions give the same head values? If not, explain the discrepancies.

## REFERENCES

- Aquaterra Consulting Pty Ltd, 2000. Groundwater Flow Modelling Guideline. Murry-Darling Basin Commission, Australia. Project 125.
- ASTM International, 2008. Standard Guide for Developing and Evaluating Groundwater Modeling Codes, D6025-96(2008). American Society of Testing and Materials. Book of Standards 04.09, 17 p.
- ASTM International, 2013. Standard Guide for Documenting a Groundwater Flow Model Application, D5718-3. American Society of Testing and Materials. Book of Standards 04.08, 6 p.
- Bakker, M., Anderson, E.I., Olsthoorn, T.N., Strack, O.D., 1999. Regional groundwater modeling of the Yucca Mountain site using analytic elements. *Journal of Hydrology* 226 (3–4), 167–178. [http://dx.doi.org/10.1016/S0022-1694\(99\)00149-3](http://dx.doi.org/10.1016/S0022-1694(99)00149-3).
- Banta, E.R., 2011. ModelMate—A Graphical User Interface for Model Analysis. U.S. Geological Survey Techniques and Methods, 6–E4, 31 p. <http://water.usgs.gov/software/ModelMate/>.
- Barlow, P.M., Moench, A.F., 1998. Analytical Solutions and Computer Programs for Hydraulic Interaction of Stream-aquifer Systems. U. S. Geological Survey. Open-File Report 98-415A, 85 p. <http://pubs.usgs.gov/of/1998/of98-415A/>.
- Bear, J., 1972. *Dynamics of Fluids in Porous Media*. Elsevier, New York, 764 p.
- Bear, J., Cheng, A.H.-D., 2010. Modeling Groundwater Flow and Contaminant Transport. In: *Theory and Applications of Transport in Porous Media*, vol. 23. Springer, 834 p.
- Berger, R.C., Howington, S.E., January 2002. Discrete fluxes and mass balance in finite elements. *Journal of Hydraulic Engineering* 128 (1), 87–92. [http://dx.doi.org/10.1061/\(ASCE\)0733-9429\(2002\)128:1\(87\)](http://dx.doi.org/10.1061/(ASCE)0733-9429(2002)128:1(87)).
- Bruggeman, G.A. (Ed.), 1999. *Analytical Solutions of Geohydrological Problems*. Developments in Water Science, vol. 46. Elsevier, Amsterdam, p. 959.
- Cardenas, M.B., 2008. Surface-ground water interface geomorphology leads to scaling of residence times. *Geophysical Research Letters* 35, L08402. <http://dx.doi.org/10.1029/2008GL033753>.
- Cardiff, M., Barrash, W., Kitanidis, P.K., Malama, B., Revil, A., Straface, S., et al., 2009. A potential-based inversion of unconfined steady-state hydraulic tomography. *Groundwater* 47 (3), 259–270. <http://dx.doi.org/10.1111/j.1745-6584.2008.00541.x>.
- Chamberlin, T.C., June 30, 1899. Lord Kelvin's address on the age of the earth as an abode fitted for life. *Science* 889–901. New Series 9(235).
- Cheng, R.T., 1978. Modeling of hydraulic systems by finite-element methods. In: *Advances in Hydro-science*, vol. 11. New York Academic Press, pp. 207–284.
- Chiang, W.-H., Kinzelbach, W., 2013. *3D-Groundwater Modeling with PMWIN: A Simulation System for Modeling Groundwater Flow and Transport Processes*. Springer-Verlag, Berlin, Heidelberg, New York, 346 p.
- Cortis, A., Berkowitz, B., 2005. Computing “anomalous” contaminant transport in porous media: The CTRW MATLAB toolbox. *Groundwater* 43 (6), 947–950. <http://dx.doi.org/10.1111/j.1745-6584.2005.00045.x>.
- Dagan, G., Fiori, A., Jankovic, I., 2003. Flow and transport in highly heterogeneous formations, part 1: Conceptual framework and validity of first-order approximations. *Water Resources Research* 39 (9), 1268. <http://dx.doi.org/10.1029/2002WR001717>.
- Dehotin, J., Vazquez, R.R., Braud, I., Debionne, S., Vaillet, P., 2011. Modeling of hydrological processes using unstructured and irregular grids-2D groundwater application. *Journal of Hydrologic Engineering* 16 (2), 108–125. [http://dx.doi.org/10.1061/\(ASCE\)HE.1943-5584.0000296](http://dx.doi.org/10.1061/(ASCE)HE.1943-5584.0000296).
- De Lange, W.J., 2006. Development of an analytic element ground water model of the Netherlands. *Groundwater* 44 (1), 111–115. <http://dx.doi.org/10.1111/j.1745-6584.2005.00142.x>.
- DHI-WASY, 2013. FEFLOW 6.2 User Manual. DHI-WASY GmbH, Berlin Germany, 202 p. [http://www.feflow.com/uploads/media/users\\_manual62.pdf](http://www.feflow.com/uploads/media/users_manual62.pdf).
- Diersch, H.-J.G., 2014. FEFLOW: Finite Element Modeling of Flow, Mass and Heat Transport in Porous and Fractured Media. Springer, 996 p.
- Dripps, W.R., Hunt, R.J., Anderson, M.P., 2006. Estimating recharge rates with analytic element models and parameter estimation. *Groundwater* 44 (1), 47–55. <http://dx.doi.org/10.1111/j.1745-6584.2005.00115.x>.

- Eriksson, L.O., Opielstrup, J., 1994. Calibration with Respect to Hydraulic Head Measurements in Stochastic Simulation of Groundwater Flow – a Numerical Experiment Using MATLAB. Starprog AB, Technical Report SKB 94-30. Swedish Nuclear Fuel and Waste Management Co (SVENSK), 50 p. <http://skb.se/upload/publications/pdf/TR-94-30webb.pdf>.
- Feinstein, D.T., Dunning, C.P., Hunt, R.J., Krohelski, J.T., 2003. Stepwise use of GFLOW and MODFLOW to determine relative importance of shallow and deep receptors. *Groundwater* 41 (2), 190–199. <http://dx.doi.org/10.1111/j.1745-6584.2003.tb02582.x>.
- Feinstein, D.T., Buchwald, C.A., Dunning, C.P., Hunt, R.J., 2006. Development and Application of a Screening Model for Simulating Regional Ground-water Flow in the St. Croix River Basin, Minnesota and Wisconsin. U.S. Geological Survey. Scientific Investigations Report 2005–5283, 50 p. <http://pubs.usgs.gov/sir/2005/5283/>.
- Ferris, J.G., Knowles, D.B., Brown, R.H., Stallman, R.W., 1962. Theory of Aquifer Tests. U. S. Geological Survey. Water-Supply Paper 1536-E, 174 p. <http://pubs.usgs.gov/wsp/wsp1536-E/>.
- Fitts, C.R., 2010. Modeling aquifer systems with analytic elements and subdomains. *Water Resources Research* 46 (7), W07521. <http://dx.doi.org/10.1029/2009WR008331>.
- Fitts, C.R., 2013. *Groundwater Science*, second ed. Academic Press, London. 672 p.
- Haitjema, H.M., 1995. *Analytic Element Modeling of Groundwater Flow*. Academic Press, Inc., San Diego, CA., 394 p.
- Haitjema, H., 2006. The role of hand calculations in ground water flow modeling. *Groundwater* 44 (6), 786–791. <http://dx.doi.org/10.1111/j.1745-6584.2006.00189.x>.
- Haitjema, H.M., Hunt, R.J., Jankovic, I., de Lange, W.J., 2006. Foreword: Ground water flow modeling with the analytic element method. *Groundwater* 44 (1), 1–122. <http://dx.doi.org/10.1111/j.1745-6584.2005.00144.x>.
- Haitjema, H.M., Feinstein, D.T., Hunt, R.J., Gusev, M., 2010. A hybrid finite difference and analytic element groundwater model. *Groundwater* 48 (4), 538–548. <http://dx.doi.org/10.1111/j.1745-6584.2009.00672>.
- Harbaugh, A.W., 1990. A Computer Program for Calculating Subregional Water Budgets Using Results from the U.S. Geological Survey Modular Three-dimensional Ground-water Flow Model. U.S. Geological Survey. Open-File Report 90-392, 46 p. <http://pubs.er.usgs.gov/publication/ofr90392>.
- Harbaugh, A.W., 1995. Direct Solution Package Based on Alternating Diagonal Ordering for the U.S. Geological Survey Modular Finite-difference Ground-water Flow Model. U.S. Geological Survey. Open-File Report 95-288, 46 p. <http://pubs.er.usgs.gov/publication/ofr95288>.
- Harbaugh, A.W., 2005. MODFLOW-2005, the U.S. Geological Survey Modular Ground-water Model – the Ground-water Flow Process. U.S. Geological Survey Techniques and Methods. 6-A16. <http://pubs.er.usgs.gov/publication/tm6A16>.
- Hunt, R.J., 2006. Ground water modeling applications using the analytic element method. *Groundwater* 44 (1), 5–15. <http://dx.doi.org/10.1111/j.1745-6584.2005.00143.x>.
- Hunt, R.J., Anderson, M.P., Kelson, V.A., 1998. Improving a complex finite difference groundwater-flow model through the use of an analytic element screening model. *Groundwater* 36 (6), 1011–1017. <http://dx.doi.org/10.1111/j.1745-6584.1998.tb02108.x>.
- Huyakorn, P.S., Pinder, G.R., 1983. *Computational Methods in Subsurface Flow*. Academic Press, New York, 473 p.
- Istok, J., 1989. *Groundwater Modeling by the Finite Element Method*. American Geophysical Union (AGU), Washington, D.C.. Water Resources Monograph 13, 495 p.
- Jankovic, I., Fiori, A., Dagan, G., 2003. Flow and transport in highly heterogeneous formations, part 3: Numerical simulations and comparisons with theoretical results. *Water Resources Research* 39 (9), 1270. <http://dx.doi.org/10.1029/2002WR001721>.
- Johnson, C., Mifflin, M., 2006. The AEM and regional carbonate aquifer modeling. *Groundwater* 44 (1), 24–34. <http://dx.doi.org/10.1111/j.1745-6584.2005.00132.x>.
- Jones, N.L., 2014. *GMS v10.0 Reference Manual*. Aquaveo, Brigham Young University, Provo, Utah, 662 p.
- Kelson, V.A., Hunt, R.J., Haitjema, H.M., 2002. Improving a regional model using reduced complexity and parameter estimation. *Groundwater* 40 (2), 132–143. <http://dx.doi.org/10.1111/j.1745-6584.2002.tb02498.x>.



- Konikow, L.F., 1978. Calibration of ground-water models. In: *Verification of Mathematical and Physical Models in Hydraulic Engineering*. American Society of Civil Engineers, New York, pp. 87–93.
- Konikow, L.F., Reilly, T.E., 1998. Groundwater modeling. In: Delleur, J.W. (Ed.), *The Handbook of Groundwater Engineering*. CRC Press, Boca Raton, FL, pp. 20–1–20–39.
- Kresic, N., Mikszewski, A., 2013. *Hydrogeological Conceptual Site Models: Data Analysis and Visualization*. CRC Press, Boca Raton, FL, 584 p.
- Langevin, C., Bean, D., 2005. Groundwater Vistas: A graphical user interface for the MODFLOW family of ground water flow and transport models. *Groundwater* 43 (2), 165–168. <http://dx.doi.org/10.1111/j.1745-6584.2005.0016.x>.
- Li, Q., Ito, K., Wu, Z., Lowry, C.S., Loheide II, S.P., 2009. COMSOL multiphysics: A novel approach to ground water modeling. *Groundwater* 47 (4), 480–487. <http://dx.doi.org/10.1111/j.1745-6584.2009.00584.x>.
- Loheide, S.P., Gorelick, S.M., 2007. Riparian hydroecology: A coupled model of the observed interactions between groundwater flow and meadow vegetation patterning. *Water Resources Research* 43 (7), W07417. <http://dx.doi.org/10.1029/2006WR005233>.
- Maslia, M.L., Randolph, R.B., 1987. *Methods and Computer Program Documentation for Determining Anisotropic Transmissivity Tensor Components of Two-dimensional Ground-water Flow*. U.S. Geological Survey. Water Supply Paper 2308, 46 p. <http://pubs.er.usgs.gov/publication/wsp2308>.
- McDonald, M.G., Harbaugh, A.W., 1988. A Modular Three-dimensional Finite-Difference Ground-water Flow Model. U.S. Geological Survey Techniques of Water-Resources Investigations. 06-A1, 576 p. <http://pubs.er.usgs.gov/publication/twri06A1>.
- McDonald, M.G., Harbaugh, A.W., 2003. The history of MODFLOW. *Groundwater* 41 (2), 280–283. <http://dx.doi.org/10.1111/j.1745-6584.2003.tb02591.x>.
- McLane, C., 2012. AnAqSim: Analytic element modeling software for multi-aquifer, transient flow. *Groundwater* 50 (1), 2–7. <http://dx.doi.org/10.1111/j.1745-6584.2011.00892.x>.
- Narasimhan, T.N., Witherspoon, P.A., 1976. An integrated finite-difference method for analyzing fluid flow in porous media. *Water Resources Research* 12 (1), 57–64. <http://dx.doi.org/10.1029/WR012i001p00057>.
- Panday, S., Langevin, C.D., Niswonger, R.G., Ibaraki, M., Hughes, J.D., 2013. MODFLOW-USG Versions 1: An Unstructured Grid Version of MODFLOW for Simulating Groundwater Flow and Tightly Coupled Processes Using a Control Volume Finite-difference Formulation. U.S. Geological Survey Techniques and Methods. 6-A45, 66 p. <http://pubs.usgs.gov/tm/06/a45/>.
- Pinder, G.F., Gray, W.G., 1976. Is there a difference in the finite element method? *Water Resources Research* 12 (1), 105–107. <http://dx.doi.org/10.1029/WR012i001p00105>.
- Pinder, G.F., Gray, W.G., 1977. *Finite Element Simulation in Surface and Subsurface Hydrology*. Academic Press, San Diego, CA, 295 p.
- Pint, T., Li, S.-G., 2006. ModTech: A GIS-enabled ground water modeling program. *Groundwater* 44 (4), 506–508. <http://dx.doi.org/10.1111/j.1745-6584.2006.00233.x>.
- Quinones-Aponte, V., 1989. Horizontal anisotropy of the principal ground-water flow zone in the Salinas alluvial fan, Puerto Rico. *Groundwater* 27 (4), 491–500. <http://dx.doi.org/10.1111/j.1745-6584.1989.tb01969.x>.
- Reeves, H.W., 2008. STRMDEPL08—An Extended Version of STRMDEPL with Additional Analytical Solutions to Calculate Streamflow Depletion by Nearby Pumping Wells. U.S. Geological Survey. Open-File Report 2008–1166, 22 p. <http://pubs.usgs.gov/of/2008/1166/>.
- Reilly, T.E., Franke, O.L., Bennett, G.D., 1987. *The Principle of Superposition and its Application in Ground-water Hydraulics*. U.S. Geological Survey Techniques of Water Resources Investigations. Chapter B6, Book 3, 28 p. <http://pubs.usgs.gov/twri/twri3-b6/>.
- Remson, I., Hornberger, G.M., Molz, F.J., 1971. *Numerical Methods in Subsurface Hydrology*. Wiley-Interscience, John Wiley & Sons, Inc., New York, 389 p.
- Rumbaugh, J.O., Rumbaugh, D.B., 2011. *Groundwater Vistas V.6*. Environmental Simulations Inc., 213 p. [http://www.groundwatermodels.com/ESI\\_Software.php](http://www.groundwatermodels.com/ESI_Software.php)

- Schlumberger Water Services, 2012. Visual MODFLOW Flex User Documentation. Schlumberger Water Services, Kitchener, Ontario, Canada, 330 p.
- Ségol, G., 1994. *Classic Groundwater Simulations: Proving and Improving Numerical Models*. PTR Prentice-Hall, Inc., Englewood Cliffs, New Jersey, 531 p.
- Sheets, R.A., Hill, M.C., Haitjema, H.M., Provost, A.M., Masterson, J.P., 2015. Simulation of water-table aquifers using specified saturated thickness. *Groundwater* 53 (1), 151–157. <http://dx.doi.org/10.1111/gwat.12164>.
- Strack, O.D.L., 1984. Three-dimensional streamlines in Dupuit-Forchheimer models. *Water Resources Research* 20 (7), 812–822. <http://dx.doi.org/10.1029/WR020i007p00812>.
- Strack, O.D.L., 1989. *Groundwater Mechanics*. Prentice-Hall, Inc., Englewood Cliffs, New Jersey, 732 p.
- Strack, O.D.L., 2003. Theory and applications of the analytic element method. *Reviews of Geophysics* 41 (2), 1005–2003. <http://dx.doi.org/10.1029/2002RG000111>.
- Strack, O.D.L., 2006. The development of new analytic elements for transient flow and multiaquifer flow. *Groundwater* 44 (1), 91–98. <http://dx.doi.org/10.1111/j.1745-6584.2005.00148.x>.
- Strack, O.D.L., Hajjema, H.M., 1981a. Modeling double aquifer flow using a comprehensive potential and distributed singularities: 1. Solution for homogeneous permeabilities. *Water Resources Research* 17 (5), 1535–1549. <http://dx.doi.org/10.1029/WR017i005p01535>.
- Strack, O.D.L., Hajjema, H.M., 1981b. Modeling double aquifer flow using a comprehensive potential and distributed singularities: 2. Solution for inhomogeneous permeabilities. *Water Resources Research* 17 (5), 1551–1560. <http://dx.doi.org/10.1029/WR017i005p01551>.
- Trefry, M.G., Muffels, C., 2007. FEFLOW: A finite-element ground water flow and transport modeling tool. *Groundwater* 45 (5), 525–528. <http://dx.doi.org/10.1111/j.1745-6584.2007.00358.x>.
- Tyson Jr., H.N., Weber, E.M., 1964. Ground-water management for the nation's future—computer simulation of ground-water basins, American Society of Civil Engineers Proceedings. *Journal of the Hydraulics Division* 90, 59–77.
- Voss, C.I., Provost, A.M., 2002. SUTRA: A Model for Saturated Unsaturated Variable-density Groundwater Flow with Solute or Energy Transport. U.S. Geological Survey. Water Resources Investigation Report 02–4231.
- Wang, H.F., Anderson, M.P., 1977. Finite differences and finite elements as weighted residual solutions to Laplace's equation. In: Gray, W.G., Pinder, G.F. (Eds.), *Finite Elements in Water Resources*, Proceedings of the First International Conference on Finite Elements in Water Resources, Princeton University, July. Pentech Press, London, pp. 2.167–2.178.
- Wang, H.F., Anderson, M.P., 1982. *Introduction to Groundwater Modeling: Finite Difference and Finite Element Methods*. Academic Press, San Diego, CA, 237 p.
- Ward, A.S., Gooseff, M.N., Singha, K., 2013. How does subsurface characterization affect simulations of hypo-rheic exchange? *Groundwater* 51 (1), 14–28. <http://dx.doi.org/10.1111/j.1745-6584.2012.00911.x>.
- Winston, R.B., 2009. ModelMuse—a Graphical User Interface for MODFLOW-2005 and PHAST. U.S. Geological Survey Techniques and Methods. 6-A29, 52 p. <http://pubs.usgs.gov/tm/tm6A29/>.
- Yager, R.M., Neville, C.J., 2002. GFLOW 2000: An analytical element ground water flow modeling system. *Groundwater* 40 (6), 574–576. <http://dx.doi.org/10.1111/j.1745-6584.2002.tb02543.x>.
- Yamamoto, H., 2008. PetraSim: A graphical user interface for the TOUGH2 family of multiphase flow and transport codes. *Groundwater* 46 (4), 525–528. <http://dx.doi.org/10.1111/j.1745-6584.2008.00462.x>.
- Zaadnoordijk, W.J., 2006. Building pit dewatering: Application of transient analytic elements. *Groundwater* 44 (1), 106–110. <http://dx.doi.org/10.1111/j.1745-6584.2005.00171.x>.
- Zheng, C., 2004. Model viewer: A three-dimensional visualization tool for ground water modelers. *Groundwater* 42 (2), 164–166. <http://dx.doi.org/10.1111/j.1745-6584.2004.tb02664.x>.
- Zlotnik, V.A., Cardenas, M.B., Toundykov, D., 2011. Effects of multiscale anisotropy on basin and hyporheic groundwater flow. *Groundwater* 49 (4), 576–583. <http://dx.doi.org/10.1111/j.1745-6584.2010.00775.x>.



## CHAPTER 4

# Model Dimensionality and Setting Boundaries

*... if one advances confidently in the direction of his dreams... he will meet with success unexpected in his common hours. He will put something behind, will pass an invisible boundary...*

*Henry David Thoreau*

### Contents

4.1 Spatial Dimensions	118
4.1.1 Two-Dimensional Models	118
4.1.1.1 Areal Models	118
4.1.1.2 Profile Models	125
4.1.2 Three-Dimensional Models	133
4.2 Selecting Boundaries	134
4.2.1 Physical Boundaries	136
4.2.1.1 Contacts with Geologic Units of Low Hydraulic Conductivity	136
4.2.1.2 Shear Zones and Faults	137
4.2.1.3 Surface Water Features	137
4.2.1.4 Freshwater–Seawater Interface	140
4.2.2 Hydraulic Boundaries	144
4.2.2.1 Streamlines (Groundwater Divides)	145
4.2.2.2 Equipotential Lines (Constant Head/Constant Flow)	145
4.3 Implementing Boundaries in a Numerical Model	145
4.3.1 Setting Boundaries in the Grid/Mesh	145
4.3.2 Specified Head Boundaries	147
4.3.3 Specified Flow Boundaries	148
4.3.4 Head-dependent Boundaries	152
4.3.4.1 Surface Water Bodies	153
4.3.4.2 Drains	155
4.3.4.3 Evapotranspiration (ET) from the Water Table	157
4.3.4.4 Lateral Boundary Flows and Distant Boundaries	158
4.4 Extracting Local Boundary Conditions from a Regional Model	159
4.5 Simulating the Water Table	162
4.5.1 Fixed Nodes	164
4.5.2 Movable Nodes	165
4.5.3 Variably Saturated Codes	166
4.6 Common Modeling Errors	170
4.7 Problems	170
References	176

## Boxes

Box 4.1	Two-Dimensional or Three-Dimensional—More about the D-F Approximation	122
Box 4.2	Profile Models	125
Box 4.3	Spreadsheet Solution of a Finite-Difference Profile Model	128
Box 4.4	The Freshwater–Seawater Interface	141
Box 4.5	Large Water Budget Errors Arising from an HDB	153
Box 4.6	What Controls the Water Table?	167

## 4.1 SPATIAL DIMENSIONS

In Chapter 3, we derived the transient governing equation for flow in three dimensions (Eqn (3.12)). Analytical solutions are often developed in one- and two dimensions but rarely in three dimensions. Most numerical groundwater models simulate flow in two or three spatial dimensions; one-dimensional numerical models are rarely used. Model dimension depends on the purpose of the model, the complexity of the hydrostratigraphy, and the flow system.

### 4.1.1 Two-Dimensional Models

In two dimensions, areal models represent the groundwater system as a single layer in map view (Fig. 4.1) and profile models represent flow in a cross section (Fig. 2.1).

#### 4.1.1.1 Areal Models

In a two-dimensional (2D) areal model, flow is simulated in two horizontal dimensions to represent flow in either a confined or unconfined aquifer (Fig. 4.1(a) and (b)). Equation (3.13a) is the governing equation for a confined aquifer and Eqn (3.13b) is the governing equation for an unconfined aquifer. The hydraulic effects of all features represented in the model (e.g., pumping wells, internal sources of water such as surface waters, and perimeter boundary conditions) fully penetrating the aquifer, i.e., extend through the full depth of the aquifer. The steady-state solution of a 2D areal model is a 2D array of heads in map view; a transient solution calculates a head array for every time step. In a confined aquifer, heads represent the potentiometric surface; in an unconfined aquifer heads represent the water table. A 2D areal model might also represent unconfined and confined conditions in different areas of the model domain (Fig. 4.1(c)).

An areal model is defined exclusively by side boundaries. The top and bottom boundaries of the model are inherent in the 2D formulation of flow and are not specified by the user. The requirement for horizontal flow means that the bottom of a 2D areal model is intrinsically a no-flow boundary. A confined aquifer is bounded at the bottom by a confining bed or other relatively impermeable material (Fig. 4.2). The top of a confined aquifer is also bounded by a confining bed. When either the top or bottom confining bed is assumed to be impermeable for the purposes of the model, there is no leakage across the

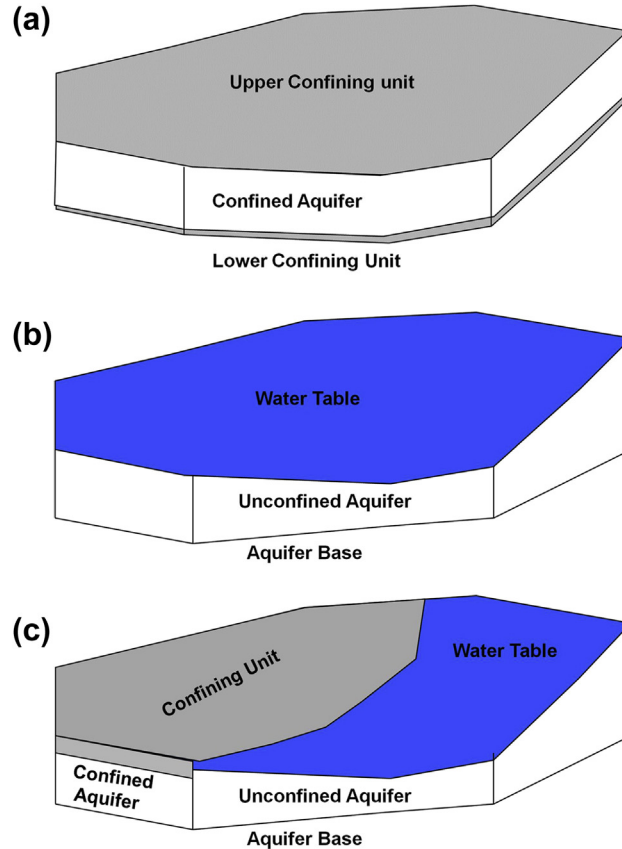


**Figure 4.1** Schematic representation of two-dimensional (2D) areal models. (a) Confined aquifer bounded by an upper and lower confining bed. The upper confining bed may be overlain by an unconfined aquifer (see Fig. 4.2), which provides a source of water to the confined aquifer via leakage through the confining bed. Heads represent the potentiometric surface defined by the elevation of water levels in wells penetrating the confined aquifer (see Fig. 4.2). (b) Head in an unconfined aquifer is equal to the elevation of the water table,  $h$ , above the base of the aquifer (see Figs. 4.2 and 4.3). The thickness of the model layer is equal to  $h$  and varies spatially. (c) A 2D areal model may simulate both confined and unconfined conditions within the same model layer.

confining bed. If the confining bed is permeable,  $R$  in Eqn (3.13a) represents *leakage*,  $q_L$ , which is the vertical flow of water through the confining bed:

$$q_L = -K'_z \frac{h_{\text{source}} - h}{b'} \quad (4.1)$$

where  $h_{\text{source}}$  is the head in the source bed, which is either an unconfined aquifer above the confining bed (Fig. 4.2) or another confined aquifer;  $h$  is the calculated head in the aquifer;  $K'_z$  and  $b'$  are the vertical hydraulic conductivity and thickness of the confining bed, respectively. Leakage can occur from aquifers located both above and below the aquifer of interest. The parameter  $K'_z/b'$  is defined as *vertical leakance*. The inverse of vertical leakance is *vertical resistance*,  $b'/K'_z$ . Although similar in concept, vertical

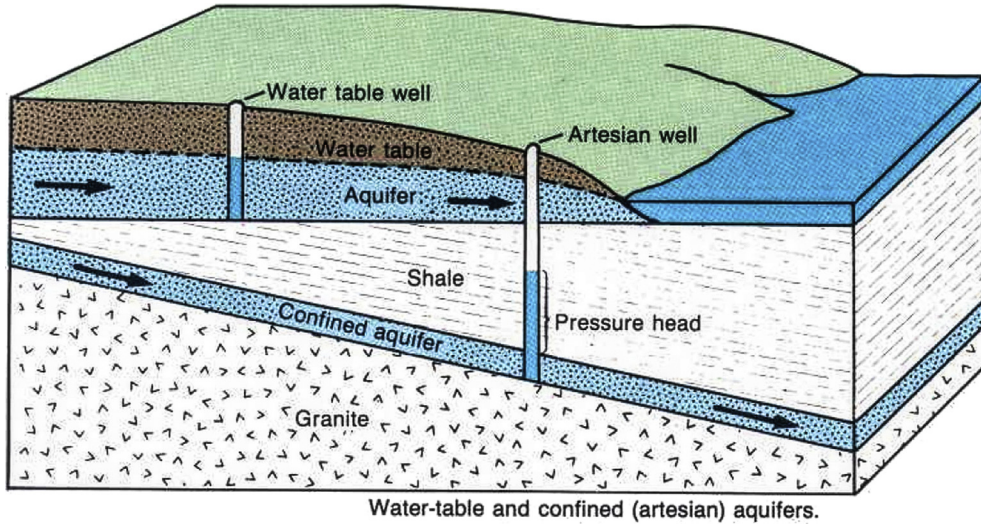


**Figure 4.2** Schematic diagram showing an unconfined aquifer and a confined aquifer within a regional groundwater flow system (Waller, 2013).

resistance has the intuitive property that resistance approaches zero as thickness,  $b'$ , goes to zero in contrast to leakance, which approaches infinity as  $b'$  goes to zero.

An unconfined aquifer is intrinsically bounded at the bottom by material that is considered impermeable and at the top by the water table. Leakage across the bottom boundary (in cases where the bottom boundary is not completely impermeable) can be simulated by Eqn (4.1) or by specifying  $q_L$  from field data. The water table is not considered a boundary because it is computed as the solution.

Two-dimensional areal models use the *Dupuit-Forchheimer (D-F) approximation*. Briefly stated, the D-F approximation assumes that flow is dominantly horizontal (Fig. B4.1.1 in Box 4.1) and vertical hydraulic gradients are negligible (though vertical flow can still be represented; see Box 4.1). When the change in head in the vertical direction is zero ( $\partial h / \partial z = 0$ ), the head at any point (x,y) in a horizontal plane is equal to the elevation of the potentiometric surface in a confined aquifer, and the elevation of the water table (measured from the base of the aquifer) in an unconfined aquifer (Fig. 4.3) (i.e., the elevation of the water-table is equal to the saturated thickness,  $b$ ). Comparisons of solutions using the D-F approximation with solutions for three-dimensional (3D) flow show that heads calculated by a D-F model are nearly indistinguishable from heads in a 3D model at distances greater than  $2.5d$  from a hydraulic feature that causes vertical flow (e.g., 3D features such as partially penetrating surface water bodies, pumping wells, and groundwater divides) (Haitjema, 2006, p. 788) where:

$$d = b\sqrt{K_h/K_v} \quad (4.2a)$$

In Eqn (4.2a),  $K_h$  and  $K_v$  are horizontal and vertical hydraulic conductivity, respectively, and  $b$  is saturated thickness. Thus, for isotropic conditions ( $K_h/K_v = 1$ ), vertical

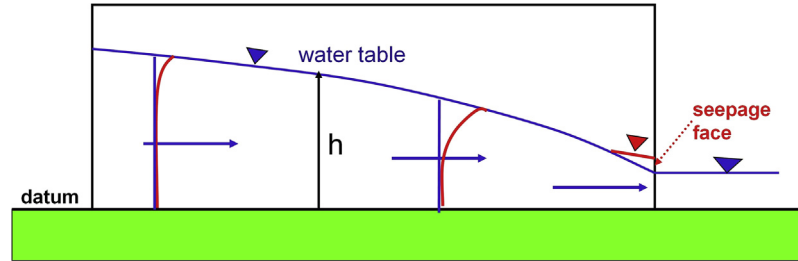


**Figure 4.3** Horizontal flow (blue arrows) in an unconfined aquifer under the Dupuit-Forchheimer (D-F) approximation. The D-F approximation is inaccurate near the discharge face and close to the water table. Equipotential lines (red lines) in the true flow field deflect at the water table and near the discharge face where there are vertical gradients and a seepage face; the D-F approximation assumes vertical equipotential lines (shown in blue). In the true flow field, the water table intersects the discharge face above the free surface of the surface water body (red line) creating a seepage face. Under the D-F approximation, the water table is continuous and meets the free surface of the surface water body without a seepage face.

flow can be neglected between two to three saturated thicknesses away from a 3D feature. In a regional groundwater flow system (e.g., Fig. B4.1.1 in Box 4.1), hydraulic features that cause vertical flow are located at system boundaries, which doubles the distance required for a single hydraulic feature and implies that D-F flow is a good approximation when the length of the system,  $L$  is greater than  $5d$  (Haitjema, 2006, p. 788):

$$L > 5b\sqrt{K_h/K_v} \quad (4.2b)$$

In many groundwater systems, the distance  $L$  is much larger than the saturated thickness,  $b$ , so that areal flow models using the D-F approximation are appropriate for a wide variety of groundwater flow problems (Box 4.1).

Under the D-F approximation, there is no seepage face. A seepage face is a discharge surface in an unconfined aquifer where pressure is equal to zero (atmospheric pressure); head along the seepage face is equal to the elevation of the face. A seepage face may form locally along hillslopes, stream banks (Fig. 4.3) and in tunnels, mines and large diameter wells (Section 6.2). D-F models perform poorly close to a discharge face where the slope of the water table is high and there are strong vertical components of flow, but the solution is accurate when the distance from the seepage face is sufficiently large, as defined by the guidelines discussed above.

The accurate simulation of the water table as a free surface (moving boundary) is complicated because it requires rigorous representation of vertical flow and a nonlinear boundary condition on the water table (Neuman and Witherspoon, 1971; Diersch, 2014, pp. 216–218, 405–406; Section 4.5). As Diersch (2014, p. 406) observed, in practice “the free-surface problem is commonly solved only in a non-rigorous manner”. D-F models are one such nonrigorous approach (Box 4.1). Other options for simulating the water table and associated seepage face are discussed in Section 4.5.



### Box 4.1 Two-Dimensional or Three-Dimensional—More about the D-F Approximation

The natural world is 3D and transient; so one might argue that 3D transient models are always the most defensible groundwater model. However, the time and cost of designing, calibrating, and performing uncertainty analysis using a 3D transient groundwater model are significant, potentially leaving little time and budget to explore questions related to model performance and forecasting. A recurring theme throughout our book is that appropriate simplification of the complex natural world necessarily underlies all environmental modeling. In Section 4.1, we discussed the D-F approximation for simulating 2D areal flow. When conditions are appropriate for a D-F model, the cost and effort of a 3D model can be avoided. Thus, the D-F approximation, when applicable, is a valuable asset to groundwater modelers. In this box, we provide some additional information about D-F models.

D-F theory dates back to the nineteenth century when Dupuit (1863) derived an expression for the potentiometric surface in which vertical changes in head were neglected. Forchheimer (1886, 1898) independently omitted vertical changes in head in equations for both confined and unconfined flow. The name of the approximation recognizes the contributions of both individuals. Although D-F theory is valid for both confined and unconfined conditions, it is especially helpful when applied to unconfined aquifers because it provides a way to calculate the elevation of the water table. Recall that a complication arises in profile (Boxes 4.2 and 4.3) and 3D models of unconfined aquifers because the water table is the upper boundary of the model (Section 4.5 and Box 4.6) but to set the water-table boundary condition, we need to know the position of the water table, which is usually poorly known. In a D-F model, however, the water table is not a boundary; instead the model calculates the elevation of the water table as the solution (e.g., Youngs, 1990).

Flowpaths in regional groundwater systems are often viewed in cross sections with vertical exaggeration (Fig. B4.1.1(a)) causing exaggerated representation of vertical flow, but when viewed without vertical exaggeration (Fig. B4.1.1(b)) flowpaths are dominantly horizontal.

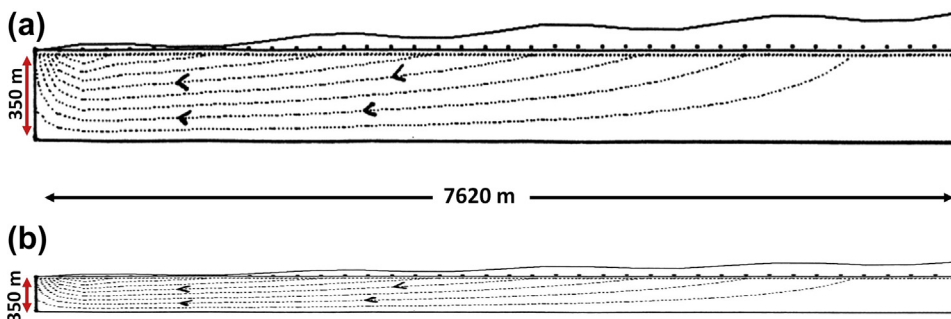


**Figure B4.1.1** Cross sections through a regional groundwater flow system showing flowpaths. (a) Vertical flow is slightly exaggerated (vertical exaggeration = 2.5). (b) Without vertical exaggeration flowpaths are dominantly horizontal. System parameters are typical of an aquifer in a humid climate (recharge = 25.4 mm/yr;  $K_h = K_v = 0.3$  m/d). The ratio of system length to thickness is approximately 25 (modified from Haitjema and Mitchell-Bruker, 2005).

### Box 4.1 Two-Dimensional or Three-Dimensional—More about the D-F Approximation—cont'd

Equation (4.2a, 4.2b) (Section 4.1) provides guidelines for determining when D-F models are appropriate. In general, the effects of features that cause 3D flow are negligible when the distance from the feature is greater than approximately  $2d$ , where  $d$  is given by Eqn (4.2a). For a homogeneous, isotropic aquifer ( $K_h/K_v = 1$ ), 3D effects are negligible when the distance from the feature is approximately two times the saturated thickness of the aquifer. Equation (4.2b) provides a guideline for the acceptable dimensions of a D-F model of regional groundwater flow (e.g., Fig. B4.1.1). For a homogeneous, isotropic aquifer system, a D-F model of regional groundwater flow performs well when the length of the system is at least five times its saturated thickness (i.e.,  $L/b > 5$ ). If  $K_h/K_v = 1000$ , the length of the system would need to be at least 160 times greater than its saturated thickness, which is not unreasonable geometry for many regional groundwater flow systems.

An often overlooked aspect of D-F theory is that vertical flow is not ignored even though vertical head gradients are assumed to be negligible. A thought experiment devised by Kirkham (1967) explains how vertical flow can occur when vertical gradients are zero. Kirkham envisioned a “slotted” porous medium where vertical slots (Fig. B4.1.2) offer no resistance to flow. Consequently there is no change in head with depth in the slots, but vertical flow can occur within the slots. The water-table curvature results from resistance to horizontal flow through the aquifer blocks located between the slots (Fig. B4.1.2). Polubarinova-Kochina (1962) also recognized that the curvature of the water table meant that D-F models must include vertical flow. Strack (1984) used ideas from Kirkham (1967) and Polubarinova-Kochina (1962)

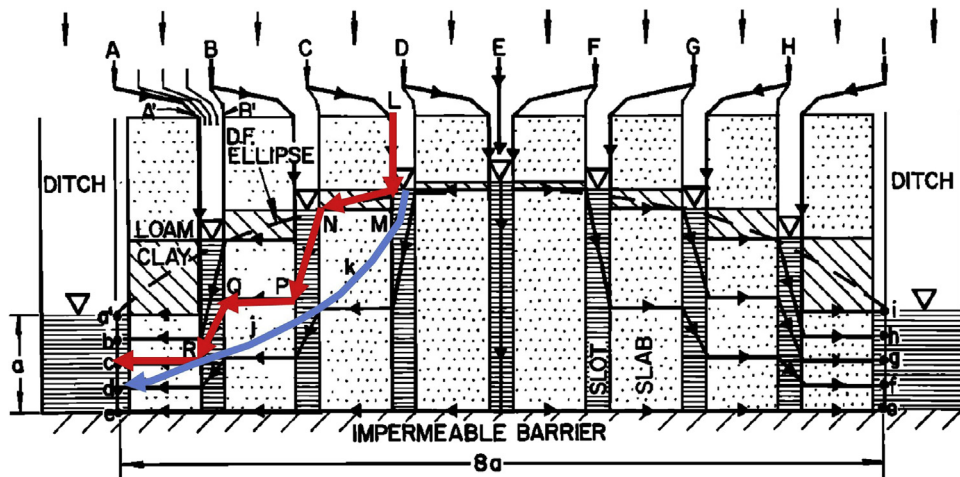


Figure B4.1.2 Kirkham's (1967) "slotted" porous medium. The slots at A through I provide no vertical resistance to flow. Vertical flow occurs along a stepped flowpath LMNPQRc (red line), which is smoothed to the path MkjRd (blue line) when the slots are closely spaced (modified from Kirkham, 1967).

(Continued)

### Box 4.1 Two-Dimensional or Three-Dimensional—More about the D-F Approximation—cont'd

to develop theory for approximating 3D flowpaths in areal 2D models; horizontal velocities are obtained from Darcy's law while vertical velocities are approximated by requiring continuity of flow. The existence of 3D flowpaths in 2D horizontal flow systems means that 3D particle tracking (Chapter 8) can be performed in D-F models.

Given that many aquifers are much longer than they are deep, D-F-theory is applicable to many regional groundwater flow problems. Nevertheless, some modeling objectives require 3D simulations. 3D models should always be used when 3D flow is important to the modeling objective (e.g., Fig. B4.1.3).

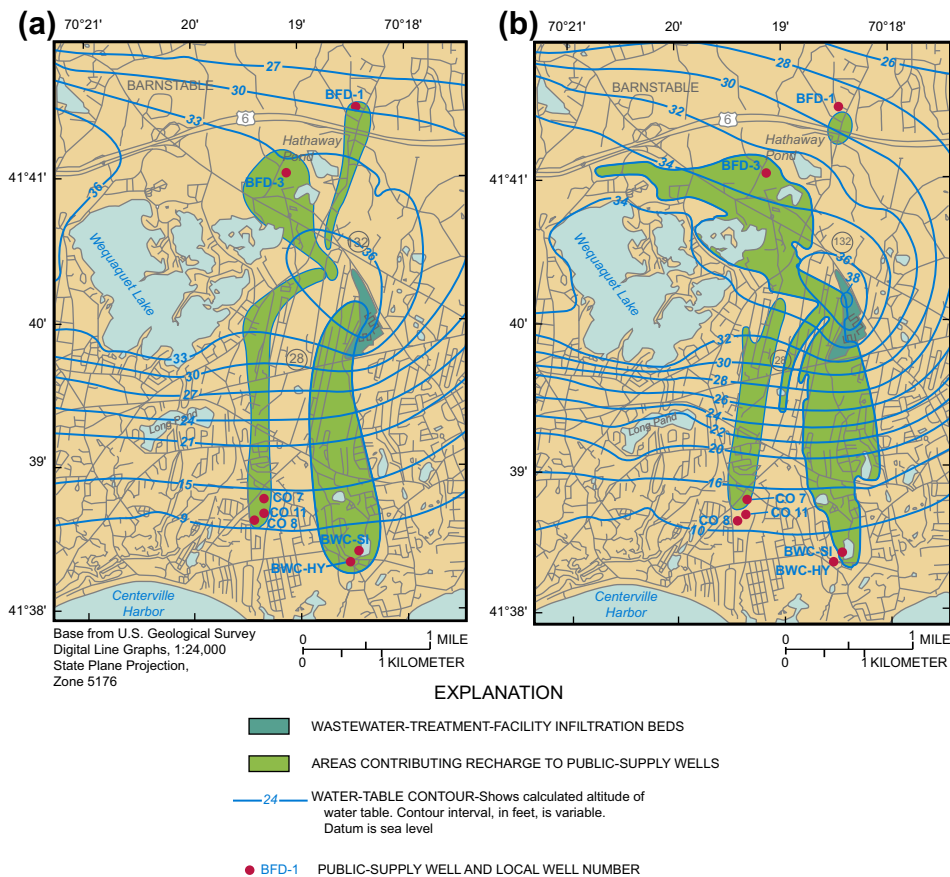


**Figure B4.1.3** Water-table contours and capture zones for seven partially penetrating, high-capacity pumping wells in a heterogeneous system computed by (a) a 2D areal model using D-F conditions; (b) a 3D eight-layer model. The pumping wells create 3D flow that affects the shapes of the capture zones (Reilly and Harbaugh, 2004).

#### 4.1.1.2 Profile Models

A profile model represents 2D flow in a vertical slice (cross section) of a groundwater flow system (Fig. B4.2.1 in Box 4.2). The governing equation is Eqn (B4.2.1) (Box 4.2). The model is defined by boundary conditions along the top, bottom, and sides of the profile.

#### Box 4.2 Profile Models

This box presents instructions for setting up profile models using standard finite-difference (FD) and finite-element (FE) groundwater flow codes. For convenience reference is made to an FD grid.

The longitudinal axis of a profile model must be oriented parallel to a groundwater flowpath because all water must flow within the profile; no water may flow perpendicular to the profile. The thickness of the profile is set to one unit or to a specified width of the aquifer where the flow parallels the profile (Fig. B4.2.1). Usually, the profile is a rectangle and there are four boundaries (i.e., top, bottom, and side boundaries) but more complicated boundary geometry can be accommodated when the profile is not rectangular. Typically, the top boundary represents the water table and the bottom boundary is simulated as a no-flow boundary but it could be simulated using specified head, specified flow, or head-dependent conditions. Side boundaries at either end of the profile often represent groundwater divides and are simulated as no-flow boundary conditions (Box 4.3). A profile model is usually constructed as a multilayer slice of a 3D model, which we call slice orientation, but could be constructed as a one-layer model, which we call layer orientation.

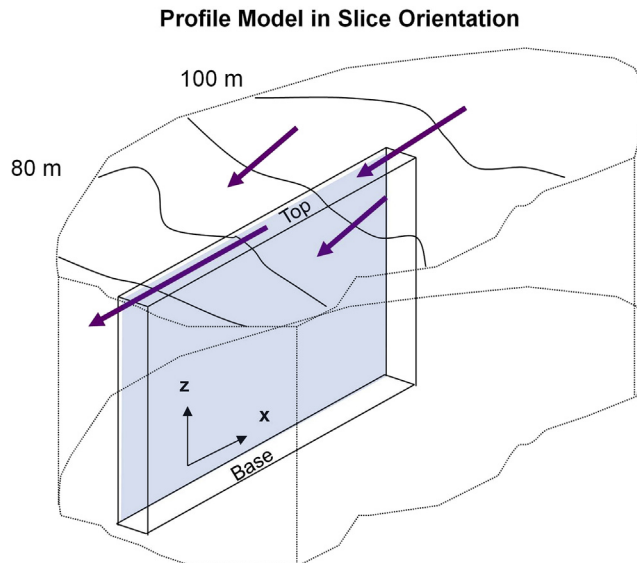


**Figure B4.2.1** Profile model aligned parallel to groundwater flow shown by purple arrows. Water-table contours (numbered in meters) are also shown. Slice orientation, simulated in a three-dimensional model, is the preferred orientation for profile modeling.

(Continued)

**Box 4.2 Profile Models—cont'd**

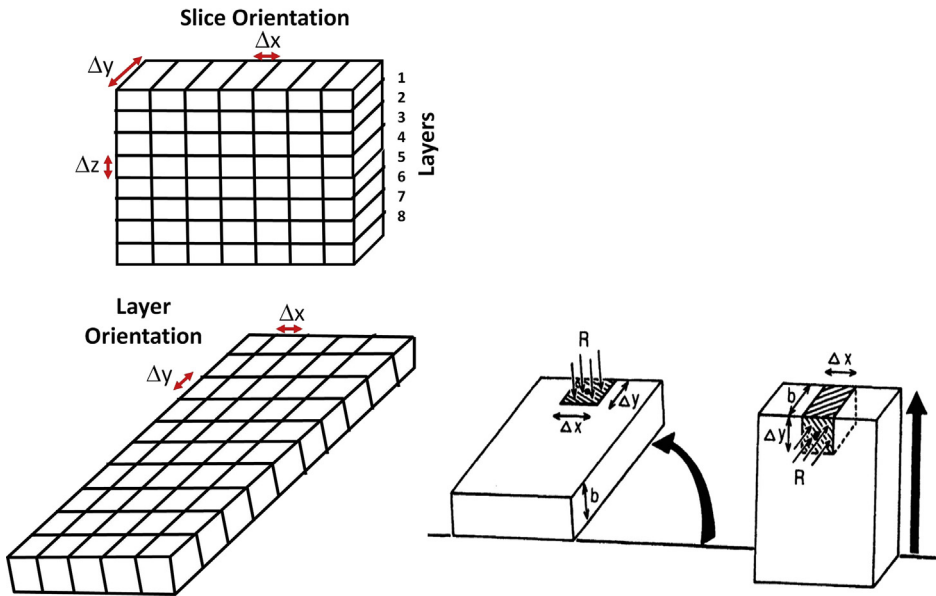


**Figure B4.2.2** In layer orientation (bottom three figures) the profile is simulated as an areal two-dimensional model. The thickness of the layer equals the width of the profile. Slice orientation (top figure) is shown for comparison.

The transient governing equation for flow in a profile in the  $x$ - $z$  plane follows from Eqn (3.12) with  $\partial h/\partial y = 0$ :

$$\frac{\partial}{\partial x} \left( K_x \frac{\partial h}{\partial x} \right) + \frac{\partial}{\partial z} \left( K_z \frac{\partial h}{\partial z} \right) = S_s \frac{\partial h}{\partial t} - W^* \tag{B4.2.1}$$

where  $W^*$  ( $1/T$ ) is volumetric recharge rate ( $L^3/T$ ) applied to the top cells ( $L^3$ ) in the profile. Transient simulations are cumbersome because flowpaths change with time and the orientation of the profile must be adjusted to conform with the changed flow field (Fig. B4.2.1). Hence, 3D models are better suited for transient models and profile models usually simulate steady-state flow where  $\partial h/\partial t = 0$  in Eqn (B4.2.1).

**Slice Orientation**

Slice orientation is the natural orientation for profile modeling. A profile in slice orientation is simply a cross section of a 3D model; the profile model has several layers and the thickness of the profile is equal to  $\Delta y$  or  $\Delta x$  depending on the orientation (e.g., Fig. B4.2.2). The 3D governing equation (Eqn (3.12)) applies and aquifer parameters ( $K_x = K_y, K_z, S_s$ ) and layer thickness are input as in a 3D model. Recharge is input according to the recharge options provided in the FD

### Box 4.2 Profile Models—cont'd

or FE code. Because the vertical slice includes several model layers, model input consists of layer by layer entry of data for a single row that represents the slice; thus, data input is somewhat more cumbersome than in layer orientation but assembly of data is facilitated in a GUI. As in 3D models, the storativity for water-table nodes equals specific yield while the storativity for nodes below the water table represents water released from compression of the aquifer and expansion of water (Section 5.5; Fig. 5.27).

#### Layer Orientation

In layer orientation (Fig. B4.2.2), the grid/mesh of the profile model is set up as an areal 2D model and thereby requires a change in perspective on the part of the modeler. Layer orientation relies on the similarity between Eqn (B4.2.1) and Eqn (3.13a), the governing equation for 2D horizontal flow in a confined aquifer. The two equations are the same if  $z$  in Eqn (B4.2.1) equals  $y$  in Eqn (3.13a). Similarly,  $K_x$ ,  $K_z$ ,  $S_s$ , and  $W^*$  in Eqn (B4.2.1) are substituted for  $T_x$ ,  $T_y$ ,  $S$ , and  $R$ , respectively, in Eqn (3.13a). The thickness of the layer,  $b$ , equals the width of the profile so that  $T_x = K_x b$  and  $T_y = K_z b$ ;  $S = S_s b$  and  $R = W^* b$ . The parameter  $S$  is the storativity, which is equal to specific yield for nodes at the water table and elsewhere represents water released from compression of the aquifer and expansion of water (Section 5.5; Fig. 5.27).

The primary advantage to layer orientation is that the raw model output can be viewed as one 2D array of head values rather than row by row for multiple layers. Layer orientation is also more convenient when using a spreadsheet to solve a profile model (Box 4.3). However, GUIs facilitate profile modeling in slice orientation because they display model input and output in cross section. Because most applied modeling is done with a GUI, slice orientation is the preferred representation for most profile models.

The solution of a profile model is a 2D array of heads in the vertical plane from which equipotential lines can be drawn and flow directions inferred (Fig. B4.3.3(c) in Box 4.3; Fig. 4.4). Profile models assume there is no flow perpendicular to the profile; they are oriented along a flowline and all flow occurs in the vertical plane of the profile.

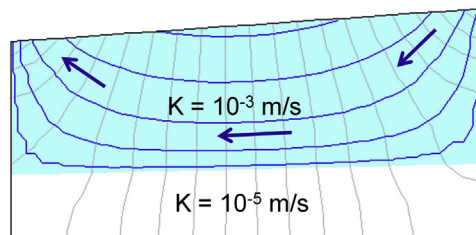


**Figure 4.4** Equipotential lines (faint gray lines) and flowpaths (heavy blue lines) with schematic flow arrows in a profile model. A two order of magnitude contrast in hydraulic conductivity effectively creates a no-flow boundary at the base of the upper layer. Figure was created using TopoDrive (Hsieh, 2001).

### Box 4.3 Spreadsheet Solution of a Finite-Difference Profile Model

Iterative solutions of the FD equation resulting from approximating simple forms of the groundwater flow equation and boundary conditions can be obtained with the aid of a spreadsheet. In spreadsheet modeling, each cell in the spreadsheet is an FD cell. The technique is suited to simple problems such as the one described by Tóth (1962) for steady-state regional groundwater flow in a cross section of a homogeneous, isotropic aquifer.

Tóth's conceptual model is shown in Fig. B4.3.1 and the mathematical model in Fig. B4.3.2. A linear water table forms the top boundary and is represented by a specified head boundary (see the cautionary discussion in Box 4.6 regarding specified head conditions at the water table). The side boundaries represent regional groundwater divides simulated by no-flow boundaries. A no-flow boundary at the bottom of the system represents impermeable material.

The governing equation is the Laplace equation:

$$\frac{\partial^2 h}{\partial x^2} + \frac{\partial^2 h}{\partial z^2} = 0 \quad (\text{B4.3.1})$$

where  $z$  is the vertical coordinate. The FD approximation for Eqn (B4.3.1) for a uniform regular grid where  $\Delta x$  and  $\Delta z$  are constant and equal is

$$h_{ij}^{m+1} = \frac{h_{i+1,j}^m + h_{i-1,j}^{m+1} + h_{i,j+1}^m + h_{i,j-1}^{m+1}}{4} \quad (\text{B4.3.2})$$

where  $m$  represents heads at the current iteration level and  $m+1$  represents heads at the new iteration level. Equation (B4.3.2) is written in the form appropriate for solution of  $h_{ij}$  by

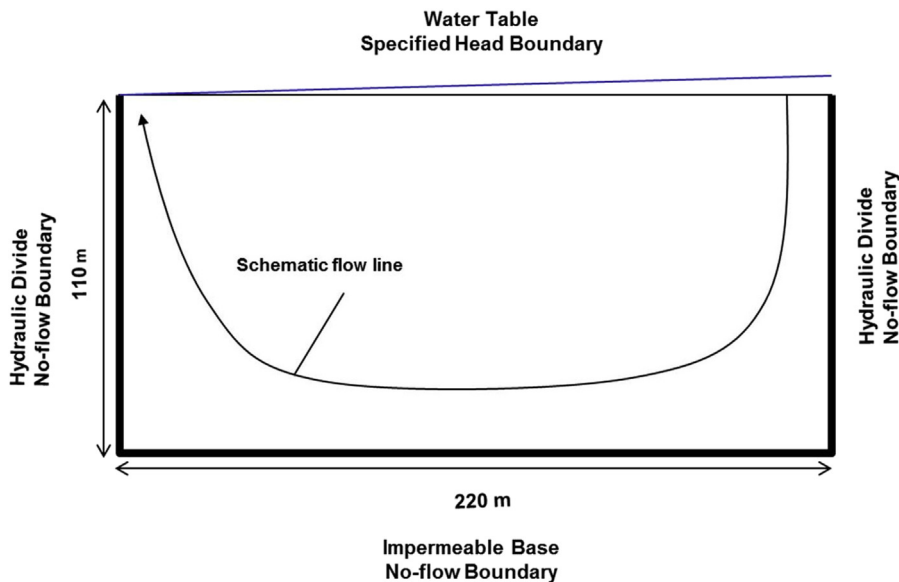
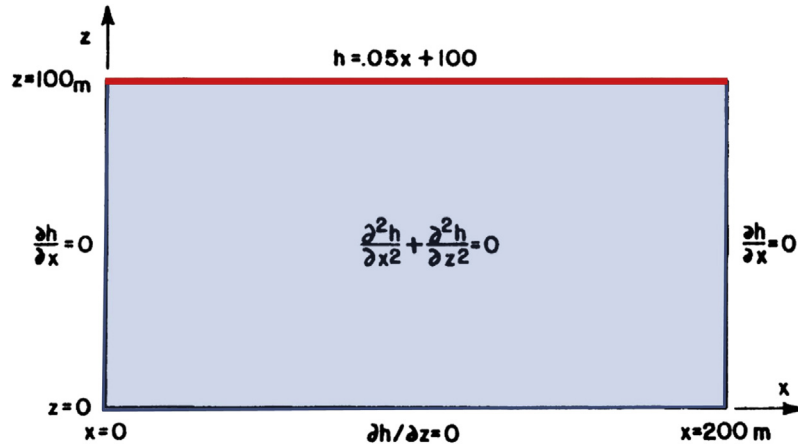


Figure B4.3.1 Conceptual model showing boundaries and schematic flowline in a cross section of a regional groundwater system (after Tóth, 1962).

### Box 4.3 Spreadsheet Solution of a Finite-Difference Profile Model—cont'd



**Figure B4.3.2** Mathematical model showing the governing equation and boundary conditions for the conceptual model in Fig. B4.3.1 (after Tóth, 1962).

Gauss-Seidel point iteration where heads are updated to the next iteration level as they are computed. Note that the head in each FD cell is equal to the average of the heads in the four neighboring cells and the solution for  $h_{i,j}^{m+1}$  is independent of hydraulic conductivity and grid spacing. The five nodes represented in Eqn (B4.3.2) comprise the 2D FD calculator known as the five-point finite-difference star operator (Fig. 3.4).

A profile model in layer orientation (Box 4.2) is set up using a spreadsheet (Fig. B4.3.3). For our version of Tóth's problem, we assume that head is equal to 100 m at the discharge area at  $(x,z) = (0,100)$  and the slope of the water table is 0.05 m/m. We use nodal spacing of 20 m ( $\Delta x = \Delta z = 20$  m) so that the spreadsheet has seven rows and 13 columns, where row 7 and columns 1 and 13 (columns A and M in Fig. B4.3.3 (b) and (c)) contain ghost (or "imaginary") nodes outside the problem domain. The ghost nodes are used to implement the no-flow boundary conditions by setting the head at the ghost node equal to the calculated head on the opposite side of the boundary. In that way, the head gradient across the boundary is zero. The spreadsheet is set up as a block-centered FD grid so that the no-flow boundary is located at the outside edge of the boundary cells. With different FD equations for the boundary cells, a point-centered grid can be used (Problem P4.1).

The FD equation for each cell in the spreadsheet is written following Eqn (B4.3.2) (Fig. B4.3.3(b)). For example, the equation in column D, row three of the spreadsheet (cell D3) is:

$$D3 = \frac{D4 + D2 + C3 + E3}{4} \quad (\text{B4.3.3})$$

Equations in the cells along the boundaries are modified to include the boundary condition. The top row of the spreadsheet contains specified head values from 100 m to 110 m, which are the heads along the top (water-table) boundary, calculated using the linear equation in Fig. B4.3.2.

(Continued)



**Box 4.3 Spreadsheet Solution of a Finite-Difference Profile Model—cont'd**

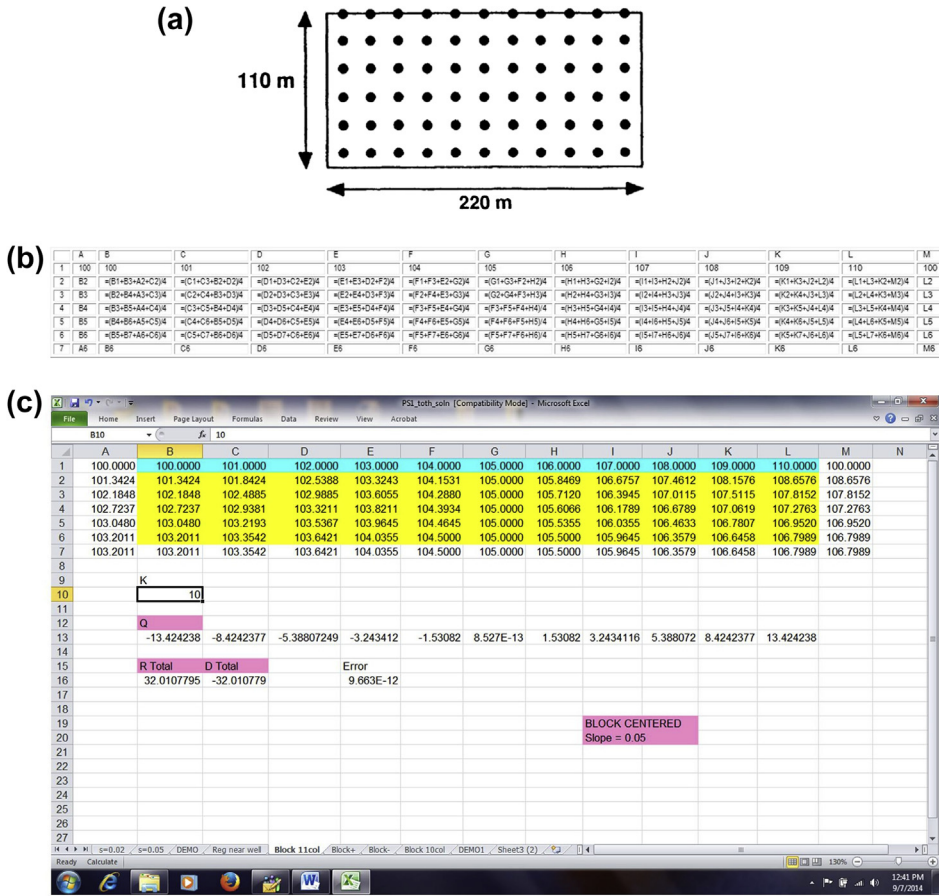


**Figure B4.3.3** Numerical model for the problem in Fig. B4.3.2. (a) Block-centered grid showing boundary location and placement of the 11 columns and six rows of nodes within the problem domain. (b) FD equations for each cell in an Excel® spreadsheet model of the problem. Specified head boundary values (in meters) are entered in the first row to represent the water table. Ghost nodes in columns A and M and row seven are outside the problem domain and are used to implement no-flow boundary conditions at the outside edge of the FD cells along the boundaries. (c) Solution showing heads in meters. For the purpose of calculating flux across the water table, hydraulic conductivity is equal to 10 m/day (cell B10). Flow (Q) at the water table is calculated in m<sup>3</sup>/day for the 1 m width of the cross section. Total recharge (RTotal) and total discharge (DTotal) across the water table and the error (i.e., the difference between RTotal and DTotal) in the water budget, are also computed.

**Box 4.3 Spreadsheet Solution of a Finite-Difference Profile Model—cont'd**

No-flow conditions across the other three boundaries are simulated by setting heads at the ghost nodes equal to the head in the adjacent cell across the boundary (Fig. B4.3.3(b)). In that way, heads in the cells in the first and last columns and the last row reflect heads across the boundary (Fig. B4.3.3(c)). The corner nodes are not included in the five-point star calculator (Eqn (B4.3.2)). Once the appropriate equations are formulated, the spreadsheet is set up to solve the equations iteratively for head in each cell (see Problem P4.1). For our problem, the flux across the water table is calculated assuming a hydraulic conductivity of 10 m/day and a profile (layer) thickness of 1 m. A statement of the water budget for this problem is: inflow across the water table (RTotal) equals discharge (DTotal) across the water table. The error in the water budget is calculated as the difference between RTotal and DTTotal. The solution (Fig. B4.3.3(c)) for heads and fluxes may be compared with the solution using point-centered boundaries (Problem P4.1).

Spreadsheet modeling is a useful teaching tool that illustrates how to write the equations for each FD cell and solve an FD model by point iteration. The interested reader will find more information about spreadsheet solutions of groundwater models in Bair and Lahm (2006). From a practical standpoint, however, spreadsheet solutions do not offer any advantages over standard computer codes even in the preliminary phases of a modeling project. Entering and checking equations for every cell in the spreadsheet is tedious and cumbersome. The time required to set up and test a complex spreadsheet model is likely to be equal to or greater than the time needed to set up and run a standard flow code.

Therefore, profile models cannot simulate radial flow to a pumping well or 3D flow around point sources and sinks or other 3D flow effects (Box 4.2).

An *axisymmetric profile model* is designed to simulate radial flow in a pie-spaced problem domain. Linear or point sources and sinks can be simulated as long as the source or sink is located at the origin of the profile (Fig. 4.5). The thickness of the profile widens from the origin ( $r = 0$ ) according to an angle  $\theta$ . Although special purpose codes are available to solve the governing equation in radial coordinates (e.g., Reilly, 1984), standard codes based on Cartesian coordinates can also simulate axisymmetric profiles by the appropriate adjustment of input parameters (e.g., see Langevin, 2008 for details of the procedure for the MODFLOW family of codes).

Profile models have been used to study regional groundwater flow in cross section (e.g., Cardenas, 2008; Winter, 1976; Freeze and Witherspoon, 1967) and hyporheic interchange beneath a stream (e.g., Woessner, 2000). Axisymmetric profile models are typically used to simulate aquifer (pumping) tests; Langevin (2008) used axisymmetric models to simulate radial flow to a pumping well, a push-pull test, and upconing of saline water as a result of pumping. However, in practice most applications of groundwater models to engineering and management problems use a 3D model to simulate 3D flow effects because it usually is not reasonable to restrict flow to one horizontal dimension or to assume radial flow throughout the problem domain.

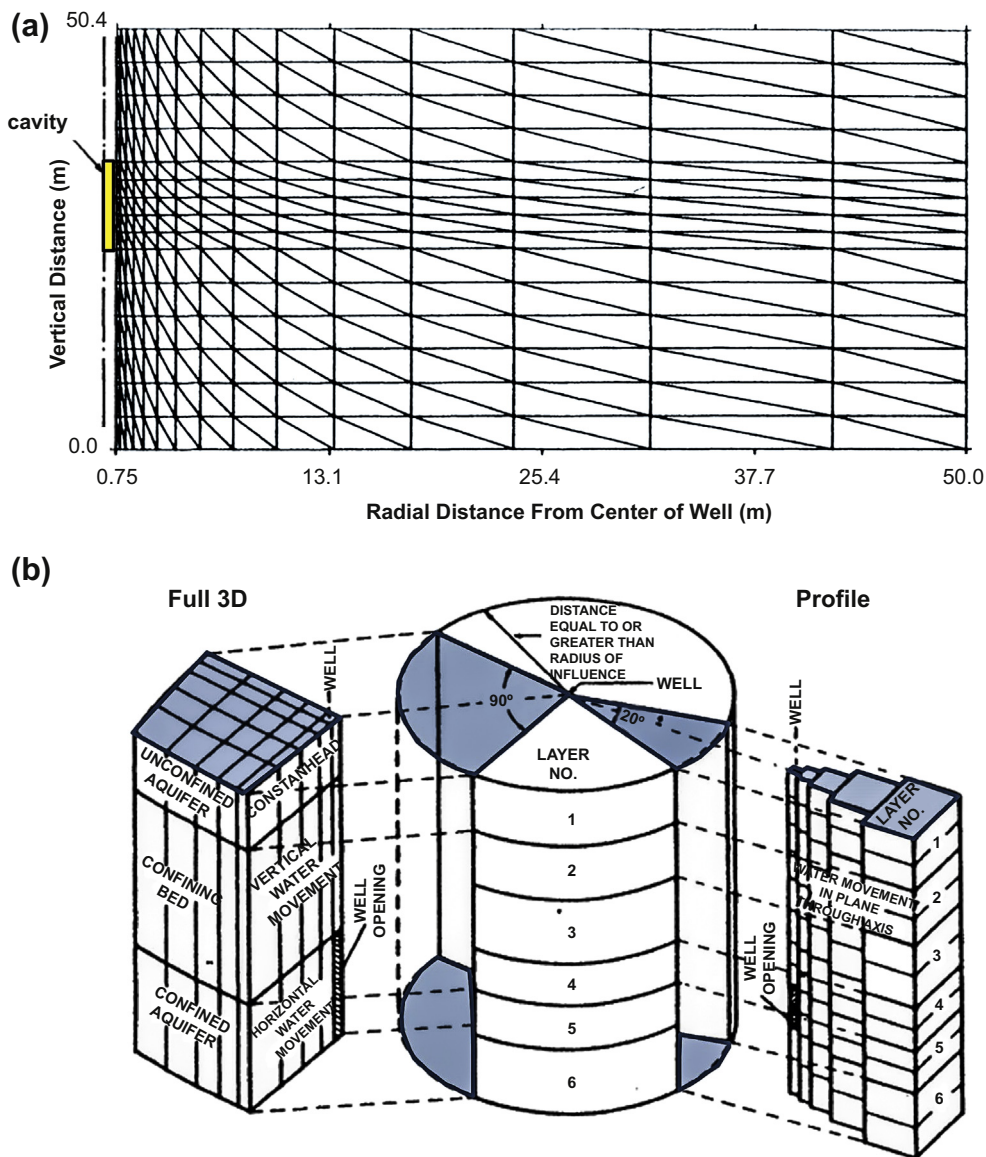


**Figure 4.5** Axisymmetric profiles. (a) An FE mesh for an axisymmetric profile model of transient groundwater flow into a cavity (i.e., a well with a central perforated interval, shown at left) (modified from Keller et al., 1989). (b) An axisymmetric profile to simulate flow to a partially penetrating pumping well at the point of the pie-shaped section of aquifer shown in the FD grid at the right. The thickness of the profile and the transmissivity assigned to a cell increase with distance from the well. Adjustments to storativity are also needed to reflect the change in profile thickness. Pumping rate is adjusted according to the angle (here equal to  $20^\circ$ ) of the aquifer wedge. The grid for a three-dimensional model, which assumes radial flow and uses symmetry to model only one quarter of the aquifer is shown on the left-hand side of the figure (modified from Land, 1977).

### 4.1.2 Three-Dimensional Models

Three-dimensional (3D) models simulate flow in all three spatial dimensions and can explicitly include all hydrostratigraphic units that affect groundwater flow. Usually each hydrostratigraphic unit is one model layer (Figs. 2.7 and 2.9(b)), but more layers are used when it is necessary to compute the vertical distribution of heads within a hydrostratigraphic unit (Section 5.3; Fig. B5.3.2 in Box 5.3). A 3D model has top and bottom as well as side boundaries and conditions along all perimeter boundaries must be specified by the user (i.e., as specified head, specified flow, or head-dependent conditions; Section 3.3). The upper boundary typically is the water table. The lower boundary usually is a contact with relatively impermeable material and is represented by a no-flow boundary condition, or leakage across the lower boundary can be simulated by specified head, specified flow, or head-dependent (Eqn (4.1)) conditions. The governing equation is Eqn (3.12) and the solution is a 3D array of heads for each time step of a transient simulation. For steady-state problems the solution is a single 3D array of heads.

*Quasi-3D models* were sometimes used in the past to simulate regional scale groundwater systems, but fully 3D models have largely supplanted quasi-3D models. In a quasi-3D model (Fig. 4.6), aquifers are each represented by one model layer but

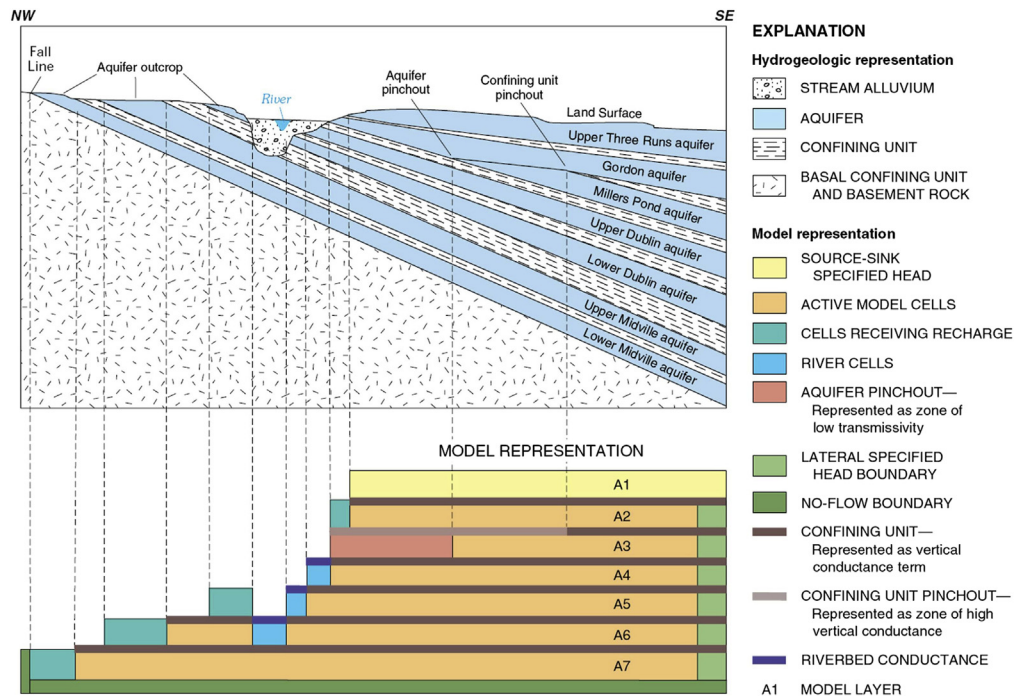


**Figure 4.6** Schematic diagram showing the hydrogeology and model layers for a seven layer quasi-3D model of the Savannah River Site, SC, USA. Confining beds are not represented in the FD grid but are indirectly included in the model by representing the vertical resistance of the confining beds by leakage and flow through the layers by leakage terms (Clark and West, 1998).

confining layers are not explicitly included in the grid/mesh. Instead, the vertical resistance to flow caused by the presence of intervening confining layers is simulated indirectly by a leakage term. The resistance to vertical flow caused by a confining unit is represented by vertical leakance ( $K'_z/b'$ ) and the vertical flux,  $q_{UL}$ , between the aquifer layers of the model is:

$$q_{UL} = -K'_z \frac{h_u - h_L}{b'} \quad (4.3)$$

where  $h_u$  is head in the upper aquifer above the confining bed and  $h_L$  is head in the lower aquifer below the confining bed;  $b'$  is the thickness of the confining bed and  $K'_z$  is its vertical hydraulic conductivity. Equation (4.3) assumes that the vertical resistance is dominated by  $K'_z$  so that flow in the aquifers is dominantly horizontal. The model is considered quasi-3D because flow in aquifers (model layers) is horizontal but vertical flow between the aquifers is represented by Eqn (4.3) without the need to represent the confining beds explicitly by layers in the grid/mesh.

In a quasi-3D model, flow is assumed to be strictly vertical through the confining beds and there is no release of water from storage within the confining bed (e.g., as a result of pumping from aquifers above and/or below the confining bed). When the hydraulic conductivity of the aquifer is more than two orders of magnitude greater than the confining bed (Fig. 4.4), the error introduced by assuming vertical flow in the confining bed is usually less than 5%; however, neglecting storage in the confining bed may cause significant error in many field applications (Steltsova, 1976). Release from storage in a confining bed can be simulated using a transient leakage term that includes the specific storage of the confining bed (see Bredehoeft and Pinder, 1970; Trescott et al., 1976; Anderson and Woessner, 1992, p. 198, for details). Particle tracking should not be used with quasi-3D models because the absence of confining beds in the grid or mesh causes errors in calculating flowpaths and travel times (Section 8.2).

In most applied modeling problems, limitations of quasi-3D models argue for full 3D models for most applications. Nevertheless, a quasi-3D approach can efficiently simulate certain multiaquifer systems that consist of a sequence of aquifers and confining beds (e.g., Fig. B4.4.1(b) in Box 4.4).

## 4.2 SELECTING BOUNDARIES

Physical and hydraulic boundaries of the conceptual model were discussed in Section 2.3 and the three types of mathematical boundary conditions (specified head including constant head; specified flow including no flow; and head-dependent conditions) were introduced in Section 3.3. Conceptually, boundary conditions define flow into and out of the problem domain. Boundary conditions that refer to hydraulic conditions along the perimeter of the model domain are called *perimeter boundary conditions* (Fig. 4.7(a)).

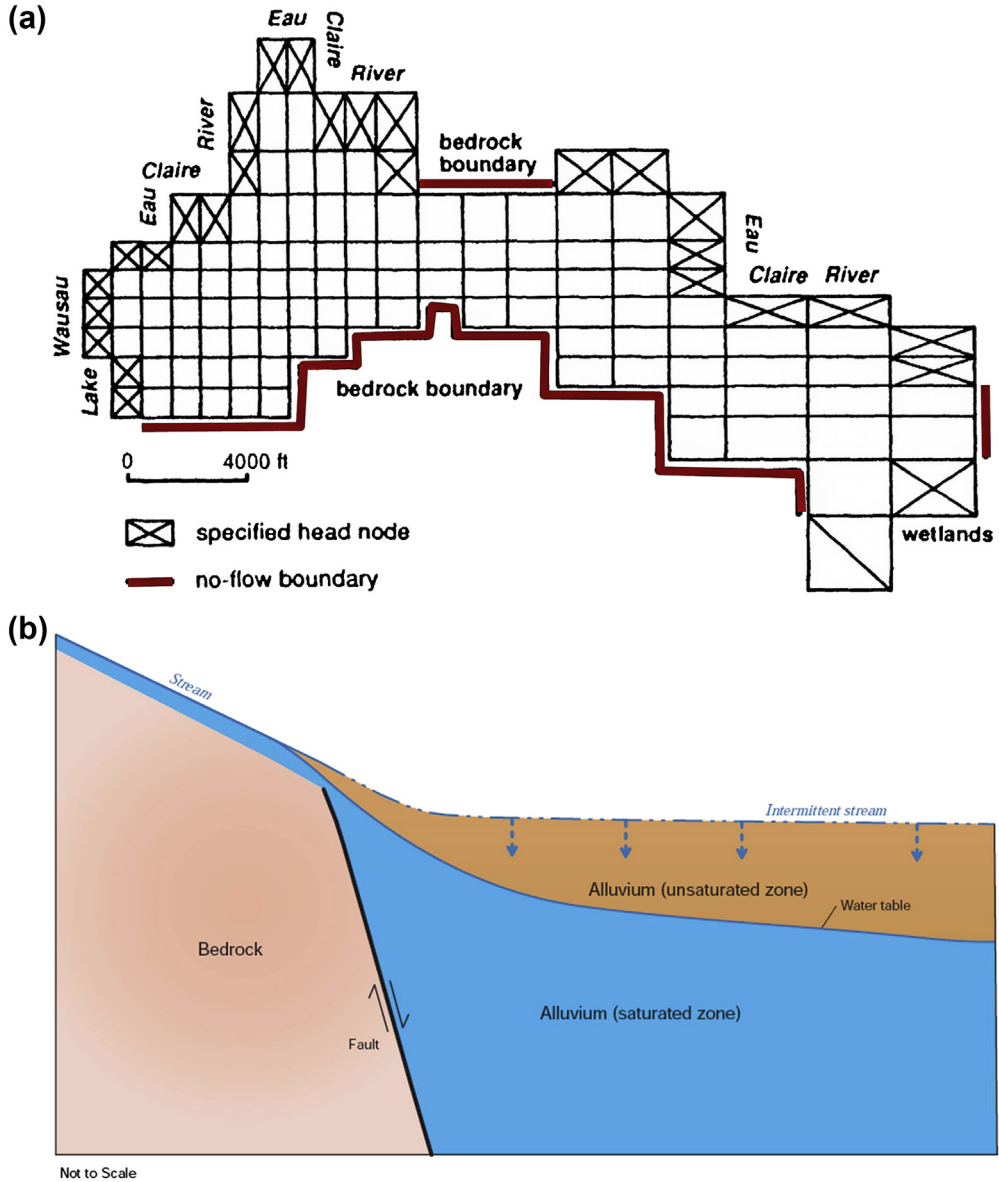


**Figure 4.7** Physical boundaries. (a) Two-dimensional areal FD grid showing perimeter boundaries defined by physical boundaries. Relatively impermeable bedrock outcrops are no-flow boundaries; specified head boundaries represent wetlands, Lake Wausau, and the Eau Claire River, WI, USA (modified from *Kendy and Bradbury, 1988*). (b) Relatively impermeable bedrock across a fault creates a physical boundary for the alluvial aquifer. The intermittent stream is separated from the water table by a thick unsaturated zone but contributes water to the aquifer via percolating conditions (Fig. 4.16(d)) (*Niswonger and Prudic, 2005*).

However, boundary conditions in groundwater flow codes can also represent internal sources and sinks (Fig. 4.7(b)), which in effect are *internal boundary conditions*. Perimeter boundary conditions are required in finite-difference (FD) and finite-element (FE) models. Only internal boundaries are specified in analytic element (AE) models (Section 3.4) because the perimeter boundary in an AE model is automatically set at infinity.

The head along a specified head boundary is fixed, which anchors the hydraulic gradient and control flux at the boundary. A specified head can have a large influence on a simulation because it has an infinite capacity to supply and remove water from the model. A specified flow boundary fixes the flux at the boundary so that boundary flows are not influenced by changes in head at the boundary. A head-dependent boundary (HDB) uses an assigned boundary head and the simulated head at the boundary to control flows across the boundary. In this section, we re-visit these three types of mathematical boundary conditions and relate them to the physical and hydraulic boundaries of the conceptual model (Section 2.3). Both physical and hydraulic boundaries can be represented by all three types of mathematical boundary conditions. In Section 4.3 we discuss how to implement the three types of mathematical boundaries in a numerical model.

Of course, boundaries in the numerical model should be consistent with boundaries in the conceptual model. Whenever possible, physical boundaries should be used instead of hydraulic boundaries. Usually physical boundaries can be found by increasing the size of the model domain to extend out to physical boundaries present in the field (Section 4.4). After boundaries are selected, the modeler should visualize the general flow pattern that will be induced by the conditions assigned to the boundaries and confirm that the flow pattern makes hydrogeologic sense and that inflow and outflow locations are consistent with what is known about the hydrogeology of the modeled area.

## 4.2.1 Physical Boundaries

Physical boundaries are the most robust and defensible type of perimeter or internal boundary as they represent physical features that are easily identified in the field (Fig. 4.7). Physical boundaries include contacts with units of low hydraulic conductivity (e.g., between valley fill and bedrock or between permeable sandstone and less permeable shale), surface water features such as rivers, lakes, wetlands, and in some coastal settings the interface between freshwater and seawater.

### 4.2.1.1 Contacts with Geologic Units of Low Hydraulic Conductivity

Low hydraulic conductivity units may form no-flow boundaries. Lateral no-flow boundaries may be placed at outcrops of relatively impermeable bedrock (Fig. 4.7(a) and (b)). The bottom boundary of most models is specified as a no flow condition at the contact with relatively impermeable material (e.g., Figs. 4.6, 2.3, 2.9(b), 2.12). When there is at least two orders of magnitude contrast in hydraulic conductivity

between hydrogeologic units, flow along the contact is dominantly horizontal and the contact could be represented as a no-flow boundary (Fig. 4.4; Freeze and Witherspoon, 1967). The justification for placing a boundary at such a contact follows from Darcy's law: given horizontal flow in two hydrogeologic units under the same horizontal hydraulic gradient, the unit with a transmissivity two or more orders of magnitude lower will convey less than 1% of the flow, which in most cases is sufficiently small that it can be neglected. In practice, the contrast in hydraulic conductivity at a geologic boundary is usually much greater than two orders of magnitude.

#### **4.2.1.2 Shear Zones and Faults**

Faults and shear zones are fractures along which movement has displaced geologic materials (Fig. 4.7(b)). Usually hydraulic conductivities of the geological materials in and near the fault (shear) zone are altered. Geologic materials may be crushed to create higher conductivity breccia or lower hydraulic conductivity fine-grained gouge in the fault; zones adjacent to the fault have either enhanced or reduced hydraulic conductivity and/or, in some settings, the hydraulic conductivity is not appreciably changed (Scholz and Anders, 1994; Caine et al., 1996). Geological characterization of faults (e.g., Caine and Minor, 2009; Rawling et al., 2001) and analysis of groundwater flow patterns (e.g., Jeanne et al., 2013; Bense and Person, 2006; Seaton and Burbey, 2006) show that groundwater flow is often disrupted and that flow patterns through the fault zone can be complicated. In some cases a fault may be a conduit or a barrier to flow (Fig. 4.8) but in geologically complicated aquifers the same fault may act as both barrier and conduit (Bense and Person, 2006).

#### **4.2.1.3 Surface Water Features**

Major surface water features, including oceans, large lakes, and streams, are physical boundaries that are perennial sources or sinks for groundwater. The stage in a major surface water body exerts hydraulic control and is not appreciably changed by stresses such as groundwater pumping (Figs. 4.7(a), 2.5(a), 2.9(b)). For example, a very large and deep lake is a physical boundary that robustly forms a constant head boundary for regional groundwater systems. A major river (Fig. 4.7(a)) can also form a robust physical boundary.

A major surface water feature that exerts strong hydraulic control may not physically penetrate the full thickness of the aquifer but nevertheless can hydraulically form a fully penetrating boundary if there is a groundwater divide beneath the feature (e.g., the rivers in Fig. 4.9(a), 2.1 and 2.6(a) and the Delaware Bay in Fig. 2.9(b)). When hydraulic control of the surface water feature is relatively weak, the divide does not fully penetrate the aquifer and some groundwater flows under the feature (e.g., the ditch in Fig. 4.9(b)). Zheng et al. (1988) found that the formation of a fully penetrating divide beneath drainage ditches was inversely proportional to the



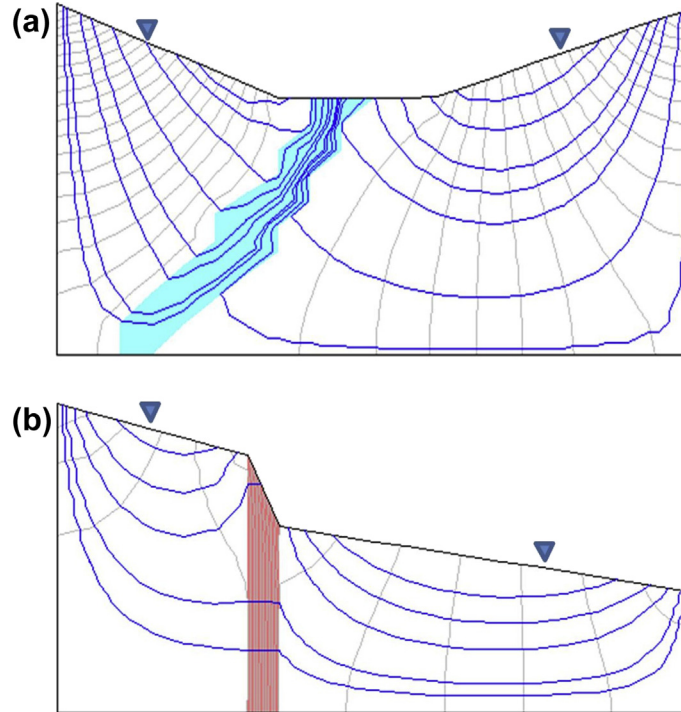


**Figure 4.8** Flow across fault zones shown in schematic cross sections of an unconfined aquifer. Simulations of the profile were done in TopoDrive (Hsieh, 2001). Equipotential lines (faint gray lines) and flowpaths (heavy blue lines) are shown. There is a two order of magnitude contrast between the hydraulic conductivity ( $K$ ) of the aquifer and the fault zone. Both aquifer and fault are isotropic. (a) Fault as a conduit. The fault zone is shaded in blue;  $K$  of the fault is larger than  $K$  of the aquifer. Groundwater flows up the fault and discharges in the valley bottom. (b) Fault as a barrier (dam). The fault zone is shaded in pink;  $K$  of the fault is smaller than  $K$  of the aquifer. There is an abrupt drop in the water table across the fault and water is dammed against the fault.

regional slope of the water table and directly proportional to the head gradient across the streambed sediments. A combination of a specified head or HDB (to represent surface water) and no-flow boundary (beneath the surface water feature) could be used to represent a strong partially penetrating surface water body. However, partially penetrating surface water bodies away from the model perimeter are best represented by head-dependent conditions so that underflow beneath the surface water feature can change as hydrologic conditions change (Section 4.3).

Surface water bodies that are not directly connected to the groundwater system are not strong physical boundaries. For example, surface water may exert little or no control over groundwater flow in deep confined aquifers and surface water in arid settings may be hydraulically disconnected from the groundwater system owing to separation by a thick unsaturated zone (Fig. 4.7(b)).

When represented with specified head or head-dependent conditions, surface water features potentially supply an infinite amount of water to the model, which may be appropriate for large perennial bodies of water. However, ephemeral and headwater streams may dry up seasonally and failure to account for their seasonal disappearance may introduce significant error into the model (Mitchell-Bruker

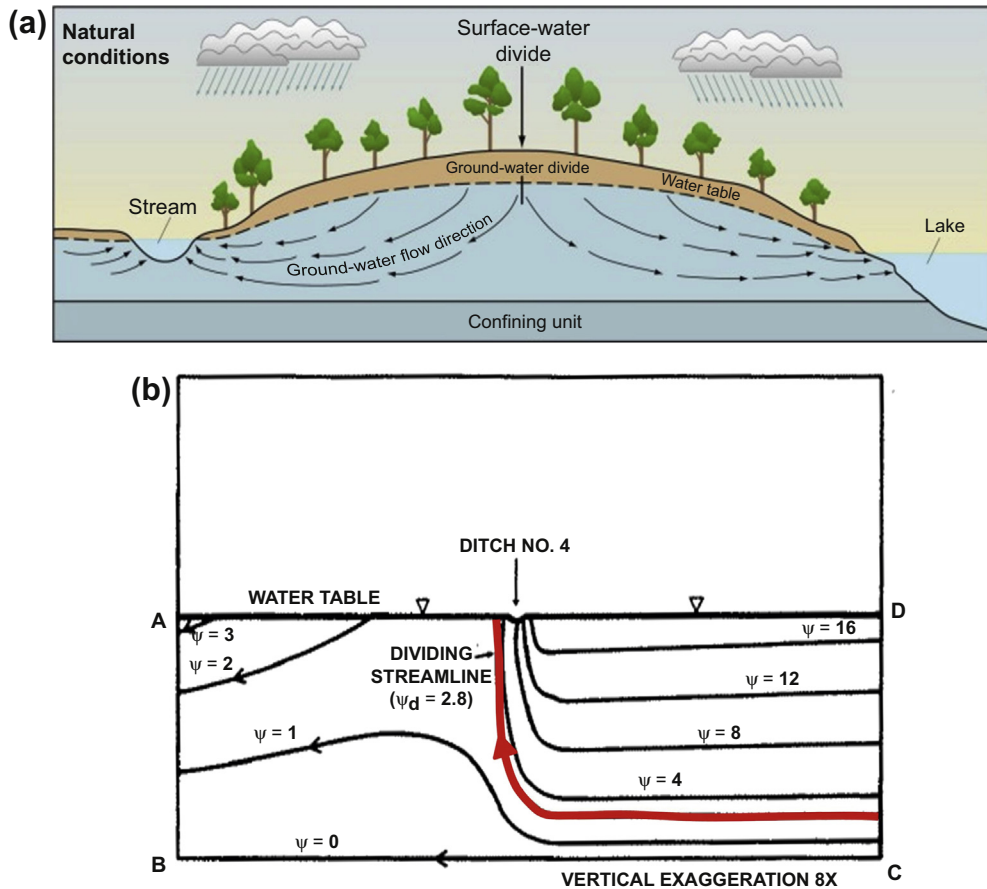


**Figure 4.9** Fully and partially penetrating surface water bodies. (a) Schematic cross section through an unconfined aquifer showing groundwater divides beneath a topographic high and beneath a stream. The stream partially penetrates the aquifer physically but is hydraulically fully penetrating. The lake (at right) is both physically and hydraulically fully penetrating (Granneman *et al.*, 2000). (b) Cross section through an unconfined aquifer showing streamlines in the vicinity of a shallow ditch. Streamlines flow beneath the ditch indicating underflow. The ditch is both physically and hydraulically partially penetrating (modified from Zheng *et al.*, 1988).

and Haitjema, 1996). Advanced options for simulating surface water features that allow for adjustment of surface water flow and stream or lake level are discussed in Chapter 6.

#### 4.2.1.4 Freshwater–Seawater Interface

In coastal aquifers, fresh groundwater discharges to the ocean along the freshwater–seawater interface (Fig. 4.10). Under field conditions, the interface moves in response to tidal fluctuations, groundwater pumping, and changes in recharge, creating a transition zone, or zone of dispersion. When the interface is relatively stable, the zone of dispersion is narrow and a no-flow boundary could be specified at a representative average position of the interface (Fig. 2.3). However, if the interface is not stable (or may not be stable under conditions represented in a forecasting simulation), a static boundary is likely not appropriate. When it is not appropriate to simulate the freshwater–seawater interface as a no-flow boundary, special purpose codes may be used to simulate a sharp interface without mixing between freshwater and seawater (Box 4.4) or to simulate mixing and flow in the interface by including density effects and dispersion (Sections 12.2 and 12.3).

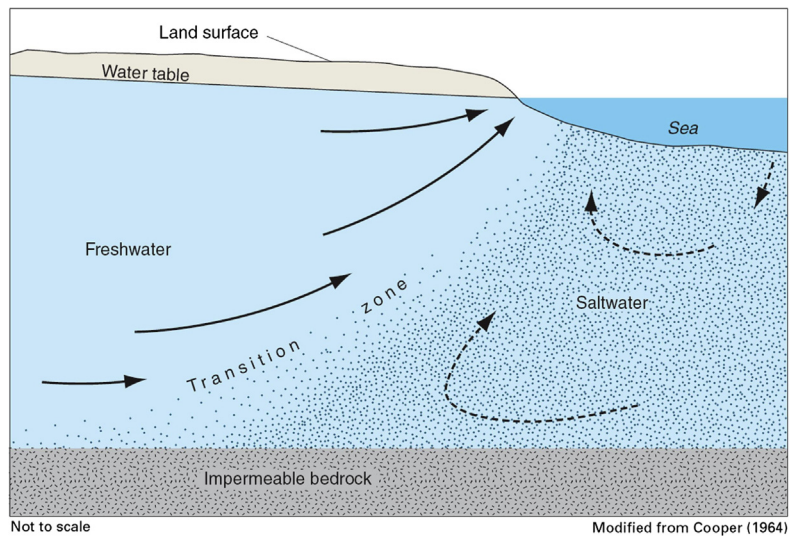


**Figure 4.10** Freshwater–seawater interface in a coastal aquifer showing the transition from freshwater to seawater in the zone of dispersion. The interface acts as a barrier to groundwater flow; freshwater flows upward along the interface and discharges to the ocean (Barlow, 2003).

### Box 4.4 The Freshwater–Seawater Interface

Groundwater is an important source of water for coastal communities throughout the world; hence, seawater intrusion is a critical concern, especially because its effects are largely irreversible. Groundwater in coastal aquifers flows seaward, mixes with subsurface saline water along the interface between freshwater and seawater, and discharges at the ocean floor (Fig. 4.10). Groundwater pumping causes the interface to move inland resulting in seawater intrusion. Mixing at the interface occurs by diffusion and dispersion creating a transition zone. Diffusion is caused by the difference in solute concentration between freshwater and seawater. Dispersion results from mixing of freshwater and seawater in response to transience in groundwater flow caused, for example, by intermittent pumping and tidal fluctuations. Such transience causes the interface to move back and forth.

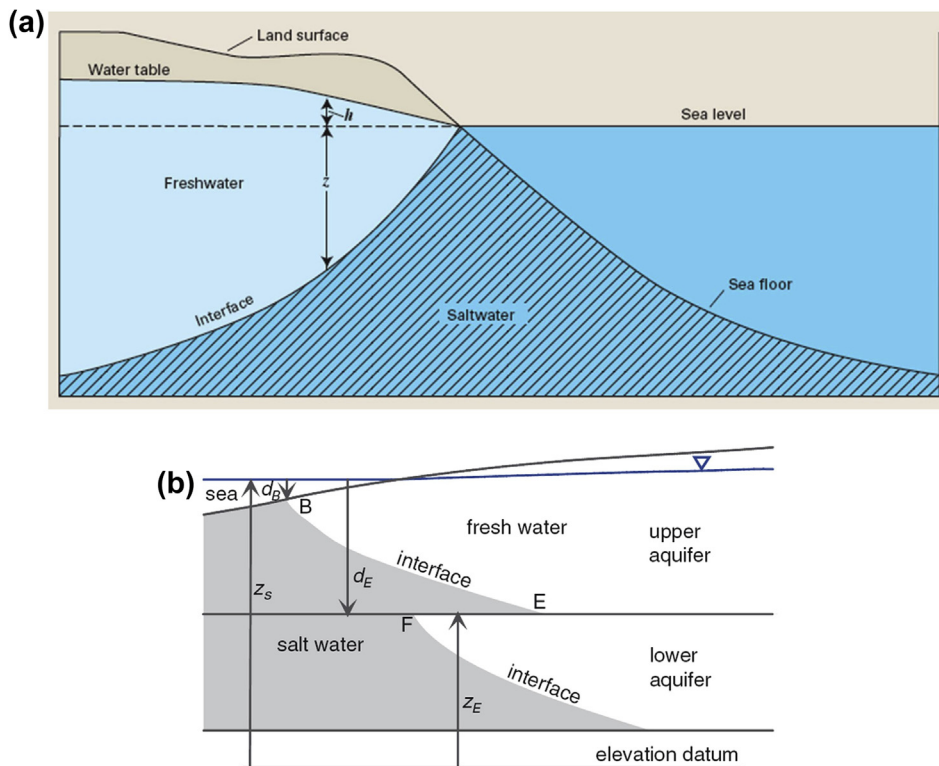


**Figure B4.4.1** The freshwater–seawater interface: (a) under hydrostatic conditions as assumed by the Ghyben–Herzberg relation (Eqn (B4.4.1b)) (Barlow, 2003); (b) in a multiaquifer system simulated using a quasi-three-dimensional model (Section 4.1). The offset in the interface between aquifers (along EF in the figure) is small when vertical resistance between layers is small (i.e., leakage is large). The offset is relatively large when there is a confining bed between aquifer layers (Fitts et al., 2015).

(Continued)

### Box 4.4 The Freshwater–Seawater Interface—cont'd

There is widespread interest in the general topic of saltwater intrusion, which includes seawater intrusion as well as movement of brines into inland freshwater aquifers (e.g., <http://www.swim-site.org/>). The literature on modeling saltwater intrusion encompasses a variety of methods from relatively simple to complex (Werner et al., 2013). The simplest expression for the freshwater–seawater interface, which derives from the well-known Ghyben–Herzberg relation, states that the depth of the interface below sea level,  $z$ , is approximately 40 times the head above sea level,  $h$  (Fig. B4.4.1(a)). This simple mathematical statement follows from the observation that under hydrostatic conditions (i.e., both freshwater and seawater are static) the head on the interface is the same from both the freshwater and the seawater sides so that:

$$\rho_s g z = \rho_f g (z + h) \quad (\text{B4.4.1a})$$

where  $\rho_s$  is the density of seawater,  $\rho_f$  is the density of freshwater, and  $g$  is gravity. Rearranging Eqn (B4.4.1a) gives the Ghyben–Herzberg relation:

$$z = \frac{\rho_f}{\rho_s - \rho_f} h = \alpha h \quad (\text{B4.4.1b})$$

For  $\rho_f = 1.0 \text{ gm/cm}^3$  (=gm/ml) and  $\rho_s = 1.025 \text{ gm/cm}^3$ ,  $\alpha = 40$ .

Of course, in reality neither freshwater nor seawater is static; both move upward and mix along the interface. Freshwater discharges to the ocean floor while seawater cycles from the ocean through the subsurface and discharges back to the ocean (as shown in Fig. 4.10). Although there is some exchange of water between freshwater and seawater in the transition zone, the interface effectively acts as a no-flow boundary. When the interface is relatively stable and the transition zone is narrow it may be appropriate (depending on the modeling objective) to represent the interface as a static no-flow boundary where freshwater discharge to the ocean floor is simulated by a head-dependent or specified head boundary condition (Fig. 2.3).

However, for some problems it is necessary to forecast the transient movement (or the final long term average, equilibrium or steady-state, position) of the interface in response to a hydrologic stress such as freshwater pumping or rising sea level. There are two categories of models for forecasting the position of the interface: sharp interface (also called interface flow) models and variable density models. Both approaches allow for the contrast in density between fresh and seawater but the sharp interface approach assumes there is no mixing along the interface and no transition zone. A variable density model couples a variable density groundwater flow model to a model for solute transport based on the advection–dispersion equation (Sections 12.2 and 12.3). Simulating the freshwater–seawater interface with a coupled model requires small nodal spacing in the vicinity of the interface and typically involves long run times. Sharp interface numerical models, which typically run much faster than coupled models, are described below. There are also a number of analytical solutions that solve for the steady-state sharp interface; the reader is referred to Werner et al. (2013; their section 4.1) and Bear and Cheng (2010, pp. 613–620) for summaries.

### Box 4.4 The Freshwater–Seawater Interface—cont'd

In the sharp interface approach, the governing equation for groundwater flow (Eqn (3.12)) is written in terms of freshwater head in the freshwater zone and native (seawater) head in the seawater zone (Fig. B4.4.2). The interface is simulated as a moving boundary between the two regimes where continuity in both head and flux are imposed along the interface. The mathematics are relatively complicated and the interested reader is referred to [Bear and Cheng \(2010, pp. 601–605\)](#) for details. The approach can be simplified by assuming horizontal flow following D-F theory (Section 4.1; Box 4.1). Then numerical codes for single density flow can be modified

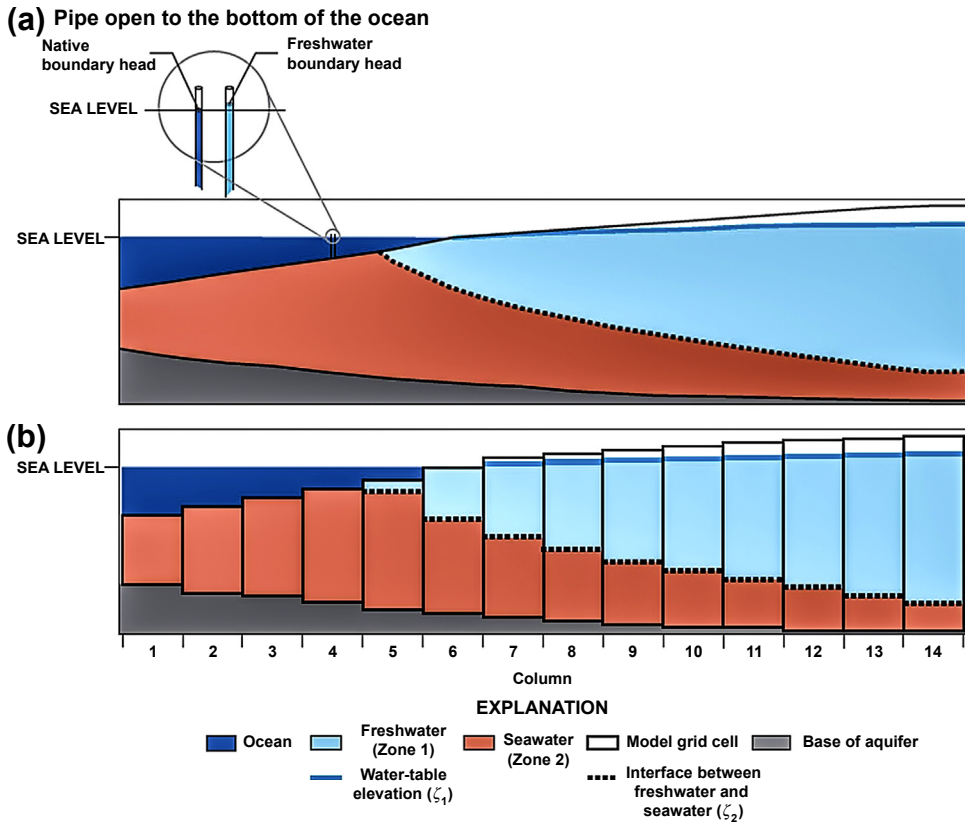


**Figure B4.4.2** Cross section of a sharp interface model as simulated with MODFLOW's SWI2 Package. (a) Conceptual model showing native (seawater) head and equivalent freshwater head at the interface. The freshwater–seawater interface (dotted line) separates freshwater (zone 1) from subsurface seawater (zone 2). (b) One-layer model of a coastal aquifer. The thickness of the layer varies in space; vertical variations in density within the layer represent freshwater and subsurface seawater. The code solves for the transient movement of the interface ([Bakker et al., 2013](#)).

(Continued)

#### Box 4.4 The Freshwater–Seawater Interface—cont'd

to solve for the interface, or interfaces in a multiaquifer system. Bakker et al. (2013) used this approach to develop the SWI2 Package for MODFLOW, which solves for the transient movement of the interface in single aquifers (Fig. B4.4.2) as well as multiaquifer systems (Fig. B4.4.1(b)).

Fitts (2013, p. 224) points out that for 2D, transient simulations, storativity (Section 5.4) at the freshwater–seawater interface for both confined and unconfined aquifers should be represented as:

$$S_y = S = n_e \frac{\rho_f}{\rho_s - \rho_f} \quad (\text{B4.4.2})$$

where  $S_y$  is specific yield (i.e., storativity of an unconfined aquifer),  $S$  is confined storativity, and  $n_e$  is effective porosity (Box 8.1). This definition of storativity is necessary because the landward movement of the interface replaces freshwater with seawater and effectively removes freshwater from storage.

Steady-state sharp interface models are also available. For example, Bakker and Schaars (2013) presented a D-F based approach to solve for the steady-state position of the interface; however, a disadvantage of their approach is that the top aquifer in a multiaquifer system cannot be unconfined. An approach similar to Bakker and Schaars (2013) is used in some AE codes where interface discharge potentials (Section 3.4) developed by Strack (1976; also see Bear and Cheng, 2010, pp. 616–619) are used to compute the steady-state position of the interface. GFLOW (Haitjema, 2007) uses Strack's formulation to simulate interface flow in a single aquifer; AnAqSim (see review by McLane, 2012) can simulate both single and multiaquifer interface flow, and also allows the top aquifer in a multiaquifer system to be unconfined (Fitts et al., 2015).

### 4.2.2 Hydraulic Boundaries

When it is not possible or convenient to specify physical boundaries around the perimeter of the problem domain, the modeler might consider using hydraulic boundaries. Hydraulic boundaries are delineated by streamlines (groundwater divides) and equipotential lines (lines of constant head).

Ideally, hydraulic boundaries, like physical boundaries, define hydraulic conditions that are invariant in time and stable in space. However, hydraulic conditions in the field may change in response to stresses so that hydraulic boundary locations and definitions in the model require reevaluation. Hydraulic boundaries are more likely than physical boundaries to be specified inappropriately. Although hydraulic boundaries are never ideal, they are more suited for steady-state problems than for transient problems because conditions along hydraulic boundaries are likely to change as a result of transient stresses. Given these issues, alternatives for setting boundary conditions (discussed in Section 4.4) should be considered before selecting a hydraulic boundary.

#### 4.2.2.1 Streamlines (Groundwater Divides)

Groundwater flows parallel to a streamline so that, by definition, no water crosses a streamline. Thus, streamlines can serve as groundwater divides that form hydraulic no-flow boundaries (Figs. 4.11(a) and 4.12). Groundwater divides that coincide with regional topographic highs (Figs. 4.9(a) and 4.11(a)) are often relatively stable features and may form perimeter boundaries. But even regional groundwater divides can shift in response to changes in pumping and to a lesser extent to changes in recharge and changes in stage at regional sinks (e.g., Sheets et al., 2005). One way to determine if a hydraulic streamline boundary is affecting modeling results is to replace the no-flow boundary with specified heads and re-run the model. If flow to or from the specified boundary nodes is insignificant, the assignment of a hydraulic no-flow boundary at that location is appropriate (Problem P4.6).

#### 4.2.2.2 Equipotential Lines (Constant Head/Constant Flow)

An equipotential line, a line of constant head, may be used to form a constant head hydraulic boundary (Fig. 4.12), or specified flow rates may be calculated across the equipotential line and used to specify boundary flows. In practice, a specified head hydraulic boundary is the least desirable type of boundary condition because heads that are not tied to a physical feature are seldom stable in space or time. Moreover, a specified head boundary potentially provides infinite amounts of water to and/or removes infinite amounts of water from the model.

### 4.3 IMPLEMENTING BOUNDARIES IN A NUMERICAL MODEL

This section presents methods for representing specified head, specified flow, and head-dependent conditions in a numerical model both as perimeter boundary conditions and internal boundaries. We refer to FD grids and FE meshes as introduced in Section 3.5 and discussed in detail in Sections 5.1, 5.2, 5.3, but for convenience we use FD notation when presenting equations for implementing boundary conditions. Generally the same equations, with slightly different notation, apply to FE models. Although the boundary options discussed below are frequently used to represent streams, lakes, springs, and wetlands, more sophisticated options are available and are discussed in Sections 6.4 through 6.7. The presentation of methods in this section is general in nature; therefore, the modeler should always consult the code's user's manual for information about code-specific boundary implementation.

#### 4.3.1 Setting Boundaries in the Grid/Mesh

In a *block-centered FD grid* (e.g., MODFLOW and MODFLOW-USG) nodes are located in the center of the FD cell/block (Fig. 4.11(b)). Specified head boundaries are located on the nodes but specified flow boundaries are located on the edge of the block surrounding



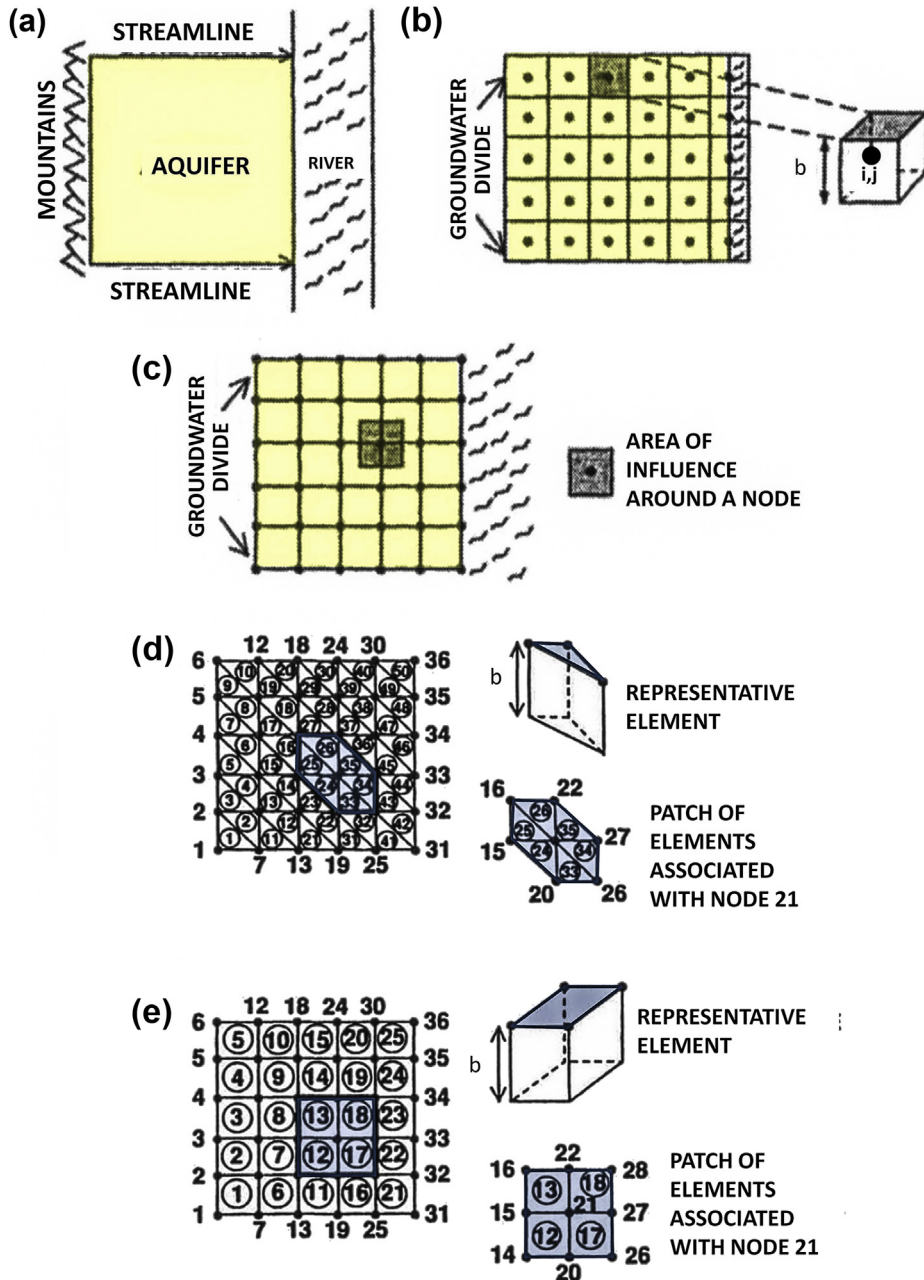


**Figure 4.11** Boundary representation in FD grids and FE meshes of a two-dimensional areal model. (a) For purposes of illustration, relatively impermeable rock at the mountain front forms a physical no-flow boundary. Streamlines, defined from a water-table map, form hydraulic no-flow boundaries. The fully penetrating river is a physical specified head boundary. (b) Block-centered FD grid showing that no-flow boundaries are located at the edges of FD cells and specified heads are located on the nodes. The grid is larger than the problem domain. (c) Point-centered FD grid showing that both no flow and specified head boundaries are placed directly on the nodes. The grid coincides with the problem domain. (d) Triangular FE mesh. Node numbers are shown; element numbers are circled. Both no flow and specified head boundaries are located directly on the nodes. (e) Quadrilateral FE mesh. Node numbers are shown; element numbers are circled. Both no flow and specified head boundaries are located directly on the nodes.

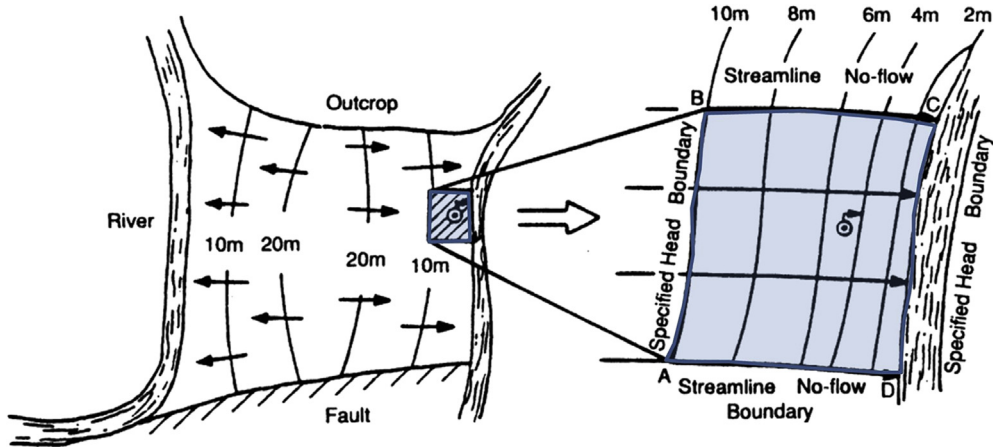


**Figure 4.12** Hydraulic boundaries. Schematic water-table contour maps for a regional problem domain (on the left) bounded by physical features and a local problem domain (on the right) with three hydraulic boundaries taken from the solution of the regional problem; the circled dot represents a pumping well (modified from *Townley and Wilson, 1980*).

the node (Fig. 4.11(b); Fig. B4.3.3(a) in Box 4.3). In a *point-centered FD grid* (e.g., HST3D; Kipp, 1987) nodes are located at the intersection of grid lines and both specified head and specified flow boundaries are placed on the nodes (Fig. 4.11(c)). (The difference between block-centered and point-centered FD models is explored in Problem P4.1.) In an FE mesh, both specified head and specified flow boundaries are placed on the nodes (Fig. 4.11(d) and (e)). Head-dependent boundaries relate flow to a user-specified boundary head and are located on the node in a point-centered FD grid and in an FE mesh and at the edge of the block in a block-centered FD grid.

### 4.3.2 Specified Head Boundaries

A specified head boundary is implemented by fixing head values at the nodes along the boundary; hence, specified boundary heads do not change in response to hydrologic stresses. In steady-state models, specified boundary heads are invariant but most codes allow the user to input a time series of heads to update boundary values during transient simulations. For example, this is done with the Time-Variant Specified-Head Package (CHD Package) in MODFLOW. Under field conditions, the head at the location of a designated specified head node may in fact change with time or the flux across the boundary may be limited by physical or hydraulic constraints. Then, a specified head boundary may cause erroneous simulated heads. Specified head boundaries are best used to represent large bodies of water (major rivers, lakes, reservoirs, and oceans) that are not affected by stresses in the system such as pumping and changes in recharge rate. Less commonly, a specified head condition can be used to solve for associated discharge in a pumping well. For example, a specified head condition allows the head in the well to be fixed at the desired elevation for problems involving dewatering without the need to know the pumping rate

that will produce that head. More commonly, however, pumping wells are simulated as specified flow conditions by specifying the pumping rate (Section 4.3.3 and Section 6.2).

In 2D areal models specified head boundaries necessarily fully penetrate the aquifer, physically (Fig. 4.3) or hydraulically. The specified boundary head represents the vertically averaged head in the aquifer at the boundary and is enforced throughout the full thickness of the aquifer. Surface water bodies in the interior of the model can be simulated using specified head conditions but the modeler should be aware that this assumes the surface water body fully penetrates the aquifer. For example, a stream represented by specified head nodes bisects a 2D areal problem domain into two independent regions each of which could be modeled separately. Similarly, placing a no-flow boundary beneath a topographic divide (Fig. 4.9(a)) effectively divides the problem domain in two. (This issue is further explored in Problems P4.3b and P4.4.) Partially penetrating surface water bodies in the model interior (e.g., Fig. 4.9(b)) are better represented using head-dependent conditions (see below).

### 4.3.3 Specified Flow Boundaries

A specified flow boundary is implemented by setting the flow at the boundary. Then heads at boundary nodes are calculated by the code and can change as the simulation progresses in time. Most codes allow the modeler to input time-varying boundary flows in transient simulations. Specified flow can be implemented along the lateral boundaries of a 2D or 3D model to represent horizontal flow across the boundary, such as groundwater entering or leaving the problem domain as underflow (e.g., Figs. 4.13(a) and (b), 2.4 and 2.15). A specified flow boundary can also be placed at the top of a 3D model to represent the vertical flow across the water table representing recharge (Fig. 4.13(a); Section 4.5), or at the bottom of the model to represent leakage to or from an underlying unit that is not included in the model. Specified flow conditions are also used to represent point sources and sinks such as pumping and injection wells (Section 6.2).

Conceptually, the same hydraulic effect can be achieved using either specified head or specified flow conditions. However, it is usually preferable to specify flow rather than head. A specified head boundary fixes the head at the boundary so that flow across the boundary is dependent on the head gradient, which is calculated by the model; hence, the calculated flow may not be representative of field conditions. A specified flow boundary, on the other hand, maintains a constant realistic flow of water into or out of the model, as designated by the modeler. Moreover, simulated heads are more sensitive to parameter changes during model calibration when a specified flow boundary is used, which helps with parameter estimation (Chapter 9).

A no-flow condition (i.e., flow is specified to be zero) is the default perimeter boundary condition in both FD and FE codes; the user must activate another option in the code to over-ride the default. Within the computer code itself, the implementation

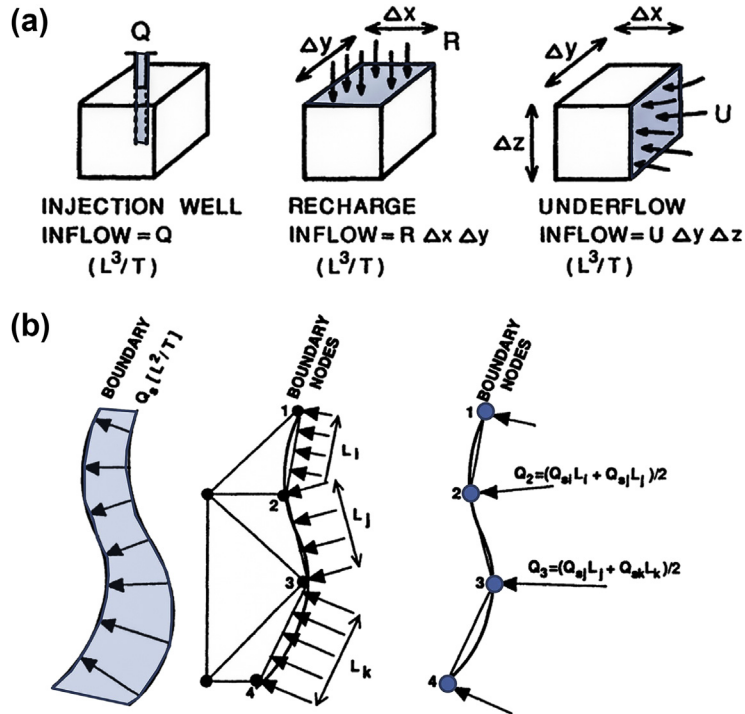


**Figure 4.13** Implementation of specified flow conditions. (a) In an FD grid, a volume of water is placed into an FD cell/block (or extracted from the cell/block) using wells ( $Q$ ) or areal recharge ( $R$ ). Lateral flows (i.e., underflow) can be introduced using a code's well or recharge option or using a head-dependent boundary. For underflow input via a well,  $Q = U\Delta x\Delta z$  where  $U$  is the lateral flux ( $L/T$ ). When underflow ( $U$ ) is input as recharge,  $R = U\Delta z/\Delta y$ . (b) In an FE mesh, diffuse flow ( $Q_b$ ) along the boundary is discretized along the sides of triangular elements and then assigned to nodes (modified from Townley and Wilson, 1980).

of no flow conditions in FD codes involves ghost nodes (Fig. B4.3.3, Box 4.3; Problem P4.1). For example, MODFLOW internally assigns default zero values of hydraulic conductivity to ghost nodes located outside the boundaries of the model in order to create no-flow conditions at the edge of the boundary cells (Fig. 4.14). In an FE code, the boundary flux is automatically set to zero when the FE equations are assembled into the global matrix equation. Details are given by Wang and Anderson (1982, pp. 117, 126–127). In both FD and FE codes, the user may implement a nonzero specified flow perimeter boundary by introducing flow into the boundary node via the code's recharge or pumping/injection well boundary conditions (Figs. 4.13(a), 4.14 and 4.15). In that way, water is introduced into the boundary node as a sink or source thereby inducing flow at the boundary.

Flow across the boundary is typically estimated from field data or information taken from the literature. In FD models, flow is input to an FD cell as a flux ( $L/T$ ) or a

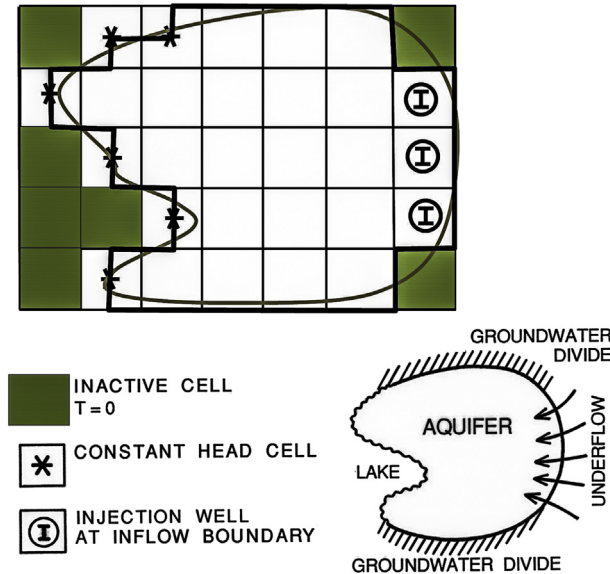


**Figure 4.14** Default no-flow boundaries in a two-dimensional block-centered FD grid are implemented by setting transmissivity ( $T$ ) equal to zero in inactive cells/ghost cells (shaded) outside the problem domain. The ghost cells with  $T = 0$  that are used to implement no flow conditions along the groundwater divides and the ghost cells to the right of the underflow boundary are not shown. Constant head and specified flow (injection wells) conditions are imposed in boundary cells to cancel the effect of the default no-flow boundaries (adapted from McDonald and Harbaugh, 1988).

volumetric flow rate ( $L^3/T$ ) (Figs. 4.13(a) and 4.14). A common application of a specified flow boundary is to represent a pumping or injection well (Section 6.2). Conceptually, water enters or leaves the cell through one of its faces and then enters the faces of adjacent active cells. For example, underflow conceptually enters or leaves through a side face; in 3D models recharge enters the top face of the cell and leakage enters or leaves through side and bottom faces. In an FE model, the flux at the boundary is proportionately distributed to each boundary node (Fig. 4.13(b)).

Although specified flow boundaries are preferred over specified head boundaries, the exclusive use of specified flow boundaries generally is not recommended even when hydrogeologically defensible. Recall that the governing equation (Eqn (3.12)) is written in terms of derivatives or differences in head. The solution is satisfied when the gradients of head are consistent with the specified boundary flux. However, when a steady-state problem is set up only in terms of gradients, the problem is nonunique because gradients are relative. In that case, many different arrays of head values can produce the same gradients. Nonuniqueness is avoided and a good solution attained by specifying head for at least one perimeter or internal boundary node to give the model a reference elevation from which to calculate heads. A head-dependent boundary condition can also serve this purpose provided the associated resistance is not extremely large (Section 4.3.4).

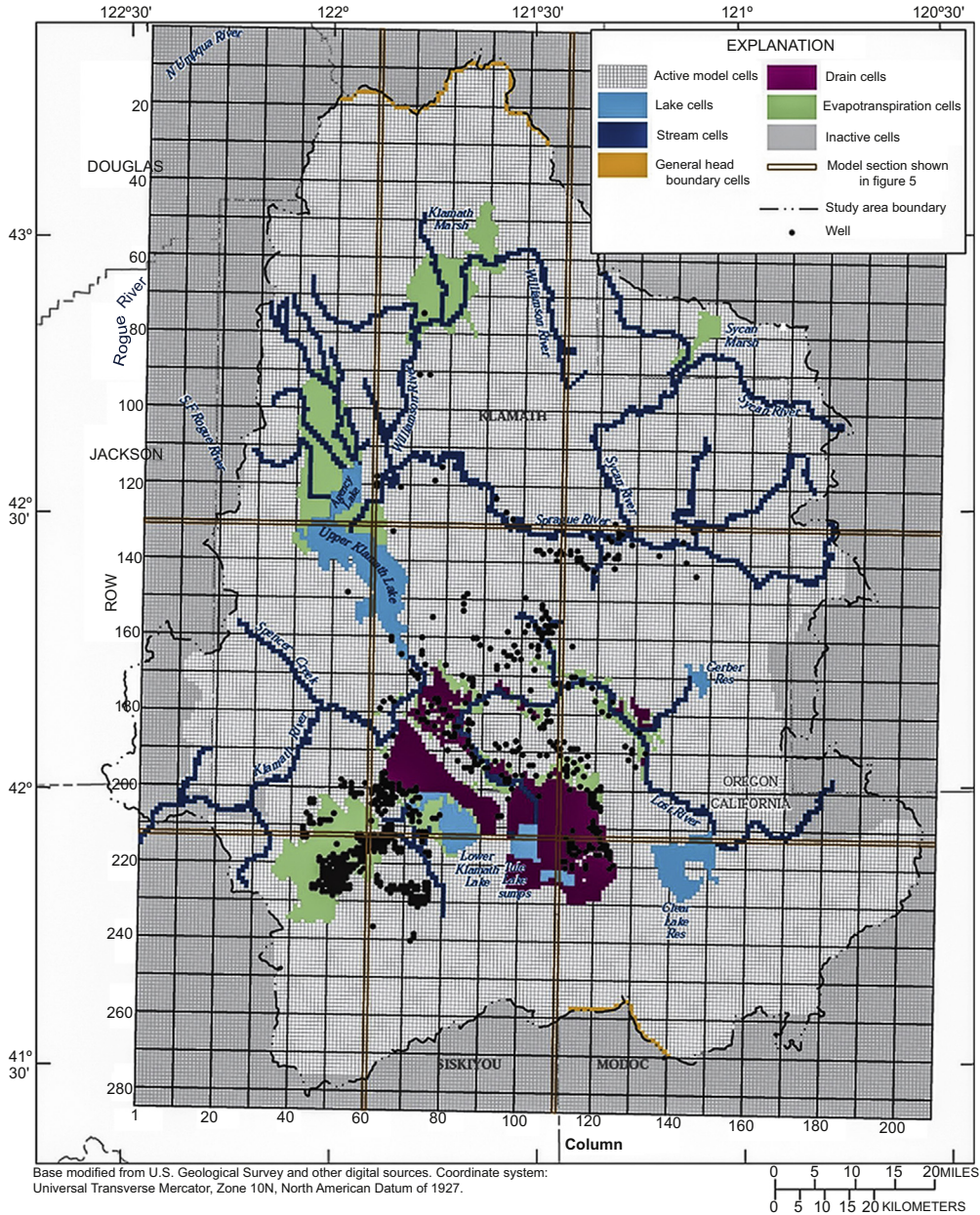


**Figure 4.15** FD grid showing implementation of head-dependent boundary (HDB) conditions for boundary flows (designated as general head boundary cells), drains, and evapotranspiration. Stream cells and lake cells use more sophisticated representation of HDB conditions as discussed in Sections 6.5 and 6.6, respectively (Gannett et al., 2012).

In a transient simulation, the heads specified in the initial conditions (Section 7.4) provide reference elevations for the solution and a unique solution can be obtained without specified head or head-dependent conditions. However, because errors in the initial heads can cause errors in the solution, the output should be reported as a difference from the initial condition (e.g., drawdown) when all boundary conditions in a transient model are set as specified flow. Hence, even in transient modeling it is usually advisable to specify a head value as an internal boundary in a model that uses all specified flow boundaries (Problem P4.5).

### 4.3.4 Head-dependent Boundaries

When a head-dependent boundary (HDB) is implemented, the code calculates flow across the boundary using the hydraulic gradient between a user-specified boundary head and the model-calculated head at a boundary node.

Mathematically, the volumetric flow rate,  $Q$  ( $L^3/T$ ), across an HDB is computed using an equation of the general form:

$$Q = C\Delta h = C(h_B - h_{i,j,k}) \quad (4.4a)$$

$$C = KA/L \quad (4.4b)$$

where  $\Delta h$  is the difference between the user-specified boundary head,  $h_B$ , and the model-calculated head near the boundary,  $h_{i,j,k}$ ;  $C$  is conductance ( $L^2/T$ ), which is computed using a representative hydraulic conductivity ( $K$ ) times a representative area ( $A$ ), divided by the distance ( $L$ ) between the locations of  $h_B$  and  $h_{i,j,k}$ . The hydraulic gradient  $\Delta h/L$  can represent either horizontal or vertical flow. An advantage of an HDB is that it gives the modeler flexibility in choosing the location of the specified boundary head,  $h_B$ , which does not have to be located directly on the boundary. Another advantage is that in transient simulations  $h_{i,j,k}$  changes with time as the simulation progresses and the simulated boundary flow ( $Q$ ) also is automatically updated.

The flexibility in specifying both the location of the boundary head and the direction of the associated hydraulic gradient means that HDB conditions can represent a wide variety of hydrogeological situations including vertical flow to and from streams, lakes, wetlands, and other surface water bodies; flow to drains; evapotranspiration from the water table; lateral and bottom boundary flows; and boundaries outside the model domain (Fig. 4.15). MODFLOW, for example, has several options for implementing HDBs including basic options provided by the River (RIV) Package, the Drain (DRN) Package, the Evapotranspiration (EVT) Package, and the General Head Boundary (GHB) Package and more advanced options provided by the Lake (LAK) Package and the Wetlands Package. The way in which conductance,  $C$ , is specified varies with the specific application of an HDB, as discussed in the sections below. Under some conditions, an HDB can generate anomalous large water budget errors (Box 4.5).

### Box 4.5 Large Water Budget Errors Arising from an HDB

A large error in the model's water budget (i.e., greater than 1.0%) is generally indicative of conceptual errors in model design, nonconvergence of the solution, and/or data entry errors (Sections 3.6 and 3.7). However, large water budget errors (up to 200%) may be generated for some formulations of HDB conditions (Sections 4.3; 6.4–6.7) even when the head solution is acceptable (i.e., the head closure criterion is met; Section 3.7). This type of water budget error does not necessarily invalidate the results of the model as long as the head closure criterion is met and flow to or from the HDB is identified as the cause of the water budget error. The way in which the error occurs is explained below.

Large errors in the computed water budget can occur as an artifact of representing the transfer of water between a perimeter or internal HDB and the aquifer. Such anomalous conditions may occur (if they occur at all) when HDB conditions are used to represent distant boundaries (Section 4.4) or large lakes (Sections 4.3 and 6.6). Recall that when implementing an HDB, the modeler assigns a boundary head and a value for conductance (Eqn (4.4)). Anomalous large volumes of water can be transferred when the assigned conductance is set very large and the gradient at the boundary is not equal to zero. The flow across the boundary is calculated using the simulated head gradient at the HDB and the large assigned conductance, which may produce an anomalously large flux of water. Even a small head gradient at the boundary could produce large fluxes of water if conductance is large. The head closure criterion is still met because the head residual at the HDB node is small.

Whether such conditions have a significant impact on the water budget depends on the relative magnitude of the sum of such anomalous computed flows compared to other components of the water budget. The water budget error can often be eliminated by reducing the value of the conductance until the model produces an acceptable water budget error while still meeting the head closure criterion and simulating appropriate responses at the HDB.

#### 4.3.4.1 Surface Water Bodies

Head-dependent conditions are frequently used in both 2D areal and 3D models to represent exchange of water at surface water bodies including streams, lakes, and wetlands (Fig. 4.15). The surface water body is not represented explicitly in the model (i.e., it does not occupy space within the grid/mesh); rather, an HDB is specified for the node influenced by the surface water feature (Fig. 4.16(a)). Recall from Section 3.3 that vertical flux,  $q_z$ , across an HDB is calculated as follows:

$$q_z = -K'_z \frac{h_{i,j,k} - h_s}{b'} \quad (4.5)$$

where here  $q_z$  is vertical flux of water to or from a surface water body,  $h_{i,j,k}$  is the groundwater head computed by the model beneath the surface water body;  $h_s$  is the surface water head specified by the modeler (i.e., the specified boundary head);  $K'_z$  is the vertical hydraulic conductivity at the interface between the groundwater system and the surface water body (usually the vertical hydraulic conductivity of streambed,



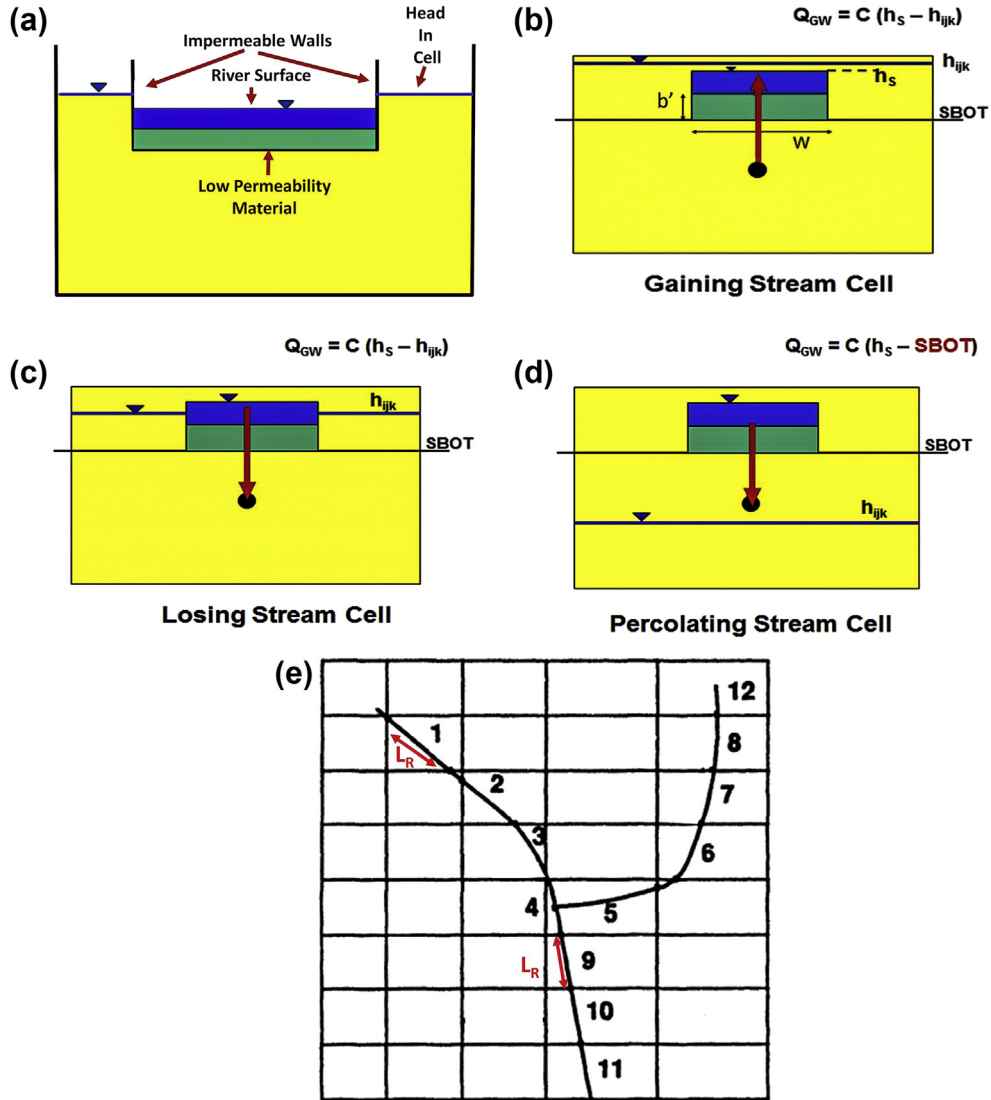


**Figure 4.16** Implementation of HDB conditions for representing surface water bodies using a stream in an FD cell for illustration. (a) Representation of the stream in an FD cell. The stream is conceptualized to be embedded in the cell and to exchange water with the aquifer but the stream does not occupy space within the grid. (Representation in an element of an FE mesh is similar.) As shown, the stage of the stream is lower than the head in the cell and the width of the stream is less than the width of the cell. (b) When the stream is gaining, the head in the aquifer,  $h_{ijk}$ , is higher than the head in the stream,  $h_s$ . The elevation of the bottom of the streambed sediments is SBOT; the thickness of the sediments is  $b'$ .  $Q_{GW}$  is the volumetric rate ( $L^3/T$ ) of groundwater discharge to the stream. (c) For a losing stream  $h_{ijk} < h_s$  and  $Q_{GW}$  is the volumetric rate ( $L^3/T$ ) of induced recharge from the stream to the aquifer. (d) Under percolating conditions, the stream is separated from the aquifer and  $Q_{GW}$  is constant. (e) Discretization of a stream into 12 reaches. The width,  $W$ , of the stream is much less than the grid spacing ( $\Delta x$ ); the length of the stream reach,  $L_R$ , is not equal to the length of the cell ( $\Delta y$ ). Each reach can have different values for  $h_s$ , SBOT,  $K'_z/b'$ , as well as  $L_R$  and  $W$  (modified from McDonald and Harbaugh, 1988).

lakebed, or wetland sediments) and  $b'$  is the thickness of the interface (usually the thickness of streambed, lakebed, or wetland sediments).

Equation (4.5) is conceptually identical to Eqn (4.1) for leakage through a confining bed. In Eqn (4.5), the connection between the surface water feature and the groundwater system is characterized by *leakance*,  $K'_z/b'$ , or its inverse *vertical resistance*,  $b'/K'_z$ , of the streambed, lakebed, or wetland sediments. Then,  $K/L$  in Eqn (4.4b) equals  $K'_z/b'$  in Eqn (4.5). To compute conductance,  $A$  in Eqn (4.4b) is the horizontal area perpendicular to flow, calculated from the width,  $W$ , and length,  $L_R$ , of the surface water segment or reach ( $A = WL_R$ ) (Fig. 4.16(e)). When the surface water feature covers the entire surface of the cell or element,  $A$  is equal to the surface area of the relevant cell or element, but the width of the surface water feature can be smaller than the width of the cell or element (Fig. 4.16(a)) and similarly the length of the surface water feature may not coincide with the length of the cell or element (Fig. 4.16(e)).

HDBs can represent both gaining (flow out of the groundwater system; Fig. 4.16(b)) and losing (flow into the groundwater system, Fig. 4.16(c)) conditions. Some specialized HDBs (e.g., the River Package for MODFLOW) disconnect the surface water feature from the aquifer when the head in the aquifer falls below the bottom of the interface sediments (SBOT in Fig. 4.16(d)). Then, *percolating conditions* occur and flow out of the surface water body is independent of groundwater head and equal to  $C(h_s - \text{SBOT})$  (Fig. 4.16(d)). When conditions are near but not at percolation, the surface water feature is said to be steeply mounded.

Most codes provide basic HDB conditions to represent vertical flux between the aquifer and surface water bodies. However, such simple HDB conditions, which use fixed surface water levels, only approximately represent the exchange of water between groundwater and surface water bodies. More advanced methods for simulating streams, lakes, and wetlands in a groundwater model are discussed in Sections 6.5, 6.6, and 6.7, respectively.

#### 4.3.4.2 Drains

Head-dependent conditions can also simulate drains including closed drains, tunnels, and mines, and springs and seeps (Figs. 4.15 and 4.17). The head in the drain is the specified boundary head,  $h_B$ , in Eqn (4.4a). In most standard representations of drains, the drain is active only when the head in the aquifer,  $h_{i,j,k}$ , is higher than the elevation of the drain,  $h_B$ . That is, drains only remove water from the problem domain; a drain does not contribute water to the model. Discharge to the drain increases as the head rises above the specified drain elevation. If  $h_{i,j,k} \leq h_B$  there is no discharge from the drain cell and  $Q$  in Eqn (4.4a) is zero by definition. For springs and seeps, the head in the drain is equal to the elevation of the land surface at the location of the spring or seep. Diffuse seepage (e.g., to wetlands) is simulated by placing drain nodes in the general area where seepage is likely to occur (Fig. 4.15) (e.g., Batelaan and De Smedt, 2004).

It is important to remember that water discharged to drains is removed from the model. This may not be appropriate for simulating seepage to springs and wetlands where water may flow overland and re-enter the groundwater system downgradient. Seepage to wetlands can be simulated using other approaches as discussed in Section 6.7. A drain package for MODFLOW (DRT1 by Banta, 2000) allows water to flow from drain nodes to the groundwater system but only at user designated locations. In general, drains are not appropriate for any surface water features that have losing reaches because water cannot leave a drain node and enter the groundwater system.

Conductance of the drain,  $C$  in Eqn (4.4b), is affected by the material surrounding the drain. For closed drains (Fig. 4.17) conductance depends on the size and density of openings in the drain, the presence of chemical precipitates around the drain, and the hydraulic conductivity and thickness of backfill around the drain. Conductance is often estimated during calibration by adjusting conductance values until simulated flows to

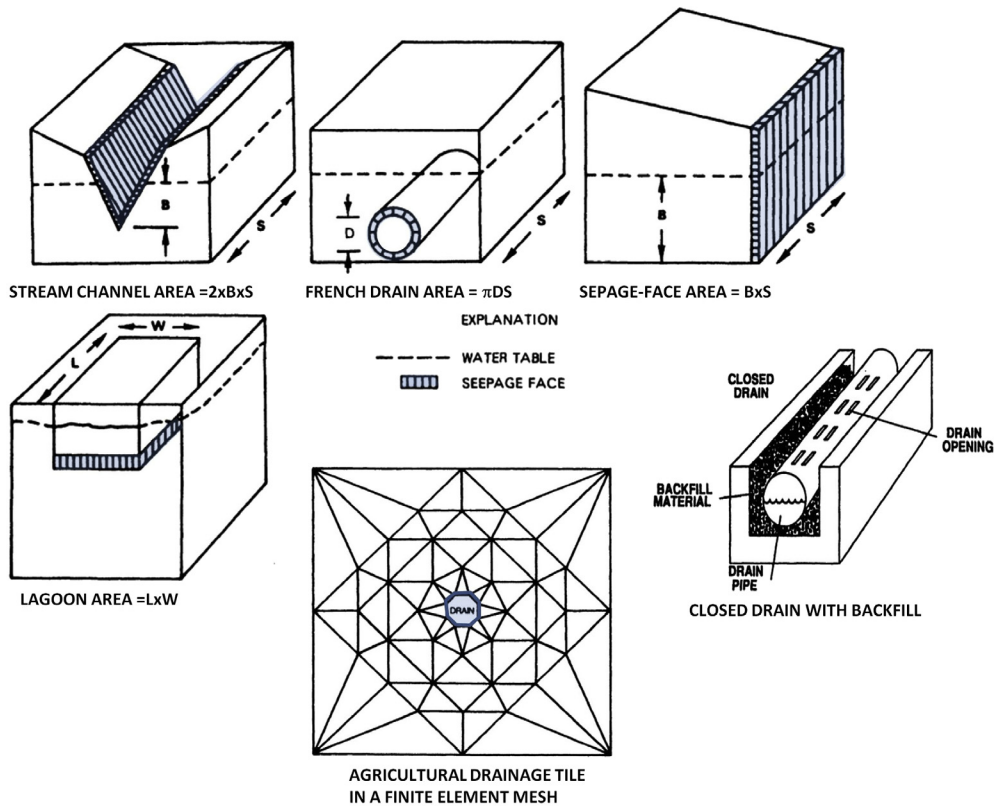


**Figure 4.17** Examples of drains with associated cross-sectional area used to compute conductance (composite of images modified from Yager, 1987; Fipps et al., 1986 and McDonald and Harbaugh, 1988).

the drain match measured flows. For mines and tunnels (e.g., Zaidel et al., 2010), drain nodes can represent a seepage face (Fig. 4.17) and conductance is related to the geological material that forms the sidewalls.

#### 4.3.4.3 Evapotranspiration (ET) from the Water Table

In many hydrogeologic settings, ET occurs mainly or exclusively from the unsaturated zone rather than from the water table. In that case, ET from the saturated zone is zero and the loss of infiltration via ET in the unsaturated zone is accounted for by inputting a net recharge rate to the groundwater model equal to precipitation minus ET (Box 5.4). However, if the water table is close to the land surface, there may be direct evaporation from the water table and/or phreatophytes (plants whose roots extend into the water table) may extract groundwater through transpiration. ET ceases when the water table drops to or below the root zone (often called the extinction depth,  $d$  in Fig. 4.18). In temperate climates, ET varies seasonally with high rates during the growing season and little or no ET during plant senescence.

In groundwater models, ET is usually expressed as a flux across the water table. In 2D areal models, ET is represented by internal HDBs; in 3D models, the water table typically is the upper boundary and ET is represented by HDB conditions at water-table nodes (Fig. 4.15). In a basic representation of ET, the modeler assigns the extinction depth ( $d$ ); a boundary head ( $h_s$ ), which is usually equal to the land surface elevation; and a maximum ET rate ( $R_{ETM}$ ). The maximum ET rate occurs when the water table equals or exceeds  $h_s$ . In between the location of the boundary head (land surface) and the extinction depth, the volumetric rate of water loss via ET varies linearly, where  $Q_{ET} = C \Delta h$  (Eqn (4.4a)) and  $C$  and  $\Delta h$  are:

$$C = \frac{R_{ETM}A}{d} = \frac{Q_{ETM}}{d} \quad (4.6a)$$

$$\Delta h = h_{i,j,k} - (h_s - d) \quad (4.6b)$$

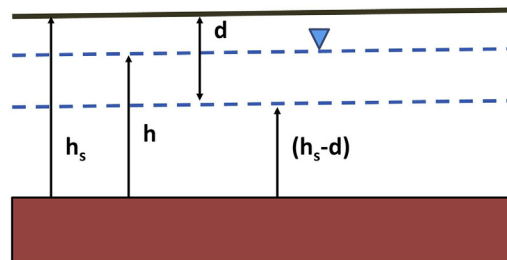


**Figure 4.18** Representation of ET as a head-dependent boundary (Eqn (4.6)) showing extinction depth ( $d$ ), land surface elevation ( $h_s$ ),  $h_s - d$ , and calculated head ( $h$ ).

In Eqn (4.6a),  $A$  is the surface area of the cell (e.g.,  $\Delta x \Delta y$ ) or element; in Eqn (4.6b),  $h_{i,j,k}$  is the head at the water table calculated by the model (Fig. 4.18). Here,  $C$  is not a conductance but is defined so that there is a linear increase in ET between the extinction depth where ET is zero, and the land surface where ET is at its maximum. Other functions can also be used to represent the relation between ET and  $\Delta h$  (e.g., Banta, 2000).

The field information for estimating the extinction depth is most often obtained from estimates of plant rooting depth. The maximum ET rate ( $R_{ETM}$ ) is commonly estimated from remote sensing and climatological information. As is true for many point measurements made in the field, local factors confound point measurements of  $R_{ETM}$  (e.g., Lott and Hunt, 2001) and in practice accurate estimation of  $R_{ETM}$  is complicated. Moreover, scaling up point measurements to represent ET in a cell or element of a groundwater model is a challenging problem. ET estimation techniques and issues are continually being researched. The discussion of these issues is beyond the scope of our text; more detail is provided by Abteu and Melesse (2012), Goyal and Harmsen (2013), and Moene and van Dam (2014), among others.

#### 4.3.4.4 Lateral Boundary Flows and Distant Boundaries

An HDB condition is often used to simulate lateral boundary flows (Fig. 4.15), including underflow (Figs. 4.13(a) and 2.15), and flows to and from a distant boundary located outside of the model domain (Fig. 4.19). In MODFLOW, lateral boundary flows and distant boundaries are represented using the General Head Boundary (GHB) Package.

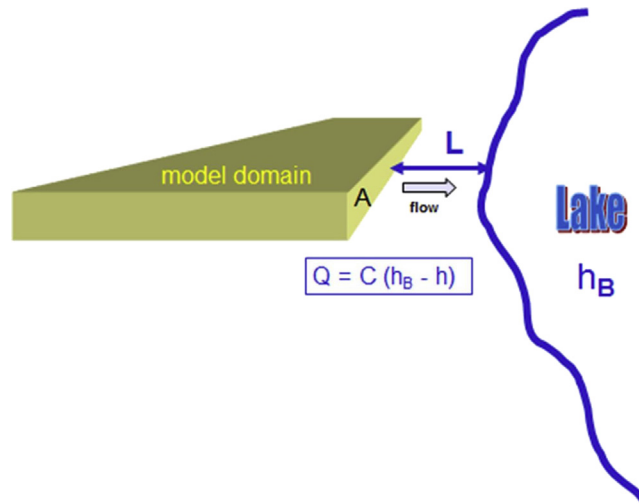


**Figure 4.19** Head-dependent boundary used to represent flow between the modeled area and a distant physical boundary, shown here as a large lake. The boundary flow ( $Q$ ) is controlled by the head at the distant boundary, shown here as the head in a large lake,  $h_B$ .  $C$  is conductance (Eqn (4.4b)).

For lateral flows at perimeter boundaries, the user-specified boundary head,  $h_B$  in Eqn (4.4a), is the head at or near the perimeter boundary and conductance (Eqn (4.4b)) reflects conditions at the boundary. An HDB can also represent lateral flows to or from a distant boundary (e.g., the lake in Fig. 4.19). In that case, the HDB effectively extends the model to a distant physical feature without expanding the grid/mesh. The head at the distant physical boundary (e.g., lake level in Fig. 4.19) is the user-specified boundary head. Conductance (Eqn (4.4b)) is computed with  $K$  equal to the average horizontal hydraulic conductivity between the perimeter boundary of the model and the distant physical boundary (e.g., the shoreline of the lake in Fig. 4.19);  $L$  is the distance between the model boundary and the distant boundary;  $A$  is the area of the face of the cell or element perpendicular to flow. In this way, the perimeter boundary of the model is tied to a physical feature without extending the grid/mesh to its physical location.

Although an HDB is usually more defensible than an inferred hydraulic boundary, professional judgment is required to decide how far a physical boundary can reasonably be located from the perimeter of the model. That is, over what distance can the average hydraulic conductivity between the distant physical feature and the perimeter of the model be reasonably estimated? Some applications of this type of HDB condition have involved large distances. For example, Handman and Kilroy (1997) used a distant HDB to represent springs located 16 miles from the perimeter of the model, where the specified boundary head was set at the elevation of the springs.

#### 4.4 EXTRACTING LOCAL BOUNDARY CONDITIONS FROM A REGIONAL MODEL

Selecting perimeter boundaries is often difficult because physical boundaries and suitable hydraulic boundaries (e.g., stable groundwater divides) may not be located near the problem domain. An HDB can be used to tie the perimeter boundary of the model to a head at a distance physical boundary (Section 4.3) or the problem domain can be expanded so that the boundaries are located on distance physical features. Expanding the problem domain requires expanding the grid/mesh and increasing the number of nodes, which increases the computational burden. In an FE mesh and an unstructured Control Volume Finite Difference (CVFD) grid, a fine nodal network may be embedded within a coarser regional network of nodes (Section 5.1) so that perimeter boundaries are placed at distant physical features while minimizing the number of nodes in the far-field area of coarse nodal spacing.

Perimeter boundaries for local scale models can also be defined by extracting heads and flows from large-scale groundwater flow models (Fig. 4.20). These techniques work well with standard FD and FE models. Two of these methods are *telescopic mesh*

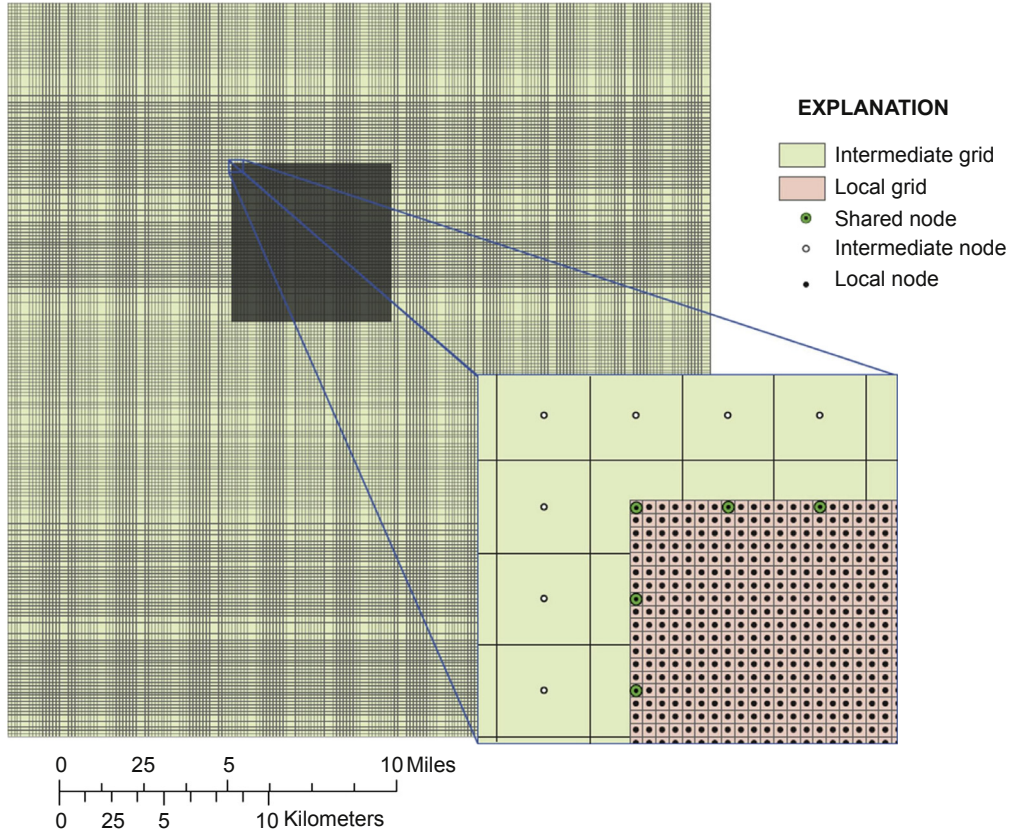


**Figure 4.20** Grid refinement for setting boundary conditions showing shared nodes in the horizontal FD grids of intermediate- and local-scale models. Hydraulic boundaries for the local-scale model are extracted from the solution of an intermediate-scale model. The grid for a regional-scale model that provides boundary information for the intermediate-scale model is not shown (Hoard, 2010).

*refinement (TMR)* (Ward et al., 1987; Leake and Claar, 1999), which applies to both FD and FE models, and *local grid refinement (LGR)*, which was developed for MODFLOW (Mehl and Hill, 2006). In TMR, boundary conditions for FD or FE models covering successively smaller geographic areas are assigned based on the heads and flows computed by a larger scale FD or FE model. Each model is run independently and boundary conditions are extracted successively after each run. Some graphical user interfaces (GUIs) (e.g., Groundwater Vistas) have a TMR option that: extracts heads and flow along a designated boundary location for the smaller scale model; calculates specified heads or

flows along the boundaries of the smaller scale model; imports that information into the smaller scale model as boundary conditions and runs the smaller scale model. Alternatively, results from a regional AE model can be used to specify boundary conditions for a local FD or FE TMR model (e.g., [Hunt et al., 1998](#); [Feinstein et al., 2003](#)). The GUI for the AE code GFLOW, for example, exports heads or flows from the solution of the AE model directly to an FD or FE model as specified head or specified flow boundaries ([Fig. 4.21](#)).

LGR is conceptually similar to TMR except there is an iterative feedback between the regional and local models to update the calculated boundary conditions (e.g., see [Feinstein et al., 2010](#); [Hoard, 2010](#)). In practice, TMR is usually preferred over LGR because LGR can be cumbersome to use, can substantially

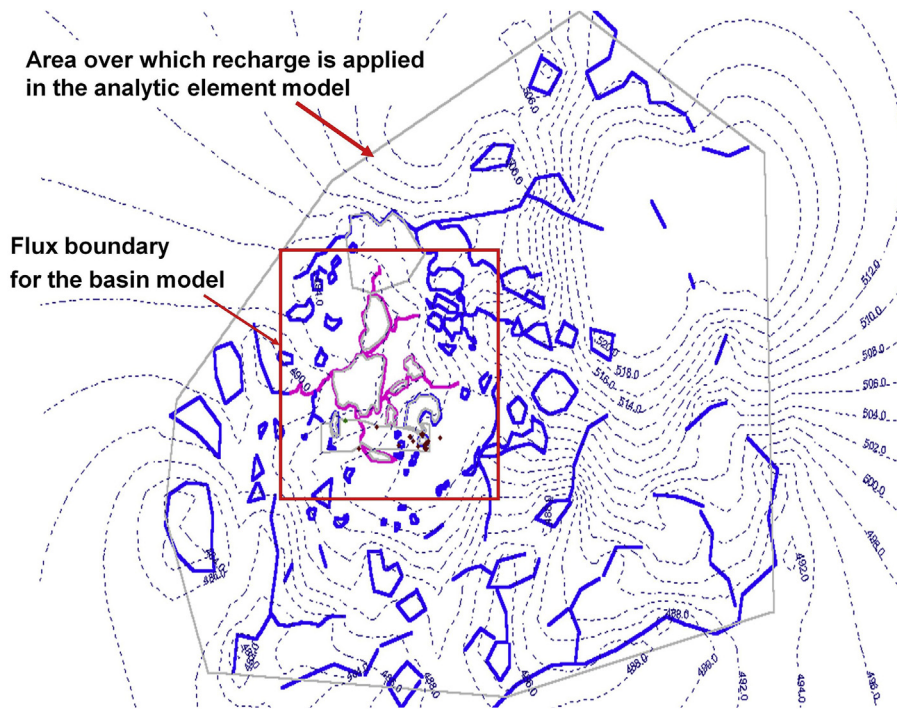


**Figure 4.21** Hydraulic boundary conditions for a 3D FD model (basin model) are extracted from the solution of a 2D regional analytic element (AE) model. Lake and stream analytic elements are outlined in blue and pink. Heads (dashed lines) calculated by the AE model were used to compute fluxes along the perimeter boundaries (outlined in red) of the FD model. Fluxes extracted from the AE model were uniformly distributed vertically along the perimeter of the five layer FD model (*modified from Hunt et al., 1998*).



increase runtimes, and may be less efficient than using a single globally refined grid (Vilhelmsen et al., 2012). TMR is appropriate for most problems provided the perimeter of the local scale model is sufficiently far from the area of interest so that results are not dominated by conditions along the boundaries. However, TMR procedures are more complicated and cumbersome when conditions along the extracted boundaries change with time. In transient TMR models, extracted boundary conditions must be updated as the rate and direction of groundwater flow across the boundaries changes with time (e.g., see Buxton and Reilly, 1986). LGR models can automate the transient updating of inset perimeter boundaries.

## 4.5 SIMULATING THE WATER TABLE

In a rigorous formulation of groundwater flow under unconfined conditions, the water table is a moving free surface boundary (Fig. 4.22(a)) whose location depends on the solution of the model. Solving the free surface boundary problem is challenging but some analytical solutions are available for special cases (Bruggeman, 1999). Simulating the water table as a moving boundary in a numerical model (e.g., Diersch, 2014, pp. 416–421) requires a code that allows for movable nodes. More often, in practice, the boundary condition on the water table is simplified to make the solution tractable using a grid/mesh with nodes that are fixed in space. In 2D areal models of unconfined groundwater flow using the D-F approximation (Section 4.1; Box 4.1), head at the water table is the dependent variable calculated as the solution (Fig. 4.3). In 2D profile models and 3D models, however, the water table is usually the upper boundary of the model. The modeler can specify the head at the water table (Box 4.3) or, more commonly, flux across the water table (Box 4.6). Generally speaking, it is preferable to specify flux (recharge) across the water table rather than head (Box 4.6). In either case, at least the approximate elevation of the water table is needed in order to locate the boundary correctly. In this section, we present some options for simulating the water table in numerical models, but first we review a few basic principles.

Groundwater flows in response to gradients in total head ( $h$ ). Total head (or head) is the sum of pressure head (Fig. 4.2) and elevation head ( $z$ ). At the water table, pressure is equal to atmospheric (zero) pressure so that head at the water table equals elevation head. The fundamental dilemma in problems with a water-table boundary is that we need to know the head at the water table to set the location of the boundary when the water table head is what we would like the model to calculate. Another complication is the associated seepage face (Figs. 4.3, 4.22(b) and (c)), whose position is also unknown. Similar to conditions along the water table, the pressure along the seepage face is zero (atmospheric), so that the head at the seepage face equals elevation of the seepage

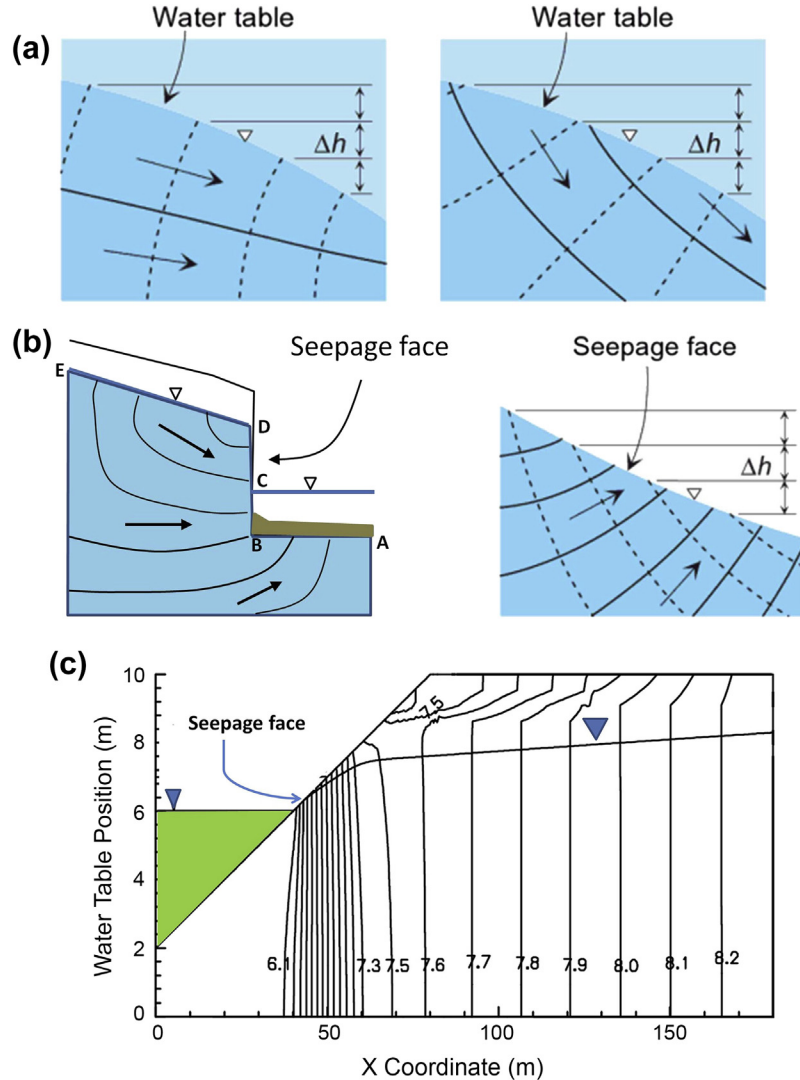


**Figure 4.22** Representation of hydraulic conditions at the water table and seepage face. (a) The water table is a streamline when there is no recharge (left hand side figure) but is not a streamline when recharge is present (right hand side figure). In both cases, the pressure head at the water table is zero. (b) A seepage face (DC) along a streambank (left hand side figure). Schematic flowlines and arrows are shown. The location of the water table (DE) and the point of intersection of the water table with the streambank (D) are unknown. Right hand side figure shows detailed schematic depiction of flow near the seepage face. The pressure head at the seepage face is zero so that head at the seepage face is equal to elevation head (modified from Fitts, 2013). (c) The water table computed as the surface of zero pressure in a variably saturated model. The aquifer is shown in cross section with vertical exaggeration = 10. Equipotential lines are computed in the unsaturated–saturated continuum and are closely spaced near the discharge face at the ocean (shaded in green). The ocean level and seepage face are also shown (modified from Ataie-Ashtiani, 2001).

face. The removal of water through a seepage face can be simulated using an HDB with drain nodes (Section 4.3; Fig. 4.17) and there are also options for simulating a seepage face along the well casing of a pumping well (Section 6.2). However, standard groundwater flow codes typically do not solve for the location of a seepage face, which is usually not a concern because for most groundwater problems the seepage face is a small feature relative to the size of the flow system. Solving for the location of the seepage face, however, can be important to engineering problems involving slope and tunnel stability, dewatering, and flow through a dam.

Below we discuss three options for simulating the water table using: (1) standard FD and FE codes with fixed nodes; (2) FE codes with movable nodes; (3) variably saturated flow codes, which simulate the unsaturated and saturated zones as a continuum. The first method is the most widely used in practice; however, if finding the location of the seepage face is a primary modeling objective, the water table and seepage face should be simulated using options 2 or 3.

#### 4.5.1 Fixed Nodes

In standard groundwater flow codes nodes are fixed in space, which means that the calculated head at the water table,  $(h_{i,j,k})_{WT}$ , is not necessarily equal to the elevation of the water table,  $z_{i,j,k}$ . Instead,  $(h_{i,j,k})_{WT}$  is expected to fall within the range  $(z_{i,j,k} \pm \Delta z/2)$  where  $\Delta z$  is the nodal spacing around  $z_{i,j,k}$  (Fig. 4.23). If the calculated head is higher

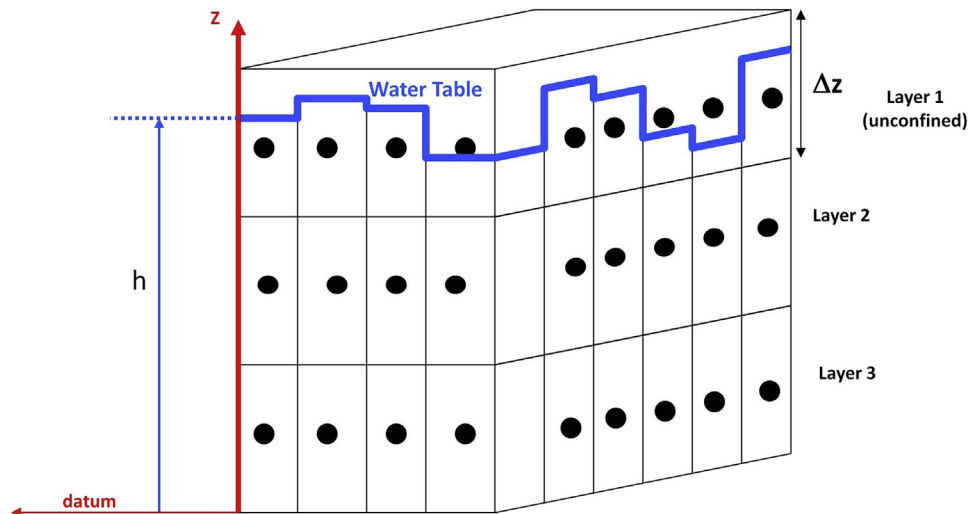


**Figure 4.23** Water table in a three-dimensional FD grid showing that head calculated at the water-table node ( $h$ ) is higher than the bottom elevation of the top layer of the model but is not necessarily equal to the elevation of the node. (A similar situation occurs in a fixed node FE mesh.)

than the top of the water-table cell (usually set at the elevation of the land surface), the water-table cell converts to confined conditions and the cell is said to be *flooded* (Section 5.3). If the calculated head is lower than the bottom of the water table cell, the cell is de-watered (see below).

Usually water-table nodes are assigned specified flow boundary conditions (Box 4.6) and then the code solves for head in the water-table cells. When  $(h_{i,j,k})_{WT}$  is not equal to the elevation of the node  $(z_{i,j,k})$ , which is usually the case, the water-table boundary is not represented exactly. Clemo (2005) presented a modification to MODFLOW-2000 to adjust the placement of the node within a cell during the simulation, but for most applications the error in the unadjusted water-table head is acceptable without such adjustments.

In the most straightforward case of using fixed nodes, the water table remains within an unconfined layer (see Section 5.3). Spatially, the water table might also be present in parts of several layers, each of which is the upper active layer in the model (e.g., Fig. 4.6). If the water table drops below the bottom of a water-table layer, nodes in the layer are de-watered. Modelers struggled with dry nodes for over two decades. In one simple approach used in older codes, the dry nodes were removed from the array of active nodes for which head is calculated. Procedures for removing dry nodes and adding them back when rewet were developed but were inherently unstable (Doherty, 2001; Painter et al., 2008) and led to incorrect solutions. A more successful approach, which is appropriate for problems where the saturated thickness of the water-table layer is not expected to change appreciably, is to simulate unconfined water-table layers as confined layers (Section 5.3). This approach linearizes the problem and produces acceptable solutions for many problems (Sheets et al., 2015; Juckem et al., 2006). The best solution is realized in modern versions of MODFLOW (e.g., MODFLOW-NWT Niswonger et al., 2011) where the problem of dry nodes is resolved more effectively and robustly by using an improved method for formulating and solving the FD equations (see review by Hunt and Feinstein, 2012; test case presented by Bedeker et al., 2012).

### 4.5.2 Movable Nodes

Movable nodes are more easily incorporated into FE codes because the FE method references the location of the node within 3D space to construct even a fixed node mesh (Section 3.5; Fig. 3.5). However, additional programming (not included in all FE codes) is required to update the location of a movable node as the solution progresses. The FE code FEFLOW (Diersch, 2014) and some special purpose FE codes (e.g., FREESURF by Neuman, 1976, Neuman and Witherspoon (1971); AQUIFEM-N by Townley, 1990) allow for movable nodes that track the water table (Fig. 4.24(a)). Movable nodes

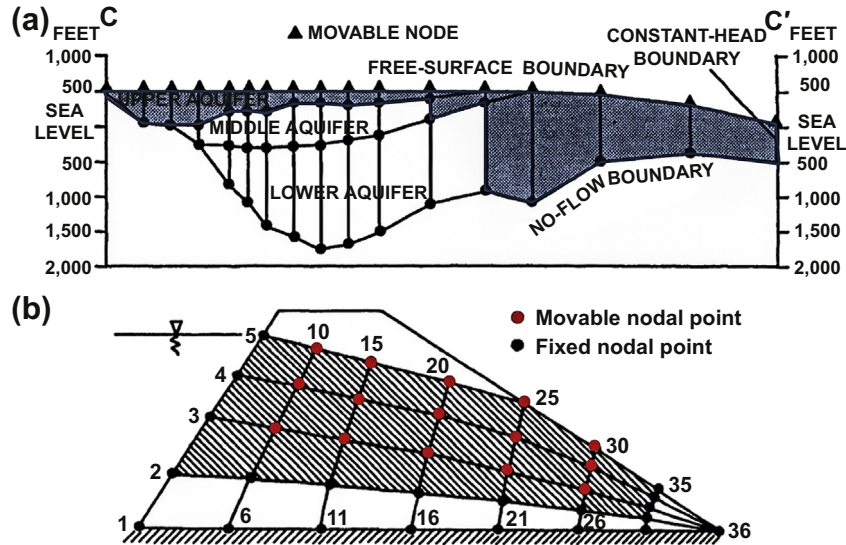


**Figure 4.24** Movable nodes and deformable elements (shaded) in FE meshes. (a) Movable nodes are placed along the water-table boundary (*modified from Mitten et al., 1988*). (b) Movable nodes are placed along the water-table boundary and along the exit face and in the interior of a permeable earthen dam. The model solves for the location of the water table and associated seepage face; nodes 25 and 30 are on the seepage face (*modified from Neuman, 1976*).

are placed exactly on the water table and the head at the node is exactly equal to the elevation of the node (i.e.  $(h_{i,j,k})_{WT} = z_{i,j,k}$ ). Movable nodes also make it possible to calculate the position of the seepage face (Fig. 4.24(b)). Of course when nodes move, the shape of the affected elements change (deform); codes that include movable nodes also account for deformable elements.

### 4.5.3 Variably Saturated Codes

The most realistic and theoretically rigorous way to simulate the water table uses a variably saturated code that represents the unsaturated and saturated zones as a continuum (Box 6.2; Section 12.2). The infiltration rate is specified across the upper boundary of the model, which is typically the land surface. The code solves for water pressure or pressure head in the subsurface continuum and the water table is determined as the surface of zero (atmospheric) pressure (Fig. 4.22(c)). The location of the seepage face is determined iteratively (Cooley, 1983; Neuman, 1973). Of course, a model that includes the unsaturated zone is more complicated than one representing only the saturated zone, requires a more complicated governing equation, and has much longer runtimes than the other two approaches.

### Box 4.6 What Controls the Water Table?

The water table is an important boundary in many groundwater models but the water-table configuration is usually poorly known. It is a common misconception that the water table is always a subdued replica of the land surface, i.e., that the water table is controlled by topography. In many hydrogeologic settings the water table is controlled by recharge rather than topography (Haitjema and Mitchell-Bruker, 2005; Shahbazi et al., 1968). The distinction is important because a water table controlled by topography is often represented by a specified head boundary condition whereas a water table controlled by recharge is usually represented by a specified flow boundary.

Groundwater modelers are tempted to specify heads at the water table by extrapolating field measurements of the water table to mimic the land surface. However, even small extrapolation errors in defining the water-table surface (for a 3D model) or the water-table profile (for a 2D profile model) can cause significant errors in the flow of water supplied to the model as recharge and removed as discharge (e.g., Stoertz and Bradbury, 1989). Recall from Section 4.3, that a specified head boundary potentially supplies infinite amounts of water to the problem domain and potentially accepts infinite amounts from the problem domain. Therefore, an incorrectly specified water-table surface potentially could provide unconstrained flows into and out of the specified boundary heads. Such flows are unlikely to represent actual flows under field conditions. Alternatively, the modeler may specify recharge as flux across the water table so that flow to or from the water table is constrained to reasonable values. Although recharge rates are difficult to measure (Section 5.4), approximate values of recharge can be estimated with some degree of confidence (Box 5.4). Moreover, initial values of recharge rates input to a model almost always are adjusted and improved during calibration.

Specified head water-table boundaries are still occasionally used to simulate topography driven groundwater flow (e.g., Zlotnik et al., 2011, 2015), which is also called Tóthian flow in reference to groundbreaking work by Tóth (1962, 1963). Tóth's work was pioneering in that it shifted the focus of hydrogeology from well hydraulics to flow system analysis. He developed a profile model for regional groundwater flow with specified heads along a linear water table (Tóth, 1962; Box 4.3); later he used a sinusoidal function (Tóth, 1963) to specify heads along the water table. The latter model produced a distinctive pattern of nested local, intermediate and regional flow cells (Fig. B4.6.1). Diagrams like Fig. B4.6.1 became icons for regional groundwater flow (Tóth, 2005).

Nested flow cells, however, are not present when the water table is controlled by recharge (Fig. B4.6.2; also see Haitjema and Mitchell-Bruker, 2005). Moreover, most practical problems in applied groundwater modeling involve recharge driven flow as can be demonstrated using a dimensionless parameter,  $h_D/d$

$$\frac{h_D}{d} = \frac{R}{K} \frac{L^2}{8bd} \quad (\text{B4.6.1})$$

developed by Haitjema and Mitchell-Bruker (2005) from the parameter grouping in Eqn (B3.2.4) (Box 3.2). Equation (B4.6.1) is used to help determine conditions under which the water table is controlled by topography versus recharge. In Eqn (B4.6.1),  $h_D$  is the head at

(Continued)

### Box 4.6 What Controls the Water Table?—cont'd

the groundwater divide for 1D flow in an unconfined aquifer bounded by two streams separated by a distance  $L$ ;  $d$  represents the terrain rise above a horizontal datum (Fig. B4.6.3);  $R$  is recharge rate;  $K$  is hydraulic conductivity; and  $b$  is thickness as shown in Fig. B4.6.3. When  $h_D$  is approximately equal to  $d$  (i.e.,  $h_D/d \cong 1$ ) the water table is not completely controlled by either topography or recharge. When  $h_D/d > 1$ , the water table intersects the land surface and is controlled by topography. Under such topography-driven flow, the water table is controlled by recharge under topographic highs and by discharge to topographic lows. When  $h_D/d < 1$ , the water table is controlled by recharge.

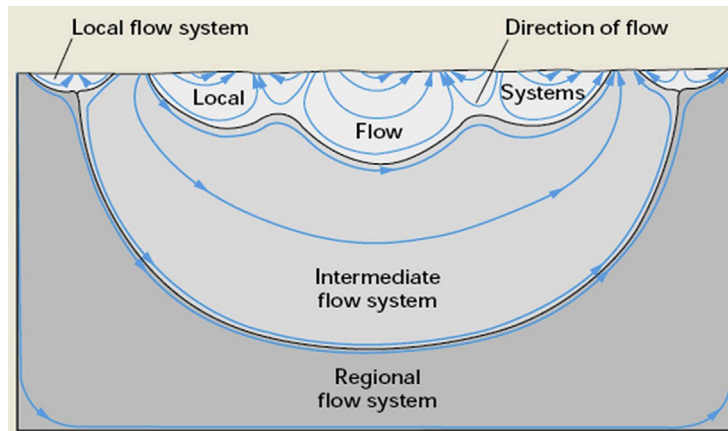


**Figure B4.6.1** Schematic diagram of a regional flow system when the water table is controlled by topography, based on Tóth's (1963) profile model. A sinusoidal specified head condition, intended to mimic topography, was imposed at the water table. The model simulates nested local, intermediate, and regional flow cells (Winter et al., 1998).

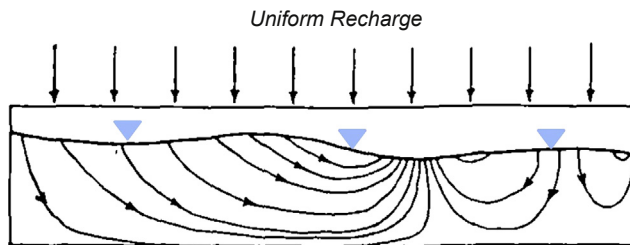


**Figure B4.6.2** Water table controlled by recharge in a 2D profile model. The water table was specified using heads determined from a Hele-Shaw analog model (Section 1.2) in which uniform recharge was infiltrated at a sinusoidal land surface. The water table does not follow the sinusoidal function of the land surface and nested flow cells are not present (modified from Shahbazi et al., 1968).

### Box 4.6 What Controls the Water Table?—cont'd

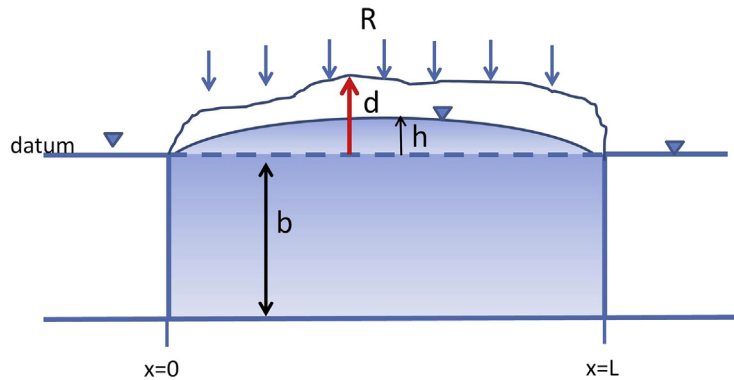


**Figure B4.6.3** Conceptual model of one-dimensional flow under the D-F approximation in an unconfined aquifer under uniform recharge,  $R$ . The maximum terrain rise,  $d$ , is the largest vertical distance between the datum (defined by the heads at the boundaries) and the land surface. The vertical scale is greatly exaggerated for purposes of illustration.

For Tóth's (1963) profile model  $h_D/d = 40$  (calculated from Eqn (B4.6.1) with  $L/b = 4$ ,  $L/d = 400$ ,  $R/K = 0.2$ ; Haitjema and Mitchell-Bruker, 2005), which means that, as expected, the water table is controlled by topography. In the Tóth model, where  $R/K = 0.2$ , low hydraulic conductivity material is subjected to high recharge. In hydrogeologic settings with more permeable hydrostratigraphic units,  $h_D/d$  is usually less than 1 and the groundwater system is recharge controlled. This follows from the observation that  $R/K$  is commonly in the range  $10^{-6}$  to  $10^{-3}$  in most field settings. For example,  $h_D/d$  is much less than 1 ( $=0.0088$ ) when  $R/K = 1.4 \times 10^{-6}$  (e.g.,  $K = 50$  m/d;  $R = 25.6$  mm/year = 10 inches/year);  $L/b = 100$  and  $L/d = 500$  (Haitjema and Mitchell-Bruker, 2005). The analysis of Haitjema and Mitchell-Bruker (2005) suggests that topography driven flow as shown in Fig. B4.6.1 is not commonly encountered in groundwater problems focused on aquifers rather than aquitards.

In most groundwater flow problems, water tables are better represented by specified flow boundary conditions rather than specified heads. Specified flow conditions allow the model to calculate the heads at the water table, are more likely to approximate the true flow to and from the water table, and are conceptually more appropriate for most aquifer systems. Topographic control of the water table occurs when a groundwater system is characterized by low hydraulic conductivity and high recharge, high vertical anisotropy, and/or deep flow systems where the ratio of system length,  $L$ , to saturated thickness,  $b$ , is small (e.g.,  $L/b = 4$  in Tóth's problem; also see Lemieux et al., 2008; Haitjema and Mitchell-Bruker, 2005). However, streambed morphology driven flow, a concept similar to topographically driven flow, can be effectively used to simulate groundwater flow in a hyporheic zone (the region below a streambed where surface water mixes with groundwater). In models of hyporheic flow, heads are specified along the top of the streambed, which forms the upper boundary of the groundwater model (e.g., Zlotnik et al., 2011).



## 4.6 COMMON MODELING ERRORS

- The modeler uses specified head and head dependent boundaries (HDBs) to represent surface water features but neglects to check whether the amount of water exchanged with the groundwater system is reasonable and consistent with the conceptual model. Specified head boundaries and HDBs (Box 4.5) may transfer unrealistic amounts of water into or out of the problem domain.
- A drain is used to simulate a surface water feature that has both gaining and losing reaches. Basic representation of a drain using an HDB does not allow water to enter the groundwater system and therefore the drain HDB cannot simulate loss of water from the drain.
- The modeler uses a 2D profile model to simulate pumping wells. A profile model assumes that there is no flow through the sides of the profile and therefore cannot simulate radial flow to a well. Pumping wells must be simulated using an axisymmetric profile model, a 2D areal model, or 3D model.
- A 2D profile model is not aligned along a groundwater flowpath. Profile models simulate flow only within the thickness of the profile and must be aligned with groundwater flow.
- The modeler selects equipotential lines to define hydraulic boundary conditions for a model designed to determine the long term impacts of pumping. Under field conditions, pumping may affect heads at the locations of the selected equipotential lines used to specify boundary conditions thereby invalidating the model's boundary conditions. Furthermore, specified head conditions based on equipotential lines provide the model with an unlimited supply of water and thereby may underestimate the impact of pumping by incorrectly keeping simulated drawdowns low.
- A model to determine the long-term impacts of pumping uses hydraulic boundary conditions defined by streamlines to set lateral no-flow boundaries. In the field, the effects of pumping may reach the hydraulic no-flow boundaries and inappropriately affect the expansion of the cone of depression, thereby causing simulated drawdowns that are too large.
- The water table is simulated using specified heads (Box 4.6). The model simulates unrealistic nested flow systems owing to unrealistic flows into and out of the water-table nodes.

## 4.7 PROBLEMS

Chapter 4 problems introduce boundary concepts and examine the effect of boundary assignment on modeling results. Some of the problems require a spreadsheet and/or a groundwater flow code (either FD or FE); some suggested codes are listed on the Web site for our book (<http://appliedgwmodeling.elsevier.com/>). Consult the code's

user's manual for specific instructions on implementing boundary conditions. Differences in boundary implementation in FD and FE approaches may cause small discrepancies in the solutions. In this chapter, we introduced pumping and injection wells to simulate boundary flows (Figs. 4.13(a), 4.14 and 4.15) and also mentioned that an internal specified flow boundary condition can represent a pumping or injection well (Section 4.3) as in Problem P4.4. Section 6.2 provides more information on wells as internal sinks.

**P4.1** Representation of no-flow and specified head boundaries in an FD grid is illustrated using a spreadsheet to simulate 2D steady-state groundwater flow in the isotropic and homogeneous aquifer shown in Figs. B4.3.1 and B4.3.2 in Box 4.3. We will solve different versions of this problem using block-centered and point-centered FD grids. The top boundary of the model is the water table, which is specified using the equation given in Fig. B4.3.2 (Box 4.3). No-flow boundaries are implemented using Eqn (B4.3.2) in Box 4.3 by incorporating ghost nodes as explained in Box 4.3. For example, along the left hand side no-flow boundary of the block-centered grid in Fig. B4.3.3 (Box 4.3) the head at ghost node A5 is set equal to the calculated head at B5; the no-flow boundary is located half-way between nodes A5 and B5. The FD equations for the block-centered grid, as implemented in the spreadsheet, are shown in Fig. B4.3.3(b) (Box 4.3). The five-point star operator (Section 3.5), shown in Fig. P4.1(a), is modified for nodes along the left hand side boundary (Fig. P4.1(b), (c)).

- a. Use a spreadsheet model to solve the FD equations for heads in a block-centered grid as given in Fig. B4.3.3(a), (b) (Box 4.3). To solve the spreadsheet in Excel<sup>®</sup>, go to: tools>options>calculations and check manual; also check the iteration box. Press F9 to begin the calculation. Use at least 1000 iterations and an error tolerance of 1E-4m. Also include a water budget calculation. Check your solution against the solution in Fig. B4.3.3(c) (Box 4.3). Draw equipotential lines (using a contour interval of 1 m) and construct flowlines on a properly scaled figure.

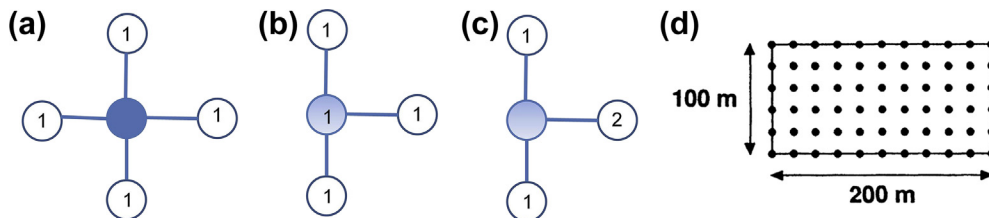


**Figure P4.1** (a) The five-point star computational module for an interior node (filled circle) in a two-dimensional FD grid. The numbers refer to the weighting of heads in the FD equation (Eqn (B4.3.2) in Box 4.3). (b) The computational module for a boundary node (shaded) in a block-centered FD grid; the no-flow boundary is to the left of the node. The head at the ghost node at  $i-1,j$  (not shown) equals the head at  $i,j$ . (c) The computational module for a boundary node (shaded) in a point-centered FD grid; the no-flow boundary is directly on the node. The head at the ghost node at  $i-1,j$  (not shown) equals the head at  $i+1,j$ . (d) Point-centered FD grid for the profile model in Box 4.3.

- b. Use a point-centered grid with 11 columns and 6 rows (Fig. P4.1(d)). Because no-flow boundaries are placed differently in a point-centered grid, the geometry of the problem domain is different (Fig. P4.1(d)) from the block-centered grid (Fig. B4.3.3(a) in Box 4.3) and the FD equations along the boundaries are also different. (Hint: Write the FD equations at the left hand side no-flow boundary of the point-centered grid using the computational module shown in Fig. P4.1(c). Construct analogous computational modules for the right hand side and bottom boundaries.)
- c. Solve the problem again using a standard FD code (e.g., MODFLOW) and an FE code (e.g., FEFLOW). Since this is the first problem requiring the use of an FD or FE code, you should test the assignment of values for solver closure criteria and assess solution convergence prior to reporting results (Section 3.7). Compare your solutions with those in parts a and b.

**P4.2** In this problem, we will construct a profile model to compute groundwater flow under a dam and solve the model using either an FD or FE code. An impermeable concrete dam 60 m long and 40 m wide is constructed over an isotropic and homogeneous silty sand ( $K = 10$  m/d) that is 26.5 m thick and fills a river valley underlain by impermeable bedrock (Fig. P4.2). The depth of the reservoir pool is 30 m and the tail water stream elevation below the dam is 10 m. The cross-sectional area of interest is 200 m long centered on the dam. As you formulate your numerical model think carefully about how to represent boundary conditions. Test values for solver closure criteria and assess solution convergence prior to reporting results (Section 3.7).

- a. Whenever possible, simulated results should be checked against some independent calculation. In this case, you can solve the problem graphically using a flow net (Boxes 5.2 and 8.2). Take the dimensions from the Figure and produce a scaled drawing of the profile without vertical exaggeration. Create a

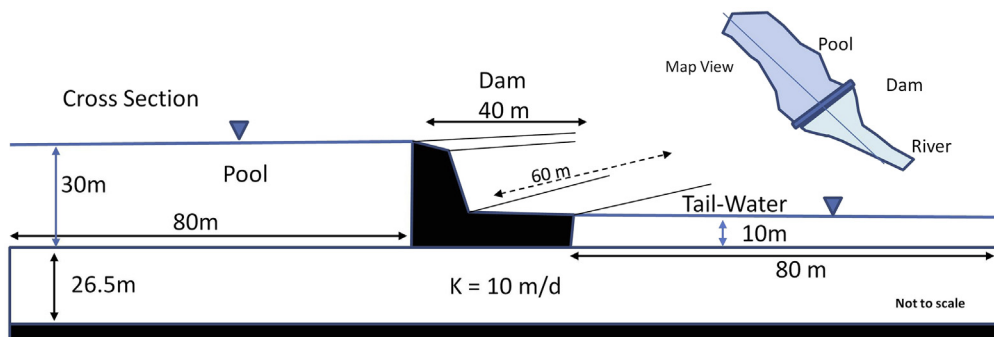


**Figure P4.2** Cross section of an aquifer with overlying dam and reservoir. The inset shows the dam in map view; the line shows the approximate location of the cross section.

flow net with curvilinear squares (see Fig. B5.2.1(a) in Box 5.2) and compute groundwater seepage per unit width under the dam (see Box 8.2).

- b.** Construct a numerical model; assign side boundaries of the profile model at  $x = 0$  and  $x = 200$  m. Use the model to calculate heads and the groundwater flow rate per unit width of the dam (from the calculated water budget).
  - c.** Compare and contrast the graphical solution in part (a) with the numerical solution in part (b) for both heads and flow. If the solutions are significantly different, there is an error in one or both solutions. Correct the error(s) and recomputed heads and seepage per unit width of the dam.
  - d.** Suppose the porous material below the dam is anisotropic so that  $K_x = 10K_z$ . Run the numerical model again but this time include anisotropy. Compute groundwater seepage per unit width of the dam. Why is the seepage rate different from the solution for isotropic and homogeneous conditions? (You can also construct a graphical solution for this problem using a transformed section. See Box 5.2.)
- P4.3** The town of Hubbertville is planning to expand its water supply by constructing a pumping well in an unconfined gravel aquifer (Fig. P4.3). The well is designed to pump constantly at a rate of 20,000 m<sup>3</sup>/day. Well construction was halted by the State Fish and Game Service who manage the Green Swamp Conservation area. The agency claimed that pumping would “significantly reduce” groundwater discharge to the swamp and damage waterfowl habitat. The town claimed the fully penetrating river boundary to the north and the groundwater divide located near the center of the valley would prevent any change in flow to the swamp.
- a.** Construct a 2D areal steady-state model of the aquifer between the river and swamp for conditions prior to pumping using the information in Fig. P4.3. Represent the river and swamp boundaries as constant head boundaries with head set at 1000 m. The side boundaries are no-flow boundaries. Justify this assignment of boundary conditions. Use a constant nodal spacing of 500 m. Run the model and produce a contour map of heads. Draw the water-table profile in a north-south cross section and label the simulated groundwater divide between the river and the swamp. Compute the discharge to Green Swamp.
  - b.** Using the steady-state heads derived in (a), locate the groundwater divide in the central portion of the valley. Run the model using first a no-flow boundary and then a specified head boundary at the location of the groundwater divide. Compare results with those in part (a). Compute the discharge to Green Swamp under each representation. What is the effect of assigning an internal boundary?
  - c.** Run the model in part (a) again but this time use a HDB to represent the river. The stage of the river is 1000 m and the width is 500 m. The vertical hydraulic

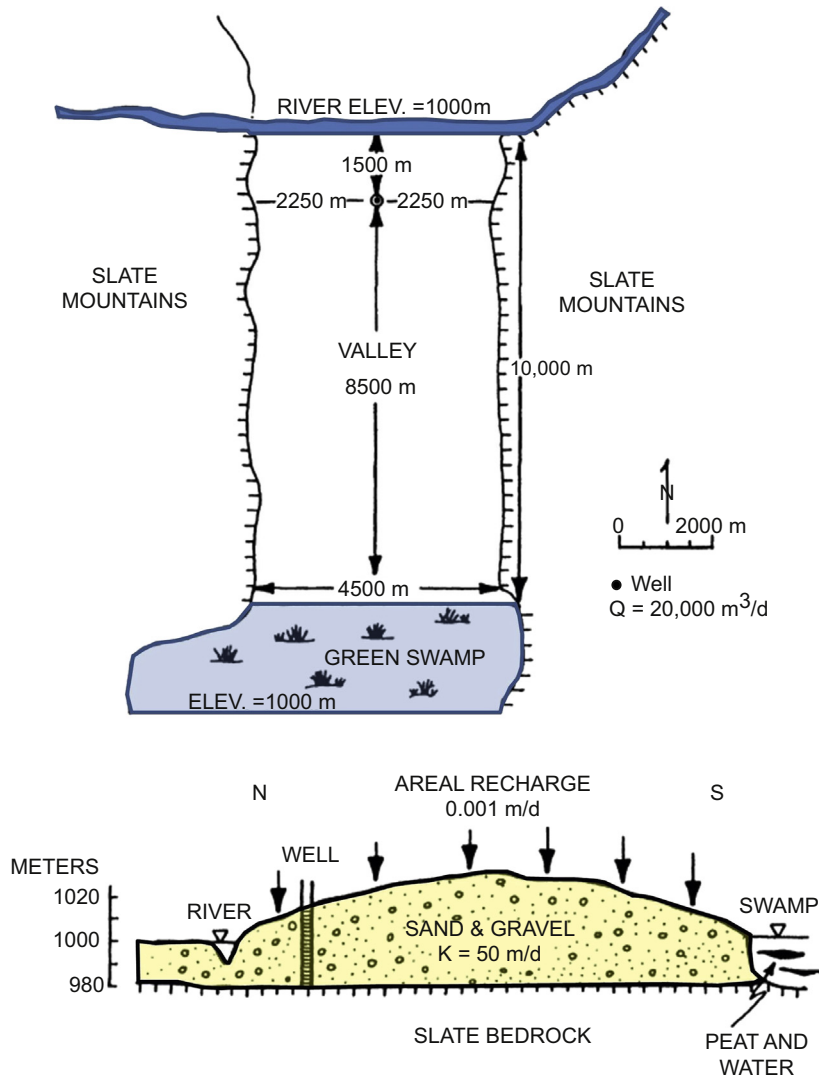


**Figure P4.3** Map and cross section of the aquifer adjoining the Green Swamp. Location of a proposed fully penetrating pumping well 1500 m from the river is also shown.

conductivity of the riverbed sediments is 5 m/day and the thickness of the sediments is 1 m. The elevation of the bottom of the sediments is 995 m. Compare results with those in part (a).

- d.** Run the model in part (c) again but this time assume the width of the river is 5 m. What is the effect of reducing the width of the river?

**P4.4** Return to the model you designed for Problem P4.3 and place a well at the location indicated in Fig. P4.3. Pump the well at a constant rate of  $20,000 \text{ m}^3/\text{day}$ .

Run the model under steady-state pumping conditions three times under each of the following three representations of model boundaries: (1) physical boundaries shown in Fig. P4.3; (2) an internal no-flow boundary at the groundwater divide between the river and the swamp; the location of the divide is determined from the solution of Problem P4.3; (3) an internal specified head boundary at the groundwater divide between the river and the swamp; the location of the divide is determined from the solution of Problem P4.3.

- a. Discuss the effects of the internal boundary conditions imposed on the groundwater divide on the resulting head distributions. Compare north-south water-table profiles drawn through the node representing the pumping well for the three pumping simulations. Compute the discharge to the Green Swamp under each set of boundary conditions.
  - b. Compare groundwater discharge to the swamp under the prepumping scenario in Problem P4.3 with the results under the pumping scenarios. In light of the modeling results, consider what might be meant by “significantly reduced” as used by the state agency (see discussion in Problem P4.3). Make a list of physical, geochemical and ecological conditions that potentially could be affected by a change in groundwater flow to the Green Swamp.
- P4.5** Replace the constant head boundaries at both the river and swamp in Problem P4.3a with specified flow boundaries. Use the water balance results from Problem P4.3a to calculate the boundary fluxes at the river and swamp. Note that all the boundaries of the model are now specified flow boundaries, including the zero flow lateral boundary conditions.
- a. Run the model with specified flow boundaries using starting heads of 1000 m and then a second time with starting heads of 2000 m. (Note: Some GUIs will warn that using all specified flow boundaries can create errors, or will not permit the model to execute under these conditions.) Compare the results with those in Problem P4.3a and explain the differences.
  - b. Take one of the models you designed in part (a) and replace one constant flux node on either the river or swamp boundary with a specified head node equal to 1000 m. Run the model to steady state. Compare the results with those in part (a) and with results from Problem P4.3a. Explain the differences.
- P4.6** It is often tempting to define boundaries of an areally extensive aquifer using hydraulic no-flow boundary conditions placed at some distance from the area of interest. The two no-flow boundaries (streamlines) define a flow tube (or under special conditions, a streamtube; see Fig. B8.2.1 in Box 8.2). One way to determine if this boundary assignment will adversely affect the modeling results is to replace the no-flow boundaries with specified heads. If flow occurs to or from these specified head nodes, the assignment of no-flow boundaries is not appropriate. This method can be illustrated using the Green Swamp problem. Let us assume that the Slate

Mountains do not exist. Instead the no-flow boundaries define a 4500 m wide flow tube within a larger regional flow system.

- a. Replace the no-flow boundaries that delineate the flow tube in Fig. P4.3(a) with specified heads taken from the solution of Problem P4.3a. Run the model to check that it reproduces the steady-state heads of Problem P4.3a. Calculate the east–west fluxes at the flow tube boundaries and the discharge to the Green Swamp. Be sure your modeled area is 4500 m wide.
- b. Simulate the steady-state flow field with the pumping well using the specified head boundaries that define the flow tube. Examine flow to and from the specified head boundaries and compare them to the prepumping rates calculated in part (a). What is the discharge to Green Swamp? Are the hydraulic boundaries that define the flow tube sufficiently removed from the pumping well so that they act as no-flow boundaries? In other words is the flow to and from the specified head nodes along the flow tube boundaries sufficiently small so that there is effectively no flow from the side boundaries into the model domain under pumping conditions?

## REFERENCES

- Abtew, W., Melesse, A., 2012. *Evaporation and Evapotranspiration: Measurements and Estimation*. Springer Dordrecht. ISBN:10: 9400747365, 290 p.
- Anderson, M.P., Woessner, W.W., 1992. *Applied Groundwater Modeling: Simulation of Flow and Advective Transport*. Academic Press, 381 p.
- Ataie-Ashtiani, B., Volker, R.E., Lockington, D.A., 2001. Tidal effects on groundwater dynamics in unconfined aquifers. *Hydrological Processes* 15 (4), 655–669. <http://dx.doi.org/10.1002/hyp.183>.
- Bair, E.S., Lahm, T.D., 2006. *Practical Problems in Groundwater Hydrology: Problem-based Learning Using Excel® Worksheets*. Pearson, Prentice Hall, Upper Saddle River, New Jersey (reference book and CD).
- Bakker, M., Schaars, F., 2013. Modeling steady sea water intrusion with single-density groundwater codes. *Groundwater* 51 (1), 135–144. <http://dx.doi.org/10.1111/j.1745-6584.2012.00955.x> (Erratum: *Groundwater* 51(4), 651).
- Bakker, M., Schaars, F., Hughes, J.D., Langevin, C.D., Dausman, A.M., 2013. Documentation of the Seawater Intrusion (SWI2) Package for MODFLOW. U.S. Geological Survey Techniques and Methods 6-A46, 47 p. <http://pubs.er.usgs.gov/publication/tm6A46>.
- Banta, E.R., 2000. MODFLOW-2000, the U.S. Geological Survey Modular Ground-water Model—documentation of Packages for Simulating Evapotranspiration with a Segmented function (ETS1) and Drains with Return Flow (DRT1). U.S. Geological Survey Open-File Report 00-466, 127 p. <http://pubs.er.usgs.gov/publication/ofr00466>.
- Barlow, P.M., 2003. *Ground Water in Freshwater-saltwater Environments of the Atlantic Coast*. U.S. Geological Survey Circular 1262, 113 p. <http://pubs.usgs.gov/circ/2003/circ1262/>.
- Batelaan, O., De Smedt, F., 2004. SEEPAGE, a new MODFLOW drain package. *Groundwater* 42 (4), 576–588. <http://dx.doi.org/10.1111/j.1745-6584.2004.tb02626.x>.
- Bear, J., Cheng, A.H.-D., 2010. Modeling groundwater flow and contaminant transport. In: *Series: Theory and Applications of Transport in Porous Media*, vol. 23. Springer, 834 p.
- Bedekar, V., Niswonger, R.G., Kipp, K., Panday, S., Tonkin, M., 2012. Approaches to the simulation of unconfined flow and perched groundwater flow in MODFLOW. *Groundwater* 50 (2), 187–198. <http://dx.doi.org/10.1111/j.1745-6584.2011.00829.x>.
- Bense, V.F., Person, M.A., 2006. Faults as conduit-barrier systems to fluid flow in siliciclastic sedimentary aquifers. *Water Resources Research* 42 (5), W05421. <http://dx.doi.org/10.1029/2005WR004480>.

- Bredehoeft, J.D., Pinder, G.F., 1970. Digital analysis of area flow in multiaquifer groundwater systems: A quasi three-dimensional model. *Water Resources Research* 6 (3), 883–888. <http://dx.doi.org/10.1029/WR006i003p00883>.
- Bruggeman, G.A.(Ed.), 1999. Analytical Solutions of Geohydrological Problems. In: *Developments in Water Science*, vol. 46. Elsevier, Amsterdam, 959 p.
- Buxton, H., Reilly, T.E., 1986. A Technique for Analysis of Ground-water Systems at Regional and Sub-regional Scales Applied on Long Island, New York. U.S. Geological Survey Water Supply Paper 2310, pp. 129–142. <http://pubs.er.usgs.gov/publication/wsp2310>.
- Caine, J.S., Evans, J.P., Forster, C.B., 1996. Fault zone architecture and permeability structure. *Geology* 24 (11), 1025–1028. <http://geology.gsapubs.org/content/24/11/1025.abstract>.
- Caine, J.S., Minor, S.A., 2009. Structural and geochemical characteristics of faulted sediments and inferences on the role of water in deformation, Rio Grande Rift, New Mexico. *Geological Society of America Bulletin* 121 (9–10), 1325–1340. <http://dx.doi.org/10.1130/B26164.1>.
- Cardenas, M.B., 2008. Surface-ground water interface geomorphology leads to scaling of residence times. *Geophysical Research Letters* 35 (8), L08402. <http://onlinelibrary.wiley.com/doi/10.1029/2008GL033753/full>.
- Clarke, J.S., West, C.T., 1998. Simulation of Ground-water Flow and Stream-aquifer Relations in the Vicinity of the Savannah River Site, Georgia and South Carolina, Predevelopment through 1992. U.S. Geological Survey Water-Resources Investigations Report 98–4062, 135 p. <http://pubs.er.usgs.gov/publication/wri984062>.
- Clemo, T., 2005. Improved water table dynamics in MODFLOW. *Groundwater* 43 (2), 270–273. <http://dx.doi.org/10.1111/j.1745-6584.2005.0021.x>.
- Cooley, R.L., 1983. Some new procedures for numerical solution of variably saturated flow problems. *Water Resources Research* 19 (5), 1271–1285. <http://dx.doi.org/10.1029/WR019i005p01271>.
- Diersch, H.-J.G., 2014. *FEFLOW: Finite Element Modeling of Flow, Mass and Heat Transport in Porous and Fractured Media*. Springer, 996 p.
- Doherty, J., 2001. Improved calculations for dewatered cells in MODFLOW. *Groundwater* 39 (6), 863–869. <http://dx.doi.org/10.1111/j.1745-6584.2001.tb02474.x>.
- Dupuit, J., 1863. *Études théoriques et pratiques sur le mouvement des eaux dans les canaux découverts et à travers les terrains perméables*. Dunod, Paris.
- Feinstein, D.T., Dunning, C.P., Hunt, R.J., Krohelski, J.T., 2003. Stepwise use of GFLOW and MODFLOW to determine relative importance of shallow and deep receptors. *Groundwater* 41 (2), 190–199. <http://dx.doi.org/10.1111/j.1745-6584.2003.tb02582.x>.
- Feinstein, D.T., Dunning, C.P., Juckem, P.F., Hunt, R.J., 2010. Application of the Local Grid Refinement Package to an Inset Model Simulating the Interactions of Lakes, Wells, and Shallow Groundwater, Northwestern Waukesha County, Wisconsin. U.S. Geological Survey Scientific Investigations Report 2010–5214, 30 p. <http://pubs.usgs.gov/sir/2010/5214/>.
- Fipps, G., Skaggs, R.W., Nieber, J.L., 1986. Drains as a boundary condition in finite elements. *Water Resources Research* 22 (11), 1613–1621. <http://dx.doi.org/10.1029/WR022i011p01613>.
- Fitts, C.R., 2013. *Groundwater Science*, second ed. Academic Press, London. 672 p.
- Fitts, C.R., Godwin, J., Feiner, K., McLane, C., Mullendore, S., 2015. Analytic element modeling of steady interface flow in multilayer aquifers using AnAqSim. *Groundwater* 55 (3), 432–439. <http://dx.doi.org/10.1111/gwat.12225>.
- Forchheimer, P., 1886. Ueber die Ergiebigkeit von Brunnen-Anlagen und Sickerschlitzten. *Zeitschrift des Architekten- und Ingenieur-Vereins zu Hannover* 32, 539–563.
- Forchheimer, P., 1898. Grundwasserspiegel bei brunnenanlagen. *Zeitschrift des österreichischen Ingenieur- und Architekten Vereins* 44, 629–635.
- Freeze, R.A., Witherspoon, P.A., 1967. Theoretical analysis of regional ground-water flow: 2. Effect of water table configuration and subsurface permeability variations. *Water Resources Research* 3 (2), 623–634. <http://dx.doi.org/10.1029/WR003i002p00623>.
- Gannett, M.W., Wagner, B.J., Lita Jr, K.E., 2012. Groundwater Simulation and Management Models for the Upper Klamath Basin, Oregon and California. U.S. Geological Survey Scientific Investigation Report 2012-5062, 92 p. <http://pubs.er.usgs.gov/publication/sir20125062>.
- Goyal, M.R.G., Harmsen, E.W., 2013. *Evapotranspiration: Principles and applications for water management*. CRC Press, Boca Raton, FL. ISBN:10: 1926895584, 628 p.



- Grannemann, N.G., Hunt, R.J., Nicholas, J.R., Reilly, T.E., Winter, T.C., 2000. The importance of ground water in the Great Lakes Region. U.S. Geological Survey Water Resources Investigations Report 00–4008, 14 p. <http://pubs.usgs.gov/wri/wri00-4008/>.
- Haitjema, H.M., 1995. Analytic Element Modeling of Groundwater Flow. Academic Press, Inc., San Diego, CA., 394 p.
- Haitjema, H.M., 2006. The role of hand calculations in ground water flow modeling. *Groundwater* 44 (6), 786–791. <http://dx.doi.org/10.1111/j.1745-6584.2006.00189.x>.
- Haitjema, H.M., 2007. Freshwater and Salt Water Interface Flow in GFLOW. GFLOW documentation. <http://www.haitjema.com/documents/FreshwaterandsaltwaterinterfaceflowinGFLOW.pdf>.
- Haitjema, H.M., Mitchell-Bruker, S., 2005. Are water tables a subdued replica of the topography? *Groundwater* 43 (6), 781–786. <http://dx.doi.org/10.1111/j.1745-6584.2005.00090.x>.
- Handman, E.H., Kilroy, K.C., 1997. Ground-water Resources of Northern Big Smoky Valley, Lander and Nye Counties, Central Nevada. U.S. Geological Survey Water Resources Investigations Report: 96–4311, 102 p. <http://pubs.er.usgs.gov/publication/wri964311>.
- Hoard, C.J., 2010. Implementation of Local Grid Refinement (LGR) for the Lake Michigan Basin Regional Groundwater–flow Model. U.S. Geological Survey Scientific Investigations Report 2010–5117, 25 p. <http://pubs.er.usgs.gov/publication/sir20105117>.
- Hsieh, P.A., 2001. TopoDrive and ParticleFlow—Two Computer Models for Simulation and Visualization of Ground–water Flow and Transport of Fluid Particles in Two Dimensions. U.S. Geological Survey Open-File Report 01–286, 30 p. <http://pubs.er.usgs.gov/publication/of01286>.
- Hunt, R.A., Anderson, M.P., Kelson, V.A., 1998. Improving a complex finite difference groundwater–flow model through the use of an analytic element model. *Groundwater* 36 (6), 1011–1017. <http://dx.doi.org/10.1111/j.1745-6584.1998.tb02108.x>.
- Hunt, R.J., Feinstein, D.T., 2012. MODFLOW–NWT – robust handling of dry cells using a Newton Formulation of MODFLOW–2005. *Groundwater* 50 (5), 659–663. <http://dx.doi.org/10.1111/j.1745-6584.2012.00976.x>.
- Jeanne, P., Guglielmi, Y., Cappa, F., 2013. Hydromechanical heterogeneities of a mature fault zone: Impacts on fluid flow. *Groundwater* 51 (6), 880–892. <http://dx.doi.org/10.1111/gwat.12017>.
- Juckem, P.F., Hunt, R.J., Anderson, M.P., 2006. Scale effects of hydrostratigraphy and recharge zonation on baseflow. *Groundwater* 44 (3), 362–370. <http://dx.doi.org/10.1111/j.1745-6584.2005.00136.x>.
- Keller, C.K., VanderKamp, G., Cherry, J.A., 1989. A multiscale study of the permeability of a thick clayey till. *Water Resources Research* 25 (11), 2299–2318. <http://dx.doi.org/10.1029/WR025i011p02299>.
- Kendy, E., Bradbury, K.R., 1988. Hydrogeology of the Wisconsin River Valley in Marathon County, Wisconsin. Wisconsin Geological and Natural History Survey, Information Circular 64, 66 p.
- Kipp Jr, K.L., 1987. HST3D: A Computer Code for Simulation of Heat and Solute Transport in Three-dimensional Ground–water Flow Systems. U.S. Geological Survey Water–Resources Investigations Report 86–4095, 517 p. <http://pubs.er.usgs.gov/publication/wri864095>.
- Kirkham, D., 1967. Explanation of paradoxes in Dupuit–Forchheimer seepage theory. *Water Resources Research* 3 (2), 609–622. <http://dx.doi.org/10.1029/WR003i002p00609>.
- Land, L.F., 1977. Utilizing a digital model to determine the hydraulic properties of a layered aquifer. *Groundwater* 15 (2), 153–159. <http://dx.doi.org/10.1111/j.1745-6584.1977.tb03160.x>.
- Langevin, C.D., 2008. Modeling axisymmetric flow and transport. *Groundwater* 46 (4), 579–590. <http://dx.doi.org/10.1111/j.1745-6584.2008.00445.x>.
- Leake, S.A., Claar, D.V., 1999. Procedure and Computer Programs for Telescopic Mesh Refinement Using MODFLOW. U.S. Geological Survey Open-File Report 99–238, 53 p. <http://pubs.er.usgs.gov/publication/of99238>.
- Lemieux, J.-M., Sudicky, E.A., Peltier, W.R., Tarasov, L., 2008. Simulating the impact of glaciations on continental groundwater flow systems: 2. Model application to the Wisconsinian glaciation over the Canadian landscape. *Journal of Geophysical Research* 113 (F3), F03018. <http://dx.doi.org/10.1029/2007JF000929>.
- Lott, R.B., Hunt, R.J., 2001. Estimating evapotranspiration in natural and constructed wetlands. *Wetlands* 21 (4), 614–628. [http://dx.doi.org/10.1672/0277-5212\(2001\)021\[0614:EEINAC\]2.0.CO;2](http://dx.doi.org/10.1672/0277-5212(2001)021[0614:EEINAC]2.0.CO;2).
- McDonald, M.G., Harbaugh, A.W., 1988. A Modular Three-dimensional Finite-Difference Ground–water Flow Model. U.S. Geological Survey Techniques of Water–Resources Investigations 06–A1, 576 p. <http://pubs.er.usgs.gov/publication/twri06A1>.

- McLane, C., 2012. AnAqSim: Analytic element modeling software for multi-aquifer, transient flow. *Groundwater* 50 (1), 2–7. <http://dx.doi.org/10.1111/j.1745-6584.2011.00892.x>.
- Mehl, S.W., Hill, M.C., 2006. MODFLOW-2005, the U.S. Geological Survey Modular Ground-water Model—Documentation of Shared Node Local Grid Refinement (LGR) and the Boundary Flow and Head (BFH) Package. U.S. Geological Survey Techniques and Methods 6–A12, 78 p. <http://pubs.er.usgs.gov/publication/tm6A12>.
- Mitchell-Bruker, S., Haitjema, H.M., 1996. Modeling steady state conjunctive groundwater and surface water flow with analytic elements. *Water Resources Research* 32 (9), 2725–2732. <http://dx.doi.org/10.1029/96WR00900>.
- Mitten, H.T., Lines, G.C., Berenbrock, C., Durbin, T.J., 1988. Water Resources of Borrego Valley and Vicinity, San Diego County, California: Phase 2—Development of a Ground-water Flow Model. U.S. Geological Survey Water-Resources Investigation Report 87–4199, 27 p. <http://pubs.er.usgs.gov/publication/wri874199>.
- Moene, A.F., van Dam, J.C., 2014. Transport in the Atmosphere-vegetation-soil Continuum. Cambridge University Press, New York. ISBN:10: 0521195683, 458 p.
- Neuman, S.P., 1973. Saturated–unsaturated seepage by finite elements. *Journal of Hydraulics Division, American Society of Civil Engineers* 99 (Hy12), 2233–2250.
- Neuman, S.P., 1976. User's Guide for FREESURF I. Department of Hydrology and Water Resources, University of Arizona, Tuscon, Arizona, 22 p.
- Neuman, S.P., Witherspoon, P.A., 1971. Analysis of nonsteady flow with a free surface using the finite element method. *Water Resources Research* 7 (3), 611–623. <http://dx.doi.org/10.1029/WR007i003p00611>.
- Niswonger, R.G., Panday, S., Ibaraki, M., 2011. MODFLOW-NWT, a Newton Formulation for MODFLOW-2005. U.S. Geological Survey Techniques and Methods 6–A37, 44 p. <http://pubs.er.usgs.gov/publication/tm6A37>.
- Niswonger, R.G., Prudic, D.E., 2005. Documentation of the Streamflow-routing (SFR2) Package to Include Unsaturated Flow beneath Streams—A Modification to SFR1. U.S. Geological Survey Techniques and Methods 6–A13, 50 p. <http://pubs.er.usgs.gov/publication/tm6A13>.
- Painter, S., Başağaoğlu, H., Liu, A.G., 2008. Robust representation of dry cells in single-layer MODFLOW models. *Groundwater* 46 (6), 873–881. <http://dx.doi.org/10.1111/j.1745-6584.2008.00483.x>.
- Polubarinova-Kochina, P.Y., 1962. Theory of Groundwater Movement. Princeton University Press, Princeton, NJ (translated from the Russian original by J.M. Roger de Wiest) 613 p.
- Rawling, G.C., Goodwin, L.B., Wilson, J.L., 2001. Internal architecture, permeability structure, and hydrologic significance of contrasting fault-zone types. *Geology* 29 (1), 43–46. [http://dx.doi.org/10.1130/0091-7613\(2001\)029<0043:IAPSAH>2.0.CO;2](http://dx.doi.org/10.1130/0091-7613(2001)029<0043:IAPSAH>2.0.CO;2).
- Reilly, T.E., 1984. A Galerkin Finite-element Flow Model to Predict the Transient Response of a Radially Symmetric Aquifer. U.S. Geological Survey Water Supply Paper 2198, 33 p. <http://pubs.er.usgs.gov/publication/wsp2198>.
- Reilly, T.E., Harbaugh, A.W., 2004. Guidelines for Evaluating Ground-water Flow Models. U.S. Geological Survey Scientific Investigation Report 2004–5038, 30 p. <http://pubs.usgs.gov/sir/2004/5038/>. Errata: [http://pubs.usgs.gov/sir/2004/5038/errata\\_sheet/](http://pubs.usgs.gov/sir/2004/5038/errata_sheet/).
- Scholz, C.H., Anders, M.H., 1994. The permeability of faults. In: Hickman, S., Sibson, R., Bruhn, R. (Eds.), Proceedings of Workshop LXIII: The Mechanical Involvement of Fluids in Faulting, Red Book Conference. U.S. Geological Survey Open File Report 94–228, Menlo Park, CA, pp. 247–253. <http://pubs.usgs.gov/of/1994/0228/report.pdf>.
- Seaton, W.J., Burbey, T.J., 2006. Influence of ancient thrust faults on the hydrogeology of the Blue Ridge Province. *Groundwater* 43 (3), 301–313. <http://dx.doi.org/10.1111/j.1745-6584.2005.0026.x>.
- Shahbazi, M., Zand, S., Todd, D.K., 1968. Effect of topography on ground water flow, vol. 77. International Association of Scientific Hydrology (Proceedings, General Assembly of Bern 1967), pp. 314–319. <http://iahs.info/Publications-News/paper-search.do>.
- Sheets, R.A., Dumouchelle, D.H., Feinstein, D.T., 2005. Ground-water Modeling of Pumping Effects Near Regional Ground-water Divides and River/aquifer Systems - Results and Implications of Numerical Experiments. U.S. Geological Survey Scientific Investigations Report 2005–5141, 31 p. <http://pubs.er.usgs.gov/publication/sir20055141>.
- Sheets, R.A., Hill, M.C., Haitjema, H.M., Provost, A.M., Masterson, J.P., 2015. Simulation of water-table aquifers using specified saturated thickness. *Groundwater* 53 (1), 151–157. <http://dx.doi.org/10.1111/gwat.12164>.

- Stoertz, M.W., Bradbury, K.R., 1989. Mapping recharge areas using a ground-water flow model — A case study. *Groundwater* 27 (2), 220–229. <http://dx.doi.org/10.1111/j.1745-6584.1989.tb00443.x>.
- Strack, O.D.L., 1976. A single-potential solution for regional interface problems in coastal aquifers. *Water Resources Research* 12 (6), 1165–1174. <http://dx.doi.org/10.1029/WR012i006p01165>.
- Strack, O.D.L., 1984. Three-dimensional streamlines in Dupuit-Forchheimer models. *Water Resources Research* 20 (7), 812–822. <http://dx.doi.org/10.1029/WR020i007p00812>.
- Streltsova, T.D., 1976. Analysis of aquifer-aquitard flow. *Water Resources Research* 12 (3), 415–422. <http://dx.doi.org/10.1029/WR012i003p00415>.
- Tóth, J., 1962. A theory of groundwater motion in small drainage basins in Central Alberta, Canada. *Journal of Geophysical Research* 67 (11), 4375–4387. <http://dx.doi.org/10.1029/JZ067i011p04375>.
- Tóth, J., 1963. A theoretical analysis of groundwater flow in small drainage basins. *Journal of Geophysical Research* 68 (16), 4795–4812. <http://dx.doi.org/10.1029/JZ068i016p04795>.
- Tóth, J., 2005. The Canadian school of hydrogeology: History and legacy. *Groundwater* 43 (4), 640–644. <http://dx.doi.org/10.1111/j.1745-6584.2005.0086.x>.
- Townley, L.R., 1990. AQUIFEM-n: A Multi-layered Finite Element Aquifer Flow Model, User's Manual and Description. CSIRO Division of Water Resources, Perth, Western Australia.
- Townley, L.R., Wilson, J.L., 1980. Description of an User's Manual for a Finite Element Aquifer Flow Model AQUIFEM-1, MIT Ralph M. Parsons Laboratory for Water Resources and Hydrodynamics. Technology Adaptation Program Report No. 79-3, 294 p.
- Trescott, P.C., Pinder, G.F., Larson, S.P., 1976. Finite-difference model for aquifer simulation in two dimensions with results of numerical experiments. U.S. Geological Survey Techniques of Water-Resources Investigations. Book 7, 116 p. <http://pubs.er.usgs.gov/publication/twri07C1>.
- Vilhelmsen, T.N., Christensen, S., Mehl, S.W., 2012. Evaluation of MODFLOW-LGR in connection with a synthetic regional-scale model. *Groundwater* 50 (1), 118–132. <http://dx.doi.org/10.1111/j.1745-6584.2011.00826.x>.
- Waller, R.M., 2013. Groundwater and the Rural Homeowner. U.S. Geological Survey, 38 p. [http://pubs.usgs.gov/gip/gw\\_ruralhomeowner/](http://pubs.usgs.gov/gip/gw_ruralhomeowner/).
- Wang, H.F., Anderson, M.P., 1982. Introduction to Groundwater Modeling: Finite Difference and Finite Element Methods. Academic Press, San Diego, CA., 237 p.
- Ward, D.S., Buss, D.R., Mercer, J.W., Hughes, S.S., 1987. Evaluation of a groundwater corrective action at the Chem-Dyne Hazardous Waste site using a telescopic mesh refinement modeling approach. *Water Resources Research* 23 (4), 603–617. <http://dx.doi.org/10.1029/WR023i004p00603>.
- Werner, A.D., Bakker, M., Post, V.E.A., Vandenbohede, A., Lu, C., Ataie-Ashiani, B., Simmons, C.T., Barry, D.A., 2013. Seawater intrusion processes, investigation and management: Recent advances and future challenges. *Advances in Water Resources* 51, 3–26. <http://dx.doi.org/10.1016/j.advwatres.2012.03.004>.
- Winter, T.C., 1976. Numerical Simulation Analysis of the Interaction of Lakes and Groundwater. U.S. Geological Survey Professional Paper 1001, 45 p. <http://pubs.er.usgs.gov/publication/pp1001>.
- Winter, T.C., Harvey, J.C., Franke, O.L., Alley, W.M., 1998. Groundwater and Surface Water, a Single Resource. U.S. Geological Survey Circular 1139, 79 p. <http://pubs.er.usgs.gov/publication/cir1139>.
- Woessner, W.W., 2000. Stream and fluvial plain ground water interactions: Rescaling hydrogeologic thought. *Groundwater* 38 (3), 423–429. <http://dx.doi.org/10.1111/j.1745-6584.2000.tb00228.x>.
- Yager, R.M., 1987. Simulation of Ground-water Flow Near the Nuclear-fuel Reprocessing Facility at the Western New York Nuclear Service Center, Cattaraugus County, New York. U.S. Geological Survey Water Resources Investigation Report 85–4308, 58 p. <http://pubs.er.usgs.gov/publication/wri854308>.
- Youngs, E.G., 1990. An examination of computed steady-state water-table heights in unconfined aquifers: Dupuit-Forchheimer estimates and exact analytical results. *Journal of Hydrology* 119 (1–4), 201–214. [http://dx.doi.org/10.1016/0022-1694\(90\)90043-W](http://dx.doi.org/10.1016/0022-1694(90)90043-W).
- Zaidel, J., Markham, B., Bleiker, D., 2010. Simulating seepage into mine shafts and tunnels with MODFLOW. *Groundwater* 48 (3), 390–400. <http://dx.doi.org/10.1111/j.1745-6584.2009.00659.x>.
- Zheng, C., Bradbury, K.R., Anderson, M.P., 1988. Role of interceptor ditches in limiting the spread of contaminants in ground water. *Groundwater* 26 (6), 734–742. <http://dx.doi.org/10.1111/j.1745-6584.1988.tb00424.x>.
- Zlotnik, V.A., Cardenas, M.B., Toundykov, D., 2011. Effects of multiscale anisotropy on basin and hyporheic groundwater flow. *Groundwater* 49 (4), 576–583. <http://dx.doi.org/10.1111/j.1745-6584.2010.00775.x>.
- Zlotnik, V.A., Toundykov, D., Cardenas, M.B., 2015. An analytical approach for flow analysis in aquifers with spatially varying top boundary. *Groundwater* 53 (2), 335–341. <http://dx.doi.org/10.1111/gwat.12205>.

## CHAPTER 5

# Spatial Discretization and Parameter Assignment

*I could be bounded in a nutshell and count myself a king of infinite space...*

*—Hamlet, Act II, Scene II*

### Contents

5.1	Discretizing Space	182
5.1.1	Orienting the Grid/Mesh	184
5.1.2	Finite-Difference Grid	184
5.1.2.1	Structured Grid	186
5.1.2.2	Unstructured Grid	191
5.1.3	Finite-Element Mesh	195
5.2	Horizontal Nodal Spacing	201
5.2.1	Solution Accuracy	202
5.2.2	Calibration Targets	202
5.2.3	Perimeter Boundary Configuration	203
5.2.4	Heterogeneity	203
5.2.5	Faults, Conduits, and Barriers	203
5.2.6	Internal Sources and Sinks	205
5.3	Model Layers	208
5.3.1	Vertical Discretization	209
5.3.2	Layer Types	214
5.3.3	Layer Elevations	215
5.3.4	Pinchouts and Faults	216
5.3.5	Dipping Hydrogeologic Units	217
5.4	Parameters	222
5.4.1	Material Property Parameters	223
5.4.1.1	Hydraulic Conductivity	223
5.4.1.2	Storage	227
5.4.1.3	Vertical Leakage, Resistance, and Conductance	229
5.4.1.4	Total Porosity and Effective Porosity	230
5.4.2	Hydrologic Parameters	230
5.4.2.1	Recharge	230
5.4.2.2	Pumping Rates	235
5.4.2.3	Evapotranspiration (ET)	235
5.5	Parameter Assignment	236
5.5.1	General Principles	236
5.5.2	Assigning Storage Parameters to Layers	237
5.5.3	Populating the Grid or Mesh	237

5.5.3.1 Zonation	238
5.5.3.2 Interpolation	238
5.5.3.3 Hybrid Approach	241
5.6 Parameter Uncertainty	241
5.7 Common Modeling Errors	243
5.8 Problems	244
References	249

## Boxes

Box 5.1 Numerical Error Inherent to Irregular FD Grids	190
Box 5.2 Vertical Anisotropy and the Transformed Section	200
Box 5.3 Upscaling Hydraulic Conductivity: Layered Heterogeneity and Vertical Anisotropy	211
Box 5.4 When Infiltration becomes Recharge	232

In previous chapters, we introduced the concept of discretizing a problem domain into nodes that define either cells/blocks in a finite-difference (FD) grid or elements in a finite-element (FE) mesh. This chapter focuses on spatial discretization and assignment of initial parameter values to the grid/mesh. Temporal discretization is discussed in Section 7.6.

## 5.1 DISCRETIZING SPACE

Designing the FD grid or FE mesh is one of the most important and difficult steps in model design. The number of nodes in the grid/mesh affects the accuracy of the solution, the computational time required to solve the model, and the amount of output that will be generated. A graphical user interface (GUI) (Section 3.6) or FE mesh generator is used to generate the grid/mesh but the modeler must input the nodal spacing and specify the type of element for an FE mesh. Some GUIs allow nodes to be added or subtracted after the grid/mesh is designed; however, re-design of the nodal network requires parameter values to be re-assigned and typically requires adjustment of boundary conditions. Therefore, it is wise to spend some time thinking about how best to design the grid/mesh to meet the modeling objective. Furthermore, the same grid/mesh will be used for all phases of the modeling project, potentially including calibration, particle tracking, and forecasting simulations. Therefore, it is important to plan ahead to make sure the grid/mesh will meet the objectives of all types of simulations to be performed during the modeling project.

In a numerical model, the problem domain is discretized using nodes and FD cells/blocks or finite elements (Figs. 3.4, 3.5, 3.10 and 4.11). The nodal network forms the computational framework of the numerical model and the nodal spacing determines the resolution of output inasmuch as heads are computed at nodes and must be interpolated between nodes. Although the terms mesh and grid are sometimes used interchangeably, we use *grid* when referring to an FD network of nodes and *mesh* when referring to an FE network. The conceptual model and location of perimeter boundaries determine

the overall dimensions of the horizontal grid/mesh. Areal two-dimensional (2D) models have only one layer defined by horizontal nodal spacing. Three-dimensional (3D) models have two or more layers but typically the horizontal nodal network is the same in all layers of the model. However, some codes allow the horizontal nodal network to vary by layer.

In general, an FE mesh provides more flexibility in discretizing the problem domain because a mesh can include triangular and/or quadrilateral (i.e., four-sided, not limited to but including rectangular) elements while standard FD grids require rectangular grids. Both grids and meshes can be structured or unstructured. In a *structured grid/mesh*, a node in 3D space is connected to at most six neighboring nodes (Fig. 5.1(a)) but in an *unstructured grid/mesh* there can be fewer or more than six connections (Fig. 5.1(b)) and the number of connections may vary from node to node. FD codes accommodate unstructured grids using the control volume finite-difference (CVFD) approach (Panday et al., 2013). Early FD methods that used this approach to form unstructured grids were called integrated finite differences (IFD). One of the earliest applications of a numerical model to a groundwater problem used an unstructured FD grid (Tyson and Weber, 1964; also see Narasimhan and Witherspoon, 1976). MODFLOW-USG, where USG stands for UnStructured Grid (Panday et al., 2013), is a recent example of a CVFD code that allows for an unstructured grid. For clarity, we distinguish between FD approaches that use CVFD, which allow for more flexible gridding via an unstructured grid, and traditional (standard) FD approaches that require a structured rectangular grid.

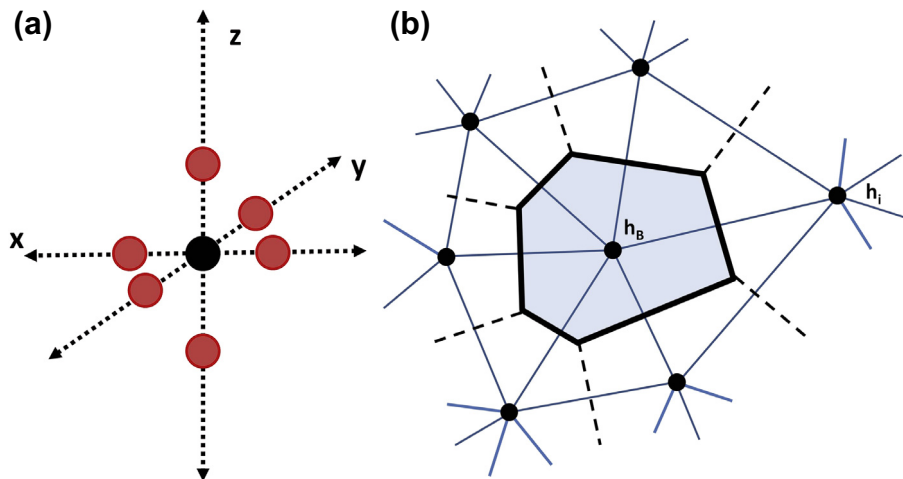


**Figure 5.1** Connections among nodes. (a) In a 3D structured grid or mesh, a node has, at most, six connections to neighboring nodes; in 2D there are a maximum of four connections (<http://doi.ieeecomputersociety.org/cms/Computer.org/dl/mags/cs/2012/03/figures/mcs20120300483.gif>). (b) A horizontal 2D unstructured FD grid where the central node is connected to six other nodes; in 3D this grid would have eight connections (modified from Tyson and Weber, 1964. This material may be downloaded for personal use only. Any other use requires prior permission of the American Society of Civil Engineers).

Discretization in the vertical direction is determined by the thickness of model layers, where each layer usually represents a hydrogeologic unit (Section 5.3). Therefore, in most numerical models the scale of discretization in the vertical direction is different from nodal spacing in the horizontal network of nodes. We defer discussion of vertical discretization to Section 5.3. Below we make some general comments about the 2D horizontal grid/mesh. Selection of horizontal nodal spacing is discussed in Section 5.2.

### 5.1.1 Orienting the Grid/Mesh

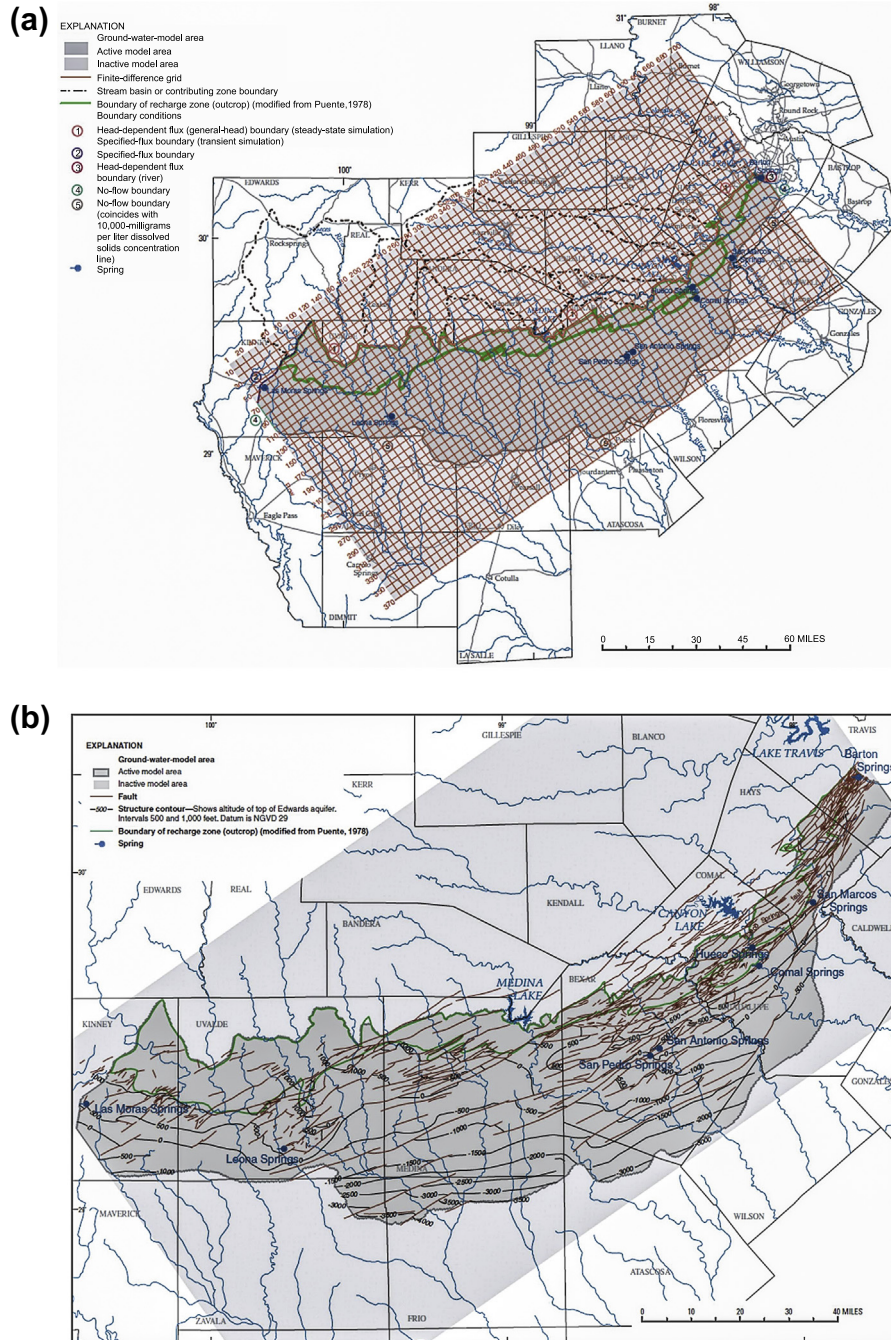
Ideally, the grid/mesh is oriented so that either the  $x$ - or  $y$ -coordinate axis is parallel to the principal direction of groundwater flow. Moreover, the coordinate axes should be co-linear with the principal directions of the hydraulic conductivity ( $K$ ) tensor (Box 3.1). The principal flow direction may be controlled by structural features such as faults and joint sets (Fig. 5.2), strike of the hydrogeologic units, or stratification (Fig. 5.3). When there is no one dominant flow direction, the grid/mesh is typically aligned with the projection used in the GIS or GUI that assembles the code's input files.

In the rare case, directions of anisotropy must be simulated as non-uniform, i.e., the principal directions of the  $K$  tensor change orientation in space so that it is not possible to align the global coordinate axes of the model co-linear with the principal directions of the  $K$  tensor (Fig. B3.1.1(b) in Box 3.1). For example, the problem of representing non-uniform anisotropy in models arises when simulating steeply dipping hydrogeologic units (Section 5.3). In such cases, the governing equation must be written to include the off-diagonal components of the  $K$  tensor (Eqn (B3.1.4) in Box 3.1) and that form of the governing equation is best solved using an FE code. FD codes, in theory, can be modified to handle non-uniform anisotropy and this is more easily done for the horizontal components of  $K$  (Anderman et al., 2002). Correcting for non-uniform vertical anisotropy is theoretically possible but in practice is difficult to program (Hoaglund and Pollard, 2003; Yager et al., 2009).

The FE method accommodates changes in directions of anisotropy more easily than the FD method (including CVFD) because each element is considered separately when assembling the coefficient matrix for an FE solution (Section 3.5) and in that way local coordinate axes within the element can be aligned with the local directions of the hydraulic conductivity tensor (see Fig. B3.1.1(b) in Box 3.1). Many, but not all, FE codes allow for non-uniformity in directions of anisotropy. In the FE code FEFLOW (Diersch, 2014) anisotropy can be aligned parallel to the global coordinate axes, parallel to dipping beds and geologic structures (e.g., as in Fig. 5.3), or parallel to local coordinate systems within elements, which is the most general case. The FE code SUTRA (Voss and Provost, 2002) also allows for the most general case of non-uniform anisotropy.

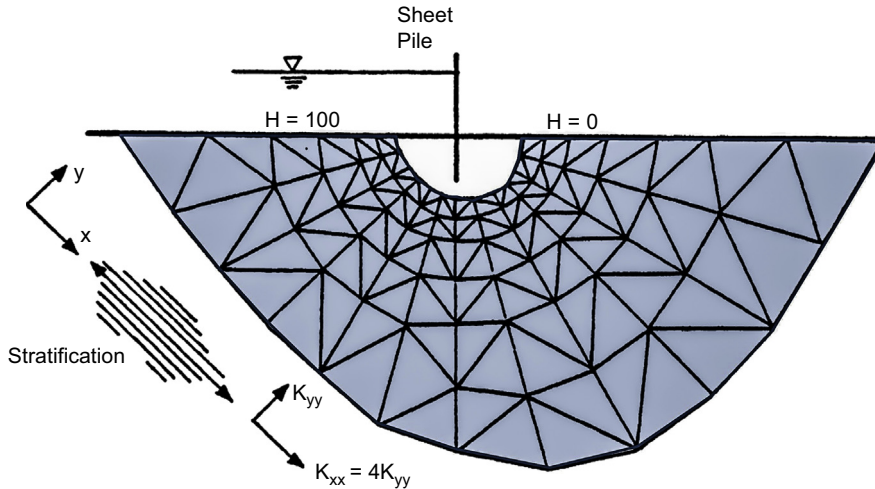
### 5.1.2 Finite-Difference Grid

A standard FD grid is rectangular and structured (Fig. 5.4(a) and (b)). An unstructured FD grid allows much more flexibility in grid design and provides much of the flexibility of an FE mesh.



**Figure 5.2** Orientation of an FD grid. (a) The FD grid for a model of the Edwards aquifer, Texas, USA, is oriented to align with northeast–southwest trending faults shown in (b). Note that the grid is larger than the problem domain defined by boundary conditions. Areas outside the boundaries contain inactive nodes (*Lindgren et al., 2004*).



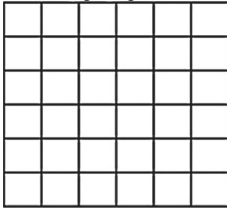
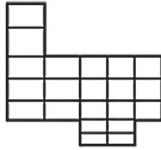
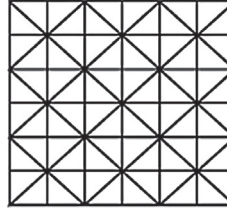
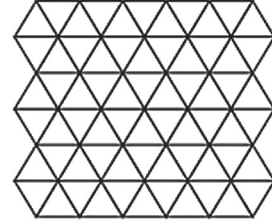
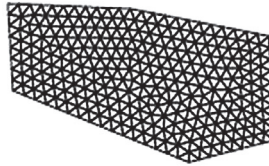
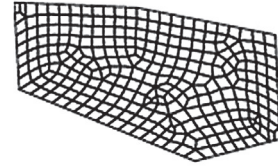
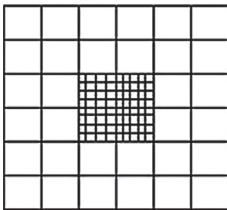
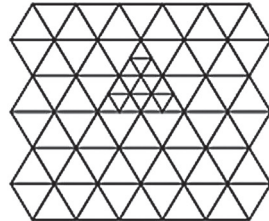
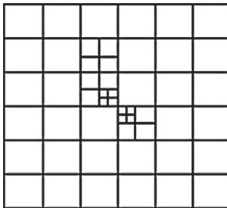
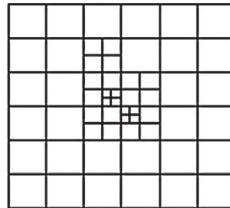


**Figure 5.3** Coordinate axes in an FE mesh are oriented to coincide with the principal components of the  $K$  tensor as shown by the stratification on the left. The detailed mesh near the sheet pile is not shown (modified from Townley and Wilson, 1980).

### 5.1.2.1 Structured Grid

A structured FD grid has rectangular cells/blocks (Figs. 4.11(b) and 3.4(c)) and can be *block centered* (Fig. 5.5(a) and 4.11(b)) or, less commonly, *point centered* (Fig. 5.5(b) and 4.11(c)). In a block-centered grid the grid lines form the edges of the cell and the nodes are centered in the cell but in a point-centered grid the grid lines pass through the nodes. In either case, the rectangular area around the node is the FD cell. The overall shape of a structured FD grid is rectangular but the groundwater system that defines the problem domain usually is not rectangular (Fig. 5.2); boundaries of the problem domain are represented within a larger rectangular area that represents the extent of the model domain (Fig. 5.2). Nodes within the model domain where the code computes values of head are *active nodes*, whereas nodes that fall outside the boundaries of the problem domain are *inactive nodes*. Inactive nodes are not part of the solution and the code does not calculate head values at those nodes (but they still take up storage space in the arrays used by the code).

In structured FD grids locations of nodes are identified using a row and column indexing convention in two dimensions and a row, column, and layer convention in three dimensions (Fig. 3.4). A 2D structured FD grid is generated by specifying arrays of values for  $\Delta x$  and  $\Delta y$  in the horizontal plane. The user should be alert to code-specific conventions for setting up the grid. For example, in MODFLOW the variable DELR ( $\Delta r$ ) represents horizontal nodal spacing between columns (equivalent to  $\Delta x$ ) while DELC ( $\Delta c$ ) represents horizontal spacing between rows (equivalent to  $\Delta y$ ). Nodes are designated using the  $i$  index for rows and  $j$  for columns (Section 3.5.1), so that the DELR array has one value for every column in the grid ( $\Delta r_j$ ) and DELC has a value for every row ( $\Delta c_i$ ) (Fig. 5.5). In a 3D model an array of  $\Delta z$  values may be input directly, or  $\Delta z$  can be calculated from top and bottom layer elevations.

**STRUCTURED GRIDS****A.** Rectangular grid**B.** Rectangular grid, irregular domain**C.** Triangular grid, isosceles triangles**D.** Triangular grid, equilateral triangles**D.** Hexagonal grid**F.** Warped triangular grid**G.** Warped quadrilateral grid**UNSTRUCTURED GRIDS****H.** Rectangular, nested grid**I.** Triangular, nested grid**J.** Radial grid**K.** Rectangular, quadtree grid, no smoothing**L.** Rectangular, quadtree grid, with smoothing**M.** Irregular polygon grid**Figure 5.4** Structured and unstructured grid designs (Panday et al., 2013).

In a *regularly spaced grid* (Fig. 5.2a), the nodal spacing is uniform in the horizontal plane ( $\Delta x = \Delta y = a$  constant) and the node is in the center of the cell. In an *irregular grid*, the nodal spacing is variable in one or both horizontal directions; the node is still in the center of the cell in a block-centered grid but is off-center in a point-centered grid (Fig. 5.5). Regularly spaced horizontal grids are more computationally accurate and operationally efficient; many post-processing routines are designed for regularly spaced horizontal networks of nodes. However, regular grids can be impractical when fine resolution is only

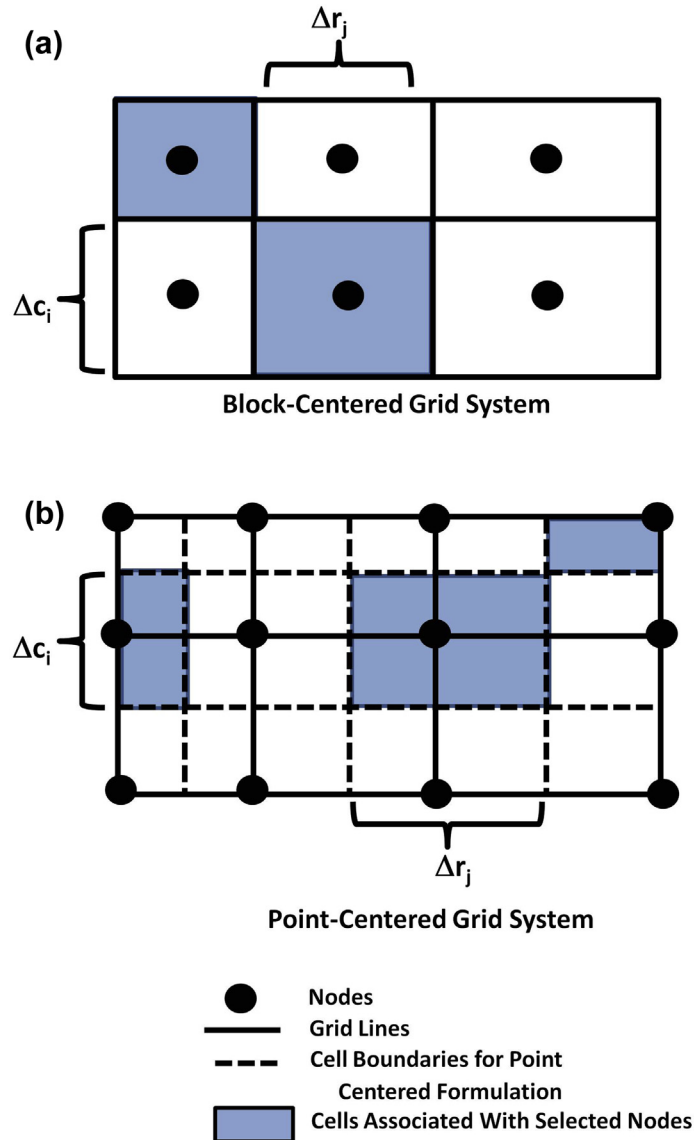


**Figure 5.5** Irregular grids shown using MODFLOW convention where  $i$  = rows and  $j$  = columns. Spacing between columns (spacing along rows) is  $\Delta r_j$  and spacing between rows (spacing along columns) is  $\Delta c_i$ : (a) block-centered grid; (b) point-centered grid (modified from McDonald and Harbaugh, 1988).

needed locally to represent surface water features, pumping wells, changes in parameters, steep hydraulic gradients, and other hydrologically significant features. When fine resolution is needed in only a portion of the model domain, an irregular grid is designed or, alternatively, a local scale grid is embedded in a larger scale grid (Fig. 5.4 (h), (i); Section 4.4, Fig. 4.20). Conceptually, embedded local scale grids are often preferred but may require more time to set up and run. Here we discuss the irregular grid used in standard FD structured grids.

An irregular grid must have the same number of rows and columns throughout the grid (Fig. 5.6), which almost always results in fine discretization outside of the focus area. When constructing an irregular grid, the nodal spacing in both horizontal dimensions should be increased or decreased gradually. A common guideline is to expand the grid by increasing the nodal spacing no more than 1.5 times the previous nodal spacing. For example, if the distance between two nodes is 1 m, the distance between the next two nodes should be no more than 1.5 m and the next nodal spacing should be no more than 2.25 m, and so on. A factor of two may be used for a few rows or columns

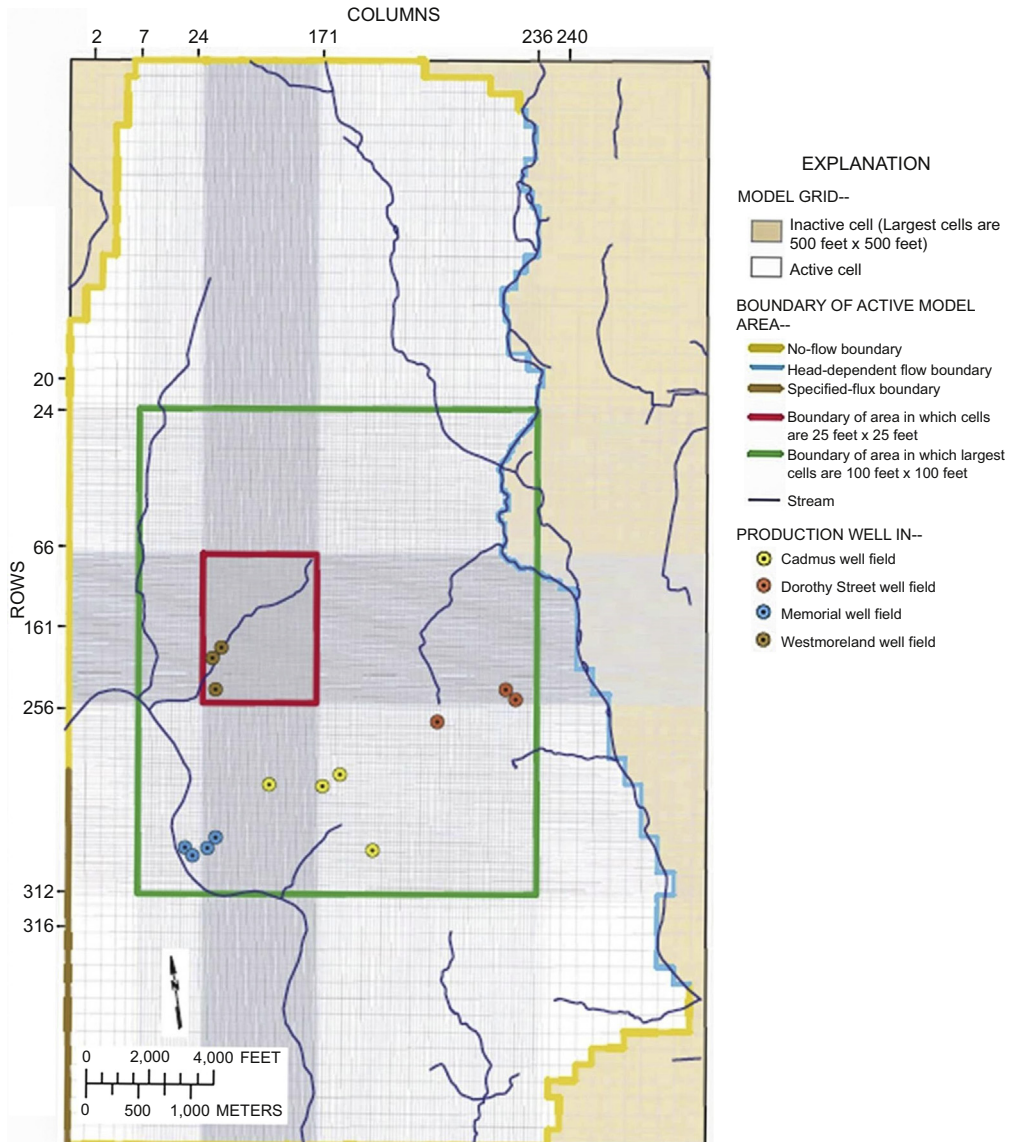


**Figure 5.6** Irregular FD grid designed to provide fine nodal spacing in the vicinity of a superfund site, New Jersey, USA (Lewis-Brown et al., 2005).

but it is advisable not to expand the entire grid using a factor of more than 1.5. The irregular grid guideline arises because the FD expression for the second derivative has a larger error when derived for irregular nodal spacing (Eqn (3.25)). The truncation error for an irregular grid is correct to the first order whereas for a regular grid the FD expression is correct to the second order. The difference in truncation error can be demonstrated by a Taylor series expansion (Remson et al., 1971, pp. 65–67). A heuristic explanation for the larger numerical error in an irregular grid is presented in Box 5.1. When variable nodal

### Box 5.1 Numerical Error Inherent to Irregular FD Grids

In this box we present a heuristic explanation for the larger error in an FD approximation based on an irregular FD grid relative to a regular FD grid (Section 5.1). Consider the one-dimensional block-centered grid in Fig. B5.1.1. The FD expression for the second derivative in the neighborhood of node  $i$  is the difference in the first derivatives as calculated at points  $i + 1/2$  and  $i - 1/2$ :

$$\frac{d^2h}{dx^2}\bigg|_i = \frac{d}{dx} \left( \frac{dh}{dx}\bigg|_{i+1/2} - \frac{dh}{dx}\bigg|_{i-1/2} \right) = \frac{1}{\Delta x} \left( \frac{h_{i+1} - h_i}{\Delta x_{i+1/2}} - \frac{h_i - h_{i-1}}{\Delta x_{i-1/2}} \right) \quad (\text{B5.1.1})$$

When  $\Delta x$  is constant (Fig. B5.1.1(a)), the points  $i + 1/2$  and  $i - 1/2$  coincide with the edges of the block so that the nodal point ( $i$ ) is centered between  $i + 1/2$  and  $i - 1/2$ . However, for an irregular grid (Fig. B5.1.1(b)),  $i + 1/2$  does not coincide with the edge of the block that contains node  $i$  and the nodal point ( $i$ ) no longer is centered between  $i - 1/2$  and  $i + 1/2$ .

The FD solution calculates the head at a location halfway between  $i + 1/2$  and  $i - 1/2$ . When the node is not centered between  $i + 1/2$  and  $i - 1/2$ , the location at which the head is calculated does not coincide with the node, thereby introducing some error into the solution.

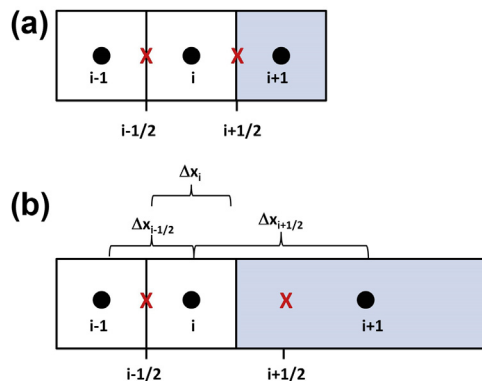


**Figure B5.1.1** (a) Regular FD grid; (b) irregular FD grid. Both are shown in one dimension. Nodes are filled circles; locations halfway between nodes are designated by red X's. The location  $i + 1/2$  is halfway between nodes  $i$  and  $i + 1$ ;  $i - 1/2$  is halfway between nodes  $i - 1$  and  $i$ ;  $\Delta x_{i+1/2}$  is the distance between nodes  $i$  and  $i + 1$ ;  $\Delta x_{i-1/2}$  is the distance between nodes  $i - 1$  and  $i$ ;  $\Delta x_i$  is the width of the cell around node  $i$ . In the regular grid,  $\Delta x_{i-1/2} = \Delta x_{i+1/2} = \Delta x$ . For illustration purposes, the irregular grid was expanded using a factor of four rather than the recommended factor of 1.5 (Section 5.1).

spacing occurs in both the  $x$ - and  $y$ -directions, numerical errors are compounded but are tolerable provided the 1.5 rule is followed when expanding the grid in both horizontal directions.

Although a regular grid is preferred for numerical accuracy and for the inherent ease of inputting data and processing output, more nodes are needed to cover the same problem domain if fine nodal spacing is used throughout. More nodes require larger input and output arrays and more computer storage and data management. However, with the increased computational power and storage in today's computers, a globally refined grid using uniform nodal spacing is possible for many groundwater problems.

### 5.1.2.2 Unstructured Grid

An unstructured FD grid in a CVFD model (Section 3.5) provides much of the flexibility in nodal design as an FE mesh by allowing discrete areas of fine nodal spacing using a nested grid (Figs. 5.4(h), (i) and 5.7), which is a desirable alternative to a structured irregular grid. Nested grids have the advantage of not requiring fine nodal spacing in areas of the problem domain outside the focus area. The concept is similar to telescopic mesh refinement (TMR) and local grid refinement (LGR) (Section 4.4), where detailed discretization in the focus area is realized in a local scale model with boundary conditions extracted from a larger-scale model. However, the TMR/LGR approach requires linking multiple numerical models and multiple sets of boundary conditions to represent nested problem domains. In contrast, in an unstructured nested grid small nodal spacing is embedded in a larger scale grid with coarser nodal spacing and there is only one problem domain, one set of boundary conditions, and one solution.

MODFLOW-USG (Panday et al., 2013) offers nested grids (Fig. 5.4(h), (i) and 5.7) as well as detailed grid resolution using quadtree refinement (Fig. 5.4(k) and (l)) around geologic or engineered features. With quadtree gridding (called octree gridding in three dimensions), a regional grid with relatively coarse nodal spacing is locally refined multiple times by subdividing each rectangular cell into as many as four smaller cells to form a nested grid around features such as pumping wells and streams and canals (Fig. 5.8).

The flexibility of an unstructured grid comes with additional complexity in input required to construct the grid. As in an FE mesh, nodes are numbered sequentially rather than located using the efficient  $i,j,k$  indexing convention of standard FD. Each cell is also numbered (Fig. 5.7). Adjacent nodes are connected and the user must input the area of the shared cell face for every cell connection. Given the complexity of assembling the data for an unstructured grid, the use of a pre-processor code is recommended (Panday et al., 2013).

An important guideline for designing an unstructured FD grid based on Cartesian coordinates is that a line connecting the centers of adjacent cells should pass through the shared face at a right angle (Fig. 5.9) and the intersection should fall approximately at the center of the face. For cylindrical grids, the intersection should coincide with the logarithmic mean of the radii. Adherence to this guideline, called the *control volume finite-difference (CVFD) requirement*, ensures that the FD equations are correct to the

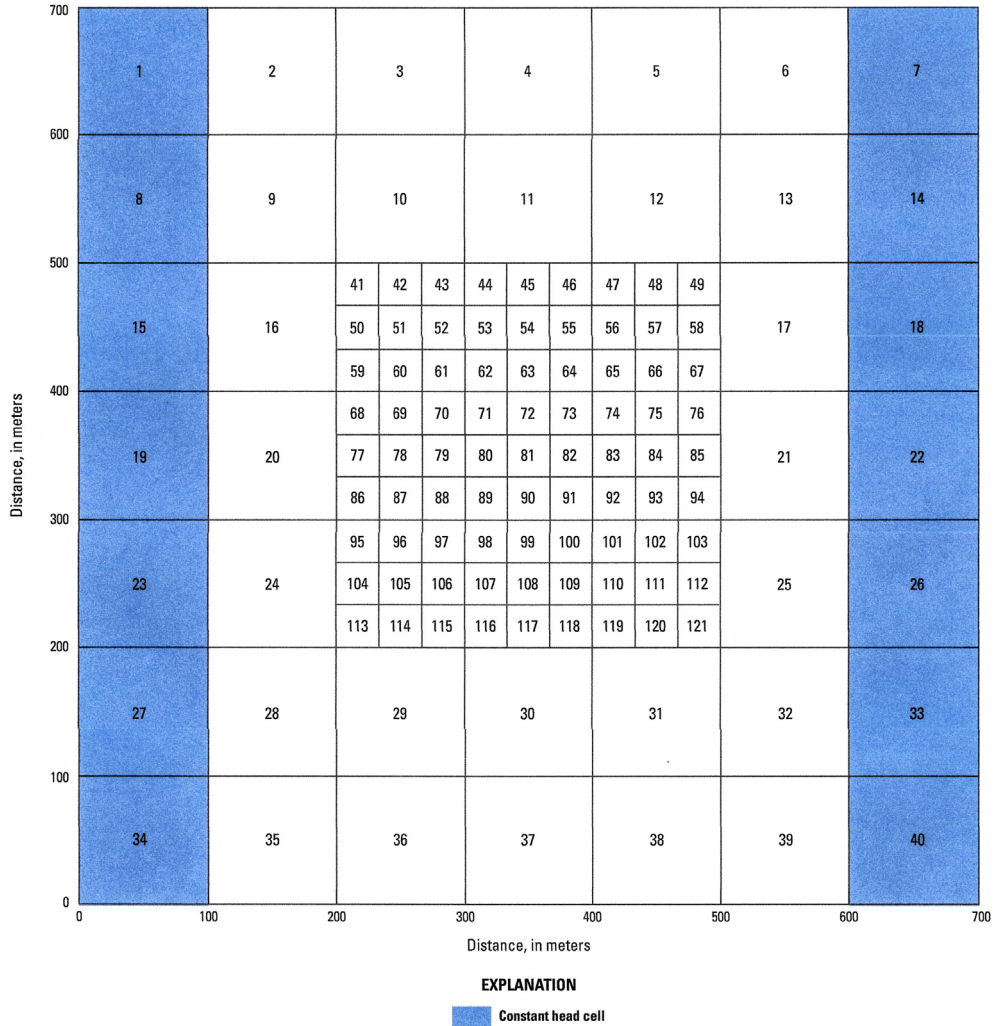
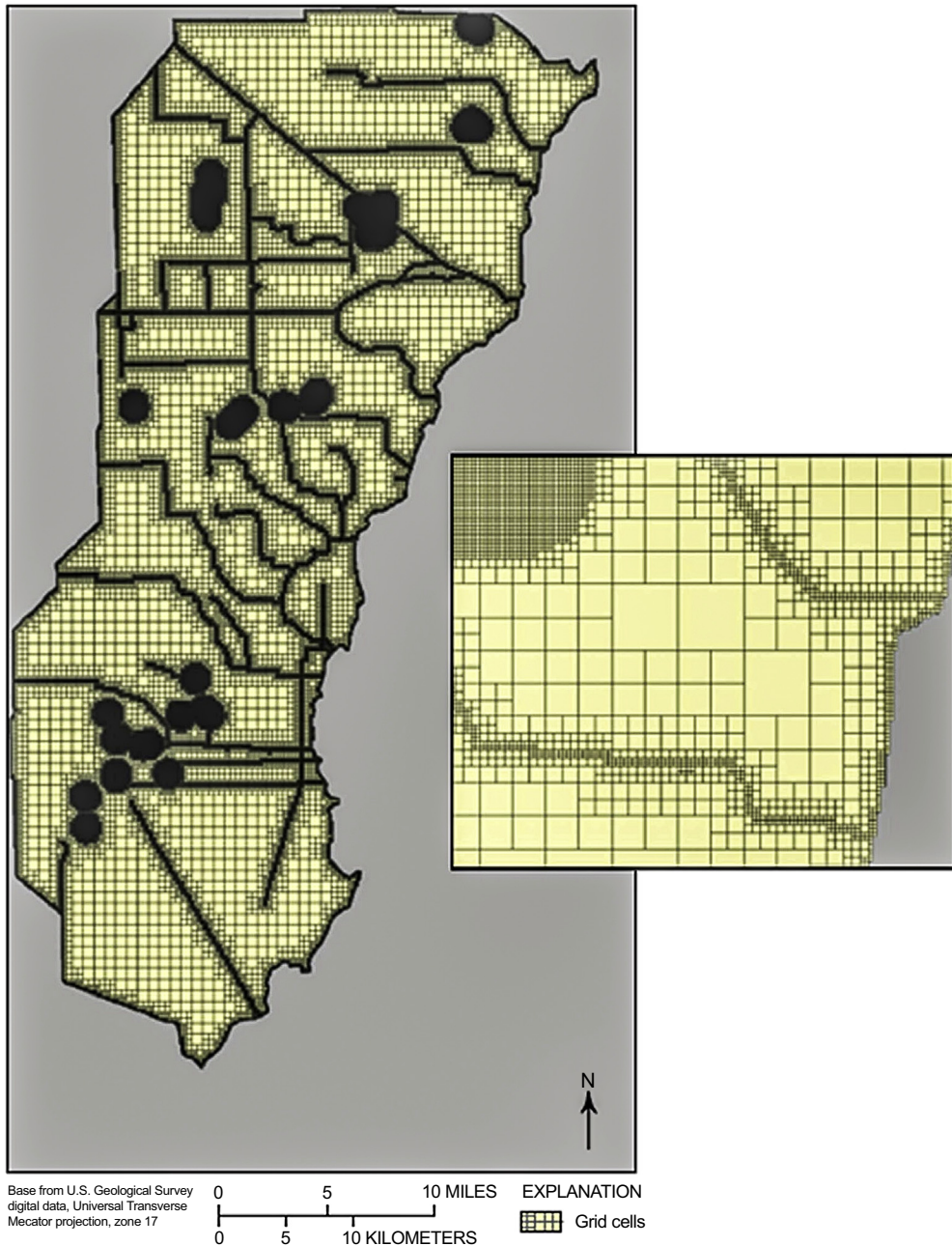


Figure 5.7 Nested cells in an unstructured FD grid; each cell is numbered (Panday et al., 2013).

second order. Strictly speaking, the guideline is violated for a nested grid (see Panday et al., 2013 for details) but small violations can be tolerated. The grids in Figs. 5.4(a)–(e) and (j) meet the CVFD requirement while the other grids in the figure do not. MODFLOW-USG includes a module called the Ghost Node Correction (GNC) Package that is designed to minimize errors caused by violation of the CVFD requirement. The GNC Package automatically places a ghost node so that the line that connects the ghost node with the active node in the adjacent cell bisects the face between the cells at a right angle (Fig. 5.10). The flux across the face is calculated based on the head at the



**Figure 5.8** Quadtree grid for a CVFD model of the Biscayne aquifer, Florida, USA, based on an 800-m structured grid. Cells are refined down four levels to a cell size of 50 m within 1000 m of a municipal well and along canals and the coastline. The quadtree grid was smoothed so that every cell is connected to no more than two cells in any direction (*Panday et al., 2013*).



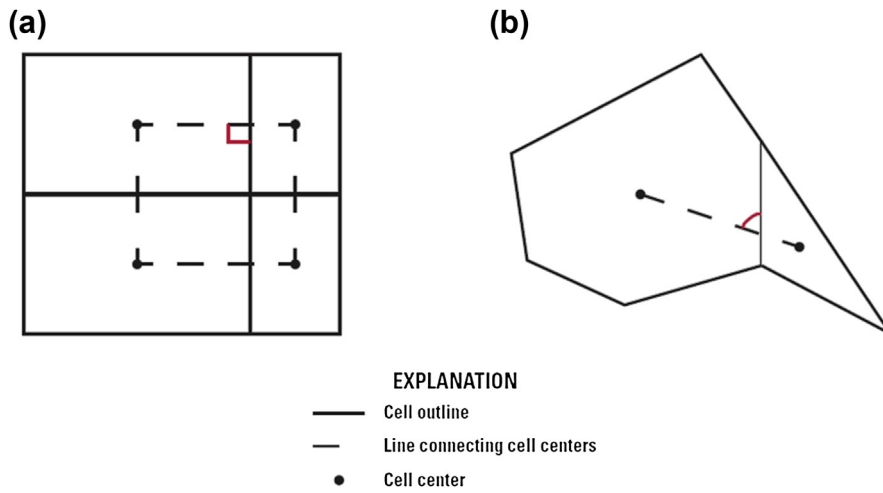


**Figure 5.9** Two types of cell connections in an unstructured FD grid. (a) A line connecting the centers of adjacent cells passes through the shared face at a right angle; (b) a connecting line does not intersect the shared face at a right angle thereby violating the CVFD requirement (Panday et al., 2013).

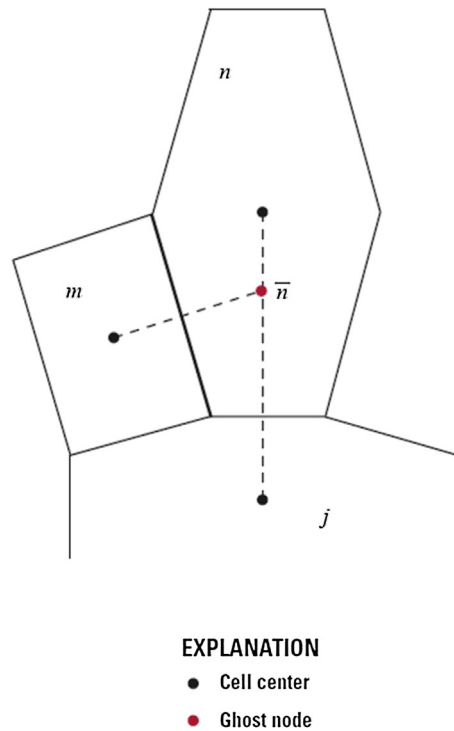


**Figure 5.10** Placement of ghost nodes in an unstructured FD grid to correct for violation of the CVFD requirement (Panday et al., 2013).

ghost node, which is approximated by interpolation. The ghost node is also used to compute connection lengths for the inter-cell conductance terms in the FD approximation of the groundwater flow equation (Eqn (3.27)). Ghost nodes themselves are not included as active nodes in the solution; heads at these nodes are computed by interpolating heads at the active nodes.

Feinstein et al. (2013) proposed a “semi-structured” unstructured grid approach whereby a uniform structured grid is maintained within a layer but a different horizontal nodal network is specified for each layer. In their example application, the uppermost layer had the smallest nodal spacing to simulate groundwater–surface water interaction while coarser discretization was used for deeper layers; four small cells in the upper layer were aligned with one large cell in the underlying layer. Their model was constructed from several separate structured grid models using standard GUIs and imported to MODFLOW-USG. Standard structured grid post-processing programs were used to post-process and visualize output from MODFLOW-USG.

From this discussion it becomes clear that accessing the flexibility in grid design of an unstructured grid requires more attention from the modeler than using a standard FD grid. As Panday et al. (2013) observed: “Unless grids are designed appropriately or proper corrections are made using the GNC Package, large errors in simulated heads and flows can result. These errors can be difficult to detect because they do not show up as errors in the simulated water budget. It is important for MODFLOW-USG users to develop an understanding of these errors, what causes them, and how to reduce them through appropriate grid design strategies and flux correction approaches.”

### 5.1.3 Finite-Element Mesh

The FE method inherently allows for both structured and unstructured meshes but a particular FE code might permit only a structured mesh; the modeler should always consult the code’s user’s manual. The construction of both structured and unstructured meshes requires more input data than the construction of a structured FD grid. Each node and element in the mesh is numbered (Fig. 3.5 (b)) and the location of the node is specified by a coordinate location  $(x,y,z)$ . Two-dimensional FEs are either triangles or quadrilaterals (Fig. 5.11). Three-dimensional elements are tetrahedrons, hexahedrons, or prisms (Fig. 5.12). Elements are fitted to the perimeter boundaries of the problem domain (Fig. 5.13(a) and (b)) with nodes located on the boundaries of the elements; nodes may also be located within elements (Figs. 5.11 and 5.12). The interpolation (basis) function that defines heads within the element (Section 3.4) determines whether the element is linear, quadratic, or cubic. The most commonly used element is the linear element. Some codes use only one type of element (Figs. 5.4(c), (d), (f), (g) and 5.13(b)) while others allow a mix (Fig. 5.14(a)). An FE mesh can accommodate nested meshes (Fig. 5.14(h) and (j)) and mesh refinement around local features of interest (Figs. 5.14(a), (b) and 4.17).

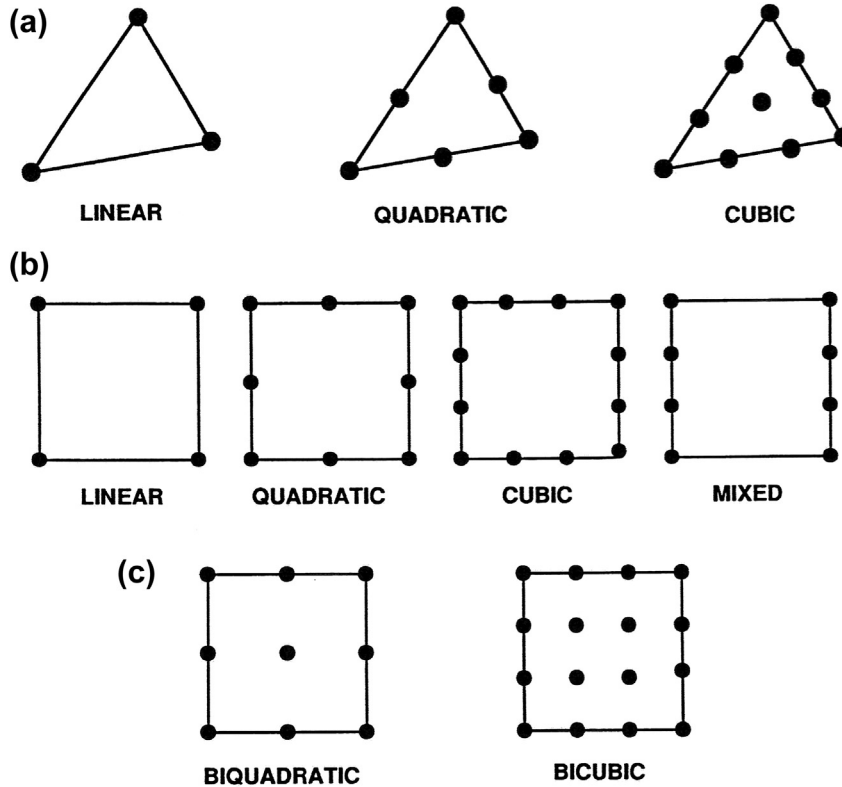


**Figure 5.11** Two-dimensional finite elements; linear, quadratic, and cubic refer to the type of basis function used (Section 3.5): (a) triangular elements; (b) quadrilateral elements (serendipity family); (c) quadrilateral elements (Lagrange family) (*adapted from Huyakorn and Pinder, 1983*).

Nodes are numbered systematically from top to bottom (or bottom to top) and from left to right sequentially across the shortest dimension of the mesh (Fig. 5.13(c)). The code may allow the user to number the nodes arbitrarily and then the code re-numbers the nodes internally according to the order in which they were listed in the input file. In that case, node numbers should be entered into the code sequentially along the shortest dimension of the problem domain. Node numbers associated with each element are input to the code in a counterclockwise fashion. The number of the element and the order in which elements are input to the code are not important for assembly of the FE equations because the code keeps track of the location of each node and links each element to its associated nodes. However, when examining model output the user will want to refer to a map of the mesh with both node and element numbers (Fig. 4.11(d) and (e)).

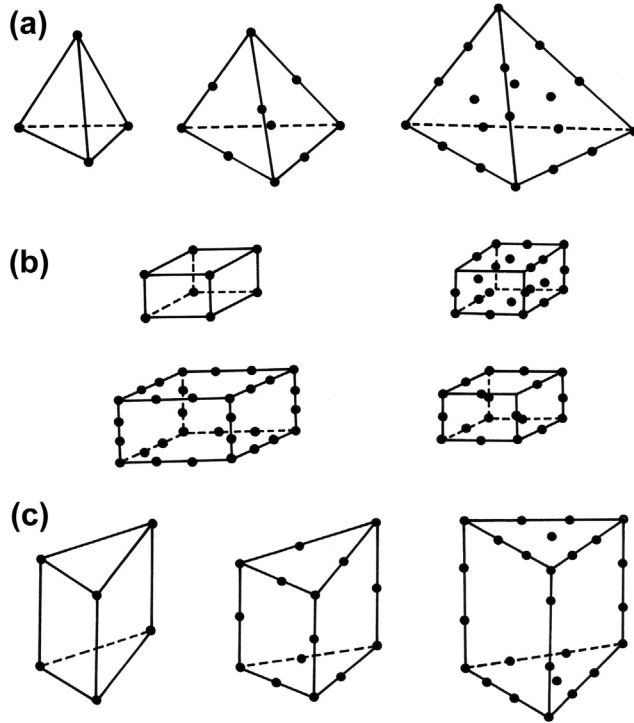


**Figure 5.12** Three-dimensional finite elements: (a) tetrahedrons; (b) hexahedrons; (c) prisms (*adapted from Huyakorn and Pinder, 1983*).

The code assembles equations for all elements into a global matrix equation (Fig. 3.9). Systematic numbering across the shortest dimension of the mesh reduces the bandwidth of the coefficient matrix and thereby reduces computer storage requirements and computational time. The semi-bandwidth (SBW) of a symmetric matrix (i.e., entries reflect across the diagonal of the matrix) is the maximum number of columns between the diagonal and the last non-zero entry, inclusive, along any row of the matrix. The bandwidth is equal to 2 times (SBW−1). The SBW is calculated from

$$\text{SBW} = R + 1 \quad (5.1)$$

where  $R$  is the maximum difference in any two nodal numbers that define a single element within the mesh (*Istok, 1989*). For example, in the mesh in Fig. 5.13(c),  $R$  is 17; the semi-bandwidth is 18 and the bandwidth is 34. Because design of an FE mesh can be time-consuming, FE codes usually include mesh generator utilities or GUIs that generate the mesh. For example, FEFLOW offers a variety of options for

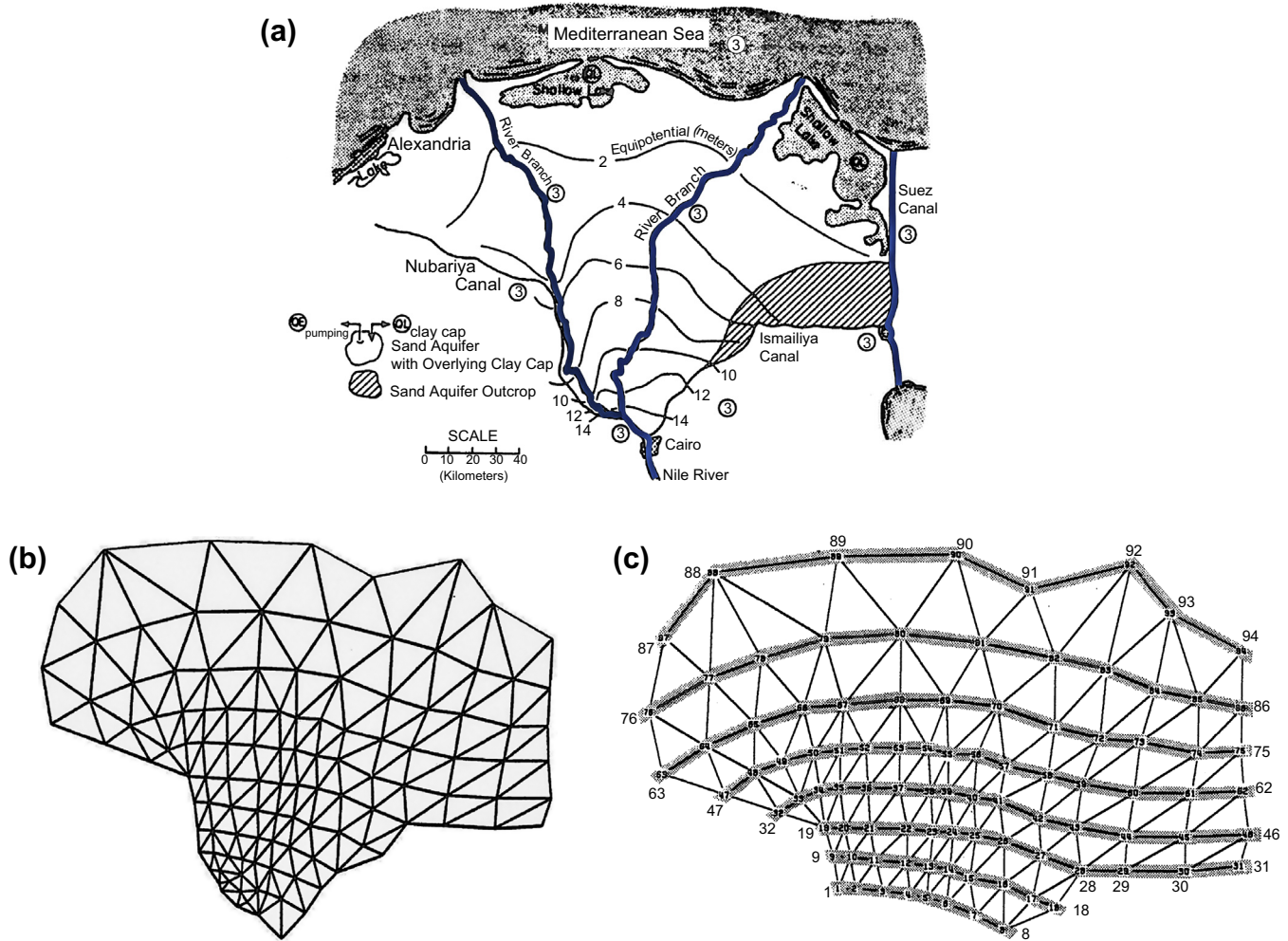


**Figure 5.13** Discretization in an FE model of the Nile Delta, Egypt. (a) Map showing head contours and boundary conditions (circled numbers) where 3 indicates a head-dependent boundary (Section 3.3). (b) Triangular elements are shaped to fit the irregular boundary. (c) Nodal numbers in a truncated version of the mesh. Nodes are numbered sequentially along the shortest dimension of the mesh (modified from Townley and Wilson, 1980).

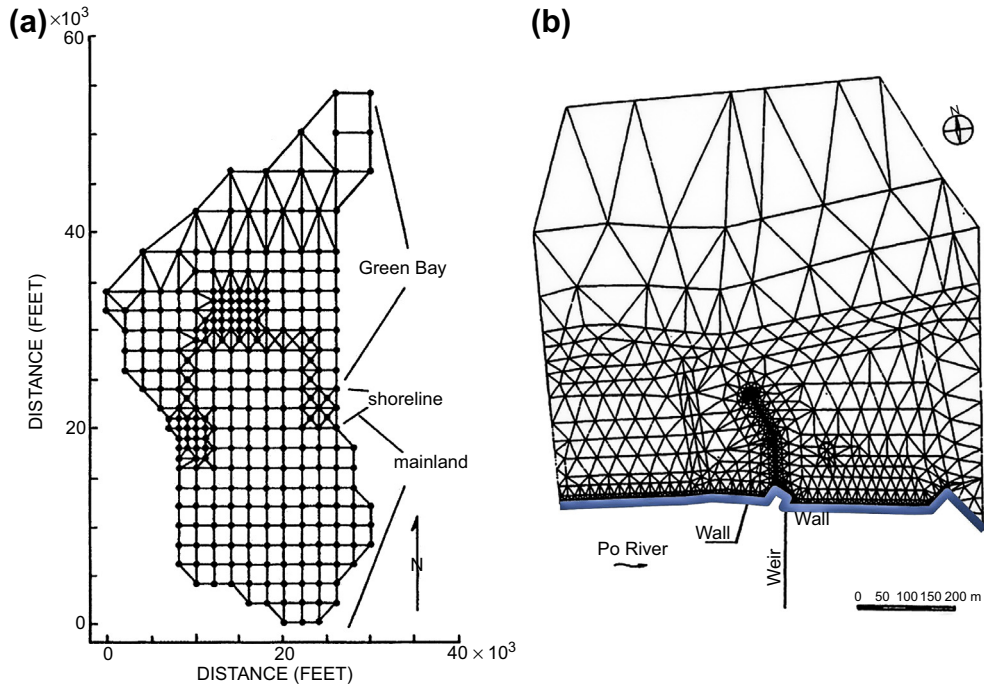


**Figure 5.14** Mesh refinement. (a) FE mesh for a peninsula jutting into Green Bay, Wisconsin, USA, constructed with a mix of triangular and quadrilateral elements. Fine nodal spacing is used to represent the shoreline area where groundwater discharges to Green Bay (*Bradbury, 1982*). (b) FE mesh showing local mesh refinement near a barrier wall designed to protect a nuclear reactor from a high water table when the Po River floods, NW Italy. The river forms the southern boundary; the river bank is represented by fine nodal spacing. The northern and southern boundaries are specified head and the eastern and western boundaries are no-flow boundaries (*modified from Gambolati et al., 1984*).

generating a mesh (*Diersch, 2014*, pp. 760–770). The FE method has some constraints on mesh design, which are discussed briefly below, but mesh generating utilities will help the modeler resolve most, if not all, of these issues.

In designing an FE mesh for isotropic materials, each element should be constructed so that the *aspect ratio*, the ratio of maximum to minimum element dimensions, is close to unity, for example by exclusive use of equilateral triangular elements. This requirement is similar to the factor of 1.5 used in constructing an irregular FD grid and is necessary to minimize numerical errors. Experience has shown that aspect ratios greater than five should be avoided. Furthermore, transition regions should be used to change element sizes gradually (*Fig. 5.14(b)*). For anisotropic porous material, the shape of the elements should be examined in the equivalent transformed isotropic domain (*Box 5.2*) and designed so that the aspect ratio in the isotropic domain does not exceed five.

### Box 5.2 Vertical Anisotropy and the Transformed Section

Vertical anisotropy in hydraulic conductivity ( $K_h/K_v$ ) is usually much larger than horizontal anisotropy ( $K_x/K_y$ ). Therefore, in this box we focus on anisotropy in the vertical plane; the same type of analysis could be done in the horizontal plane. We define the vertical anisotropy ratio as  $K_h/K_v$  where  $K_h (=K_x)$  is horizontal hydraulic conductivity, but readers should be aware that other authors sometimes define vertical anisotropy to be  $K_v/K_h$ .

A steady-state, homogeneous, anisotropic system can be mathematically transformed into an isotropic system by coordinate transformation, creating what is sometimes called a transformed section. The equations that govern the transformation of coordinates are used in design of an FE mesh (Section 5.1), checking the size of vertical nodal spacing (Eqn (5.4), Section 5.3), Dupuit–Forchheimer analysis (Eqn (4.2), Section 4.1; Box 4.1), and flow net construction (Box 8.2).

The coordinates in the true anisotropic system are  $x$  and  $z$ . In the transformed isotropic system the coordinates are  $X$  and  $Z$ , where

$$X = x \quad (\text{B5.2.1a})$$

$$Z = z\sqrt{K_x/K_z} \quad (\text{B5.2.1b})$$

Equations (4.2) and (5.4) follow from Eqn (B5.2.1b). (For analysis in a 2D horizontal plane,  $X = x$  and  $Y = y\sqrt{T_x/T_y}$ , where  $T_x$  and  $T_y$  are transmissivities.)

From Eqns (B5.2.1a,b):

$$\frac{\partial}{\partial x} = \frac{\partial}{\partial X} \quad (\text{B5.2.2a})$$

$$\frac{\partial}{\partial z} = \sqrt{\frac{K_x}{K_z}} \frac{\partial}{\partial Z} \quad (\text{B5.2.2b})$$

In the true ( $x$ - $z$ ) coordinate system, the partial differential equation for steady-state flow in a homogeneous, anisotropic system with no areal recharge is

$$K_x \frac{\partial^2 h}{\partial x^2} + K_z \frac{\partial^2 h}{\partial z^2} = 0 \quad (\text{B5.2.3})$$

Equation (B5.2.3) transforms to the Laplace equation in the  $X$ - $Z$  coordinate system:

$$\frac{\partial^2 h}{\partial x^2} + \frac{\partial^2 h}{\partial z^2} = 0 \quad (\text{B5.2.4})$$

By requiring that flow in the transformed section is the same as in the true section, it can be shown (e.g., see Fitts, 2013, p. 285) that the equivalent isotropic hydraulic conductivity,  $K_X (=K_Z)$ , in the transformed section is

$$K_X = K_Z = \sqrt{K_x/K_z} \quad (\text{B5.2.5})$$

Flow nets (Box 8.2) can be constructed in the transformed section by drawing equipotential lines at right angles to flow lines (Fig. B5.2.1(a)) and then transformed back to the true coordinates (Fig. B5.2.1(b)). In the transformed section, the effects of vertical flow are exaggerated compared to flow in the true  $x$ - $z$  coordinate system. In other words, in the true coordinate system vertical anisotropy creates resistance to flow in the vertical direction, which diverts flow into the horizontal direction.

### Box 5.2 Vertical Anisotropy and the Transformed Section—cont'd

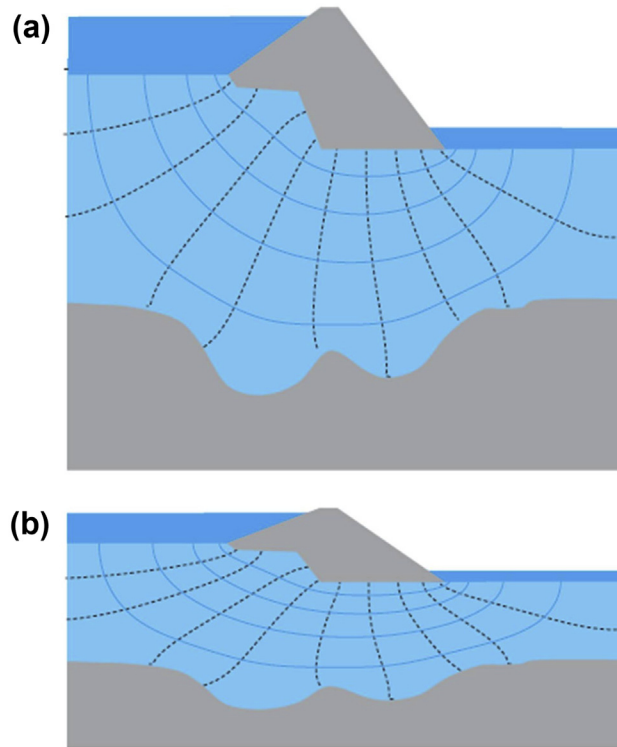


**Figure B5.2.1** Flow nets showing flow beneath a dam. Equipotential lines are heavy dotted lines and flow lines are shown by solid light blue lines. Flow is from left to right. (a) In the transformed (isotropic) section ( $X-Z$  coordinates) equipotential lines and flow lines meet at right angles. (b) In the true (anisotropic) system ( $x-z$  coordinates), equipotential lines and flow lines are not at right angles (*Fitts, 2013*).

## 5.2 HORIZONTAL NODAL SPACING

In [Section 5.1](#), we discussed some general features of the horizontal grid/mesh. In this section we discuss selecting the horizontal nodal spacing. Design of the horizontal nodal network is guided by the modeling objective. For example, if the objective is to simulate groundwater–surface water exchange (e.g., simulations of conjunctive use), small nodal spacing around important surface water features likely will be needed. If the objective is to compute flowpaths in heterogeneous porous material, a sufficient number of nodes must be used to discretize the heterogeneities that affect flow. If the objective is to simulate an aquifer test, fine nodal spacing around the pumping well will be



required. The optimal nodal spacing also balances the need for an accurate solution (provided by a relatively large number of nodes) with reasonable runtimes and ease of data management and visualization of results (provided by a relatively small number of nodes).

The overall size of the problem domain is the first consideration in deciding on the number of nodes required; obviously more nodes are required to provide reasonable coverage of large geographical areas. Additionally, at least six other factors influence the design of the horizontal nodal network and the horizontal nodal spacing: (1) solution accuracy; (2) locations of calibration targets; (3) configuration of perimeter boundaries; (4) spatial variability (heterogeneity) in parameters; (5) faults, conduits, and barriers; and (6) sources and sinks. Factors 4, 5, and 6 typically cause abrupt changes in hydraulic gradient so that fine nodal spacing is required when it is necessary to capture head changes around the associated feature.

Each of these six factors is discussed below.

### 5.2.1 Solution Accuracy

Recall that a numerical approximation of the governing equation replaces the continuous space of the partial differential equation with a discrete representation of the solution at nodes (Section 3.4); theoretically, the smaller the nodal spacing the more accurate the solution. Ideally, the effect of nodal spacing on the solution should be evaluated by a sensitivity test whereby nodal spacing is reduced in sequential runs of the model until there is an acceptably small difference in computed heads and flows. Testing different nodal networks is most easily done for simple problems (Problem P5.1) but, in practice, formal sensitivity analysis of nodal spacing is rarely done because reducing the nodal spacing requires not only construction of a new grid/mesh but also re-discretization of parameters, boundary conditions, and source/sinks. For steady-state models, another option is to compare results from the numerical solution with the solution of an analytic element (AE) model (Sections 3.4, 4.4), which does not depend on nodes. Large discrepancies between an FD/FE model and an AE model suggest that the nodal spacing of the FD grid/FE mesh should be refined (e.g., [Hunt et al., 2003a](#); [Haitjema et al., 2001](#)).

### 5.2.2 Calibration Targets

During model calibration, field observations, including heads and fluxes, are used as calibration targets, which are compared to simulated equivalent values computed by the model. Ideally, calibration head targets should be located on nodes so that the head computed by the code (which is always computed for the node) can be compared directly to the measured value without introducing interpolation errors. However, it

may not be practical to position nodes on the locations of any or all head or flux targets. In recognition of this design problem, some GUIs (e.g., Groundwater Vistas) include an option to interpolate the head target to a node when post-processing model results.

### 5.2.3 Perimeter Boundary Configuration

The nodal spacing should be small enough so that cells or elements capture boundary irregularities that are important to the problem. Close correspondence between the perimeter boundaries of the model and the geometry of boundaries for the modeled area allow for better representation of perimeter boundary conditions (Figs. 5.2(a), 5.6 and 5.13).

### 5.2.4 Heterogeneity

Nodal spacing determines the maximum level of heterogeneity that can be included in the model inasmuch as a different parameter value can be assigned to each cell, element, or node (Section 5.5). Accurate representation of spatial variability in hydraulic conductivity is important for transport models (Section 12.3) and in determining flowpaths using particle tracking codes (Chapter 8) where it is critical to simulate changes in velocity for accurate representation of flowpaths. Representation of heterogeneity in hydraulic conductivity can also be important in a groundwater flow model when flowpaths are used as calibration targets (Section 9.3, Box 10.2). Haitjema et al. (2001) conducted numerical experiments to test the effect of nodal spacing on the velocity field computed by the FD code MODFLOW. In their example problem, hydraulic conductivities differed by a factor of 10 or more from the surrounding porous material. Based on that example, they concluded that zones representing heterogeneities ideally should be discretized into at least 50 FD cells for accurate representation of flowpaths and travel times.

Designing the nodal network to capture spatial variability in areally distributed recharge is usually less important than heterogeneity in hydraulic conductivity (e.g., Haitjema, 1995, pp. 278–279). However, accounting for heterogeneity in recharge by zonation may be necessary for some modeling problems (Section 5.5).

### 5.2.5 Faults, Conduits, and Barriers

Representation of geologic faults (Section 4.2; Fig. 4.8) typically requires smaller nodal spacing than used over the rest of the problem domain. A barrier fault can be simulated by non-connecting nodes (Fig. 5.15(a)) or by low-permeability elements/cells (Figs. 5.15(b) and 4.8(b)). A permeable fault or conduit can be simulated by high-conductivity elements/cells (Fig. 4.8(a)).

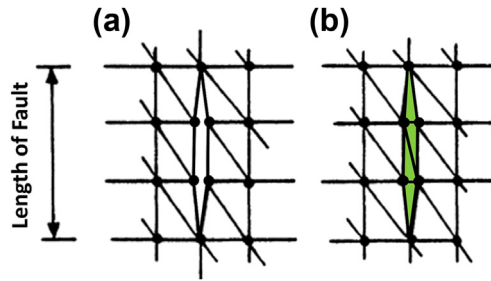


**Figure 5.15** Faults in an FE mesh. (a) Non-connected nodes represent an impermeable fault. (b) Thin elements (shaded) represent a fault. Hydraulic conductivity, or transmissivity, values assigned to the elements determine whether the fault is permeable or impermeable (modified from Townley and Wilson, 1980).

FEFLOW (Diersch, 2014) includes an option to use *discrete feature elements (DFEs)* to simulate geologic and engineered features that are smaller than the nodal spacing of the mesh and have a higher transmission of flow than the surrounding porous media such as wells, conduits, and open faults (Fig. 5.16). One-dimensional DFEs are planar (for

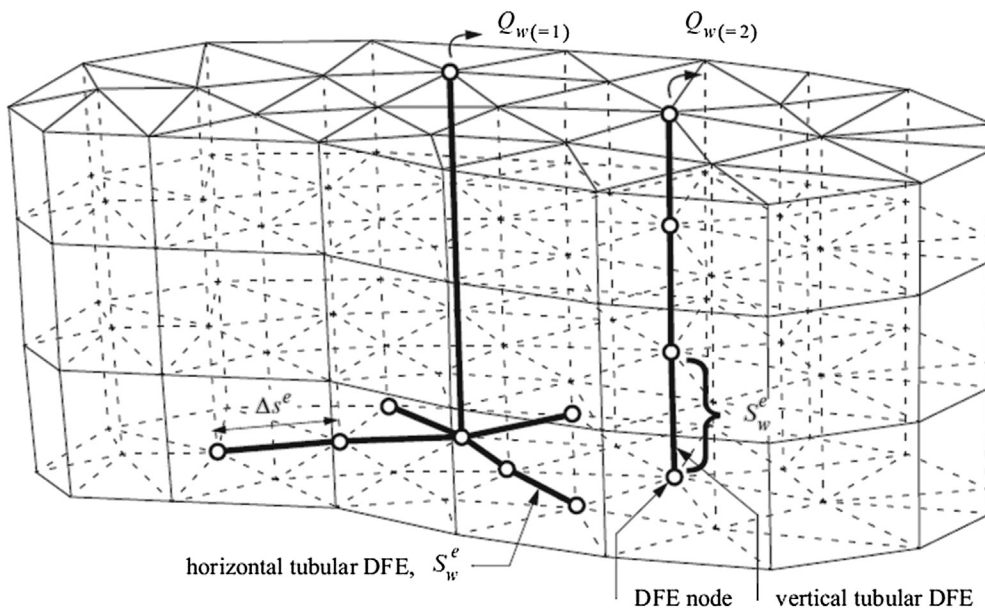


**Figure 5.16** Tubular discrete feature elements (DFEs) to represent a multi-layer pumping well and a horizontal pumping well in an FE mesh (Diersch, 2014).

channels, mine shafts, tunnels, and streams) or tubular (for wells, conduits, tunnels, and drains). Two-dimensional DFEs are used to represent fractures and permeable faults. A DFE shares the nodes of the elements that make up the mesh and is placed along the edge or face of elements or interconnected nodes within the mesh (Fig. 5.16). Diersch (2014, Chapters 4 and 12) provides a detailed discussion of DFEs. Also see the discussion of DFEs in Section 6.2.2.

Special packages simulate barriers and conduits in MODFLOW. The Horizontal-Flow Barrier (HFB) Package simulates discrete and narrow geologic features that impede groundwater flow (Hsieh and Freckleton, 1993). The physical barrier is not represented by discretization but its properties are used to modify intra-nodal conductivities in the FD approximation of the groundwater flow equation. The Conduit Flow Process (CFP) (Shoemaker et al., 2008; reviewed by Reimann and Hill, 2009; also see Reimann et al., 2012) simulates a network of conduits (Fig. 5.17) within a continuous porous medium. The CFP simulates turbulent and laminar pipe flow in the conduits coupled to laminar flow in the surrounding continuous porous medium simulated by MODFLOW-2005. The Connected Linear Network (CLN) Process in MODFLOW-USG is similar in function to the CFP for simulating conduit flow.

### 5.2.6 Internal Sources and Sinks

If the modeling objective requires accurate representation of the steep hydraulic gradients usually present around sources and sinks, relatively small nodal spacing around those features is required. The sources and sinks most often included in a groundwater model are streams, lakes, wetlands, springs, and pumping and injection wells. All of these features except for lakes and wetlands typically are smaller than the nodal spacing used over the rest of the problem domain.

Haitjema et al. (2001) showed that 95% of the inflow to (or outflow from) a surface water feature separated from an underlying aquifer by a sediment layer occurs within a distance of  $3\lambda$ , where  $\lambda$  is the *characteristic leakage length* (Fig. 5.18(a)). The expression for  $\lambda$  is derived from an analytical solution (see Haitjema et al., 2001, p. 933, for details) and is defined as follows:

$$\lambda = \sqrt{Tc} \quad (5.2)$$

where  $c = b'/K'_z$

In Eqn (5.2),  $T$  is transmissivity of the aquifer (hydraulic conductivity times saturated thickness) and  $c$  is the vertical resistance (Section 4.3) between the surface water body and the aquifer calculated as the ratio of the thickness of stream, lake, or wetland sediments,  $b'$ , to the vertical hydraulic conductivity of the sediments,  $K'_z$ . Surface water features are

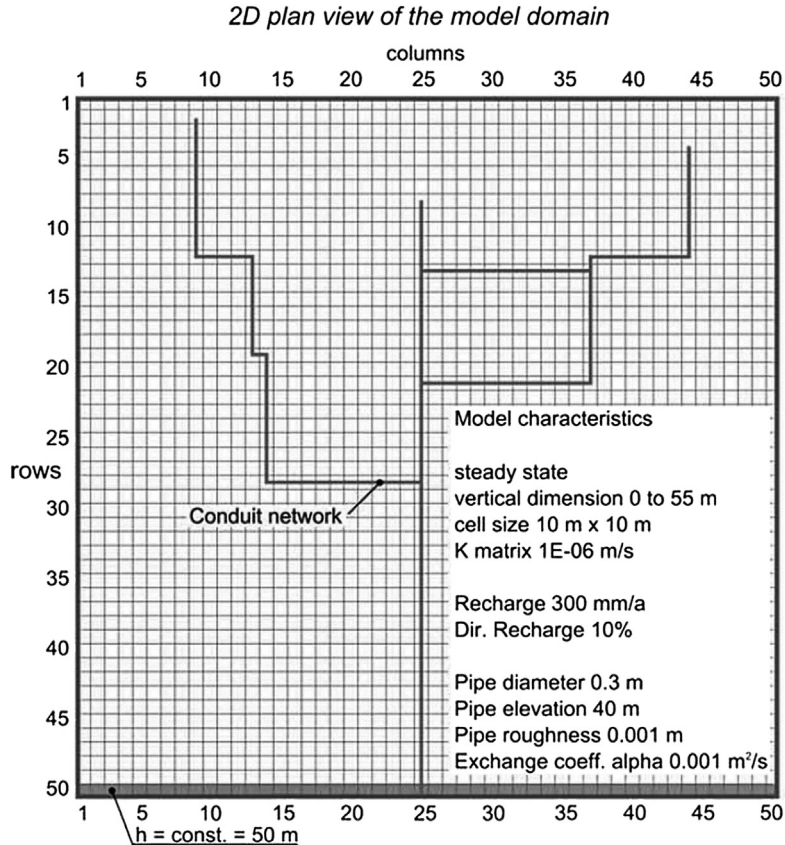


**Figure 5.17** Conduits in an FD grid simulated using the Conduit Flow Process (Reimann and Hill, 2009).

typically represented by internal head-dependent boundary conditions (Section 4.4, Fig. 4.6) and it follows that the head-dependent cells/elements should be smaller than  $3\lambda$  in order to capture spatial variability in flow rates and to simulate associated groundwater heads in the aquifer. In numerical experiments using MODFLOW, Haitjema et al. (2001) concluded that surface water features should be represented by head-dependent cells with nodal spacing equal to  $\lambda$  or smaller, ideally around  $0.1\lambda$ , in order to represent flow rates and heads accurately (see also Hunt et al., 2003a). For wide surface water bodies, the area of fine nodal spacing may be limited to the inflow/outflow zone of width  $3\lambda$ .

Pumping and injection wells are point sinks and sources, respectively. In almost all models, the diameter of a pumping or injection well will be smaller than the nodal

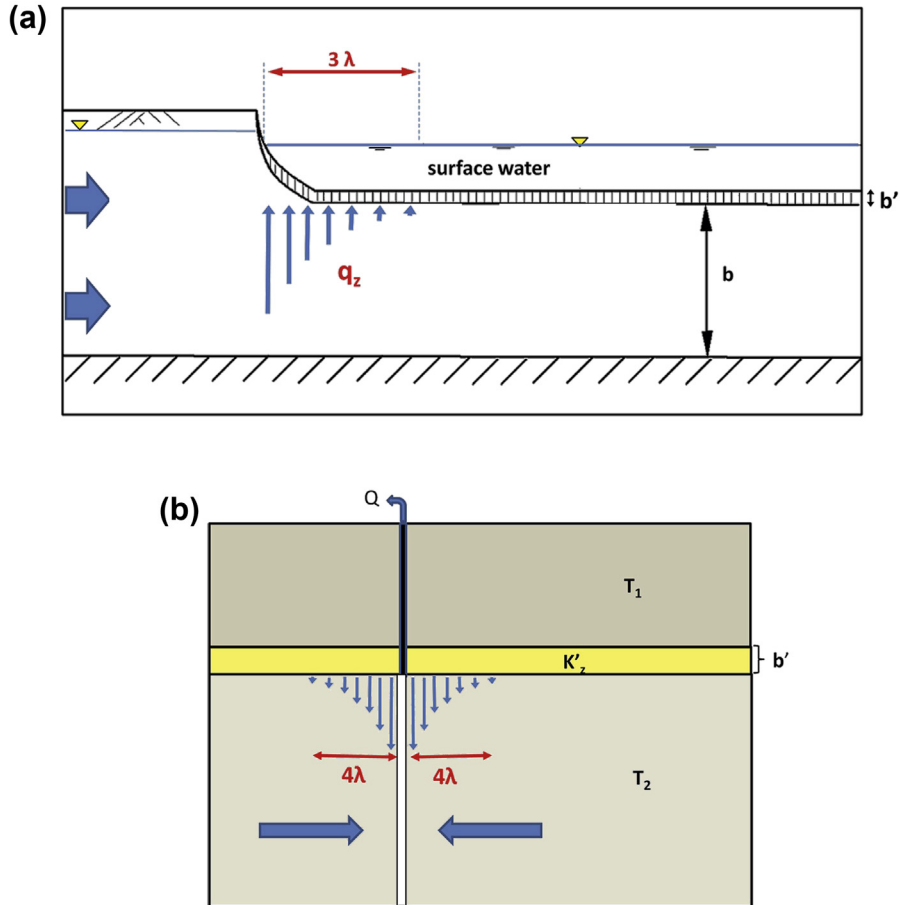


**Figure 5.18** Characteristic leakage length,  $\lambda$ , for (a) a surface water body represented as a head-dependent boundary condition (adapted from Haitjema, 2006); (b) a pumping well in a leaky confined aquifer.

spacing. Some FE codes use tubular DFEs to simulate pumping wells (Fig. 5.16) and similar options are available for MODFLOW (the CF Process in MODFLOW and the CLN Process in MODFLOW-USG; see the discussion of DFEs and the MODFLOW options in Section 5.2.5).

In a standard FD grid or FE mesh, fine nodal spacing around the well node improves the resolution of heads in and around the well. The recommended guideline for accurate representation of head gradients around pumping/injection wells is that the nodal spacing around the well node should be less than  $\xi r_w$ , where  $\xi$  is a factor that ranges between 4.8

and 6.7 depending on the grid/mesh design (Box 6.1) and  $r_w$  is the radius of the well. If the modeling objective does not require detailed resolution of head gradients, coarse nodal spacing around the well may be adequate for the modeling objective and it may suffice to estimate heads in and around the well using the Thiem analytical solution (Box 6.1).

Haitjema (2006) showed that a pumping well finished in a semi-confined (leaky) aquifer induces leakage through the confining bed, where 95% of the leakage occurs within a radius of  $4\lambda$  around the well (Fig. 5.18(b)). In that case,  $\lambda$  is defined as follows:

$$\lambda = \sqrt{\frac{T_1 T_2 c}{T_1 + T_2}} \quad (5.3)$$

where  $c = b'/K'_z$

and  $T_1$  and  $T_2$  are aquifer transmissivities shown in Fig. 5.18(b);  $c$  is the vertical resistance of the confining layer. Nodal spacing within the zone of leakage ideally should be of the order  $0.1\lambda$  and not larger than  $\lambda$  to capture variability in leakage rates (Haitjema et al., 2001). Equation (5.3) reduces to Eqn (5.2) by setting  $T_1$  equal to infinity to represent the surface water body in Fig. 5.18(a); then  $T_2$  in the denominator of Eqn (5.3) is negligible compared to  $T_1$ , and  $T_2$  equals  $T$  in Eqn (5.2).

### 5.3 MODEL LAYERS

Most groundwater flow codes are designed for 3D flow but allow the user to simulate 2D flow by using only one model layer (Section 4.1, Fig. 4.1, Boxes 4.1 and 4.2). For some regional scale problems, a 2D model may be adequate; 3D models are typically required when vertical variability in hydrostratigraphy is important and/or when it is necessary to simulate vertical changes in head (e.g., Fig. B4.1.3(b) in Box 4.1). In 3D simulations, typically each layer represents a hydrostratigraphic unit (Figs. 5.19, 2.7 and 4.6) but more than one layer can be used to represent a single hydrostratigraphic unit if it is necessary to simulate vertical variation in hydraulic conductivity or to capture vertical changes in head within the unit (Section 5.3.1).

In the most straightforward design, the 2D horizontal nodal spacing is the same for all layers. Horizontal and vertical hydraulic conductivities and storage parameters are assigned to each cell, element, or node in the horizontal nodal network that constitutes the layer. When solving the numerical approximation of the governing equation, values of  $\Delta z$  could be used directly (Eqn (3.25)) but commonly the code internally assimilates  $\Delta z$  into parameters that describe vertical transmission properties (Eqn (3.27)). Vertical transmission properties between layers are calculated by using vertical leakance (the average  $K_z$  between the layers divided by the distance between the centers of the layers) multiplied by the area of the horizontal face of the cell/element (e.g., Eqn (3.26)).

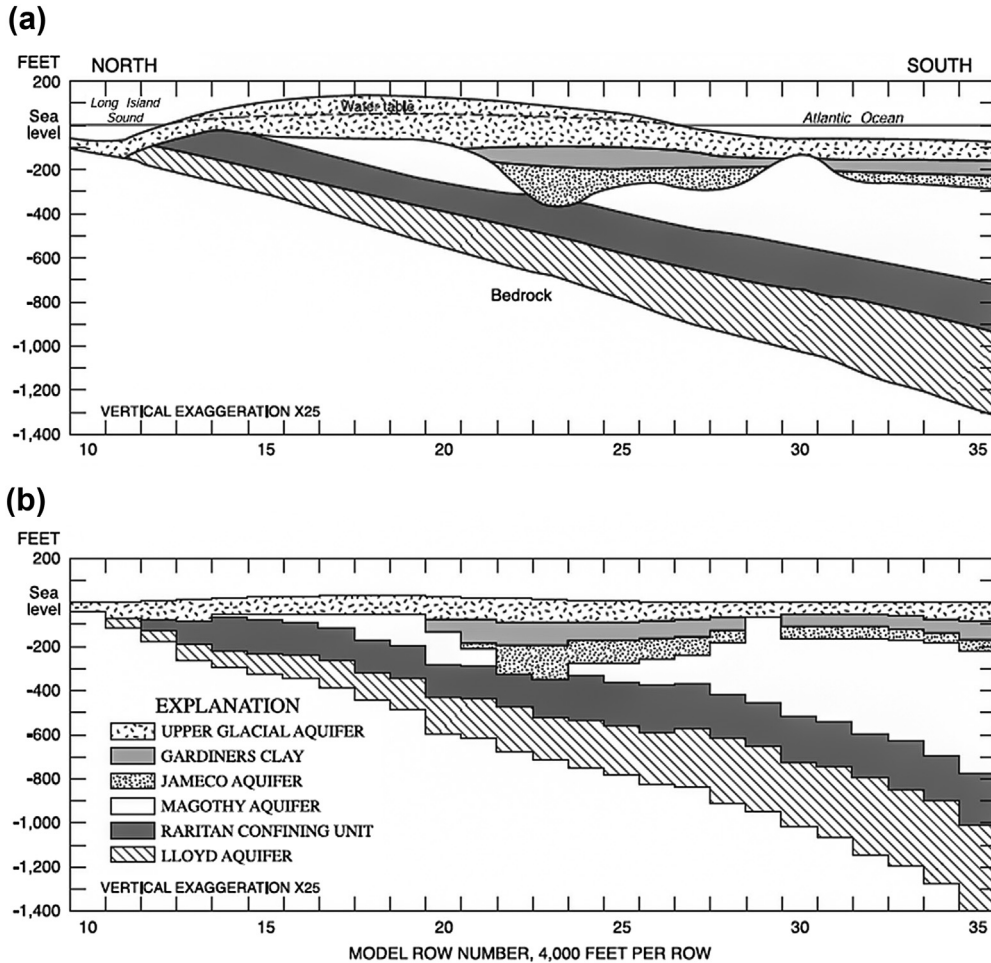


**Figure 5.19** Representation of layers as hydrogeologic units, Long Island, NY, USA. (a) Hydrogeologic cross section showing the hydrogeologic units; (b) representation of the dipping units as deformed model layers (see Fig. 5.20) (Reilly and Harbaugh, 2004; modified from Buxton et al., 1999).

### 5.3.1 Vertical Discretization

The number of model layers and the vertical nodal spacing ( $\Delta z$ ) depend on the magnitude of vertical head gradients and the vertical variability in  $K$ . Although there is no general rule for selecting values for  $\Delta z$ , there is a general guideline for using a minimum of three layers in two situations, as discussed below.

1. A minimum of three layers should be used when capturing vertical changes in head or  $K$  within a hydrostratigraphic unit (e.g., Fig. B5.3.2 in Box 5.3) is important for



the modeling objectives. Three layers are needed to represent the variability in vertical leakance within the hydrostratigraphic unit. Vertical leakance is the average  $K_z$  between two layers divided by the distance between the centers of the layers. Heads in a model layer are computed using leakance values both above and below the node. Therefore, using three layers to represent a hydrostratigraphic unit ensures that heads in the middle layer of the sequence are computed using values of vertical leakance based entirely on  $K_z$  of the hydrostratigraphic unit.

2. When there is a large contrast in  $K$  between any two layers, there should be three or more transition layers in the unit of lower  $K$  if particle tracking (Chapter 8) is anticipated as part of the modeling project. The transition layers help ensure that head gradients are appropriately represented (Fig. B5.3.2 in Box 5.3) and velocities are accurately computed between layers. Accurate velocities are needed for accurate representation of flowpaths and travel times.

Additional layers typically are not needed to simulate vertical flow beneath surface water features represented by head-dependent boundary conditions because vertical flows can be reasonably simulated by adjusting vertical conductance during model calibration (Section 5.4; Nemeth and Solo-Gabriele, 2003). In that case, additional layers capture vertical changes in head but do not necessarily improve simulated flows, which are still matched by adjusting vertical conductance.

Unlike horizontal spacing guidelines, abrupt changes in  $\Delta z$  are usually not problematic because most model domains are dominated by horizontal flow (Haitjema, 2006; Box 4.1). Therefore, there are no general guidelines for vertical discretization analogous to the 1.5 rule for expanding nodal spacing in the horizontal plane (Section 5.2). Relatively fine vertical discretization may be required, however, for accurate representation of large local changes in vertical hydraulic conductivities and vertical gradients.

In most settings significantly larger vertical nodal spacing relative to horizontal nodal spacing does not necessarily cause numerical errors. This is because most models incorporate some vertical anisotropy, which reduces the vertical component of flow and directs it into the horizontal direction. Vertical anisotropy effectively transforms the vertical dimension (Box 5.2) so that increasing vertical nodal spacing by a factor of  $\sqrt{K_h/K_v}$  relative to horizontal nodal spacing gives the same numerical accuracy as an isotropic grid/mesh with  $\Delta z = \Delta x = \Delta y$ . In other words, for a problem with vertical anisotropy the vertical nodal spacing,  $\Delta z_{\text{adjusted}}$ , could be increased according to:

$$\Delta z_{\text{adjusted}} = \Delta z \sqrt{K_h/K_v} \quad (5.4)$$

where  $\Delta z = \Delta x = \Delta y$  and  $K_h$  and  $K_v$  are horizontal and vertical hydraulic conductivity, respectively. For example if  $K_h/K_v = 100$ , the vertical nodal spacing could be 10 times larger than  $\Delta x$  and  $\Delta y$  without losing numerical accuracy. The concepts underlying Eqn (5.4) come from analysis of a transformed section (see Box 5.2).

### Box 5.3 Upscaling Hydraulic Conductivity: Layered Heterogeneity and Vertical Anisotropy

Point measurements of hydraulic conductivity are made at a scale smaller than the nodal spacing of most groundwater flow models. Point measurements can be adjusted to fit the larger nodal spacing in a numerical model by *upscaling*. A simple example of upscaling is presented in this box. For convenience, we refer to an FD cell, but the principles discussed also apply to finite elements.

In early work, [Maasland \(1957\)](#) and [Marcus and Evenson \(1961\)](#) observed that layered heterogeneity is related to the anisotropy of a composite sequence of geologic units. The layered sequence in [Fig. B5.3.1](#) is heterogeneous because each geologic unit in the sequence has a different value of hydraulic conductivity. Conceptually, measurements made at a small enough scale sample a homogeneous and isotropic volume of porous material. If the hydraulic conductivities of homogeneous and isotropic strata that make up a layered sequence could be measured, those hydraulic conductivity values could be *scaled up to hydraulically equivalent horizontal and vertical hydraulic conductivities* appropriate for representing the composite sequence of geologic units in cells or elements in a layer of a numerical model.

Suppose we want to calculate equivalent horizontal and vertical conductivities at each node ( $i,j$ ) in a horizontal nodal network within a given model layer of thickness  $B_{ij}$  ([Fig. B5.3.1](#)). Each isotropic stratum, ideally a *lamina* (the thinnest recognizable layer in sediment), in the layered sequence is homogeneous in the area around the node. The thickness of a lamina in the sequence is  $b_{i,j,k}$ , where  $k$  is a vertical index, and its hydraulic conductivity is  $K_{i,j,k}$ . The thickness of the model layer at node ( $i,j$ ) is  $B_{i,j}$ , where

$$B_{i,j} = \sum_{k=1}^m b_{i,j,k} \quad (\text{B5.3.1})$$

and  $m$  is the number of laminae in the layered sequence.

By realizing that the horizontal flow (specific discharge) through the layered sequence (as represented by Darcy's law) is equal to the sum of the flows through the laminae ([Freeze and Cherry, 1979](#), p. 34; [Haitjema, 1995](#), p. 129; [Todd and Mays, 2005](#), p. 101), it follows that the hydraulically equivalent horizontal hydraulic conductivity,  $K_h$ , is

$$(K_h)_{i,j} = \sum_{k=1}^m \frac{K_{i,j,k} b_{i,j,k}}{B_{i,j}} \quad (\text{B5.3.2})$$

(Continued)

### Box 5.3 Upscaling Hydraulic Conductivity: Layered Heterogeneity and Vertical Anisotropy—cont'd

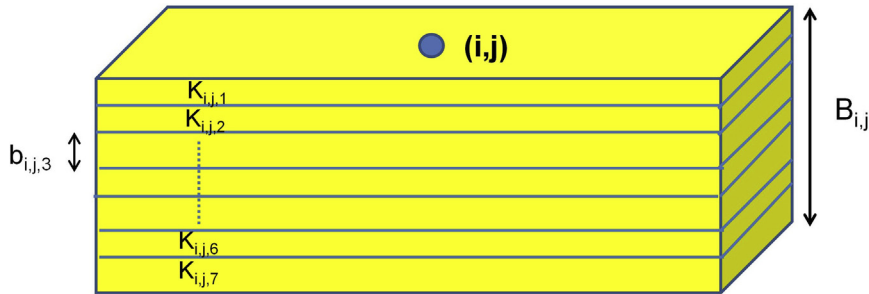


**Figure B5.3.1** Layered sequence of seven isotropic units that form a model layer of thickness  $B_{ij}$  at node  $(i,j)$  in the horizontal nodal network. The layered heterogeneity in the sequence of isotropic layers can be represented by a homogeneous and anisotropic block, which may be an FD cell or a finite element. Equations (B5.3.2) and (B5.3.3) can be used to calculate the equivalent horizontal and vertical hydraulic conductivity, respectively, for the block.

The equivalent vertical hydraulic conductivity,  $K_v$ , is

$$(K_v)_{ij} = \frac{B_{ij}}{\sum_{k=1}^m \frac{b_{i,j,k}}{K_{i,j,k}}} \quad (\text{B5.3.3})$$

Equation (B5.3.3) follows from conservation of mass, which requires that the vertical flow (specific discharge) is constant throughout the layered sequence (Freeze and Cherry, 1979, p. 33; Todd and Mays, 2005, p. 102).

It is apparent from Eqns (B5.3.2) and (B5.3.3) that values of equivalent  $K_h$  and  $K_v$ , and hence the vertical anisotropy ratio ( $K_h/K_v$ ), depend on the number of laminae included in the calculation and the contrast in hydraulic conductivity among laminae (Problem P5.2b). Equations (B5.3.2) and (B5.3.3) can also be used to compute equivalent hydraulic conductivities for a model layer when the layered sequence consists of anisotropic units rather than laminae. In that case, the set of  $K_h$  values for the layered sequence of units is input to Eqn (B5.3.2) to calculate the equivalent  $K_h$  for the model layer and  $K_v$  values are used in Eqn (B5.3.3) to calculate the equivalent  $K_v$  for the model layer (Problem P5.3).

Upscaling using Eqns (B5.3.2) and (B5.3.3) is difficult in practice because it usually is not practical to measure hydraulic conductivities at the scale required by those equations, i.e., at the scale of a lamina. Furthermore, laminae are seldom laterally continuous at the scale of a cell/element but are discontinuous and inter-finger (Fig. 5.26). Upscaling procedures that utilize available field measurements, which are at scales larger than a lamina, require different techniques; there is a relatively large literature on this topic (e.g., Dagan et al., 2013; Nøtinger et al., 2005; Renard and Marsily, 1997; also see references 23–27 in Zhou et al., 2014), which is beyond the scope of our book. However, in practice, values of horizontal hydraulic conductivity are refined and the vertical anisotropy ratio is estimated during model calibration (Chapter 9).

### Box 5.3 Upscaling Hydraulic Conductivity: Layered Heterogeneity and Vertical Anisotropy—cont'd

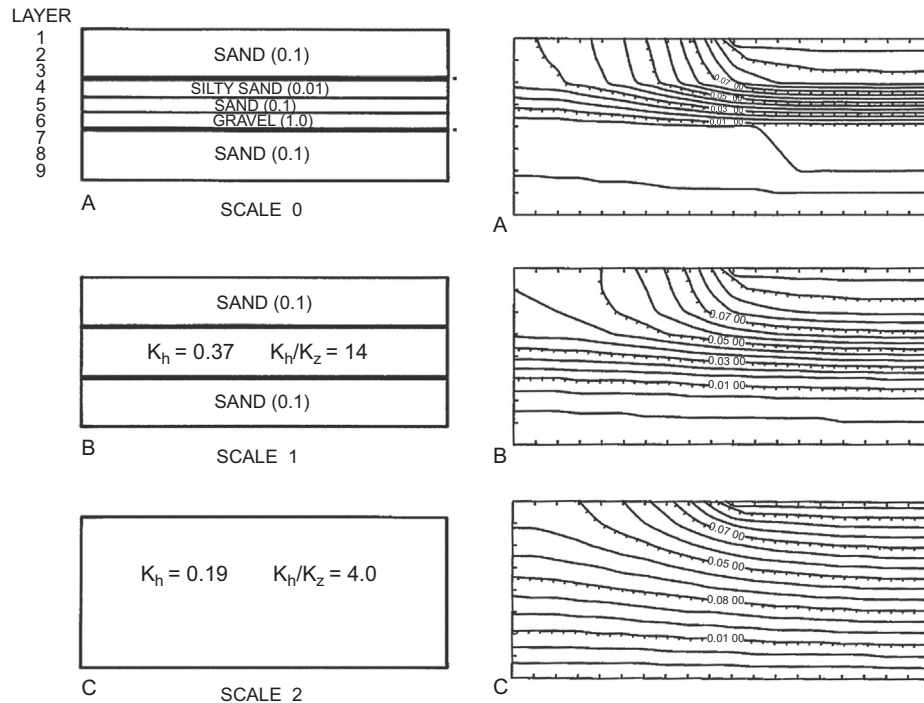


**Figure B5.3.2** Effects of layered heterogeneity. Representation of layered heterogeneity at three different scales is shown at the left. At scale 0 the layers are isotropic; values of  $K$  (cm/s) are given in parentheses. The equivalent horizontal hydraulic conductivity,  $K_h$ , and vertical anisotropy ratio,  $K_h/K_v$ , at scales 1 and 2 were calculated using Eqns (B5.3.2) and (B5.3.3). Equipotential lines (contour interval = 0.0034 cm) under 2D flow are shown in the figures at the right; in each representation the sides and left-hand side of the top boundary are under no flow conditions while the right-hand side of the top boundary is specified at  $h = 0.1$  cm and the bottom boundary is specified at  $h = 0$ . All three models were discretized into nine layers with each layer 20 cm thick. The same relative effects would be observed if the layers were scaled to represent flow at a larger scale, e.g., if each layer were 20 m thick (*modified from Anderson, 1987*).

Nevertheless, the modeler should always use Eqns (B5.3.2) and (B5.3.3) to confirm that calibrated vertical anisotropy ratios are reasonable for the geologic setting simulated.

In unconsolidated aquifers (e.g., alluvial deposits or glacial outwash) measured values of the vertical anisotropy ratio usually range between 2 and 100 (Todd and Mays, p. 103, who cite Morris and Johnson, 1967). For example, field measurements of the vertical anisotropy ratio in glacial outwash in Wisconsin, USA, range from 20 (Weeks, 1969) to around 5

(Continued)

### Box 5.3 Upscaling Hydraulic Conductivity: Layered Heterogeneity and Vertical Anisotropy—cont'd

(Kenoyer, 1988). Models that include unconsolidated aquifers are often designed for larger vertical scales than the scale of field measurements (e.g., Cao et al., 2013; Morgan and Jones, 1995; Guswa and LaBlanc, 1985; Winter, 1976) and those models use larger anisotropy ratios, often 100 or more (also see Problem P5.3). For example, Cao et al. (2013) used a vertical anisotropy ratio of 10,000 to represent unconsolidated alluvial sediments with interbedded clay layers in a three-layer regional model of the North China plain where mean layer thickness ranged from 110 to 160 m. The vertical anisotropy ratio in layered bedrock systems can be 1000 or more. Feinstein et al. (2010, p. 110) used  $K_H/K_V$  up to 2000 for aquifers and up to 20,000 for confining beds in a regional model of the Lake Michigan Basin, where fractures and permeable beds alternated with shale beds within the layers represented as confining beds.

Although large vertical anisotropy ratios may be unavoidable in some large-scale regional models, at the site scale, or even at the scale of a groundwatershed, it is often preferable to include low-permeability layers explicitly as model layers rather than lump their effect into the vertical anisotropy ratio assigned to a composite model layer. The modeler should be aware that, depending on boundary conditions, a high vertical anisotropy ratio may cause flow to be diverted horizontally (Box 5.2), even when vertical flow is imposed by the boundary conditions (Fig. B5.3.2).

### 5.3.2 Layer Types

A model layer may be confined, unconfined, or convertible. For modeling purposes, a layer is *confined* if the head is above the top of the layer and the saturated thickness of the layer does not change with time or stress applied. Then, transmissivity ( $T_x$ ,  $T_y$ ) is calculated for each cell, element, or node by multiplying hydraulic conductivity by saturated thickness.

Values of  $K_z$  are assigned to calculate leakance between layers. The storage parameter (Section 5.4) for a confined layer is confined storativity (specific storage multiplied by layer thickness). The code may allow the user to specify either storativity or, more conveniently, specific storage for each cell, element, or node. Simulated heads in a confined layer are, by definition, above the top of the layer. If the head in a confined layer drops below the top of the layer anytime during the simulation, the code typically requires that the layer remain confined (i.e., the saturated thickness is fixed at the thickness of the layer) or convert to unconfined conditions. Keeping layers under confined conditions, however, can result in an unrealistic saturated thickness. Therefore, layers that convert should be designated as convertible layers, which are discussed below.

In some settings, a layer under unconfined conditions (i.e., a water table layer) can be simulated as a confined layer if it is reasonable to assume that the saturated thickness is relatively constant in time. Representing an unconfined aquifer with constant saturated thickness is called the *specified-thickness approximation*, which linearizes the solution and is often helpful for stabilizing iterative solutions and speeding model convergence.

Sheets et al. (2015) presented a comprehensive analysis of the approximation, concluding that: “The reduced execution time and increased stability obtained through the approximation can be especially useful when many model runs are required, such as during inverse model calibration, sensitivity and uncertainty analyses, multimodel analysis, and development of optimal resource management scenarios.” However, any confined layer that represents a water table layer should be assigned values of specific yield to represent storativity.

A layer is *unconfined* when the head in the layer is below the top of the layer. The saturated thickness of an unconfined layer is equal to the elevation of the water table measured from the bottom of the layer. Saturated thickness changes during the simulation as the water table fluctuates. Values of hydraulic conductivity ( $K_x$ ,  $K_y$ ,  $K_z$ ) and specific yield are assigned to each cell, element, or node in the layer.

A *convertible layer* designation allows the code to switch from confined to unconfined conditions, or vice versa, without user intervention. If a layer is convertible, the code checks whether the head is above or below the top of the layer as the simulation progresses and treats the layer as confined or unconfined, accordingly. Values of both confined and unconfined storage parameters (Section 5.5) are input for convertible layers. The top several layers of a model can be designated as convertible while the bottom layers are designated as confined if it is unlikely that the water table will ever drop down into those layers. However, to maintain consistent input structure for all layers and to allow for the flexibility for a layer to switch between confined and unconfined conditions, it is usually preferable to designate all layers as convertible.

### 5.3.3 Layer Elevations

In a structured FD grid, the top and bottom elevations of the layers are typically input by the modeler and the code uses those values to compute layer thickness, although some codes might accept  $\Delta z$  directly as input. When the top and bottom elevations of a layer are constant in space,  $\Delta z$  is constant for the layer. However, most FD codes that use a structured grid (e.g., MODFLOW) allow the top and bottom elevations of a layer to vary by node so that in effect  $\Delta z$  varies spatially causing distortion of the layer (Fig. 5.20). The distortion introduces some error into the numerical solution, which is usually not a concern for groundwater flow modeling but may be a concern for particle tracking (Section 8.2). In an unstructured FD grid/FE mesh, the  $z$ -coordinate location of each node is required as input to generate the grid/mesh. Unstructured FD grids assume a layered sequence of nodes. An FE mesh is not restricted to a layered geometry (Fig. 5.3), but layers can be used when they best represent the geology (Fig. 5.16).

The bottom of a layer is the bottom of the hydrostratigraphic unit or is based on layered heterogeneities within the hydrostratigraphic unit. The top of a confined layer is also determined from the hydrostratigraphy. Conceptually, the top of an unconfined

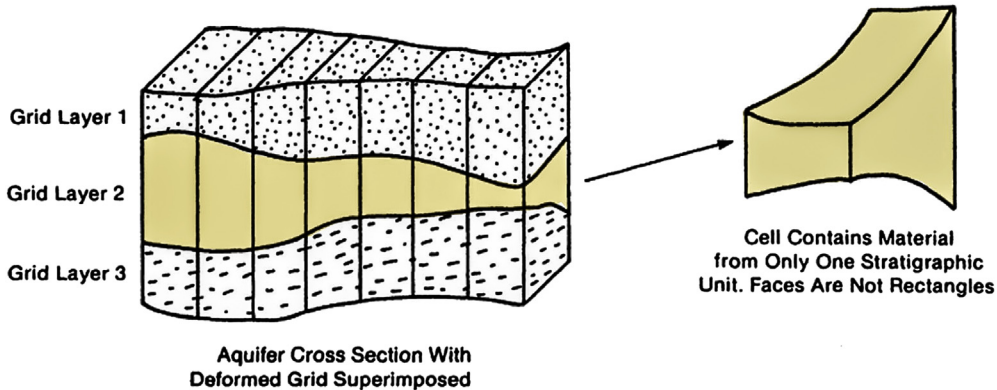


**Figure 5.20** Hydrogeologic units as deformed layers in an FD grid. Each cell in the layer has different top and bottom elevations so that  $\Delta z$  effectively varies with space, causing an irregularly shaped (deformed) layer as in Fig. 5.19 (modified from McDonald and Harbaugh, 1988).

layer is the water table, but since the water table is not accurately known the top is specified at an elevation above the water table, usually the elevation of the land surface. If the head in an unconfined layer rises above the modeler-specified top of the layer, the code will convert the layer to confined conditions, which may adversely affect the solution. Unintended conversions from unconfined to confined conditions are typically most problematic in transient simulations because upon conversion the code will use values of confined storativity instead of specific yield. Values of confined storativity are much lower than specific yield (Section 5.4).

To avoid unintended conversion to confined conditions, the top elevation of the top layer can be set arbitrarily higher (e.g., hundreds of meters higher) than the anticipated maximum elevation of the water table. However, in practice, the top elevation is usually set equal to the elevation of the land surface by using a GUI or GIS. Setting the top of the model at the elevation of the land surface is highly recommended so that the modeler can determine more easily if the computed head is above the land surface. GUIs typically include an option to display locations where the simulated head is above the land surface as flooded nodes. Flooded nodes may be appropriate in topographically low areas near surface water bodies and wetland areas. If not appropriate, flooded nodes can be eliminated by reducing recharge and/or increasing hydraulic conductivity of the system. Alternatively, a head-dependent boundary condition (e.g., drain nodes to represent wetlands) can be used to remove water when the simulated head reaches a modeler-specified elevation (e.g., land surface) provided there is justification for including such a feature.

### 5.3.4 Pinchouts and Faults

A commonly encountered complication in representing model layers is the presence of pinchouts, which occur when hydrostratigraphic units are discontinuous. In structured

grids and meshes, pinchouts can be simulated by adjustment of aquifer parameter values within a layer (Fig. 5.21(a); also see Fig. 4.6). Alternatively, a layer may continue as an arbitrarily thin layer ( $<1$  m) into an area where the unit is absent. Where absent, the arbitrarily thin layer is assigned properties representative of an adjacent layer. The unstructured FD grid in MODFLOW-USG permits conceptually more satisfying representation of pinchouts (Fig. 5.21(b)). The vertical offset of units along faults can also be represented in MODFLOW-USG (Fig. 5.22) where resistance along the fault is simulated with the Horizontal Flow Barrier (HFB) Package. FE meshes have similar flexibility for representing pinchouts and faults (Fig. 5.15), including DFEs for simulating flow in and around conduit faults (Fig. 5.16).

### 5.3.5 Dipping Hydrogeologic Units

It is usually acceptable to simulate hydrogeologic units that dip less than  $10^\circ$  as horizontal layers. When units dip more than  $10^\circ$  special procedures are warranted. The best option for simulating steeply dipping ( $>10^\circ$ ) hydrogeologic units is to use an FE code that solves the general form of the governing equation that includes the off-diagonal components of the hydraulic conductivity tensor (Eqn (B3.1.4) in Box 3.1; Section 5.1.1). FD and FE codes that do not allow for the general treatment of anisotropy can simulate some simple configurations of dipping beds in profile where the model's global coordinate system can be easily tilted to align with the  $K$  tensor (Fig. 5.3) or when a correction factor can be applied to the nodal spacing in order to represent dipping beds as horizontal layers (Carleton et al., 1999, pp. 24–25). However, for complex geologic settings where the dip changes (e.g., for folded beds, Fig. B3.1.1(b) in Box 3.1; Fig. 5.23(b)), an FE code that allows for alignment of  $K$  with local coordinate axes in each element of the mesh is required (e.g., see the results of Yager et al., 2009).

Both structured and unstructured FD grids are designed to represent horizontal layers (Figs. 5.23(c), 2.9(b), 2.11 and 4.6) so that the principal components of the hydraulic conductivity ( $K$ ) tensor can be aligned with the model's coordinate system (Box 3.1). Dipping hydrogeologic units slope at an angle (the dip angle) from the horizontal causing misalignment of the  $K$  tensor relative to the model's coordinate axes (Fig. 5.23(a)); the same situation occurs in structured FE meshes (Fig. 5.23(b)). When the dip is less than  $10^\circ$ , the error caused by the misalignment is less than 20% (Hoaglund and Pollard, 2003). Errors caused by misalignment can be significant, however, for steeply dipping hydrogeologic units. Nevertheless, FD (including CVFD) models can be used to simulate dipping beds provided the modeler is aware of the presence of errors caused by misalignment of the  $K$  tensor with the model's coordinate axes. A relatively large number of such models have been documented in the literature (see the references cited in Table 2 in Yager et al., 2009 for a partial list). Some guidelines for designing FD grids to simulate dipping units are given below.



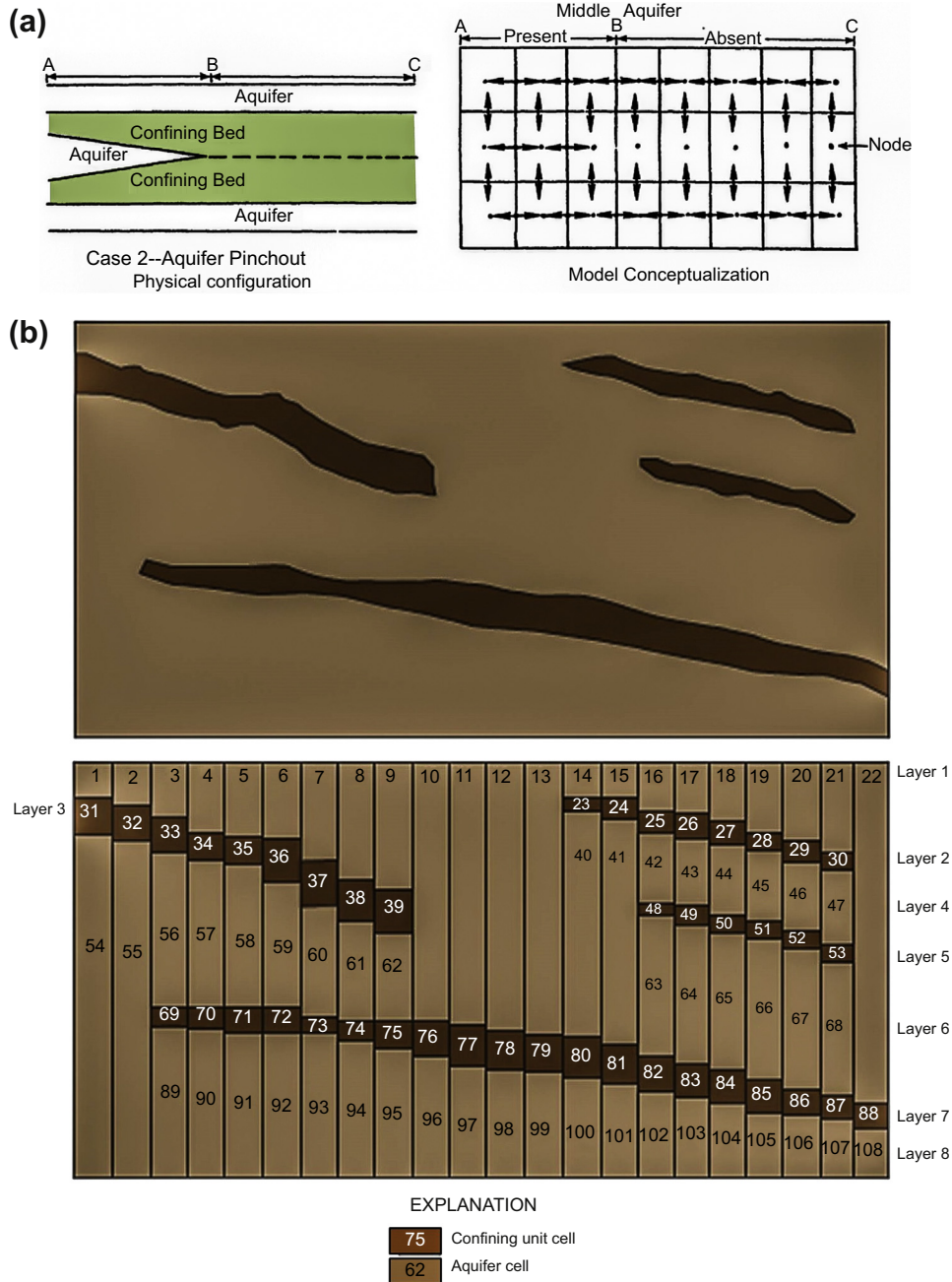


**Figure 5.21** Pinchouts. (a) Confining bed and pinchout aquifer shown at left are represented by the second model layer shown at the right. Hydraulic properties assigned to nodes within the layer reflect the change from aquifer to confining bed (*modified from Leahy, 1982*). (b) Pinchouts in cross section in an unstructured FD grid (*Panday et al., 2013*).

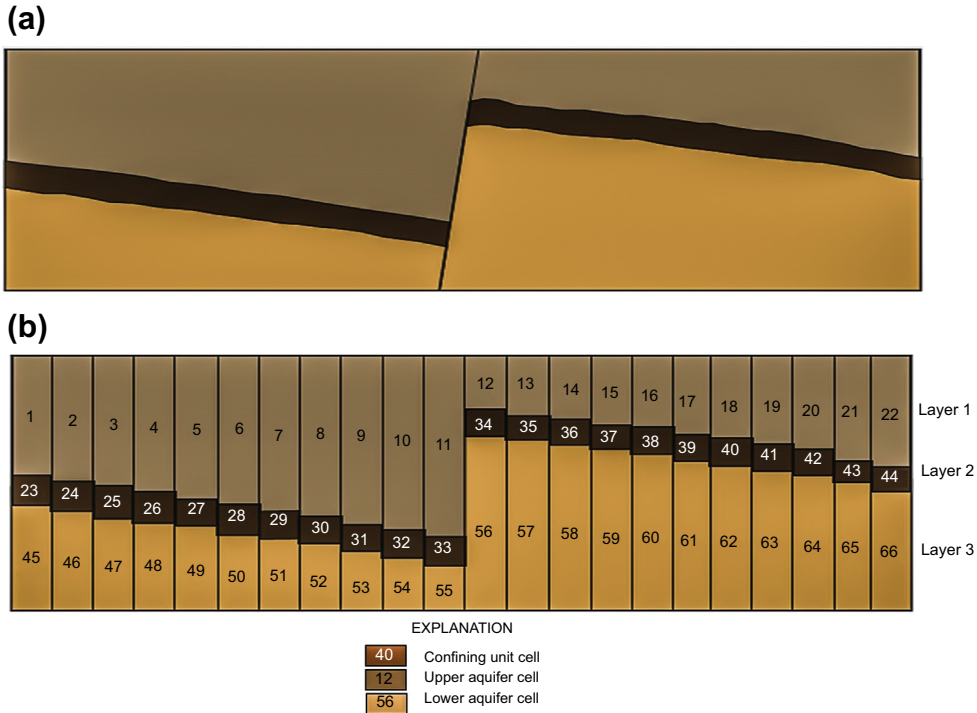


**Figure 5.22** Representation of faults in an unstructured FD grid. (a) Offset of units along a fault shown in cross section; (b) representation in an unstructured FD grid (Panday et al., 2013).

There are two general ways to simulate dipping hydrogeologic units in an FD grid: (1) spatial variation of material property parameters within layers is used to represent the change from one dipping hydrogeologic unit to the next (Fig. 5.23(a) and (c)); (2) each layer is represented as a single hydrogeologic unit (Figs. 5.24, 5.19(b) and 4.6). Each of these options is discussed below. In both options errors are introduced because  $K$  is not aligned with the  $x$  and  $z$  coordinate axes. Nevertheless, these options provide ways to incorporate the spatial changes in  $K$  caused by dipping beds using a standard FD code.

Dipping units can be simulated by assigning appropriate values of material property parameters to cells within a layer to represent the change from one dipping unit to the next (Fig. 5.23(a) and (c)). Then, horizontal changes in geology caused by the dip of the beds are captured by changes in the array of hydraulic conductivity values. This method is a conceptually pleasing way to represent the hydrogeology because the dip of the beds is reflected in the changes in geology within the grid. However, the method requires relatively complex bookkeeping to keep track of the spatial variation of hydraulic conductivity. That is, spatial variation in hydraulic conductivity must correspond to the locations of the relevant hydrogeologic units and is tied to the top and bottom elevations of the dipping hydrogeologic units, which are not explicitly included in the model.

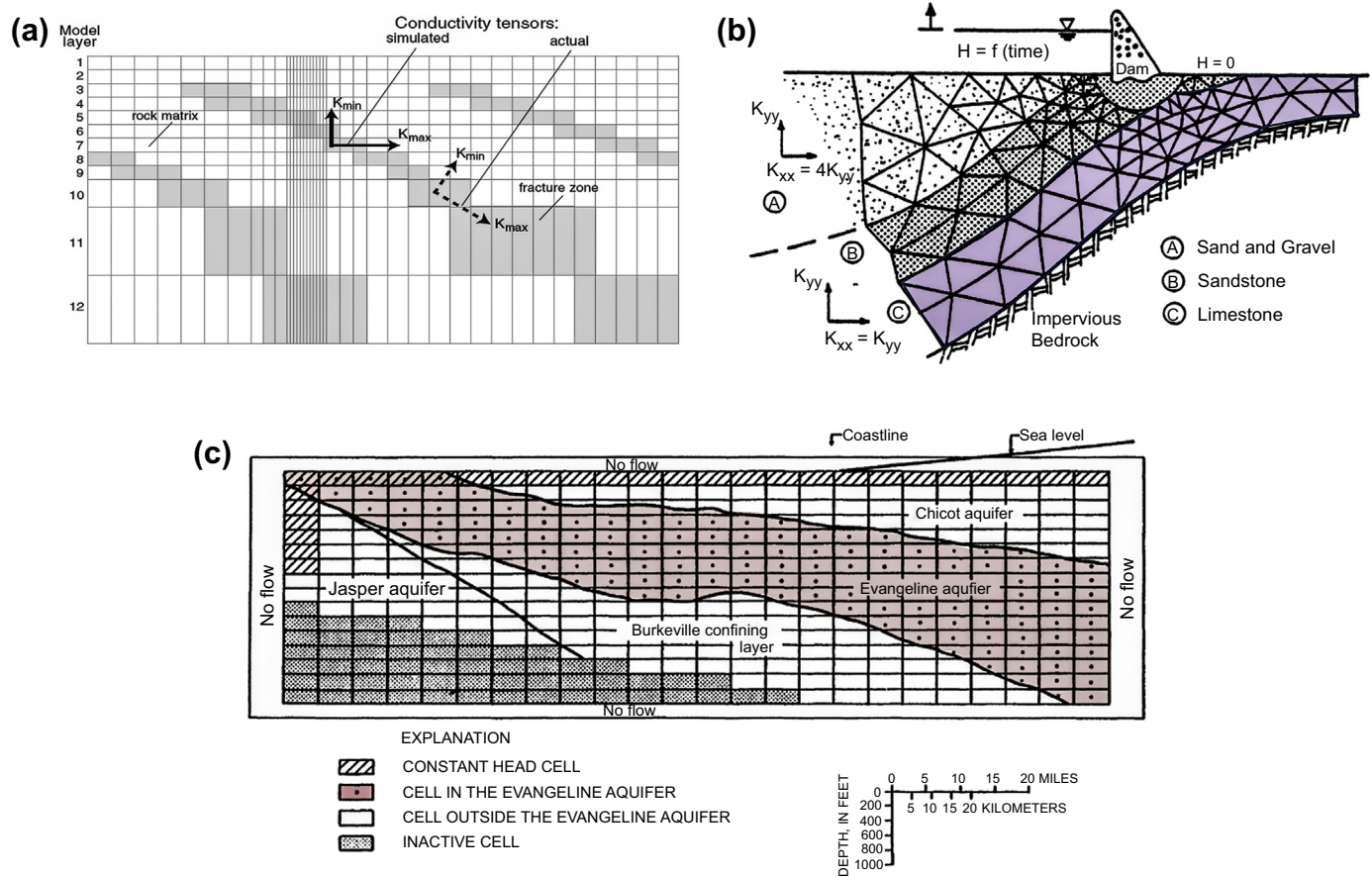


**Figure 5.23** Misalignment of the hydraulic conductivity tensor with the model's coordinate axes. (a) FD grid in profile showing dipping beds of fractured rock (shown by shading) superimposed over horizontal model layers. The horizontal change in geology caused by the dip of the units is captured by spatial variation in  $K$  within the layer.  $K_{min}$  is vertical hydraulic conductivity and  $K_{max}$  is horizontal hydraulic conductivity (Yager *et al.*, 2009). (b) FE mesh showing dipping and folded beds (hydrogeologic units B and C) beneath a dam in a 2D profile model. Under field conditions, the principal components of the  $K$  tensor ( $K_x$ ,  $K_y$ ) for hydrogeologic units B and C align with the dipping and folded bedding planes. In the model, units B and C are assumed to be isotropic so that  $K_{xx}$  and  $K_{yy}$  are equal and are aligned with the global coordinate system. For hydrogeologic unit A, the principal components of the hydraulic conductivity tensor are aligned with the global coordinate axes where  $K_{xx}$  is parallel to horizontal bedding in the sand and gravel and  $K_{yy} = K_{xx}/4$ . The fine resolution in the mesh beneath the dam is not shown (modified from Townley and Wilson, 1980). (c) FD grid in profile showing dipping hydrogeologic units represented by spatial variation in hydraulic conductivity within model layers (modified from Groschen, 1985).

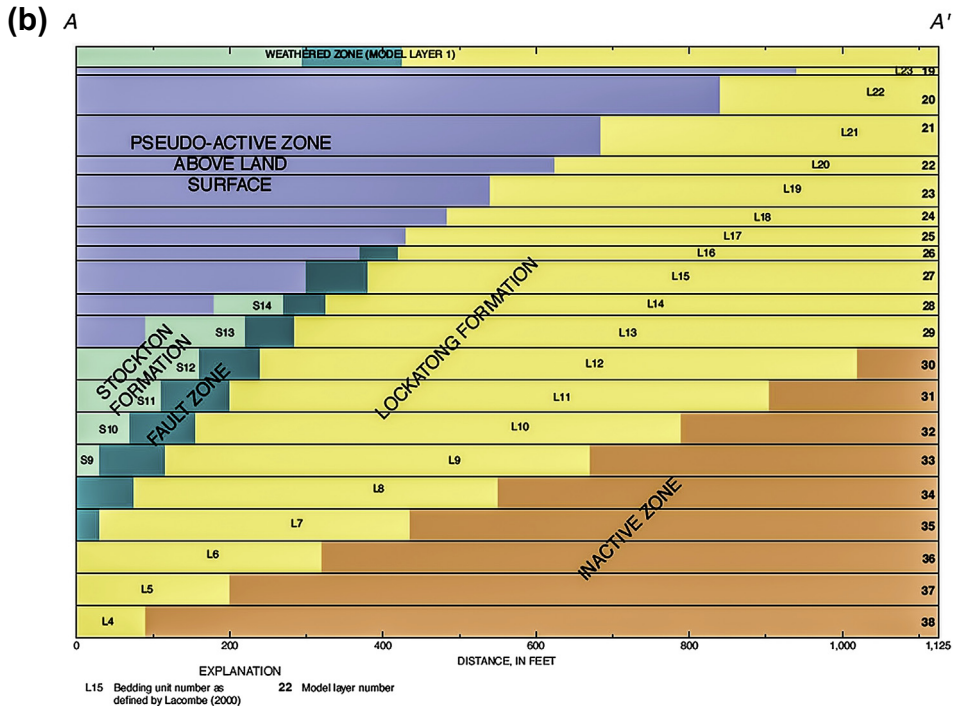
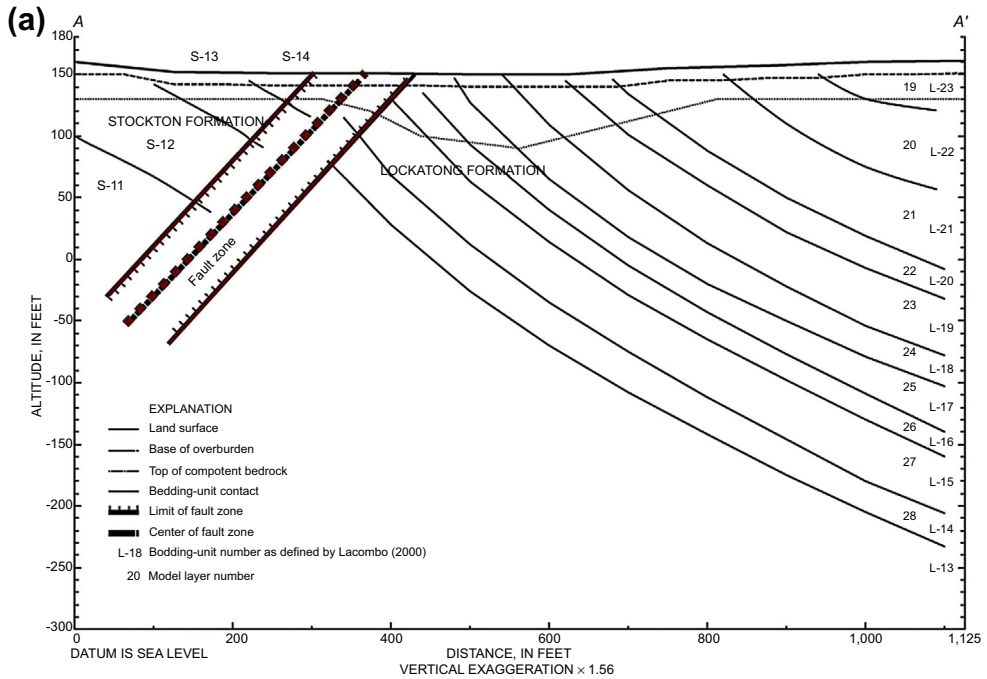


**Figure 5.24** Example representation of dipping hydrogeologic units as horizontal layers in an FD grid. The full grid is three dimensional with 71 layers. (a) Hydrogeologic cross section showing the dipping beds and fault zone. The dip angle in this setting ranges from 15° to 70° with the largest dips occurring near the fault zone. (b) Horizontal model layers that represent the geology in (a) showing areas of active (yellow and green), pseudo-active (purple), and inactive (tan) cells (modified from Lewis-Brown and Rice, 2002).

A conceptually less pleasing but operationally attractive alternative allows dipping hydrogeologic units to be represented in the usual manner as discrete layers in the model (Figs. 5.24, 5.19(b) and 4.6). Usually the layers are *deformed layers*, i.e., the nodes in a layer are aligned horizontally in the nodal network but each cell in the layer is assigned different top and bottom elevations (Figs. 5.19(b) and 5.20). This alternative for representing dipping hydrogeologic units is sometimes identified as using deformed layers although the layers used in this approach may not be deformed (Fig. 5.24(b)) and deformed layers are not necessarily dipping layers (Fig. 2.9(b)). For simple geologic settings characterized by uniformly sloping beds (Figs. 5.19(b) and 4.6), the approach is relatively straightforward. However, for complex geology (Fig. 5.24(a)) the layering is conceptually and operationally more complex in order to simulate the correct hydraulic conditions in each layer. Each layer may have up to three zones (Fig. 5.24(b)) arranged to span the entire horizontal extent of the model, inasmuch as each layer must occupy the full extent of the problem domain. (1) A zone of active nodes represents flow in the unit. (2) Nodes in a pseudo-active zone are assigned aquifer parameter values that allow water to flow vertically from the surface or a surficial aquifer but do not allow horizontal transmission of water. In the pseudo-active zone, the layer has a nominal thickness ( $<1$  m) and a high vertical hydraulic conductivity,  $K_z$  (i.e., a high leakance; low resistance). Nodes in the pseudo-active layer are called *pass-through nodes* because their only purpose is to transmit recharge to active nodes. Pass-through nodes transmit recharge to lower layers where a hydrostratigraphic unit crops out at the land surface (Fig. 4.6) or subcrops beneath an overlying horizontal surficial layer (Fig. 5.24). The high  $K_z$  of pass-through nodes can cause numerical instability, however, especially where they connect to internal boundary conditions that have high leakance (low resistance). (3) Finally, a zone of inactive nodes can be used to delineate the downdip terminus of the layer by imposing no flow conditions downdip where permeability of the unit is effectively zero at large depths.

## 5.4 PARAMETERS

In the next three sections we discuss parameters and assignment of initial parameter values to the grid/mesh. In this section, we briefly review the parameters used in modeling groundwater flow. In Section 5.5 we discuss parameter assignment whereby initial parameter values are assigned to each cell, element, or node. Some or all of these parameter values will be adjusted during model calibration (Chapter 9). In Section 5.6, we introduce parameter uncertainty, which is discussed again in Chapters 9 and 10.

The governing equation for groundwater flow (Eqn (3.12)) includes (1) the dependent variable, head, which is calculated by the model; (2) the independent variables, which are the spatial coordinates,  $x, y, z$  that provide the framework for the nodal network, and time,  $t$ , which provides the temporal framework; and (3) parameters. Parameters include *material property parameters*, which describe hydraulic characteristics

of the porous media, and *hydrologic parameters*, which specify stresses to the system as sources and sinks such as recharge rates, and pumping and injection rates.

An important consideration in parameter assignment is the recognition that both material property and hydrologic parameters are typically *scale dependent*, i.e., the value of the parameter depends on the scale at which the measurement is made. Parameter values obtained from field and laboratory measurements are usually at a different scale than the nodal spacing of a numerical model. *Scaling errors* are introduced by assigning parameter values to the nodal network without correction for scale dependency. *Upscaling* procedures (Box 5.3) adjust small-scale parameter values to fit the larger nodal spacing in a numerical model; likewise, large-scale parameter values (e.g., at a regional scale) may have to be downscaled for use at the site scale.

### 5.4.1 Material Property Parameters

Traditionally, two material property parameters describe hydraulic characteristics of the porous medium: (1) hydraulic conductivity, which describes transmission properties; and (2) storativity, which describes the transient uptake and release of water to or from storage. Also, effective porosity is needed for time of travel estimates using particle tracking (Chapter 8, Box 8.1).

#### 5.4.1.1 Hydraulic Conductivity

Hydraulic conductivity ( $K$ ) is the primary material property parameter that governs groundwater flow. Solutions are usually sensitive to  $K$ . Moreover, the large range in  $K$  values for geologic materials (e.g., over 12 orders of magnitude; Fig. 5.25) complicates a simple assignment of values. For screening models or preliminary model runs, it may be appropriate to assume that  $K$  is a constant value (i.e., that the porous material is homogeneous and isotropic). However, geologic materials in the field are heterogeneous (properties vary in space) and anisotropic (properties vary with direction) and most models include some heterogeneity and usually anisotropy as well. In many settings, the assumption that  $K$  is isotropic in the horizontal plane ( $K_x = K_y$ ) is appropriate. However, if the aquifer is fractured (Figs. 5.2, 2.14(a) and (b)), or contains sedimentary structures such as imbrication or other features that impart a preferential direction of flow (Fig. 2.8), horizontal anisotropy ( $K_x/K_y$ ) may be important. Horizontal anisotropy is also important for simulating dipping hydrogeologic units (Section 5.3) where the horizontal  $K$  parallel to the strike is typically greater than the horizontal  $K$  perpendicular to the strike (Yager et al., 2009). Horizontal anisotropy may be estimated from field measurements (Quinones-Aponte, 1989; Neuman et al., 1984) but is usually inferred or estimated from the geology.

Vertical anisotropy ( $K_h/K_v$ ), where  $K_h$  and  $K_v$  are horizontal and vertical  $K$ , respectively, is common to most hydrogeologic settings, and is caused by bedding planes and laminae (stratification) within a model layer (Figs. 5.26 and B5.3.2 in Box 5.3), as well

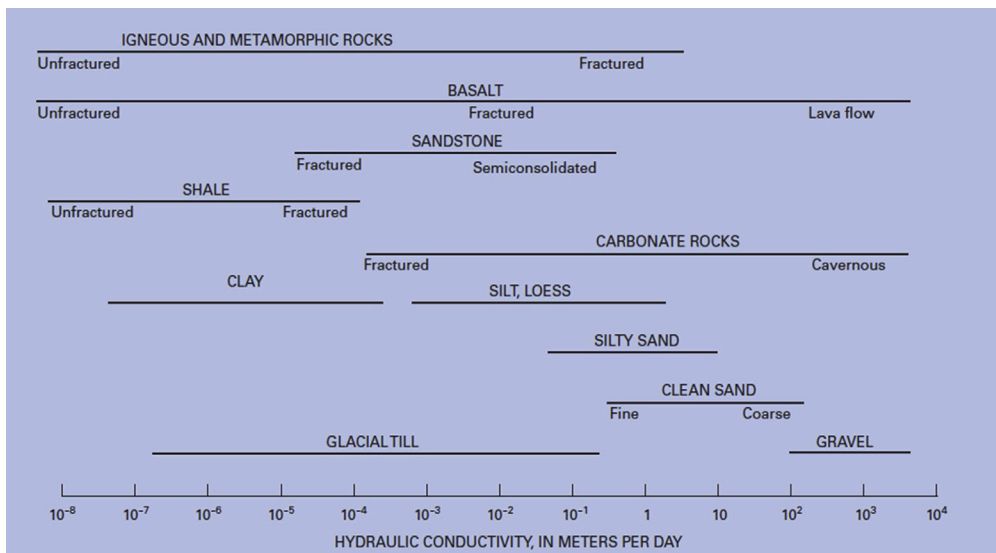


Figure 5.25 Range in hydraulic conductivity of geologic materials (Healy et al., 2007; modified from Heath, 1983).

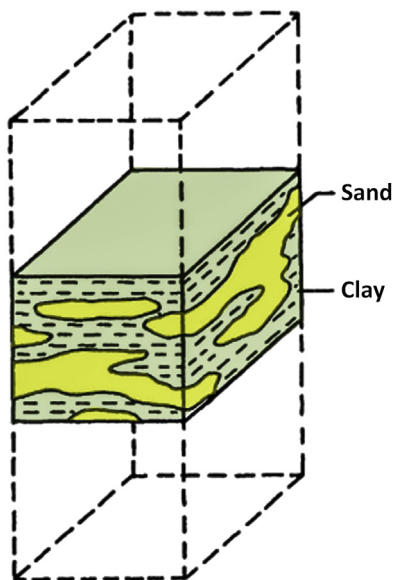


Figure 5.26 Schematic representation of discontinuous and interfingering laminae in a cell block in a layer of an FD grid (modified from McDonald and Harbaugh, 1988).

as fractures, heterogeneity, and other structures that cause preferential flow in the horizontal direction. Vertical anisotropy can be measured with specially designed aquifer tests (e.g., Weeks, 1969; Neuman, 1975; Kruseman and de Ridder, 1990; Sterrett, 2008) or tracer tests (e.g., Kenoyer, 1988) but these tests are rarely performed in practice. Vertical anisotropy is often scale dependent and depends both on the number of layers and structures sampled in the field and on the thickness of associated model layers (Box 5.3). Hence, field measurements typically are not representative of vertical anisotropy at the scale of a model and usually  $K_h/K_v$  is estimated during model calibration (Box 5.3).

Detailed information on spatial and directional variability in hydraulic conductivity is rarely available in either two or three dimensions, especially at the resolution of the nodal spacing in most groundwater flow models. Point values of hydraulic conductivity are commonly estimated from aquifer (pumping) tests, single-well (slug) tests, well performance tests and/or laboratory permeameter tests, and grain size analyses. Each method typically produces a different estimate of  $K$  inasmuch as each method samples the aquifer at a different scale and has different limiting assumptions and inherent errors.

In an aquifer test a well is pumped for a relatively long time, typically 24–72 h, and head is measured in one or more observations wells. Analysis of drawdown gives an estimate of the bulk average transmissivity and storativity for the volume of aquifer within the cone of depression. The values of aquifer parameters obtained from these tests average the effects of small-scale heterogeneities, fractures, layering, and other hydrogeologic features that affect transmission and storage of water in the aquifer. Aquifer tests can be designed to measure properties in confining beds as well. Parameter values obtained from aquifer tests may be appropriate for some site-scale models and may even be appropriate for regional-scale models if the cone of depression extends over a sufficiently large portion of the aquifer so that pumping “samples” the aquifer at a regional scale. However, a standard aquifer test does not provide information on spatial variation in  $K$  at the site scale. Below we discuss methods that can provide information about site-scale heterogeneity.

In hydraulic tomography, wells in a 3D network are sequentially pumped while water-level response is monitored in the remaining wells (Yeh and Lee, 2007). Sequential pumping in a 3D network of wells provides additional information over a single-well test because the pumping stress is applied at multiple points in space. An inverse code (Chapter 9) is used to estimate spatial variation in material property parameters (e.g., Berg and Illman, 2013; Cardiff et al., 2009). Bohling and Butler (2010) pointed out that inverse solutions of hydraulic tomography are non-unique and urged care when interpreting their results.



Single-well (slug) tests measure the response of head in a well to a sudden increase or decrease in water level caused by introducing/removing a metal or plastic cylinder or known volume of water (slug) to/from the well. These tests measure properties immediately around the well so that the values of parameters obtained from these tests are considered point rather than spatially integrated measurements. Multilevel slug tests (Butler, 2009) sample the spatial variation in  $K$  in three dimensions. In a multilevel slug test, water is injected into or removed from multiple levels of a well or borehole, usually installed by direct push (ASTM, 2010). Sections of a screened well or open borehole can be isolated by packers or fitted with multiple piezometers for testing (e.g., Liu et al., 2009, 2010; Dogan et al., 2011).

A well performance (specific capacity) test is typically performed soon after a well is drilled. Water is pumped from the finished well, typically for a few hours or less. The pumping rate (yield), initial static and final pumping water levels in the well, length of pumping, and specific capacity (pumping rate divided by drawdown) are reported. Specific capacity can be used to estimate values of transmissivity (e.g., Dunkle et al., 2015; Arihood, 2009; Sterrett, 2008; McLin, 2005); hydraulic conductivity is estimated from transmissivity and unit thickness. Well performance test results are usually included in a well construction report (WCR) that is often filed with a regulatory agency and publicly accessible. WCRs also report well ownership, location, drilling method, well construction and completion, and a geologic log from which information about hydrostratigraphy and thickness of units can be compiled. Data reported in WCRs should be used with caution as the elevation of the measuring point is usually not accurately measured and reported water levels may include drawdown from unquantified well losses that affect reported final pumping levels (Sterrett, 2008). Nevertheless, given the lack of information typically available for the subsurface, WCRs can provide useful information for estimating initial values of hydraulic conductivity for groundwater modeling.

Laboratory methods to estimate  $K$  include grain size analysis of unconsolidated sediment and permeameter tests of both sediment and rock. Parameter values from laboratory tests are point measurements because they sample a small portion of the aquifer. Hydraulic conductivity values from grain size analyses rely on generic empirical relations of grain size to permeability such as Hazen's equation, which may not represent site conditions (Rosas et al., 2014). In a permeameter test, hydraulic conductivity is estimated from measurements of flow rate and head in a column of porous media under steady-state (constant head) or transient (falling head) conditions. Hydraulic conductivity values obtained from permeameter tests are often several orders of magnitude smaller than values measured in situ (Bradbury and Muldoon, 1990) owing to rearrangement of grains during repacking the sediment into the permeameter. Even intact cores of sediment or rock and in situ measurements made in the field with a portable permeameter (Davis et al., 1994) can be unrepresentative of field conditions owing to scaling effects

caused by large-scale features such as fractures, gravel lenses, or bedding that are not captured at the scale of the permeameter sample. In practice, therefore, for modeling purposes, laboratory methods are best suited for determining relative differences in hydraulic conductivity.

#### 5.4.1.2 Storage

Storage parameters describe the release and uptake of water from storage in porous material in transient simulations (Chapter 7). The three storage parameters: storativity, specific storage, and specific yield are discussed below.

Storativity,  $S$ , sometimes called storage coefficient, is a dimensionless parameter that represents the change in volume of water,  $\Delta V_w$ , in a unit area of porous material,  $A$ , that occurs in response to a unit change in head,  $\Delta h$ ,

$$S = \frac{-\Delta V_w}{A\Delta h} \quad (5.5)$$

The convention in Eqn (5.5) is that  $\Delta V$  is intrinsically positive when  $\Delta h$  is negative, or, in other words, water is released from storage when head decreases and water is taken into storage when head increases. Under confined conditions, water is released from storage solely by aquifer compression and expansion of water, so that

$$S = \rho g b (\alpha + \theta \beta) \quad (5.6)$$

where  $\rho$  is density of water,  $g$  is gravity,  $b$  is thickness of the aquifer,  $\alpha$  is compressibility of the aquifer,  $\theta$  is total porosity, and  $\beta$  is compressibility of water. *Specific storage*,  $S_s$  ( $L^{-1}$ ), is confined storativity divided by aquifer thickness,  $b$ :

$$S_s = S/b \quad (5.7)$$

In an unconfined aquifer, most water is released from storage by drainage of water out of the pore space at the water table. Only a small amount of water is released as a result of the compression of the aquifer matrix and expansion of water. Water drained from pore space is represented by *specific yield*,  $S_y$ , which describes gravity drainage of water in response to a decline in the water table. More generally, it represents the volume of water,  $\Delta V_w$ , drained from a volume of porous material,  $\Delta V_{pm}$ . Under field conditions,  $\Delta V_{pm}$  equals  $A\Delta h$ , where  $\Delta h$  is the change in elevation of the water table:

$$S_y = \frac{\Delta V_w}{\Delta V_{pm}} = \frac{\Delta V_w}{A\Delta h} \quad (5.8)$$

Storativity of an unconfined aquifer,  $S_u$ , is

$$S_u = S_y + S_s b \cong S_y \quad (5.9)$$

where  $b$  is saturated thickness and  $S_s$  is defined by Eqns (5.6) and (5.7). In practice, unconfined storativity is effectively equal to  $S_y$  because  $S_y$  is so much larger than  $S_s b$ . Rather than refer to confined and unconfined storativity, some authors (e.g., Barlow and Leake, 2012, p. 5) restrict the use of storativity to confined conditions. For an applied modeler, the primary storage parameters input to a code are specific storage,  $S_s$  (Eqn. (5.7)), and specific yield,  $S_y$  (Eqn (5.8)). Internally, a groundwater flow code multiplies  $S_s$  by saturated thickness of the layer (e.g., Eqn (3.28)) and then uses confined storativity for confined layers and specific yield for unconfined layers (Section 5.5). Values of confined storativity and specific yield at a freshwater–seawater interface require special consideration (see Box 4.4).

Storativity for confined aquifers and specific yield are usually estimated from aquifer tests. Specific yield can also be measured by drainage experiments in the laboratory by measuring the volume of water,  $\Delta V_w$ , drained from a volume of saturated porous material,  $\Delta V_{pm}$  (Eqn (5.8)). Values of confined  $S$  are small, ranging from  $10^{-2}$  to  $10^{-5}$  (Fitts, 2013, p. 220). Values for  $S_y$  are much larger (Table 5.1) and typically range from 0.01 to 0.30 (Freeze and Cherry, 1979, p. 61; also see Fitts, 2013, p. 222). When field measurements are not available, values for specific yield may be taken from literature values (e.g., Table 5.1; also see Johnson, 1966) inasmuch as the range of possible values is relatively small. Specific storage can be calculated from measured values of confined storativity

**Table 5.1** Typical values of specific yield ( $S_y$ ) (Morris and Johnson, 1967)

Material	No. of analyses	Range	Arithmetic mean
Sedimentary materials			
Sandstone (fine)	47	0.02–0.40	0.21
Sandstone (medium)	10	0.12–0.41	0.27
Siltstone	13	0.01–0.33	0.12
Sand (fine)	287	0.01–0.46	0.33
Sand (medium)	297	0.16–0.46	0.32
Sand (coarse)	143	0.18–0.43	0.30
Gravel (fine)	33	0.13–0.40	0.28
Gravel (medium)	13	0.17–0.44	0.24
Gravel (coarse)	9	0.13–0.25	0.21
Silt	299	0.01–0.39	0.20
Clay	27	0.01–0.18	0.06
Limestone	32	0–0.36	0.14
Wind-laid materials			
Loess	5	0.14–0.22	0.18
Eolian sand	14	0.32–0.47	0.38
Rock			
Schist	11	0.22–0.33	0.26
Tuff	90	0.02–0.47	0.21

**Table 5.2** Typical values of specific storage ( $S_s$ ) (adapted from Domenico, 1972)

Material	Specific storage ( $S_s$ ) ( $m^{-1}$ )
Plastic clay	$2.0 \times 10^{-2} - 2.6 \times 10^{-3}$
Stiff clay	$2.6 \times 10^{-3} - 1.3 \times 10^{-3}$
Medium-hard clay	$1.3 \times 10^{-3} - 9.2 \times 10^{-4}$
Loose sand	$1.0 \times 10^{-3} - 4.9 \times 10^{-4}$
Dense sand	$2.0 \times 10^{-4} - 1.3 \times 10^{-4}$
Dense sandy gravel	$1.0 \times 10^{-4} - 4.9 \times 10^{-5}$
Rock, fissured, jointed	$6.9 \times 10^{-5} - 3.3 \times 10^{-6}$
Rock, sound	Less than $3.3 \times 10^{-6}$

using Eqn (5.7) or estimated from literature values (Table 5.2). Because storage parameters are typically not well constrained by field data, uncertainty in values of storage is usually evaluated during model calibration.

#### 5.4.1.3 Vertical Leakance, Resistance, and Conductance

Surface water features often are simulated in a groundwater model by head-dependent boundary conditions (Section 4.3) whereby the rate of exchange of water between surface water and groundwater is affected by sediments present at the sediment–water interface. The vertical hydraulic conductivity and thickness of the sediments is used to calculate flow rate through the sediments (Eqn (4.5)), where vertical leakance is the vertical hydraulic conductivity of the sediments divided by their thickness ( $K'_z/b'$ ); vertical resistance, ( $b'/K'_z$ ), is the inverse of leakance. Vertical conductance is leakance times the horizontal area of the sediments within the cell (Eqn (4.4b)).

Vertical leakance is difficult to measure in the field; point measurements are strongly affected by local heterogeneity in  $K'_z$ , which makes upscaling problematic (e.g., Rosenberry et al., 2008). In practice, vertical leakance (or conductance) is estimated during model calibration. Generic guidelines for the relative magnitude of  $K'_z$  can be helpful when checking that calibrated values are reasonable for the hydrogeologic setting being simulated. For example, littoral sediments (sediments disturbed by waves and currents) have relatively higher  $K'_z$  than finer sediments deposited in deeper and calmer water. In areas where surface water recharges an aquifer, sediments may have lower  $K'_z$  than areas where groundwater discharge occurs owing to clogging of pore space by fine-grained sediment suspended in surface water (Lee, 1977; Rose, 1993).

Head-dependent conditions only approximately represent the relevant geometry and flow system around surface water features and fine spatial discretization may be required to represent properties associated with surface water features (Section 5.2). Consequently, adjusting vertical leakance (or conductance) during calibration offsets artifacts introduced by discretization such that calibrated leakance values likely will not agree even with

perfectly accurate field measurements of leakance (McDonald and Harbaugh, 1988, pp. 6–5 and 6–6). Consequently, leakance values are typically calibrated to match field measurements of flux. Similarly, the leakance of drains and springs simulated by head-dependent conditions (Section 4.3) is also typically adjusted during calibration to match measured flows.

#### **5.4.1.4 Total Porosity and Effective Porosity**

Neither total porosity (a measure of total void space within a volume of porous material) nor effective porosity (a measure of interconnected void space) appears in the governing equation of groundwater flow (Eqn (3.12)). Although total porosity is in the definition of confined storativity (Eqn (5.6)), confined storativity is usually estimated from aquifer tests or taken from literature values rather than computed from Eqn (5.6). Effective porosity, however, is important in particle tracking where it is used to calculate velocity (Section 8.1). Hence, we defer discussion of effective porosity to Chapter 8 (Box 8.1).

### **5.4.2 Hydrologic Parameters**

Hydrologic parameters describe stresses to the system. The main hydrologic stresses are recharge, pumping/injection, and evapotranspiration.

#### **5.4.2.1 Recharge**

Recharge is water that infiltrates at the land surface, flows through the unsaturated zone, and crosses the water table to enter the groundwater system. Methods of measuring and estimating recharge are many and varied (Table 5.3) and are discussed in detail by Healy (2010). Initial values of steady-state recharge to the water table can be broadly specified as a fraction of the local annual precipitation or estimated from soil characteristics (e.g., using the HELP model; Schroeder et al., 1994). Recharge can also be estimated as outflow from an unsaturated flow model (e.g., HYDRUS; Simunek et al., 2011; and the UZF Package; Niswonger et al., 2006) (Box 5.4), from output of General (Global) Circulation Models (e.g., Toews and Allen, 2009), or as the residual in a soil water balance (Box 5.4).

Although large-scale recharge estimates can be bounded by reasonable ranges, spatial and temporal variability in recharge is difficult to quantify. The modeling purpose dictates when spatial and temporal variation in recharge is important. For example, if contaminant transport or high-resolution delineation of groundwater flowpaths is a primary modeling objective, recharge should be specified in space and time with relatively high resolution. For regional groundwater problems, it is usually sufficient to assign an average recharge rate uniformly over the entire problem domain, although spatial variation in recharge may be required for accurate simulation of baseflow (e.g., Juckem et al., 2006) or groundwater levels (Cao et al., 2013) even at the regional scale.

**Table 5.3** Methods of estimating recharge and discharge. Most methods can be used for estimating both recharge and discharge although a given method may be better suited for one than the other (modified from [NRC, 2004](#); [Scanlon et al., 2002](#))

Hydrologic zone where actual measurement is made	Method	
	Arid and semi-arid climates	Humid climates
Surface water	Channel water budget Baseflow discharge Seepage meters Heat tracers Isotopic tracers Solute mass balance Watershed modeling	Channel water budget <sup>b</sup> Baseflow discharge <sup>b</sup> Seepage meters Heat tracers Isotopic tracers Solute mass balance Watershed modeling
Unsaturated zone (measurable discharge would mainly be upward exfiltration to vegetation)	Lysimeters <sup>a</sup> In situ sensors (neutron probes, TDR, etc.)  Zero-flux plane <sup>a</sup> Darcy's law Tracers (historical ( <sup>36</sup> Cl, <sup>3</sup> H, <sup>2</sup> H, <sup>18</sup> O), environmental (Cl)) Numerical modeling Thermal analysis Surface geophysics (DC, EM, radar) Cross-hole geophysics (DC, EM, radar) Gravity geophysics	Lysimeters <sup>a</sup> In situ sensors (neutron probes, TDR, etc.)  Zero-flux plane <sup>a</sup> Darcy's law Tracers (applied)  Numerical modeling  Surface geophysics (DC, EM, radar) <sup>a</sup> Cross-hole geophysics (DC, EM, radar) <sup>a</sup>
Groundwater	   Elastic compression measurements (e.g., GIS, InSAR)  Tracers (historical (CFCs, <sup>3</sup> H/ <sup>3</sup> He), environmental (Cl, <sup>14</sup> C)) Numerical modeling	Water table fluctuations (observation wells, geophysics)   Darcy's law Tracers (historical (CFCs, <sup>3</sup> H/ <sup>3</sup> He))  Numerical modeling

<sup>a</sup>Method appropriate only for recharge estimation.

<sup>b</sup>Method appropriate only for discharge estimation.

### Box 5.4 When Infiltration becomes Recharge

Groundwater recharge, which is water that crosses the water table, is one of the most important parameters (Section 5.4) for groundwater modeling. Groundwater recharge originates as *infiltration* at the land surface (terrestrial infiltration) or as infiltration beneath a surface water body or water that is temporarily ponded on the land surface (ponded infiltration). In both cases, some water is usually lost via evapotranspiration; the remainder eventually arrives at the water table as recharge. The recharge process is of interest in agricultural problems and streamflow generation as well as in groundwater problems. Thus, it is not surprising that infiltration and recharge have been studied by soil physicists and surface water hydrologists in addition to groundwater hydrologists (e.g., see the overview by Freeze and Cherry, 1979, pp. 211–221).

Recharge is difficult to measure in the field but there are many methods for estimating recharge indirectly (Table 5.3). Field measurements, when available, typically are point values that must be upscaled to the model domain. Given tools currently available, our preferred method is to calculate an initial estimate of recharge as the residual in a soil water balance. The soil water balance method is appealing because it provides a physical basis for estimating recharge in space and time, uses commonly available data (e.g., land cover, soil properties and root depths, precipitation, and air temperature), and can be applied to model domains of any size. Also, software that calculates recharge in a format suitable for input to a groundwater flow model is readily available (e.g., Westenbroek et al., 2010). In this method, the soil root zone is defined to extend from the land surface to the zero flux plane (Fig. B5.4.1), an imaginary surface that demarcates upward movement of water in response to evapotranspiration from downward movement to the water table. Infiltration at the land surface is calculated as precipitation minus runoff; losses from evapotranspiration within the soil zone are subtracted (e.g., using the well-known Thornthwaite–Mather method; see Westenbroek et al., 2010); and the residual water crosses the zero flux plane and flows through the unsaturated zone to the water table to become recharge.

Although the approach is appealing, there are three concerns in using a soil water balance to estimate recharge. (1) Any quantity calculated as a water balance residual is affected by the cumulative errors in estimating all the other components in the water balance. (2) The soil water balance method does not account for rejected recharge. The concept of rejected recharge was introduced by Theis (1940) and is explained as follows. In areas where the ambient water table is close to the land surface (usually within 1 m), infiltration during storm events may cause the water table to rise to the land surface, thereby saturating the soil zone from below. Saturated soil transmits water only up to a rate equal to the saturated hydraulic conductivity. If the rainfall rate exceeds the saturated hydraulic conductivity, excess rainfall is “rejected” and runs off the land surface as *saturation excess overland flow* (Box 6.3), which is distinct from infiltration excess (Hortonian) overland flow that occurs when the soil’s infiltration capacity is exceeded. Accounting for rejected recharge can give appreciably lower values of recharge than estimated from a simple soil water balance (Fig. B5.4.2(a)). (3) The residual from the soil water balance is water that flows out the bottom of the root zone. Therefore, the method does not account for the time required

### Box 5.4 When Infiltration becomes Recharge—cont'd

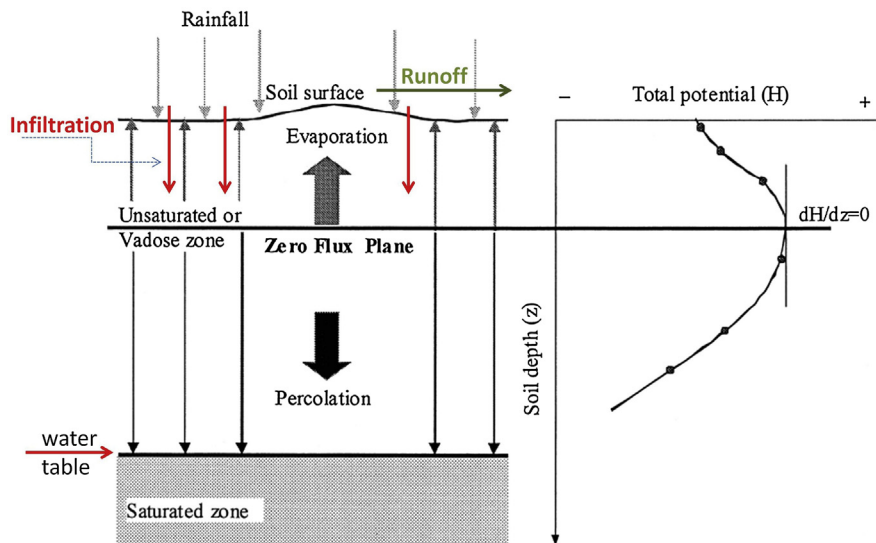


**Figure B5.4.1** Schematic profile of the subsurface (left-hand side) and plot of total head (potential) in the subsurface continuum (right-hand side) showing the zero flux plane in the unsaturated (vadose) zone. The soil root zone is the upper part of the unsaturated zone between the land (soil) surface and the zero flux plane. Here, evaporation includes both evaporation and transpiration (i.e., evapotranspiration). Runoff shown here represents infiltration excess overland flow rather than rejected recharge. Recharge crosses the water table at the top of the saturated zone. The gradient in total head ( $dH/dz$ ) changes direction at the zero flux plane (whereas pressure head = 0 at the water table) (modified from Khalil et al., 2003).

for water to flow from the zero flux plane to the water table. In areas with deep water tables (e.g., depths  $>5$  m in coarse soils), transit through the unsaturated zone affects the timing and magnitude of recharge at the water table (Fig. B5.4.2(b)).

These issues can appreciably affect the results of a groundwater model if recharge calculated from a soil water balance is input directly as recharge at the water table. To address the first concern, it is usual practice to adjust recharge estimated from a soil water balance during calibration of the groundwater flow model. In order to retain the relative spatial differences in recharge over a watershed, a single multiplier can be defined as a calibration parameter for the recharge array derived from a soil water balance. In that way, a physically based recharge pattern is retained but the absolute values of recharge are obtained by parameter estimation during calibration (Chapter 9). To address the last two concerns, the groundwater model must account for unsaturated zone processes at some level, even if in a simplified representation (e.g., Niswonger et al., 2006).

(Continued)



## Box 5.4 When Infiltration becomes Recharge—cont'd

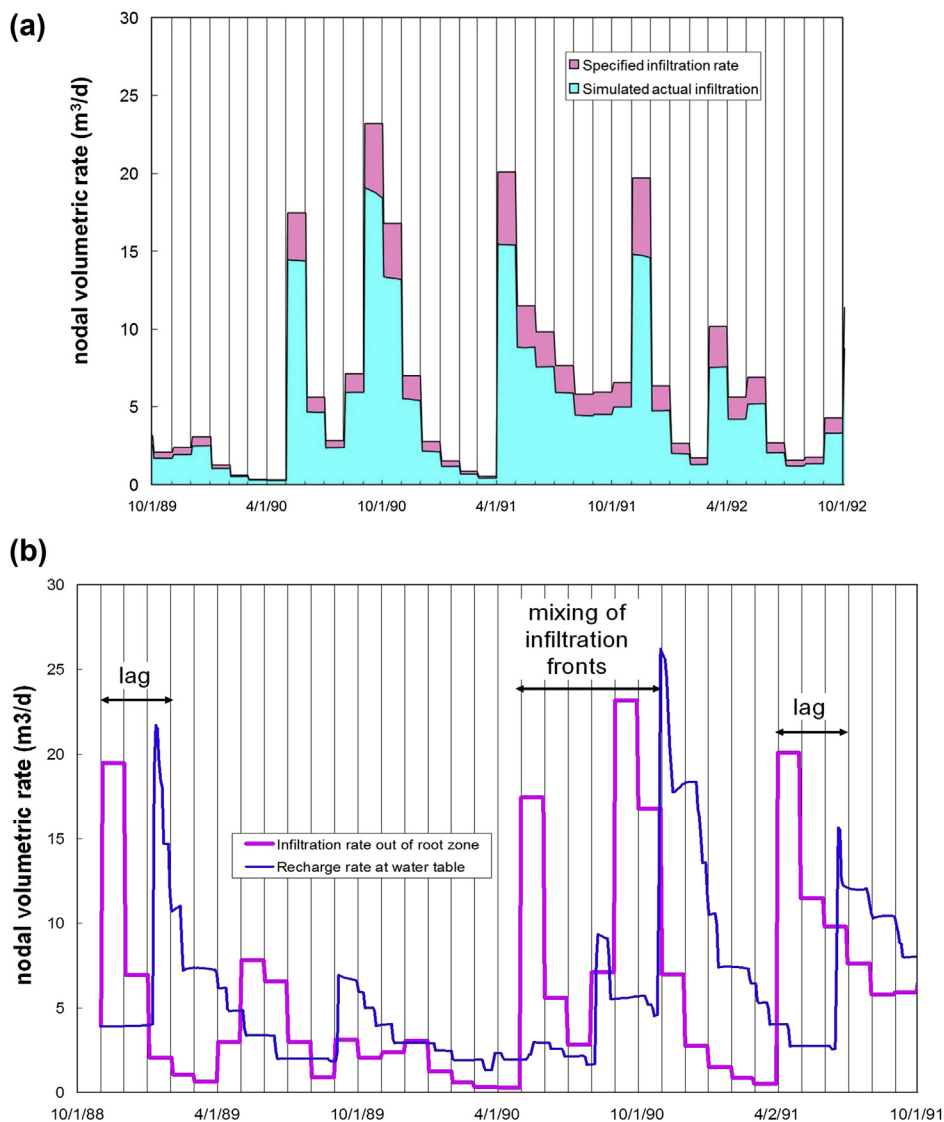


**Figure B5.4.2** Comparison of recharge estimated from a soil water balance with recharge calculated by a one-dimensional (column) unsaturated flow approximation for each node by using the MODFLOW-UZF Package (Niswonger et al., 2006) for a humid temperate climate in northern Wisconsin, USA. The tops of the soil columns were placed at the zero flux plane (Figure B5.3.1). Recharge rates from the soil water balance were calculated by using a soil water balance approach. (a) Results when the unsaturated zone was less than 1 m thick. Recharge at the water table simulated by using the UZF Package (blue bars) was less than recharge estimated from a soil water balance (blue + pink) that did not account for rejected recharge and associated saturation excess overland flow. (b) Results when the unsaturated zone was greater than 15 m thick show differences in the timing and magnitude of recharge events. Infiltration derived from the soil water balance is shown by the pink line; water passing the simulated water table by using the UZF Package is shown by the blue line. Note that recharge (blue line) during October 1990 does not return to the baseline observed in the summer owing to the mixing of the fall 1990 infiltration front with the previous spring's infiltration (modified from Hunt et al., 2008).

Spatial distribution of recharge is controlled by many interrelated factors such as precipitation, local topography, soil infiltration capacity, and topography as well as depth to the water table and unsaturated zone properties and conditions. Distributing recharge spatially can be difficult because most field measurements that constrain recharge (e.g., stream baseflow) integrate large areas of the model domain and thereby provide insight on the average rate over the area but not the distribution within the area. Temporal distribution of recharge can be confounded by unsaturated zone processes that serve to lag and coalesce individual infiltration events (Box 5.4).

Often piecewise constant recharge rates are assigned to zones within the problem domain (Section 5.5). A soil water balance approach (Box 5.4) helps delineate recharge zones and estimate relative, if not absolute, values of recharge among zones. Initial values of recharge assigned to the nodal network are usually adjusted during model calibration (e.g., Cao et al., 2013) and are constrained by measurements of groundwater discharge such as stream baseflow because much of the water that enters the model as recharge typically leaves the model as discharge to surface water. Even when recharge parameters vary spatially, a single calibration parameter is often used to multiply all values in the model's recharge array to match measured baseflow (e.g., Hunt et al., 2003b; Feinstein et al., 2010).

#### **5.4.2.2 Pumping Rates**

Pumping (or injection) rates are straightforward to measure and frequently recorded (e.g., for municipal pumping wells); if not recorded water usage can be estimated, for example by using crop type to estimate irrigation pumping.

#### **5.4.2.3 Evapotranspiration (ET)**

ET is the combined loss of water by direct evaporation and transpiration by plants, which occurs most commonly where the water table is at or close to the land surface. Similar to recharge, there is a wide variety of possible techniques for measuring ET, and detailed discussion is outside the scope of our text. In terms of applied groundwater modeling, ET from the water table is typically simulated as a head-dependent boundary condition (Section 4.3), where required input parameters are the maximum ET rate and the extinction depth where ET ceases. Reasonable values for these parameters are expected to be site specific; ranges are available in the literature (e.g., see Moene and Dam, 2014; Goyal and Harmsen, 2013; Abteu and Melesse, 2012).

Evaporation, and when vegetation is present also transpiration, also occurs from surface water features, which in turn can affect groundwater flow. Direct evaporation of water from streams is typically negligible due to small free water surface area, and thus is commonly neglected in groundwater models. Evaporation from relatively large surface water bodies such as lakes should be included (Section 6.6). Evaporation from even relatively small lakes can be scale dependent owing to changes in wind regime (e.g., Granger and Hedstrom, 2011) resulting from different fetch lengths and degree of sheltering.

Consequently, rates of lake evaporation may vary for lakes in the same model (e.g., [Hunt et al., 2013](#)). ET rates from wetlands can be affected by changes in wind regime resulting from changes in surface roughness so that actual ET rates are higher than potential ET rates derived from point values calculated by commonly used meteorological methods ([Lott and Hunt, 2001](#)). Regardless of whether ET is simulated as a head-dependent boundary condition or directly specified as a flux out of the model, point measurements of ET should be scaled up to the nodal spacing and assessed during calibration to ensure representativeness for a given site ([Healy, 2010](#), p. 31).

## 5.5 PARAMETER ASSIGNMENT

Initial parameter values assigned to the model are based on field and laboratory measurements and guided by hydrogeologic judgment. After adjusting for scale effects ([Section 5.4](#)), point estimates of parameter values are zoned or interpolated to populate the grid/mesh. During model calibration, some or all parameter values are adjusted so that simulated values of heads and fluxes more closely match measurements from the field site ([Chapter 9](#)).

### 5.5.1 General Principles

Both FD (including CVFD) and FE models calculate heads at nodal points. However, parameter values may be assigned to cells, elements, or nodes; the convention for parameter assignment is code specific. Some general principles about parameter assignment are given below but the modeler should always consult the code's user's manual for code-specific information.

When assigning initial parameter values, site-specific, field-based values are preferred, but parameter values for the general region in which the site is located as well as generic parameter values from the literature are often helpful in selecting initial estimates. Generic values for the primary material property parameters of hydraulic conductivity, specific yield, and specific storage are given in [Fig. 5.25](#), [Tables 5.1](#) and [5.2](#), respectively.

In a block-centered FD grid, parameter values are associated with all active nodes ([Fig. 5.2\(a\)](#), [5.6](#), [3.4](#) and [4.15](#)). The code usually internally sets parameter values to zero for inactive nodes ([Fig. 4.14](#)). In a block-centered grid, parameters are representative of the volume of material in the block. In a point-centered grid, parameters are assigned to the area of influence around a node ([Fig. 5.5\(b\)](#)) although other conventions are possible. In FE modeling, parameter values are usually assigned to the elements (e.g., [Fig. 5.23\(b\)](#); and in FEFLOW; [DHI-WASY GmbH, 2012](#)), although some codes (e.g., MODFE; [Torak, 1993](#)) assign some parameters to nodes and some to elements. When linear triangular elements are used exclusively, it may be easier to assign values to the nodes because there are always fewer nodes than elements, provided nodal assignment is permitted by the code. For example, the mesh in [Fig. 5.13\(c\)](#) has 155 elements but only 96 nodes. When aquifer properties vary sharply, parameter values should be

assigned to the elements. Moreover, boundaries between two types of porous media should always coincide with element boundaries (Fig. 5.23(b)).

### 5.5.2 Assigning Storage Parameters to Layers

Special attention is required when assigning storage parameters (Section 5.4) to model layers. Values of specific yield are assigned to unconfined layers and values of confined storativity or specific storage are assigned to confined layers. In most cases the layer will be designated as convertible (Section 5.3), and both specific yield and specific storage (or confined storativity) are input and the code uses the appropriate parameter depending on the current state of the layer (i.e., as either confined or unconfined). Specific yield is the appropriate storage parameter only for model layers where a water table is present (i.e., for unconfined layers). If an unconfined aquifer is represented by several model layers, only layers in which the water table is present are unconfined (Fig. 5.27). Layers below a water table layer are modeled as confined layers and use a confined storage parameter.

### 5.5.3 Populating the Grid or Mesh

Field and laboratory measurements typically are available at only a limited number of locations in the problem domain, but the model requires that values be assigned to every cell, element, or node in the grid/mesh. There are two main methods for extending point estimates of parameters to the entire nodal network: zonation and interpolation. A hybrid approach that uses both zonation and interpolation is also available. Regardless of the approach used, parameter distributions should be consistent with the geological history and depositional environment of the conceptual model for the site being modeled.

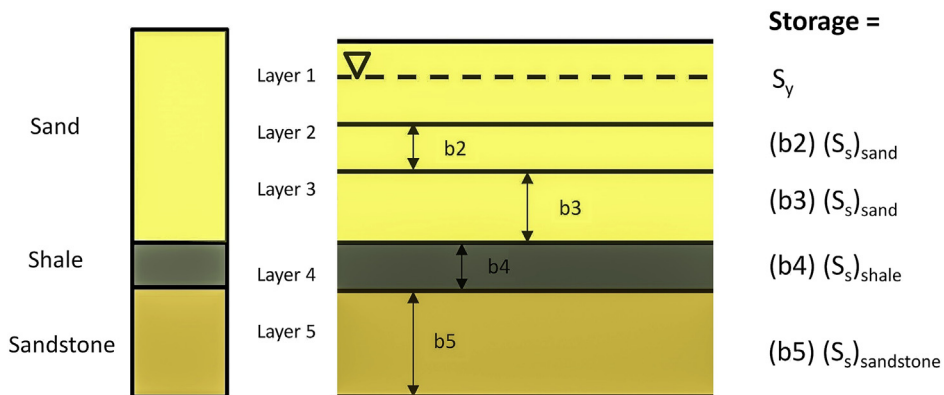


**Figure 5.27** Assignment of storage parameters in a five-layer model with three hydrogeologic units: an upper sand aquifer under unconfined conditions, a shale confining unit, and a confined sandstone aquifer. Under the conditions shown the water table (dashed line) is only in layer 1 and layers below layer 1 are fully saturated. Storage in layer 1 is represented by specific yield ( $S_y$ ); layers 2, 3, 4, and 5 are under confined conditions with confined storativity equal to specific storage ( $S_s$ ) times the thickness of the layer. In practice, all layers should be designated as convertible layers (Section 5.3) and then both specific yield and specific storage (or confined storativity) would be input for all layers. The code would automatically use specific yield only for unconfined layers (i.e. layers where a water table is present).

### 5.5.3.1 Zonation

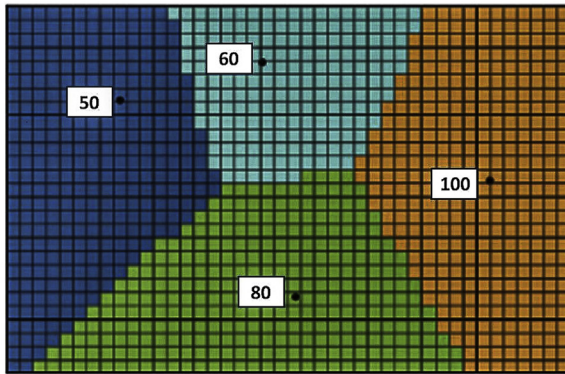
In zonation, parameter values are assigned as piecewise constant values to defined areas (zones) in the model domain (Figs. 5.28(a) and 5.29). Zones are piecewise constant in that nodes within the same zone are given the same parameter value; spatial changes in parameter values occur only among zones. Delineation of zones relies on information contained in the conceptual model that identifies areas in the problem domain where parameters are likely to be the same. The geometric mean of expected values of a given parameter within the zone is assigned to the zone if heterogeneity is thought to be random, whereas the arithmetic mean is used if trends are present. A different pattern of zones is usually required for each parameter. For example, zones of hydraulic conductivity are usually different from recharge zones (Fig. 5.29(a) and (b)).

### 5.5.3.2 Interpolation

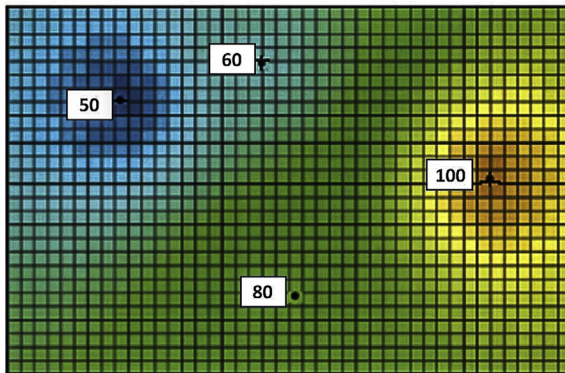
Interpolation uses parameter values at specified locations to compute values at every nodal point in the grid/mesh. Interpolation allows for gradation in properties within a hydrogeologic unit or hydrofacies and thereby represents spatial variability as trends within the unit. There are two main types of interpolation methods: deterministic and geostatistical. Deterministic interpolation uses point values directly while geostatistical interpolation uses point values and statistical properties of the parameter such as the spatial autocorrelation among measured points to generate a contour map of the parameter distribution in space.

Two commonly used deterministic interpolators are inverse distance and polynomial fitting. Inverse distance is an exact interpolator because it retains the measured value at a nodal point (Fig. 5.28(b)). Polynomial fitting is an inexact interpolator because least-squares fitting of a polynomial usually calculates a value different from the measured value at the measurement location. Inexact interpolators help eliminate the effects of extremes in measured values and associated sharp peaks and troughs in the property contours, which may or may not be desired for the conditions represented.

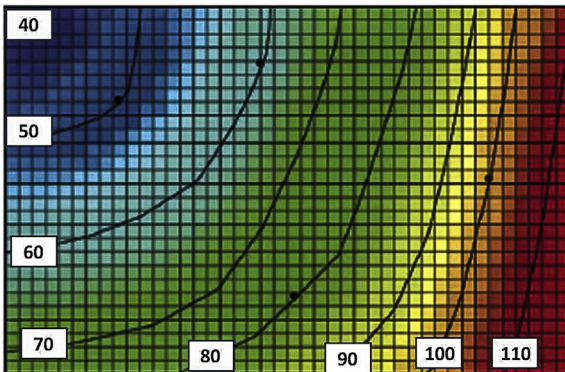
Geostatistical interpolation via kriging is the most commonly used interpolation scheme because it generates reasonably smooth distributions for most data sets while retaining the measured value at the corresponding location in the grid. Kriging was first used in applications to ore deposits and is named after Danie G. Krige (1919–2013) of South Africa, who pioneered the method. In *kriging*, the parameter is assumed to be a random function whose spatial correlation (spatial structure) is defined by a variogram (Fig. 5.30), which shows the change in the parameter with distance. Higher correlation between measurement points is expected when measurements are available at small separation distances. Kriging also provides an estimate of the interpolation error by computing the standard deviation of the kriged values. Such error estimates can be used to inform plausible ranges of parameter values for model calibration and forecast uncertainty analysis. Kriging also preserves initial parameter values at the specified nodal location. Marsily (1986, Chapter 11) gives an overview of kriging applied to groundwater problems along with selected applications. A popular approach for parameterizing the



Cell value is the nearest measured value



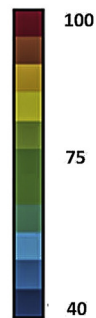
Cell value is the inverse-distance-squared weighted average of measured values



Cell value is the distance-weighted average of the two adjacent contours

**EXPLANATION**

HYDRAULIC CONDUCTIVITY  
IN FEET PER DAY



— CONTOUR OF HYDRAULIC  
CONDUCTIVITY IN FEET PER DAY,  
CONTOUR INTERVAL IS 10 FT

100 ● DATA POINT LOCATION AND  
VALUE OF HYDRAULIC  
CONDUCTIVITY, IN FEET PER DAY

**Figure 5.28** Parameter assignment of hydraulic conductivity in an FD grid: (a) zonation; (b) inverse distance interpolation; (c) linear interpolation (*Reilly and Harbaugh, 2004*).

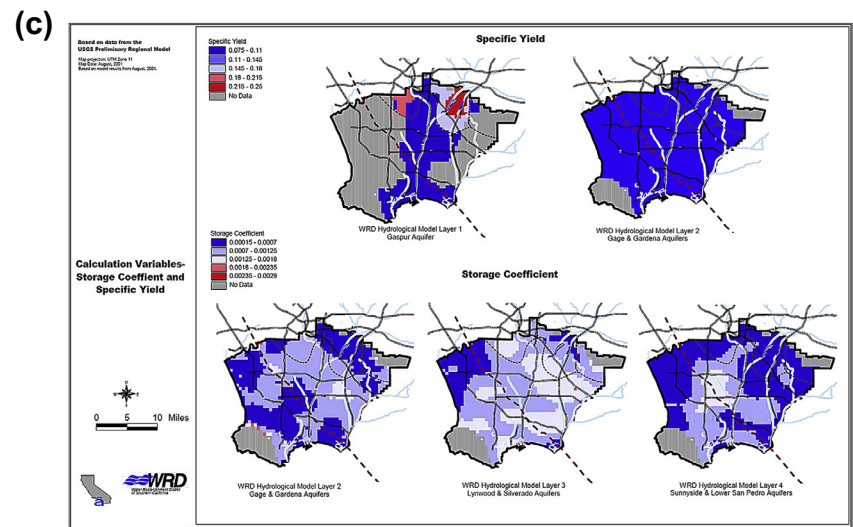
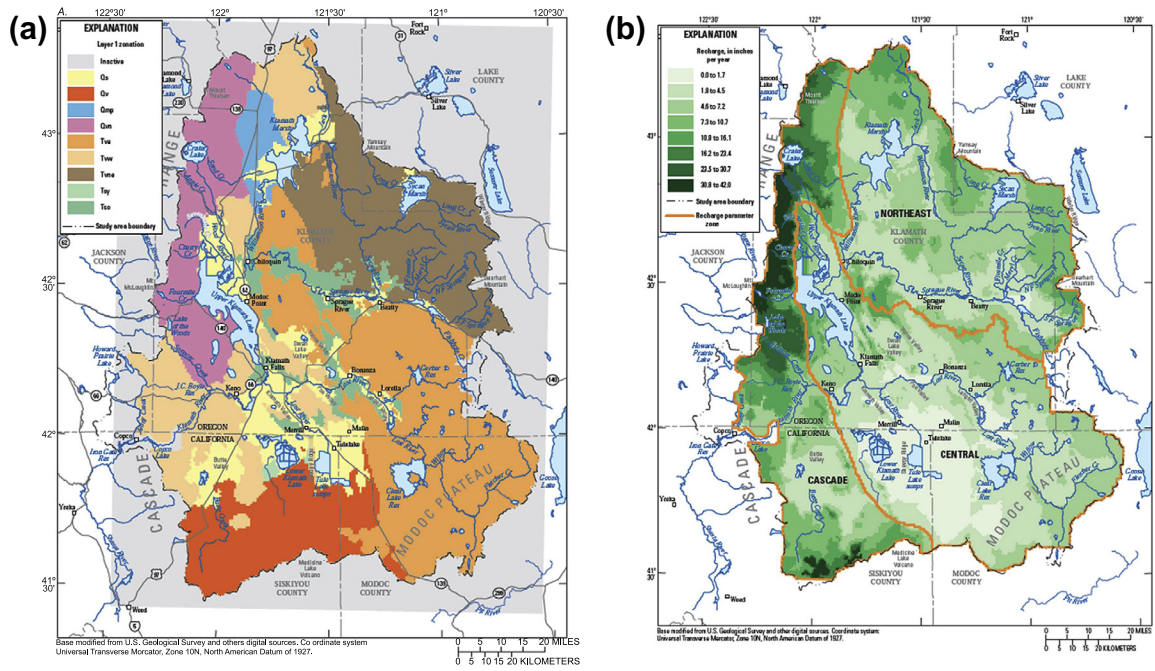


**Figure 5.29** Examples of parameter zonation: (a) hydraulic conductivity zones (Gannett et al., 2012); (b) recharge zones (Gannett et al., 2012); (c) storage parameters (Johnson and Njuguna, 2002).

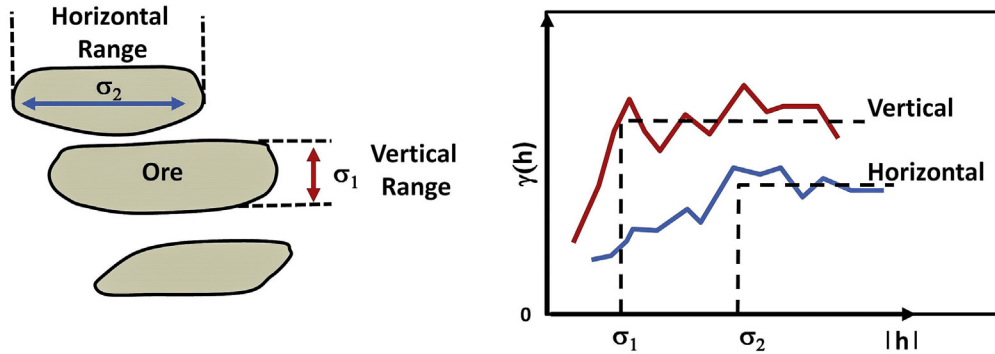


**Figure 5.30** Variograms defined by the separation distance of measurement points,  $h$ , and the variance of the separation distance or variogram function,  $\gamma$ . Variograms and kriging were first used in mining applications where the sill,  $\sigma$ , represents the horizontal and vertical dimensions of an ore body. In hydrogeologic applications, the sill represents the dimensions of heterogeneities (*modified from Journal and Huijbregts, 1978*).

nodal network via interpolation involves pilot points (Section 9.6; Box 9.3; [Doherty et al., 2010](#)). Available estimates of parameter values are used to estimate values at a number of discrete locations, or pilot points, distributed throughout the model domain. Then, parameter values at pilot points are interpolated by kriging and values are assigned to all cells, elements, or nodes. Interpolation routines are included in GUIs (Section 3.6) and GISs (Box 2.1). The popular program SURFER (Golden Software) provides multiple interpolation methods including inverse distance and kriging.

### 5.5.3.3 Hybrid Approach

In a given model, some parameters may be zoned and others interpolated. Moreover, both approaches can be used to represent variability in the same parameter type. For example, most geologic settings do not exclusively have the sharp boundaries and geometries of a zoned problem domain, yet interpolation does not represent discrete differences in parameter values that may be present in the field. A hybrid approach uses zonation to represent discrete areas where geologically reasonable and interpolation to represent spatial variability within zones. A hybrid approach is an attractive option for many problems (e.g., [Doherty and Hunt, 2010a,b](#); [Hunt et al., 2007](#); [Webb and Anderson, 1996](#)).

## 5.6 PARAMETER UNCERTAINTY

Parameter values are never known with certainty and are affected by confounding factors such as measurement error, interpolation error, and scaling error. It can be helpful to visualize parameter uncertainty by estimating errors in the initial parameter values assigned to the grid/mesh. For example, a maximum, minimum, and average value, along with confidence intervals, variances, or standard deviations can be tabulated for each parameter value. Uncertainty in parameter values can be visualized in a box and whisker plot ([Fig. 5.31](#)).



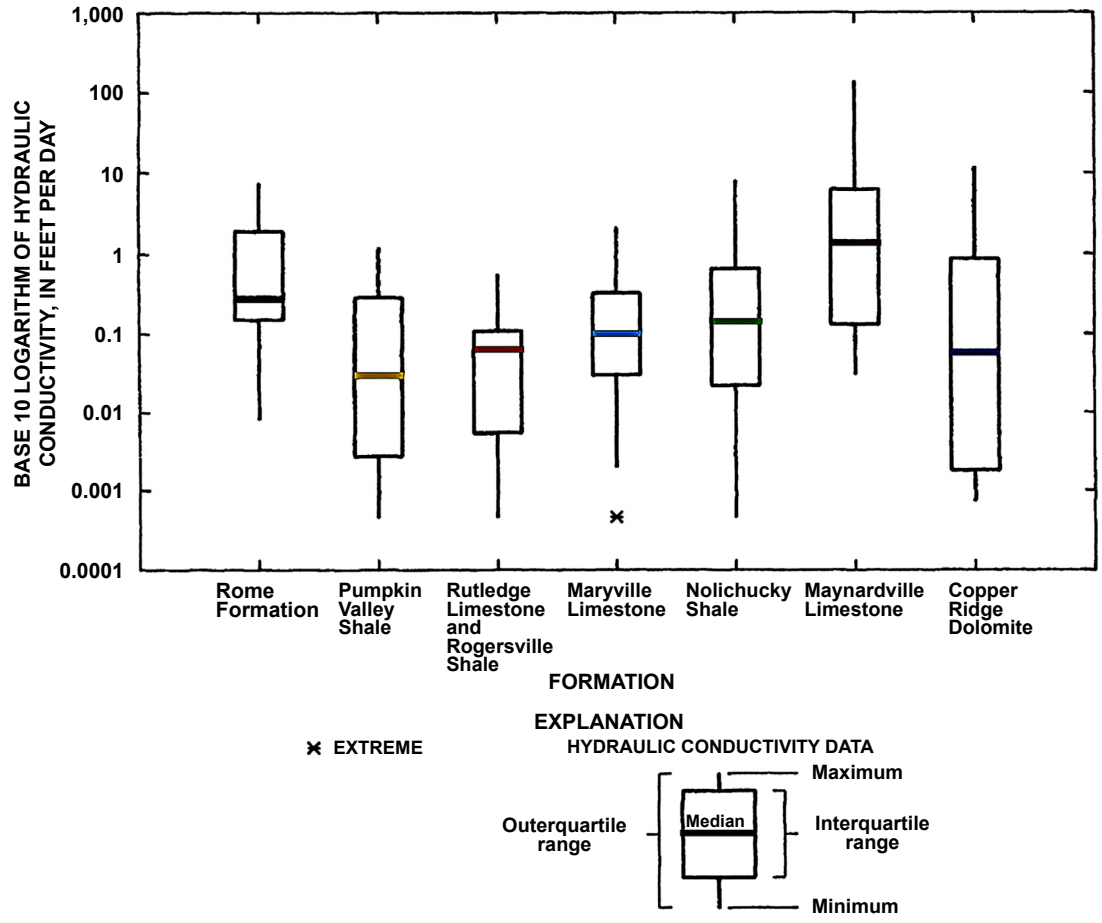


**Figure 5.31** Box and whisker plot showing ranges in hydraulic conductivity in hydrogeologic units for a model of Bear Creek Valley, TN , USA (modified from *Connell and Bailey, 1989*).

Hydraulic conductivity ranges over 12 orders of magnitude (Fig. 5.25); specific yield varies mainly within one order of magnitude (Table 5.1). Consequently, there is inherently less uncertainty in values of specific yield relative to hydraulic conductivity. This is fortunate because measured values of specific yield are often unavailable for a given site. Specific storage (representing confined storativity) has a larger range (Table 5.2) than specific yield (Table 5.1), but field estimates of storativity are often available. Moreover, simulations may be relatively insensitive to changes in confined storativity, inasmuch as water derived from storage under confined conditions is typically small.

Because parameter values are imperfectly known, often with large uncertainty, initial estimates of values assigned to the model are refined during calibration (Chapter 9). The effect of uncertainty in parameter values on model forecasts is evaluated during a formal uncertainty analysis (Chapter 10).

## 5.7 COMMON MODELING ERRORS

- The grid/mesh is aligned with geographical, site, or political boundaries rather than the primary direction of groundwater flow.
- Nodal spacing is too large around surface water bodies for accurate representation of groundwater–surface water exchange. The characteristic leakage length,  $\lambda$  (Eqn (5.2)), should be used as a guide when designing the nodal spacing around surface water features when it is important for accurate representation of fluxes to and from surface water.
- A MODFLOW-USG unstructured grid is created that violates the CVFD requirement and the modeler fails to use ghost-node correction. The resulting errors in simulated heads and flows are not detected because they do not cause errors in the simulated water budget.
- A structured FD grid with deformed layers is used to represent steeply dipping and folded hydrogeologic units when an FE model that includes non-uniform anisotropy is needed.
- The simulated water table is above the land surface in an area known to be dry land. The modeler failed to check for flooded nodes.
- Values of specific yield are input to represent storage in layers under confined conditions. The modeler incorrectly assumed that specific yield is the appropriate storage parameter for all layers that represent a surficial unconfined aquifer. Rather, model layers are under confined conditions except when a water table is present in the layer. Specific storage (or confined storativity) is the appropriate storage parameter for a confined layer. The error can be avoided by always using convertible layers, which require input of both specific storage (or confined storativity) and specific yield.

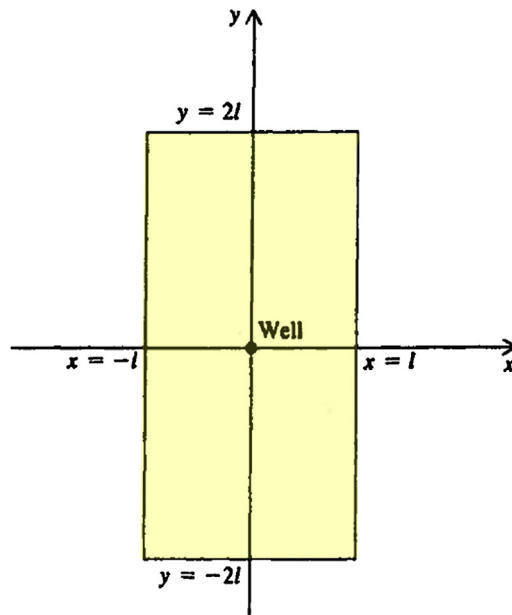
- Storativity is input when the code expects specific storage (or vice versa).
- Parameter zone sizes and geometries do not conform to the hydrogeology of the modeled area.
- Point measurements of parameters are assigned to the grid/mesh without upscaling.

## 5.8 PROBLEMS

Problems for this chapter examine the effect of nodal spacing on the head solution, differences between areal 2D and 3D models, and the effects of interpolation methods and data density on parameter distributions.

**P5.1** Develop a 2D areal model (consider using a spreadsheet model with Gauss/Seidel iteration; see Box 4.3) to solve for heads in the upper right-hand quadrant of the island shown in Fig. P5.1. The aquifer is confined, homogeneous, and isotropic with transmissivity,  $T$ , equal to 10,000 ft<sup>2</sup>/day. Recharge,  $R$ , occurs uniformly through a leaky confining bed at a rate of 0.00305 ft/day. The half-width of the island,  $l$ , is 12,000 ft. The head at the perimeter of the island is at sea level (use  $h = 0$  ft). The heads are symmetric across the groundwater divides that separate the island into four quadrants (Fig. P5.1). Use a point-centered FD grid (or an FE mesh) so that the node at the observation well in the center of the island (Fig. P5.1) is located directly on the groundwater divides that form the left-hand side and lower boundary of the quadrant model.

**Figure P5.1** Areal view of a rectangular island. The lines that divide the island into four quadrants are groundwater divides that form in this homogeneous and isotropic aquifer in response to the imposed flow regime (Wang and Anderson, 1982).



Include a water budget in your model. The inflow to the model is the volume of water entering from recharge. For the purposes of the water budget you should use the area of the grid/mesh (which may not conform exactly with the dimensions of the problem domain) in computing the volume of recharge entering the model. Inflow should equal outflow, which is the volume discharging to the ocean. The outflow rate can be calculated using Darcy's law applied along the discharge boundaries.

- Write the mathematical model for this problem including the governing equation and boundary conditions of the quadrant model.
- Solve the model using an error tolerance equal to  $1\text{E}-4$  ft and test two designs for the nodal network: (1) a  $4 \times 7$  array of nodes ( $\Delta x = \Delta y = 4000$  ft); (2) a  $13 \times 25$  array of nodes ( $\Delta x = \Delta y = 1000$  ft). For each nodal network, print out the head solution to the fourth decimal place.
- Compare your solutions in part (b) to the analytical solution (from Carslaw and Jaeger, 1959, p. 151):

$$h(x, y) = \frac{R(a^2 - x^2)}{2T} - \frac{16Ra^2}{T\pi^3} \sum_{n=0}^{\infty} \frac{(-1)^n \cos\left(\frac{(2n+1)\pi x}{2a}\right) \cosh\left(\frac{(2n+1)\pi y}{2a}\right)}{(2n+1)^3 \cosh\left(\frac{(2n+1)\pi b}{2a}\right)} \quad (\text{P5.1.1})$$

where  $a = l$  and  $b = 2l$ .

(Hint: Write a computer program to solve Eqn (P5.1.1). Prior to solving Eqn (P5.1.1), you can do a quick check of your numerical solution by checking the head at the center of the island, which is 20 ft according to Eqn (P5.1.1).)

- Compare the results of the water budget computation for each nodal network in (b). You will find that outflow from the island is considerably less for the larger nodal spacing (4000 ft). Explain why.
- Run your model with a nodal spacing of 500 ft and again with a nodal spacing of 250 ft. Compare head values and the volumetric discharge rate at the shoreline for all four nodal networks. Do you think a nodal spacing of 1000 ft is adequate for this problem? Justify your answer.

**P5.2** Refer to Box 5.3 to answer (a) and (b) below.

- Derive Eqns (B5.3.2) and (B5.3.3) in Box 5.3 using mass balance and Darcy's law. (Hint: Consult Freeze and Cherry, 1979, pp. 32–34; or Todd and Mays, 2005, pp. 101–102, if you need help.)
- Devise a layered system of homogeneous and isotropic units and use Eqns (B5.3.2) and (B5.3.3) in Box 5.3 to show that the vertical anisotropy ratio,  $K_h/K_v$ , for the layered sequence is scale-dependent. That is, show that the ratio depends on the resolution of heterogeneity of the vertical sequence of geologic units (the number of layers in the sequence). Different values of  $K_h/K_v$  are computed when heterogeneity is captured at smaller scales by including more layers in the sequence.

- P5.3** An industrial facility in an arid setting is disposing of fluids in a 900 m by 900 m pond that is leaking at a rate of 0.2 m/d (Fig. P5.2). Recharge from precipitation in this area is negligible. The pond is located in the center of the horizontal problem domain and is underlain by a sequence of sediment layers consisting of sand, clay, and sand and gravel. Wet areas around the pond perimeter at the land surface are causing some local water-logging of the soils and impacting vegetation. The owners of the pond believe that the water-logging is caused by seepage out of the pond through the berms around the sides of the pond. The state regulatory agency, however, suspects that leakage through the bottom of the pond has created a water table mound that intersects the land surface. The objective of modeling is to determine whether the groundwater mound beneath the pond reaches the land surface and is water-logging the soil.
- a. The consulting firm hired by the industrial facility recommends a 2D areal steady-state unconfined model as a quick and easy way to address the modeling objective. As a newly hired hydrogeologist of the consulting firm, you are instructed to construct the model. The width of the problem domain is

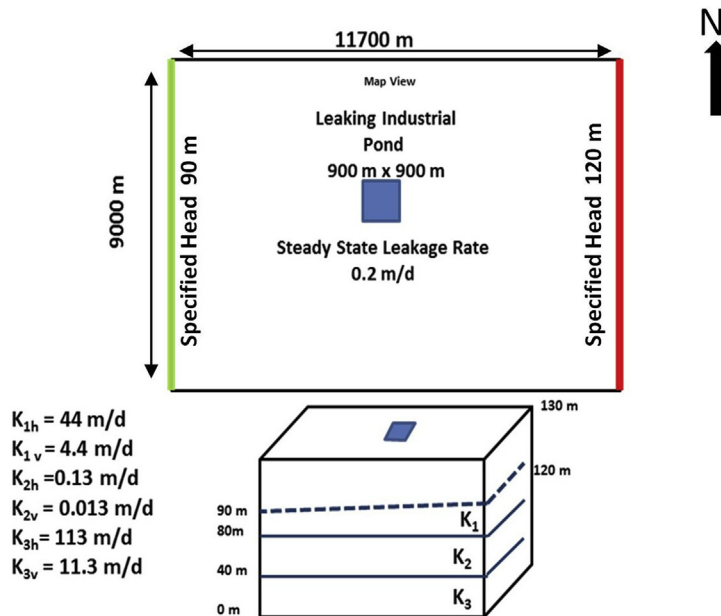


**Figure P5.2** The model domain for Problem P5.3 in map view and as a 3D block. The width of the problem domain is 11,700 m. Heads along the side boundaries are 120 and 90 m.  $K_1$  is the hydraulic conductivity in layer 1 where the horizontal hydraulic and vertical conductivities ( $K_x$  and  $K_z$ ) are  $K_{1h}$  and  $K_{1v}$ , respectively.  $K_2$  and  $K_3$  are the hydraulic conductivities for layers 2 and 3, respectively. The blue square is the pond. The dashed line represents the water table. The average saturated thickness of layer 1 is 25 m. The land surface elevation is 130 m above datum.

11,700 m. Use no flow boundary conditions at the north and south ends of the problem domain and specified heads along the sides (Fig. P5.2). Use a uniform nodal spacing of 900 m. Use Eqns (B5.3.2) and (B5.3.3) in Box 5.3 to compute the average horizontal and vertical hydraulic conductivity for the layer. Although the vertical hydraulic conductivity is not used in a one-layer 2D areal model, the vertical anisotropy ratio of the layer is of interest. Produce a contour map of the water table (use 1-m contour intervals) using the computed heads. Under this representation does the water table intersect the land surface?

- b.** The state regulatory agency insists that a 3D model be developed to examine how vertical flow and anisotropy influence the height of the groundwater mound. They point out that the low hydraulic conductivity of layer 2 and the vertical anisotropy present in the layered sequence of units might cause the mound to rise to the surface. Construct a three-layer steady-state model based on the information in Fig. P5.2. Specified head and no flow boundaries extend to all layers. Generate an equipotential surface (using 1-m contour intervals) for each layer. Also show the head distribution in a cross section that passes through the specified head boundaries and the pond. Examine your results and answer the following:
  - i. Explain why the results of the 2D model are different from the 3D model. What are the main factors that control the height of the water table mound under the pond? Discuss whether the 2D model is appropriate for this problem.
  - ii. Is it likely that the water table intersects the land surface away from the pond? If so, use shading on a map of the land surface in the vicinity of the pond to show the area affected by leakage.
- c.** When the modeling report is sent out for review, reviewers question whether the large nodal spacing of 900 m sufficiently captures the head gradient that defines the mound. They say that the surface area affected by the mound is underestimated. Use the three-layer model developed in (b) to assess the effect of nodal spacing on the solution. Reduce the nodal spacing uniformly over the grid/mesh to 300 m, or construct an irregular FD grid, unstructured FD grid, or FE mesh with fine nodal spacing in the vicinity of the pond. Run the model and generate equipotential maps for each layer (use a 1-m contour interval) and a cross section that passes through the pond and constant head boundaries. If the mound intersects the land surface, show the area impacted by shading on a map of the land surface. Compare and contrast results with those of parts (a) and (b).
- d.** What is your conclusion about the cause of water-logging? Support your answer with modeling results.
- e.** In this problem we assumed that all parameters were known, and we examined how layering (and anisotropy) and nodal spacing affected the height and

configuration of the water table. Make a list of factors (in addition to dimensionality and nodal spacing) that would add uncertainty to a forecast of the height of the water table mound in this problem. Speculate how the uncertainty might affect modeling results and conclusions.

**P5.4** A regional groundwater model (Fig. P5.3) of an arid basin is developed to determine whether withdrawal of water to supply a distant city is sustainable for the next 15 years. As part of the field investigation the geology was mapped and aquifer (pumping) tests were conducted to measure hydraulic conductivities in the basin. During the aquifer tests, each of the wells indicated on the map was pumped and drawdown was measured in observation wells (not shown on the map). Measured values of hydraulic conductivity are representative of the nodal spacing used in the model, which was 1000 m. The sediment in the alluvial fan is predominately fine sand, sand, and gravel. The area in between the two fans shown in Fig. P5.3 is mainly silt and clay. Field locations of sites where hydraulic conductivity was measured are shown in Fig. P5.3 and the corresponding values are given in Table P5.1.

- a. Use the hydraulic conductivity values in Table P5.1 to draw a contour map by hand of the distribution of hydraulic conductivity using linear interpolation. Use your hydrogeologic intuition and knowledge to infer likely boundaries of sedimentary facies present in this geologic setting to help shape your contour lines.

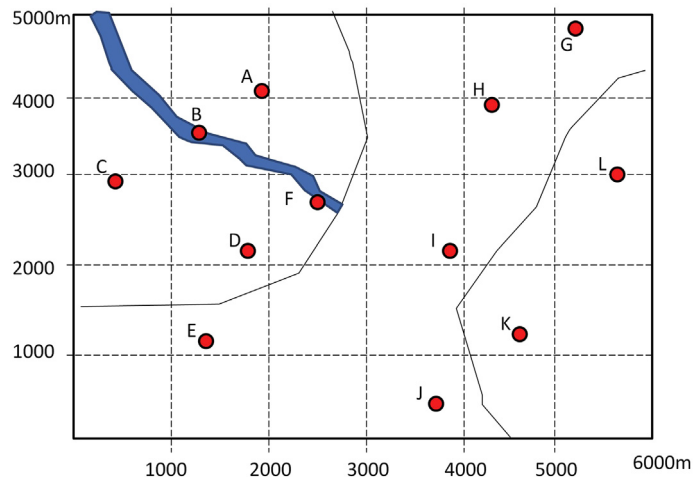


**Figure P5.3** Problem domain of an arid valley for Problem P5.4, showing geologic boundaries of two alluvial fans and locations of field measured hydraulic conductivities (red dots) reported in Table P5.1. The area shown in blue is the inferred location of a gravel-rich buried channel that is tapped by wells B and F.

**Table P5.1** Hydraulic conductivity values from aquifer (pumping) tests. Well locations are given by coordinate locations and are shown in Fig. P5.3

Well #	x (m)	y (m)	K (m/d)
A	1950	4100	56
B	1300	3500	100
C	400	2900	45
D	1800	2200	20
E	1300	1200	5
F	2500	2700	76
G	5200	4800	1
H	4300	3900	6
I	3800	2200	10
J	3700	500	15
K	4700	1300	43
L	5600	3000	28

- b. Input the point hydraulic conductivity data (Table P5.1) into geostatistical and deterministic interpolation programs and produce contour and color flood maps of hydraulic conductivity. Compare and contrast your results with the hand-contoured interpretation from (a). How does each method handle trends in hydraulic conductivity present at the domain boundary?
- c. Remove every other data point from Table P5.1 so that the data set is reduced by half. Repeat contouring following instructions in (a) and (b). Do the results from the interpolation programs you used produce a reasonable distribution of the hydraulic conductivity for this setting? Comment on the challenges of assigning hydraulic conductivity values to a model with a uniform horizontal nodal spacing of 1000 m when field data are sparse.

## REFERENCES

- Abtew, W., Melesse, A., 2012. Evaporation and Evapotranspiration: Measurements and Estimation. Springer Dordrecht. ISBN: 9400747365; 290 p.
- Anderman, E.R., Kipp, K.L., Hill, M.C., Valstar, J., Neupauer, R.M., 2002. MODFLOW-2000, the US Geological Survey Modular Groundwater Model: Documentation of the Model-layer Variable Direction Horizontal Anisotropy (LVDA) Capability of the Hydrogeologic-unit Flow (HUF) Package. US Geological Survey Open-File Report 02-409, 61 p. <http://pubs.er.usgs.gov/publication/ofr02409>.
- Anderson, M.P., 1987. Treatment of heterogeneities in groundwater modeling. In: Solving ground water problems with models, V. 1. Proceedings, National Ground Water Association Conference and Exposition, Denver, CO, pp. 444-463. [info.ngwa.org/gwol/pdf/870142823.pdf](http://info.ngwa.org/gwol/pdf/870142823.pdf).
- Arihood, L.D., 2009. Processing, Analysis, and General Evaluation of Well-driller Records for Estimating Hydrogeologic Parameters of the Glacial Sediments in a Ground-water Flow Model of the Lake Michigan Basin. U.S. Geological Survey Scientific Investigations Report 2008-5184, 26 p. <http://pubs.er.usgs.gov/publication/sir20085184>.



- ASTM International, 2010. Standard Practice for Direct Push Installation of Prepacked Screen Monitoring Wells in Unconsolidated Aquifers. ASTM D6725-04, 15 p.
- Barlow, P.M., Leake, S.A., 2012. Streamflow depletion by wells—understanding and managing the effects of groundwater pumping on streamflow. U.S. Geological Survey Circular 1376, 84 p. <http://pubs.usgs.gov/circ/1376/>.
- Berg, S.J., Illman, W.A., 2013. Field study of subsurface heterogeneity with steady-state hydraulic tomography. *Groundwater* 51 (1), 29–40. <http://dx.doi.org/10.1111/j.1745-6584.2012.00914.x>.
- Bohling, G.C., Butler, J.J., 2010. Inherent limitations of hydraulic tomography. *Groundwater* 48 (6), 809–824. <http://dx.doi.org/10.1111/j.1745-6584.2010.00757.x>.
- Bradbury, K.R., 1982. Hydrogeologic Relationships between Green Bay of Lake Michigan and Onshore Aquifers in Door County (Ph.D. Dissertation). University of Wisconsin-Madison, Wisconsin, 287 p.
- Bradbury, K.R., Muldoon, M.A., 1990. Hydraulic conductivity determinations in unlithified glacial and fluvial materials. In: Nielson, D.M., Johnson, A.I. (Eds.), *Ground Water and Vadose Zone Monitoring*, vol. 1053. ASTM Special Technical Publication, pp. 138–151.
- Butler, J.J., 2009. Pumping tests for aquifer evaluation—time for a change? *Groundwater* 47 (5), 615–617. <http://dx.doi.org/10.1111/j.1745-6584.2008.00488.x>.
- Buxton, H.T., Smolensky, D.A., Shernoff, P.K., 1999. Feasibility of Using Ground Water as a Supplemental Supply for Brooklyn and Queens. U.S. Geological Survey Water-Resources Investigations Report 98-4070, New York, 33 p. <http://pubs.er.usgs.gov/publication/wri984070>.
- Cao, G., Zheng, C., Scanlon, B.R., Liu, J., Li, W., 2013. Use of flow modeling to assess sustainability of groundwater resources in the North China Plain. *Water Resources Research* 49 (1), WR011899. <http://dx.doi.org/10.1029/2012>.
- Cardiff, M., Barrash, W., Kitanidis, P.K., Malama, B., Revil, A., Straface, S., Rizzo, E., 2009. Potential-based inversion of unconfined steady-state hydraulic tomography. *Groundwater* 47 (2), 259–270. <http://dx.doi.org/10.1111/j.1745-6584.2008.00541.x>.
- Carleton, G.B., Welty, C., Buxton, H.T., 1999. Design and Analysis of Tracer Tests to Determine Effective Porosity and Dispersivity in Fractured Sedimentary Rocks, Newark Basin. U.S. Geological Survey Water-Resources Investigations Report 98-4126A, New Jersey, 80 p. <http://pubs.er.usgs.gov/publication/wri984126A>.
- Carslaw, H.S., Jaeger, J.C., 1959. *Conduction of Heat in Solids*, second ed. Oxford University Press, London. 510 p.
- Connell, J.F., Bailey, Z.C., 1989. Statistical and Simulation Analysis for Hydraulic-conductivity Data for Bear Creek and Melton Valleys, Oak Ridge Reservation, Tennessee. U.S. Geological Survey Water Resources Investigations Report 89-4062, 49 p. <http://pubs.er.usgs.gov/publication/wri894062>.
- Dagan, G., Fiori, A., Jankovic, I., 2013. Upscaling of flow in heterogeneous porous formations: Critical examination and issues of principle. *Advances in Water Resources* 51, 67–85. <http://dx.doi.org/10.1016/j.advwatres.2011.12.017>.
- Davis, J.M., Wilson, J.L., Phillips, F.M., 1994. A portable air-minipermeameter for rapid in situ field measurements. *Groundwater* 32 (2), 258–266. <http://dx.doi.org/10.1111/j.1745-6584.1994.tb00640.x>.
- DHI-WASY GmbH, 2012. FEFLOW 6.1 User Manual. DHI-WASH GmbH, Berlin, 116 pp.
- Diersch, H.-J.G., 2014. FEFLOW: Finite Element Modeling of Flow, Mass and Heat Transport in Porous and Fractured Media. Springer, 996 p.
- Dogan, M., Van Dam, R.L., Bohling, G.C., Butler Jr, J.J., Hyndman, D.W., 2011. Hydrostratigraphic analysis of the MADE Site with full-resolution GPR and direct-push hydraulic profiling. *Geophysical Research Letters* 38 (6), L06405. <http://dx.doi.org/10.1029/2010GL046439>.
- Doherty, J.E., Fienen, M.N., Hunt, R.J., 2010. Approaches to Highly Parameterized Inversion: Pilot-point Theory, Guidelines, and Research Directions. U.S. Geological Survey Scientific Investigations Report 2010-5168, 36 p. <http://pubs.usgs.gov/sir/2010/5168/>.
- Doherty, J., Hunt, R.J., 2010a. Approaches to Highly Parameterized Inversion: A Guide to Using PEST for Groundwater-model Calibration. U.S. Geological Survey Scientific Investigations Report 2010-5169, 60 p. <http://pubs.usgs.gov/sir/2010/5169/>.

- Doherty, J., Hunt, R.J., 2010b. Response to comment on: Two statistics for evaluating parameter identifiability and error reduction. *Journal of Hydrology* 380 (3–4), 489–496. <http://dx.doi.org/10.1016/j.jhydrol.2009.10.012>.
- Domenico, P.A., 1972. *Concepts and Models in Groundwater Hydrology*. McGraw-Hill, NY, 405 p.
- Dunkle, K.M., Hart, D.H., and Anderson, M.P., 2015. New ways of using well construction reports for hydrostratigraphic analyses. *Groundwater*, early view. <http://dx.doi.org/10.1111/gwat.12326>.
- Feinstein, D.T., Fienen, M., Reeves, H., Langevin, C., 2013. Application of a “semi-structured” approach with MODFLOW-USG to simulate local groundwater/surface-water interactions at the regional scale as basis for a decision-support tool. In: *MODFLOW and More 2013: Translating Science into Practice*, Proceedings of the 7th International Conference of the International Ground Water Modeling Center. Colorado School of Mines, Golden, CO, pp. 600–604.
- Feinstein, D.T., Hunt, R.J., Reeves, H.W., 2010. Regional groundwater-flow model of the Lake Michigan Basin in support of Great Lakes Basin water availability and use studies. U.S. Geological Survey Scientific Investigations Report 2010–5109, 379 p. <http://pubs.usgs.gov/sir/2010/5109/>.
- Fitts, C.R., 2013. *Groundwater Science*, second ed. Academic Press, 696 p.
- Freeze, R.A., Cherry, J.A., 1979. *Groundwater*. Prentice Hall, 604 p.
- Gambolati, G., Toffolo, F., Uliana, F., 1984. Groundwater response under an electronuclear plant to a river flood wave analyzed by a nonlinear finite element model. *Water Resources Research* 20 (7), 903–913. <http://dx.doi.org/10.1029/WR020i007p00903>.
- Gannett, M.W., Wagner, B.J., Lite Jr, K.E., 2012. *Groundwater Simulation and Management Models for the Upper Klamath Basin, Oregon and California*. U.S. Geological Survey Scientific Investigations Report 2012–5062, 92 p. <http://pubs.usgs.gov/sir/2012/5062/>.
- Goyal, M.R.G., Harmsen, E.W., 2013. *Evapotranspiration: Principles and Applications for Water Management*. CRC Press, Boca Raton, FL, ISBN 1926895584, 628 p.
- Granger, R.J., Hedstrom, N., 2011. Modelling hourly rates of evaporation from small lakes. *Hydrology and Earth System Sciences* 15, 267–277. <http://dx.doi.org/10.5194/hess-15-267-2011>.
- Groschen, G.E., 1985. Simulated Effects of Projected Pumping on the Availability of Freshwater in the Evangeline Aquifer in an Area Southwest of Corpus Christi, Texas. U.S. Geological Survey Water Resources Investigation Report 85–4182, 103 p. <http://pubs.er.usgs.gov/publication/wri854182>.
- Guswa, J.H., Le Blanc, D.R., 1985. Digital Models of Ground-water Flow in the Cape Cod Aquifer System, Massachusetts. U.S. Geological Survey Water Supply Paper 2209, 64 p. <http://pubs.er.usgs.gov/publication/wsp2209>.
- Haitjema, H.M., 1995. *Analytic Element Modeling of Groundwater Flow*. Academic Press, San Diego, CA, 394 p.
- Haitjema, H.M., 2006. The role of hand calculations in ground water flow modeling. *Groundwater* 44 (6), 786–791. <http://dx.doi.org/10.1111/j.1745-6584.2006.00189.x>.
- Haitjema, H., Kelson, V., de Lange, W., 2001. Selecting MODFLOW cell sizes for accurate flow fields. *Groundwater* 39 (6), 931–938. <http://dx.doi.org/10.1111/j.1745-6584.2001.tb02481.x>.
- Healy, R.W., 2010. *Estimating Groundwater Recharge*. Cambridge University Press, Cambridge, UK, ISBN 978-0-521-86396-4, 245 p.
- Healy, R.W., Winter, T.C., LaBaugh, J.W., Franke, O.L., 2007. *Water Budgets: Foundations for Effective Water-resources and Environmental Management*. U.S. Geological Survey Circular 1308, 90 p. <http://pubs.usgs.gov/circ/2007/1308/>.
- Heath, R.C., 1983. *Basic Ground-water Hydrology*. U.S. Geological Survey Water Supply Paper 2220, 84 p. <http://pubs.er.usgs.gov/publication/wsp2220>.
- Hoaglund, J.R., Pollard, D., 2003. Dip and anisotropy effects on flow using a vertically skewed model grid. *Groundwater* 41 (6), 841–846. <http://dx.doi.org/10.1111/j.1745-6584.2003.tb02425.x>.
- Hsieh, P.A., Freckleton, J.R., 1993. Documentation of a Computer Program to Simulate Horizontal-flow Barriers Using the U.S. Geological Survey’s Modular Three-dimensional Finite-difference Ground-water Flow Model. U.S. Geological Survey Open-File Report 92–477, 32 p. <http://pubs.er.usgs.gov/publication/of92477>.
- Hunt, R.J., Doherty, J., Tonkin, M.J., 2007. Are models too simple? Arguments for increased parameterization. *Groundwater* 45 (3), 254–261. <http://dx.doi.org/10.1111/j.1745-6584.2007.00316.x>.

- Hunt, R.J., Haitjema, H.M., Krohelski, J.T., Feinstein, D.T., 2003a. Simulating ground water-lake interactions: Approaches and insights. *Groundwater* 41 (2), 227–237. <http://dx.doi.org/10.1111/j.1745-6584.2003.tb02586.x>.
- Hunt, R.J., Prudic, D.E., Walker, J.F., Anderson, M.P., 2008. Importance of unsaturated zone flow for simulating recharge in a humid climate. *Groundwater* 46 (4), 551–560. <http://dx.doi.org/10.1111/j.1745-6584.2007.00427.x>.
- Hunt, R.J., Saad, D.A., Chapel, D.M., 2003b. Numerical Simulation of Ground-water Flow in La Crosse County, Wisconsin and into Nearby Pools of the Mississippi River. U.S. Geological Survey Water-Resources Investigations Report 03–4154, 36 p. <http://pubs.usgs.gov/wri/wri034154/>.
- Hunt, R.J., Walker, J.F., Selbig, W.R., Westenbroek, S.M., Regan, R.S., 2013. Simulation of Climate-change Effects on Streamflow, Lake Water Budgets, and Stream Temperature Using GSFLOW and SNTMP, Trout Lake Watershed, Wisconsin. U.S. Geological Survey Scientific Investigations Report 2013-5159, 118 p. <http://pubs.usgs.gov/sir/2013/5159/>.
- Huyakorn, P.S., Pinder, G.F., 1983. *Computational Methods in Subsurface Flow*. Academic Press, 473 p.
- Istok, J., 1989. Groundwater modeling by the finite element method, American. Geophysical Union. *Water Resources Monograph* 13, 495 p.
- Johnson, A.I., 1966. Compilation of Specific Yield for Various Materials. U.S. Geological Survey Open-File Report, 119 p. <http://pubs.usgs.gov/of/1963/0059/report.pdf>.
- Johnson, T., Njuguna, W., 2002. Available aquifer storage determinations using MODFLOW and GIS, Central and West Coast Groundwater Basins, Los Angeles County, California. In: Water Replenishment District of Southern California, Presented at the 22nd Annual Esri International User Conference, July 8–12, 2002. <http://proceedings.esri.com/library/userconf/proc02/pap0330/p0330.htm>.
- Journel, A.G., Huijbregts, C.J., 1978. *Mining Geostatistics*. Academic Press, 600 p.
- Juckem, P.F., Hunt, R.J., Anderson, M.P., 2006. Scale effects of hydrostratigraphy and recharge zonation on baseflow. *Groundwater* 44 (3), 362–370. <http://dx.doi.org/10.1111/j.1745-6584.2005.00136.x>.
- Kenoyer, G.J., 1988. Tracer test analysis of anisotropy in hydraulic conductivity of granular aquifers. *Groundwater Monitoring & Remediation* 8 (3), 67–70. <http://dx.doi.org/10.1111/j.1745-6592.1988.tb01086.x>.
- Khalil, M., Sakai, M., Mizochuchi, M., Miyazaki, T., 2003. Current and prospective applications of zero flux plane (ZFP) method. *Journal Japan Society Soil Physics* 95, 75–90. <https://www.js-soilphysics.com/data/pdf/095075.pdf>.
- Kruseman, G.P., de Ridder, N.A., 1990. *Analysis and Evaluation of Pumping Test Data*. International Institute for Land Reclamation and Improvement, 377 p.
- Leahy, P.P., 1982. A Three-dimensional Ground-water-flow Model Modified to Reduce Computer Memory Requirements and Better Simulate Confining - Bed and Aquifer Pinchouts. U.S. Geological Survey Water Resources Investigation Report 82–4023, 59 p. <http://pubs.er.usgs.gov/publication/wri824023>.
- Lee, D.R., 1977. A device for measuring seepage flux into lakes and estuaries. *Limnology and Oceanography* 22 (1), 140–147. <http://dx.doi.org/10.4319/lo.1977.22.1.0140>.
- Lewis-Brown, J.C., Rice, D.E., 2002. Simulated Ground-water Flow, Naval Air Warfare Center West Trenton. U.S. Geological Survey Water-Resources Investigations Report 02–4019, New Jersey, 44 p. <http://pubs.er.usgs.gov/publication/wri024019>.
- Lewis-Brown, J.C., Rice, D.E., Rosman, R., Smith, N.P., 2005. Hydrogeologic Framework, Ground-water Quality, and Simulation of Ground-Water Flow at the Fair Lawn Well Field Superfund Site, Bergen County. U.S. Geological Survey, Scientific Investigations Report 2004-5280, New Jersey pp. 109. <http://pubs.usgs.gov/sir/2004/5280/>.
- Lindgren, R.J., Dutton, A.R., Hovorka, S.D., Worthington, S.R.H., Painter, S., 2004. Conceptualization and simulation of the Edwards aquifer, San Antonio region, Texas. U.S. Geological Survey Scientific Investigations Report 2004–5277, 143 p. <http://pubs.usgs.gov/sir/2004/5277/>.
- Liu, G., Butler Jr, J.J., Bohling, G.C., Reboulet, E., Knobbe, S., Hyndman, D.W., 2009. A new method for high-resolution characterization of hydraulic conductivity. *Water Resources Research* 45 (8), W08202. <http://dx.doi.org/10.1029/2009WR008319>.

- Liu, G., Zheng, C., Tick, G.R., Butler Jr, J.J., Gorelick, S.M., 2010. Relative importance of dispersion and rate-limited mass transfer in highly heterogeneous porous media: Analysis of a new tracer test at the MADE Site. *Water Resources Research* 46 (3), W03524. <http://dx.doi.org/10.1029/2009WR008430>.
- Lott, R.B., Hunt, R.J., 2001. Estimating evapotranspiration in natural and constructed wetlands. *Wetlands* 21 (4), 614–628. [http://dx.doi.org/10.1672/0277-5212\(2001\)021\[0614:EEINAC\]2.0.CO;2](http://dx.doi.org/10.1672/0277-5212(2001)021[0614:EEINAC]2.0.CO;2).
- Maasland, M., 1957. Soil Anisotropy and Land Drainage. In: Luthin, J.N. (Ed.), *Drainage of Agricultural Lands*. American Society of Agronomy, Madison, WI, pp. 216–285.
- Marcus, H., Evenson, D.E., 1961. Directional Permeability in Anisotropic Porous Media, *Water Resources Center Contribution*, vol. 31. University of California, Berkeley.
- de Marsily, G., 1986. *Quantitative Hydrogeology*. Academic Press, 440 p.
- McDonald, M.G., Harbaugh, A.W., 1988. A Modular Three-dimensional Finite-difference Ground-water Flow Model. *Techniques of Water-Resources Investigations 06-A1*, USGS, 576 p. <http://pubs.er.usgs.gov/publication/twri06A1>.
- McLin, S.G., 2005. Estimating aquifer transmissivity from specific capacity using MATLAB. *Groundwater* 43 (4), 611–614. <http://dx.doi.org/10.1111/j.1745-6584.2005.0101.x>.
- Moene, A.F., van Dam, J.C., 2014. *Transport in the Atmosphere-vegetation-soil Continuum*. Cambridge University Press, New York. ISBN: 0521195683, 458 p.
- Morgan, D.S., Jones, J.L., 1995. Numerical Model Analysis of the Effects of Ground-water Withdrawals on Discharge to Streams and Springs in Small Basins Typical of the Puget Sound Lowland. U.S. Geological Survey Open-File Report 95-470, Washington, 73 p. <http://wa.water.usgs.gov/pubs/ofr/ofr.95-470/descript.html>.
- Morris, D.A., Johnson, A.I., 1967. Summary of Hydrologic and Physical Properties of Rock and Soil Materials as Analyzed by the Hydrologic Laboratory of the U.S. Geological Survey 1948–1960. U.S. Geological Survey Water Supply Paper 1839-D, 42 p. <http://pubs.er.usgs.gov/publication/wsp1839D>.
- Narasimhan, T.N., Witherspoon, P.A., 1976. An integrated finite-difference method for analyzing fluid flow in porous media. *Water Resources Research* 12 (1), 57–64. <http://dx.doi.org/10.1029/WR012i001p00057>.
- Nemeth, M.S., Solo-Gabriele, H.M., 2003. Evaluation of the use of reach transmissivity to quantify exchange between groundwater and surface water. *Journal of Hydrology* 274 (1–4), 145–159. [http://dx.doi.org/10.1016/S0022-1694\(02\)00419-5](http://dx.doi.org/10.1016/S0022-1694(02)00419-5).
- Neuman, S.P., 1975. Analysis of pumping test data from anisotropic unconfined aquifers considering delayed gravity response. *Water Resources Research* 11 (2), 329–342. <http://dx.doi.org/10.1029/WR011i002p00329>.
- Neuman, S.P., Walter, G.R., Bentley, H.W., Word, J.J., Gonzalez, D.D., 1984. Determination of horizontal aquifer anisotropy with three wells. *Groundwater* 22 (1), 66–72. <http://dx.doi.org/10.1111/j.1745-6584.1984.tb01477.x>.
- Niswonger, R.G., Prudic, D.E., Regan, R.S., 2006. Documentation of the Unsaturated-zone Flow (UZFI) Package for Modeling Unsaturated Flow between the Land Surface and the Water Table with MODFLOW-2005. U.S. Geological Survey Techniques and Methods Report 6-A19, 62 p. <http://pubs.er.usgs.gov/publication/tm6A19>.
- Nøttinger, R., Artus, V., Zargar, G., 2005. The future of stochastic and upscaling methods in hydrogeology. *Hydrogeology Journal* 13 (1), 184–201. <http://dx.doi.org/10.1007/s10040-004-0427-0>.
- NRC (National Research Council), 2004. In: Anderson, M.P., Wilson, J.L. (Eds.), *Groundwater Fluxes across Interfaces*. National Academy Press, 85 p.
- Panday, S., Langevin, C.D., Niswonger, R.G., Ibaraki, M., Hughes, J.D., 2013. MODFLOW-USG Version 1: An Unstructured Grid Version of MODFLOW for Simulating Groundwater Flow and Tightly Coupled Processes Using a Control Volume Finite-difference Formulation. U.S. Geological Survey Techniques and Methods. Book 6, Chapter A45, 66 p. <http://pubs.usgs.gov/tm/06/a45>.
- Quinones-Aponte, V., 1989. Horizontal anisotropy of the principal ground-water flow zone in the Salinas alluvial fan, Puerto Rico. *Groundwater* 27 (4), 491–500. <http://dx.doi.org/10.1111/j.1745-6584.1989.tb01969.x>.
- Reilly, T.E., Harbaugh, A.W., 2004. Guidelines for Evaluating Ground-water Flow Models. U.S. Geological Survey Scientific Investigations Report 2004-5038, 30 p. <http://pubs.er.usgs.gov/publication/sir20045038>.

- Reimann, T., Birk, S., Rehr, C., Shoemaker, W.B., 2012. Modifications to the conduit flow process mode 2 for MODFLOW-2005. *Groundwater* 50 (1), 144–148. <http://dx.doi.org/10.1111/j.1745-6584.2011.00805.x>.
- Reimann, T., Hill, M.E., 2009. MODFLOW-CFP: A new conduit flow process for MODFLOW-2005. *Groundwater* 47 (3), 321–325. <http://dx.doi.org/10.1111/j.1745-6584.2009.00561.x>.
- Remson, I., Hornberger, G.M., Molz, F.J., 1971. *Numerical Methods in Subsurface Hydrology*. Wiley-Interscience, 389 p.
- Renard, P., de Marsily, G., 1997. Calculating equivalent permeability: A review. *Advances in Water Resources* 20 (5/6), 253–278. [http://dx.doi.org/10.1016/S0309-1708\(96\)00050-4](http://dx.doi.org/10.1016/S0309-1708(96)00050-4).
- Rosas, J., Lopez, O., Missimer, T.M., Coulibaly, K.M., Dehwah, A.H.A., Sesler, K., Lujan, L.R., Mantilla, D., 2014. Determination of hydraulic conductivity from grain-size distribution for different depositional environments. *Groundwater* 52 (3), 399–413. <http://dx.doi.org/10.1111/gwat.12278>.
- Rose, W.R., 1993. Hydrology of Little Rock Lake in Vilas County, North-Central Wisconsin. U.S. Geological Survey Water-Resources Investigations Report 93-4139, 22 p. <http://pubs.er.usgs.gov/publication/wri934139>.
- Rosenberry, D.O., LaBaugh, J.W., Hunt, R.J., 2008. Use of monitoring wells, portable piezometers, and seepage meters to quantify flow between surface water and ground water (Chapter 2). In: *Field Techniques for Estimating Fluxes between Surface and Ground Water*. U.S. Geological Survey Techniques and Methods Report 4-D2, pp. 43–70, 128 p. <http://pubs.usgs.gov/tm/04d02/pdf/TM4-D2-chap2.pdf>.
- Scanlon, B.R., Healy, R.W., Cook, P.G., 2002. Choosing appropriate techniques for quantifying groundwater recharge. *Hydrogeology Journal* 10 (1), 18–39. <http://dx.doi.org/10.1007/s10040-001-0176-2>.
- Schroeder, P.R., Dozier, T.S., Zappi, P.A., McEnroe, B.M., Sjostrom, J.W., Peton, R.L., 1994. The Hydrologic Evaluation of Landfill Performance (HELP) Model, Engineering Documentation for Version 3, EPA/600/R-94/168b, US Environmental Protection Agency, Risk Reduction Engineering Laboratory, Cincinnati, OH.
- Sheets, R.A., Hill, M.C., Haitjema, H.M., Provost, A.M., Masterson, J.P., 2015. Simulation of water-table aquifers using specified saturated thickness. *Groundwater* 53 (1), 151–157. <http://dx.doi.org/10.1111/gwat.12164>.
- Shoemaker, W.B., Kuniandy, E.L., Birk, S., Bauer, S., Swain, E.D., 2008. Documentation of a Conduit Flow Process (CFP) for MODFLOW-2005. U.S. Geological Survey Techniques and Methods. Book 6, Chapter A24, 50 p. <http://pubs.er.usgs.gov/publication/tm6A24>.
- Šimůnek, J., van Genuchten, M.Th., Šejna, M., 2011. The HYDRUS Software Package for Simulating Two- and Three-dimensional Movement of Water, Heat, and Multiple Solutes in Variably-saturated Media. Technical Manual, Version 2.0. PC Progress, Prague, Czech Republic, 258 p.
- Sterrett, R.J. (Ed.), 2008. *Groundwater & Wells*, third ed. Johnson Division, St. Paul, MN. 812 p.
- Theis, C.V., 1940. The source of water derived from wells. *Civil Engineering* 10 (5), 277–280 (Reproduced in Anderson, M.P., editor, 2008, *Benchmark Papers in Hydrology, 3: Groundwater*. Selection, Introduction and Commentary by Mary P. Anderson, IAHS Press, pp. 281–286.).
- Todd, D.K., Mays, L.W., 2005. *Groundwater Hydrology*, third ed. John Wiley & Sons, Inc. 636 p.
- Toews, M.W., Allen, D.M., 2009. Evaluating different GCMs for predicting spatial recharge in an irrigated arid region. *Journal of Hydrology* 374 (3–4), 265–281. <http://dx.doi.org/10.1016/j.jhydrol.2009.06.022>.
- Torak, L.J., 1993. A MODular Finite-element Model (MODFE) for Areal and Axisymmetric Ground-water-flow Problems, Part 1—Model Description and User's Manual. U.S. Geological Survey Techniques of Water-Resources Investigations. Book 6, Chapter A3, 136 p. <http://pubs.usgs.gov/twri/twri6a3/>.
- Townley, L.R., Wilson, J.L., 1980. Description of and user's manual for a finite element aquifer flow model AQUIFEM-1, MIT Ralph M. Parsons Laboratory for Water Resources and Hydrodynamics. Technology Adaptation Program Report No. 79-3 294.
- Tyson Jr, H.N., Weber, E.M., 1964. Ground-water management for the nation's future—Computer simulation of ground-water basins, American Society of Civil Engineers Proceedings. *Journal of the Hydraulics Division* 90, 59–77.
- Voss, C.I., Provost, A.M., 2002. SUTRA: A Model for Saturated Unsaturated Variable-density Ground-water Flow with Solute or Energy Transport. U.S. Geological Survey Water Resources Investigation Report 02-4231, 429 p. <http://pubs.er.usgs.gov/publication/wri024231>.

- Wang, H.F., Anderson, M.P., 1982. Introduction to Groundwater Modeling: Finite Difference and Finite Element Methods. Academic Press, San Diego, CA, 237 p.
- Webb, E.K., Anderson, M.P., 1996. Simulation of preferential flow in three-dimensional, heterogeneous conductivity fields with realistic internal architecture. *Water Resources Research* 32 (3), 533–545. <http://dx.doi.org/10.1029/95WR03399>.
- Weeks, E.P., 1969. Determining the ratio of horizontal to vertical permeability by aquifer-test analysis. *Water Resources Research* 5 (1), 196–214. <http://dx.doi.org/10.1029/WR005i001p00196>.
- Westenbroek, S.M., Kelson, V.A., Dripps, W.R., Hunt, R.J., Bradbury, K.R., 2010. SWB - a Modified Thornthwaite-Mather Soil Water Balance Code for Estimating Groundwater Recharge. U.S. Geological Survey Techniques and Methods 6A31, 65 p. <http://pubs.usgs.gov/tm/tm6-a31/>.
- Winter, T.C., 1976. Numerical Simulation Analysis of the Interaction of Lakes and Ground Water. U.S. Geological Survey Professional Paper 1001, 45 p. <http://pubs.er.usgs.gov/publication/pp1001>.
- Yager, R.M., Voss, C.I., Southworth, S., 2009. Comparison of alternative representations of hydraulic-conductivity anisotropy in folded fractured-sedimentary rock: Modeling groundwater flow in the Shenandoah Valley (USA). *Hydrogeology Journal* 17 (5), 1111–1131. <http://dx.doi.org/10.1007/s10040-008-0431-x>.
- Yeh, T.-C.J., Lee, C.-H., 2007. Time to change the way we collect and analyze data for aquifer characterization. *Groundwater* 45 (2), 116–118. <http://dx.doi.org/10.1111/j.1745-6584.2006.00292.x>.
- Zhou, H., Gomez-Hernandez, J.J., Li, L., 2014. Inverse methods in hydrogeology: Evolution and recent trends. *Advances in Water Resources* 63, 22–37. <http://dx.doi.org/10.1016/j.advwatres.2013.10.014>.

## CHAPTER 6

# More on Sources and Sinks

*Among the many problems in heat-conduction analogous to those in ground-water hydraulics are those concerning sources and sinks, sources being analogous to recharging wells and sinks to ordinary discharging wells*

*C.V. Theis (1935)*

*Eventually, all things merge into one, and a river runs through it.*

*Norman Fitzroy Maclean, A River Runs Through It*

### Contents

6.1 Introduction	258
6.2 Pumping and Injection Wells	259
6.2.1 FD Well Nodes	262
6.2.2 FE Well Nodes and Multinode Wells	262
6.2.3 Multinode Wells in FD Models	264
6.3 Areally Distributed Sources and Sinks	270
6.4 Drains and Springs	272
6.5 Streams	273
6.6 Lakes	279
6.7 Wetlands	283
6.8 Common Modeling Errors	291
6.9 Problems	292
References	296

### Boxes

Box 6.1 Guidelines for Nodal Spacing around a Well Node	267
Box 6.2 Watershed Modeling	285
Box 6.3 Surface Water Modeling	289

In Section 4.3 we discussed sources and sinks represented as specified head, specified flow, or head-dependent boundary (HDB) conditions; in Section 5.2 we presented guidelines for selecting the nodal spacing around sources and sinks. In this chapter we present some additional information about representing sources and sinks, including pumping and injection wells, drains and springs, streams, lakes, and wetlands. We also discuss nonpoint (areally distributed) sources and sinks including recharge from infiltration, leakage, underflow, and evapotranspiration (ET) across the water table.

## 6.1 INTRODUCTION

The addition or removal of water from a groundwater flow model is represented either as a perimeter or internal boundary condition (Sections 4.2 and 4.3) or by a sink/source term ( $W^*$  in Eqn (3.12)). Streams, wetlands, lakes, drains, springs, and evapotranspiration (ET) from the water table are typically represented by HDB conditions (Section 4.3) and sometimes by specified head and specified flow conditions. Areally distributed recharge from infiltration through the unsaturated zone and pumping (or injection) of water via wells is represented by a sink/source term or by specified head or specified flow boundary conditions (Section 4.3).

Code developers have taken two different general approaches for programming sources and sinks into a groundwater flow model. Some codes rely on separate packages to assemble the input data, compute terms relevant to a particular type of source or sink, and keep track of output related to that source or sink. For example, MODFLOW has separate input for packages that represent pumping and injection wells, streams, lakes, wetlands, drains, ET from the water table, and flow to and from the unsaturated zone. Although input for packages is assembled separately, packages are included with the main computer program and exchange of input and output data with the main part of the code occurs automatically.

In the second approach (used in FEFLOW, [Diersch, 2014](#); and COMSOL), the modeler must select the appropriate general sink/source terms or boundary conditions (Section 4.3) from the options provided by the code and must input the appropriate values for associated parameters. Under this approach, the code is programmed for a general sink/source term as well as specified head and specified flow boundary conditions and a general HDB condition. The user must decide how best to represent a particular source or sink via options available in the code. For example, if a stream is to be represented using HDB conditions, the general HDB option in the code would be used. In that way, several types of sinks and sources may be represented by the same general sink/source and boundary options programmed in the code. The modeler must use hydrogeologic judgment guided by the general principles for representing sinks and sources given in Sections 4.2 and 4.3 to decide which boundary option in the code is best suited for representing a particular source or sink. Additionally, the modeler must formulate the correct input data to simulate the feature using the option selected. This approach for representing sources and sinks in a groundwater model requires a more thorough understanding of both hydrogeologic processes and the specifics of how the code is programmed compared to the package approach described above.

For applied groundwater modeling, the first approach (using packages) is often more convenient, especially for a beginning to intermediate-level modeler. Packages serve to direct the modeler to primary processes that are important in groundwater modeling. The input data for a package are tailored to a specific process and relate directly to parameters that describe the process. The package approach also provides convenient internal tracking



and reporting of the simulated process in model output. However, for advanced applications, the second approach can provide more flexibility for customizing input data to a particular source or sink. The limitations in some of the basic MODFLOW packages motivated development of new MODFLOW packages. For example, the Streamflow-Routing (SFR) Packages were developed to address limitations in the River Package (Section 6.5).

In this chapter, we use the finite-difference (FD) code MODFLOW and the finite-element (FE) code FEFLOW as examples to frame the discussion of the two approaches for representing sources and sinks and also to represent differences between FD and FE methods. Pumping and injection wells are discussed in Section 6.2, nonpoint (areally distributed) sources and sinks in Section 6.3, drains and springs in Section 6.4, streams in Section 6.5, lakes in Section 6.6, and wetlands in Section 6.7.

## 6.2 PUMPING AND INJECTION WELLS

In Section 4.3, we discussed how pumping and injection wells are used to implement specified flow boundary conditions along the perimeter of a model (Figs 4.13(b) and 4.14). We also mentioned that a pumping or injection well can be simulated using a specified head node (Section 4.3) to represent dewatering, for example. In this section we discuss pumping and injection wells in the interior of the model domain (Fig. 6.1) that represent point sources and sinks that exist in the field.

Pumping wells include domestic, industrial, irrigation, and municipal water supply wells; they also include wells for dewatering tunnels, quarries and mines, and pumping wells

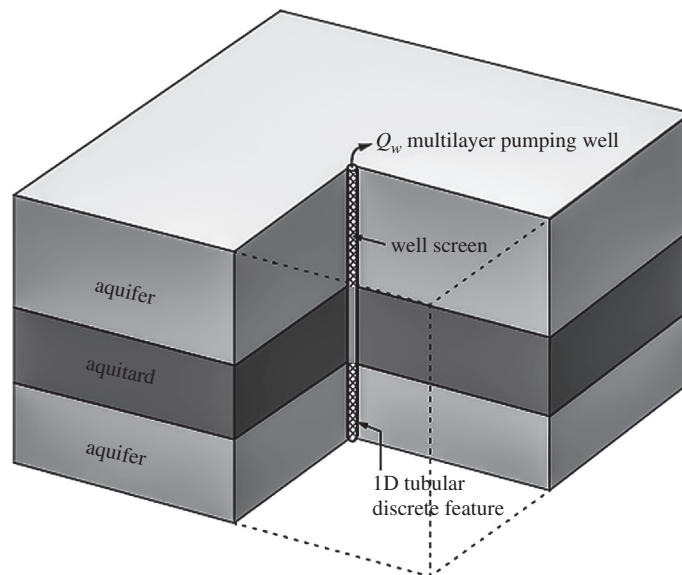


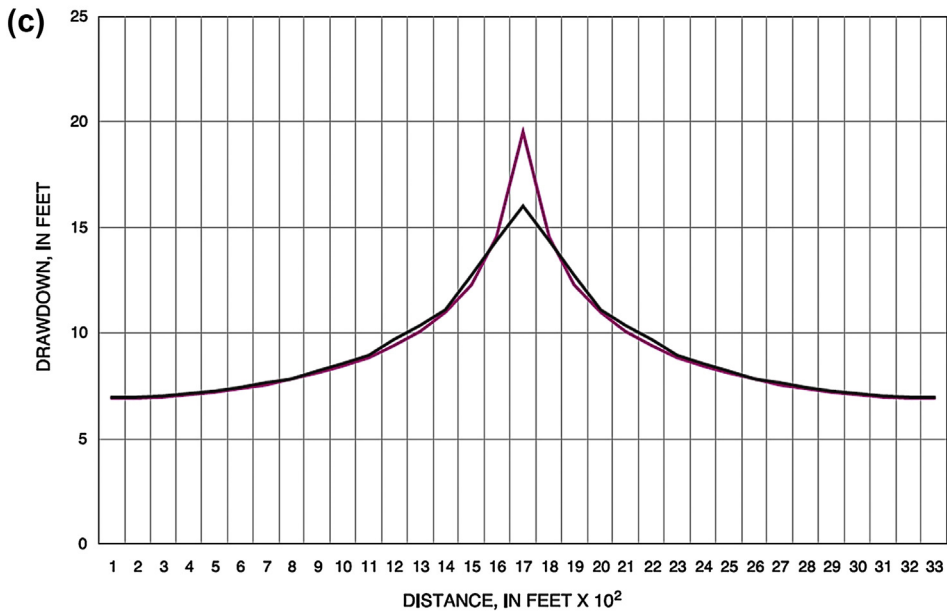
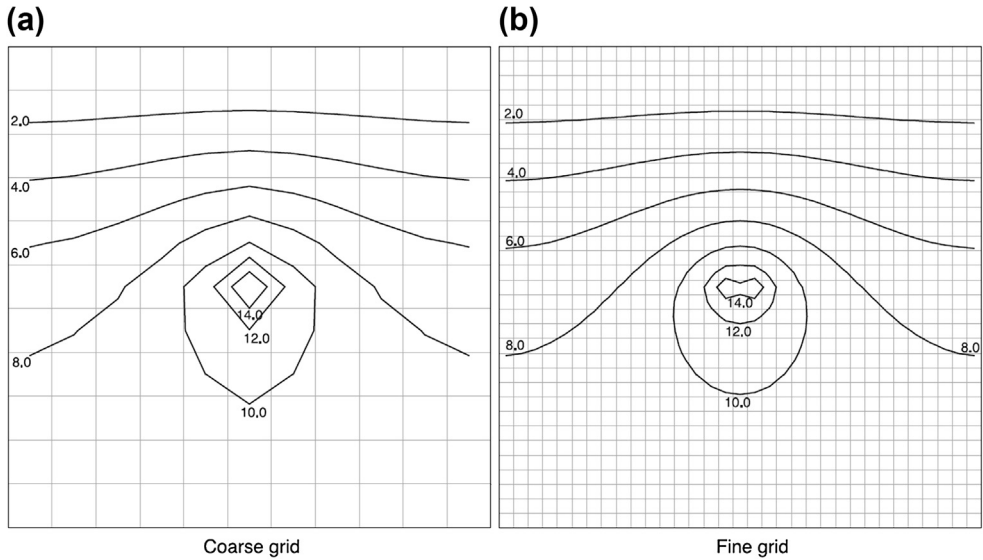
**Figure 6.1** Representation of a well in a layered FE model. The well is open to the aquifer through the screened sections and is simulated using 1D tubular discrete feature element (DFE) (Diersch, 2014).

for groundwater remediation. Injection wells are used for aquifer storage and recovery, groundwater heat pump systems, creation and maintenance of hydraulic barriers, disposal of waste fluids, and hydraulic fracturing (fracking). Usually, pumping and injection wells are vertical but inclined and horizontal wells can also be simulated (Fig. 5.16). Horizontal wells are sometimes used for water supply (e.g., the Ranney<sup>®</sup> radial collector well—[Haitjema et al., 2010](#); [Kelson, 2012](#)) and in hydraulic fracturing. When two or more wells are located in close proximity, a single well node may represent the combined discharge or injection of multiple wells. In regional models, typically only major high-capacity wells are simulated; low-yield wells such as individual domestic wells withdraw only a small volume of water and their effect on a regional flow system is usually negligible. Even at a local scale, it may not be necessary to include pumping from domestic wells. For example, water pumped from domestic wells in a surficial unconfined aquifer is often a small percentage of the water budget and/or most of the water pumped is returned locally to the groundwater system via on-site disposal to a septic system.

The locations of wells in the model domain should be plotted on the base map displayed in the Graphical User Interface (GUI) that is used to assemble input data and process output. Ideally, the model node coincides with the field location of the well but in practice it is seldom possible to locate all nodes directly at the field location of the well. Well nodes are placed in the layers that correspond to the elevations of well screens and open intervals (Fig. 6.1).

In both FD and FE models, the head computed at a well node does not perfectly represent the actual head in the pumping or injection well (Box 6.1). In both FD and FE models, a pumping/injection well creates a singularity in the solution, which means that the derivative does not exist there. Under pumping conditions in a typical grid/mesh, the simulated head will be biased high relative to the head in the well; thus, calculated drawdown will be underestimated (Fig. 6.2(c)). For injection, the opposite effect occurs and the simulated head will be biased low. If more accuracy is needed, heads in and near the pumping/injection well can be calculated using the Thiem analytical solution (e.g., [Charbeneau and Street, 1979](#)); see Box 6.1 and Section 6.2.3. Using an analytical solution has the advantage that simulated heads are corrected without refining the nodal spacing around the well. For many modeling objectives, it is sufficient to estimate those heads using the Thiem equation (Box 6.1) (or to use uncorrected heads). However, if simulation of heads in the immediate vicinity of the well is a primary modeling objective, it may be advisable to use small nodal spacing near important pumping centers (Box 6.1). For example, local scale models can be designed with small nodal spacing to simulate conventional aquifer tests, aquifer tests with hydraulic tomography, and single well tests (Section 5.4; [Yang et al., 2015](#)).

To simulate pumping/injection, the user specifies the pumping or injection rate at the well node as a volumetric rate ( $L^3/T$ ). The sign of the volumetric rate indicates whether water is extracted by pumping or injected into the groundwater system. Codes differ in the sign used to represent the flow direction (e.g., withdrawals are negative in MODFLOW's Well Package but positive in FEFLOW). Pumping and/or injection rates



EXPLANATION

- FINE GRID
- COARSE GRID

**Figure 6.2** Effect of nodal spacing on simulated heads near pumping wells in a 2D areal FD model. In figures (a) and (b) two wells, separated by a distance of 200 ft, are each pumping at a rate of 100,000 ft<sup>3</sup>/day. (a) Nodal spacing is 300 ft; the well node represents both pumping wells. (b) Nodal spacing is 100 ft; each well pumps from a separate well node. (c) The model design is the same as in (a) and (b) except that there is only one well pumping at a rate of 200,000 ft<sup>3</sup>/day. The figure shows the drawdown along the row that contains the well node (Reilly and Harbaugh, 2004).

and schedules can be estimated using discharge information from operators/owners or regulatory agencies charged with monitoring water use. In areas with numerous ungauged high-capacity wells, power records combined with pump size and efficiency estimates are often used to estimate discharges. Groundwater obtained from private domestic wells is usually not metered. In that case, daily per person water use estimates for the household can approximate the net pumping rate. Irrigation pumping can be calculated from crop acreage taken from air photos or other estimates of water application rates.

In two-dimensional (2D) areal models, wells are simulated by default as fully penetrating, i.e., the well is open to the entire saturated thickness of the layer. Effects of partially penetrating wells are usually ignored because the effects are limited to a radius of about  $1.5b\sqrt{K_h/K_v}$ , where  $b$  is the saturated thickness of the aquifer and  $K_h/K_v$  is the vertical anisotropy (Hantush, 1964; Haitjema 1995, p. 394). Furthermore, errors associated with spatial discretization in the grid/mesh often overwhelm errors caused by ignoring partial penetration. In three-dimensional models, details on the construction of each well are necessary to determine the elevations of the top and bottom of the well screens. Three-dimensional models can simulate the effects of partial penetration by representing an aquifer with several layers so that pumping or injection nodes can be placed in the specific layer where pumping occurs; however, the well fully penetrates the selected layer, unless specialized options are used (e.g., MODFLOW's Multi-Node Well Packages, Section 6.2.3).

### 6.2.1 FD Well Nodes

A pumping or injection well in an FD grid is conceptualized as a point sink or source located at a well node (Fig. 6.3(a)). However, the node in an FD model represents the entire cell/block; therefore, water discharged from a pumping well or recharged via an injection well is removed or introduced to the entire volume of the cell/block. This means that point injection or withdrawal of water is simulated conceptually in the same way as areally distributed recharge or discharge over the area of the cell (Fig. 6.3(b)). In both cases, the code adds a volume of water distributed over the top face of the FD cell/block per unit of time ( $L^3/L^2T$ ). Most FD codes (e.g., the Well Package in MODFLOW) allow the user to input well discharge or injection as a volumetric rate ( $L^3/T$ ) and the code converts the volumetric rate to a flux by dividing by the area of the top of the cell.

### 6.2.2 FE Well Nodes and Multinode Wells

In FE codes, wells are usually simulated by assigning a pumping or injection rate to a node as a specified flow (Neumann) internal boundary condition (e.g., FEFLOW's well boundary condition). An FE node under specified flow conditions is sometimes called a Neumann node (Istok, 1989, p. 155). Water is extracted from or injected to

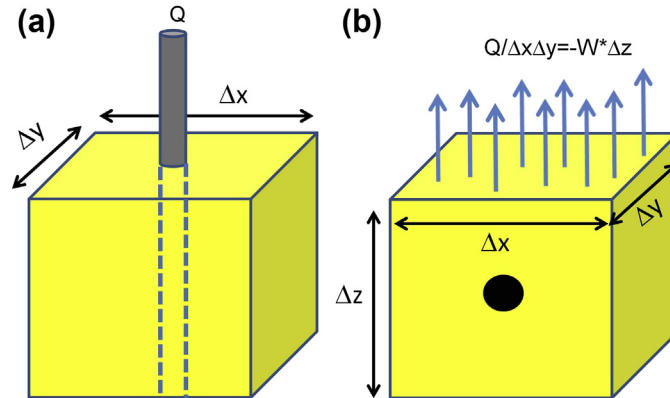


**Figure 6.3** Representation of a pumping or injection well in an FD grid. (a) Conceptual representation of the well as a point source or sink; (b) representation of discharge from a pumping well ( $Q$ ) in an FD model as areally distributed discharge where  $W^*$  ( $T^{-1}$ ) is a general sink/source term (see Eqn 3.12).

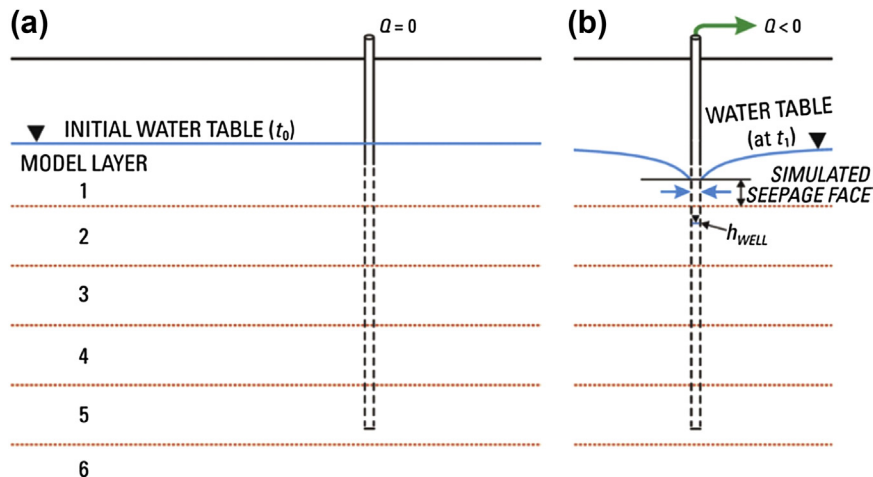


**Figure 6.4** Multinode wells. (a) The well fully penetrates the top four layers and is partially penetrating in layer 5. (b) Formation of a seepage face along the well bore causes additional head loss in the well; note that discharge from the well follows MODFLOW convention where a negative value of  $Q$  represents pumping (Konikow *et al.*, 2009).

nodes rather than distributed over an area as is done in an FD model. If the well is not located on a node, the flow is divided among the nodes of the element that contains the well, usually assuming linear variation within the element (Istok, 1989; Torak, 1993 provide details).

A multinode (multilayer) well represents a vertical well that penetrates more than one model layer and is simulated by connecting two or more well nodes (Figs 6.1 and 6.4;

also Fig. 5.16). FEFLOW simulates multinode wells using one-dimensional (1D) tubular discrete feature elements (DFEs) as shown in Fig. 6.1 and Fig. 5.16 (Diersch, 2014, pp. 221–223; also see discussion of DFEs in Section 5.2). By definition, a DFE represents a feature that is smaller than the nodal spacing and transmits more groundwater flow than the surrounding porous medium. A high conductivity is assigned to the DFE (of the order  $10^6$  m/s) to ensure relatively uniform heads at the nodes forming the well axis while maintaining a small gradient within the DFE toward the discharge location of the well. The formulation also allows for storage in the well casing, which can be significant immediately after pumping begins, but casing storage is small over long pumping periods and is often neglected in practice (Diersch, 2014, pp. 222, 426). Flow in the DFE (i.e., along the axis of the well bore) is simulated using the Hagen–Poiseuille equation for laminar flow (Diersch, 2014, p. 222). The total pumping or injection rate is assigned to the node located at the discharge or injection point of the well. The tubular DFE that represents the well shares and connects nodes within the mesh (Fig. 5.16). In that way the DFE is coupled to the solution of the groundwater flow equation and depth-variable inflow or outflow from the well is automatically accommodated.

### 6.2.3 Multinode Wells in FD Models

The Connected Linear Network (CLN) Process in MODFLOW-USG (Panday et al., 2013) is similar in function to DFEs. The CLN Process can be applied using either a structured or unstructured FD grid (Section 5.2). A cylindrical linear conduit in the CLN Process is similar to a 1D tubular DFE in an FE mesh except that the CLN nodes are not shared between the linear network and the porous medium. Rather the CLN solution is coupled to the solution of the groundwater flow equation that solves for heads at the nodes in the porous medium. The CLN Process solves for laminar flow of water within the cylindrical linear conduit that represents the well and also calculates exchange of water between CLN nodes and nodes in the porous medium. The CLN node is pumped using the Well Package in MODFLOW.

There are three other ways to simulate multinode wells in the structured grid of a standard FD model: (1) user-assigned apportioning of pumping or injection among layers, (2) high vertical hydraulic conductivity assigned to cells containing well nodes, and (3) specialized equations that represent processes within a multilayer well. Neville and Tonkin (2004) presented a comparative analysis of the three approaches. Each approach is discussed below in the context of pumping wells, but the same procedures apply for injection wells.

1. Well nodes are placed in each layer penetrated by the well and the user inputs the pumping rate at each well node by apportioning the total pumping rate ( $Q_T$ ) among the individual layers penetrated by the well based on layer transmissivity. Thus, the total discharge  $Q_T$  equals the sum of the pumping rates from the individual

layers ( $Q_{i,j,k}$ ). The transmissivity-weighted pumping rates for each layer ( $Q_{i,j,k}$ ) are approximated as:

$$Q_{i,j,k} = \frac{T_{i,j,k}}{\sum T_{i,j,k}} Q_T \quad (6.1)$$

where  $T_{i,j,k}$  is the transmissivity of a layer and  $\sum T_{i,j,k}$  is the sum of the transmissivities of all layers penetrated by the well (McDonald and Harbaugh, 1988). Equation (6.1) is an approximation because it does not reflect that  $Q_{i,j,k}$  is a function of the head at the well node ( $h_{i,j,k}$ ), which is computed as part of the solution. Also, conventional FD equations do not recognize that a well penetrating more than one aquifer or stratigraphic layer forms a preferential/small resistance pathway between layers. The code computes different heads for each well node when the head in a multiaquifer well is actually a composite average of the heads in all the layers it penetrates (Papadopoulos, 1966). Neville and Tonkin (2004) concluded that this approach is too simplistic for simulating multinode wells for most applied modeling problems.

2. The vertical hydraulic conductivity of the cell/block that contains the well node is set to a very high value in order to minimize the head differential within the simulated well. The user still must input pumping rates for each well node using Eqn (6.1). Neville and Tonkin (2004) concluded that this approach generates acceptable solutions provided two conditions are met: (1) The vertical hydraulic conductivity of the cells containing the well nodes must be set sufficiently high so that the calculated heads in all cells are approximately equal and (2) the areal dimensions of the FD cell representing the well must be similar to the dimensions of the well, ideally following the nodal spacing guideline given by Eqn B6.1.6 in Box 6.1. Even when guidelines are followed, stacking of high-vertical-conductivity cells may cause numerical instability and problems in solution convergence. In addition, the approach does not allow for well loss, which is additional drawdown resulting from turbulent flow and resistance in the well screen, well bore (skin effects), or a seepage face at the well bore (Fig. 6.4 (b)).
3. In practice, the preferred way to simulate wells that penetrate more than one layer of a standard FD grid is to use the Thiem equation to approximate head around well nodes, as is done in the Multi-Node Well (MNW2) Package (Konikow et al., 2009) in MODFLOW. The MNW2 Package is a revised and expanded version of the MNW1 Package (Halford and Hanson, 2002), which itself was built from an earlier package (the Multi-Aquifer Well (MAW1) Package) based on ideas by Bennett et al. (1982). Neville and Tonkin (2004) tested the MAW1 Package and compared results to an analytical solution. They found that the method gave excellent results and appeared to be relatively insensitive to cell size, suggesting that the method can represent wells in a regional model with a relatively coarse grid.

The MAW1, MNW1, and MNW2 Packages calculate a composite average head at the nodes of a multinode well and apportion pumping (or injection) among the well

nodes. MODFLOW-NWT (Niswonger et al., 2011; see review by Hunt and Feinstein, 2012) uses the multinode well packages with the Well Package in MODFLOW to simulate multinode wells. It also has an option that reduces the pumping rate in simulations of flow in thin unconfined layers when there is a seepage face along the well bore (Fig. 6.4(b)).

A brief description of the MNW2 Package follows; most of the options discussed are also available in the MNW1 Package. The Thiem equation is used to represent flow near the well under quasi-steady-state (steady-shape) conditions (Eqn B6.1.1 in Box 6.1). The Thiem equation for flow to a multinode well ( $Q_n$ ) is written as:

$$Q_n = \frac{2\pi T_n}{\ln(r_e/r_w)} (h_w - h_n) \quad (6.2a)$$

or

$$Q_n = CWC_n (h_w - h_n) \quad (6.2b)$$

where  $h_w$  is the actual head in the well and  $h_n$  is the head calculated for the FD cell containing the well node;  $CWC_n$  is the cell-to-well conductance ( $L^2/T$ ); anisotropic aquifer transmissivity,  $T_n$ , equals  $b\sqrt{K_x K_y}$ ;  $r_w$  is the radius of the well and  $r_e$  is the effective well radius (defined in Box 6.1). Also

$$Q_T = \sum_{n=1}^m Q_n \quad (6.3)$$

where  $m$  is the total number of nodes in the well. However,  $h_w$ ,  $h_n$ , and  $Q_n$  are unknown. In MNW2,  $h_n$  is calculated by solving the general FD equations. Then  $h_w$  and  $Q_n$  are computed by iteration. In odd-numbered iterations, the most recently computed values of  $Q_n$  are used in Eqns (6.2) and (6.3) to compute  $h_w$ . In even-numbered iterations, the most recently computed value of  $h_w$  is used to compute  $Q_n$ . Equation (6.2b) is computed in MODFLOW's General Head Boundary (GHB) Package where the boundary head is equal to  $h_w$ .

The solution process described above considers only the theoretical drawdown or aquifer loss calculated by the Thiem equation. The MNW2 Package can also include additional drawdown caused by well loss. The  $CWC_n$  term in Eqn (6.2b) is modified as follows:

$$CWC_n = \left[ A + B + CQ_n^{(P-1)} + \Delta h_p Q_n^{-1} \right]^{-1} \quad (6.4)$$

The first head-loss term, A, accounts for theoretical loss computed by the Thiem equation (Eqn (6.2a)) and corrects for the fact that the well has a radius less than the areal dimensions of the cell in which the well is located (Box 6.1). The second and third terms represent well loss; B accounts for head losses that occur adjacent to and within the borehole and well screen (skin effects) and C accounts for nonlinear head losses due to turbulent flow near the well. The linear well loss coefficient (B) includes the effects of head loss from flow through parts of the aquifer disturbed during drilling, and flow



through the gravel pack and well screen. The coefficient  $C$  and power term ( $P$ , dimensionless) are typically estimated for specific wells by step-drawdown tests. The additional head loss caused by partial penetration is represented by  $\Delta h_p$ , which is calculated from analytical solutions (described by Barlow and Moench, 2011). MNW2 also has a procedure to handle the presence of a seepage face along the well bore (Fig. 6.4(b)). For details on how MNW2 calculates well loss, partial penetration, and the seepage face, the reader is referred to Konikow et al. (2009).

### Box 6.1 Guidelines for Nodal Spacing around a Well Node

In both FD and FE models, the head computed at a well node does not accurately represent the head in the pumping or injection well (Section 6.2; Fig. 6.2). Rather the computed head equals the head at the *effective well radius*, sometimes called the *virtual well radius* (Figs B6.1.1(a) and B6.1.2). In this box, we discuss: (1) how the effective well radius can be used to estimate the head in a pumping/injection well for relatively coarse nodal spacing and (2) how to design fine nodal spacing around a well node so that the calculated head better approximates the head in and near the well.

The principles discussed in this box apply to both FD and FE models, although the mathematics of handling well nodes differs between the methods (Section 6.2). For convenience, we consider 2D horizontal flow in an FD grid and use FD notation to present the methods, but the same principles apply to an FE mesh. In the discussion below, we refer to a pumping well for convenience, but the principles also apply to injection wells.

*Estimating head in the well.* The Thiem analytical solution is often used with a numerical model to calculate heads in the vicinity of the pumping well. The Thiem equation was derived for steady-state radial flow to a pumping well in a homogeneous and isotropic aquifer, but is locally valid even before true steady state is reached. Specifically, the Thiem equation can be

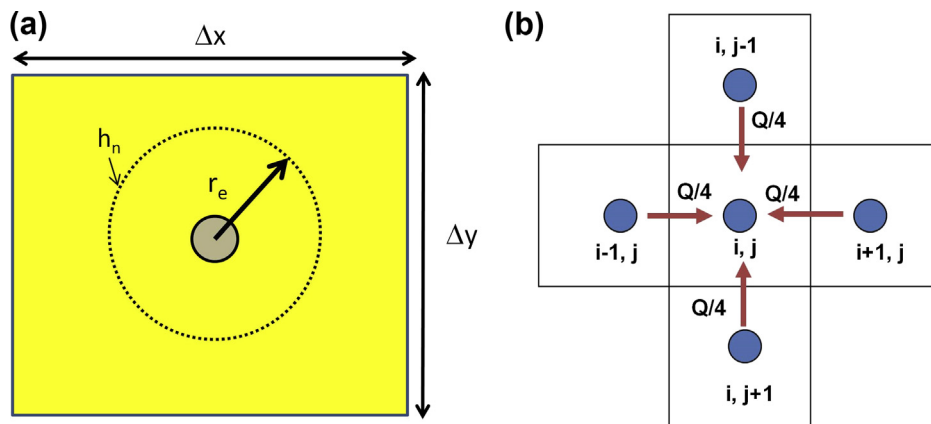


**Figure B6.1.1** Well node in an FD grid. (a) The well node is shown at the center of an FD cell; the effective well radius,  $r_e$ , is the radius at which the head is equal to the average head in the cell,  $h_n (=h_{i,j})$ . (b) FD cells in the vicinity of the well node ( $i,j$ ). The pumping rate is  $Q$ . The cell containing the pumping node receives one-fourth of the pumping discharge from each of the four neighboring cells.

(Continued)

### Box 6.1 Guidelines for Nodal Spacing around a Well Node—cont'd

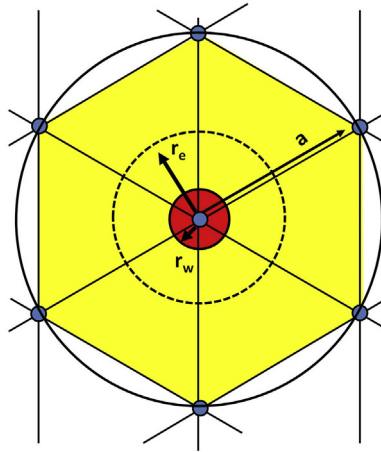


**Figure B6.1.2** Well node in an FE mesh consisting of equilateral triangular elements. The well node is surrounded by six neighboring nodes; each is located at a distance equal to  $a$  (Eqn B6.1.7) from the well node. The radius of the well is  $r_w$  and the effective well radius is  $r_e$  (modified from *Diersch et al., 2011*).

used to calculate heads near a pumping well when the rate of removal of water from storage near the well is zero. Under those conditions, quasi-steady-state conditions, called *steady-shape conditions*, apply near the well and the Thiem equation is applicable (*Heath and Trainer, 1968*). *Butler (1988)* (also see *Bohling et al., 2002, 2007*) pointed out that steady-shape conditions are reached when  $t = 100 r^2 S / 4T$ , where  $t$  is the time since pumping began,  $r$  is distance from the pumping well,  $S$  is the storativity, and  $T$  is the transmissivity. This rule comes from the guideline for using the Cooper–Jacob approximation to the Theis equation for transient radial flow to a well; the approximation is valid when  $u$  (which equals  $r^2 S / 4Tt$ ) is less than 0.01.

The Thiem equation is written as follows:

$$h_w = h_{ij} - \frac{Q}{2\pi T} \ln \frac{r_e}{r_w} \quad (\text{B6.1.1})$$

where  $h_w$  is the head in the well and  $h_{ij}$  is the head computed by the FD code for the cell containing the well node, which is equal to the head at  $r_e$ .  $Q$  is the total pumping (or injection) rate at the well node and  $T$  is the transmissivity of the cell. The radius of the well is  $r_w$  and  $r_e$  is the effective well radius. (In an FD model, the head at  $r_e$  is equal to the average head in the cell,  $h_{ij}$ .) Eqn B6.1.1 can be used to estimate the head in the well,  $h_w$ , from the head calculated at the node,  $h_{ij}$ , given a value for  $r_e$ .

When there is a regular grid in the vicinity of the well node so that  $\Delta x = \Delta y = a$ , it can be demonstrated that  $r_e = 0.208a$  (*Prickett, 1967*). To verify this relation refer to *Fig. B6.1.1(b)*, which shows a portion of a 2D areal grid in the vicinity of a well node. Assuming that draw-down is symmetric in the vicinity of the well node ( $ij$ ), the volumetric flow rate through each side of the cell is  $Q/4$ . We apply Darcy's law to calculate flow through the right-hand-side face of the cell:

$$\frac{Q}{4} = aT \frac{h_{i+1,j} - h_{ij}}{a} \quad (\text{B6.1.2})$$

### Box 6.1 Guidelines for Nodal Spacing around a Well Node—cont'd

Applying the Thiem equation between  $r = \Delta x = a$  (where head is equal to  $h_{i+1,j}$ ) and  $r = r_e$  (where head is equal to  $h_{i,j}$ ) yields:

$$\frac{Q}{4} = \frac{\pi T}{2} \frac{h_{i+1,j} - h_{i,j}}{\ln(a/r_e)} \quad (\text{B6.1.3})$$

Equating Eqns. B6.1.2 and B6.1.3 gives

$$\frac{a}{r_e} = e^{\pi/2} = 4.81$$

or

$$r_e = 0.208a \quad (\text{B6.1.4})$$

By modifying the Thiem equation for unconfined conditions, a formula analogous to Eqn B6.1.1 is written as follows:

$$h_w = \sqrt{h_{i,j}^2 - \frac{Q}{\pi K} \ln \frac{r_e}{r_w}} \quad (\text{B6.1.5})$$

where  $r_e$  is approximated by Eqn B6.1.4. It should be remembered that effects of well loss (Eqn (6.4); Section 6.2) are not included in Eqns B6.1.1 or B6.1.5.

*A Guideline for Designing Nodal Spacing.* Equation B6.1.4 provides a guideline for designing nodal spacing around a well when the modeling objective requires accurate heads and flows immediately around the pumping well. Suppose we set  $r_e$  (where head is equal to  $h_{i,j}$ ) in Eqn B6.1.4 equal to  $r_w$ . In that way we require that the computed head ( $h_{i,j}$ ) is equal to the head at  $r_w$  (the head in the well). Then, it follows that

$$a = 4.81r_w \quad (\text{B6.1.6})$$

That is, the nodal spacing around the well node (node  $i,j$ ) should be around 4.81 times the radius of the well, or less, for the head calculated at the well node ( $h_{i,j}$ ) to approximate the head in the well ( $h_w$ ). If the nodal spacing guideline in Eqn B6.1.6 is observed when designing the grid, it is not necessary to use Eqns B6.1.1 or B6.1.5 to estimate the head in the well.

In an FE mesh with equilateral triangular elements (Fig. B6.1.2):

$$a = \xi r_w \quad (\text{B6.1.7})$$

where  $\xi$  depends on the number of nodes,  $n$ , connected to the well node,  $\xi = 4.81$  for  $n = 4$ ,  $\xi = 6.13$  for  $n = 6$ , and  $\xi = 6.66$  for  $n = 8$  (DHI-WASY GmbH, 2010, p. 50).

Nodal spacing defined by Eqns B6.1.6 and B6.1.7 is advisable when using a groundwater flow model to analyze the results of aquifer tests, hydraulic tomography, or single-well tests (Section 5.4). Fine nodal spacing around pumping/injection wells might also be required to calculate accurate groundwater velocities in the immediate vicinity of the well node for particle tracking solutions (Chapter 8) and when a groundwater flow model is linked to a solute or heat transport model (Sections 12.2 and 12.3). For most other groundwater flow problems, such fine nodal spacing (i.e., equal to  $a$  in Eqns B6.1.6, B6.1.7) around pumping/injection wells is usually unnecessary inasmuch as the computed head for a relatively coarse grid (e.g., Fig. 6.2(a) and (c)) is sufficient for many modeling objectives. If necessary, the Thiem equation (Eqns B6.1.1, B6.1.5) can be used to improve calculated values of head at and near the well node.

### 6.3 AREALLY DISTRIBUTED SOURCES AND SINKS

The most common areally distributed (nonpoint) source of water is recharge to the water table, which originates from infiltration at the land surface and reaches the water table after flowing through the unsaturated zone (Fig. 6.5(a) and (b); Box 5.4). Other types of areally distributed flows include leakage through the bottom boundary of the model to or from an underlying unmodeled unit, underflow through the side boundaries of the model (Fig. 6.5(c)), and ET. Depending on the options chosen, nonpoint sources and sinks may be input to the model as a flux (L/T) or a volumetric rate ( $L^3/T$ ). For example, some codes have options for input of recharge as a flux across the water table (e.g., the Recharge Package in MODFLOW). If input as a flux, the code multiplies the recharge flux by the area of the cell or element that receives recharge to calculate the volumetric rate of water added to the node (Fig. 6.5(a)).

Recharge can also be input as a volumetric rate using a specified flow boundary condition. FE codes that accept recharge input as a flux multiply user-specified rates by the area of the element associated with the node and apportion water to nodes (Fig. 6.5(b)). Details of the procedure are given by Torak (1993) and Istok (1989). In FEFLOW, recharge can be input as a flux to the top or bottom layer of the model as a “material property”, or as a volumetric rate via the well boundary condition (a type of specified flux boundary condition); if recharge is input as a well boundary condition, the user must convert the recharge flux to a volumetric rate for input to the code. Conceptually, the effect on the local flow system is different when recharge enters the groundwater system as distributed recharge to the water table (in an FD model) vs point recharge to a node (in an FE model). However, in practice the solution is insensitive to this conceptual difference. In effect, both FD and FE codes input a volumetric rate of water to a node when simulating areally distributed recharge. The difference is that the node in an FD model represents the space occupied by the entire FD cell/block.

Recharge is normally input directly to unconfined layers (Section 5.3) and only to cells or elements where the water table is present. For some models, the water table may occur only in the top layer of the model, but in many models the water table is also present in some lower layers (e.g., Fig. 4.6), or the water table may drop down into lower layers during iteration of a steady-state solution or in response to stresses in a transient simulation (Section 4.5). To handle those situations, some codes allow the modeler to apply recharge to the top active cells in the model rather than exclusively to the top layer. In that way, the code automatically updates the distribution of recharge when the water table moves between layers.

The mechanics of how recharge is included in the numerical approximation of the governing equation is code specific and the interested reader should consult the code's

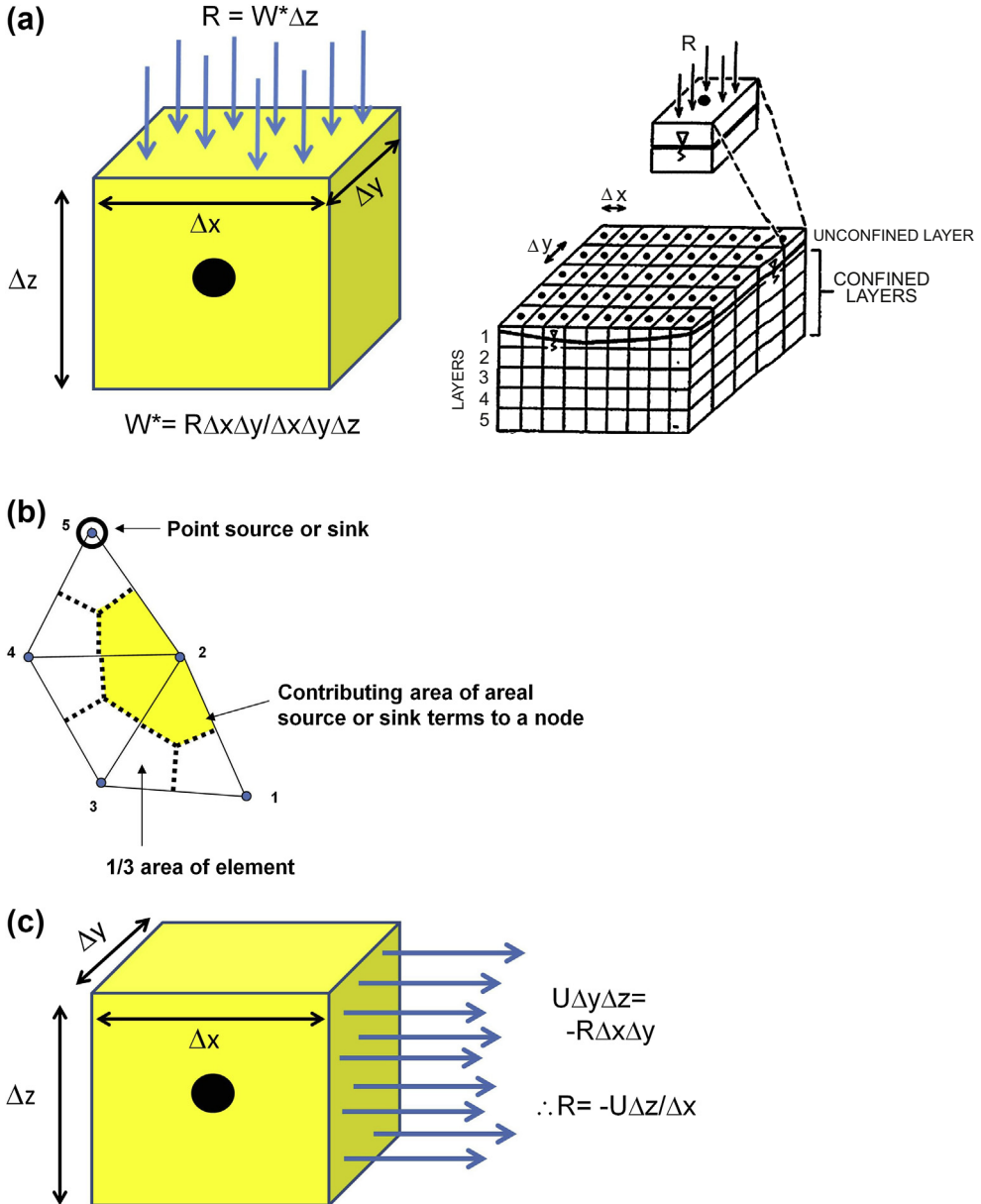


**Figure 6.5** Distributed recharge. (a) Recharge from infiltration is applied as a flux (L/T) to the top (unconfined) layer of a three-dimensional FD cell.  $W^*$  is the sink/source term in the general governing equation (Eqn (3.12)). (b) Recharge to the shaded area in the FE mesh is applied as a volumetric recharge rate ( $L^3/T$ ) to node 2. The specified flow rate assigned to node 2 is a weighted average based on the rates in the shaded area. (c) Discharge assigned (as negative recharge) to a side face of an FD block to represent underflow,  $U$ , (Fig. 2.15). If input as a rate (L/T) via the code's recharge array, side fluxes must be adjusted as shown when assembling input data. In an FE code, underflow is assigned to a node as a specified flow boundary condition using a volumetric rate ( $L^3/T$ ).

user's manual for details. Generally speaking, if recharge is input as a source term in the governing equation (Eqn (3.12)), it is included internally in the matrix  $\{f\}$  in Eqn (3.30) for FD approximations of the governing equation. In an FE formulation, an additional matrix containing the recharge terms is added to the right-hand side of Eqn (3.30). Wang and Anderson (1982, pp. 145–147) give details for a steady-state, 2D example. Numerically it may be simpler to include recharge as a specified flow boundary condition in an FE formulation.

Flow through the bottom of an FD block in a structured grid is mathematically identical to flow through the top of a block or element and is also identical in an unstructured FD grid and FE mesh as long as the area of the bottom face of the block or element is the same as the top face. For lateral inflow input as recharge, the modeler may have to adjust the rate input to the code. For example, the code may be programmed to multiply the rate by the top face ( $\Delta x \Delta y$ ) of an FD block, which is appropriate for simulating recharge from infiltration (Fig. 6.5(a)). However, lateral flow, such as underflow (Fig. 6.5(c)), occurs through a side face ( $\Delta x \Delta z$  or  $\Delta y \Delta z$ ), which generally will have a different area than the top face of the block or element. In that case, the modeler should adjust the rate input to the code so that the code computes the correct volume of water applied to the node. These issues do not arise when lateral flows are represented by a general HDB condition (Section 4.3), which is generally the preferred way to represent lateral flow of water to/from the model.

Loss of water across the water table occurs as ET, which is usually simulated as an HDB condition (Section 4.3). MODFLOW has a variety of packages to simulate ET, including the original Evapotranspiration Package (McDonald and Harbaugh, 1988). Other ET packages include the Evapotranspiration Segments (ETS1) Package by Banta (2000); also see Doble et al. (2009); Baird and Maddock (2005); Ajami et al. (2012). In FEFLOW, ET is simulated using a general HDB condition and the modeler must formulate input using the principles in Section 4.3.

## 6.4 DRAINS AND SPRINGS

When a high water table limits land use, drains (Fig. 4.17) may be constructed to lower the water table. For example, drainage tiles are used to dewater agricultural fields; large excavations and underground workings such as mines, quarries, and tunnels may be dewatered using drains and/or pumping wells. Such features that remove water from the groundwater system are usually simulated with HDB conditions (Section 4.3).

A drain-type formulation of an HDB condition can also be used to simulate flowing wells (e.g., Brooks, 2006) and seepage faces (Fig. 4.17), springs, seeps, diffuse flow into

wetlands, and headwater streams. Springs, seeps and diffuse flow into groundwater-fed wetlands are typically points or areas of groundwater discharge in topographic depressions and low-lying areas of the land surface. For flowing wells, springs, and seeps, the elevation of the drain is set equal to the land surface elevation at the location of the feature (Section 4.3).

The conductance (Eqn (4.4b)) of discharge features simulated as drains is usually estimated during calibration by comparing simulated discharge to measured flows. For example, springflow can be measured using stream gaging equipment for large flows; portable flumes and weirs to channel smaller flows; and seepage meters (Lee, 1977; Rosenberry et al., 2008) for submerged springs. An alternative to estimating conductance as a calibration parameter is to set the drain conductance to an arbitrarily high value so that aquifer properties in the area around the drain control flow from the discharge feature.

A drain removes water from the model, which may not be appropriate if, under field conditions, water discharged to the feature being simulated flows overland and reenters the groundwater system downgradient. Code developers have handled this situation by allowing a portion of the drained water to reenter the groundwater system at user-specified nodes (e.g., the Drain Return (DRT1) Package by Banta, 2000). A better approach is to represent the discharge feature as the first node in a stream network so that the water drained from the groundwater system can be routed downgradient as streamflow and potentially reenter the groundwater flow system as seepage from the stream (Section 6.5).

A drain formulation assumes no seepage out of the feature when the head in the aquifer is at or below the drain elevation specified by the modeler. In some field situations, wetlands may recharge the groundwater system at certain times of the year and remove water at other times; in these cases, a drain formulation is not appropriate if recharge from a wetland is sufficiently large. When important for the modeling objective, wetlands can be simulated using options for streams (Section 6.5) and lakes (Section 6.6) or by simulating both groundwater and surface water flow through a wetland layer (Section 6.7).

## 6.5 STREAMS

Streams can be both sources and sinks of groundwater. Groundwater discharges into a gaining stream (Fig. 6.6(a); Fig. 4.16(b)) and is recharged by water from a losing stream (Fig. 6.6(b); Figs 4.7 and 4.16(c) and (d)). *Baseflow* is streamflow derived from groundwater; it is typically measured during dry conditions when the stream is not receiving water from overland runoff or other sources, or is estimated from hydrograph separation. The exchange of water between an aquifer and a stream can be spatially (e.g., Lowry et al., 2007; Woessner, 2000) and temporally (e.g., Hunt et al., 2006) complex. In

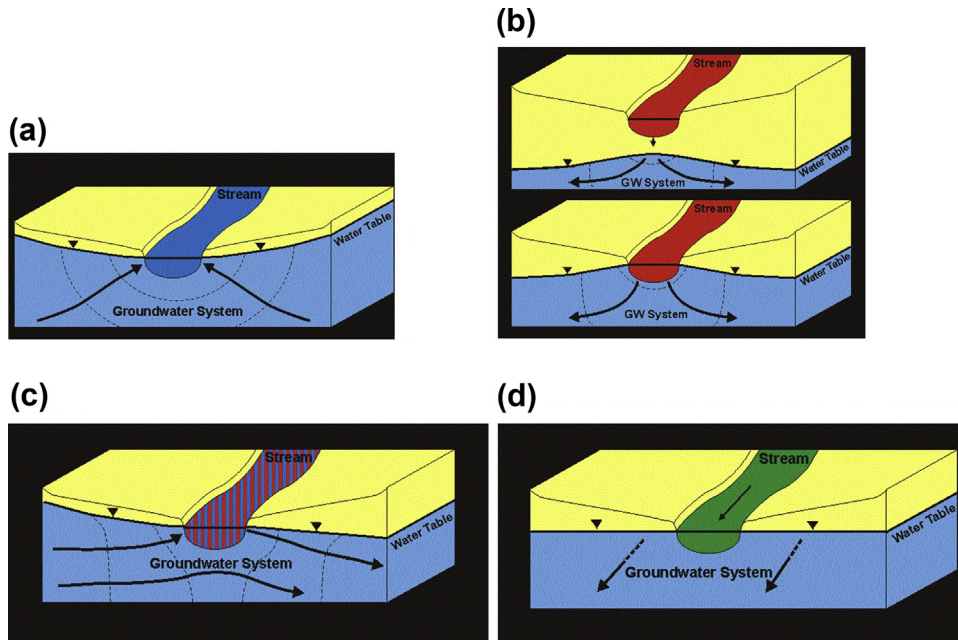


**Figure 6.6** Conceptual models of stream and groundwater exchange showing the water table position relative to the stream stage: (a) gaining stream; (b) losing stream; (c) flow through stream; (d) parallel flow stream (after *Woessner, 2000*).

in addition to gaining and losing reaches, sections of the stream may have flow-through and parallel flow conditions (Fig. 6.6(c) and (d)) and the distribution and spatial extent of conditions can change with time. The direction of flow between the groundwater system and a stream is determined by the relative elevations of stream stage and the groundwater head adjacent to and below the stream.

Streams that fully occupy a cell/element are occasionally simulated as specified head nodes (Figs 4.7(a)); however, most streams are narrower and shallower than the nodal spacing, and specified head nodes are infinite sources/sinks of water for the groundwater system. Usually the better approach is to simulate streams using HDB conditions (Sections 4.2 and 4.3) whereby the stream is conceptualized to be hydraulically connected to a cell/element but does not physically occupy space within the grid/mesh (Fig. 4.16). Stream dimensions are defined within each cell/element where the stream is present:  $W$  is the width of the stream;  $L$  is its length in the cell/element;  $b$  is the thickness of the streambed sediments. Under HDB conditions, exchange of water between the stream and the aquifer occurs vertically through the streambed; no exchange occurs through the sides of the channel. In MODFLOW, for example, the River Package calculates the flow of water between the stream and the aquifer,  $Q_{GW}$ , using Eqn (4.5)



with riverbed conductance,  $C$ , equal to leakance  $K_z'/b'$  times the area the river occupies within the cell ( $LW$ ):

$$Q_{GW} = -K_z' \frac{h_{i,j,k} - h_s}{b'} LW \quad (6.5)$$

where  $h_{i,j,k}$  is the groundwater head calculated by the model at the HDB node connected to the stream and  $h_s$  is the head in the stream specified by the user (Fig. 4.16(b) and (c)). When  $Q_{GW}$  is negative, water discharges into the stream and is removed from the groundwater system; when  $Q_{GW}$  is positive, water enters the groundwater system from the stream. In simple representations, (e.g., using the River Package in MODFLOW)  $h_s$  is assumed constant and equal to a user-specified value for a specified period of time, although it typically varies spatially along the length of the stream.

Equation (6.5) is used for both gaining and losing conditions, but when the head in the aquifer falls below the bottom of the streambed sediments, the stream is said to be disconnected from the aquifer and percolating conditions occur. Under percolating conditions (Fig. 4.16(d)), the head at the bottom of the streambed is assumed equal to the elevation of the bottom of the streambed sediments (SBOT in Fig. 4.16(d)) and flow from the stream to the groundwater system ( $Q_{GW}$ ) is constant:

$$Q_{GW} = C(h_{i,j,k} - SBOT) \quad (6.6)$$

where  $C = (K_z'/b')(LW)$  and  $h_{i,j,k} < SBOT$ . During model calibration, simulated values of  $Q_{GW}$  (Eqns (6.5) and (6.6)) are compared with field estimates. The flux between the stream and the groundwater system can be measured locally at specific locations using seepage meters placed in the streambed, estimated from Darcy's law with measured vertical gradients and streambed hydraulic conductivity (e.g., [Rosenberry et al., 2008](#)), and estimated by temperature flux methods (e.g., [Lapham, 1989](#); [Constantz et al., 2008](#)).

The net gain or loss is estimated for each stream reach by subtracting the upstream flow from the downstream flow. The distance between measurements must be sufficiently large so that measurements are not confounded by errors associated with measuring small differences in flows. Streamflow measured with errors around 5% are considered good estimates but errors up to 20% are tolerable ([Herschy, 1995](#); [Harmel et al., 2006](#)). Long-term streamflow records at gaging stations are especially useful for computing increases or decreases in streamflow between stations. Typically both synoptic measurements and stream gage data are processed to remove sources of streamflow not derived from groundwater. Synoptic measurements can be adjusted using a nearby index stream gage (e.g., [Gebert et al., 2007](#)); baseflow separation techniques (e.g., [Westenbroek et al., 2012](#); [Sloto and Crouse, 1996](#)) are typically used to process streamflow time series to generate time series of baseflow.

The simple process of simulating stream/groundwater exchange described above has several disadvantages, the chief of which is that when the stream stage ( $h_s$ ) is time invariant it can be a source/sink of infinite amounts of water. Time invariant stream stage is not appropriate for headwater (ephemeral) streams (e.g., [Mitchell-Bruker and Haitjema, 1996](#)) or small streams when pumping wells are nearby. Moreover, temporal fluctuations in stream stage may have a significant effect on groundwater heads and then stream stages in the model should vary with time. There are several advanced methods for simulating streams that allow for fluctuations in stream stage. The SFR packages (SFR1 by [Prudic et al., 2004](#); SFR2 by [Niswonger and Prudic, 2005](#)) for MODFLOW allow the user to specify a constant stream stage, but more commonly an SFR package is used to calculate stream stage as the simulation progresses. The SFR packages also calculate and rout streamflow downgradient. Several methods for calculating stream discharge are included; the most commonly used method relies on Manning's equation:

$$Q_s = \frac{C_f}{n} AR^{2/3} S_0^{1/2} \quad (6.7)$$

where  $Q_s$  is the streamflow ( $L^3/T$ ),  $C_f$  is a units conversion factor equal to 1.0 for  $m^3/s$  or 1.486 for  $ft^3/s$ ,  $n$  is Manning's roughness coefficient,  $A$  is the cross-sectional area of the stream channel ( $L^2$ ),  $R$  is the hydraulic radius of the stream channel ( $L$ ), and  $S_0$  is the slope of the water surface, which is usually assumed to be equal to the slope of the stream channel ( $L/L$ ). The SFR packages also allow for the addition and subtraction of water from runoff, engineered diversions of streamflow, and precipitation and evaporation from the water surface within each stream segment. Because this representation keeps track of streamflow by stream reach, the volume of water lost from the stream (e.g., by recharging the groundwater system) is limited to water captured upstream; thus, ephemeral streams and upgradient stream reaches are allowed to dry up when appropriate rather than forced to supply unrealistic volumes of leakage as can happen when the stream stage is held constant in time ([Mitchell-Bruker and Haitjema, 1996](#)).

The SFR packages include multiple options for calculating stream stage from calculated stream discharge. The most commonly used method assumes a wide rectangular stream channel in which stream width,  $W$ , is much greater than stream depth,  $d_s$ . Then [Eqn \(6.7\)](#) can be written:

$$Q_s = \frac{C_f}{n} W d_s^{5/3} S_0^{1/2} \quad (6.8)$$

Using the value of  $Q_s$  calculated by the code together with known stream geometry and slope, the stream depth,  $d_s$ , is calculated from [Eqn \(6.8\)](#). Then  $d_s$  is added to the modeler-specified elevation of the top of the streambed to give stream stage. A more complex cross-sectional geometry for the stream channel can be defined by eight points ([Fig. 6.7](#)) and then a more complicated expression is used to calculate stream

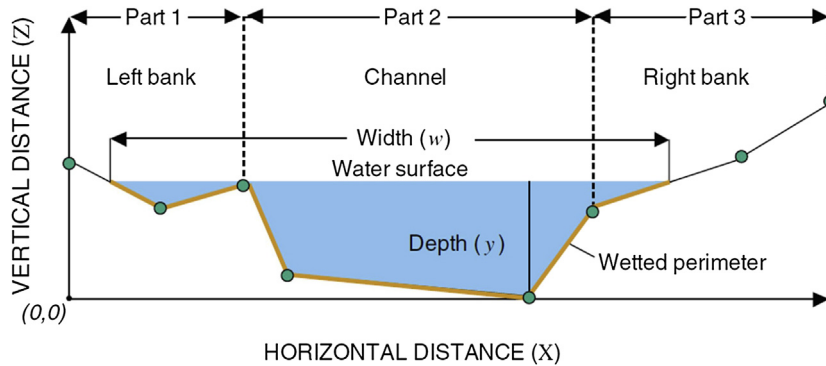


**Figure 6.7** Complex stream channel geometry approximated using eight points along the channel (Prudic et al., 2004).

depth; the reader is referred to Prudic et al. (2004) and Niswonger and Prudic (2005) for details, as well as for discussion of the other options for calculating stream depth.

The SFR2 Package (Niswonger and Prudic, 2005) allows some stream properties (e.g., vertical hydraulic conductivity and thickness of the streambed sediments) to be entered for the cell as opposed to assigning those properties to entire stream segments as is required in SFR1. SFR2 also includes the capability to rout water through an unsaturated zone when the stream is under percolating conditions (Figs 4.16(d)). The time required for water from the stream to flow through the unsaturated zone can be important for transient models, especially in arid settings where the distance between the streambed and the water table is large (Fig. 4.7).

Hughes et al. (2012, 2014) developed a streamflow package for MODFLOW, called the Surface–Water Routing (SWR1) Process, that allows for more sophisticated handling of 1D and 2D surface water flow. The SWR1 Process routs streamflow using options such as a diffusive wave approximation of the Saint Venant equations; surface water stages are then coupled to the groundwater flow equation in MODFLOW. The SWR1 Process handles more surface water routing situations than the SFR packages, including surface flow through wetlands (Section 6.7).

Including stream stage calculation in a groundwater model increases the complexity of input and output and adds nonlinear equations that can affect solution stability. Therefore, when modeling with MODFLOW it is common to use the simpler River Package and the Drain Package for features farther from the area of interest (where effects of omitting fluctuation in stream stage are expected to be unimportant to the modeling objective) and one of the SFR Packages to represent near-field streams (Fig. 6.8(a)).

In FEFLOW streams are typically simulated using a general HDB condition. For more advanced applications, FEFLOW is linked to a surface water code (MIKE11). For both FD and FE modeling, the availability of sophisticated options for simulating

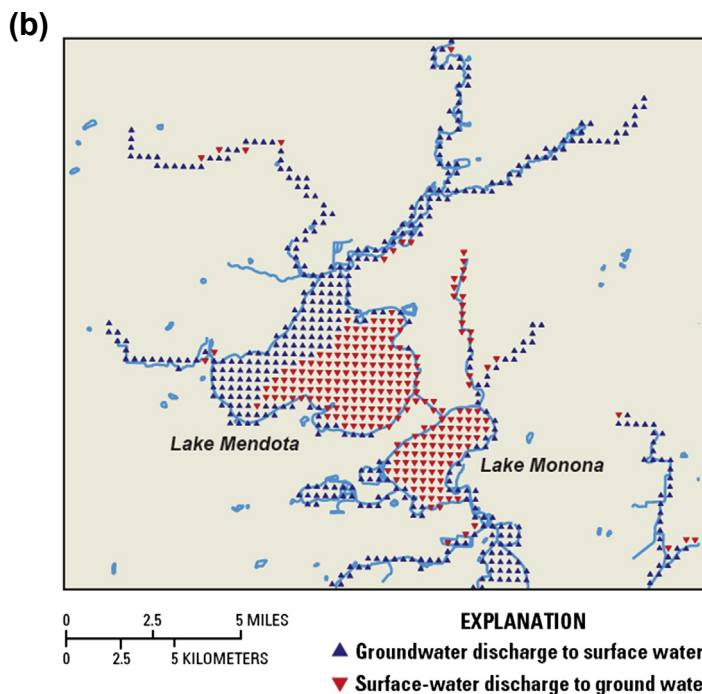
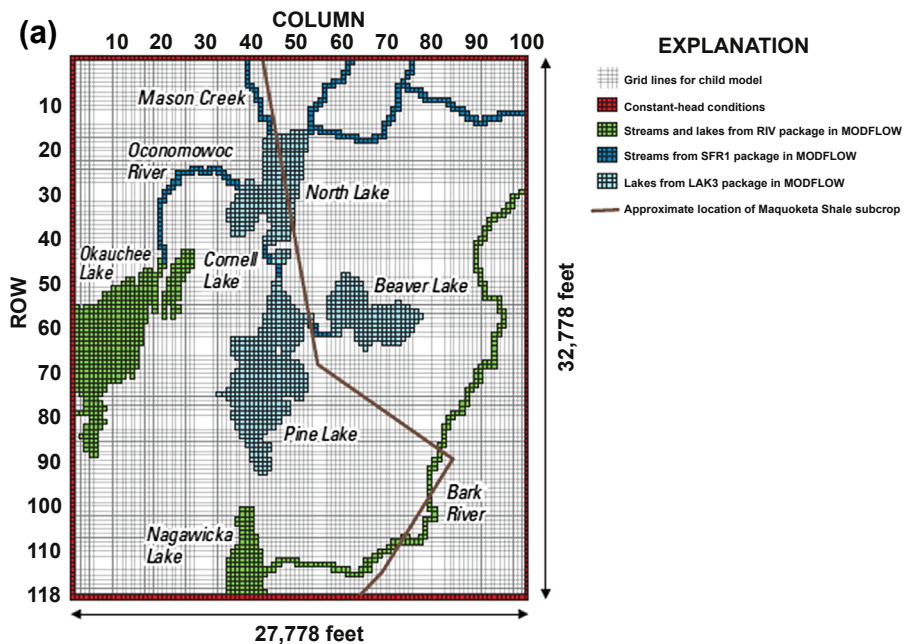


**Figure 6.8** Representation of streams and lakes in an FD grid. (a) The River Package in MODFLOW was used to represent far-field streams and far-field lakes as fixed level lakes; the SFR and Lake Packages were used to simulate near-field streams and lakes, respectively (Feinstein et al., 2010). (b) The River Package in MODFLOW was used to represent fixed level lakes. Areas of outflow from the lakes to the groundwater system in response to pumping are indicated by red triangles; blue triangles indicate areas of groundwater inflow (modified from Hunt et al., 2001).

streams within a groundwater model makes it possible to simulate groundwater basins with complex connected surface water systems. Consequently, groundwater-based codes often can be used effectively in watershed modeling (see [Box 6.2](#), which immediately follows [Section 6.7](#)).

## 6.6 LAKES

Lakes can be represented as specified heads or using HDB conditions (Sections 4.2 and 4.3). Both of those options require the user to specify lake level, which is then held constant. In some problems, however, calculation of lake level is important to the modeling objective. For those problems, fluctuations in lake level can be simulated using options available in some groundwater flow codes, as discussed below.

Lakes can be broadly classified as *drainage lakes*, which have significant surface water inflows and/or have an outflowing stream, and *seepage lakes*, which do not have significant inflowing or outflowing streams. Lakes can also be classified according to groundwater regime as recharge, discharge, and flow-through ([Born et al., 1979](#)) ([Fig. 6.9\(a\)–\(c\)](#)). A recharge lake adds water to the groundwater system, a discharge lake acts as a sink, and a flow-through lake exchanges water with the groundwater system as inflow and outflow. However, the exchange of water between the groundwater system and a lake is often more complex in space and time than the three basic categories (e.g., see [Fig. 6.9\(d\)](#)). Moreover, flow regimes may change seasonally and in response to drought and periods of high precipitation.

Broadly speaking, lakes can be simulated in a groundwater model by specifying the lake level (called a fixed lake level model) or by allowing the model to calculate lake level (called a fluctuating lake level model) ([Hunt et al., 2003](#)). A fixed lake level may be represented with specified heads set to the lake surface elevation, or, more commonly, by using the same type of HDB conditions used for streams ([Section 6.5](#)). Under HDB conditions the lake does not occupy space in the grid/mesh and exchange of water with the aquifer is assumed to occur only vertically through the bottom of the lake. Therefore, it is not possible to simulate lake basin geometry or flow through the sides of the lake but flow through the bottom of the lake can be calculated ([Fig. 6.8\(b\)](#)).

There are two options for representing fluctuating lake levels: high-conductivity nodes and special-purpose lake water budget equations (e.g., the Lake Package in MODFLOW as coded by [Merritt and Konikow, 2000](#), and in the analytic element code GFLOW using a lake element described by [Hunt et al., 2003](#)). For seepage lakes, assigning high values of hydraulic conductivity (K) to cells or elements containing the lake allows the model to calculate water levels at the nodes representing the lake and thus lake levels are allowed to change during the simulation (e.g., [Anderson et al., 2002](#); [Hunt et al., 2003](#); [Chui and Freyberg, 2008](#)). High K values assigned to lake nodes can work well to simulate lake levels in seepage lakes, but the method is not suited for

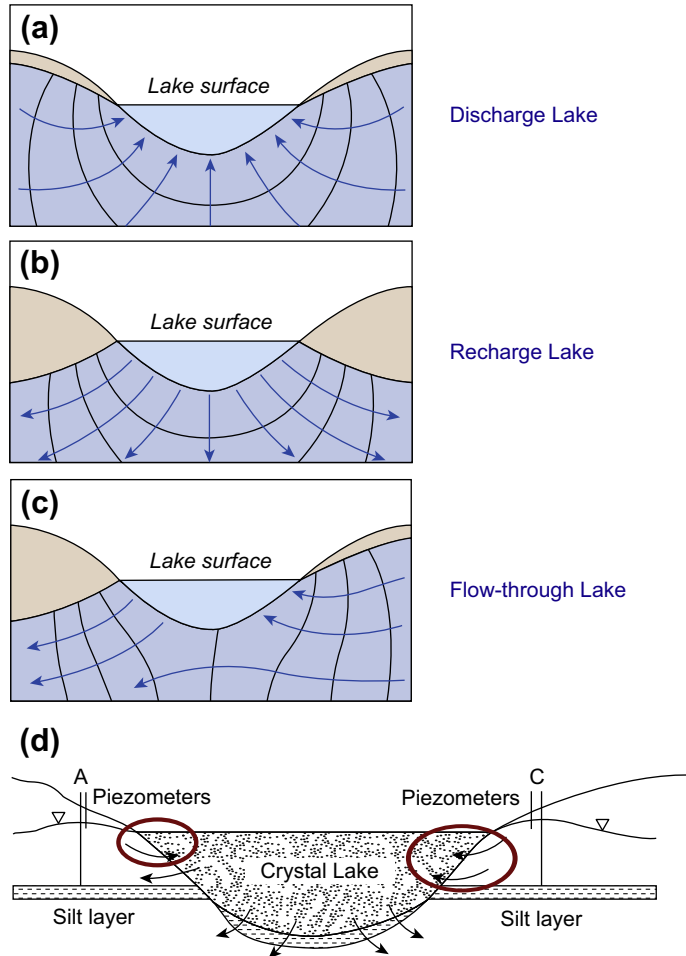


**Figure 6.9** Lakes classified by groundwater flow regime. (a) A discharge lake receives inflow from groundwater. (b) A recharge lake recharges the groundwater system. (c) A flow-through lake receives groundwater inflow through some of the lakebed and recharges the groundwater system through the remainder of the lakebed (*Winter et al., 1998*). (d) A lake with a complex flow regime has shallow discharge conditions (circled arrows), intermediate flow-through conditions, and deep recharge (modified from *Anderson and Cheng, 1993*).

drainage lakes, requires postprocessing to calculate fluxes between the aquifer and the lake, and may have relatively long run times to achieve acceptable water budget errors (e.g., see *Anderson et al., 2002*).

Alternatively, special-purpose lake water budget equations allow for simulation of fluctuating lake levels in both seepage and drainage lakes. In MODFLOW, the Lake Package (LAK3; *Merritt and Konikow, 2000*) simulates fluctuating lake levels and calculates lake budgets in seepage and drainage lakes for both steady-state and transient

simulations. The lake occupies space within the grid and interfaces both laterally and vertically with adjacent aquifer cells (Fig. 6.10(a)). In this approach, lake nodes are specified as inactive in the solution of the groundwater flow equation but the geometry of the lake is represented in the grid. Then, head at lake nodes (lake level) is calculated separately and coupled to the groundwater solution as specified heads in an HDB condition. LAK3 computes lake levels from a water budget equation that includes groundwater inflow and outflow, streamflow in and out of the lake, precipitation to and evaporation from the lake surface, runoff to the lake, and any other withdrawals or additions of water to the lake. The SFR Package is used to automate delivery of streamflow to the lake and to rout outflow from a drainage lake downstream.

In the Lake Package, exchange of water between the lake nodes and the aquifer is determined from Darcy's law by using hydraulic gradients calculated by the code and leakage values assigned to the lakebed by the modeler (Fig. 6.10(b)). The code computes groundwater flow horizontally and vertically to or from the lake,  $Q_{GW}$ , as

$$Q_{GW} = KA \frac{h_l - h_a}{\Delta l} = C(h_l - h_a) \quad (6.9)$$

where  $K$  is either the horizontal or vertical hydraulic conductivity between the lake and a location within the aquifer (Fig. 6.10(c));  $A$  is the cross-sectional area of the cell

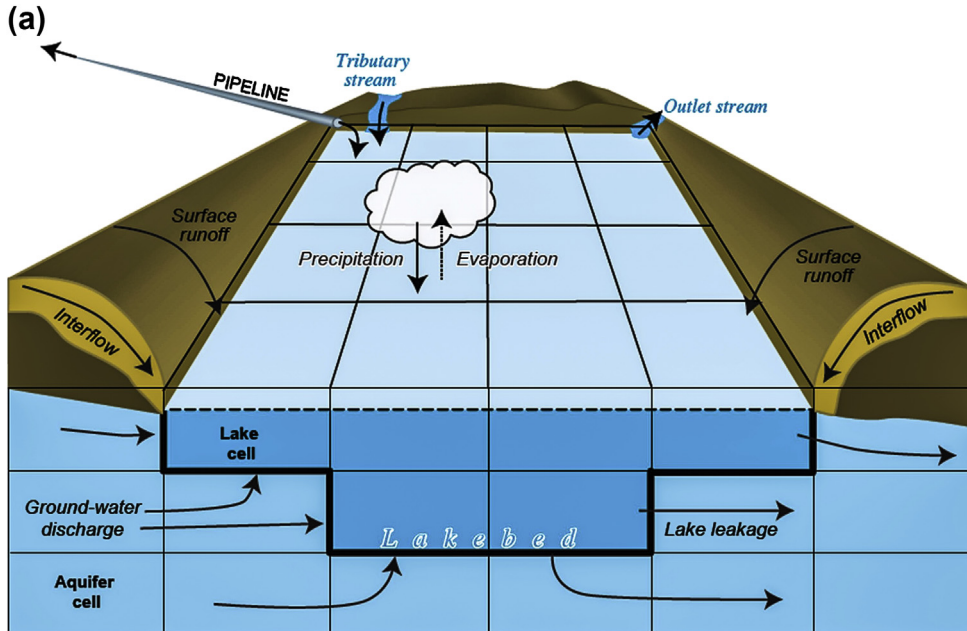


**Figure 6.10** Representation of a lake in MODFLOW with the LAK3 Package. (a) Lake nodes occupy space in the FD grid. Water budget components are also shown.

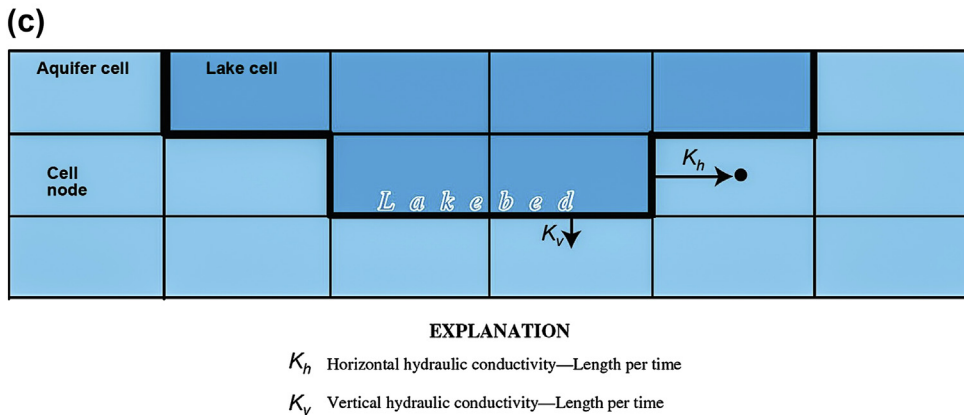
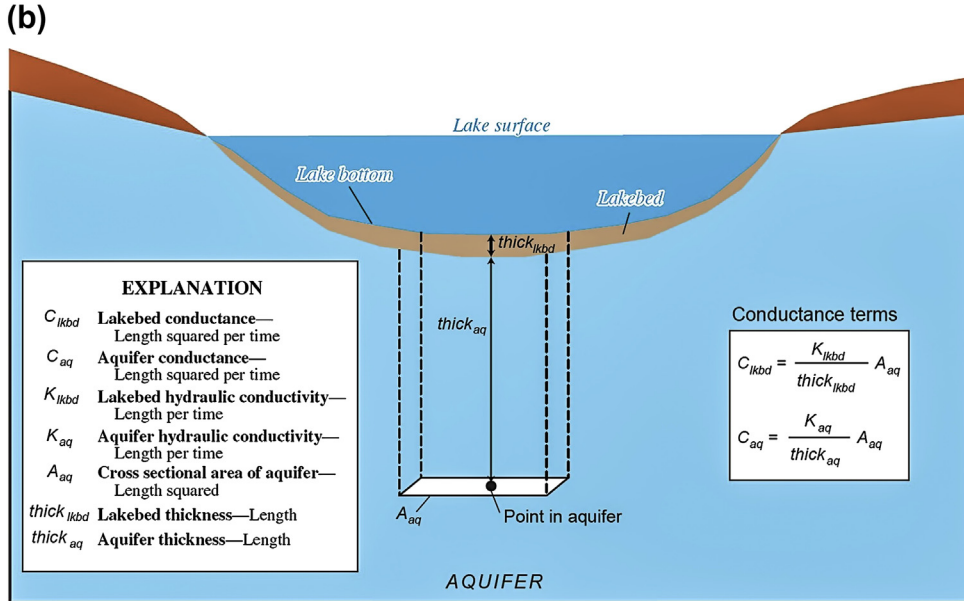


**Figure 6.10 Cont'd.** (b) General equations for calculating conductance,  $C_{lkbd}$  and  $C_{aq}$  are used in Eqn (6.16) to compute average conductance values; (c) both horizontal and vertical flow between the lake and groundwater are simulated (Parts (a), (b) and (c) are from Markstrom et al., 2008; modified from Merritt and Konikow, 2000).

perpendicular to the flow direction;  $h_l$  is lake stage;  $h_a$  is head in the aquifer cell adjacent to the lake;  $\Delta l$  is the distance between the points at which  $h_l$  and  $h_a$  are calculated;  $C$  is the conductance.

Conductance includes the resistance (inverse of leakance) of the lakebed sediments and also the resistance in the aquifer itself over the distance between the lakebed sediment–aquifer interface and the active cell in the adjacent aquifer (Fig. 6.10(b)).



The code computes  $C$  as a series including the lakebed and the portion of the aquifer interfacing with the lake:

$$\frac{1}{C} = \frac{1}{C_{\text{lkbd}}} + \frac{1}{C_{\text{aq}}} \quad (6.16)$$

where  $C_{\text{lkbd}}$  and  $C_{\text{aq}}$  are defined in Fig. 6.10(b). The interested reader is directed to Merritt and Konikow (2000) and Markstrom et al. (2008) for additional details about the Lake Package.

Similar to representing streams, sophisticated simulation of fluctuating lake stage as described above is typically restricted to cases where lake–groundwater interactions are important for the modeling purpose. In a MODFLOW model with many lakes, lakes of lesser importance (e.g., in the far-field) are typically represented by simple HDB conditions (e.g., using the River Package or General Head Boundary (GHB) Package in MODFLOW), while lakes that are important to the modeling purpose are represented using the Lake Package (Fig. 6.8(a)).

## 6.7 WETLANDS

Typically, wetlands are simulated as shallow lakes (Section 6.6); as high  $K$  nodes (Merritt, 1992); as streams (Section 6.5); or as drains (Section 6.4). However, when it is important to the modeling objective to represent flow through the wetland itself, the modeler may consider using the SWR1 Process (Section 6.5) or the Wetlands Package in MODFLOW (Restrepo et al., 1998; Wilsnack et al., 2001). These code enhancements allow for simulation of flows within both the wetland and the groundwater system.

The SWR1 Process, which is designed for streamflow routing in channels (Section 6.5), can also simulate flow in a 2D surface water feature, such as a wetland. In SWR1, the wetland overlies the subsurface grid of the groundwater flow (MODFLOW) model. In the Wetlands Package, the upper layer of the model represents surface water and wetland soils (Fig. 6.11). The user may choose to simulate only surface water flow through the wetland layer or both surface water flow and flow through the wetland sediments. Overland flow is represented using the Kadlec (1990) equation:

$$q_{\text{OL}} = K_{\text{W}}(h - L_{\text{S}})^{\beta} S_{\text{f}}^{\alpha} \quad (6.11)$$

where  $q_{\text{OL}}$  is overland flow per unit width,  $K_{\text{W}}$  is the hydraulic conductance coefficient for overland flow,  $h$  is head,  $L_{\text{S}}$  is land surface elevation,  $S_{\text{f}}$  is hydraulic gradient,  $\beta$  is an exponent related to microtopography and the stem density–depth distribution, and  $\alpha$  is an exponent that reflects the degree of laminar or turbulent flow. For example, when  $\alpha = \beta = 1$ , Eqn (6.11) reduces to Darcy’s law and when  $\alpha = 0.5$  and  $\beta = 5/3$ , Eqn (6.11) is Manning’s equation (Eqn (6.8)). The wetland layer is coupled to the underlying layer of the groundwater model through conductance terms; see

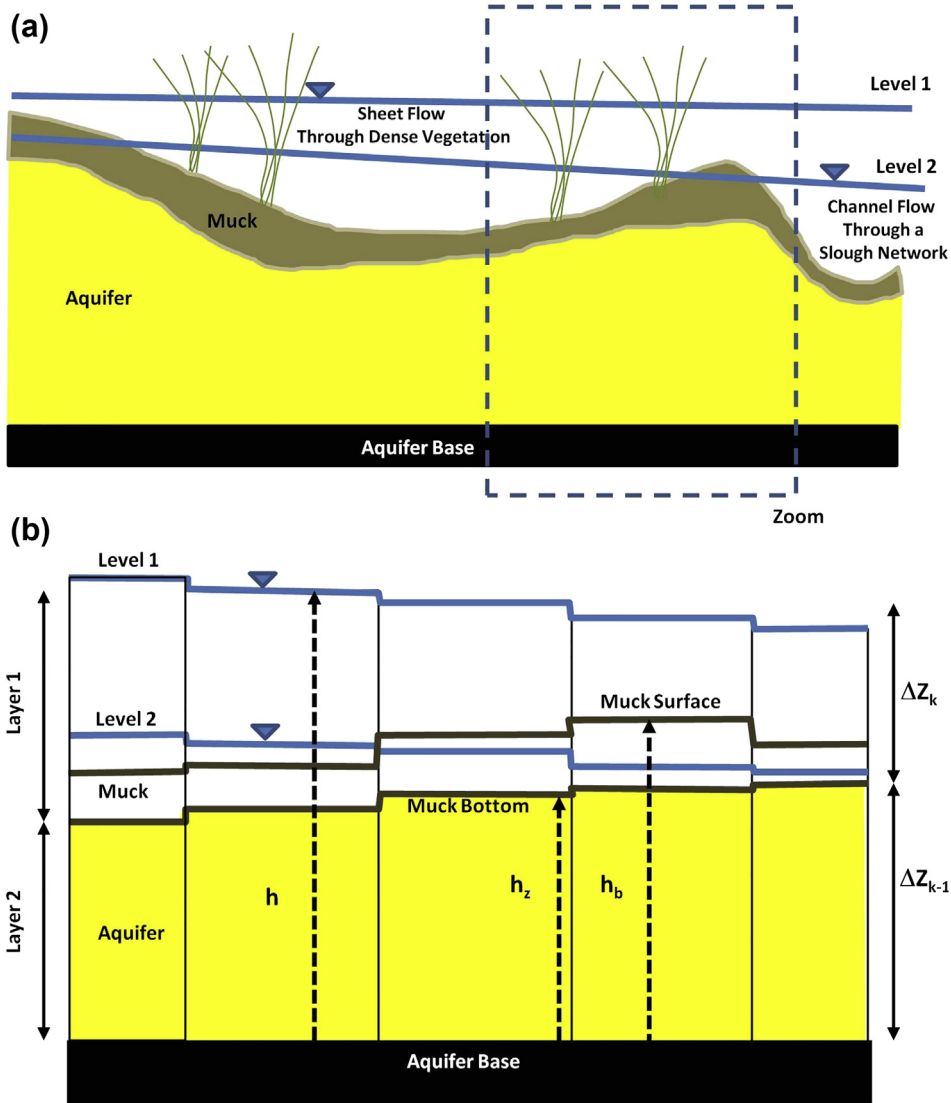


**Figure 6.11** Representation of wetlands in MODFLOW with the Wetlands Package. (a) Schematic representation of field conditions. (b) Two-layer model consisting of an upper wetland layer coupled to a subsurface layer. The upper layer simulates the wetland including overland surface water flow and flow through the wetland sediments (modified from Restrepo et al., 1998).

Restrepo et al. (1998) and Wilsnack et al. (2001) for details. Preferential flowpaths through the wetland layer can be represented by varying the cell-by-cell anisotropy ratio; ET and removal of water from the wetland layer by sinks such as pumping can also be simulated.

### Box 6.2 Watershed Modeling

The watershed is the hydrologic unit typically used in water resources assessment, planning, and management. Watershed models include groundwater-based models of the kind discussed in our book (e.g., [Reeves, 2010](#)) and full hydrologic watershed models (e.g., [Hunt et al., 2013](#)), here called hydrologic response models (following [Freeze and Harlan, 1969](#); among others), which include a topography-based rainfall-runoff model ([Beven, 2012](#)).

A groundwatershed, or groundwater basin, is bounded by groundwater divides and may not align with the topographic watershed that controls surface water flow ([Fig. B6.2.1](#)); therefore, surface water divides may only approximate the boundaries of a groundwater basin. A groundwater-based watershed model is built with a groundwater flow code where groundwatershed divides are explicitly simulated and perimeter boundary conditions are determined

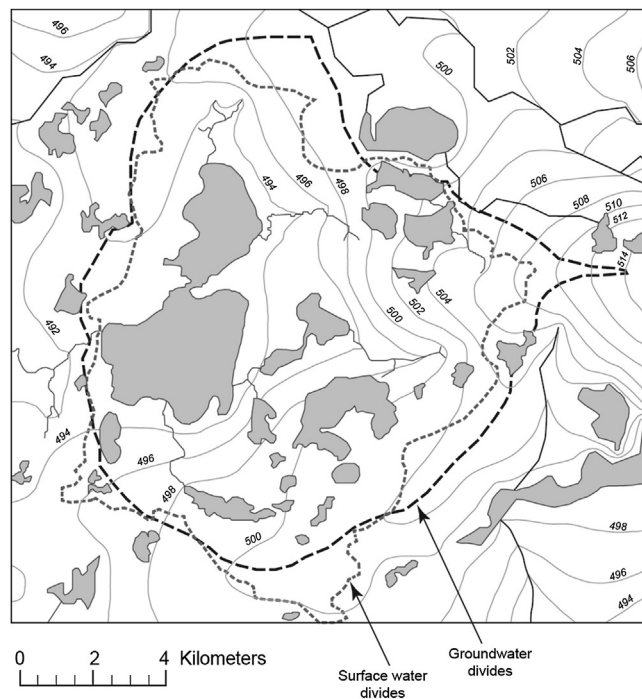


**Figure B6.2.1** Trout Lake surface watershed (outlined with dotted line) and groundwatershed (outlined with dashed line) in glaciated terrain in a temperate climate (northern Wisconsin, USA). Water table contours (m) are also shown. A regional analytic element model was used to define hydraulic perimeter boundary conditions for the rectangular problem domain of the FD model shown in the figure; also see [Fig. 4.21](#). Groundwater divides (shown by the dashed line) were delineated based on heads calculated by the FD model (*modified from [Pint et al., 2003](#)*).

(Continued)

### Box 6.2 Watershed Modeling—cont'd

from the solution of a larger regional model (Section 4.4; Figs 4.20 and 4.21). Specialized options (Sections 4.3, 6.5, 6.6 and 6.7) are used to simulate exchange between surface water and groundwater; groundwater divides that delineate the groundwatershed may be determined from the solution (Fig. B6.2.1). Though often less important in steady-state models, representation of unsaturated zone processes should be included in transient groundwater-based watershed models to simulate the correct timing of hydrologic responses (Fig. B6.3.2 in Box 6.3). Options that internally link representation of 1D vertical unsaturated flow to a groundwater model are commonly used (e.g., Zhu et al., 2012; Niswonger et al., 2006).

In contrast, a hydrologic response model represents hydrologic processes at the land surface of a topographically defined watershed and includes simulation of both surface and sub-surface sources of streamflow (Fig. B6.2.2). Development of a hydrologic response model was an early goal of hydrologic modelers (Freeze and Harlan, 1969; also see Beven, 2002) and is still an active area of research (e.g., De Lange et al., 2014; Schmid et al., 2014; Liggett et al., 2012). However, differences in spatial scales and response times among the various processes in the hydrologic cycle complicate designing and solving such watershed models. Early watershed codes (e.g., the Stanford Watershed Model by Crawford and Linsley, 1966) routed precipitation through streams with losses to and gains from the groundwater system using a “black box”

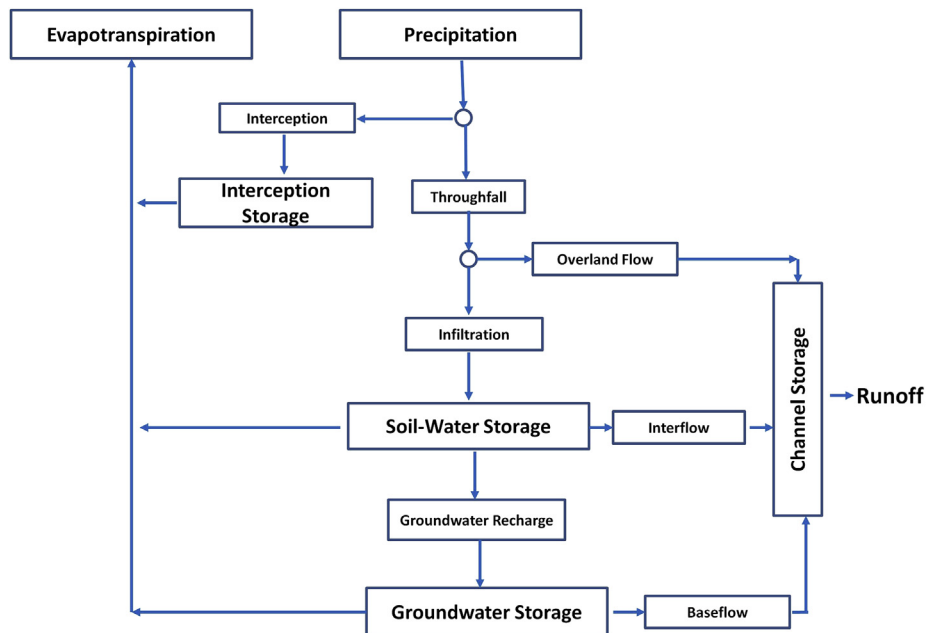
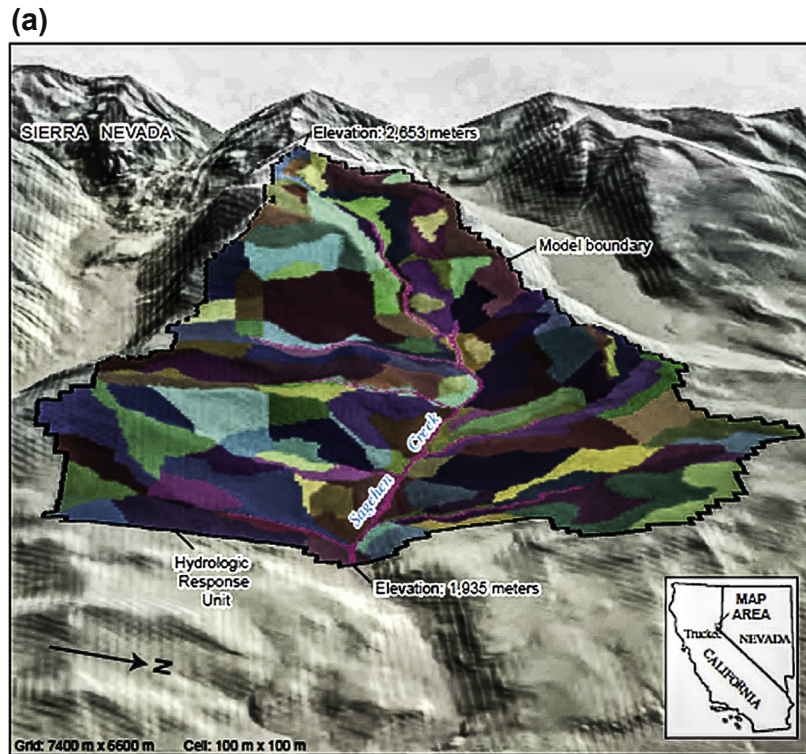


Figure B6.2.2 Components of the hydrologic cycle for a hydrologic response model (modified from Freeze and Harlan, 1969).

### Box 6.2 Watershed Modeling—cont'd

approach (Box 6.3). Models that rigorously simulate the entire subsurface as a continuum were also developed early in the history of modeling (e.g., Freeze, 1971). Later, investigators developed codes that coupled a surface water code to a subsurface code based on the Richard's equation for variably saturated flow in the subsurface continuum (e.g., Panday and Huyakorn, 2004; HydroGeoSphere, see review by Brunner and Simmons, 2012; FEFLOW, Diersch, 2014, Table 10.3, p. 478). However, such subsurface models require small time steps and small spatial discretization and are computationally intensive with long run times.

Run times can be reduced by linking 1D models for vertical flow through the unsaturated zone to a groundwater model linked to a surface water model. For example, GSFLOW (Markstrom et al., 2008) couples a rainfall-runoff code that simulates processes at the land surface including streamflow and lakes with MODFLOW for groundwater flow; 1D vertical



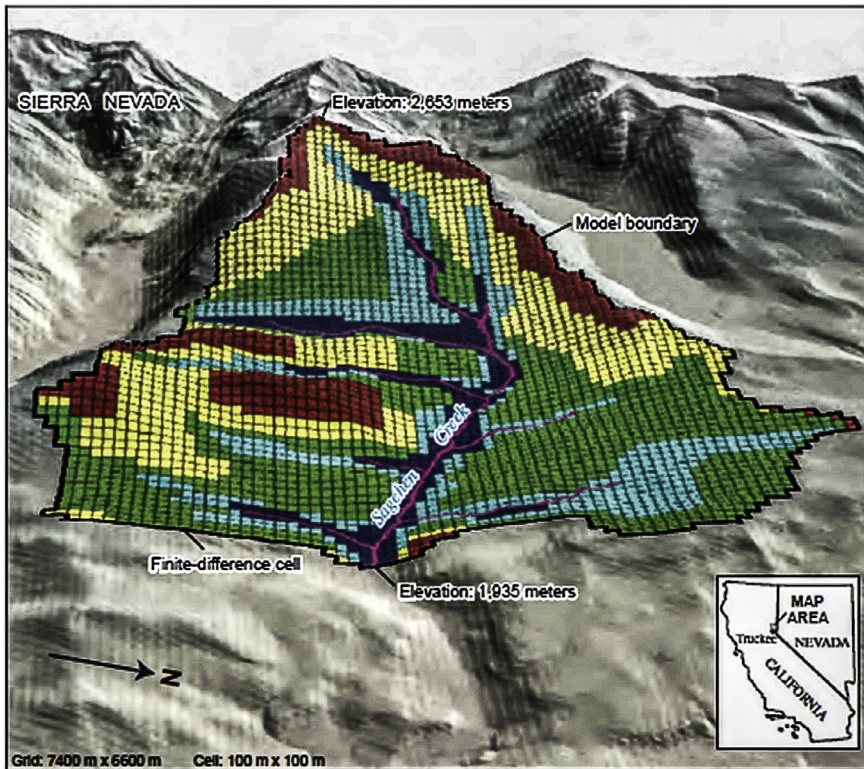
**Figure B6.2.3** Components of a GSFLOW model of the snowmelt-dominated montane watershed near Truckee, CA, USA. (a) Hydrologic Response Units (HRUs; Box 6.3) used in the rainfall-runoff model to represent surface and soil zone processes.

(Continued)

**Box 6.2 Watershed Modeling—cont'd**

unsaturated flow is simulated by the Unsaturated Zone Flow (UZF) Package (Niswonger et al., 2006) (Fig. B6.2.3). Similar options are available in MIKE SHE (Graham and Butts, 2006; also see reviews by Hughes and Liu, 2008; Jaber and Shukla, 2012).

(b)



Grid: 7400 m x 6600 m Cell: 100 m x 100 m  
 Shaded relief base from USGS 10-meter National Elevation Data, illumination from the northwest at 45°. Universal Transverse Mercator projection. Zone 11. North American Datum of 1983. Perspective Information: Altitude is 6,300 meters above land surface, viewing angle is 24 degrees, vertical exaggeration = 2x.

**EXPLANATION**  
 Hydraulic conductivity value—Meters per day

Layer 1	Layer 2
0.026	0.00045
0.052	0.0009
0.065	0.0027
0.13	0.009
0.39	0.027

**Figure B6.2.3 Cont'd.** (b) FD grid and values of hydraulic conductivity used in MODFLOW (Markstrom et al., 2008).

### Box 6.3 Surface Water Modeling

Surface water models, or *rainfall-runoff models* (e.g., [Beven, 2012](#); [Loague, 2010](#)), simulate two processes: streamflow generation and streamflow routing. *Streamflow generation* simulates the processes involved in routing rainfall to a stream channel accounting for losses and additions along the way. Surface water hydrologists long struggled to understand the processes involved in streamflow generation and there is a rich legacy of papers and ideas ([Beven, 2006](#); [Kirkby, 1978](#)).

*Streamflow routing* is the process of moving water downgradient in a stream channel while accounting for groundwater inflow to the channel and outflow from the channel to the groundwater system ([Section 6.5](#)). The main output of a rainfall-runoff model is a streamflow hydrograph (i.e., [Fig. B6.3.1](#), middle plot).

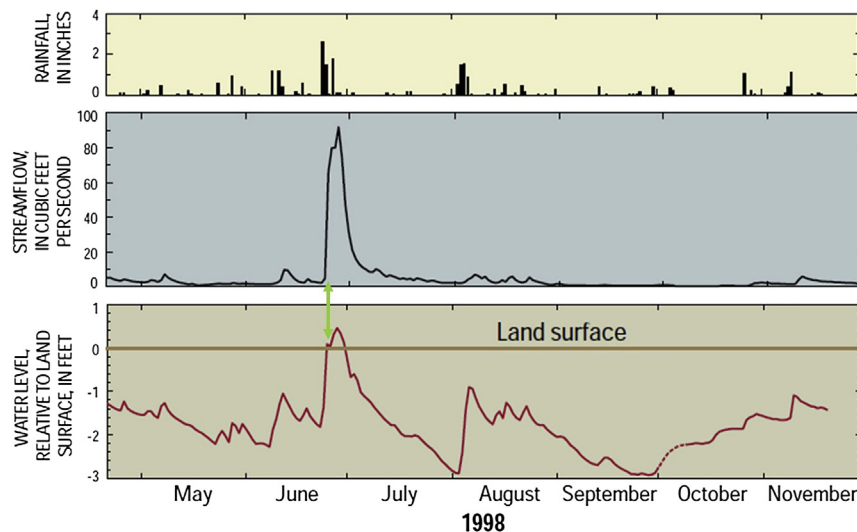


**Figure B6.3.1** Field data from a watershed in a humid temperate climate (central Wisconsin, USA) showing the importance of the variable source area in generating peak streamflows. When the water table is below land surface (bottom graph) precipitation infiltrates and becomes groundwater recharge and streamflows (middle graph) are dominated by groundwater-derived baseflow. When the water table rises to the land surface (green arrow) in response to high precipitation (upper graph), precipitation runs off rather than infiltrates. The resulting peak streamflow (middle graph) is over 9 times higher than average streamflow (modified from [Hunt et al., 2000](#)).

Rainfall-runoff models can be broadly categorized into lumped, semidistributed, and fully-distributed models ([Beven, 2012](#)). In a lumped model, streamflow routing and each streamflow generation process, including groundwater flow, is represented as a compartment or a “black box” that represents the average response of a process over a watershed. For example, groundwater response over the entire watershed might be simulated as a single linear reservoir.

(Continued)

### Box 6.3 Surface Water Modeling—cont'd

Spatial variability in groundwater response might be simulated as a simple function of the land surface. In a semidistributed model, watersheds are divided into hydrologic response units (HRUs), which are areas that respond similarly to hydrologic events (Fig. B6.2.3 (a) in Box 6.2). Each process is discretized (distributed) based on the HRUs; for example, each HRU in the watershed might have its own linear reservoir to represent flow to and from groundwater. The most sophisticated and computationally demanding representation of watershed processes is the fully distributed rainfall-runoff model. In this representation, parameters are distributed over the watershed using discretization schemes based on a grid/mesh with resolutions similar to groundwater models; groundwater flow is typically represented by a model of the type discussed in our book.

A major difference between groundwater models and surface water models is that observations in a surface water model consist primarily of a small number of streamflow hydrographs, whereas observations in a groundwater model are spatially distributed heads and fluxes. Hence, surface water modelers commonly have temporally dense but spatially sparse calibration data, whereas in a groundwater model the data typically are larger in number of locations but more temporally sparse. Moreover, streamflow hydrographs usually constrain only around three to six calibration parameters out of potentially thousands of parameters input to a watershed model (Jakeman and Hornberger, 1993; Doherty and Hunt, 2009). Hence, the ability to meet objectives of surface water modeling, such as forecasting of peak streamflows, has typically been poor (e.g., Beven, 2009).

Hydrologists have long recognized the importance of including groundwater processes in surface water models. For example, in an important contribution for understanding streamflow generation, Freeze (1972a,b; summarized in Kirkby, 1978) used a numerical subsurface model to demonstrate the importance of groundwater-related processes in streamflow generation during storm events. When the water table rises to the land surface in low-lying areas during storm events, a storm-derived *variable source area* forms where saturation excess overland flow occurs as a result of rejected recharge (Box 5.4). Saturation excess overland flow moves quickly to the stream channel and causes a rapid rise in streamflow. The concept of the variable source area, which was developed in the 1960s, helped explain the rapid rise in streamflow and the high peaks observed during storm events, which were not explained by other phenomena. The transition from infiltration (where water enters the subsurface) to saturation excess overland flow (where water runs off the land surface) is a major threshold for stormflow generation that causes peak streamflows (Fig. B6.3.1). Thus, low-lying areas where the water table is near the land surface (e.g., wetlands near streams) are important source areas for peak streamflows; the timing of runoff generation depends on when the water table in those areas rises to the land surface converting them into stormflow source areas.

Runoff contributed by variable source areas can be appreciable (Fig. B6.3.1) and models that do not include this process of runoff generation may produce incorrect forecasts of both peak and nonpeak flows (Fig. B6.3.2). When groundwater processes are omitted or oversimplified in a rainfall-runoff model, the available parameters take on surrogate roles (a similar phenomenon occurs in groundwater modeling; Sections 5.3, 9.6; Box 5.3) in order to fit peak



### Box 6.3 Surface Water Modeling—cont'd

streamflows during history matching. Because surrogate parameters may adversely affect forecasts of peak flows, there is renewed interest in coupled groundwater and surface water models and hydrologic response models (Box 6.2).

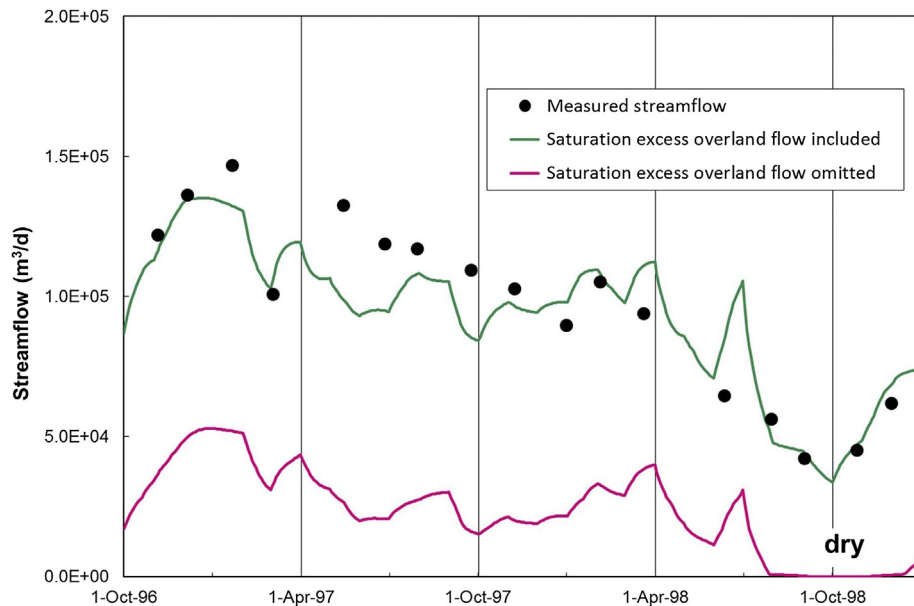


**Figure B6.3.2** Importance of saturation excess overland flow on nonpeak streamflows in a humid temperate climate (northern Wisconsin, USA). Streamflow is simulated at the outlet of a large lake, which receives inflow from five tributary streams. Two simulations used the same spatially and temporally distributed precipitation rate; results from the simulation that omitted saturation excess overland flow (pink line) are biased low when compared to measured flows at the lake outlet (shown by black dots). When saturation excess overland flow is routed to the five tributary streams there is a better match between simulated streamflow (green line) and measured flows (modified from *Hunt et al., 2008*).

## 6.8 COMMON MODELING ERRORS

- The modeler specifies the wrong sign when the discharge rate of a well is input causing injection of water instead of pumping. The modeler should check simulated head contour lines and the computed water budget to verify that pumping is appropriately represented.
- The modeler uses a code that includes procedures for reducing well discharge in unconfined layers affected by a seepage face along the well bore but fails to realize that

the code reduces modeler-specified pumping rates in response to the formation of a seepage face. Hence, the simulated well discharge is less than specified by the modeler. The modeler should always check discharge rates reported in model output to make sure that simulated wells are pumping the correct volume of water.

- Recharge is specified for only the top layer of the model when the water table also occurs in lower layers (e.g., see Fig. 4.6). The amount of water input to the model is less than the modeler intended because the code did not rout recharge to the water table in the highest active layer.
- Dry cells or inactive cells above water table nodes (e.g., see Fig. 4.6) prevent application of recharge to the water table because the code does not allow water table cells below inactive cells to receive recharge. The amount of water input to the model is less than the modeler-intended because the code could not rout recharge to the water table in the highest active layer.
- Ephemeral streams are simulated as HDB conditions allowing unrealistic volumes of water into the model. The modeler should use drain nodes or a code that allows stream cells to go dry (e.g., the SFR Package in MODFLOW) to simulate ephemeral streams.
- Drains are used to simulate features that lose appreciable water to the groundwater system under field conditions. Drains are inappropriate when simulating features that recharge the groundwater system. The modeler should use another type of HDB condition.
- Incorrect values of lakebed leakance are input to the Lake Package in MODFLOW but go undetected because the modeler neglected to check the listing of lakebed properties in the code's output.

## 6.9 PROBLEMS

Problems for this chapter explore nodal spacing in the vicinity of wells, representation of rivers and drains as HDB nodes, and simulation of a quarry reservoir using three different approaches.

**P6.1** Fig. P6.1 shows a 10-m-thick confined aquifer with three no-flow boundaries and one specified head boundary set at 100 m measured from the base of the aquifer, which is at an elevation of zero. The dimensions of the problem domain are 8100 m by 8550 m. Hydraulic conductivity of the aquifer is 5 m/d. A well (shown by the blue dot) is pumped at 1060 m<sup>3</sup>/d. A second well, well A (shown by the red dot), is not pumped and is used as a monitoring well.

- a. Design a 2D areal steady-state model for this problem using a regular grid/mesh with a relatively large nodal spacing (e.g., 900 m by 900 m for a block-centered FD grid). Be sure the two wells are located on nodes. Execute the model and generate a contour map of the head distribution. Report the simulated heads at the pumping well and the monitoring well.

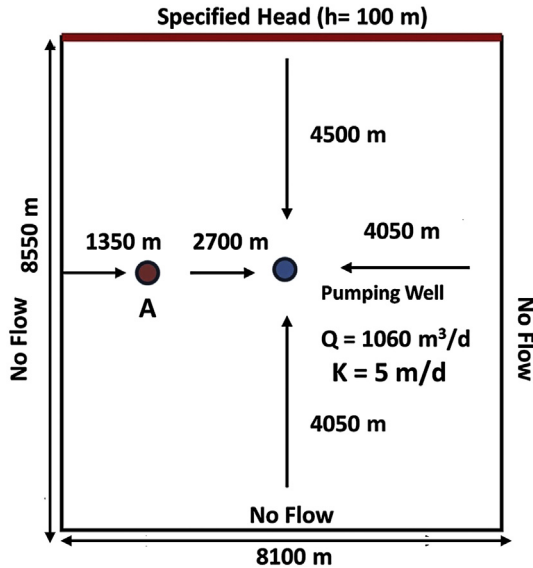


**Figure P6.1** Areal 2D model domain showing the locations of a pumping well (blue dot) and a monitoring well (red dot) that fully penetrate a 10-m-thick confined aquifer.

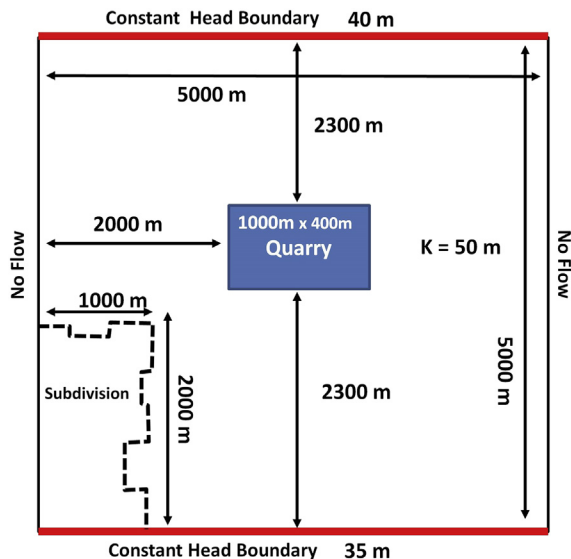
- b. Change the nodal spacing to about a third of the initial spacing (e.g., 300 m by 300 m for a block-centered FD grid). Again be sure that the two wells are located on nodes. Execute the model and generate a contour map of head distribution. Report the simulated heads at the pumping well and the monitoring well.
- c. Change the nodal spacing once again to values about an order of magnitude smaller (e.g., 30 m by 30 m for a block-centered FD grid). Again be sure that the two wells are located on nodes. Execute the model and generate a contour map of head distribution. Report the simulated heads at the pumping well and the monitoring well.
- d. Discuss the effect of the nodal spacing on the head in the monitoring well. Is the simulated head at the monitoring well approximately the same for the various models? What is your conclusion regarding the appropriate nodal spacing for this problem?
- e. Assume that the radius of the pumping well is 0.3 m. Use variable nodal spacing or a nested FE mesh or nested unstructured FD grid designed so that the nodal spacing around the pumping well follows the guidelines in [Box 6.1](#). Compare and contrast your results with those derived from models in parts (a), (b), and (c).
- f. Visualize the flow field if the well is not pumping. Are the boundary conditions realistic? How would the addition of uniform areally distributed leakage over the problem domain affect the flow system under nonpumping conditions?

**P6.2** A sand and gravel quarry that will be mined above and below the water table is being planned for an area upgradient of a 100-home subdivision. The housing development draws water from wells penetrating the same unconfined aquifer in which the quarry will be developed. Upon completion of mining the quarry will fill with groundwater. There is concern that the reservoir that will be left upon completion of mining will affect groundwater flow directions and/or the quantity of water flowing to the subdivision boundary. The quarry operators say that the reservoir will not affect local groundwater conditions.

Design a 2D areal model for this problem; use uniform nodal spacing of 125 m. Assume that the base of the unconfined aquifer is at an elevation of zero, the aquifer is mined down to the base, and steady-state conditions are adequate to assess the effects of the reservoir. The aquifer is homogeneous and isotropic with hydraulic conductivity equal to 50 m/d.

- Calculate groundwater heads beneath the subdivision under steady-state conditions without the reservoir. There are a number of methods to represent quarry reservoirs that penetrate a water table aquifer for the conditions shown in Fig. P6.2. First simulate the effect of the quarry reservoir on groundwater levels by assigning a specified head in the reservoir of around 38 m. Use your steady-state solution without the reservoir to verify that this is the average groundwater head in the vicinity of the quarry prior to the formation of the reservoir. Are heads in the vicinity of the subdivision boundary affected by the reservoir?
- Simulate the effect of the quarry reservoir using a zone of high hydraulic conductivity ( $K$ ). You will likely have to try several values of  $K$  until the head in the reservoir reaches a minimum and stops changing as you increase  $K$ . Also, check that there is a negligible hydraulic gradient in the portion of

**Figure P6.2** Areal 2D model domain of an unconfined aquifer showing a reservoir (in blue) created by mining a sand and gravel quarry. A subdivision is shown in the lower left-hand corner of the figure.



- the model that represents the reservoir. Be sure to check the water budget for model convergence. Examine the heads in the vicinity of the subdivision boundary and comment on simulated values relative to the results in part (a).
- Simulate the quarry reservoir as a fully penetrating lake using the LAK3 Package in MODFLOW. Groundwater flux occurs only through the sides of the reservoir. Use the model to calculate groundwater heads assuming no surface water inflow or outflow and no evaporative losses from the surface of the reservoir. Run the simulation again and include evaporation of 0.001 m/d from the surface of the reservoir. Examine the heads in the vicinity of the subdivision boundary and comment on simulated values relative to the results in parts (a) and (b).
  - Compare and comment on the results obtained from the three methods of simulating the reservoir and list the advantages and disadvantages of each method.
- P6.3** This problem illustrates the use of HDB conditions to simulate a river and drains in an unconfined aquifer between two lakes (Fig. P6.3). The river is 200 m wide as is

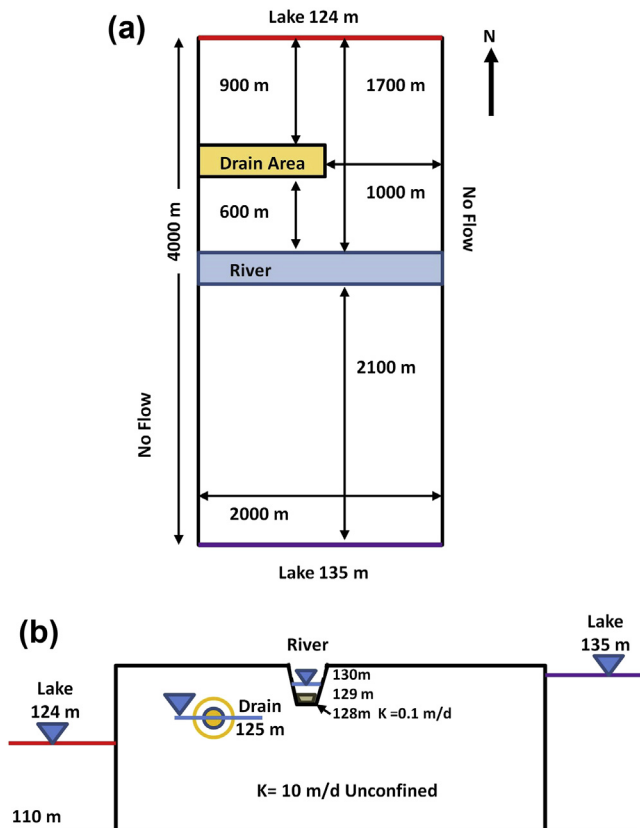


**Figure P6.3** (a) Areal 2D model domain of an unconfined aquifer between two lakes crossed by a 200-m-wide river with a constant stage of 130 m. Drains are installed in a 200 m wide area (shaded in tan) to lower the water table to 125 m. (b) A north-south cross section through the drain area.

the area where drains have been installed (shaded in tan). The riverbed sediments have a thickness of 1 m and a vertical hydraulic conductivity of 0.1 m/d.

- a. Design a steady-state model and calculate the rate of groundwater flow to and/or from the river and to the drains. The conductance of the drains is unknown. Test the sensitivity of the model to drain conductance and select a value to use in the simulation.
- b. Run the model again assuming a river width of 50 m instead of 200 m. How does this change affect the total groundwater flow to or from the river?
- c. Change the river nodes to drain nodes with a drain elevation of 130 m. Run the model again and describe the effect of this change on the head distribution. Under what field situations would such a representation of a river be valid?

**P6.4** Models designed in Chapter 4 for the setting shown in Fig. P4.3 assumed that the base of the aquifer is impermeable. How would you incorporate a uniform upward rate of leakage from bedrock into the unconfined aquifer in a 2D areal view model? How would you simulate this leakage at the node representing the pumping well?

## REFERENCES

- Ajami, H., Maddock, T., Meixner, T., Hogan, J.F., Guertin, D.P., 2012. RIPGIS-NET: A GIS tool for riparian groundwater evapotranspiration in MODFLOW. *Groundwater* 50 (1), 154–158. <http://dx.doi.org/10.1111/j.1745-6584.2011.00809.x>.
- Anderson, M.P., Cheng, X., 1993. Long- and short-term transience in a groundwater/lake system in Wisconsin, U.S.A. *Journal of Hydrology* 145, 1–18. [http://dx.doi.org/10.1016/0022-1694\(93\)90217-W](http://dx.doi.org/10.1016/0022-1694(93)90217-W).
- Anderson, M.P., Hunt, R.J., Krohelski, J., Chung, K., 2002. Using high hydraulic conductivity nodes to simulate seepage lakes. *Groundwater* 40 (2), 117–122. <http://dx.doi.org/10.1111/j.1745-6584.2002.tb02496.x>.
- Baird, K.J., Maddock, T., 2005. Simulating riparian evapotranspiration: A new methodology and application for groundwater models. *Journal of Hydrology* 312 (1–4), 176–190. <http://dx.doi.org/10.1016/j.jhydrol.2005.02.014>.
- Banta, E.R., 2000. MODFLOW-2000, the U.S. Geological Survey Modular Ground-water Model—documentation of Packages for Simulating Evapotranspiration with a Segmented Function (ETS1) and Drains with Return Flow (DRT1). U.S. Geological Survey Open-File Report 00–466, 127 p. <http://pubs.er.usgs.gov/publication/ofr00466>.
- Barlow, P.M., Moench, A.F., 2011. WTAQ Version 2—A Computer Program for Analysis of Aquifer Tests in Confined and Water-table Aquifers with Alternative Representations of Drainage from the Unsaturated Zone. U.S. Geological Survey Techniques and Methods 3–B9, 41 p. <http://pubs.usgs.gov/tm/tm3b9/>.
- Bennett, G.D., Kontis, A.L., Larson, S.P., 1982. Representation of multiaquifer well effects in three-dimensional groundwater flow simulation. *Groundwater* 20 (3), 334–341. <http://dx.doi.org/10.1111/j.1745-6584.1982.tb01354.x>.
- Beven, K.J., 2002. Towards an alternative blueprint for a physically-based digitally simulated hydrologic response modeling system. *Hydrological Processes* 16, 189–206. <http://dx.doi.org/10.1002/hyp.343>.
- Beven, K.J. (Ed.), 2006. *Benchmark Papers in Hydrology, 1: Streamflow Generation Processes*. Selection, Introduction and Commentary by Keith J. Beven. IAHS Press, p. 431.

- Beven, K.J., 2009. Environmental Modelling: An Uncertain Future? An Introduction to Techniques for Uncertainty Estimation in Environmental Prediction. Routledge, 310 p.
- Beven, K.J., 2012. Rainfall-runoff Modeling: The Primer, second ed. Wiley-Blackwell. 488 p.
- Bohling, G.C., Zhan, X., Butler Jr., J.J., Zheng, L., 2002. Steady shape analysis of tomographic pumping tests for characterization of aquifer heterogeneities. *Water Resources Research* 38 (12), 1324. <http://dx.doi.org/10.1029/2001WR001176>.
- Bohling, G.C., Butler Jr., J.J., Zhan, X., Knoll, M.D., 2007. A field assessment of the value of steady-shape hydraulic tomography for characterization of aquifer heterogeneities. *Water Resources Research* 43 (5), W05430. <http://dx.doi.org/10.1029/2006WR004932>.
- Born, S.M., Smith, S.A., Stephenson, D.A., 1979. Hydrogeology of glacial-terrain lakes, with management and planning applications. *Journal of Hydrology* 43 (1-4), 7-43. [http://dx.doi.org/10.1016/0022-1694\(79\)90163-X](http://dx.doi.org/10.1016/0022-1694(79)90163-X).
- Brooks, L., 2006. Hydrology and Simulation of Ground-water Flow, Lake Point, Tooele County, Utah. U.S. Geological Survey Scientific Investigation Report 2006-5310, 28 p. <http://pubs.usgs.gov/sir/2006/5310/>.
- Brunner, P., Simmons, C.T., 2012. HydroGeoSphere: A Fully Integrated, Physically Based Hydrological Model. *Groundwater* 50 (2), 170-176. <http://dx.doi.org/10.1111/j.1745-6584.2011.00882.x>.
- Butler Jr., J.J., 1988. Pumping tests in nonuniform aquifers—the radially symmetric case. *Journal of Hydrology* 101 (1-4), 15-30. [http://dx.doi.org/10.1016/0022-1694\(88\)90025-X](http://dx.doi.org/10.1016/0022-1694(88)90025-X).
- Charbeneau, R.J., Street, R.L., 1979. Modeling groundwater flow fields containing point singularities: A technique for singularity removal. *Water Resources Research* 15 (3), 583-594. <http://dx.doi.org/10.1029/WR015i003p00583>.
- Chui, T.F.M., Freyberg, D.L., 2008. Simulating a lake as a high-conductivity variably saturated porous medium. *Groundwater* 46 (5), 688-694. <http://dx.doi.org/10.1111/j.1745-6584.2008.00463.x>.
- Constantz, J.E., Niswonger, R.G., Stewart, A.E., 2008. Analysis of Temperature Gradients to Determine Stream Exchanges with Ground Water. In: *Field Techniques for Estimating Fluxes Between Surface and Ground Water*. U.S. Geological Survey Techniques and Methods Report 4-D2, pp. 115-128, <http://pubs.usgs.gov/tm/04d02/pdf/TM4-D2-chap4.pdf>.
- Crawford, N.H., Linsley, R.K., 1966. Digital Simulation in Hydrology, Stanford Watershed Model IV. Technical Report No. 39, Department of Civil Engineering, Stanford University, 210 p.
- Diersch, H.-J.G., 2014. FEFLOW: Finite Element Modeling of Flow, Mass and Heat Transport in Porous and Fractured Media, Springer, 996 p.
- Diersch, H.-J.G., Bauer, D., Heidemann, W., Ruhaak, W., Schatzki, P., 2011. Finite element modeling of borehole heat exchanger system, Part 2: Numerical simulation. *Computers & Geosciences* 37 (8), 1136-1147. <http://dx.doi.org/10.1016/j.cageo.2010.08.002>.
- Doble, R.C., Simmons, C.T., Walker, G.R., 2009. Using MODFLOW 2000 to model ET and recharge for shallow ground water problems. *Groundwater* 47 (1), 129-135. <http://dx.doi.org/10.1111/j.1745-6584.2008.00465.x>.
- Doherty, J., Hunt, R.J., 2009. Two statistics for evaluating parameter identifiability and error reduction. *Journal of Hydrology* 366, 119-127. <http://dx.doi.org/10.1016/j.jhydrol.2008.12.018>.
- Feinstein, D.T., Dunning, C.P., Juckem, P.F., Hunt, R.J., 2010. Application of the Local Grid Refinement Package to an Inset Model Simulating the Interactions of Lakes, Wells, and Shallow Groundwater, Northwestern Waukesha County, Wisconsin. U.S. Geological Survey Scientific Investigations Report 2010-5214, 30 p. <http://pubs.usgs.gov/sir/2010/5214/>.
- Freeze, R.A., 1971. Three-dimensional, transient, saturated-unsaturated flow in a groundwater basin. *Water Resources Research* 7 (2), 347-366. <http://dx.doi.org/10.1029/WR007i002p00347>.
- Freeze, R.A., 1972a. Role of subsurface flow in generating surface runoff, 1. Base flow contributions to channel flow. *Water Resources Research* 8 (3), 609-623. <http://dx.doi.org/10.1029/WR008i003p00609> (Reproduced in Loague, K., editor, 2010, *Benchmark Papers in Hydrology*, 4: Rainfall-Runoff Modelling. Selection, Introduction and Commentary by Keith Loague, IAHS Press, pp. 256-270.).
- Freeze, R.A., 1972b. Role of subsurface flow in generating surface runoff, 2. Upstream source areas. *Water Resources Research* 8 (5), 1272-1283. <http://dx.doi.org/10.1029/WR008i005p01272> (Reproduced in Loague, K., editor, 2010, *Benchmark Papers in Hydrology*, 4: Rainfall-Runoff Modelling. Selection, Introduction and Commentary by Keith Loague, IAHS Press, pp. 271-283.).

- Freeze, R.A., Harlan, R.L., 1969. Blueprint for a physically-based, digitally-simulated hydrologic response model. *Journal of Hydrology* 9, 237–258. [http://dx.doi.org/10.1016/0022-1694\(69\)90020-1](http://dx.doi.org/10.1016/0022-1694(69)90020-1).
- DHI-WASY GmbH, 2010. FEFLOW: Finite element subsurface flow and transport simulation system. White Papers 5, 108 p.
- Gebert, W.A., Radloff, M.J., Considine, E.J., Kennedy, J.L., 2007. Use of streamflow data to estimate base flow/ground-water recharge for Wisconsin. *JAWRA Journal of the American Water Resources Association* 43 (1), 220–236. <http://dx.doi.org/10.1111/j.1752-1688.2007.00018.x>.
- Graham, D.N., Butts, M.B., 2006. Flexible integrated watershed modeling with MIKE SHE. In: Singh, V.P., Frevert, D.K. (Eds.), *Watershed Models*. CRC Press, Boca Raton, Florida, pp. 245–271.
- Haitjema, H.M., 1995. *Analytic Element Modeling of Groundwater Flow*. Academic Press, Inc., San Diego, CA, 394 p.
- Haitjema, H., Kuzin, S., Kelson, V., Abrams, D., 2010. Modeling flow into horizontal wells in a Dupuit-Forchheimer model. *Groundwater* 48 (6), 878–883. <http://dx.doi.org/10.1111/j.1745-6584.2010.00694.x> (erratum *Groundwater* 49(6), p. 949).
- Halford, K.J., Hanson, R.T., 2002. User Guide for the Drawdown-limited, Multi-node Well (MNW) Package for the U.S. Geological Survey's Modular Three-dimensional Finite-difference Ground-water Flow Model, Versions MODFLOW-96 and MODFLOW-2000. U.S. Geological Survey Open-File Report 02–293, 33 p. <http://pubs.er.usgs.gov/publication/ofr02293>.
- Hantush, M.S., 1964. Hydraulics of wells. In: Chow, V.T. (Ed.), *Advances in Hydroscience*, 1. Academic Press, New York, pp. 281–432.
- Harmel, R.D., Cooper, R.J., Slade, R.M., Haney, R.L., Arnold, J.G., 2006. Cumulative uncertainty in measured streamflow and water quality data for small watersheds. *Transactions of the American Society of Agricultural and Biological Engineers (ASABE)* 49 (3), 689–701. <http://dx.doi.org/10.13031/2013.20488>.
- Heath, R.C., Trainer, F.W., 1968. *Introduction to Ground Water Hydrology*. John Wiley and Sons, New York (Reprinted 1981 by Water Well Journal Publishing Co., Worthington, OH, 285 p.).
- Herschy, R.W., 1995. *Streamflow Measurement*, second ed. Elsevier. 524 p.
- Hughes, J.D., Liu, J., 2008. MIKE SHE: Software for integrated surface water/ground water modeling. *Groundwater* 46 (6), 797–802. <http://dx.doi.org/10.1111/j.1745-6584.2008.00500.x>.
- Hughes, J.D., Langevin, C.D., Chartier, K.L., White, J.T., 2012. Documentation of the Surface-water Routing (SWR1) Process for Modeling Surface-water Flow with the U.S. Geological Survey Modular Ground-water Model (MODFLOW-2005). U.S. Geological Survey Techniques and Methods 6–A40, 113 p. <http://pubs.usgs.gov/tm/6a40/>.
- Hughes, J.D., Langevin, C.D., White, J.T., 2014. MODFLOW-based coupled surface water routing and groundwater-flow simulation. *Groundwater early view*. <http://dx.doi.org/10.1111/gwat.12216>.
- Hunt, R.J., Graczyk, D.J., Rose, W.J., 2000. Water Flows in the Necedah National Wildlife Refuge. U.S. Geological Survey Fact Sheet FS-068–00, 4 p. <http://pubs.er.usgs.gov/usgspubs/fs/fs06800>.
- Hunt, R.J., Prudic, D.E., Walker, J.F., Anderson, M.P., 2008. Importance of unsaturated zone flow for simulating recharge in a humid climate. *Groundwater* 46 (4), 551–560. <http://dx.doi.org/10.1111/j.1745-6584.2007.00427.x>.
- Hunt, R.J., Haitjema, H.M., Krohelski, J.T., Feinstein, D.T., 2003. Simulating ground water-lake interactions: Approaches and insights. *Groundwater* 41 (2), 227–237. <http://dx.doi.org/10.1111/j.1745-6584.2003.tb02586.x>.
- Hunt, R.J., Strand, M., Walker, J.F., 2006. Measuring groundwater-surface water interaction and its effect on wetland stream benthic productivity, Trout Lake watershed, northern Wisconsin, USA. *Journal of Hydrology* 320 (3–4), 370–384. <http://dx.doi.org/10.1016/j.jhydrol.2005.07.029>.
- Hunt, R.J., Feinstein, D.T., 2012. MODFLOW-NWT: Robust handling of dry cells using a Newton formulation of MODFLOW-2005. *Groundwater* 50 (5), 659–663. <http://dx.doi.org/10.1111/j.1745-6584.2012.00976.x>.
- Hunt, R.J., Bradbury, K.R., Krohelski, J.T., 2001. The Effects of Large-scale Pumping and Diversion on the Water Resources in Dane County, Wisconsin. U.S. Geological Survey Fact Sheet 127–01, 4 p. <http://pubs.er.usgs.gov/publication/fs12701>.



- Hunt, R.J., Walker, J.F., Selbig, W.R., Westenbroek, S.M., Regan, R.S., 2013. Simulation of Climate-change Effects on Streamflow, Lake Water Budgets, and Stream Temperature Using GSFLOW and SNTEMP, Trout Lake Watershed, Wisconsin. U.S. Geological Survey Scientific Investigations Report 2013–5159, 118 p. <http://pubs.usgs.gov/sir/2013/5159/>.
- Istok, J., 1989. Groundwater modeling by the finite element method, American Geophysical Union (AGU), Washington, D.C. Water Resources Monograph 13, 495 p. <http://dx.doi.org/10.1029/WM013>.
- Jaber, F.H., Shukla, S., 2012. MIKE SHE: Model use, calibration, and validation. Transactions of the ASABE 55 (4), 1479–1489. <http://dx.doi.org/10.13031/2013.42255>.
- Jakeman, A.J., Hornberger, G.M., 1993. How much complexity is warranted in a rainfall-runoff model? Water Resources Research 29 (8), 2637–2649. <http://dx.doi.org/10.1029/93WR00877>.
- Kadlec, R.H., 1990. Overland flow in wetlands: Vegetation resistance. Journal of Hydraulic Engineering 116 (5), 691–705. [http://dx.doi.org/10.1061/\(ASCE\)0733-9429\(1990\)116:5\(691\)](http://dx.doi.org/10.1061/(ASCE)0733-9429(1990)116:5(691)).
- Kelson, V., 2012. Predicting collector well yields with MODFLOW. Groundwater 50 (6), 918–926. <http://dx.doi.org/10.1111/j.1745-6584.2012.00910.x>.
- Kirkby, M.J. (Ed.), 1978. Hillslope Hydrology. John Wiley & Sons, 389 p.
- Konikow, L.F., Hornberger, G.Z., Halford, K.J., Hanson, R.T., 2009. Revised Multi-node Well (MNW2) Package for MODFLOW Ground-water Flow Model. U.S. Geological Survey Techniques and Methods 6–A30, 67 p. <http://pubs.usgs.gov/tm/tm6a30/>.
- De Lange, W.J., Prinsen, G.F., Hoogewoud, J.C., Veldhuizen, A.A., Verkaik, J., Oude Essink, G.H.P., van Walsum, P.E.V., Delsman, J.R., Hunink, J.C., Massop, H.Th.L., Kroon, T., 2014. An operational, multi-scale, multi-model system for consensus-based, integrated water management and policy analysis: The Netherlands Hydrological Instrument. Environmental Modelling & Software 59, 98–108. <http://dx.doi.org/10.1016/j.envsoft.2014.05.009>.
- Lapham, W.W., 1989. Use of Temperature Profiles Beneath Streams to Determine Rates of Vertical Ground-water Flow and Vertical Hydraulic Conductivity. U.S. Geological Survey Water-Supply Paper 2337, 35 p. <http://pubs.er.usgs.gov/publication/wsp2337>.
- Lee, D.R., 1977. A device for measuring seepage flux in lakes and estuaries. Limnology and Oceanography 22 (1), 140–147. <http://dx.doi.org/10.4319/lo.1977.22.1.0140>.
- Liggett, J.E., Werner, A.D., Simmons, C.T., 2012. Influence of the first-order exchange coefficient on simulation of coupled surface–subsurface flow. Journal of Hydrology 414–415, 503–515. <http://dx.doi.org/10.1016/j.jhydrol.2011.11.028>.
- Loague, K. (Ed.), 2010. Benchmark Papers in Hydrology, 4: Rainfall-runoff Modelling. Selection, Introduction and Commentary by Keith Loague, IAHS Press, 506 p.
- Lowry, C., Walker, J.F., Hunt, R.J., Anderson, M.P., 2007. Identifying spatial variability of groundwater discharge in a wetland stream using a distributed temperature sensor. Water Resources Research 43 (10), W10408. <http://dx.doi.org/10.1029/2007WR006145>.
- Markstrom, S.L., Niswonger, R.G., Regan, R.S., Prudic, D.E., Barlow, P.M., 2008. GSFLOW—Coupled Ground-water and Surface-water Flow Model Based on the Integration of the Precipitation-runoff Modeling System (PRMS) and the Modular Ground-water Flow Model (MODFLOW—2005). U.S. Geological Survey Techniques and Methods 6–D1, 240 p. <http://pubs.usgs.gov/tm/tm6d1/>.
- McDonald, M.G., Harbaugh, A.W., 1988. A Modular Three-dimensional Finite-difference Ground-water Flow Model. U.S. Geological Survey Techniques of Water-Resources Investigations 06–A1, 576 p. <http://pubs.usgs.gov/twri/twri6a1/>.
- Merritt, M.L., 1992. Representing canals and seasonally inundated wetlands in a ground water flow model of a surficial aquifer. In: Interdisciplinary Approaches in Hydrology and Hydrogeology (M.E. Jones and A. Laenen, Eds.). American Institute of Hydrology, pp. 31–45.
- Merritt, M.L., Konikow, L.F., 2000. Documentation of a Computer Program to Simulate Lake-aquifer Interaction Using the MODFLOW Ground-water Flow Model and the MOC3D Solute-transport Model. U.S. Geological Survey Water-Resources Investigations Report 00–4167, 146 p. <http://pubs.er.usgs.gov/publication/wri004167>.
- Mitchell-Bruker, S., Haitjema, H.M., 1996. Modeling steady state conjunctive groundwater and surface water flow with analytic elements. Water Resources Research 32 (9), 2725–2732. <http://dx.doi.org/10.1029/96WR00900>.

- Neville, C.J., Tonkin, M.J., 2004. Modeling multiaquifer wells with MODFLOW. *Groundwater* 42 (6), 910–919. <http://dx.doi.org/10.1111/j.1745-6584.2004.t01-9->.
- Niswonger, R.G., Prudic, D.E., 2005. Documentation of the Streamflow-routing (SFR2) Package to Include Unsaturated Flow beneath Streams—A Modification to SFR1. U.S. Geological Survey Techniques and Methods 6–A13, 50 p. <http://pubs.usgs.gov/tm/2006/tm6A13/>.
- Niswonger, R.G., Prudic, D.E., Regan, R.S., 2006. Documentation of the Unsaturated-zone Flow (UZFI) Package for Modeling Unsaturated Flow between the Land Surface and the Water Table with MODFLOW-2005. U.S. Geological Survey Techniques and Methods 6–A19, 72 p. <http://pubs.er.usgs.gov/publication/tm6A19>.
- Niswonger, R.G., Panday, S., Ibaraki, M., 2011. MODFLOW-NWT, A Newton Formulation for MODFLOW-2005. U.S. Geological Survey Techniques and Methods 6–A37, 44 p. <http://pubs.usgs.gov/tm/tm6a37/>.
- Panday, S., Huyakorn, P.S., 2004. A fully coupled physically-based spatially-distributed model for evaluating surface/subsurface flow. *Advances in Water Resources* 27 (4), 361–382. <http://dx.doi.org/10.1016/j.advwatres.2004.02.016>.
- Panday, S., Langevin, C.D., Niswonger, R.G., Ibaraki, M., Hughes, J.D., 2013. MODFLOW-USG Versions 1: An Unstructured Grid Version of MODFLOW for Simulating Groundwater Flow and Tightly Coupled Processes Using a Control Volume Finite-difference Formulation. U.S. Geological Survey Techniques and Methods 6–A45, 66 p. <http://pubs.usgs.gov/tm/06/a45>.
- Papadopoulos, I.S., 1966. Nonsteady flow to multiaquifer wells. *Journal of Geophysical Research* 71 (20), 4791–4797. <http://dx.doi.org/10.1029/JZ071i020p04791>.
- Pint, C.D., Hunt, R.J., Anderson, M.P., 2003. Flow path delineation and ground water age, Allequash Basin, Wisconsin. *Groundwater* 41 (7), 895–902. <http://dx.doi.org/10.1111/j.1745-6584.2003.tb02432.x>.
- Prickett, T.A., 1967. Designing pumped well characteristics into electric analog models. *Groundwater* 5 (4), 38–46. <http://dx.doi.org/10.1111/j.1745-6584.1967.tb01625.x>.
- Prudic, D.E., Konikow, L.F., Banta, E.R., 2004. A New Streamflow-routing (SFR1) Package to Simulate Stream-aquifer Interaction with MODFLOW-2000. U.S. Geological Survey Open-File Report: 2004-1042, 95 p. <http://pubs.usgs.gov/of/2004/1042/>.
- Reeves, H.W., 2010. Water Availability and Use Pilot—A Multiscale Assessment in the U.S. Great Lakes Basin. U.S. Geological Survey Professional Paper 1778, 105 p. <http://pubs.usgs.gov/pp/1778/>.
- Reilly, T.E., Harbaugh, A.W., 2004. Guidelines for Evaluating Ground-water Flow Models. U.S. Geological Survey Scientific Investigations Report 2004-5038, 30 p. <http://pubs.usgs.gov/sir/2004/5038/>.
- Restrepo, J.I., Montoya, A.M., Obeysekera, J., 1998. A wetland simulation module for the MODFLOW ground water model. *Groundwater* 36 (5), 764–770. <http://dx.doi.org/10.1111/j.1745-6584.1998.tb02193.x>.
- Rosenberry, D.O., LaBaugh, J.W., Hunt, R.J., 2008. Use of Monitoring Wells, Portable Piezometers, and Seepage Meters to Quantify Flow between Surface Water and Ground Water. In: *Field Techniques for Estimating Fluxes between Surface and Ground Water*. U.S. Geological Survey Techniques and Methods Report 4–D2 (Chapter 2), pp. 43–70. <http://pubs.usgs.gov/tm/04d02>.
- Schmid, W., Hanson, R.T., Leake, S.A., Hughes, J.D., Niswonger, R.G., 2014. Feedback of land subsidence on the movement and conjunctive use of water resources. *Environmental Modelling & Software* 62, 253–270. <http://dx.doi.org/10.1016/j.envsoft.2014.08.006>.
- Sloto, R.A., Crouse, M.Y., 1996. HYSEP: A Computer Program for Streamflow Hydrograph Separation and Analysis. U.S. Geological Survey Water-Resources Investigations Report 96-4040, 46 p. <http://pubs.er.usgs.gov/publication/wri964040>.
- Theis, C.V., 1935. The relation between lowering of the piezometric surface and rate and duration of discharge of a well using ground-water storage. *Transactions of the American Geophysical Union* 16, 519–524. <http://onlinelibrary.wiley.com/doi/10.1029/TR016i002p00519/full>.
- Torak, L.J., 1993. A Modular Finite-element Model (MODFE) for Areal and Axisymmetric Ground-Water-Flow Problems, Part 1: Model Description and User's Manual. U.S. Geological Survey Techniques of Water Resources Investigations. Chapter A3 Book 6, 136 p. <http://pubs.usgs.gov/twri/twri6a3/>.
- Wang, H.F., Anderson, M.P., 1982. *Introduction to Groundwater Modeling: Finite Difference and Finite Element Methods*. Academic Press, San Diego, CA, 237 p.

- Westenbroek, S.M., Doherty, J.E., Walker, J.F., Kelson, V.A., Hunt, R.J., Cera, T.B., 2012. Approaches in Highly Parameterized Inversion: TSPROC, A General Time-series Processor to Assist in Model Calibration and Result Summarization. U.S. Geological Survey Techniques and Methods (Chapter 7), Book 7, Section C, 73 p. <http://pubs.usgs.gov/tm/tm7c7/>.
- Wilsnack, M.M., Welter, D.E., Montoya, A.M., Restrepo, J.I., Obeysekera, J., 2001. Simulating flow in regional wetlands with the MODFLOW wetlands package. JAWRA Journal of the American Water Resources Association 37 (3), 655–674. <http://dx.doi.org/10.1111/j.1752-1688.2001.tb05501.x>.
- Winter, T.C., Harvey, J.C., Franke, O.L., Alley, W.M., 1998. Ground Water and Surface Water, a Single Resource. U.S. Geological Survey Circular 1139, 79 p. <http://pubs.er.usgs.gov/publication/cir1139>.
- Woessner, W.W., 2000. Stream and fluvial plain ground water interactions: Rescaling hydrogeologic thought. Groundwater 38 (3), 423–429. <http://dx.doi.org/10.1111/j.1745-6584.2000.tb00228.x>.
- Yang, L., Wang, X.-S., Jiao, J.J., 2015. Numerical modeling of slug tests with MODFLOW using equivalent well blocks. Groundwater 53 (1), 158–163. <http://dx.doi.org/10.1111/gwat.12181>.
- Zhu, Y., Liangsheng, S., Lin, L., Jinzhong, Y., Ming, Y., 2012. A fully coupled numerical modeling for regional unsaturated–saturated water flow. Journal of Hydrology 475, 188–203. <http://dx.doi.org/10.1016/j.jhydrol.2012.09.048>.

## CHAPTER 7

# Steady-State and Transient Simulations

*Time, that black and narrow isthmus between two eternities.*

*Charles Caleb Colton*

*And time...must have a stop.*

*Henry IV, Pt. 1*

### Contents

7.1 Steady-State Simulations	303
7.1.1 Starting Heads	304
7.1.2 Boundary Conditions	304
7.1.3 Characterizing Steady-State Conditions	305
7.2 Steady State or Transient?	307
7.3 Transient Simulations	310
7.4 Initial Conditions	312
7.5 Perimeter Boundary Conditions for Transient Simulations	314
7.6 Discretizing Time	316
7.6.1 Time Steps and Stress Periods	316
7.6.2 Selecting the Time Step	318
7.7 Characterizing Transient Conditions	320
7.8 Common Modeling Errors	324
7.9 Problems	324
References	326

In the previous six chapters, we described the design of a numerical model and alluded to steady-state and transient (time-dependent) conditions. Almost all models start with a steady-state simulation and some modeling objectives also require a transient simulation. In this chapter, we discuss the characteristic features of a steady-state simulation, some of which were introduced earlier (the problems in Chapters 4–6 were all formulated as steady-state problems), but most of the chapter discusses transient simulations.

### 7.1 STEADY-STATE SIMULATIONS

In a steady-state model,  $\partial h/\partial t$  in the governing equation (Eqn (3.12)) is zero, and hydrologic parameters (Section 5.4) and computed heads and fluxes are constant in time (time

invariant). A steady-state solution alone is often sufficient to address many modeling objectives, such as analyzing average groundwater flow patterns and flow rates; estimating average annual leakage from a losing stream; calculating regional water table gradients; simulating flow directions influenced by long-term pumping. Steady-state models can also be used to forecast the effects of a time-averaged stress such as a long drought or projected long-term pumping. Furthermore, a steady-state model is usually the first step in transient modeling inasmuch as most transient models use a steady-state solution as initial conditions (Section 7.4). A steady-state simulation is usually the default simulation option when entering input into a graphical user interface (GUI) (Section 3.6) that executes a groundwater flow code.

### 7.1.1 Starting Heads

Numerical models that are solved iteratively (Sections 3.5 and 3.7) require *starting heads* at all nodes at the beginning of a steady-state simulation. (Direct numerical solutions as described in Section 3.5 typically do not require starting heads.) The starting heads influence the number of iterations required for the solution to converge but in most cases the final steady-state solution is not dependent on the values of the starting heads as long as the solution has converged to sufficient accuracy (Section 3.5).

Starting heads can be constant over the grid/mesh or arbitrary values can be specified. Arbitrary starting heads are usually based either on land surface elevation or on specified head internal and perimeter boundary conditions. Fewer iterations are required for convergence when the starting heads are relatively close to the final head solution. Poor choices of starting heads can cause the iterative solver to overshoot the solution during the initial iterations, which can result in dry nodes (Section 4.5) that can affect convergence and final head solutions. Therefore, starting heads should always be specified within the range of the solution. Starting heads are typically based on assigned specified head boundary conditions and are almost always set above the bottom elevation of the base of the model, and usually set above the bottom elevation of the top layer in three-dimensional models. Some GUIs automate the generation of default starting heads, typically by using specified head values at internal and perimeter boundaries or using the top elevation of the uppermost layer.

### 7.1.2 Boundary Conditions

Internal and perimeter boundary conditions (Sections 4.2 and 4.3) in steady-state models are time invariant, as are values of material properties and hydrologic parameters (Section 5.4). Care must be taken when assigning boundary conditions because a steady-state solution is strongly affected by its boundaries. This is because a steady-state solution has no water contributed by storage so all water is derived from internal and perimeter boundaries (and

areally distributed sources). Or put another way, steady state represents heads at infinite time, which means that hydrologic stresses reach the perimeter boundaries and conditions at the boundaries propagate completely throughout the model.

### 7.1.3 Characterizing Steady-State Conditions

Interpretive steady-state models that are designed as generic or simple screening models may not require calibration (Section 1.3), but most steady-state models are calibrated (Chapter 9) to field-measured observations of the groundwater system, typically heads and flows. When calibration is required, the modeler must assemble a set of field observations to compare to simulated steady-state heads (Fig. 9.3) and flows. However, judgment is needed because field measurements from groundwater systems are rarely in true steady state; rather, heads and flows continually change in response to changes in natural and induced recharge and discharge (Fig. 7.1). Therefore, in most cases the modeler must develop representative steady-state calibration targets from inherently transient field data. There are two options for assembling a steady-state calibration data set.

1. Time-averaged values of head that represent mean annual, seasonal, monthly, or some other selected period of time important for the modeling objective, may be calculated from head measurements in observation wells (Fig. 7.2). Mean baseflows can be computed from streamflow measurements (Fig. 9.4(b)). One criterion to judge

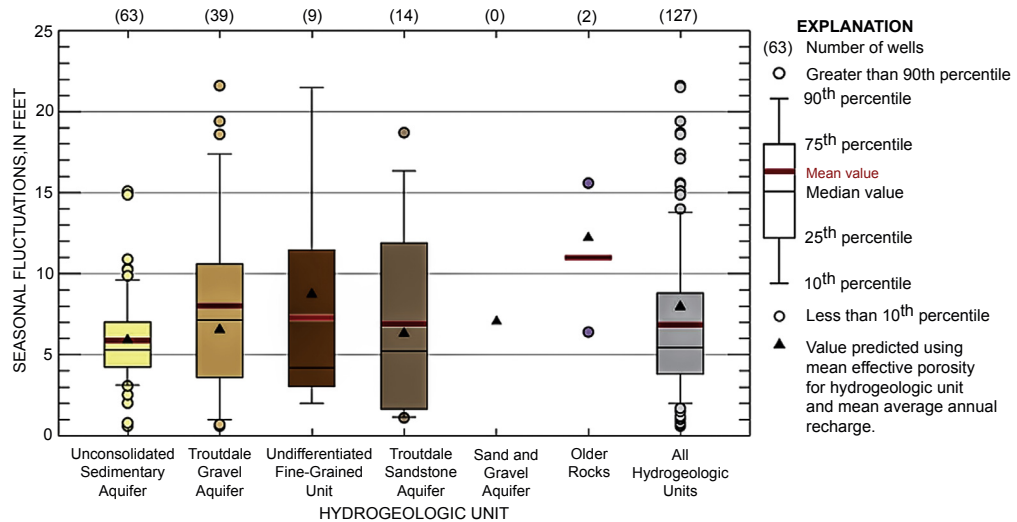


**Figure 7.1** Box and whisker plot showing the mean, median, and range in head in observation wells in hydrogeologic units for a temperate climate in Oregon, USA (Snyder, 2008).

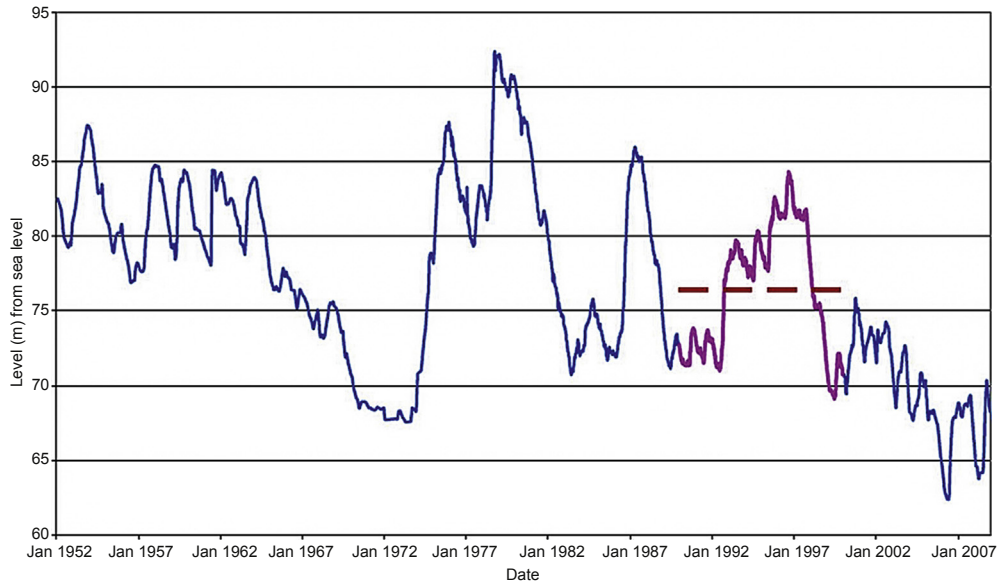


**Figure 7.2** Hydrograph for a monitoring well in New Zealand. The period 1990–2000 was used to derive an average head target (shown by dashed line) for a steady-state model (Scott and Thorley, 2009).

if a period of time represents steady-state conditions is to assess whether field measurements at the beginning of the period are similar to measurements at the end of the period. Similar values of heads at the beginning and end of a time period suggest that the change in storage during the period is negligible and the average heads during the period may be used (e.g., Dripps et al., 2006).

2. When changes in head over time are small, field measurements from a representative time period can be used directly as steady-state calibration data. Ideally the measurements reflect a time period when water levels and flows are approximately constant, i.e., at quasi- or pseudo-steady state. For example, heads measured at some representative time might be judged to represent long-term average conditions. Another option is to use seasonal quasi-steady-state heads. For example, in some northern latitudes, mountain valley groundwater systems are dominated by snowmelt recharge so that mid- to late-March is a period of pseudo-steady state when hydrographs level off at the end of winter before spring recharge occurs. In other temperate climates, mid-fall may be a period of quasi-steady state (Fig. 7.3). Bounding and successive steady-state simulations (Section 7.2) are calibrated to quasi-steady-state heads.

The output of a steady-state model is a spatial array of heads, usually output by the code as two-dimensional arrays of heads in layers and associated flows at internal and perimeter boundaries. A GUI and/or visualization software displays simulated heads by

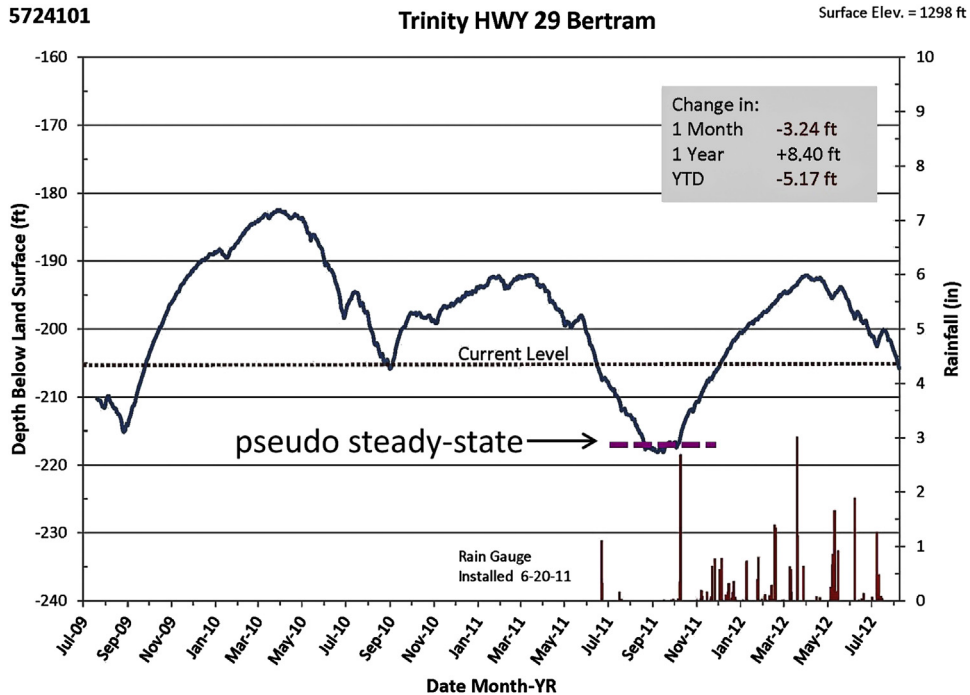


**Figure 7.3** Hydrograph for a monitoring well in the Trinity aquifer, Texas, USA (July 2009–July 2012), showing pseudo-steady-state conditions at the end of summer 2011 when pumping rates are low and before fall rains occur (*modified from Central Texas Groundwater Conservation District, The Hydro Blog, August 2012, <http://www.centraltexasgcd.org/the-hydro-blog/>*).

layer in areal (Figs 2.5 and 9.3) and profile (Fig. 4.22(c)) views. Simulated steady-state water budgets (Section 3.6) are reported in units consistent with units input for parameter values (e.g., volumetric flow rates in  $\text{m}^3/\text{d}$ ,  $\text{ft}^3/\text{d}$ ,  $\text{m}^3/\text{s}$ , or other units).

## 7.2 STEADY STATE OR TRANSIENT?

In Box 4.1, we addressed a fundamental decision in model design—whether a three-dimensional model is needed. In this section, we discuss another fundamental decision—whether a transient model is needed. Steady-state models are inherently simpler to create, execute, and postprocess than transient models, and for that reason alone steady-state models are typically preferred provided they adequately address the modeling objective. Steady-state models need only a single set of calibration data and produce only one set of results while transient models require multiple calibration data sets and produce more output than steady-state models. Transient models also require additional input, namely values for storage parameters (Section 5.4) and initial conditions (Section 7.4).



However, for many situations a transient model is clearly required—e.g., to calculate water-level fluctuations in response to changes in daily or seasonal pumping rates, daily or seasonal variations in recharge, seasonal extraction of groundwater by phreatophytes; or to evaluate the effects of transience on transport of contaminants from a source area. The decision of steady state or transient is also determined by the time frame pertinent to the modeling objective. For example, a transient model would be needed to assess how short-duration pumping of irrigation wells affects baseflows and water levels in domestic wells, but a steady-state model might suffice if the modeling purpose requires only information on the long-term or average annual effects of pumping.

Below we discuss two simple calculations that can help the modeler decide whether a transient model is needed. Both of these indicators (as well as a parameter for estimating the time to steady-shape conditions; see Box 6.1) are expressed as a ratio of  $L^2$ , where  $L$  is a characteristic system length, to *hydraulic diffusivity*,  $Kb/S$  ( $= T/S$ ), where  $K$  is hydraulic conductivity;  $b$  is saturated thickness;  $S$  is storativity (specific yield,  $S_y$ , for an unconfined aquifer); and  $T$  is transmissivity. Hydraulic diffusivity is an important parameter in assessing the importance of transience response to many different types of stresses including the effects of aquifer pumping on streamflow (Barlow and Leake, 2012, p. 8). Hydraulic stresses propagate faster through aquifers with higher hydraulic diffusivity. Because confined storativity is much less than specific yield (Section 5.4), hydraulic diffusivity is usually higher in confined aquifers than unconfined aquifers. For a given value of  $K$ , the approach to steady state is faster for smaller values of storativity (Fig. 7.4).

The *groundwater system time constant*,  $T^*$ , is derived from dimensionless analysis of the governing equation (Eqn (3.12)) (Domenico and Schwartz, 1998, p. 173):

$$T^* = \frac{SL^2}{Kb} \quad (7.1)$$

where  $L$  is usually taken to be the distance between system boundaries, and  $T^*$  has units of time. If the time at which we wish to observe the system is significantly larger than  $T^*$ , the system will appear to be at steady state and can be simulated using a steady-state model. Stated another way, transient effects initiated at  $t = 0$  (where  $t$  is time) are readily apparent only if we observe the system at times less than  $T^*$  ( $t < T^*$ ). Confined aquifers, which have relatively large values of hydraulic diffusivity due to their low storativity, generally have smaller time constants than unconfined aquifers.

A related (dimensionless) parameter is *aquifer response time*,  $\tau$  (Haitjema, 2006, p. 789; also see Haitjema, 1995; pp. 280–292; and Townley, 1995), which is derived from analytical solutions for one-dimensional, and radial flow in aquifers subjected to periodic fluctuations in areal recharge and/or periodic fluctuations in head at the boundary,

$$\tau = \frac{1}{4P} \frac{SL^2}{Kb} = \frac{T^*}{4P} \quad (7.2)$$

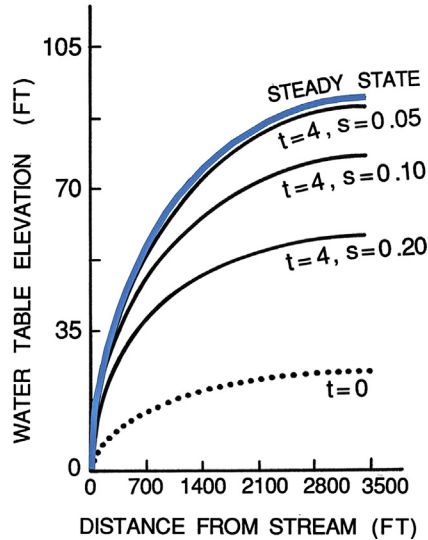


**Figure 7.4** Water table profiles showing the effect of storage on the approach to steady state for a one-dimensional model of an unconfined aquifer using different values of storativity,  $S$ , (=specific yield). The aquifer receives recharge at a constant rate, and groundwater discharges to a stream located at distance equal to zero. The transient response is initiated by an increase in recharge rate; the head at  $t = 0$  represents initial conditions;  $t$  is time in months. At steady state, the solution is independent of storativity (Zucker *et al.*, 1973).

where  $L$  is the distance between major surface water features and  $P$  is the period of the forcing function (=365 days for seasonal fluctuations). Equation (7.2) is used to assess when steady-state conditions can approximate transient system response to periodic stresses, as described below.

Groundwater systems are almost never at steady state, but for many problems the modeling objective can be effectively addressed by analyzing steady-state conditions. *Time-averaged steady-state conditions* represent average heads for some designated time period (Fig. 7.2) such as the average annual water table. Two steady states that represent the end range of conditions observed in the field are called *bounding steady states*. For example, two separate steady-state models could be developed to assess seasonal groundwater conditions (e.g., periods of seasonally high- and low-groundwater levels) or conditions representing wet and dry years. The field data for a bounding steady-state condition are head observations at pseudo-steady state (Section 7.1; Fig. 7.3). Successive steady states consist of two or more steady-state solutions that represent different pseudo-steady-state field conditions.

The groundwater system responds slowly to periodic changes in recharge or boundary conditions when  $\tau$  is large (i.e., hydraulic diffusivity,  $Kb/S$ , is small) and quickly when  $\tau$  is small ( $Kb/S$  is large). Haitjema (1995, pp. 292–293) compared bounding steady-state solutions with transient solutions with respect to changes in head and discharge at the

boundary with  $P = 365$  days. Based on those findings, [Haitjema \(2006\)](#) provided the following guidelines (derived for  $P = 365$  days):

1. When  $\tau > 1.0$ , a steady-state model of time-averaged conditions is appropriate.
2. When  $0.1 < \tau < 1.0$ , a transient model is required.
3. When  $\tau < 0.1$ , bounding or successive steady-state solutions may be used.

In general, small values of  $\tau$  characterize highly permeable unconfined aquifers and most confined aquifers; thus bounding or successive steady-state solutions are applicable to represent annual periodicity. Moderately permeable to low permeability unconfined systems will likely exhibit local transient effects that are not captured by successive steady-state solutions and thus typically require transient solutions. Justification for these guidelines is presented in detail by [Haitjema \(1995, pp. 280–292\)](#).

### 7.3 TRANSIENT SIMULATIONS

A transient simulation is initiated by introducing a stress (e.g., a change in pumping or recharge rate; [Fig. 7.5 \(a\)](#)) or combination of stresses (pumping and recharge) to the starting head distribution (i.e., the initial conditions). Perimeter boundary conditions always affect a steady-state solution ([Section 7.1](#)) but affect a transient solution only if the stresses introduced at the beginning of a simulation reach a perimeter boundary ([Section 7.5](#)). If the newly stressed conditions persist for enough time, typically the groundwater system will reach a new steady-state condition ([Fig. 7.4](#)). Transient simulations require consideration of the following factors:

1. Values of storage parameters ([Section 5.4](#)) must be assigned to all hydrogeologic units in the model, in addition to hydraulic conductivity.
2. Representative initial conditions must be formulated ([Section 7.4](#)).
3. The effects of hydrologic stresses may propagate out to the perimeter boundaries of the model, which may not be appropriate for the field conditions being simulated ([Section 7.5](#)).
4. Time, as well as space, must be appropriately discretized ([Section 7.6](#)).
5. Field observations used in model calibration must represent the length of time simulated ([Section 7.7](#)).
6. A transient simulation usually requires longer run times than a steady-state simulation ([Section 3.7](#)) because the model must be solved at each time step (iterative solutions require multiple trial solutions per time step) and most transient models require multiple time steps.
7. Steady-state simulations generate only one set of heads but transient simulations calculate heads for each time step, typically producing more output ([Fig. 7.5](#); [Section 7.7](#)).

Storage parameters were discussed in [Section 5.4](#) and run times were discussed in [Section 3.7](#). The other factors listed above are discussed in [Sections 7.4–7.7](#).

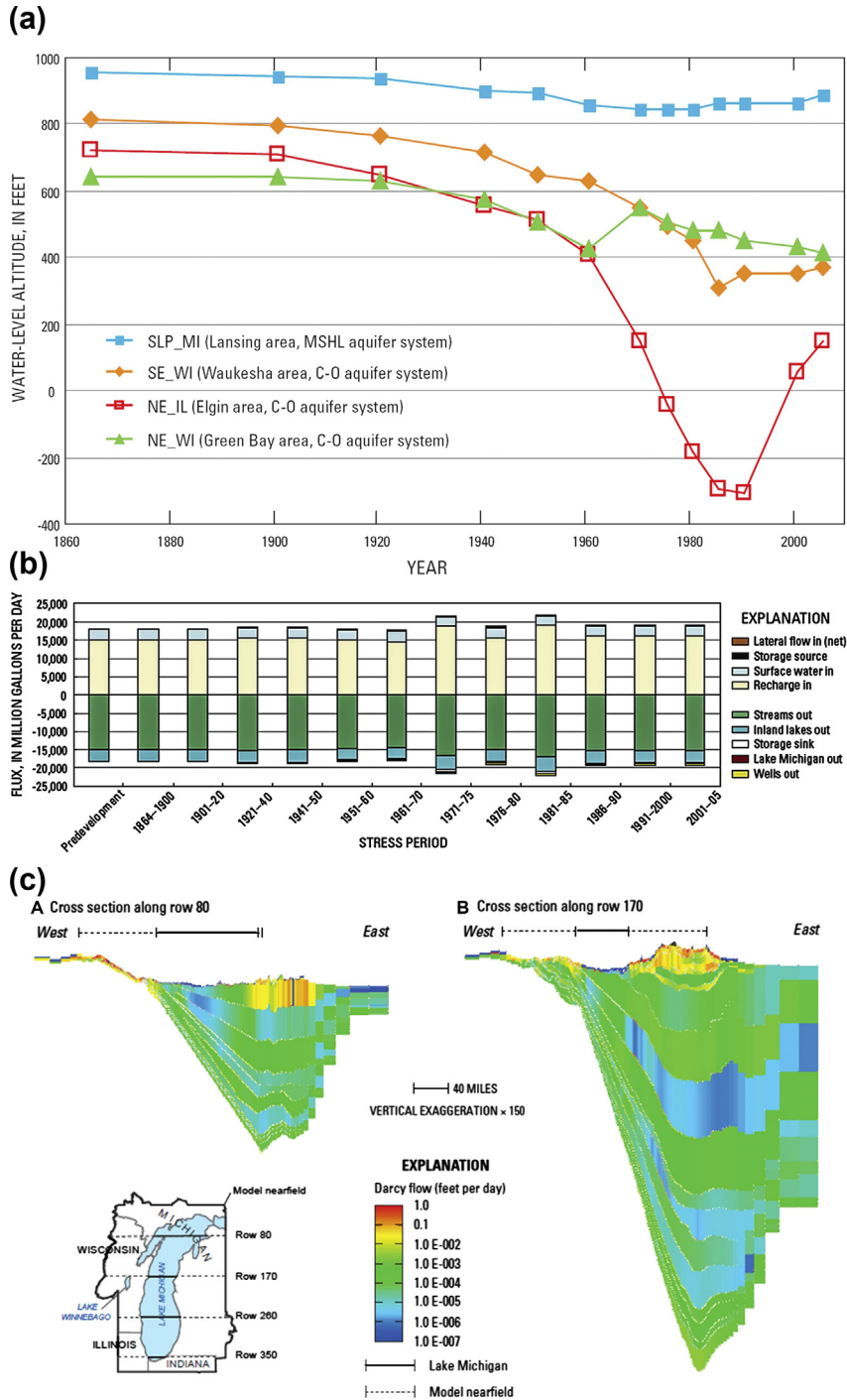


**Figure 7.5** Examples of output from a transient model of the Lake Michigan Basin, USA. (a) Calculated groundwater levels at pumping centers shown from predevelopment conditions to recent time. (b) Simulated water budgets at selected times. (c) Simulated flows in selected cross sections for 2005 (Feinstein et al., 2010).

## 7.4 INITIAL CONDITIONS

A transient model requires the modeler to specify *initial conditions*, i.e., heads at every node at the beginning of the simulation. Initial conditions are conceptually different from the starting heads in a steady-state model (Section 7.1) because a steady-state solution is theoretically independent of the values of the starting heads while early time transient results are strongly influenced by initial conditions input by the modeler. In this way, initial conditions can be considered a boundary condition in time. It is a standard practice to use heads generated by a steady-state model as the initial conditions for a transient model. Novice modelers often want to input field-measured heads as initial conditions, but this is inappropriate as explained by Franke et al. (1987):

*Use of model-generated head values ensures that the initial head data and the model hydrologic inputs and parameters are consistent. If the field-measured head values were used as initial conditions, the model response in the early time steps would reflect not only the model stress under study but also the adjustment of model head values to offset the lack of correspondence between model hydrologic inputs and parameters and the initial head values.*

Two types of steady-state conditions can form initial conditions. For *static steady-state conditions*, head is constant throughout the problem domain and there is no flow of water anywhere in the system (Fig. 7.6(a)). These initial conditions are commonly used for simulations that calculate drawdown in response to pumping (e.g., Prickett and Lonquist, 1971) where relative drawdowns are of interest rather than absolute values of head. The most commonly used initial conditions are *dynamic steady-state conditions*, where heads vary spatially but are constant in time (Fig. 7.6(b)); these conditions are dynamic in that water flows through the system whereas there is no flow of water under static steady-state conditions. Dynamic steady-state conditions are computed from a steady-state simulation. (For example, the solution of Problem P4.3 is the initial condition for Problem P7.2.)

In addition to the two types of steady-state initial conditions discussed above, there is a transient initial condition known as *dynamic cyclic equilibrium conditions* (Fig. 7.6(c)) where heads fluctuate cyclically, but the cycle is similar over time. Each cycle might represent monthly head fluctuations in an average year; if average monthly recharge rates are the same in all years, each cycle of heads is identical (see Problem P7.2b). The initial conditions are dynamic because heads change monthly but are also at equilibrium because the cycles themselves do not change with time. That is, when the cycles represent monthly fluctuations within a year, the heads in January of each cycle are the same, as are the heads in February, and so on through December. Dynamic cyclic equilibrium initial conditions are generated by assigning arbitrary initial starting heads and running a transient model with a set of cyclic stresses (e.g., monthly average recharge rates) until the resulting heads come to a cyclic equilibrium. The transient simulation of interest is started from any point in time during an equilibrium cycle. For example, Maddock

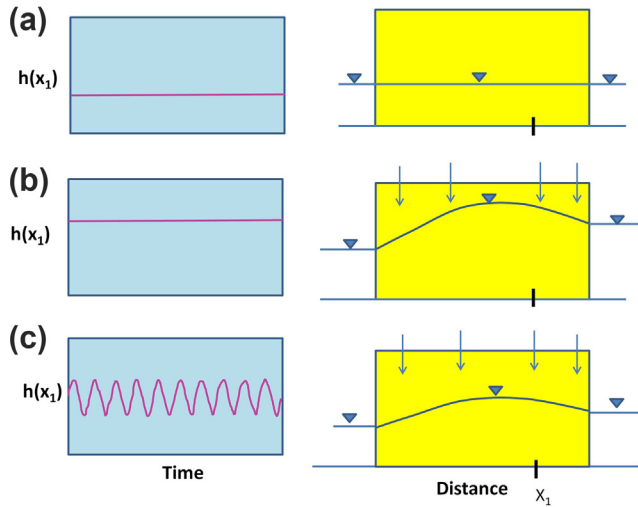


**Figure 7.6** Schematic depiction of three types of initial conditions, shown for one-dimensional horizontal flow in an unconfined aquifer between two streams. The spatial variation of head,  $h(x)$ , is shown on the right; corresponding hydrographs at the location  $x_1$  are shown at left. (a) Static steady state; head is constant in space and time; (b) Dynamic steady state; head varies in space but is constant in time; (c) Dynamic cyclic equilibrium conditions; head varies in both space and time. The water table configuration on the right is for one point in time.

and Vionnet (1998) used this type of initial condition to represent groundwater level fluctuations in annual cycles each representing four seasons for a transient simulation to determine the effects of pumping on streamflow. Ataie-Ashtiani et al. (2001) used cyclic initial conditions to represent tidal fluctuations in an unconfined coastal aquifer.

When dynamic cyclic equilibrium conditions are developed, the transient model includes a *spin-up period* at the beginning of the simulation prior to the time period of interest (Fig. 7.7). For Maddock and Vionnet's (1998) model, for example, the spin-up period required 100 cycles before dynamic cyclic equilibrium conditions were generated. Spin up is frequently used in surface water modeling and in integrated hydrologic modeling (e.g., Ajami et al., 2014), sometimes with the objective of producing cyclic equilibrium conditions, but spin up is used less commonly in groundwater modeling.

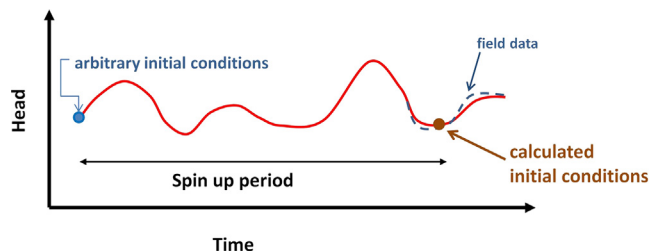


**Figure 7.7** Schematic hydrograph showing transient model spin up to generate initial conditions. Arbitrary initial conditions at the beginning of the spin up might be based on historical information about predevelopment water levels (blue dot). Simulated results are shown by the red line. Results for the spin-up period are not used but heads at the end of the spin up are matched to field observations (dashed blue line). The calculated heads at the end of the spin-up period (shown by the brown dot) effectively provide initial conditions for the rest of the transient simulation.

The results at the end of a spin up do not have to be dynamic cyclic equilibrium conditions. For example, in a research application, [Lemieux et al. \(2008\)](#) used spin up to generate heads at the end of the last interglacial period to serve as initial conditions for a transient model of groundwater flow during the last ice age. In applied groundwater modeling, starting heads for a spin-up simulation are often assigned based on predevelopment heads ([Fig. 7.5\(a\)](#)). The transient model is run using estimated values of stresses (e.g., pumping and recharge rates) assigned to the spin-up period but no attempt is made to match heads during spin up. Simulated heads are matched to recent field-measured heads at the end of the spin-up period, and the simulated heads effectively become the initial conditions for the rest of the simulation ([Fig. 7.7](#)). The rationale for using spin up is that the influence of potentially erroneous starting heads diminishes as the simulation progresses and is reduced to an acceptable level by the end of the spin up. In other words, errors in the initial conditions produced at the end of the spin-up period are minimized provided the spin-up period is sufficiently long. Groundwater systems with low hydraulic diffusivity take longer to propagate stresses and thus require longer spin-up periods than groundwater systems with high hydraulic diffusivity. [Reilly and Harbaugh \(2004, p. 18–19\)](#) suggested using [Eqn \(7.1\)](#) to estimate when the initial conditions cease to influence the transient solution. That is, the solution is not affected by initial conditions when the spin-up time is greater than  $T^*$ . Nevertheless, the modeler should test the effect of the length of the spin-up period on the results, especially if results early in the transient simulation (i.e., soon after the end of the spin-up period) are important for the modeling objective.

## 7.5 PERIMETER BOUNDARY CONDITIONS FOR TRANSIENT SIMULATIONS

Perimeter boundary conditions (Section 4.2) for a transient model are typically the same boundary conditions that produced the initial conditions. Important transient changes to the system generally are simulated by changing internal stresses and/or by changing conditions at internal boundary conditions or introducing new internal boundaries. However, in some cases perimeter boundaries might be updated by the modeler during the transient simulation to reflect changes known or expected to occur along the boundary.

Perimeter boundary conditions always affect a steady-state solution ([Section 7.1](#)) and, therefore, the effects of boundary conditions used to generate dynamic steady-state and dynamic cyclic equilibrium initial conditions are implicitly included in a transient simulation. However, perimeter boundary conditions directly affect the transient solution only when transient stresses reach a boundary. When stresses reach a physical boundary (Section 4.2), the simulated response may be realistic and appropriate. For example, a relatively impermeable fault zone or impermeable rock might be represented in a model

by a no-flow boundary, which would appropriately simulate the effects of a cone of depression intersecting the boundary (e.g., Fig. 3.2). Similarly, when the cone of depression caused by pumping intersects a surface water body represented by a head-dependent boundary (HDB) condition (Section 4.3), the model would simulate flow of water from surface water to the groundwater system, which is appropriate if the surface water level under field conditions is not affected by the pumping.

However, problems arise when the condition specified at the boundary does not realistically or appropriately characterize transient conditions in the field. For example, under field conditions the surface water level represented by the HDB condition discussed in the example above, might decline in response to pumping. The specified boundary head in a standard HDB condition, however, remains constant throughout the simulation and consequently too much water would be drawn from the boundary. If the change in boundary head in response to pumping were known a priori, it could be updated over time. However, changes in conditions at a boundary usually are not known, and a more complicated option that allows for calculating fluctuations in surface water levels might be necessary (Sections 6.5 and 6.6).

In general, a boundary where heads are specified (including HDBs) potentially provides or receives an infinite amount of water. Specified flow and no-flow perimeter boundary conditions limit the amount of exchange that can occur at the boundary, but time-invariant specified flow perimeter boundary conditions may also bias the effects of stresses imposed in the model domain. Moreover, exclusive use of specified flow perimeter boundary conditions may be hydrogeological defensible but should be avoided because errors in the initial heads can cause errors in the solution (Section 4.3). If perimeter boundaries are all specified flow boundaries, it is advisable to specify a head value as an internal boundary in order to tie the solution to an absolute value of head.

Ideally, the modeler has the flexibility to set perimeter boundaries sufficiently distant that the effects of simulated transience depend primarily on internal boundary conditions rather than conditions at the perimeter, which are usually more poorly constrained. However, this may not be possible. In order to detect potentially inappropriate boundary effects, the influence of boundaries on the solution should be monitored as the solution progresses. The effects of the boundaries can be evaluated by checking the change in flow rates across specified head and head-dependent boundaries and the change in heads at specified flow boundaries as the simulation progresses. If the changes are significant, the solution is being affected by the boundary conditions. The effects of the boundary conditions can also be evaluated by changing specified head and head-dependent boundaries to specified flow and vice versa, and rerunning the transient model. If differences between the two solutions are acceptably small, the boundary is considered to have a negligible effect on the solution. If boundary conditions are inappropriately affecting the solution, the grid/mesh can be expanded so that the perimeter boundaries are set



farther from the simulated stresses or more complicated options for representing the boundary conditions (Sections 6.5 and 6.6) may be considered.

A final comment about perimeter boundary conditions for a transient simulation concerns the relatively rare case where it is appropriate to use arbitrary distant boundaries. If the length of the transient simulation is such that the effects of the stresses do not extend to the boundaries, a transient problem can be formulated with arbitrary perimeter boundary conditions, usually no-flow conditions. The placement and conditions along the perimeter boundaries are arbitrary since the boundaries are set far enough from the area of interest so that the simulation is not influenced by conditions along the perimeter. Of course, the use of distant perimeter boundaries requires that the grid/mesh extends out as far as the boundaries even though there is little or no interest in simulating heads in the distant parts of the model domain. An irregular grid/mesh with large nodal spacing near the perimeter minimizes the total number of nodes required. Even so, stresses may reach the boundaries provided the simulation is run long enough.

If a transient model is poorly conceived, it may not reach steady state even with long simulation times. For example, suppose an aquifer is pumped at a constant rate. At steady state, water supplied to the well comes exclusively from sources of water at the perimeter boundaries and/or inside the problem domain (e.g., recharge, leakage, and surface water). If the modeler does not include such sources of water, steady-state conditions are never reached and water comes exclusively from storage. In some cases this may be appropriate; for example, pumping from storage is the underlying assumption of the Theis analytical solution for radial flow to a pumping well in a confined aquifer of infinite areal extent. However, in a numerical model with no-flow perimeter boundaries and no internal sources of water, a pumping well will withdraw water from storage until the aquifer is completely dewatered, if the simulation time is long enough.

## 7.6 DISCRETIZING TIME

### 7.6.1 Time Steps and Stress Periods

Both steady-state and transient simulations require discretization of space by means of a grid/mesh, but in a transient simulation, time also must be discretized. The total amount of time represented in a transient simulation is divided into smaller portions of time called *time steps*. In some transient problems, stresses are introduced at the beginning of the simulation and held constant throughout the entire simulation. For example, the modeling objective might be to simulate the response to pumping a well at a constant rate or to simulate response to a long-term drought. However, more often stresses such as pumping and recharge change during the simulation (e.g., to reflect seasonal pumping and/or recharge), and then the total simulation period is divided into blocks of time usually known as *stress periods* (following MODFLOW terminology). By definition, stresses remain constant during a stress period (Fig. 7.8) but the timing, locations,

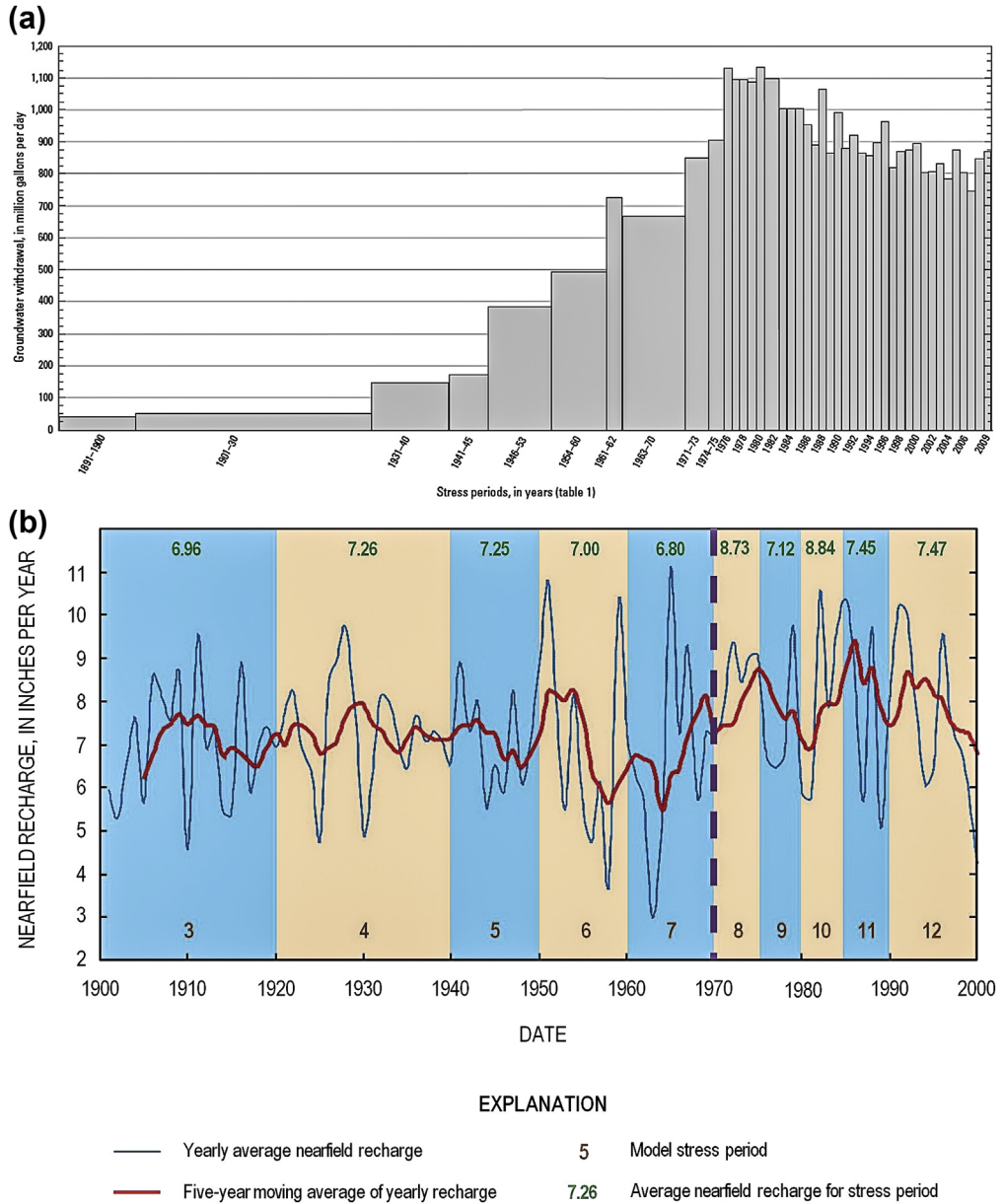


**Figure 7.8** Stress periods for: (a) groundwater withdrawals from pumping; the simulation used 78 stress periods of variable length between 1891 and 2009 (*Kasmarek, 2012*); (b) recharge; recharge rates were estimated from residuals in a soil-water balance model (Box 5.4). Rates for stress periods 3–12 are shown (*Feinstein et al., 2010; Reeves, 2010*).

and rates of stresses as well as boundary conditions can change from one stress period to the next as specified by the modeler. Each stress period is subdivided into time steps in order to simulate changes in head within the stress period and to help stabilize the numerical solution. In MODFLOW, one stress period is specified if stresses are constant throughout the simulation.

A transient simulation begins by simulating the response on initial heads (Section 7.4) to stresses in the first stress period after one time step has elapsed. For the second time step, the code replaces the initial heads with the head solution from the end of first time step and calculates heads at the end of second time step, which become the starting heads for the third time step. This process continues until the end of the simulation (if one stress period long) or to the end of the stress period when the heads from the last time step become the starting heads for the first time step in the second stress period. The process continues until all the stress periods have been simulated.

### 7.6.2 Selecting the Time Step

Selecting the length of the time step is important to model design because the size of the time step can affect the error in the water balance calculated by the model as well as the stability of the solution. The choice of time step may be dictated by the type of model and/or the code. For example, a groundwater model coupled to an unsaturated flow model often has numerical instabilities related to the size of the time step (Box 6.2). If time steps are too large, the numerical solution calculates unrealistic oscillating values of pressure head. Similarly, oscillation can affect numerical solutions of the advection–dispersion equation for solute transport when time steps are too large. Numerical oscillations can usually be eliminated by decreasing the size of the time step. Some solute transport codes (e.g., MT3DMS: Zheng and Wang, 1999) calculate the time step required to keep oscillations under control and automatically set the time steps. Groundwater flow codes, however, are much less prone to numerical instability and most flow codes require the user to specify the time steps, or time-step parameters, as discussed below.

In theory, small time steps are preferred so that the numerical model more closely approximates the partial differential equation (Eqn (3.12)). However, the total simulation period can extend over years or decades making uniformly small time steps computationally impractical. Instead, time steps of variable length are typically used with small time steps at the beginning of a stress period to capture the initial response to a stress, and longer time steps after the initial stress response has been absorbed by the system. Variable length time steps are computed using a time-step multiplier that increases the time step as the simulation progresses up to a maximum specified value after which the time step is held constant. Torak (1993) recommended that for nonlinear problems and problems that have rapid changes in stresses, time steps should be increased by multiples of no

more than 1.1–1.5. Marsily (1986, p. 399) recommended multiples of 1.2–1.5 where 1.414 ( $=\sqrt{2}$ ) is often a good initial choice.

Some codes may require the modeler to specify an initial time step,  $\Delta t_i$ , to start the simulation and/or at the beginning of each stress period. A good order-of-magnitude estimate for a reasonable initial time step is the maximum time step allowed for an explicit solution of the numerical approximation of the two-dimensional, homogenous, and isotropic governing equation when  $\Delta x = \Delta y = a$  (Marsily, 1986, p. 399; Wang and Anderson, 1982, p. 70):

$$\Delta t_i = \frac{Sa^2}{4Kb} \quad (7.3)$$

where  $K$  is hydraulic conductivity,  $b$  is layer thickness, and  $S$  is storativity. For an irregular grid/mesh,  $\Delta t_i$  can be approximated by selecting a representative value of nodal spacing and representative cell or element properties. Time steps of the order  $\Delta t_i$  at the beginning of a stress period capture rapid changes in head caused by changes in stresses and/or the introduction of new stresses (Fig. 7.9). If these rapid head changes are not important to the modeling objective, it might be appropriate to use a larger initial time step and ignore results from the first few time steps.

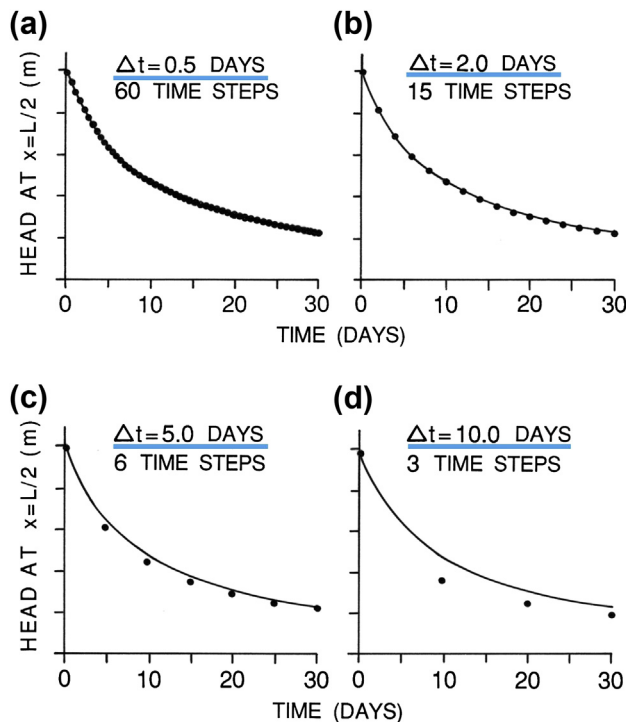


**Figure 7.9** Effect of the size of the time step ( $\Delta t$ ) on the numerical solution (dots) for the decay of a groundwater mound compared to an analytical solution (solid line). Small time steps in (a) and (b) give results that match the analytical solution very well. The larger time step in (c) also provides an acceptable match to the analytical solution. The time step in (d) produced results that do not match the solution within the first 30 days (modified from Townley and Wilson, 1980).

MODFLOW computes the initial time step in a stress period from user-specified values for the time-step multiplier ( $M$ ), the number of time steps in the stress period ( $N$ ), and the length of the stress period ( $T_{SP}$ ):

$$\Delta t_i = T_{SP} \frac{(1 - M)}{(1 - M)^N} \quad (7.4)$$

Each stress period begins with a small time step of  $\Delta t_i$  and the time-step multiplier is used to increase the time step as the stress period progresses. Then the time step is reduced to  $\Delta t_i$  again at the beginning of the next stress period. A general guideline is that there should be at least six time steps per stress period, as suggested by Prickett and Lonquist (1971) who showed that numerical solutions agreed with the Theis analytical solution after about six time steps (Fig. 7.10(a)). The six time steps per stress period rule was discussed more recently by Reilly and Harbaugh (2004) (Fig. 7.10(b)). Also see Fig. 7.9(c).

Adaptive time stepping is also used in FEFLOW (Diersch, 2014, pp. 304–308), where:

$$\Delta t_{n+1} = \Delta t_n \left( \frac{\varepsilon}{\|d_{n+1}\|} \right)^B \quad (7.5)$$

In Eqn (7.5),  $\Delta t_n$  is the current time step;  $\Delta t_{n+1}$  is the next time step;  $\varepsilon$  is the closure criterion (error tolerance; Sections 3.5.4 and 3.7.3);  $d_{n+1}$  is the local truncation error where the double bars signify the norm (average value);  $B$  is equal to either 1/3 or 1/2 depending on the solution method (Table 8.7, p. 306, in Diersch, 2014). The user specifies a small initial time step and a value for  $\varepsilon$  between  $10^{-3}$  and  $10^{-4}$ . By adjusting  $\varepsilon$ , the modeler can control the time-stepping process. When  $\varepsilon$  is too large the solution will oscillate; when  $\varepsilon$  is too small computations become unacceptably expensive.

It is a good modeling practice to make several trial runs of the model using different numbers of time steps, different time-step multipliers, and different solver settings. Then the effect on both heads and the water budget at times that are important to the modeling objective should be evaluated and the final time discretization parameters can be selected.

## 7.7 CHARACTERIZING TRANSIENT CONDITIONS

Calibration data for a transient simulation should include long-term hydrographs (e.g., Fig. 7.2; also see Taylor and Alley, 2001) and information on the transient response of fluxes distributed throughout the modeled area. Long-term monitoring

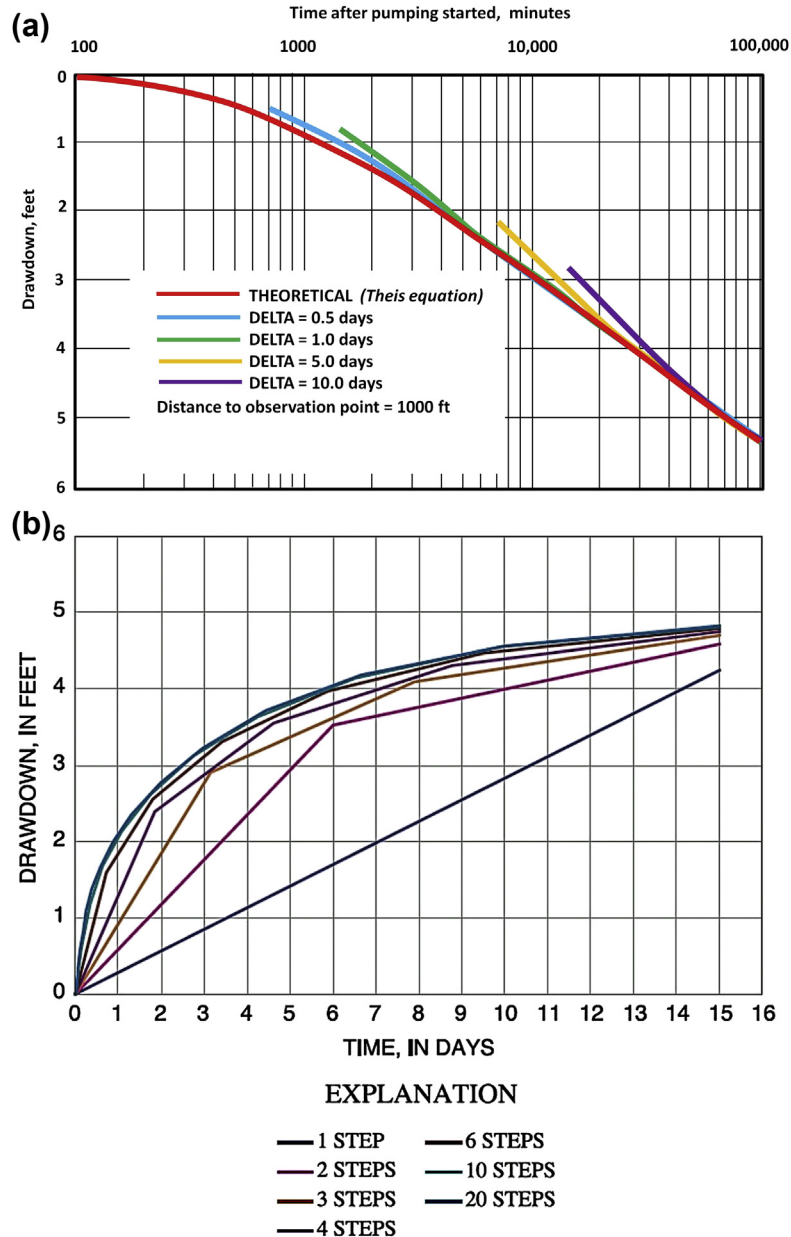


**Figure 7.10** Effect of the number of time steps on numerical solutions of drawdown in response to pumping. (a) Numerical solutions using four different time steps (DELTA) are compared to the Theis analytical solution. Drawdown is shown at an observation point 1000 ft from the pumping well (modified from Prickett and Lonquist, 1971: *Comparison of theoretical and digital computer solutions near a pumped well with DELTA as a variable*, by Thomas A. Prickett and Carl G. Lonquist, Bulletin 55, Illinois State Water Survey, Champaign, IL). (b) Numerical solutions for drawdown in a pumping well using from 1 to 20 time steps. Except for the 1 time step simulation each time step was 1.5 times longer than the last. The solutions for 10 and 20 time steps are indistinguishable at the scale of the plot. The solution for 6 time steps is in good agreement with the 10 and 20 time step solutions (Reilly and Harbaugh, 2004).

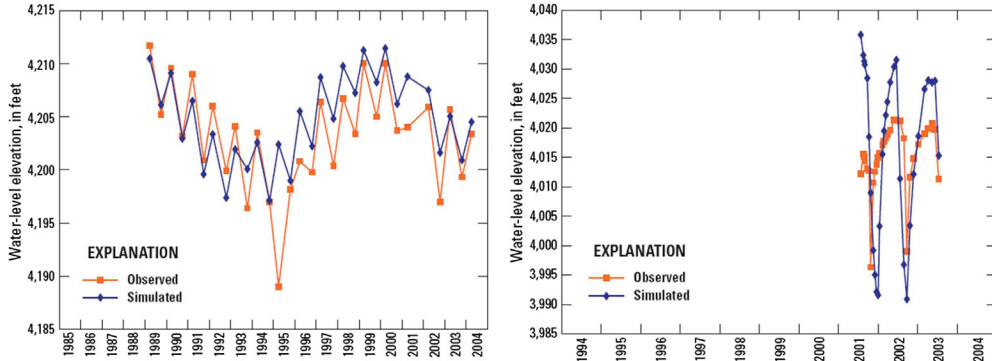


**Figure 7.11** Simulated and observed water levels for two monitoring wells in California, USA, with different periods of record (*Gannett et al., 2012*).

data are helpful in identifying transient patterns and trends even if the length of the transient simulation is shorter than the record of observations. During calibration, simulated heads are compared with measured heads for whatever length of time a record is available within the simulated period (Fig. 7.11). Bar graphs of the mean and range in water level at each observation well are also helpful (Fig. 9.4(c) and (d)). Measured groundwater flows (e.g., baseflow, Fig. 9.4(a); Table 7.1) also form part of the calibration data set. In practice, calibration data are compiled from whatever water-level and streamflow records are available (Table 7.1). Additionally, head data of historical water levels may be useful if initial conditions are based on predevelopment conditions (Section 7.4).

Once the observed data set is compiled, the modeler must decide how much of the transient model output should be stored, processed, and analyzed during model calibration (Chapter 9) and forecasting (Chapter 10). Transient head data are usually postprocessed for display in contour maps for selected time periods and/or hydrographs that show the fluctuation in head at selected locations (Fig. 7.5(a); Fig. 9.4(a)). Time series processing codes (e.g., TSPROC, *Westenbroek et al., 2012*) automate the processing and evaluation of transient model input and output. Given the magnitude of output generated during a transient simulation, examination is usually restricted to key times important to the modeling purpose when heads, fluxes (Fig. 7.5(c)), and water budgets are examined. Simulated water budgets (Fig. 7.5(b); Fig. 3.12) should be checked to ensure that the solution has converged for the time step examined (Section 3.7). The change in storage reported in the water budget tracks the progress toward steady state; change in storage decreases as the solution approaches steady state and equals zero at steady state (Fig. 3.12).

**Table 7.1** Types of transient calibration data for confined aquifers in a regional model of the Lake Michigan Basin, USA (modified from [Feinstein et al., 2010](#)). Higher observation weights reflect increased importance of the observation in model calibration (Section 9.5)

	Number of observations	Observation weight
<b>Target subset</b>		
<b><i>“Predevelopment”—before 1940</i></b>		
USGS network water levels	11	1
Water levels taken from drillers’ logs	51	0.25
Wisconsin Cambrian–Ordovician head contours	233	0.04
Michigan Pennsylvanian head contours	115	0.04
Michigan Marshall head contours	103	0.04
Indiana miscellaneous water levels	19	0.16
Illinois Cambrian–Ordovician head contours	231	0.04
<b><i>USGS network wells—“historical” water levels</i></b>		
Southern Lower Peninsula, Michigan	1761	0.01–0.04
Northern Lower Peninsula, Michigan	272	0.01
Upper Peninsula, Michigan	426	0.01–0.04
Northeastern Wisconsin	1964	0.01–0.04
Southeastern Wisconsin	1149	0.01–0.04
Northern Indiana	294	0.01
Far-field	2422	0.0025–0.01
<b><i>Northeastern Illinois Cambrian–Ordovician</i></b>		
2000 water-level contours	248	0.01
Drawdown, 1864–2000 contours	248	0.01
Recovery, 1980–2000 contours	267	0.0025–0.01
<b><i>Decadal head changes in USGS network wells</i></b>		
Southern Lower Peninsula, Michigan	1	49
Northeastern Wisconsin	22	1–4
Southeastern Wisconsin	40	1
<b><i>Vertical head differences</i></b>		
USGS network wells	41	0.25–4
USGS RASA packer tests in early 1980s	31	4
<b><i>Baseflow targets at USGS streamgages in 2000</i></b>		
Southern Lower Peninsula, Michigan	17	3.60E–11
Northern Lower Peninsula, Michigan	11	3.60E–11
Upper Peninsula, Michigan	9	3.60E–11
Northeastern Wisconsin	12	3.60E–11
Southeastern Wisconsin	4	3.60E–11
Northern Indiana	3	3.60E–11
Northeastern Illinois	6	3.60E–11
<b>Total</b>	10,011	



## 7.8 COMMON MODELING ERRORS

- A costly transient model is constructed when less expensive bounding steady-state solutions would satisfactorily address the modeling objective.
- Initial conditions for a transient simulation are specified using field-measured heads rather than model-generated initial conditions.
- The spin-up period for a transient simulation is not long enough to overcome erroneous starting initial conditions.
- Simulated outputs from the first time step in a stress period are used for decision-making when the modeling objective requires consideration of the average effect of the stress, or conditions at the end of the stress period.
- Transient effects propagate out to a model boundary represented by a hydraulic boundary condition, and the modeler fails to realize that the computed heads and flows are unreasonable for the field situation being simulated.
- Fewer than six time steps are specified for a stress period when the modeling objective requires good resolution of head changes at the beginning of the stress period.

## 7.9 PROBLEMS

Problems for this chapter explore the effect of the time step on the transient solution. Also, the Hubbertville problem from Chapter 4 (P4.3, P4.4) is revisited, and the effect of pumping the aquifer for 1 year on the discharge to Green Swamp is assessed.

- P7.1** Revisit Problem P6.1b. Use a model with uniform nodal spacing of 100 m to generate dynamic steady-state initial heads and run a transient model with  $S = 3E-5$ . Calculate heads and drawdown after 1 day of continuous pumping.
- a. Make three separate runs using 1, 5, and 10 time steps of uniform length; save the heads at the end of each time step. For each simulation, plot drawdown or heads in a profile that passes through the well; put all profiles on a single graph. Compare and contrast results.
  - b. Run the model with 10 variable length time steps using smaller time steps at early times in a 1-day stress period. Plot a profile of these data on the same graph as prepared previously. What is the effect of using time steps of varying length?
- P7.2** Revisit Problems P4.3 and P4.4 in Chapter 4. The town currently proposes to complete the well and pump it for 1 year to meet emergency demands for water supply. They argue that operation of the well will be a long-term test so that the effect of pumping on discharge to the swamp can be assessed. You are asked to forecast the effects on discharge to the swamp and water table before the town is given permission to start pumping.
- a. Convert the steady-state pumping model in Problem P4.3 into a transient model using  $S_y = 0.1$  and initial heads equal to the steady-state solution

generated without the pumping well. Forecast the head distribution and reduction in flow to the swamp after 1 year of continuous pumping under the average daily recharge rate given in Fig. P4.3. Place an observation well near the groundwater divide. Heads at the observation well should be calculated at the end of each month starting with February and ending with January. Each month is a stress period, each divided into 10 time steps. Prepare a profile of the head distribution for each month and hydrographs for the observation well and pumping well. The profile should be oriented north–south and pass through the pumping node and observation well. How does discharge to Green Swamp change under this set of conditions relative to the discharge computed in Problem P4.3?

- b. Your model and results from Problem P7.2a have been reviewed and it is suggested that your model is inappropriate because you assumed a constant average annual recharge rate. Historical records of water table fluctuations in this valley suggest that the water table rises 2 m each year in early spring and then declines over the rest of the year to a low in January. Estimated monthly average recharge rates are given in Table P7.1. Use dynamic steady-state heads under nonpumping conditions as initial conditions for a transient simulation beginning on January 1. Use the transient model to calculate heads at the end of each month assuming the well is continuously pumped, and recharge fluctuates monthly according to the rates in Table P7.1. Prepare a hydrograph showing fluctuations in head in the observation well and in the pumping well. Also graph simulated monthly head profiles; each profile should pass through the swamp, observation well, pumping well, and river.

**Table P7.1** Estimated average monthly recharge rates for the Hubbertville aquifer

Month	Rate (m/day)
January	0.001
February	0.003
March	0.004
April	0.003
May	0.001
June	0.0005
July	0.00005
August	0.00005
September	0.00005
October	0.00005
November	0.00005
December	0.0005

- c. Compare and contrast the effects on discharge to the Green Swamp as computed in Problems P4.3 (steady state no pumping), P4.4 (steady state pumping well), P7.2a (1 year of pumping with constant average annual recharge), and P7.2b (1 year of pumping with variable recharge). Compare the hydrographs produced in Problems P7.2a and P7.3b. Are your model results intuitive? Why or why not?

## REFERENCES

- Ajami, H., McCabe, M.F., Evans, J.P., Stisen, S., 2014. Assessing the impact of model spin-up on surface water-groundwater interactions using an integrated hydrologic model. *Water Resources Research* 50 (3), 2636–2656. <http://dx.doi.org/10.1002/2013WR014258>.
- Ataie-Ashtiani, B., Volker, R.E., Lockington, D.A., 2001. Tidal effects on groundwater dynamics in unconfined aquifers. *Hydrological Processes* 12, 655–669. <http://dx.doi.org/10.1002/hyp.183>.
- Barlow, P.M., Leake, S.A., 2012. Streamflow depletion by wells—understanding and managing the effects of groundwater pumping on streamflow. U.S. Geological Survey Circular 1376, 84 p. <http://pubs.usgs.gov/circ/1376/>.
- Central Texas Groundwater Conservation District, August 2012. The Hydro Blog. <http://www.centraltexasgcd.org/the-hydro-blog/>.
- Diersch, H.-J.G., 2014. FEFLOW: Finite Element Modeling of Flow, Mass and Heat Transport in Porous and Fractured Media. Springer, 996 p.
- Domenico, P.A., Schwartz, F.W., 1998. *Physical and Chemical Hydrogeology*, second ed. John Wiley & Sons, Inc. 506 p.
- Dripps, W.R., Hunt, R.J., Anderson, M.P., 2006. Estimating recharge rates with analytic element models and parameter estimation. *Groundwater* 44 (1), 47–55. <http://dx.doi.org/10.1111/j.1745-6584.2005.00115.x>.
- Feinstein, D.T., Hunt, R.J., Reeves, H.W., 2010. Regional Groundwater-Flow Model of the Lake Michigan Basin in Support of Great Lakes Basin Water Availability and Use Studies. U.S. Geological Survey Scientific Investigations Report 2010–5109, 379 p. <http://pubs.usgs.gov/sir/2010/5109/>.
- Franke, O.L., Reilly, T.E., Bennett, G.D., 1987. Definition of Boundary and Initial Conditions in the Analysis of Saturated Ground-Water Flow Systems—An Introduction. U.S. Geological Survey Techniques of Water-Resources Investigation 03–B5, 15 p. <http://pubs.usgs.gov/twri/twri3-b5/>.
- Gannett, M.W., Wagner, B.J., Lite Jr., K.E., 2012. Groundwater Simulation and Management Models for the Upper Klamath Basin, Oregon and California. U.S. Geological Survey Scientific Investigations, Report 2012-5062, 92 p. <http://pubs.usgs.gov/sir/2012/5062/>.
- Haitjema, H.M., 1995. *Analytic Element Modeling of Groundwater Flow*. Academic Press, Inc., San Diego, CA, 394 p.
- Haitjema, H., 2006. The role of hand calculations in ground water flow modeling. *Groundwater* 44 (6), 786–791. <http://dx.doi.org/10.1111/j.1745-6584.2006.00189.x>.
- Kasmarek, M.C., 2012. Hydrogeology and Simulation of Groundwater Flow and Land-Surface Subsidence in the Northern Part of the Gulf Coast Aquifer System, Texas, 1891–2009 (ver. 1.1, December 2013). U.S. Geological Survey Scientific Investigations Report 2012–5154, 55 p. <http://dx.doi.org/sir20125154>.
- Lemieux, J.-M., Sudicky, E.A., Peltier, W.R., Tarasov, L., 2008. Simulating the impact of glaciations on continental groundwater flow systems: 2. Model application to the Wisconsinian glaciation over the Canadian landscape. *Journal of Geophysical Research* 113, F03018. <http://dx.doi.org/10.1029/2007JF000929>.
- Maddock III, T., Vionnet, L.B., 1998. Groundwater capture processes under a seasonal variation in natural recharge and discharge. *Hydrogeology Journal* 6 (1), 24–32. <http://dx.doi.org/10.1007/s100400050131>.
- Marsily, G. de, 1986. *Quantitative Hydrogeology*. Academic Press, 440 p.

- Prickett, T.A., Lonquist, C.G., 1971. Selected Digital Computer Techniques for Groundwater Resource Evaluation. Illinois Water Survey Bulletin 55, Champaign, IL, 62 p.
- Reeves, H.W., 2010. Water Availability and Use Pilot—A Multiscale Assessment in the U.S. Great Lakes Basin. U.S. Geological Survey Professional Paper 1778, 105 p. <http://pubs.usgs.gov/pp/1778/>.
- Reilly, T.E., Harbaugh, A.W., 2004. Guidelines for Evaluation Ground-Water Flow Models. U.S. Geological Survey Scientific Investigations Report 2004—5038, 30 p. <http://pubs.usgs.gov/sir/2004/5038/>.
- Scott, D., Thorley, M., 2009. Steady-State Groundwater Models of the Area Between the Rakaia and Waimakariri Rivers. Environment Canterbury, New Zealand, ISBN 978-1-86937-940-7. Report R09/20, 37 p.
- Snyder, D.T., 2008. Estimated Depth to Ground Water and Configuration of the Water Table in the Portland, Oregon Area. U.S. Geological Survey Scientific Investigations Report 2008—5059, 40 p. <http://pubs.usgs.gov/sir/2008/5059/>.
- Taylor, C.J., Alley, W.M., 2001. Ground-water-level monitoring and the importance of long-term water-level data. U.S. Geological Survey Circular 1217, 68 p. <http://pubs.usgs.gov/circ/circ1217/>.
- Torak, L.J., 1993. A Modular Finite-Element Model (MODFE) for Areal and Axisymmetric Ground-Water-Flow Problems: 3. Design and Philosophy and Programming Details. U.S. Geological Survey Techniques of Water Resources Investigations. Chapter A5 Book 6, 243 p. <http://pubs.usgs.gov/twri/twri6a5/>.
- Townley, L.R., 1995. The response of aquifers to periodic forcing. *Advances in Water Resources* 18 (3), 125–146. [http://dx.doi.org/10.1016/0309-1708\(95\)00008-7](http://dx.doi.org/10.1016/0309-1708(95)00008-7).
- Townley, L.R., Wilson, J.L., 1980. Description of an User's Manual for a Finite Element Aquifer Flow Model AQUIFEM-1. MIT Ralph M. Parsons Laboratory for Water Resources and Hydrodynamics, Technology Adaptation Program Report No. 79—3, 294 p.
- Wang, H.F., Anderson, M.P., 1982. Introduction to Groundwater Modeling: Finite Difference and Finite Element Methods. Academic Press, San Diego, CA, 237 p.
- Westenbroek, S.M., Doherty, J.E., Walker, J.F., Kelson, V.A., Hunt, R.J., Cera, T.B., 2012. Approaches in highly parameterized inversion: TSPROC, a general time-series processor to assist in model calibration and result summarization. U.S. Geological Survey Techniques and Methods, 7—C7, 73 p. <http://pubs.usgs.gov/tm/tm7c7/>.
- Zheng, C., Wang, P.P., 1999. MT3DMS: A Modular 3-D Multi-species Transport Model for Simulation of Advection, Dispersion and Chemical Reactions of Contaminants in Groundwater Systems; Documentation and User's Guide. Contract Report SERDP-99—1. U.S. Army Engineer Research and Development Center, Vicksburg, MS, 169 pp.
- Zucker, M.B., Remson, I., Ebert, J., Aguado, E., 1973. Hydrologic studies using the Boussinesq equation with a recharge term. *Water Resources Research* 9 (3), 586–592. <http://dx.doi.org/10.1029/WR009i003p00586>.



## CHAPTER 8

# Particle Tracking

*As many fresh streams meet in one salt sea;  
As many lines close in the dial's centre;  
So may a thousand actions, once afoot,  
End in one purpose, and be all well borne  
Without defeat.*

*Henry V, Act I*

### Contents

8.1 Introduction	331
8.2 Velocity Interpolation	338
8.2.1 Effect of Spatial Discretization	338
8.2.2 Effect of Temporal Discretization	340
8.2.3 Interpolation Methods	341
8.3 Tracking Schemes	346
8.3.1 Semianalytical Method	347
8.3.2 Numerical Methods	348
8.4 Weak Sinks	349
8.5 Applications	351
8.5.1 Flow System Analysis	357
8.5.2 Capture Zones and Contributing Areas	358
8.5.3 Advective Transport of Contaminants	363
8.6 Particle Tracking Codes	364
8.7 Common Errors in Particle Tracking	365
8.8 Problems	366
References	370

### Boxes

Box 8.1 Effective Porosity	332
Box 8.2 Flow Nets	335
Box 8.3 More on Capture Zones and Contributing Areas	360

Particle tracking (PT) is a postprocessing tool for calculating flowpaths and travel times, both of which may be used as calibration targets (Section 9.3). PT is also used for representing the advective transport of solutes, including contaminants.

## 8.1 INTRODUCTION

A particle tracking (PT) code is a postprocessor for a groundwater flow model that calculates the velocity field and tracks the movement of imaginary particles through the model domain. A PT code takes the computed head distribution and hydraulic conductivities from a groundwater flow model and, with the addition of user-specified values of effective porosity (Box 8.1), calculates velocities at nodal points of the grid/mesh (Fig. 8.1).

### Box 8.1 Effective Porosity

Particle tracking (PT) requires values of effective porosity,  $n$ , to calculate groundwater velocity (Eqn (8.1)). Effective porosity is a relatively simple concept but is difficult to define quantitatively. Only selected aspects of effective porosity pertinent to PT are discussed in this box. For additional information, the reader is referred to [Zheng and Bennett \(2002, pp. 56–57; pp. 16–17\)](#) and [Stephens et al. \(1998\)](#).

Effective porosity can be qualitatively defined as the ratio of the volume of interconnected pore volume available for flow to the total volume of porous material. Then, by definition, effective porosity is smaller than total porosity, which is the ratio of total pore volume to total volume of porous material. Total porosity can be measured in the laboratory or estimated from grain size analysis (e.g., [Frings et al., 2011](#)) and many tabulations are available (e.g., [Kresic, 2007, Appendix C, pp. 767–775](#)). Effective porosity can also be measured in the laboratory using column experiments, but conclusions based on experimental results are contradictory and ambiguous. For example, in experiments conducted by [van der Kamp et al. \(1996\)](#), values of effective porosity were dependent on the type of tracer. They attributed the differences in measurements to “phenomena such as ion exclusion, enclosed pores, and bound water” (p. 1821). They also found that in some experiments effective porosity was greater than their measured values of total porosity. In practice, it is customary to use effective porosity to represent both total and effective porosity for all types of porous material rather than define two different porosity values (Zheng and Bennett, p. 57). This assumption is most likely to be valid for sand aquifers.

Ideally, effective porosity ( $n$ ) is determined from a field tracer test performed at the site being modeled. Then,  $n$  is calculated from the following equation:

$$n = \frac{q}{v} = \frac{KI}{v} \quad (\text{B8.1.1})$$

where  $q$  is specific discharge,  $K$  is hydraulic conductivity,  $I$  is hydraulic gradient, and velocity,  $v$ , is the ratio of distance to time of travel of the tracer. [Gelhar et al. \(1992\)](#) tabulated values of effective porosity estimated from field tracer tests for a variety of aquifers ([Table B8.1.1](#)). Values for unconsolidated sediments range from around 0.40 (alluvial sediments; fine sand, and glacial till) to 0.004 (layered medium sand) and from 0.60 (fractured dolomite and limestone) to 0.005 (fractured chalk) for rock.

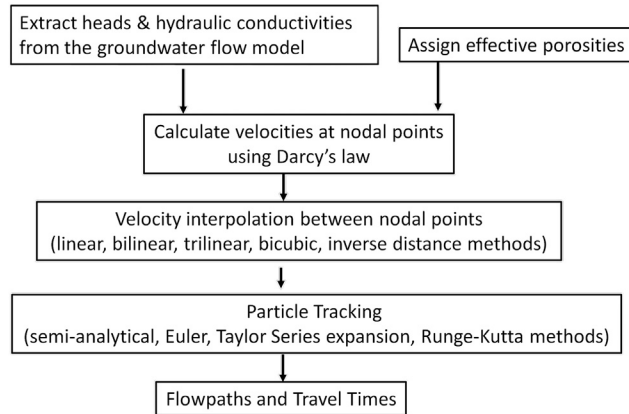
However, tracer tests are rarely performed in practice. Rather, effective porosity is estimated as some fraction of total porosity, taken from literature values such as those in [Table B8.1.1](#), or estimated during model calibration. In applied groundwater modeling, effective porosity is typically best described as the number required to achieve agreement with observations of travel times ([Zheng and Bennett, 2002, p. 17](#)).

### Box 8.1 Effective Porosity—cont'd

**Table B8.1.1** Values of effective porosity from field tracer tests compiled by [Gelhar et al. \(1992\)](#)  
**Unconsolidated material** **Effective porosity**

Gravel with cobbles	0.22
Gravel	0.17
Gravel, sand, and silt	0.38
Very heterogenous sand and gravel	0.35
Glaciofluvial sand and gravel (2 different tests)	0.10; 0.07–0.40
Glaciofluvial sand (3 different tests)	0.38
Glacial outwash	0.35
Sand and gravel	0.32
Sand, gravel, and silt (2 different tests)	0.25
Sand and gravel with clay lenses	0.30
Fine sand and glacial till	0.40
Medium to coarse sand with some gravel	0.39
Sand, silt, and clay	0.25
Medium to fine sand with clay and silt	0.25
Layered medium sand	0.004
Sand (3 different sites)	0.24; 0.35; 0.38
Sand and sandstone with some silt and clay	0.23
Alluvium (2 different sites)	0.30; 0.40
Alluvium (gravels)	0.22
Alluvium (clay, silt, sand, and gravel)	0.20
Clay, sand, and gravel (4 different tests)	0.021–0.24
<b>Rock</b>	
Sandstone	0.32–0.48
Limestone (3 different sites)	0.12; 0.23; 0.35
Dolomite	0.034
Chalk	0.023
Fractured limestone	0.01
Fractured limestone and calcareous sandstone	0.25
Fractured dolomite (4 different sites)	0.007, 0.11; 0.024; 0.12; 0.18
Fractured dolomite and limestone	0.06–0.60
Fractured chalk	0.005
Fractured granite	0.02–0.08
Basaltic lava and sediments (2 different tests)	0.10



**Figure 8.1** Workflow of the particle tracking process.

Nodal velocities are interpolated to other points in the flow field and imaginary particles are introduced and tracked in continuous space to delineate flowpaths. A PT code keeps track of the locations of all particles, removing particles that enter internal sinks (e.g., wells) or exit through perimeter boundaries. In two-dimensional, steady-state problems with no areal recharge, flowpaths are streamlines (Section 3.4) and when superimposed over equipotential lines may form a *flow net* but only under certain conditions (Box 8.2). In practice, flow nets alone are too limited for applied groundwater modeling. The modeler should be alert to the difference between flow nets, which are valid only under restrictive conditions (see Boxes 8.2 and 5.2), and flowpaths produced by PT, which can be calculated from output of any groundwater model, even the most complex.

During PT, particles are moved according to the average linear velocity of groundwater ( $\mathbf{v}$ )

$$\mathbf{v} = -\frac{\mathbf{K}}{n}(\mathit{grad} \ h) \quad (8.1)$$

where  $\mathbf{v}$  is a vector;  $\mathbf{K}$  is the hydraulic conductivity tensor (Section 3.2, Box 3.2),  $\mathit{grad} \ h$  is the gradient of  $h$ , a vector, and  $n$  is effective porosity (Box 8.1).

Most graphical user interfaces (GUIs) include an option to postprocess results from a groundwater flow model to produce a display of velocity vectors in both map (Fig. 8.2(a)) and cross-sectional views. General flow directions can be inferred from these graphics, but they do not represent flowpaths. The modeler should examine maps of velocity vectors, but should also perform PT to help visualize groundwater flow. Tracking particles from boundary cells or elements produces a picture of flowpaths from initial starting position to discharge location (Fig. 8.2(b)). Flowpaths should be compared with flowlines generated for the conceptual model (Section 2.3); any

## Box 8.2 Flow Nets

In introductory hydrogeology classes, groundwater flow is often visualized in a flow net (e.g., Fig. B8.2.1; Fig. B5.2.1 in Box 5.2) and students are required to construct a flow net as a learning exercise. Flow nets are rarely used in applied groundwater modeling, however, because they require overly restrictive simplifying assumptions. We discuss flow nets in this box in order to alert the reader to the difference between the restrictive concept of a flow net and the general nature of flowpaths in particle tracking.

A plot of streamlines and equipotential lines may form a flow net (Fig. B8.2.1), but these plots are limited to cases of two-dimensional, steady-state flow in an aquifer with no recharge. The streamfunction,  $\psi$ , (Section 3.4) defines streamlines just as a solution for head defines equipotential lines. Under homogenous and isotropic conditions, streamlines and equipotential lines intersect at right angles and form curvilinear squares (Fig. B8.2.1). For anisotropic media, coordinate transformation (Box 5.2) allows streamlines to be drawn at right angles to equipotential lines in a transformed section and then the flow net can be transformed back to the true coordinates (see Fig. B5.2.1 in Box 5.2). Flow nets can also be constructed for heterogeneous aquifers where hydraulic conductivity is piecewise constant (e.g., Fig. B8.2.2).

Flow nets can be drawn by hand by contouring field-measured heads and then drawing streamlines at right angles to equipotential lines. However, field-based flow nets are only valid for the restrictive conditions that apply to all flow nets, as discussed above. Flow nets can also be generated using analytical (e.g., Newsom and Wilson, 1988) and numerical (e.g., Bramlett and Borden, 1990) solutions. By contouring  $\psi$ , a set of streamlines is produced that can be superimposed over a set of equipotential lines to create a flow net. Analytical models that generate flow nets are limited to simple problems. Numerical models produce flow nets for more complex problems involving heterogeneous (in piecewise constant  $K$  zones) and anisotropic aquifers (Fig. B8.2.2). However, all flow nets are limited to two-dimensional, steady-state flow with no recharge.

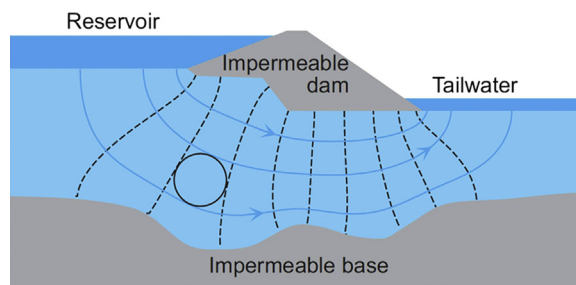
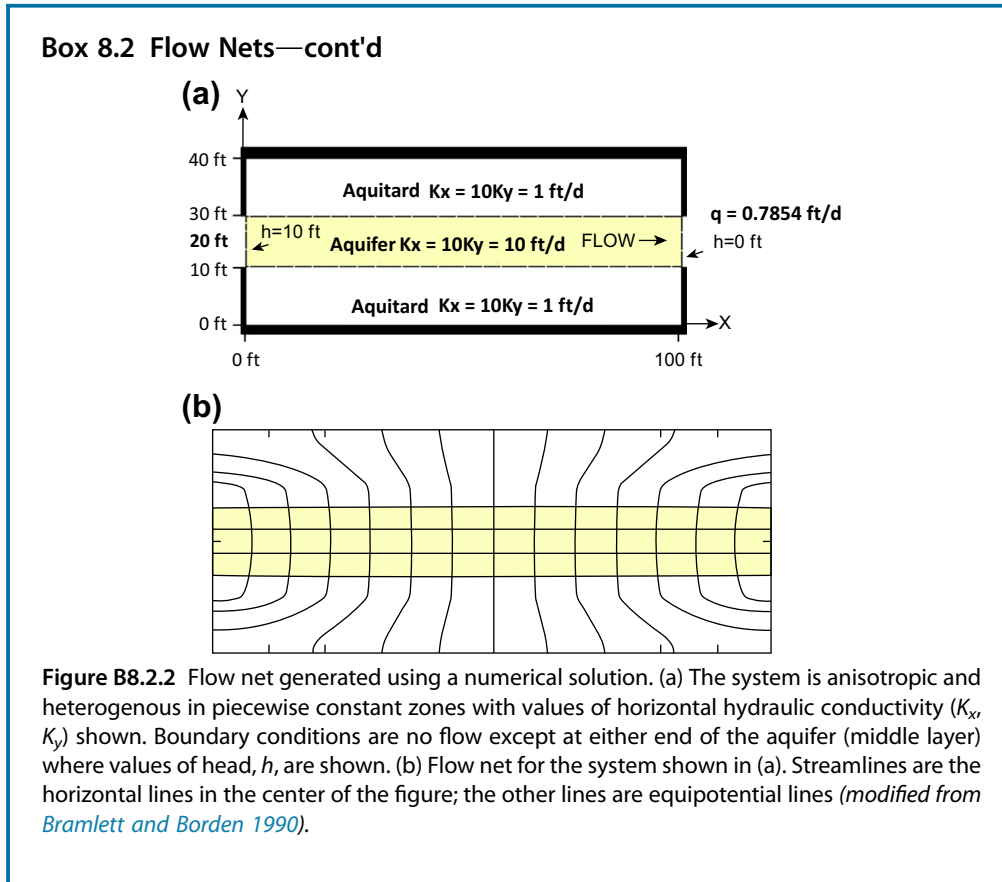


**Figure B8.2.1** Schematic flow net with equipotential lines of constant head (dashed lines) and streamlines (blue lines with arrowheads) representing constant values of the streamfunction,  $\psi$ . If the contour interval of  $\psi$  is constant, the flow rate,  $\Delta Q$  ( $L^3/T$ ), through a streamtube is constant and can be calculated (see Section 3.4, Eqn (3.21)) (Fitts, 2013).

(Continued)



inconsistencies should be resolved before attempting to calibrate the model. Sometimes flowpath visualization helps identify conceptual errors in the groundwater flow model that were not evident from the head distribution. PT can help the modeler identify recharge and discharge areas; contributing areas to rivers, lakes, and springs and capture zones of pumping wells; and assess the effects of partially penetrating wells and streams. PT codes also compute the travel time of each particle. Travel times provide a rough approximation of groundwater age (i.e., the residence time of a parcel of groundwater in the flow system), which reflects time since the sampled water entered the groundwater system. PT is also helpful in model calibration especially when flowpaths are used as calibration criteria (e.g., Reynolds and Marimuthu, 2007; Hunt et al., 2005).

PT represents the *advective transport* of solutes (including contaminants). Advective transport is the movement of solute calculated solely from the average linear velocity

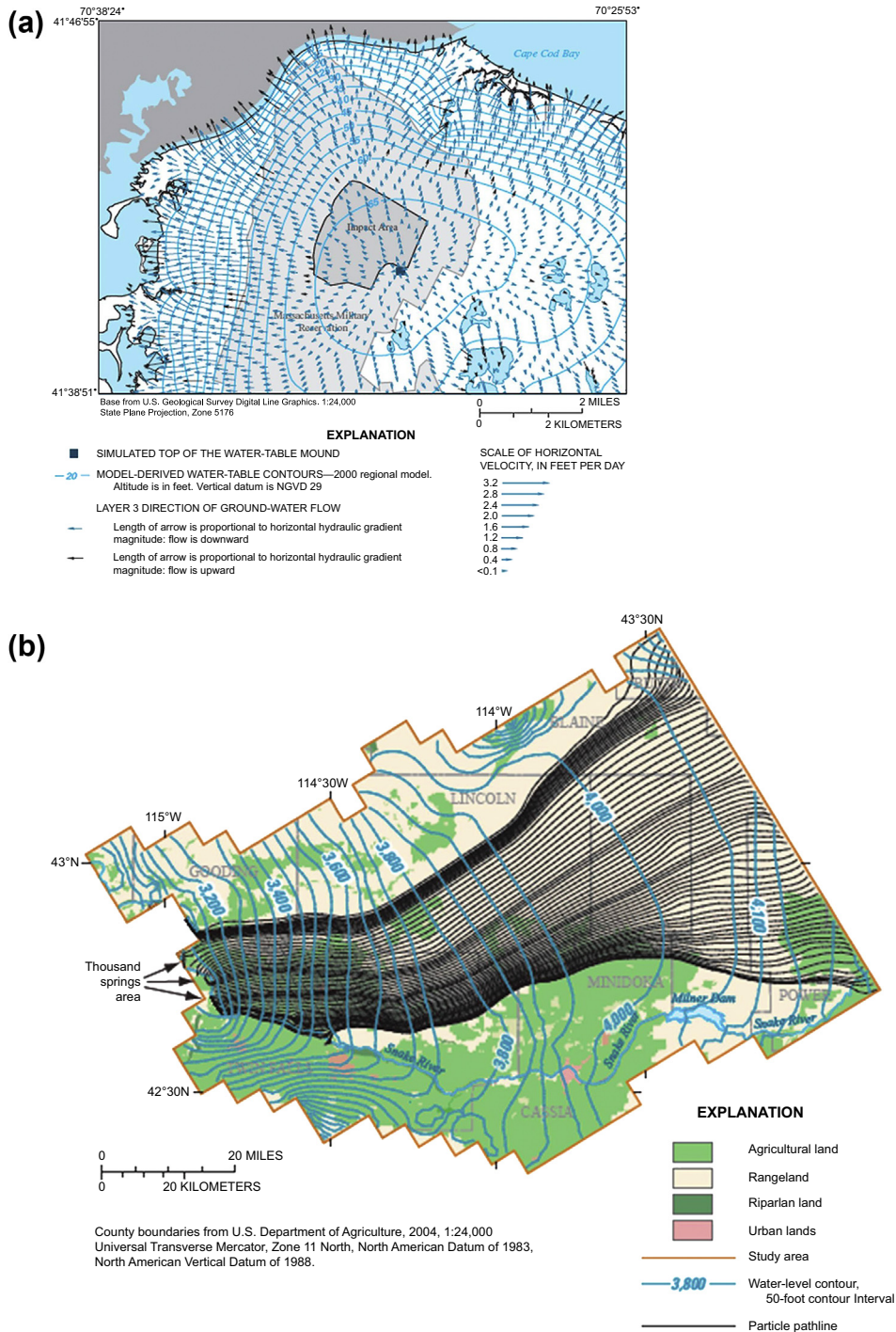


**Figure 8.2** Velocities and flowpaths. (a) Simulated horizontal groundwater velocity vectors around a water table mound (*Walter and Masterson, 2003*); (b) Flowpaths produced by a particle tracking code originate at a boundary and discharge to a large group of springs at the Snake River, South Central Idaho, USA (*Skinner and Rupert, 2012*).

of groundwater (Eqn (8.1)). In PT, the particles represent the solute. If the solute is chemically nonreactive, particles are transported following the average linear velocity. Linear chemical adsorption can be represented by decreasing the particle velocity using a retardation factor ( $R_d$ ) appropriate to the particular solute being simulated;  $R_d$  is discussed in more detail in Section 8.5. Standard PT codes can simulate linear chemical adsorption but do not simulate more complex chemical reactions or dispersion of the solute. Because dispersion is not represented, travel times computed in PT do not represent the first arrival of a solute at a receptor; instead they approximate the travel time of the center of mass of a solute plume. If dispersion and/or complex chemical reactions are important, a solute transport model based on the advection–dispersion equation is required (Section 12.3). But for many problems, advective transport with PT is an adequate approximation of solute transport.

There are two parts to PT: velocity interpolation and tracing flowpaths by tracking particles. Differences among PT codes relate to the different procedures used for interpolation and tracking. Brief overviews of velocity interpolation and tracking methods are given in Sections 8.2 and 8.3, respectively. Only the basics of PT are presented in this chapter; the reader is referred to Chapter 6 of Zheng and Bennett (2002) for a more detailed presentation of PT theory.

## 8.2 VELOCITY INTERPOLATION

### 8.2.1 Effect of Spatial Discretization

PT uses the discretization, hydraulic conductivities, and simulated heads of the groundwater flow model (Fig. 8.1). Therefore, the accuracy of computed flowpaths is a function of the accuracy of the head distribution calculated by the flow model. When velocities vary greatly in space, finer nodal spacing will generate a more accurate velocity distribution for PT (Fig. 8.3). Spatial variations in velocity are caused by spatial variation in hydraulic gradients, such as around sources/sinks, spatial variation in hydraulic conductivity (Fig. 8.4; Fig. B4.1.3 in Box 4.1), and spatial variation in effective porosity. Fine nodal spacing may not be necessary for the objectives of the groundwater flow model itself, but may be required for PT to produce accurate delineation of flowpaths (Haitjema et al., 2001), contributing areas and well capture zones (Fig. 8.4; Fig. B4.1.3 in Box 4.1), and for calculation of travel times. For accurate PT, the guidelines for horizontal nodal spacing presented in Section 5.2 and Box 6.1 and the guidelines for model layers in Section 5.3 should be observed.

Other aspects of spatial discretization that cause problems in PT involve quasi-3D models and fully 3D models that use distorted layers. PT should not be done for quasi-3D models (Section 4.1.2; Fig. 4.6) because the omission of the physical space that represents confining beds from the grid/mesh of the groundwater flow model causes problems in velocity interpolation and particle tracking. Heads are not calculated within

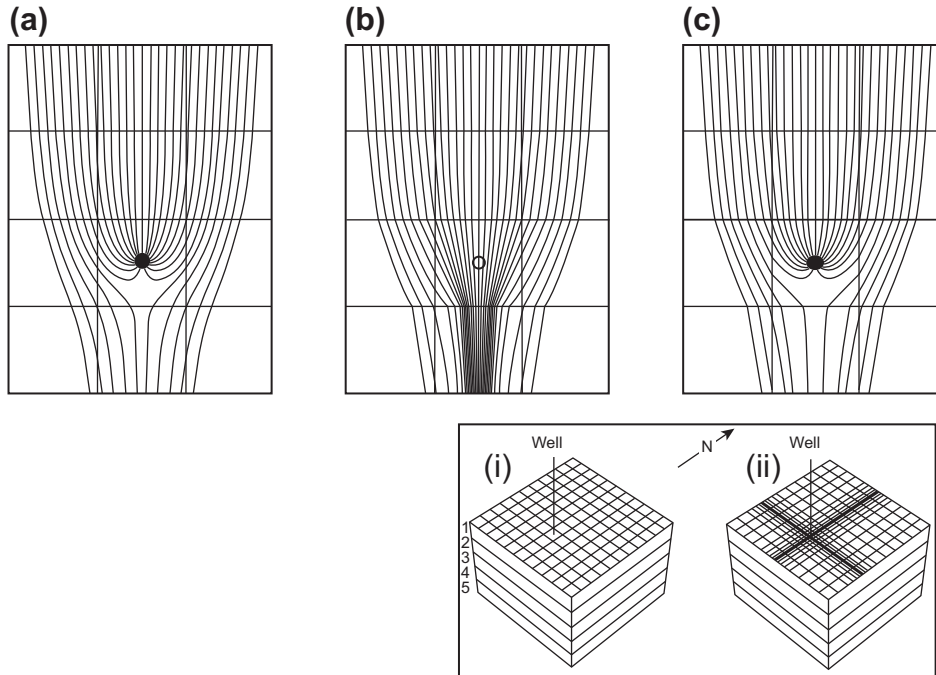


**Figure 8.3** Comparison of flowpaths associated with a weak sink (pumping well) in a 5-layer model; the well is in layer 3. Flow is from top to bottom of the figures with forward tracking of particles. In the boxed inset at the bottom of the figure: (i) the coarse grid is 500 ft by 500 ft in the horizontal dimension and has 10-ft spacing in the vertical dimension; (ii) the fine grid has 10-ft spacing in the cell containing the well. (a) Flowpaths in the finely discretized grid ((ii) in the inset); (b) Flowpaths in the coarse grid ((i) in the inset) showing that all flow bypasses the well (i.e., no particles are captured by the well); (c) Flowpaths in the coarse grid but with a velocity refinement procedure (Zheng, 1994).

confining beds of a quasi-3D model; hence, velocities computed from output of the flow model are not representative of velocities in the groundwater flow system. Furthermore, because the grid/mesh does not include the physical space occupied by confining beds, flowpaths are not represented correctly in a quasi-3D model and therefore travel times cannot be accurately computed.

Distorted layers, which are frequently used in three-dimensional models (Section 5.3; Fig. 5.20), also can cause problems (Zheng, 1994). The thickness of a distorted layer varies in space so that the top and bottom elevations of the layer do not align with the orthogonal coordinate system assumed in PT, causing errors in velocity interpolation and PT (and also in the solution of the groundwater flow equation, Section 5.3). Therefore, whenever possible, layers should be of uniform thickness (i.e., each layer has a constant  $\Delta z$ ) when PT is important to the modeling objective. If distorted layers are unavoidable, a correction procedure for tracking performed using the Euler integration and Runge-Kutta methods (Section 8.3) is available (Zheng, 1994) and is implemented in some PT codes (e.g., PATH3D by Zheng, 1989; Section 8.6).

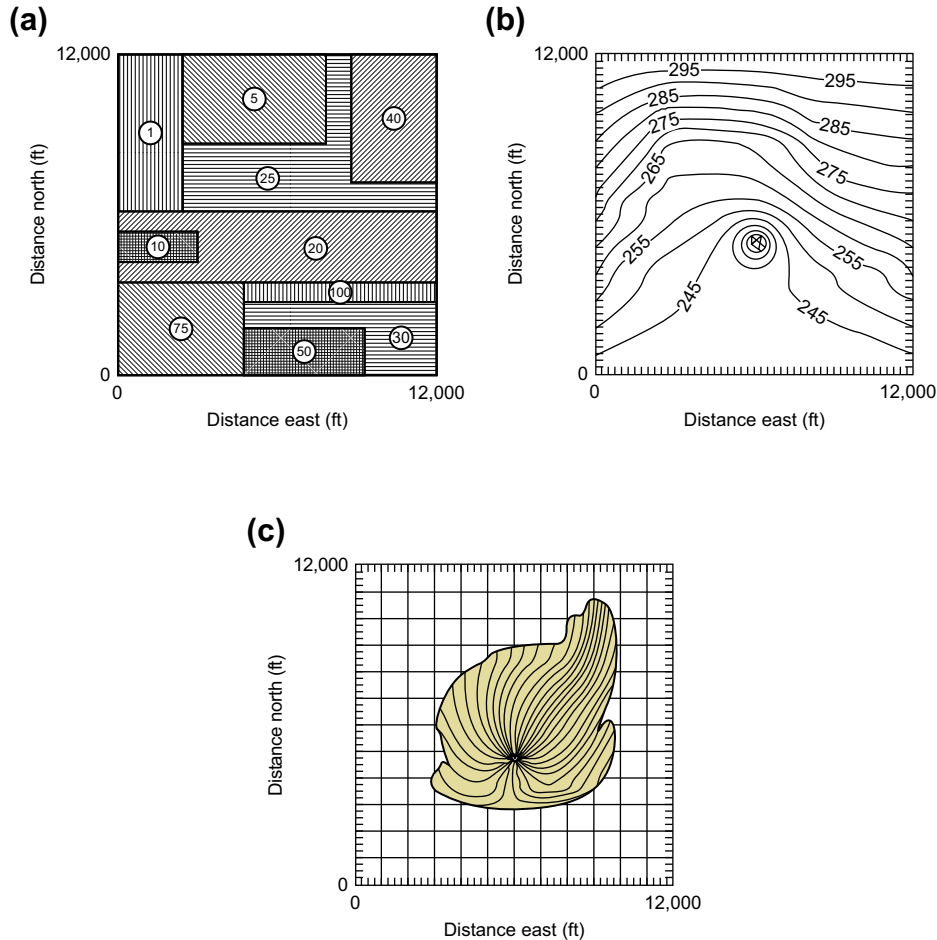


**Figure 8.4** Capture zone for a well pumping a heterogeneous aquifer. (a) Zoned hydraulic conductivity ( $K$ ) distribution where circled numbers are values of  $K$  in ft/day; (b) Potentiometric surface; (c) 20-year capture zone (modified from Shafer, 1987).

### 8.2.2 Effect of Temporal Discretization

In steady-state flow, velocities are calculated only once and remain constant throughout PT. In transient PT, velocities are calculated at designated times. Heads computed at the end of a time step are used to calculate velocities during that time step (Fig. 8.5). Zheng and Bennett (2002, p. 135) note that this approach is like assuming that each time step represents steady-state velocity conditions and "...is generally adequate as long as the head change between successive time steps is not dramatic." The groundwater system time constant,  $T^*$ , and the aquifer response time,  $\tau$ , (Eqns (7.1) and (7.2)) can help the modeler decide whether to use a steady-state or transient model (Section 7.2). Under

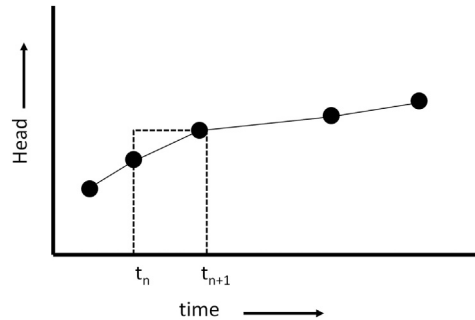


**Figure 8.5** Velocity interpolation for a transient simulation uses the ending head distribution of a time step to calculate a velocity field for particle tracking to represent conditions during that time step. In other words, the head distribution at  $t_{n+1}$  represents heads (and associated velocities) between  $t_n$  and  $t_{n+1}$ .

transient conditions, velocities fluctuate under field conditions and accurate PT depends on the time discretization of the groundwater flow model (Section 7.6). If the time step in the groundwater flow model is too long, the calculated heads and resultant velocities will poorly represent heads and velocities during the time step. In that case, one approach is to compute intermediate velocities during a time step for use in PT by interpolating heads with respect to time. Intermediate velocities are calculated from the heads at the beginning and end of the time step so that the velocity field varies during the time step for the purposes of PT. PT results obtained by interpolating velocities within a time step closely approximate results obtained using constant velocities within smaller time steps (Zheng and Bennett, 2002). However, using either procedure (interpolating velocities within time steps or smaller time steps in the groundwater flow model) increases computational effort.

Rayne et al. (2013) recommended that particles in a transient PT simulation be released continuously at all time steps of all stress periods rather than released only at the beginning of the simulation. The resulting capture zone (Fig. 8.6(a)) can be quite different from the capture zone produced when particles are introduced only at one time period (Fig. 8.6(b)). Capture zones produced from continuous release of particles (e.g., Fig. 8.6(a)) are likely to provide a better representation of field conditions. Therefore, a general recommendation for transient PT is to release particles at all time steps of all stress periods.

### 8.2.3 Interpolation Methods

Heads at nodal points are computed by the groundwater flow model and used in Eqn (8.1) to compute velocities at each nodal point (Fig. 8.7). In a PT code, particles are moved in continuous space so velocities are needed at locations throughout the model



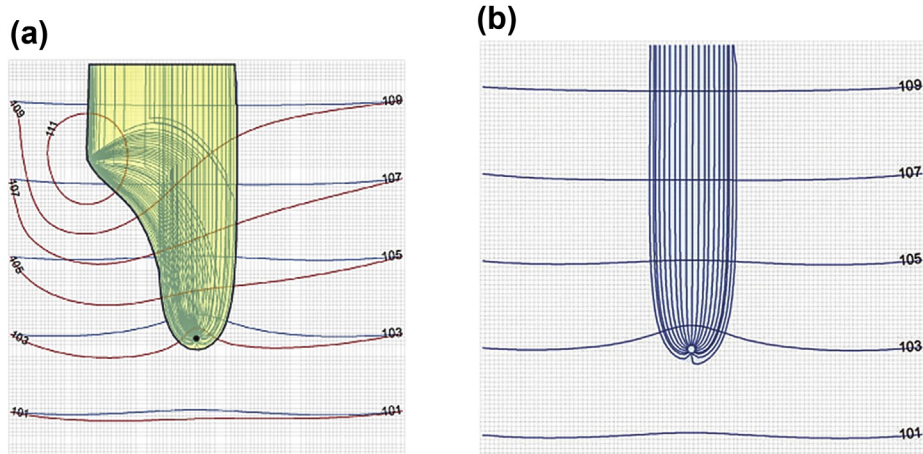


**Figure 8.6** Capture zone for a transient simulation in a homogenous confined aquifer where the pumping rate is constant but recharge varies with space and time; there are four stress periods of four time steps each. (a) The correct capture zone (yellow shading) for the pumping well (black dot) defined by flowpaths generated by back tracking particles released at the pumping well at all time steps. Flowpaths (green lines) are shown only for the last time step of each stress period. Contour lines of head are shown for stress period 4 (blue lines) and stress period 2 (red lines). (b) Incorrect capture zone (blue shading) defined by reverse tracking of particles released only at the beginning of the PT simulation (i.e., at the last time step of the last stress period of the groundwater flow model) (Rayne et al., 2013).

domain and not just at the nodal points. Interpolation schemes are used to compute components of the velocity vector,  $v_x$ ,  $v_y$ ,  $v_z$ , at particle locations, which rarely coincide with nodal locations.

Typically, linear, bilinear, or trilinear interpolation schemes are used for rectangular finite-difference (FD) cells and quadrilateral elements (transformed to rectangular elements), although other schemes such as bicubic interpolation are sometimes used (Shafer, 1990; Zheng and Bennett, 2002). Triangular finite elements (FE) require a slightly different interpolation approach as is discussed at the end of this section. Painter et al. (2012, 2013), Muffels et al. (2014), and Pollock (2015) described the challenges of developing an interpolation method to represent the velocity field in unstructured grids.

A linear interpolation formula for  $v_x$ , for example, is a function of changes in  $v_x$  in the  $x$ -direction only

$$v_x = (1 - f_x)v_{x(i-1/2,j)} + f_x v_{x(i+1/2,j)} \quad (8.2)$$

where  $f_x = (x_p - x_{i-1/2,j})/\Delta x_{i,j}$  and  $x_p$  is the  $x$ -coordinate of the particle (Fig. 8.7). Similar equations can be written for  $v_y$  and  $v_z$ .

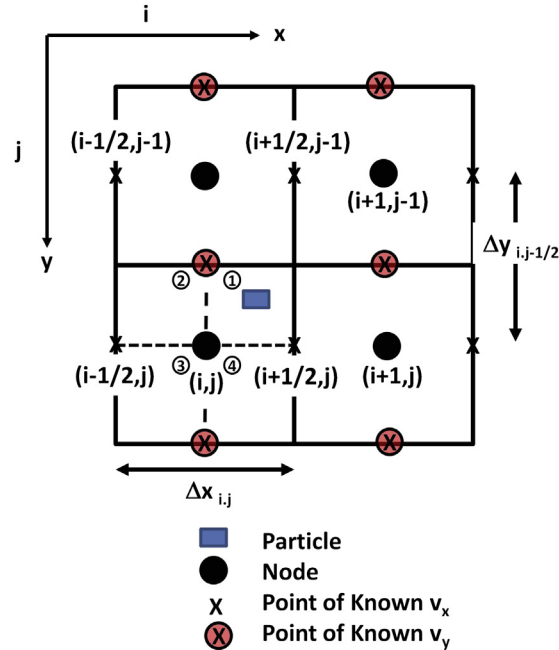


**Figure 8.7** A portion of a finite-difference grid showing the locations of nodes and internalnodal positions (shown by x's), where velocity components  $v_x$  and  $v_y$  are calculated. The quadrants (circled and numbered) associated with node  $(i, j)$  are used in bilinear interpolation of velocities.

In two-dimensional PT, *bilinear interpolation* considers linear changes in velocity in two directions for each velocity component. Each cell/element is divided into four quadrants (Fig. 8.7). The usual bilinear interpolation formula for  $v_x$  for a point in quadrant 1 is as follows:

$$v_x = (1 - F_y)[(1 - f_x)v_{x(i-1/2, j-1)} + f_x v_{x(i+1/2, j-1)}] + F_y[(1 - f_x)v_{x(i-1/2, j)} + f_x v_{x(i+1/2, j)}] \quad (8.3)$$

where  $F_y = (y_p - y_{i, j-1})/\Delta y_{i, j-1/2}$ .

Equation (8.3) is best understood if the calculation is done in three steps:

Step 1. An intermediate value of velocity is calculated using the two  $v_x$  values closest to the particle (Fig. 8.7):

$$(v_x)_1 = (1 - f_x)v_{x(i-1/2, j)} + f_x v_{x(i+1/2, j)}$$

Step 2. Another intermediate value of velocity is calculated using the next two nearest  $v_x$  values.

$$(v_x)_2 = (1 - f_x)v_{x(i-1/2, j-1)} + f_x v_{x(i+1/2, j-1)}$$

Step 3. The final value of  $v_x$  is calculated using the values from steps 1 and 2.

$$v_x = F_y(v_x)_1 + (1 - F_y)(v_x)_2.$$

An equation similar to Eqn (8.3) is written for  $v_y$ . Equations for the other three quadrants are analogous. In three-dimensions, a trilinear scheme is used and  $v_x$ ,  $v_y$  and  $v_z$  are interpolated between two adjacent layers.

In a linear interpolation scheme,  $v_x$  is continuous along the  $x$ -axis but discontinuous along other axes. Similarly  $v_y$  and  $v_z$  are continuous along their respective axes. Linear interpolation satisfies the continuity equation (Eqn (3.2)). Bilinear and trilinear interpolation generate continuous velocity fields but do not preserve discontinuities in velocity at boundaries between units of different hydraulic conductivity and do not conserve mass within a cell/element. Goode (1996) observed that the ideal interpolation scheme should give smoothly varying velocities where hydraulic properties vary smoothly but discontinuous velocities at media boundaries. He proposed an interpolation scheme that combines linear and bilinear interpolation.

*Inverse distance interpolation* (Fig. 8.8) is another type of bilinear interpolation. Like standard bilinear interpolation (Eqn (8.3)), it incorporates linear changes in both directions of a two-dimensional problem domain

$$v_x = \left( \sum_{m=1}^4 (v_x)_m / (r_x)_m \right) / \sum_{m=1}^4 (1/r_x)_m \quad (8.4a)$$

$$v_y = \left( \sum_{m=1}^4 (v_y)_m / (r_y)_m \right) / \sum_{m=1}^4 (1/r_y)_m \quad (8.4b)$$

where  $(r_x)_m$  and  $(r_y)_m$  are the distances of the particle from the four nearest locations of known velocity (i.e., at nodal points) (Fig. 8.8).

Triangular elements, often used in FE codes, require a different interpolation approach (Fig. 8.9). Heads at nodes generated by an FE flow model are used with defined element basis or weighting functions (interpolation functions) to calculate heads at any location within an element. Derivatives of the element heads are used to define local gradients and velocity components are computed from the local gradients, element hydraulic conductivity values, and an assigned effective porosity:

$$v_x^e(x, y) = -K_x^e \partial h^e(x, y) / (n^e \partial x) \quad (8.5a)$$

$$v_y^e(x, y) = -K_y^e \partial h^e(x, y) / (n^e \partial y) \quad (8.5b)$$

where  $v_x^e(x, y)$  and  $v_y^e(x, y)$  are the velocity components at a point,  $(x, y)$ ;  $K_x^e$  and  $K_y^e$  are components of the element hydraulic conductivity;  $h^e$  is the head at a point  $(x, y)$  in the element; and  $n^e$  is the effective porosity of the material within the element (Zheng and Bennett, 2002).

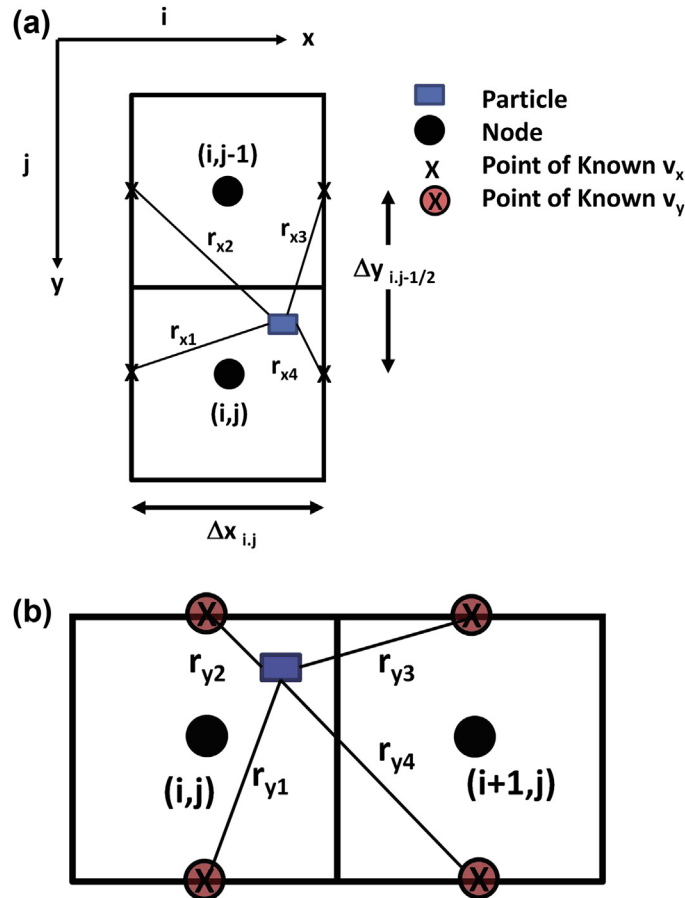
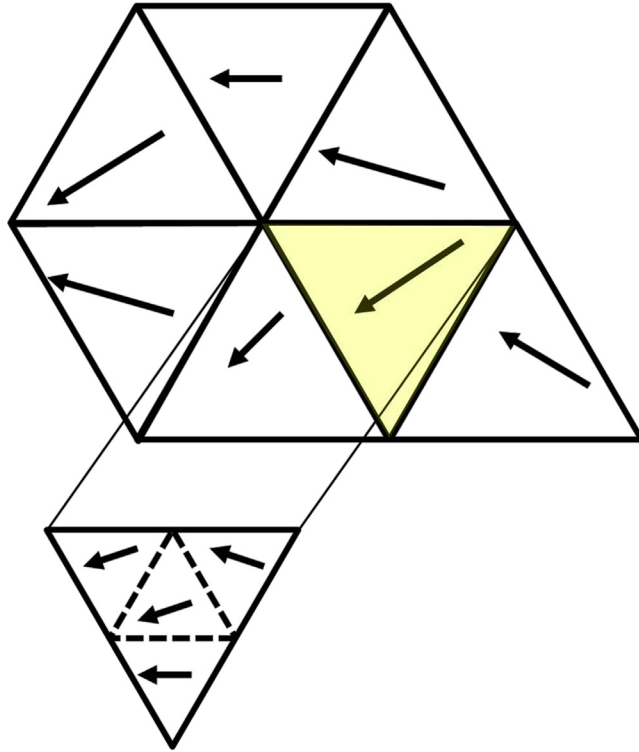


**Figure 8.8** Definition diagram for inverse distance interpolation: (a) Points used in the calculation of  $v_x$ ; (b) Points used in the calculation of  $v_y$  (modified from [Franz and Guiguer, 1990](#)).

This approach yields velocities that are discontinuous at element boundaries and mass conservation at boundaries is not satisfied ([Zheng and Bennett, 2002](#); [Cordes and Kinzelbach, 1992](#)). Alternatively, elements are subdivided into smaller domains and velocity vectors are computed for four subtriangles within the triangular element ([Fig. 8.9](#)). [Cordes and Kinzelbach \(1992\)](#) report that this approach improves mass balance and representation of the velocity field. The resulting piecewise velocity field requires smoothing to create a continuous field for PT ([Diersch, 2014](#)).

Velocity interpolation in unstructured grids ([Section 5.1](#)) presents additional challenges ([Painter et al., 2012](#); [Muffels et al., 2014](#); [Pollock, 2015](#)) and is an active area of research. Discussion of velocity interpolation in an unstructured grid/mesh is beyond the scope of this chapter. However, PT codes for unstructured grids and meshes are briefly discussed in [Section 8.6](#).

**Figure 8.9** Improvement of interpolation of velocity by subdividing triangular finite elements into four subtriangles in which separate velocity vectors are computed (modified from Cordes and Kinzelbach, 1992).



### 8.3 TRACKING SCHEMES

Flowpaths are determined by tracking particles in continuous space within the interpolated velocity field. Standard PT codes use an orthogonal coordinate system to reference particle locations. The first step in the tracking process is to calculate the distance a particle will move in each coordinate direction ( $dx$ ,  $dy$ ,  $dz$ ) during a specified time interval,  $dt$ . Distances are computed as follows:

$$dx = v_x dt \quad (8.6a)$$

$$dy = v_y dt \quad (8.6b)$$

$$dz = v_z dt \quad (8.6c)$$

One semianalytical and three numerical methods are commonly used to solve Eqn (8.6). The three numerical methods are Euler integration, Taylor Series expansion, and Runge-Kutta methods. Both semianalytical and numerical approaches are incorporated into PT codes that interface with structured and unstructured FD grids and FE meshes (Section 8.6). The semianalytical and Runge-Kutta schemes are the most widely used methods in PT.

### 8.3.1 Semianalytical Method

An analytical solution or, more commonly, a semianalytical solution, of Eqn (8.6) is possible if a linear velocity interpolation scheme is used. Presentation of the equations for a semianalytical solution is rather complex; the reader is referred to Zheng and Bennett (2002, Chapter 6) for details. We consider movement along the x-axis to illustrate some of the equations involved in the method. A semianalytical solution of Eqn (8.6a) is:

$$x_e = x_p + \frac{1}{A_x} \left[ (v_x)_p \exp(A_x \Delta t) - (v_x)_1 \right] \quad (8.7)$$

where  $A_x = [(v_x)_2 - (v_x)_1] / \Delta x_{i,j}$  and  $(v_x)_1$  and  $(v_x)_2$  are the velocities at either end of the cell/element in the x-direction;  $x_p$  is the initial x-coordinate of the particle and  $x_e$  is the exit coordinate of the particle along the x-axis (Fig. 8.10). Note that  $\Delta t$  in Eqn (8.7) is the time increment used in PT, which is usually different from the time step of the groundwater flow model. In fact,  $\Delta t$  in Eqn (8.7) must be selected so that the particle does not cross a cell/element boundary within a single tracking step. This is necessary because tracking based on Eqn (8.7) (and similar equations in the y- and z-directions) assume  $A_x$ ,  $A_y$ , and

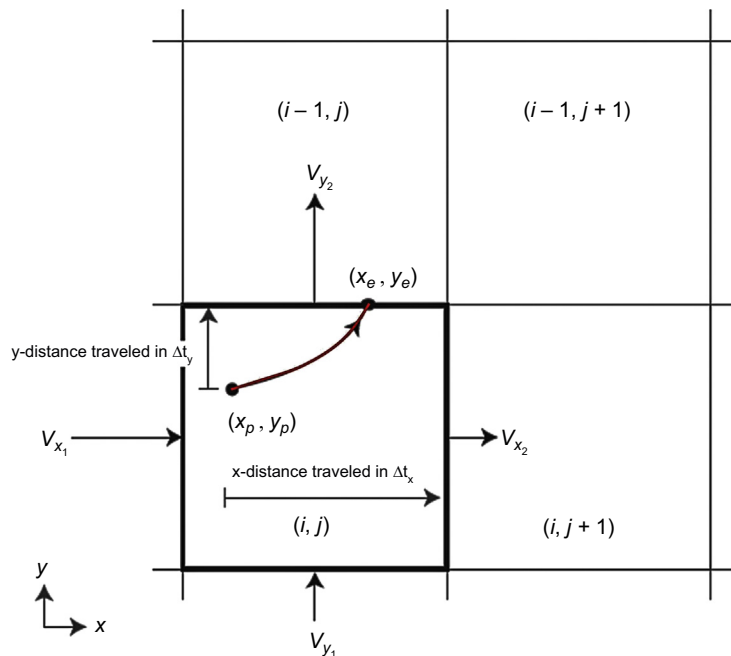


**Figure 8.10** Semianalytical particle tracking within a finite-difference cell showing the computation of travel time and flowpath from the particle location  $(x_p, y_p)$  to an exit point  $(x_e, y_e)$  (modified from Pollock, 2012). In this figure, MODFLOW numbering convention is used where  $i$  = row and  $j$  = column (Fig. 5.5).

$A_z$  are constant and cell-specific. The new particle location in the  $x$ -direction ( $x_e$ ) is calculated directly from Eqn (8.7). Similar equations are written for  $y_e$  and  $z_e$ . The particle is moved in one tracking step from its initial position to its exit location at the cell/element boundary. The semianalytical approximation is well-suited to steady-state problems because velocities at the cell/element boundaries and the associated  $A$  values are constant for steady-state conditions and are calculated only once. In transient simulations, velocities change with time and values of  $A$  must be updated during the tracking process, which adds considerably to the computational burden.

The semianalytical method as described above assumes that once a particle enters a cell or element it will exit through a cell/element boundary. Complications arise if this is not the case, for example, if the cell/element is a sink. Zheng and Bennett (2002, Chapter 6) discuss modifications in the procedure to handle such situations.

### 8.3.2 Numerical Methods

Numerical methods are well-suited for a wide variety of hydrogeological problems; Euler integration is the simplest tracking method. To illustrate the mathematics, we again use particle movement in the  $x$ -direction as an example, where  $dx = \Delta x = x_p - x_0$ :

$$x_p = x_0 + (v_x)_0 \Delta t \quad (8.8)$$

where  $x_0$  is the initial position of the particle and  $x_p$  is the position after tracking for a time period of  $\Delta t$ . Analogous equations are written for the  $y$ - and  $z$ -coordinates. Numerical errors tend to be large unless small tracking steps ( $\Delta t$ ) are used.

In a Taylor Series expansion, the new position of the particle,  $x_p$ , is calculated from

$$x_p = x_0 + (dx/dt)\Delta t + (d^2x/dt^2)(\Delta t^2/2) \quad (8.9)$$

analogous equations are written for the  $y$ - and  $z$ -coordinates. Equation (8.9) is essentially the Euler formula (Eqn (8.8)) with an additional higher order term that represents the time rate of change of velocity or the acceleration. Additional details are given by Kincaid (1988) and Zheng and Bennett (2002).

The fourth-order Runge-Kutta method is widely used in PT. The method calculates the velocity of the particle at four points for each tracking step: at the initial position of the particle ( $p_1$ ), at two intermediate points ( $p_2$  and  $p_3$ ), and at a trial end point ( $p_4$ ) (Fig. 8.11) where

$$x_{p_2} = x_{p_1} + v_{xp_1} \frac{\Delta t}{2} \quad (8.10a)$$

$$x_{p_3} = x_{p_1} + v_{xp_2} \frac{\Delta t}{2} \quad (8.10b)$$

$$x_{p_4} = x_{p_1} + v_{xp_3} \Delta t \quad (8.10c)$$

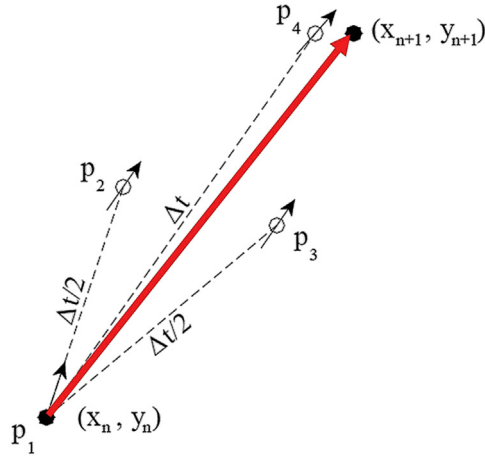


**Figure 8.11** Schematic diagram for the fourth-order Runge-Kutta method showing trial locations of the particle  $p_1$  after moving one full ( $p_4$ ) and two half steps ( $p_2, p_3$ ). The final particle location is  $(x_{n+1}, y_{n+1})$  (modified from Zheng and Bennett, 2002).

Analogous equations are written for the  $y$ - and  $z$ -coordinates. See Zheng and Bennett (2002, Chapter 6) for details. The final  $x$ -coordinate position of the particle ( $x_{n+1}$ ) is calculated using an average of velocities at all four points:

$$x_{n+1} = x_n + \frac{\Delta t}{6} (v_{xp_1} + 2v_{xp_2} + 2v_{xp_3} + v_{xp_4}) \quad (8.11)$$

Accuracy of results from the Runge-Kutta and the Euler methods depends on the size of the tracking step (Zheng and Bennett, 2002). Smaller steps give better results but require more computational time. Zheng and Bennett (2002) describe methods to adjust the size of the time step during PT by using step-doubling or inverse distance methods (Franz and Guiguer, 1990) (Fig. 8.12). In step doubling, particles are advanced using a designated tracking step and then tracking is repeated using two half-tracking steps (Fig. 8.12(a)). Alternatively, reverse tracking from the computed particle location is performed (Fig. 8.12(b)). The difference in particle locations is determined and if the difference (i.e., the error,  $\Delta s$ ) is considered unacceptable, the tracking step size is reduced and the process repeated until an acceptable error is obtained (see Zheng and Bennett, 2002, Chapter 6, for details).

## 8.4 WEAK SINKS

Special care is needed in PT around weak sinks (e.g., a well pumping at a low rate). Particles can either be captured by a sink or pass through it (Fig. 8.13; Fig. 8.3(a), (b)). A *strong sink* always captures particles because flow through all faces of the cell/element in which the sink is located is inward (Fig. 8.13(b)). PT codes remove particles that enter a cell/element



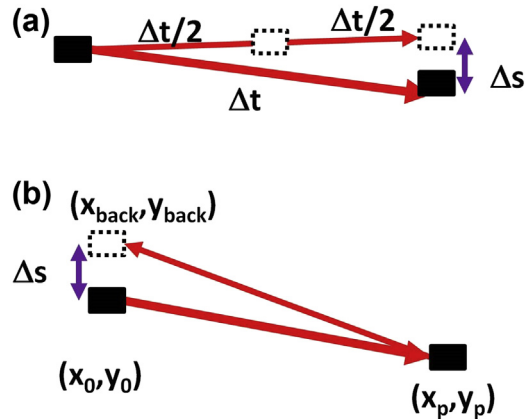


**Figure 8.12** Methods to control the tracking step in particle tracking where  $\Delta s$  is the error. For additional discussion of these methods see [Section 8.6](#). (a) Use of two half-tracking steps ( $\Delta t/2$ ) in PATH3D (modified from [Zheng, 1989](#)); (b) reverse tracking used in FLOWPATH (modified from [Franz and Guiguer, 1990](#)).

containing a strong sink. However, fluxes and gradients at the faces of a cell/element containing a *weak sink* are not uniformly inward ([Fig. 8.13\(a\)](#)). Weak sinks are problematic because the fate of a particle entering the cell or element depends on where it enters the cell/element; some particles will be captured by the sink while others will pass through and exit the cell/element.

The *strength of a sink* is defined by  $S_{\text{snk}}$ :

$$S_{\text{snk}} = \frac{Q_{\text{snk}}}{Q_{\text{in}}} \quad (8.12)$$

where  $Q_{\text{snk}}$  is the discharge rate ( $L^3/T$ ) at the sink and  $Q_{\text{in}}$  ( $L^3/T$ ) is the total volumetric inflow rate to the sink cell/element.  $S_{\text{snk}}$  equals 1 for a strong sink and is less than 1 for a

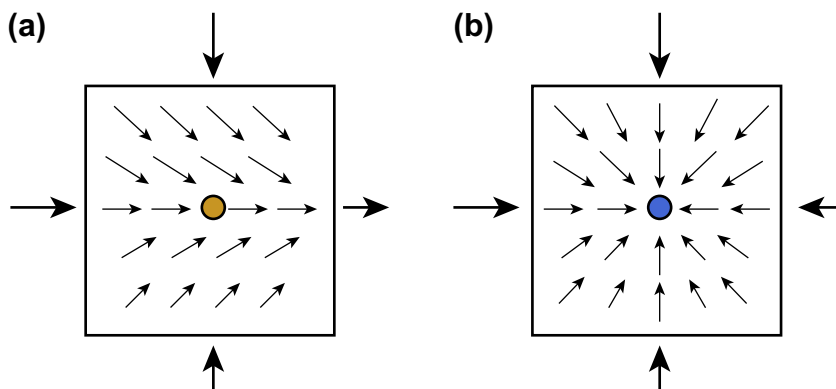


**Figure 8.13** Schematic diagram of flows in model cells associated with (a) a weak sink and (b) a strong sink. Flow rate is proportional to the length of the arrow (modified from [Spitz et al., 2001](#)).

weak sink. A PT code may control particle capture in weak sinks by setting thresholds based on the value of  $S_{\text{snk}}$ . For example, MODPATH (Pollock, 1989, 2012) allows the user to select one of three options for particles that enter a weak sink: (1) the particle is always captured; (2) the particle is never captured; (3) capture depends on the value of  $S_{\text{snk}}$ . If the third option is selected, the user specifies the value of  $S_{\text{snk}}$  required for capture. For example, by selecting a value of  $S_{\text{snk}} = 0.4$ , particles would be captured when  $S_{\text{snk}}$  is equal to or greater than 0.4 and allowed to bypass the sink when  $S_{\text{snk}}$  is less than 0.4. Visser et al. (2009), however, pointed out that specifying the value of  $S_{\text{snk}}$  required for capture introduces undesired subjectivity into PT analysis (also see Shoemaker et al., 2004).

One way to eliminate weak sinks is to use fine nodal spacing in the vicinity of the sink (Fig. 8.3 (c)). Following the guidelines in Box 6.1 for nodal spacing around a well node, for example, would produce a strong sink for most pumping rates (Spitz et al., 2001). A second approach is to use a velocity refinement scheme to provide better resolution of local velocities near the sink. Zheng (1994) used an analytical solution to refine velocities in the sink cell while still using a coarse FD grid (Fig. 8.3(c)). Spitz et al. (2001) created a submodel with refined nodal spacing around the cell representing the weak sink; flows from the original model were used as constant-flux boundary conditions for the submodel. In their method, the submodel is coupled with the original model and the coupled model is run with successively finer discretization in the submodel until the simulated well becomes a strong sink. Other schemes for improving velocity calculations in the vicinity of weak sinks were described by Charbeneau and Street (1979) and Paschke et al. (2007).

Although our discussion here focuses on weak sink wells, the concepts and approaches also apply to weak sink surface water features. Visser et al. (2009), Abrams (2013), and Abrams et al. (2013) proposed methods specifically designed for weak sink streams.

## 8.5 APPLICATIONS

PT codes can track particles both forward (forward PT) and backward (backward or reverse PT) in time. In *forward tracking*, particles are placed in the model domain (e.g., at the water table, in recharge areas, or at inflow boundaries) and tracked forward in time (Figs 8.2(b) and 8.14(a)). In *reverse tracking*, particles are placed in discharge locations such as a stream or pumping well and back-tracked to determine the contributing area, capture zone (Fig. 8.15), or source of water (Fig. 8.16). Particles representing contaminants can also be tracked forward in time from a source area (Fig. 8.17) or backward in time to help identify potential sources (Fig. 8.16). Forward and backward tracking helps visualize groundwater flow in both local and regional settings. Typically, flowpaths are shown in 2D map or cross-sectional views (Figs 8.15 and 8.16). In 3D PT, such representations are projections onto a horizontal or vertical plane. Flowpaths can also be shown in

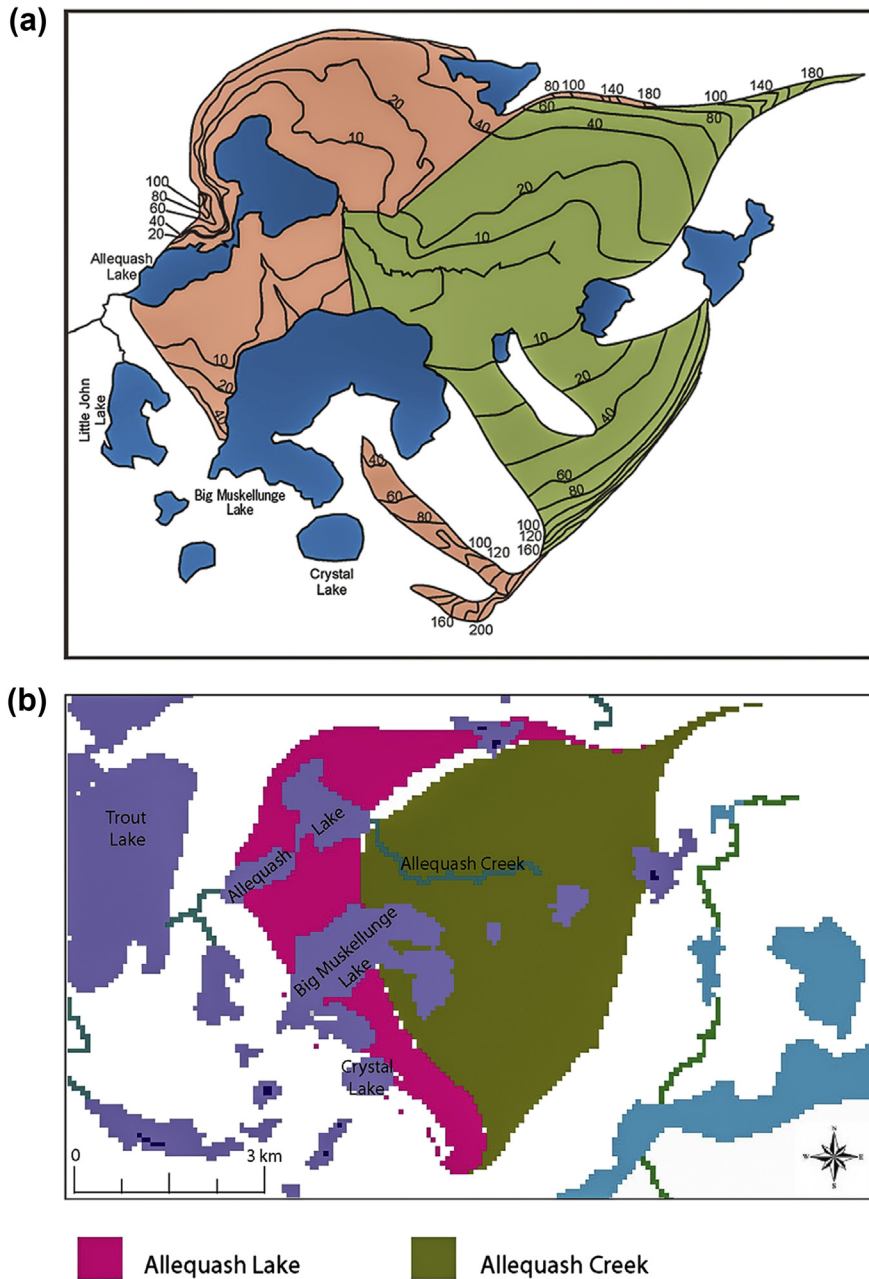


**Figure 8.14** Contributing areas. (a) Forward particle tracking to delineate the contributing area to Allequash Lake (salmon pink) and Allequash Creek (green) in a humid temperate climate in Northern Wisconsin, USA. Contours indicate time of travel in years. Particles were placed at the water table in every active cell in the model and tracked forward in time. All weak sinks were converted to strong sinks (Pint et al., 2003). (b) Contributing areas as shown in (a) but allowing all particles to pass through weak sinks (Masbruch, 2005).

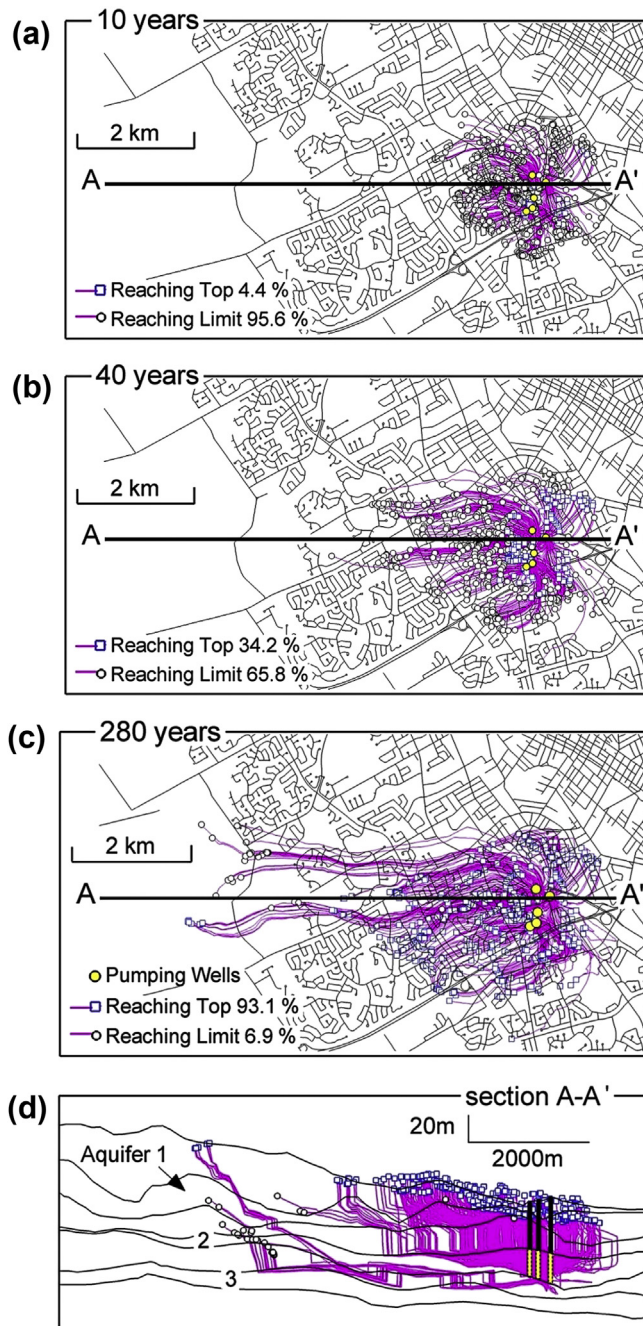


**Figure 8.15** Reverse particle tracking showing capture zone projections for a well field of five wells. The configuration of the capture zones is irregular owing to the highly heterogenous aquifer and the three-dimensional flow field. (a), (b), and (c) show horizontal plane projections at 10, 40, and 280 years, respectively; the blue squares show the position of particles that have reached the surface; for example, 93.1% of particles have reached the surface after 280 years. Open circles show the end position of particles that have not reached the surface; for example, 6.9% of particles have not reached the surface after 280 years. (d) a vertical plane projection at 280 years (*modified from Frind and Molson, 2004; Frind et al., 2002*).

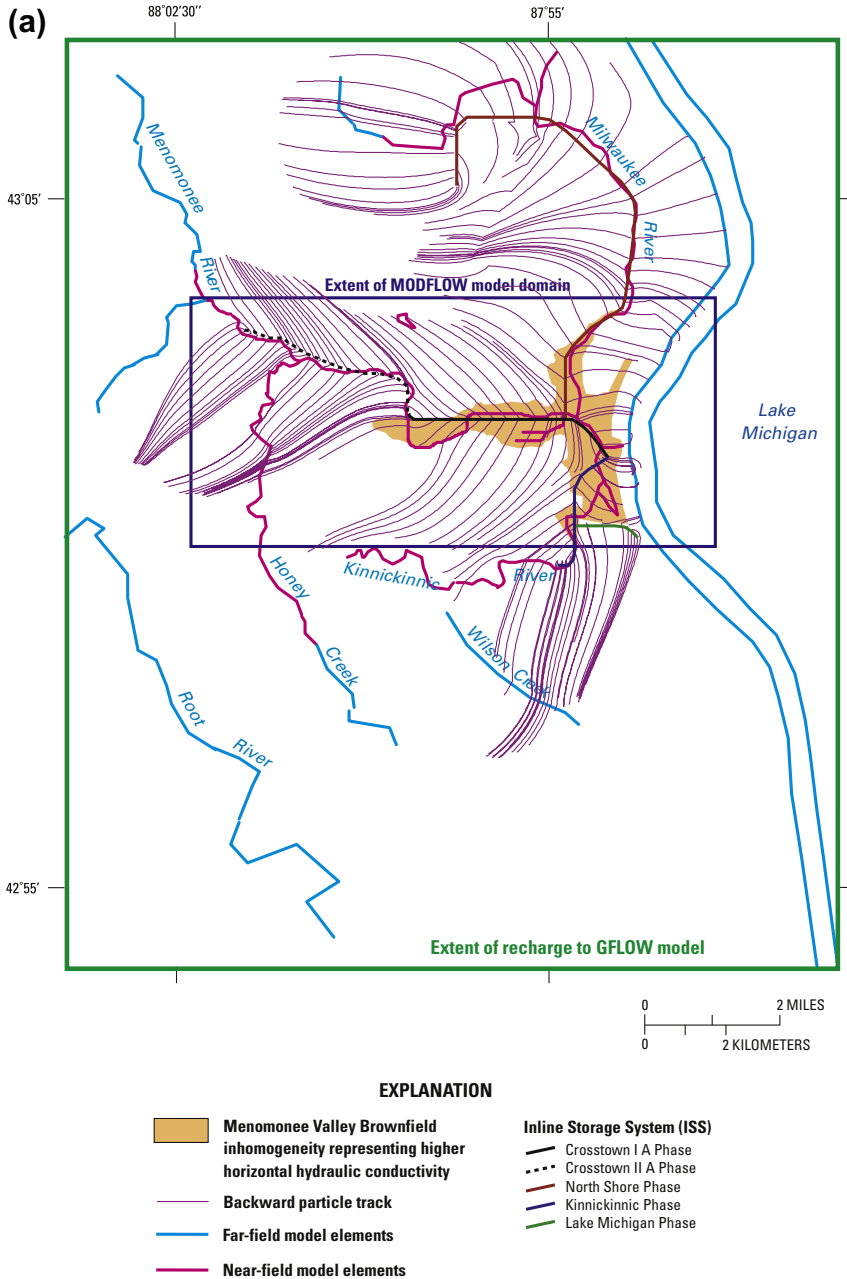


**Figure 8.16** Reverse particle tracking to identify sources of water to a deep sewer tunnel system. (a) Map view showing extent of a MODFLOW model set in a regional analytic element (GFLOW) model. The tunnel is shown as line segments representing the In-line Storage System (ISS) (see the legend).

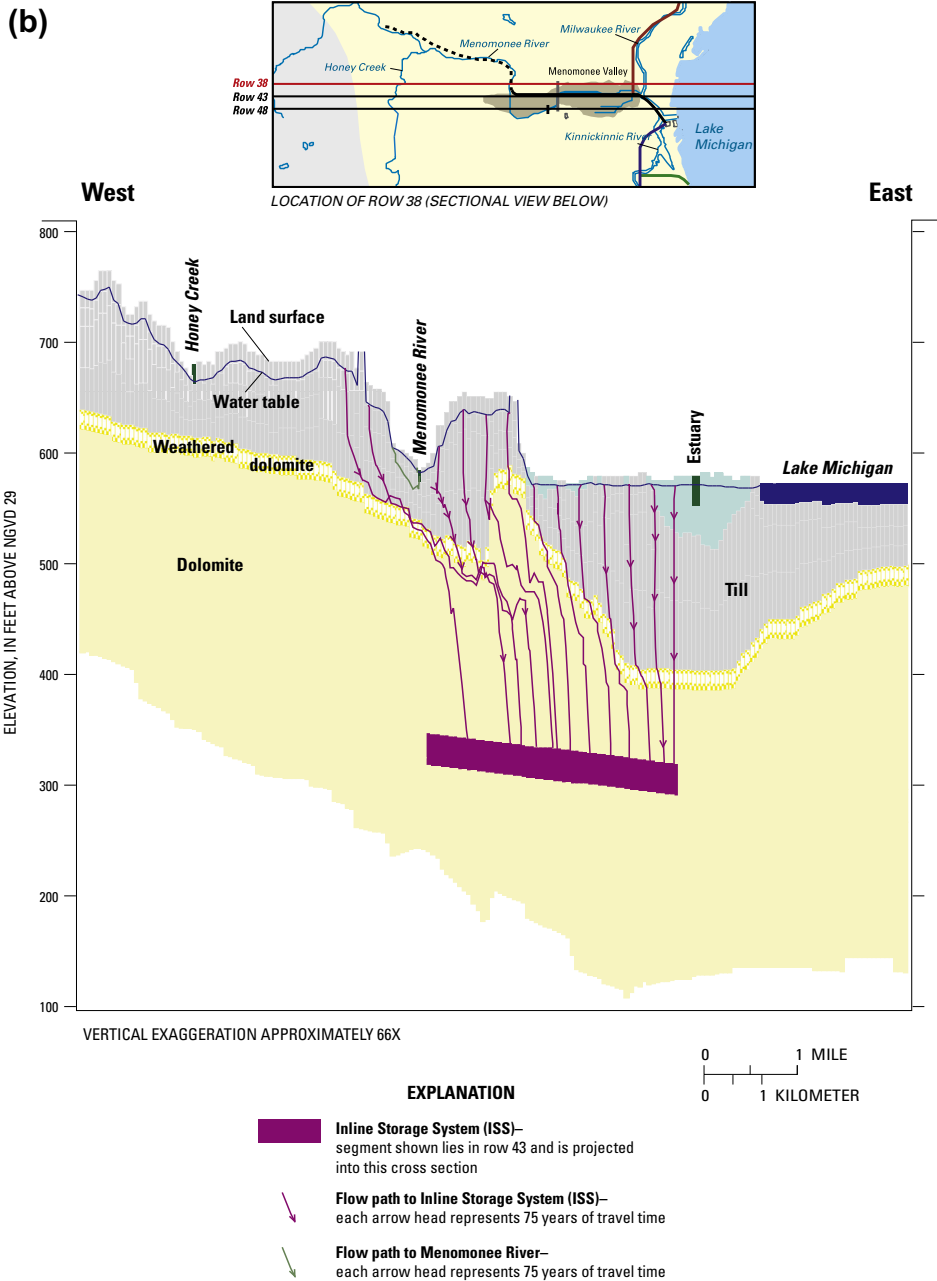
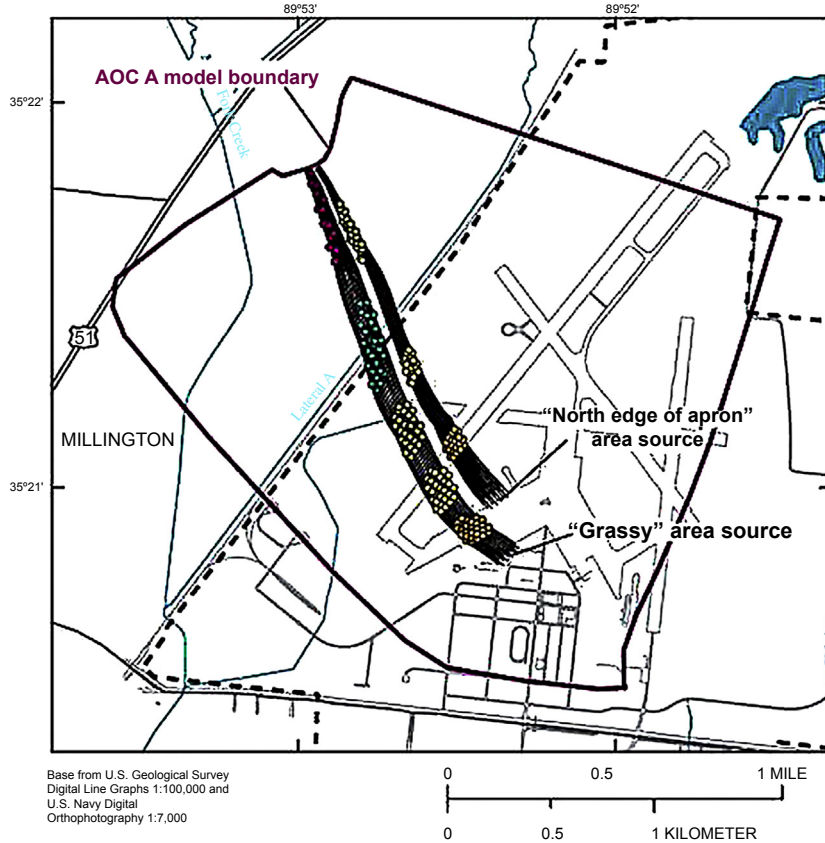


**Figure 8.16.b, Cont'd.** (b) West—east cross section. The tunnel (Inline Storage System (ISS)) is shown in purple. Travel times are indicated by the arrowheads; each arrowhead represents 75 years of travel time (Dunning et al., 2004).



**EXPLANATION**

<p>————— ADVECTIVE PARTICLE TRACKING FLOW LINE</p> <p>----- NAVAL SUPPORT ACTIVITY MID-SOUTH BOUNDARY</p> <p>- - - - - MILLINGTON CITY BOUNDARY</p>	<p><b>TIME OF TRAVEL PLOTS</b></p> <p>● AFTER 10 YEARS</p> <p>● AFTER 20 YEARS</p> <p>● AFTER 30 YEARS</p> <p>● AFTER 40 YEARS</p> <p>● AFTER 50 YEARS</p>
---	--

**Figure 8.17** Advective particle tracking from contaminated areas (labeled as grassy area source and north edge of apron area source) at a former airfield, showing flowpaths and travel times (Haugh et al., 2004).

three-dimensions (Fig. 8.18). Flowpaths, represented by particle tracks, can converge but never cross; in 3D models, particle tracks may appear to cross when projected onto a plane. Travel times may be represented by arrowheads (Fig. 8.16(b)), dots (Fig. 8.17), or colors (Fig. 8.18). The effects of changes in parameter values, such as recharge rates, on the configuration of flowpaths can also be examined (Fig. 4.1.3 in Box 4.1; Fig. 10.15).

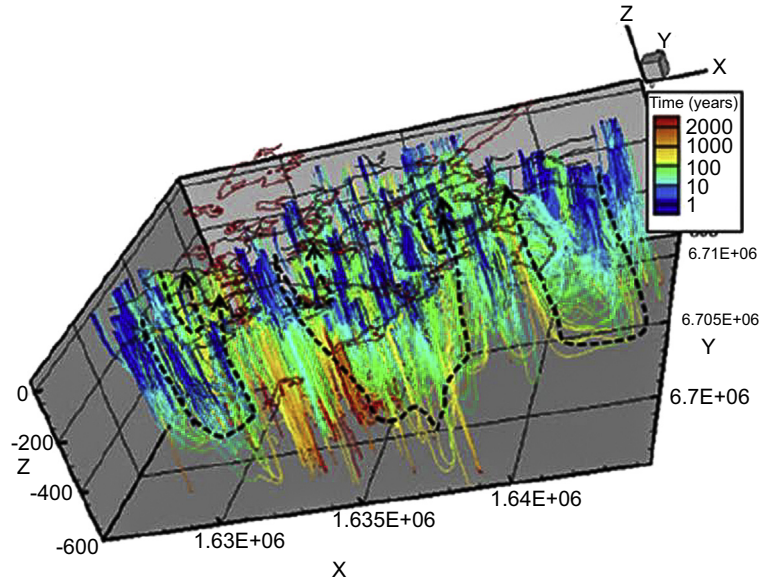


**Figure 8.18** Flowpaths in three-dimensions. Particles released at the surface move down through the bedrock and back up to Quaternary deposits at the surface. Travel times are indicated by colors. Main flowpaths are shown by dashed black lines with arrowheads. Streams and lakes at the surface are outlined in red (Bosson *et al.*, 2013).

### 8.5.1 Flow System Analysis

PT is used to delineate basin-scale flowpaths (Figs 8.2(b) and 8.18) and contributing areas to rivers, lakes (Fig. 8.14; Box 8.3), and springs (Fig. B10.2.2 in Box 10.2), to identify sources of water (Fig. 8.16), and to estimate travel times (Fig. 8.18).

The travel time calculated in PT can only give an approximate groundwater age for a parcel of water along a flowpath. Mixing of waters of different ages affects the mean (apparent) groundwater age in a sample of groundwater collected in the field (e.g., Bethke and Johnson, 2002a,b, 2008; Weissmann *et al.*, 2002; Goode, 1996) but PT does not represent mixing of flowpaths. Rather, PT assumes that a parcel of water (represented by a particle in the PT code) moves as a discrete volume along a flowpath (i.e., as “piston-flow” or “plug-flow”). Thus, the advective groundwater age calculated in PT differs from the mean groundwater age obtained by analyzing a tracer in a mixed-age groundwater sample (McCallum *et al.*, 2014). Nevertheless, age estimates from PT are often sufficient for many problems. Moreover, mixing of waters of different ages can be inferred from PT (Fig. 8.19). When mixing of flowpaths of different ages is a concern, groundwater age is best estimated using a solute transport model based on the advection-dispersion equation (Section 12.3; also see Molson and Frind, 2012; DHI-WASY, 2012).



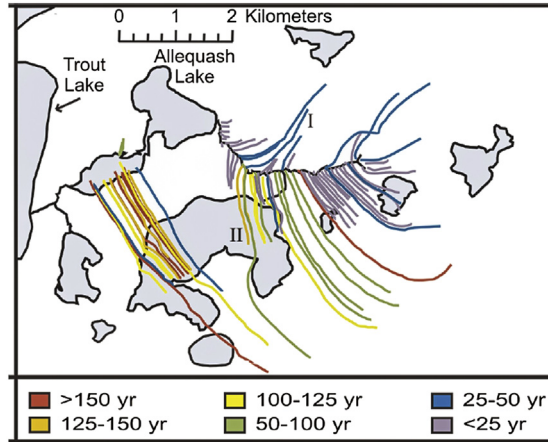


**Figure 8.19** Advective age of particles along different flowpaths. Flowpaths of vastly different ages discharge in close proximity suggesting that mixing of waters of different ages occurs in the discharge location. (For example, flowpath I discharges near flowpath II.) Groundwater sampled in discharge areas will have a mean or apparent age that is different from the advective age of an individual flowpath (Pint *et al.*, 2003).

## 8.5.2 Capture Zones and Contributing Areas

PT is frequently used to delineate capture zones of wells and contributing areas to rivers, lakes, and springs, most commonly for steady-state flow. Some basic information about capture zones and contributing areas is presented below; more information is provided in Box 8.3.

For our purposes, a *capture zone* delineates the portion of groundwater flow captured by a pumping well (Figs 8.3, 8.4 and 8.6; Fig. B8.3.1 in Box 8.3; Fig. B4.1.3 in Box 4.1) whereas a *contributing area* delineates the area in which groundwater flows to a spring or surface water body (Fig. 8.14; Fig. B8.3.3 in Box 8.3; Fig. B10.2.2 in Box 10.2). For regulatory purposes, capture zones are usually calculated for a specific time of capture. For example, a 20-year capture zone shows the extent of capture 20 years after the onset of pumping (Fig. 8.4(c); also see Fig. 8.15 and Fig. B8.3.1(b) in Box 8.3). Capture zones are usually shown as horizontal projections in map view (Fig. 8.15 (a), (b), (c); Fig. B8.3.1(b) in Box 8.3) but flowpaths related to well capture can also be shown in cross section (Fig. 8.15 (d)).

Capture zones and contributing areas may be delineated by reverse PT whereby particles are introduced at the discharge location (e.g., a well, spring, drain, or surface water body) and tracked backward for a prescribed period of time or until all particles reach a source location. However, results from reverse PT may be sensitive to placement of the particles (and PT code settings) when particles originate at locations of converging flowpaths such as a pumping well (Fig. 8.20) or gaining stream. Capture zones can be

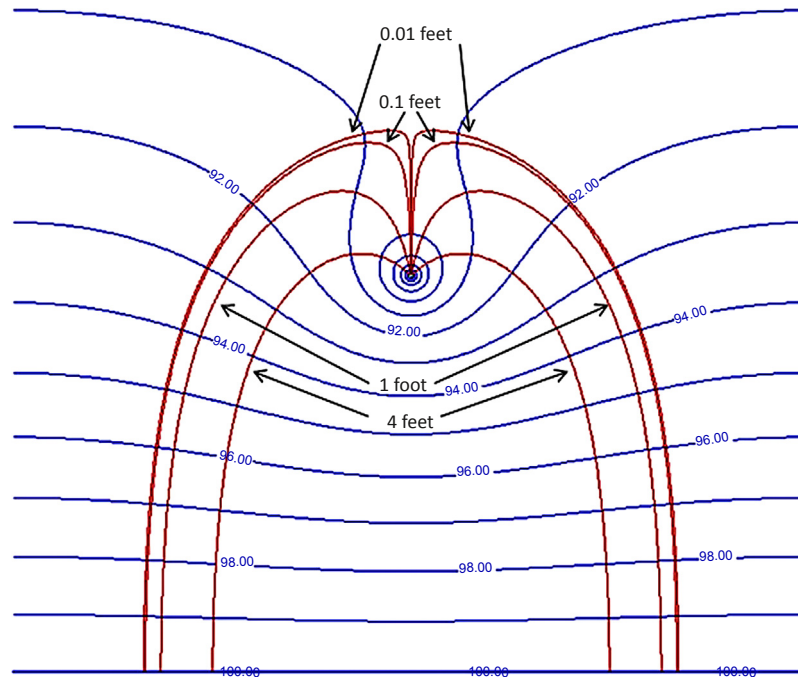


**Figure 8.20** Different capture zones (red lines) are computed by reverse particle tracking when particles are released from slightly different locations around the well node. Equipotential lines are shown in blue. Particles were released 0.01, 0.1, 1, and 4 ft off-center of the well. Particles released 4 ft and 1 ft off-center underestimate the width and downgradient extent of the capture zone. Particles released 0.1 and 0.01 ft off-center produce virtually the same capture zone width, but the 0.01 ft release points show slightly greater downgradient capture (*courtesy of Kurt Zeiler, Brown and Caldwell*).

delimited by forward tracking a large number of particles from a source area (Fig. 8.14), but reverse PT is often easier to perform. A compromise is to use backward tracking and then verify the simulated capture zone or contributing area with forward tracking, or by executing another backward tracking run with more particles and/or with particles originating from slightly different locations within the area of converging flowpaths (Fig. 8.20).

PT to delineate capture zones and contributing areas is complicated around weak sinks (Section 8.4). The shape and extent of the capture zone or contributing area may be sensitive to the value of  $S_{\text{snk}}$  (Eqn (8.12)) that the modeler selects as the threshold for capture (e.g., compare Fig. 8.14(a) and (b)). Such changes in capture also can affect groundwater residence times (Visser et al. 2009; Abrams et al., 2013). Abrams et al. (2013) suggested settings for the PT code MODPATH to reduce confounding effects of weak surface water sinks on capture zones and residence time calculations.

### Box 8.3 More on Capture Zones and Contributing Areas

In Section 8.5, we used the term “capture zone” to refer to a pumping well, while “contributing area” was used to refer to lakes, rivers, and springs. However, capture zone is often used in a general way to refer to the portion of the groundwater flow field that discharges water to any sink be it a well, lake, river, or spring. Nevertheless, we will maintain the distinction made in Section 8.5 for clarity.

Computing the extent of existing and potential future capture zones is a common task for groundwater modelers. Capture zones are used to examine regulatory compliance such as wellhead protection and in water management and aquifer remediation when wells are pumped to capture and treat a contaminant plume. Capture zones are three-dimensional features (Fig. B8.3.1(a)) but are typically shown in map view (Fig. B8.3.1(b)). Moreover, the capture

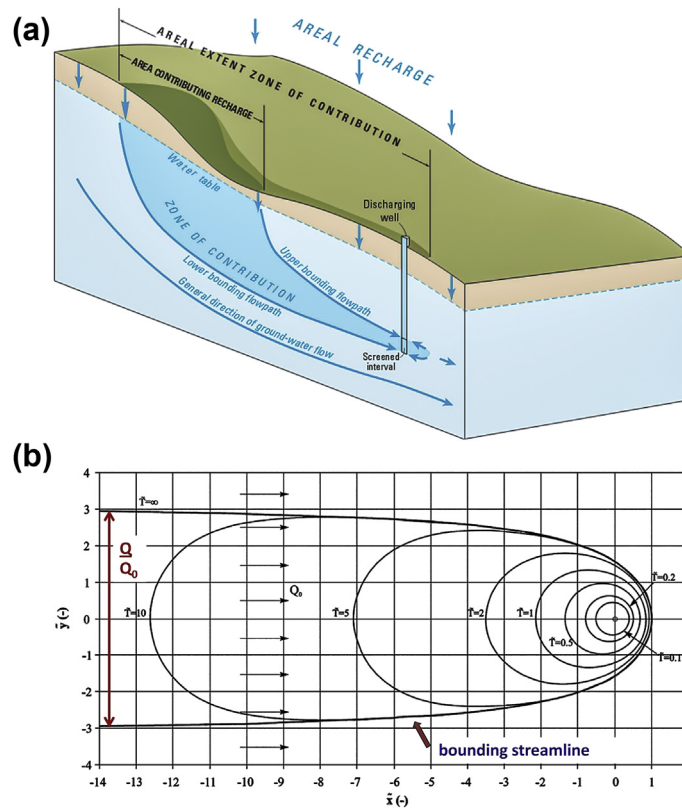


**Figure B8.3.1** Capture zones. (a) Capture zone (labeled as zone of contribution) shown in 3D with bounding flowpaths (Paschke et al., 2007). (b) Time of travel (TOT) capture zones and bounding streamline shown in map view for a two-dimensional, steady-state, uniform flow field with ambient flow of  $Q_0$  ( $L^2/T$ ; discharge rate per unit thickness) and pumping rate of  $Q$  ( $L^3/T$ ); recharge rate is zero.  $\bar{t}$  is a dimensionless time parameter ( $=2\pi\tau Q_0^2/nbQ$  where  $t$  is the time particles along a TOT line take to reach the well;  $n$  is the effective porosity; and  $b$  is the average saturated thickness of the aquifer prior to pumping) (modified from Ceric and Haitjema, 2004).

### Box 8.3 More on Capture Zones and Contributing Areas—cont'd

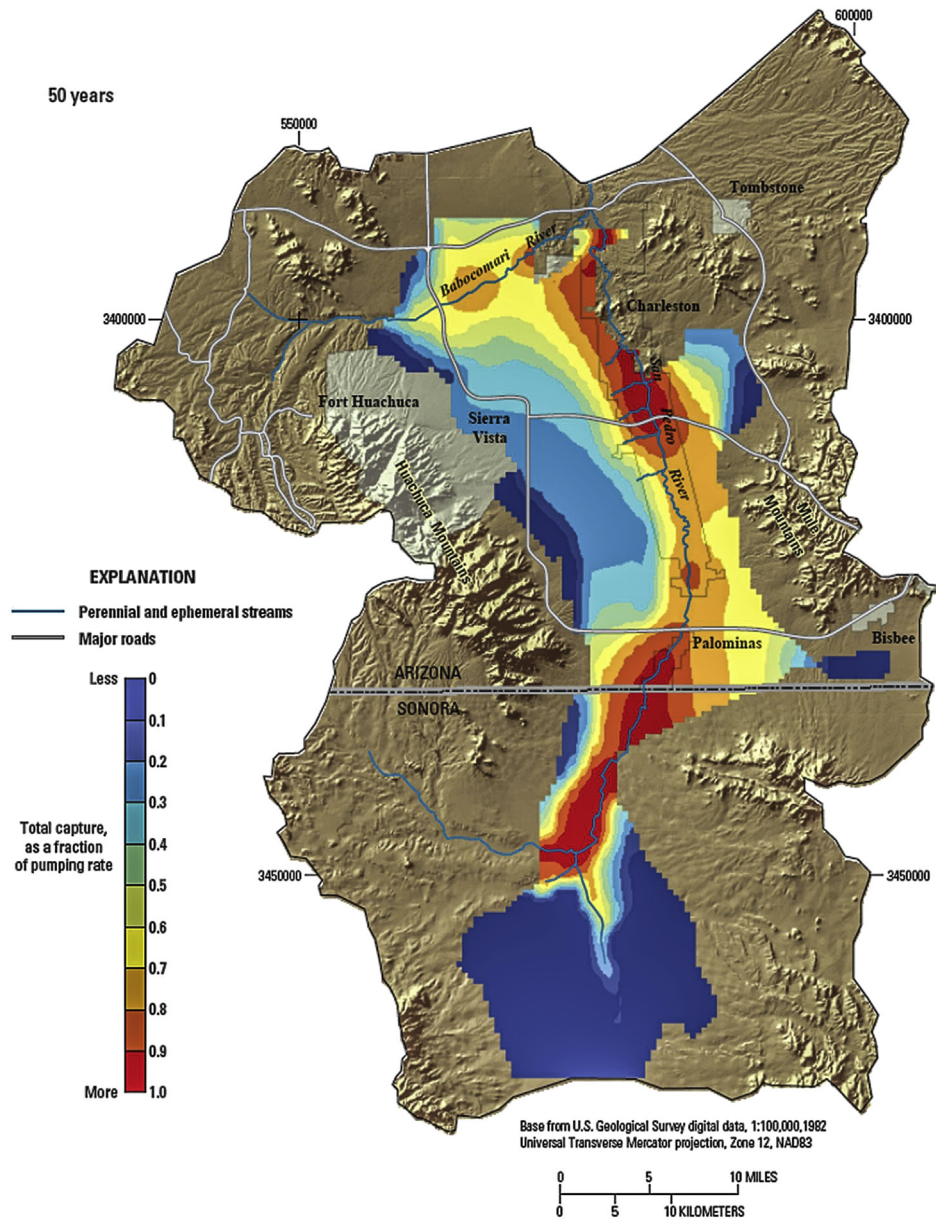


**Figure B8.3.2** Stream capture zones resulting from pumping at a constant rate for 50 years from the lower basin-fill in a semiarid basin, Arizona, USA. The color at any location represents the fraction of the withdrawal rate by a well at that location that is contributed by streamflow depletion (*Barlow and Leake, 2012*).

(Continued)

### Box 8.3 More on Capture Zones and Contributing Areas—cont'd

pattern may change with time under transient flow conditions (Fig. 8.6). Under steady-state flow conditions, capture zones are typically represented for a specific time of capture (i.e., the time elapsed since the onset of pumping) (Figs 8.4(c) and 8.15). A composite of capture zones under steady-state conditions can be represented in a depiction of time of travel (TOT) capture zones (Fig. B8.3.1(b)), which represents the extent of capture for specific times after pumping begins.

Haitjema (1995, 2006) presented guidelines for evaluating capture zone simulations including describing the geometry of a capture zone for a well pumping at a constant rate in a two-dimensional uniform flow field when areal recharge is zero (i.e., for the conditions shown in Fig. B8.3.1(b)). For example, the width of the capture zone at steady state is  $Q/Q_0$  where  $Q$  ( $L^3/T$ ) is the pumping rate and  $Q_0$  is the ambient flow rate ( $L^2/T$ , reflecting discharge rate per unit thickness). However, when areal recharge is included in the analysis, capture zones are smaller and equations that assume zero recharge compute capture zones that are too large. Because most aquifers in nonarid settings receive some areal recharge, Zhou and Haitjema (2012) advised against using equations that assume zero recharge for TOT capture zones beyond 5 years. Nevertheless, such analytical tools may be useful to obtain a first approximation of a capture zone to help design and evaluate numerical models that include more complex conditions such as aquifer heterogeneities and complex sources and sinks.

When wells extract groundwater from an aquifer connected to a stream, there is the potential for loss in streamflow (known as streamflow depletion) in addition to capture of terrestrial recharge. Stream capture zones can be delineated (Fig. B8.3.2) by particle tracking to represent the fraction of pumped well water derived from streamflow. Stream capture, like well capture, is calculated for a specific time after the onset of pumping.

By definition, contributing areas are 2D features projected onto the land surface, but a 3D contributing zone could be defined (Fig. B8.3.3). Contributing areas and zones are typically represented for steady-state conditions so that they can be delineated by dividing or bounding flowpaths (flowlines), which separate the flow discharging to the sink from the rest of the flow field (Fig. B8.3.3). The same concept pertains to capture zones (Fig. B8.3.1(a)).

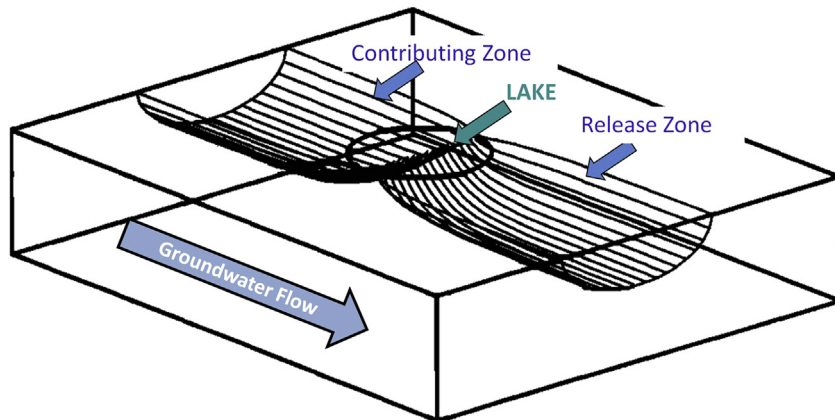


**Figure B8.3.3** Contributing and release zones around a circular lake delineated by bounding flowpaths. The release zone delineates flow leaving the lake through the groundwater system (modified from Townley and Trefry, 2000).

### 8.5.3 Advective Transport of Contaminants

Another application of PT is to simulate advective transport of contaminants (Section 8.1). Particles, which represent the contaminant, move according to the average linear velocity (Eqn (8.1)). Therefore, particle arrival times at a receptor (e.g., a well or surface water body) approximate the arrival of the center of mass rather than the leading edge of the contaminant plume (Fig. 8.21). Contaminants may be tracked forward in time along flowpaths (Fig. 8.17) or backward to help identify potential source areas (Fig. 8.16).

Standard PT codes do not typically include dispersion or chemical reactions other than linear adsorption. Linear adsorption retards the velocity of the contaminant (Fig. 8.21) and is simulated using a dimensionless *retardation factor*,  $R_d$ . The retarded velocity,  $v_c$ , is equal to  $v/R_d$  where  $v$  is the average linear velocity in Eqn (8.1) and  $R_d$  is greater than 1.  $R_d$  can be estimated from the *distribution coefficient*,  $K_d$ , which is usually given in units of ml/gm:

$$R_d = 1 + \frac{\rho_b}{\theta} K_d \quad (8.13)$$

where  $\rho_b$  is bulk mass density of the porous material ( $M/L^3$ ) and  $\theta$  is the total porosity. There are two types of porosity in transport problems: total porosity and effective porosity (Zheng and Bennett, 2002, pp. 56–57; Box 8.1). Total porosity includes immobile pore water, which contains solute, that should be accounted for when determining the total mass in the system. Nevertheless, in practice, although not rigorously correct, it is customary to use effective porosity to represent total porosity in Eqn (8.13) for purposes of transport modeling (Zheng and Bennett, 2002, p. 621).

$K_d$  is typically measured in laboratory batch experiments whereby dissolved concentrations are plotted against sorbed concentrations at different sampling intervals;  $K_d$  is equal to the slope of the best-fit line through the data points. The concept of a retardation

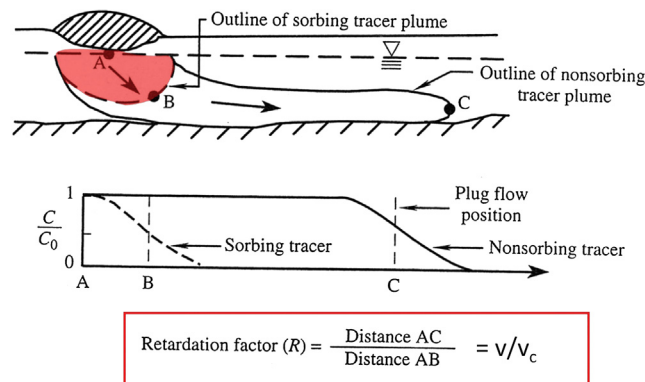


**Figure 8.21** Schematic diagram showing the retarding effect of linear adsorption and definition of the retardation factor. In particle tracking, solutes are transported by plug flow (modified from Zheng and Bennett, 2002).

factor can also be used to represent other chemical processes that retard contaminant transport such as ion exchange and some chemical reactions that involve forward and backward reactions.

## 8.6 PARTICLE TRACKING CODES

Most PT codes are designed to postprocess results from a specific groundwater flow code. MODPATH (Pollock, 1989, 2012) and PATH3D (Zheng, 1989) are 3D PT codes that use heads from MODFLOW, but they could be modified to accept a head solution from any block-centered FD code. Both MODPATH and PATH3D use linear interpolation. MODPATH uses a semianalytical solution tracking scheme that avoids errors associated with numerical integration but is not ideal for transient simulations. MODPATH version 6 (Pollock, 2012) allows PT in a variety of different grids and allows for local grid refinement (LGR, Section 4.4). PATH3D uses a fourth-order Runge-Kutta approximation for tracking. Numerical errors are minimized by automatic adjustment of the tracking step according to an error criterion set by the user. The position of the particle is calculated using a full tracking step and two half steps (Fig. 8.12(a)). If the discrepancy in particle position ( $\Delta s$ ) is greater than the error criterion ( $\Delta s_0$ ), the time step is reduced and the tracking step is repeated. PATH3D is efficient for both steady-state and transient problems. Anderman and Hill (2001) developed the Advective Transport-Observation Package in MODFLOW-2000 to represent advective transport of contaminants. This package uses the same methods as MODPATH.

Recently two PT codes were developed for the unstructured FD grid in MODFLOW-USG (Panday et al., 2013). ModPATH3DU (Muffels et al., 2014) uses universal kriging (Section 5.5) to interpolate heads in the vicinity of a particle from which velocities are calculated. The code has options for both semianalytical tracking (based on MODPATH by Pollock, 1989, 2012) and a numerical method based on a fourth-order Runge-Kutta approximation (based on PATH3D by Zheng, 1989), as well as Euler interpolation. The tracking algorithm can be specified cell by cell so that the modeler can select different tracking algorithms as appropriate throughout the grid. MODPATH-USG (Pollock, 2015) extends the semianalytical tracking approach in MODPATH to a subset of the unstructured grids available in MODFLOW-USG. Painter et al. (2012, 2013) developed WALKABOUT for PT in fully unstructured grids. Results for relatively simple flow fields generated flowpaths similar to those from analytical solutions.

ZOOPT is a steady-state, three-dimensional PT code for the flow code ZOOMQ3D (Jackson, 2002; Jackson and Spink, 2004). It uses linear interpolation and a semianalytical tracking method modified by applying the Runge-Kutta method at prescribed model features such as weak sinks and nodes with vertical variations in hydraulic conductivity. The code is also compatible with FD LGR (Section 4.4), which is incorporated in the groundwater flow code ZOOMQ3D.

FLOWPATH (Franz and Guiguer, 1990) includes a block-centered FD flow code for two-dimensional and steady-state conditions. FLOWPATH uses inverse distance interpolation (Fig. 8.8) with Euler integration. The size of a tracking step is controlled by an error criterion. During the error check, the particle is moved backward from its new location  $(x_p, y_p)$  for the length of the tracking step (Fig. 8.12(b)). The discrepancy ( $\Delta s$ ) between the initial position of the particle  $(x_0, y_0)$  and the position achieved during backward tracking  $(x_{back}, y_{back})$  is calculated from the following equation:

$$\Delta s = \left[ (x_0 - x_{back})^2 + (y_0 - y_{back})^2 \right]^{1/2} \quad (8.14)$$

The error tolerance ( $E$ ) is

$$E = 0.05a \quad (8.15)$$

where  $a$  is the average nodal spacing. If  $\Delta s$  is greater than the error tolerance, the tracking step is reduced by 50% and the particle is again moved from its initial position  $(x_0, y_0)$  but using a smaller tracking step.

GWPATH (Shafer, 1990) uses an analytical interpolation scheme and the Runge-Kutta method for tracking. WHPA (Blandford and Huyakorn, 1990) is a collection of programs developed for the U.S. EPA for delineating wellhead protection areas. It has three options for calculating a flow field using analytical solutions. It includes a 2D PT code (GPTRAC) that accepts a head solution from a user-supplied flow code, which can be either a block- or point-centered FD code or an FE code with rectangular elements. It uses linear interpolation of velocity and an analytical solution for moving particles.

The FE code FEFLOW (Diersch, 2014) incorporates PT as a postprocessor within the user interface. Velocities are interpolated using basis functions and particles are tracked using a fourth-order Runge-Kutta approximation with adaptive step control. A PT method for FE models developed by Suk and Yeh (2009, 2010) produces velocity fields by creating subelements. Their method takes into account changes in velocity during a time step. Suk (2012) compared results from their method with results from MODPATH (Pollock, 1989, 2012).

## 8.7 COMMON ERRORS IN PARTICLE TRACKING

- A capture zone or contributing area is delineated by reverse PT using too few particles. Flowpaths produced by reverse PT can be sensitive to number and placement of particles especially when particles originate in areas of converging flow (e.g., near a pumping well or gaining stream).
- The modeler assumes that time of travel calculated by PT directly corresponds to estimates of groundwater age from tracers sampled in the field.



- The modeler assumes that the arrival time of a contaminant at a receptor calculated by PT accurately characterizes the time of first arrival. First arrival times are affected by dispersion, which is not included in a PT code.
- The modeler fails to account for weak sink effects on capture zones and aquifer residence time calculations.
- The modeler is not aware that distorted layers can adversely affect flowpaths and travel times calculated by PT.
- PT is performed for a quasi-3D groundwater flow model. Quasi-3D models do not explicitly include confining layers in the grid/mesh and therefore groundwater flowpaths and travel times are not correct because travel through the omitted units is not represented.
- The horizontal nodal spacing in the groundwater flow model is too coarse around sources and sinks and the flowpaths calculated by PT are not representative of field conditions.
- The horizontal nodal spacing is too coarse to capture important changes in hydraulic conductivity in a heterogenous aquifer and the flowpaths calculated by PT are not representative of field conditions.
- The modeler processes PT results from a 2D flow model and depicts particle tracks that cross. Flowpaths may converge but never cross. When particle tracks in a 3D model are projected onto a plane, flowpaths may appear to cross, but particle tracks depictions in a 2D model never cross.
- The modeler fails to test the sensitivity of PT travel time results to values of effective porosity.

## 8.8 PROBLEMS

We revisit the Hubbertville problem to trace groundwater flowpaths. We also explore PT in two- and three-dimensions, computation of travel times, and the effects of weak sinks and spatial discretization on PT results.

**P8.1** The town of Hubbertville wants to site a landfill upgradient from the proposed water supply well described in Problem P4.3 (Chapter 4). The landfill would be on a few acres owned by the town and located 5000 m due south and 500 m due west of the well site shown in Fig. P4.3. If the landfill should leak, leachate could enter groundwater flowing beneath the landfill.

- a. Run the steady-state groundwater flow model with the well pumping and use a PT program to delineate the flowpath that contaminated groundwater would most likely follow. Assume an effective porosity of 0.15. Initiate tracking from the water table directly below the landfill site by placing particles in the appropriate cells or elements. Would the supply well be affected if the landfill should leak?

- b.** How many days will it take for leachate to travel 1000 m downgradient from the area beneath the landfill?
- P8.2** Use a PT program that allows backward tracking to define the steady-state capture zone around the Hubbertville supply well (see Problem P8.1). Check the backward tracked capture zone by using forward tracking. Generate maps showing the 5-day, 30-day, and 1-year capture zones.
- P8.3** PT in a cross-sectional model is useful to illustrate vertical flowpaths. We revisit Problem P4.2 (Chapter 4) to investigate flowpaths under a dam.
- a.** Using the results of Problem P4.2b and assuming an effective porosity of 0.15 place a number of evenly spaced particles at the boundary representing the pond side of the dam and forward track the particles under the dam to the river side of the dam. Verify that the particle tracks intersect equipotential lines at right angles.
- b.** Repeat PT using an anisotropic hydraulic conductivity field (P4.2 (d)). Are the flowpaths intuitive? Why or why not?
- P8.4** PT can also be used to compare representations of groundwater flow in 2D versus 3D. In Problem P5.1 (c) and (d) two representations of the hydrogeological setting around a leaking pond were simulated. Assume effective porosities as follows: layer 1 = 0.20; layer 2 = 0.10; layer 3 = 0.15. PT will help visualize how multiple layers and anisotropy affect the flow field. Place particles at the location of the pond and forward track them to the boundary. Describe how flowpaths are different in the 2D versus 3D flow fields. Are the results intuitive?
- P8.5** Examine three-dimensional flowpaths in the three-layer model domain shown in [Fig. P8.1](#). This setting, which covers an area 15,000 m by 10,000 m, represents a deep, confined, faulted anisotropic aquifer at steady-state conditions. Groundwater flow is from left to right in [Fig. P8.1](#). There is a proposal to inject oil field wastes at either site I1 or I2, and to extract water from P1 for use at associated energy production sites. There is concern that the injection of wastes will adversely affect the quality of extracted groundwater. You are asked to design an injection scheme that eliminates or reduces the capture of injected water by the pumping well. Note that because this is a steady-state problem, the specified head boundary conditions affect the solution. However, because the problem is intended to provide an illustration of 3D PT, we will accept the boundaries as indicated in [Fig. P8.1](#).
- a.** Create a flow model and place both the pumping well, P1, and injection well, I1, in the third layer. Generate the steady-state head distribution. Without doing PT, evaluate the simulated heads, and using your knowledge of the hydraulic conductivity distribution and the boundary conditions sketch a few flowpaths between the injection site and either the pumping well or the right-hand model boundary.

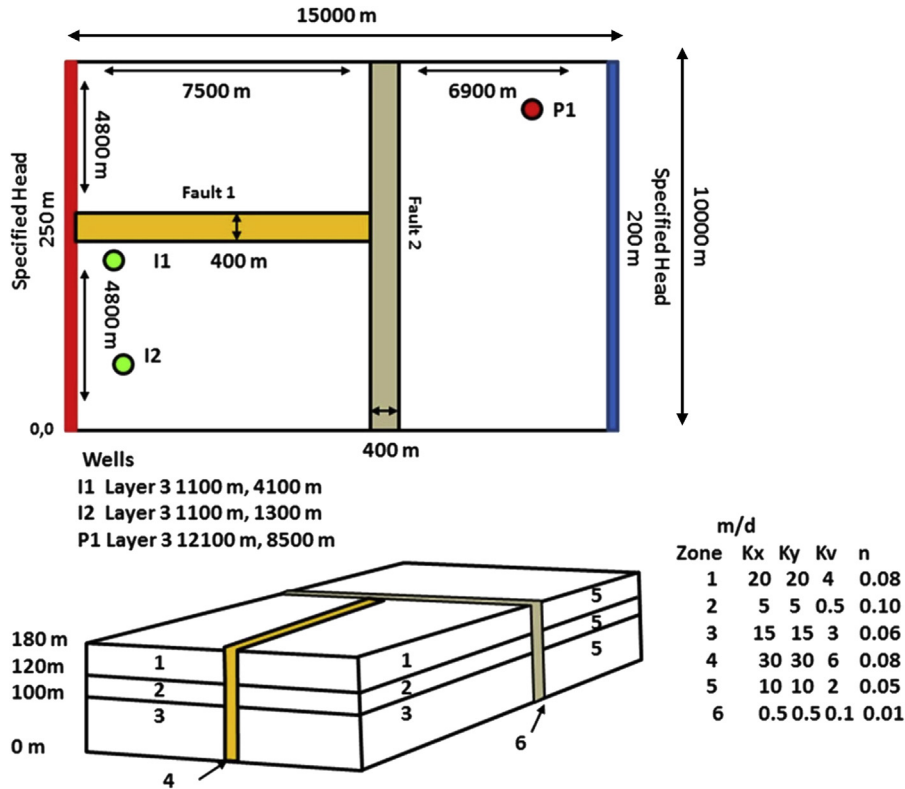


**Figure P8.1** Model domain of a portion of saturated rock located at depth below an area undergoing oil and gas development. The domain is composed of three layers that have similar properties on the left side of fault 2. The geologic material to the right of fault 2 is the same in each layer and represents a different rock type that has been faulted into this location. Faults each represent a zone 400-m wide and extend completely through each layer. Specified head boundaries are located on the left- and right-hand sides and extend to each layer in the domain. The remaining boundaries are no flow. Locations of injection wells I1 and I2 and pumping well P1 are also shown.

- b. Use a PT code with the effective porosity values given in Fig. P8.1 to calculate flowpaths by placing a circular set of particles around the injection well; use forward PT. Test the sensitivity of your results to number and placement of particles. How are these results similar or dissimilar to the flowpaths in (a)? Do the PT results suggest that injected wastewater is likely to reach the pumping well? Plot the flowpaths in 3D using a GUI or postprocessor and examine particle pathways. Comment on the challenges of visualizing and interpreting flowpaths in 3D.
- c. Repeat the flow modeling and PT process for the injection of the wastes at location I2. Compare and contrast results with those of (b).

- d. Examine how the placement of the pumping well within the fault block on the right-hand side of fault 2 affects the flowpaths. How would flowpaths change if you pumped the water from layer 1 instead of layer 3? How would flowpaths change if P1 were closer to fault 2?
- e. Use a PT code to compute the travel time for each particle used in (b) and (c). Under steady-state conditions, what are the maximum and minimum travel times for water injected at I1 and I2 to reach either P1 or the right-hand side boundary?
- P8.6** We will examine the influence of weak sinks on PT results by modifying the 900 m by 900 m nodal spacing used in Problem P6.1 (Chapter 6). Add a specified head boundary on the south side to create a steady-state flow field (Fig. P8.2). Modify your files for Problem P6.1 to set the head along the south boundary at 120 m and then using an effective porosity of 0.08 place a line of particles just inside the model domain adjacent to that boundary. Run the steady-state one-layer confined groundwater flow model with the well pumping at  $1060 \text{ m}^3/\text{day}$ .
- Run a PT code using threshold settings to allow all particles to pass through weak sinks. Plot the flowpaths and determine if the pumping node is a strong or weak sink.
  - Change the threshold to capture all particles when they enter a weak sink and rerun the model. Plot the flowpaths and determine if the code represented the pumping node as a strong or weak sink.

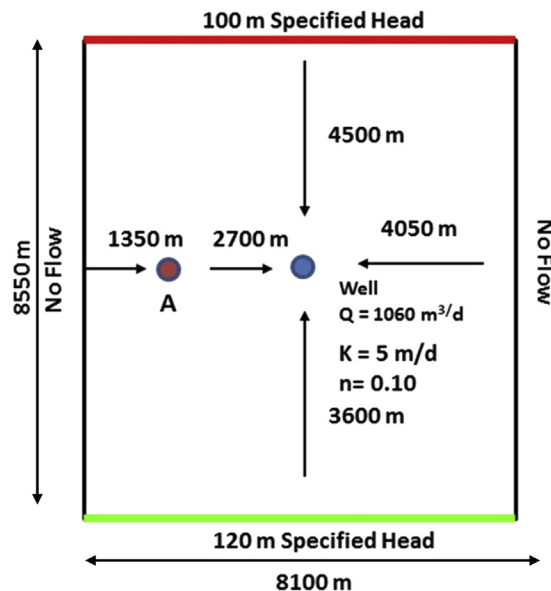


**Figure P8.2** Model domain of a 10-m thick single layer confined aquifer. Location of the pumping well is shown. The letter A (red dot) represents a monitoring well location.

- c. By modifying your input files for Problem P6.1 (a), (b), (c), or (d) you can evaluate the effect of discretization on particle capture. Delineate the capture zone for the pumping well. You will likely need to add additional particles along the southern boundary to assure sufficient particle pass-through in the area surrounding the well node. Run your flow and PT codes and examine how the size of the well capture zone changes with spatial discretization.

## REFERENCES

- Abrams, D., 2013. Correcting transit time distributions in coarse MODFLOW-MODPATH models. *Groundwater* 51 (3), 474–478. <http://dx.doi.org/10.1111/j.1745-6584.2012.00985.x>.
- Abrams, D., Haitjema, H., Kauffman, L., 2013. On modeling weak sinks in MODPATH. *Groundwater* 51 (4), 597–602. <http://dx.doi.org/10.1111/j.1745-6584.2012.00995.x>.
- Anderman, E.T., Hill, M.C., 2001. MODFLOW-2000, the U.S. Geological Survey Modular Groundwater Model Documentation of the Advective-Transport Observation (ADV2) Package, Version 2. U.S. Geological Survey Open-File Report 01-54, 68 p. <http://pubs.er.usgs.gov/publication/ofr0154>.
- Barlow, P.M., Leake, S.A., 2012. Streamflow Depletion by Wells—Understanding and Managing the Effects of Groundwater Pumping on Streamflow. U.S. Geological Survey Circular 1376, 84 p. <http://pubs.usgs.gov/circ/1376/>.
- Bethke, C.M., Johnson, T.M., 2002a. Paradox of groundwater age. *Geology* 30 (2), 107–110. <http://geology.gsapubs.org/content/30/2/107.abstract>.
- Bethke, C.M., Johnson, T.M., 2002b. Ground water age. *Groundwater* 40 (4), 337–339. <http://dx.doi.org/10.1111/j.1745-6584.2002.tb02510.x>.
- Bethke, C., Johnson, T., 2008. Groundwater age and groundwater age dating. *Annual Review of Earth and Planetary Science* 36, 121–152. <http://dx.doi.org/10.1146/annurev.earth.36.031207.124210>.
- Blandford, T.N., Huyakorn, P.S., 1990. WHPA: A Modular Semi-analytical Model for the Delineation of Wellhead Protection Areas. U.S. Environmental Protection Agency, Office of Ground-Water Protection, 247 p.
- Bosson, E., Selroos, J.-O., Stigsson, M., Gustafsson, L.-G., Destouni, G., 2013. Exchange and pathways of deep and shallow groundwater in different climate and permafrost conditions using the Forsmark site, Sweden, as an example catchment. *Hydrogeology Journal* 21 (1), 225–237. <http://dx.doi.org/10.1007/s10040-012-0906-7>.
- Bramlett, W., Borden, R.C., 1990. Numerical generation of flow nets — the FLOWNS model. *Groundwater* 28 (6), 946–950. <http://dx.doi.org/10.1111/j.1745-6584.1990.tb01731.x>.
- Ceric, A., Haitjema, H.M., 2004. On using simple time of travel capture zone delineation methods. *Groundwater* 43 (3), 408–412. <http://dx.doi.org/10.1111/j.1745-6584.2005.0035.x>.
- Charbeneau, R.J., Street, R.L., 1979. Modeling groundwater flow fields containing point singularities: Streamline, travel times, and breakthrough curves. *Water Resources Research* 15 (6), 1445–1450. <http://dx.doi.org/10.1029/WR015i006p01445>.
- Cordes, C., Kinzelbach, W., 1992. Continuous groundwater velocity fields and path lines in linear, bilinear, and trilinear finite elements. *Water Resources Research* 28 (11), 2903–2911. <http://dx.doi.org/10.1029/92WR01686>.
- DHI-WASY GmbH, 2012. FEFLOW 6.1 User Manual. DHI-WASH GmbH, Berlin, 116 p.
- Diersch, H.-J.G., 2014. FEFLOW: Finite Element Modeling of Flow, Mass and Heat Transport in Porous and Fractured Media. Springer, 996 p.
- Dunning, C.P., Feinstein, D.T., Hunt, R.J., Krohelski, J.T., 2004. Simulation of Ground-water Flow, Surface-water Flow and a Deep Sewer Tunnel System in Menomonee Valley. Wisconsin, Milwaukee. U.S. Geological Survey Scientific Investigations Report 2004-5031, 39 p. <http://pubs.usgs.gov/sir/2004/5031/>.
- Fitts, C.R., 2013. *Groundwater Science*, second ed. Academic Press, London, 672 p.

- Franz, T., Guiguer, N., 1990. FLOWPATH, Two-dimensional Horizontal Aquifer Simulation Model. Waterloo Hydrogeologic Software, Waterloo, Ontario, 74 p.
- Frind, E.O., Molson, J.W., 2004. A new particle tracking algorithm of finite element grids, Keynote Lecture. In: FEM MODFLOW: Finite-Element Models, MODFLOW and More. International Association of Hydrological Sciences and United States Geological Survey, Karlovy Vary (Carlsbad), Czech Republic, 4 p.
- Frind, E.O., Muhammad, D.S., Molson, J.W., 2002. Delineation of three-dimensional well capture zones for complex multi-aquifer systems. *Groundwater* 40 (6), 586–598. <http://dx.doi.org/10.1111/j.1745-6584.2002.tb02545.x>.
- Frings, R.M., Schüttrumpf, H., Vollmer, S., 2011. Verification of porosity predictors for fluvial sand-gravel deposits. *Water Resources Research* 47 (7), W07525. <http://dx.doi.org/10.1029/2010WR009690>.
- Gelhar, L.W., Welty, C., Rehfeldt, K.R., 1992. A critical review of data on field-scale dispersion in aquifers. *Water Resources Research* 28 (7), 1955–1974. <http://dx.doi.org/10.1029/92WR00607>.
- Goode, D.J., 1996. Direct simulation of groundwater age. *Water Resources Research* 32 (2), 289–296. <http://dx.doi.org/10.1029/95WR03401>.
- Haitjema, H.M., 1995. Analytic Element Modeling of Groundwater Flow. Academic Press, Inc., San Diego, CA, 394 p.
- Haitjema, H., 2006. The role of hand calculations in ground water flow modeling. *Groundwater* 44 (6), 786–791. <http://dx.doi.org/10.1111/j.1745-6584.2006.00189.x>.
- Haitjema, H., Kelson, V., de Lange, W., 2001. Selecting MODFLOW cell sizes for accurate flow fields. *Groundwater* 39 (6), 931–938. <http://dx.doi.org/10.1111/j.1745-6584.2001.tb02481.x>.
- Haugh, C.J., Carmichael, J.K., Ladd, D.E., 2004. Hydrogeology and Ground-Water-Flow Simulation in the Former Airfield Area of Naval Support Activity Mid-South, Millington, Tennessee. U.S. Geological Survey Scientific Investigations Report 2004-5040, 31 p. <http://pubs.usgs.gov/sir/2004/5040/>.
- Hunt, R.J., Feinstein, D.T., Pint, C.D., Anderson, M.P., 2005. The importance of diverse data types to calibrate a watershed model of the Trout Lake Basin, northern Wisconsin, USA. *Journal of Hydrology* 321 (1–4), 286–296. <http://dx.doi.org/10.1016/j.jhydrol.2005.08.005>.
- Jackson, C.R., 2002. Steady-State Particle Tracking in the Object-Oriented Regional Groundwater Model ZOOMQ3D. British Geological Survey Commissioned Report CR/02/201c, Environmental Agency National Groundwater Contaminated Land Centre, Technical Report NC/01/38/2, 32 p.
- Jackson, C.R., Spink, A.E.F., 2004. User's Manual for the Groundwater Flow Model ZOOMQ3D. British Geological Survey, Nottingham, UK, 107 pp. (IR/04/140). <http://nora.nerc.ac.uk/11829/>.
- van der Kamp, G., Van Steenpoort, D.R., Wassenaar, L.I., 1996. The radial diffusion method: 1. Using intact cores to determine isotopic composition, chemistry, and effective porosities for groundwater in aquitards. *Water Resources Research* 32 (6), 1815–1822. <http://dx.doi.org/10.1029/95WR03719>.
- Kincaid, C.T., 1988. FASTCHEM™ Package, V.3: User's Guide to the ETUBE Pathline and Streamtube Database Code. EPRI EA-5870-CCM, Electric Power Research Institute.
- Kresic, N., 2007. Hydrogeology and Groundwater Modeling, second ed. CRC Press, Boca Raton, FL, 807 p.
- Masbruch, M.D., 2005. Delineation of Source Areas and Characterization of Chemical Variability Using Isotopes and Major Ion Chemistry, Allequash Basin, Wisconsin. M.S. thesis. Department of Geology and Geophysics, University of Wisconsin—Madison, 131 p.
- McCallum, J.L., Cook, P.G., Simmons, C.T., 2014. Limitations of the use of environmental tracers to infer groundwater age. *Groundwater*, early view. <http://dx.doi.org/10.1111/gwat.12237>.
- Molson, J.W., Frind, E.O., 2012. On the use of mean groundwater age, life expectancy and capture probability for defining aquifer vulnerability and time-of-travel zones for source water protection. *Journal of Contaminant Hydrology* 127, 76–87. <http://dx.doi.org/10.1016/j.jconhyd.2011.06.001>.
- Muffels, C., Wang, X., Neville, C.J., Tonkin, M., 2014. User's Guide for Mod-PATH3DU, a Groundwater Path and Travel-time Simulator, Version 1.0.0. S.S. Papadopulos and Associates, Inc., Bethesda, Maryland. <http://www.sspa.com/software/mod-path3du>.
- Newsom, J.M., Wilson, J.L., 1988. Flow of ground water to a well near a stream—effect of ambient groundwater flow direction. *Groundwater* 26 (6), 703–711. <http://dx.doi.org/10.1111/j.1745-6584.1988.tb00420.x>.

- Painter, S.L., Gable, C.W., Kelkar, S., 2012. Pathline tracing on fully unstructured control-volume grids. *Computational Geosciences* 16 (4), 115–1134. <http://dx.doi.org/10.1007/s10596-012-9307-1>.
- Painter, S.L., Robinson, B.A., Dash, Z.V., 2013. Calculation of resident groundwater concentration by post-processing particle-tracking results. *Computational Geosciences* 17 (2), 189–196. <http://dx.doi.org/10.1007/s10596-012-9325-z>.
- Panday, S., Langevin, C.D., Niswonger, R.G., Ibaraki, M., Hughes, J.D., 2013. MODFLOW—USG Version 1: An Unstructured Grid Version of MODFLOW for Simulating Groundwater Flow and Tightly Coupled Processes Using a Control Volume Finite-Difference Formulation. U.S. Geological Survey Techniques and Methods, Book 6, Chapter A45, 66 p. <http://pubs.usgs.gov/tm/06/a45>.
- Paschke, S.S., Kauffman, L.J., Eberts, S.M., Hinkle, S.R., 2007. Overview of regional studies of the transport of anthropogenic and natural contaminants to public-supply wells. In: Paschke, S.S. (Ed.), *Hydrogeologic Settings and Ground-water Flow Simulations for Regional Studies of the Transport of Anthropogenic and Natural Contaminants to Public-Supply Wells—Studies Begun in 2001*, pp. 1–1–1–18. U.S. Geological Survey Professional Paper 1737–A. <http://pubs.usgs.gov/pp/2007/1737a/>.
- Pint, C.D., Hunt, R.J., Anderson, M.P., 2003. Flowpath delineation and ground water age, Allequash Basin, Wisconsin. *Groundwater* 41 (7), 895–902. <http://dx.doi.org/10.1111/j.1745-6584.2003.tb02432.x>.
- Pollock, D.W., 1989. Documentation of computer programs to compute and display pathlines using results from the U.S. Geological Survey modular three-dimensional finite-difference ground-water model. U.S. Geological Survey Open File Report 89-381, 81 p. <http://pubs.er.usgs.gov/publication/ofr89381>.
- Pollock, D.W., 2012. User guide for MODPATH Version 6–A Particle-Tracking Model for MODFLOW. U.S. Geological Survey Techniques and Methods 6–A41, 59 pp. <http://pubs.usgs.gov/tm/6a41/>.
- Pollock, D.W., 2015. Extending the MODPATH algorithm to rectangular unstructured grids. *Groundwater*, early view. <http://dx.doi.org/10.1111/gwat.12328>.
- Rayne, T.W., Bradbury, K.R., Zheng, C., 2013. Correct delineation of capture zones using particle tracking under transient conditions. *Groundwater* 52 (3), 332–334. <http://dx.doi.org/10.1111/gwat.12141>.
- Reynolds, D.A., Marimuthu, S., 2007. Deuterium composition and flow path analysis as additional calibration targets to calibrate groundwater flow simulation in a coastal wetlands system. *Hydrogeology Journal* 15 (3), 515–535. <http://dx.doi.org/10.1007/s10040-006-0113-5>.
- Shafer, J.M., 1987. Reverse pathline calculation of time related capture zones in nonuniform flow. *Groundwater* 25 (3), 283–289. <http://dx.doi.org/10.1111/j.1745-6584.1987.tb02132.x>.
- Shafer, J.M., 1990. GWPAT.H. Version 4.0. J.M. Shafer, Champaign, IL.
- Shoemaker, W.B., O'Reilly, A.M., Sepúlveda, N., Williams, S.A., Motz, L.H., Sun, Q., 2004. Comparison of Estimated Areas Contributing Recharge to Selected Springs in North-Central Florida by Using Multiple Ground-water Flow Models. U.S. Geological Survey Open-File Report 03–448, 31 p. <http://pubs.er.usgs.gov/publication/ofr03448>.
- Skinner, K.D., Rupert, M.G., 2012. Numerical Model Simulations of Nitrate Concentrations in Groundwater Using Various Nitrogen Input Scenarios, Mid-Snake Region, South-Central Idaho. U.S. Geological Survey Scientific Investigations Report 2012-5237, 30 p. <http://pubs.usgs.gov/sir/2012/5237/>.
- Spitz, F.J., Nicholson, R.S., Pope, D.A., 2001. A nested discretization method to improve pathline resolution by eliminating weak sinks representing wells. *Groundwater* 39 (5), 778–785. <http://dx.doi.org/10.1111/j.1745-6584.2001.tb02369.x>.
- Stephens, D.B., Hsu, K.-C., Prieksat, M.A., Ankey, M.D., Blandford, N., Roth, T.L., Kelsey, J.A., Whitworth, J.R., 1998. A comparison of estimated and calculated effective porosity. *Hydrogeology Journal* 6 (1), 156–165. <http://dx.doi.org/10.1007/s100400050141>.
- Suk, H., 2012. Practical implementation of new particle tracking method to the real field of groundwater flow and transport. *Environmental Engineering Science* 29 (1), 70–78. <http://dx.doi.org/10.1089/ees.2011.0153>.
- Suk, H., Yeh, G.T., 2009. Multidimensional finite-element particle tracking method for solving complex transient flow problems. *Journal of Hydrologic Engineering* 14 (7), 759–766. [http://dx.doi.org/10.1061/\(ASCE\)HE.1943-5584.0000047](http://dx.doi.org/10.1061/(ASCE)HE.1943-5584.0000047).

- Suk, H., Yeh, G.T., 2010. Development of particle tracking algorithms for various types of finite elements in multi-dimensions. *Computers and Geosciences* 36 (4), 564–568. <http://dx.doi.org/10.1016/j.cageo.2009.09.011>.
- Townley, L.R., Trefry, M.G., 2000. Surface water-groundwater interaction near shallow circular lakes: Flow geometry in three dimensions. *Water Resources Research* 36 (4), 935–948. <http://dx.doi.org/10.1029/1999WR900304>.
- Visser, A., Heerink, R., Broers, H.P., Bierkens, M.F.P., 2009. Travel time distributions derived from particle tracking in models containing weak sinks. *Groundwater* 47 (2), 237–245. <http://dx.doi.org/10.1111/j.1745-6584.2008.00542.x>.
- Walter, D.A., Masterson, J.P., 2003. Simulation of Advective Flow Under Steady-State and Transient Recharge Conditions, Camp Edwards, Massachusetts Military Reservation, Cape Cod, Massachusetts. U.S. Geological Survey Water-Resources Investigations Report 03-4053, 51 p. <http://pubs.usgs.gov/wri/wri034053/>.
- Weissmann, G.S., Zhang, Y., La Bolle, E.M., Fogg, G.E., 2002. Dispersion of groundwater age in an alluvial aquifer system. *Water Resources Research* 38 (10), 16-1–16-8. <http://dx.doi.org/10.1029/2001WR000907>.
- Zheng, C., 1989. PATH3D, A Ground-water Path and Travel-Time Simulator, Version 3.0 User's Manual. S.S. Papadopoulos & Associates, Inc., Bethesda, MD.
- Zheng, C., 1994. Analysis of particle tracking errors associate with spatial discretization. *Groundwater* 32 (5), 821–828. <http://dx.doi.org/10.1111/j.1745-6584.1994.tb00923.x>.
- Zheng, C., Bennett, G.D., 2002. *Applied Contaminant Transport Modeling*, second ed. John Wiley & Sons, New York. 621 p.
- Zhou, Y., Haitjema, H., 2012. Approximate solutions for radial travel time and capture zone in unconfined aquifers. *Groundwater* 50 (5), 799–803. <http://dx.doi.org/10.1111/j.1745-6584.2011.00883.x>.



## CHAPTER 9

# Model Calibration: Assessing Performance

*Clearly, many branches of science need an exquisite precision...and the infinitesimal decimals of calibration, so space launches, for example, are not scheduled for leap-second dates. But society as a whole neither needs that obsessive...measurement nor is well served by it.*

*Jay Griffith, A Sideways Look at Time*

### Contents

9.1 Introduction	376
9.2 Limitations of History Matching	378
9.3 Calibration Targets	380
9.3.1 Head Targets	381
9.3.2 Flux Targets	382
9.3.3 Ranking Targets	384
9.4 Manual History Matching	385
9.4.1 Comparing Model Output to Observations	385
9.4.2 Choosing the Parameters to Adjust	393
9.4.3 Manual Trial-and-Error History Matching	394
9.4.4 Limitations of a Manual Approach	395
9.5 Parameter Estimation: Automated Trial-and-Error History Matching	396
9.5.1 Weighting the Targets	400
9.5.2 Finding a Best Fit	402
9.5.3 Statistical Analysis	410
9.6 Highly Parameterized Model Calibration with Regularized Inversion	411
9.6.1 Increasing the Number of Calibration Parameters	412
9.6.2 Stabilizing Parameter Estimation	414
9.6.2.1 Adding Soft Knowledge: Tikhonov Regularization	414
9.6.2.2 Collapsing Problem Dimensionality: Subspace Regularization	420
9.6.3 Speeding the Parameter Estimation Process	424
9.7 A Workflow for Calibration and Model Performance Evaluation	426
9.8 Common Modeling Errors	431
9.9 Problems	432
References	436

### Boxes

Box 9.1 Historical Context for Parameter Estimation	397
Box 9.2 Tips for Running a Parameter Estimation Code	408
Box 9.3 Tips for Effective Pilot Point Parameterization	416
Box 9.4 A “Singularly Valuable Decomposition”—Benefits for Groundwater Modeling	421

Box 9.5 Code/Model Verification and Model Validation

427

Box 9.6 Additional Parameter Estimation Tools

430

## 9.1 INTRODUCTION

Groundwater modeling would be straightforward if it were possible to characterize the natural world perfectly. Then boundary and parameter assignment would incorporate all relevant spatial and temporal information and the model would exactly simulate the real groundwater system. However, groundwater systems are never known exactly and, rather than reflecting the environmental system itself, we must map this system into a *model space* (Beven, 2009, p. 11). Model space is used here to define the range of feasible models and model inputs that are potentially appropriate for a field site. During the translation that occurs during this mapping, the already simplified view of the natural world represented by a conceptual model is further simplified so that a numerical model is computationally tractable. In order to judge how well this mapping of an environmental system to a model space was performed, model performance must be evaluated using field observations that can be compared with model output (*hard data*) as well as everything else we know about the system (*soft data*).

In the *forward problem*, parameters such as hydraulic conductivity, specific storage, storativity/specific yield, and recharge rate are specified, and heads and fluxes are calculated. However, in practice, field-measured values of heads and fluxes are usually known with a relatively higher degree of confidence and parameter values are less well known. In this context, the groundwater model is posed as an *inverse problem*, where head observations form the dependent variable in the governing equation and are used to solve for parameter values. Inverse problems are typically solved by *history matching*, a term that originated in the petroleum industry and refers to the matching model outputs to a historical time series of measured values by adjusting model inputs. For our purposes, history matching refers to matching field measurements (including at least heads and fluxes) in both steady-state and transient simulations (Chapter 7). The objective of history matching is to identify a set of parameters that produces a satisfactory match to the field observations. Parameters are adjusted within reasonable ranges in sequential forward runs of the model until the model produces an acceptable match. In its most general form (Fig. 9.1), history matching includes these steps:

1. select calibration targets from the set of field observations;
2. run the model using best estimates of input parameters (material property parameters and hydrologic parameters; Section 5.4);
3. compare simulated outputs to the targets;
4. adjust values of input parameters to obtain better fits of simulated values to targets;
5. select the model with the best fit possible given limitations on time and resources.

We distinguish between two phases of history matching: the first involving manual trial-and-error history matching shown in Fig. 9.1; and a subsequent phase where history matching is performed using software. History matching is important for evaluating a

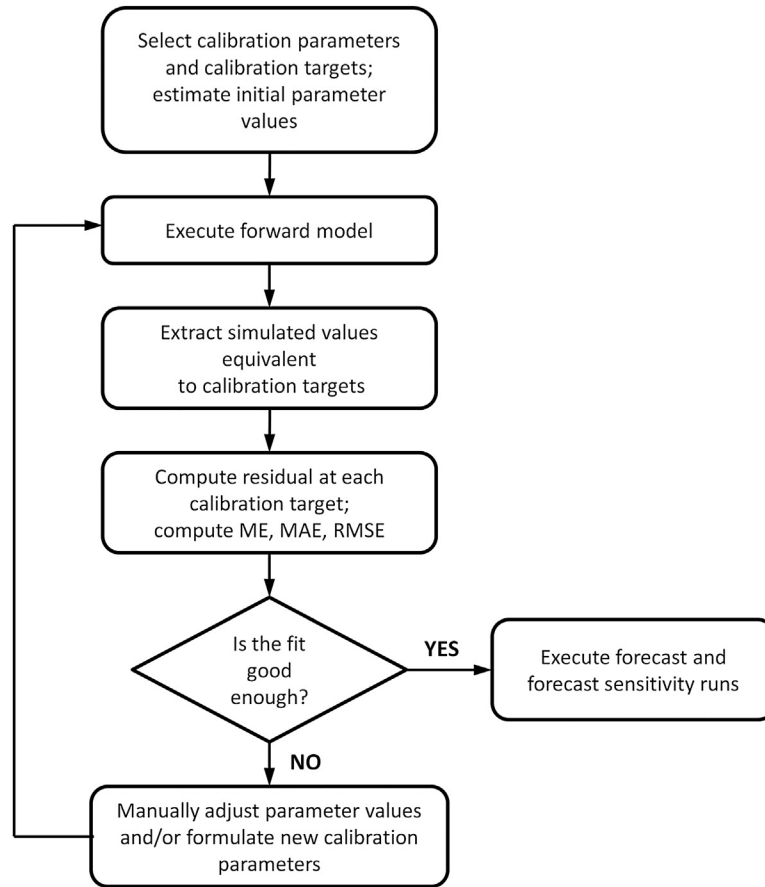


**Figure 9.1** General workflow for manual trial and error, the first phase of history matching a model intended for forecasting (ME, mean error; MAE, mean absolute error; RMSE, root mean squared error).

model's fit for purpose: if a model cannot reproduce the measured heads and fluxes with sufficient accuracy, one can have little confidence that the calibrated model will adequately reproduce unmeasured heads and fluxes or forecast future conditions.

History matching can be considered a *hard knowledge* evaluation of model performance because field measurements can be directly compared with simulated values, sometimes also called *simulated equivalent values*. However, a good fit does not mean that the match is acceptable; the match is acceptable only if the parameters and assumptions used to obtain the fit are reasonable. Therefore, model performance evaluation also includes a *soft knowledge* evaluation of *hydrogeologic reasonableness*. Soft knowledge relies on expert knowledge about the system that is not directly comparable to quantitative model outputs, and draws on geological and hydrologic information of the site and basic hydrogeologic theory embodied in the conceptual model (Section 2.3). For example, if we know that the aquifer consists of gravel, a model calibrated with hydraulic conductivity values typical of silt and clay would be rejected even if the model satisfactorily reproduced field

observations. Similarly, in most cases a model that produced a good fit but used recharge rates larger than precipitation rates would be rejected as hydrogeologically unreasonable. Effective soft knowledge assessment draws on the literature, knowledge of site conditions, hydrogeological principles, and professional experience. Guidelines for this type of assessment are not easily reduced to simple instructions or steps. Rather, soft knowledge assessments rely on “hydrosense” (Hunt and Zheng, 2012) that is developed with experience solving hydrogeological problems and designing and running models.

In practice, assessment of hydrogeological reasonableness using soft knowledge is done in concert with history matching. The combined evaluation of both hard and soft knowledge is *model calibration*, where a final *calibrated model* has an acceptable fit to observations and contains reasonable parameters and assumptions. If a model does not pass both assessments it cannot be considered calibrated. Typically, most effort and reporting focuses on the model’s ability to fit observations (history matching), because assessments using hard knowledge can be easily communicated using summary statistics and visualization. Evaluation of a model’s adherence to soft knowledge is not easily quantified and is often conveyed with words (e.g., “the calibrated parameter value is consistent with values reported for the site...”). In practice, model assessment using hard knowledge of model fit is sandwiched between two soft knowledge assessment activities: development of the conceptual model and evaluation of calibrated parameters for reasonableness. Although soft knowledge assessment of the calibrated parameter values is important, the focus of this chapter is on the five steps listed above that constitute history matching.

## 9.2 LIMITATIONS OF HISTORY MATCHING

Groundwater models simulate a portion of a complex natural world, much of which is unseen and uncharacterized (Freeze et al., 1990). Hence, the groundwater modeling problem is inherently tied to an *open system* (Oreskes et al., 1994) that, by definition, is impossible to characterize completely. As a result, a groundwater model is always a simplification of the true hydrogeologic system. Because the natural world is complex both in properties and processes, models almost always have more unknown parameter values than field measurements. As such, the inverse problem is said to be *underdetermined* by observations and therefore mathematically *ill-posed* (e.g., Freeze and Cherry, 1979; McLaughlin and Townley, 1996). A well-posed problem has a solution that depends continuously on the data, and is unique (Hadamard, 1902). In practice, what we know is typically not sufficient to constrain the problem to one unique solution. Rather, the modeler often must consider a “family” of possible reasonable models because groundwater models are fundamentally *nonunique*. In the broadest sense, a modeling problem might be considered an expression of multiple working hypotheses about how the system works, where model evaluation is a form of hypothesis testing rather than a matter of finding the optimal model (Beven, 2009, p. 18). In practice, however, decision-makers often require a single “best” model for the decision of interest. Therefore,

the selected best calibrated model should ideally: (1) be based on the strongest conceptual model; (2) utilize all the information contained in the available observations; (3) avoid inappropriate simplification of natural world processes and structure important for the forecast(s) of interest; (4) be sufficiently discretized in space and time; and (5) have manageable run times given financial and time constraints of the project.

Fully understanding groundwater model nonuniqueness is critical for identifying an appropriate model, as well as forming the family of defensible models. We cannot objectively define a uniquely best model because all field-based groundwater modeling efforts necessarily use data sets that are incomplete and contain errors (e.g., [Table 9.1](#)). There will always be a number of possible defensible models that can reasonably simulate what we know about the real-world system that the model aims to represent. Hence, selection of a model that is considered the best representation of this reality will always be subjective ([Doherty and Hunt, 2009a,b](#)) even if unlimited resources and time were available.

This does not mean that all models are potentially acceptable nor is the selection of a “best” model based on whim. Rather, the corollary to a number of possible reasonable models is a much larger number of unreasonable ones. A skilled modeler discerns those dead-ends quickly and focuses on the reasonable subset. Therefore, although subjectivity operates within the realm of the family of reasonable models, those models outside this realm can be more objectively discarded. Models that fail calibration because they fail to achieve a satisfactory history match, use unreasonable parameter values, and/or do not conform to the conceptual model, may be discarded.

**Table 9.1** Estimated accuracy of head data by measurement method (modified from [Nielson, 1991](#)). Measurement method is but one source of error for head targets

Measurement method	Accuracy, in feet	Major interference or disadvantage
<b><i>Nonflowing wells</i></b>		
Steel tape and chalk	0.01	Cascading water
Electric tape	0.02–0.1	Cable wear; hydrocarbons on water
Pressure transducers	0.01–0.1	Temperature change; electronic drift; blocked capillary
Acoustic probe	0.02	Cascading water; floating hydrocarbons on water
Ultrasonics	0.02–0.01	Temperature change; well materials
Floats	0.02–0.05	Float or cable drag; float size or lag
Poppers	0.1	Background noise in/around well; well depth
Air lines	0.25–1.0	Air line or fitting leaks; gage inaccuracies
<b><i>Flowing wells</i></b>		
Transducers	0.02	Temperature changes; electronic drift
Casing extensions	0.1	Limited range; awkward
Manometer/pressure gage	0.1–0.5	Gage inaccuracies; calibration required

Haitjema (2015) pointed out that the logical endpoint of calibration cannot be finding the *true model*, one that contains completely accurate properties of the field site. Nor is the logical endpoint even an *optimal model*, one that uses the most sophisticated methods to squeeze out every bit of information from every observation. Rather, in practice, the logical endpoint of modeling is an *appropriate model*—a model that balances sophistication and realistic representation with resources and time available. The concept of the appropriate model can be illustrated by the following example. If 80% of the project objective can be met with a model that used only 10% of the financial resources, can the decision the model was designed to address be made without expending additional resources on the remaining 20% of the objective? Can the uncertainty associated with the unknown 20% be handled in other ways, such as engineering safety factors? Or put another way, is it worth spending the remaining 90% of the resources to attempt to address the remaining 20% of the objective? The concept of the appropriate model recognizes that 80% of the answer may suffice for many problems that require modeling. However, at a minimum, an appropriate groundwater flow model must be a defensible representation of the groundwater system that, at a minimum, approximates large-scale observed groundwater flow directions and head trends.

### 9.3 CALIBRATION TARGETS

Commonly a modeler has a number of (imperfect) observations, typically heads and fluxes, which collectively give a partial snapshot of true field conditions at a site. Not all observations are equally certain; some may be relatively precise and accurate while others are decidedly approximate. The modeler selects all or some of these observations from similar conditions/time periods as *calibration targets*. Calibration targets are compared with simulated values during history matching to describe model fit, and contain the hard knowledge about the system. Hence, requiring that simulated values match the calibration targets forces the model to respond like the field system, at least for the conditions represented in the simulation. Information contained within the calibration targets, in turn, constrains model parameters that are adjusted during history matching.

Inclusion of several different types of calibration targets maximizes the amount of information that can be considered during calibration. At a minimum, both head and flux targets should routinely be used during history matching because one type of observation (e.g., heads) alone cannot mathematically constrain the inverse solution of the groundwater flow equation uniquely (Box 3.2, see also Haitjema, 2006). Ideally, the model should use as many types of available observations as can be compared to model outputs (Hunt et al., 2006). In addition to heads and fluxes, observations for history matching might include results from advective particle tracking (Chapter 8), as shown in Fig. 9.2, borehole flow measurements, indirect flux measurements based on isotope compositions, temperature, and solute concentrations, and observations from remote sensing (e.g., the

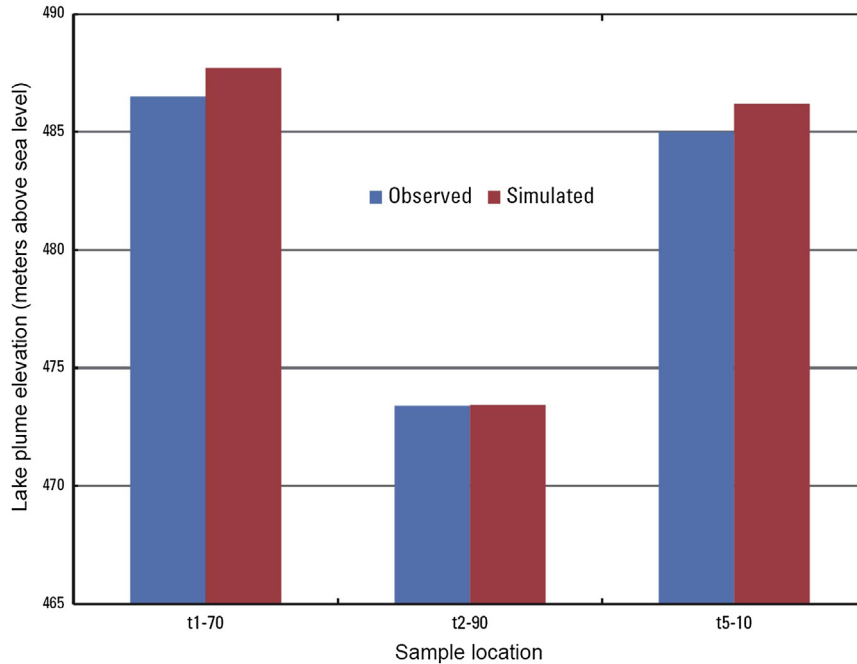


**Figure 9.2** History matching to the depth of the interface between a plume of lake water and terrestrially recharged groundwater at three locations. The interface was located in the field by using measurements of stable isotopes of water (observed) and in the model by advective particle tracking (simulated) (modified from [Hunt et al., 2013](#)).

occurrence of saturated soils), and geophysics (e.g., extent of a contaminant plume). An objective of calibration is to extract the maximum information from all observations available while balancing the potentially contradictory information from different observations. Though many types of targets are desirable, our discussion will focus on the minimum recommended and most commonly used types, head and flux targets.

### 9.3.1 Head Targets

Head is the only type of target that is a direct output of the groundwater flow equation, and at least some measurements of head are available in most groundwater investigations. Ideally, head values provide the modeler with a relatively large number of observations distributed in space and time (Fig. 7.11). Even with large numbers of head measurements, it is important to note that head data have associated uncertainty. *Measurement errors* include uncertainty associated with the accuracy of the water level measuring device (Table 9.1), potential operator error, and errors that result from inaccurate surveying of the elevation of a well's measuring point. *Interpolation errors* occur when the field head

target is not located on a node in the grid or mesh. Comparison of simulated and observed heads can be improved by the use of postprocessing algorithms (included in some graphical user interfaces (GUIs)) that interpolate simulated heads in order to make a target location-specific comparison. Heads may be measured in wells with screens that partially penetrate a model layer or penetrate more than one model layer (Section 6.2). Heads measured in wells with long screens may be appropriate for history matching vertically averaged head output from a two-dimensional areal model. However, vertically distinct head measurements at a given location are better suited for 3-D modeling. Such data are obtained from nested and multilevel piezometers, where multiple discrete measuring points are open to different elevations (e.g., Meyer et al., 2014). The difference in head between vertically separated observation points can also be processed for use as *head difference targets*. Head difference targets increase the signal-to-noise ratio of the head data and are especially useful for calibration of vertical hydraulic conductivity (Doherty and Hunt, 2010, p. 13) but are typically used together with unprocessed head targets. *Transient errors* are introduced when a single value of head is used as a target when multiple measurements over a period of time show temporal changes in head (Fig. 7.1). Steady-state models may be calibrated using temporally averaged head targets where the measurements span time periods meaningful for the modeling objective (Figs 7.2 and 7.3). However, in some locations heads can fluctuate 10s of meters over a selected time period, and a steady-state model is inappropriate (Section 7.2). In transient models, *temporal head difference targets* can be calculated from a time series (Fig. 7.11) as the difference between observed heads measured at two different times and are often superior to absolute head targets in transient models (Doherty and Hunt, 2010, p. 13).

Head target uncertainty is usually expressed as a *standard deviation* (the square root of the average of squared differences of the values from their average value) or *variance* (the square of the standard deviation) around the observed head value. Head target uncertainty can also be expressed as the 95% confidence interval (approximately  $\pm$  two standard deviations) around the reported value. Clearly, information on the magnitude of the types of errors described above helps quantify the uncertainty associated with a head target. Surveying error should be recorded when a well's measurement point is surveyed; instrument and operator errors should be estimated and recorded when the well is monitored for head. Details of well construction are needed to assess scaling error, and time series of head measurements are required to assess temporal error. Total combined errors of head targets are never perfectly known; thus a modeler commonly states an assessment of head target certainty without detailed breakdown of all components of uncertainty present.

### 9.3.2 Flux Targets

Flux observations include a variety of types of flows such as baseflow, springflow, infiltration from a losing stream, groundwater inflow to a lake, and evapotranspiration across



the water table, and all may be used as calibration targets. Spatially integrated values of groundwater fluxes to and from streams are often estimated from stream gage data or miscellaneous stream discharge measurements. Point estimates of fluxes can be upscaled from direct field measurements or computed using field data and Darcy's law. Fluxes can also be estimated indirectly using tracers (e.g., McCallum et al., 2012; Gardner et al., 2011; Cook et al., 2008; Hunt et al., 1996; Krabbenhoft et al., 1994). Typically, the modeler has many fewer flux observations than head measurements. Nevertheless, flux observations at different locations in the problem domain are extremely helpful during calibration because they give insight into processes in different areas represented in the model. Not all locations of flux targets are equally valuable for calibration: for example, a baseflow measurement at the most downstream location of a model domain commonly has high importance because it integrates the most model area, while locations upstream represent the distribution of groundwater flow within smaller areas of the model domain (Hunt et al., 2006).

For transient models, flux targets are most useful when averaged over time periods suited to the modeling objective (e.g., mean monthly baseflow; defined using flow duration/cumulative probability curves). Time periods used for averaging should correspond to the time period for temporal averaging of head targets when possible. *Spatial flux difference targets* (differences between fluxes at different locations measured during a similar time period) and *temporal flux difference targets* (difference between fluxes at the same location at different times) help maximize the extraction of information contained within raw observed flow data. Difference targets should be used together with standard flux targets whenever possible.

Similar to head targets, flux targets have associated measurement error, and in practice their measurement error is commonly larger than for heads because it is more difficult to measure fluxes accurately in the field. Transient errors in streamflow targets are usually relatively large because surface water flows tend to be more temporally variable than groundwater fluxes. Indirect estimation of flux involves a number of assumptions, which introduce additional error to the flux target. In practice, therefore, each flux target will have its own associated measurement error.

Flux target uncertainty is commonly expressed as *coefficient of variation* (standard deviation divided by the expected, or average, value) relative to the observed value (e.g.,  $\pm 20\%$ ). This type of reporting normalizes the uncertainty to the magnitude of the flux, which is useful for reporting uncertainty of flux targets of different magnitudes. For steady-state models, a coefficient of variation is often assigned to a single flux target to express the uncertainty based on the range of flux measurements in the time series. Similar to head targets, flux target uncertainty can also be expressed as the 95% confidence interval (approximately plus or minus two standard deviations) around the reported value. For example, uncertainty in steady-state flux targets is shown by error bars in Fig. 9.7(a). When possible field data are used to quantify the magnitude of

uncertainty (for example, time series data from a stream gage), but in many cases uncertainty is assigned using professional judgment and based on the importance of the target to the modeling objective.

### 9.3.3 Ranking Targets

Not all targets are equally certain or important to the modeling purpose (e.g., [Townley, 2012](#)), and no model can match all calibration targets equally well. Therefore, it is necessary to decide which targets are most important. This is done by *ranking* the targets, where the rank expresses the modeler's judgment of the importance of simulating a specific target during history matching. The modeler tries to find a good match to the higher ranked targets and may accept a model that poorly matches lower ranked targets. The set of ranked targets is the single most important expression of what the modeler holds to be important for calibration, and by extension, the modeling objective. The ranked targets affect both the identification of an appropriate model and the forecasts (Chapter 10) made using the final calibrated model.

From the perspective of statistical theory, ranking targets according to their measurement error is a primary consideration (e.g., [Hill and Tiedeman, 2007](#)), and target measurement error is a recommended first approximation for specifying target importance. However, this first ranking typically is adjusted to reflect practical considerations related to the type and location of the target ([Doherty and Hunt, 2010](#), p. 12). For example, there may be hundreds of one type of target (commonly heads) and only one or a few of another (commonly fluxes and/or head difference targets). If measurement error were used as the only ranking criterion, model fit would be overwhelmingly dominated by a large number of head values, which would imply that matching all head targets is more important than matching the fewer flux targets. Likewise, head and flux measurements from the area of primary modeling interest (the *near-field*) are likely most relevant to the modeling purpose and forecast. Targets distributed in the model domain outside the area of interest (the *far-field*) typically have relatively less importance due simply to their location. Therefore, even though near-field and far-field targets might have the same measurement error, they would not be considered equally valuable for finding the best appropriate model. As a result, far-field targets are assigned a lower rank. The ranking might also include consideration of target type; if the modeling purpose required forecasts of future fluxes at a near-field flux target location, for example, a modeler would likely be willing to trade worse fit in heads simulated at far-field targets in order to get a better simulation of the flux target of interest.

Ultimately, the best appropriate model is the one that provides the best forecasts of interest for the system. As such, the ranking of targets should anticipate the needs of the forecasting simulation (Chapter 10). Consequently, because each model is uniquely characterized by its purpose, there is no universally appropriate way to rank targets; rather, it is recognized that this ranking will always include subjective elements that rely on professional experience and

the modeling objective (Doherty and Hunt, 2010, p. 12). In the first phase of history matching (manual trial-and-error calibration; Section 9.4), subjectivity is obvious because targets are ranked qualitatively in order of importance. In the second phase of history matching (automated trial-and-error calibration; Section 9.5), targets are quantitatively ranked using numerical weights (e.g., Table 7.1) but still rely on the subjective judgment of the modeler.

## 9.4 MANUAL HISTORY MATCHING

Once calibration targets are selected and ranked, the groundwater flow model is executed using a set of initial parameter values based on the conceptual model. For some screening models and heuristic modeling exercises where observations do not exist (e.g., Beven, 2009, p. 49), the first forward run might produce results sufficient for the modeling objective. In that case, all subsequent work focuses on forecasting and estimating uncertainty in the forecasts (Chapter 10). Typically, however, multiple runs are necessary to obtain an acceptable history match. The first step in the history matching process involves measuring and improving model fit with *manual trial-and-error* history matching where the modeler manually changes parameter values and evaluates output after each forward run. The second step uses computer codes that automate trial-and-error history matching (Sections 9.5 and 9.6). In both phases, an assessment of the fit is made using both qualitative and quantitative methods. Given the importance to all aspects of history matching, we start by discussing methods for assessing model fit.

### 9.4.1 Comparing Model Output to Observations

Visual comparisons of simulated values and targets together with calculation of summary statistics are efficient ways to assess model fit. These methods are used to report results obtained via both manual and automated trial and error history matching. Most straightforward is a plot of the observed and simulated water table (e.g., Fig. 9.3) and/or potentiometric surface(s) in each layer of the model. However, observed surfaces are not equivalent to the hard data represented by the point measurements themselves because subjective decisions were needed for their creation. For transient models, observed and simulated hydrographs (Fig. 7.11) depict the model's ability to capture the dynamics of the groundwater system (Fig. 9.4). *Scatter plots* (Fig. 9.5(a)) show calibration targets versus simulated values and allow for a quick assessment of model fit; *categorized scatter plots* (Fig. 9.5(b)) are useful for distinguishing between data with different sources. In addition to fit, scatter plots also visualize *bias* in the calibration. Bias is absent when points in the scatter plot are more or less equally distributed around the central line shown on the plot, which indicates one-to-one correspondence between simulated and observed values (i.e., this line is not a regression line fitted to the data set). If simulated heads in a scatter plot are biased high, for example, it could mean that recharge rates are too high and/or hydraulic conductivities are too low.

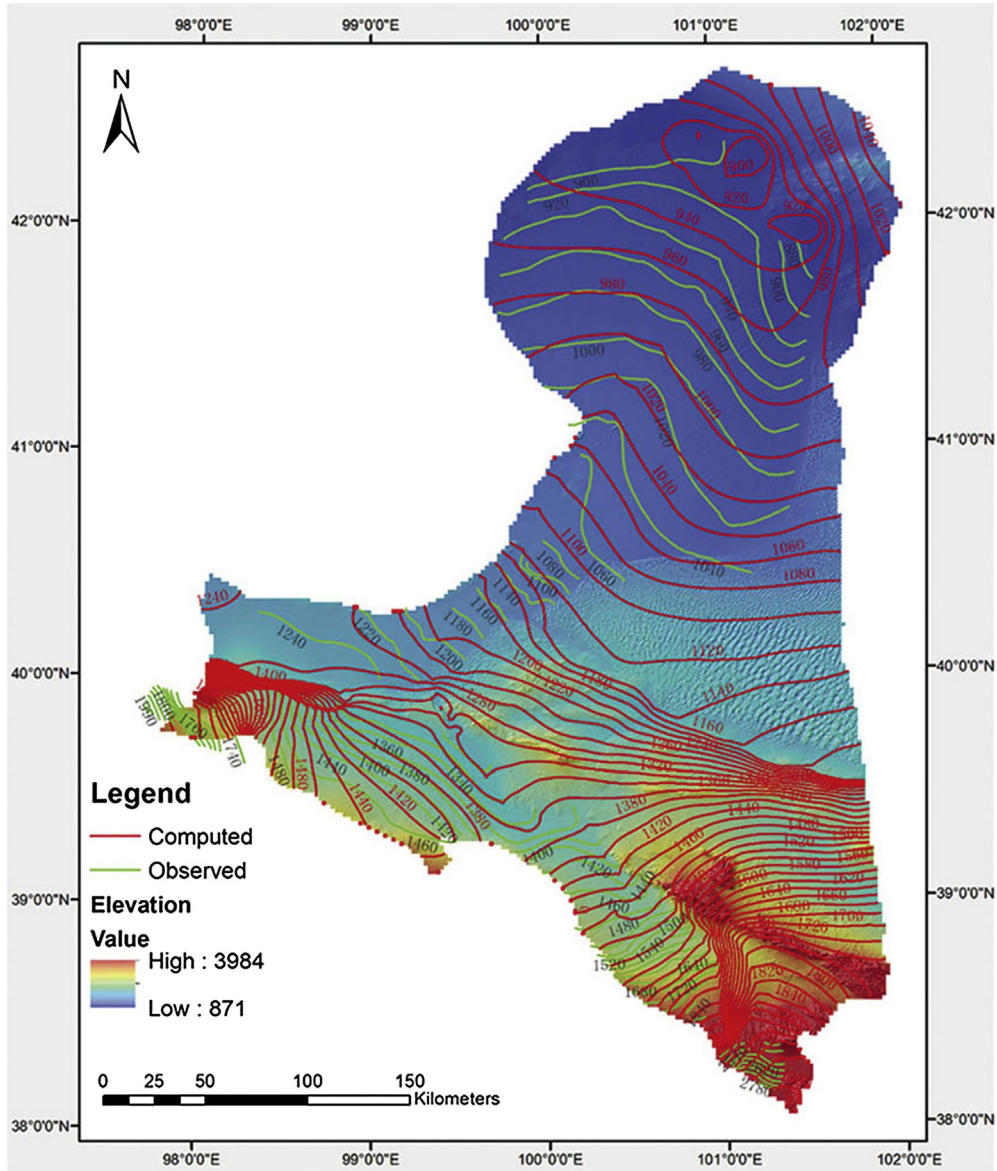


**Figure 9.3** Map view of observed (green) and simulated (red) water table (shown by contours) in an arid inland river basin in China. Topographic elevations are shown by color shading (Yao *et al.*, 2014).

Plots of *residual errors* (or *residuals*) are also useful for visualizing calibration results. Residual error is the difference between the target's observed value and its simulated value; for example, the residual in head is  $(h_m - h_s)$ , where  $h_m$  is the measured (observed) head and  $h_s$  is the simulated head. Residual errors can be plotted spatially in map view

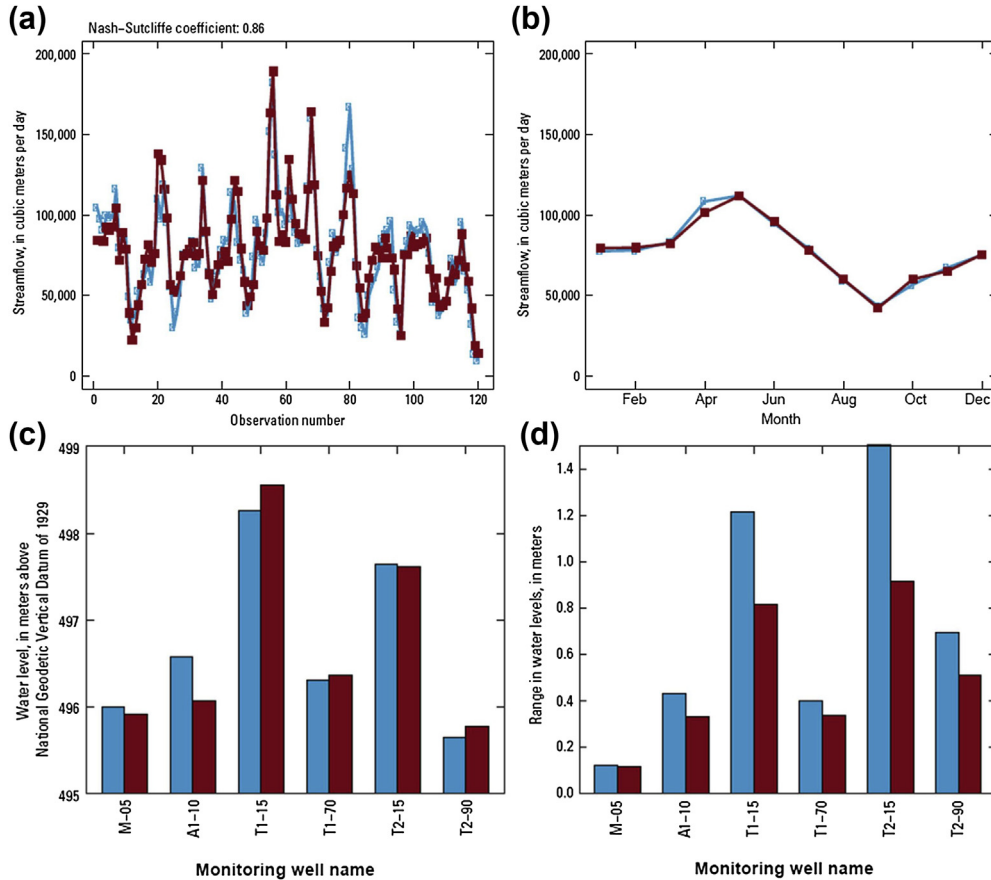


**Figure 9.4** Four ways to visualize the comparison of history matching observed (blue) to simulated (reddish-brown) targets in a transient model. (a) Hydrograph of observed and simulated streamflow with Nash–Sutcliffe coefficient (Eqn (9.4)) reported; Fig. 7.11 shows an example of this type of plot using observed and simulated heads. (b) Monthly plot of mean observed and simulated streamflow over the same months in different years using data shown in panel (a). (c) Comparison of mean observed and simulated heads. (d) Comparison of the observed and measured range of values for mean head values shown in panel c (modified from Hunt et al., 2013).

(e.g., heads: Fig. 9.6(a); fluxes: Fig. 9.6(b)) or in a cross section to illustrate the magnitude and spatial distribution of residuals. Residuals can also be shown by using graphs (Fig. 9.7). For transient simulations, residuals can be shown on a hydrograph (Fig. 7.11) of each target or a summary plot for groups of targets, such as by hydrogeologic unit (Fig. 7.1).

Although valuable, visual representations of results are necessarily subjective. Therefore, quantitative *summary statistics* are also calculated to measure the goodness of fit. The search for the best appropriate model focuses on finding a model that minimizes those statistics.

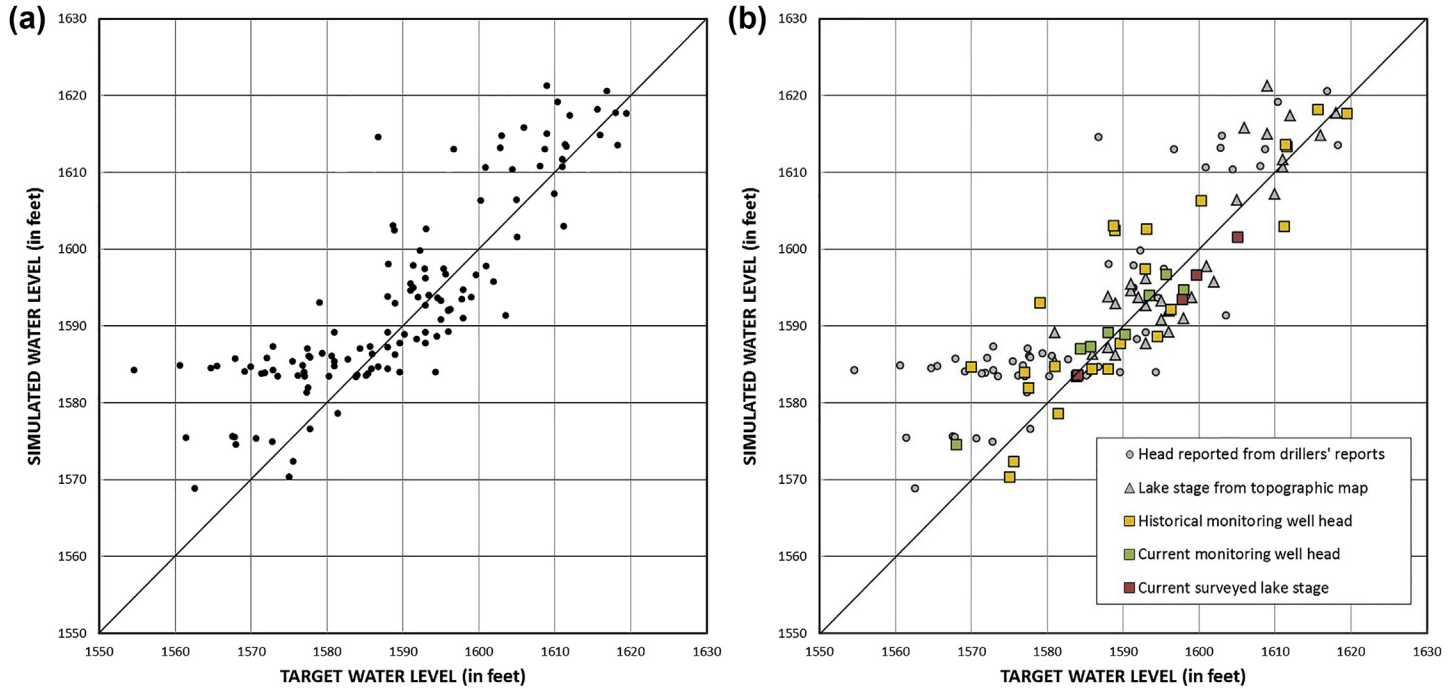


**Figure 9.5** Scatter plot (a) and categorized scatter plot (b) of simulated to observed fit of water levels. The categories in (b) can convey the modeler's assessment of target quality, here ranging between observations roughly estimated (small, gray dots) and more accurate observations (larger, colored symbols). The 1:1 perfect fit line is also shown for reference to visualize bias (modified from Juckem et al., 2014).

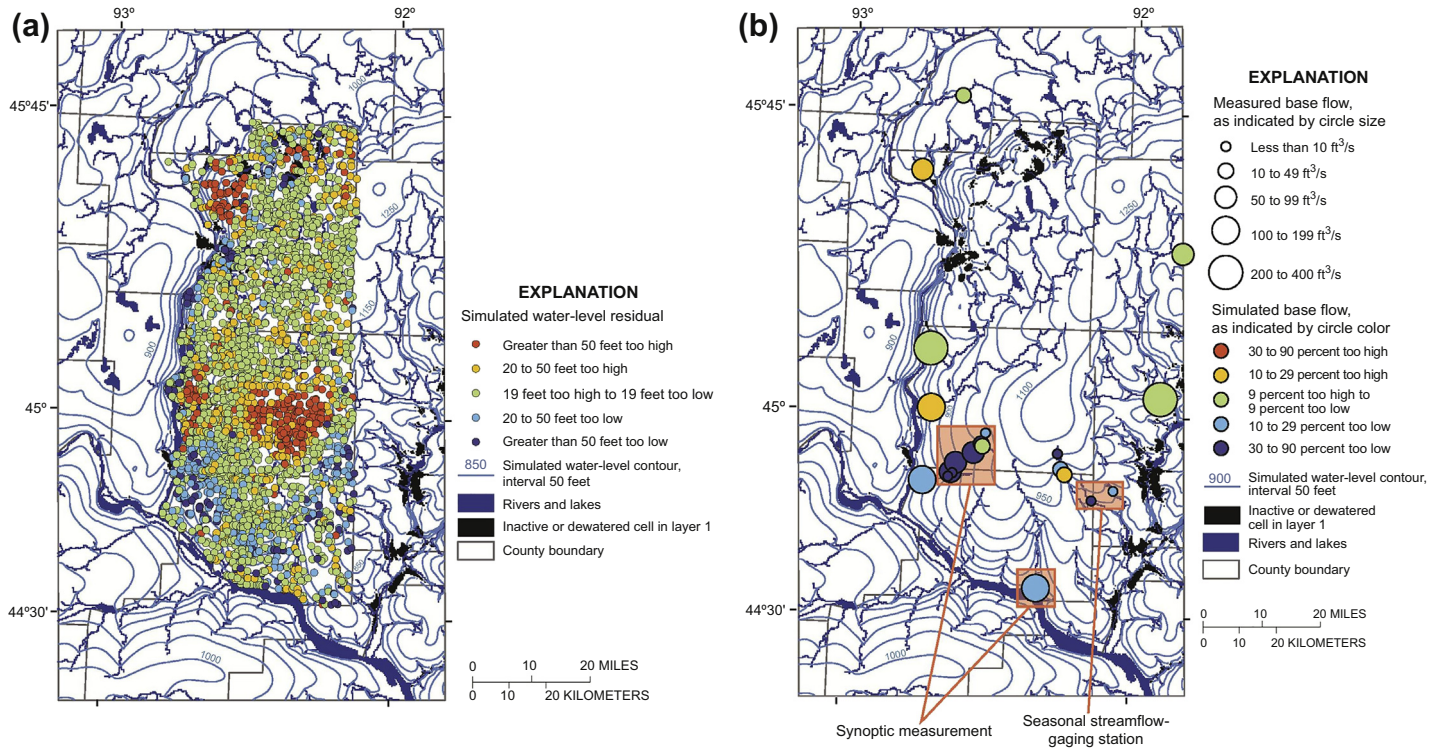


**Figure 9.6** Two examples of representing residual errors. (a) Similar size symbols with different colors can be effective when many data are shown, as is the case for head data from the large-scale groundwater model shown in the figure. With such a representation the spatial bias of simulated heads is effectively conveyed. (b) Different sizes and colors can be used when data are few, such as with flux targets in the same model domain as shown in (a). Color relates to degree of fit and symbol size relates to magnitude of the measured flux target—information important when judging the fit of a regional model. Small data sets of lesser quality from synoptic measurements and seasonal stream gages are highlighted to distinguish them from higher quality long-term streamflow measurements (*modified from Juckem, 2009*).

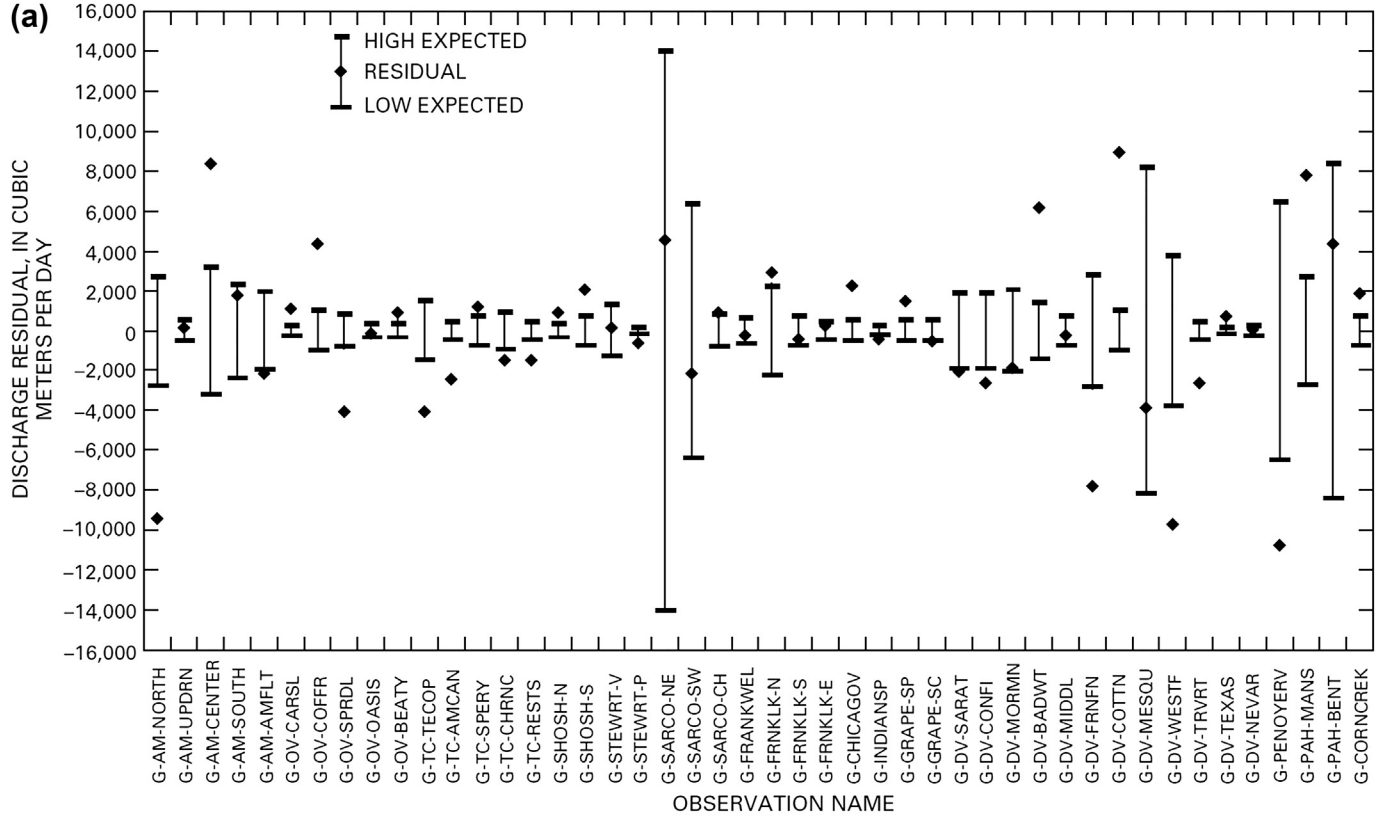
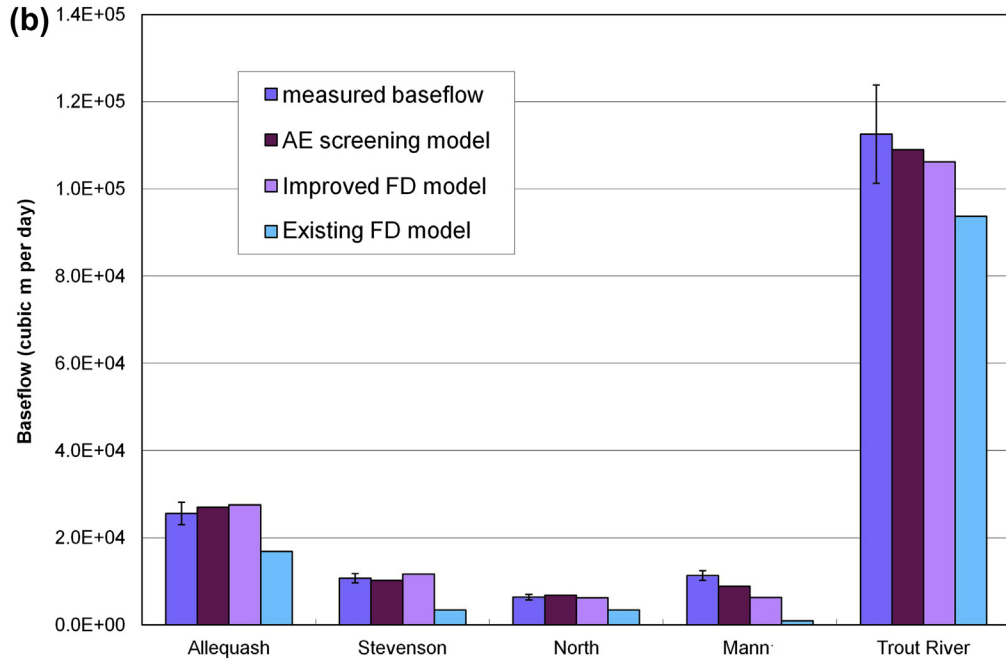


Figure 9.7 History match of flux targets: (a) flux targets with residual error related to uncertainty in measured values (D’Agnese et al., 2002);





**Figure 9.7 Cont'd (b)** spatial flux difference targets of baseflow in five streams for three different models showing uncertainty in measured values (*modified from Hunt et al., 1998*).

Examples of summary statistics, commonly reported together, are given below; the examples use head data as example observations, but the statistics can be calculated for any type of observation.

1. The *mean error (ME)* is the mean difference of the residual errors (measured heads  $h_m$  minus simulated heads  $h_s$ ):

$$ME = \frac{1}{n} \sum_{i=1}^n (h_m - h_s)_i \quad (9.1)$$

where  $n$  is the number of targets. The *ME* is simple to calculate but is not an ideal statistic. It provides a general description of model bias but because both negative and positive differences are included in the mean, the errors may cancel each other, thus reducing the overall error reported. A small *ME* suggests that the overall model fit is not biased (the simulated values are on average not too high or too low), but this by itself is a weak indicator of goodness of model fit.

2. The *mean absolute error (MAE)* is the mean of the absolute value of the residual. Using head as the example:

$$MAE = \frac{1}{n} \sum_{i=1}^n |(h_m - h_s)_i| \quad (9.2)$$

Taking the absolute value of the residuals ensures that positive and negative residuals do not cancel. As a result, the *MAE* is usually larger than the *ME*, and is generally a better indicator of model fit than the *ME*.

3. The *root mean squared error (RMSE)* is the average of the squared residuals.

$$RMSE = \left[ \frac{1}{n} \sum_{i=1}^n (h_m - h_s)_i^2 \right]^{0.5} \quad (9.3)$$

*RMSE* is less robust to the effects of outlier residuals; thus, the *RMSE* is typically larger than the *MAE*.

For transient models, other summary statistics can be used to compare individual simulated to observed hydrographs, such as the Nash–Sutcliffe coefficient of efficiency (*NS*):

$$NS = 1 - \frac{\sum_{i=1}^n |(h_m - h_s)_i|^2}{\sum_{i=1}^n |(h_m - \bar{h}_m)_i|^2} \quad (9.4)$$

where  $\bar{h}_m$  is the mean of observed head. *NS* ranges from  $-\infty$  to 1; values close to 1 indicate a good fit. For a value of 0, the mean of the data is as good a predictor as the transient series of simulated values. For a value less than 0, the mean of the data would be a better predictor. In practice, lower values such as 0.5 might be deemed acceptable depending on the difficulty of the problem, and many times it is the improvement in *NS* results after a new history match that is of primary focus rather than the value itself.

Even with quantitative summary statistics, deciding that a model's history match is good enough for the modeling purpose is not straightforward because "good enough" remains subjective. Some guidelines use summary statistics as goodness of fit criteria (e.g., [Murray–Darling Basin Commission, 2001](#); [ASTM, 2008](#)). For example, a model might be considered sufficiently calibrated if the *RMSE* is less than some set percentage of the calibration target range of values. That is, if head targets range from 50 to 150 m, an acceptable *RMSE* is on the order of 10 m using 10% as a criterion. However, no reasoning supports an assertion that simply meeting such a criterion defines an appropriately calibrated model. Nor are there established industry guidelines regarding the acceptable magnitude of the *ME*, *MAE*, or *RMSE*, other than it is desirable to minimize these values. Although the utility of standard criteria is recognized, uniform calibration standards have not been adopted by the modeling community. In part, this reflects the awareness that all modeling requires subjective judgment (e.g., [Silver, 2012](#); [Fiene, 2013](#)). Moreover, it is unlikely that a universally appropriate methodology could be formulated because the acceptability of a calibration is directly dependent on the modeling objective, and there are many possible modeling objectives.

## 9.4.2 Choosing the Parameters to Adjust

As discussed above, the first forward model run using best estimates for model parameter values is unlikely to obtain a model fit sufficient for the modeling purpose. Therefore, parameter values must be adjusted from the modeler's initial estimate to obtain a better fit. The translation of real-world properties to the model requires assigning parameter values to every node in the grid/mesh (Section 5.5). For purposes of calibration, the modeler reduces the set of all possible parameters (Section 5.4) to a set of *calibration parameters* that are allowed to vary during history matching. Calibration parameters may include any model input: vertical and horizontal hydraulic conductivities, boundary conditions, recharge rates, as well as other sources and sinks of water. Calibration parameters will not be equally valuable for improving model fit; during manual trial-and-error, the modeler identifies *insensitive parameters* that minimally affect the model output of simulated targets, and *sensitive parameters* that have a larger effect. Because the goal of adjusting parameter values is to find a sufficiently good history match, the modeler focuses on adjusting sensitive parameters. The final set of *optimal calibration parameter* values reflects the solution to the inverse problem supported by hard knowledge (Fig. 9.1). However, even then, this set should be recognized as *conditionally optimal* because it is dependent on the calibration data (and their errors), and criteria for judging what is optimal, selected by the modeler (Beven, 2009, p. 106).

One might ask why not make all parameters calibration parameters? When the number of calibration parameters (the unknowns) is greater than the number of observations (the knowns), the inverse problem is considered mathematically ill-posed and underdetermined (Section 9.2). One general approach to obtain an *overdetermined*, and therefore hopefully mathematically tractable, problem is to reduce the number of calibration parameters to a number fewer than the number of calibration targets. This approach for obtaining a tractable inverse problem has been extensively developed (e.g., see Hill and Tiedeman, 2007).

The advantage to simplifying the model by reducing the number of calibration parameters a priori is that at some point excluding enough calibration parameters will always result in a tractable inverse problem. Excluding parameters from the history matching process is also conceptually straightforward. However, when simplifications introduced during parameterization are done poorly, model outputs are adversely affected in ways not obvious to the modeler or easily corrected (Doherty and Welter, 2010). This is because the degree of simplification is a subjective choice of the modeler and, once set, further analysis of model error is difficult. As a result, it becomes difficult to assess whether large residuals are caused by poor choices of parameter values or if caused by defects in the model resulting from "incorrect hypotheses, unmodeled processes, or unknown correlations between processes" (Gaganis and Smith, 2001); this latter source of model misfit is called *structural error* (sometimes called "model error"). Although structural error appears

self-evident, in practice complexities that are left out while defining the model are often “quietly forgotten” (Beven, 2009, p. 6).

A straightforward method of reducing the number of calibration parameters involves *zonation* (Section 5.5), whereby areas of the model domain are assigned the same parameter value; adjusting the calibration parameter for the zone adjusts the parameter at all nodes in the zone simultaneously. Hence, zonation creates areas of *piecewise constant* parameters so that when the parameter is changed it affects model input for all nodes within the zone. The piecewise constant structure inherent to zonation is a modeling artifact—a simplification that helps models handle a complex natural world. When present, zones exist only approximately in the field. One concern is that the structural error imparted by zonation on model results can be large (e.g., Moore and Doherty, 2005). Yet zones are commonly used to reduce the number of calibration parameters, and thus zonation helps obtain a well-posed inverse problem.

Although impossible to quantify completely, it is clear that structural error associated with a model is not random. Its magnitude is a direct function of the type and degree of simplification imposed by the modeler (e.g., Beven, 2005). For example, a model with only one zone has relatively large structural error and will be less successful in fitting targets than a model with more zones. Recognizing the relation of the total number of parameters to structural error, and its effect on model calibration and forecasting, is important because structural error is usually the largest component of model error in sparsely parameterized groundwater models (Sun et al., 1998; Gaganis and Smith, 2001; Moore and Doherty, 2005). When the level of simplification imposed by the modeler unacceptably degrades a model’s performance, the model is considered *oversimplified*. The issue of oversimplification is not new to groundwater modeling—the development of numerical models was driven by attempts to overcome oversimplification inherent in the limiting assumptions typical of analytical solutions (e.g., Freeze and Witherspoon, 1966). This selection and grouping of calibration parameters for history matching is called *parameterization*; we revisit the topic of parameterization and its effect on model performance in Section 9.6.

### 9.4.3 Manual Trial-and-Error History Matching

Similar to the initial forward run of the model, a second run of the forward model using different calibration parameters is unlikely to provide a satisfactory history match. The process of trying additional parameter sets becomes an iterative *manual trial-and-error* matching procedure whereby the modeler manually adjusts parameter values and compares model output to targets using successive forward runs of the model. By manually adjusting parameters, the modeler explores how changes to the number, magnitude, and location of calibration parameters influence the fit between simulated values and targets. In this way, manual trial-and-error history matching not only improves the fit but also provides important insight into how the simulated groundwater system behaves.

Some parameters and boundary conditions may be known with a high degree of certainty and, therefore, should be modified only slightly from initial values, if at all, during this phase of history matching. The modeler identifies insensitive parameters by observing that changes (made within a predetermined reasonable range) produce little change in model outputs. Therefore, during subsequent trial runs insensitive parameters are set as invariant, or *fixed*, values that are based on field data, literature values, professional judgment, and/or other soft knowledge. A parameter that is insensitive during history matching may be sensitive in forecasting simulations, however. Therefore, a parameter that is fixed during history matching may need to be freed during the forecasting phase of modeling (Chapter 10).

When changing multiple parameters in the same forward run of the model, the modeler may also identify parameters that are *correlated*. Two or more parameters are correlated when the effects of changes in one parameter can be offset by changes to others such that model outputs are not appreciably changed. For example, examination of the groundwater flow equation (e.g., Eqns (3.12) and (3.13(a,b))) (and hydrogeologic intuition) indicates that decreases in hydraulic conductivity and increases in recharge both increase heads. Therefore, both are sensitive parameters when considered independently. However, a decrease in hydraulic conductivity can be offset with a commensurate decrease in recharge rate resulting in no net effect on simulated heads. This is an important insight for model calibration because it means that history matching to head data only is fundamentally nonunique. Head data alone can only constrain the ratio of recharge and hydraulic conductivity (Box 3.2; [Haitjema, 2006](#)); unique individual values for both recharge and hydraulic conductivity cannot be obtained. However, if a flux target (e.g., observed baseflow) is considered along with head data, parameter correlation is reduced and unique estimates of both hydraulic conductivity and recharge can be obtained. In cases where additional observations are not available to break parameter correlation, the modeler attempts to determine best estimates for correlated parameters manually. Such manual intervention can be difficult in practice because parameter correlation is harder to identify than insensitivity, especially if many parameters and processes are simulated.

#### 9.4.4 Limitations of a Manual Approach

Manual trial-and-error calibration remains a fundamental first step for history matching because it gives the modeler much insight about the site modeled and how parameter changes affect different areas of the model and types of observations. In this way, manual trial-and-error helps develop a modeler's "hydrosense." Manual trial-and-error is also an efficient first test of the conceptual model because it can quickly demonstrate that a specific conceptual model is ill-suited to match field observations and thus does not belong in the family of reasonable models. These positive aspects notwithstanding, manual trial-and-error history matching is an imperfect process because even though

some insight is gained, feedbacks between sources and sinks and other correlated parameters and processes in most groundwater systems are complex. As a result, it is impossible to track effects of all changes in calibration parameters to system-wide effects on all observations. The inherent subjectivity and deficiencies of manual trial-and-error calibration were summarized by [Carrera and Neuman \(1986\)](#):

*The method of calibration used most often in real-world situations is manual trial and error. However, the method is recognized to be labor intensive (therefore expensive), frustrating (therefore often left incomplete), and subjective (therefore biased and leading to results the quality of which is difficult to evaluate).*

The last point is critically important: the very ad hoc nature of manual trial and error makes comprehensive testing and identification of all insensitive and correlated parameters difficult. As a result, using manual trial-and-error calibration alone is problematic. It cannot guarantee that the modeler has found the quantifiable best fit for a given conceptual model. At the end of even the most rigorous manual trial-and-error procedure it is likely that untested sets of parameters might yield a better model. For some modeling purposes, this lack of a guarantee of best fit is undesirable but not problematic. In other cases, failure to present a defensible best model can have serious repercussions, especially when groundwater models are used in regulatory and legal arenas (e.g., [Bair, 2001](#); [Bair and Metheny, 2011](#)). In recognition of this fact, mathematically rigorous automated trial-and-error methodologies ([Box 9.1](#); [Sections 9.5 and 9.6](#)) were developed. Yet, even with these methods, it should be recognized that advanced methods can never fully replace insight and hydrosense gained from the manual trial-and-error process. Instead, advanced methods are best applied after a model is at least roughly calibrated using a manual trial-and-error approach.

## 9.5 PARAMETER ESTIMATION: AUTOMATED TRIAL-AND-ERROR HISTORY MATCHING

*Parameter estimation* is an indirect solution of the inverse problem ([Box 9.1](#)) that is effectively automated trial-and-error calibration because computer algorithms perform the same general steps as described in [Section 9.4](#) and shown in [Fig. 9.1](#). Parameter estimation starts with an initial set of reasonable parameters derived from a manual history match and perfects the ad hoc and subjective manual results using a computer program (inverse code) and statistical methods. Parameter estimation codes also formalize the history matching process in that the modeler must explicitly address elements loosely handled in a manual trial-and-error process. These include:

1. the computer code(s) for the forward runs;
2. the calibration parameters;
3. calibration targets and their weights;
4. criteria for when to stop looking for a better fit.

### Box 9.1 Historical Context for Parameter Estimation

The inverse problem is called “inverse” because what we know (heads) must be inverted to find what we do not know (e.g., aquifer material properties). In other words, in solving the inverse problem for groundwater flow, we can find values for the parameters because we assume heads are known. Pioneering papers by Stallman (1956a,b) proposed a direct solution to this inverse problem. The direct approach was explored by Nelson (1960, 1961, 1962), among others (e.g., Emsellem and de Marsily, 1971; Neuman, 1973). In the direct method, the partial differential equation for groundwater flow is written with hydraulic conductivity as the dependent variable; heads must be specified completely in space and time. However, heads are never completely known, which necessitates interpolation of field-measured heads. Interpolation introduces small errors into the head distribution that can cause large errors when solving the inverse problem for hydraulic conductivity. Therefore, even though the direct approach is appealing owing to its mathematical elegance and computational efficiency, it was found to be unstable for most realistic problems.

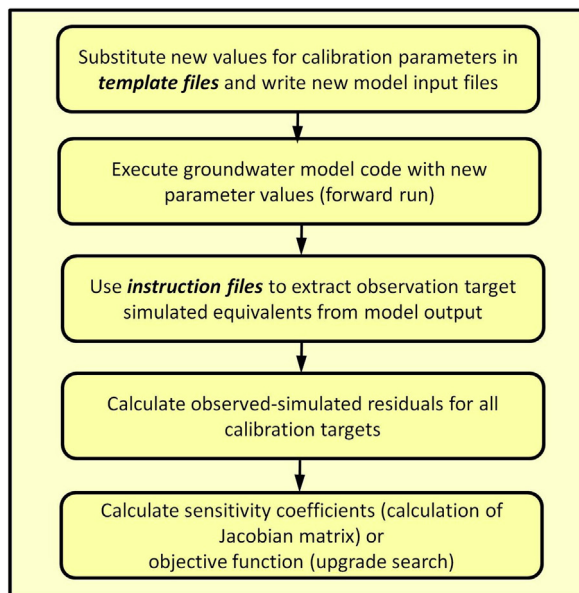
The inverse problem, however, can also be solved indirectly. The indirect method essentially automates the manual trial-and-error process where properties are estimated iteratively using statistical regression and computer algorithms. Yeh and Tauxe (1971), Cooley and Sinclair (1976), and Cooley (1977, 1979) advocated an indirect approach to solve for groundwater parameters, now called *parameter estimation*. Richard Cooley (Cooley, 1977, 1979; Cooley and Naff, 1990) developed a pioneering inverse code using nonlinear regression, an approach later extended to the parameter estimation code MODINV (Doherty, 1990), MODFLOWP (Hill, 1992), and UCODE (Poeter et al., 2005). PEST (Parameter ESTimation; Doherty 2014a,b) replaced MODINV in 1994, and currently the PEST software suite is widely used for applied groundwater modeling. Late in the twentieth century, groundwater modelers began routinely applying inverse codes to sparsely parameterized problems and a wider use of parameter estimation was advocated (e.g., Yeh, 1986; Carrera, 1988; Poeter and Hill, 1997). Researchers in other fields such as geophysics were also addressing inverse problems at this time by applying advanced statistical theory and mathematics (e.g., Aster et al., 2013) to solve highly parameterized problems. Many of these advanced methods (e.g., singular value decomposition, Tikhonov regularization) are now available to groundwater modelers through the PEST software suite ([www.pesthomepage.org](http://www.pesthomepage.org)).

It is clear that indirect methods for solving the inverse problem are valuable and essential tools for groundwater modeling. There is a textbook focusing primarily on calibration of sparsely parameterized models (Hill and Tiedeman, 2007), and guidelines for highly parameterized groundwater modeling are available (Doherty and Hunt, 2010). Large increases in computer power and access to parallel processing have expanded parameter estimation to complex models with 1000s of calibration parameters (e.g., BeoPEST: Schreüder, 2009; GENIE: Muffels et al., 2012; PEST++: Welter et al., 2012), and cloud computing (e.g., Hunt et al., 2010). Inverse codes include modern programming techniques, provide simplified access to advanced methods (e.g., PEST++, Welter et al., 2012), and have been updated to incorporate the Bayesian geostatistical approach (bgaPEST—Fiene et al., 2013) and the null-space Monte Carlo method (Tonkin and Doherty, 2009; Doherty et al., 2010b). Inverse methods are still evolving and finding better ways to solve the inverse problem continues to be an active area of research (e.g., Zhou et al., 2014).

For example, parameter estimation requires the modeler to translate an observation's subjective importance (i.e., its rank; Section 9.3) into a numerical weight (Table 7.1). Parameter estimation also requires the modeler to quantify the reasonable ranges for the calibration parameters. Perhaps most importantly, parameter estimation quantitatively determines when a fit is sufficiently good. Thus, parameter estimation utilizes the power of modern computing methods to alleviate the labor intensive aspects of manual trial-and-error calibration (e.g., Figs 9.8 and 9.9). For example, a typical parameter estimation algorithm automates: (1) adjustment of calibration parameters; (2) evaluation of output; (3) tracking the effect of changes in all calibration parameters on all calibration targets; and (4) estimating better values for calibration parameters. Because the calibration steps in Fig. 9.9 are formalized in the input for the parameter estimation code, the quantitative description of the calibration can be expressed in a way that is transparent and easily documented.

Although the general steps in parameter estimation (Fig. 9.9) are formalized in the code, the automated process cannot be considered automatic calibration because the modeler is fully involved in all aspects of defining the calibration. If the fit is unacceptable, the modeler modifies the target types, weights, and calibration parameters, after which the parameter estimation process is repeated. The modeler will also perform a soft knowledge assessment of the calibration by deciding whether the calibrated parameter values are hydrogeologically reasonable and conform to the conceptual model. If the best fit model is still unacceptable, a new conceptual model and a new numerical model must be formulated and the calibration process, starting with manual trial-and-error history matching, is repeated.

**Figure 9.8** A schematic workflow diagram of the mechanics of each forward run automated by a universal nonlinear regression parameter estimation code. The shaded background in the figure indicates that the steps are performed internally by the code without user intervention. Two types of ASCII (American Standard Code for Information Interchange) files are required before the parameter estimation code can be run: (1) a template file that specifies where to place new values of calibration parameters in the model input file; and (2) an instruction file that extracts relevant model outputs for comparison to observed calibration targets. Both required files are typically created by a graphical user interface (GUI).





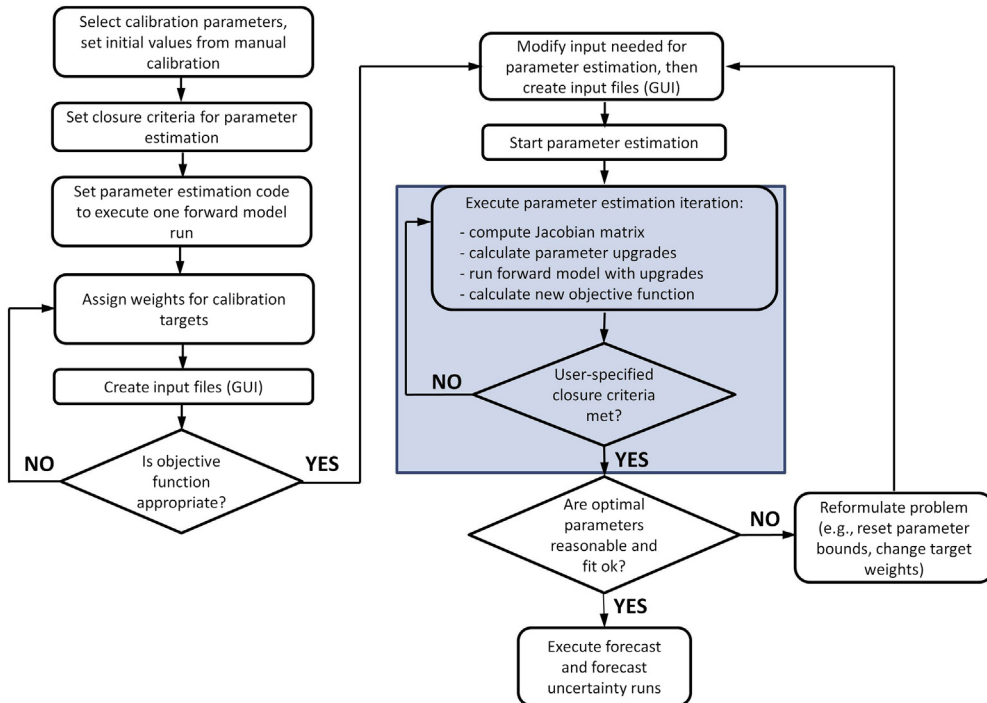


**Figure 9.9** A schematic diagram of a general workflow for parameter estimation, the second phase of history matching for a model designed for forecasting. Shaded box contains steps automated by the parameter estimation code; steps in the unshaded areas require modeler action. An objective function is appropriate when all targets are included but targets important to the modeling objective are more prominently weighted (GUI, graphical user interface).

As outlined above, parameter estimation appears to be straightforward, and general guidelines are well developed (Box 9.2). However, automating the inverse problem is difficult and many approaches have been developed. Zhou et al. (2014) broadly group inverse methods into deterministic and stochastic approaches. Deterministic inverse methods seek a single representation of parameters that produces a best fit to the calibration targets. Stochastic inverse methods generate multiple realizations of parameter distributions, all of which give acceptable fits to the calibration parameters; the ensemble of realizations is carried forward to make forecasts (Chapter 10) and convey parameter uncertainty. We focus here primarily on deterministic inverse methods that are programmed into “universal” parameter estimation codes. Universal parameter estimation codes are widely used for applied modeling because they can interface with any computer code that can: (1) run in batch mode (reach completion and write model output without user intervention) and (2) read input and write output files. The input/output file format required is most commonly American Standard Code for Information Interchange

(ASCII) files, which is the computer file type recognized by simple text editors. Most GUIs for groundwater flow codes build input and can execute a universal parameter estimation code. The essential elements of formalizing the calibration problem for universal parameter estimation codes are considered in more detail below and in [Section 9.6](#). Tips for running the code are given in [Box 9.2](#).

Parameter estimation theory uses advanced mathematical and statistical methods, and can be quite sophisticated. Fortunately, advanced parameter estimation techniques are accessible to the applied modeler through widely available software, and their appropriate use does not require detailed knowledge of underlying theory. In this section, we discuss some general concepts relevant to all deterministic inverse methods, but in [Section 9.6](#) we emphasize specific approaches embodied in the PEST (Parameter *EST*imation) suite of codes ([Doherty, 2014a,b](#); [Welter et al., 2012](#); [Fiene et al., 2013](#)). Similar to our use of MODFLOW and FEFLOW to illustrate concepts of groundwater modeling, PEST is used to illustrate concepts of calibration. The PEST software suite is currently widely used for parameter estimation of applied groundwater models, and includes many advanced capabilities (some of which are discussed in [Section 9.6](#)). Although not a stochastic inverse code in the sense discussed by [Zhou et al. \(2014\)](#), PEST has an option that allows generation of multiple realizations of parameters in a Monte Carlo framework ([Section 10.5](#)).

Those who wish to delve further into the details of parameter estimation theory should consult references provided at the end of this chapter, and associated literature cited therein. [Zhou et al. \(2014\)](#) provides a review of inverse modeling applied to groundwater systems and many references. User manuals or guidance documents provided with specific codes (e.g., [Doherty, 2014a,b](#); [Doherty and Hunt, 2010](#); for PEST) typically include the theoretical background, as well as instructions and examples for creating input and running the code itself.

### 9.5.1 Weighting the Targets

In [Section 9.3](#), we ranked targets qualitatively considering errors, uncertainty, and the importance of the target for addressing the modeling purpose. This same approach is used to rank targets for parameter estimation except that targets are now numerically weighted ([Table 7.1](#)). In an ideal statistical world, assigned individual target weights directly express the associated measurement error of the observation. However, as discussed in [Section 9.3](#), the ideal rarely holds when models are applied in practice; thus, initial measurement-based weights are often adjusted to reflect other modeling considerations such as the need to balance the numbers of each type of target, the spatial distribution (e.g., declustering—[Bourgault, 1997](#)), and the importance of the target to the modeling purpose, such as location in the near-field or far-field.

Mathematically, weights are used to increase or decrease the contribution of individual residuals to the total sum of model error called the *objective function* (often represented

by  $\Phi$ ). Most universal parameter estimation codes calculate the objective function as the sum of squared weighted residuals. That is, the residual calculated for each target is multiplied by its weight, squared (making all residuals positive), and then summed. A quantitative best fit model has the minimum value of the objective function. If the targets include only head observations, the objective function,  $\Phi$ , is:

$$\Phi = \sum_{i=1}^n [w_{hi}(h_m - h_s)_i]^2 \quad (9.5)$$

where  $w_{hi}$  is the weight for the  $i$ th head observation;  $h_m$  is the measured (observed) head target;  $h_s$  is the simulated head. For better posed history matching, both head and flux observations are used as targets and the objective function is written:

$$\Phi = \left\{ \sum_{i=1}^n [w_{hi}(h_m - h_s)_i]^2 + \sum_{i=1}^n [w_{fi}(f_m - f_s)_i]^2 \right\} \quad (9.6)$$

where  $w_{hi}$  is the weight for the  $i$ th head observation;  $h_m$  is the measured (observed) head target;  $h_s$  is the simulated equivalent head;  $w_{fi}$  is the weight for the  $i$ th flux observation;  $f_m$  is the measured (observed) flux target;  $f_s$  is the simulated equivalent flux.

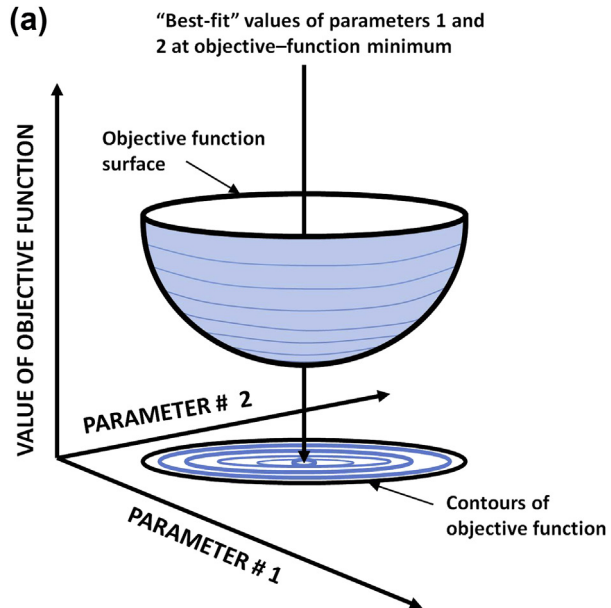
From Eqns (9.5) and (9.6), it is evident that the objective function can be expanded to include any type of observation that has a simulated equivalent quantity. Indeed, including as many observation types in the objective function as possible helps constrain the parameter estimation process and ensure better correspondence between the simulated and real-world systems (Hunt et al., 2006). Moreover, raw observations as in Fig. 9.4(a) can be processed (e.g., Fig. 9.4(b)–(d)) and also included in the objective function to emphasize aspects of the system deemed important. Equations (9.5) and (9.6) show that assigned weights directly influence the objective function — a higher weight increases the importance of the residual by giving it a larger contribution to the objective function.

The best fit model has the minimum value of the objective function, which is directly dependent on the weights assigned to each target. It follows that targets with relatively small measurement errors and that are important for the forecast should be assigned relatively larger weights. Weighting also quantifies a modeler's judgment regarding the importance of target type relative to other types (e.g., heads versus fluxes, far-field heads versus near-field heads, baseflow targets versus miscellaneous streamflow measurements). The goal of target weighting is to achieve a balanced initial objective function (Fig. B9.2.1 in Box 9.2) where all targets have a presence. However, the objective function does not need to be perfectly balanced; rather, it should reflect the modeling purpose, where targets important to the modeling objective are more prominent. Because expression of what the modeler holds important for the modeling purpose is part of the art of modeling, there is no one set of definitive rules for weighting. Different views of weighting are explored by Doherty and Hunt (2010) and Hill and Tiedeman (2007).

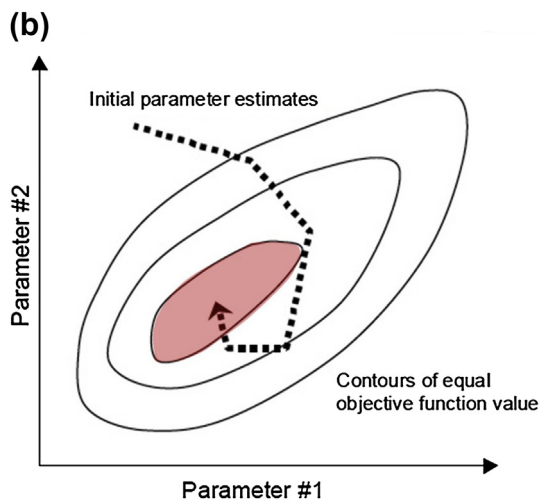
## 9.5.2 Finding a Best Fit

The objective function provides a single numerical value that encapsulates the model's fit to all targets and the importance assigned to each target by the modeler. Because a best fit corresponds to the minimum of the objective function, finding the best fit becomes a search for a minimum on a multidimensional *objective function surface* (Fig. 9.10). For a

**Figure 9.10** (a) Idealized objective function surface for a two-parameter problem (modified from Himmelblau, D.M., 1972, *Applied Nonlinear Programming*, McGraw-Hill, New York, reproduced with permission of McGraw-Hill Education).



(b) improvement in the solution via parameter upgrade in successive parameter estimation iterations (shown by the dashed line) leading to the objective function minimum (from Doherty, 2014a).

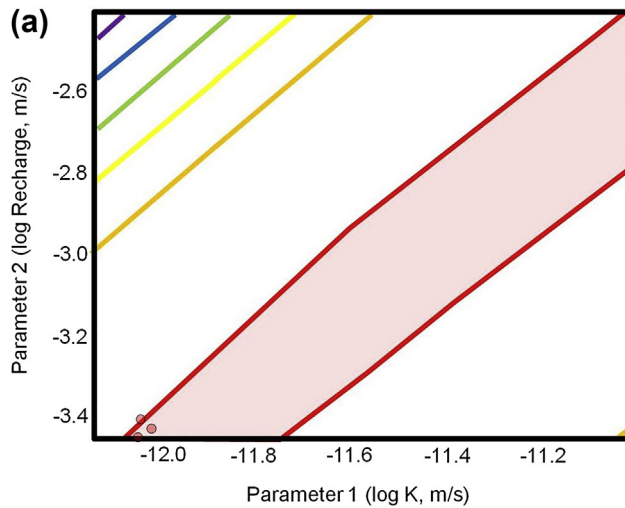


simple two-parameter model as shown in Fig. 9.10, the objective function surface is easily visualized as contours of the objective function. Most history matching occurs with more than two parameters, however, which results in a multidimensional surface difficult to visualize. Nevertheless, concepts discussed below for the simple case of a two-parameter model are similar for a multidimensional surface. To find the objective function minima, the parameter estimation code performs a series of forward model runs, each with a different set of values for calibration parameters. The algorithm then calculates the objective function using an equation like Eqn (9.6). The search for optimal parameters typically is not random; *derivative-based nonlinear* search techniques used for most applied modeling evaluate the slopes of the objective function surface and adjust parameters to force the forward model to progress toward the global minimum of the objective function. The search technique must accommodate nonlinearity because the responses of heads and flows to changes in parameters are usually nonlinear (e.g., Eqn (3.12)).

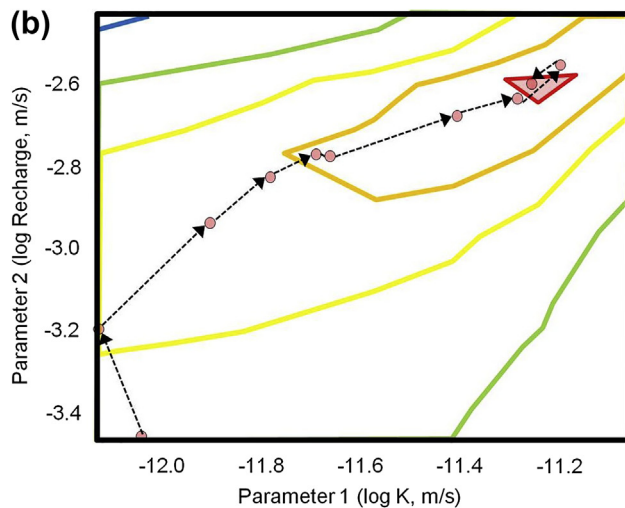
One widely used method to search the objective function surface for the minimum is based on the *Gauss–Marquardt–Levenberg (GML) method*, also known as the *damped least squared method* (Levenberg, 1944; Marquardt, 1963; Hill and Tiedeman, 2007; Doherty, 2014a). *Derivative-based methods* such as GML assume that simulated values of targets vary as a continuous function in response to changes in calibration parameters. That is, the GML method assumes that model inputs (parameters) and outputs (simulated values of targets) are continuously differentiable. In general, the groundwater flow equation conforms to this assumption. As discussed previously, however, nonuniqueness inherent to groundwater models means that multiple combinations of parameters can provide similar fits to the targets. In the two-parameter case, nonuniqueness can be visualized as a set of optimal values lying in the “trough” of the objective function surface (Fig. 9.11(a)). However, even when the inverse problem is well posed (e.g., giving the unique best fit in Fig. 9.11(b)), a multidimensional objective function surface can have multiple local minima in addition to the global minimum (Fig. 9.12) that represents the best model fit. For some models, guaranteeing that an objective function minimum is the global minimum can be difficult, especially when the derivatives are noisy (i.e., not perfectly continuously differentiable due to machine or code precision issues or solver closure selected—compare Figs. 9.13(a) and (b)). *Global methods* do not rely on derivatives to explore the objective function surface; however, they are much more computationally expensive than gradient-based methods, and thus typically consider a relatively small number of calibration parameters (usually  $<100$ ). As a result, derivative-based methods are more commonly used than global methods for most applied modeling problems.

Universal parameter estimation codes can manipulate model input files and process model output files from any groundwater flow code. Therefore, they can calculate the objective function slope required by derivative-based methods using almost any code, not just the subset that internally include such capabilities. Observation-to-parameter

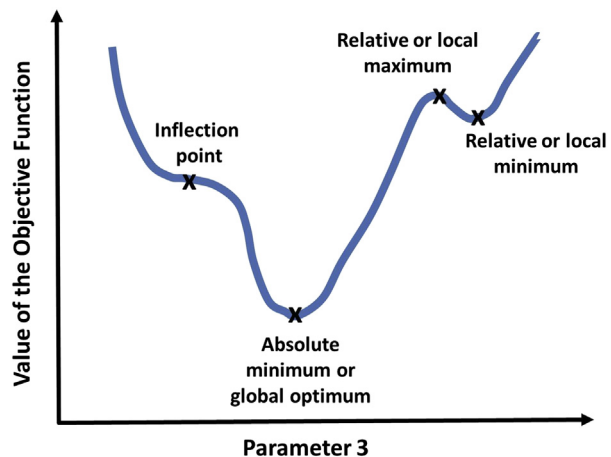
**Figure 9.11** Objective function surfaces from a two-parameter model of a field site where contour lines with warmer colors represent lower objective function value: (a) example of a solution that did not converge; that is, the objective function surface has no unique minimum (shaded pink trough). Nonconvergence was caused by using only head data as calibration targets;



(b) the objective function surface for a solution that converged. The solution included both heads and groundwater temperature as observation targets. Dashed lines represent the approach to the surface minimum and reddish circles represent parameter upgrades (modified from Bravo et al., 2002).



**Figure 9.12** Cross section of an objective function surface showing local and global minima (modified from Zheng and Bennett, 2002).



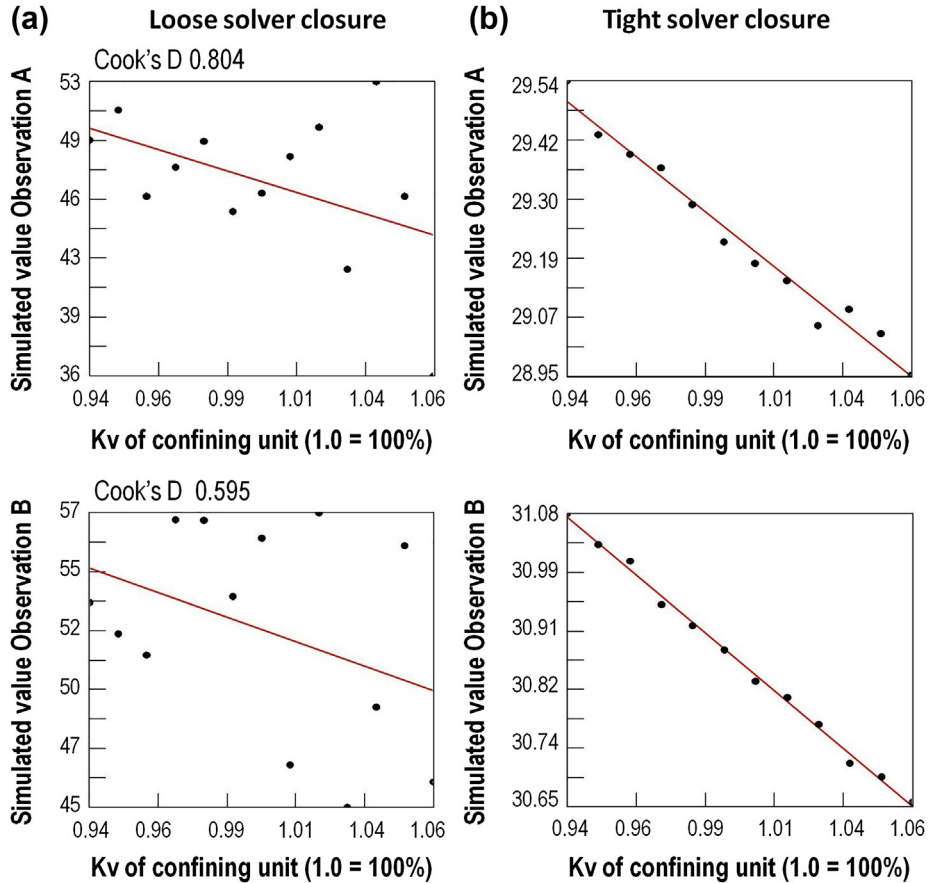


**Figure 9.13** Plot of change in model outputs (y-axes) to small increments of change in one model parameter (x-axes) for two different observations. Each dot represents one model run; the straight line is the best fit through the dots. Because the true parameter sensitivity derivative is approximated using a 1% parameter perturbation sequential 1% perturbations should provide a coherent change (e.g., the monotonically changing line shown in (b)). Poor derivatives calculated by perturbation (a) can confound derivative-based parameter estimation methods; tighter solver closure as shown in (b) provides more coherent derivatives. An influence statistic (Cook's D, [Box 9.6](#)) for the two observations is also listed, where higher values represent more influence on the regression (*modified from Feinstein et al., 2008*).

derivatives relate the change in the simulated value of the target ( $\Delta_{\text{observation}}$ ) to a change in the value of the calibration parameter ( $\Delta_{\text{parameter}}$ ), and are known as *sensitivity coefficients* (also called *parameter sensitivity*):

$$\text{sensitivity coefficient}_{ij} = \frac{\Delta_{\text{observation}_i}}{\Delta_{\text{parameter}_j}} \quad (9.7)$$

where  $\Delta observation_i$  is the change in simulated value of the  $i$ th target and  $\Delta parameter_j$  is the change in value of the  $j$ th calibration parameter. The set of sensitivity coefficients forms a two-dimensional array of values of  $i$  rows and  $j$  columns commonly known as the *Jacobian matrix* or *sensitivity matrix* (Fig. 9.14). The heads computed by using initial parameter values at the start of the parameter estimation process form the basis for comparison; changes in output are calculated by changing parameter values from their initial values. After the initial forward run, a series of forward runs is performed where each individual calibration parameter is changed by a small amount (usually 1%) and the model is run while all other parameters are held constant at their initial values.

Changes in the simulated values for each target ( $\Delta observation_i$ ) are calculated by subtracting the model output from the run with the perturbed parameter from the output of the initial model run that used unperturbed parameters. The sensitivity for the parameter that was perturbed is calculated from Eqn (9.7) and entered into the Jacobian matrix. The minimum number of forward runs needed to calculate a Jacobian matrix is equal to the number of calibration parameters plus one (i.e., the initial unperturbed run). Perturbation-based sensitivity information stored in the Jacobian matrix only approximate the actual derivatives of the observations to changes in each parameter, but has been found to be sufficiently accurate for applied models (Yager, 2004).

Once the Jacobian matrix is calculated, the slope of the objective function surface as represented by the derivative information is used to identify changes in calibration parameters that move toward the objective function minimum. From these slopes: revised estimates of the calibration parameters are selected; a new forward run is performed, and a new objective function is calculated. In practice, the complex objective function surface and deviations from linearity preclude a simple determination of a single best new set of calibration parameters; therefore, a small number (usually  $<10$ ) of candidate parameter sets are calculated and run in the forward model. An objective function is then calculated from each candidate parameter set, and the one with the lowest value is used to update the calibration parameters. A first update to initial parameter values does not complete the parameter estimation process because the groundwater inverse problem is nonlinear and sensitivities contained in the initial Jacobian matrix cannot accurately represent the sensitivities of the solution using the new parameter values. Therefore, a new Jacobian matrix is calculated using the parameters that gave the lowest objective function, which becomes the new unperturbed base case, and the slopes are used to develop a new set of candidate calibration parameters. The set of runs that starts with the calculation of a new Jacobian matrix and includes the set of forward runs for the corresponding new parameter estimates is called a *parameter estimation iteration*. Replacing a parameter set with a new parameter set that lowers the objective function constitutes a *parameter upgrade*—indicating that parameters are not merely updated but improved.



		Parameters (columns)					
		k_unconsol	k_bedrock	recharge	c_drainagelakes	c_seepagelakes	c_stream
Observations (rows)	Head_11_poor	-1.15129	0.00000	0.308674	-6.864546E-06	3.222347E-04	-7.712651E-07
	Head_12_poor	-2.87823	-5.756463E-02	1.80995	-0.172709	-5.642061E-02	2.47528
	Head_13_fair	-12.9520	-0.402952	8.10971	-4.250797E-04	2.104297E-02	11.8007
	Head_16_fair	7.59851	-0.230259	2.94640	5.831008E-02	2.083643E-02	10.5920
	Head_18_fair	-33.3875	2.300745E-14	8.67094	-5.791823E-02	1.759003E-02	0.518045
	Head_23_fair	-8.00148	-1.533830E-14	2.20281	0.172619	3.733688E-03	0.575639
	Head_36_fair	0.633211	0.00000	-0.182398	6.825390E-06	-3.094240E-04	-0.115128
	Head_39_fair	-21.0687	-5.756463E-02	11.6735	-0.114699	3.664815E-02	11.3978
	Head_46_fair	1.26643	-1.533830E-14	2.14669	-5.775567E-02	9.476421E-03	5.06567
	Head_50_fair	-1.72694	-5.756463E-02	4.86862	-0.172693	3.120432E-04	9.95868
	Head_52_fair	-39.6620	-5.756463E-02	15.6582	-0.115823	3.457457E-02	10.0162
	Head_55_best	-52.9019	-5.756463E-02	20.1199	-0.171774	1.216745E-02	20.7809
	Head_56_best	-80.7632	0.00000	24.6799	5.718392E-02	1.862524E-02	16.5210
	Head_57_poor	-44.6701	7.669149E-15	12.0242	-1.301467E-04	6.561156E-03	2.01475

**Figure 9.14** An example of a Jacobian matrix with 6 columns of parameters and 14 rows of observations. Each entry in the matrix is a parameter sensitivity (sensitivity coefficient) calculated from Eqn (9.7). The numbers in the left-hand column are the labels for head targets where best, fair, and poor indicate the quality of the target.

The search for parameter upgrades continues until one of three modeler-designated parameter estimation *closure criteria* is met: (1) the model fit cannot be further improved; (2) changes to the upgraded parameters are sufficiently small that one is not substantively different from another; or (3) the maximum number of parameter estimation iterations specified by the modeler has been reached. Because initial parameter values specified by the modeler may or may not be near final optimal values, there is no general guideline for how much the initial objective function should be reduced. Rather, in practice an acceptable value of the final objective function is the decision of the modeler. Thus, even though the trial-and-error process is automated, deciding when to end the parameter estimation is not automatic but depends on choices made by the modeler.

### Box 9.2 Tips for Running a Parameter Estimation Code

Calibration guidelines presented in this chapter and by others (e.g., Hill and Tiedeman, 2007 for sparsely parameterized models) primarily pertain to conceptual aspects of modeling. Successful parameter estimation also involves more mechanistic aspects because input to a parameter estimation code can be lengthy and involve complex statistical concepts. Fortunately, most codes use default settings that are appropriate for many applied groundwater modeling problems, and utility software and graphical user interfaces simplify access to a code. Nevertheless, proper application of a parameter estimation code still requires attention to user manuals and guidelines included with the code itself. Running example problems or tutorials included with the code will give the user familiarity with its operation and troubleshooting options. Regardless of the code chosen, the following practices can facilitate efficient execution of the parameter estimation process.

- Run all input checking utilities (e.g., PESTCHEK.exe for PEST) before starting the parameter estimation run. Such utilities are tuned to identify and describe common errors that will cause parameter estimation to fail.
- When extracting values from the model output to align with the observation targets, carry the maximum numerical precision possible even if numerical precision is higher than reasonable for the associated field-measured observation. This will ensure a more accurate derivative calculation during construction of the Jacobian matrix, which in turn facilitates a better parameter upgrade by the derivative method.
- Use the parameter estimation code's option to log transform all calibration parameters that do not go negative (e.g., hydraulic conductivity). This dampens changes in extremely sensitive parameters and enhances parameter estimation performance.
- Recognize that tighter closure criteria in the solver of the groundwater code for the forward problem may appreciably speed and improve the parameter estimation process even if the forward run time increases. Gradient-based methods like Gauss–Marquardt–Levenberg rely on coherent/linear derivatives, but loose closure criteria can affect derivative quality (Fig. 9.13) even if the overall computed water budget is acceptable.
- Perform an initial check run that makes one pass through the parameter estimation steps including model input file creation, forward model run, extraction of model output, and

### Box 9.2 Tips for Running a Parameter Estimation Code—cont'd

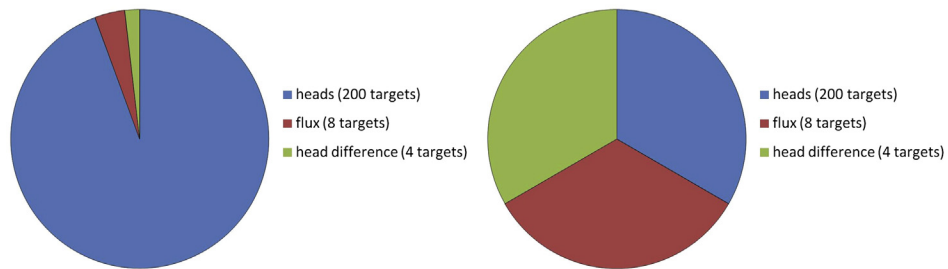


**Figure B9.2.1** Pie charts of an initial objective function that is: (a) unbalanced because the number of head targets is much larger than other targets and (b) more balanced because no one target type dominates or is dominated by other groups. The more balanced objective function was obtained by simply normalizing the observation weights by the number of targets in each group.

calculation of residuals in order to verify that the steps are performed correctly. Moreover, this initial pass-through will give a value for the starting objective function, which should be evaluated for balance among target types (Fig. B9.2.1), and to make sure the initial objective function reflects the modeler's view of the importance of different observation target types.

- After the first Jacobian matrix is calculated, parameter sensitivities reported as zero, if any, should be evaluated. An unexpected zero sensitivity indicates a possible error in the handling of the parameter estimation file where a model input file is being created but is not being called by the associated model run file.
- If the chain of programs run for a forward model run contains intermediate utility codes that preprocess input for the groundwater model, it is good practice to have the output of the utility code be deleted at the top of that batch file/script used to call the forward model run. This ensures that the parameter estimation process is not using an old version of utility output, which may not be discovered until the completion of the parameter estimation run and poor results are obtained.
- Set the initial range of possible parameter values defined by their upper and lower bounds larger than what is realistic to assess potential issues with the conceptual model and effects of processes omitted from the model. Near the conclusion of parameter estimation, set the upper and lower bounds to the expected realistic range (e.g., 95% confidence interval) to ensure realistic parameters and to provide first estimates of parameter uncertainty for evaluating forecast uncertainty (Chapter 10).
- Recognize that at the end of the parameter estimation process the results are not necessarily better than a manual trial-and-error calibration, and may even be worse. For example, the parameter estimation process may find that unreasonable parameter values gave the best model fit whereas unreasonable parameter values would have been excluded at the beginning of a manual trial-and-error calibration. The modeler should never allow the parameter estimation to dictate what parameter set is best if a modeler's hydrosense indicates otherwise. Parameter estimation simply reflects the history matching problem as defined by information provided by the modeler. Often this information can be improved after initial parameter estimation results are obtained and reviewed.

### 9.5.3 Statistical Analysis

Prior to the widespread availability of parameter estimation methods, groundwater models were calibrated exclusively by manual trial and error. Then, parameter sensitivity was evaluated by a manual *sensitivity analysis*. The sensitivity of a given parameter was determined by fixing all calibration parameters at their calibrated values except for the selected parameter, which was varied in sequential forward runs of the model by incrementally increasing and decreasing its value by some percent from its calibrated value (e.g.,  $\pm 25\%$ ). This type of sensitivity analysis showed how much the model moved out of calibration by changes in selected calibration parameters—a subset of all possible calibration parameters subjectively selected by the modeler. This approach was limited, not only to the subset of parameters manually adjusted, but also by reporting the change using a summary of all calibration target residuals, regardless of importance to the modeling objective. Hill and Tiedeman (2007, p. 184–185) discussed other limitations of this traditional type of sensitivity analysis. Modern parameter estimation codes make such sensitivity analysis unnecessary because parameter sensitivity coefficients are automatically calculated for all calibration targets and included in the Jacobian matrix. Hence, parameter sensitivities can be more thoroughly evaluated.

*Parameter sensitivity analysis* uses the Jacobian matrix to develop quantitative statistical insights about the model. *Insensitive parameters* (Section 9.4) are now defined as those having sensitivity coefficients less than a modeler-specified threshold. For practical purposes, an insensitive parameter is defined as those having a sensitivity coefficient more than two orders of magnitude lower than the sensitivity of the most sensitive parameter (Hill and Tiedeman, 2007, p. 50). In addition, information contained in the Jacobian matrix allows calculation of *parameter correlation coefficients* between calibration parameters. In a simple parameter sensitivity analysis, the modeler ranks calibration parameters by sensitivity and identifies both insensitive parameters and correlated parameters (e.g., correlation coefficient  $> 0.95$ ). *Parameter identifiability* (Doherty and Hunt, 2009a; Fig. 10.10) combines parameter insensitivity and correlation information, and reflects the “ease with which particular parameter values in a model might be calibrated” (Beven, 2009, p. 273). An identifiable parameter is both sensitive and relatively uncorrelated and thus is more likely to be estimated (identified) than an insensitive and/or correlated parameter. Parameter sensitivity analysis can also include evaluating the *statistical influence*, which quantitatively relates the importance of observations to calibration parameters and the determination of best fit (e.g., Yager, 1998; Hunt et al., 2006; Hill and Tiedeman, 2007).

Parameter estimation has greatly reduced the effort needed to perform sensitivity analyses, and introduced new quantitative measures such as identifiability and influence. General guidelines for performing parameter sensitivity analysis (e.g., Hill and Tiedeman, 2007) and sophisticated software tools are available. However, there is debate among

modelers over how much effort should be expended on parameter sensitivity analyses because they only identify underlying calibration issues; they cannot overcome them. Model calibration still requires intervention by the modeler to overcome problems of parameter insensitivity and correlation. As we will see in [Section 9.6](#), advanced parameter estimation methods can automatically overcome parameter insensitivity and correlation without modeler intervention. Just as calculating the Jacobian matrix is an interim step toward identifying upgraded parameters, parameter sensitivity analysis is an interim step in finding a best model for forecasts. Therefore, in many cases modeling resources may be better spent on other methods of parameter estimation that allow the modeler to overcome problems only identified in parameter sensitivity analysis. This should, in turn, allow additional resources to be spent on uncertainty analyses of the forecast (Chapter 10).

## 9.6 HIGHLY PARAMETERIZED MODEL CALIBRATION WITH REGULARIZED INVERSION

As the conceptual model is formulated, the numerical model is designed, and parameters are assigned to the nodal network, the modeler must make decisions on how to simplify the natural world for the purposes of the model. So far in this chapter, we have described the traditional approach for making the inverse problem tractable: the modeler reduces the complexity of the natural world to a small number of calibration parameters and thereby simplifies the problem to a sparsely parameterized model (e.g., as advocated by [Hill \(2006\)](#)). Once history matching of the sparsely parameterized model is complete, the modeler must assess the suitability of the simplification by evaluating parameter sensitivity, correlation, and the distribution of residuals that result from the conceptualization. If the fit of simulated values to targets is judged inadequate, more calibration parameters may be added. If the number of calibration parameters is too large to identify a best fit, insensitive and correlated parameters are set to fixed values to reduce the number of calibration parameters. The sparsely parameterized approach requires the modeler to spend time and effort initially deciding how best to simplify the model. If the first attempt at simplification fails to produce an acceptable calibration, more time and effort must be spent reformulating the calibration parameters for additional attempts at history matching. Moreover, if the conceptual model itself is found wanting after failed attempts to calibrate successively simpler (or more complex) models, the entire process must start over with the development of a new conceptual model.

Recognition of the disadvantages of sparsely parameterized methods in other fields of science led to the development of alternatives. One branch of these methods is *regularized inversion* ([Engl et al., 1996](#)), which is attractive because it addresses many of the issues of arbitrarily simplified groundwater models ([Hunt et al., 2007](#)). “Inversion” refers

to solving the inverse problem. “Regularization” describes any general process that makes a mathematical function (like the objective function surface in Fig. 9.11(b)) more stable or smooth. Regularization can be broadly interpreted as any method that helps provide an approximate and meaningful answer to an ill-posed problem. With this definition, it follows that the traditional approach of specifying a relatively few number of parameters acts as a regularization strategy, albeit an informal and subjective one. In the form most commonly used for applied groundwater modeling, regularized inversion consists of:

1. assigning a large number of parameters to the model domain—many more than are used in the traditional sparsely parameterized approach; the model is said to be *highly parameterized* and all parameters are selected as calibration parameters;
2. constraining the larger parameter set with mathematical regularization, which allows the parameter estimation problem to be solved.

When properly performed, regularized inversion provides a systematic and quantitative framework for achieving parameter simplification whereby the mathematical rationale for the simplification is formally documented, transparent, and readily conveyed to others. Moreover, regularized inversion produces a single best fit appropriate model, which is required for many models used in decision-making. It also is attractive because it achieves parameter parsimony in more rigorous ways than zonation and other ad hoc simplification approaches.

It is important to note that regularized inversion was not simply overlooked by previous generations of modelers, but was recognized to be computational challenging due to the high number of parameters considered. Major advances in computing power, numerical solution techniques, and advanced techniques for formulating the parameter estimation problem made regularized inversion possible. Doherty and Hunt (2010) discuss detailed methodology for application of regularized inversion to groundwater flow models; many GUIs have regularized inversion capabilities. The main tenets and approaches are discussed below.

### 9.6.1 Increasing the Number of Calibration Parameters

The inherent subjectivity of traditional ad hoc parameter simplification introduces unquantifiable degrees of structural error (Section 9.4). Zonation, for example, defines the geometry of a set number of piecewise constant zones, thereby creating boundaries where properties change abruptly. The abrupt change across boundaries is usually not geologically realistic, and geographical delineations of zone boundaries are usually not well supported by field data. As a result, there is always uncertainty whether the zones are optimally constructed. Specifying too few zones decreases the ability of the

observations to inform the parameter estimation process because the coarse model structure does not have receptacles to use the information and may bias the forecasts made using the calibrated model. Sparsely parameterized models may produce an acceptable history match, but in effect their parameters are *surrogates* for the true complexity in the natural world. Although surrogate parameters may be given names intended to reflect their physical significance, the values of those parameters needed to get good model performance will depend on the model structure used (Beven, 2009, p. 9). Such surrogacy may produce acceptable forecasts when, for example, observations used for history matching are the same type and time period as the forecast. When this is not the case, however, artifacts from the simplification process can degrade the forecast to an unknown degree because effects of simplification cannot be completely characterized (Doherty and Welter, 2010). *Highly parameterized approaches* were developed in an effort to avoid the problems of difficult to measure parameter oversimplification on model performance. Rather than reducing the number of model parameters a priori, the modeler retains all parameters that are of potential use for calibration and forecasting as calibration parameters. Therefore, the emphasis is on retaining model *flexibility* afforded by using many parameters. The concept of flexibility allows for more avenues to pursue model fit. Furthermore, more information contained within the observations can be extracted because observations are less likely to be competing with other observations to constrain the same calibration parameter. In addition, flexibility also facilitates more encompassing analysis of forecast uncertainty (Chapter 10).

Highly parameterized approaches have sometimes been characterized as the pursuit of model *complexity* (e.g., Hill, 2006). The definition of model complexity, however, is not straightforward (Gómez-Hernández, 2006) and involves more than the number of parameters in a model. For example, highly parameterized models provide more flexibility, but that does not equate to each parameter having a unique value, or that the resulting hydraulic conductivity field is highly heterogeneous. In a model described by Fienen et al. (2009a), each node was assigned a calibration parameter yet the high parameterization collapsed to a relatively simple three zone conceptualization after calibration. An advantage of the highly parameterized approach over traditional zonation is that the simple conceptualization is not specified beforehand, but is identified after information in the observations is considered during calibration. Application of the highly parameterized approach requires a large number of model runs, however, to assess the effect of each parameter on model output. Therefore, the goal is to find a middle ground where the calibration parameters provide sufficient flexibility so that the maximum amount of information is extracted from the calibration targets and structural error is reduced, but the parameters are not so numerous as to confound or preclude calibration. Finding this middle ground is part of the art of modeling and continues to be actively discussed (e.g., Hunt and Zheng, 1999; Hill, 2006; Gómez-Hernández, 2006;

Hunt et al., 2007; Voss, 2011; Doherty and Christensen, 2011; Doherty, 2011; Simmons and Hunt, 2012; Doherty and Simmons, 2013).

A highly parameterized model includes as much detail as necessary to address the modeling purpose. For example, parameterization could include heterogeneity in hydraulic properties at a level of detail important for a forecast, such as representing high hydraulic conductivity preferential flowpaths, which are important in transport simulations. In some cases, properties in every model cell/element in an area of interest are specified as calibration parameters (e.g., Fienen et al., 2009a). In practice, there are still practical limits to how many calibration parameters can be included in the inverse problem. Therefore, the computational burden is commonly reduced by the use of *pilot points* (Marsily et al., 1984; Certes and Marsily, 1991; Ramarao et al., 1995; McLaughlin and Townley, 1996; Doherty, 2003; Alcolea et al., 2006; Doherty et al., 2010a). In this approach, parameter values are estimated at discrete locations (pilot points) distributed throughout the model domain. Once the pilot point locations and parameter values are assigned, spatial interpolation (Section 5.5) such as kriging is used to assign parameter values to all remaining nodes or elements. The number and locations of pilot points are selected to balance parameter flexibility while reducing the computational burden and addressing the modeling objective (Fig. 9.15; Box 9.3). Pilot points can be assigned to zones so that known geologic boundaries can be represented. A pilot point approach is a compromise between extremely large numbers (hundreds of thousands) of possible parameters and the traditional sparsely parameterized approach using an arbitrarily small number of parameters (usually fewer than 100).

## 9.6.2 Stabilizing Parameter Estimation

Regularization, in the broadest sense, includes any mechanism that stabilizes the ill-posed inverse problem. For example, reducing the number of calibration parameters by using pilot points is a form of regularization because fewer parameters make the parameter estimation process more tractable. Two main types of regularization are commonly used in applied groundwater modeling: adding soft knowledge and reducing problem dimensionality. These methods can be used by themselves but are most commonly used in combination.

### 9.6.2.1 Adding Soft Knowledge: Tikhonov Regularization

In Section 9.1 we emphasized that model calibration consists of both a hard knowledge and a soft knowledge assessment. In manual trial-and-error calibration and simple parameter estimation (Section 9.5), soft knowledge assessment is done independently of the hard knowledge assessment. That is, the model is first calibrated using hard knowledge via history matching and then the calibrated parameters are assessed for hydrogeological reasonableness using soft knowledge. Or put another way: a calibrated model is one that



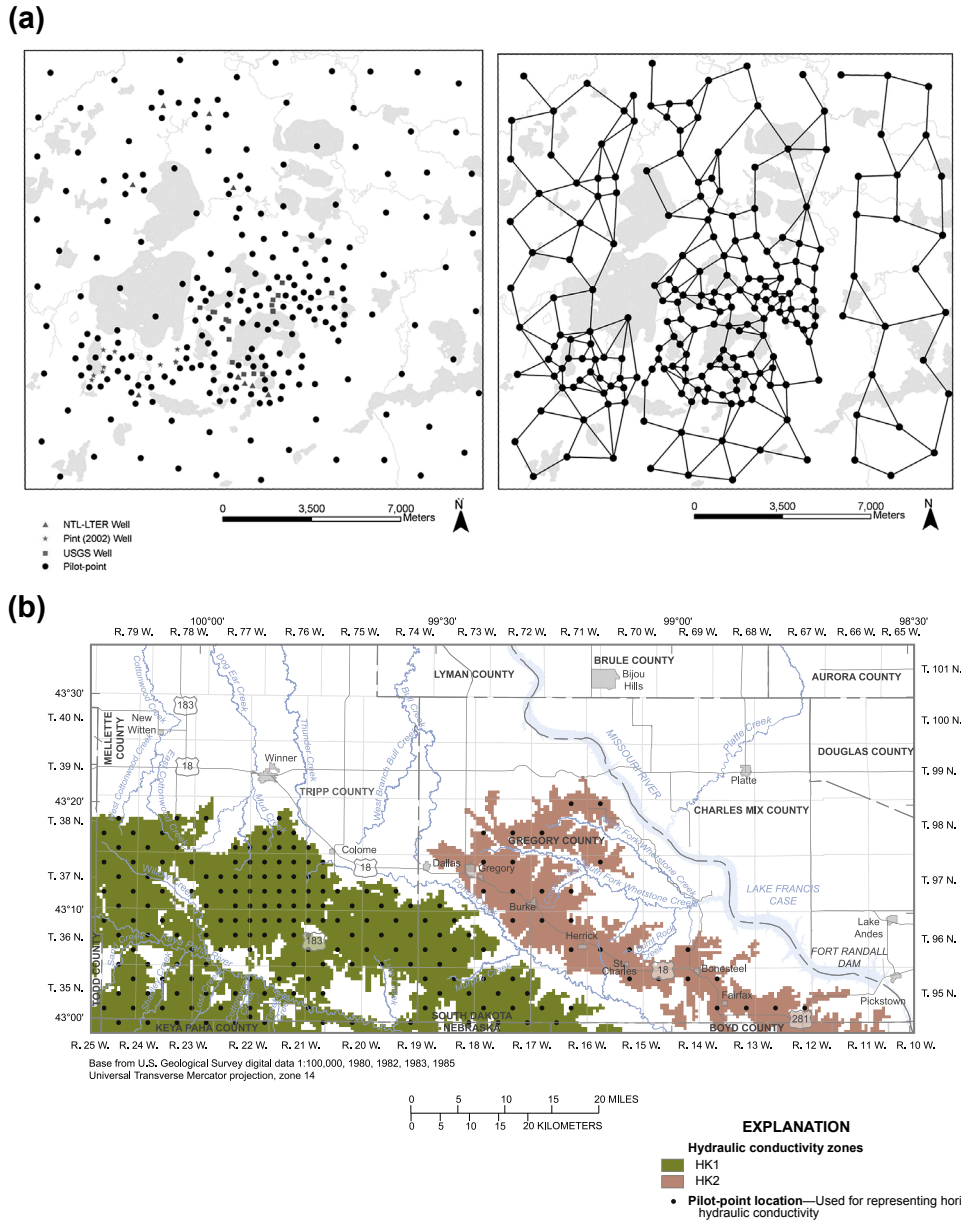


**Figure 9.15** Pilot Points. (a) Network of pilot points in a watershed-scale groundwater flow model (left); linkages between pilot points (right) used to calculate Tikhonov regularization constraints for preferred homogeneity (*modified from Muffels, 2008*). (b) Network of pilot points used to represent two hydraulic conductivity zones where Tikhonov regularization is applied to pilot points within the same zone (*modified from Davis and Putnam, 2013*).

### Box 9.3 Tips for Effective Pilot Point Parameterization

There is no universal set of rules for the placement of pilot points used for parameterization. However, [Doherty et al. \(2010a\)](#) provided the following suggestions based on a mathematical analysis of pilot point parameterization schemes:

1. Generally place pilot points in a uniform pattern to ensure some minimal level of coverage over the entire model domain. Then place additional pilot points in areas of interest. Avoid large gaps between pilot points so that single pilot points are not representing large areas of the domain. The separation between pilot points should be equal to or greater than the characteristic length of any heterogeneities in hydraulic properties in the model domain.
2. Pilot points that are used to estimate horizontal hydraulic conductivity should be placed between observation targets along the direction of the groundwater gradient.
3. Place pilot points at wells where aquifer test data are available so that hydraulic property estimates derived from aquifer test results can serve as initial and/or preferred parameter values.
4. Place pilot points that are used to estimate storage parameters at locations where fluctuations in head have been measured.
5. Place pilot points that are used to estimate hydraulic conductivity parameters between outflow boundaries and upgradient observation wells.
6. Increase pilot point density where calibration target data density is high. But do not place pilot points at locations containing head observations to minimize “bulls eyes” in the hydraulic conductivity.
7. If the number of pilot points is limited by computing resources (e.g., long-forward run times and few resources to run the problem), consider using fewer pilot points to represent vertical hydraulic conductivity in confining or semiconfining units and more pilot points to represent horizontal hydraulic conductivity.

Pilot points can be placed in zones (Section 5.5); some zones may have many pilot points and others just one. When a single pilot point is assigned to a zone, the parameter estimation process assigns one value to each node in that zone; thus the pilot point parameter acts as a piecewise constant zone, which is insensitive to the location of the pilot point. When more than one pilot point is located in a zone, spatial interpolation from pilot points to the nodal points, and associated regularization ([Section 9.6](#)), do not take place across zonal boundaries.

has the best fit to hard data but also whose parameters have the smallest deviation from soft knowledge available for a modeled area. This informal representation of a soft knowledge penalty, however, can be mathematically included along with the expression of goodness of fit from [Eqn \(9.6\)](#):

$$\Phi_{total} = \Phi_{hard\ data\ misfit} + \Phi_{soft\ knowledge\ deviation} \quad (9.8)$$

which can also be expressed as:

$$\Phi_{total} = \sum_{i=1}^n (w_i r_i)^2 + \sum_{j=1}^q (f_j(p)) \quad (9.9)$$

The first term to the right of the equals sign is the measurement objective function from Eqn (9.6), which is calculated as the sum of squared weighted residuals, where  $n$  residuals,  $r_i$ , are calculated from hard knowledge and  $w_i$  are their respective weights. The second term quantifies the penalty resulting from deviations from soft knowledge as the sum of  $q$  deviations from  $j$  soft knowledge conditions  $f_j$ , where  $f_j$  is a function of model parameters  $p$ . A calibrated model, therefore, is found by minimizing both the measurement objective function (hard data) and the soft knowledge penalty.

The Russian mathematician Andrey Tikhonov developed an approach for mathematically including soft knowledge at the beginning of the calibration process (Tikhonov 1963a,b; Tikhonov and Arsenin, 1977), now known as *Tikhonov regularization*. With Tikhonov regularization, the modeler's soft knowledge can be used along with hard knowledge during parameter estimation. Soft knowledge includes intuitive knowledge, professional judgment, regional literature values, and geological expertise—information that is often qualitative or marginally relevant to the site being modeled. Yet, this approach is widely used because even such qualitative information can help stabilize an ill-posed parameter estimation problem, particularly when the type of information conveyed by the soft knowledge is not contained in the targets.

Tikhonov regularization formally incorporates soft knowledge into the calibration process by augmenting the objective function, here called the *measurement objective function* (described by Eqn (9.6)), with a second *regularization objective function* that expresses the soft knowledge penalty (i.e., the two additive components of Eqn (9.9), respectively). The regularization objective function captures the parameters' deviation from the modeler's understanding of the system as expressed by *preferred conditions* for parameters (e.g., Doherty, 2003, pp. 171–173); thus, minimizing the regularization objective function reduces the soft knowledge penalty. Preferred conditions are usually expressed as a preferred parameter value (e.g., “this area is thought to have a hydraulic conductivity of 4 m/d”) and/or a preferred difference, most often a difference of zero indicating a preferred homogeneity condition (e.g., “these two areas are thought to have the same properties”). The more the parameter estimation process deviates from the preferred conditions, the larger the value of the regularization objective function. The model is calibrated by minimizing both the measurement and regularization objective functions ( $\Phi_{total}$ , Eqn (9.9)); when both minima are obtained a unique solution to the inverse solution is obtained (see De Groot-Hedlin and Constable, 1990).

Note that obtaining a unique solution is directly dependent on the modeler's formulation of the problem—if the modeler changes observation weights or regularization

preferred conditions, minimization of both the measurement and regularization measurement functions must be performed again. Mathematically, the regularization objective function is tracked separately from the targets and related measurement objective function. Thus, parameter estimation using Tikhonov regularization is a “dual constrained minimization” process. Functionally, the modeler-specified preferred conditions constitute a suite of fallback values for parameters (or for relations between parameters) that are applied when information contained in the observations is insufficient for unique estimation of a parameter (e.g., insensitive parameters). When the hard knowledge from observations informs the parameter value, deviation from these fallback preferred values is allowed. Such deviations, however, penalize the combined objective function by increasing the value of the regularization objective function. Therefore, deviations from soft knowledge are only allowed if they provide sufficiently large reduction in the measurement objective function (better fit to the targets) to offset the increase in the combined objective function.

Tikhonov regularization also allows the modeler to specify how strongly to enforce the soft knowledge constraints. This is done through the *target measurement objective function*. This additional input provided by the modeler (e.g., in PEST via the variable PHIMLIM) limits the level of fit the calibration process is allowed to achieve (Doherty, 2003; Fioren et al., 2009b). When the target measurement objective function is unrealistically below the lowest possible measurement objective function (Fig. 9.16(a)), soft knowledge is weakly enforced. This can lead to unreasonably extreme values for parameters. Higher values of the target measurement objective function cause the soft knowledge to be more strongly enforced and the resulting parameter field is smoother (Fig. 9.16(b)). In practice, a very low value for the target measurement objective function is typically specified in an initial run to minimize soft knowledge and obtain a best fit to hard data (e.g., Fig. 9.16(a)). The best fit value of the measurement objective function is then used to estimate a target measurement objective function that is somewhat higher than the best fit (e.g., around 10% higher, Fig. 9.16(b)).

As expected given the issues described in Section 9.1, there are many possible models that could be considered calibrated depending on the modeler’s expression of the strength of soft knowledge. The trade-off between soft knowledge and hard knowledge can be shown graphically by a *Pareto front* diagram (Fig. 9.17). A Pareto front is commonly used in economics to describe the trade-off between two objectives when it is not possible for both to be attained simultaneously. In Fig. 9.17, the calibration that favors the soft knowledge preferred condition (smallest value on  $y$ -axis scale) gives the worst model fit (i.e., the largest value on the  $x$ -axis scale); the calibration that favors the hard knowledge and gives the best history match (smallest value on  $x$ -axis scale) deviates the most from the soft knowledge. The best calibrated model selected from the Pareto front is an expression of the modeler’s subjective judgment as to the optimal trade-off between hard and soft knowledge, which is the essence of the art of modeling. For

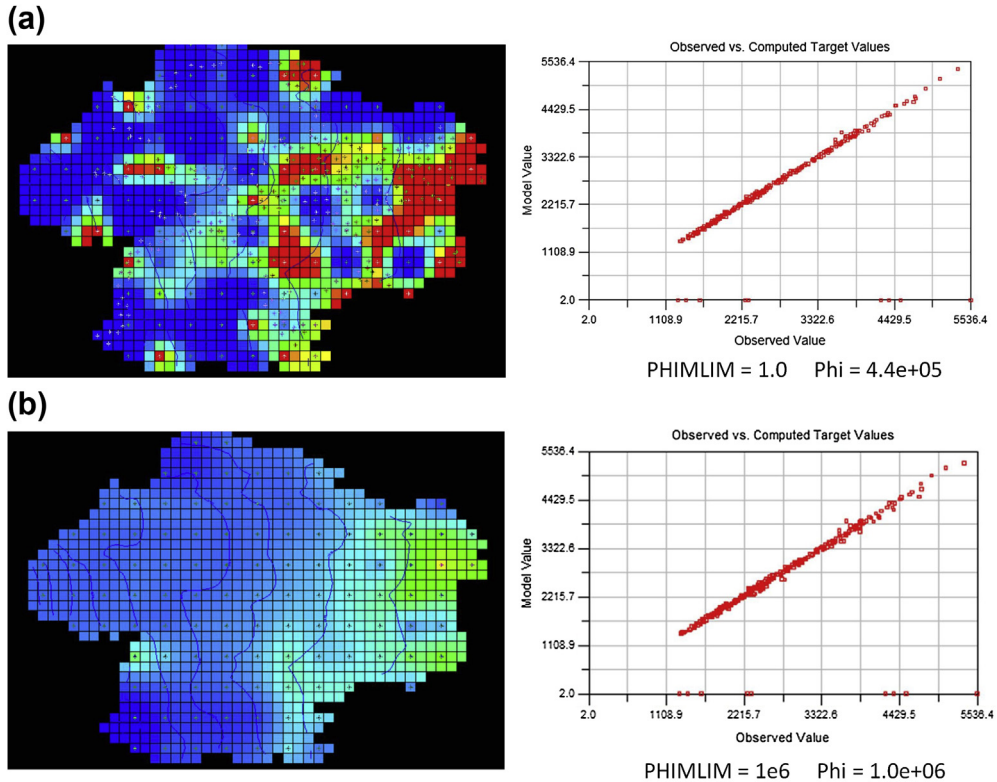


**Figure 9.16** Visualization of parameter estimation using alternative Tikhonov regularization, where the same parameter estimation problem is solved using two different values of the target objective function (PHIMLIM variable in PEST). (a) When the target objective function is set unrealistically low (PHIMLIM = 1), user soft knowledge is disregarded and optimality of the inverse solution is defined solely by the model's fit to calibration targets (i.e., minimization of the measurement objective function,  $\Phi$ ). The resulting field has extreme contrasts and parameter "bulls eyes" that reflect the code's unchecked pursuit of the best fit. (b) When the target objective function is set to a value around 10% higher than the best  $\Phi$  obtained (PHIMLIM = 1e6), the resulting fit is slightly worse (as shown by a slightly larger spread around the 1:1 line in the scatter plot of heads), but heterogeneity in the optimal parameter field is reduced. Whether the heterogeneity expressed is reasonable is the decision of the modeler; thus both models might be considered part of the Pareto front shown in Fig. 9.17 (modified from USGS unpublished data).

most groundwater models, we can assume that neither extreme of the Pareto front is optimal. That is, a history match that is too good reflects noise associated with the field measurements and/or inadequacies of the model rather than the properties of the natural system, and the model is said to be *overfit*. At the other extreme of the Pareto front, hard knowledge from the targets is unacceptably diminished and the model is dominated by a modeler's preconceived notions of the system; such a model is said to be *underfit*. When

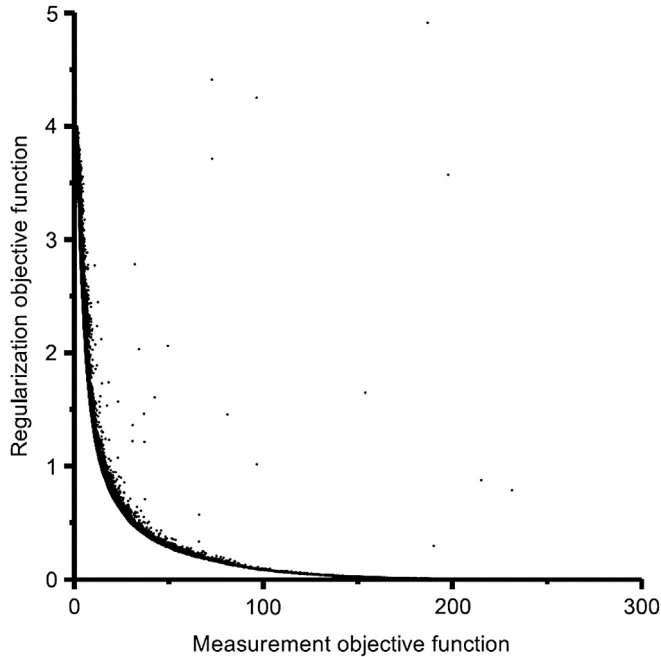


**Figure 9.17** A Pareto front diagram. Multiple calibrations by Tikhonov regularized inversion of the same model are shown by dots, which coalesce into a thick black line along a “front”; the only difference among calibrations is the strength of the soft knowledge constraint expressed during parameter estimation. The Pareto front illustrates the inherent trade-off between a perfect model fit (zero on x-axis) and perfect adherence to the modeler’s soft knowledge (zero on y-axis). The “best” model is the modeler’s subjective pick of one calibration from the many calibration results along the Pareto front (*modified from Moore et al., 2010*).

properly balanced, the soft knowledge constraint defines an *optimal parameter field* where heterogeneity is included at locations and in ways that are supported by the calibration targets. Therefore, changes to the target measurement objective function allow the modeler to evaluate whether departures from initial values of the parameters based on soft knowledge used to construct the conceptual model are supported by observations and are hydrogeologically realistic (e.g., [Fiinen et al., 2009b](#)). Put another way, although the complexity of the natural world can never be known, Tikhonov regularization gives the modeler a mathematically defensible way to include as much parameter complexity as their observations support.

### 9.6.2.2 Collapsing Problem Dimensionality: Subspace Regularization

In contrast to Tikhonov regularization, which adds information to the calibration process in order to achieve numerical stability, subspace methods achieve numerical stability by

reducing the dimensionality of the Jacobian matrix through subtraction of parameters and/or by combining parameters (Aster et al., 2013). Only those parameters and linear combinations of parameters that are sufficiently constrained by the targets are estimated. The determination of which parameters to estimate is automated using *singular value decomposition* (SVD—Box 9.4) of the Jacobian matrix (e.g., Moore and Doherty, 2005; Tonkin and Doherty, 2005).

Although understanding the theoretical underpinnings is not critical for using SVD for model calibration, a brief discussion is included here to familiarize the reader with terminology associated with SVD. SVD uses linear algebra for matrix decomposition; it conveys the maximum signal energy (information from the observations) into as few coefficients (calibration parameters) as possible, and thus is widely used in applications in engineering, signal processing, and statistics. Recall from Section 9.5 that the Jacobian matrix consists of sensitivity coefficients (Eqn (9.7)) that relate all parameters (i.e., *base parameters*) to all observations. SVD operates on the Jacobian matrix to divide parameter space into a set of linearly independent combinations of parameters. Each of

#### Box 9.4 A “Singularly Valuable Decomposition”<sup>1</sup>—Benefits for Groundwater Modeling

When large numbers of parameters are added to a model, some will be insensitive and others highly correlated with other parameters. As a result, even though a parameter is important to the modeling objective, it does not mean that it is *identifiable* (capable of being estimated given the available calibration targets). Doherty and Hunt (2010) point out that what is needed is an intelligent calibration tool—one that detects what can and cannot be inferred from the calibration targets. This tool should estimate what it can leave out and what it cannot—all automatically, without user intervention. Singular value decomposition (SVD) is such a tool, fondly referred to as a “singularly valuable decomposition” by Kalman (1996).

SVD is a way of processing matrices into a smaller set of independent linear approximations that represent the underlying structure of the matrix; thus, it is called a *subspace method*. It is used widely for such tasks as image processing, for example, as commonly experienced in the sequentially updated resolution of images displayed by an Internet browser (similar to Fig. B9.4.1). In this way, SVD gives the user progressively more useful information, even from a blurry image, earlier rather than waiting for the entire image to download.

In the context of groundwater model calibration, rather than solving for all details of an inverse problem (represented by all calibration parameters), SVD utilizes a reduced representation of the problem. It recognizes that certain combinations of observations are uniquely informative and also creates linear combinations of the parameters. Similar to the image processing example, this subspace represents a blurry view of the subsurface, but a view that defines where combinations of informative observations (the *solution space*) run out, thereby defining the combinations of parameters that cannot be estimated (the *null space*). SVD-based parameter estimation fixes initial values of insensitive parameters and does not

(Continued)

### Box 9.4 A “Singularly Valuable Decomposition”<sup>1</sup>—Benefits for Groundwater Modeling—cont'd

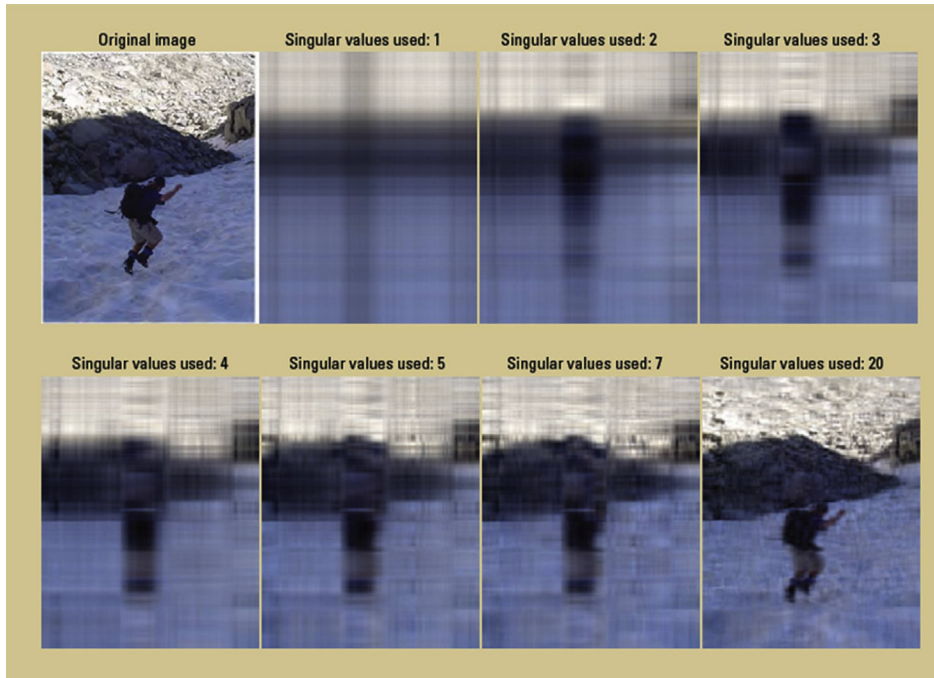


**Figure B9.4.1** Singular value decomposition of a photographic image. When the matrix is perfectly known (defined by 240 pixels/singular values in the image), it reflects the highest resolution and thus the highest number of singular values can be shown visually. For reference, the image with 20 singular values represents less than 10% of the information contained in the original image in the upper left, yet it contains enough information that the subject matter can be easily identified. A similar concept applies to groundwater problems—if too few singular values are selected, a needlessly coarse and blurry representation of the groundwater system results. When the information content of the calibration data set is increased, a larger number of data-supported singular values can be included, resulting in a sharper “picture” of the groundwater system. In practice, most field observations only support a relatively blurry depiction of subsurface properties (from *Doherty and Hunt, 2010*; image and SVD processing by Michael N. Fioren, USGS).

use them in the parameter estimation process. Therefore, parameter combinations in the solution space become the heart of the calibration process. Because only parameter combinations that can be estimated are used in the parameter estimation process, solution of the inverse problem is unique and unconditionally stable. By using parameter combinations, known as superparameters, such as in SVD-Assist (Section 9.6), the size of the Jacobian matrix is reduced, as is processing time.

<sup>1</sup> Kalman, D., 1996. A singularly valuable decomposition—The SVD of a matrix. *College Mathematics Journal* 27(1), 2–23.



these combinations is multiplied by a factor known as a *singular value*, and summed to reproduce the full parameter field. In this way, singular values constitute a reduced set of linear combinations of the full suite of calibration parameters (here called *base parameters*).

Singular values are usually listed in decreasing order (i.e., singular value of index 1 is more constrained by information contained in observations than singular value 2). In practice, those parameters associated with singular values of lower index tend to represent spatially averaged parameters; those associated with higher index tend to represent local system detail. After SVD, *singular value truncation* is performed where parameter combinations associated with singular values that are greater than a user-specified threshold (i.e., have lower index number) are considered supported by the observation data and assigned to the *solution space*; parameters and parameter combinations that cannot be estimated from the targets (e.g., insensitive parameters) are not included in the solution space and are assigned to the *null space* (Fig. 9.18). A parameter or combination of parameters residing in the null space is considered uninformed by the observations and retains the

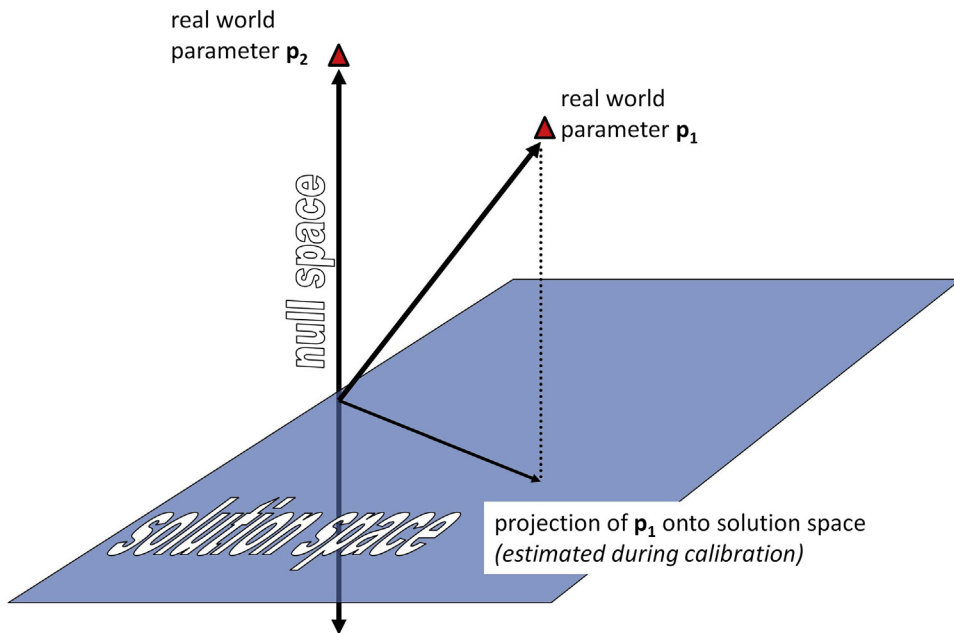


**Figure 9.18** A schematic depiction of the relation of two parameters ( $p_1$  and  $p_2$ ) to the solution space and null space defined by a set of calibration targets. Because neither parameter lies on the plane of the solution space, the parameters are not perfectly constrained by the observations. Parameter  $p_1$  is partially informed by the observations; thus it has a projection into the solution space and can be estimated during parameter estimation. Parameter  $p_2$ , however, cannot be projected onto the solution space and cannot be estimated given the calibration targets (modified from Doherty et al., 2010b).

initial values specified by the modeler during calibration. Therefore, it is important when using SVD that initial parameter values are hydrogeologically reasonable. By using linear combinations of parameters rather than individual parameters, correlated parameters that cannot be estimated individually can be estimated in combination with associated correlated parameters. In this way, SVD automatically accounts for the insensitive and correlated parameters that a modeler must otherwise address manually using the methods discussed in [Sections 9.4 and 9.5](#).

If too many combinations of parameters are estimated (too many singular values), the problem will still be ill-posed and numerically unstable. If too few parameters are estimated, the model fit may be unnecessarily poor, and forecasting errors may be larger than for an optimally parameterized model. Even when the problem includes an appropriate number of singular values, SVD can still be ruthless in its search for a best fit ([Doherty and Hunt, 2010](#)). Therefore, when used alone, SVD can result in overfitting, producing calibrated parameter fields that lack geologically realistic characteristics. As a result, SVD is often used in conjunction with Tikhonov regularization, which produces geologically realistic parameter distributions owing to soft knowledge constraints. When the two approaches are combined, the degree of fitting is controlled by the soft knowledge input under Tikhonov regularization, but the fitting is performed on an inverse problem that is unconditionally stable ([Box 9.4](#)).

### 9.6.3 Speeding the Parameter Estimation Process

Although SVD can provide an unconditionally stable and unique model calibration, it does not alleviate the high computational burden of a highly parameterized approach because the full Jacobian matrix is computed for each parameter estimation iteration. Recall from [Section 9.5](#) that the minimum number of model runs required for calculation of the full Jacobian matrix is equal to the number of calibration parameters plus one. Fortunately, parameter estimation is an “embarrassingly parallel” problem ([Foster, 1995](#)). That is, to construct the Jacobian matrix each parameter is perturbed independently from all others, and thus one run does not require information from other runs to start or complete. Large speedups in total run time can be achieved by distributing the runs across multiple processors and calculating the Jacobian matrix and parameter upgrade searches simultaneously (e.g., [Schreüder, 2009](#); [Doherty, 2014a](#)). Advances in run management and computational networking allow the runs to be distributed over multiple processor cores on a single personal computer or, for larger problems, over the Internet (e.g., [Muffels et al., 2012](#)) and in the cloud computing environment ([Hunt et al., 2010](#)).

In addition to the brute force approach of simply adding more computer units to perform parameter estimation, the SVD process itself can be sped up using *SVD-Assist* (SVDA) ([Tonkin and Doherty, 2005](#)), whereby the solution and null subspaces are

defined just once by using the Jacobian matrix calculated from initial parameter values. Before the parameter estimation process starts, a set of *superparameters* is defined from sensitivities calculated from the full set of calibration (base) parameter values using SVD, thereby reducing the full parameter space to a subset of the solution space that relates to the full set of base parameters. Being derived from SVD, superparameters are comprised of linear combinations of parameters informed by the observation targets. Significant speedups in the parameter estimation process are obtained because, once defined by SVD, the number of superparameters is less than the set of base parameters but can be estimated as if they were ordinary base parameters. Derivatives in the Jacobian matrix are calculated using the smaller number of superparameters rather than the full set of base parameters. However, it is possible that a Jacobian matrix calculated from final optimized parameters would be appreciably different from that calculated from the initial values because of nonlinearity. If sufficiently different, the underlying assumption of SVDA is violated because superparameters defined using initial values would not approximate those calculated from optimal values. In that case, following the initial SVDA run, the Jacobian matrix is recalculated from calibrated parameter values, superparameters are redefined, and another SVDA parameter estimation run is performed with the newly defined superparameters. A parameter estimation code (PEST++—Welter et al., 2012) automates these relinearization and singular value redefinition steps, thereby freeing the modeler from performing this check.

The number of superparameters may be sufficiently small for their values to be estimated using traditional calibration methods for well-posed inverse problems (Section 9.5). In most cases, however, Tikhonov regularization (with default conditions applied to the base calibration parameters) should be included in a *hybrid SVDA/Tikhonov* (Fig. 9.19) parameter estimation process. Doherty and Hunt (2010) suggest this as the preferred method for applied modeling because: (1) large reductions in run times are achieved because the number of runs needed for most parameter estimation iterations is related to the number of superparameters; (2) simultaneous application of Tikhonov regularization constraints allows the user to interject soft knowledge into the parameter estimation process and thus rein in the pursuit of a best fit to calibration targets. SVD and SVDA have been incorporated into some GUIs and codes (PEST++—Welter et al., 2012), and utility software is also available (e.g., SVDAPREP—Doherty, 2014a). Because of the complementary increase in speed and likelihood of obtaining geologically realistic parameter fields, the hybrid SVDA/Tikhonov approach is currently the most efficient and numerically stable means of attaining a hydrogeologically reasonable, highly parameterized groundwater model. However, the decision as to what constitutes hydrogeologically reasonable is subjective (e.g., Fig. 9.17) and the modeler may perform several iterations through the loop shown in Fig. 9.19, where alternate Tikhonov regularization schemes are tested to refine the trade-off of soft and hard knowledge (e.g., Fig. 9.16).

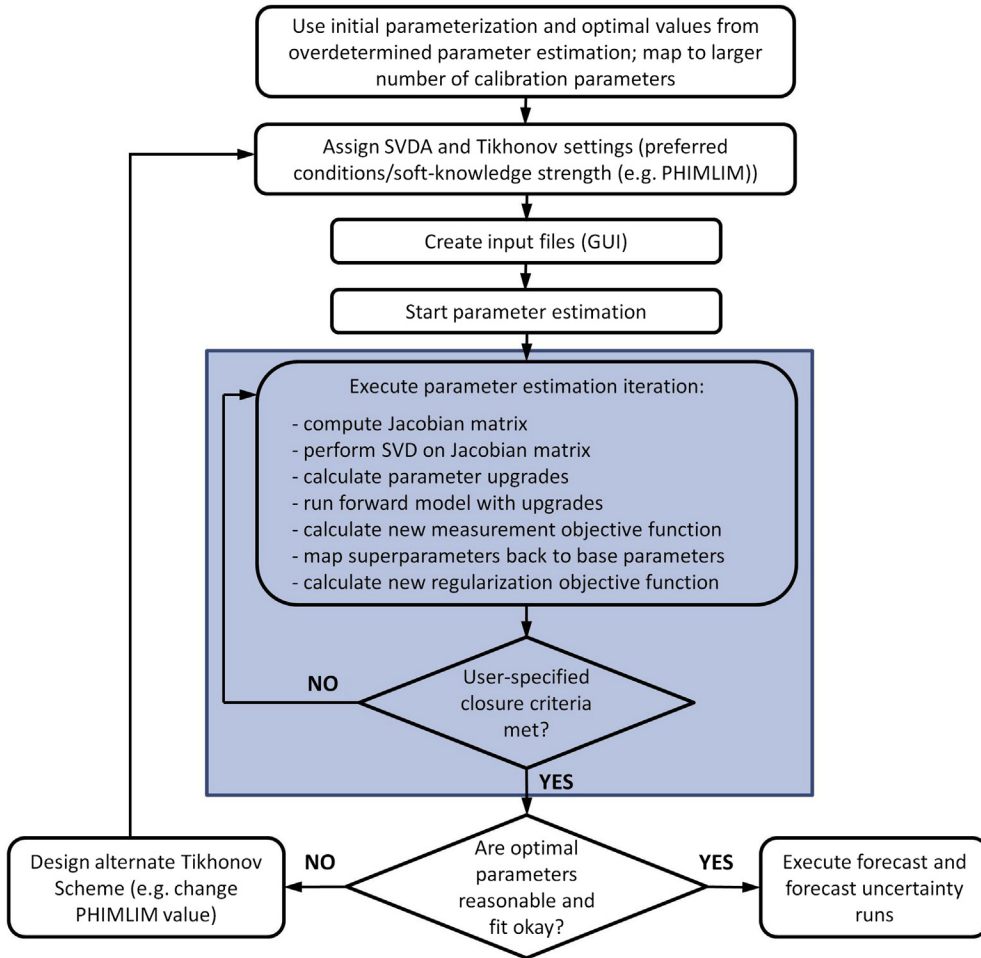


**Figure 9.19** A schematic diagram of a general workflow for parameter estimation using a hybrid SVD-Assist (SVDA)/Tikhonov regularization approach. Shaded box contains the steps performed internally by the parameter estimation code without user intervention; unshaded steps require modeler action. The trade-off between soft knowledge and the model's fit to hard knowledge is adjusted by changing the target objective function for Tikhonov regularization (the PHIMLIM parameter in PEST); (GUI, graphical user interface; SVD, singular value decomposition).

## 9.7 A WORKFLOW FOR CALIBRATION AND MODEL PERFORMANCE EVALUATION

Model calibration, which includes history matching and an assessment of parameter reasonableness, is in essence an exercise in evaluating model performance. Most groundwater modelers accept that a groundwater model can never be validated (Box 9.5).

### Box 9.5 Code/Model Verification and Model Validation

When discussing model calibration, the terms verification and validation (Section 1.5) are often used. Given the state of modeling in the twenty-first century and the availability of new approaches for calibration (Sections 9.5 and 9.6), these concepts have become largely unnecessary. Nevertheless, the terms continue to be used (e.g., Moriasi et al., 2012; Anderson and Bates, 2001; Beven and Young, 2013) and are discussed here to provide the reader with a context for their use in applied groundwater modeling.

*Code verification* refers to establishing that a computer program (code) is correctly written so that it accurately solves the relevant partial differential equation. Most codes for groundwater modeling that are in use today have been verified by the developer of the code and thus code verification by the user is unnecessary. Code verification is usually documented in the user's manual.

An interest in *model verification* (as opposed to code verification) arose from the practice among streamflow modelers to divide field observations into groups using a split sample method. One portion of the sample of observations was used to calibrate the model to a specific time period and the other portion of the sample was used to test the calibrated model. It is sometimes recommended that groundwater models be calibrated against one time period and "verified" against another, or for different time periods that represent different hydraulic conditions (e.g., average annual heads versus heads from a short-term aquifer test); or that a groundwater flow model be "verified" by demonstrating that calibrated heads and fluxes can reasonably reproduce observations of another dependent variable such as concentrations (using a solute transport model) or temperatures (using a heat transport model). Doherty and Hunt (2010), however, point out that while these exercises demonstrate that a calibrated model is able to reproduce certain aspects of system response under field conditions, the data used in a verification exercise are more valuable when incorporated into the calibration. In most cases, any additional confidence gained by withholding data will be overwhelmed by the uncertainty that remains. Nonuniqueness and uncertainty can be reduced by including more and varied calibration targets in the calibration. Different time periods and data types contain information pertinent to different aspects of the modeled system. Therefore, history matching exercises (and the final calibrated model) are poorer by the omission of data. Using concepts discussed in Section 9.6, including data withheld for the purpose of verification could add dimensions to the parameter solution space, and thereby decrease the dimensionality of the null space. Where data are scarce, uncertainty margins will be wide—an inescapable consequence of not having data. Therefore, for most groundwater modeling projects, verification will not lead to increased confidence in the model's performance. Rather, time and resources are better spent in parameter estimation using the full set of observations followed by forecast uncertainty analysis (Chapter 10).

The term *model validation* implies that the model is in some sense "correct" and therefore capable of making accurate (valid) forecasts. In the twentieth century, attempts were made to establish validation protocols, especially for siting geologic repositories for high-level nuclear waste. However, concerns over nonuniqueness and model uncertainty led to the current

(Continued)

**Box 9.5 Code/Model Verification and Model Validation—cont'd**

view that a model cannot be validated; it can only be invalidated (e.g., Konikow and Bredehoeft, 1992). Furthermore, it can only be invalidated at a certain level of confidence (Oreskes et al., 1994; Oreskes and Belitz, 2001). In short, validation has been replaced with other types of model performance evaluation such as parameter estimation and forecast uncertainty analysis. These activities can build confidence in the model while recognizing that it is impossible to guarantee that the model is 100% correct. Rather, the goal is to assess a model's fit for purpose, which evaluates whether it is conditionally suitable for use in a stated type of application (Beven and Young, 2013). The situation is well summarized by Doherty (2011): "When it makes a prediction, a model cannot promise the right answer. However, if properly constructed, a model can promise that the right answer lies within the uncertainty limits which are its responsibility to construct."

Therefore, calibration is the primary way to assess model performance. Calibration of groundwater models should start with manual trial-and-error history matching (Fig. 9.1), followed by automated trial-and-error history matching (parameter estimation, Fig. 9.9). A general workflow for calibration would typically calibrate the steady-state model first, focusing on hydraulic conductivity, recharge, and leakance/resistance parameters. If transient modeling is required, the transient model is typically calibrated separately after the steady-state calibration, where history matching is attempted by adjusting only storage parameters. Temporal difference targets (Section 9.3) are best suited for the primary focus for transient history matching. The quality of the match can be judged by the representation of system dynamics (Fig. 7.11; Fig. 9.4(a) and (d)), and history matching is not confounded by the need to overcome systematic misfit in absolute model outputs inherited from the steady-state calibration. A separate calibration of steady-state and transient models prevents the steady-state best fit from being degraded during transient calibration when adjustment of storage parameters alone can obtain a good fit to the transient observation targets. Moreover, the number of calibration parameters estimated with the transient model is limited to storage parameters; a small number of transient calibration parameters is desirable because transient models typically have appreciably longer forward run times than steady-state models. In some cases, the separate calibration approach may not yield a satisfactory transient history match; in these cases the steady-state and transient models are run together, and model outputs are evaluated using a combined objective function that includes both steady-state and transient observations.

If simple methods alone are used for parameter estimation (Section 9.5), final calibrated parameter values must be assessed for reasonableness using a manual soft knowledge assessment. For most applied modeling, the preferred approach is to use PEST with Tikhonov regularization to include soft knowledge formally in the parameter estimation solution. SVD helps stabilize the solution (Section 9.6) and SVDA speeds up the calibration process. Moreover, modern desktop computers have multiple processors that

allow for parallel processing (running multiple workers) on a single machine. Because most parameter estimation codes have parallel processing capabilities, the user can take advantage of the pleasingly parallel aspects of parameter estimation. If multiple networked computers are used for parallel processing of proprietary software, the modeler must ensure that each additional machine has appropriate software licenses. Open source software typically can be copied to multiple machines without such licensing concerns.

The results of the calibration should be documented by reporting summary statistics ( $ME$ ,  $MAE$ ,  $RMSE$  for steady-state models: Eqns (9.1)–(9.3); NS for transient models: Eqn (9.4), Fig. 9.4(a)), a plot of observed versus simulated values (Fig. 9.5; Fig. 7.11), a map and spatial plot showing locations and magnitudes of residuals (Fig. 9.6), and an evaluation of the simulated water budget (Fig. 7.5(b)). Summary statistics and residual plots are typically represented using unweighted residuals because they represent the true departure from observed values and are not obscured by weights, which are subjectively chosen by the modeler. The modeler should report and discuss both the rank (weight—e.g., Table 7.1) of the observation targets and the choice of calibration parameters, and discuss how soft knowledge was included in the calibration. If Tikhonov regularization was used, a Pareto front diagram (Fig. 9.17) is helpful.

Evaluation of model performance must also identify data gaps and uncertainties in the conceptual model and limitations of the numerical model. The modeler evaluates recalcitrant misfit of targets and the spatial and temporal distribution of residuals by examining scatter plots of observed versus simulate values (Fig. 9.5) and spatial maps of residuals (Fig. 9.6). Additional statistical tools are also available that can evaluate how the selected conceptual model performed (Box 9.6). If such examination leads to the conclusion that the best fit model is inadequate, it is likely that the underlying assumptions and/or conceptual model are inadequate, or that the calibration targets poorly represent the hydrogeological site conditions. The usefulness of any forecast based on an inadequate calibrated model is questionable. If potentially significant flaws in the conceptual model are suspected, the modeler may decide to examine *alternative conceptual models* (Section 1.6). Alternative conceptual models allow the modeler to expand the evaluation to other plausible representations of the system, within constraints of the available data and what is known about the system. One or more new conceptual models would form the basis of new or refined numerical models. With each new model, the model assessment processes begin again, including calibration. The advantage of parameter estimation is that the quantitative best fit for a given conceptual model is identified efficiently and in a mathematically rigorous way, and shortcomings in the conceptual model are transparent. Therefore, parameter estimation facilitates testing more than one conceptual model. An alternative conceptual model may supplant the original conceptual model and become the preferred basis for forecasting simulations. Or as we will see in Chapter 10, several conceptual models may be carried forward to help represent uncertainty in the forecasts. Uncertainty estimates have become an important part of applied modeling.

### Box 9.6 Additional Parameter Estimation Tools

The quantitative framework inherent in parameter estimation allows for evaluating a model beyond approaches discussed in Sections 9.4–9.6. Two additional statistical metrics are briefly discussed in this box: (1) parameter and observation influence; (2) global sensitivity. Both of these metrics are included in currently available software, but are not as widely used as other methods covered in this chapter. Parameter estimation is an active area of research and we expect that these and many more tools will eventually be incorporated into the standard applied modeling software toolkit.

An objective of parameter estimation is to maintain the same importance (ranking) of observations as in manual trial-and-error calibration (Section 9.5). Before calibration begins, the leverage an observation exerts on the parameters can be calculated (e.g., Hill and Tiedeman, 2007, p. 134; INFSTAT utility in PEST—Doherty, 2014b). With this information the modeler can identify observations that have the potential to dominate the parameter estimation process, and thus can assess whether its influence is consistent with the modeling purpose. When an observation has too much leverage, its weight (Section 9.5) can be reduced to lessen its effect. After calibration is performed, the modeler may question results if the parameter values fall outside the range of values considered representative for the site. Information regarding which observation(s) are better fit by using parameter values outside the range of reasonable values may be helpful in evaluating the calibration. Yager (1998) describes the use of the influence statistic DFBETAS (Belsley et al., 1980), which statistically measures an observation's effect on a single parameter. With this information, observations can be ranked in order of influence on an estimated parameter (e.g., Hunt et al., 2006). The SSSTAT (using subspace methods discussed in Section 9.6) tool in the PEST software suite (Doherty, 2014b) is designed to trace observation influence to parameters in underdetermined inverse problems.

The sensitivity coefficient (Eqn (9.7)) measures local sensitivity because it is based on small perturbations around a given parameter value. Local sensitivity, while computationally efficient, also assumes linearity, which means that sensitivity coefficients calculated for one set of parameters apply for the entire range of possible input and output, which may not be a good assumption. Global sensitivity analyses (e.g., Saltelli et al., 2008) address nonlinear sensitivity for a wide range of parameter values. According to Mishra et al. (2009) global sensitivity analyses are well suited for determining parameters that have the greatest impact on overall uncertainty and factors that cause extreme forecasts.

Mishra et al. (2009) compared results from global sensitivity to local sensitivity analyses and the Method of Morris (Morris, 1991), which provides a “bridge” between local and global methods. Global methods are more computationally intensive, and the number of runs required is unknown a priori because it depends on problem-specific factors such as degree of nonlinearity and number of parameters. A practical alternative is to “simplify the model via reduction in spatial dimensions, simplification of processes, screening for key parameters based on expert judgment...”, to help guide subsequent work. Another such bridge is the Distributed Evaluation of Local Sensitivity Analysis statistic (Rakovec et al., 2014). The insight such methods provide can facilitate more efficient direct sampling-based uncertainty analyses such as Monte Carlo.



Whereas reporting results from a single calibrated model was standard practice in the past, it is now widely recognized that modeling must include some expression of uncertainty in the conceptual model, calibrated numerical model, and forecast conditions. Uncertainty analyses are explored in Chapter 10.

## 9.8 COMMON MODELING ERRORS

- Too much time and effort are spent on model design and construction; calibration is started too late and the project is nearly out of time and money. Consequently, the final model does not have an acceptable history match and/or has unreasonable parameters.
- Calibration is deemed complete simply because a summary statistic (e.g., a limit on the MAE) is met. Alternatively, an appropriate model is discarded because a summary statistic is not met.
- Calibration is deemed complete after a history matching exercise but optimized calibration parameters include unreasonable values.
- History matching only includes manual trial-and-error when the modeling objective requires a quantitative best fit. Model calibration should include parameter estimation.
- Weights assigned to calibration targets for parameter estimation do not reflect the same importance the modeler used for manual trial-and-error history matching. Consequently, the results of parameter estimation do not reflect the modeler's judgment of observation importance.
- The modeler accepts a history match produced by an oversimplified model that does not fully leverage information contained in the observations and degrades the model's forecasting ability.
- The initial model used for parameter estimation is overly complex and has not been tested via manual trial-and-error calibration. Models should illuminate system complexity, not create it (Saltelli and Funtowicz, 2014).
- Parameter results are accepted without evaluation simply because they are produced by a computer algorithm. The modeler should examine parameter estimation results for hydrogeological reasonableness.
- Too much time and effort are given to performing parameter estimation statistical analyses leaving little or no time for the primary modeling objectives of forecasting and related uncertainty analyses.
- SVD is not used on an ill-posed problem and the parameter estimation cannot find a best fit.
- SVD is used without some form of additional regularization (e.g., Tikhonov regularization). The process reports best fit calibrated parameters that are outside the range of reasonable values when a model with values within the range produces a fit that is only negligibly worse.

## 9.9 PROBLEMS

Chapter 9 problems are designed to provide experience in using trial-and-error and automated history matching to calibrate models. The best calibrated model from these problems will be used in the problems in Chapter 10 for forecasting and forecast uncertainty analysis.

**P9.1** Design a 2-D areal model of an unconfined sand and gravel aquifer; the dimensions of the problem domain are 1500 m by 1500 m (Fig. P9.1). Use a uniform nodal spacing of 100 m. The modeling objective is to forecast the effects on heads and river flows from proposed pumping of well M (Fig. P9.1). It is desirable to minimize the effects of pumping on river flows because farms downstream rely on river water for irrigation.

The north, east, and west boundaries of the problem domain are no flow boundaries representing impermeable bedrock. The south boundary is represented by a 100 m wide gravel-bottomed eastward sloping ditch that carries water out of the basin. The ditch leaks large quantities of water continuously. Leakage also enters the problem domain from many other such ditch systems south of the modeled area (see Fig. P9.1). The eastward flowing river just south of the northern boundary of the model is 100 m wide. The average stage (m above sea level) is given in Fig. P9.1 at the points indicated. The river has an average depth of 2 m and a bottom composed of 2 m of sand and fine gravel with a vertical hydraulic conductivity of 30 m/d. The river flows adjacent to an outcrop of impermeable bedrock in the area labeled “area not contributing groundwater” (Fig. P9.1). The entire area receives an average daily recharge of 0.0001 m/d.

The driller’s logs for wells shown in Fig. P9.1 generally listed river sand and gravel with isolated lenses of silt and clay from land surface to the aquifer base. The geologic logs for wells N and E (Fig. P9.1) show over 50% silt and clay, which are interpreted as overbank and oxbow sediments. Aquifer tests of wells finished in sand and gravel yielded hydraulic conductivities ranging from 30 to 120 m/d with an average of  $75 \text{ m/d} \pm 40\%$ . The steady-state groundwater discharge to the river was  $45,550 \text{ m}^3/\text{d} \pm 10\%$ . Inflow from the river to the aquifer was  $350 \text{ m}^3/\text{d} \pm 10\%$ . All head measurements (Table P9.1) used as calibration targets contain a measurement error of about  $\pm 0.002 \text{ m}$  and a survey error of  $\pm 0.02 \text{ m}$ .

- a. Use information in the geologic logs (described above) to delineate zones of hydraulic conductivity. Then calibrate a 2-D areal model to the steady-state heads in Table P9.1 and river fluxes given above using manual trial-and-error history matching. The number and assigned hydraulic conductivity values of the zones can be varied. Justify your values. Keep a simulation log (Section 3.7, Table 3.1) in which you record each trial calibration run and the effect

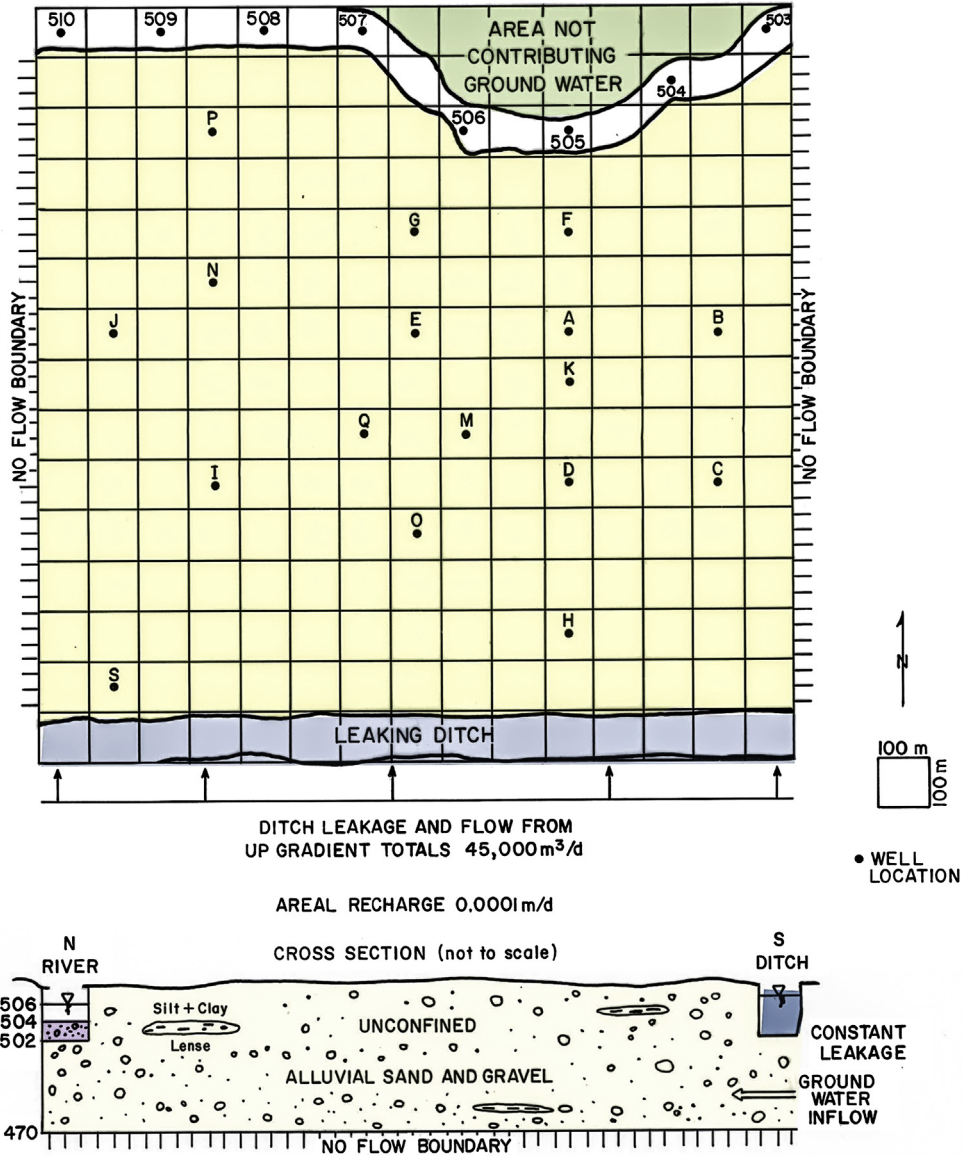


**Figure P9.1** Map view and cross section of an unconfined sand and gravel aquifer. The areal dimensions of the problem domain are 1500 m by 1500 m and the nodal spacing is uniformly 100 m. Impermeable bedrock along the northern boundary of the problem domain and north of the river does not contribute water to the river. Numbers refer to river stage in meters above sea level. Letters refer to pumping and observation wells (Table P9.1). The cross section is oriented N–S along column 9. Elevations are given in meters above sea level.

**Table P9.1** Head targets for the aquifer shown in Fig. P9.1

Well	Row	Column	Head (m) I <sup>a</sup>	Head (m) II <sup>b</sup>
P	3	4	509.12	509.11
G	5	8	508.19	507.99
F	5	11	508.17	507.79
N	6	4	512.83	512.83
J	7	2	515.71	515.71
E	7	8	513.17	513.04
A	7	11	512.22	508.8
B	7	14	511.95	511.29
K	8	11	513.88	512.21
Q	9	7	518.32	518.18
M	9	9	517.12	516.68
I	10	4	519.28	518.86
D	10	11	516.71	516.17
C	10	14	516.03	515.66
O	11	8	519.02	518.86
H	13	11	519.70	519.55
S	14	2	521.96	521.95

<sup>a</sup>I, Steady-state heads.

<sup>b</sup>II heads after 3 days of pumping well A; all heads are averages for a 100 m by 100 m area centered on the well.

of changing parameter values on the resulting history match. Calibration will mostly require adjusting values of hydraulic conductivity. Calculate summary statistics (Eqns (9.1)–(9.3)) to judge your calibration. Also show simulated and measured values on a scatter plot and residuals on a map. Use the heads from the best calibrated model to generate a water table contour map, showing both field and simulated equipotential lines. List the values of the parameters for the best calibrated model. Discuss the calibration results; are your parameter values hydrogeologically reasonable? Justify your selection of the best calibrated model.

- b.** Repeat the process using parameter estimation (i.e., automated trial and error) with the zone configuration from the manual trial-and-error calibration. Describe how you formulated the objective function and justify the weights used. Compare and contrast the RMSE of heads and the river discharge from manual trial-and-error calibration in part (a) with the results from parameter estimation. Also compare and contrast the final calibrated hydraulic conductivity values and comment on differences and similarities.

**P9.2** History matching sometimes includes calibration to transient conditions. Transient data form a second set of calibration data.

The specific yield of the sand and gravel aquifer was estimated to be about 0.10. Design a transient model to simulate results of a three-day aquifer test whereby well A (Fig. P9.1) is pumped continuously at a constant rate of 20,000 m<sup>3</sup>/d. The cumulative three-day groundwater discharge to the river during the test was about 125,700 m<sup>3</sup> ± 10% and cumulative river inflow to the aquifer was 1030 m<sup>3</sup> ± 10%.

- a. Use the parameter values and zones from the steady-state calibration of Problem P9.1(b) and final heads as initial conditions. Run the transient model and examine the heads and the cumulative flux to and from the river after 3 days of simulated pumping. Attempt to calibrate to the observations using only the specific yield and river fluxes. Do the simulated heads match the transient calibration head targets (Table P9.1) and the flows to and from the river measured during the aquifer test?
  - b. If your head and flux matches were unacceptable in part (a) recalibrate the steady-state model by altering the zonation as needed using automated trail-and-error methods. Then attempt transient calibration using zones and hydraulic conductivities from the new steady-state model and adjust values of specific yield. Justify your objective function design, and the final aquifer parameter values.
  - c. Comment on your methods and the calibration results. How confident are you that the model is calibrated so that it could appropriately forecast the response of the aquifer to pumping a new well at location M?
- P9.3** The previous calibration methods used zones of hydraulic conductivity. In this problem, we will use pilot points with parameter estimation. Use initial parameter values from your best calibrated steady-state model from Problem P9.2 (a) and (b).
- a. Remove all the zones and use a regular grid of pilot points; calibrate the steady-state model again. Derive initial hydraulic conductivities for the pilot points from your results (Problem P9.2(b)). Compare and contrast your results with those of Problems P9.1(a), P9.1(b)).
  - b. Use the calibrated parameter values from Problem P9.3(a) and the heads as the initial conditions and place a pumping well at A to simulate the three-day aquifer test. Calibrate the transient model to river fluxes using specific yield. Compare and contrast your results with results from Problem P9.2(b).
  - c. Pick a best model (base model) and support your selection. This model will be used in Chapter 10 for forecasting and uncertainty analysis.
- P9.4** Read the report by [Doherty and Hunt \(2010\)](#) (given in the reference list), which advocates highly parameterized models. Construct a flow chart of the process they advocate for parameter estimation.

## REFERENCES

- Alcolea, A., Carrera, J., Medina, A., 2006. Pilot points method incorporating prior information for solving the groundwater flow inverse problem. *Advances in Water Resources* 29 (11), 1678–1689. <http://dx.doi.org/10.1016/j.advwatres.2005.12.009>.
- Anderson, M.G., Bates, P.D. (Eds.), 2001. *Model Validation: Perspectives in Hydrological Science*. John Wiley & Sons Ltd., London, UK, 512 pp.
- Aster, R.C., Borchers, B., Thurber, C.H., 2013. *Parameter Estimation and Inverse Problems*, second ed. Elsevier Academic Press. 301 p.
- ASTM (International), 2008. Standard guide for calibrating a groundwater flow model application D5981 – 96(2008). American Society of Testing and Materials, ASTM International, 6 p.
- Bair, E.S., 2001. Models in the courtroom. In: Anderson, M.G., Bates, P.D. (Eds.), *Model Validation: Perspectives in Hydrological Science*. John Wiley & Sons Ltd., London, pp. 55–77.
- Bair, E.S., Metheny, M.A., 2011. Lessons learned from the landmark “A Civil Action” trial. *Groundwater* 49 (5), 764–769. <http://dx.doi.org/10.1111/j.1745-6584.2008.00506.x>.
- Belsley, D.A., Kuh, E., Welsch, R.E., 1980. *Regression Diagnostics: Identifying Influential Data and Source of Collinearity*. John Wiley, New York, 292 p.
- Beven, K.J., 2005. On the concept of model structural error. *Water Science & Technology* 52 (6), 167–175. <http://www.iwaponline.com/wst/05206/wst052060167.htm>.
- Beven, K.J., 2009. *Environmental Modelling: An Uncertain Future? An Introduction to Techniques for Uncertainty Estimation in Environmental Prediction*. Routledge, 310 p.
- Beven, K., Young, P., 2013. A guide to good practice in modeling semantics for authors and referees. *Water Resources Research* 49 (8), 5092–5098. <http://dx.doi.org/10.1002/wrcr.20393>.
- Bourgault, G., 1997. Spatial declustering weights. *Mathematical Geology* 29 (2), 277–290. <http://dx.doi.org/10.1007/BF02769633>.
- Bravo, H.R., Jiang, F., Hunt, R.J., 2002. Using groundwater temperature data to constrain parameter estimation in a groundwater flow model of a wetland system. *Water Resources Research* 38 (8), 28–1–28–14. <http://dx.doi.org/10.1029/2000WR000172>.
- Carrera, J., 1988. State of the art of the inverse problem applied to flow and solute transport equations. In: Custodio, E., et al. (Eds.), *Groundwater Flow and Quality Modelling*. D. Reidel Publication Company, pp. 549–583.
- Carrera, J., Neuman, S.P., 1986. Estimation of aquifer parameters under transient and steady state conditions: 1. Maximum likelihood method incorporating prior information. *Water Resources Research* 22 (2), 199–210. <http://dx.doi.org/10.1029/WR022i002p00199>.
- Certes, C., Marsily, G. de, 1991. Application of the pilot points method to the identification of aquifer transmissivities. *Advances in Water Resources* 14 (5), 284–300. [http://dx.doi.org/10.1016/0309-1708\(91\)90040-U](http://dx.doi.org/10.1016/0309-1708(91)90040-U).
- Cook, P.G., Wood, C., White, T., Simmons, C.T., Fass, T., Brunner, P.A., 2008. Groundwater inflow to a shallow, poorly-mixed wetland estimated from a mass balance of radon. *Journal of Hydrology* 354 (1–4), 213–226. <http://dx.doi.org/10.1016/j.jhydrol.2008.03.016>.
- Cooley, R.L., 1977. A method of estimating parameters and assessing reliability for models of steady state groundwater flow, 1. Theory and numerical properties. *Water Resources Research* 13 (2), 318–324. <http://dx.doi.org/10.1029/WR013i002p00318>.
- Cooley, R.L., 1979. A method of estimating parameters and assessing reliability for models of steady state groundwater flow, 2. Application of statistical analysis. *Water Resources Research* 15 (3), 603–617. <http://dx.doi.org/10.1029/WR015i003p00603>.
- Cooley, R.L., Sinclair, P.J., 1976. Uniqueness of a model of steady-state groundwater flow. *Journal of Hydrology* 31 (3–4), 245–269. [http://dx.doi.org/10.1016/0022-1694\(76\)90127-X](http://dx.doi.org/10.1016/0022-1694(76)90127-X).
- Cooley, R.L., Naff, R.L., 1990. *Regression Modeling of Ground-water Flow*. U.S. Geological Survey Techniques of Water-Resources Investigations, 03–B4, 232 p. <http://pubs.usgs.gov/twri/twri3-b4/>.
- D’Agnes, F.A., O’Brien, G.M., Faunt, C.C., Belcher, W.R., San Juan, C., 2002. A Three-dimensional Numerical Model of Predevelopment Conditions in the Death Valley Regional Ground-water Flow

- System, Nevada and California. U.S. Geological Survey Water-Resources Investigations Report, 02-4102, 114 p. <http://pubs.usgs.gov/wri/wri024102/>.
- Davis, K.W., Putnam, L.D., 2013. Conceptual and Numerical Models of Groundwater Flow in the Ogallala Aquifer in Gregory and Tripp Counties, South Dakota, Water Years 1985–2009. U.S. Geological Survey Scientific Investigations Report 2013-5069, 82 p. <http://pubs.usgs.gov/sir/2013/5069/>.
- De Groot-Hedlin, C., Constable, S., 1990. Occam's inversion to generate smooth, two-dimensional models from magnetotelluric data. *Geophysics* 55 (12), 1613–1624. <http://dx.doi.org/10.1190/1.1442813>.
- Doherty, J., 1990. MODINV – Suite of Software for MODFLOW Preprocessing, Postprocessing, and Parameter Optimization. User's Manual: Australian Centre for Tropical Freshwater Research (various pagings).
- Doherty, J., 2003. Ground water model calibration using pilot points and regularization. *Groundwater* 41 (2), 170–177. <http://dx.doi.org/10.1111/j.1745-6584.2003.tb02580.x>.
- Doherty, J., 2011. Modeling: Picture perfect or abstract art? *Groundwater* 49 (4), 455. <http://dx.doi.org/10.1111/j.1745-6584.2011.00812.x>.
- Doherty, J., 2014a. PEST, Model-independent Parameter Estimation—User Manual (fifth ed., with slight additions). Watermark Numerical Computing, Brisbane, Australia.
- Doherty, J., 2014b. Addendum to the PEST Manual. Watermark Numerical Computing, Brisbane, Australia.
- Doherty, J., Christensen, S., 2011. Use of paired simple and complex models to reduce predictive bias and quantify uncertainty. *Water Resources Research* 47 (12), W12534(21). <http://dx.doi.org/10.1029/2011WR010763>.
- Doherty, J., Hunt, R.J., 2009a. Two statistics for evaluating parameter identifiability and error reduction. *Journal of Hydrology* 366 (1–4), 119–127. <http://dx.doi.org/10.1016/j.jhydrol.2008.12.018>.
- Doherty, J., Hunt, R.J., 2009b. Response to comment on: Two statistics for evaluating parameter identifiability and error reduction. *Journal of Hydrology* 380 (3–4), 489–496. <http://dx.doi.org/10.1016/j.jhydrol.2009.10.012>.
- Doherty, J., Hunt, R.J., 2010. Approaches to Highly Parameterized Inversion: A Guide to Using PEST for Groundwater-model Calibration. U.S. Geological Survey Scientific Investigations Report 2010-5169, 60 p. <http://pubs.usgs.gov/sir/2010/5169/>.
- Doherty, J., Simmons, C.T., 2013. Groundwater modeling in decision support: Reflections on a unified conceptual framework. *Hydrogeology Journal* 21 (7), 1531–1537. <http://dx.doi.org/10.1007/s10040-013-1027-7>.
- Doherty, J., Welter, D.E., 2010. A short exploration of structural noise. *Water Resources Research* 46 (5), W05525. <http://dx.doi.org/10.1029/2009WR008377>.
- Doherty, J.E., Fienen, M.N., Hunt, R.J., 2010a. Approaches to Highly Parameterized Inversion: Pilot-point Theory, Guidelines, and Research Directions. U.S. Geological Survey Scientific Investigations Report 2010-5168, 36 p. <http://pubs.usgs.gov/sir/2010/5168/>.
- Doherty, J.E., Hunt, R.J., Tonkin, M.J., 2010b. Approaches to Highly Parameterized Inversion: A Guide to Using PEST for Model-parameter and Predictive-uncertainty Analysis. U.S. Geological Survey Scientific Investigations Report 2010–5211, 71 p. <http://pubs.usgs.gov/sir/2010/5211/>.
- Emsellem, Y., Marsily, G. de, 1971. An automatic solution for the inverse problem. *Water Resources Research* 7 (5), 1264–1283. <http://dx.doi.org/10.1029/WR007i005p01264>.
- Engl, H.W., Hanke, M., Neubauer, A., 1996. *Regularization of Inverse Problems*. Kluwer Academic, Dordrecht, The Netherlands, 321 p. ISBN 978-0-7923-4157-4.
- Feinstein, D.T., Hunt, R.J., Reeves, H.W., 2008. Calibrating a big model: Strategies and limitations. In: *MODFLOW and More 2008: Ground Water and Public Policy*, Proceedings of the 9th International Conference of the International Ground Water Modeling Center. Colorado School of Mines, Golden, CO, pp. 430–434.
- Fienen, M.N., 2013. We speak for the data. *Groundwater* 51 (2), 157. <http://dx.doi.org/10.1111/gwat.12018>.
- Fienen, M., Hunt, R., Krabbenhoft, D., Clemo, T., 2009a. Obtaining parsimonious hydraulic conductivity fields using head and transport observations—A Bayesian geostatistical parameter estimation approach. *Water Resources Research* 45 (8), W08405(23). <http://dx.doi.org/10.1029/2008WR007431>.

- Fienen, M.N., Muffels, C.T., Hunt, R.J., 2009b. On constraining pilot point calibration with regularization in PEST. *Groundwater* 47 (6), 835–844. <http://dx.doi.org/10.1111/j.1745-6584.2009.00579.x>.
- Fienen, M.N., D’Oria, M., Doherty, J.E., Hunt, R.J., 2013. Approaches in Highly Parameterized Inversion: bgaPEST, A Bayesian Geostatistical Approach Implementation with PEST. U.S. Geological Survey Techniques and Methods. Book 7, Section C, (Chapter 9), 86 p. <http://pubs.usgs.gov/tm/07/c09/>.
- Foster, I., 1995. *Designing and Building Parallel Programs*. Addison-Wesley Pearson Education, Upper Saddle River, New Jersey, 430 p. ISBN 9780201575941.
- Freeze, R.A., Cherry, J.A., 1979. *Groundwater*. Prentice-Hall, 604 p.
- Freeze, R.A., Witherspoon, P.A., 1966. Theoretical analysis of regional groundwater flow, 1. Analytical and numerical solutions to the mathematical model. *Water Resources Research* 2 (4), 641–656. <http://dx.doi.org/10.1029/WR002i004p00641>.
- Freeze, R.A., Massmann, J., Smith, L., Sperling, T., James, B., 1990. Hydrogeological decision analysis: 1. A framework. *Groundwater* 28 (5), 738–766. <http://dx.doi.org/10.1111/j.1745-6584.1990.tb01989.x>.
- Gaganis, P., Smith, L., 2001. A Bayesian approach to the quantification of the effect of model error on the predictions of groundwater models. *Water Resources Research* 37 (9), 2309–2322. <http://dx.doi.org/10.1029/2000WR000001>.
- Gardner, W.P., Harrington, G., Solomon, D.K., Cook, P., 2011. Using terrigenic  $^4\text{He}$  to identify and quantify regional groundwater discharge to streams. *Water Resources Research* 47 (6), W06523(13). <http://dx.doi.org/10.1029/2010WR010276>.
- Gómez-Hernández, J.J., 2006. Complexity. *Groundwater* 44 (6), 782–785. <http://dx.doi.org/10.1111/j.1745-6584.2006.00222.x>.
- Hadamard, J., 1902. Sur les problèmes aux dérivées partielles et leur signification physique. *Princeton University Bulletin*, 49–52.
- Haitjema, H., 2006. The role of hand calculations in ground water flow modeling. *Groundwater* 44 (6), 786–791. <http://dx.doi.org/10.1111/j.1745-6584.2006.00189.x>.
- Haitjema, H.M., 2015. The cost of modeling. *Groundwater* 53 (2), 179. <http://dx.doi.org/10.1111/gwat.12321>.
- Hill, M.C., 1992. A Computer Program (MODFLOWP) for Estimating Parameters of a Transient, Three-dimensional, Ground-water Flow Model Using Nonlinear Regression. U.S. Geological Survey Open-File Report 91-484, 358 p. <http://pubs.er.usgs.gov/publication/ofr91484>.
- Hill, M.C., 2006. The practical use of simplicity in developing ground water models. *Groundwater* 44 (6), 775–781. <http://dx.doi.org/10.1111/j.1745-6584.2006.00227.x>.
- Hill, M.C., Tiedeman, C.R., 2007. *Effective Groundwater Model Calibration—with Analysis of Data, Sensitivities, Predictions, and Uncertainty*. Wiley-Interscience, Hoboken, NJ, 455 p.
- Himmelblau, D.M., 1972. *Applied Nonlinear Programming*. McGraw-Hill, New York, 477 p.
- Hunt, R.J., Anderson, M.P., Kelson, V.A., 1998. Improving a complex finite difference ground water flow model through the use of an analytic element screening model. *Groundwater* 36 (6), 1011–1017. <http://dx.doi.org/10.1111/j.1745-6584.1998.tb02108.x>.
- Hunt, R.J., Zheng, C., 1999. Debating complexity in modeling. *Eos (Transactions, American Geophysical Union)* 80 (3), 29. <http://dx.doi.org/10.1029/99EO00025>.
- Hunt, R.J., Krabbenhoft, D.P., Anderson, M.P., 1996. Groundwater inflow measurements in wetland systems. *Water Resources Research* 32 (3), 495–507. <http://dx.doi.org/10.1029/95WR03724>.
- Hunt, R.J., Feinstein, D.T., Pint, C.D., Anderson, M.P., 2006. The importance of diverse data types to calibrate a watershed model of the Trout Lake Basin, northern Wisconsin, USA. *Journal of Hydrology* 321 (1–4), 286–296. <http://dx.doi.org/10.1016/j.jhydrol.2005.08.005>.
- Hunt, R.J., Doherty, J., Tonkin, M.J., 2007. Are models too simple? Arguments for increased parameterization. *Groundwater* 45 (3), 254–261. <http://dx.doi.org/10.1111/j.1745-6584.2007.00316.x>.
- Hunt, R.J., Luchette, J., Schreüder, W.A., Rumbaugh, J.O., Doherty, J., Tonkin, M.J., Rumbaugh, D.B., 2010. Using a cloud to replenish parched groundwater modeling efforts. *Rapid Communication for Groundwater* 48 (3), 360–365. <http://dx.doi.org/10.1111/j.1745-6584.2010.00699.x>.
- Hunt, R.J., Zheng, C., 2012. The current state of modeling. *Groundwater* 50 (3), 329–333. <http://dx.doi.org/10.1111/j.1745-6584.2012.00936.x>.



- Hunt, R.J., Walker, J.F., Selbig, W.R., Westenbroek, S.M., Regan, R.S., 2013. Simulation of Climate-change Effects on Streamflow, Lake Water Budgets, and Stream Temperature Using GSFLOW and SNTMP, Trout Lake Watershed, Wisconsin. U.S. Geological Survey Scientific Investigations Report 2013-5159, 118 p. <http://pubs.usgs.gov/sir/2013/5159/>.
- Juckem, P.F., 2009. Simulation of the Groundwater-flow System in Pierce, Polk, and St. Croix Counties, Wisconsin. U.S. Geological Survey Scientific Investigations Report 2009-5056, 53 p. <http://pubs.usgs.gov/sir/2009/5056/>.
- Juckem, P.F., Fienen, M.N., Hunt, R.J., 2014. Simulation of Groundwater Flow and Interaction of Groundwater and Surface Water on the Lac du Flambeau Reservation, Wisconsin. U.S. Geological Survey Scientific Investigations Report 2014-5020, 34 p. <http://dx.doi.org/10.3133/sir20145020>.
- Kalman, D., 1996. A singularly valuable decomposition: The SVD of a matrix. *College Mathematics Journal* 27 (1), 2–23. <http://dx.doi.org/10.2307/2687269>.
- Konikow, L.F., Bredehoeft, J.D., 1992. Ground-water models cannot be validated. *Advances in Water Resources* 15 (1), 75–83. [http://dx.doi.org/10.1016/0309-1708\(92\)90033-X](http://dx.doi.org/10.1016/0309-1708(92)90033-X).
- Krabbenhoft, D.P., Bowser, C.J., Kendall, C., Gat, J.R., 1994. Use of oxygen-18 to assess the hydrology of groundwater-lake systems. In: Baker, L.A. (Ed.), *Environmental Chemistry of Lakes and Reservoirs*, American Chemical Society Advances in Chemistry Series, vol. 237, pp. 67–90.
- Levenberg, K., 1944. A method for the solution of certain non-linear problems in least squares. *Quarterly of Applied Mathematics* 2, 164–168.
- Marquardt, D., 1963. An algorithm for least-squares estimation of nonlinear parameters, *SIAM. Journal on Applied Mathematics* 11 (2), 431–441. <http://dx.doi.org/10.1137/0111030>.
- Marsily, G. de, Lavendan, C., Boucher, M., Fasanino, G., 1984. Interpretation of interference tests in a well field using geostatistical techniques to fit the permeability distribution in a reservoir model. In: Verly, G., David, M., Journel, A.G., Marechal, A. (Eds.), *Geostatistics for Natural Resources Characterization*. NATO, C 182, Boston, Massachusetts, pp. 831–849.
- McCallum, J., Cook, P., Berhane, D., Rumpf, C., McMahon, G., 2012. Quantifying groundwater flows to streams using differential flow gaugings and water chemistry. *Journal of Hydrology* 416–417, 118–132. <http://dx.doi.org/10.1016/j.jhydrol.2011.11.040>.
- McLaughlin, D., Townley, L.R., 1996. A reassessment of the groundwater inverse problem. *Water Resources Research* 32 (5), 1131–1161. <http://dx.doi.org/10.1029/96WR00160>.
- Meyer, J.R., Parker, B.L., Cherry, J.A., 2014. Characteristics of high resolution hydraulic head profiles and vertical gradients in fractured sedimentary rocks. *Journal of Hydrology* 517, 493–507. <http://dx.doi.org/10.1016/j.jhydrol.2014.05.050>.
- Mishra, S., Deeds, N., Ruskauuff, G., 2009. Global sensitivity analysis techniques for probabilistic ground water modeling. *Groundwater* 47 (5), 727–744. <http://dx.doi.org/10.1111/j.1745-6584.2009.00604.x>.
- Moore, C., Doherty, J., 2005. Role of the calibration process in reducing model predictive error. *Water Resources Research* 41 (5), 1–14. <http://dx.doi.org/10.1029/2004WR003501>.
- Moore, C., Wöhling, T., Doherty, J., 2010. Efficient regularization and uncertainty analysis using a global optimization methodology. *Water Resources Research* 46 (8), W08527. <http://dx.doi.org/10.1029/2009WR008627>.
- Moriassi, D.N., Wilson, B.N., Douglas-Mankin, K.R., Arnold, J.G., Gowda, P.H., 2012. Hydrologic and water quality models: Use, calibration and validation. *Transactions American Society of Agricultural and Biological Engineers* 55 (4), 1241–1247. <http://dx.doi.org/10.13031/2013.42265>.
- Morris, M.D., 1991. Factorial sampling plans for preliminary computational experiments. *Technometrics* 33 (2), 161–174. <http://www.jstor.org/stable/1269043>.
- Muffels, C.T., 2008. Application of the LSQR Algorithm to the Calibration of a Regional Groundwater Flow Model—Trout Lake Basin, Vilas County, Wisconsin (M.S. thesis). University of Wisconsin-Madison, 106 p.
- Muffels, C.T., Schreüder, W.A., Doherty, J.E., Karanovic, M., Tonkin, M.J., Hunt, R.J., Welter, D.E., 2012. Approaches in Highly Parameterized Inversion—GENIE, A General Model-independent TCP/IP Run Manager. U.S. Geological Survey Techniques and Methods. Book 7, Chapter C6, 26 p. <http://pubs.usgs.gov/tm/tm7c6/>.

- Murray–Darling Basin Commission (MDBC), January 2001. Groundwater Flow Modelling Guideline. Report prepared by Aquaterra.
- Nelson, R.W., 1960. In place measurement of permeability in heterogeneous media, 1. Theory of a proposed method. *Journal of Geophysical Research* 65 (6), 1753–1760. <http://dx.doi.org/10.1029/JZ065i006p01753>.
- Nelson, R.W., 1961. In place measurement of permeability in heterogeneous media, 2. Experimental and computational considerations. *Journal of Geophysical Research* 66 (6), 2469–2478. <http://dx.doi.org/10.1029/JZ066i008p02469>.
- Nelson, R.W., 1962. Conditions for determining areal permeability distributions by calculation. *Society of Petroleum Engineers Journal* 2 (3), 223–224. <http://dx.doi.org/10.2118/371-PA>.
- Neuman, S.P., 1973. Calibration of distributed parameter groundwater flow models viewed as a multiple-objective decision process under uncertainty. *Water Resources Research* 9 (4), 1006–1021. <http://dx.doi.org/10.1029/WR009i004p01006>.
- Nielson, D.M., 1991. *Practical Handbook of Ground-Water Monitoring*. Lewis, Chelsea, MI, 717 p.
- Oreskes, N., Belitz, K., 2001. Philosophical issues in model assessment. In: Anderson, M.G., Bates, P.D. (Eds.), *Model Validation: Perspectives in Hydrological Science*. John Wiley & Sons Ltd., London, UK, pp. 24–41.
- Oreskes, N., Shrader-Frechette, K., Belitz, K., 1994. Verification, validation, and confirmation of numerical models in the earth sciences. *Science* 263 (5147), 641–646. <http://dx.doi.org/10.1126/science.263.5147.641>.
- Poeter, E.P., Hill, M.C., 1997. Inverse models—a necessary next step in ground-water modeling. *Groundwater* 35 (2), 250–260. <http://dx.doi.org/10.1111/j.1745-6584.1997.tb00082.x>.
- Poeter, E.P., Hill, M.C., Banta, E.R., Mehl, S., Christensen, S., 2005. UCODE\_2005 and Six Other Computer Codes for Universal Sensitivity Analysis, Calibration, and Uncertainty Evaluation. *U.S. Geological Survey Techniques and Methods*, 6 A11, 47 p. 283 p. <http://pubs.usgs.gov/tm/2006/tm6a11/>.
- Rakovec, O., Hill, M.C., Clark, M.P., Weerts, A.H., Teuling, A.J., Uijlehoet, R., 2014. Distributed Evaluation of Local Sensitivity Analysis (DELSA), with application to hydrologic models. *Water Resources Research* 50 (1), 409–426. <http://dx.doi.org/10.1002/2013WR014063>.
- Ramarao, B.S., Lavenue, A.M., Marsily, G. de, Marietta, M.G., 1995. Pilot point methodology for automated calibration of an ensemble of conditionally simulated transmissivity fields, 1. Theory and computational experiments. *Water Resources Research* 31 (3), 475–493. <http://dx.doi.org/10.1029/94WR02258>.
- Saltelli, A., Ratto, M., Andres, T., Campolongo, F., Cariboin, J., Gatelli, D., Saisana, M., Tarantola, S., 2008. *Global Sensitivity Analysis: The Primer*. Wiley-Interscience, Hoboken NJ, 302 p.
- Saltelli, A., Funtowicz, S., 2014. When all models are wrong. *Issues in Science and Technology* 79–85. Winter 30. <http://www.issues.org/30.2/>.
- Schreüder, W.A., 2009. Running BeoPEST. In: *Conference Proceedings from the 1st PEST Conference*, November 1–3, 2009, Potomac, MD. Lulu Press, Inc., Raleigh, NC, USA, 7 p.
- Silver, N., 2012. *The Signal and the Noise: Why Most Predictions Fail but Some Don't*. Penguin Press, New York, NY, 534 p.
- Simmons, C.T., Hunt, R.J., 2012. Updating the debate on model complexity. *GSA Today* 22 (8), 28–29. <http://dx.doi.org/10.1130/GSATG150GW.1>.
- Stallman, R.W., 1956a. Numerical analysis of regional water levels to define aquifer hydrology. *Eos, Transactions American Geophysical Union* 37 (4), 451–460. <http://dx.doi.org/10.1029/TR037i004p00451>.
- Stallman, R.W., 1956b. Use of Numerical Methods for Analyzing Data on Ground-water Levels. *International Association of Scientific Hydrology Pub.* 41, Tome II, pp. 227–331. (Reproduced in Freeze, R. A. and Back, W., editors, 1983: *Physical Hydrogeology, Benchmark Papers in Geology*, v. 72, Hutchinson Ross Publishing Company, Stroudsburg, Pennsylvania, pp. 193–197).
- Sun, N.Z., Yang, S.L., Yeh, W.W-G., 1998. A proposed stepwise regression method for model structure identification. *Water Resources Research* 34 (10), 2561–2572. <http://dx.doi.org/10.1029/98WR01860>.
- Tikhonov, A.N., 1963a. Solution of incorrectly formulated problems and the regularization method. *Soviet Mathematics Doklady* 4, 1035–1038.

- Tikhonov, A.N., 1963b. Regularization of incorrectly posed problems. *Soviet Mathematics Doklady* 4, 1624–1637.
- Tikhonov, A.N., Arsenin, V.Y., 1977. *Solutions of Ill-Posed Problems*. Halstead Press–Wiley, New York, 258 p.
- Tonkin, M.J., Doherty, J., 2005. A hybrid regularized inversion methodology for highly parameterized models. *Water Resources Research* 41 (10), W10412. <http://dx.doi.org/10.1029/2005WR003995>.
- Tonkin, M.J., Doherty, J., 2009. Calibration-constrained Monte-Carlo analysis of highly parameterised models using subspace techniques. *Water Resources Research* 45 (12), W00B10. <http://dx.doi.org/10.1029/2007WR006678>.
- Townley, L.R., 2012. Calibration and sensitivity analysis. In: Barnett, B., Townley, L.R., Post, V., Evans, R.E., Hunt, R.J., Peeters, L., Richardson, S., Werner, A.D., Knapton, A., Boronkay, A. (Eds.), *Australian Groundwater Modelling Guidelines*, Waterlines Report 82. National Water Commission, Canberra, pp. 57–78, 191 p. ISBN 978-1-921853-91-3.
- Voss, C.I., 2011. Editor's message: Groundwater modeling fantasies—Part 1, adrift in the details. *Hydrogeology Journal* 19 (7), 1281–1284. <http://dx.doi.org/10.1007/s10040-011-0789-z>.
- Welter, D.E., Doherty, J.E., Hunt, R.J., Muffels, C.T., Tonkin, M.J., Schreüder, W.A., 2012. Approaches in Highly Parameterized Inversion: PEST++, A Parameter ESTimation Code Optimized for Large Environmental Models. *U.S. Geological Survey Techniques and Methods*, 7(C5), 47 p. <http://pubs.usgs.gov/tm/tm7c5/>.
- Yager, R.M., 1998. Detecting influential observations in nonlinear regression modeling of groundwater flow. *Water Resources Research* 34 (7), 1623–1633. <http://dx.doi.org/10.1029/98WR01010>.
- Yager, R.M., 2004. Effects of model sensitivity and nonlinearity on nonlinear regression of ground water flow. *Groundwater* 42 (2), 390–400. <http://dx.doi.org/10.1111/j.1745-6584.2004.tb02687.x>.
- Yeh, W., 1986. Review of parameter identification procedures in groundwater hydrology: The inverse problem. *Water Resources Research* 22 (2), 95–108. <http://dx.doi.org/10.1029/WR022i002p00095>.
- Yeh, W.W-G., Tauxe, G.W., 1971. Optimal identification of aquifer diffusivity using quasilinearization. *Water Resources Research* 7 (4), 955–962. <http://dx.doi.org/10.1029/WR007i004p00955>.
- Yao, Y., Zheng, C., Liu, J., Cao, G., Xiao, H., Li, H., Li, W., 2014. Conceptual and numerical models for groundwater flow in an arid inland river basin. *Hydrological Processes* 29 (6), 1480–1492. <http://dx.doi.org/10.1002/hyp.10276>.
- Zheng, C., Bennett, G.D., 2002. *Applied Contaminant Transport Modeling*, second ed. John Wiley & Sons, New York, 621 p.
- Zhou, H., Gómez-Hernández, J.J., Liangping, L., 2014. Inverse methods in hydrogeology: Evolution and recent trends. *Advances in Water Resources* 63, 22–37. <http://dx.doi.org/10.1016/j.advwatres.2013.10.014>.

## CHAPTER 10

# Forecasting and Uncertainty Analysis

*A good forecaster is not smarter than everyone else, he merely has his ignorance better organized.*

—Anonymous

*There are known knowns. These are things we know that we know. There are known unknowns. That is to say, there are things that we now know we don't know. But there are also unknown unknowns. These are things we do not know we don't know.*

—Donald Rumsfeld

### Contents

10.1 Introduction	443
10.2 Characterizing Uncertainty	447
10.3 Addressing Uncertainty	453
10.4 Basic Uncertainty Analysis	458
10.4.1 Scenario Modeling	458
10.4.2 Linear Uncertainty Analysis	460
10.4.2.1 Examples of Linear Uncertainty Analysis	465
10.5 Advanced Uncertainty Analysis	469
10.5.1 Analysis Using One Conceptualization	469
10.5.2 Analysis Using Multiple Conceptualizations	477
10.6 Reporting Forecast Uncertainty	480
10.7 Evaluating Forecasts: Postaudits	481
10.8 Common Modeling Errors	483
10.9 Problems	483
References	485

### Boxes

Box 10.1 Historical Overview of Uncertainty Analysis in Groundwater Modeling	446
Box 10.2 Travel Time in Heterogeneous Aquifers: Impossible to Forecast Accurately?	455
Box 10.3 Cost-Benefit Analyses of Future Data Collection	468
Box 10.4 Using Monte Carlo Methods to Represent Forecast Uncertainty	472

## 10.1 INTRODUCTION

For most applied groundwater modeling problems, the model's purpose is addressed by making a *forecast* of the response of the system to future conditions, or (less frequently) a *backcast* or *hindcast* to past conditions (Fig. 10.1). We use the term forecast over *prediction*

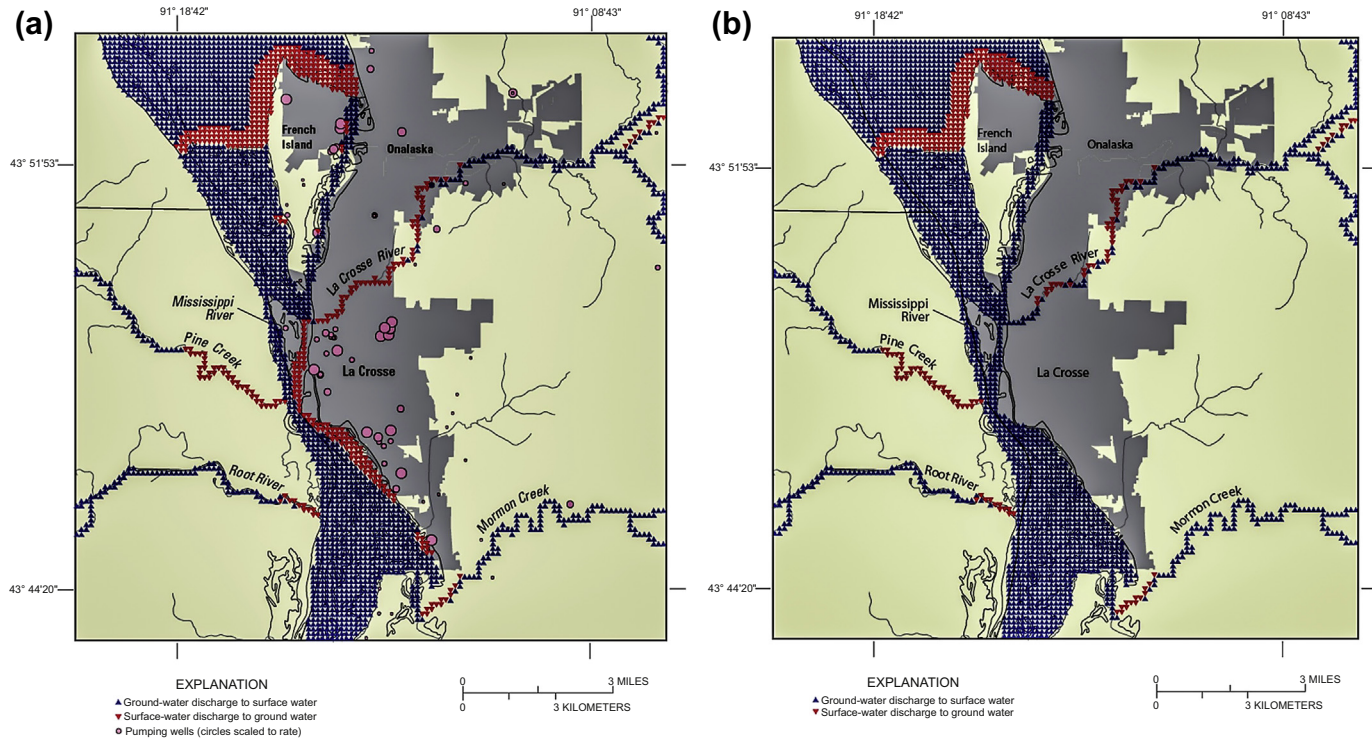


**Figure 10.1** A simple example of hindcasting groundwater–surface water interaction in a humid temperate climate (Wisconsin, USA). A model calibrated to current pumping conditions (a) is re-run to simulate groundwater–surface water interaction before pumping (b). Red symbols identify areas of induced flow from surface water in response to pumping, a dam, and high hydraulic conductivity fluvial sediments in the river valleys. Blue symbols represent areas of groundwater discharge to surface water. Comparison of (a) and (b) shows the expansion of losing stream conditions caused by pumping. The effect of the dam is evident during both time periods (horizontal red band near top of figures) (modified from [Hunt et al., 2003](#)).

to reflect the fact that all estimates of future conditions have uncertainty; the term forecast more accurately represents that inherent uncertainty. There is also widespread understanding of forecast probability (e.g., “70% chance of rain”) among scientists and the general public, whereas “prediction” connotes more certainty. A forecast is considered acceptable when it adequately represents all that is known at the time of the forecast, even though what was forecast may not come to pass owing to factors unknown when the forecast was made.

In a forecasting simulation, future changes in the groundwater system are typically simulated using a calibrated model, which is called the *base model*. The base model is founded on a conceptual model supported by field data, and is calibrated by history matching to provide the subjective (weighted) best fit to calibration targets and soft knowledge. It is not considered a true or complete representation of actual groundwater conditions. Instead, it is recognized to contain parameter error from both observation measurement error and parameter simplification errors such that the model is unable to capture all system detail (Chapter 9). Not all forecasts require calibrated models, however. Uncalibrated interpretive models (Section 1.3) can also be used to explore how changes in properties or assumptions influence outcomes of interest, or used to explore best- or worst-case scenarios (e.g., [Doherty and Simmons, 2013](#)). However, in this chapter, we focus on forecasting using a base model.

Groundwater modeling forecasts are often used to plan future actions because they help characterize the likelihood that something “bad” might happen ([Freeze et al., 1990](#); [Tartakovsky, 2013](#)), such as an ecologically sensitive stream going dry or a water withdrawal exceeding what is sustainable. The role of forecasting in this context is to assess likelihood of an event, which is a concept very different from predicting what will happen in the future ([Doherty, 2011](#)). Modeling expresses our lack of knowledge because even a perfectly calibrated model cannot guarantee that a forecast is accurate. Yet with a reasonable model, formal cost-benefit or risk-assessment analyses can be performed by including a quantification of uncertainty (e.g., [Tartakovsky, 2013](#)). It is critical that the model be reasonable. As noted by [Silver \(2012\)](#):

*It is forecasting's original sin to put politics, personal glory, or economic benefit before the truth of the forecast. Sometimes it is done with good intentions, but it always makes the forecast worse.*

Here, truth means that the forecast is an unbiased and fair depiction of what is expected to occur. It is the obligation of the modeler to provide the best forecast possible, report uncertainty bounds around the forecast, and communicate those limits in an understandable way to other modelers, clients, managers, and regulators. Indeed, it has been argued that model forecasts submitted without uncertainty estimates should be rejected out of hand ([Beven and Young, 2013](#)).

Although the importance of characterizing uncertainty has been recognized for a long time (e.g., [Knight, 1921](#)), there is still “uncertainty about uncertainty estimation in environmental modeling” ([Beven, 2005](#)). Many of the tools used to quantify uncertainty in groundwater modeling were developed in other branches of science. For example,

### Box 10.1 Historical Overview of Uncertainty Analysis in Groundwater Modeling

Uncertainty has long been recognized to limit the applicability of groundwater modeling results. For example, early applications of analytical solutions to groundwater problems were recognized as being primarily useful constructs for answering a specific engineering question rather than providing realistic representations of a complex natural world. Freeze (1975) brought awareness of uncertainty in groundwater models to a new level by demonstrating that uncertainty in subsurface properties could be quantified in a rigorous, formal way. His work helped launch a new subdiscipline in groundwater hydrology: “stochastic analysis” (e.g., see Fig. 3 in Dagan, 1986). A model is *stochastic* if any of its parameters have a probabilistic distribution; otherwise, the model is *deterministic*. For example, a stochastic model might use a formal stochastic formulation of the partial differential equation for groundwater flow (Section 12.5). The straightforward Monte Carlo method (Sections 10.5, 12.5), however, is a more widely used way to solve a groundwater problem stochastically. The theory and application of geostatistics and probabilistic concepts to assess uncertainty in groundwater systems has been developed by many researchers (e.g., see books by Dagan, 1989; Gelhar, 1993; Kitanidis, 1997; Zhang, 2002; Rubin, 2003).

Concurrent with the exploration of stochastic models, other approaches to describe uncertainty were being developed for groundwater systems, leveraging the quantitative statistical framework provided by the indirect inverse solution (or “parameter estimation”—Box 9.1) approach advocated by Cooley (1977, 1979). Early efforts focused on the overdetermined inverse problem (e.g., a modeling problem where there are fewer calibration parameters than calibration targets). The overdetermined problem was extensively researched, including nonlinear confidence intervals and Monte Carlo methods (e.g., Vecchia and Cooley, 1987), and assessing data importance for forecasts using linear methods (e.g., Tonkin et al., 2007a). A detailed exploration of overdetermined approaches to model uncertainty is given in Hill and Tiedeman (2007). Uncertainty analysis was also addressed using probabilistic formulations such as Bayes’ theorem (Section 10.2) (e.g., Carrera and Neuman, 1986a,b,c; Kitanidis, 1986, 1995; Woodbury and Ulrych, 1993, 2000; Yeh and Liu, 2000; Gaganis and Smith, 2001; Fioren et al., 2010 Appendix 1, and many others).

It became apparent, however, that many societal decisions needed more tools for quantifying uncertainty. In addition to characterizing uncertainty resulting from model error, more general uncertainty concepts that included consideration of structural error resulting from model simplification (Cooley, 2004; Moore and Doherty, 2005) and risk assessment (Freeze et al., 1990, 1992; Massmann et al., 1991; Tartakovsky, 2013) were developed. More information about decision-making in the context of uncertainty is given by Zheng and Bennett (2002), Stauffer et al. (1999), Sperling et al. (1992), and Morgan et al. (1992). It also became apparent that many complex groundwater systems were better represented by highly parameterized models. Because highly parameterized problems are underdetermined and mathematically ill-posed (Section 9.2), other approaches—different from those used for overdetermined problems—were needed. Many of those approaches were derived from other branches of science where similar problems arise, such as geophysics (Aster et al., 2013) and environmental modeling (Beven, 2009).

Currently, many theoretical explorations of groundwater model uncertainty are not suited for general application to applied groundwater modeling. Some are too simple for realistic

### Box 10.1 Historical Overview of Uncertainty Analysis in Groundwater Modeling—cont'd

models; others have not yet been developed into practical tools. Some methods require multiple models of the groundwater system (Section 10.5), which is a disadvantage in decision-making, where one “best” model is often preferred. However, with the release and continuing development of the Parameter ESTimation (PEST) software suite ([www.pesthomepage.org](http://www.pesthomepage.org)), a subset of practical methods for groundwater modeling became available based on approaches used in geophysical problems (Menke, 1989; Tarantola, 2004; Aster et al., 2013). Therefore, we have focused on the use of these widely available software tools. Methods for uncertainty analysis within PEST include linear (Section 10.4) and nonlinear (Section 10.5) analyses, and are designed for underdetermined and mathematically ill-posed problems. Theoretical considerations and mathematical formulations of PEST tools are documented over a wide range of literature (e.g., Doherty, 2015; Moore and Doherty, 2005; Christensen and Doherty, 2008; Tonkin et al., 2007b; Tonkin and Doherty, 2009; Doherty and Hunt, 2009a,b, 2010; Doherty and Welter, 2010; Moore et al., 2010; Fienen et al., 2010; Doherty et al., 2010, Appendix 4; White et al., 2014, and references contained therein). Detailed guidelines for applying PEST software tools to groundwater uncertainty analysis are given by Doherty et al. (2010).

However, there are many other approaches available, including geostatistical approaches that are not calibration constrained and are widely used in petroleum reservoir modeling. As such, the presentation in this box can only provide a snapshot of time: “One thing that the history of science teaches us is that even in 20 years time we will not be using the same methods and theories as now” (Beven, 2009).

real-time forecasting of flood stages, projecting changes in atmospheric CO<sub>2</sub>, making weather forecasts, and anticipating changes in stock market value, all commonly include uncertainty analyses. A brief historical overview in Box 10.1 gives a short history of uncertainty techniques in groundwater modeling. Such a historical snapshot is necessarily incomplete, however, as the topic is large and evolving, and there is no agreed upon fundamental set of approaches applicable to the wide range of modeling objectives being addressed. Finally, it should be noted that throughout this chapter “uncertainty” and “error” are used interchangeably for convenience, though there are advantages to considering them conceptually separate (e.g., White et al., 2014).

## 10.2 CHARACTERIZING UNCERTAINTY

For any forecast, two broad sources of uncertainty can be considered: (1) uncertainty associated with the model itself; and (2) uncertainty associated with accurate specification of future conditions. The first source of uncertainty stems from assumptions used in the conceptual model, measurement error in observations used to calibrate the model, simplifications required by calibration, and simplification error resulting from defects in the parameterization of the model selected (Sections 9.4 and 9.6). It can be shown that the measurement error and parameter simplification error are additive (e.g., Moore and



Doherty, 2005); more importantly, as one decreases, the other increases. In the science of information theory (e.g., Wallace and Boulton, 1968), this trade-off is depicted as a *Minimum Message Length (MML)* curve, where conveying salient information is hindered by messages that are too short (not enough information) or too long (information is degraded by noise and extraneous unimportant information). In a groundwater modeling context, the curve illustrates that the simpler the model, the larger the associated parameter simplification error (Section 9.6); conversely, overly complex models are dominated by noise resulting from measurement uncertainty (Fig. 10.2(a)). Therefore, a forecast

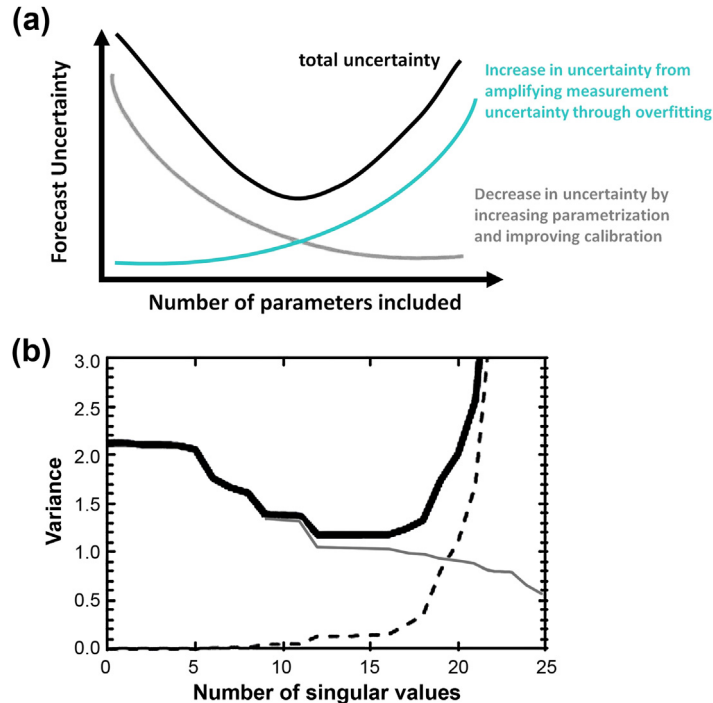


**Figure 10.2** Minimum Message Length (MML) curves as described by Wallace and Boulton (1968) and Moore and Doherty (2005). (a) A typical MML conceptualization showing sources of uncertainty in the base model as measurement error (blue-green line) and structural error (gray line) and their relation to model complexity and forecast uncertainty. Increasing complexity results in increasing the measurement error component of uncertainty because the noise within the measurements is amplified (right-hand portion of the figure). Very simple models (left-hand portion of the figure), on the other hand, are also characterized by relatively high forecast uncertainty because the model's ability to forecast is adversely affected by parameter simplification error. The minimum forecast uncertainty is found when the total uncertainty in the base model (thick black line; the sum of measurement uncertainty and structural uncertainty) is minimized (*modified from Hunt, 2012*). (b) MML curve (thick black line) for a groundwater model of an arid setting (Yucca Mountain, Nevada, USA). Model complexity is represented by the number of singular values (parameters or parameter combinations) included in the error analysis (x-axis). The error variance in the forecast (thick black line) caused by error in the base model is the sum of structural error (thin solid line) and measurement error (dashed line). Forecast error is high when the model is oversimplified (0–10 singular values), and again when the model is overly complex (>18 singular values). The smallest total error occurs when 11–16 singular values are used (*James et al., 2009*).

using an overly simple model has a large uncertainty due to the large parameterization error (“variance” in Fig. 10.2(b)) resulting from oversimplification. Overly complex models will also have high error resulting from overfitting. Therefore, it is desirable to minimize forecast uncertainty by finding the minimum total error that occurs between the extremes. In this way, the MML curve formulation can be considered a restatement of *Occam’s Razor*, where a best approach is to keep things simple, but not too simple (e.g., Hunt et al., 2007).

The second source of uncertainty arises when forecasts need to estimate future stresses and properties—both those we know about (“known unknowns”) and those we cannot anticipate (“unknown unknowns”). Examples of uncertain future parameters include future recharge rates, future pumping schedules, and locations of future sources and sinks, as well as related nonhydrogeological factors such as political, economical, and sociological actions that affect future hydrogeological conditions (Hunt and Welter, 2010). In some cases, the forecasts are so dependent on other assumptions about future conditions that they are better considered “what if” scenarios, or *projections*, rather than forecasts (Beven and Young, 2013).

Forecast uncertainty has also been described using two broad categories: (1) *intrinsic (aleatoric) uncertainty* and (2) *epistemic uncertainty* (Rubin, 2003, p. 4). The word “alea” is Latin for dice, and reflects irreducible uncertainty—that is, variability inherent to the problem that cannot be reduced by more measurements or more knowledge. An example is random variability in the throw of dice; hydrologic examples are given in Table 10.1. Such uncertainty is well suited for description using probabilities. The second category of uncertainty, epistemic uncertainty, represents all other uncertainty, i.e., uncertainty that potentially can be reduced by new measurements, a new model, or new knowledge. (“Epistemic” is derived from the Greek word for knowledge or science.) Measurement errors (e.g., Table 9.1) reflect the lack of perfect agreement of a hydrologic measurement despite repeated sampling, and in this way can be considered an example of intrinsic error (Table 10.1). In practice, measurement error effects on uncertainty are further modified by other considerations such as declustering and weighting to reflect the importance to the modeling objective (Section 9.3) and often treated like epistemic error. Structural and parameter simplification error associated with model assumptions and design (Section 9.4 and 9.6) are also considered epistemic error (Table 10.1), as are nonrandom factors such as uncertainties about future conditions (e.g., climate change).

Though important, epistemic uncertainties are considered difficult to quantify. For example, we can estimate future boundary conditions that might occur (e.g., scenarios), but “we cannot very easily assess whether one scenario is more likely than another, or whether we have missed some likely potential futures because of lack of knowledge or understanding (...Rumsfeld’s unknown unknowns)” (Beven, 2009, p. 25). Thus, even when epistemic uncertainty is treated as intrinsic uncertainty—as in some cases of climate change—associated probabilities will likely be incomplete, imprecise, or change with time. As a result, any probabilistic representation of epistemic error ultimately requires subjective assumptions (Beven and Young, 2013).

**Table 10.1** Examples of intrinsic and epistemic uncertainties in hydrologic modeling (adapted from [Beven and Young, 2013](#))

Uncertainty from	Intrinsic/aleatory component	Epistemic component
Rainfall observation	Gauge errors, after allowing for consistent bias associated with height, wind speed, shield design, etc. Radar reflectivity residuals, drop-size distribution, attenuation, bright band, and other anomalies	Neglect of, or incorrect corrections for, gauge errors and radar estimates.  Errors associated with lack of knowledge of spatial heterogeneity
Remote sensing and sensor data	Random error in correction of sensor values to fields of digital numbers (sensor drift, atmospheric corrections, etc.) Random error in converting digital numbers to hydrological relevant variables	Inappropriate correction algorithms or assumptions about parameters  Inappropriate conversion algorithms in obtaining hydrologically relevant variables
Soil-water balance recharge and evapotranspiration estimates	Random measurement errors in meteorological variables	Biases in meteorological variables relative to effective values required to estimate catchment average evapotranspiration Choice of assumptions in process representations The choice of functions in simulation or forecasting equation Neglect of local factors
Aquifer Properties	Point observation/measurement errors	Errors associated with lack of knowledge of spatial heterogeneity and laterally continuous preferential flowpaths  Errors arising from neglect of or inappropriate handling of scale effects
Head observations	Point observation/measurement errors	Commensurability errors of simulated equivalent outputs with respect to observed values arising from inappropriate handling of scale effects
Discharge observations	Fluctuation in stage observations Measurement error in direct discharge observations for rating curve definition	Poor methodology and operator error Unrecorded nonstationary changes in cross section from vegetation growth and sediment transport Inappropriate choice of rating curve, particularly in extrapolating beyond the range of available discharge observations

The calibration approach of Chapter 9 and the uncertainty description to this point were discussed without reference to an overarching statistical framework. Forecast uncertainties, however, are by their very nature statistical. Therefore, below we provide a brief overview of one useful statistical framework—Bayesian methods. The reader is directed to Hill and Tiedeman (2007), Beven (2009), and Aster et al. (2013) for other statistical frameworks that are also widely used.

The calibration approach of Chapter 9 can be described in terms of a probabilistic approach, one that selects an appropriate model that is most probable given what is known. This concept of calibration-informed weighting of groundwater model results is formally expressed by the widely used *Bayes' theorem* (e.g., Gaganis and Smith, 2001; Rojas et al., 2008), and can be expressed as Bayes' rule:

$$P(A|B) = \frac{P(B|A)P(A)}{P(B)} \quad (10.1)$$

which describes the probability of hypothesis A given information B. In Bayesian terminology, the *posterior* belief, expressed as the probability  $P(A|B)$ , is a function of our *prior* belief  $P(A)$  and the *likelihood*,  $P(B|A)$ , that B will occur if A is true. In this way, it reflects a conditional probability of A given B, stated as  $P(A|B)$ , and B given A,  $P(B|A)$ . Fig. 10.3 visualizes this Bayesian updating in terms of calibration as described in Chapter 9. Our posterior belief (the probability that calibration parameter A is optimal) is updated after our prior belief (our initial estimate of the calibration

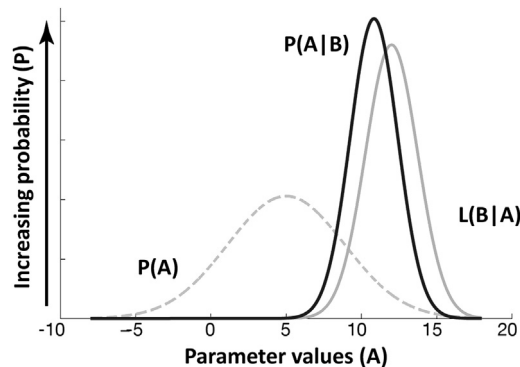


**Figure 10.3** A schematic picture of Bayesian updating using a one-parameter distribution, where the possible range of the parameter spans from  $-10$  to  $20$ . The probability density function representing the prior distribution  $P(A)$  of the calibration parameter is diffuse (gray dashed line), meaning the variance is relatively high and, correspondingly, uncertainty in the parameter is high. The likelihood function  $L(B|A)$  (solid gray line), on the other hand, has lower variance, suggesting a history-matching process brings a higher level of certainty to the estimation of the parameter than given by the prior distribution only. The resulting posterior distribution  $P(A|B)$  (solid black line) is a convolution of the prior and likelihood functions. The peak is higher indicating more certainty resulted after history matching, is shifted significantly from the prior toward the likelihood, and is narrower, representing less uncertainty (modified from Fioren et al., 2009, 2013).

parameter,  $P(A)$ ) has been tested for likelihood using the observations from the system (calibration targets). That is, what is the probability we perfectly match our observations B given parameter A? As more calibration observations become available, this posterior belief is further informed. An important feature of Bayesian methods is that Bayes theorem does not require belief that the world is intrinsically uncertain, but rather it recognizes our perceptions of the world are incomplete and thus are approximations of reality.

The advantage of a probabilistic representation is that it conveys estimates of parameter values and their uncertainty made prior to model calibration (the *prior*) using expert knowledge. In this way, a Bayesian approach recognizes the utility of subjective soft knowledge in addition to information gained from history matching. Expert knowledge can be expressed in many ways. In some cases, the method assumes “no prior,” which means that all parameter values are equally likely. Even common sense can serve as a prior—a check against taking the output of a model too credulously (Silver, 2012).

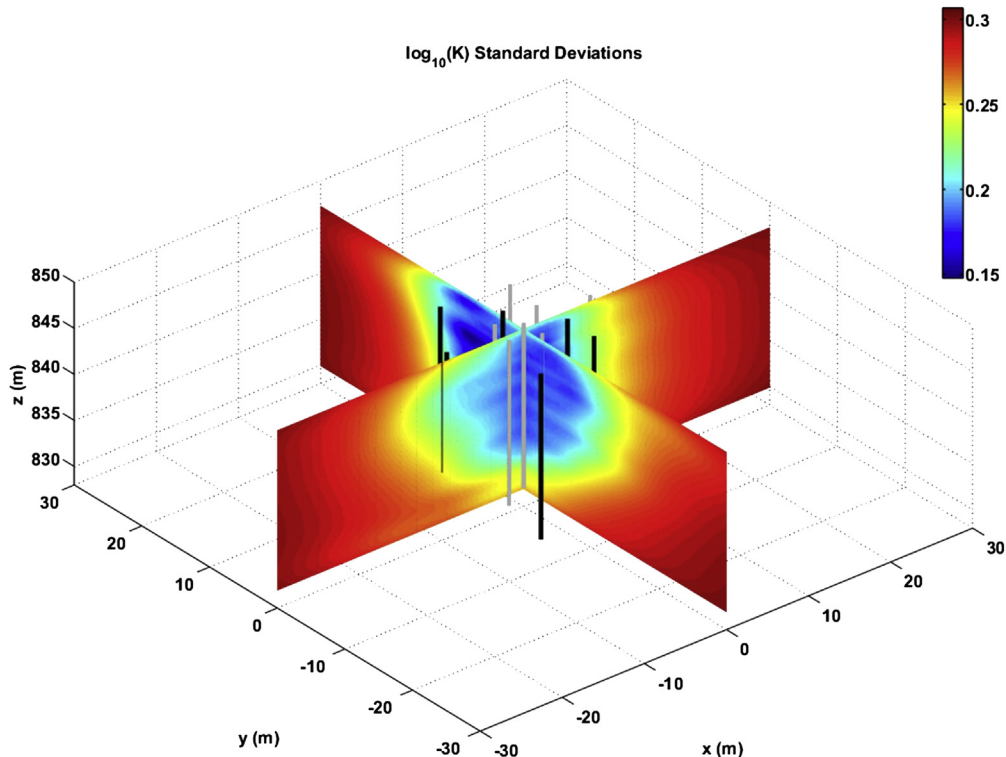


**Figure 10.4** An example of a Bayesian posterior uncertainty evaluation of log hydraulic conductivity (shown by colors) after a number of aquifer (pumping) tests were performed using hydraulic tomography. Areas stressed by multiple aquifer tests are characterized by lower uncertainty (lower standard deviation of  $\log(K)$ , blue areas). Areas distant from the pumping locations have higher uncertainty (Cardiff *et al.*, 2013).

Regardless of how originally formulated, this prior uncertainty is updated by gaining new information (e.g., during history matching) resulting in a new (*posterior*) estimate of parameters and their uncertainty (Fig. 10.3). However, similar to the concept of multiple possible models illustrated in Fig. 9.17, a Bayesian approach does not expect ever to identify a parameter set with 100% probability—rather the end result is a most probable set of parameters with associated uncertainty.

This formulation, however, is well suited for extending a Bayesian approach to forecast uncertainty. For example, uncertainties associated with all model inputs can be expressed as probability distributions. As a result, both forecast probabilities and probabilities associated with calibration parameters (Fig. 10.4) can be updated as new information about the system becomes available. The updating could be performed in a variety of ways, such as a literature review, new field measurements, or additional calibration. In practice, history matching is the most common way to update the prior probabilities. Bayesian methods typically require a large number of forecast simulations to express the estimated uncertainty. Yet if the problem is constructed appropriately, the use of a single parameter set followed by postcalibration uncertainty analysis can be a more computationally efficient way to obtain an outcome similar to a Bayesian analysis (Doherty et al., 2010; Aster et al., 2013). Regardless of how obtained, a modeler's subjective choices still underpin the uncertainties reported (e.g., Fioren, 2013)—in many ways similar to how subjective choices influence calibration, as discussed in Chapter 9.

### 10.3 ADDRESSING UNCERTAINTY

The generally ubiquitous nature of uncertainty notwithstanding, it is recognized that uncertainty can be influenced by the type of forecast. One way to reduce uncertainty is to frame the modeling purpose in terms of relatively less uncertain forecasts to avoid adding unnecessary uncertainty to model forecasts (Hunt, 2012). The following examples demonstrate how defining the forecast can influence the resulting uncertainty.

1. Forecasts that require no structural changes to the base model are relatively less uncertain than forecasts requiring structural changes. Structural changes include changes to the domain geometry, and/or boundary conditions, and/or sources or sinks (e.g., dam removal, or addition of pumping wells, quarries, tunnels, slurry walls, and/or artificial lakes). For example, a model designed to forecast the effect of changing pumping rates from wells simulated in the base model will have less uncertainty than a forecast simulating a new (proposed) well field. Structural changes can also include changes in underlying assumptions, such as when a forecast requires a transient simulation and the base model is calibrated to steady-state conditions. Additional uncertainty is added from the aquifer storage parameters needed for transient simulations because those parameters cannot be estimated during steady-state calibration.

2. Forecasts that depend on detailed knowledge of aquifer heterogeneities, such as travel times (Chapter 8), will have greater uncertainty than larger scale forecasts that integrate heterogeneities because field characterization of such detail is difficult. Travel times are also relatively more uncertain than forecasts of heads because travel times require an additional parameter (effective porosity, Box 8.1) and application of interpolation and tracking schemes (Chapter 8). A forecast of flowpath is more certain than travel time (Box 10.2) because hydraulic gradients that determine flowpaths can be tested during calibration but values of effective porosity, which are required to calculate travel time, typically are not. Hence, delineation of a well capture zone is more certain than the time required for a particle to reach the well. Similarly, a forecast of arrival of a contaminant at a receptor or boundary, which requires an estimate of travel time, will have relatively high uncertainty (Box 10.2).
3. Forecasts formulated in terms of differences in model outputs (e.g., “future baseflow is forecast to decrease by 10%”) are less uncertain than absolute forecasts (e.g., “future baseflow is forecast to be 1000 m<sup>3</sup>/day”).
4. Forecasting representative average conditions over a period of time (Fig. 10.5) is less uncertain than forecasting absolute conditions or extreme ranges of conditions.
5. A forecast similar in length to the length of time of the history match used to calibrate the base model has relatively less uncertainty than a longer forecast because the range and dynamics of system drivers are more likely to be represented in the forecast.
6. Forecasts that rely on sensitive parameters are more certain than forecasts relying on insensitive parameters. Recall from Section 9.6 that insensitive parameters are fixed at constant values and are not estimated during calibration. A forecast uncertainty assessment, however, encompasses all parameters potentially important for the forecast—including those considered insensitive for history matching.

Although appropriate formulation of the forecast can reduce uncertainty, addressing uncertainty more formally requires a quantitative estimate of the uncertainty that surrounds a forecast. In a broad sense, parameter sensitivity (Sections 9.4 and 9.5) relates to forecast uncertainty. An *uncertainty analysis*, however, is a more encompassing characterization of uncertainty—one that moves beyond those factors easiest to analyze (Saltelli and Funtowicz, 2014). Yet, it is also recognized that “you cannot be certain about uncertainty” (Knight, 1921). Therefore, in practice, the objective of an uncertainty analysis is to report a representative estimate of uncertainty surrounding a forecast, and convey the modeler’s assessment of how well the model can be expected to address the modeling purpose. For example, results from an ensemble of forecast simulations could be reported to show a range of reasonable forecasts. If only a single forecast is reported, it should be accompanied by an estimate of associated uncertainty around the forecasted model output.

### Box 10.2 Travel Time in Heterogeneous Aquifers: Impossible to Forecast Accurately?

Moore and Doherty (2005) examined a relatively difficult type of forecast—forecasting the exit location of a particle at a model boundary. First they created a two-dimensional synthetic aquifer using a random field generator. Then they placed an imaginary particle in the flow field and traced its path using a particle tracking code. The particle exited 206.8 m from the left-most edge of the bottom model boundary (Fig. B10.2.1), which became the “truth” for basis of

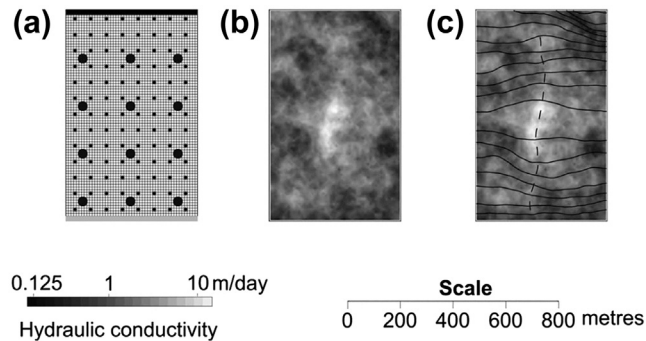


**Figure B10.2.1** Details of the synthetic aquifer: (a) model domain and grid with the 12 head observation locations (representing wells) shown as large circles and pilot point locations shown as small circles. (b) The “true” hydraulic conductivity field. (c) Head contours (solid lines) and particle track (dotted line) calculated for the true hydraulic conductivity field (*modified from Moore and Doherty, 2005; Moore et al., 2010*).

comparison. Next they selected 12 head values from the simulated “true” head distribution, added a small amount of assumed measurement error, and then used the 12 head observations as targets to estimate the hydraulic conductivity field. Using uniform observation weights, the model was calibrated to the head targets, where the best-fit values of hydraulic conductivity produced a very good match to the targets. However, the forecast of the exit location of the particle was more than 4 m away from the true exit location. The error was due to smoothing of the true hydraulic conductivity field during calibration. They also pointed out that introducing more heterogeneity in hydraulic conductivity cannot compensate for a lack of information in the head targets: a model that was overfit by introducing heterogeneity to achieve an almost perfect match to head targets yielded an exit location forecast off by over 50 m.

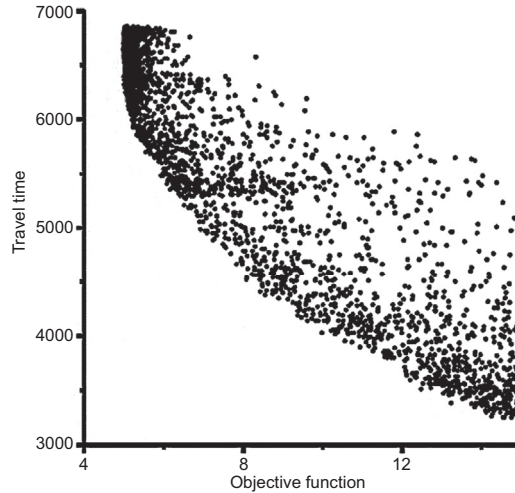
Moore et al. (2010) revisited this problem to calculate the time for the particle to reach the boundary, where the true travel time through the synthetic aquifer is 3256 days. The smoothing of the true heterogeneity in the calibrated model had a larger effect on the forecast of travel time than the forecast of exit location, yielding a travel time of 6823 days—more than a factor of 2 higher than the true travel time. Then they used a Pareto front approach to ask the question: “How much do we need to degrade the calibration in order to attain a simulated travel time near the actual travel time?” Fig. B10.2.2 shows that the true particle travel time forecast is simulated only by accepting a relatively degraded calibration (i.e., a calibration with a larger value for the objective function but still statistically acceptable). A travel time close to the true value of 3256 days is achieved only for high values of the objective function

(Continued)



### Box 10.2 Travel Time in Heterogeneous Aquifers: Impossible to Forecast Accurately?—cont'd

**Figure B10.2.2** A Pareto front diagram showing a forecast of particle travel time in days (vertical axis) versus the calibration objective function (horizontal axis). Each dot represents a forecast made with a different calibrated model. Well-calibrated models have low objective functions and poorly calibrated models have relatively higher objective functions. The true travel time through the synthetic aquifer (Fig. B10.2.1) is 3256 days, which is only sampled when the objective function is at its upper limit of feasibility (modified from Moore *et al.*, 2010).



(rightmost end of the x-axis). Or put another way, the better the model performed in history matching (moved leftward along the x-axis), the worse it performed for the travel time forecast—an artifact that can result in models that are overfit (Section 9.6).

This example provides some important general insights for forecasting: (1) the type of forecast decided the relative uncertainty, and forecasts of exit locations are relatively less uncertain than forecasts of travel time; (2) although head data are common calibration targets, their ability to constrain forecasts such as flowpath and travel time may be poor; (3) our ability to represent laterally continuous preferential flowpaths accurately is often lacking, yet some forecasts depend on such characterizations.

The synthetic test case had more observations relative to the total number of nodes than many groundwater models of real aquifers, suggesting that a forecast of time of arrival of an actual contaminant at a site boundary or a drinking water well will have relatively high uncertainties. Hence, even a sophisticated uncertainty analysis may not capture the error introduced by the unavoidable smoothing of the real hydraulic conductivity field. Forecasts of time of arrival at a boundary or receptor can also be expected to be biased longer than actual times because parameter fields in the model are smoothed and tend to smear out preferential flowpaths. Finally, it should be noted that the above discussion of travel times refers to the advective travel time computed by a particle tracking code (Chapter 8); it includes simplification error from neglecting potentially important processes because the worst-case scenario of first arrival of a contaminant requires consideration of dispersion and a full solute transport model (Section 12.3). Therefore, not only are travel times difficult to forecast, forecasting travel times also requires additional thought to develop a conservative worst case for arrival times at a boundary or receptor.

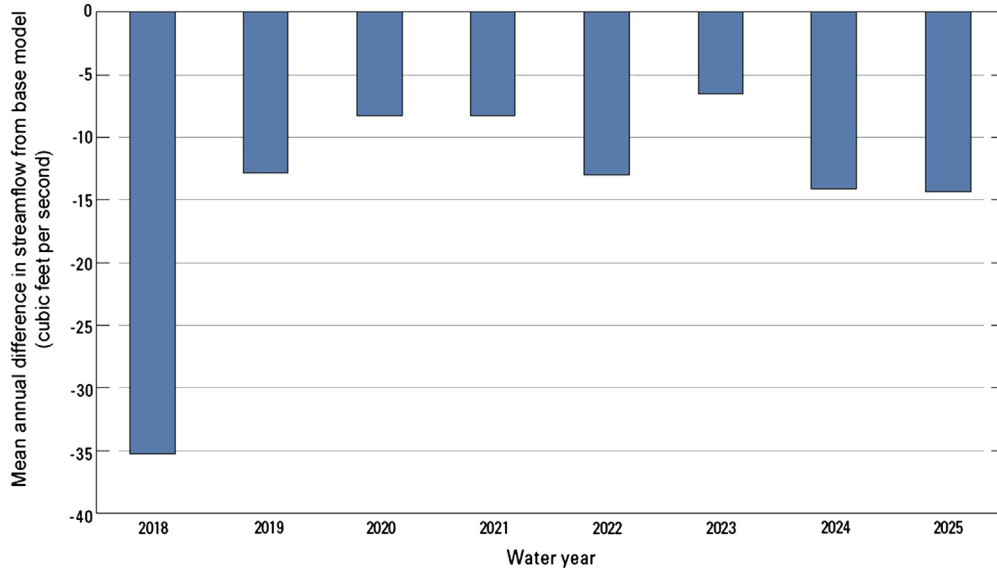


**Figure 10.5** An example of a forecast of future reductions in streamflow resulting from continuing an existing pumping regime. The forecast has relatively less uncertainty because it is reported as a mean annual value rather than the range of all simulated values. In addition, the forecast can be expected to contain less uncertainty because it is presented as a difference rather than absolute model output, and concerns a quantity (pumping stress) included in the calibration history matching (*modified from Ely et al., 2011*).

Much work has been devoted to the topic of uncertainty analysis (e.g., [Box 10.1](#)); yet, it must be remembered that “uncertainty estimation is only a means to an end: the end of making better decisions” ([Beven, 2009](#); p. 30). We focus here on uncertainty analysis for applied groundwater modeling where forecasts might be used to address regulatory requirements and/or guide management decisions. In many such cases, the goal of forecasting is to inform risk management and estimating the probability or likelihood of the occurrence of some event. Uncertainty analyses can be computationally frugal *basic uncertainty analyses* ([Section 10.4](#)) or computationally demanding *advanced uncertainty analyses* ([Section 10.5](#)). The reporting of forecast uncertainty is often the same between the two, such as a standard deviation or 95% confidence interval, but the amount of effort devoted to the uncertainty analysis is different. Required investment of time and money can also depend, however, on other factors ([Barnett et al., 2012](#); page 10). Cases that are societally controversial, or where forecast failure has dire consequences, may require advanced methods. Advanced uncertainty analysis may also be warranted when omitting important system details potentially could influence risk factors that are important to the modeling objective. For example, when forecasting travel time and other transport phenomena (e.g., [Bradbury et al., 2013](#); [Hunt et al., 2014](#)), basic analyses may not fully encompass uncertainty caused by

omitting natural world detail important to the forecast (Box 10.2). In these cases, more sophisticated approaches that better represent important system detail are warranted.

## 10.4 BASIC UNCERTAINTY ANALYSIS

A basic uncertainty analysis focuses on a small set of dominant factors expected to drive forecast uncertainty and uses approximate but computationally efficient representations of uncertainty (Fig. 10.6). Using the two sources of uncertainty described in Section 10.2, *scenario modeling* addresses uncertainty in future conditions and *linear uncertainty analysis* addresses uncertainty stemming from the base model.

### 10.4.1 Scenario Modeling

In scenario modeling, all initial parameters and hydrologic conditions from the base model are retained except for those explored as part of the forecast. The base model, modified for a set of future conditions, represents a *scenario* or *projection* of the future. The scenario is executed as a forward run, a relatively small number of times (typically

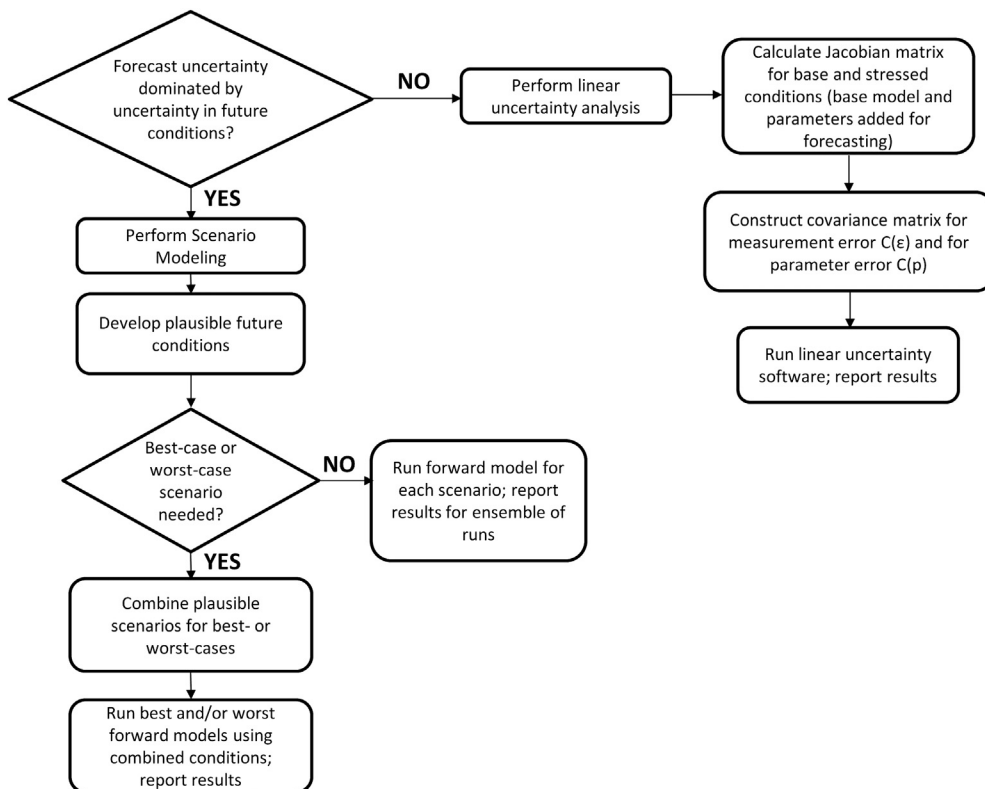
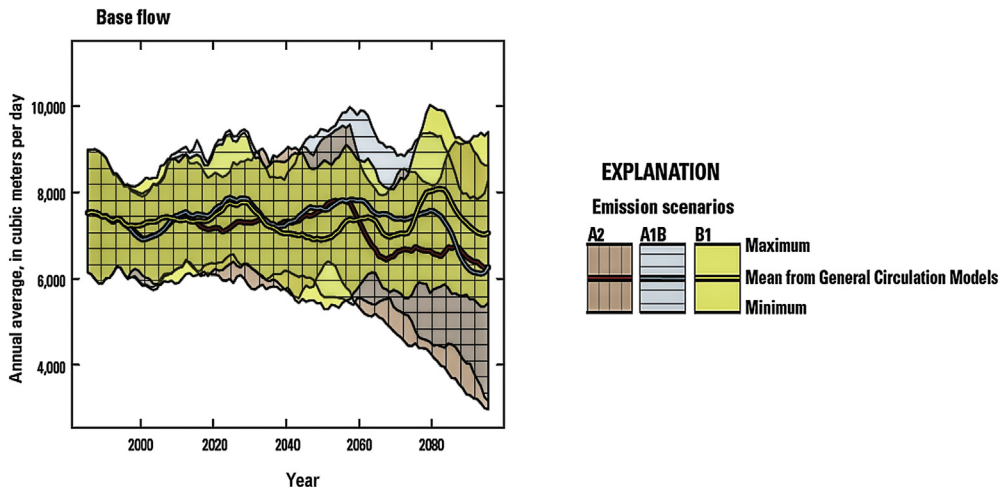


Figure 10.6 Schematic diagram of a potential workflow for performing basic uncertainty analysis.

fewer than 20). Each run is executed with different assumed values (determined by the modeler) for future conditions. One objective of scenario modeling is to produce an ensemble of results that defines a representative envelope of uncertainty around the forecast. For example, several different pumping rates and/or variations in recharge rates during wet and drought periods might each constitute a scenario.

A scenario might assume that system dynamics are constant over time (e.g., the system and drivers have the same mean and variance over time, called *stationarity*); alternatively, a scenario can encompass conditions with dynamics that differ from the base model. Simulations using different future climates are examples of scenarios that are nonstationary. Future scenarios can also be formulated to simulate future maximum and minimum responses, and might include combinations of future stresses. The intent of such an analysis is to bracket the forecasts of the base model with a range of forecasts that represent a reasonable envelope of *best-* or *worst-case* scenarios. Often construction of such a scenario is straightforward (“what is the effect of extreme drought on groundwater discharge?”). In other cases, the response of a complex model to altering multiple parameters and stresses may not be obvious, and other more advanced methods such as a maximization–minimization uncertainty analysis (Section 10.5) may be required.

An example of scenario modeling is shown in Fig. 10.7, where the purpose of the model was to assess effects of possible future climates on stream baseflow. To represent the uncertainty inherent to future climate predictions, 15 forecasts were made using precipitation and temperature output from three potential CO<sub>2</sub> emission scenarios (derived



**Figure 10.7** A forecast of baseflow summarizing 15 scenario forward runs (maximum, minimum, and average conditions in each of three emission scenarios). Forecast uncertainty is shown by the envelope around the means of the three scenarios (colored lines). The forecasts derived from the mean of each emission scenario were based on the mean results from 5 different General Circulation Models. Note how the uncertainty envelope increases with time (Hunt et al., 2013).

using five different General Circulation Models or GCMs). The range in the 15 forecasts is illustrated by the outer envelope of results in Fig. 10.7; the mean result for a given emission scenario is shown by a colored line. Important points regarding uncertainty are illustrated by the results: (1) there can be no expectation of one “best” forecast given the uncertainty about future climates; (2) uncertainty in the forecasts increases with time; (3) there is appreciable difference in climate among the five GCMs even for the same emission scenario; (4) effects of CO<sub>2</sub> emissions on baseflow are forecast to be most pronounced during the later portion of the twenty-first century. Note that since there is so much variability in the future climate driver, no attempt was made to include the additional uncertainty contributed to the forecasts from the base model; it is negligible for this forecast compared to the uncertainty in the climate driver.

### 10.4.2 Linear Uncertainty Analysis

Linear uncertainty analyses require few alterations to the base model. They are typically computationally frugal because only sensitivities are required, and are appropriate for both overdetermined and underdetermined inverse problems. The Jacobian matrix described in Section 9.5 is the basis of linear uncertainty analysis. Recall that the Jacobian matrix is composed of parameter sensitivities, which relate changes in model parameters to changes in model outputs. Linear methods are computationally easy to implement because the Jacobian matrix is calculated only once. However, they do require the calculation of additional sensitivities for each forecast and the modeler’s assessment of uncertainty in parameters and observations (the “prior”). In the simplest case, measurement error propagates uncertainty to calibration parameters (e.g., Fig. 10.8), which in turn can be related to uncertainty in model forecasts (e.g., see Hill and Tiedeman, 2007, p. 159). However, as shown in Fig. 10.2, measurement error is only one component of model uncertainty; parameter simplification error can be an important contributor to forecast uncertainty, especially if the model is sparsely parameterized.

In recognition of its importance, a method for estimating parameter simplification error was developed by Cooley (2004) where multiple realizations of a complex hydraulic conductivity field were translated to simpler zones. However, this analysis was computationally demanding, and at the end the modeler had to decide if the simplification error was acceptable. If not, the model parameterization, calibration process, and evaluation of parameter simplification error had to begin again. Moore and Doherty (2005) discuss a more computationally efficient approach for including both measurement error uncertainty and simplification uncertainty in a linear uncertainty analysis. Given there is readily available software for applied modeling, we use the Moore and Doherty (2005) formulation here as an example of including both simplification and measurement error in forecast uncertainty estimates.

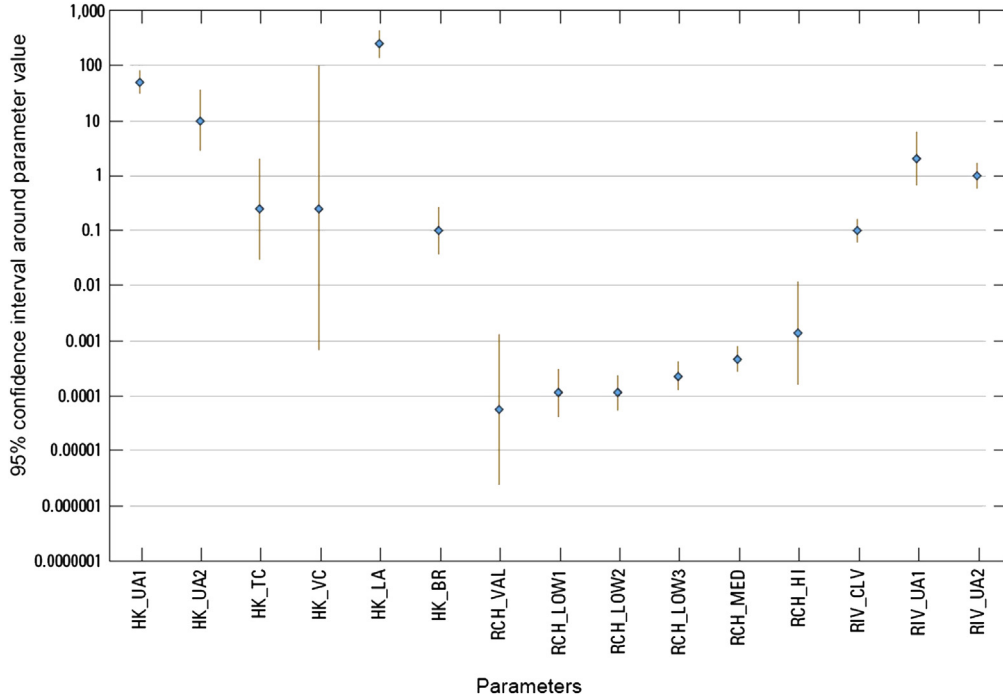


**Figure 10.8** A visual representation of final calibrated model parameters and their associated 95% confidence interval calculated by linear uncertainty methods. HK = hydraulic conductivity (ft/d), RCH = recharge (ft/d), and RIV = conductance (ft<sup>2</sup>/d) (modified from *Ely and Kahle, 2004*).

Assume that uncertainty is reported as the error variance of the forecast, where the variance is calculated by comparing a true value of the variable (e.g., head) in question ( $\xi$ ) to that forecast by a model ( $s$ ). *Moore and Doherty (2005)* calculated the error variance for forecast  $s$  as

$$\sigma_{\xi-s}^2 = \mathbf{y}^t(\mathbf{I} - \mathbf{R})\mathbf{C}(\mathbf{p})(\mathbf{I} - \mathbf{R})^t\mathbf{y} + \mathbf{y}^t\mathbf{G}\mathbf{C}(\boldsymbol{\epsilon})\mathbf{G}^t\mathbf{y} \quad (10.2)$$

where

$\sigma_{\xi-s}^2$  = the error variance of the forecast  $s$

$\mathbf{y}$  = vector of parameter sensitivities to forecast  $s$

$\mathbf{I}$  = Identity matrix

$\mathbf{R}$  = Resolution matrix

$\mathbf{C}(\mathbf{p})$  = covariance matrix of parameter uncertainty representing expert knowledge

$\mathbf{G}$  = matrix used to compute parameters for the best history match

$\mathbf{C}(\boldsymbol{\epsilon})$  = covariance matrix of measurement error of targets

$t$  represents the matrix transpose operation

The derivation of Eqn (10.2) is outside the scope of our textbook; a summary of the mathematical background may be found in Appendix 4 of Doherty et al. (2010). For our purposes, note that there are two additive terms on the right-hand side of Eqn (10.2): (1) terms to the right of the addition sign represent forecast uncertainty resulting from measurement error in the targets; and (2) terms to the left represent uncertainty from parameter simplification error (Section 9.6). The contributions of the two components are depicted in Fig. 10.2(b), which were calculated using Eqn (10.2).

The equivalent Bayes' formulation of Eqn (10.2) for uncertainty in a forecast  $s$  is given by

$$\sigma_s^2 = \mathbf{y}^t \mathbf{C}(\mathbf{p}) \mathbf{y} - \mathbf{y}^t \mathbf{C}(\mathbf{p}) \mathbf{X}^t [\mathbf{X} \mathbf{C}(\mathbf{p}) \mathbf{X}^t + \mathbf{C}(\boldsymbol{\epsilon})]^{-1} \mathbf{X} \mathbf{C}(\mathbf{p}) \mathbf{y} \quad (10.3)$$

$\sigma_s^2$  = variance of uncertainty of forecast  $s$

$\mathbf{y}$  = vector of parameter sensitivities to forecast  $s$

$\mathbf{C}(\mathbf{p})$  = covariance matrix of parameter uncertainty representing expert knowledge

$\mathbf{X}$  = Jacobian matrix of parameter sensitivities

$\mathbf{C}(\boldsymbol{\epsilon})$  = covariance matrix of measurement error of targets

$t$  represents the matrix transpose operation

$-1$  represents that matrix inverse operation

Equation (10.3) is a form of a widely used matrix relation called Schur's complement (Golub and Van Loan, 2012, p. 119); the mathematical background for Eqn (10.3) is reported by others (e.g., Appendix A of Christensen and Doherty, 2008; Appendix 1 of Fioren et al., 2010). For our purposes, note that in Eqn (10.3) the posterior forecast uncertainty  $\sigma_s^2$  is calculated by reducing the prior uncertainty (the first term,  $\mathbf{y}^t \mathbf{C}(\mathbf{p}) \mathbf{y}$ ) by the second term, which reflects information gained from the observations through parameter sensitivities after accounting for observation error,  $\mathbf{C}(\boldsymbol{\epsilon})$ .

In practice, both Eqns (10.2) and (10.3) are solved using parameter estimation software (e.g., GENeral LINear PREDiction (GENLINPRED) uncertainty/error analyzer in the PEST software suite—Doherty et al., 2010, p. 26). Therefore, we focus here on understanding the important elements that a modeler must input to solve each equation. The key component for representing measurement error in the observations is the covariance matrix  $\mathbf{C}(\boldsymbol{\epsilon})$ , which has a row and column for each target. Thinking of a matrix as a table, a covariance matrix is symmetric in that it has the same labels (target name) along the top as along the side. Variance of the measurement error representing the total “noise” that confounds true measurement is entered for each target along the diagonal of the matrix; any interaction (covariance) between measurement errors is represented by off-diagonal elements. If there is no interaction between measurement errors, the off-diagonal entry is zero. As noted by Moore and Doherty (2005), “for better or for worse this  $\mathbf{C}(\boldsymbol{\epsilon})$  is normally assumed to be a diagonal matrix” and

measurement error is considered fully explained by what the modeler enters along the diagonal for the measurement itself. In this way,  $C(\boldsymbol{\epsilon})$  is better thought of as a variance matrix.

In practice, the  $C(\boldsymbol{\epsilon})$  matrix is typically entered into the linear uncertainty analysis by setting observation weights for parameter estimation (Section 9.5) equal to the observation error expected, which reflects our ability to measure the observation and the ability of the model to simulate it (e.g., a steady-state model simulating transient field measurements). It is important to note that weights used for specifying the  $C(\boldsymbol{\epsilon})$  matrix may be different from those used for calibration, because calibration weights reflect additional factors such as the targets' location in the near-field or far-field and their importance for the modeling objective.

The key components for representing parameter simplification error are the resolution matrix ( $\mathbf{R}$ ) and the  $C(\mathbf{p})$  matrix (Eqn. (10.2)), and the  $C(\mathbf{p})$  matrix (Eqn. (10.3)). The resolution matrix  $\mathbf{R}$  represents the correspondence between estimated parameters and true parameters, and is calculated as part of the parameter estimation operation. Therefore, for both Eqns (10.2) and (10.3), the  $C(\mathbf{p})$  matrix is the primary input required from the modeler to calculate the parameter simplification error. The  $C(\mathbf{p})$  matrix is a covariance matrix of parameter error that represents the *innate parameter variability* (e.g., 95% confidence interval, standard deviation, or variance) resulting from the translation of the heterogeneity of the natural world to a model. As such, it reflects the expert knowledge of system properties represented in the model. Recall that choices made during parameterization impart uncertainty because the model is required to represent a complex natural world with a simplified version of that world (Gaganis and Smith, 2001; Beven, 2005). Any model parameter is, therefore, an imperfect simplification of the natural world. Quantitative representation of parameter simplification error hinges on the modeler specification of the  $C(\mathbf{p})$  matrix.

A simple example illustrates how choices of model simplification can influence the assignment of innate parameter variability. Suppose a model domain representing a heterogeneous aquifer is divided into three types of sediments: (1) well-sorted eolian sand; (2) medium-sorted fluvial sand; and (3) poorly sorted sand and gravel from supraglacial deposits. Soft knowledge and intuition tell us that the innate parameter variability associated with a parameter used to represent a given type of sediment will differ among the sediment types. Eolian (wind-blown) sand is characterized by a small range of grain sizes; thus, a parameter that describes eolian sand is expected to have relatively small innate parameter variability. The wide range of sediment sizes in supraglacial sediments (sediments that slump off an ice block) is expected to have relatively large innate parameter variability because of the poor sorting during deposition. Parameter variability for fluvial sediments typically is between these two end members. Moreover, if the heterogeneity was represented by only one encompassing parameter (“unconsolidated sediment”), the innate parameter variability would



be higher. From this simple example, it is clear that assigning innate parameter variability, although not random, has subjective elements.

In practice, the  $C(\mathbf{p})$  matrix is assigned based on expert knowledge, which might be formalized by using geostatistical approaches. In its simplest form, however,  $C(\mathbf{p})$  is a diagonal matrix, containing the modeler's estimate of the uncertainty along the center diagonal, expressed as the standard deviation, which represents the expected innate variability in the parameter. Because the nondiagonal elements are typically zero, input to the parameter estimation code can be as simple as a parameter uncertainty file containing two columns (for example, a  $C(\mathbf{p})$  matrix for the previous simple example is given in Table 10.2). Uncertainty software may also have an option to use the parameter upper and lower bounds applied during history matching to represent a 95% confidence interval for the parameter (see Box 9.2), which then can be used for automating the creation of the  $C(\mathbf{p})$  matrix. Such straightforward formulation is appropriate for many applied groundwater modeling problems.

However, because  $C(\mathbf{p})$  is a covariance matrix, additional sophistication can be added if the modeler chooses by entering nonzero values for the off-diagonal entries to represent spatial correlation between parameters. James et al. (2009) describe the  $C(\mathbf{p})$  matrix as follows:

*Specifically, [the  $C(\mathbf{p})$  matrix] characterizes the current state of geological knowledge and geological uncertainty associated with a study site. Geologic uncertainty is expressed through nonzero diagonal elements. Geologic knowledge is expressed through nonzero off diagonal elements (indicating that something is known of the spatial correlation of hydraulic properties) and finite diagonal elements (indicating that there are bounds on geological uncertainty).*

Regardless if one uses a diagonal matrix such as shown in Table 10.2 or a more sophisticated formulation as described by James et al. (2009), the strength of representing parameter simplification error via the  $C(\mathbf{p})$  matrix is that it is expressed with

**Table 10.2** An example of a simple  $C(\mathbf{p})$  matrix for a three-parameter model ( $K$  = hydraulic conductivity). (a) Input for the matrix; (b) the  $C(\mathbf{p})$  matrix constructed from information in (a)

(a) Input for $C(\mathbf{p})$ matrix		
Parameter	Parameter placement in the $C(\mathbf{p})$ matrix	Innate parameter variability (standard deviation, m/d)
$K_{\text{fluvial sand}}$	row 1, column 1	5
$K_{\text{eolian sand}}$	row 2, column 2	0.2
$K_{\text{supraglacial sand \& gravel}}$	row 3, column 3	50
(b) Resulting $C(\mathbf{p})$ matrix		
5	0	0
0	0.2	0
0	0	50

mathematical rigor for subsequent quantification of uncertainty (Doherty and Hunt, 2009b). For example, as simpler or more complex parameterizations are chosen, the  $C(\mathbf{p})$  matrix can be updated to reflect the change in expected innate parameter variability. Many uncertainty procedures for groundwater modeling do not include a quantitative expression of parameter simplification error in forecast uncertainty (as is included in Eqns (10.2) and (10.3)). However, simplification error is commonly the dominant contributor to forecast uncertainty, especially when the forecast is sensitive to system details such as small-scale heterogeneity (e.g., Box 10.2) (Gaganis and Smith, 2001; Moore and Doherty, 2005; Ye et al., 2010). Thus, one could argue that omission of parameter simplification error can cause uncertainty to be underestimated.

#### 10.4.2.1 Examples of Linear Uncertainty Analysis

Though involving advanced statistical concepts, in practice, linear uncertainty analysis is straightforward and can be performed with widely available software. In the simplest case, the result of a linear uncertainty analysis is the uncertainty around a forecast model output—for example, standard deviation, variance, or 95% confidence interval (e.g., 95% confidence interval around a forecast of mine inflow—Kelson et al., 2002). The assumption of linearity results in uncertainties that are symmetric around the forecast value. In some cases, the symmetry results in unrealistic ranges of possible forecasts; for example, a linear uncertainty analysis may forecast drawups for an added pumping well when the uncertainty range is applied. Therefore, uncertainty estimates calculated by linear uncertainty methods may need to be censured to remove unrealistic results, or other more advanced nonlinear methods may be required.

A first type of linear uncertainty analysis is evaluating the relation of forecast uncertainty to the parameters in the base model and the quality of the observations used to calibrate the base model (e.g., Gallagher and Doherty, 2007; Doherty and Hunt, 2009a; James et al., 2009; Dausman et al., 2010; Fienen et al., 2010, 2011). The following examples were generated using the PEST GENLINPRED utility (Doherty et al., 2010). As noted above, linear analysis requires parameter sensitivities to the forecast ( $y$  in Eqns (10.2) and (10.3)) and the modeler's assessment of uncertainty in the observations and in the parameters. The first is obtained by adding forecasts to the list of observations used in the parameter estimation and recalculating the Jacobian matrix. In the examples presented below, parameter estimation weights were specified for each observation were used to populate the  $C(\boldsymbol{\epsilon})$  matrix, and the  $C(\mathbf{p})$  matrix was derived from the parameter upper and lower bounds.

In Fig. 10.9, the estimated potential for error in forecasts of lake stage in a groundwater model was calculated using initial (precalibration) values of the calibration parameters and calibrated parameter values, where total uncertainty in the drought lake stage forecast equals the sum of the row of bars in Fig. 10.9. A comparison of the results from a linear uncertainty analysis, as represented by the error variance in the forecast

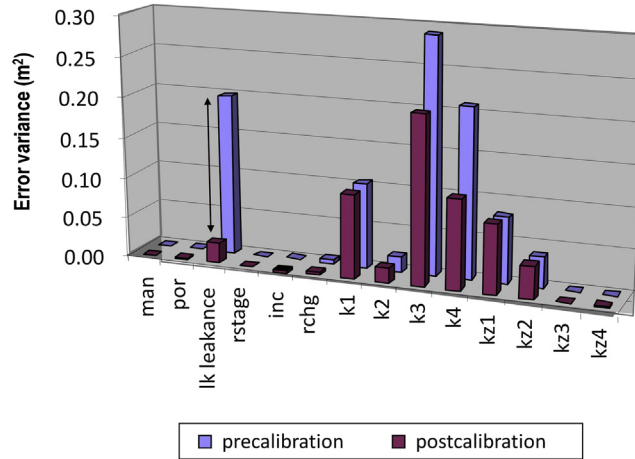


**Figure 10.9** Precalibration and postcalibration parameter contribution to total error variance (sum of all bars in a row) for a forecast of lake level under drought conditions (using MODFLOW's Lake Package, Section 6.6). The error variance (calculated from Eqn (10.2)) represents uncertainty around the model forecast. The bars show the contribution of each parameter to the total forecast error (precalibration =  $0.96 \text{ m}^2$ ; postcalibration  $0.60 \text{ m}^2$ ). Forecast uncertainty is lower after calibration, as shown by the reduction in height in the bars for a number of calibration parameters used in the forecast simulation. Note that postcalibration reduction in forecast uncertainty was most notable for the lakebed leakance (lk leakage) parameter. Thus, less gain is expected from future data-collection activities targeting only this parameter because the value of the parameter is already well constrained by existing history matching data, i.e., the parameter has good identifiability (*modified from Hunt and Doherty, 2006*). Parameter types are: man = Manning's  $n$ , por = effective porosity, lk leakage = lakebed leakance, rstage = far-field river stage boundary, inc = stream elevation increment boundary condition, rchg = recharge, k1 through k4 = horizontal hydraulic conductivity of layers 1 through 4, kz1 through kz4 = vertical hydraulic conductivity of layers 1 through 4.

of lake stage during drought conditions, suggests that calibration reduced the forecast uncertainty, but the reduction was not equal across all model parameters (x-axis). Moreover, the results show that if more reductions in forecast uncertainty were desired, additional field work to characterize horizontal hydraulic conductivity of layers 3, 4, and 1 (k3, k4, and k1 in Fig. 10.9) would be more effective than additional work to characterize the lakebed leakance (lk leakage in Fig. 10.9).

Linear uncertainty methods can also be used to visualize the information content of a specified set of observation targets using parameter identifiability (Fig. 10.10). As defined by Doherty and Hunt (2009a), larger identifiability (longer length of the stacked bars) represents higher information contained in the observed data for those parameters. Warmer colors indicate higher confidence in the ability of the observation data to constrain the parameter. Using the concepts in Chapter 9, the warmer colors represent parameters more firmly rooted in the solution space defined by the observation data.

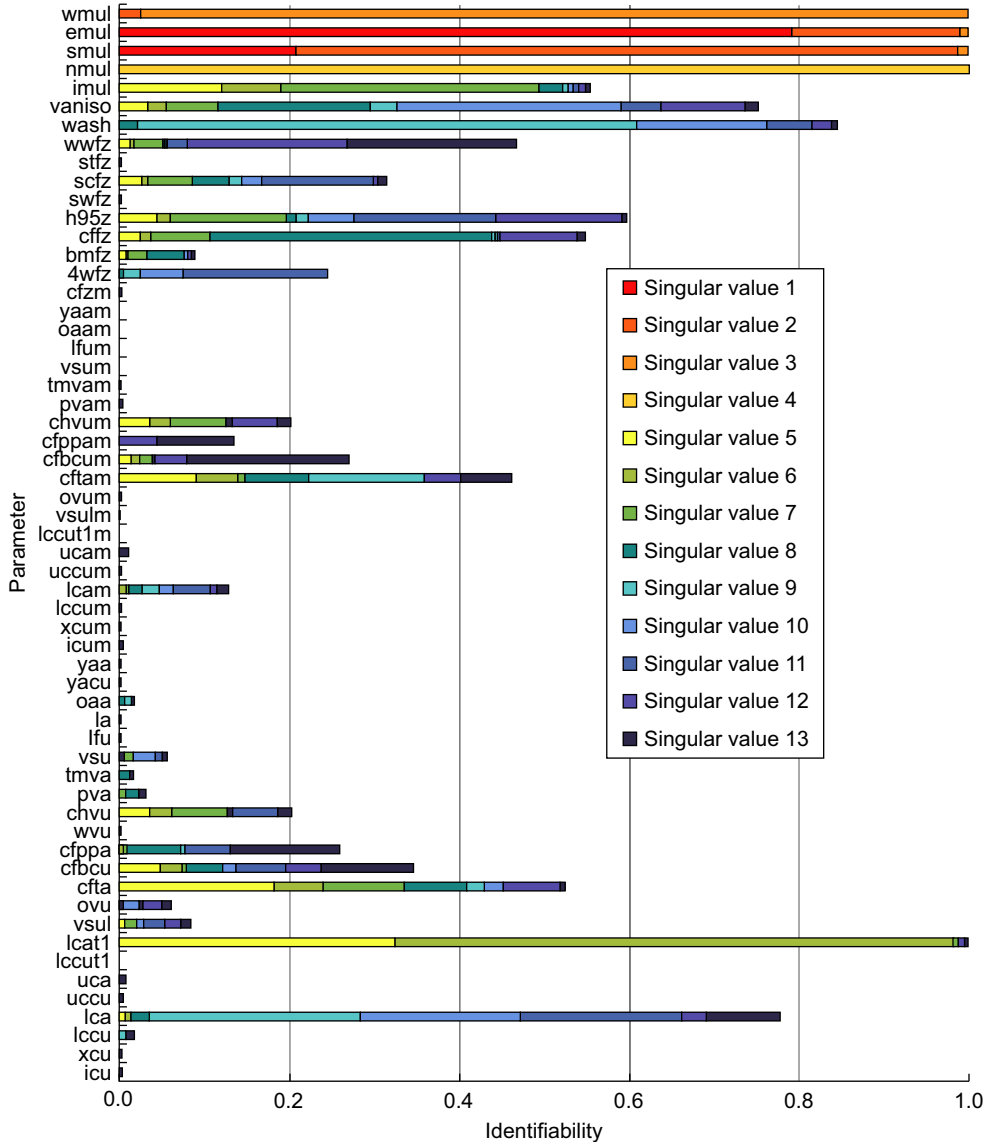


**Figure 10.10** Linear uncertainty analysis for a groundwater flow model of an arid hydrologic setting (Yucca Mountain, Nevada, USA). Parameter identifiability is used to judge parameters that are not constrained by the observation targets. A value of 1.0 indicates a completely identifiable parameter, i.e., one that is well constrained by the calibration targets and can be estimated by history matching. An identifiability of 0.0 represents complete unidentifiability—that is, the observations have no information to constrain the parameter and it cannot be estimated by history matching. Identifiability between the two extremes is more qualitative, whereby small bars are less identifiable and larger bars are relatively more identifiable. The color coding represents the strength of identifiability. Warmer colors represent parameters more supported by observation targets; cooler colors are parameters less supported by observation targets (James *et al.*, 2009).

Conversely, shorter bars indicate parameters that have a larger null-space component and are not as constrained by the observation data. Visualization of parameters that can be constrained by calibration, and those that cannot, can be valuable for assessing sources of forecast uncertainty and shortcomings in the existing observation data.

Another application of linear methods is discussed in [Box 10.3](#), where linear methods are used to assess the worth of future data collection. Reductions in forecast uncertainty that result from adding *potential observations* are evaluated for the purpose of evaluating proposed data collection schemes for their ability to reduce forecast uncertainty without

### Box 10.3 Cost-Benefit Analyses of Future Data Collection

Hydrologists are often asked what kind of monitoring network can most effectively support science-based water-resources management decisions. Commonly, hydrologic monitoring locations often are selected to fill gaps in the existing network or for convenience of access (e.g., near a road). A model calibrated to such available data, however, might be poorly suited for forecasting. [Fiene et al. \(2011\)](#) suggest that one of the most underappreciated uses of models is for calculating the reduction in uncertainty resulting from future data collection. Modeling tools are available that can help rank locations and types of data that are most important for a specific forecast. Put another way, these tools help the hydrologist determine observation data that most reduce uncertainty for a specific forecast. Such insights can help guide decisions for expansion of an existing monitoring network.

The capability to assess the worth of potential future observations (e.g., fluxes and heads) uses linear uncertainty analysis ([Section 10.4](#)) to identify the factors that contribute most to forecast uncertainty. This, in turn, allows formulation of *cost-benefit analyses* that can guide selection of the most cost-effective strategy of data gathering and/or modeling to reduce forecast uncertainty. The method is based on the concept of *potential observations*, which are those that might be included in future monitoring. Within the parameter estimation framework, potential observations are simply added to the real observations from the site area but are given zero weight. Evaluation of the worth of potential observations using linear analysis does not require that we actually know the observed value at the proposed monitoring locations – any arbitrary value can be used. It requires only that we know the proposed observations' location to calculate sensitivity. Such sensitivity is easily calculated using parameter estimation and is encapsulated in the Jacobian matrix ([Section 9.5](#)). Moreover, the Jacobian matrix can be calculated before or after the calibration process; thus, this approach is applicable to initial models developed in early stages of an investigation.

An advantage of a cost-benefit analysis is that limited monitoring resources can be focused on reducing forecast uncertainty, and relating those improvements to the cost of additional collection of field data. Data worth can be posed in terms of the addition of new data or subtraction of existing information by reducing monitoring efforts ([Beven, 1993, 2009](#)). Monitoring reduction is recognized as being potentially problematic because the ability to provide forecasts for future societal questions may be diminished by the loss of information, even if not critical for current forecasts. Detailed examples of the use of models in determining data worth are given by [Fiene et al. \(2010, 2011\)](#).

the expense of actually collecting the proposed data (e.g., Dausman et al., 2010; Fioren et al., 2010, 2011). Plots such as those in Fig. 10.10 could be updated for a number of potential future data collection activities spanning a range of cost and effort. This allows the modeler to convey the cost-benefit relation that forms the trade-off of additional field data collection and model forecast uncertainty reduction.

Though linear uncertainty results are typically quickly obtained, computationally frugal, and can be powerful, it must be noted that most groundwater modeling problems are not strictly linear (e.g., Vecchia and Cooley, 1987; Cooley, 1997). That is, the governing equation for groundwater flow and the output it produces are linear in the case of confined groundwater flow (Eqn. (3.13a)), but are nonlinear for unconfined groundwater flow (Eqn(3.12) and (3.13b)). Furthermore, in the context of uncertainty analysis, we refer to linearity in the inverse problem, which can also be linear or nonlinear. The degree of linearity in the underlying groundwater model is not a direct measure of the degree of linearity in the inverse problem (Mehl, 2007), because the function of interest is not the head solution but derivatives of heads with respect to parameter values (i.e., the parameter sensitivities discussed in Section 9.5). Although few groundwater modeling problems are strictly linear, recall that it is not possible to calculate true uncertainty even with an advanced uncertainty analysis because a model is never a true model of the groundwater system. Therefore, qualitative aspects of the analysis can be just as important as quantitative forecast error estimates (Gallagher and Doherty, 2007). Approximate estimates from linear uncertainty methods are often sufficient for purposes of engineering practice and decision-making, and can minimize computational cost while providing a theoretical basis.

## 10.5 ADVANCED UNCERTAINTY ANALYSIS

Advanced uncertainty methods provide similar uncertainty outputs (e.g., variance or 95% confidence intervals) as linear analyses but advanced uncertainty methods are more computationally demanding and generally require a higher level of user interaction with the software. Software is available for most of these approaches, either through the PEST Software Suite (Box 10.1) or other sources. New advanced methods are still being actively researched and new off-the-shelf software is being developed. In this section, we focus on advanced methods that have software readily available, which include both those that can be applied to a single base model and also those using multiple model conceptualizations.

### 10.5.1 Analysis Using One Conceptualization

Software is available for advanced methods that extend the linear uncertainty approach (Section 10.4) to nonlinear methods. In cases where a rigorous analysis of the best- or worst-case scenario is desired, a forecast uncertainty analysis can be posed as a constrained *maximization—minimization problem* (Figs. 10.11 and 10.12). In this method, a forecast is

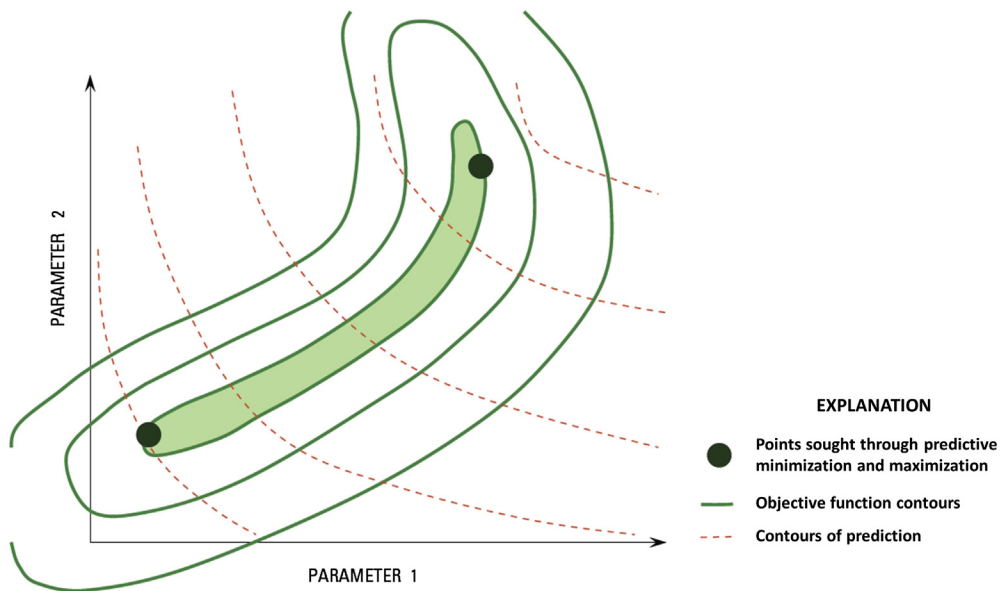


Figure 10.11 Schematic illustration of nonlinear calibration-constrained forecast maximization–minimization for a two-parameter problem (Doherty et al., 2010).

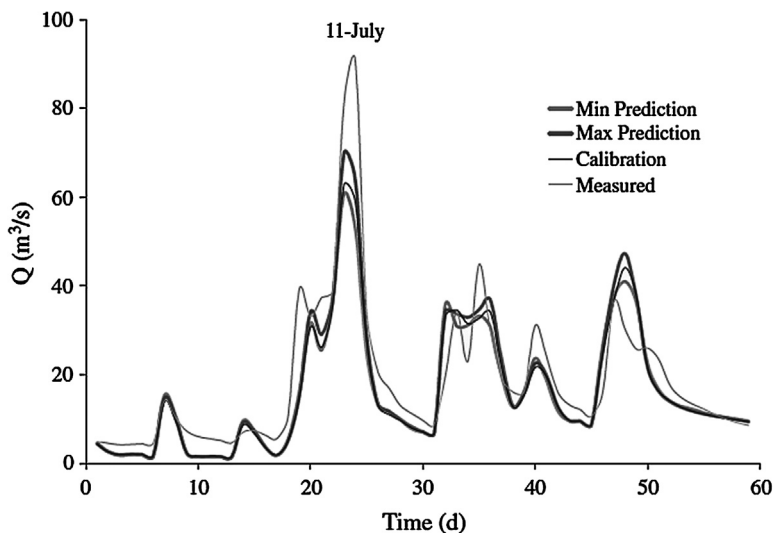


Figure 10.12 A comparison of measured streamflow to maximum and minimum forecasts calculated by using a constrained maximization and minimization approach shown in Fig. 10.10 (modified from Bahremand and De Smedt, 2010).

maximized or minimized subject to the constraint that the degradation of the objective function (Section 9.5) rises no higher than a user-specified value (Vecchia and Cooley, 1987; Christensen and Cooley, 1999; Cooley and Christensen, 2006; Tonkin et al., 2007b). That is, of the infinite number of possible forecasts, only those based on parameters consistent with the observation data need to be considered. Therefore, the forecast uncertainty simulation is designed to find the maximum or minimum output of interest that also conforms to the realm of what is reasonable (which in practice is an objective function constraint that is slightly higher than the objective function minimum achieved during the history matching phase of model calibration).

Fig. 10.11 illustrates a generalized two-parameter maximization–minimization problem. Dashed lines represent the forecast of interest for a range of values for parameters 1 (x-axis) and 2 (y-axis). The objective function surface (solid green lines) is also shown; there are multiple combinations of parameters 1 and 2 that provide an objective function low enough for the parameters to be considered to calibrate the model (green-shaded area). For uncertainty analysis, the minimum and maximum values of the forecast (two dots) are those that are reasonable given the constraints on the parameters provided by the calibration targets. That is, only those parameters considered calibrated are used for evaluating the forecast range. For many applied groundwater modeling problems, however, the maximization–minimization problem can be difficult to solve, especially in highly parameterized models (i.e., where there are many more axes than the two shown in Fig. 10.11). As described by James et al. (2009), most difficulties stem from a highly complex objective function surface, model instabilities, noisy derivatives in the Jacobian matrix, and high computational burden.

The conceptually straightforward *Monte Carlo Method* (Box 10.4) is the most common type of advanced uncertainty analysis, with many applications reported in the groundwater literature (e.g., Bair et al., 1991; Varljen and Shafer, 1991; Cooley, 1997; Hunt et al., 2001; Bogena et al., 2005; Starn et al., 2010; Yoon et al., 2013; Juckem et al., 2014). The method was pioneered in 1946 by Stanislaw Ulam, a physicist at Los Alamos National Laboratory in New Mexico (Eckhardt, 1987). Ulam was seeking a way “to change processes described by certain differential equations into an equivalent form interpretable as a succession of random operations.” In reference to the Monte Carlo Casino in Monaco, the code name “Monte Carlo” was selected to reflect the roots of the method in the probabilistic concepts of gambling.

For our purposes, the Monte Carlo method is considered a nonlinear method because it does not assume a linear relation between model inputs and forecast outputs a priori. Rather, it uses a large number of forward forecast simulations to explore uncertainty without making any assumptions about linearity. In basic linear uncertainty methods, a relatively small number of runs are typically executed. In a Monte Carlo analysis the forward model is typically run thousands to millions of times to define



### Box 10.4 Using Monte Carlo Methods to Represent Forecast Uncertainty

Hunt et al. (2001) forecast the area of contribution for a large spring complex using stochastic modeling with Monte Carlo methods. A three-layer groundwater flow model with particle tracking was used to identify a probability envelope for the area of contribution for the spring complex based on the estimated uncertainty in hydraulic conductivity. A stochastic version of MODFLOW (Ruskauff et al., 1998) was used to generate 200 realizations of the hydraulic conductivity field by randomly sampling a uniform distribution (Fig. 10.13) of horizontal hydraulic conductivity values defined from field data. Values varied between 1.5 and 4.6 m/d in layer 2 and between 0.2 and 3 m/d in layer 3. Twenty-five realizations were sufficient for convergence (Fig. B10.4.1(a)), but at least 100 realizations are recommended in stochastic modeling in order to ensure a representative probability distribution of model outputs.

Some of the 200 realizations did not yield a calibrated model (Fig. B10.4.1(b)) as judged by the mean absolute error (MAE) in heads; these simulations were removed, leaving 136 “conditioned” realizations. That is, the 136 realizations are conditional on the requirement that the MAE stay within range of an acceptable calibration, judged to be for  $MAE \leq 7.68$  m. Results from the 136 runs of the forward model were summarized by plotting the mean and standard deviations of the head field. All 136 forward runs were then used to track particles placed upgradient of the spring at the top of layers 2 and 3. A stochastic particle-tracking program (Stochastic MODPATH, Ruskauff et al., 1998) computed the probability of spring capture by summing how many times a model cell contributed particles to the spring and then dividing the sum by the 136 total realizations. Therefore, a result of 1.0 (100% probability) represents the case where a cell contributed to the spring in all 136 runs.

The map of the probability of spring capture (Fig. B10.4.2) shows that the area of contribution for the spring extends beyond the surface-water divide. Importantly, stochastic modeling allowed uncertainty to be represented to decision-makers interested in protecting the area of contribution for spring. The presentation of probability of capture in a readily understood graphic (Fig. B10.4.2) allowed decision-makers to assess the size and location of the spring’s area of contribution, which in turn facilitated the cost-benefit analysis that related trade-offs of protecting the spring to zoning restrictions on land use within the area of contribution.

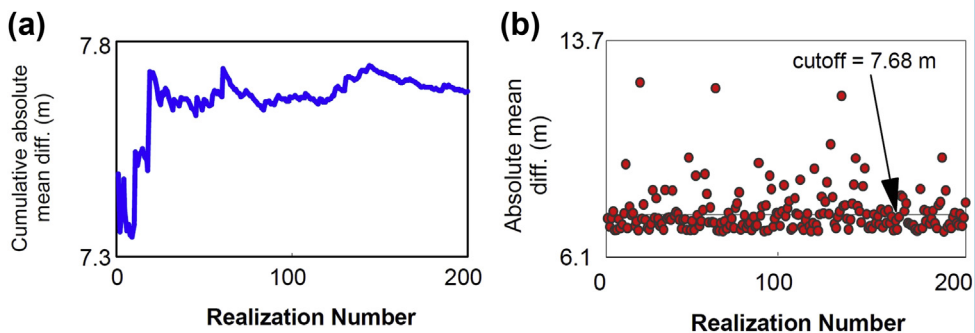


**Figure B10.4.1** Results of Monte Carlo simulations: (a) convergence of the Monte Carlo process is indicated by the relatively stable moving average MAE after 25 realizations; (b) large errors in head (large MAE) were addressed by conditioning the 200 runs by removing runs where the MAE was greater than 7.68 m (Hunt and Steuer, 2000).

### Box 10.4 Using Monte Carlo Methods to Represent Forecast Uncertainty—cont'd

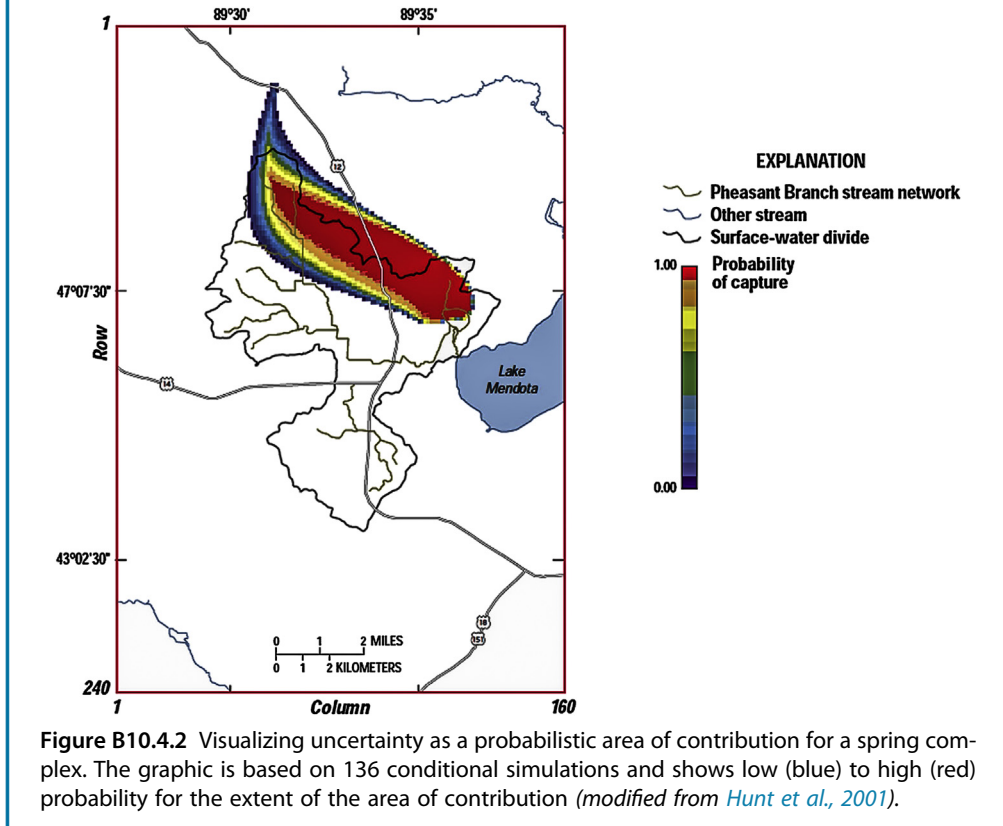


**Figure B10.4.2** Visualizing uncertainty as a probabilistic area of contribution for a spring complex. The graphic is based on 136 conditional simulations and shows low (blue) to high (red) probability for the extent of the area of contribution (modified from Hunt et al., 2001).

an uncertainty envelope around the forecast and statistically characterize the results. Moreover, parameters are defined probabilistically using modeler-specified distributions of parameter values, often represented by *probability density functions (pdf)* or a *cumulative density function (cdf)* (Fig. 10.13). The mechanics of generating a Monte Carlo data set in the context of groundwater modeling is covered in detail by Kitanidis (1997) and Zheng and Bennett (2002).

A schematic for a general Monte Carlo procedure is shown in Fig. 10.14, though in practice specially designed software is often used (e.g., Stochastic MODFLOW—Ruskauff et al., 1998; FePEST capabilities of FEFLOW). The distribution of parameters is sampled to create *realizations* of the parameter field, each of which

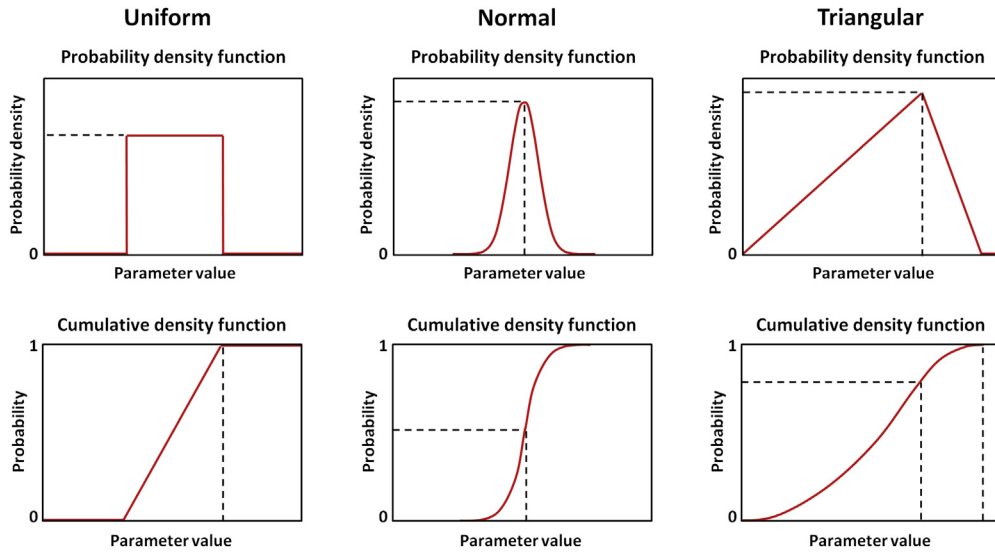


**Figure 10.13** Schematic representations of three different types of Probability Density Functions (PDFs—top row) and Cumulative Density Functions (CDFs—bottom row) used for parameters sampled in Monte Carlo analysis (after *NIST, 2012*).

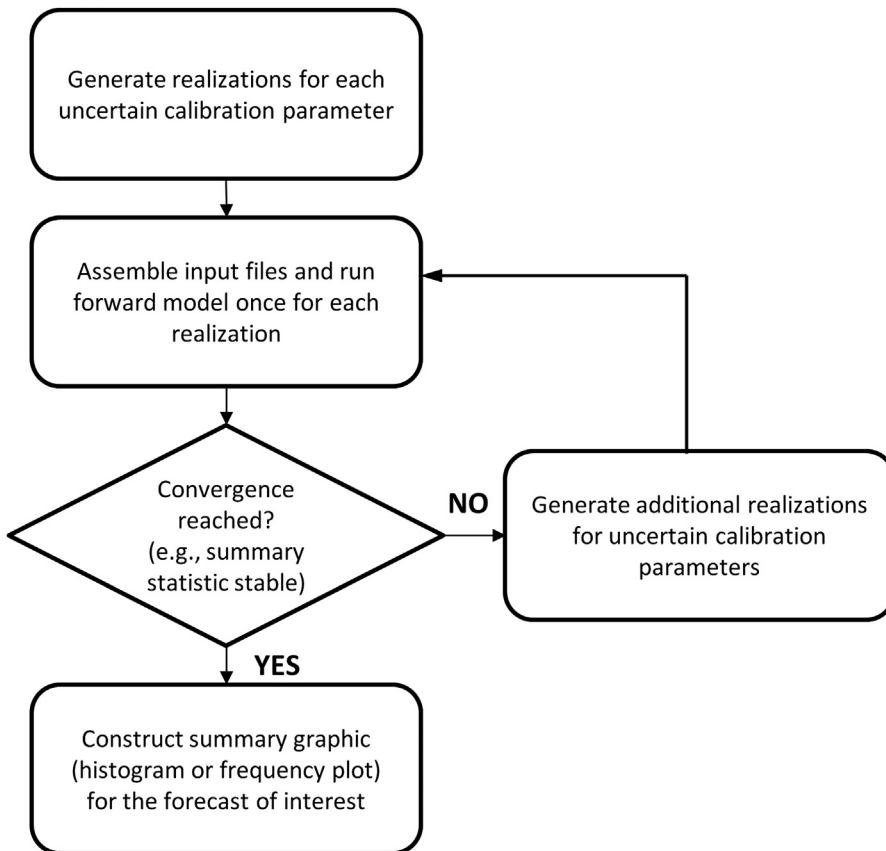


**Figure 10.14** Schematic workflow for performing Monte Carlo uncertainty analysis.

represents a different possible parameter set. A forward model is run once for each realization. The results of each forward run are tallied and the ensemble of results is summarized, usually in graphical form (e.g., Figs. B10.4.1 and B10.4.2 in Box 10.4). To determine whether a sufficient number of realizations have been considered, a second set of runs may be performed using a larger number of realizations and the statistics of both sets are compared. When the resulting ensembles of results have similar statistics (e.g., a similar mean absolute error in Fig. B10.4.1(a) in Box 10.4), the Monte Carlo process is said to have *converged*. The ensemble of Monte Carlo runs is typically reduced by *conditioning* such that realizations that fail to meet modeler-specified criteria (e.g., a calibration statistic such as mean absolute error, Fig. B10.4.1(b) in Box 10.4) are removed before compiling the results and reporting forecast uncertainty. Similar to bounding possible parameters in a maximization—minimization problem, conditioning guides the reporting of uncertainty estimates to include only forecast simulations consistent with what is known about the system, as expressed by fit to observation data. The resulting visualization of probability efficiently conveys uncertainty that surrounds a model output (e.g., Fig. 10.15).

To make the sampling of parameter combinations computationally more efficient, parameter combinations that tend to provide a reasonable fit to the calibration objective function can be favored, such as in *Markov Chain Monte Carlo* (MCMC) simulation. MCMC methods analyze the parameter probability functions to characterize a representative “desired” distribution. Therefore, rather than randomly sampling all possible parameter distributions as in Monte Carlo methods, the sampling is restricted to those in the desired distribution. Upon completion, MCMC results are used to construct standard statistical measures such as the 95% confidence interval around a forecast (Fig. 10.16). Examples using MCMC codes are described by Lu et al. (2004), Fienen et al. (2006), Hassan et al. (2009), Keating et al. (2010), Mariethoz et al. (2010), and Laloy et al. (2013).

Alternatively, a *null-space Monte Carlo* (NSMC) approach (Tonkin and Doherty, 2009) can be employed where the number of possible runs is reduced a priori to those that do not have an adverse effect on the calibration (i.e., reside in the null space, Section 9.6). Therefore, rather than running a complete ensemble of runs and removing runs afterward by conditioning, the full suite of realizations can be reduced before the Monte Carlo process begins (Fig. 10.17). NSMC methods are especially helpful for forecasts that depend on hydrologic system detail and require fine-scale parameterization (such as flowpaths and travel times). NSMC is incorporated into graphical user interfaces (e.g., GMS<sup>®</sup>, GroundwaterVistas<sup>®</sup>) and been applied to practical problems by Herckenrath et al. (2011), Yoon et al. (2013), Tavakoli et al. (2013) and Sepúlveda and Doherty (2015). Details of the NSMC method and tips for implementing it in PEST-based software are described in detail by Doherty et al. (2010).

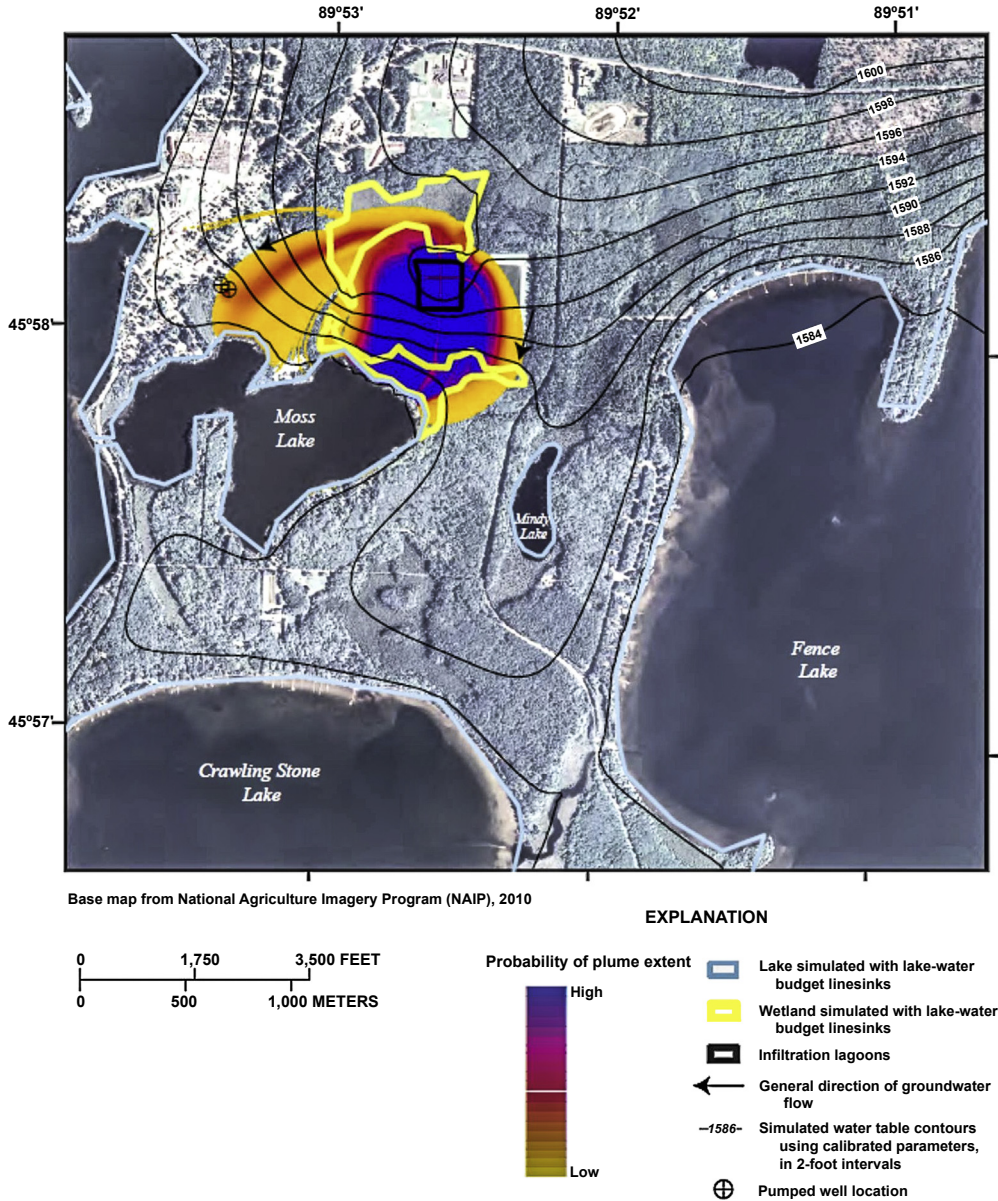


**Figure 10.15** Simulated probability due to uncertainty in advective transport parameters affecting a plume emanating from treatment lagoons. Blue color represents high probability flowpaths; orange colors represent low probability flowpaths (Juckem et al., 2014).

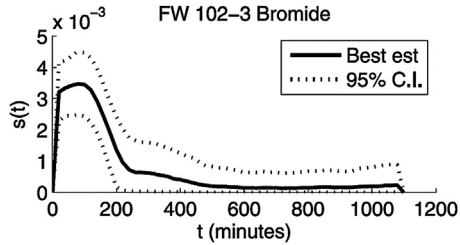


**Figure 10.16** Markov Chain Monte Carlo results showing the best estimate (solid line) and upper and lower 95% confidence intervals (dashed lines) for hypothetical injection and advective transport of bromide (modified from *Fioren et al., 2006*).

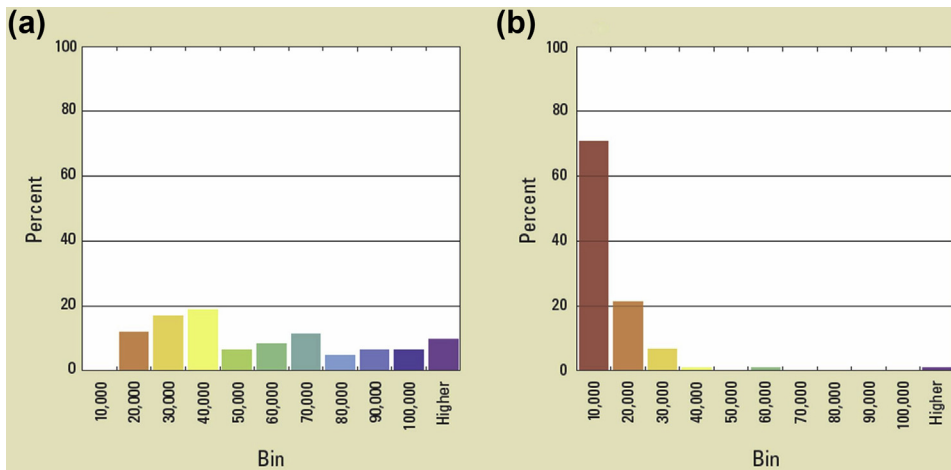


**Figure 10.17** Distribution of objective functions computed from 100 realizations with stochastic parameters: (a) before null-space projection and recalibration; (b) after null-space projection. Realizations sampled from (b) are much more likely to meet conditioning criteria. As a result, null-space Monte Carlo reduces the computational burden needed for the Monte Carlo process to converge (*Doherty et al., 2010*).

## 10.5.2 Analysis Using Multiple Conceptualizations

The uncertainty methods discussed above use alternative parameterizations based on one assumed model structure. However, forecast uncertainty may also include conceptualizations that are plausible but not readily accommodated via alternative parameterizations of the same model structure. For example, alternative models that include or omit a fault might require different nodal spacing and hence different model structures. Similarly, models with different physical processes included and omitted would be considered to have different model conceptualizations. To evaluate uncertainty that results from

different conceptual models, *multiple conceptualizations* can be considered in the uncertainty analysis. Detailed description of these methodologies is beyond the scope of our book; further information can be found in Pappenberger and Beven (2006), Poeter and Hill (2007), Vrugt et al. (2008), Singh et al. (2010), and Keating et al. (2010), and references cited below.

When considering multiple conceptualizations, the objective is to retain and weight (or rank) in terms of likelihood all the models that are acceptable or *behavioral*, and to reject models that are not behavioral. Behavioral models are those that reproduce historical observations within some tolerance limit and contain features consistent with the conceptual model. An inherent difficulty with ranking multiple conceptualizations is defining the optimal way to assess *likelihood* of each alternative forecast model—a topic that is being actively researched. One issue is that most criteria for determining likelihood still use calibration targets even though conditions simulated by the base model do not necessarily reflect conditions of the forecast. Therefore, likelihood criteria based on calibration data can only be considered surrogates for the true forecast likelihood.

Singh et al. (2010) divide uncertainty analysis using multiple conceptualizations into two broad categories, where the goal of both is to develop a forecast probability. First, there are those that use Monte Carlo sampling across multiple conceptual models and parameterizations. Of these, *General Likelihood Uncertainty Estimation (GLUE)* (Beven and Binley, 1992; Beven, 2009) is most widely used. GLUE was developed for surface-water modeling, but has also been applied to groundwater models (e.g., Christensen, 2004; Hassan et al., 2008; Singh et al., 2010; Ye et al., 2010). In a general sense, the approach is similar to Monte Carlo methods applied to one calibrated model. In GLUE, however, it is acknowledged that in an open system a given end state of that system can be reached by many potential means. Therefore, multiple conceptual models (and associated model structures) can be expected to represent processes and hydrologic responses equally well. These equally acceptable models are called *equifinal*, a term derived from General Systems Theory (von Bertalanffy, 1968). GLUE extends the simple Bayes' theorem approaches by recognizing that initial assumptions about the natural world, such as expressed by our choice of model structure, error structure, and parameterization, directly influence what is deemed behavioral and thus affect the analysis of forecast uncertainty. GLUE allows more flexibility in the likelihood function used to develop the set of behavioral models, though still typically evaluates the family of possible outcomes of equifinal models and weights their forecasts based on the history-matching comparison to field observations. By using a Monte Carlo approach to simulate many forward model runs, each conceptualization and associated forecast can be assigned a probability.

The second broad category uses statistical “information criteria” to develop the forecast probabilities obtained from multiple model conceptualizations and

parameterizations. These statistical metrics include Akaike (Akaike, 1973), Bayesian (Schwarz, 1978), and Kashyap (Kashyap, 1982) Information Criterion (AIC, BIC, and KIC, respectively). These metrics are less computationally intensive than the Monte Carlo approaches, but assume an error structure and use properties of the model such as number of parameters and observations to determine model quality. For example, *Maximum Likelihood Bayesian Model Averaging (MLBMA)* (e.g., Neuman, 2003) uses BIC and KIC statistics along with model fit to weight forecasts from each conceptualization. *Akaike Information Criterion-based Model Averaging (AICMA)* (Poeter and Anderson, 2005) is similar in concept to MLBMA but uses AIC criteria to weight forecasts from different model conceptualizations. One issue for applied groundwater modeling is that the statistical theory underlying information criteria approaches was not developed for groundwater modeling. For example, the original theoretical development defines “parameter” as an independent new process or other major change to the model—a stark contrast to groundwater models where a new pilot point or zone is considered an additional parameter. Therefore, the information criteria penalty assessed according to the number of model parameters may give preference to oversimplified groundwater models.

In Chapter 9 and elsewhere in the text, we stressed the desirability of not restricting a model’s representation of the natural world to a single conceptualization. However, multiple conceptualizations currently are not widely used in applied groundwater modeling for uncertainty analysis. This is due to a number of factors: (1) there is an associated high computational burden to evaluate multiple models; (2) software for modeling applied problems is immature; and (3) there is a troublesome lack of agreement among methods (e.g., Table 3 in Singh et al., 2010). One source of the lack of agreement among methods likely relates to the penalty for the number of model parameters in information criteria methods; penalty criteria are absent in GLUE. A simple parameter penalty approach based on the number of groundwater model parameters is not consistent with information criteria statistical theory, especially for highly parameterized models of naturally complex systems. In recognition of this issue, Singh et al. (2010) reduced the number of model parameters used in their information criteria evaluations to 15 linear combinations of the calibration parameters constrained by observation targets (i.e., solution space parameters defined by singular value decomposition—Section 9.6). However, even with such an adjustment to make groundwater model parameters more in line with the statistical theory, agreement between GLUE and the information criteria methods was poor. Therefore, although considering multiple conceptual models is encouraged, formal methods for performing an uncertainty analysis using multiple models are still developing. Hence, hydrosense and professional judgment are needed when multiple models are considered.



## 10.6 REPORTING FORECAST UNCERTAINTY

Regardless of the method(s) used to estimate uncertainty, effective communication of results to decision-makers is critically important to the successful completion of the modeling project. Just as there is no reasonable expectation that a model can represent all details of the field situation, there can be no expectation that the uncertainty analysis gives a precise report of true uncertainty. Therefore, the objective of uncertainty reporting is to clearly present the modeler's estimate of the representative uncertainty given what is known about the system, the type of forecast(s), and the modeler's experience with the model and model calibration.

Because uncertainty is a wide-ranging concept in popular and scientific literature, unambiguous communication is important. We suggest that terminology described by the International Panel on Climate Change (IPCC, 2014) becomes the standard for applied modeling because it provides a widely scrutinized vocabulary for environmental modeling where uncertainty in specific outcomes is assessed using expert judgment and statistical analysis. The IPCC suggest that specific terms be applied to the assessment of forecast probability (Table 10.3). In addition, model forecasts and associated uncertainty results should be reported with a precision (e.g., significant figures) that aligns with the modeling assumptions and quality of observations available. Presenting results with unrealistic precision can undermine the confidence in the calibration, forecast(s), and uncertainty analysis.

In many cases, the terms in Table 10.3 will augment but not replace other more encompassing statistical descriptions of forecast uncertainty. In these cases, the modeler must realize that decision-makers, regulators, and other users of model results may not be familiar with theoretical aspects of uncertainty analysis. Therefore, it is incumbent on the modeler to provide a presentation of uncertainty in a format most directly

**Table 10.3** Uncertainty terms and related forecast probability (IPCC, 2014)

Phrase used	Associated forecast probability
Virtually certain	>99%
Extremely likely	>95%
Very likely	>90%
Likely	>66%
More likely than not	>50%
About as likely as not	33–66%
Unlikely	<33%
Very unlikely	<10%
Extremely unlikely	<5%
Exceptionally unlikely	<1%

applicable to the decision of interest, and translate uncertainty to the stakeholders' forecasts of interest. This can be especially important when the model is used in adversarial proceedings; that is, "a modeler will minimize the effect of the opposition's claims of uncertainty by actually quantifying the uncertainty" (Myers, 2007).

To convey the maximum amount of information quickly, visual presentations (e.g., graphs—Fig. 10.5; maps—Fig. 10.1, 10.15; B10.4.2 in Box 10.4) are preferred over tables and text. Ideally, the visual depiction should either convey the uncertainty limits around a single forecast (e.g., error bars, box-and-whisker plots) or represent the uncertainty in the ensemble of results from multiple simulations of a specific forecast (Figs. 10.7; B10.4.2 in Box 10.4). Relating uncertainty in a forecast to its component parts (Fig. 10.9) can articulate what is and is not known given the modeling performed. If uncertainty around a forecast is too large, the worth of additional data collection can be weighed according to its ability to constrain model parameters important for the forecast (Fig. 10.10), or for other potential forecasts of interest.

For many forecasts, uncertainty is best represented probabilistically; for example, a probabilistic map view of capture effectively summarizes the probability that groundwater will flow to a spring (Fig. B10.4.2 in Box 10.4). In cases where decisions are thresholds that precipitate action, determinations of a reasonable best- or worst-case scenario are helpful because they can be expressed as an envelope of forecasts given what is known about the system and expected in the future (Fig. 10.7). This can be done as a constrained maximization—minimization problem where the bounds of what is reasonable for a forecast are determined by an acceptable calibration degradation specified by the modeler (Fig. 10.11). Or, the full range of forecast values can be displayed as a Pareto front diagram (Fig. B10.2.2 in Box 10.2). Such a presentation frees the modeler from the need to specify an allowable degradation, which in turn lets the decision-maker directly decide the likelihood that an action threshold would be crossed. Regardless of visualization chosen, results of uncertainty analyses are best related in terms that can be directly used by the decision-maker without extraneous extrapolation or inference.

## 10.7 EVALUATING FORECASTS: POSTAUDITS

A *postaudit* is a comparison between conditions simulated in a forecast and conditions that actually occurred. Therefore, postaudits require collection of field data at a future time simulated in the forecast. Several postaudits were performed in the 1980s to 1990s (e.g., Konikow and Person, 1985; Konikow, 1995) when sufficient time had passed after the first forecasts were made with early groundwater flow models in the 1960s and 1970s.

However, even though it is likely that there have been tens of thousands of forecasts by groundwater models since the 1960s, few postaudits are reported in the literature. There are many reasons for this, both practical and philosophical. Practically speaking, models are most often designed to solve an immediate problem so that a management

decision can be made. After the model has served this purpose, it is typically “shelved.” Usually, these models are not updated. Alternatively, some models are designed to be continually updated as long-term tools in *adaptive management*. Adaptive management is a structured, iterative process of decision-making with the objective of reducing uncertainty over time via system monitoring and model improvement. Or, put in more general terms, adaptive management means being prepared to change strategy as the future unfolds in a system regularly monitored and reviewed (Beven, 2009, p. 239).

In other fields such as weather forecasting, it is recognized that real-time information (information about what is currently happening in the system) can be used in the forecast simulation to improve the forecast. This is done by *data assimilation* for *adaptive forecasting* (Beven, 2009, p. 22), where data assimilation refers to using new data as they become available to update the model. In these types of modeling, it is expected that the model will be continually updated and therefore a postaudit is unnecessary. Similarly, models are increasingly being used for long-term management (see Jorgensen, 1981 for an early use of groundwater models for long-term management; see also De Lange, 2006). Sometimes these types of long-term modeling efforts are driven by regulatory requirements, such as in Europe where groundwater management models are required by law (e.g., the European Water Framework Directive — Hulme et al., 2002; Shepley et al., 2012). Updates are expected or required, and a formal postaudit snapshot contributes little.

On more philosophical grounds, postaudits can illustrate the pit falls in attempting to forecast future conditions. Early postaudits (Konikow, 1995) showed that model forecasts fail owing to modeler error, improper conceptual models, and failure to estimate future stresses accurately. Experience gained from formal and informal postaudits underscored the importance of the now widely understood influence of unanticipated changes that frequently occur after the forecast is made. For example, in one case, the trend in baseflow assumed for the forecast did not reflect the baseflow conditions that actually occurred, which made for poor model forecasts (Konikow and Person, 1985).

Unanticipated changes can also include changes in sources and sinks such as installation of new high-capacity wells, drainage tiles, canals, as well as unanticipated changes in recharge rates, pumping rates, and other stresses. These factors can change the groundwater system such that any forecast that did not include them falls short, regardless of the sophistication of the base model(s) and associated uncertainty analysis. In this way, postaudits will often tell us what we already know: “surprise is a part of science” (Bredehoeft, 2005). Surprise is endemic to our modeling efforts and will always be an unquantifiable uncertainty added to all model forecasts (e.g., Hunt and Welter, 2010). Although postaudits may help optimize the performance of an existing pump-and-treat system, for example, and are integrated into the concept of adaptive management, ultimately they cannot overcome uncertainty intrinsic to forecasts made in a world dominated by “unknown unknowns.”

## 10.8 COMMON MODELING ERRORS

- A model forecast is presented without discussion or reporting of representative uncertainty.
- A type of forecast is chosen (e.g., absolute model output, extreme ranges in future conditions) that has relatively higher uncertainty than other types of forecasts (e.g., relative model outputs, average conditions—Section 10.3) that would have also addressed the modeling objective effectively.
- Uncertainty analysis is performed as an afterthought and is focused only on those factors easiest to analyze. For example, an uncertainty analysis that only includes uncertainty associated with the base model, when uncertainty in future events is also a significant contributor to total forecast uncertainty, underestimates expected uncertainty.
- Parameter simplification error is not considered in the uncertainty analysis. Simplification error is especially important in sparsely parameterized models where it is typically the largest component of uncertainty.
- The model forecast and resulting uncertainty are reported with more precision (e.g., significant figures) than is warranted by the modeling assumptions and observation. Presenting overly precise results undermines confidence in the modeling effort.
- Uncertainty analysis is reported in a way that stakeholders cannot understand.
- Uncertainty results are provided to decision-makers in ways that are easy for the modeler to report, but not easy to apply to the decision of interest.
- Reported forecasts and uncertainty are overestimated or underestimated to yield a result that advances a stakeholder's preference.
- Uncertainty analysis is performed by changing one parameter at a time when the decision-making requires a best- or worst-case scenario that relies on combinations of factors.
- Forecasts and uncertainty are not discussed in terms of probabilities when it is possible to do so. Estimates of uncertainty expressed as a probability are best for translating model uncertainty to cost-benefit analyses.

## 10.9 PROBLEMS

The problems for Chapter 10 use the base model developed in Chapter 9 for forecasting and forecast uncertainty analysis.

- P10.1** Use parameter values and initial conditions from the base model from the problems in Chapter 9 and run a transient model to forecast the head distribution resulting from continuously pumping a new well at location M (Fig. P9.1) at a constant rate of  $30,000 \text{ m}^3/\text{d}$  for 1 year. Do not calibrate the transient model. Compare the simulated heads with measured heads reported in Table P10.1; you would not

**Table P10.1** Measured heads after 1 year of pumping

Well	Row	Column	Head (m) <sup>a</sup>
P	3	4	508.53
G	5	8	506.84
F	5	11	506.25
N	6	4	509.78
J	7	2	511.62
E	7	8	507.68
A	7	11	507.27
B	7	14	507.63
K	8	11	507.76
Q	9	7	510.00
M	9	9	504.36
I	10	4	512.82
D	10	11	509.44
C	10	14	510.12
O	11	8	511.08
H	13	11	512.94
S	14	2	515.85

<sup>a</sup>heads after 1 year of pumping well M, all heads are averages.

have these values when a forecast is made, but are available here because they were generated for a synthetic problem. Compare the simulated heads with measured heads reported in [Table P10.1](#). Discuss the criteria you would use to decide if your model is a reasonable representation of the hydrogeologic conditions at the site. Is a transient calibration necessary?

- P10.2** The forecast in problem P10.1 assumed that hydrologic conditions remained constant except for the introduction of the new pumping well. Perform a linear uncertainty analysis ([Fig. 10.6](#)) to quantify uncertainty in the forecast including structural error and future uncertainty. (For example, future political, sociological, and economical conditions might make it necessary to increase or decrease the pumping rate of well M, or necessitate seasonal variations in the pumping rate. Also, the areal recharge rate might change in the future.) Use graphics to display your results and prepare a visual presentation to convey results to stakeholders, who include the farmers downstream of the well and the local regulatory agency.
- P10.3** Use one or more of the advanced uncertainty analyses discussed in [Section 10.5](#) to quantify uncertainty and present results visually in a form suitable for the stakeholders mentioned in problem P10.2.
- P10.4** Compare and contrast the results of your results from problems P10.1, P10.2, and P10.3. Which analysis would you present to the stakeholders?

## REFERENCES

- Akaike, H., 1973. Information theory as an extension of the maximum likelihood principle. In: Petrov, B.N. (Ed.), Second International Symposium on Information Theory. Akademiai Kiado, Budapest, Hungary, pp. 267–281.
- Aster, R.C., Borchers, B., Thurber, C.H., 2013. Parameter Estimation and Inverse Problems, second ed. Academic Press, Waltham, MA. 360 p.
- Bair, E.S., Safreed, C.M., Stasny, E.A., 1991. A Monte Carlo-based approach for determining travel time-related capture zones of wells using convex hulls as confidence regions. *Groundwater* 29 (6), 849–855. <http://dx.doi.org/10.1111/j.1745-6584.1991.tb00571.x>.
- Barnett, B., Townley, L.R., Post, V., Evans, R.E., Hunt, R.J., Peeters, L., Richardson, S., Werner, A.D., Knapp, A., Boronkay, A., 2012. Australian Groundwater Modelling Guidelines. Waterlines Report, vol. 82. National Water Commission, Canberra, ISBN 978-1-921853-91-3, 191 p.
- Bahreman, A., De Smedt, F., 2010. Predictive analysis and simulation uncertainty of a distributed hydrological model. *Water Resources Management* 24 (12), 2869–2880. <http://dx.doi.org/10.1007/s11269-010-9584-1>.
- Beven, K., Binley, A., 1992. The future of distributed models: Model calibration and uncertainty prediction. *Hydrological Processes* 6 (3), 279–298. <http://dx.doi.org/10.1002/hyp.3360060305>.
- Beven, K.J., 1993. Prophecy, reality and uncertainty in distributed hydrological modeling. *Advances in Water Resources* 16 (1), 41–51. [http://dx.doi.org/10.1016/0309-1708\(93\)90028-E](http://dx.doi.org/10.1016/0309-1708(93)90028-E).
- Beven, K.J., 2005. On the concept of model structural error. *Water Science and Technology* 52 (6), 167–175. <http://www.iwaponline.com/wst/05206/wst052060167.htm>.
- Beven, K.J., 2009. Environmental Modelling: An Uncertain Future? An Introduction to Techniques for Uncertainty Estimation in Environmental Prediction. Routledge, 310 p.
- Beven, K.J., Young, P., 2013. A guide to good practice in modeling semantics for authors and referees. *Water Resources Research* 49 (8), 5092–5098. <http://dx.doi.org/10.1002/wrcr.20393>.
- Bogena, H., Kunkel, R., Montzka, C., Wendland, F., 2005. Uncertainties in the simulation of groundwater recharge at different scales. *Advances in Geosciences* 5, 25–30. <http://dx.doi.org/10.5194/adgeo-5-25-2005>.
- Bradbury, K.R., Borchardt, M.A., Gotkowitz, M., Spencer, S.K., Zhu, J., Hunt, R.J., 2013. Source and transport of human enteric viruses in deep municipal water supply wells. *Environmental Science and Technology* 47 (9), 4096–4103. <http://dx.doi.org/10.1021/es100698m>.
- Bredehoeft, J.D., 2005. The conceptual model problem—surprise. *Hydrogeology Journal* 13 (1), 37–46. <http://dx.doi.org/10.1007/s10040-004-0430-5>.
- Cardiff, M., Barrash, W., Kitanidis, P.K., 2013. Hydraulic conductivity imaging from 3-D transient hydraulic tomography at several pumping/observation densities. *Water Resources Research* 49 (11), 7311–7326. <http://dx.doi.org/10.1002/wrcr.20519>.
- Carrera, J., Neuman, S.P., 1986a. Estimation of aquifer parameters under transient and steady state conditions: 1. Maximum likelihood method incorporating prior information. *Water Resources Research* 22 (2), 199–210. <http://dx.doi.org/10.1029/WR022i002p00199>.
- Carrera, J., Neuman, S.P., 1986b. Estimation of aquifer parameters under transient and steady state conditions: 2. Uniqueness, stability, and solution algorithms. *Water Resources Research* 22 (2), 211–227. <http://dx.doi.org/10.1029/WR022i002p00211>.
- Carrera, J., Neuman, S.P., 1986c. Estimation of aquifer parameters under transient and steady state conditions: 3. Application to synthetic and field data. *Water Resources Research* 22 (2), 228–242. <http://dx.doi.org/10.1029/WR022i002p00228>.
- Christensen, S., 2004. A synthetic groundwater modelling study of the accuracy of GLUE uncertainty intervals. *Nordic Hydrology* 35, 45–59. <http://www.iwaponline.com/nh/035/nh0350045.htm>.
- Christensen, S., Cooley, R.L., 1999. Evaluation of prediction intervals for expressing uncertainties in groundwater flow model predictions. *Water Resources Research* 35 (9), 2627–2639. <http://dx.doi.org/10.1029/1999WR900163>.
- Christensen, S., Doherty, J., 2008. Predictive error dependencies when using pilot points and singular value decomposition in groundwater model calibration. *Advances in Water Resources* 31 (4), 674–700. <http://dx.doi.org/10.1016/j.advwatres.2008.01.003>.

- Cooley, R.L., 1977. A method of estimating parameters and assessing reliability for models of steady state groundwater flow, 1. Theory and numerical properties. *Water Resources Research* 13 (2), 318–324. <http://dx.doi.org/10.1029/WR013i002p00318>.
- Cooley, R.L., 1979. A method of estimating parameters and assessing reliability for models of steady state groundwater flow, 2. Application of statistical analysis. *Water Resources Research* 15 (3), 603–617. <http://dx.doi.org/10.1029/WR015i003p00603>.
- Cooley, R.L., 1997. Confidence intervals for ground-water models using linearization, likelihood, and bootstrap methods. *Groundwater* 35 (5), 869–880. <http://dx.doi.org/10.1111/j.1745-6584.1997.tb00155.x>.
- Cooley, R.L., 2004. A theory for modeling ground-water flow in heterogeneous media. U.S. Geological Survey Professional Paper 1679, 220 p. <http://pubs.er.usgs.gov/publication/pp1679>.
- Cooley, R.L., Christensen, S., 2006. Bias and uncertainty in regression-calibrated models of groundwater flow in heterogeneous media. *Advances in Water Resources* 29 (5), 639–656. <http://dx.doi.org/10.1016/j.advwatres.2005.07.012>.
- Dagan, G., 1986. Statistical theory of groundwater flow and transport: Pore to laboratory, laboratory to formation, and formation to regional scale. *Water Resources Research* 22 (9S), 120S–134S. <http://dx.doi.org/10.1029/WR022i09Sp0120S>.
- Dagan, G., 1989. *Flow and Transport in Porous Formations*. Springer-Verlag, Heidelberg, Berlin, New York, 465 p.
- Dausman, A.M., Doherty, J., Langevin, C.D., Sukop, M.C., 2010. Quantifying data worth toward reducing predictive uncertainty. *Groundwater* 48 (5), 729–740. <http://dx.doi.org/10.1111/j.1745-6584.2010.00679.x>.
- De Lange, W.J., 2006. Development of an analytic element ground water model of the Netherlands. *Groundwater* 44 (1), 111–115. <http://dx.doi.org/10.1111/j.1745-6584.2005.00142.x>.
- Doherty, J., 2011. Modeling: Picture perfect or abstract art? *Groundwater* 49 (4), 455. <http://dx.doi.org/10.1111/j.1745-6584.2011.00812.x>.
- Doherty, J., Hunt, R.J., 2009a. Two statistics for evaluating parameter identifiability and error reduction. *Journal of Hydrology* 366 (1–4), 119–127. <http://dx.doi.org/10.1016/j.jhydrol.2008.12.018>.
- Doherty, J., Hunt, R.J., 2009b. Response to comment on: Two statistics for evaluating parameter identifiability and error reduction. *Journal of Hydrology* 380 (3–4), 481–488. <http://dx.doi.org/10.1016/j.jhydrol.2009.10.012>.
- Doherty, J.E., 2015. *Calibration and Uncertainty Analysis for Complex Environmental Models*. Watermark Numerical Computing, Brisbane, Australia, 227 p.
- Doherty, J.E., Hunt, R.J., 2010. Approaches to highly parameterized inversion: A guide to using PEST for groundwater-model calibration. U.S. Geological Survey Scientific Investigations Report 2010-5169, 60 p. <http://pubs.usgs.gov/sir/2010/5169/>.
- Doherty, J.E., Hunt, R.J., Tonkin, M.J., 2010. Approaches to highly parameterized inversion: A guide to using PEST for model-parameter and predictive-uncertainty analysis. U.S. Geological Survey Scientific Investigations Report 2010-5211, 71 p. <http://pubs.usgs.gov/sir/2010/5211/>.
- Doherty, J., Simmons, C.T., 2013. Groundwater modeling in decision support: Reflections on a unified conceptual framework. *Hydrogeology Journal* 21 (7), 1531–1537. <http://dx.doi.org/10.1007/s10040-013-1027-7>.
- Doherty, J., Welter, D.E., 2010. A short exploration of structural noise. *Water Resources Research* 46 (5), W05525. <http://dx.doi.org/10.1029/2009WR008377>.
- Eckhardt, R., 1987. Stan Ulam, John von Neumann, and the Monte Carlo method. *Los Alamos Science* 15, 131–137. <http://la-science.lanl.gov/lascience15.shtml>.
- Ely, D.M., Kahle, S.C., 2004. Conceptual model and numerical simulation of the ground-water-flow system in the unconsolidated deposits of the Colville River Watershed, Stevens County, Washington. U.S. Geological Survey Scientific Investigations Report 2004-5237, 72 p. <http://pubs.usgs.gov/sir/2004/5237/>.
- Ely, D.M., Bachmann, M.P., Vaccaro, J.J., 2011. Numerical simulation of groundwater flow for the Yakima River basin aquifer system, Washington. U.S. Geological Survey Scientific Investigations Report 2011-5155, 90 p. <http://pubs.usgs.gov/sir/2011/5155/>.
- Fienen, M.N., 2013. We speak for the data. *Groundwater* 51 (2), 157. <http://dx.doi.org/10.1111/gwat.12018>.

- Fienen, M.N., Luo, J., Kitanidis, P.K., 2006. A Bayesian geostatistical transfer function approach to tracer test analysis. *Water Resources Research* 42 (7), W07426. <http://dx.doi.org/10.1029/2005WR004576>.
- Fienen, M., Hunt, R., Krabbenhoft, D., Clemo, T., 2009. Obtaining parsimonious hydraulic conductivity fields using head and transport observations: A Bayesian geostatistical parameter estimation approach. *Water Resources Research* 45 (8), W08405. <http://dx.doi.org/10.1029/2008WR007431>.
- Fienen, M.N., Doherty, J.E., Hunt, R.J., Reeves, H.W., 2010. Using prediction uncertainty analysis to design hydrologic monitoring networks—Example applications from the Great Lakes Water Availability Pilot Project. U.S. Geological Survey Scientific Investigations Report 2010-5159, 44 p. <http://pubs.usgs.gov/sir/2010/5159/>.
- Fienen, M.N., Hunt, R.J., Doherty, J.E., Reeves, H.W., 2011. Using models for the optimization of hydrologic monitoring. U.S. Geological Survey Fact Sheet 2011-3014, 6 p. <http://pubs.usgs.gov/fs/2011/3014/>.
- Fienen, M.N., Doria, M., Doherty, J.E., Hunt, R.J., 2013. Approaches in highly parameterized inversion: bgaPEST, a Bayesian Geostatistical Approach Implementation with PEST. U.S. Geological Survey Techniques and Methods. Book 7, Section C, Chapter 9, 86 p. <http://pubs.usgs.gov/tm/07/c09/>.
- Freeze, R.A., 1975. A stochastic-conceptual analysis of one-dimensional groundwater flow in nonuniform homogeneous media. *Water Resources Research* 11 (5), 725–741. <http://dx.doi.org/10.1029/WR011i005p00725>.
- Freeze, R.A., Massmann, J., Smith, L., Sperling, T., James, B., 1990. Hydrogeological decision analysis: 1. A framework. *Groundwater* 28 (5), 738–766. <http://dx.doi.org/10.1111/j.1745-6584.1990.tb01989.x>.
- Freeze, R.A., Massmann, J., Sperling, T., Smith, L., 1992. Hydrogeological decision analysis: 4. The concept of data worth and its use in the development of site investigation strategies. *Groundwater* 30 (4), 574–588. <http://dx.doi.org/10.1111/j.1745-6584.1992.tb01534.x>.
- Gaganis, P., Smith, L., 2001. A Bayesian approach to the quantification of the effect of model error on the predictions of groundwater models. *Water Resources Research* 37 (9), 2309–2322. <http://dx.doi.org/10.1029/2000WR000001>.
- Gallagher, M., Doherty, J., 2007. Predictive error analysis for a water resource management model. *Journal of Hydrology* 334 (3–4), 513–533. <http://dx.doi.org/10.1016/j.jhydrol.2006.10.037>.
- Gelhar, L.W., 1993. *Stochastic Subsurface Hydrology*. Prentice Hall, 390 p.
- Golub, G.H., Van Loan, C.F., 2012. *Matrix Computations*, fourth ed. Johns Hopkins University Press, 784 p.
- Hassan, H.E., Bekhit, H.M., Chapman, J.B., 2008. Uncertainty assessment of a stochastic groundwater flow model using GLUE analysis. *Journal of Hydrology* 362 (1–2), 89–109. <http://dx.doi.org/10.1016/j.jhydrol.2008.08.017>.
- Hassan, A.E., Bekhit, H.M., Chapman, J.B., 2009. Using Markov Chain Monte Carlo to quantify parameter uncertainty and its effect on predictions of a groundwater flow model. *Environmental Modelling and Software* 24 (6), 749–763. <http://dx.doi.org/10.1016/j.envsoft.2008.11.002>.
- Herckenrath, D., Langevin, C.D., Doherty, J., 2011. Predictive uncertainty analysis of a saltwater intrusion model using null-space Monte Carlo. *Water Resources Research* 47 (5), W05504. <http://dx.doi.org/10.1029/2010WR009342>.
- Hill, M.C., Tiedeman, C.R., 2007. *Effective Groundwater Model Calibration—with Analysis of Data, Sensitivities, Predictions, and Uncertainty*. Wiley-Interscience, Hoboken, N.J., 455 p.
- Hulme, P., Fletcher, S., Brown, L., 2002. Incorporation of groundwater modeling in the sustainable management of groundwater resources. In: Hiscock, K.M., Rivett, M.O., M Davison, R. (Eds.), *Sustainable Groundwater Development*. Geological Society of London, pp. 83–90. Special Publication 193.
- Hunt, R.J., 2012. Uncertainty. In: *Australian Groundwater Modelling Guidelines*. Waterlines Report Series No. 82. National Water Commission, Canberra, Australia, ISBN 978-1-921853-91-3, pp. 92–105.
- Hunt, R.J., Steuer, J.J., 2000. Simulation of the recharge area for Frederick springs, Dane County, Wisconsin. U.S. Geological Survey Water-Resources Investigations Report 00-4172, 33 p. <http://pubs.er.usgs.gov/publication/wri004172>.



- Hunt, R.J., Steuer, J.J., Mansor, M.T.C., Bullen, T.D., 2001. Delineating a recharge area for a spring using numerical modeling, Monte Carlo techniques, and geochemical investigation. *Groundwater* 39 (5), 702–712. <http://dx.doi.org/10.1111/j.1745-6584.2001.tb02360.x>.
- Hunt, R.J., Saad, D.A., Chapel, D.M., 2003. Numerical simulation of ground-water flow in La Crosse County, Wisconsin and into nearby pools of the Mississippi river. U.S. Geological Survey Water-Resources Investigations Report 03-4154, 36 p. <http://pubs.usgs.gov/wri/wri034154/>.
- Hunt, R.J., Doherty, J., 2006. A strategy of constructing models to minimize prediction uncertainty. In: MODFLOW and More 2006-Managing Ground Water Systems, Proceedings of the 7th International Conference of the International Ground Water Modeling Center. Colorado School of Mines, Golden, CO, pp. 56–60.
- Hunt, R.J., Doherty, J., Tonkin, M.J., 2007. Are models too simple? Arguments for increased parameterization. *Groundwater* 45 (3), 254–262. <http://dx.doi.org/10.1111/j.1745-6584.2007.00316.x>.
- Hunt, R.J., Welter, D.E., 2010. Taking account of “unknown unknowns”. *Groundwater* 48 (4), 477. <http://dx.doi.org/10.1111/j.1745-6584.2010.00681.x>.
- Hunt, R.J., Walker, J.F., Selbig, W.R., Westenbroek, S.M., Regan, R.S., 2013. Simulation of climate-change effects on streamflow, lake water budgets, and stream temperature using GSFLOW and SNTMP, Trout Lake Watershed, Wisconsin. U.S. Geological Survey Scientific Investigations Report 2013-5159, 118 p. <http://pubs.usgs.gov/sir/2013/5159/>.
- Hunt, R.J., Borchardt, M.A., Bradbury, K.R., 2014. Viruses as groundwater tracers: Using ecohydrology to characterize short travel times in aquifers. *Groundwater* 52 (2), 187–193. <http://dx.doi.org/10.1111/gwat.12158>.
- Intergovernmental Panel on Climate Change, 2014. Climate change 2014: Synthesis report. In: Fifth Assessment Report of the Intergovernmental Panel on Climate Change. Cambridge University Press, Cambridge and New York, 116 p. [http://www.ipcc.ch/pdf/assessment-report/ar5/syr/AR5\\_SYR\\_FINAL\\_All\\_Topics.pdf](http://www.ipcc.ch/pdf/assessment-report/ar5/syr/AR5_SYR_FINAL_All_Topics.pdf).
- James, S.C., Doherty, J.E., Eddebarh, A., 2009. Practical postcalibration uncertainty analysis: Yucca mountain, Nevada. *Groundwater* 47 (6), 851–869. <http://dx.doi.org/10.1111/j.1745-6584.2009.00626.x>.
- Jorgensen, D.G., 1981. Geohydrologic models of the Houston District, Texas. *Groundwater* 19 (4), 418–428. <http://dx.doi.org/10.1111/j.1745-6584.1981.tb03489.x>.
- Juckem, P.F., Fienen, M.N., Hunt, R.J., 2014. Simulation of groundwater flow and interaction of groundwater and surface water on the Lac du Flambeau Reservation, Wisconsin. U.S. Geological Survey Scientific Investigations Report 2014-5020, 34 p. <http://dx.doi.org/10.3133/sir20145020>.
- Kashyap, R.L., 1982. Optimal choice of AR and MA parts in autoregressive moving average models. *IEEE Transactions on Pattern Analysis and Machine Intelligence* 4 (2), 99–104. <http://dx.doi.org/10.1109/TPAMI.1982.4767213>.
- Keating, E.H., Doherty, J., Vrugt, J.A., Kang, Q., 2010. Optimization and uncertainty assessment of strongly nonlinear groundwater models with high parameter dimensionality. *Water Resources Research* 46 (10), W10517. <http://dx.doi.org/10.1029/2009WR008584>.
- Kelson, V.A., Hunt, R.J., Haitjema, H.M., 2002. Improving a regional model using reduced complexity and parameter estimation. *Groundwater* 40 (2), 132–143. <http://dx.doi.org/10.1111/j.1745-6584.2002.tb02498.x>.
- Kitanidis, P.K., 1986. Parameter uncertainty in estimation of spatial functions: Bayesian analysis. *Water Resources Research* 22 (4), 499–507. <http://dx.doi.org/10.1029/WR022i004p00499>.
- Kitanidis, P.K., 1995. Quasi-linear geostatistical theory for inverting. *Water Resources Research* 31 (10), 2411–2419. <http://dx.doi.org/10.1029/95WR01945>.
- Kitanidis, P.K., 1997. Introduction to Geostatistics: Application in Hydrogeology. Cambridge University Press, UK, 249 p.
- Knight, F.H., 1921. Risk, Uncertainty, and Profit. Hart, Schaffner, and Marx Prize Essays 31. Houghton Mifflin Co., New York, NY, 381 p.
- Konikow, L.F., 1995. The value of postaudits in groundwater model applications. In: El-Kadi, A. (Ed.), *Groundwater Models for Resource Analysis and Management*. CRC-Lewis Publisher, Boca Raton, Florida, pp. 59–78.

- Konikow, L.F., Person, M., 1985. Assessment of long-term salinity changes in an irrigated stream-aquifer system. *Water Resources Research* 21 (11), 1611–1624. <http://dx.doi.org/10.1029/WR021i011p01611>.
- Laloy, E., Rogiers, B., Vrugt, J.A., Mallants, D., Jacques, D., 2013. Efficient posterior exploration of a high-dimensional groundwater model from two-stage Markov Chain Monte Carlo simulation and polynomial chaos expansion. *Water Resources Research* 49 (5), 2664–2682. <http://dx.doi.org/10.1002/wrcr.20226>.
- Lu, Z., Higdon, D., Zhang, D., 2004. A Markov chain Monte Carlo method for the groundwater inverse problem. In: Miller, C.T., Pinder, G.F. (Eds.), *Developments in Water Science*, vol. 55, Part 2. Elsevier, pp. 1273–1283. [http://dx.doi.org/10.1016/S0167-5648\(04\)80142-4](http://dx.doi.org/10.1016/S0167-5648(04)80142-4).
- Mariethoz, G., Renard, P., Caers, J., 2010. Bayesian inverse problem and optimization with iterative spatial resampling. *Water Resources Research* 46 (11), W11530. <http://dx.doi.org/10.1029/2010WR009274>.
- Massmann, J., Freeze, R.A., Smith, L., Sperling, T., James, B., 1991. Hydrogeological decision analysis: 2. Applications to ground-water contamination. *Groundwater* 29 (4), 536–548. <http://dx.doi.org/10.1111/j.1745-6584.1991.tb00545.x>.
- Mehl, S., 2007. Forward model nonlinearity versus inverse model nonlinearity. *Groundwater* 45 (6), 791–794. <http://dx.doi.org/10.1111/j.1745-6584.2007.00372.x>.
- Menke, W., 1989. *Geophysical Data Analysis: Discrete Inverse Theory*, revised ed. Academic Press, Inc., New York, 289 p.
- Moore, C., Doherty, J., 2005. Role of the calibration process in reducing model predictive error. *Water Resources Research* 41 (5), W05020. <http://dx.doi.org/10.1029/2004WR003501>.
- Moore, C., Wöhling, T., Doherty, J., 2010. Efficient regularization and uncertainty analysis using a global optimization methodology. *Water Resources Research* 46 (8), W08527. <http://dx.doi.org/10.1029/2009WR008627>.
- Morgan, M.G., Henrion, M., Small, M., 1992. *Uncertainty: A Guide to Dealing with Uncertainty in Quantitative Risk and Policy Analysis*. Cambridge University Press, Cambridge, UK, 346 p.
- Myers, T., 2007. Minimizing the insufficient data argument: Uncertainty analysis in adversarial decision making. In: *NGWA Ground Water and Environmental Law Conference July 24–26, 2007, Proceedings*. Water Well Publishing, Dublin, OH, pp. 127–140.
- National Institute of Standards and Technology, 2012. *NIST/SEMATECH e-Handbook of Statistical Methods*. <http://www.itl.nist.gov/div898/handbook/> (accessed 11.11.14.).
- Neuman, S.P., 2003. Maximum likelihood Bayesian averaging of uncertain model predictions. *Stochastic Environmental Research and Risk Assessment* 17 (5), 291–305. <http://dx.doi.org/10.1007/s00477-003-0151-7>.
- Pappenberger, F., Beven, K.J., 2006. Ignorance is bliss: Or seven reasons not to use uncertainty analysis. *Water Resources Research* 42 (5), W05302. <http://dx.doi.org/10.1029/2005WR004820>.
- Poeter, E., Anderson, D., 2005. Multimodel ranking and inference in ground water modeling. *Groundwater* 43 (4), 597–605. <http://dx.doi.org/10.1111/j.1745-6584.2005.0061.x>.
- Poeter, E.P., Hill, M.C., 2007. *MMA, A computer code for Multi-Model Analysis*. U.S. Geological Survey Techniques and Methods 6–E3, 113 p. <http://pubs.usgs.gov/tm/2007/06E03/>.
- Rojas, R., Feyen, L., Dassargues, A., 2008. Conceptual model uncertainty in groundwater modeling: Combining generalized likelihood uncertainty estimation and Bayesian model averaging. *Water Resources Research* 44 (12), W12418. <http://dx.doi.org/10.1029/2008WR006908>.
- Rubin, Y., 2003. *Applied Stochastic Hydrogeology*. Oxford University Press, Inc, New York, NY, 391 p.
- Ruskauff, G.J., Rumbaugh, J.O., Rumbaugh, D.B., 1998. *Stochastic MODFLOW and MODPATH for Monte Carlo Simulation*. Environmental Simulations Incorporated, Herndon, VA, 58 p.
- Saltelli, A., Funtowicz, S., 2014. When all models are wrong. *Issues in Science and Technology* 30, 79–85. <http://www.issues.org/30.2/>.
- Schwarz, G., 1978. Estimating the dimension of a model. *Annals of Statistics* 6 (2), 461–464. <http://projecteuclid.org/euclid.aos/1176344136>.
- Sepúlveda, N., and J. Doherty, 2015. Uncertainty analysis of a groundwater flow model in east-central Florida. *Groundwater* 53(3), 464–474. <http://dx.doi.org/10.1111/gwat.12232>.

- Shepley, M.G., Whiteman, M.I., Hulme, P.J., Grout, M.W. (Eds.), 2012. Groundwater Resources Modeling: A Case Study from the UK. The Geological Society of London, p. 378. Special Publication 364.
- Silver, N., 2012. The Signal and the Noise: Why Most Predictions Fail but Some Don't. Penguin Press, New York, NY, 534 p.
- Singh, A., Mishra, S., Ruskauff, G., 2010. Model averaging techniques for quantifying conceptual model uncertainty. *Groundwater* 48 (5), 701–715. <http://dx.doi.org/10.1111/j.1745-6584.2009.00642.x>.
- Sperling, T., Freeze, R.A., Massmann, J., Smith, L., James, B., 1992. Hydrogeological decision analysis: 3. Application to design of a ground-water control system at an open pit mine. *Groundwater* 30 (3), 376–389. <http://dx.doi.org/10.1111/j.1745-6584.1992.tb02006.x>.
- Starn, J.J., Bagtzoglou, A.C., Robbins, G.A., 2010. Using atmospheric tracers to reduce uncertainty in groundwater recharge areas. *Groundwater* 48 (6), 858–868. <http://dx.doi.org/10.1111/j.1745-6584.2010.00674.x>.
- Stauffer, F.W., Kinzelbach, W., Kovar, K., Hoehn, E. (Eds.), 1999. Calibration and Reliability in Groundwater Modeling: Coping with Uncertainty. IAHS Publication No. 265. International Association of Hydrological Sciences, IAHS Press, Wallingford, Oxfordshire, 525 p.
- Tarantola, A., 2004. Inverse Problem Theory and Model Parameter Estimation. Society for Industrial and Applied Mathematics, Philadelphia, PA, 352 p.
- Tartakovsky, D.M., 2013. Assessment and management of risk in subsurface hydrology: A review and perspective. *Advances in Water Resources* 51, 247–260. <http://dx.doi.org/10.1016/j.advwatres.2012.04.007>.
- Tavakoli, R., Yoon, H., Delshad, M., El Sheikh, A.H., Wheeler, M.F., Arnold, B.W., 2013. Comparison of ensemble filtering algorithms and null-space Monte Carlo for parameter estimation and uncertainty quantification using CO<sub>2</sub> sequestration data. *Water Resources Research* 49 (12), 8108–8127. <http://dx.doi.org/10.1002/2013WR013959>.
- Tonkin, M.J., Tiedeman, C.R., Ely, M.D., Hill, M.C., 2007a. OPR–PPR, a computer program for assessing data importance to model predictions using linear statistics. U.S. Geological Survey Techniques and Methods TM-6E2, 115 p. <http://pubs.usgs.gov/tm/2007/tm6e2/>.
- Tonkin, M.J., Doherty, J., 2009. Calibration-constrained Monte-Carlo analysis of highly parameterized models using subspace techniques. *Water Resources Research* 45 (12), W00B10. <http://dx.doi.org/10.1029/2007WR006678>.
- Tonkin, M.J., Doherty, J., Moore, C., 2007b. Efficient nonlinear predictive error variance for highly parameterized models. *Water Resources Research* 43 (7), W07429. <http://dx.doi.org/10.1029/2006WR005348>.
- Varljen, M.D., Shafer, J.M., 1991. Assessment of uncertainty in time-related capture zones using conditional simulation of hydraulic conductivity. *Groundwater* 29 (5), 737–748. <http://dx.doi.org/10.1111/j.1745-6584.1991.tb00565.x>.
- Vecchia, A.V., Cooley, R.L., 1987. Simultaneous confidence and prediction intervals for nonlinear regression models with application to a groundwater flow model. *Water Resources Research* 23 (7), 1237–1250. <http://dx.doi.org/10.1029/WR023i007p01237>.
- von Bertalanffy, L., 1968. General Systems Theory: Foundations, Development, Applications. George Braziller, Inc., USA, ISBN 0-8076-0453-4.
- Vrugt, J.A., ter Braak, C.J.F., Gupta, H.V., Robinson, B.A., 2008. Equifinality of formal (DREAM) and informal (GLUE) Bayesian approaches in hydrologic modeling? *Stochastic Environmental Research and Risk Assessment* 23 (7), 1011–1026. <http://dx.doi.org/10.1007/s00477-008-0274-y>.
- Wallace, C.S., Boulton, D.M., 1968. An information measure for classification. *Computer Journal* 11 (2), 185–194. <http://dx.doi.org/10.1093/comjnl/11.2.185>.
- White, J.T., Doherty, J.E., Hughes, J.D., 2014. Quantifying the predictive consequences of model error with linear subspace analysis. *Water Resources Research* 50 (2), 1152–1173. <http://dx.doi.org/10.1002/2013WR014767>.
- Woodbury, A.D., Ulrych, T.J., 1993. Minimum relative entropy – Forward probabilistic modeling. *Water Resources Research* 29 (8), 2847–2860. <http://dx.doi.org/10.1029/93WR00923>.

- Woodbury, A.D., Ulrych, T.J., 2000. A full-Bayesian approach to the groundwater inverse problem for steady state flow. *Water Resources Research* 36 (8), 2081–2093. <http://dx.doi.org/10.1029/2000WR900086>.
- Ye, M., Pohlmann, K.F., Chapman, J.B., Pohl, G.M., Reeves, D.M., 2010. A model-averaging method for assessing groundwater conceptual model uncertainty. *Groundwater* 48 (5), 716–728. <http://dx.doi.org/10.1111/j.1745-6584.2009.00633.x>.
- Yeh, T., Liu, S., 2000. Hydraulic tomography: Development of a new aquifer test method. *Water Resources Research* 36 (8), 2095–2105. <http://dx.doi.org/10.1029/2000WR900114>.
- Yoon, H., Hart, D.B., McKenna, S.A., 2013. Parameter estimation and predictive uncertainty in stochastic inverse modeling of groundwater flow: Comparing null-space Monte Carlo and multiple starting point methods. *Water Resources Research* 49 (1), 536–553. <http://dx.doi.org/10.1002/wrcr.20064>.
- Zhang, D., 2002. *Stochastic Methods for Flow in Porous Media*. Academic Press, San Diego, CA, 350 p.
- Zheng, C., Bennett, G.D., 2002. *Applied Contaminant Transport Modeling*, second ed. John Wiley & Sons, New York, NY, 621 p.



## CHAPTER 11

# The Modeling Report, Archive, and Review

*The writer does the most who gives his reader the most knowledge, and takes from him the least time.*

*Sydney Smith (1771–1845)*

### Contents

11.1 Introduction	495
11.2 The Modeling Report	498
11.2.1 Title	498
11.2.2 Executive Summary and Abstract	499
11.2.3 Introduction	500
11.2.4 Hydrogeologic Setting and Conceptual Model	500
11.2.4.1 Hydrogeologic Setting	501
11.2.4.2 System Properties	501
11.2.4.3 Observations	502
11.2.4.4 Conceptual Model	502
11.2.5 Numerical Model	502
11.2.5.1 Governing Equation and Code	503
11.2.5.2 Design	503
11.2.5.3 Model Execution	504
11.2.5.4 Calibration	504
11.2.6 Forecasting Simulations and Uncertainty Analysis	506
11.2.7 Discussion	507
11.2.8 Model Assumptions, Simplifications, and Limitations	508
11.2.9 Summary and Conclusions	508
11.2.10 References Cited	508
11.2.11 Appendices	509
11.3 Archiving the Model	509
11.4 Reviewing the Modeling Report	510
11.5 Common Errors in Report/Archive Preparation and Review	513
11.6 Problems	513
References	514

### 11.1 INTRODUCTION

A modeling project concludes with preparation of both a modeling report and archive. A comprehensive report is essential to the effective completion of a modeling study; it

not only presents modeling results but must also explain (and defend) choices made during the formulation and development of the groundwater model and, together with the modeling archive, provides additional model specific data that allow for a thorough review including replication of the modeling results. The requirement for replication of results is critically important.

Modeling is performed to meet regulatory requirements, to help in environmental decision-making and water-resources management and planning, or to evaluate a scientific hypothesis. In experimental sciences, there are well-established codes of conduct for how results and methods are published and made available to others. It is considered unethical to withhold any important details that would hinder others from replicating and reproducing the results (Johansson, 2015). These same standards are applied to all aspects of computational sciences (Peng, 2011; Morin et al., 2012). Hence, the documentation and associated material that accompanies a modeling result (i.e., the modeling report, appendices, and access to the archive) are as important as the modeling itself. Simply put, replication is a cornerstone of the scientific method (Johansson, 2015); a model result that cannot be replicated does not conform to the scientific method, and cannot be considered to be based on sound science and sound engineering practice. Therefore, a model must be sufficiently documented to withstand critical scientific review; at a minimum, the report and its supporting material (appendices and the modeling archive) must include a complete set of model input that when run gives the reported model output. Geospatial coordinates specific to the model grid/mesh must be provided so that it can be located in a geographic information system. Documentation must also include model output that supports model results, and output that directly corresponds to what a reviewer would obtain when the model is run with the input given (Section 11.4).

The audience for whom the work is performed generally includes the stakeholders who require modeling results to make decisions. Care must be taken to state the forecasted groundwater response objectively; wording should be clear and concise using clearly defined and readily understood terms (e.g., Sections 1.3 and 10.6). The report should be reviewed by colleagues and may also be subjected to outside peer reviews. The review process is intended to provide quality control and be helpful to the modeler (Section 11.4). Given that the report likely will be read by technical reviewers as well as stakeholders, the audience for a modeling report will have varying levels of hydrogeological and modeling expertise and understanding. The report should clearly address the technical level of the target audience while maintaining scientific rigor. For example, the decision to include details of modeling mechanics in the main text rather than in an appendix (see Hunt and Schwartz, 2014) will be dictated by the intended audience. Typically, a modeling report is mainly technical but includes an executive summary and discussion section written for less technical readers.

The modeling report may be distilled for incorporation into a larger project report or published as a stand-alone report, or as a research thesis, dissertation or peer-reviewed journal paper. [Barnett et al. \(2012\)](#) suggested that an interim report should be prepared after each of the following phases of the project: (1) constructing the conceptual model and designing the numerical model; (2) model calibration; (3) forecasting simulations and uncertainty analysis. Regardless of format, the final report and supporting interim reports should be archived together with the code(s), information on data input and output, processing methods, and key decision points. Understandable and clear listing of the field measurements used to perform history matching—locations, dates, data types, and notes regarding qualitative ranking (Section 9.3)—are of primary importance. Those data are typically more valuable to future modeling efforts than the archived model itself. The archive should provide sufficient information for another modeler to reproduce the results in the modeling report. Hence, the archives should include input and output files of selected model runs, with a listing of the steps needed to execute the model and associated pre- and postprocessing utility programs. An archive may also include graphics and visualizations beyond those in the modeling report as well as a simulation log, which is a written record of actions and decisions made during the modeling project (Table 3.1, Section 3.7).

Groundwater modeling guidelines prepared by governmental agencies or professional societies serve a variety of purposes. They may recommend a general framework, or protocol for modeling and reporting results, and provide advice for designing a model. Guidelines developed for regulatory purposes, often by a state regulatory agency, may aim to ensure that policies, laws, rules and regulations are met (e.g., [OEPA, 2007](#)) and provide a framework to ensure consistent and complete reporting. Some guideline documents describe a generic approach to groundwater modeling. For example, ASTM guideline document D5718-13 ([ASTM, 2013](#)) provides general information on documenting a groundwater flow model application and archiving data. [Neuman and Wierenga \(2003\)](#) developed guidelines for staff of the U.S. Nuclear Regulatory Commission that describe a generic strategy for groundwater modeling including site characterization, development of the conceptual and numerical models, parameter estimation, forecasting, and uncertainty analysis. Recent guidelines for Australia ([Barnett et al., 2012](#)) also describe a general approach to groundwater modeling; the document is intended as a reference “for groundwater modellers, project proponents (and model reviewers), regulators, community stakeholders and model software developers who may be involved in the process of developing a model and/or modelling studies.” A guideline document from the U.S. Geological Survey ([Reilly and Harbaugh, 2004](#)) is intended to help reviewers and users evaluate “the accuracy or reasonableness” of groundwater flow models. Guidelines can be useful to develop credible models, but report formats and content are usually only briefly outlined. In [Section 11.2](#), we discuss the content typically expected in a modeling report.



## 11.2 THE MODELING REPORT

The author(s) of a modeling report should be explicitly listed on the front cover/title page to identify who is responsible for the content. The authors should be familiar with the standard elements of writing (e.g., [Strunk and White, 2009](#)) and would benefit from training in technical science writing (e.g., [Greene, 2013](#)). Experience is one of the best ways to improve technical writing; suggestions from a senior modeler can be invaluable. Authors should follow the basic format of a technical report, which starts with an abstract or executive summary, and is followed by the body of the report ending with a list of reference citations and appendices. Correct and complete reference citations are essential for conveying the scientific foundations for assertions made in the report. It is also essential to credit the original authors of all material and figures not solely created or significantly modified by the authors. Quotation marks must be used when including exact words of others and when including text published elsewhere, even if from your own published work. Failure to acknowledge the work of others is plagiarism and failure to acknowledge your own previously published work is self-plagiarism ([Anderson, 2006](#)). When paraphrasing the ideas of others, credit to the original source must be given. Although seemingly not related to understanding a modeling effort, poor writing and reference quality, lack of acknowledgments, and self-plagiarism undermine the credibility of the modeling results.

Within the main body of the report and accompanying appendices, the following 10 topics should be discussed (modified from [Reilly and Harbaugh, 2004](#)):

1. The purpose of the study and the role of simulation in addressing the purpose;
2. A description of the hydrologic system under investigation;
3. Mathematical methods and their appropriateness to the problem under investigation;
4. Hydrogeologic character of the boundary conditions;
5. Discretization of the problem domain;
6. Aquifer system properties;
7. Hydrologic stresses (e.g., pumping, recharge, changes in river stage);
8. Initial conditions (for transient simulations);
9. Discretization of time (for transient simulations);
10. Calibration criteria, procedure, and results;
11. Limitations of the model and impact of the limitations on results and conclusions.

A suggested outline for relating this material is given in [Fig. 11.1](#) and suggested report topics are discussed below.

### 11.2.1 Title

In selecting a title for the report, it must be remembered that constructing a model is never the purpose of a modeling study (Section 2.1). A title like “The Construction of

Title
Executive Summary or Abstract
Introduction
Hydrogeologic Setting and Conceptual Model
Hydrogeologic Setting
Parameters
Measured Heads; Sources and Sinks
Conceptual Model
Numerical Model
Governing Equation and Code
Design
Calibration
Forecasting Simulations and Uncertainty Analysis
Discussion
Summary and Conclusions
References cited
Appendices

**Figure 11.1** Generic outline of a modeling report.

a Hydrogeologic Model of the Groundwater Conditions in Central Nebraska” does not tell the reader why a model was needed or what was done. The title should reflect the goals and specific modeling objectives. For example, the modeling objective may be to assess the impact of historical and future groundwater pumping and irrigation water use on low streamflows. In that case, a good report title would be “Simulation of Groundwater Flow and Effects of Groundwater Irrigation on Stream Base Flow in the Elkhorn and Loup River Basins, Nebraska, 1895–2055,” which is the title of a report by [Stanton et al. \(2010\)](#). The modeler should create an informative title, not one that masks the contents of the report.

### 11.2.2 Executive Summary and Abstract

The modeler’s distillation of the modeling project is the most read component of any modeling report, and as a result must be well-thought-out and clearly written. At a minimum, it should unambiguously state the modeling purpose and summarize the most important findings of the project. It briefly summarizes the purpose, methods, results, and conclusions. Given its importance for concisely summarizing important facets of the modeling process, it is typically written after the rest of the report has been finalized.

This distillation typically takes one of two forms, an executive summary or an abstract. An executive summary can be up to several pages long but should be less than 5% of the full report length excluding appendices. Conceptually, an executive summary is a condensed version of the report intended for the busy “executive” (or administrator or legislator) who does not have the time, and/or in some cases expertise, to read the entire report. It should describe the modeling process and results in nontechnical terms. Topics should be presented in the same order as in the body of report and important

topics should be summarized in short, concise paragraphs. It can refer to figures and tables in the body of the report, or key figures or tables can be reproduced in the executive summary itself.

An abstract is shorter than an executive summary and summarizes the objectives, methods, results, and conclusions. The abstract is intended as a brief overview of the report and is written with the expectation that the audience will read the body of the report. Abstracts are intended to be short (e.g., as short as four or five sentences) and usually no more than a page in length. Abstracts for journal papers are usually fewer than 500 words. Abstracts rarely include figures, tables, or references.

### 11.2.3 Introduction

The introduction includes a statement of the modeling purpose following the guidelines in Section 2.1, a discussion of the importance of the problem, long-term goals and specific modeling objectives, their relation to previous work, and the general approach used to accomplish the goals and objectives. A goal is a long-term general planning or management objective that may not be fully met during the modeling project. Objectives are modeling-specific tasks designed to address issues or questions; objectives are completed during the modeling project. Succinctly-stated modeling objectives should be listed in the order they would logically be completed to achieve the project objectives. The success of the project will be judged by the degree to which the stated objectives are met.

The introduction should relate the modeling project to previous work, including earlier modeling efforts. A literature review includes as many pertinent previous studies as practical and provides basic geological, hydrological, and hydrogeological information used in constructing the conceptual and numerical models. In general, it is good practice to cite any previous work relevant to the site being modeled that relates to model conceptualization, construction, and calibration. The introduction should also include a review of any past modeling efforts, briefly listing their purpose and conclusions in a sentence or short paragraph. Citations to work from both the published literature (e.g., peer-reviewed state and federal agency reports, journal papers) and gray literature (e.g., consulting reports, papers in conference proceedings, theses, and dissertations) should be included in the literature review. The final section of the introductory material should conclude with a brief paragraph on the overall approach or strategy used to accomplish the modeling objectives.

### 11.2.4 Hydrogeologic Setting and Conceptual Model

This section presents what was known about the hydrogeologic system prior to the present modeling effort. It should contain sections describing: (1) the hydrogeologic setting (e.g., climate, geology, hydrostratigraphy); (2) system properties; (3) observation data

(e.g., heads and fluxes, with error estimates); (4) a conceptual model of the system including a water budget and discussion of simplifying assumptions used to construct the conceptual model.

#### **11.2.4.1 Hydrogeologic Setting**

The general climate and site location should be described. A location map of the study area with surface topography and surface water bodies labeled should be presented at the beginning of this section. The physical and hydraulic conditions that were used to form the boundary conditions of the numerical model should be described (Section 2.3) and defended. Field data used to justify the selection of the boundaries should be presented either in the main body of the report or in an appendix. Diagrams with schematic flow arrows may be used to show general flow directions at the model's perimeter boundaries and in the interior of the modeled area.

The description of the hydrogeologic setting includes the definition of site-specific hydrostratigraphic units, a map showing areal distribution of hydrostratigraphic units, and cross sections that show the depth, thickness, and orientation of the units. It is recommended that at least one cross section be constructed without vertical exaggeration to convey the actual dimensions of the problem; the vertical exaggeration used for other figures should be defined on the cross sections. A geologic map and geologic cross sections may be used to show geologic formations in lieu of hydrostratigraphic units (Section 2.3) as long as the relation between site geologic formations and hydrostratigraphic units can be easily identified (Fig. 2.7). If the modeling report is the first to describe the hydrogeology of an area, presentation of aquifer parameters and head data may provide justification for the definition of hydrostratigraphic units. If the work has redefined the hydrostratigraphy of an area, the original classification should be cited, and revisions clearly presented. A discussion of depositional environments and geologic history will assist in conceptualizing the spatial variation of geologic units, their hydraulic properties, and importance for modeling (e.g., [Fiene et al., 2009](#)).

#### **11.2.4.2 System Properties**

The intent of this section is to present values of material property parameters and hydrologic parameters (Section 5.4) that form the basis of the groundwater model. Effective porosity (Box 8.1) should be discussed if particle tracking was done as part of the modeling effort. Methods used to obtain the values listed, estimated ranges in values, and a rationale for assigning spatial variation of properties in the study area should be included. Properties presented in this section are premodeling values as they relate to the conceptual model and are derived from field and literature values. Changes made in system properties during model calibration are typically discussed in the section on model calibration when reasonableness of parameter values (Section 9.1) is discussed.

### **11.2.4.3 Observations**

The observations of head and fluxes and other field measurements used as calibration targets should be discussed, and in some cases presented in map view; if sufficient data are available, information should also be shown in cross section. If several aquifers are being modeled, data should be presented for each aquifer (Fig. 2.5). The directions of groundwater flow and the locations of recharge and discharge areas should be qualitatively shown, including important sources and sinks such as streams, lakes, wetlands, springs, drains, irrigated areas, and pumping wells. Recharge and discharge rates at sources and sinks can be tabulated, or more formally addressed in the context of model calibration targets. Even if the model is to be run only at steady state, transience in the system may be discussed to justify the assumption of steady-state conditions (Sections 7.1, 7.2). If the model is transient, temporal variations in system dynamics should be characterized (Section 7.7). For example, temporal variations in springflow and streamflow could be tabulated or graphed. Transient information on important stresses such as pumping wells should also be included.

### **11.2.4.4 Conceptual Model**

The conceptual model, based on the material described previously, is presented with graphics (schematic diagrams, graphs, and tables) and explanatory text. The nature of the graphics used to present the conceptual model will vary according to the purpose of the model, the hydrogeologic setting, and the existing literature and available data. A figure showing hydrostratigraphic units and generalized arrows to represent the flow system is particularly helpful (Figs 2.9(b), 2.12, 2.15). An estimation of the long-term average fluxes needed for evaluating the simulated water budget may be sufficient for a steady-state model; seasonal or annual fluxes might be needed for evaluating simulated transient water budgets. The reporting of important fluxes should be accompanied by a description of how each was calculated or estimated. Water budget information should be summarized in tabular form (Table 2.2; Fig. 2.16) and ideally includes ranges in values to indicate the expected uncertainty inherent to such an estimate (Table 2.3). If alternative conceptual models were used, differences among the alternative conceptualizations should be explained, preferably with visualizations that efficiently convey how they differ from the primary conceptual model.

### **11.2.5 Numerical Model**

This section can include the governing equation used to solve the mathematical model, but at a minimum should include: (1) information about the modeling codes used; (2) the design of the numerical model including the grid/mesh, information on nodal spacing, boundary and initial conditions (for transient models), (3) initial values of parameters input to the model; (4) calibration targets, procedures, and history matching results.

### **11.2.5.1 Governing Equation and Code**

The mathematical model (Sections 3.2, 3.3) consists of a governing equation, boundary conditions, and initial conditions if the problem is transient. However, in practice, modeling codes are sufficiently mature that formal recitation of the exact governing equation(s) (e.g., Eqn (3.12)) is not needed. Rather, it is more important to report the version of the code used along with a short explanation of why the code was selected. Code description can also include discussion of specific code options and the solver used as well as utility and associated codes. When the model has exhibited sensitivity to solver settings, values of closure criteria and their effect on water budget error, or comparisons to other solution schemes should be discussed.

Standard codes (e.g., MODFLOW, FEFLOW, and PEST) are not typically modified for most applied modeling projects, but any modifications to the code should be documented. If extensive recoding was done, a summary of the changes should be included in this subsection and a copy of the modified portions of the code included in an appendix. This material, along with associated example problems used to benchmark the modifications, must be made available upon request. If a new code was developed, a separate report or appendix should be prepared to describe the code and its verification (Section 3.6; [ASTM, 2008](#)). A report that documents a new code should describe the governing equation, how boundary conditions are implemented, explicit model input descriptions, the numerical method, code verification, and include a user's manual. Proprietary codes can be problematic for some applied modeling projects because the source code is usually not made available to reviewers or the general public. Verification might be required to demonstrate that a code correctly solves the governing equations with associated boundary conditions. If a proprietary code is not made available, the report should include a comparison to a nonproprietary code for a similar modeling problem. Otherwise, the report should state that the modeler did not confirm that the code properly represents all features and processes claimed.

### **11.2.5.2 Design**

This section of the report describes how the conceptual model was translated into the numerical model, including how space and time were discretized, how model boundaries were simulated (Section 4.3), and how parameters were assigned to the grid or mesh (Section 5.5). If only a portion of the study area was modeled, the rationale for selecting the subarea should be presented. The selection of a two- or three-dimensional model (Section 4.1; Box 4.1) and steady-state or transient conditions (Section 7.2) should be justified based on the conceptual model and modeling purpose.

The grid/mesh should be superimposed on a map of the study area. If the full grid/mesh is too refined to be viewed easily, a simplified representation of the actual grid/mesh should be included. The depiction should include geospatial coordinates and other information that indicates the locations of important surface water boundaries

and key topographic and geologic features. Types of perimeter boundaries and sources and sinks are discussed, as are assumptions made in locating and simulating boundaries, and sources and sinks (Section 4.3 and Chapter 6). A summary statement of the overall dimensions of the grid/mesh and the number of nodes, as well as the number and type of elements for a finite-element model, and the number of layers should be given. A diagram that shows the relation between hydrostratigraphic units and model layers is also valuable (Fig. 2.7).

The method and rationale used to assign initial parameter values and stresses should be discussed. Figures may be used to show the distribution of parameters on the grid/mesh (Fig. 5.29). The likely ranges in values or the mean and standard deviation or variance of each parameter is also given (e.g., using a table or box plot, Fig. 5.31). This discussion can also present known sources of uncertainty in material property and hydrologic parameter values.

#### **11.2.5.3 Model Execution**

When running the code the modeler selects a solver and assigns closure criteria, including for the simulated water budget (Section 3.7). The acceptable percent error in the simulated water budget should be reported along with related information on the solver and closure criteria. Only results of converged models should be presented; if a model did not converge in all areas (e.g., during a small number of time steps in a transient run), an explanation of the likely causes and possible resulting limitations should be presented.

#### **11.2.5.4 Calibration**

Most modeling applications require one or more calibrated models, defined as those models that reasonably simulate field observations and have parameters that are reasonable given what is known about the system. Model fit is assessed through history matching (Chapter 9), which is done in two phases: (1) an initial calibration by manual trial and error (Section 9.4); (2) parameter estimation using a parameter estimation code (Sections 9.5, 9.6). In addition, criteria used to justify that the history matching adequately produced a reasonable representation of the hydrogeological system also need to be documented. The report should present a clear description of all criteria for the calibration process including soft knowledge (Section 9.1) used in determining whether parameters are reasonable.

The report should list the calibration targets (Section 9.3), estimates of error associated with the targets (e.g., Table 9.1), and weights used for parameter estimation (e.g., Table 7.1). Targets should be identified by type (e.g., head, flux, head difference, etc.) and quality, and when possible the target description should include locations shown on a map. The rationale for selecting targets, definition of how error was estimated, and how targets were weighted should be included. A general description of the nature and type of targets including how indirect targets (e.g., those derived from isotope

analyses and age tracers, flowpaths, temperature, or solute concentrations) were evaluated should be discussed.

The calibration process should be briefly described, including important insights gained during the manual trial-and-error and parameter estimation phases of calibration. The name and version of the parameter estimation code should be listed. Some audiences may also benefit from a short description of the underlying parameter estimation methodology used (e.g., sparsely parameterized or overdetermined; highly parameterized or underdetermined; Chapter 9). The components of the initial objective function used in parameter estimation (e.g., Eqn (9.6)) should be described and related to modeling objectives (e.g., Fig. B9.2.1 in Box 9.2). When pilot point methods are used during calibration a graphic illustrating the number and distribution should be included (Fig. 9.15). When soft knowledge is used formally to constrain the parameter estimation process (Section 9.6), the relation of adherence to soft knowledge constraints versus model fit can be presented (Figs 9.16, 9.17).

The results of the calibration should be discussed and displayed graphically and in tables. Graphics should include categorized scatter plots of observed (target) *vs* simulated values (e.g., Figs 9.2 through 9.7). The match to flux targets is often presented in a plot showing calibration targets with estimated error bars around the field measurement and the simulated fluxes (Fig. 9.7). Residual error in each target should also be plotted on a map (Fig. 9.6). Bias, if any, in the calibration should be discussed. Values of summary statistics (e.g., ME, MAE, and RMSE; Eqns (9.1), (9.2) and (9.3)) as well as the final value of the objective function for parameter estimation provide a transparent metric of the quality of the history matching. Overall model performance can be illustrated in representative plots and tables in the main body of the report while comparisons for each target can be included in an appendix.

If the model is calibrated to transient conditions, additional calibration information is presented. Typically, a transient model is first calibrated to steady-state conditions, which are used as initial conditions (Section 7.4). The results of the steady-state calibration should be presented as discussed above. Results of the transient calibration are typically presented in a hydrograph, or time series of heads and fluxes, which document the dynamics of the system that are important for judging transient model performance (Figs 7.3, 7.11; Eqn (9.4)). When transient fluctuations in a very large number of head and flux targets are used for calibration, a selected number of representative observations may be presented to illustrate spatial and temporal goodness of fit.

The final set of calibrated parameter values obtained from the parameter estimation phase of calibration should be presented and compared to the initial values derived from the conceptual model. Calibrated parameter values should fall within the expected range or an explanation for the mismatch (e.g., model too simple so calibration parameters became surrogates, Section 9.6; improper conceptual model, and/or overly narrow estimate of initial parameter values) should be presented. Calibration of alternative



conceptual models should be presented and compared with the calibration of the primary conceptual model. Additional tables, maps, or graphs that compare calibration statistics of alternative models with the original calibrated model can facilitate the comparison among alternative models.

Modeling reports can also include a section on statistical analysis of the calibration (Section 9.5), which can be helpful if in-depth reporting on the statistical mechanics of history matching is required. For simple parameter estimation, a sensitivity analysis can convey how the model outputs changed when parameter values were changed, for example, by reporting sensitivity coefficients (Eqn (9.7)). Parameter identifiability (Fig. 10.10) illustrates calibration parameters that are most constrained by the observations available. However, detailed reporting of statistical analyses for advanced parameter estimation (Section 9.6) is not typically needed for applied modeling projects.

The second part of the calibration discussion is an assessment of the hydrogeological reasonableness of the calibrated model using soft knowledge (Sections 9.1, 9.7). It is important to evaluate the degree to which soft knowledge of the site conditions support the parameters that give an acceptable history match; such an evaluation should be illustrated and discussed. Figures or tables that show the similarity between field measurements and simulated data sets should be prepared including horizontal and vertical flow in model layers (equipotential maps and interpreted flow directions), well hydrographs (transient), the location and magnitude of flux targets, locations of gaining and losing surface water bodies, mapped and modeled groundwater recharge and discharge areas, premodeling site groundwater budgets and simulated budgets, field-based material property values and final calibrated values, and other pertinent comparisons of observed and modeled conditions. It is the quantifiable and qualitative analyses of model fits that are used to determine model reasonableness, and both must be presented and discussed in sufficient detail to allow the reader to evaluate the calibration.

For most modeling objectives, a best calibrated (base) model (Section 10.2) from the family of reasonable models (Section 9.1; Fig. 9.17) is used to make a series of forecasts. Therefore, the overall intent of the calibration discussion in the modeling report is to provide sufficient description of the base model that the reader will have an appreciation for the strengths and limitations of the base model.

### 11.2.6 Forecasting Simulations and Uncertainty Analysis

This component of the modeling report should clearly relate the simulated forecast(s) to the modeling purpose. It should include information on how the forecast was constructed including the parameters and assumptions that were changed from the base model for the purpose of the forecasts. A discussion of the future conditions selected for the forecasts should be included (Section 10.4). Typically forecasts are based on a subset of potential future events and conditions. Forecasting simulations report possible

outcomes based on the changes. Every forecast contains uncertainties; hence, the need to include assessments of forecast uncertainty is widely recognized (Chapter 10).

The choice of basic or advanced forecast uncertainty methods (Sections 10.4, 10.5) should be briefly discussed and methods referenced. Some forecasts benefit from inclusion of best case and worst case scenarios. Plots and tables showing the range and variability in forecast results should be presented (e.g., Figs 10.7, 10.12, 10.16). Analysis of how measurement and structural error led to forecast uncertainty can be formally related to a forecast (Fig. 10.2). In most cases, uncertainty is best conveyed in terms of the estimated probability of the forecast (Fig. 10.15; Box 10.4). If linear uncertainty analysis is used (Section 10.4), the modeler's determination of the error around the observations and innate parameter variability associated with the chosen model structure should be presented (e.g., Table 10.2). Analyses and plots of how well individual parameters are identified by the calibration data can help assess their influence on the degree of forecast uncertainty (Fig. 10.10); such analysis can also suggest which parameters could benefit from better definition as a means to reduce forecast uncertainty. Because there are many possible ways to assess uncertainty, the description in the main body of the report should be restricted to important outcomes and insights; detailed explanation of the specifics of the uncertainty analysis is often best communicated in appendices.

Forecast results should be presented with an explanation of the likelihood of occurrence (e.g., worst case or probable case) and sources of uncertainty (in the base model and in future stresses; Section 10.2) should be discussed to provide context for the forecast. The choice of emphasizing scenario uncertainty and/or base model uncertainty (Section 10.2) should be aligned with uncertainties expected to dominate the model's ability to meet the modeling objective.

The intended audience often includes decision-makers, regulators, and other stakeholders who have limited knowledge of uncertainty theory. Whenever possible, the report should relate the forecast and associated uncertainty using terms accessible to the audience. The modeling report should present uncertainty in terms that most directly relate to the decision of interest (Fig. B10.4.2 in Box 10.4) and should use language that relates to probability of the forecast (Section 10.6). Visualization, preferably using forecast probability, is often the most effective way to convey a forecast and its associated uncertainty.

### 11.2.7 Discussion

The discussion section evaluates the modeling results and concisely addresses the model's ability to address its intended purpose (e.g., if the stated modeling objectives were met). The strengths and weaknesses of the conceptual model(s) chosen should be conveyed. Suggestions for actions that could improve model performance and reduce forecast uncertainty are often valuable. For example, the model provides a quantitative framework to inform cost-benefit decisions related to filling data gaps by identifying the most

valuable additional field data (Box 10.3). The modeler's assessment of the reliability of the calibration and simulated forecasts should be discussed. Recall that when a model makes a forecast, "a model cannot promise the right answer. However, if properly constructed, a model can promise that the right answer lies within the uncertainty limits which are its responsibility to construct" (Doherty, 2011). Therefore, the discussion section should identify what can and cannot be supported based on the work performed.

### 11.2.8 Model Assumptions, Simplifications, and Limitations

The report should provide context for the simplifications and assumptions in the model, and discuss how they limit the model's ability to meet modeling goals and objectives (e.g., Hunt and Welter, 2010). This material can reiterate some of the qualitative aspects that may not be reflected in the modeling results and accompanying uncertainty analyses (e.g., selection of steady-state conditions to represent a transient system). This section should include additional cautions regarding the results. Depending on the specific model, it might include statements of how a smaller nodal spacing or more model layers, additional data and parameter estimates, or transient simulations, are likely to influence model outcomes.

### 11.2.9 Summary and Conclusions

The summary should briefly address the purpose of the project, modeling objectives and results, and state what was learned from the modeling effort; a list of concisely stated important points is often most effective (Hunt and Schwartz, 2014). When an executive summary is included at the beginning of the report, a summary at the end may not be needed.

Conclusions should primarily focus on the project purpose and modeling objectives, and should be based on material presented earlier in the report. This section may also include summary insights about the modeling process and the adequacy of the conceptual model. Specifics as to future field data collection activities and how the conceptual model could be redesigned are valuable to provide options for addressing questions left unanswered and possibilities for future work.

### 11.2.10 References Cited

The list of references allows the reader to identify material used to support model construction, calibration, and forecasting. References cited in the text are typically listed alphabetically by the first author's last name, or sometimes listed and numbered in the order they were cited in the text. In the main body of the report, standard reference citing usually includes the author(s) followed by the date of publication, or the number of the reference if the numbering convention is used. The reference citation typically includes the names of the authors, date of publication, title of publication, name of the journal, company or

agency producing the work, and volume/issue number or city of publication, and the total number of pages in a cited report or range of page numbers in a journal article. Scientific journals and some agencies have strict requirements as to how references are cited.

### 11.2.11 Appendices

Appendices contain any relevant documentation not presented in the body of the report. They include detailed explanation of concepts and steps covered cursorily in the body of the report, and additional or supplemental information such as data input files and key output files; code modifications or a listing of the code; geologic logs; well inventories; water level measurements; determinations of parameters; and water budget calculations. An appendix that provides a concise summary of the process used to select input for the parameter estimation code (e.g., calibration target weights, calibration parameter bounds) is appropriate. Appendices of most modeling reports should include sufficient information so that model results can be replicated and/or reproduced using a different groundwater code (Table 11.1). If data input and output files are not included in the appendices, the location of these files must be listed in the report (e.g., a Web site or model archive, Section 11.3) so that an interested reader can access them.

## 11.3 ARCHIVING THE MODEL

The purpose of the modeling archive is “to ensure that the results are reproducible in the future either by the model developer or other interested parties” (Reilly and Harbaugh, 2004, p. 26). According to ASTM (2013), the archive consists of “sufficient information generated during the modeling effort that a post modeling audit could be adequately performed by a third party and such that future reuse of the model is possible.” Despite best efforts, the modeling report may not clearly convey all aspects of the modeling effort to a reviewer. The archive should include the name and contact information for the lead modeler(s) in order to facilitate timely response to questions about the archive and model files. A well-constructed and well-documented archive provides critical documentation supporting the scientific soundness of the modeling. The archive should allow both replication of the modeling results presented in the report and, if called for, reproduction using a different code (Table 11.1).

**Table 11.1** Minimum information required for model replication and reproducibility

---

#### **Replication**

---

All files needed to run a model and obtain results

Model output files that allow evaluation that the model was run as described

---

#### **Reproducibility**

---

Graphical user interface files and other files required to construct model input files

---

The archive should include all raw and processed field data and related metadata used to create the model (Barnett et al., 2012). In addition, the groundwater flow code and parameter estimation code used in the study should be included, and the modeler produced simulation log (Section 3.7; Table 3.1). It will be helpful to include installation and model files for the Graphical User Interface (GUI) as in many cases the model representation in the GUI is the most convenient and powerful way for someone else to access the model. The final modeling report is included in the archive as are input and output files for final calibration and forecasting simulations that were used to obtain model outputs (graphs, figures, and statistics) presented in the report. Original data sets and other data information (e.g., Geographical Information System (GIS) coverages) should be included. If desired, the interim modeling reports and other products can also be included. Ideally both paper and electronic copies of all material are included in the archive and copies are stored in multiple secure locations. Instructions for retrieving the data should accompany the files and be accessible at other locations.

The archive should allow the model to be revived by future investigators or accessed by model reviewers, stakeholders and regulators but this poses some challenges as electronic storage media and data formats are continually changing. It is recognized that paper records, though they present challenges related to retrieving data, have a long shelf life and should be one component of a robust archive. O'Reilly (2010) recommends four steps to keep electronically stored data in archives safe: "choose file formats that won't become obsolete, use storage media that won't deteriorate or become inaccessible, make multiple copies stored apart, and check your archived data regularly to ensure it is still readable." Data sets should be stored in the original formats and one or more open generic formats; Barnett et al. (2012) suggest the use of ASCII text files and Jones et al. (2014) a compressed binary format (e.g., MODFLOW). It is recommended that some of the stored files be opened on a regular schedule (annually) to assure they remain accessible. In addition to the data files that are archived, the original modeling code or GUI can also become obsolete. As formats and software changes, files and codes may need to be periodically updated and archived in new formats. If it is critically important to have access to a model after an extended period (e.g., a model used in legal proceedings), it is recommended that professionals in archiving data be consulted when setting up and maintaining the archive. Otherwise, the sophistication of the archiving procedures can be matched to the resources available. The field measurements that describe the system should be a primary focus of even a simple modeling archive inasmuch as they underlie all modeling efforts and remain valuable sources of information long after the modeling is complete.

## 11.4 REVIEWING THE MODELING REPORT

The modeling report is typically reviewed by professionals chosen by the modeler or official reviewers such as staff of a regulatory agency, clients, anonymous peer reviewers,

outside expert panel, and/or an opposing expert in a legal action. [ASTM \(2013\)](#), [Neuman and Wierenga \(2003\)](#), [Reilly and Harbaugh \(2004\)](#), and [Barnett et al. \(2012\)](#) recommend that model review should consider: (1) the modeling purpose and objectives; (2) major defining and limiting considerations; (3) theoretical basis for the model; (4) parameter estimation methodology and results; (5) data quality and quantity; (6) key assumptions; (7) model performance measures; (8) model documentation and user's guide; (9) retrospective ([U.S. EPA 1994](#)). [Barnett et al. \(2012\)](#) proposed that models undergo three levels of review: an appraisal, in-depth peer review, and a postaudit (Section 10.7). They developed a series of questions as a compliance check list to assess if the model adequately met goals and objectives:

Are the model objectives clearly stated?

Are the objectives satisfied?

Is the conceptual model consistent with objectives?

Is the conceptual model based on all available data, presented clearly and reviewed by an appropriate reviewer?

Does the model design conform to best practices?

Is the model history matching satisfactory?

Are the final parameter values and estimated fluxes plausible?

Do the model predictions conform to best practices?

Is the uncertainty associated with the predictions reported?

Is the model fit for the purpose?

[Barnett et al. \(2012\)](#) also provide a more detailed set of questions to guide appraisals by a reviewer knowledgeable about the overall nature of the project and a peer reviewer knowledgeable about groundwater modeling. Here we address the peer review process.

During an in-depth peer review, access is given to all the materials in the appendices and modeling archive. The reviewer evaluates how well the project completed each step in the modeling process (Fig. 1.1). The reviewer evaluates the entire modeling effort focusing on the success of model calibration (both history matching and soft knowledge assessment), model assumptions and limitations, and validity of conclusions drawn from the modeling results. Reviewer(s) may also be asked to comment on the technical expertise of the author(s) of the modeling report, including education and experience.

The reviewer should pay special attention to the data sets and interpretations that underlie the conceptual model. The conceptual model, which is tailored to the modeling purpose, provides an efficient framework for all subsequent review. The reviewer should become familiar with the site being modeled and ideally should visit the site in person. A site visit puts the modeling conceptualization and assumptions in context and often provides background important for understanding the hydrogeologic setting. Review

of how the conceptual model was translated into the numerical model requires sufficient familiarity with the code so that input files and values selected for code-specific solver parameters can be evaluated.

The reviewer should examine the supplied input and output files (Table 11.1) using the relevant GUI and other required software to run the model and verify that results agree with those presented in the modeling report. In some cases, the complexity of the model and special requirements such as the need for parallel processing and large servers may preclude the reviewer from running the code. Under those circumstances, the modeling team responsible for the simulations should work closely with the reviewer and provide needed runs and data analyses. When a proprietary code was used, both code and input files should be made available to the reviewers. When agreements do not provide for direct access to the code, the modeler or group who produced the model should work with the reviewer to generate needed model executions and analyses. Review of model output is facilitated by a GUI or postprocessor that displays contour maps of head, velocity vector plots, hydrographs, and summary statistics (Section 9.4) related to the calibration. Graphs generated in a GUI or postprocessor can quickly synthesize large files of output data. In some cases it may be necessary to review the raw model output for convergence, warnings, and error reports. Simulated water budgets should be examined for consistency and reasonableness and compared with other estimates. A large water budget error and/or an anomalous entry in the simulated water budget may indicate a flaw in the design of the numerical model and/or an error in input data (Section 3.6).

When modeling results are used in the regulatory and legal arenas, interpretations of field conditions and model results may support different or even contradictory conclusions. However, all parties typically recognize that the same system is being represented and such differences in model results usually are the result of differences in assumptions about the conceptual and numerical models, and choices for spatial and temporal parameter assignment. When opposing parties cannot reach consensus on model formulation, their work is often reviewed by an independent person or group in an attempt to resolve differences, including settings where decisions are made by hearing examiners or judges and/or juries. The well-known trial concerning contaminated groundwater at Woburn, Massachusetts, is an excellent example of potential pitfalls that can occur when models are brought into the courtroom (Bair, 2001). The process leading to litigation might be somewhat streamlined if opposing parties were required to reach a consensus on the portions of the modeling process not in dispute and to identify important disputed issues. Fortunately, models provide a framework for such discussion (Hunt and Welter, 2010). Moreover, there is a growing awareness of the importance of communicating with and engaging stakeholders and decisions makers in the modeling process, which may help resolve disputes before they end up in the courtroom.

## 11.5 COMMON ERRORS IN REPORT/ARCHIVE PREPARATION AND REVIEW

- The report is not targeted to stakeholders or other end users. The information in the report is either overly complex or too simple for the target audience.
- The report is poorly written and/or poorly organized such that the modeling process and results cannot be understood and/or evaluated. Furthermore, a poorly written report brings the credibility of the author(s) into question.
- A model is transmitted to reviewers and/or stakeholders with missing or incorrect input or output, or without the GUI file that was used to construct the input. In addition to causing delay and expense to others, such negligence reflects poorly on the modeling effort.
- Archives are poorly organized and incomplete. Archives are of greatest value when they are carefully designed; archive maintenance should be performed on a regular schedule to modernize data format and verify access.
- Model review is conducted by poorly qualified evaluators. When professionals who have limited knowledge of the formulation, execution, and analyses of groundwater models act as reviewers their comments may improperly represent the modeling effort by either understating or overstating the value of the modeling results.
- A model and its report are prepared with a limited budget as a preliminary analysis of groundwater conditions but model reviewers evaluate it in the context of a fully budgeted detailed modeling project. Requests by clients for a preliminary groundwater model of a site may produce a model that will be criticized for its simplicity and incompleteness. Therefore, reports that document preliminary modeling efforts should clearly state modeling objectives and limitations.

## 11.6 PROBLEMS

**P11.1** Record keeping is essential in modeling.

- a. Describe the method of record keeping you used when modeling problems in Chapters 9 and 10. Could another modeler take your records and notes in their current condition and reconstruct the steps you used to produce calibrated steady-state and transient models? If not, do the problem again and this time keep a simulation log.
- b. Make a list of the important decisions/assignments in the calibration process that need to be documented in a modeling report.

**P11.2** Using your notes and the results from Problems P10.1, 10.2, and 10.3 prepare a short modeling report using the outline recommended in this chapter. Include a title, a description of the conceptual model and the code you used, discussion of the translation of the conceptual model to the numerical model, and results of the numerical model including methods of calibration. Conclude the report with a discussion of whether the results are a reasonable representation of the groundwater conditions represented in the conceptual model.



## REFERENCES

- ASTM International, 2008. Standard guide for developing and evaluating groundwater modeling codes, D6025–96(2008). American Society of Testing and Materials, Book of Standards 04 (09), 17 p.
- ASTM International, 2013. Standard guide for documenting a groundwater flow model application D5718–13. ASTM International, 100 Barr Harbor Drive, PO Box C700, West Conshohocken, PA 19428–2959, 6 p.
- Anderson, M.P., 2006. Plagiarism, copyright violation and dual publication: Are you guilty? *Groundwater* 44 (5), 623. <http://dx.doi.org/10.1111/j.1745-6584.2006.00246.x>.
- Bair, E.S., 2001. Models in the courtroom. In: Anderson, M.G., Bates, P.D. (Eds.), *Model Validation: Perspectives in Hydrological Science*. John Wiley & Sons Ltd, London, pp. 55–77.
- Barnett, B., Townley, L.R., Post, V., Evans, R.F., Hunt, R.J., Peeters, L., Richardson, S., Werner, A.D., Knapton, A., Boronkay, A., 2012. Australian Groundwater Modelling Guidelines. Waterlines Report No. 82, National Water Commission, Canberra, 191 p. [http://nwc.gov.au/\\_data/assets/pdf\\_file/0016/22840/Waterlines-82-Australian-groundwater-modelling-guidelines.pdf](http://nwc.gov.au/_data/assets/pdf_file/0016/22840/Waterlines-82-Australian-groundwater-modelling-guidelines.pdf).
- Doherty, J., 2011. Modeling: Picture perfect or abstract art? *Groundwater* 49 (4), 455. <http://dx.doi.org/10.1111/j.1745-6584.2011.00812.x>.
- Fienen, M., Hunt, R., Krabbenhoft, D., Clemo, T., 2009. Obtaining parsimonious hydraulic conductivity fields using head and transport observations—A Bayesian geostatistical parameter estimation approach. *Water Resources Research* 45 (8), W08405(23). <http://dx.doi.org/10.1029/2008WR007431>.
- Greene, A.E., 2013. *Writing Science in Plain English*. The University of Chicago Press, Chicago, 124 p.
- Hunt, R.J., Welter, D.E., 2010. Taking account of “unknown unknowns”. *Groundwater* 48 (4), 477. <http://dx.doi.org/10.1111/j.1745-6584.2010.00681.x>.
- Hunt, R.J., Schwartz, F.W., 2014. For whom do we write? Suggestions for getting read in the twenty-first century. *Groundwater* 52 (2), 163–164. <http://dx.doi.org/10.1111/gwat.12167>.
- Johansson, J.R., 2015. Introduction to scientific computing with Python, <https://github.com/jrjohansson/scientific-python-lectures/blob/master/Lecture-0-Scientific-Computing-with-Python.ipynb> (accessed 26.02.15).
- Jones, N.L., Lemon, A.M., Kennard, M.J., 2014. Efficient storage of large MODFLOW models. *Groundwater* 52 (3), 461–465. <http://dx.doi.org/10.1111/gwat.12060>.
- Morin, A., Urban, J., Adams, P.D., Foster, I., Sali, A., Baker, D., Sliz, P., 2012. Shining light into black boxes. *Science* 336 (6078), 159–160. <http://dx.doi.org/10.1126/science.1218263>.
- Neuman, S.P., Wierenga, P.J., 2003. *A Comprehensive Strategy of Hydrogeologic Modeling and Uncertainty Analysis for Nuclear Facilities and Sites*. NUREG/CF-6805, 236 p. <http://www.nrc.gov/reading-rm/doc-collections/nuregs/contract/cr6805/>.
- Ohio Environmental Protection Agency (OEPA), 2007. *Ground Water Flow and Fate and Transport Modeling*. Technical Guidance Manual for Ground Water Investigations chapter 14, 32 p. <http://www.epa.state.oh.us/ddagw/tgmweb.aspx>.
- O’Reilly, D., 2010. Future Proof Your Data Archive. <http://www.cnet.com/how-to/future-proof-your-data-archive/>.
- Peng, R.D., 2011. Reproducible research in computational science. *Science* 334 (6060), 1226–1227. <http://dx.doi.org/10.1126/science.1213847>.
- Reilly, T.E., Harbaugh, A.W., 2004. *Guidelines for Evaluating Ground-Water Flow Models*. U.S. Geological Survey Scientific Investigations Report 2004–5038, 30 p. <http://pubs.usgs.gov/sir/2004/5038/>.
- Stanton, J.S., Peterson, S.M., Fienen, M.N., 2010. *Simulation of Groundwater Flow and Effects of Ground-water Irrigation on Stream Base Flow in the Elkhorn and Loup River Basins, Nebraska, 1895–2055-Phase Two*. U.S. Geological Survey Scientific Investigations Report 2010–5149, 78 p. <http://pubs.usgs.gov/sir/2010/5149/>.
- Strunk Jr., W., White, E.B., 2009. *The Elements of Style*, fifth ed. Allyn and Bacon, Boston. 105 p.
- U.S. Environmental Protection Agency (EPA), 1994. *Assessment Framework for Ground-water Model Applications*. Solid Waste and Emergency Response, OSWER, EPA 500–8–94–003, 46 p.

## CHAPTER 12

# Beyond Basic Modeling Concepts

*I have yet to see any problem, however complicated, which when you looked at it in the right way did not become more complicated.*

*Poul Anderson*

*O, that way madness lies; let me shun that;*

*King Lear (Act III, Scene IV)*

### Contents

12.1 Introduction	515
12.2 Complex Groundwater Flow Processes	518
12.2.1 Flow through Fractures and Conduits	518
12.2.2 Aquifer Compaction	518
12.2.3 Variably Saturated Flow	519
12.2.4 Variable Density Flow	520
12.2.5 Multiphase Flow	521
12.2.6 Linked and Coupled Models	521
12.3 Transport Processes	522
12.4 Surface Water Processes	523
12.5 Stochastic Groundwater Modeling	524
12.6 Decision-Support and Optimization	525
12.7 Final Comments	526
References	527

### 12.1 INTRODUCTION

Groundwater flow models, described in Chapters 1–10, can solve many practical problems; however, the groundwater modeler eventually will encounter a problem that involves processes beyond simple groundwater flow. In Section 3.1 we briefly mentioned variably saturated flow, variable density flow, and multiphase flow. Simulating any of these three processes requires a more complicated flow equation than the basic groundwater flow equation (Eqn (3.12)). Simulating solute and heat transport and rigorous simulation of surface water routing require linking or coupling a groundwater flow model to transport models or rainfall-runoff models, respectively. Moreover, complex subsurface processes such as flow through conduits and fractures and aquifer compaction are typically not included in a basic groundwater flow simulation, although

some flow codes have options or add-on packages for those processes. Also, there are codes for simulating groundwater flow and transport with stochastic characterization of aquifer heterogeneity and codes designed to optimize decisions in management problems.

The first edition of this book (Anderson and Woessner, 1992) included a final chapter that briefly summarized theory and approaches for simulating complex groundwater problems. Now, however, there are many more ways to simulate complex processes in groundwater models. For example, there are options in groundwater flow codes for unsaturated flow and for coupling groundwater and streamflow routing models. Modern programming languages such as Python are well-suited for groundwater problems (e.g., Bakker, 2014) and can expand modeling tools to incorporate cutting-edge and well-tested methods of other sciences. There are also many more textbooks, reports, and journal papers to help the practitioner learn how to model complex problems where groundwater is an important but not the only process of interest. Given this explosion of information since the first edition, a single comprehensive chapter on advanced topics is simply not possible. Instead this chapter is intended to provide starting points for those who want to go beyond the fundamental concepts of groundwater flow modeling covered in Chapters 1–10. In this chapter we: (1) refer readers back to those sections in our book that briefly discuss simulation of advanced processes; (2) provide additional thoughts and some references to help readers get started in modeling complex processes in groundwater systems. Additional references and resources, such as Python versions of problems at the end of chapters in our book, are available at <http://appliedgwmodeling.elsevier.com>.

First, we cover complex subsurface flow processes: flow through conduits and fractures; aquifer compaction; variably saturated flow; and variable density flow. Then, we discuss transport of heat and solutes in groundwater, which requires linking or coupling a groundwater flow model to one or more transport models. Next, we discuss surface water processes; simple simulation of surface water can be handled by options and packages within a groundwater code, but rigorous surface water modeling requires coupling a groundwater code to a surface water code. Finally we discuss stochastic groundwater modeling and groundwater modeling in decision-support and optimization frameworks.

Before undertaking modeling of complex processes, the modeler should first consider whether simulation of additional processes beyond groundwater flow is necessary. Does the modeling purpose justify the additional time and expense that will be required? Is the appropriate model (Section 9.2) simpler and less costly? Simulating complex processes requires more knowledge and skill on the part of the modeler, as well as additional parameters and appropriate values for those parameters. The inclusion of additional parameters comes at a cost during model calibration (Fig. 10.2) unless information is also available to constrain the new parameters. Otherwise, a groundwater problem that was originally ill-posed and underdetermined (Section 9.2) becomes a more complicated problem that is still fundamentally ill-posed and undetermined. Moreover, the complications of simulating complex processes increase the computational burden; the potential for

numerical instability in the solution; the amount of output to analyze; and uncertainty in results. The conclusions in 1990 of a panel of modeling experts convened by the National Research Council (NRC, 1990, p. 14) are relevant:

*Ground water models do and should vary in complexity. The complexity of the model used to analyze a specific site should be determined by the type of problem being analyzed. While more complex models increase the range of situations that can be described, increasing complexity requires more input data, requires a higher level and range of skill of the modelers, and may introduce greater uncertainty in the output if input data are not available or of sufficient quality to specify the parameters of the model.*

Nevertheless, even complex models poorly constrained by observations can have value if only to explore the effect of a complex process on a forecast and its associated uncertainty. Using the tools in Chapters 9 and 10 such as parameter identifiability (Fig. 10.10) or the more advanced tools described in Box 9.6, the modeler can identify and focus on the factors most important to the forecast, i.e., those factors that dominate forecast uncertainty.

Throughout the book, we illustrate groundwater flow modeling concepts using the finite-difference (FD) code MODFLOW and the finite-element (FE) code FEFLOW. Fortunately, both MODFLOW and FEFLOW can handle many complex processes by turning on advanced options within the code, by adding modules, or by linking or coupling to other codes. In the discussion below, we mention specific advanced options for those codes, but the reader is urged to consult Web sites maintained by the developers of MODFLOW and FEFLOW for up-to-date listings of capabilities and related information.

Although we use MODFLOW and FEFLOW for illustration, concepts covered in our book, including this chapter, are relevant to any groundwater modeling code. Summary descriptions of MODFLOW and FEFLOW and several other codes including the popular code Transport Of Unsaturated Groundwater and Heat (TOUGH) are given by Bear and Cheng (2010, pp. 583–591) and Barnett et al. (2012; Table 4-1, pp. 42–44). TOUGH is a multiprocess control volume FD code that simulates “the coupled transport of water, vapor, non-condensable gas, and heat in porous and fractured media” (Lawrence Berkeley National Laboratory: <http://esd.lbl.gov/research/projects/tough/>). TOUGH is intended for simulation of “coupled thermal, hydrological, geochemical, and mechanical processes in permeable media” with application to “nuclear waste disposal, environmental remediation problems, energy production from geothermal, oil and gas reservoirs as well as gas hydrate deposits, geological carbon sequestration, vadose zone hydrology.” It currently has limited capabilities for representing other potentially important drivers such as surface water processes; options for simulating chemical reactions are also limited to those relevant to its primary applications for simulating fluids in geothermal reservoirs and around geological repositories proposed for high-level nuclear waste. More information about TOUGH can be found in a review paper by Finsterle et al. (2014) and on the TOUGH Web site.

## 12.2 COMPLEX GROUNDWATER FLOW PROCESSES

### 12.2.1 Flow through Fractures and Conduits

When fractures are uniformly distributed and well connected, the flow system may be appropriately simulated as an equivalent porous medium (EPM) (Box 2.2) using the methods described in Chapters 1–10 of our book. Effective aquifer parameters (for hydraulic conductivity, storage, and porosity) are defined so that the model reproduces the pattern and rates of flow observed in the field. The EPM approach assumes that fractured porous material can be treated as a continuum and that a representative elementary volume (REV; Section 3.2) of material characterized by effective aquifer parameters can be defined.

The difficulty in applying the EPM approach arises in determining the appropriate size of the REV needed to define equivalent hydraulic properties (e.g., [Muldoon and Bradbury, 2005](#)). The EPM approach may adequately represent the behavior of a regional flow system, but poorly reproduce local groundwater flow. When fractures are sparse and the hydraulic conductivity of the unfractured matrix is low, the EPM approach may not be appropriate even with a large REV ([Gale, 1982](#)). Flow through discrete fractures and conduits within a porous matrix can be simulated by discrete feature elements in FEFLOW (Section 5.2, Fig. 5.16; Section 6.2) and by the conduit flow process for MODFLOW and a similar option in MODFLOW-USG (Section 5.2). Specialty codes are available for simulating flow through a network of discrete fractures (e.g., FracMan: <http://www.fracman.com/>). Simulation of flow through a discrete network of fractures and conduits in carbonate rock (e.g., limestone and dolostone; karst systems, Fig. 2.14(a)) presents additional challenges owing to changes in secondary permeability resulting from dissolution and precipitation, which can change the geometry and permeability of the network (e.g., [Nogues et al., 2013](#)).

Other useful references on groundwater flow in fractures and conduits include [Ghasemizadeh et al. \(2012\)](#), [Sahimi \(2012\)](#), [Franciss \(2010\)](#), [Neuman \(2005\)](#), [Berkowitz et al. \(1988\)](#), [National Research Council \(1996, 2001\)](#), and [Bear et al. \(1993\)](#).

### 12.2.2 Aquifer Compaction

Aquifer compaction and associated land surface subsidence were important in the history of hydrogeology for understanding the concept of storage and defining storage parameters (e.g., see discussion of papers A1, A3, and A7 in [Anderson, 2008](#)). Aquifer compaction is the reduction in aquifer volume resulting from compaction of compressible fine-grained sediments within or adjacent to the aquifer in response to pumping ([Leake and Prudic, 1991](#)). As used in groundwater modeling, “compaction” refers to a decrease in aquifer thickness as a result of an increase in vertical compressive stress; the process is commonly called “consolidation” by soils engineers ([Leake and Galloway, 2007](#)). From a physical process point of view, poroelastic effects are relevant: “Poro-elastic effects

include fluid-to-solid coupling whereby a change in pore pressure causes a change in volume of porous material, which is manifested as land surface subsidence. Solid-to-fluid coupling occurs when a change in stress causes a change in pore pressure, which is manifested as water-level fluctuations” (Anderson, 2008, p. 17). Theoretical details are given by Wang (2000) and summarized by Bear and Cheng (2010, pp. 237–249).

Values of material property parameters change when aquifers and confining beds compact in response to changes in pore pressure. Aquifer compaction is irreversible when the skeletal structure of the porous material is permanently rearranged. Then, water removed from storage by pumping is permanently lost and the aquifer is considered mined (Leake and Prudic, 1991). For most applied groundwater models, the effect of compaction is typically small and can be neglected. However, in some cases, the altered geometry and loss of aquifer storage caused by compaction may be important, such as in cases of prolonged pumping from groundwater systems with highly compressible units (e.g., Holzer and Galloway, 2005; Kasmarek, 2012). Some codes have specialized capabilities to handle the changes in aquifer properties resulting from compaction. For example, MODFLOW’s Subsidence and Aquifer-System Compaction (SUB) Package (Hoffmann et al., 2003) and a similar package for water-table aquifers (SUB-WT; Leake and Galloway, 2007) account for both recoverable and permanent compaction as water is released from storage, including storage in compressible fine-grained interbeds.

### 12.2.3 Variably Saturated Flow

Our book focuses on modeling flow in the saturated zone below the water table where pore space is represented as being completely filled (saturated) with water (Section 3.1). A dilemma in modeling groundwater systems arises when selecting the upper boundary, which is often placed at the water table (Section 4.5) when the natural boundary for the subsurface is land surface (Box 6.2). Ideally, we would like to model the entire subsurface continuum so that infiltration at the land surface is routed through the unsaturated zone while accounting for losses from evapotranspiration (Box 5.4, Box 6.2). Then, processes that affect the amount and timing of groundwater recharge would be simulated holistically using gradients in pressure head and calculated as flow across the water table, i.e., the surface where pressure is zero (atmospheric) (e.g., see Fig. 4.22(c)).

However, simulating flow in the subsurface continuum requires a variably saturated flow model; complications arise because under unsaturated conditions hydraulic conductivity is a function of moisture content. Typically, a variably saturated flow code is based on the well-known Richards equation (e.g., see Bear and Cheng, 2010, p. 305), which is numerically and computationally more difficult to solve than the groundwater flow equation. Moreover, soil moisture characteristic curves, which define the relation between soil moisture and pressure, as well as curves that define the pressure dependence of unsaturated hydraulic conductivity, are required. Such site-specific functional relations

are not easily obtained; [Diersch \(2014, Appendix D\)](#) summarizes some generic relations that can be applied to site-specific soils. Furthermore, scaling issues present challenges when designing nodal spacing for a variably saturated flow model (Box 6.2).

We briefly discussed variably saturated and unsaturated flow in Section 4.5 and Box 6.2. In Box 5.4 (Fig. B5.4.2) we presented an example of recharge generated using a one-dimensional approximation for simulating unsaturated flow developed by [Niswonger et al. \(2006\)](#) for MODFLOW. Several options for simulating unsaturated flow are available in FEFLOW (see Table 10.3, p. 478, in [Diersch, 2014](#)). The reader is also referred to the book by [Szymkiewicz \(2013\)](#) and chapters in [Zheng and Bennett \(2002, Chapter 16\)](#), [Bear and Cheng \(2010, Chapter 6\)](#), and [Diersch \(2014, Chapter 10\)](#).

### 12.2.4 Variable Density Flow

By variable density flow, we mean flow of miscible fluids, i.e., fluids that mix with groundwater. Examples of miscible flow are: mixing of highly concentrated dissolved contaminants with groundwater; liquid phase flow at elevated temperatures in a geothermal reservoir; seepage of thermally altered water into groundwater of ambient temperature; seawater intrusion into coastal aquifers; brine disposal into freshwater aquifers; freshwater storage in saline aquifers.

Modeling variable density flow requires coupling a variable density groundwater flow model to a solute transport model, and also to a heat transport model ([Section 12.3](#)) if the fluids are affected by spatial and/or temporal changes in temperature. Nevertheless, “the greatest difference between uniform-density and variable-density problems is not in the transport equation, but rather in the equations governing the underlying groundwater flow regime, and in the fact that the flow and transport equations are two-way coupled” ([Zheng and Bennett, 2002, p. 445](#)). The governing equation for variable density flow is written with pressure as the dependent variable (e.g., see [Appendix A](#) in [Zheng and Bennett, 2002](#)). The problem is “two-way coupled” because flow is dependent on density, which is dependent on solute concentration, and velocity in the solute transport equation is dependent on the solution for groundwater flow. A starting point for learning about modeling variable density flow is [Zheng and Bennett \(2002; Chapter 15 and Appendix A\)](#). Also see [Holzbecher \(1998\)](#), [Diersch \(2014, Chapter 11\)](#) and review papers by [Simmons \(2005\)](#), [Diersch and Kolditz \(2002a\)](#), and [Simmons et al. \(2001\)](#).

Flow of miscible fluids is complex because changes in concentration of solute can appreciably affect fluid density, which may also be affected by the temperature of the fluid ([Section 3.1](#)). In applied groundwater modeling, the most common type of variable density flow problem involving miscible fluids is seawater intrusion in coastal aquifers. Recent attention has focused on the effect of potential climate change on seawater intrusion (e.g., [Loáiciga et al., 2012](#); [Langevin and Zygnerski, 2012](#)). Sharp interface models, which assume there is no mixing between freshwater and seawater, were discussed in [Box 4.4](#).

If the interface cannot be approximated as a sharp front, a variable density code is required to simulate mixing in the transition zone (Fig. 4.10). Several variable density codes suited to modeling seawater intrusion are currently available (e.g., see Table 1, p. 11, in [Werner et al., 2013](#)). The code SEAWAT ([Langevin et al., 2007, 2004](#)), which was derived from MODFLOW and MT3DMS, is specifically designed for applied modeling of seawater intrusion under various temperature regimes. SUTRA ([Voss and Provost, 2002](#)) is a generic variable density FE code that can be applied to seawater intrusion problems (e.g., [Gingrich and Voss, 2005](#)). Likewise, FEFLOW has options for variable density flow built directly into the code ([Diersch and Kolditz, 2002b](#)). The literature on seawater intrusion is enormous; some recent review papers that include discussion of modeling seawater intrusion include [Werner et al. \(2013\)](#) and [Carrera et al. \(2010\)](#). Also see [Bear and Cheng \(2010, Chapter 10\)](#).

### 12.2.5 Multiphase Flow

Immiscible fluids (both liquids and gases) move as separate phases within the subsurface. Some examples of immiscible (multiphase) flow include: gasoline or dry cleaning solvents in groundwater; air and water in the unsaturated zone; oil, gas, and water in a petroleum reservoir; water and steam in a geothermal reservoir.

The most common type of multiphase flow in applied groundwater modeling involves nonaqueous phase liquids (NAPLs). NAPLs may be either lighter (LNAPL) or denser (DNAPL) than groundwater. Models simulating NAPLs in groundwater are complicated because a separate set of equations for flow and transport of solute is needed for groundwater and each NAPL. Moreover, for each NAPL there typically is an associated gaseous zone in the unsaturated zone as well as a miscible transition zone in the saturated zone where some NAPL mixes with groundwater. Furthermore, geometry of hydrostratigraphic units (e.g., dip) can be more important for DNAPL movement than hydraulic gradients.

The transport code MT3DMS can be linked to another code (e.g., HSSM by [Weaver, 1996](#)) for simulation of LNAPL (see [Zheng, 2009](#)). A classic reference for visualizing NAPL flow in the subsurface is [Schwille \(1988\)](#); also see [Mayer and Hassanizadeh \(2005\)](#). Multiphase modeling in porous media was reviewed by [Helmig et al. \(2013\)](#), [Abriola \(1989\)](#), and [Pinder and Abriola \(1986\)](#) and discussed by [Christ et al. \(2006\)](#) and [Gerhard et al. \(2007\)](#), among others.

### 12.2.6 Linked and Coupled Models

A basic groundwater flow model, or one that simulates variably saturated flow or variable density flow, may be linked or coupled to a solute or heat transport model ([Section 12.3](#)) or a rainfall-runoff model ([Box 6.3; Section 12.4](#)). When a flow model is linked to a transport or rainfall-runoff model, the flow model is solved first and results are input to the other



model, which is solved in the same time step as the flow model. In other words, the models are solved sequentially without feedback within the time step. When results from one model significantly affect parameters in the other model within a time step (e.g., temporal changes in temperature and/or solutes affect density and viscosity, which affect hydraulic conductivity; or fluctuations in stream stage affect groundwater flow), it is necessary to couple the flow model to the transport model or rainfall-runoff model. When coupled, the models are solved iteratively within the time step and input to each model is updated to reflect output from the other. Of course, a flow model (basic groundwater flow, variably saturated flow, or variable density flow) can be linked or coupled to both transport model(s) and a rainfall-runoff model as part of a hydrologic response model (Box 6.2).

### 12.3 TRANSPORT PROCESSES

Simulating the transport of heat and solutes (including contaminants) involves solving linked or coupled groundwater flow and transport models. In applied groundwater modeling, solute transport is based on the advection–dispersion equation. The heat transport equation is of the same form as the advection–dispersion equation. In fact, the solute transport code MT3DMS, which links to the flow code MODFLOW, can be used for transport of heat by variable conversion (Zheng, 2009) when temperature–dependent changes in viscosity and density are negligible. FEFLOW includes options for transport of both heat and solutes (Diersch, 2014, Chapters 11, 12, 13).

Although transport based on the advection–dispersion equation is the norm in applied groundwater modeling “there are a number of conceptual weaknesses and flaws in the underlying theory” (Konikow, 2011) and other approaches have been proposed (e.g., Hadley and Newell, 2014). When simulating solute transport in highly heterogeneous or fractured media, the advection–dispersion equation is a poor predictor of transport processes. One way to improve forecasting with the advection–dispersion equation is to include a term to describe the exchange of heat or solute between fractures or highly permeable preferential flowpaths and the surrounding porous matrix. This is done using a dual-porosity (also called dual domain) approach introduced in the 1960s (see Anderson, 2008; pp. 104–105, for the historical background). Zheng et al. (2011) and Zheng and Bennett (2002), among others, discuss the dual-porosity approach applied to simulating transport in aquifers with highly conductive preferential flowpaths. Both MT3DMS and FEFLOW have a dual-porosity option.

A basic solute transport code solves for the concentration of a single chemical species. To simulate reactions between two or more chemical species, geochemical reaction modules interface with the transport code. For example, MT3DMS interfaces with RT3D (Clement, 1997, 2003) or PHT3D (Prommer et al., 2003; Prommer and Post, 2010; also see reviews by Appelo and Rolle, 2010; Zheng, 2009). FEFLOW also has options for including multispecies reactions (Diersch, 2014, Chapter 12).

The literature on modeling heat and solute transport in groundwater is immense. Some useful starting points are the textbook by [Zheng and Bennett \(2002\)](#) and summary paper by [Konikow \(2011\)](#). Theory is discussed by [Diersch \(2014, Chapters 11, 12, 13\)](#) and [Bear and Cheng \(2010, Chapter 7\)](#). Additionally, [Saar \(2011\)](#) and [Anderson \(2005\)](#) review the theory and application of heat transport models to groundwater problems.

## 12.4 SURFACE WATER PROCESSES

Surface water processes occur in a variety of settings including streams, lakes, wetlands, and the ocean and are an integral part of groundwater modeling inasmuch as groundwater and surface water are typically well connected in nonarid hydrogeological settings. In basic groundwater modeling, interest in surface water processes is typically limited to simulating the exchange of water between an aquifer and surface water.

In most applied groundwater models, simple surface water exchange with groundwater systems can be adequately simulated via boundary conditions that are available in all groundwater flow codes (Sections 4.2, 4.3). In [Box 4.4](#) and in [Section 12.2](#), we discussed variable density groundwater flow in coastal aquifers where groundwater interfaces with seawater. In [Chapter 6](#) we discussed some advanced options for representing surface water processes in groundwater models, including streamflow routing in channels via the Manning equation ([Section 6.5](#)), representation of lakes using MODFLOW's Lake Package ([Section 6.6](#)), and overland flow in wetlands via the Kadlec equation ([Section 6.7](#)). Surface water modelers use a variety of rainfall-runoff models that typically include a highly simplified representation of the groundwater system ([Box 6.3](#)) to forecast streamflow ([Beven, 2012](#); [Loague, 2010](#)). Likewise, groundwater modelers use simplified representations of surface water processes in groundwater models. Although such simplifications can be appropriate for many situations, some problems require coupling a rainfall-runoff model to a groundwater model. Even though computationally expensive, applications of such coupled models likely will become increasingly common (e.g., [Fig. B6.3.1](#), [Box 6.3](#)).

There is a large literature on modeling groundwater–surface water interaction including models of conjunctive use of groundwater and surface water that date from the 1960s (e.g., [Jenkins, 1968](#)) to the present (e.g., [Schmid et al., 2014](#); [Hanson et al., 2012](#); [Schoups et al., 2006](#)), as well as models that address the relatively new interest in groundwater–surface water exchange in the hyporheic zone (the subsurface region surrounding a stream channel where surface water mixes with groundwater). Groundwater modeling of the hyporheic zone progresses historically from relatively simple representations (e.g., [Harvey and Bencala, 1993](#); [Woessner, 2000](#)) to relatively complex ([Sawyer and Cardenas, 2009](#); [Zhou et al., 2014](#)). [Anderson and Siegel \(2013\)](#) give an historical overview of modeling groundwater–surface water interaction; the reader will find citations to recent models of groundwater–surface water interaction throughout our book, especially in [Chapters 4](#) and [6](#).

## 12.5 STOCHASTIC GROUNDWATER MODELING

Freeze's (1975) analysis of uncertainty in groundwater flow models helped launch the discipline of stochastic groundwater hydrology (e.g., see Fig. 3 in Dagan, 1986). In the last quarter of the twentieth century a large number of journal papers were published on the topic; there are also several books on geostatistics and stochastic modeling in hydrogeology (Dagan, 1989; Gelhar, 1993; Kitanidis, 1997; Zhang, 2002; Rubin, 2003).

In stochastic modeling, one or more parameters have a probabilistic distribution (Box 10.1). For example, spatial variability (heterogeneity) in hydraulic conductivity may be represented by  $Y = \ln K$ , where  $K$  is hydraulic conductivity and  $Y$  is a random space function. By representing  $K$  in this manner, the governing equation for groundwater flow becomes a stochastic partial differential equation because  $K$  is represented as a random space function. The probabilistic representation of flow can be carried into a transport model so that the stochastic partial differential equation for solute transport (i.e., the advection-dispersion equation) is solved for the expected value of concentration. Much attention was focused on analytical solutions of the stochastic advection-dispersion equation but by the end of the twentieth century, the analytical approach was not being used in applied groundwater modeling (e.g., see Dagan, 2002; Renard, 2007). Instead, numerical solutions using the Monte Carlo method emerged as the favored approach for solving stochastic groundwater models.

An advantage of stochastic modeling is that probabilities and multiple realizations capture inherent uncertainties of the unseen subsurface and provide theoretical rigor lacking in a deterministic approach. Multiple realizations may be generated using geostatistical methods, geologic process models, and multiple-point geostatistics; Michael et al. (2010) presented an approach that combines all three methods. In geostatistical methods (e.g., see the review by Marsily et al., 2005), uncertain parameters are represented by random variables with assigned statistics (e.g., mean value, standard deviation, and variogram). In practice, the uncertain parameter is usually hydraulic conductivity, for which multiple possible realizations of the hydraulic conductivity field are generated using kriging (Section 5.5, Fig. 5.30), the Monte Carlo method, and a random field generator (Section 10.5). Such geostatistical methods are used to generate realizations in Stochastic MODFLOW and MODPATH (Ruskauff et al., 1998).

Alternatively, geologic process models, which simulate deposition of sediment, have been used to generate multiple realizations of a hydrogeologic setting; inferences about the parameter field can then be made using hydrogeologic judgment (Kolterman and Gorelick, 1996; Marsily et al., 2005). Multiple-point geostatistics (Hu and Chuginova, 2008) use a training image (Mariethoz and Caers, 2014) rather than a variogram to describe the structure of geological heterogeneity. A training image is developed from geological and/or geophysical information and can include preferential flowpaths of high hydraulic conductivity important for solute transport. Multiple realizations are generated but only those realizations that are consistent with the basic patterns of the

training image are retained. Connectivity metrics (reviewed by [Renard and Allard, 2013](#)) can be used to assess the connection among geological heterogeneities (e.g., along preferential flowpaths of high hydraulic conductivity) in the realizations.

In the context of parameter estimation, a stochastic approach means that “all alternative solutions to the inverse problem are considered likely realizations of the aquifer heterogeneity, and all solutions are treated as an ensemble of realizations that must be further analyzed to make uncertainty-qualified predictions” ([Zhou et al., 2014](#), p. 26). In inverse stochastic modeling ([Zhou et al., 2014](#); [Gómez-Hernández et al., 2003](#)), special methods are used to solve the inverse problem for a set of acceptable calibrated models.

Their superior theoretical rigor notwithstanding, stochastic methods require subjective judgment. For example, although training images can reduce the number of plausible realizations for stochastic modeling, the modeler must select the images that reflect plausible aquifer heterogeneity. Hence, subjective decisions are required in stochastic modeling as in deterministic modeling (e.g., Fig. 9.16), albeit uncertainty resulting from heterogeneity is more rigorously handled in a stochastic framework ([Gómez-Hernández, 2006](#)). Stochastic modeling is computationally intensive, especially when the groundwater model is highly parameterized (Section 9.6). Moreover, clients, regulators, decision-makers, and other stakeholders typically are not willing to consider more than one realization (multiple models) of a groundwater system in the decision-making process. However, with increased computer power, the ability to evaluate multiple stochastic realizations will improve and stakeholders may become more willing to accept an uncertainty analysis based on multiple models (Section 10.5).

## 12.6 DECISION-SUPPORT AND OPTIMIZATION

Many groundwater modeling applications are driven by regulatory requirements and/or water management planning, including economics (e.g., [Guillaume et al., 2012](#); [Srinivasan et al., 2010](#)). Groundwater modelers have formally incorporated groundwater models into the decision-making process (e.g., [Freeze et al., 1990](#)), including probabilistic assessments to evaluate risk (e.g., [Enzenhoefer et al., 2014](#)). There is also a large literature on using formal optimization methods in conjunction with groundwater models where the objective is to find an optimal solution given a set of societal constraints ([Ahlfeld and Mulligan, 2000](#)). For example, a typical groundwater management question is to find the maximum pumping rate for a well field while maintaining a specified streamflow in a nearby stream. There are versions of MODFLOW that address management problems including the Groundwater Management Process ([Ahlfeld et al., 2005, 2009](#); [Banta and Ahlfeld, 2013](#)) and the Farm Process ([Schmid et al., 2006](#); [Schmid and Hanson, 2009](#)). In addition to [Ahlfeld and Mulligan \(2000\)](#), useful starting points for learning about optimization methods applied to groundwater modeling are [Zheng and Bennett \(2002, Chapter 17\)](#) and [Bear and Cheng \(2010, Chapter 11\)](#).

The need for groundwater modelers to engage and include stakeholders is becoming well recognized (e.g., [Tidwell and Van Den Brink, 2008](#)). Such feedback and interaction can take place when groundwater models are updated and maintained as ongoing management tools such as in adaptive management (Sections 1.6, 10.7). For example, countrywide groundwater models are used for water resources planning and management in Denmark ([Refsgaard et al., 2010](#)) and the Netherlands ([De Lange et al., 2014](#); [De Lange, 2006](#)) and efforts are underway in the United Kingdom to develop a network of such groundwater models ([Shepley et al., 2012](#)). Groundwater models are also being formally included in decision support systems (DSSs). A DSS is “a metadiscipline, which integrates knowledge and practices across multiple scientific fields (e.g., hydrology, ecology, economics, various social sciences)” ([Jakeman et al., 2011](#)). Clearly, when linking across multiple disciplines the weak link will undermine not only that part of the system represented by the weak link but could adversely affect the entire DSS. Therefore, there has been much interest in improving the underlying models that underpin a DSS; best practices such as covered in our book help ensure that the groundwater component of a DSS is sound.

As part of a DSS, the runtime of the groundwater model becomes important because a DSS is intended to answer “what if?” questions quickly. There is an expectation that results will be presented within a few seconds. If a groundwater model’s runtime is too long, it will not be useful in a DSS. Even under the best circumstances, typical groundwater models have runtimes longer than a few seconds. Yet simple groundwater models with short runtimes constructed specifically for integration into a DSS may not adequately simulate processes important for the decision of interest. In one approach for addressing this issue, researchers are working toward distilling fast-running simple groundwater models from longer running complex models. In other words, a model that is designed to be appropriately simple for a specific forecast is derived from a complex model. In the broadest sense, the simple model becomes a transfer function—a simplifying construct that provides a useful approximation of a more complex system and generates representative forecasts (ideally accompanied by an indication of forecast uncertainty). One family of such forecast generators is described in Box 1.1. Examples of recent advances in the theoretical development of paired simple and complex models for groundwater forecasts and forecast uncertainty are described by [Razavi et al. \(2012\)](#), [Watson et al. \(2013\)](#), [White et al. \(2014\)](#), and [Burrows and Doherty \(2014\)](#).

## 12.7 FINAL COMMENTS

Efforts to adapt models to address the needs of stakeholders are aimed at addressing societal issues effectively and efficiently. Models that simulate complicated coupled hydraulic, thermal, chemical, and mechanical subsurface processes are being used to simulate hydraulic fracturing associated with development of unconventional oil and gas;

carbon sequestration in the subsurface; groundwater flow and transport around proposed geologic repositories for high-level nuclear waste; and remediation of contaminated aquifers. There is also increased interest in coupling subsurface and surface water models to plan for the hydrologic effects of potential climate change and sustainable conjunctive use of surface water and groundwater. Hence, groundwater modelers will increasingly be drawn into interdisciplinary modeling efforts. One example of extending groundwater concepts to societal issues is epitomized by the field of ecohydrology, which is the integration of groundwater hydrology and ecology for the purposes of societal decision-making (Hunt et al., in press; Hunt and Wilcox, 2003). Ecohydrological issues are wide-ranging and can include seemingly disparate topics as the effects of hydrologic, agricultural, and urbanization stresses on wildlife and wetlands; changes in groundwater discharge on fish habitat; and microbial reactions at the periphery of a contaminant plume on aquifer remediation strategies (Hancock et al., 2009).

The broadening of modeling objectives to societally relevant topics brings new challenges to groundwater modeling: “Today, there is less emphasis on pure research in small teams and more emphasis on larger and more complex problems of global importance undertaken by multidisciplinary teams. The challenge of emerging new problems is unprecedented in the history of hydrogeological sciences” (Schwartz, 2012). As increasingly complex problems are addressed using integrated and coupled models, groundwater modeling is moving beyond a single person to teams of scientists, engineers, and other specialists (Hunt and Zheng, 2012; Langevin and Panday, 2012). Applied groundwater modelers can expect to be called upon to integrate, defend, and explain their modeling work to other scientists, economists, engineers, and modelers. Consequently, not only do groundwater modelers need to be well-versed in the basics of modeling groundwater flow as covered in our book, but also be aware of the overarching philosophy and practices of other types of environmental modeling and decision-making (e.g., Beven, 2009; Soetaert and Herman, 2009). The best practices described in our book serve as a first step toward effective groundwater modeling, and the methods described for groundwater models provide an entry into the larger world of effective societal problem solving using environmental models.

*Once more unto the breach, dear friends, once more...*

*Henry V, Act III*

## REFERENCES

- Abriola, L.M., 1989. Modeling multiphase migration of organic chemicals in groundwater systems—A review and assessment. *Environmental Health Perspectives* 83, 117–143. <http://dx.doi.org/10.2307/3430652>.
- Ahlfeld, D.P., Baker, K.M., Barlow, P.M., 2009. GWM-2005—A Groundwater-Management Process for MODFLOW-2005 with Local Grid Refinement (LGR) Capability. U.S. Geological Survey Techniques and Methods, 6—A33, 65 p. <http://pubs.usgs.gov/tm/tm6a33/>.

- Ahlfeld, D.P., Barlow, P.M., Mulligan, A.E., 2005. GWM—A Ground—Water Management Process for the U.S. Geological Survey Modular Ground—Water Model (MODFLOW—2000). U.S. Geological Survey Open—File Report 2005—1072, 124 p. <http://pubs.usgs.gov/of/2005/1072/>.
- Ahlfeld, D.P., Mulligan, A.E., 2000. Optimal Management of Flow in Groundwater Systems: An Introduction to Combining Simulation Models and Optimization Methods. Academic Press, 185 p.
- Anderson, M.P., 2005. Heat as a ground water tracer. *Groundwater* 43 (6), 951—968. <http://dx.doi.org/10.1111/j.1745-6584.2005.00052.x>.
- Anderson, M.P. (Ed.), 2008. *Benchmark Papers in Hydrology, 3: Groundwater. Selection, Introduction and Commentary by Mary P. Anderson.* IAHS Press, 625 p.
- Anderson, M.P., Siegel, D.I., 2013. Seminal advances in hydrogeology 1963 to 2013: The O.E. Meinzer Award Legacy. In: Bickford, M.E. (Ed.), *The Web of Geological Science: Advances, Impacts and Interactions.* Geological Society of America, Denver, CO, pp. 463—500. Special Paper 500, (Chapter 14).
- Anderson, M.P., Woessner, W.W., 1992. *Applied Groundwater Modeling: Simulation of Flow and Advective Transport.* Academic Press, 381 p.
- Appelo, C.A.J., Rolle, M., 2010. PHT3D: A reactive multicomponent transport model for saturated porous media. *Groundwater* 48 (5), 627—632. <http://dx.doi.org/10.1111/j.1745-6584.2010.00732.x>.
- Bakker, M., 2014. Python scripting: The return to programming. *Groundwater* 52 (6), 821—822. <http://dx.doi.org/10.1111/gwat.12269>.
- Banta, E.R., Ahlfeld, D.P., 2013. GWM—VI — Groundwater Management with Parallel Processing for Multiple MODFLOW versions. U.S. Geological Survey Techniques and Methods 6—A48. <http://pubs.usgs.gov/tm/6a48/>.
- Barnett, B., Townley, L.R., Post, V., Evans, R.F., Hunt, R.J., Peeters, L., Richardson, S., Werner, A.D., Knapton, A., Boronkay, A., 2012. *Australian Groundwater Modelling Guidelines.* Waterlines Report No. 82. National Water Commission, Canberra, 191 p. [http://nwc.gov.au/\\_\\_data/assets/pdf\\_file/0016/22840/Waterlines-82-Australian-groundwater-modelling-guidelines.pdf](http://nwc.gov.au/__data/assets/pdf_file/0016/22840/Waterlines-82-Australian-groundwater-modelling-guidelines.pdf).
- Bear, J., Cheng, A.H.-D., 2010. *Modeling Groundwater Flow and Contaminant Transport, Theory and Applications of Transport in Porous Media.* Springer, 834 p.
- Bear, J., Tsang, C.-F., Marsily, G. de, 1993. *Flow and Contaminant Transport in Fractured Rock.* Academic Press, 560 p.
- Berkowitz, B., Bear, J., Braester, C., 1988. Continuum models for contaminant transport in fractured porous formations. *Water Resources Research* 24 (8), 1225—1236. <http://dx.doi.org/10.1029/WR024i008p01225>.
- Beven, K.J., 2009. *Environmental Modelling: An Uncertain Future?* Routledge, London, 310 p.
- Beven, K.J., 2012. *Rainfall-Runoff Modeling: The Primer,* second ed. Wiley-Blackwell, 488 p.
- Burrows, W., Doherty, J., 2014. Efficient calibration/uncertainty analysis using paired complex/surrogate models. *Groundwater*. <http://dx.doi.org/10.1111/gwat.12257> early view.
- Carrera, J., Hidalgo, J.J., Slooten, L.J., Vázquez-Suñé, E., 2010. Computational and conceptual issues in the calibration of seawater intrusion models. *Hydrogeology Journal* 18 (1), 131—145. <http://dx.doi.org/10.1007/s10040-009-0524-1>.
- Christ, J.A., Ramsburg, C.A., Pennell, K.D., Abriola, L.M., 2006. Estimating mass discharge from dense nonaqueous phase liquid source zones using upscaled mass transfer coefficients: An evaluation using multiphase numerical simulations. *Water Resources Research* 42 (11), W11420. <http://dx.doi.org/10.1029/2006WR004886>.
- Clement, T.P., 1997. *A Modular Computer Model for Simulating Reactive Multi-species Transport in Three-Dimensional Ground Water Systems.* Draft Report, PNNL-SA-28967. Pacific Northwest National Laboratory, Richland, Washington.
- Clement, T.P., 2003. *RT3D v2.5 Updates to User's Guide.* Pacific Northwest National Laboratory, Richland, Washington.
- Dagan, G., 1986. Statistical theory of groundwater flow and transport: Pore to laboratory, laboratory to formation, and formation to regional scale. *Water Resources Research* 22 (9S), 120S—134S. <http://dx.doi.org/10.1029/WR022i09Sp0120S>.

- Dagan, G., 1989. *Flow and Transport in Porous Formation*. Springer-Verlag, Heidelberg, Berlin, New York, 465 p.
- Dagan, G., 2002. An overview of stochastic modeling of groundwater flow and transport: From theory to applications. *Eos* 83 (53), 621–625. <http://dx.doi.org/10.1029/2002EO000421>.
- De Lange, W.J., 2006. Development of an analytic element ground water model of the Netherlands. *Groundwater* 44 (1), 111–115. <http://dx.doi.org/10.1111/j.1745-6584.2005.00142.x>.
- De Lange, W.J., Prinsen, G.F., Hoogewoud, J.C., Veldhuizen, A.A., Verkaik, J., Oude Essink, G.H.P., van Walsum, P.E.V., Delsman, J.R., Hunink, J.C., Massop, H.ThL., Kroon, T., 2014. An operational, multi-scale, multi-model system for consensus-based, integrated water management and policy analysis: The Netherlands Hydrological Instrument. *Environmental Modelling & Software* 59, 98–108. <http://dx.doi.org/10.1016/j.envsoft.2014.05.009>.
- Diersch, H.J.G., 2014. *FEFLOW: Finite Element Modeling of Flow, Mass and Heat Transport in Porous and Fractured Media*. Springer, 996 p.
- Diersch, H.J.G., Kolditz, O., 2002a. High-density flow and transport in porous media: Approaches and challenges. *Advances in Water Resources* 25 (8–12), 899–944. [http://dx.doi.org/10.1016/S0309-1708\(02\)00063-5](http://dx.doi.org/10.1016/S0309-1708(02)00063-5).
- Diersch, H.J.G., Kolditz, O., 2002b. Variable-density flow and transport in porous media: Approaches and challenges. In: *FEFLOW White Papers Vol. II*. <http://www.feflow.info/manuals.html>.
- Enzenhofer, R., Bunk, T., Nowak, W., 2014. Nine steps to risk-informed wellhead protection and management: A case study. *Groundwater* 52 (S1), 161–174. <http://dx.doi.org/10.1111/gwat.12161>.
- Finsterle, S., Sonnenthal, E.L., Spycher, N., 2014. Advances in subsurface modeling using the TOUGH suite of simulators. *Computers & Geosciences* 65, 2–12. <http://dx.doi.org/10.1016/j.cageo.2013.06.009>.
- Franciss, F.O., 2010. *Fractured Rock Hydraulics*. Taylor & Francis Group, London, UK. CRC Press, Balkema, The Netherlands, 179 p.
- Freeze, R.A., 1975. A stochastic-conceptual analysis of one-dimensional groundwater flow in nonuniform homogeneous media. *Water Resources Research* 11 (5), 725–741. <http://dx.doi.org/10.1029/WR011i005p00725> (Reprinted in Anderson, M.P. (Ed.), 2008, *Benchmark Papers in Hydrology*, 3: *Groundwater*. Selection, Introduction and Commentary by Mary P. Anderson. IAHS Press, pp. 331–347.).
- Freeze, R.A., Massmann, J., Smith, L., Sperling, T., James, B., 1990. Hydrogeological decision analysis: 1. A framework. *Groundwater* 28 (5), 738–766. <http://dx.doi.org/10.1111/j.1745-6584.1990.tb01989.x>.
- Gale, J.E., 1982. Assessing the permeability characteristic of fractured rock. *Geological Society of America Special Paper* 189, 163–181.
- Gelhar, L.W., 1993. *Stochastic Subsurface Hydrology*. Prentice Hall, Englewood Cliffs, NJ, 390 p.
- Gerhard, J.L., Pang, T.W., Kueper, B.H., 2007. Time scales of DNAPL migration in sandy aquifers examined via numerical simulation. *Groundwater* 45 (2), 147–157. <http://dx.doi.org/10.1111/j.1745-6584.2006.00269.x>.
- Ghasemizadeh, R., Hellweger, F., Butscher, C., Padilla, I., Vesper, D., Field, M., Alshwabken, A., 2012. Review: Groundwater flow and transport modeling of karst aquifers, with particular reference to the North Coast Limestone aquifer system of Puerto Rico. *Journal of Hydrogeology* 20 (8), 1441–1461. <http://dx.doi.org/10.1007/s10040-012-0897-4>.
- Gingerich, S.B., Voss, C.I., 2005. Three-dimensional variable-density flow simulation of a coastal aquifer in southern Oahu, Hawaii, USA. *Hydrogeology Journal* 13 (2), 436–450. <http://dx.doi.org/10.1007/s10040-004-0371-z>.
- Gómez-Hernández, J.J., 2006. Complexity. *Groundwater* 44 (6), 782–785. <http://dx.doi.org/10.1111/j.1745-6584.2006.00222.x>.
- Gómez-Hernández, J.J., Hendricks Franssen, H.J.W.M., Sahuquillo, A., 2003. Stochastic conditional inverse modeling of subsurface mass transport: A brief review and the self-calibration method. *Stochastic Environmental Research Risk Assessment* 17 (5), 319–328. <http://dx.doi.org/10.1007/s00477-003-0153-5>.
- Guillaume, J.H.A., Qureshi, M.E., Jakeman, A.J., 2012. A structured analysis of uncertainty surrounding modeled impacts of groundwater-extraction rules. *Hydrogeology Journal* 20 (5), 915–932. <http://dx.doi.org/10.1007/s10040-012-0864-0>.



- Hadley, P.W., Newell, C., 2014. The new potential for understanding groundwater contaminant transport. *Groundwater* 52 (2), 174–186. <http://dx.doi.org/10.1111/gwat.12135> (Also see discussion by S.P. Neuman (<http://dx.doi.org/10.1111/gwat.12245>) and reply by Hadley and Newell, 2014, *Groundwater* 52(5), 653–658. <http://dx.doi.org/10.1111/gwat.12246>).
- Hancock, P.J., Hunt, R.J., Boulton, A.J., 2009. Hydrogeocology: The interdisciplinary study of groundwater dependent ecosystems. *Hydrogeology Journal* 17 (1), 1–3. <http://dx.doi.org/10.1007/s10040-008-0409-8>.
- Hanson, R.T., Flint, L.E., Flint, A.L., Dettinger, M.D., Faunt, C.C., Cayan, D., Schmid, W., 2012. A method for physically based model analysis of conjunctive use in response to potential climate changes. *Water Resources Research* 48 (6), W00L08. <http://dx.doi.org/10.1029/2011WR010774>.
- Harvey, J.W., Bencala, K.E., 1993. The effect of streambed topography on surface-subsurface water exchange in mountain catchments. *Water Resources Research* 29 (1), 89–98. <http://dx.doi.org/10.1029/92WR01960> (Reprinted in Anderson, M.P. (Ed.), 2008, *Benchmark Papers in Hydrology, 3: Groundwater. Selection, Introduction and Commentary by Mary P. Anderson.* IAHS Press, pp. 458–467.).
- Helmig, R., Flemisch, B., Wolff, M., Ebigbo, A., Class, H., 2013. Model coupling for multiphase flow in porous media. *Advances in Water Resources* 51, 52–66. <http://dx.doi.org/10.1016/j.advwatres.2012.07.003>.
- Hoffmann, J., Leake, S.A., Galloway, D.L., Wilson, A.M., 2003. MODFLOW-2000 Ground-Water Model: User Guide to the Subsidence and Aquifer-system Compaction (SUB) Package. U.S. Geological Survey Open-File Report 2003-233, 44 p. <http://pubs.usgs.gov/of/2003/ofr03-233/>.
- Holzbecher, E.O., 1998. *Modeling Density-driven Flow in Porous Media—Principles, Numerics, Software.* Springer-Verlag, Berlin, 286 p.
- Holzer, T.L., Galloway, D.L., 2005. Impacts of land subsidence caused by withdrawal of underground fluids in the United States. *Reviews in Engineering Geology* 16, 87–99. [http://dx.doi.org/10.1130/2005.4016\(08\)](http://dx.doi.org/10.1130/2005.4016(08)).
- Hu, L.Y., Chugunova, T., 2008. Multiple-point geostatistics for modeling subsurface heterogeneity: A comprehensive review. *Water Resources Research* 44 (11), W11413. <http://dx.doi.org/10.1029/2008WR006993>.
- Hunt, R.J., Wilcox, D.A., 2003. Ecohydrology—Why Hydrologists Should Care. *Groundwater* 41 (3), 289. <http://dx.doi.org/10.1111/j.1745-6584.2003.tb02592.x> (see also comment by R.W. Talkington and response by Hunt and Wilcox, 2003, *Groundwater* 41 (5), 562–565. <http://dx.doi.org/10.1111/j.1745-6584.2003.tb02393.x>).
- Hunt, R.J., Zheng, C., 2012. The current state of modeling. *Groundwater* 50 (3), 329–333. <http://dx.doi.org/10.1111/j.1745-6584.2012.00936.x>.
- Hunt, R.J., Hayashi, M., Batelaan, O., Ecohydrology and its relation to integrated groundwater management. In: Jakeman, A.J., Barreteau, O., Hunt, R.J., Rinaudo, J.D., Ross, A. (Eds.), *Integrated Groundwater Management*, Springer Publishing, New York, NY (in press).
- Jakeman, A.J., El Sawah, S., Guillaume, J.H.A., Pierce, S.A., 2011. Making progress in integrated modeling and environmental decision support. In: Hrebicek, J., Schimak, G., Denzer, R. (Eds.), *Environmental Software Systems. Frameworks of Environment*, 9th IFIP WG.11 International Symposium, IFIP AICT 359. IFIP (International Federation for Information Processing), Springer, pp. 15–25.
- Jenkins, C.T., 1968. Electric analog and digital computer model analysis of stream depletion by wells. *Groundwater* 6 (6), 37–46. <http://dx.doi.org/10.1111/j.1745-6584.1968.tb01258.x>.
- Kasmarek, M.C., 2012. Hydrogeology and Simulation of Groundwater Flow and Land-surface Subsidence in the Northern Part of the Gulf Coast Aquifer System, Texas, 1891–2009 (ver. 1.1, December 2013). U.S. Geological Survey Scientific Investigations Report 2012-5154, 55 p. <http://pubs.usgs.gov/sir/2012/5154/>.
- Kitanidis, P.K., 1997. *Introduction to Geostatistics: Applications in Hydrogeology.* Cambridge University Press, Cambridge, UK, 249 p.
- Koltermann, C.E., Gorelick, S.M., 1996. Heterogeneity in sedimentary deposits: A review of structure-imitating, process-imitating, and descriptive approaches. *Water Resources Research* 32 (9), 2617–2658. <http://dx.doi.org/10.1029/96WR00025>.

- Konikow, L.F., 2011. The secret to successful solute-transport modeling. *Groundwater* 49 (2), 144–159. <http://dx.doi.org/10.1111/j.1745-6584.2010.00764.x>.
- Langevin, C.D., Oude Essink, G.H.P., Panday, S., Bakker, M., Prommer, H., Swain, E.D., Jones, W., Beach, M., Barcelo, M., 2004. Chapter 3, MODFLOW-based tools for simulation of variable-density groundwater flow. In: Cheng, A., Ouazar, D. (Eds.), *Coastal Aquifer Management: Monitoring, Modeling, and Case Studies*. Lewis Publishers, pp. 49–76.
- Langevin, C.D., Panday, S., 2012. Future of groundwater modeling. *Groundwater* 50 (3), 333–339. <http://dx.doi.org/10.1111/j.1745-6584.2012.00937.x>.
- Langevin, C.D., Zygmierski, M., 2012. Effect of sea-level rise on salt water intrusion near a coastal well field in southeastern Florida. *Groundwater* 51 (5), 781–803. <http://dx.doi.org/10.1111/j.1745-6584.2012.01008.x>.
- Langevin, C.D., Thorne Jr., D.T., Dausman, A.M., Sukop, M.C., Guo, W., 2007. SEAWAT Version 4: A Computer Program for Simulation of Multi-species Solute and Heat Transport. U.S. Geological Survey Techniques and Methods Book 6. Chapter A22, 39 p. <http://pubs.usgs.gov/tm/tm6a22/>.
- Leake, S.A., Galloway, D.L., 2007. MODFLOW Ground-water Model—User Guide to the Subsidence and Aquifer-system Compaction Package (SUB-wt) for Water-table Aquifers. U.S. Geological Survey Techniques and Methods, 6–A23, 42 p. <http://pubs.usgs.gov/tm/2007/06A23/>.
- Leake, S.A., Prudic, D.E., 1991. Documentation of a Computer Program to Simulate Aquifer-system Compaction Using the Modular Finite-difference Ground-water Flow Model. U.S. Geological Survey Techniques and Methods Book 6. Chapter A2, 68 p. <http://pubs.usgs.gov/twri/twri6a2/>.
- Loague, K. (Ed.), 2010. Benchmark Papers in Hydrology. Rainfall-Runoff Modelling. Selection, Introduction and Commentary by Keith Loague, vol. 4. IAHS Press, p. 506.
- Loáiciga, H.A., Pingel, T.J., Garcia, E.S., 2012. Sea water intrusion by sea-level rise: Scenarios for the 21st century. *Groundwater* 50 (1), 37–47. <http://dx.doi.org/10.1111/j.1745-6584.2011.00800.x>.
- Mariethoz, G., Caers, J., 2014. *Multiple-point Geostatistics: Stochastic Modeling with Training Images*. Wiley-Interscience, Hoboken, NJ, 384 p.
- Marsily, G. de, Delay, F., Goncalves, J., Renard, P., Teles, V., Violette, S., 2005. Dealing with spatial heterogeneity. *Hydrogeology Journal* 13 (1), 161–183. <http://dx.doi.org/10.1007/s10040-004-0432-3>.
- Mayer, A., Hassanizadeh, S.M. (Eds.), 2005. *Soil and Groundwater Contamination: Nonaqueous Phase Liquids—Principles and Observations*. Water Resources Monograph, vol. 17. American Geophysical Union, Washington, DC, 216 p. <http://dx.doi.org/10.1029/WM017>.
- Michael, H.A., Li, H., Boucher, A., Sun, T., Caers, J., Gorelick, S.M., 2010. Combining geologic-process models and geostatistics for conditional simulation of 3-D subsurface heterogeneity. *Water Resources Research* 46 (5), W05527. <http://dx.doi.org/10.1029/2009WR008414>.
- Muldoon, M., Bradbury, K.R., 2005. Site characterization in densely fractured dolomite: Comparison of methods. *Groundwater* 43 (6), 863–876. <http://dx.doi.org/10.1111/j.1745-6584.2005.00091.x>.
- National Research Council (NRC), 1990. *Ground Water Models: Scientific and Regulatory Applications*. National Academy Press, Washington, DC, 303 p.
- National Research Council (NRC), 1996. *Rock Fractures and Fluid Flow: Contemporary Understanding and Applications*. National Academies Press, Washington, DC, 551 p.
- National Research Council (NRC), 2001. *Conceptual Models of Flow and Transport in the Fractured Vadose System*. National Academy Press, Washington, DC, 374 p.
- Neuman, S.P., 2005. Trends, prospects and challenges in quantifying flow and transport through fractured rocks. *Hydrogeology Journal* 13 (1), 124–147. <http://dx.doi.org/10.1007/s10040-004-0397-2>.
- Niswonger, R.G., Prudic, D.E., Regan, R.S., 2006. Documentation of the Unsaturated-zone Flow (UZFI) Package for Modeling Unsaturated Flow between the Land Surface and the Water Table with MODFLOW-2005. U.S. Geological Survey Techniques and Methods Report, 6–A19, 62 p. <http://pubs.usgs.gov/tm/2006/tm6a19/>.
- Nogues, J.P., Fitts, J.P., Celia, M.A., Peters, C.A., 2013. Permeability evolution due to dissolution and precipitation of carbonates using reactive transport modeling in pore networks. *Water Resources Research* 49 (9), 6006–6021. <http://dx.doi.org/10.1002/wrcr.20486>.

- Pinder, G.F., Abriola, L.M., 1986. On the simulation of nonaqueous phase organic compounds in the subsurface. *Water Resources Research* 22 (9), 109S–119S. <http://dx.doi.org/10.1029/WR022i09Sp0109S>.
- Prommer, H., Barry, D.A., Zheng, C., 2003. MODFLOW/MT3DMS-Based reactive multicomponent transport modeling. *Groundwater* 41 (2), 247–257. <http://dx.doi.org/10.1111/j.1745-6584.2003.tb02588.x>.
- Prommer, H., Post, V.E.A., 2010. A Reactive Multicomponent Model for Saturated Porous Media, Version 2.0, User's Manual. <http://www.pht3d.org>.
- Razavi, S., Tolson, B., Burn, D., 2012. Review of surrogate modeling in water resources. *Water Resources Research* 48 (7), W07401. <http://dx.doi.org/10.1029/2011WR0011527>.
- Refsgaard, J.C., Højberg, A.L., Møller, I., Hansen, M., Søndergaard, V., 2010. Groundwater modeling in integrated water resources management—visions for 2020. *Groundwater* 48 (5), 633–648. <http://dx.doi.org/10.1111/j.1745-6584.2009.00634.x>.
- Renard, P., 2007. Stochastic hydrogeology: What professionals really need? *Groundwater* 45 (5), 531–541. <http://dx.doi.org/10.1111/j.1745-6584.2007.00340.x>.
- Renard, P., Allard, D., 2013. Connectivity metrics for subsurface flow and transport. *Advances in Water Resources* 51, 168–196. <http://dx.doi.org/10.1016/j.advwatres.2011.12.001>.
- Rubin, Y., 2003. *Applied Stochastic Hydrogeology*. Oxford University Press, New York, NY, 391 p.
- Ruskauff, G.J., Rumbaugh, J.O., Rumbaugh, D.B., 1998. Stochastic MODFLOW and MODPATH for Monte Carlo Simulation. Environmental Simulations Incorporated, Herndon, VA, 58 p.
- Saar, M.O., 2011. Review: Geothermal heat as a tracer of large-scale groundwater flow and as a means to determine permeability fields. *Hydrogeology Journal* 19 (1), 31–52. <http://dx.doi.org/10.1007/s10040-010-0657-2>.
- Sahimi, M., 2012. *Flow and Transport in Porous Media and Fractured Rock: From Classical Methods to Modern Approaches*. John Wiley & Sons, 733 p.
- Sawyer, A., Cardenas, M., 2009. Hyporheic flow and residence time distributions in heterogeneous cross-bedded sediment. *Water Resources Research* 45 (8), W08406. <http://dx.doi.org/10.1029/2008WR007632>.
- Schmid, W., Hanson, R.T., 2009. The Farm Process Version 2 (FMP2) for MODFLOW-2005-modifications and Upgrades to FMP1. U.S. Geological Survey Techniques and Methods, Book 6. Chapter A32, 102 p. <http://pubs.usgs.gov/tm/tm6a32/>.
- Schmid, W., Hanson, R.T., Leake, S.A., Hughes, J.D., Niswonger, R.G., 2014. Feedback of land subsidence on the movement and conjunctive use of water resources. *Environmental Modelling & Software* 62, 253–270. <http://dx.doi.org/10.1016/j.envsoft.2014.08.006>.
- Schmid, W., Hanson, R.T., Maddock III, T., Leake, S.A., 2006. User Guide for the Farm Process (FMP1) for the U.S. Geological Survey's Modular Three-Dimensional Finite-Difference Ground-Water Flow Model, MODFLOW-2000. U.S. Geological Survey Techniques and Methods, 6–A17, 127 p. <http://pubs.usgs.gov/tm/2006/tm6A17/>.
- Schoups, G., Addams, C.L., Minjares, J.L., Gorelick, S.M., 2006. Sustainable conjunctive water management in irrigated agriculture: Model formulation and application to the Yaqui Valley, Mexico. *Water Resources Research* 42 (10), W10417(19). <http://dx.doi.org/10.1029/2006WR004922>.
- Schwartz, F.W., 2012. Volume 50 and beyond. *Groundwater* 50 (1), 1. <http://dx.doi.org/10.1111/j.1745-6584.2011.00894.x>.
- Schwille, F., 1988. *Dense Chlorinated Solvents in Porous and Fractured Media: Model Experiments*. translated from the German by J.F. Pankow. Lewis Publishers, Boca Raton, Florida, USA, 146 p.
- Shepley, M.G., Whiteman, M.I., Hulme, P.J., Grout, M.W., 2012. *Groundwater Resources Modelling: A Case Study from the UK*, vol. 364. The Geological Society, London. Special Publication, 378 p.
- Simmons, C.T., 2005. Variable density groundwater flow: From current challenges to future possibilities. *Hydrogeology Journal* 13 (1), 116–119. <http://dx.doi.org/10.1007/s10040-004-0408-3>.
- Simmons, C.T., Fenstemaker, T.R., Sharp Jr., J.M., 2001. Variable-density groundwater flow and solute transport in heterogeneous porous media: Approaches, resolutions and future challenges. *Journal of Contaminant Hydrology* 53 (1–4), 245–275. [http://dx.doi.org/10.1016/S0169-7722\(01\)00160-7](http://dx.doi.org/10.1016/S0169-7722(01)00160-7).
- Soetaert, K., Herman, P.M.J., 2009. *A Practical Guide to Ecological Modelling*. Springer, 372 p.

- Srinivasan, V., Gorelick, S.M., Goulter, L., 2010. A hydrologic-economic modeling approach for analysis of urban water supply dynamics in Chennai, India. *Water Resources Research* 46 (7), W07540. <http://dx.doi.org/10.1029/2009WR008693>.
- Szymkiewicz, A., 2013. *Modelling Water Flow in Unsaturated Porous Media: Accounting for Nonlinear Permeability and Material Heterogeneity*. Springer, 237 p.
- Tidwell, V.C., Van Den Brink, C., 2008. Cooperative modeling: Linking science, communication, and ground water planning. *Groundwater* 46 (2), 174–182. <http://dx.doi.org/10.1111/j.1745-6584.2007.00394.x>.
- Voss, C.I., Provost, A.M., 2002. SUTRA: A Model for 2D or 3D Saturated-Unsaturated, Variable-density Ground-water Flow with Solute or Energy Transport. U.S. Geological Survey Open-File Report 02–4231, 250 p. <http://pubs.er.usgs.gov/publication/wri024231>.
- Wang, H.F., 2000. *Theory of Linear Poroelasticity with Applications to Geomechanics and Hydrogeology*. Princeton University Press, 287 p.
- Watson, T.A., Doherty, J.E., Christensen, S., 2013. Parameter and predictive outcomes of model simplification. *Water Resources Research* 49 (7), 3952–3977. <http://dx.doi.org/10.1002/wrcr.20145>.
- Weaver, J., 1996. *The Hydrocarbon Spill Screening Model (HSSM) Volume 1 User's Guide (Version 1.1 Rev. October 1996)*. U.S. Environmental Protection Agency, Office of Research and Development, Athens, Georgia.
- Werner, A.D., Bakker, M., Post, V.E.A., Vandenbohede, A., Lu, C., Ataie-Ashtiani, B., Simmons, C.T., Barry, D.A., 2013. Seawater intrusion processes, investigation and management: Recent advances and future challenges. *Advances in Water Resources* 51, 3–26. <http://dx.doi.org/10.1016/j.advwatres.2012.03.004>.
- White, J.T., Doherty, J.E., Hughes, J.D., 2014. Quantifying the predictive consequences of model error with linear subspace analysis. *Water Resources Research* 50 (2), 1152–1173. <http://dx.doi.org/10.1002/2013WR014767>.
- Woessner, W.W., 2000. Stream and fluvial plain ground water interactions: Rescaling hydrogeologic thought. *Groundwater* 38 (3), 423–429. <http://dx.doi.org/10.1111/j.1745-6584.2000.tb00228.x>.
- Zhang, D., 2002. *Stochastic Methods for Flow in Porous Media*. Academic Press, San Diego, CA, 350 p.
- Zheng, C., 2009. Recent developments and future directions for MT3DMS and related transport codes. *Groundwater* 47 (5), 620–625. <http://dx.doi.org/10.1111/j.1745-6584.2009.00602.x>.
- Zheng, C., Bianchi, M., Gorelick, S.M., 2011. Lessons learned from 25 years of research at the MADE site. *Groundwater* 49 (5), 649–662. <http://dx.doi.org/10.1111/j.1745-6584.2010.00753.x>.
- Zheng, C., Bennett, G.D., 2002. *Applied Contaminant Transport Modeling*, second ed. John Wiley & Sons, New York. 621 p.
- Zhou, H., Gómez-Hernández, J.J., Liangping, L., 2014. Inverse methods in hydrogeology: Evolution and recent trends. *Advances in Water Resources* 63, 22–37. <http://dx.doi.org/10.1016/j.advwatres.2013.10.014>.
- Zhou, Y., Ritzi, R.W., Soltanian, M.R., Dominic, D.F., 2014. The influence of streambed heterogeneity on hyporheic flow in gravelly rivers. *Groundwater* 52 (2), 206–216. <http://dx.doi.org/10.1111/gwat.12048>.

# INDEX

## A

- A Civil Action, 13
- Abstract. *See* Modeling report
- Active nodes, 165, 186, 192, 195, 222, 236
- Adaptive forecasting, 482
- Adaptive management, 18, 482, 526
- Adaptive time stepping, 320
- Advanced uncertainty analysis. *See* Uncertainty
- Advection–dispersion equation, 142, 318, 338, 357, 522, 524
- Advective groundwater age. *See* Particle tracking (PT)
- Advective transport, of contaminants. *See* Particle tracking (PT)
- AE. *See* Analytic element (AE)
- AEM. *See* Analytic element method (AEM)
- AE model. *See* Analytic element model (AE model)
- AIC. *See* Akaike Information Criterion (AIC)
- AICMA. *See* Akaike Information Criterion-based Model Averaging (AICMA)
- Akaike Information Criterion (AIC), 479
- Akaike Information Criterion-based Model Averaging (AICMA), 479
- Aleatory (intrinsic) error. *See* Error
- Alluvial deposits (fan and sediments), 21, 44–45, 60, 213–214, 248, 332
- Alternative conceptual model. *See* Conceptual model
- Alternative parameterizations, 477
- American Standard Code for Information Interchange (ASCII), 398, 399–400, 510
- Analog model, 5, 168
- Analytic element (AE), 8, 80–84, 144, 161, 279, 354
- Analytic element method (AEM), 8, 80–81, 83, 84, 85
- Analytic element model (AE model), 8, 11, 14, 17, 80–85, 136, 161, 202, 285, 354
- Analytical model, 6, 8, 11, 14, 78–85, 108, 335
- Analytical solutions, 6, 8, 14, 19, 78–80, 81–82, 85, 98, 99, 107, 108, 118, 142, 162, 205, 208, 245, 260, 265, 267, 308, 316, 319, 320–321, 347, 351, 364, 365, 394, 446, 524
- AnAqSim code, 84–85, 144
- Ancillary information, 30, 57–59
- Anisotropy, 21, 51, 73, 84, 85, 98, 169, 173, 184, 199–201, 210–214, 217, 223, 225, 243, 245, 247, 262, 266, 284, 335–336, 367
  - horizontal, 77, 184, 200, 210, 223
  - non-uniform, 184, 243
  - vertical (anisotropy ratio), 51, 169, 184, 200–201, 210–214, 223, 225, 245, 247, 262, 284
- ANN model. *See* Artificial neural network model (ANN model)
- Appropriate model, 22, 27, 28, 60, 108, 123, 139, 153, 223, 225, 237, 273, 310, 319, 376, 379, 380, 384, 387, 392, 412, 431, 435, 451, 516
- Aquiclude, 38, 41
- AQUIFEM-N code, 165
- Aquifer, 4, 6, 8, 9, 11, 17, 18, 21, 31, 34, 35, 37–38, 41, 42, 51, 55–56, 58, 62, 63, 70, 71, 72, 75, 76–77, 78–80, 83, 84, 85, 96, 106, 108, 109–110, 118–120, 122–124, 125–127, 128, 132, 133–134, 135, 137–138, 139, 140, 141–142, 144, 148, 153, 154–155, 163, 168–169, 171, 172, 173–174, 175, 185, 193, 201, 205–206, 208, 213, 217, 218, 222, 223, 225, 226, 227, 228, 229, 230, 236–237, 243, 244, 248–249, 259–260, 262, 265, 266, 267, 269, 273–275, 279, 280, 281–283, 292, 294, 296, 307, 308, 309, 313, 316, 323, 324, 332, 335, 340, 342, 353, 360, 362, 366, 367, 377, 397, 416, 427, 432–434, 435, 450, 452, 453, 454, 455–456, 463, 498, 501, 502, 515–516, 518–519, 520, 522, 523, 525, 527
  - alluvial, 21, 63, 135, 213
  - compressible, 518–519

- Aquifer (*Continued*)  
 confined, 31, 38, 56, 76, 83, 108, 109–110, 118–119, 120, 127, 138, 144, 207, 228, 292–293, 308, 310, 316, 323, 342, 367, 369  
 heterogeneous, 58, 77, 335, 340, 353, 366, 455–456, 463  
 leaky confined, 207, 208  
 loss, 266  
 response time, 80, 308, 340  
 semi-confined, 208  
 test, 6, 201, 225, 228, 230, 248, 260, 269, 416, 427, 432, 435, 452  
 unconfined (conditions), 21, 31, 55, 62, 77, 79, 83, 118–121, 122, 138, 139, 144, 162, 165, 168–169, 173, 214–216, 217, 227–228, 237, 243, 246, 260, 266, 269, 270, 271, 291, 294, 295, 296, 308–309, 310, 313, 432–433, 469  
 unconsolidated, 213–214
- Aquifer Storage and Recovery (ASR), 260
- Aquifuge, 38, 41
- Aquitard, 38, 40–41, 43, 54, 169
- Aquitardifer, 41, 43
- Arbitrary distant boundaries. *See* Boundary conditions
- Archive, modeling, 18, 495–496, 497, 509–511, 513
- Areal models. *See* Two-dimensional (2D) models
- Argus ONE GIS, 34
- Arid setting, 53, 54, 59, 138, 231, 246, 248, 277, 386, 448, 467
- Arithmetic mean, 228, 238
- Artificial neural network model (ANN model), 6, 7
- Artificial recharge. *See* Recharge
- ASCII. *See* American Standard Code for Information Interchange (ASCII)
- Aspect ratio, 199
- Atmospheric pressure, 121, 162, 166, 519
- Automated trial-and-error. *See* Calibration; Parameter estimation
- Average conditions, 54, 306, 310, 454, 459, 483
- Average linear velocity, 334, 336, 338, 363
- Axissymmetric profile model. *See* Profile (cross-sectional model)
- B**
- Backcast. *See* Hindcast (methods and models)
- Backward tracking. *See* Particle tracking (PT)
- Balanced objective function. *See* Objective function
- Bandwidth. *See* Matrix
- Barriers, 45, 52, 56, 81–82, 103, 137, 138, 140, 199, 202, 203–205, 217, 260
- Base model, 9, 17, 435, 445, 448, 453, 454, 458, 459, 460, 465, 469, 478, 482, 483, 506, 507  
 parameters, 9, 445, 458, 459, 465, 483, 506  
 uncertainty, 435, 448, 453, 454, 458, 460, 482, 483, 506, 507
- Base parameters. *See* Base model, parameters
- Baseflow, 54, 230, 231, 235, 273, 275, 289, 305, 308, 322, 323, 382–383, 391, 395, 401, 454, 459–460, 482, 499
- Basic uncertainty analysis. *See* Uncertainty, basic analysis
- Basis function, 89–90, 91, 195–196, 365
- Batch mode (file), 399, 409
- Bayes theorem, 446, 451–452, 478
- Bayesian approach, 397, 452–453
- Bayesian Information Criterion (BIC), 479
- Bayesian methods, 6, 451–453, 462
- Bayesian model averaging, 479. *See also* Maximum Likelihood Bayesian Model Averaging (MLBMA)
- Behavioral models, 478
- Benchmarking, 503
- BeoPEST code. *See* PEST Software Suite
- Best-case worst-case scenario modeling, 445, 456, 459, 469, 481, 483, 507
- Best fit model, 376, 396, 398, 401, 403, 409, 412, 429, 431
- Best model, 378–379, 396, 411, 420, 435, 447
- bgaPEST code. *See* PEST Software Suite
- Bias, 13, 14–15, 260, 291, 315, 385, 388, 389, 391, 396, 413, 445, 450, 456, 505
- BIC. *See* Bayesian Information Criterion (BIC)
- Bicubic element. *See* Element
- Bicubic interpolation. *See* Particle tracking (PT), velocity interpolation
- Bilinear interpolation. *See* Particle tracking (PT), velocity interpolation
- Biquadratic element. *See* Element
- Black-box model. *See* Data-driven model (Black-box model)

- Block-centered finite-difference (FD) grid. *See also*  
 Grid, block-centered finite difference  
 nodes, 85–88, 129–130, 145–147, 150, 171,  
 186–187, 190, 236, 292–293, 364–365
- Boundary conditions, 6, 8, 11, 14, 17, 35–36, 70,  
 77–78, 79, 83, 88, 106, 108, 118, 125,  
 128–129, 134, 136, 142, 144–145,  
 148–150, 152, 159–162, 165, 167, 169,  
 170, 171–173, 175, 182, 185, 191, 198,  
 202, 203, 206, 214, 216, 222, 245, 247,  
 258, 259, 262, 270–272, 285, 293,  
 304–305, 309–310, 312, 314–316, 318,  
 324, 336, 351, 367, 393, 395, 449, 453,  
 466, 498, 501, 503, 523
- arbitrary distant, 316
- Cauchy, 77–78
- conceptual model, 17, 32, 35–36
- constant head, 77, 100, 134, 137, 144, 145, 150,  
 173, 175, 226, 247, 335
- Dirichlet, 77, 78
- distant, 153, 158–159, 315–316
- equipotential line. *See* Boundary conditions,  
 hydraulic
- extracting local boundary conditions from a  
 regional model, 159–162
- fault, 37, 62, 98, 135, 137, 138, 314–315
- finite difference  
 block-centered, 85, 129, 145–147, 150,  
 171–172, 236, 292, 293  
 point-centered, 146–147, 171–172, 244, 365
- finite elements, 98, 101, 136, 145, 146, 148–150,  
 159–161, 165–166, 183, 186, 191, 197–198,  
 199, 204
- General Head Boundary (GHB) Package. *See*  
 MODFLOW code (Modular Groundwater  
 Flow Model), packages
- head-dependent boundary (HDB), 77, 100, 107,  
 125, 133, 134, 136, 138, 143, 147, 148, 150,  
 151, 152–153, 155, 157, 158, 159, 164, 170,  
 173, 198, 206, 210, 216, 229, 235, 236, 257,  
 258, 272, 274–275, 277, 279, 281, 283, 292,  
 295, 315
- hydraulic, 134, 136, 144–145, 147, 159, 160, 161,  
 170, 176, 324  
 equipotential line, 144–145, 170  
 streamline, 36, 139, 144–145, 146, 163,  
 170, 175
- hydrogeologic, 36
- impermeable, 35, 81, 120, 128, 133, 135, 136,  
 146, 172, 204, 296, 314, 432–433
- internal, 78, 83, 136, 150, 152, 173, 175, 222,  
 258, 262, 314, 315
- irregular, 198, 203
- mixed, 77
- moving, 121, 143, 162
- Neumann, 77, 78, 262
- no-flow, 77, 82, 106, 118, 125, 127, 128–130,  
 133, 134–135, 136–137, 138, 140, 142, 145,  
 146, 148–150, 170, 171, 172, 173, 175–176,  
 199, 213, 222, 247, 292, 312, 315, 316, 336,  
 368, 432
- perimeter, 51, 78, 83, 118, 133, 134–136, 144,  
 145, 148–149, 150, 153, 159, 161, 162, 182,  
 195, 202, 203, 258, 259, 285, 304–305, 306,  
 310, 314–316, 334, 501, 504
- physical, 42, 135–138, 144, 158–159, 175, 314
- saltwater interface. *See* seawater interface, below
- seawater interface, 136, 140, 141–144, 228,  
 520, 523
- selection, 14, 134–145, 501
- specified flow (conditions), 77, 125, 133, 134,  
 136, 145, 147, 148–152, 161, 165, 167–169,  
 171, 175, 257, 258, 259, 262, 270–272, 315
- specified head, 14, 77, 82, 99, 100, 125, 128–130,  
 133, 134–136, 138, 139, 142, 145–148, 150,  
 152, 153, 160–161, 167–169, 170, 171, 173,  
 175, 176, 199, 247, 257, 258, 259, 274, 279,  
 281, 292, 294, 304, 315, 367, 368, 369
- streamline, 139, 144–145, 163, 170, 175, 360
- type 1, 77
- type 2, 77
- type 3, 77
- water table, 122, 129, 162, 165, 166, 167
- Bounds, on parameter value, 409, 464, 465, 509
- Bulk mass density, 363
- ## C
- C/C++, 9
- C(e) matrix, 461, 462–463, 465
- C(p) matrix, 461, 462, 463–465
- Calibration, 9, 10, 11, 12, 16–18, 19, 20, 22, 27,  
 28, 42, 45, 49, 54, 56, 58, 59, 60, 101, 102,  
 103–104, 105, 122, 148, 156, 167, 182,  
 202, 203, 210, 212–213, 215, 222, 225,  
 229–230, 233, 235, 236, 238, 243, 273,  
 275, 290, 305, 306, 307, 310, 320, 322,  
 323, 331, 332, 336, 376, 377, 378, 379,

- 380–381, 382, 383, 384, 385, 386, 392, 393–394, 395–396, 397, 398, 399–400, 403, 404, 405–406, 408–409, 410–414, 416, 417, 418, 419, 420, 421–422, 423–425, 426–431, 432, 434, 435, 444, 445, 446–447, 451–453, 454, 455–456, 457, 460, 461, 463, 465–466, 467, 468, 470, 471, 472, 475, 478, 479, 480, 481, 483–484, 497, 498, 500, 501, 502, 504–506, 507, 508, 509, 510, 511, 512, 513, 516, 525. *See also* Parameter estimation
- automated trial-and-error, 385, 396–411, 428, 432, 434, 435
- best fit, 376, 396, 398, 399, 401, 403, 409, 410, 412, 418, 419, 420, 424, 425, 428, 429, 431, 445, 455
- goodness of fit, 387, 392, 416, 505
- history matching, 9, 18, 291, 376–381, 382, 384, 385, 387, 390, 392, 393, 394–395, 396, 398, 399, 401, 403, 409, 411, 413, 414, 418–419, 426, 427, 428, 431, 432, 434, 445, 451, 452–453, 454, 456, 457, 461, 464, 466, 467, 471, 478, 497, 502, 504, 505, 506, 511
- manual trial-and-error, 376, 377, 385, 393, 394–395, 396, 398, 409, 410, 414, 428, 430, 431, 434, 504, 505
- objective function. *See* Objective function
- optimal calibration (forecast, model, parameter), 60, 378, 380, 393, 403, 408, 412, 418–420, 424, 425, 451, 478, 525
- parameters, 9, 16, 18–19, 42, 45, 49, 60, 101, 102, 103–104, 105, 148, 222, 229, 233, 235, 236, 238, 243, 273, 290, 307, 378, 379, 380, 385, 393–400, 403, 405–406, 408–409, 410, 411–414, 417, 418, 419, 420–422, 423–425, 427, 428, 429, 430, 431, 434, 435, 445, 446, 447, 451–452, 453, 454, 460, 461, 465–466, 467, 468, 470, 471, 475, 479, 501, 502, 504–506, 507, 509, 516
- reasonableness assessment, 42, 45, 377, 378, 414, 426, 428, 431, 497, 501, 506, 512
- statistics, 378, 384, 385, 387, 391, 392, 396, 405, 408, 410, 421, 429, 430, 431, 434, 446, 451, 455, 475, 505, 506, 510, 512
- steady-state, 103–104, 305, 306, 382, 383, 428, 429, 432, 435, 453, 502, 505, 513
- targets. *See* Calibration target
- transient, 49, 103–104, 305, 307, 320, 322, 323, 382, 428, 429, 434–435, 453, 463, 483–484, 502, 505
- underdetermined, 378, 393, 430, 446–447, 460, 505, 516
- underfit, 419
- workflow, 10, 16, 17, 377, 398, 399, 426–431
- Calibration target, 16, 18, 54, 58, 101, 202–203, 305, 331, 376, 380–385, 386, 392, 393, 394, 396, 398, 399, 403, 404, 405–406, 410, 411, 413, 416, 419–420, 421, 423, 425, 427, 428, 429, 431, 432, 435, 445, 446, 452, 455, 456, 463, 467, 471, 478, 479, 502, 504, 505, 509
- flux. *See* Flux target
- head. *See* Head target
- lake inflow, 382
- lake plume, 381
- ranking, 384–385
- residual, 56, 386–387, 389, 390, 391, 392, 393, 410, 411, 429, 434, 505
- selection, 18, 376, 380–385, 504
- spring flow, 54, 382, 502
- temporal, 54, 382, 428, 429, 502, 505
- water budget, 56, 429, 506, 509
- weighting of, 323, 385, 398, 400–401, 429, 430, 431, 434, 445, 451, 455, 463, 478, 504
- Capture zone, 21, 124, 336, 338, 340, 341, 342, 351, 353, 358–362, 365–366, 367, 370, 454
- composite, 362
- stream, 358, 360, 361, 362
- well, 21, 124, 336, 338, 340, 342, 351, 353, 358, 359, 360–362, 365, 367, 370, 454
- Categorized scatter plots, 385, 388, 505
- Cauchy boundary conditions. *See* Boundary conditions
- Cdf. *See* Cumulative density function (cdf, Cumulative distribution function)
- CFP. *See* Conduit Flow Process (CFP); MODFLOW code (Modular Groundwater Flow Model), processes
- Characteristic leakage length, 80, 205, 207, 243
- Chemical analyses and tracers, 57–58
- artificial tracers, 58
- environmental tracers, 58, 231
- isotopes, 58, 380–381, 504
- major cations and anions, 57
- organic compounds, 58



- pH, 57
- specific conductance, 57
- temperature, 57, 58, 70, 78, 232, 275, 379, 380, 404, 427, 459, 505, 520, 521, 522
- total dissolved solids (TDS), 57, 70
- CLN Process. *See* Connected Linear Network (CLN) Process; MODFLOW code (Modular Groundwater Flow Model), processes
- Closed form analytical solution, 6
- Closure criterion, 96, 97, 99, 100, 102, 105–107, 110, 153, 172, 320, 408, 503, 504
  - parameter estimation, 408
- Cloud computing, 397, 424
- Code, 8–9, 11, 12, 15, 17, 18, 19, 21, 22, 33–34, 42, 54, 60, 70, 71, 76, 78, 81, 83, 84, 89, 91, 92–93, 95, 96–107, 125, 127, 131, 136, 140, 143–144, 145, 147, 148–149, 152, 155, 161, 162, 164, 165–166, 170, 172, 183, 184, 186, 191, 195, 196, 197, 202, 203, 207, 208, 214, 215, 216, 217, 219, 225, 228, 236, 237, 244, 258, 259, 260, 262, 265, 268, 270, 271, 272, 273, 276, 277, 279, 281, 283, 285–287, 291–292, 304, 306, 318, 319, 322, 331, 334, 336, 337, 338, 339, 341, 344, 345, 346, 349, 351, 357, 358, 359, 363, 364–365, 366, 368, 369, 370, 385, 396, 397, 398, 399–400, 401, 403, 408–409, 410, 414, 425, 426, 427–428, 429, 455–456, 464, 471, 475, 496, 497, 502, 503, 504, 505, 509, 510, 512, 513, 516, 517, 518, 519, 521, 522, 523
- Code verification. *See* Verification
- Coefficient of variation, 383
- Collector wells. *See* Well, radial collector (Ranney)
- Complexity. *See* Model complexity
- Composite capture zone. *See* Capture zone
- Compressibility, 127, 227, 231, 510, 518, 519
  - aquifer, 227, 518–519
  - water, 227, 518–519
- Computational effort, 341
- Computer program. *See* Code
- COMSOL software package, 98, 258
- Conceptual model, 4, 5, 10, 11, 16, 17, 18, 19, 20, 22, 27, 29–60, 62, 63, 79, 99, 102, 106, 107, 128, 129, 134, 136, 143, 169, 170, 182, 237, 238, 274, 334, 336, 376, 377, 378, 379, 385, 395, 396, 398, 408–409, 411, 420, 429, 431, 445, 447, 469, 477–479, 482, 497, 500–502, 503, 505–506, 507, 508, 511–512, 513
  - alternative, 59, 60, 62, 429, 477, 502, 505–506
  - ancillary information, 30, 57
  - boundaries, 17, 31, 32, 35–36, 37, 51, 54, 62, 79, 99, 106, 128, 134, 136, 153, 169, 170, 182, 334, 376, 503
  - components, 32, 35–60, 63
  - definition and general features, 29–34
  - evolving hypothesis, 16, 30, 59
  - flow direction, 17, 35, 51, 53, 62, 334
  - groundwater budget components, 17, 35, 53, 54–57, 58, 60, 63
  - hydrogeologic site, 31, 32
  - hydrogeological properties, 37–50
  - hydrologic system, 30, 33, 54
  - hydrostratigraphy, 17, 32, 35, 37–50, 59, 60, 62, 500, 501, 502
  - multiple, 17, 478–479
  - sources and sinks, 32, 35, 51–54, 99, 274
- Conditionally optimal parameter, 393
- Conditioning, 472, 475, 477
- Conductance, 57, 88, 89, 94, 95, 103, 152, 153, 155, 156–157, 158, 159, 210, 229–230, 266, 273, 275, 282, 283, 296, 461
  - horizontal, 88, 155, 159
  - vertical, 88, 210, 229–230
- Conduit flow, 7, 42, 45, 70, 71, 137, 205, 515, 516, 518
- Conduit Flow Process (CFP). *See* MODFLOW code (Modular Groundwater Flow Model), processes
- Cone of depression, 80, 108, 110, 170, 225, 315
- Confidence building, 16, 428
- Confidence intervals, 241, 382, 383, 409, 446, 457, 461, 463, 464, 465, 469, 475, 477
- Confined aquifer. *See* Aquifer
- Confined layer. *See* Layer
- Confining bed, 37–38, 41, 42, 46, 47, 118–119, 133, 134, 141, 155, 208, 214, 218, 225, 244, 338–339, 519
  - horizontal flow, 41, 134
  - vertical flow, 119, 134
  - vertical hydraulic conductivity, 41, 119, 134
- Conjunctive use of groundwater and surface water, 201, 523, 527

- Connected Linear Network (CLN) Process.  
*See* MODFLOW code (Modular Groundwater Flow Model), processes
- Conservation of mass, 70, 72, 94, 99, 212, 345
- Consolidation process, 518–519
- Constant head boundary. *See* Boundary conditions
- Constrained maximization–minimization, 469–471, 481
- Contaminant plume, 9, 360, 363, 381, 527
- Contaminant transport. *See* Solute transport
- Continuity equation (mass balance), 58, 94, 231, 245, 344–345
- Contour plot, 46, 51, 108, 124, 125, 147, 171, 173, 198, 213, 238, 247, 248, 249, 285, 291, 292, 293, 322, 323, 335, 342, 352, 386, 403, 404, 434, 455, 512
- Contributing areas, 336, 338, 351–352, 357, 358–362, 365
- Control volume finite-difference (CVFD) method. *See* Numerical methods
- Control volume finite-difference (CVFD) requirement, 191, 192, 194, 243
- Convergence, 95, 96, 97, 100, 102, 105–107, 172, 214, 265, 295, 304, 322, 356, 358–359, 365, 366, 404, 472, 475, 477, 504, 512
- Monte Carlo analysis, 472, 475, 477
- numerical model, 95–96, 106, 107, 172, 265, 304, 512
- solution, 95–96, 97, 100, 102, 105–107, 172, 265, 304, 322, 404
- Convertible layer. *See* Layer
- Convolution, 451
- Cook's D, 405
- Cooper–Jacob approximation, 268
- Coordinate system, 74–76, 184, 200, 217, 220, 339, 346
- global, 74–76, 184, 217, 220
- local, 74–76, 184, 217
- rotation, 76
- Correlated parameter. *See* Parameter
- Cost–benefit analysis, 445, 468, 469, 472, 483
- Coupled groundwater and surface water models, 98, 277, 283, 284, 287, 291
- Coupled models, 70, 98, 142, 318, 351, 517, 520, 521–522, 523, 526, 527
- Covariance matrix. *See* Matrix
- Cross section, 5, 11, 22, 32, 45, 47, 51, 109, 118, 122, 125, 126–127, 128, 130, 131, 138, 139, 143, 156, 163, 172, 173, 174, 209, 218, 219, 221, 247, 276, 281, 295, 311, 334, 351, 355, 358, 367, 387, 404, 433, 450, 501, 502
- Cross-sectional model. *See* Profile (cross-sectional model)
- Crystalline rock, 42
- Cubic element. *See* Element
- Cumulative density function (cdf, Cumulative distribution function), 473–474
- Curvilinear squares, 173, 335
- CVFD method. *See* Numerical methods; control volume finite-difference (CVFD) method
- CVFD requirement. *See* Control volume finite-difference (CVFD) requirement
- ## D
- D–F approximation. *See* Dupuit–Forchheimer (D–F) approximation (conditions)
- Dam, 138, 164, 166, 172–173, 201, 220, 367, 444, 453
- Damped least squared method. *See* PEST Software Suite
- Darcy's law, 58, 70, 71, 73, 74–76, 77, 94, 99, 124, 137, 211, 231, 245, 268, 275, 281, 283, 383
- Darcy–Weisbach equation, 7
- Data assimilation, 482
- Data-driven model (Black-box model), 5, 6, 14, 286–287, 289
- Decision support system (DSS), 526
- Declustering, 400, 449
- Deformable element. *See* Element
- Deformable grid. *See* Grid
- Deformed layer. *See* Layer
- Dense nonaqueous phase liquid (DNAPL), 521
- Density-dependent flow. *See* Variable density flow
- Dependent variable, 6, 70, 73, 78, 83, 89, 91, 162, 222, 376, 397, 427, 520
- Depositional setting, 44–45
- Derivative-based methods, 403, 405, 408
- Derivative-based nonlinear search techniques. *See* Parameter estimation
- Deterministic interpolation, 238, 249
- Deterministic model, 5, 399, 400, 446, 524, 525
- Dewatering, 4, 14, 103, 147, 164, 165, 259, 272, 316
- DFBETAS, 430
- DFE (Discrete feature element). *See* Element

- Diagonal matrix. *See* Matrix
- Diffuse flow, 149, 272–273
- Diffusion, 141
- Dimensionality (one, two, three, multi), 18, 11,  
13, 14, 28, 29, 35, 50, 73, 74, 76, 79, 80,  
84, 85, 86, 87, 89, 90, 118–134, 135, 141,  
146, 150, 169, 171, 172, 183, 186, 189,  
190, 191, 195, 196, 197, 199, 204–205,  
210, 221, 225, 226, 227, 224, 241, 245,  
248, 262, 264, 265, 266–267, 271, 274,  
292, 304, 306, 307, 308, 309, 313, 319,  
334, 335, 339, 343, 344, 353, 356–357,  
360, 362, 363, 364, 365, 366, 367, 382,  
402–403, 406, 414, 420–421, 427, 430,  
432, 433, 455, 501, 503, 504, 520
- Dipping beds, 76, 184, 217, 219–222
- Dipping hydrogeological units, 184, 209, 217,  
219–222, 223, 243
- Direct inverse approach. *See* Inverse solution
- Direct solution. *See* Numerical solutions
- Dirichlet conditions. *See* Boundary conditions
- Discharge, 4, 21, 31, 34, 36, 51, 54, 55, 56, 57, 59,  
60, 62, 73, 74, 82, 83–84, 121, 129–131,  
138, 140, 141–142, 147, 154, 155, 156,  
163, 167–168, 173, 175, 176, 199,  
211–212, 229, 231, 235, 245, 260, 262,  
263, 264, 267, 271, 273, 275, 276, 279,  
280, 291–292, 305, 309, 324–325, 326,  
332, 334, 336, 337, 350, 351, 358, 360,  
362, 383, 432, 434, 435, 444, 450, 459,  
502, 506, 527
- areally distributed, 262, 263
- diffuse, 51, 155, 272–273
- lake, 59, 279–283, 336, 502
- line, 51
- point, 51
- stream, 4, 31, 59, 121, 154, 163, 235, 271–276,  
279, 309, 336, 351, 358, 383, 444, 502
- Discharge potential, 83–84, 144
- Discontinuous beds, 40–41, 46
- Discrete feature element (DFE). *See* Element
- Discretization, 14, 18, 82, 83, 85, 91, 92, 98, 102,  
149, 154, 182–201, 202, 203, 205,  
209–210, 213, 222, 229, 241, 262, 287,  
290, 310, 316–320, 338–341, 351, 357,  
366, 370, 379, 382, 414, 498, 503, 518
- spatial, horizontal, 182–208, 210
- spatial, vertical, 91, 92, 184, 209–214, 229, 262
- temporal, 182, 340–341
- Dispersion, of solutes, 84, 140–141, 338,  
363, 366, 456
- Disposal of waste fluids, 260
- Dissolved solids, 57, 70
- Distant boundaries. *See* Boundary conditions
- Distorted layer. *See* Layer, distorted (deformed)
- Distributed discharge. *See* Discharge, areally  
distributed
- Distributed Evaluation of Local Sensitivity Analysis  
statistic, 430
- Distributed recharge. *See* Recharge, areally  
distributed
- Distribution coefficient ( $K_d$ ), 363
- Divide. *See* Groundwater, divide; Surface water,  
divide
- Dividing streamline. *See* Streamline
- DNAPL. *See* Dense nonaqueous phase liquid  
(DNAPL)
- Drain, 151, 152, 155–157, 164, 170, 205, 216,  
230, 257, 258, 259, 272–273, 277, 283,  
292, 295–296, 358, 502
- Drain (DRN) Package. *See* MODFLOW code  
(Modular Groundwater Flow Model),  
packages
- Drainage lake, 279, 280–281
- Drawdown, 11, 14, 28, 81, 108, 110, 152, 170,  
225, 226, 248, 260, 261, 265, 266, 267,  
268, 312, 321, 323, 324
- Drawup, 465
- Dry nodes (cells), 104, 165, 292, 304
- DSS. *See* Decision support system (DSS)
- Dual constrained minimization process.  
*See* Parameter estimation
- Dual domain. *See* Porosity, dual
- Dual porosity. *See* Porosity
- Dupuit, Jules, 122
- Dupuit-Forchheimer (D-F) approximation  
(conditions), 77, 84, 120–124, 143–144,  
162, 169
- Dynamic cyclic equilibrium. *See* Initial conditions
- Dynamic steady-state conditions. *See* Initial  
conditions
- ## E
- Ecohydrology, 527
- Effective well radius. *See* Well
- Effluent stream. *See* Stream
- Electrical geophysical methods, 46

- Element, 8, 19, 75–76, 82, 83, 86, 89–91, 92, 94, 99, 106, 154, 155, 158, 159, 166, 182, 183, 184, 195, 196, 197, 199, 203–205, 206, 208, 211–212, 214, 215, 217, 222, 236–237, 241, 263, 270, 272, 274, 279, 319, 334, 342, 343, 344, 345, 347–348, 349–350, 365, 366, 384, 396, 400, 414, 462, 464, 498, 504
- bicubic, 196
- biquadratic, 196
- cubic, 195, 196
- deformable, 166
- discrete feature element (DFE), 204–205, 207, 217, 259, 264, 518
- planar, 204
- tubular, 204–205, 207, 259, 264
- equilateral triangular, 199, 268–269
- hexahedron, 195, 197
- linear, 195, 196
- mixed, 195, 199
- number, 86, 89, 90, 146, 196, 197, 198
- patch, 90, 91
- prism, 195, 197
- quadratic, 195, 196
- quadrilateral (Lagrange family), 196
- quadrilateral (Serendipity family), 196
- tetrahedron, 195, 197
- triangular, 86, 89, 90, 91, 146, 149, 183, 196, 198, 199, 236, 268–269, 342, 344, 345, 346
- Elevation head. *See* Head
- Embarrassingly parallel problem, 424
- Engineering calculator. *See* Interpretive model
- Eolian deposits, 42, 463
- Ephemeral stream. *See* Stream
- Epistemic error. *See* Error
- EPM. *See* Equivalent porous medium (EPM)
- Equifinal model, 478
- Equipotential line. *See* Boundary conditions, hydraulic
- Equivalent freshwater head, 143
- Equivalent horizontal hydraulic conductivity. *See* Hydraulic conductivity (permeability)
- Equivalent porous medium (EPM), 42, 71, 518
- Equivalent vertical hydraulic conductivity. *See* Hydraulic conductivity (permeability)
- Error, 4, 12, 15, 18, 20, 56, 58, 59, 91, 95, 96, 97, 99–100, 101, 102, 105, 106–107, 108, 110, 130–131, 134, 139, 152–153, 165, 167, 170, 171, 173, 175, 190–191, 192, 195, 199, 202, 210, 215, 217, 219, 223, 225, 232, 238, 241, 243, 245, 262, 275, 280, 291–292, 314, 315, 318, 320, 324, 336, 339, 348, 349, 350, 364, 365–366, 376, 377, 379, 381–382, 383, 384, 385, 386, 389, 390, 391, 392, 393, 394–395, 396, 397, 398, 400, 408–409, 410, 412, 413, 414, 424, 428, 430, 431, 432, 434, 435, 445, 446, 447–449, 450, 455–456, 460, 461, 462–463, 464–465, 466, 472, 475, 478, 479, 481, 482, 483, 484, 501, 503, 504, 505, 507, 512, 513
- aleatory (intrinsic), 449, 450
- conceptualization, 4, 100, 102, 106, 107, 153, 336, 393–394, 395, 396, 398, 409, 447, 448, 482
- epistemic, 449, 450
- forecast, 448, 466, 469
- interpolation, 202, 238, 241, 365, 381, 397
- intrinsic. *See* aleatory, above
- mean absolute error (MAE), 377, 391–392, 429, 431, 472, 475, 505
- mean error (ME), 377, 391, 392, 429, 505
- measurement, 18, 58, 167, 241, 275, 379, 381–382, 383, 384, 400, 401, 432, 445, 447–448, 449, 450, 455, 460, 461, 462–463, 505, 507
- operator, 381, 382, 450
- parameter simplification, 412, 445, 447–448, 449, 460, 462, 463, 464, 465, 483
- residual, 91, 96, 97, 105–106, 110, 386, 389, 390, 391, 392, 505
- root mean squared error (RMSE), 377, 392, 429, 434, 505
- round-off, 55, 95, 96
- scaling, 223, 241, 382
- simplification, of processes, 456
- structural, 393–394, 412–413, 446, 448, 449, 484, 507
- surveying, 381, 382, 432
- tolerance. *See* Error criterion
- truncation, 190, 320
- variance, 448, 449, 461, 465–466
- water budget, 99, 100, 106–107, 108, 131, 152, 153, 280, 503, 512

- Error criterion, 96, 105, 106, 364, 365. *See also*  
 Closure criterion  
 head, 96, 105, 106  
 flow, 107  
 particle tracking, 364, 365  
 water budget, 100, 106, 107
- ET. *See* Evapotranspiration (ET)
- Ethics, 13–15, 496
- Euler integration, 339, 346, 348, 349, 364, 365
- European Water Framework Directive, 13, 482
- Evaporation, from surface water bodies, 31, 54,  
 157, 236, 276, 281, 295
- Evapotranspiration (ET), 51, 54, 55, 56, 57, 63,  
 151, 152, 157–158, 230, 232–233,  
 235–236, 257, 258, 270, 272, 284, 382,  
 450, 519
- Evapotranspiration (ET) Package.  
*See* MODFLOW code (Modular  
 Groundwater Flow Model), packages
- Excess overland flow. *See* Infiltration excess  
 overland flow; Saturation excess overland  
 flow
- Execution time, 95, 102, 105, 107, 215, 471, 504
- Executive summary. *See* Modeling report
- Expert knowledge, 377, 452, 461, 462, 463, 464
- Extinction depth, 157, 158, 235
- Extracting local boundary conditions.  
*See* Boundary conditions
- F**
- Facies models, 44
- Far-field, 36, 82, 83, 159, 278, 283, 323, 384, 400,  
 401, 463, 466
- Farm Process (FMP2). *See* MODFLOW code  
 (Modular Groundwater Flow Model),  
 processes
- Fault, 35, 37, 45, 52, 62, 82, 98, 135, 137, 138,  
 184, 185, 202, 203–205, 216–217, 219,  
 221, 314, 367, 368, 369, 477  
 as a barrier to flow, 45, 52, 82, 135, 137, 138, 202,  
 203, 217, 314, 367, 368, 369  
 as a boundary, 35, 37, 62, 98, 135, 137, 202, 221,  
 314, 367, 368, 369  
 as a conduit for flow, 45, 52, 137, 138, 202,  
 203–205, 217, 367, 368, 369  
 grid alignment, 135, 184, 185, 217, 219, 221  
 finite-difference representation, 98, 135, 185,  
 203, 217, 219, 221, 477  
 finite-element representation, 98, 203, 204, 205,  
 217, 477
- FD. *See* Finite-difference (FD)
- FE. *See* Finite-element (FE)
- FEFLOW code, 9, 76, 95, 98, 99, 100–101, 165,  
 172, 184, 197, 204, 236, 258, 259, 260,  
 262, 264, 270, 272, 277, 287, 320, 365,  
 400, 473, 503, 517, 518, 520, 521, 522  
 adaptive time stepping, 320  
 alignment of anisotropy, 76, 184  
 boundary conditions  
 ET, 270, 272  
 recharge, 258, 270, 520  
 stream, 258, 259, 277  
 well, 262, 264, 270  
 closure criterion, 320  
 density-driven flow, 521–522  
 direct solver, 95  
 discrete feature element (DFE), 205, 207, 219,  
 259, 264, 518  
 dual porosity option, 518, 522  
 error, local truncation, 320  
 FePEST code, 473  
 graphical user interface, 101  
 hydraulic conductivity tensor alignment, 184  
 linked to MIKE, 277  
 material property assignment, 236, 270  
 mesh generator, 197  
 movable nodes, 165  
 multispecies reactions, 522  
 orientating the mesh, 184  
 particle tracking post processor, 365  
 sink/source terms, 98, 258–259, 262, 270, 272,  
 277, 287  
 solute transport, 522  
 solution oscillation, 320  
 time step, 320, 365  
 unsaturated flow, 520  
 variable density flow, 521  
 variably saturated flow representation, 287, 520  
 water budget, 99
- Fence diagram, 32, 47, 48
- FePEST code. *See* FEFLOW code
- Finite-difference (FD), 8, 9, 11, 21, 85–89, 91–95,  
 96, 98, 101, 108, 109, 125–126, 128–129,  
 130, 131, 132, 133, 135–136, 145–147,  
 148–149, 150–151, 154, 159–161, 164,  
 165, 170–171, 172, 182–183, 184, 185,  
 186, 188, 189, 190, 191, 192, 194, 195,

- 199, 202, 203, 205, 206, 207, 211, 215, 216, 217, 218, 219, 220, 221, 224, 236, 239, 243, 244, 247, 259, 260, 261, 262, 263, 264–268, 270, 271–272, 277, 278, 281, 285, 288, 292, 293, 342, 343, 346, 351, 364, 365, 517
- Finite-element (FE), 8, 9, 21, 76, 85–86, 89, 90, 91, 92–93, 95, 96, 98, 99, 101, 125, 127, 136, 145, 146, 147, 148–149, 154, 159–160, 164–166, 170–171, 172, 182, 183, 184, 186, 191, 195–201, 202, 204, 207, 211–212, 215, 217, 220, 236, 243, 244, 247, 259, 260, 262, 264, 267–269, 270, 271–272, 277, 293, 342, 344, 346, 365, 504, 517, 521
- Five-point finite-difference star operator, 85, 129, 131, 171
- Fixed lake level model, 278, 279
- Fixed nodes, 164–165
- Fixed parameter, 395, 410, 411, 421, 454
- Flooded cell (node), 165, 216, 243
- Flow net, 84, 172, 200–201, 334, 335–336
  - anisotropic medium, 84, 200–201, 335–336
  - isotropic medium, 200–201, 335
- Flowing well. *See* Well
- Flowpath, 9, 17, 18, 21, 51, 58, 84, 122–124, 125–127, 134, 138, 170, 201, 203, 210, 230, 284, 331, 334, 335, 336, 337, 338, 339, 342, 346, 347, 351, 356, 357, 358, 359, 360, 362, 363, 364, 365, 366, 367, 368, 369, 414, 450, 454, 456, 475, 476, 505, 522, 524–525
- Flowpath chemistry, 58
- FLOWPATH code, 350, 365
- Flow system, 3, 11, 17, 29, 33, 46, 51, 54, 58, 94, 118, 120, 121, 122–124, 125, 164, 167–169, 170, 176, 229, 260, 270, 273, 293, 336, 339, 357, 502, 518
  - definition, 167–168
  - intermediate, 167–168, 280
  - local, 167–168, 260, 270, 351, 518
  - regional, 8, 11, 28, 29, 32, 36, 54, 80, 120, 121, 122–124, 128, 131, 133, 137, 167–168, 176, 260, 351, 518
  - Tóthian, 128, 167
- Flow-through lake, 279, 280
- Flow-through stream. *See* Stream
- Fluctuating lake level model, 279, 280, 283
- Flume, 273
- Fluvial deposit, 44, 60, 444, 463
- Flux target, 56, 203, 328, 380–381, 382–384, 387, 389, 390, 391, 395, 401, 435, 504, 505, 506
  - calibration, 56, 202–203, 380–384, 395, 504–506
  - difference target, 383, 384, 391
  - error, 56, 203, 383, 384, 389, 390, 504, 505
  - forecasting, 384
  - ranking, 384
  - weighting, 323, 401, 409, 504
- Forchheimer, Philipp, 122
- Forecast/forecasting model, 4, 6, 9–11, 12, 13, 16, 17, 18, 19–20, 21, 22, 27, 28, 29, 59, 102, 122, 140, 142, 182, 238, 243, 248, 290–291, 304, 322, 324–325, 377, 379, 384, 385, 394, 395, 399, 401, 409, 411, 413, 414, 424, 427–428, 429, 430, 431, 432, 435, 443, 445, 446, 447–449, 450, 451, 453–454, 455–456, 457–460, 461, 462, 465–466, 468–469, 470, 471, 472, 473, 475, 477, 478–479, 480–482, 483–484, 496, 497, 506–508, 510, 517, 522, 523, 526
  - advanced uncertainty analysis, 457, 469–479, 484
  - basic uncertainty analysis, 457, 458–469
  - best model. *See* Best model, Best fit model
  - General Likelihood Uncertainty Estimation, 478
  - linear uncertainty analysis, 458, 460–469, 471, 484, 507
  - Markov Chain Monte Carlo method, 475, 477
  - Monte Carlo Method, 397, 398, 400, 446, 471, 472–473, 474, 475, 477, 478, 479, 524
  - multiple conceptualizations, 477–479
  - Null-space Monte Carlo approach, 397, 475, 477
  - postaudit, 18, 481–482
  - reporting results, 445, 454, 457, 461, 475, 480–481, 483, 497, 506, 507, 508, 511
  - scenario modeling, 458–460
- Fortran, 9
- Forward problem, 376, 408
- Forward run, 376, 385, 394, 395, 396, 398, 406, 408, 410, 416, 428, 458, 459, 472, 475
- Forward tracking. *See* Particle tracking (PT)
- FracMan code, 518
- Fracture, 41, 42–43, 45, 51–52, 70, 71, 137, 205, 214, 220, 223, 225, 227, 332–333, 515, 516, 517, 518, 522
- Fracture flow, 42, 45, 51, 70, 71, 223, 225, 515, 516, 518, 522
- FREESURF code, 165

- Freshwater–seawater interface, 140–144, 228, 520  
Fully penetrating well. *See* Well
- G**
- Gaining stream. *See* Stream  
Galerkin’s method, 91  
Gauss–Marquardt–Levenberg (GML) method.  
  *See* PEST Software Suite  
Gauss–Seidel point iteration, 129, 244  
General (Global) Circulation Model (GCM), 230,  
  459–460  
General Head Boundary (GHB) Package.  
  *See* MODFLOW code (Modular  
  Groundwater Flow Model), packages  
General Likelihood Uncertainty Estimation  
  (GLUE), 478, 479  
General Systems Theory, 478  
Generic models, 11, 19, 20, 21, 28–29, 35, 40, 60,  
  305, 497, 521  
GENIE code, 397  
GENLINPRED. *See* PEST Software Suite  
Geographic information system (GIS), 32, 33–34,  
  47, 50, 101, 184, 216, 231, 241, 496, 510  
Geologic formation, 41, 501  
Geologic history, 42, 45, 49, 237, 501  
Geologic maps, 31, 35, 60, 62, 501  
Geologic process models, 524  
Geometric mean, 238  
Geophysical data (including borehole), 30, 43,  
  46–47, 57–58, 231, 266, 381, 397,  
  446–447, 524  
Geostatistics, 238, 249, 397, 446–447, 464, 524  
GFLOW code, 84, 144, 161, 279, 354  
GHB Package. *See* General Head Boundary  
  (GHB) Package; MODFLOW code  
  (Modular Groundwater Flow Model),  
  packages  
Ghost (imaginary) node, 129–131, 149, 171, 192,  
  194–195  
Ghost Node Correction (GNC) Package.  
  *See* MODFLOW code (Modular  
  Groundwater Flow Model), packages  
Ghyben–Herzberg relation, 141–142  
GIS. *See* Geographic information system (GIS)  
Glaciated terrain, 45, 285  
Global Circulation Model. *See* General (Global)  
  Circulation Model (GCM)  
Global coordinate system. *See* Coordinate system  
Global matrix. *See* Matrix  
Global minimum, of the objective function.  
  *See* Objective function  
Global sensitivity methods, 430  
GLUE. *See* General Likelihood Uncertainty  
  Estimation (GLUE)  
GML method. *See* PEST Software Suite;  
  Gauss–Marquardt–Levenberg (GML)  
  method  
GMS. *See* Groundwater Modeling System (GMS)  
GNC Package. *See* MODFLOW code (Modular  
  Groundwater Flow Model), packages;  
  Ghost Node Correction (GNC) Package  
Goodness of fit. *See* Calibration  
Governing equation, 6, 17, 70, 71–77, 78, 79, 83,  
  85, 86, 91, 94, 95, 99, 108, 109, 118,  
  125–127, 128–129, 131, 133, 143, 150,  
  166, 184, 200, 202, 208, 217, 222, 230,  
  245, 270–272, 303, 308, 319, 376, 469,  
  502, 503, 520, 524  
GPTRAC, 365  
Gradient. *See* Hydraulic gradient  
Grain size analysis, 225, 226, 332  
Graphical user interface (GUI), 33–34, 99,  
  101–102, 107, 127, 160–161, 175, 182,  
  184, 195, 197, 203, 216, 241, 260, 304,  
  306, 334, 368, 382, 398, 399, 400, 408,  
  412, 425–426, 475, 509, 510, 512, 513  
Gravel, 60, 62, 173, 220, 227, 228, 229, 246, 248,  
  267, 294, 333, 377, 432–433, 435,  
  463, 464  
Grid, 17, 76, 85, 86, 87, 88, 91, 92–93, 95, 98–99,  
  103, 108, 109–110, 125, 127, 128–130,  
  132, 133–134, 135, 145–147, 149, 150,  
  151, 153, 154, 159, 160, 162, 164, 171,  
  172, 182–195, 199, 201, 202, 206,  
  207–208, 210, 215–221, 222, 224, 236,  
  237, 238–239, 241, 243, 244, 245, 247,  
  260, 262, 263, 264, 265, 267–269, 272,  
  274, 278, 279, 281, 283, 288, 290, 292,  
  293, 304, 315–316, 319, 331, 338–339,  
  342, 343, 345, 346, 351, 364, 366, 382,  
  393, 435, 455, 496, 502, 503–504  
  block-centered finite difference, 85, 87, 91,  
  129–130, 145–147, 150, 171–172, 186,  
  187–188, 190, 236, 292, 293, 364  
  boundary. *See* Boundary conditions  
  deformable, 216, 222, 243

- Grid (*Continued*)
- design, 17, 182, 184, 187, 188, 189, 190,
    - 191–192, 195, 201, 202, 203, 208, 214, 215, 217, 267, 269, 292, 293, 502, 503–504
  - finite-difference, 76, 85, 86–88, 91, 93, 125,
    - 128–130, 132, 133, 135, 145–147, 149, 150, 151, 160, 164, 171, 182–183, 184–195, 199, 202, 206, 207, 215–216, 217, 218, 219–221, 224, 236, 239, 243, 244, 247, 262, 263, 265, 267, 272, 278, 281, 288, 292, 293, 342, 343, 346, 351, 364
  - irregular, 187–188, 189–190, 191, 316, 319
  - local grid refinement (LGR), 160, 161–162, 191, 364
  - nested, 187, 191, 192, 293
  - octree grid refinement, 191
  - orientation, 125–127, 184, 185
  - parameter assignment, 17, 101, 103–104, 182, 188, 203, 208, 214, 215, 217–222, 236, 237–241, 244, 264, 271, 277, 393, 502, 503–504
  - point-centered finite difference, 129, 146, 147, 171, 172, 186, 187–188, 236, 244
  - populating, 236, 237–241
  - quadtree grid refinement, 187, 191, 193
  - regular, 128, 187, 190, 191, 268, 292, 435
  - semi-structured, 195
  - size, 193, 265
  - spacing, 85–86, 99, 108, 129, 154, 159, 182–184, 186–191, 195, 201–202, 207–208, 210, 243, 244, 247, 269, 292, 293, 316, 319, 339, 351, 366, 502
  - structured, 183, 184, 186–191, 193, 195, 215, 216, 217, 243, 264, 272, 346
  - unstructured, 92–93, 183, 184, 187, 191–195, 215, 217, 218, 219, 243, 247, 264, 272, 293, 342, 345, 346, 364
- Groundwater, 3–4, 5, 6, 8–10, 11–12, 13, 14, 16–17, 19–20, 21–22, 28–29, 30–31, 32–34, 35–36, 37, 41, 42, 46, 49, 51–53, 54–59, 60, 62, 63, 70–77, 78, 80, 81, 83–84, 85, 91, 92, 95, 96, 98–99, 100–102, 105, 109, 118, 120–121, 122–124, 125, 128, 131, 132, 133, 136, 137, 138, 139, 140, 141–143, 144, 145, 148, 150, 153–154, 155, 156, 157, 158, 159, 162, 164, 167–169, 170, 171, 173, 175, 183, 184, 186, 191, 195, 199, 201, 203, 205–206, 208, 211, 214, 215, 222, 223, 225, 226, 228, 229, 230–231, 232–233, 235, 238, 243, 244, 246, 247, 248, 258, 260, 262, 264, 269, 270, 272–275, 276, 277, 278–279, 280–281, 282, 283, 285–287, 289–291, 292, 294, 295, 296, 304, 305, 306, 307, 308, 309, 310, 311, 313, 314, 315, 317, 318, 319, 322, 325, 331–332, 334–341, 342, 347, 351, 357, 358, 359, 360, 362, 364, 365, 366, 367, 369, 376, 378, 379, 380, 381, 382–383, 385, 389, 394, 395–396, 397, 400, 403, 404, 406, 408–409, 410, 411–412, 414, 415, 416, 419, 421–422, 425, 426, 427, 428, 432, 435, 443, 444, 445, 446–447, 448, 451, 456, 457, 459, 464, 465, 467, 469, 471, 472, 473, 478, 479, 481, 482, 496, 497, 499, 501, 502, 506, 509, 510, 511, 512, 513, 515–517, 518–522, 523, 524–526, 527
- age, 21, 31, 58, 336, 357–358, 365
  - basin, 31, 34, 248, 279, 285, 499
  - budget (water budget), 17, 31, 32, 34, 35, 53, 54–57, 58, 60, 62–63, 97, 99–100, 106–107, 108, 122, 130–131, 152, 153, 171, 173, 195, 243, 245, 260, 281, 291, 295, 307, 311, 320, 322, 408, 429, 501, 502, 503, 504, 506, 509, 512
  - budget residual, 106
  - divide, 11, 35, 80, 120, 125, 128, 137, 139, 144, 145, 150, 159, 168, 173, 175, 244, 285–286, 290, 325
  - flow system. *See* Flow system
  - velocity. *See* Average linear velocity
- GroundWater Desktop, 33, 102
- Groundwater divide. *See* Groundwater
- Groundwater Management (GWM) Process.  
*See* MODFLOW code (Modular Groundwater Flow Model), processes
- Groundwater Modeling System (GMS), 101, 475
- Groundwater–surface water interaction, 54, 56, 58, 80, 91, 98, 195, 201, 444, 523
- Groundwater system time constant, 308, 340
- Groundwatershed, 214, 285–286
- Groundwater Vistas, 101, 160, 203, 475
- GSFLOW code, 287
- GUI. *See* Graphical user interface (GUI)
- Guidelines (for modeling), 18, 20, 78, 121, 123, 189–190, 191–192, 201, 207, 209–210, 217, 229, 257, 258, 265, 267–269, 293,



- 310, 320, 338, 351, 362, 378, 392, 397,  
399, 408, 410, 447, 457, 497, 500, 511
- GWPATH code, 365
- ## H
- Hagen–Poiseuille equation, 264
- Hantush–Jacob solution, 7
- Hard knowledge, 377, 378, 380, 393, 414, 417,  
418–419, 425, 426
- Hazen’s equation, 226
- HDB. *See* Boundary conditions, head-dependent  
boundary (HDB)
- Head, 5–6, 9, 14–15, 31, 36, 38, 51, 56, 70, 71, 72,  
73, 74–75, 80, 82, 83, 85, 86, 88, 89–90,  
91, 94, 95, 96, 97, 99, 100, 104, 105–106,  
106–107, 108, 109, 110, 118–119, 120,  
121, 122–123, 125, 127, 128–131, 133,  
134, 135, 136, 137, 138, 139, 142–143,  
144, 145–146, 147–148, 149, 150, 151,  
152–154, 155, 157, 158, 171, 173,  
175–176, 182, 186, 190, 192, 195,  
198–199, 202–203, 206, 207–208,  
209–210, 214, 215, 216, 222, 225, 226,  
227, 229–230, 233, 235, 236, 243, 244,  
245, 246–247, 257, 258, 259, 260, 261,  
263, 264, 265–269, 273–275, 276, 279,  
281–282, 283, 285, 290, 291, 292–293,  
294–295, 296, 303–306, 308–309, 310,  
312–313, 314, 315, 316, 318, 319, 320,  
322–323, 324–325, 331, 335, 336, 338,  
340–341, 342, 344, 364, 365, 367–368,  
369, 376–377, 379, 380, 381–382, 383,  
384, 385, 386–387, 389, 391, 392, 395,  
397, 401, 403, 404, 406, 407, 409, 416,  
419, 427, 432, 434, 435, 450, 454–456,  
461, 468, 469, 472, 483–484, 501–502,  
504, 505, 512, 519
- closure criterion, 96, 97, 105–107, 110, 153
- elevation, 162–163
- error criterion. *See* closure criterion, above
- freshwater, 142–143
- gradient, 5, 73, 74–75, 77, 103, 120, 123, 129,  
136, 138, 148, 150, 152, 153, 162, 202,  
207–208, 209–210, 233, 247, 264, 283, 294,  
302, 332, 338, 344, 350, 416, 454, 519, 521
- loss, 226, 263, 265, 266–267, 295, 519
- pressure, 121, 162–163, 166, 233, 318, 519
- total, 162, 233, 435, 455, 504
- Head target, 203, 305–306, 379, 381–382, 383,  
384, 387, 389, 392, 395, 401, 407, 409,  
434, 435, 455, 504
- calibration, 202–203, 379, 380–381, 382, 392,  
435, 455
- difference, 382, 383, 384, 386, 504
- error, 379, 381–382, 392, 432, 461, 504
- ranking, 384–385, 400
- weighting, 171, 323, 344, 401, 409, 455, 504
- Head-dependent boundary (HDB). *See* Boundary  
conditions, head-dependent boundary  
(HDB)
- Head-specified well. *See* Well
- Headwater stream. *See* Stream
- Hele-Shaw analog model, 5, 168
- HELP code, 230
- Heterogeneity, 6, 8, 11, 12, 21, 58, 73, 77, 81, 84,  
85, 98, 124, 201, 202, 203, 211–214, 215,  
223, 225, 229, 238, 241, 245, 333,  
335–336, 340, 353, 362, 366, 413, 414,  
416, 419, 420, 450, 454, 455–456, 463,  
465, 516, 522, 524–525
- Heterogeneous aquifer. *See* Aquifer
- Hexahedron element. *See* Element
- HFB Package. *See* Horizontal-Flow Barrier (HFB)  
Package; MODFLOW code (Modular  
Groundwater Flow Model), packages
- High-capacity well. *See* Well
- High-conductivity node (cell/element), 203,  
264, 279
- Highly parameterized. *See* Parameter estimation
- Hindcast (methods and models), 9, 11, 14, 18,  
443–444
- History matching. *See* Calibration
- Homogeneous, 21, 41, 42, 77, 79, 83, 96, 108,  
109, 123, 128, 171, 172, 173, 200,  
211–212, 223, 244, 245, 267, 294, 319,  
335, 342, 354, 415, 417
- Horizontal anisotropy. *See* Anisotropy
- Horizontal nodal spacing. *See* Discretization,  
spatial, horizontal
- Horizontal well. *See* Well
- Horizontal-Flow Barrier (HFB) Package.  
*See* MODFLOW code (Modular  
Groundwater Flow Model), packages
- HRU. *See* Hydrologic response unit (HRU)
- HSSM code, 521
- HST3D code, 147
- Humid hydrologic setting, 34

- Hybrid approach, to parameter assignment, 241, 425–426
- Hydraulic barriers, 45, 52, 81–82, 103, 137–138, 140, 199, 202–203, 205, 260
- Hydraulic boundaries. *See* Boundary conditions
- Hydraulic conductivity (permeability), 21, 28, 31, 33, 37, 38, 41, 45, 46, 49–50, 52, 58, 73–74, 76, 78, 79, 82, 88, 95, 108, 127, 129–131, 134, 136–138, 149, 152, 156, 159, 168–169, 184, 200, 203–204, 205, 208, 211–214, 215, 216, 217, 219–220, 222–227, 232, 236, 238, 239, 240, 242, 243, 246–247, 248–249, 275, 279, 288, 292, 294, 308, 310, 319, 331, 332, 334, 335, 338, 340, 344, 364, 366, 367, 376, 377, 385, 395, 397, 408, 413, 414, 415, 416, 417, 428, 432, 434, 435, 444, 452, 455–456, 460, 461, 464, 472, 518, 519, 522, 524–525
- anisotropy. *See* Anisotropy
- equivalent horizontal, 211–213
- equivalent vertical, 211–212
- horizontal, 41, 43, 58, 137, 159, 200, 208, 211–213, 220, 246–247, 249, 281, 336, 366, 393, 416, 466, 472
- lake bed, 155, 281
- orientation of grid/mesh, 184
- methods to determine, 223–227
- misalignment of tensor, 217, 220
- primary, 41, 42
- secondary, 41, 43
- streambed, 153–155, 275, 277
- tensor, 73, 74, 76, 184, 186, 217, 220, 334
- unsaturated, 519
- upscaling, 211–214, 223, 229
- vertical, 41, 43, 58, 119–120, 134, 152, 153, 200, 205, 208, 210–211, 220, 222, 229, 246–247, 264–265, 277, 281, 296, 382, 393, 416, 432, 466
- Hydraulic diffusivity, 308, 309, 314
- Hydraulic fracturing (fracking), 260, 526
- Hydraulic gradient, 103, 120, 136, 137, 152, 188, 202, 205, 281, 283, 294, 332, 338, 454, 521
- Hydraulic tomography, 225, 260, 269, 452
- Hydric soils, 59
- Hydrochemical facies, 58
- Hydrofacies, 41, 42, 44, 45, 46–47, 49, 238
- Hydrogeologic maps, 51
- Hydrogeologic reasonableness, 377, 378, 414, 431, 497, 506
- Hydrogeological cross section, 5, 11, 22, 32, 45, 51, 118, 122, 125, 126–128, 130, 131, 138–139, 143, 163, 172, 173, 174, 209, 221, 247, 311, 334, 351, 355, 358, 367, 387, 433, 501, 502
- Hydrogeological unit. *See* Hydrostratigraphic unit (Hydrogeologic or Geohydrologic unit)
- Hydrograph, 31, 51, 273, 289–290, 300, 306–307, 313, 320, 322, 325–326, 385, 387, 392, 505, 506, 512
- discharge, 273, 320, 325, 326, 505, 506
- head (water level), 31, 51, 273, 289, 306–307, 313, 320, 322, 325–326, 385, 387, 392, 505, 512
- stream stage, 273–274, 289–290, 387
- Hydrologic budget, 31, 54, 57, 60, 63
- Hydrologic parameters. *See* Parameter
- Hydrologic response model, 285–286, 291, 522
- Hydrologic response unit (HRU), 287, 290
- Hydrologic system conceptual model. *See* Conceptual model
- Hydrologic watershed model, 231, 279, 285–290
- Hydrosense, 13, 21, 378, 395, 396, 409, 479
- Hydrostatic conditions, 141–142
- Hydrostratigraphic unit (Hydrogeologic or Geohydrologic unit), 17, 41–42, 43, 45–47, 49, 54, 60, 133, 137, 169, 184, 208, 209–210, 215–216, 217, 219, 220, 221, 222–223, 237, 238, 242, 243, 305, 310, 387, 501–502, 504, 521
- Hydrostratigraphy, 32, 35, 37–50, 59, 62, 118, 208, 215, 226, 500–501
- Hydrostructural unit, 45
- HYDRUS code, 230
- Hyporheic zone, 11, 131, 169, 523
- ## I
- Identifiability. *See* Parameter
- Identity matrix. *See* Matrix
- IFD. *See* Integrated finite differences (IFD)
- Igneous and metamorphic terrains, 41, 42, 45, 52
- Ill-posed. *See* Inverse problem
- Imaginary node. *See* Ghost (imaginary) node
- Impermeable, 35, 38, 41, 81, 108, 118, 120, 128, 133, 135, 136, 146, 172, 204, 296, 314, 432, 433
- Inactive nodes, 185, 186, 222, 236. *See also* Nodes

- Independent variable, 73, 222
- Indirect inverse solution. *See* Inverse solution
- Infiltration, 51, 63, 157, 166, 168, 230, 232–234, 235, 257, 258, 270, 271, 272, 289–290, 382, 519
- Infiltration excess overland flow, 232–234. *See also* Saturation excess overland flow
- Infiltration galleries, 51
- Influence, statistical, 405, 410, 430
- Influent stream. *See* Stream
- Information criteria, 478–479
- Information theory, 448
- INFSTAT utility. *See* PEST Software Suite
- Initial conditions, 6, 17, 70, 85, 94, 108, 152, 304, 307, 309, 310, 312–314, 320, 324–325, 435, 483, 498, 502, 503, 505
- arbitrary, 312–313
  - dynamic cyclic equilibrium, 312–313, 314
  - dynamic steady state, 312, 313, 314, 324, 325
  - spin-up, 313, 314, 324
  - static steady state, 312, 313
- Instruction file, 398
- Injection well. *See* Well
- Innate parameter variability, 463–464, 465, 507
- Input parameters, 101, 131, 235, 376, 502
- Insensitive parameters. *See* Parameter
- Integrated finite differences (IFD). *See* Control volume finite-difference (CVFD) method
- Integrated hydrologic model, 313, 527
- Interfingering laminae, 211–212, 223–224
- Interglacial period, 314
- Intermediate groundwater flow system. *See* Flow system
- Internal boundary conditions. *See* Boundary conditions
- International Panel on Climate Change (IPCC), 480
- Interpolation, 89–90, 182, 195, 203, 236, 237, 238–241, 244, 248–249, 334, 338–346, 347, 364, 365, 382, 397, 414, 416, 454
- error. *See* Error, interpolation
  - head, 89–90, 182, 192, 195, 202–203, 236, 244, 338, 341, 344, 364–365, 381–382, 397, 454
  - methods, 237, 238, 239, 241, 244, 249, 338–347, 364, 365, 454
  - parameter, 236–238, 239, 241, 244, 248, 414, 416, 454
  - velocity, 334, 338–346, 347, 364, 365
- Interpretive model, 9, 11, 19, 21, 28–29, 35, 60, 84, 223, 305, 385, 430, 445, 497
- engineering calculator, 11, 19, 21, 35
  - generic, 11, 19, 21, 28–29, 35, 60, 305, 497
  - screening, 11, 19, 21, 28, 84, 223, 305, 385, 430
  - uncalibrated, 11, 445
- Intrinsic (aleatory) error. *See* Error, aleatory (intrinsic)
- Introduction. *See* Modeling report
- Inverse distance interpolation. *See* Particle tracking (PT), velocity interpolation
- Inverse problem, 376, 396, 397, 399, 406, 411–412, 414, 421–422, 446, 460, 469, 525. *See also* Parameter estimation
- ill-posed, 378, 393, 412, 414, 417, 431, 446–447, 516
  - non-uniqueness, 225, 403
  - well-posed, 378, 403, 425
- Inverse solution, 225, 380, 396–397, 417, 419, 446
- direct, 397, 469
  - indirect, 396–397, 446
- Inversion, 411–426
- IPCC. *See* International Panel on Climate Change (IPCC)
- Irregular grid. *See* Grid
- Isotopes. *See* Chemical analyses and tracers
- Isotropic conditions, 77, 83, 108–109, 120, 123, 128, 138, 171, 172, 173, 199–201, 210, 211–213, 220, 223, 244, 245, 267, 294, 319, 335
- Iteration, 95–96, 97, 100, 104, 105, 109–110, 128–129, 131, 161, 166, 171, 214, 244, 266, 270, 304, 310, 394, 397, 402, 406, 408, 424, 425, 482, 522
- closure criterion, 96, 97, 99, 100, 102, 105–107, 110, 153, 172, 320, 403, 405, 408, 503, 504
  - numerical solution, 95, 96, 304
  - parameter estimation, 105, 397, 402–403, 405–406, 408, 424–425
  - point, 96, 109–110, 129, 131
- Iterative solution. *See* Numerical solutions
- J**
- Jacobian matrix. *See* Parameter estimation
- K**
- K. *See* Hydraulic conductivity (permeability)
- K tensor. *See* Hydraulic conductivity (permeability)

- $K_d$ . *See* Distribution coefficient ( $K_d$ )
- Karst, 6, 42, 45, 52, 518
- Kashyap Information Criterion (KIC), 479
- Known unknowns, 12, 449, 482
- Kriging, 238, 241, 364, 414, 524
- ## L
- Lake cells, 151
- Lake (LAK3) Package. *See* MODFLOW code (Modular Groundwater Flow Model), packages
- Land surface subsidence, 56, 518–519
- Laplace equation, 77, 83–84, 86, 128, 200
- Lateral boundary flows, 158–159, 175
- Lawrence Berkeley National Laboratory (LBNL), 517
- Layer, 8, 43, 84, 86, 88, 91, 92, 97, 103–104, 105, 118, 119, 124–127, 129, 131, 133–134, 141, 143, 161, 164, 165, 183, 184, 186, 195, 204, 205, 208–222, 223, 224, 225, 228, 237, 243, 245–247, 259, 260, 262, 263, 264–266, 270, 271, 273, 283–284, 291–292, 304, 306–307, 319, 332–333, 336, 338–339, 344, 366, 367–368, 382, 385, 466, 472, 504, 506, 508
- confined, 119, 127, 134, 165, 208, 214–216, 228, 237, 243, 291, 366, 369
- convertible, 214, 215, 237, 243
- discretization, 84, 86, 92, 103, 105, 110, 124–127, 133, 143, 161, 165, 183, 186, 195, 208–225, 237, 243, 260, 262–266, 283–284, 292, 304, 307, 336, 338–339, 344, 367–368, 385, 466, 472, 504, 508
- distorted (deformed), 209, 216, 222, 243, 338, 339, 366
- orientation, 125–126, 127, 129, 204, 208, 216–222
- storage, 237
- thickness, 119, 126, 131, 143, 165, 184, 211–212, 214, 215, 217–220, 225, 228, 237, 246, 262, 319, 339
- unconfined, 119, 141, 164–165, 188, 214, 215–216, 228, 237, 243, 266, 270, 271, 291–292
- vertical hydraulic conductivity of, 134, 205, 208, 210, 211–214, 217, 220, 222, 225, 245–247, 264, 382, 466
- Leakage, 4, 41, 80, 82, 118–120, 133–134, 141, 148, 150, 155, 205, 207, 208, 243, 244, 246, 247, 257, 270, 276, 293, 296, 304, 316, 432
- Leakance, 119–120, 133, 141, 155, 208, 210, 214, 222, 229–230, 275, 281, 282, 292, 428, 466
- horizontal, 155, 208, 222, 229, 281, 466
- vertical, 119–120, 133–134, 155, 208, 210, 222, 229–230, 281
- Leaky beds, 41, 207, 208, 244
- Least squares fitting (also damped), 238, 403
- Legal arena, 13, 99, 396, 512
- LGR. *See* Grid, local grid refinement (LGR)
- Light nonaqueous phase liquid (LNAPL), 521
- Likelihood, 425, 445, 451–452, 457, 478, 481, 507
- Line discharge. *See* Discharge
- Linear adsorption, 363
- Linear combination of parameters, 421, 423, 424, 425, 479
- Linear element. *See* Element
- Linear interpolation, 90, 239, 248, 342, 344, 364, 365
- Linear uncertainty analysis. *See* Uncertainty, linear analysis
- Linearity (Linear), 5, 7, 79, 80, 83, 91, 95, 98, 108, 129, 131, 157, 158, 165, 195–196, 214, 236, 263, 264, 266, 289–290, 334, 336, 338, 342, 343, 344, 347, 363, 406, 408, 421, 423, 424, 430, 446–447, 460, 465, 468, 469, 471, 479
- Linked models, 33–34, 70, 269, 277, 287, 521–522
- Literature review. *See* Modeling report
- LNAPL. *See* Light nonaqueous phase liquid (LNAPL)
- Local flow system. *See* Flow system
- Local grid refinement (LGR). *See* Grid, MODFLOW code (Modular Groundwater Flow Model), packages
- Local minimum of the objective function. *See* Objective function
- Local sensitivity, 430
- Log-transformed parameter, 408
- Losing stream. *See* Stream
- ## M
- MAE. *See* Error; mean absolute error (MAE)
- Manning's equation, 276, 283, 466, 523
- Manual-trial-and-error. *See* Calibration
- Markov Chain Monte Carlo (MCMC) method, 475, 477

- Mass Balance equation. *See* Continuity equation (mass balance)
- Material property parameters. *See* Parameter
- Mathematical model, 4, 5–9, 17, 22, 29, 35, 70, 78–85, 108–109, 128–129, 245, 502–503  
analytical, 6, 8, 17, 29, 70, 78–85, 108  
boundary conditions, 6, 17, 35, 70, 79, 108, 245  
data-driven (black-box), 5, 6–7, 14, 526  
deterministic, 5  
governing equation, 6, 17, 70, 79, 108, 129, 245, 502, 503  
initial conditions, 6, 17, 70, 108, 503  
numerical, 6, 70, 78, 85–96, 502  
process based models (physically based models), 5, 6–7  
stochastic, 5, 399, 446, 472, 473, 477, 516, 524, 525
- MATLAB software package, 6, 98
- Matrix, 42, 71, 74–76, 88–89, 91, 92, 94, 95, 96, 105, 149, 184, 197, 227, 272, 406–407, 409, 410, 411, 421–422, 424–425, 460, 461, 462–463, 464, 465, 468, 471, 518, 522  
bandwidth, 197  
covariance, 461, 462, 463, 464  
diagonal, 74–75, 197, 462, 464  
global, 74–76, 88, 91, 92, 94, 95, 96, 149, 184, 197  
identity, 461  
innate parameter variability. *See* C(p) matrix  
Jacobian. *See* Parameter estimation  
measurement error. *See* C( $\epsilon$ ) matrix  
resolution, 422, 461, 463  
semi-bandwidth, 197  
sensitivity. *See* Parameter estimation; Jacobian (sensitivity) matrix  
solution methods, 89, 95, 96  
symmetric, 75, 197, 462
- Maximization–minimization problem, 469, 471, 475
- Maximum Likelihood Bayesian Model Averaging (MLBMA), 479
- Maximum terrain rise, 169
- MCMC method. *See* Markov Chain Monte Carlo (MCMC) method
- ME. *See* Error, mean error (ME)
- Mean absolute error (MAE). *See* Error
- Mean error (ME). *See* Error
- Measurement error. *See* Error
- Measurement objective function. *See* Objective function
- Mesh, 17, 86, 89–90, 92, 101, 102, 127, 132, 134, 145–147, 149, 153–154, 159, 162, 164, 165–166, 182–184, 186–187, 191, 195–202, 204–205, 207–208, 210, 215, 217, 220, 222, 236, 237–241, 243, 244, 245, 247, 260, 262, 264, 267–269, 271, 272, 274, 279, 290, 292, 293, 304, 315–316, 331, 338–339, 345–346, 366, 382, 393, 496, 502, 503–504  
deformable, 165–166  
design of, 17, 86, 89, 132, 134, 145–147, 149, 154, 159, 164, 182, 184, 186, 187, 197, 200, 202, 204–205, 208, 210, 215, 217, 274, 290, 292, 315–316, 496, 502, 504  
generator, 182, 197  
irregular, 247, 316, 319  
mixed element, 195–196, 199  
orientation, 127, 184, 186, 243  
parameter assignment, 204, 210, 215, 217, 222, 236, 237, 241, 271, 393, 503  
quadrilateral element, 146, 199  
refinement, 195, 199  
structured, 132, 183, 195, 216–217, 272, 292  
triangular element, 86, 149, 196–197, 198, 199, 268–269  
unstructured, 159, 183, 187, 191, 195, 247, 272, 293, 345  
well, placement of, 204–205, 207, 259–260, 262, 264, 267–269. *See also* Well
- Method of Morris, 430
- Method of weighted residuals, 91
- MIKE11 code, 277
- MIKE SHE code, 288
- Mines, 14, 42, 121, 155, 157, 205, 248, 259, 272, 465
- Minimum Message Length (MML) curve, 448–449
- Misfit, of model, 60, 393, 428, 429
- MLBMA. *See* Maximum Likelihood Bayesian Model Averaging (MLBMA)
- MML curve. *See* Minimum Message Length (MML) curve
- Model complexity, 8, 12, 13, 14, 60, 71, 78, 80, 83, 84, 85, 86, 96, 98, 101, 105, 107, 118, 143, 334, 335, 362, 378, 397, 411, 413, 431, 448–449, 459, 512, 513, 515, 516, 517, 518, 519–522, 526, 527

- Model space, 376
- Model validation. *See* Validation, model
- Model verification. *See* Verification
- Model Viewer software, 102
- Modeling ethics. *See* Ethics
- Modeling objective (purpose), 5, 9–11, 13, 14, 17, 19, 21–22, 27, 28–29, 57, 59–60, 70, 78, 99, 100, 102, 118, 124, 130, 131, 140, 142, 162, 182, 201, 205, 208, 210, 214, 229, 230, 245, 246, 260, 269, 273, 277, 279, 283, 290, 303–305, 307, 308, 309, 313, 314, 320, 322, 324, 338–339, 363, 377, 380, 382, 383–384, 392, 393, 396, 400–401, 410–411, 414, 421, 428, 430, 431, 432, 443, 447, 449, 453–454, 457, 459, 463, 483, 498–499, 500, 502, 503, 506, 507–508, 509, 511, 513, 525, 526
- Modeling report, 15, 18, 20, 21, 102, 247, 495–513
  - abstract, 498, 499–500
  - appendices, 496, 509
  - assumptions, simplifications and limitations, 480, 483, 508
  - discussion, 498, 507–508
  - executive summary, 496, 498, 499–500
  - forecasting simulations and uncertainty analyses, 497, 499, 506–507, 510
  - hydrogeologic setting and conceptual model, 499–502
  - introduction, 499–500
  - literature review, 500
  - numerical model, 497, 502–506
  - references cited, 499, 508–509
  - reviewing, 500, 510–513
  - summary and conclusions, 499, 508
  - title, 498–499
- Modeling workflow, 10, 16–20, 27, 334, 377, 398–399, 426–431, 458, 474
- MODFLOW code (Modular Groundwater Flow Model), 9, 11, 34, 85, 88, 92–93, 95, 97, 98, 100–101, 106, 131, 143–144, 145, 147, 149, 152, 155, 156, 158, 160, 165, 172, 183, 186, 188, 203, 205, 206, 207, 215, 258, 259, 260, 262, 263, 264, 265–266, 270, 272, 274–275, 276, 277, 278, 279, 280, 281, 283–284, 287–288, 292, 295, 316, 318, 320, 347, 354, 364, 400, 466, 472, 473, 503, 510, 517, 518, 519, 520, 521, 522, 523, 524, 525
- block-centered finite differences, 85, 86, 87, 89, 145–147, 188
- governing equation, 88–89
- packages
  - Drain (DRN) Package, 152, 277
  - Drain Return (DRT1) Package, 156, 273
  - Evapotranspiration (ET) Package, 152, 272
  - Evapotranspiration Segments (ETS1) Package, 272
  - General Head Boundary (GHB) Package, 152, 158, 266, 283
  - Ghost Node Correction (GNC) Package, 192, 195
  - Horizontal-Flow Barrier (HFB) Package, 103, 205, 217
  - Lake (LAK3) Package, 280–281, 295
  - Local Grid Refinement (LGR) Package, 160, 191
  - Multi-Aquifer Well (MWP1) Package, 265
  - Multi-Node Well (MNW1) Package, 262, 265, 266
  - Multi-Node Well (MNW2) Package, 262, 265, 266, 267
  - Recharge (RCH) Package, 270
  - River (RIV) Package, 152, 155, 259, 274–275, 277–278, 283
  - Seawater Intrusion (SWI2) Package, 143–144
  - Stream Flow Routing (SFR1) Package, 259, 276, 277–278, 281, 292
  - Stream Flow Routing (SFR2) Package, 259, 276, 277–278, 281, 292
  - Subsidence and Aquifer Compaction for water table aquifers (SUB-WT) Package, 519
  - Time-variant Specified-head (CHD) Package, 147
  - Unsaturated Zone Flow (UZF) Package, 230, 234, 288
  - Well (WEL) Package, 260, 262, 264, 266
  - Wetlands Package, 152, 283–284
- processes
  - Conduit Flow Process (CFP), 205, 207, 518
  - Connected Linear Network (CLN) Process, 205, 207, 264
  - Farm Process (FMP2), 525
  - Groundwater Management (GWM) Process, 525
  - Surface-Water Routing (SWR1) Process, 277, 283

- versions
    - MODFLOW-2000, 165, 364
    - MODFLOW-2005, 205
    - MODFLOW-NWT, 165, 266
    - MODFLOW-SURFACT, 101
    - MODFLOW-USG, 92, 98, 101–102, 145, 183, 191, 192, 195, 205, 207, 217, 243, 264, 364, 518
    - MODFLOWP, 397
      - Stochastic, 473, 524
  - MODFLOW-USG. *See* MODFLOW, versions
  - MODHMS code, 101
  - MODINV code, 397
  - MODPATH code, 101, 351, 359, 364, 365, 472, 524
  - ModPATH3DU code, 364
  - MODPATH –USG code, 364
  - ModTech, 101
  - Monitoring network design, 323, 468
  - Monte Carlo method, 397, 446, 471–473, 475, 478, 524
  - Mountain front recharge, 51, 54
  - Movable nodes, 162, 164, 165–166
  - Moving boundary, 35, 121, 143, 162
  - MT3DMS code, 101, 318, 521, 522
  - Multi-aquifer well. *See* Well
  - Multi-layer well. *See* Well
  - Multi-node well. *See* Well
  - Multiphase flow, 70, 515, 521
  - Multiple conceptualizations, 17, 469, 477, 478, 479
  - Multiple-point geostatistics, 524
  - Multiple working hypotheses, 59, 378
- N**
- NAPL. *See* Nonaqueous phase liquid (NAPL)
  - Nash–Sutcliffe coefficient of efficiency (NS), 387, 392, 429
  - Near-field, 36, 82, 83, 84, 108, 277, 278, 384, 400–401, 463
  - Nested grid. *See* Grid
  - Nested well (piezometer). *See* Well
  - Network design. *See* Monitoring network design
  - Neumann boundary conditions. *See* Boundary conditions
  - Ninety-five percent (95%) confidence interval, 382, 383, 409, 457, 461, 463, 464, 465, 469, 475, 477
  - No prior, 452
  - Nodal spacing, 85–87, 108, 129, 142, 159, 164, 173, 182–183, 184, 186, 187, 189–191, 195, 199, 200, 201–208, 209, 210–211, 217, 223, 225, 236, 243, 244, 245, 247–248, 249, 257, 260–261, 264, 265, 267–269, 274, 292–294, 316, 319, 324, 338, 351, 365, 366, 369, 432–433, 477, 502, 508, 520
    - guidelines for, 142, 151, 164, 183–184, 189–191, 195, 201–211, 217, 243–245, 247–249, 257, 260–261, 264–265, 267–269, 274, 292–294, 316, 338, 351, 366, 369, 477
    - irregular, 87, 187, 189–191, 195, 199, 247, 316, 319
    - regular, 128, 187, 190, 191, 268, 292
    - uniform, 85, 86–87, 108, 187, 191, 247, 249, 294, 324, 432, 433
  - Nodes, 8, 77, 85, 86, 87, 88, 89, 90, 91, 92–93, 95, 96, 98, 99, 105, 106, 108, 109, 110, 127, 129–131, 145–147, 148–149, 150, 152, 153, 155, 156, 157, 159, 160, 162, 164–166, 170, 171, 175–176, 182, 183, 184, 185, 186, 187, 189, 190, 191, 192, 195, 196, 198, 201–203, 204, 205, 207–208, 210, 211, 212, 214, 215, 216, 218, 222, 234, 236, 237, 238, 241, 243, 244, 245, 259, 260–269, 270, 271, 272, 273, 274, 275, 279, 281, 283, 292–293, 296, 304, 312, 316, 325, 343, 344, 351, 364, 369, 370, 382, 393, 394, 413, 414, 416, 456, 504
  - No-flow boundary. *See* Boundary conditions
  - Nonaqueous phase liquid (NAPL), 71, 521
  - Nonconvergence, 97, 106, 107, 153, 404
    - groundwater flow model, 97, 106, 153
    - inverse problem, 404
  - Nonlinear calibration–constrained forecast, 470
  - Nonlinear uncertainty analysis. *See* Uncertainty, nonlinear analysis
  - Nonlinearity, 95, 105, 108, 121, 266, 277, 318, 397, 398, 402–403, 406, 425, 430, 446–447, 465, 469, 471
    - groundwater flow equation, 95, 105, 108, 318, 469
    - inverse problem, 397, 399, 402–403, 406, 425, 430
    - uncertainty, 446–447, 465, 469–471
  - Nonstationary, 450, 459
  - Non-uniform anisotropy. *See* Anisotropy

- Non-uniqueness. *See* Parameter estimation
- Null space, 421, 423, 427, 468, 475, 477
- Null-space Monte Carlo approach (NSMC approach). *See* PEST Software Suite
- Numerical methods, 8, 17, 18, 78, 85, 96, 346, 348–349, 364, 503
- control volume finite differences (CVFD)
    - method, 91–94, 95, 96, 98, 101, 159, 183, 184, 191–192, 194, 217, 236, 243
  - finite differences (FD). *See* Finite-difference (FD)
  - finite elements (FE). *See* Finite-element (FE)
  - integrated finite differences, 92, 183. *See also*
    - control volume finite differences (CVFD)
    - method, above
- Numerical solutions, 78, 85, 95, 96, 99, 173, 202, 215, 245, 304, 318, 319, 320, 321, 336, 412, 524
- direct, 95–96, 304, 397
  - iterative, 96, 397
- O**
- Objective function, 399, 400–401, 402–403, 404, 406, 408, 409, 412, 417, 418, 419, 420, 426, 428, 434, 435, 455–456, 471, 475, 477, 505
- balanced, 401, 409, 414, 435, 505
  - formulation, 400–401
  - global minimum, 402–404
  - local minimum, 402–403
  - measurement, 417–418, 419–420
  - regularization, 412, 414, 416, 417–418, 420–424, 431
  - surface, 402–403, 404, 406, 412, 471
  - target measurement. *See* Objective function, measurement
  - value, 402, 406, 408–409, 418–420, 434, 455–456, 471
  - weighting, 400–401, 409, 417
- Observation target. *See* Calibration; Flux target; Head target
- Observation well. *See* Well
- Occam's Razor, 449
- OCTAVE code, 98
- Octree grid refinement. *See* Grid
- Open source software, 33, 429
- Open system groundwater model, 378, 478
- Optimal model, 14, 215, 378, 380, 525
- Optimal parameter field, 419, 420, 424, 425
- Optimization, 101, 425, 431, 516, 525–526
- Orientating the grid. *See* Grid, orientation
- Outliers, 392
- Overfit. *See* Parameter estimation
- Overland flow, 156, 232–234, 283, 284, 290–291, 523
- Overdetermined problem. *See* Parameter estimation
- Oversimplified, 290, 394, 413, 431, 448, 449, 479
- P**
- Parallel flow stream. *See* Stream
- Parallel processing, 105, 397, 429, 512
- Parameter, 5, 9, 14, 73, 76, 222–236, 376, 393–394, 501, 503, 504
- assignment, 236–241
  - correlated, 238, 393, 395, 396, 410, 411, 424
  - flexibility, 414
  - hydrologic, 223, 230–236, 303, 304, 376, 501, 504
  - identifiability, 410, 466, 467, 506, 517
  - insensitive, 393, 395, 410, 418, 421, 423, 454
  - material property, 219, 222, 223–230, 236, 376, 501, 504, 519
  - scale dependence, 223, 225, 235, 245
  - sensitive, 148, 223, 393, 395, 408, 410, 454
  - uncertainty, 241–243, 399, 409, 461, 462
  - upgrade, 402, 404, 406, 408, 424
- Parameter estimation, 18, 101, 148, 233, 396–411, 412–413, 414–426, 427, 428, 430, 431, 434, 435, 462, 463, 464, 465, 468, 497, 504, 505, 506, 511, 525. *See also*
- Calibration
    - automated trial-and-error, 396–411, 428, 432, 434–435
  - closure criteria, 408
  - code (universal), 399–400, 401, 403
  - derivative-based nonlinear search techniques, 403
  - dual constrained minimization process, 418
  - highly parameterized, 397, 411–414, 424, 425, 435, 446, 471, 479, 505, 525
  - identifiability. *See* Parameter
  - insensitive parameter. *See* Parameter
  - inverse problem. *See* Inverse problem
  - Jacobian (sensitivity) matrix, 406–407, 408–409, 410, 411, 421, 422, 424, 425, 460, 462, 465, 468, 471
  - nonconvergence, 404
  - nonuniqueness, 379, 403, 427
  - objective function. *See* Objective function
  - optimal parameter field, 419–420
  - overdetermined problem, 393, 446, 460
  - overfit, 419, 424, 449, 455–456



- parameter sensitivity analysis, 410–411
- sensitive parameter. *See* Parameter
- sensitivity matrix. *See* Jacobian matrix, above
- speeding the solution, 424–426, 428
- stabilizing the solution, 414–424
- statistical analysis, 410–411
- targets (observations). *See also* Flux target; Head target
  - ranking, 384–385, 430
  - weighting, 323, 385, 396, 398, 400–401, 431, 434, 455, 463, 465, 504, 509
- tips for running code, 408–409
- underdetermined, 378, 393, 430, 446, 505, 516
- underfit, 419
- workflow, 398–399, 426
- Parameterization, 8, 16, 393, 394, 414, 447, 449, 460, 463, 465, 475, 477
- Pareto front diagram, 418–420, 429, 455–456, 481
- Parsimony, 29, 60, 412
- Partially penetrating well. *See* Well
- Particle tracking (PT), 28, 41, 45, 49, 84, 101, 124, 134, 182, 210, 215, 223, 230, 269, 331–370, 380–381, 455, 472, 501
  - advective groundwater age, 357, 358
  - advective transport, of contaminants, 331, 336–338, 363–364, 476, 477
  - average linear velocity, 334, 336, 338, 363
  - backward (reverse) tracking, 342, 349, 351, 353, 354, 358–359, 363, 365, 367
  - capture zone, 21, 124, 336, 338, 340, 341, 342, 351, 353, 358–362, 365, 366, 367, 370
  - code, 9, 17, 18, 203, 337, 364–365, 455, 456
  - contributing areas, 336, 338, 351–352, 357, 358–362, 365
  - effect of spatial discretization, 338–340, 366, 370
  - effect of temporal discretization, 340–341
  - flowpath. *See* Flowpath
  - forward tracking, 339, 351–352, 359, 367
  - groundwater age, 336, 357, 365
  - projection onto a 2D plane, 351, 356
  - reverse tracking. *See* Particle tracking (PT); backward (reverse) tracking
  - strong sinks, 349–350, 351, 352, 369
  - tracking schemes, 346–349
    - Euler integration, 339, 346, 348, 349, 364, 365
    - Runge–Kutta method, 339, 346, 348, 349, 364, 365
    - semianalytical solution, 347–348, 364
    - Taylor Series expansion, 346, 348
  - tracking step, 347–348, 349, 350, 364, 365
  - travel time, 9, 17, 18, 134, 203, 210, 331, 332, 336, 338, 339, 347, 355–356, 357, 366, 369, 454, 455–456, 457, 475
  - velocity interpolation, 338–346
    - bicubic, 342
    - bilinear, 342, 343, 344
    - inverse distance, 344, 345, 349, 365
    - linear, 90, 239, 248, 342, 343, 344, 364, 365
    - trilinear, 342, 344
  - weak sinks, 339, 349–351, 352, 359, 364, 366, 369
- Pass-through nodes, 222
- Patch of elements. *See* Element
- PATH3D code, 101, 339, 350, 364
- Pdf. *See* Probability density function (pdf)
- Percolating conditions, 135, 154–155, 275, 277
- Perennial stream. *See* Stream
- Performance evaluation, 18, 377, 426–429
- Perimeter boundaries. *See* Boundary conditions
- Permeability. *See* Hydraulic conductivity (permeability)
- Permeameter, 225, 226–227
- PEST Software Suite, 9, 101, 397, 400, 408, 418, 419, 425, 426, 428, 430, 447, 462, 465, 469, 475, 503
  - BeoPEST code, 397
  - bgaPEST code, 397
  - damped least squared method, 403
  - FePEST code, 473
  - Gauss–Marquardt–Levenberg (GML) method, 403, 408
  - GENLINPRED utility, 462, 465
  - INFSTAT utility, 430
  - linear uncertainty analysis, 447
  - MODINV, 397
  - multiple realizations (Monte Carlo Framework), 400
  - nonlinear uncertainty analysis, 447
  - null-space Monte Carlo (NSMC) method, 397, 475, 477
  - PEST++, 9, 101, 397, 425
  - PESTCHEK.exe, 408
  - PHIMLIM variable, 418, 419, 426
  - regularized inversion, 411–426
  - singular value decomposition (SVD), 397, 421–422, 426
  - singular value decomposition assist (SVDA). *See* SVD-Assist (SVDA) below

- PEST Software Suite (*Continued*)  
 singular value truncation, 423, 424  
 SSSTAT tool, 430  
 subspace regularization, 420–424  
 superparameters, 422, 425  
 SVD-Assist (SVDA), 422, 423, 425, 426, 428  
 SVDAPREP, 425  
 Tikhonov regularization, 425–426, 428  
 user manual, 400
- PetraSim code, 101
- Petroleum reservoir modeling, 11, 447, 521
- pH. *See* Chemical analyses and tracers
- PHIMLIM. *See* PEST Software Suite
- Phreatophyte, 157, 308
- PHT3D code, 522
- Physical boundaries. *See* Boundary conditions
- Physical models, 5  
 analog, 5  
 electrical, 5  
 viscous fluid, Hele-Shaw, parallel plate, 5, 168
- Piezometer, 58, 226, 382
- Pilot point, 241, 414, 415, 416, 435, 455, 479, 505
- Pinchout, 216–217, 218
- Planar discrete feature element (DFE).  
*See* Element, discrete feature element (DFE)
- Plume, 9, 338, 360, 363, 381, 476, 527
- PMWIN code, 101, 103
- Point discharge. *See* Discharge
- Point-centered grid. *See* Grid
- Poisson equation, 83, 84
- Polynomial fitting, 238
- Ponded infiltration, 232
- Poro-elastic effects, 518–519
- Porosity, 41, 42, 363, 518  
 dual, 522  
 effective, 41, 45, 49, 144, 223, 230, 332, 333, 334, 338, 344, 360, 363, 454, 466, 501  
 primary, 41, 42  
 secondary, 41, 42–43  
 total, 227, 230, 332, 363
- Postaudit, 18, 481–482, 511
- Posterior, 451–452, 453, 462
- Potential observations, 468
- Potentiometric surface map, 38, 51, 340
- Prediction. *See* Forecast/forecasting model
- Predictive model. *See* Forecast/forecasting model
- Preferential flow (path), 223, 225, 284, 414, 450, 456, 522, 524–525
- Preferred conditions for parameters, 417, 418
- Pressure head. *See* Head
- Princeton Transport Code, 34
- Principle of superposition, 80–81, 83, 108
- Prior information, 451–453, 460
- Prism, element. *See* Element
- Probability density function (pdf), 451, 473, 474
- Problem domain, 5, 6, 8, 70, 75  
 active, 99, 150, 185  
 boundaries of, 51, 78, 86, 134, 144, 148, 159, 167, 170, 186, 195, 241  
 conceptual model, 51  
 infinite, 83  
 nested, 191  
 subdivision of, 89, 146, 182, 183, 191, 202, 235, 432
- Process-based (physically based) mathematical model, 5–9, 70
- Profile (cross-sectional model), 58, 118, 122, 125–132, 138, 162, 167, 169, 170, 171, 220  
 application, 131  
 axisymmetric, 131–132, 170  
 layer orientation, 125–127, 129  
 slice orientation, 125–127
- Purpose of modeling, 9–11  
 of model. *See* Modeling objective (purpose)  
 of report. *See* Modeling report
- Pump and treat, 360, 482
- Pumping rate. *See* Well
- Pumping test (aquifer test). *See* Aquifer
- Push-pull test, 131
- Python, 516
- ## Q
- Quadratic element. *See* Element
- Quadrilateral element (Lagrange family).  
*See* Element
- Quadrilateral element (Serendipity family).  
*See* Element
- Quadrilateral finite-element mesh. *See* Mesh
- Quadtree grid refinement. *See* Grid
- Quantifiable best fit. *See* Calibration, best fit
- Quasi-3D model, 133–134, 141, 338–339, 366
- Quasi-steady state. *See* Steady-state conditions
- ## R
- $R_d$ . *See* Retardation factor ( $R_d$ )
- Radial collector wells (Ranney). *See* Well

- Radial flow, 131, 132, 170, 267–268, 308, 316
- Rainfall–runoff model, 285, 287, 289–290, 515, 521–522, 523
- Random access memory (RAM), 105
- Ranking targets. *See* Calibration target; Flux target; Head target; Parameter estimation, targets (observations)
- RCRA (Resource Conservation Recovery Act), 29
- Realizations of parameter field, 399, 400, 460, 472, 473, 477, 524–525
- Reasonableness assessment. *See* Calibration
- Recharge lake, 279, 280
- Recharge, 4, 6, 13, 18, 21, 22, 28, 31, 34, 35, 38, 51, 54, 55, 56, 58, 59, 62, 72, 77, 79, 81–82, 83, 99, 100, 104, 106, 122, 126, 130, 140, 145, 147, 148, 149, 150, 154, 157, 162, 163, 167–169, 200, 203, 216, 222, 223, 230–235, 238, 240, 244–245, 246, 257, 258, 262, 270–272, 273, 279, 280, 289–290, 292, 305, 306, 308, 309, 310, 312, 314, 316–317, 325, 326, 334, 336, 342, 351, 356, 360, 362, 376, 378, 381, 385, 393, 395, 428, 432, 449, 450, 459, 461, 466, 482, 484, 498, 502, 506, 519, 520
- areally distributed, 106, 149, 200, 203, 258, 259, 262, 270–272
- artificial, 51
- methods for estimating, 230–231, 232–235, 308, 335, 342, 362, 384
- rejected, 290
- spatial variability in, 34, 54, 59, 82, 202, 203, 206, 238, 240, 524
- temporal variability of, 54, 230, 234, 308–311, 314, 316–317, 325, 342, 459, 482, 519
- Recharge driven flow, 167, 169
- Recharge (RCH) Package. *See* MODFLOW code (Modular Groundwater Flow Model), packages
- References cited. *See* Modeling report
- Regional groundwater flow system. *See* Flow system
- Regularization, 392, 411–426, 428, 429, 431
- Regularization objective function. *See* Objective function
- Regularized inversion. *See* PEST Software Suite
- Regularly spaced grid. *See* Grid, regular
- Rejected recharge. *See* Recharge
- Replication of modeling results, 496, 509
- Reproducibility of modeling results, 6, 19, 176, 377, 427, 478, 496, 497, 509, 518
- Report. *See* Modeling report
- Reporting forecast uncertainty, 445, 453, 454, 457, 461, 471, 475, 480–481, 483–484, 496, 497, 506–507, 510. *See also* Modeling report
- Representative elementary volume (REV), 71, 72, 73, 518
- Residual error. *See* Error
- Resistance, 119–120, 123, 133–134, 142, 150, 155, 200, 205, 208, 217, 222, 229–230, 265, 282, 428
- vertical, 119, 123, 133, 134, 141, 155, 200, 205, 208, 229
- Resolution matrix. *See* Matrix
- Response time, 286. *See also* Aquifer, response time
- Retardation factor ( $R_d$ ), 338, 363
- REV. *See* Representative elementary volume (REV)
- Reverse particle tracking. *See* Particle tracking (PT), backward (reverse) tracking
- Reviewing modeling report. *See* Modeling report
- Richards equation, 519
- River (RIV) Package. *See* MODFLOW code (Modular Groundwater Flow Model), packages
- Risk assessment, 445, 446, 457, 525
- Root mean squared error (RMSE). *See* Error
- Round-off error. *See* Error
- RT3D code, 522
- Runge-Kutta method. *See* Particle tracking (PT), tracking schemes
- Runoff, 51, 55, 70, 104, 232–233, 273, 276, 281, 285, 287, 289–290, 515, 521–523

## S

- S. *See* Storage
- $S_y$ . *See* Storage
- $S_s$ . *See* Storage
- Safety factor, 380
- Saltwater intrusion. *See* Seawater intrusion
- Sand, 5, 28, 42, 44, 213, 220, 228, 229, 237, 246, 248, 332–333, 463, 464
- Saturated thickness, 31, 79, 120–121, 123, 165, 169, 214, 215, 228, 246, 262, 308, 360

- Saturation excess overland flow, 232, 234, 290–291
- Saturated zone, 51, 70, 157, 164, 166, 233, 519, 521
- SBW. *See* Matrix; semi-bandwidth
- Scale dependent parameter. *See* Parameter, scale dependence
- Scaling errors. *See* Error
- Scatter plots, 385, 388, 419, 429, 505
- Scenario, 215, 445, 449, 456, 458–460, 469, 481, 483, 507
- Scientific method, 16, 496
- SCM. *See* Site conceptual model (SCM)
- Screening models, 11, 19, 21, 28, 84, 223, 305, 385, 430
- SEAWAT code, 101, 521
- Seawater intrusion, 70, 85, 141–142, 520–521
- Secondary porosity. *See* Porosity
- Seep, 155, 272–273
- Seepage face, 56, 98, 121, 157, 162–164, 166, 263, 265, 266, 267, 272, 291–292
- Seepage lake, 279, 280
- Seepage meter, 231, 273, 275
- Seismic geophysical method, 46
- Semianalytical particle tracking method.  
*See* Particle tracking (PT), tracking schemes
- Semi-arid hydrologic setting, 231, 361
- Semi-bandwidth (SBW). *See* Matrix
- Sensitive parameters. *See* Parameter
- Sensitivity analysis, 202, 410–411, 430, 506
- Sensitivity coefficient, 405–406, 407, 410, 421, 430, 506
- Sensitivity matrix. *See* Parameter estimation, Jacobian (sensitivity) matrix
- Septic field, 260
- SFR Packages. *See* MODFLOW code (Modular Groundwater Flow Model), packages, Stream flow–Routing Packages
- Sharp interface model, 140, 142–144, 520
- Shear zones, 137
- Simplifying assumptions, 11, 30, 71, 335, 501
- Simplification error. *See* Error
- Simulated equivalent values, 202, 377, 401, 450
- Simulation log, 102–105, 432, 497, 510
- Single phase fluid, 71
- Single-well test. *See* Well
- Singular value decomposition (SVD). *See* PEST Software Suite
- Singular value decomposition assist (SVDA).  
*See* PEST Software Suite, SVD–Assist (SVDA)
- Singular value truncation. *See* PEST Software Suite
- Sink, 8, 32, 35, 51–54, 72, 76, 78, 80, 81, 83, 94, 98, 99, 106, 131, 136, 137, 145, 148, 149, 171, 202, 205–208, 223, 257–296, 334, 338, 339, 348, 349–351, 352, 359, 360, 362, 364, 366, 393, 396, 449, 453, 482, 502, 504
- areally distributed, 257, 258, 259, 262, 263, 270–272, 293
- point, 8, 51, 131, 148, 206, 257, 259, 262–264, 273, 351
- strength, 350
- strong, 349–350, 351, 352, 369
- weak, 137, 339, 349–351, 352, 359, 364, 366, 369
- Site conceptual model (SCM), 29, 31, 32, 36, 46
- Skin effects. *See* Well
- SLAEM/MLAEM code, 84–85
- Slice orientation. *See* Profile (cross-sectional model)
- Slug test. *See* Well
- Soft data, 376
- Soft knowledge, 16, 377–378, 395, 398, 414–420, 424, 425–426, 428–429, 445, 452, 463, 504, 505, 506, 511
- Software license, 429
- Soil water balance approach, 230, 232–234, 235, 317, 450
- Solute transport, 28, 70, 71, 78, 84, 98, 101, 142, 269, 318, 336, 338, 357, 363, 427, 456, 515, 520, 521, 522, 523, 524
- Solution
- accuracy, 97, 99, 106, 121, 182, 191, 202, 210, 211, 216, 260, 269, 304, 406
- analytical, 6, 8, 14, 19, 28, 78–80, 81–82, 98, 99, 107, 142, 162, 205, 208, 260, 265–267, 308, 316, 319, 320, 321, 335, 351, 365, 394, 446, 524
- channels/conduits, 39–41, 52
- convergence, 95, 96, 97, 100, 102, 105–107, 153, 172, 214, 265, 304, 322, 405
- methods, 89, 95–96
- space, 421–422, 423, 425, 427, 466, 479
- Solver, 95–96, 100, 102, 104, 105, 106, 107, 172, 304, 320, 403, 405, 408, 503, 504, 512

- Source, 8, 29, 30, 31, 32, 33, 35, 51–54, 55, 56, 58, 72, 76, 78, 81, 83, 94, 98, 99, 118, 119, 131, 136, 137, 141, 148, 149, 202, 205–206, 223, 257–296, 305, 316, 338, 351, 354, 356, 357, 358–359, 362, 363, 366, 393, 396, 453, 482, 502, 504
- areally distributed, 203, 257, 258, 259, 262, 263, 270–272, 305
- point, 8, 51, 131, 148, 206, 259–269
- Source bed, 119
- Sparsely parameterized model, 394, 397, 408, 411, 412, 413, 414, 460, 483, 505
- Spatial dimensions, 118–134, 430
- Spatial discretization. *See* Discretization
- Specific capacity test. *See* Well
- Specific conductance. *See* Chemical analyses and tracers
- Specific discharge, 73, 74, 211–212, 332
- Specific storage ( $S_s$ ). *See* Storage
- Specific yield ( $S_y$ ). *See* Storage
- Specified flow boundary. *See* Boundary conditions
- Specified head boundary. *See* Boundary conditions
- Specified-thickness approximation, 214
- Spin-up period, 313, 314, 324
- Spreadsheet model, 6, 79, 109, 110, 127, 128–131, 170, 171, 244
- Spring, 7, 21, 31, 51, 54, 56, 57, 82, 145, 155, 156, 159, 205, 230, 257, 258, 259, 272–273, 336, 337, 357, 358, 360, 382, 472–473, 481, 502
- Spring (season), 234, 306, 325
- Spring flow target. *See* Calibration target
- SSSTAT tool. *See* PEST Software Suite
- Standard deviation, 238, 241, 382, 383, 452, 457, 463, 464, 465, 472, 504, 524
- Stanford Watershed Model, 286
- Starting heads. *See* Steady-state simulation
- Static steady-state conditions. *See* Initial conditions
- Stationarity, 459
- Statistical analysis, 410–411, 431, 480, 506
- Statistical influence, 405, 410, 430
- Steady-shape conditions, 266, 268, 308
- Steady-state conditions, 8, 76, 77, 78, 79–80, 83, 96, 105, 106, 107, 133, 144, 147, 226, 304–310, 311, 312–313, 314–316, 340, 348, 358, 360–362, 365, 453, 502, 503, 505, 508
- bounding, 306, 309, 310, 324
- used as initial conditions, 307, 312–314, 505
- pseudo, 306, 307, 309
- quasi, 266, 268, 306
- time-averaged, 304, 305, 309, 310
- Steady-state simulation, 13, 28, 51, 80, 84, 95, 103, 105, 106, 107, 118, 126–128, 133, 142, 144, 147, 150, 171, 200, 202, 230, 267, 270, 272, 280, 286, 303–310, 312–313, 314, 316, 322, 324, 334, 348, 360–362, 364, 365, 382, 383, 428, 429, 435, 453, 463, 502, 508
- boundary conditions for, 304–305
- calibration data set for, 305, 306, 307, 428, 504
- starting heads for, 105, 106, 304, 312
- successive solutions, 306, 309, 310
- Step drawdown test. *See* Well
- Stochastic analysis, 446, 524–525
- Stochastic model, 5, 399, 446, 472, 473, 477, 516, 524–525
- Stochastic MODFLOW. *See* MODFLOW code (Modular Groundwater Flow Model), versions
- Stochastic MODPATH code, 472
- Storage, 41, 49, 54, 55, 56, 72, 73, 88, 94, 99, 100, 107, 134, 144, 208, 214, 215, 223, 225, 227–229, 237, 240, 243, 244, 264, 268, 304, 306, 307, 309, 310, 316, 322, 416, 428, 453, 518, 519, 520
- specific storage ( $S_s$ ), 72, 73, 76, 88, 126–127, 134, 214, 227–229, 236, 237, 243, 376
- specific yield ( $S_y$ ), 77, 127, 144, 215, 216, 227, 228, 236, 237, 243, 308, 309, 376, 435
- storage coefficient, 31, 227. *See also* storativity ( $S$ ), below
- storativity ( $S$ ), 76, 127, 132, 144, 214, 215, 216, 223, 225, 227–228, 230, 237, 243, 244, 268, 308, 309, 319, 376
- Storativity ( $S$ ). *See* Storage
- Stratigraphic column, 47, 50
- Stream, 4, 11, 21, 31, 36, 57, 59, 78, 79–80, 121, 131, 135, 137, 139–140, 145, 148, 151, 152, 153, 154, 155, 161, 168, 172, 189, 191, 205, 235, 257, 258, 259, 273–279, 281, 283, 286, 289–291, 292, 304, 309, 313, 336, 351, 357, 358, 361–362, 382–383, 384, 387, 389, 391, 444, 445, 457, 459, 466, 470, 499, 502, 522, 523, 525
- bed, 138, 153–155, 169, 274, 275, 276, 277
- capture, 358, 361–362

- Stream (*Continued*)
- cells, 151, 292
  - channel, 276–277, 289–290, 523
  - contributing area, 336, 351–352, 357, 358–362, 365
  - depletion, 361–362
  - drainage network, 31
  - effluent. *See* Stream, gaining
  - ephemeral, 139, 276, 292
  - flow, 11, 31, 59, 79, 121, 131, 139, 140, 145, 146, 152, 155, 163, 168, 169, 170, 175, 205, 232, 235, 257, 258, 273, 274–275, 276, 277, 279, 281, 283, 286, 287, 289–291, 304, 305, 308, 313, 322, 335, 336, 351, 358, 360, 362, 365, 382, 383, 387, 389, 401, 427, 444, 457, 459, 470, 499, 502, 516, 522, 523, 525
  - flow-through, 274
  - gage, 273, 275, 383, 384, 389
  - gaining, 154, 273–274, 275, 358, 365
  - groundwater exchange with, 11, 54, 153, 154, 155, 170, 201, 229, 243, 273, 275, 276, 286, 315, 523
  - headwater, 139, 273, 276
  - influent. *See* Stream, losing
  - losing, 31, 154, 155, 156, 273, 275, 304, 382, 444, 506
  - parallel flow, 274
  - perennial, 31, 137, 139
  - quality, 31
- Streamflow generation, 232, 289–290
- Stream flow–Routing (SFR) Packages.  
*See* MODFLOW code (Modular Groundwater Flow Model), packages
- Streamfunction, 83–84, 335
- Streamline, 36, 84, 139, 144, 145, 146, 163, 170, 175, 334, 335–336, 360, 512
- as a boundary. *See* Boundary conditions, hydraulic dividing, 139, 144, 145
- Streamtube, 175, 335
- Strength of a sink. *See* Sink
- Stress period, 100, 105, 316–318, 319, 320, 324, 325, 341, 342
- Strong sink. *See* Particle tracking (PT); Sink
- Structural error. *See* Error
- Structured grid. *See* Grid
- Structured mesh. *See* Mesh
- Subsidence and Aquifer Compaction for Water Table Aquifers (SUB-WT) Package.  
*See* MODFLOW code (Modular Groundwater Flow Model), packages
- Subspace regularization. *See* PEST Software Suite
- Successive steady-state solutions. *See* Steady-state simulation
- Summary and conclusions. *See* Modeling report
- Summary statistics, 378, 385, 387, 391, 392, 429, 431, 505, 512
- Superfund sites, 29, 189
- Superparameters. *See* PEST Software Suite
- Superposition, 80–81, 83, 108
- Supraglacial deposits, 463, 464
- Surface water, 14, 17, 31, 34, 35, 51, 54, 56, 58, 80, 81, 83, 91, 98, 99, 100, 118, 120, 121, 136, 137–140, 148, 152, 153–155, 156, 169, 170, 188, 195, 201, 205–206, 207, 208, 210, 216, 229, 231, 232, 235, 243, 273, 276, 277–279, 283–284, 285–291, 292, 309, 313, 315, 316, 351, 358, 359, 363, 383, 444, 472, 501, 503, 506, 515, 516, 517, 523, 527
- as boundary, 17, 35–36, 83, 134–135, 136, 137, 138, 139, 140, 148, 153–155, 167, 169
  - divide, 139, 285, 472
  - features (bodies), 17, 31, 34, 51, 54, 56, 58, 81, 83, 91, 98, 99, 100, 120, 136, 137–140, 148, 152, 153–155, 156, 170, 188, 201, 205–206, 210, 216, 229, 235, 243, 309, 351, 501, 506
- Surface water–groundwater processes, 54, 80, 91, 195, 201, 243, 283, 444, 523, 527
- Surface–Water Routing (SWR1) Process.  
*See* MODFLOW code (Modular Groundwater Flow Model), processes
- SURFER program, 241
- Surrogate parameters, 290–291, 413, 478, 505
- SUTRA code, 76, 184, 521
- SVD. *See* PEST Software Suite, singular value decomposition (SVD)
- SVDA (SVD-Assist). *See* PEST Software Suite
- SVDAPREP. *See* PEST Software Suite
- SWB code. *See* Soil water balance approach
- SWR1 process. *See* MODFLOW code (Modular Groundwater Flow Model), processes, Surface–Water Routing (SWR1) Process
- Synoptic measurements, of streamflow, 275, 389

## T

- Target. *See* Calibration target; Flux target; Head target; Parameter estimation, targets (observations)
- Target measurement objective function.  
*See* Objective function, measurement
- Taylor Series expansion, 190, 346, 348
- TDS. *See* Chemical analyses and tracers; total dissolved solids (TDS)
- Telescopic mesh refinement (TMR),  
159–162, 191
- Temperate climate, 157, 234, 285, 289, 291, 305, 306, 352, 444
- Temperature, 57, 58, 70, 78, 232, 275, 379, 380, 404, 427, 459, 505, 520–521, 522
- Template file, 398
- Tensor. *See* Hydraulic conductivity (permeability)
- Terrestrial infiltration, 232
- Tetrahedron, element. *See* Element
- Theis equation, 6, 78, 108, 268, 316, 320, 321
- Thiem equation, 76, 208, 260, 265, 266, 267–269
- Three-dimensional models (3D models), 6, 8, 11, 13, 14, 35, 50, 73, 90, 91, 120, 122–124, 125–127, 131–132, 133–134, 148, 150, 153, 157, 162, 164, 167, 170, 183, 186, 195, 197, 208, 244, 247, 262, 304, 307, 338–339, 353, 356, 364, 366, 367, 382, 503
- Tidal effects, 140, 141, 313
- Tikhonov regularization. *See* PEST Software Suite
- Time-averaged steady-state conditions.  
*See* Steady-state conditions
- Time constant of groundwater system, 308, 340
- Time-dependent simulations. *See* Transient simulations (model)
- Time invariant, 144, 276, 304, 315
- Time of travel (TOT), 223, 332, 352, 360, 362, 365
- Time step, 17, 88, 96, 99, 100, 105, 106, 107, 118, 133, 287, 310, 316–320, 321, 322, 324, 325, 340–341, 342, 347, 349, 364, 365, 504, 522
- Time step multiplier, 318, 320
- Title. *See* Modeling report
- TMR. *See* Telescopic mesh refinement (TMR)
- Tomography. *See* Hydraulic tomography
- TopoDrive code, 127, 138
- Topographic maps, 31, 35
- Topography-driven flow, 167–169
- TOT. *See* Time of travel (TOT)
- Total dissolved solids (TDS). *See* Chemical analyses and tracers
- Total head. *See* Head
- Total porosity. *See* Porosity
- Tóth's problem, 128–129, 167, 169
- Tóthian flow, 128, 167
- TOUGH2 code, 101
- Tracer. *See* Chemical analyses and tracers
- Track record, of code, 99, 100–101
- Tracking schemes. *See* Particle tracking (PT)
- Tracking step. *See* Particle tracking (PT)
- Training images, 524–525
- Transfer function, 526
- Transformation, of coordinates, 74, 76, 173, 199, 200–201, 210–211, 335
- Transient simulations (model), 6, 8, 17, 28, 35, 49, 51, 70, 73, 74, 78, 80, 85, 91, 99, 100, 105, 106, 107, 118, 122, 126, 132, 133, 143, 144, 147, 148, 152, 162, 216, 227, 270, 277, 280, 286, 303–326, 340, 342, 348, 362, 364, 376, 382, 383, 385, 387, 392, 428, 429, 434, 435, 453, 483–484, 498, 508
- boundary conditions for, 17, 35, 70, 106, 118, 133, 147, 148, 152, 304–305, 309, 312, 314–316, 502, 503, 504, 513
- calibration of, 103, 122, 307, 310, 322, 376, 382, 385, 387, 392, 428, 429, 434, 435, 453, 463, 484, 505
- evaluation of, 106, 308, 315, 322, 428
- governing equation for, 73, 118, 126, 268, 503
- initial conditions for, 17, 70, 152, 304, 307, 309, 310, 312–314, 324, 498, 502
- storage. *See* Storage
- stress period, 105, 310, 316–318, 342, 504
- time step, 17, 105, 107, 118, 133, 310, 316–320, 341, 342, 504
- Transition zone, 140, 141–142, 521
- Transmissivity, 31, 76, 79, 83, 132, 137, 150, 204, 205, 214, 225, 226, 244, 264–265, 266, 268, 308
- Transparency of reporting, 398, 412, 429–431, 505
- Transport Of Unsaturated Groundwater and Heat (TOUGH) code. *See* TOUGH2 code

- Transport process (model), 9, 28, 30, 55, 70, 71, 78, 98, 101, 142, 203, 230, 269, 308, 318, 336, 338, 357, 363–364, 414, 427, 450, 456, 457, 476, 477, 516, 517, 520, 521–523, 524, 527
- Travel time, 9, 17, 18, 134, 203, 210, 331, 332, 336, 338, 339, 347, 355, 356, 357, 366, 369, 443, 454, 455–456, 457, 475
- Trial-and-error calibration. *See* Calibration
- Triangular element. *See* Element
- Triangular mesh. *See* Mesh, triangular element
- Trilinear interpolation. *See* Particle tracking (PT), velocity interpolation
- True model, 380, 469
- Truncation, 190, 320, 423
- TSPROC code, 322
- Tubular discrete feature element (DFE).  
*See* Element, discrete feature element (DFE)
- Tunnel, 51, 121, 155, 157, 164, 205, 259, 272, 354, 355, 453
- Two-dimensional (2D) models, 8, 11, 31, 74, 76, 82, 84, 85, 86, 100, 118–132, 135, 146, 148–150, 156, 161, 162, 167–168, 170, 171, 172, 173, 183, 195–196, 205, 208, 213, 217, 220, 244, 246–247, 261–262, 265–266, 268, 286, 292–296, 306–308, 316, 319, 324–325, 334–335, 343–344, 351, 360, 362, 365–367, 382, 406, 432–433, 455, 484, 501
- areal, 31, 82, 84, 100, 118–124, 127, 135, 148, 149, 153, 157, 161–162, 170, 173, 183, 244, 246–247, 261, 262, 265, 266, 267, 268, 292–296, 308, 316, 382, 432–433, 484, 501
- profile (cross-sectional), 118, 122, 125–127, 128–131, 132, 156, 162, 167–169, 170, 171, 172, 173, 213, 217, 220, 276, 281, 307, 324–325, 334, 351, 367
- U**
- UCODE code, 101, 397
- Uncalibrated interpretive model. *See* Interpretive model
- Uncertainty, 9, 11–13, 15, 17, 18, 20, 22, 56, 59, 102, 105, 122, 215, 222, 229, 241–243, 248, 380, 382, 383–384, 385, 390–391, 399, 400, 409, 411, 412–413, 427–428, 429, 430, 431, 432, 435, 443–484, 497, 502, 504, 506–508, 511, 517, 524, 525, 526
- advanced analysis, 457, 469–479
- aleatory (intrinsic), 449–450, 482
- basic analysis, 457, 458–469
- behavioral, 478
- best-case scenario, 445, 459, 469, 481, 483, 507
- C(e) matrix, 461, 462–463, 465
- C(p) matrix, 461, 462, 463, 464, 465
- conditional, 443–445, 447, 449, 451, 454, 458–459, 466, 472–473, 475, 478, 481, 482, 483
- cost-benefit analysis, 445, 468, 472, 483
- covariance matrix, 461, 462, 463, 464
- epistemic component, 449–450
- future data collection, 466, 468–469
- GLUE, 478, 479
- information criteria metrics, 478–479
- likelihood, 445, 451–452, 457, 478, 481
- linear analysis, 458, 460–469
- Markov Chain Monte Carlo (MCMC) analysis, 475, 477
- maximization–minimization, 459, 469–471, 475, 481
- MLBMA, 479
- Monte Carlo, 397, 400, 430, 446, 471, 472–473, 474–475, 477, 478, 479, 524
- multiple conceptualizations, 477–479
- nonlinear analysis, 430, 446–447, 465, 469
- null-space Monte Carlo (NSMC), 475, 477
- postcalibration, 453, 466
- potential observations, 468
- precalibration, 465–466
- probabilistic, 446, 449, 451, 452–453, 457, 471, 473, 481, 524
- reduction of, 430, 457, 466, 468–469
- reporting of, 383, 457, 475, 480–481, 483
- scenario modeling, 449, 456, 458–460, 469, 481
- software, 447, 460, 462, 464, 465, 469, 473, 479
- worst-case scenario, 445, 456, 459, 469, 481, 483, 507
- Unconfined aquifer. *See* Aquifer
- Unconfined layer. *See* Layer
- Unconsolidated aquifer. *See* Aquifer
- Under-determined problem. *See* Calibration
- Underfit. *See* Calibration
- Underflow, 51, 54, 55–56, 138, 139, 148, 149, 150, 158, 257, 270, 271, 272
- Uniform distribution, 472
- Unknown unknowns, 12, 393, 449, 482
- Unsaturated hydraulic conductivity. *See* Hydraulic conductivity (permeability)



- Unsaturated-saturated continuum, 163, 164, 166
- Unsaturated zone (vadose zone), 54, 70, 135, 138, 157, 166, 230, 231, 232–234, 235, 258, 270, 277, 286–288, 517, 519, 521
- Unstructured grid. *See* Grid
- Unstructured mesh. *See* Mesh
- Upgrade, of parameter. *See* Parameter
- Upscaling hydraulic conductivity. *See* Hydraulic conductivity (permeability)
- User's manual, for a code, 19, 98, 99, 102, 106, 145, 170–171, 195, 236, 270–272, 427, 503
- V**
- Vadose zone. *See* Unsaturated zone (vadose zone)
- Validation, model, 19–20, 427–428
- Variable density flow, 70, 142, 515, 516, 520–522, 523
- Variable source area, 289–290
- Variably saturated code, 164, 166–169, 519
- Variably saturated flow, 70, 163, 164, 287, 515, 516, 519–520, 521–522
- Variance, 241, 382, 448–449, 451, 459, 461, 462–463, 465–466, 469, 504
- Variogram, 238, 241, 524
- Variogram separation distance, 241
- Velocity interpolation. *See* Particle tracking (PT)
- Verification, 19–20, 426, 427, 503  
code, 19, 99, 427–428, 503  
model, 19, 427–428
- Vertical anisotropy. *See* Anisotropy
- Vertical conductance. *See* Conductance
- Vertical discretization. *See* Discretization, spatial, vertical
- Vertical exaggeration, 51, 122, 163, 172, 501
- Vertical leakance. *See* Leakance
- Vertical resistance. *See* Resistance
- Virtual well radius. *See* Well, effective well radius
- Viscosity, 522
- Visual MODFLOW-flex (VM-Flex) GUI, 101
- Visualization, 51, 101–102, 202, 306, 336, 378, 419, 468, 475, 481, 497, 502, 507
- Void space, 41, 42–43, 49, 230
- Volumetric flow rate, 150, 152, 268, 307
- 291, 295, 307, 311, 320, 322, 408, 429, 501, 502, 504, 509, 512. *See also*  
Groundwater, budget
- Water budget errors. *See* Error
- Water quality, 31. *See also* Chemical analysis
- Water reuse, 51
- Water table, 5, 21, 31, 35, 51, 58–59, 62, 63, 70, 77, 98, 99, 104, 118, 119, 120, 121, 122–124, 125, 127, 128–131, 133, 135, 138, 146, 147, 148, 152, 157–158, 162–169, 170, 171, 173, 175, 199, 214–215, 216, 227, 230, 232–234, 235, 237, 243, 246, 247, 248, 257, 258, 270, 272, 274, 277, 285, 289–290, 292, 294, 295, 304, 309, 313, 324, 325, 337, 351–352, 366, 383, 385–386, 434, 519  
boundary. *See* Boundary conditions  
controlling factors, 138, 162–169  
map, 146  
simulation of, 165, 234, 235
- Watershed modeling, 231, 279, 285, 289–290, 415
- Weak sink. *See* Particle tracking (PT); Sink
- Weighted residual, 91, 401, 417
- Weighting targets. *See* Calibration target; Parameter estimation, targets (observations)
- Weirs, 273
- Well, 4, 11, 36, 42, 46, 50, 51, 58, 62, 63, 72, 73, 81, 82, 100, 108, 109, 110, 118, 119, 120, 121, 124, 131, 132, 147, 148, 149, 150, 164, 167, 170, 171, 173, 174, 175, 176, 188, 191, 193, 201, 204–205, 206–208, 225, 226, 231, 236, 248, 257, 258, 259–269, 270, 272, 276, 291–292, 293, 296, 305–306, 307, 316, 321–322, 324, 325, 326, 334, 338, 340, 342, 349, 351, 353, 358–359, 360, 363, 365, 367, 368, 370, 381–382, 416, 432–433, 434, 435, 453, 456, 465, 482, 483, 484, 500, 502, 509, 525  
capture zone. *See* Capture zone  
discharge specified, 264, 267  
domestic, 260, 262, 308  
effective well radius, 266, 267–269  
field, 4, 62, 63, 353, 459, 525  
flowing, 272–273, 379  
fully penetrating, 84, 108, 110, 118, 148, 174, 260, 262, 263, 291, 293, 294  
head-specified, 147–148, 258
- W**
- WALKABOUT code, 364
- Water budget, 17, 34, 54–57, 60, 97, 99–100, 106–107, 108, 130–131, 152, 153, 171, 173, 195, 231, 243, 245, 260, 279–281,

Well (*Continued*)

- high-capacity, 124, 205, 260, 262, 482
  - horizontal, 204, 260
  - injection, 51, 56, 72, 148, 149, 150, 171, 205, 206, 207, 257, 258, 259–269, 367, 368
  - loss, 226, 265, 266–267, 269
  - multi-aquifer, 265
  - multi-layer, 204, 259, 263–264
  - multi-node, 262–269
  - nested, 51
  - node, 201, 204, 207, 208, 260, 261, 262, 264–269, 292, 307, 323, 351, 359, 370
  - observation (monitoring), 28, 51, 73, 119, 225, 231, 244, 248, 305, 322, 325, 379, 381, 382, 416, 433, 455
  - partially penetrating, 82, 120, 129, 132, 262, 263, 267, 336, 382
  - performance test, 225, 226
  - pumping, 51, 58, 72–73, 80, 100, 108, 110, 118, 120, 124, 131–132, 147–148, 164, 170, 173, 174–175, 176, 188, 191, 201, 204, 205, 206, 207, 208, 226, 235, 257, 258, 259–269, 272, 276, 291, 292, 293, 296, 316, 321, 325, 326, 336, 339, 340, 342, 349, 351, 358, 360–362, 365, 366, 367, 368, 369, 370, 432, 433, 434, 435, 453, 465, 484, 502
  - radial collector (Ranney), 260
  - single-well test, 225, 226, 260, 269
  - skin effects, 265, 266
  - slug test, 225, 226
  - specific capacity test, 226
  - step drawdown test, 267
  - virtual well radius, 267
- Well construction report (WCR), 226
- Well (WEL) Package. *See* MODFLOW code (Modular Groundwater Flow Model), packages
- Well posed inverse problem. *See* Inverse problem
- Wellhead protection, 360, 365
- Wetland, 51, 58, 135, 136, 145, 152, 153, 155, 156, 205, 216, 236, 257, 258, 259, 273, 277, 283–291, 502, 523, 527
- Wetland Package. *See* MODFLOW code (Modular Groundwater Flow Model), packages
- WHPA code, 365
- Windows in confining beds, 41
- Workflow, 10, 16–20, 27, 334, 377, 398, 399, 426–431, 458, 474
- Worst-case scenario modeling, 445, 456, 459, 469, 481, 483, 507
- Z**
- Zero flux plane, 231, 232–234
- Zero parameter sensitivity, causes for, 405, 409, 410
- Zonation, 8, 203, 222, 237, 238, 239, 240, 241, 338, 394, 412, 413–414, 435, 444
- anisotropy, 200–201
  - hydraulic conductivity, 8, 74–76, 203, 211–214, 222, 238, 239, 240
  - parameter, 8, 203, 236, 237, 238, 240, 396–411, 444
  - using pilot points with, 414
  - recharge, 230–234, 235, 238, 240
  - storativity (storage coefficient), 227, 240, 243, 244
- Zone of dispersion, between freshwater and seawater, 140, 141–143
- ZONEBUDGET, 100
- ZOOMQ3D, 364
- ZOOPT code, 364